

Stellar Spectral Classification

Princeton Series in Astrophysics

Edited by David N. Spergel

Theory of Rotating Stars, *by Jean-Louis Tassoul*

Theory of Stellar Pulsation, *by John P. Cox*

Galactic Dynamics, Second Edition, *by James Binney and Scott Tremaine*

Dynamical Evolution of Globular Clusters, *by Lyman Spitzer, Jr.*

Supernovae and Nucleosynthesis: An Investigation of the History of Matter,
from the Big Bang to the Present, *by David Arnett*

Unsolved Problems in Astrophysics, edited *by John N. Bahcall and Jeremiah
P. Ostriker*

Galactic Astronomy, *by James Binney and Michael Merrifield*

Active Galactic Nuclei: From the Central Black Hole to the Galactic Environment,
by Julian H. Krolik

Plasma Physics for Astrophysics, *by Russell M. Kulsrud*

Electromagnetic Processes, *by Robert J. Gould*

Conversations on Electric and Magnetic Fields in the Cosmos, *by Eugene
N. Parker*

High-Energy Astrophysics, *by Fulvio Melia*

Stellar Spectral Classification, *by Richard O. Gray and Christopher J. Corbally*

Stellar Spectral Classification

Richard O. Gray

Christopher J. Corbally

with

Adam J. Burgasser

Margaret M. Hanson

J. Davy Kirkpatrick

Nolan R. Walborn

PRINCETON UNIVERSITY PRESS
PRINCETON AND OXFORD

Copyright © 2009 by Princeton University Press

Published by Princeton University Press, 41 William Street, Princeton, New Jersey 08540

In the United Kingdom: Princeton University Press, 6 Oxford Street, Woodstock,
Oxfordshire OX20 1TW

All Rights Reserved

ISBN: 978-0-691-12510-7

ISBN (pbk.): 978-0-691-12511-4

British Library Cataloging-in-Publication Data is available

This book has been composed in Times

Printed on acid-free paper ∞

press.princeton.edu

Printed in the United States of America

1 3 5 7 9 10 8 6 4 2

10 9 8 7 6 5 4 3 2 1

To Robert F. Garrison,
friend, teacher, and mentor

Contents

<i>Preface</i>	xi
Important Note on Terminology and Units	xv
Chapter 1. The History and Philosophy of Stellar Spectral Classification	000
1.1 Early History	000
1.2 Later Developments	000
1.3 The MK Process	000
Chapter 2. An Overview of the Normal Stars	000
2.1 Introduction	000
2.2 The Spectral Sequence	000
2.3 Multicolor Photometry and Stellar Classification	000
2.4 Physical Principles Underlying the MK Sequence	000
Chapter 3. The OB Stars—Nolan R. Walborn	000
3.1 Introduction	000
3.2 The Optical	000
3.3 The Ultraviolet	000
3.4 The Infrared—Margaret M. Hanson	000
3.5 Peculiar Categories	000
3.6 X-Ray Line Spectra	000
3.7 Calibration and Astrophysical Modeling	000
Chapter 4. The B-type Stars	000
4.1 Introduction	000
4.2 Optical Classification	000
4.3 The Ultraviolet	000
4.4 Chemically Peculiar B-type Stars	000
4.5 Be Stars and B Shell Stars	000
4.6 Other B-type Emission-line Stars	000
4.7 B-type Stars in Advanced Evolutionary States	000

Chapter 5. The A-type Stars	000
5.1 Introduction	000
5.2 Optical Spectral-type Criteria	000
5.3 Ultraviolet and Infrared Classification Schemes	000
5.4 Chemically Peculiar Stars	000
5.5 Herbig Ae/Be Stars	000
5.6 A-type Stars in Advanced Evolutionary Stages	000
5.7 A-type Shell Stars	000
Chapter 6. The F-type Stars	000
6.1 Introduction	000
6.2 Optical Classification	000
6.3 Classification in the Ultraviolet and Infrared	000
6.4 Population II F-type Stars	000
6.5 Chemically Peculiar F-type Stars	000
6.6 F-type Stars in Advanced Evolutionary Stages	000
Chapter 7. The G- and K-type Stars	000
7.1 Introduction	000
7.2 Optical Classification	000
7.3 The Infrared	000
7.4 The Search for a Solar Twin; Chromospheric Activity	000
7.5 T Tauri Stars	000
7.6 Chemically Peculiar G- and K-giants	000
7.7 Population II and III Stars	000
7.8 The High Luminosity, Yellow Variables	000
Chapter 8. The M-type, S-type, and Carbon Stars	000
8.1 Introduction	000
8.2 The M-type Stars	000
8.3 The Carbon Stars	000
8.4 The S-type Stars	000
8.5 Symbiotic and Algol Stars	000
Chapter 9. M Dwarfs and L Dwarfs—J. Davy Kirkpatrick	000
9.1 Introduction	000
9.2 The Discovery of M Dwarfs and L Dwarfs	000
9.3 Spectroscopic Classification	000
9.4 Physical Interpretation of Types	000
9.4 Peculiar Objects	000
Chapter 10. The T-type Dwarfs—Adam J. Burgasser	000
10.1 Introduction	000
10.2 Recognition of the T Dwarf Class and Early Discoveries	000

CONTENTS	ix
10.3 T Dwarf Spectral Characteristics	000
10.4 Near-Infrared Classification	000
10.5 Optical Classification	000
10.6 Mid-Infrared Classification	000
10.7 Additional Considerations for T-Dwarf Classification	000
10.8 Beyond the T Dwarfs	000
Chapter 11. Wolf-Rayet Stars and the Luminous Blue Variables	000
11.1 The Wolf-Rayet Stars	000
11.2 Luminous Blue Variables	000
11.3 Evolutionary Connections	000
Chapter 12. Endpoints of Stellar Evolution	000
12.1 Proto-Planetary Nebulae and Planetary Nebula Nucleus Stars	000
12.2 White Dwarf Stars	000
12.3 Novae	000
12.4 Supernovae	000
Chapter 13. Further Techniques	000
13.1 Introduction	000
13.2 Composite Spectra	000
13.3 Classification Systems in the Thermal Infrared	000
13.4 Other Classification systems	000
13.5 Automated Methods of Spectral Classification	000
13.6 Low Dispersion Techniques and Natural Groups	000
Glossary	000
Appendix A: MK Standard Stars	000
Appendix B: Calibrations of the MK System	000
Appendix C: The Book Website	000
General Index	000
Object Index	000

Preface

Stellar spectral classification has played a seminal role in the development of modern astronomy. A perusal of this book will show that it continues to be at the forefront of many important discoveries and developments in stellar astrophysics, not the least of which is the current exciting work involving the L and T dwarfs. As a consequence, it is a pity that many professional astronomers were exposed to MK spectral classification only in an introductory class taken during their freshman year at university, or perhaps as an aside in a course on astrophysics, and thus are unacquainted with its wide scope of application and its power as a tool for astrophysical insight.

We, the two primary authors of this book, have felt for some time the need for a new and comprehensive survey of stellar spectral classification. The last major monograph on the subject was written by Carlos and Mercedes Jaschek in the late 1980s, just at the end of the photographic era, when astronomers were transitioning to digital detectors. That book came too early to cover the recent developments in the spectroscopy of low-mass stars and brown dwarfs, and of course, could not cover results from the Hubble Space Telescope, FUSE, ISO, and Spitzer which still lay in the future. Moreover, with this new book, we can present the philosophical foundation of the MK spectral classification system and the critical importance of standard stars, while including a discussion of the physical basis for spectral and luminosity classification. And thus the power, vitality, and beauty of spectral classification as a technique will become quite clear.

We hope that this book will prove to be an interesting and indeed inspiring introduction to the subject. For, even though the MK system is celebrating its 65th birthday as this book reaches print, there is still much work to be done to perfect the system, and still many discoveries to be made. The primary purpose of this book is to introduce a new generation of astronomers to spectral classification, but we hope it will also serve as a useful introduction to the field of stellar astronomy itself. If our readers learn only a fraction of what we have learned in writing the book, we will consider it a success. We have written it with both the graduate student and the professional astronomer in mind, but it should also be accessible to an advanced undergraduate.

The book begins with a review of the history of stellar spectral classification and its major contributions to the fields of stellar astrophysics and Galactic struc-

ture. The first chapter then goes on to discuss the philosophical foundations of the MK system as well as giving practical guidance on using the technique of MK classification. It also discusses the extension of the system to other wavelength regions and stellar types. The purpose of the second chapter is to give the non-spectroscopist an overview of the spectral sequence as well as a basic understanding of the physics behind the changes in the appearance of stellar spectra with temperature. It also introduces some of the terminology commonly used in stellar classification. Stellar astronomers can give this chapter a miss, but undergraduates, graduate students, and others may profit from it, as it brings together basic important information usually taught (if taught at all) in a number of different classes. The main part of the book commences with Chapter 3, on the OB stars, written by Nolan Walborn, with the infrared section written by Margaret Hanson. Nolan has made major and fundamental advances in the study of the OB stars, and Margaret is well-known for her work on OB stars in the infrared. Chapters 4–8 continue with the traditional spectral sequence (OBAFGKM), including, in Chapter 8, in addition to a discussion of the M-type giants, a review of the carbon and S-type stars. Chapters 9 and 10 discuss the spectral classification of low-mass stars and brown dwarfs. Chapter 9, on the M and L dwarfs, was written by Davy Kirkpatrick, a pioneer in brown-dwarf spectroscopy, and Chapter 10 by Adam Burgasser, one of the prime movers in T-dwarf research. Chapter 11 covers the Wolf–Rayet stars and the luminous blue variables, and Chapter 12 stars in advanced evolutionary stages, including the white dwarfs, novae, cataclysmic variables, and supernovae. Finally, Chapter 13 discusses composite spectra due to two or more stars, and makes the linkage between stellar spectroscopy and the spectroscopy of galaxies. Chapter 13 also considers classification in the thermal infrared, and techniques of automated classification, and their application to the large-scale surveys now underway, such as the Sloan Digital Sky Survey, and surveys in the future, such as *Gaia*. The book has a wealth of figures, many of which have not appeared in the literature before. Indeed, it is our hope that these figures might act as a sort of spectral classification “key” for the baffled astronomer confronted with an unusual spectrum. At the end of the book, we have included a glossary, some handy appendices, and what we hope is a useful index.

We are grateful for the support and encouragement received during the nearly two and a half years it took to write and edit this book. First, we would like to acknowledge our gratitude to Bob Garrison, to whom this book is dedicated, for his support as a teacher, friend, and mentor to both of us over the years. We also are very grateful for the contributions of our coauthors, Nolan Walborn, Margaret Hanson, Davy Kirkpatrick, and Adam Burgasser, as they have added immeasurably to the value of this book. We would also like to thank Alex Fullerton, Pat Boeshaar, and Jim Liebert for critiquing draft versions of certain chapters in this book and for their valuable suggestions. Also Joe Pollock for pointing out to us the *NY Tribune* 1873 article, a quote from which begins Chapter 1, Nancy Houk and Francesco Rossi for conference and atlas pictures, and many other astronomers for generously giving permission for use of illustrations and spectra (including spectra

in online repositories) and for answering queries. We would like to thank Jeanette Hopkins for guidance on various matters related to publishing books. We are deeply grateful for the support, encouragement and help of Ingrid Gnerlich, Senior Editor, Physical and Earth Sciences, and Brigitte Perner, Senior Production Editor at Princeton University Press. We are also grateful for the skilled work of the copy editor, Lee A. Young. ROG would like to thank the Vatican Observatory Research Group both in Tucson, AZ, and at Castel Gandolfo, as well as IPAC (Caltech) and the Dominion Astrophysical Observatory for hospitality on his sabbatical during which time he was writing portions of this book. He would also like to thank the chair of the department of Physics and Astronomy, Appalachian State University, Tony Calamai, for a generous amount of release time during the writing and editing of this book. Both ROG and CJC would like to thank Vatican Observatory Directors George Coyne and Jose Funes for their material support and encouragement. Finally, both of us, but obviously especially ROG, would like to thank Mary Gray from the bottom of our hearts for her constant support, encouragement, and patience during the writing of this book, especially as she was writing and editing a book of her own during this time! Without her, this book would have been impossible, and we really mean that!

Richard O. Gray & Christopher J. Corbally, Boone NC, July 2008

Important Note on Terminology and Units

Stellar spectroscopy for historical reasons has its own set of physical units and conventions, which may be somewhat unfamiliar to readers from other fields of physics or even astronomy. The practice in stellar spectroscopy is to use the cgs (centimeter–gram–second) system instead of the more familiar MKS system. Thus the acceleration of gravity (g) at the surface of the star is in units of cm s^{-2} (although it usually appears as the logarithm, $\log g$), energy in ergs, and luminosity in erg s^{-1} . Stellar spectroscopists commonly use the *electron volt* (eV) for energy in the context of atomic physics (excitation energies, ionization potentials, etc.); $1 \text{ eV} = 1.602 \times 10^{-12} \text{ erg}$. Wavelength is traditionally measured in angstroms ($1 \text{ \AA} = 1 \times 10^{-10} \text{ m}$) for the ultraviolet and optical parts of the spectrum, and microns ($1 \mu\text{m} = 1 \times 10^{-6} \text{ m}$) in the infrared. It is customary to indicate the wavelength of a spectral line in angstroms with the Greek letter λ as a prefix, thus $\lambda 4226$ instead of 4226 \AA . Two or more wavelengths in a series are denoted, for instance, $\lambda\lambda 4076, 4101$ and 4121 . The units employed for monochromatic flux are $\text{erg cm}^{-2} \text{ s}^{-1} \text{ \AA}^{-1}$. However, the mass, radius, and luminosity of a star are often expressed in solar units ($M_{\odot}, R_{\odot}, L_{\odot}$) where

$$\begin{aligned} 1 M_{\odot} &= 1.981 \times 10^{33} \text{ g} \\ 1 R_{\odot} &= 6.955 \times 10^{10} \text{ cm} \\ 1 L_{\odot} &= 3.839 \times 10^{33} \text{ erg s}^{-1} \end{aligned}$$

We follow all these conventions in this book!

Terminology for wavelength regions is used inconsistently in stellar astronomy. Throughout much of this book (with the exceptions of Chapters 9 and 10 on the M-, L-, and T-type dwarfs) by *optical* we mean the part of the spectrum visible to the eye, conventionally $3900\text{--}7000 \text{ \AA}$. The ultraviolet is commonly split into a number of pieces, the *near-ultraviolet* (NUV) and the *far-ultraviolet* (FUV), but how those terms are used often depends on the context. For instance, for ground-based observations, the NUV is used to refer to the wavelength region from the atmospheric cutoff (about 3000 \AA) to 3900 \AA , but the IUE, HST, and GALEX satellites all have their own definitions of NUV and FUV. See §3.3 for more details. For the infrared, except for Chapters 9 and 10, we conform to the common practice of defining the *near-infrared* (NIR) to be the spectral region extending from H α (6563 \AA) to $1 \mu\text{m}$ (10000 \AA), the *infrared* or *mid-infrared* to be the region encom-

passing the *J*, *H*, *K*, and *L* bands (about 1–4 μm), and the *thermal-infrared* from 4 μm up to the submillimeter region (beginning about 200 μm). But astronomers who work on cool stars use this terminology differently. In Chapters 9 and 10 the *optical* or the *red-optical* stretches from 4000 to ~ 10000 Å, the *near-infrared* from about 1 μm to about 4 μm , and *mid-infrared* from about 4–15 μm . We have conformed to these uses, even though this results in somewhat inconsistent terminology in the book, so that readers will not have to make the transition when they turn to the literature.

Another instance of idiosyncratic terminology used in this book is the terms *early-type* and *late-type* to refer to stars hotter and cooler, respectively, than the Sun. Thus, the O-, B-, A-, and F-type stars are early-type, and the G-, K-, M-, L-, and T-types are late-type. In addition, we refer to main-sequence stars as *dwarfs* (not to be confused with white dwarfs). The term *subdwarf* is a term that has been used in various contexts in stellar spectroscopy. We tend to avoid this term; see the Glossary entry for extra information.

Stellar Spectral Classification

Chapter One

The History and Philosophy of Stellar Spectral Classification

1.1 EARLY HISTORY

1.1.1 The Pioneers of Spectral Classification

Thus, ladies and gentlemen, I have endeavored to set before you what the spectroscope has done for astronomy. . . . And much as it has done in the last 10 years we are yet upon the mere threshold of its discoveries.¹

Prof. C. A. Young, speaking those concluding words before the American Institute at Cooper Union on “The Astronomical Conquests of the Spectroscope,” was quite right. They were all witnessing exciting times for astronomy. Just ten years earlier, in 1863, each of Giovanni Battista Donati, George Airy, William Huggins, Lewis M. Rutherfurd, and Angelo Secchi had published pioneering papers on their stellar spectroscopic observations. Joseph Fraunhofer in Munich had first observed solar and stellar spectra in 1814, but after his death in 1826 the science of stellar spectroscopy languished. Brief revivals occurred from J. Lamont setting up Fraunhofer’s equipment in Munich again, from William Swan, also a Scottish scientist, and from I. Porro in Paris, but the lasting revival had to wait Donati’s modest descriptions of stellar spectra that began in 1860 in Florence.

With similar inspiration to Donati’s, perhaps just “in the air” of the times, pioneering research fields in stellar spectroscopy were launched by the other four stellar spectroscopists who published in 1863. It was Airy who started the Royal Greenwich Observatory’s extensive program to measure the Doppler motions of stars.

Huggins, from his observatory near London and with his assistant William Miller, pursued the coincidences between laboratory spark spectra and the lines found in stellar spectra. From these comparisons he concluded that “a common chemistry . . . exists throughout the universe” (Huggins 1909). He was also interested in the nature of nebulae, believing that the bright emission lines of some of these were due to nitrogen, not a mysterious ‘nebulium.’ He also investigated novae and cometary spectroscopy.

Rutherfurd was clearly a skilled instrumentalist who experimented with celestial photography and making diffraction gratings. From his private observatory in

¹C. A. Young, as reported in the *New York Tribune*, Tuesday, January 28, 1873, p. 3.

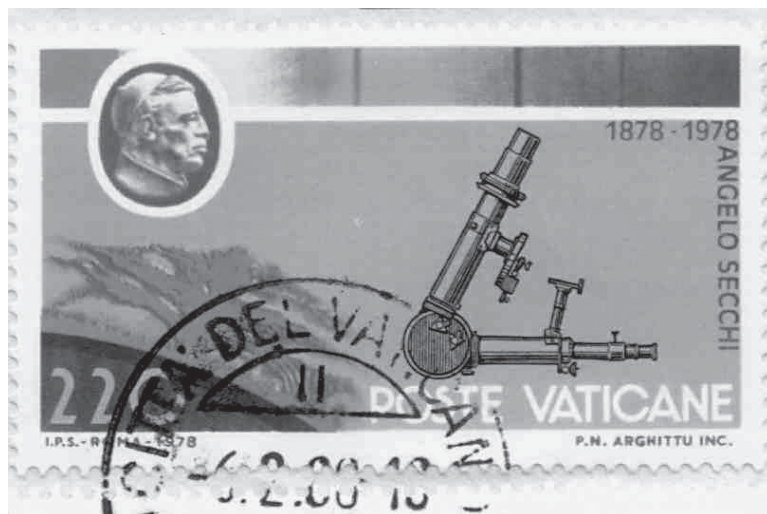


Figure 1.1 Vatican stamp commemorating the centenary of Father Angelo Secchi's death. Reproduced by permission of the Vatican City.

New York state he amassed sufficient spectra to attempt the classification of stars into three groups: those showing color like the Sun with many lines and bands; those like Sirius, which are white stars with lines unlike the Sun; and those like Rigel, which are also white but show no lines. Modern equivalent groups would be the late-type stars, the late-B to early-F stars, and the OB stars.

Secchi, after travels in the United States, returned to Italy and became director of the Roman College Observatory. His wide interests covered meteorology, terrestrial magnetism, sunspots and other solar chromospheric phenomena, double stars and comets, besides spectroscopy, as the stamp in Figure 1.1 commemorates. In 1863 he classified the spectra of stars into two classes, basically the early- ("I") and the late-types ("II").² In 1866 he added what are now the M-types ("III"), and two years later he identified some faint red stars as type "IV," the carbon stars. Later yet he felt compelled to separate some emission-line stars into a further class, "V". Discovering the carbon stars and correlating their bands with the "reversed spectrum of carbon," the laboratory emission spectrum, was a great achievement of Secchi. He also identified the strong lines in class I as due to hydrogen and surmised from their breadth in Sirius that "this could lead one to estimate the considerable pressure that the gas possesses in the atmosphere of this star" (Secchi 1870).

If we have written a little more on Secchi than on the other spectroscopic pioneers, one reason is because he was the most prolific in observations, with at least 4,000 classified stars to his name. He illustrates a first principle of classification—amass as many specimens as possible. These showed him that there were varieties

²The terms "early" and "late" refer to hotter and cooler stars respectively. They came from an understanding of stellar evolution that proved incorrect, but the terms stuck as convenient, a concession made in the 1922 IAU adoption of the Draper classification system.

of stellar spectra that could not be covered by his classes. His examination of the spectra also led him to consider the astrophysics behind the diversity that he found in them.

A competition among these four pioneers is invidious. In a solidly researched and well detailed history of astronomical spectroscopy, on which this shortened account depends, John Hearnshaw (1986, p. 52ff) reviews who might be considered the first stellar spectroscopist, but more telling are the similarities and differences he finds between each. Airy's recording of line positions eventually led to radial velocity work, though Secchi mentioned the possibility while Huggins actually attempted it. Rutherford, who prided himself on his efficient instrumentation, included what later became photometric color indices in his approach to classification, while Secchi relied purely on the spectral features. Huggins was interested in the composition of stars and in the physical conditions that led to the spectra seen, and Secchi's own observations brought these same questions to mind. They were all founders, all "caught up in the wave of enthusiasm for spectroscopy that followed Bunsen and Kirchhoff's announcement in 1859 and 1860 of the solution of the mystery of the Fraunhofer lines and their interpretation in terms of radiation theory spectrum analysis" (Brück 1979). Each of the founders had his own emphasis. So while Hearnshaw (1986, p. 77) makes a good case that Huggins be regarded as the founder of stellar spectroscopy, Secchi's pure and prolific approach makes him the father of stellar spectral classification along with the branches of astrophysics that his methodology encouraged.

1.1.2 More Foundational Classification Schemes

Hermann Carl Vogel's spectroscopic research first began at Bothkamp near Kiel, where he was appointed director in 1870, and continued at Potsdam some four years later (Figure 1.2). He combined Secchi's classes III and IV, since they were both based on broad bands, and went on to subdivide the resulting three classes. However, the discovery of helium both in stars and on earth was to revise his scheme in 1895, subdividing his class Ia.

One of the namers of "helium," Norman Lockyer in London, was also to offer his own spectral classification scheme that was developed around 1890. However, the differentiation of stars into ascending and descending temperature branches was based on his "meteoritic hypothesis" for the origin and subsequent evolution of stars (Figure 1.3). In this putting of theory before classification he joined Vogel in what gave rise to his particular scheme. Still, while Lockyer's undisciplined theories and so his classifications were never generally accepted, he did at least distinguish the spectra of giants and supergiants (heating on his ascending branch) from those of dwarfs (cooling, as the Sun was supposed to be doing).

An amateur astronomer, F. McLean, started an objective prism survey down to 3.5 magnitude from his backyard in Tunbridge Wells, Kent, and completed the survey two years later in 1897 when he visited the Cape Observatory, South Africa. His spectral classification system was able from the beginning to include the stars

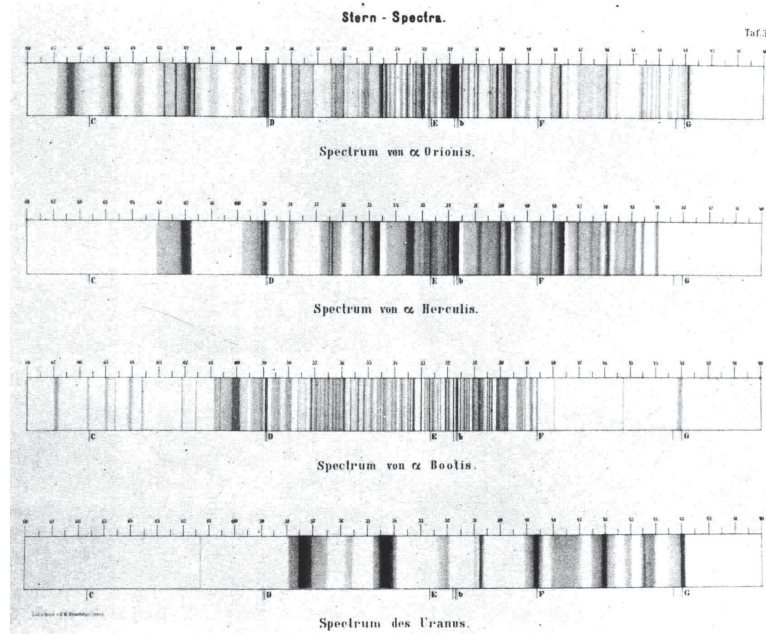


Figure 1.2 Stellar spectra drawn by Vogel at Bothkamp. Reproduced by permission of the Royal Society.

with neutral helium absorption. It was modeled on Secchi's, with Vogel-like revisions, and his groups corresponded to the MK series of B, A, F, G-K, M, and carbon stars. The spectra of stars seemed to be grouping themselves into consistent order, even under the eyes of different classifiers. These observers were also now using photography effectively to give themselves better quality spectra with which to work. One resulting remarkable discovery of McLean was to find that some lines in "helium stars" corresponded to the spark spectra for oxygen.

1.1.3 The Draper system

The developments in spectral classification that took place at the Harvard College Observatory, Cambridge, Massachusetts from 1885 for about four decades are most significant in our story (Figure 1.4). Here we have the energy of Edward C. Pickering who, as director, had the foresight to start an all-sky, spectroscopic survey. That foresight found an ally in Mrs. Anna Palmer Draper, who wanted to give a suitable memorial to the stellar spectroscopic activities of her late husband, Henry.

Accordingly, Mrs. Williamina Fleming was assigned to examine the first survey's spectra, from which came both a classification and an estimate of magnitude for the 10,351 stars in the Draper Memorial Catalogue of 1890. For its classification scheme Pickering and Fleming subdivided the four Secchi types so that thirteen "letter" types resulted, and to these were added O for Wolf-Rayet (WR)

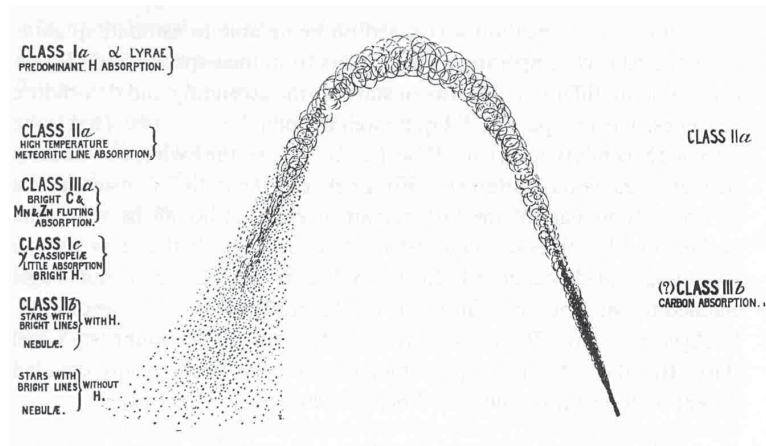


Figure 1.3 Lockyer's temperature curve for spectral evolution, showing his ascending branch of supergiants and giants and the descending branch of dwarfs. Reproduced by permission of the Royal Society.



Figure 1.4 A photograph taken in 1892 at the Harvard College Observatory showing Williamina Fleming (standing) and Annie Jump Cannon (far right, looking through eyepiece). Courtesy, Curator of astronomical photographs at Harvard College Observatory.

spectra with bright lines, P for planetary nebula spectra, and Q for spectra remaining unclassified. So these Draper Memorial types introduced the letters with which we are familiar today. Most of the letters persisted; the O and B types were later put at the head; some were dropped, others changed, such as the C stars with double lines probably due to an instrumental fault; and as always, there was plenty of

scope to refine the types by further subdivision. However this was a most significant start, again helped by a much increased database of spectra.

The brighter stars were assigned to Miss Antonia Maury. To classify these more detailed spectra Maury reverted to Roman numerals for her 22 groups, I to XXII, the last being the WR stars. She was the first to place the Orion or B stars ahead of those with strongest hydrogen, the A stars. While she had in mind an evolutionary sequence in doing this, it was not explicitly a temperature sequence. Another innovation was that Maury's groups were further divided according to the appearance of the lines in their spectra. So the addition of lowercase letters would refer to whether the lines were average width (a), hazy (b), or sharp (c). The hazy no doubt included rapid rotators and unresolved double-lined binaries. The c stars were comparatively few in number but were the indication of a "collateral division" among stars, which we now know to be luminosity. Not everyone appreciated such details and divisions, which amounted to some 74 types; the supporters of Vogel's system back in Europe were particularly critical of all these complications in spectral classification.

Miss Annie Jump Cannon entered the Harvard scene to tackle the classification of the southern bright stars. Her 1901 classification scheme reverted to the letter types of Fleming, but updated for the Orion lines in the B stars and the Pickering series lines in the O stars. The letters were in the now familiar MK order—OBAFGKM (Table 1.1), so in this she followed Maury but put the WR stars firmly at the head. To cope with better precision available in the spectra, rather than adding letters along the lines of Maury adding Roman numerals, she was the first to subdivide the letters into decimal types. The notation for these decimal types settled into the now familiar A0, A2, etc. Among the stars not fitting into this scheme Cannon commented on those with peculiar silicon (also noted by Maury) or strontium, and particularly the metallic-line A stars, now called the Am stars.

With the publishing of the last of four catalogues in 1912 the Draper Catalogue was complete, as was its classification scheme. A Committee on the Classification of Stellar Spectra was formed to gather comments on whether this was the most useful scheme to date. The 28 replies from prominent spectroscopists in 7 countries were published by the committee's secretary, F. Schlesinger (1911). Most were favorable to the Draper system, with some understandable support for the Potsdam scheme of Vogel. Interestingly, Henry Norris Russell supported the non-alphabetical order of the letters since "This helps to keep the novice from thinking that it is based on some theory of evolution" (*ibid.*); and of significance was Karl Schwarzschild's recommendation to keep the number of variables limited since "ultimately the spectrum of a star might depend on nothing other than its mass, its age and its temperature" (*ibid.*). The tentative adoption of the Draper system became formal in Rome at the first General Assembly of the International Astronomical Union in 1922 (IAU 1922).

Work on peculiar stars continued at Harvard, particularly by Fleming up until her death in 1911. In October of that year Cannon started what Newall (1920) well described as "a piece of work of colossal magnitude," the Henry Draper (HD) Catalogue program (as distinct from the earlier Draper Catalogue of Stellar Spectra)

Table 1.1 The Principal Early Spectral Classifications

Secchi type	Vogel class	McLean division	Lockyer genus	Pickering class ^a	Maury group	Cannon class ^b
(V)	—	—	—	P	—	P
(V)	IIb	(Ia)	Argonian	O	XXII	Oa
(V)	IIb	(Ia)		O	XXII	Ob
(V)	IIb	(Ia)		O	XXII	Oc
(V)–IO	IIb	(Ia)		O	XXII	Od
(V)–IO	IIb	(Ia)		O	XXII	Oe
IO ^c	Ib	Ia		B	I	Oe5
IO	Ib	Ia	Alnitamian	B	II	B0
IO	Ib	Ia		B	III	B1
IO	Ib	Ia	Crucian	B	IV	B2
IO	Ib	Ia	Taurian	B	IV	B3
IO	Ib	Ib		BA	V	B5
IO–I	Ib	Ib	Algolian	BA	VI	B8
IO–I	Ib	Ib	Rigelian	BA	VI	B9
V	Ic1, Ic2	—	Crucian	D	L	OeSp–B9p
I	Ia2	II	Markabian	A	VII	A0
I	Ia2	II	Sirian	A	VIII	A0
I	Ia2	II	Cygnian	A	VIII	A2
I	Ia2	II		AF	IX	A2
I	Ia3	III		AF	IX–X	A3
I	Ia3	III		AF	X	A5
I	Ia3	III		F	XI	F0
I	Ia3	III		F	XI–XII	F2
I–II	Ia3–IIa	III	Procyonian	FG	XII	F5
II	IIa	IV	Polarian	G	XIII	F8
II	IIa	IV		G	XIV	G0
II	IIa	IV		GK	XIV–XV	G5
II	IIa	IV	Arcturian	K	XV	K0
II	IIa	IV		K	XV–XVI	K2
II–III	IIa–IIIa	IV–V	Aldebarian	KM	XVI	K5
III	IIIa	V	Antarian	Ma	XVII	M0 (Ma)
III	IIIa	V		Ma	XVIII	M0 (Ma)
III	IIIa	V		Mb	XIX	M3 (Mb)
III	IIIa	V		(Mc)	—	M6,5 (Mc)
III	IIIa	V		Md	XX	Md
—	—	—		—	—	S
IV	IIIb	VI			XXI (?)	R0
IV	IIIb	VI			XXI (?)	R3
IV	IIIb	VI			XXI (?)	R5
IV	IIIb	VI			XXI (?)	R8
IV	IIIb	VI	Piscian	Na	XXI	N0 (Na)
IV	IIIb	VI			XXI	N3 (Nb)
IV	IIIb	VI			XXI	Nc
—	—	—	—	—	—	Pec
—	—	—	—	—	—	Con

^aIn collaboration with Mrs. Fleming.^bThe Draper Classification.^cSecchi's Orion subtype.

From Hearnshaw (1986), as adapted from Curtiss (1932).

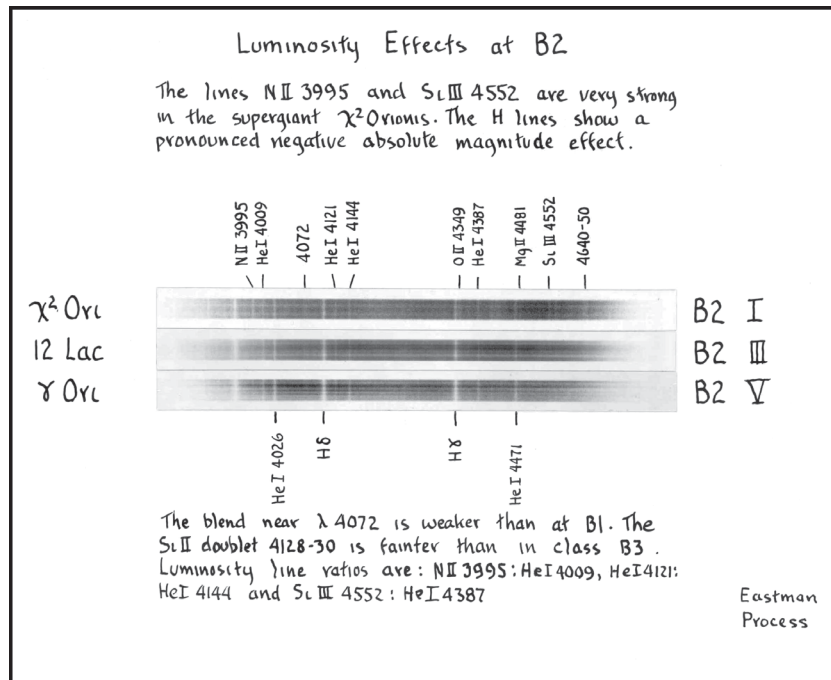


Figure 1.5 A plate from the spectral atlas of Morgan, Keenan, & Kelleman (1943), showing a luminosity montage at B2. Reproduced courtesy University of Chicago Press.

to classify spectra of 225,300 stars. Four years later the classifying was essentially complete and the catalogue eventually all published by 1924 at the cost of \$1 per star—real value for money! Its classification scheme was that of the Draper Catalogue, but with a little revision at the bottom end of the sequence. The earlier types were holding up well, even with such an enormous increase in data.

The HD catalogue was extended under Harlow Shapley, who was interested in questions of galactic structure. The additional 46,850 spectral types for fainter stars in the northern hemisphere, comprising the Henry Draper Extension (HDE), were again on the Draper system, even if G-star types were a bit earlier and M star types a bit later when compared with the main HD catalogue. By the time of her death in 1941 Cannon had classified over 395,000 stars (Hearnshaw 1986, p. 138). While this monument to her achievement will eventually be surpassed numerically by a machine, her profound impact on stellar and Galactic astronomy will certainly remain.

1.1.4 Preparing for the MK System

In the MKK Atlas of 1943 (Figure 1.5), which inaugurated the current MK system of stellar spectral classification, six investigators were acknowledged as having the most important influence on it: Antonia Maury, Annie Cannon, Norman Lockyer, Walter Adams, Bertil Lindblad, and E. Gwyn Williams. This was because the MK

system, while inheriting the revised Draper system, brought the second dimension of luminosity firmly into the classification of stars.

We have indicated the development in temperature ordering, initiated by Lockyer, and the general acceptance of the letter and decimal type classes for spectral type, showing Maury's and Cannon's influence. In this story there have also been pointers to how the realization of a second dimension arose by the three astronomers just mentioned. Others involved in this development whom we have not yet mentioned must include Walter Adams and Arnold Kohlschütter working at the Mt. Wilson Observatory, with Adams later becoming its director. They repeated the discovery by Monck, Hertzsprung, and Russell of the relationship between the intrinsic luminosity of a star and its proper motion and parallax, but also noticed that there were spectral differences between the low and high luminosity stars. They identified some luminosity sensitive lines, and by using ratios of these lines with ones that were insensitive they calibrated a star's luminosity ratios against its absolute magnitude. The technique of spectroscopic parallaxes was born and with it a new way to probe Galactic structure. As an historical note, it was Adams who chaired the Spectral Classification Committee of the Rome IAU in 1922. An earlier historical curiosity was Russell at an RAS meeting in 1913 attributing the terms "giant" and "dwarf," perhaps erroneously (Hearnshaw 1986, p. 215), to Hertzsprung while discussing the diagram that later would carry both their names (thanks to Bengt Strömgren).

Lindblad is acknowledged in the MKK Atlas both for his connecting the width of the wings of Balmer $H\gamma$ with the luminosity of an early-type star and for discovering the luminosity sensitivity of the CN molecular bands in late-type stars. He started this work around 1921 at Mt. Wilson Observatory, thus inheriting the work of Adams and others, and continued it at Uppsala and Stockholm. From 1931 E. G. Williams also spent a couple of years at Mt. Wilson studying the lines in O and B stars. He showed that line ratios, rather than absolute line intensities, could improve the Draper subtypes for these stars. Among those line ratios were those for the neutral helium singlet-to-triplet series, as discovered earlier by Struve (1928). Struve (1929) also was critical in developing the explanation of the Stark effect for the luminosity sensitivity of hydrogen and helium lines. Another who could have been acknowledged by MKK includes Plaskett (1922), since he clearly separated WR from O stars, but no doubt a line has to be drawn somewhere of whom to mention, as here too.

1.1.5 The MK System

The most obvious new feature of the MK system is its fully-fledged luminosity classes, I to V, attached to the various temperature classes. These were introduced by W. W. Morgan after he had realized that in the $\log g - \log T$ diagram,³ as in the observational H-R diagram, each grouping of stars from the main sequence

³ g stands for the *surface gravity* of the star, which is correlated with luminosity class, in that class V stars (dwarfs) have high gravities and class I stars (supergiants) have low gravities. T stands for the *effective temperature* of the star, which is correlated with spectral class. Thus, the $\log g - \log T$ diagram is the theoretical

and upwards in luminosity formed a sequence of near constant $\log g$. Stars readily wanted to be grouped according to gravity as well as according to temperature, and this grouping could be done by criteria in their spectra. This discovery was confirmed by Morgan finding that the color photometry of normal stars followed that of their spectral classification, so no third parameter was needed for such normal stars. This insight was taken to heart by Morgan's collaborator, Philip. C. Keenan, and celebrated in the 55 prints, produced by Miss Edith Kellman, of blue-violet slit spectra from the Yerkes 40" refractor that comprised the 1943 MKK *Atlas of Stellar Spectra*. Just over half of these prints, 23, showed luminosity effects at different spectral types, so the emphasis of the Atlas was clear.

The MKK Atlas certainly also brought refinements to the criteria employed in classification. However, a large set of standard star spectra, "specimens," were included to demonstrate that the classifications were ultimately based on a morphological match with those standards rather than on the criteria, however much refined. So there were advances both in technique and in philosophy within the new system.

Thirteen of the MKK Atlas plates showed peculiarities in spectra. These plates indicated that the scheme was by no means the final word. A greater discrimination was possible and indeed there was "incompleteness in the system itself" (Morgan 1984). Other populations of stars were to be introduced (see §1.2), and new atlases were to be offered by both Morgan and Keenan, for instance, the Keenan–McNeil atlas—Figure 1.6 (Keenan & McNeil 1976)—and the Morgan, Abt, & Tapscott atlas (Figure 1.7, Morgan, Abt, & Tapscott 1978), but this MKK Atlas, with its grid of standard stars as a firm foundation, has remained definitive of the approach to classification by the MK System.

1.2 LATER DEVELOPMENTS

The publication of the MKK Atlas in 1943 introduced to astronomy a new and powerful tool, and Morgan and his colleagues were eager to use this tool to solve some of the "big questions" of the day. One such "big question" was the detection of spiral structure in the Milky Way Galaxy. Spiral structure in the Milky Way's neighbor, the Andromeda Galaxy, is correlated with the distribution of blue giant and supergiant stars, many of which are clustered in *OB associations*, and thus Morgan reasoned that if the distribution of this same class of stars could be plotted in the solar neighborhood, the local spiral structure could be discerned. Work therefore concentrated on deriving accurate absolute magnitudes for the B-type stars, so that their distances could be determined (e.g., Bidelman 1954). In 1951, at a meeting of the American Astronomical Society, Morgan, Sharpless, and Osterbrock announced the detection of spiral structure in the Milky Way (see Figure 1.8). A more detailed analysis was later published in Morgan, Whitford, & Code (1953).

counterpart of the observational Hertzsprung–Russell (H–R) diagram, which plots luminosity versus spectral class. See Chapter 2 for more details on both parameters.

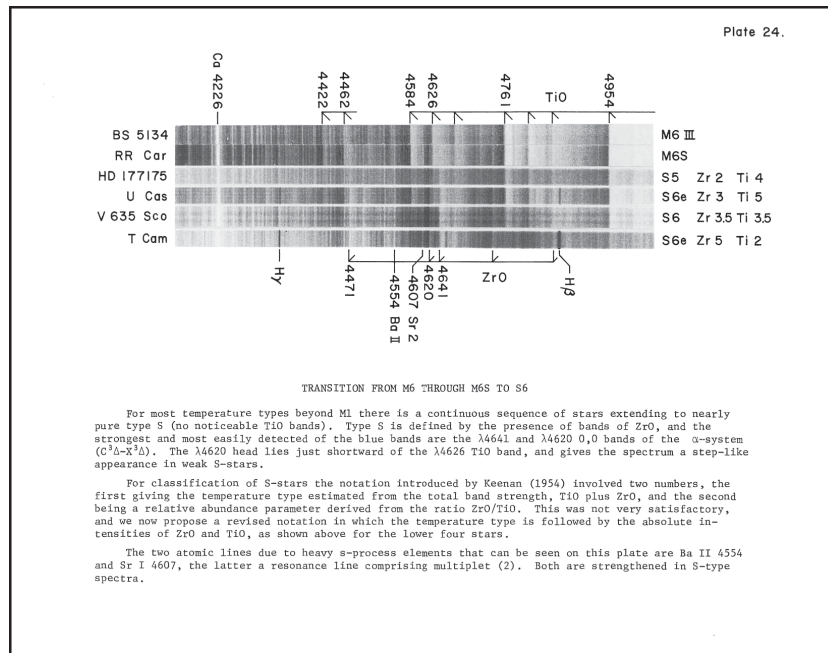


Figure 1.6 A plate from the spectral classification atlas of Keenan & McNeil (1976). Reproduced courtesy Raymond McNeil.

Morgan's inspiration that spectral classification could be used as a tool to probe the spiral structure of the Milky Way Galaxy marked the coming of age of the MK spectral classification system as a powerful technique for investigating problems in the fields of Galactic structure and stellar astrophysics. One of Morgan's graduate students, Nancy Grace Roman (Figure 1.9), made a critically important contribution to the study of Galactic structure and evolution. At that time (the early 1950s), astronomers were aware of the existence of two populations of stars in the Milky Way Galaxy, called Population I and Population II. The discovery of these two populations came about through the work of Walter Baade (Baade 1944) who, taking advantage of the blackout conditions in southern California during the war, was able to use the Mount Wilson 100-inch reflector to obtain high-resolution photographs that resolved the nucleus of the Andromeda Galaxy, its dwarf elliptical satellites M32 and NGC 205, as well as the ellipticals NGC 147 and NGC 185 into stars. Baade realized from these photographs that the stellar population in these spheroidal systems was dominated by K-type giants, very unlike the stellar population of the spiral arms of the Andromeda Galaxy and indeed the disk of our own Milky Way Galaxy, which are dominated by B supergiants. This led Baade to suggest that the stars in both Andromeda and the Milky Way could be divided into two populations. In Population I, Baade included the stellar types typical of the Galactic disk, i.e. stars in open clusters, OB stars, and most stars of the solar neighborhood, including the Sun. Population II, on the other hand, included

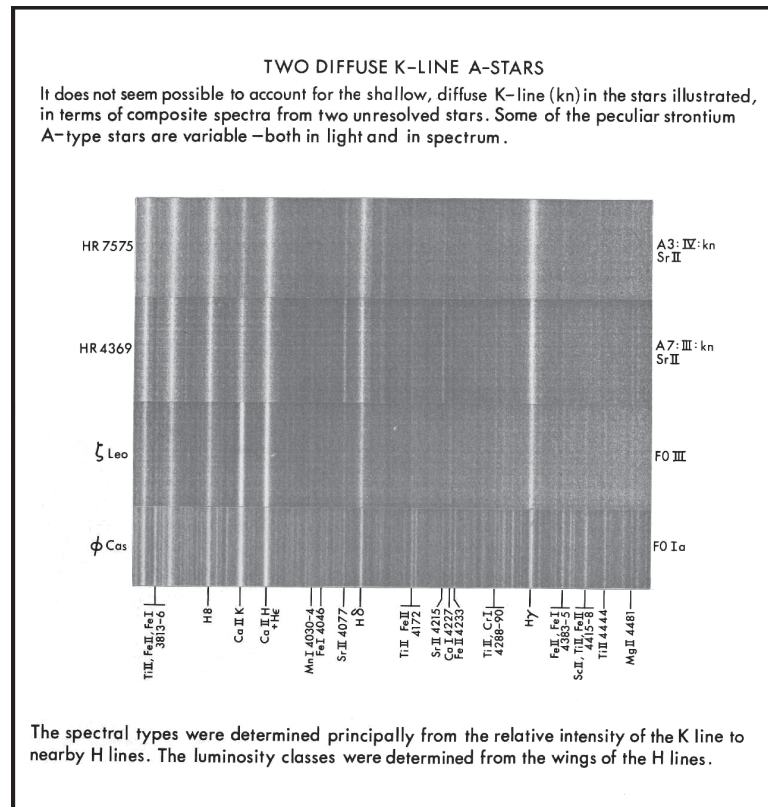


Figure 1.7 A plate from the spectral classification atlas of Morgan, Abt, & Tapscott (1978). Reproduced courtesy Helmut Abt.

some K-type giants, “cluster variables” (i.e. RR Lyrae variables), subdwarfs (i.e. stars that appear to lie below the main sequence on the Hertzsprung–Russell diagram), and stars in globular clusters. One distinguishing feature between the two populations in the Milky Way Galaxy was the velocity relative to that of the Sun. Population II objects are high-velocity objects, whereas Population I stars have low velocities.⁴

It was at this point that the work of Roman supplied a critical missing link. Roman (Roman 1950, 1952, 1954) studied samples of F, G, and K-type stars and discovered, through spectral classification, a set of weak-lined dwarf and giant stars that she found had, as a group, systematically higher velocities than the normal strong-lined stars. These weak-lined (low metal abundance), high-velocity stars were identified as Population II stars passing through the solar neighborhood. This discovery supplied the critical link between stellar kinematics and chemical

⁴The phrase “relative to the Sun” is important here, as the Sun executes a circular orbit around the center of the Galaxy with an orbital velocity of about 240 km/s. Stars executing similar orbits will have low velocities relative to the Sun, whereas stars with orbits out of the plane of the disk and/or elliptical orbits will have high relative velocities.

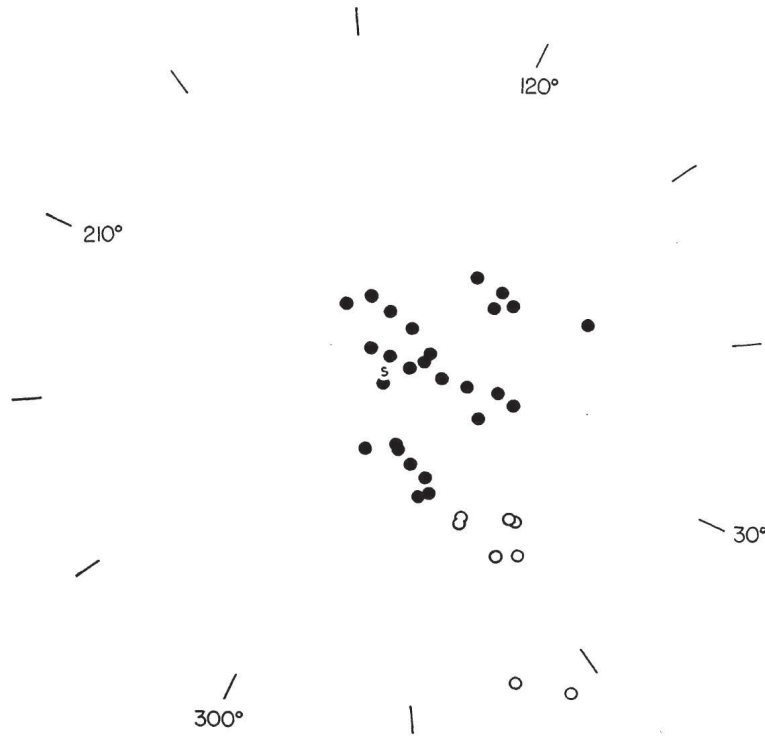


Figure 1.8 The delineation of spiral structure in the Milky Way Galaxy by Morgan, Whitford, & Code (1953) by plotting the space distribution of blue giants. The Sun is marked by an “S” at the center, and the Galactic center is at a longitude of 327° in this figure, toward the bottom of the page. The dark circles represent aggregates (OB associations) of blue giants, whereas the open circles represent single stars. The Sun appears to be on the inner edge of a linear feature, now known as the Orion–Cygnus arm. The linear feature lying between the Sun and the Galactic center is the Sagittarius arm. There is also an indication of yet another spiral arm, external to the Orion–Cygnus arm, now known as the Perseus arm. Reproduced by permission of the AAS.

composition that laid the groundwork for our current understanding of the formation and chemical evolution of the Galaxy. That is to say, the metal-rich nature of the Population I stars could now be understood as a consequence of the fact that they had been formed out of gas enriched with metals produced in the cores of earlier generations of stars. The resulting correlations between position in the Galaxy (bulge and halo for Population II stars, disk for Population I stars), kinematics (elliptical orbits not confined to the disk for Population II stars, versus circular orbits in the disk for Population I stars), and age (as now deduced through metal abundances and H–R diagrams of the two populations; old for Population II stars, relatively young for Population I stars) led to the modern picture of the formation and evolution of the Galaxy.

This ability of spectral classification to probe the structure and evolution of the Galaxy inspired many of the developments and applications of the MK Spectral



Figure 1.9 Nancy Roman. Reproduced with the permission of the Swarthmore College Bulletin. Photographer Jean Gwaltney.

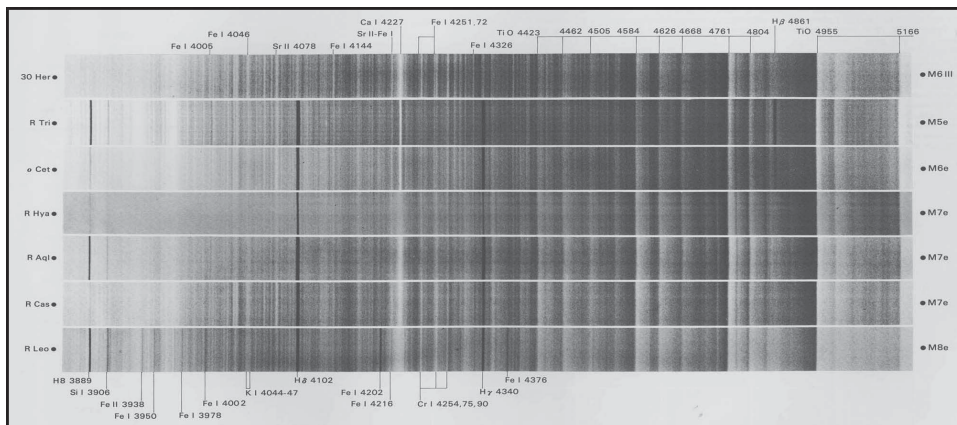


Figure 1.10 A page from the Yamashita spectral atlas illustrating the spectra of the Mira variables (Yamashita, Nariai, & Norimoto 1977). Reproduced courtesy University of Tokyo Press.

Classification system in the two decades that followed. An important development during this period was the invention, by W. W. Morgan and Harold Johnson, of the *UBV* photometric system (see §2.3 and Johnson & Morgan 1953), and its calibration in terms of MK spectral types. This seminal paper contained *UBV* observations of hundreds of field stars as well as many stars in the Pleiades and two other open clusters. These observations enabled the absolute-magnitude calibration of the B-type stars, the development of the “Q Method” for determining the

reddening of B-type stars due to interstellar dust, and the definition of the “standard main sequence.” The luminosity classification of the B-type stars was also refined in this paper, including the subdivision of the supergiant “I” class into luminosity types Ia and Ib (see §2.2.4). These developments made practical the determination of accurate distances to B-type stars, OB associations, and open clusters, and thus helped astronomers to refine and extend the spiral structure discovered by Morgan and associates in 1951. These studies reached their culmination with the discovery of the major Sagittarius–Carina spiral arm, and the presentation of the detailed local spiral structure based on optical tracers by Humphreys (1976).

In the decades of the 1960s through the 1980s, major efforts were made to study both spectroscopically and photometrically the bright O and B field stars (Lesh 1968; Hiltner, Garrison, & Schild 1969; Garrison, Hiltner, & Schild 1977) and many open clusters and OB associations (see Humphreys 1978) in the Milky Way Galaxy, and the most luminous OB supergiants in the Magellanic Clouds and the Andromeda Galaxy. These decades also saw the initiation of ambitious objective-prism surveys, such as those of Sanduleak, Stephenson, & Pesch (for instance, the Luminous Stars in the Northern and Southern Milky Way surveys, and the Case Low-Dispersion Northern Sky Survey) and MacConnell (for instance, his H α and M-supergiant surveys) as well as the HD reclassification project, carried out by Nancy Houk (see, for instance, Houk 1994). These studies have had far-reaching consequences for the study of Galactic structure and stellar evolution. It is impossible in the space available to review the many results from these investigations, but a few of the more outstanding include the following: the establishment of the Humphreys–Davidson limit for the most luminous stars in a galaxy (see §11.2), the recording of the progenitor spectrum of SN1987A (Sanduleak –69° 202), the delineation of the detailed local spiral structure (see above), the discovery of the WO class of Wolf–Rayet stars (Sanduleak 1971), and the construction of a composite zero-age main sequence based on cluster H–R diagrams (Garrison 1978).

During these years, and continuing on to the present date, the MK system itself has undergone refinement and extension. These modifications to the MK system have included (1) an extension to both hotter and cooler stellar types, (2) the addition of dimensions other than those of temperature and luminosity, and (3) the extension to other wavelength regions, including the ultraviolet and the infrared. These extensions and refinements will be discussed in detail in later chapters, but it is worthwhile here to place them in the context of the historical development of the MK system.

On the original MKK (1943) system, the hottest O-type standard star, ζ Pup, was classified as O5, and the coolest main-sequence star was classified as M2 V. Later spectral atlases extended these limits to O4 (MAT atlas) and M5.5 (Keenan & McNeil atlas, based on the work of Boeshaar 1976). Walborn (see Chapter 3) first extended the hot limit to O3 in order to describe the spectra of certain stars in the η Carinae region (Walborn 1971), and then much more recently to O2 (Walborn et al. 2002), again based on the same hot O-type stars in the Carina Nebula, but this time using spectral features revealed in new, high signal-to-noise digital spectra. On the

cool side, the main sequence was first extended in a systematic way to very late M-type dwarfs (M9) by Boeshaar & Tyson (1985) and then later by Kirkpatrick, Henry & McCarthy (1991) (see Chapter 9 for more details). The discovery of brown dwarfs necessitated the further extension of the MK spectral classification system first to the L-type dwarfs (see Chapter 9 and Kirkpatrick et al. 1999) and then to the ultra-cool T-type dwarfs (see Chapter 10 and Burgasser et al. 2002). It is possible that the MK system will need to be extended to even cooler objects, once those objects are discovered and observed spectroscopically.

The MK spectral classification system, at its outset, was designed to be a two-dimensional system with the dimensions corresponding to temperature and luminosity. But stars show a wild diversity that cannot be accommodated in a strictly two-dimensional classification system. As a consequence, additional dimensions, usually confined to limited regions of the H–R diagram, have been added. Keenan & McNeil (1976) and later Keenan (1985) first introduced the use of abundance indices to classify the metal-weak, metal-strong, and chemically peculiar G and K-type giants. A perusal of the later chapters of this book will reveal a number of instances in which the MK system has been extended by the use of additional indices or dimensions, related not only to chemical abundances, but also to the presence and strength of emission lines and other spectral features.

The canonical MK system is based on spectra in the blue-violet spectral region. This choice was dictated by the spectral sensitivity of photographic emulsions of the first half of the twentieth century, but it has turned out to be a good choice for a number of reasons. One reason is that the blue-violet region has a much higher density of spectral lines than the red, and this is especially true for lines sensitive to the luminosity dimension. However, there are advantages to either setting up parallel classification systems in the ultraviolet and the infrared, or extending the applicability of the MK system to those spectral regions. For instance, the hottest stars are brightest in the ultraviolet, and thus the ultraviolet should be the natural realm for classification for those stars. Likewise, the coolest stars peak in the red and near-infrared, and so are best observed and classified there. Morgan himself advocated setting up completely autonomous classification systems in the ultraviolet and infrared (Morgan 1984), but as a matter of fact, the MK system and spectral types have, with a few exceptions, transferred quite successfully to those spectral regions. For some spectral classes this has been quite a surprise. For instance, the ultraviolet spectral region of the O-type stars is dominated by wind features, and it was thought that these features would be poorly correlated with the optical-region spectral types. But it turns out that these wind features correlate beautifully with spectral sequences established in the blue-violet (see Chapter 3).

Spectral classification systems for the O and B-type stars have been set up in the ultraviolet (see Chapters 3 and 4 and Walborn et al. 1985; Walborn, Parker, & Nichols 1995; Rountree & Sonneborn 1993) and the infrared (see §3.4 and Hanson, Conti, & Rieke 1996). We will also present spectral sequences in the ultraviolet for the A-, F-, and G-type stars and in the infrared for A-type and cooler stars in later chapters of this book.

The large-scale photometric and spectroscopic surveys that are currently in progress, or in the planning stages, such as the Sloan Digital Sky Survey, *Gaia*, and RAVE (the RAdial Velocity Experiment) are one of the hallmarks of the current era of astronomical research. These surveys are returning and will return massive amounts of data, including stellar spectra. For instance, the sixth data release of the Sloan Digital Sky Survey brings the total number of stellar spectra observed in that project to nearly 300,000. While this is comparable to the number of stellar spectra Annie J. Cannon dealt with in her lifetime, *Gaia* will collect low-resolution spectra of hundreds of millions of stars. Such enormous quantities of spectral data cannot be classified using the traditional visual techniques employed by MK spectral classification; automatic methods of classification will have to be used. Such methods are currently under development, and are the subject of §13.5 of this book.

1.3 THE MK PROCESS

1.3.1 The Importance of Classification

Classification lies at the foundation of many of the natural and physical sciences because of the need to organize vast quantities of data into a manageable system. What, for instance, would the state of modern biology be without a comprehensive system for organizing the hundreds of thousands of species of plants, animals, and bacteria? But classification plays other roles besides mere organization. Classification is often the beginning of understanding and insight, achieved by perceiving relationships between disparate groups of objects. Classification can also identify the truly peculiar object, the object that does not fit comfortably into the general reference frame. Such objects are worthy of further study, as the peculiarity can often yield deep insights into the meaning and nature of normality.

The MK Spectral Classification System has served as the general reference frame for the classification of stellar spectra for over 60 years. In the previous two sections, we have reviewed the history of this system of classification; in this section, we delve more deeply into its philosophy and practice.

1.3.2 The Importance and Use of Standard Stars

The MK system is an example of a classification system set up using the principles of the *MK Process*. The MK Process is an Aristotelian, inductive approach to classification in general (Garrison 2001), which means that it is a methodology that formulates a classification system based on *specimens*, and that these specimens serve to define the system. In the case of the MK system, these specimens are the spectra of *standard stars*. Consistent with the MK Process, the MK system uses only the information present in the spectrum for classification purposes, and does not admit external information, such as information from photometry, theory, calibrations, or any other source into the determination of the classification of a particular star.

The autonomous nature of the MK system has been the key to its long-term stability and success, and means that the MK type is actually a fundamental datum of astronomy. The importance of keeping the classification system independent of theory and calibrations is clear. If the classification is based, even in part, on theory or a calibration, then when that theory or calibration changes (as it inevitably will), the classification will also then need to be changed. If, on the other hand, the classification is based only on comparison of the spectrum with the defining standards, the classification will be unchanged even when the theory or calibration changes. The resulting independence of the classification system means that when it is confronted with theory or another autonomous classification system (for instance, one based on photometry), that confrontation will be fruitful, and can yield new information and insights.

MK standard stars are those stars that have been selected to best exemplify the spectral class they represent. Spectral classification is carried out by comparing the unknown with the standard spectra; the classification is determined once the best match is found. Quite often, the unknown spectrum is found to fall between two or more standard spectra. In this case, interpolation is allowed. For instance, along the main sequence, there are standards for spectral types G0 V and G2 V. A star with a spectrum that appears intermediate to these two *spectral boxes* will be given a spectral type of G1 V.

For a system based on the MK Process to work in a practical way, the standards that define that system must be universally accepted. When the first MKK atlas was published (Morgan, Keenan, & Kelleman 1943), it was accompanied by a list of standard stars. Later publications by Morgan & Keenan (Johnson & Morgan 1953; Morgan & Keenan 1973; Keenan & McNeil 1976; Morgan, Abt, & Tapscott 1978; Keenan & McNeil 1989) extended and refined the MK system. These publications added standards to the original corpus, and dropped some that had been found to be unsuitable. In addition, with the improvement in the quality of stellar spectra, the spectral types of some of the original spectral standards have been changed, but never enough to dislocate the system. The definition of standards has never been the exclusive preserve of Morgan and Keenan (Figure 1.11). Careful workers in the field, including R. F. Garrison (Figure 1.12), N. R. Walborn and R. O. Gray, have introduced new standards and have also refined the spectral types of existing standards. The introduction of new standards has, of course, played a vital role in the extension of the MK system, via the MK Process, to both hotter and cooler regimes. For instance, the extension of the MK system to the L and T dwarfs (see Chapters 9 and 10) has required the designation of standards for those types. If these new standards are carefully chosen, they will define an internally consistent system, and should survive. If not, they will ultimately be rejected by other classifiers. There is, therefore, in a sense, a “natural selection” process for standard stars!

Historically, the founders of the MK system, W. W. Morgan and P. C. Keenan, practiced somewhat incompatible policies for establishing standards. Morgan always insisted that a given spectral box be defined by a single standard star. Keenan,

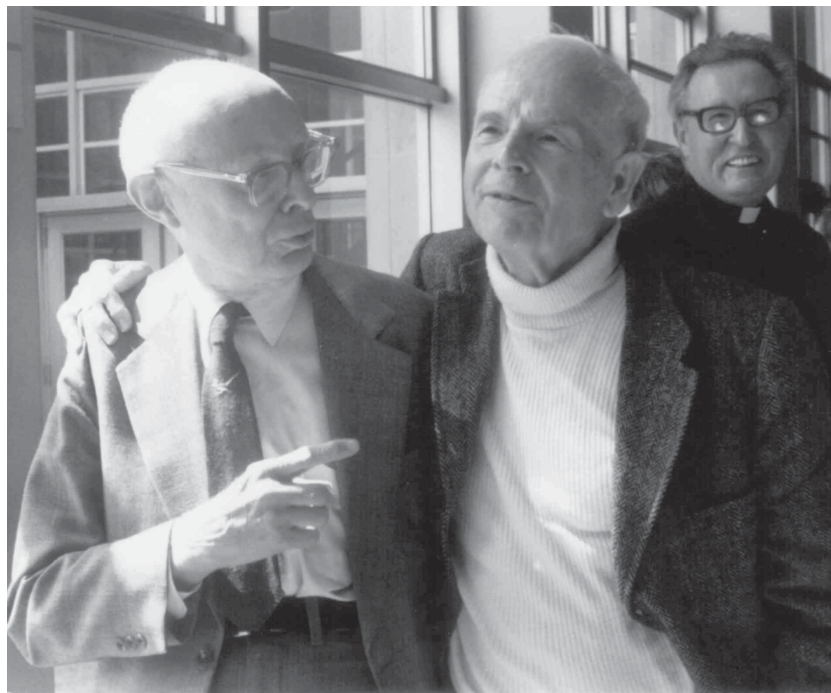


Figure 1.11 Keenan (left) and Morgan at the time of the MK Process conference, held in Toronto, June 1983. In the background is Father Martin McCarthy of the Vatican Observatory. Photo courtesy Nancy Houk.



Figure 1.12 Robert Garrison, Janet Rountree (Lesh), and W. W. Morgan, taken at the MK Process conference, June 1983. Photo courtesy Nancy Houk.

on the other hand, followed the practice of defining multiple standards for a single spectral box; in the Perkins Catalog (Keenan & McNeil 1989), for instance, Keenan & McNeil defined seven (!) standards for spectral class K0 III. Keenan (1994) justified this practice on the need for standards to be available all around the sky, including both the northern and southern hemispheres, but also due to the fact (Keenan 1984) that for the cool stars, and especially for the supergiants,

spectral variability at some level is common, and that it is necessary to have as many spectral standards as possible in order to define an average type.

Partly in response to these differences in practice, R. F. Garrison has put considerable effort into systematizing a hierarchy of standards for the MK system (Garrison 1994). One of the purposes of this hierarchy is to ensure the stability of the MK system while at the same time support a flexible enough structure to allow extension and refinement of the MK system in the future. Garrison defines three levels of standards in this hierarchy: (1) the *Anchor Points*, (2) the *Primary Standards*, and (3) the *Secondary Standards*. The Anchor Points are standard stars whose classifications have not changed since the original publication of the MKK system in 1943. But to ensure that these Anchor Points are truly stable and consistent with the MK System of today, they must also have a reliable modern published type by either Morgan or Keenan, R. O. Gray for the A-type stars, Walborn for the O-type stars, or by Garrison himself. As Garrison states, these stars “represent the MK System as it was then and is now.” These are the stars that provide the fundamental anchoring definitions for the system. The Anchor-Point standards do not populate a full grid of spectral boxes, however. For instance, there is no Anchor-Point standard for the F8 III box, and many other spectral boxes are unfilled. The Primary Standards help to fill in this grid, and consist of “the best known specimen of each spectral type and luminosity class.” Finally, since the Anchor Points and Primary Standards are distributed randomly across the sky, with no attention paid to availability in either the northern or southern hemisphere, or to seasonal access, a set of Secondary Standards with reliable spectral types, checked largely by Garrison himself, but drawn from the lists of other experienced classifiers, is being compiled. These are, as far as possible, situated to be accessible to both hemispheres, and to be spaced in right ascension 6–8 hours apart. Garrison’s hierarchical system thus upholds Morgan’s stricture of having a single standard define a given spectral box (i.e., the Anchor Points), but at the same time recognizes the practicality of Keenan’s approach by establishing standards all around the sky. Appendix A reproduces Garrison’s hierarchy as it now stands.

The advent of large telescopes and sensitive detectors has resulted in a mini-crisis in the use of standard stars. Many of the MK standards, including the secondary standards in Garrison’s hierarchy, are bright, and will saturate the detectors of even one-meter-class telescopes. Solutions to this problem include observing standards through neutral-density filters or with a stopped-down aperture. But neutral density filters may not be truly neutral, and can introduce artifacts into the spectrum. And stopping down a telescope to a smaller aperture changes the beam size, and thus the optical behavior of the spectrograph. A better solution would be to establish faint secondary standards that can be observed with a large telescope. This suggestion led to the establishment of the *Standard Star Working Group*⁵ of the International Astronomical Union, one goal of which was the establishment of MK (and other) standards at the 10th and 15th magnitudes. This is a fairly easy task to accomplish for main-sequence stars, as it is only necessary to select

⁵<http://stellar.phys.appstate.edu/ssn>

suitable stars on open-cluster main sequences. But to find suitable unreddened giant and supergiant standards at 15th magnitude is very difficult indeed. Another problem is the reluctance of telescope time-allocation committees (TACs) to grant time for adequate observations of standard stars on large telescopes. This practice is understandable, but regrettable and ultimately short-sighted.

1.3.3 The Practice of Spectral Classification

The photographic emulsions available at the time of the original MKK system dictated many of the features of that system. For instance, those emulsions were sensitive only in the blue-violet part of the spectrum, and thus the canonical wavelength region for the MK system became (and continues to be) from about 3800 Å to the vicinity of H β (about 5000 Å). Because of the difficulties involved in producing calibrated tracings from these photographic spectra, classification was carried out using the original glass plates. This necessitated widening the spectra (perpendicular to the dispersion), as lines, line profiles, and molecular bands are difficult to see in narrow spectra. The spectrum was widened by trailing the star along the slit during the exposure. Dispersions of 60–150 Å/mm (corresponding, on Kodak IIa-O plates developed with a fine-grain developer, to spectral resolutions of about 1–3 Å) were most commonly used.

Because MK classification is carried out through comparison of the unknown spectrum with the MK standards, the most common way to proceed was to lay one plate (carrying the standard) on top of the plate carrying the unknown spectrum, emulsion to emulsion, and to view both through a dissecting microscope. This is the way that the two primary authors of this monograph learned spectral classification. It was a peaceful, relaxing process; both of us remember long, warm, summer days spent at the David Dunlap Observatory classifying our plates taken at Las Campanas in Chile. Another common technique to compare two or more photographic spectra was to use the spectra comparator (Abt 2003). Classification of photographic spectra could also be an aesthetic experience; while the spectra of rapidly rotating A-type stars are rather ugly, the stark simplicity of the spectra of A- and B-type supergiants is exquisite. Other types of spectra, such as those of the carbon stars, are similarly beautiful. Some of this is lost with modern digital spectra, but not all, fortunately. With photographic spectra, it was vitally important to ensure that the spectral material was as homogeneous as possible. What this meant is that it was necessary not only to obtain the spectra of standards and unknowns using the same telescope and spectrograph, but also to ensure uniformity of photographic development techniques. Standards and unknowns needed to be exposed to the same density so that they could be directly intercompared.

Today almost all spectral classification is carried out using digital spectra obtained with CCDs. The primary spectral region for ground-based spectral classification for O–M-type stars is still the blue-violet region, and the reason for this is no longer the sensitivity of the detector, but rather that this region has the highest concentration of temperature- and luminosity-sensitive criteria, plus, for the

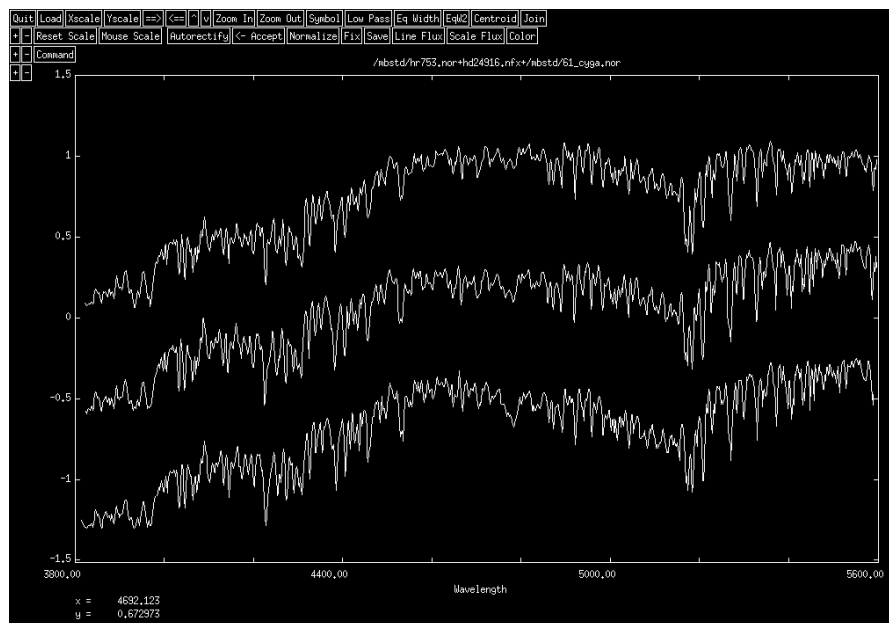


Figure 1.13 Using the authors' program xmk22 to classify spectra. The top and bottom spectra are MK standards for K3 V and K5 V, respectively; the middle spectrum is the unknown. The unknown has been successfully bracketed by the two standards; its spectral type is K4 V. This program is available on the book's website in both its Linux/UNIX version (xmk22) and a Windows version (Winmk)—see Appendix C.

cool stars, a splendid array of molecular bands, including bands of CH, CN, C₂, MgH, and TiO, amongst others. However, the sensitivity of new detectors from the X-ray to the far infrared has opened those regions of the electromagnetic spectrum to spectral classification, and we will describe later in this chapter, and throughout this book, extensions of the MK system to other wavelength regions. The spectral resolution in the blue-violet that seems to be ideal for use with digital spectra is about the same as was used with photographic spectra, i.e., about 1–4 Å (per 2 pixels). Attention to the signal-to-noise (S/N) of the digital spectra is also important; bearing in mind that the equivalent S/N of a well-widened, well-exposed photographic spectrum is on the order of 200–300 (Garrison 2001), precise spectral classification using digital spectra requires $S/N > 100$. Of course, for faint stars, compromise is necessary.

The spectral classification of digital spectra is still carried out by comparing the unknown to the MK standards. For most astronomers engaged in spectral classification, this comparison is still performed visually, but now on the computer screen (see Figure 1.13). However, efforts are now being made to develop techniques to classify spectra automatically, without human intervention; these techniques will be described in some detail in Chapter 13. The best of those techniques are faithful to the MK Process, and involve direct comparison of the unknown with the standards. With digital spectra, it is no longer necessary to widen the spectrum.

However, attention must still be paid to homogeneity of the spectral material; ideally the standards should be observed with the same equipment as the unknowns, and be processed identically. Fortunately, digital spectra allow this requirement to be somewhat relaxed; with modern software it is often possible to manipulate one set of spectra obtained with one instrument to match the resolution of another set of spectra, obtained with another instrument. But still, caution is necessary, as it can be difficult to entirely correct for factors such as scattered light and to exactly reproduce the line-spread function of a spectrograph by digital manipulation.

Spectral classification, whether carried out with photographic or digital spectra, requires the careful comparison of unknown and standard. This comparison is a *unitary* process, which means that all features of the spectrum are used in finding the match between unknown and standard, although this comparison is usually aided by certain *classification criteria*, i.e., lines, blends, line ratios, etc. Morgan (1984) described the process in the following way: “The classification act itself consists of comparisons with the series of standard spectra that define the boxes, with the question ‘Is the unknown spectrum (x) “like” or “not like” this particular spectrum?’” Spectral classification is usually an iterative procedure; a rough temperature type is obtained, then a rough luminosity type, and then the unknown is compared in detail with surrounding standards. If the unknown is metal-weak or metal-strong, or chemically peculiar in some way, the comparison process can be even more involved. The complexity of this process is often underestimated by those who have never carried it out, and many think that this procedure is easily transferred to the computer. In reality, however, visual classification, which uses the powerful ability of the human brain to recognize and process complex patterns (such as, for instance, the human face) still has the advantage over the computer. Some continue to decry spectral classification as a subjective process. This is Keenan’s (Keenan 1984) answer:

First, I want to correct a misunderstanding which I hope is not shared by many. It has been said that when classification is carried out by visual inspection of spectrograms the process is purely subjective, and that the classifier is free to make arbitrary changes in the scheme of types assigned to the stars. This is *untrue!* It is subjective only in the sense that the ability of the human eye to match complex patterns is used, but the network of patterns defining the system is the same whether the comparison is made visually or by summing measured intensity ratios, or by deriving an electronic pattern recognition index. If I or anyone else made arbitrary changes in a system, that system would soon cease to be useful.

1.3.4 Extending the MK Classification System

The MK Classification system may be extended in two ways. The first is to extend the system to new classes of stars. Examples mentioned earlier in this

chapter included the extensions of the MK system to both hotter and cooler stars, in particular hot O-type stars, and the cool L- and T-type dwarfs. Other examples include the extension to Population II stars, to certain types of peculiar stars, and even to populations of stars in external galaxies. The second way of extending the MK system is to different wavelength regions, for instance the ultraviolet, the infrared, and even the X-rays (see Chapter 3). How these extensions can and should be carried out is the subject of this section.

Excellent examples of how the MK system can be extended to new classes of stars are the subjects of Chapters 9 and 10: the extensions to the L- and T-type dwarfs. The authors of those chapters (Davy Kirkpatrick and Adam Burgasser) played crucial roles in those extensions. Both have a deep knowledge of and appreciation for the MK Process, and both used that philosophical system in their work. Both have described in their chapters how the classification systems were set up. In essence, they followed the advice of Morgan (1984) who stated “It could be said, with some truth, that the spectral forms have helped to classify themselves, by showing where they are most comfortable.” What they did was to take a sample of spectra of the new class, and literally spread those spectra out on the floor or desk (see Figure 10.5), and then arrange them into a sequence. This was done without reference to theoretical expectations or preconceived notions; they simply allowed the spectra “to classify themselves.” This process not only established the first rough outlines of the new classification systems, but also identified candidate standards and certain objects that did not fit, but were peculiar in some way. In both cases, the sequences that emerged turned out to be temperature sequences, and the peculiar objects are now being understood in terms of surface-gravity and/or metal-abundance differences. Of course the historical development of the OBAFGKM sequence of the MK system was much more complicated than this (see §1.1), but it is possible to establish that sequence without reference to theory. The authors tested this in 1999 at the Vatican Observatory Summer School, held at Castel Gandolfo, just outside of Rome. We had 25 highly intelligent beginning astronomy graduate students (from 24 countries!), most of whom had had little or no exposure to the MK system. We divided the class into 4 groups and gave each a set of stellar spectra observed in the red, centered on the $H\alpha$ line, and asked them to arrange those spectra in the most logical order without giving any further guidance. All of the groups, quite independently, came up with the OBAFGKM sequence, simply because they allowed the spectra to show “where they are most comfortable.” They also identified a number of peculiar objects. Many of those peculiar objects turned out to be giants and supergiants, and thus they had the beginnings of a luminosity dimension.

Extensions of the MK system have also been made to metal-weak stars, and to the chemically peculiar cool giant stars. How such extensions should be made was a subject of disagreement between Morgan and Keenan. Morgan (1984) insisted that parallel, but independent classification systems should be set up to classify stars of different degrees of metal richness or weakness. For instance, for weak-metal-line stars, Morgan advocated setting up three *systems*, denoted (m-1), (m-2),



Figure 1.14 William Bidelman, taken at the MK Process conference, June 1983. Photo courtesy Nancy Houk.

and (m-3) for progressively greater line weakening. Morgan also stated: “For such systems to be completely autonomous, we cannot require them to be attachable to the MK System—or to each other. They complement each other; but they each must live separate, independent lives.” Keenan (1987) has pointed out, however, that “the great majority of the so-called ‘peculiar’ stars fall into groups that are not sharply bounded but actually shade into the normal stars of the original MK system” and thus can be best classified by extending the MK system with the addition of further dimensions, rather than by setting up autonomous classification systems. It seems to the present authors that Morgan’s approach is best applied to setting up classification systems in other wavelength regions, as these regions may sample different layers of the stellar atmosphere than the optical. There is thus ample reason to keep such classification systems independent of the original MK system. But setting up independent and autonomous systems in other contexts is not necessarily the best approach. Nature, at least on the macroscopic scale, is much more often characterized by continua than by jumps and discontinuities, and it is only right that our classification systems should reflect that reality, instead of imposing boundaries where they do not exist in the natural world.

The discussion in the previous paragraph suggests that classification systems set up in other wavelength regions should be kept independent of the original MK system in the blue-violet. What that means is that when one is seeking to set up such a classification system, it is really necessary to start from scratch. One should not assume, for instance, that a good standard in the blue-violet is also going to be a suitable standard for the ultraviolet or the infrared. Indeed, the procedure one follows should be similar to that followed by Kirkpatrick and Burgasser when they

set up the classification systems for the L and T dwarfs (see above and Chapters 9 and 10). Obtain as large a sample as possible of spectra of stars in the wavelength region of choice, and then attempt to find sequences. Spectral classes should be defined, as much as possible, by the appearance or disappearance of some major spectral feature (for instance, the boundary between the O and B classes in the original MK system was fixed at the point where lines of He II disappear from spectra of classification resolution). These spectral classes need not correspond to the original MK classes. Chances are, there will be a fairly close correspondence unless one chooses a spectral region where the predominant features are not *photospheric*. But in any case, the notation used should be easily distinguishable from that used in the original MK system. Standards, likewise, should be chosen from the spectral material at hand to exemplify the newly formed spectral classes. Once the classification system is well-defined, detailed comparisons may then be made with the original MK system. If the correspondence between the two systems is close, then it may prove unnecessarily redundant to retain a distinct nomenclature. This is actually what happened when classification of the O-type stars was attempted in the ultraviolet. The O-star ultraviolet spectra are dominated by non-photospheric features, such as P Cygni profiles from the strong stellar winds. Nevertheless, sequences identified in the ultraviolet corresponded so closely with the original MK temperature and luminosity sequences, that a distinct nomenclature was found unnecessary (see Chapter 3), and classifications performed in the ultraviolet are essentially interchangeable with those carried out in the optical. On the other hand, Kirkpatrick (see §9.3.2) has found that spectral sequences in the near-infrared for the L dwarfs do not conform exactly with those in the optical, and thus an independent classification scheme needs to be established for the optical. Likewise, in the optical, Burgasser (see §10.5.2) has used a distinct notation for the T dwarfs, which are normally classified in the near-infrared.

Unfortunately, the practice outlined in the above paragraph has not been used in all cases. A prime example is the classification of the Wolf-Rayet stars (Chapter 11), in which spectral types in the optical have been used to “order” Wolf-Rayet spectra in the ultraviolet. In some cases (in particular the WN stars) this does not result in good sequences, implying the need for an independent classification system in the ultraviolet.

1.3.5 The Mandate of the MK System

In order to make proper use of any system of classification, it is necessary to understand the *mandate* of that system. The mandate of the original MK system is to describe the blue-violet spectrum of stars at classification resolution (1–4 Å) in terms of a set of standard stars. It is important for users to understand that this mandate does *not* include providing the basic physical parameters of stars such as the effective temperature, the radius, the mass, the luminosity, or the metallicity. Nor is determining the spectral type of a star equivalent to measuring its color on the Johnson *UBV* or any other photometric system (see §2.3). While the MK



Figure 1.15 Nancy Houk, at the microscope reclassifying spectra of HD stars for the Michigan Spectral Catalogue. Photo courtesy Nancy Houk.

system may be *calibrated* in terms of these quantities (see Appendix B), those calibrations are not part of the MK system, and *should not be used to judge the rightness or wrongness of a particular MK type or the suitability of a particular standard*. To do so would be to admit external information into the classification process, and destroy the independence of the MK system. An example will be useful in illustrating this point.

The Sun is the MK standard for the spectral type G2 V. The Sun, of course, is difficult to observe directly using spectrographs or photometers designed for stars, and so the normal practice is to observe the reflected spectrum from a solar-system body without an atmosphere. Bright asteroids such as Vesta or Ceres, or ice-covered moons such as Callisto, are commonly used for this purpose. However, because these bodies are not perfectly white or grey, their Johnson $B-V$ colors do not give us the $B-V$ index of the Sun (see §2.3 for more information on the Johnson UBV system). If we want to determine the $B-V$ index for the Sun, or if we want to compare the Sun with its peers in terms of, for instance, sunspot activity, rotational velocity, etc., it is useful to find what are called “solar twins.” The subject of solar twins is discussed in much more detail in §7.4.1. Hardorp (Hardorp 1978) was one of the first to try to find solar twins. He did this by observing a number of bright solar-type stars with a 20-Å resolution spectral scanner in the near ultraviolet (3640–4100 Å). Surprisingly, he found that no G2 V star in his sample matched the spectrum of the Sun, and those stars that did match had a $B-V$ averaging 0.66 instead of the 0.63 derived from the mean color of other G2 V

stars. He suggested that this was due to an error in the spectral type of the Sun, and that the “MK system of spectral classification should be revised to take this into account” (Hardorp 1980). Almost all recent determinations of the $B-V$ index of the Sun have settled on a value near 0.63 (see, for instance, de Strobel 1996; Sekiguchi & Fukugita 2000), and it now appears that Hardorp’s results were due to his use of a sample of solar-type stars that are metal-rich compared to the Sun (de Strobel 1996). If the MK system had been modified according to Hardorp’s suggestion, we would have had to rescind that modification a few years later, and the stability, usefulness, and internal consistency of the MK system would have been compromised. But what if Hardorp had turned out to be right? This would have implied that the Sun is, indeed, different from its peers, and this would have been an important discovery made possible by the autonomy of the MK system. But this still would not have justified the removal of the Sun as the G2 V standard for the blue-violet MK system, *as the sun appears entirely normal with respect to its peers in the blue-violet*. It would, however, have implied that an independent classification system set up in Hardorp’s spectral region would have the potential to yield interesting astrophysical information when confronted with the blue-violet MK system.

Bibliography

- Abt, H.A. 2003, in *The Garrison Festschrift*, eds. R.O. Gray, C.J. Corbally, & A.G.D. Philip (Schenectady: L. Davis Press), p. 123
- Baade, W. 1944, *ApJ*, 100, 137
- Bidelman, W.P. 1954, *PASP*, 66, 249
- Boeshaar, P.C. 1976, Ph.D. thesis, Ohio State Univ.
- Boeshaar, P.C., & Tyson, J.A. 1985, *AJ*, 90, 817
- Brück, H.A. 1979, in *Spectral Classification of the Future*, IAU Coll. 47, eds. M.F. McCarthy, A.G.D. Philip, & G.V. Coyne (Vatican: Vatican Observatory), p. 7
- Burgasser, A., et al. 2002, *ApJ*, 564, 421
- Curtiss, R.H. 1932, *Handbuch der Astrophysik* (Berlin: Springer-Verlag), 5, Ch. 1
- de Strobel, G.C. 1996, *A & A Rev*, 7, 243
- Garrison, R.F. 1978, in *The HR Diagram: The 100th Anniversary of Henry Norris Russell*, IAU Symp. #80, eds. A.G.D. Philip & D.S. Hayes (Dordrecht: D. Reidel), p. 147
- Garrison, R.F. 1994, in *The MK Process at 50 Years: A Powerful Tool for Astrophysical Insight*, eds. C.J. Corbally, R.O. Gray, & R.F. Garrison, Astronomical Society of the Pacific Conference Series, Vol. 60 (San Francisco: Astronomical Society of the Pacific), p. 3
- Garrison, R.F. 2001, "Classification of Stars" in *Encyclopedia of Astronomy and Astrophysics*, ed. Paul Murdin (Bristol: Nature Publishing Group and Institute of Physics Publishing), Vol. 1, p. 351
- Garrison, R.F., Hiltner, W.A., & Schild, R.E. 1977, *ApJS*, 35, 111
- Hanson, M.M., Conti, P.S., & Rieke, M.J. 1996, *ApJS*, 107, 281
- Hardorp, J. 1978, *AA*, 63, 383
- Hardorp, J. 1980, *AA*, 91, 221
- Hearnshaw, J.B. 1986, *The Analysis of Starlight* (Cambridge: CUP)
- Hiltner, W.A., Garrison, R.F., & Schild, R.E. 1969, *ApJ*, 157, 313
- Houk, N. 1994, in *The MK Process at 50 Years: A Powerful Tool for Astrophysical Insight*, eds. C.J. Corbally, R.O. Gray, & R.F. Garrison, Astronomical Society of the Pacific Conference Series, Vol. 60 (San Francisco: Astronomical Society of the Pacific), p. 285
- Huggins, W. 1909, *The Scientific Papers of Sir William Huggins*, Publ. of Sir Wm Huggins Obs., Vol. II (Wesley & Son)
- Humphreys, R.M. 1976, *PASP*, 88, 647
- Humphreys, R.M. 1978, *ApJS*, 38, 309
- Humphreys, R.M., & Davidson, K. 1979, *ApJ*, 232, 243

- IAU 1922, *Transactions of the IAU*, Vol. I B, ed. A. Fowler (New Zealand Journal of Science), 1, 95
- Johnson, H.L., & Morgan, W.W. 1953, ApJ, 117, 313
- Keenan, P.C. 1984, in *The MK Process and Stellar Classification*, ed. R.F. Garrison (David Dunlap Observatory: University of Toronto), p. 29
- Keenan, P.C. 1985, in *Calibration of Fundamental Stellar Quantities*, IAU Symposium No. 111, eds. D.S. Hayes, L.E. Pasinetti, & A.G.D. Philip (Dordrecht: Reidel), p. 121
- Keenan, P.C. 1987, PASP, 99, 713
- Keenan, P.C. 1994, in *The MK Process at 50 Years: A Powerful Tool for Astrophysical Insight*, eds. C.J. Corbally, R.O. Gray, & R.F. Garrison, Astronomical Society of the Pacific Conference Series, Vol. 60 (San Francisco: Astronomical Society of the Pacific), p. 15
- Keenan, P.C., & McNeil, R.C. 1976, *An Atlas of Spectra of the Cooler Stars: Types G, K, M, S and C* (Columbus: Ohio State University)
- Keenan, P.C., & McNeil, R.C. 1989, ApJS, 78, 245
- Kirkpatrick, J.D., Henry, T.J., & McCarthy, D.W. 1991, ApJS, 77, 417
- Kirkpatrick, J.D., et al. 1999, ApJ, 519, 802
- Kurtz, M.J. 1984, in *The MK Process and Stellar Classification*, ed. R.F. Garrison (Toronto: David Dunlap Observatory), 136
- Lesh, J.R. 1968, ApJS, 17, 371
- McCarthy, M.F. 1979, in *Spectral Classification of the Future*, IAU Coll. 47, eds. M.F. McCarthy, A.G.D. Philip, & G.V. Coyne (Vatican: Vatican Observatory) RA, 9, 103
- Morgan, W.W. 1984, in *The MK Process and Stellar Classification*, ed. R.F. Garrison (David Dunlap Observatory: University of Toronto), p. 18
- Morgan, W.W., Abt, H.A., & Tapscott, J.W. 1978, *Revised MK Spectral Atlas of Stars Earlier than the Sun* (Chicago and Tucson: Yerkes Observatory, University of Chicago, and Kitt Peak National Observatory)
- Morgan, W.W., & Keenan, P.C. 1973, ARAA, 11, 29
- Morgan, W.W., Keenan, P.C., & Kellman, E. 1943, *An Atlas of Stellar Spectra* (Chicago: University of Chicago Press)
- Morgan, W.W., Whitford, A.E., & Code, A.D. 1953, ApJ, 118, 318
- Newall, H.F. 1920, MNRAS, 80, 429
- Plaskett, H.H. 1922, *Publ. Dominion Astrophys. Observ. Victoria*, 1, 325
- Roman, N.G. 1950, ApJ, 112, 554
- Roman, N.G. 1952, ApJ, 116, 122
- Roman, N.G. 1954, AJ, 59, 307
- Rountree, J., & Sonneborn, G. 1993, *Spectral Classification With the International Ultraviolet Explorer: An Atlas of B-Type Spectra*, NASA Reference Publication 1312
- Sanduleak, N. 1971, ApJ, 164, L71
- Schlesinger, F. 1911, ApJ, 33, 260
- Secchi, A. 1870, *Comptes Rendus*, 71, 252

- Sekiguchi, M., & Fukugita, M. 2000, AJ, 120, 1072
- Struve, O. 1928, Nature, 122, 994
- Struve, O. 1929, ApJ, 70, 237
- Walborn, N. 1971, ApJ, 167, L31
- Walborn, N.R., Nichols-Bohlin, J., & Panek, R.J. 1985, International Ultraviolet Explorer Atlas of O-Type Spectra from 1200 to 1900 Å, NASA RP 1155
- Walborn, N.R., Parker, J.Wm., & Nichols, J.S. 1995, International Ultraviolet Explorer Atlas of B-Type Spectra from 1200 to 1900 Å, NASA RP 1363
- Walborn, N., et al. 2002, ApJ, 123, 2754
- Yamashita, Y., Nariai, K., & Norimoto, Y. 1977, *An Atlas of Representative Stellar Spectra* (Tokyo: University of Tokyo Press).

Chapter Two

An Overview of the Normal Stars

2.1 INTRODUCTION

Stellar spectra are astonishingly diverse. In the optical part of the spectrum, the vast majority are primarily absorption-line spectra, but even these range from the starkly simple A-type spectra, dominated by a few strong hydrogen lines, to the complex molecular spectra of M-type stars and carbon stars. For most stars, a solar mix of elemental abundances is a good first estimate, but there are some stars in which trace elements, such as the rare earths, or more common elements, such as carbon, are bizarrely enhanced. Some stars are hydrogen deficient, whereas others show marked underabundances of most metals. Certain stellar spectra, on the other hand, are dominated by emission lines. Wolf–Rayet stars, for example, show broad, strong emission lines in their spectra, clearly deriving from a massive stellar wind, whereas in the flare stars, common among the early M-type dwarfs, the emission lines are produced in active regions that might cover a significant fraction of the stellar surface.

This surprising diversity of spectral forms is a reflection of the wide range of physical phenomena that go into the formation of stellar spectra. It is remarkable, therefore, that the vast majority of stellar spectra can be comprehended on the basis of only two physical parameters—temperature and gas pressure (or its proxies, surface gravity and density). The purpose of this chapter is to take a first look at the variety of stellar types explained by those two physical parameters. First, we survey the two-dimensional array of *normal* stellar types from a descriptive, morphological point of view (the basis of the MK spectral classification system); second, we briefly examine an independent technique for classifying stars, i.e., multicolor photometry; and then, finally, we explore, using simple concepts from physics, how those two physical parameters can account for the observed array of spectral forms of normal stars.

2.2 THE SPECTRAL SEQUENCE

2.2.1 The Main Sequence

In Chapter 1 we traced the history of the MK spectral classification system, including the realization that the sequence of spectral types OBAFGKM represents a temperature sequence. That this ordering of spectral types is a temperature sequence is abundantly clear from Figure 2.1, which shows how the optical spectral

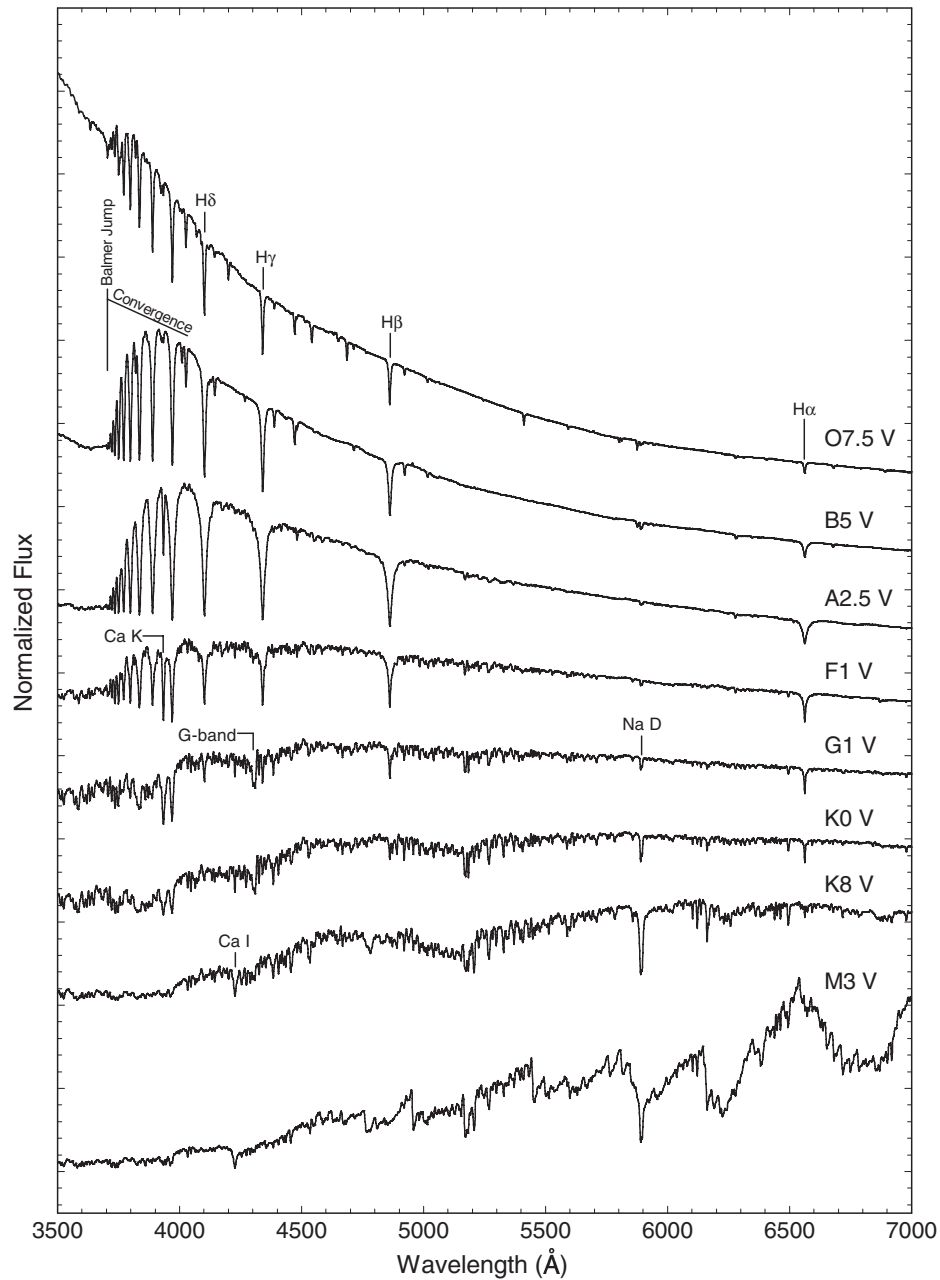


Figure 2.1 The OBAFGKM spectral sequence for main-sequence (dwarf) stars illustrating that the spectral sequence is ordered in terms of temperature. Here, the normalized stellar flux (the *energy distribution*) is plotted against wavelength. Some of the more prominent spectral features are marked, including the Balmer jump and convergence. The source of these spectra is the Indo-US coude-feed spectral library (Valdes et al. 2004). The spectra have been normalized at a common wavelength, and separated by one continuum unit for clarity, except for the bottom spectrum, which is offset by 2 units.

energy distributions of main-sequence (*dwarf*¹) stars vary with spectral type. This sequence is presented in more detail in Figures 2.2 and 2.3 in the blue-violet spectral region traditionally used for MK spectral classification. Figure 2.2 illustrates stars hotter than the Sun (these stars are commonly referred to as the *early-type stars*), and Figure 2.3 stars cooler than the Sun, the *late-type stars*. Note that these figures use two different spectral formats. In Figure 2.2 the spectra are presented in “rectified” format, in which the intensity of the continuum points (i.e. the points not affected by line absorption) has been normalized to unity. This is a convenient format to use as it permits the use of line ratios over a wide wavelength range in spectral classification. However, in the late-type stars, the density of the spectral lines is so great that there are no true continuum points, and so rectification of the spectrum is not the best representation. Instead, the most convenient format for these spectra in classification is the “normalized flux” format, in which the stellar fluxes have been normalized to unity at one common point. The spectra in Figure 2.3 have been normalized to unity at a common wavelength of 5445 Å.

A glance at Figure 2.2 indicates that the salient feature of the sequence of early-type spectra is the behavior of the hydrogen Balmer lines (the $H\beta$, $H\gamma$, $H\delta$, $H\epsilon$, $H8$, and $H9$ lines in the Balmer series are visible in these spectra). Note that in the O-type stars, the hottest normal stars, the Balmer lines (which in the O-type stars are actually blended with lines of the Pickering series of He II—see §2.4.2) are quite weak. With decreasing temperature (later spectral type), the Balmer lines increase in strength, coming to a maximum in the early A-type stars, at a spectral type of about A2. They then fade rapidly with decreasing temperature, and cease to dominate the blue-violet spectrum in K-type and later stars. In §2.4 we will use elementary concepts from atomic and statistical physics to understand this behavior. For the moment, it is sufficient to note that this behavior comes about through the interplay of the ionization and excitation of hydrogen.

Lines of other species show a similar behavior. For instance, lines of neutral helium (He I) are very weak in the early O-type stars, but grow in strength with decreasing temperature, coming to a maximum at a spectral type of B2 on the main sequence. They then fade and essentially disappear from classification-resolution spectra by A0. In the O-type stars, lines of singly ionized helium (He II) are already declining in strength; their peak would be attained only in stars substantially hotter than the hottest known O-type star.

Another outstanding feature of the spectral sequence is the appearance and rapidly growing strength of lines due to metals. While lines of doubly and triply² ionized metals appear in the spectra of the O-type stars, and singly and doubly ionized metals in the B-type stars, lines of metals begin to dominate the appearance of the blue-violet spectrum only in the A-type stars. The strongest metal line in this

¹The terms *dwarf*, *giant*, and *supergiant* are commonly used to refer to stars that inhabit different parts of the *Hertzsprung–Russell diagram* (see Glossary). Stars on the main sequence are called dwarfs, whereas giants and supergiants have evolved off the main sequence.

²Notation such as Fe I, Fe II, Fe III, etc. is used to represent different ionization states of an atomic species. Thus, Fe I refers to neutral iron, Fe II to singly ionized iron (Fe^{+1}), Fe III to doubly ionized iron, etc.

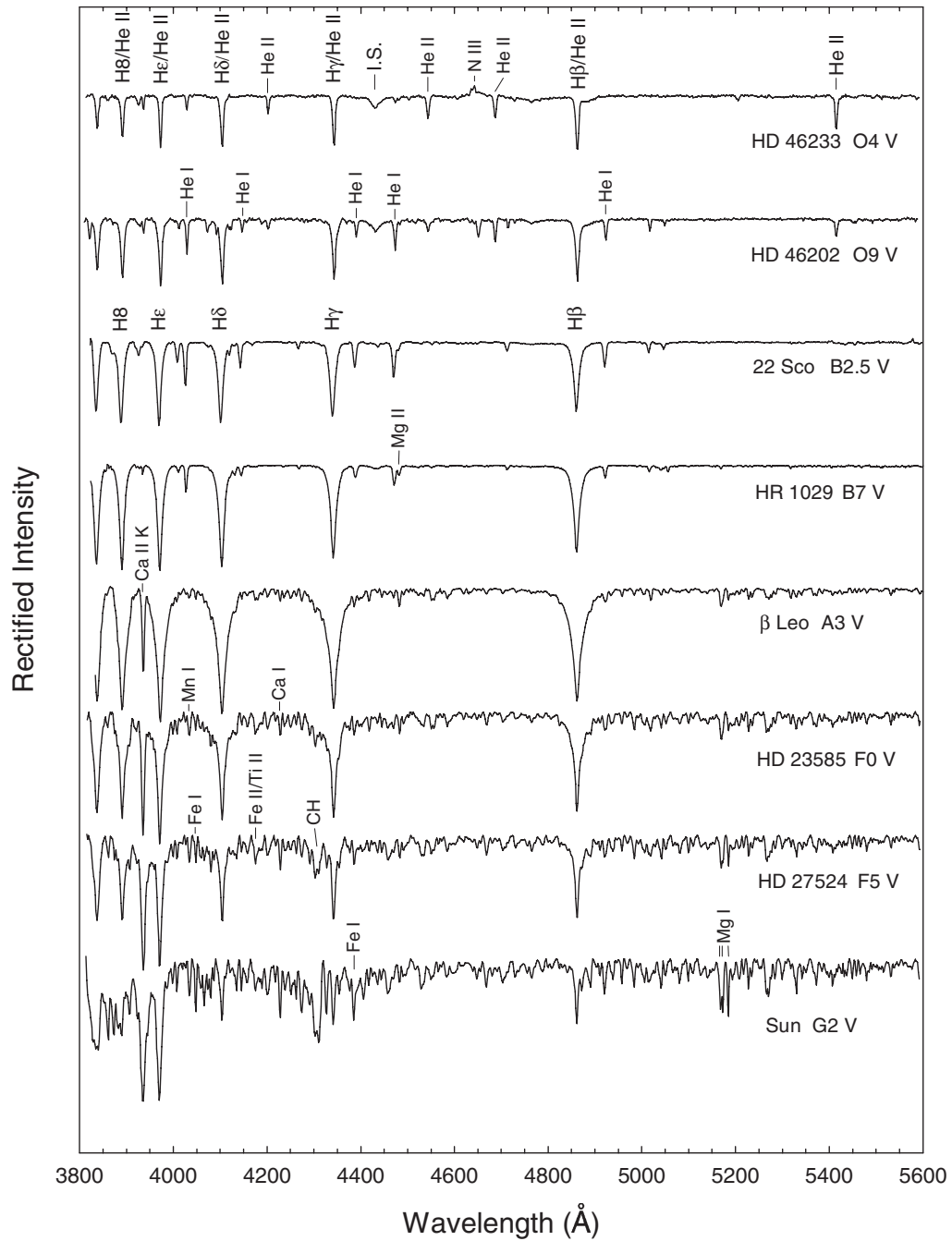


Figure 2.2 The Main Sequence from O4 to G2. Spectra in Figures 2.2–2.5 were obtained with the GM spectrograph on the 32" telescope of the Dark Sky Observatory. These rectified spectra have a resolution of 3.6 \AA , and have been offset by 0.7 continuum units for clarity.

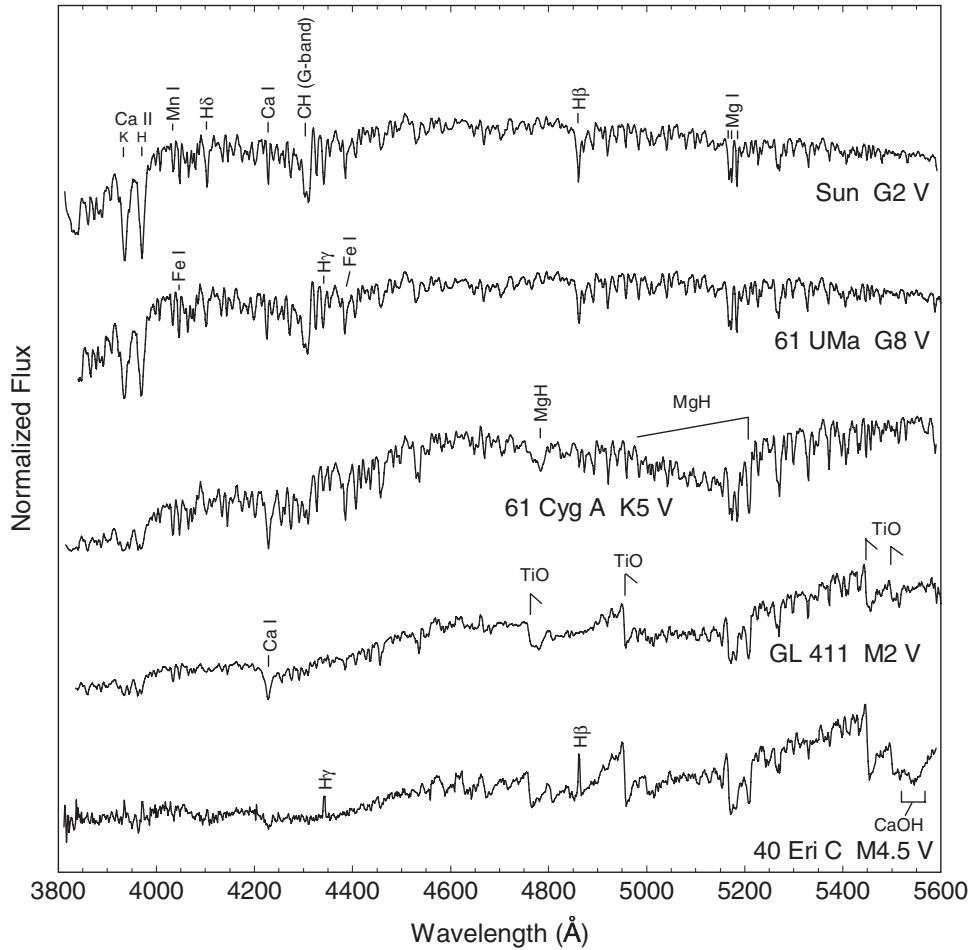


Figure 2.3 The Main Sequence from G2 to M4.5. These flux-calibrated spectra have been normalized at 5445 Å, and given integer vertical offsets for clarity.

spectral region, the Ca II K-line, first appears at a spectral type of B9 (some stars of earlier types show an interstellar Ca II K-line), and grows rapidly with decreasing temperature. Some of the metal lines commonly used in spectral classification are marked in Figures 2.2 and 2.3. Notice that most of these lines, especially the lines due to neutral species, grow in strength with decreasing temperature until a spectral type of K5, after which many begin to decline in strength. While this behavior appears superficially like that of the hydrogen and helium lines, the physics governing these line strengths is considerably more complex. We will consider this physics in more detail in §2.4.

Finally, spectral features due to molecules make their first appearance in the early F-type stars. The feature marked “CH” in the F5 star in Figure 2.2 is due to the diatomic molecule CH and is called the G-band. This molecular band grows rapidly in strength and comes to a maximum in the dwarfs at a spectral type of K2,

after which it fades away. In the K-type stars, molecular bands due to CN and MgH are prominent in the blue-violet region. The M-type spectra are dominated by strong bands of TiO. In even later spectra (as we will see in Chapters 8, 9 and 10), and in spectra of stars with unusual abundances (see, for instance, Chapter 8), many other molecules make their appearance, including polyatomic molecules. Note the band due to CaOH in the M4.5 dwarf in Figure 2.3.

2.2.2 Supergiants

Figures 2.4 and 2.5 present similar sequences for Ib supergiant stars and can be compared directly with Figures 2.2 and 2.3 for the dwarfs. Note that superficially the sequences appear very similar. However, there are a number of important differences. Consider the Balmer lines. In the supergiants, we see a behavior similar to what we saw in the dwarfs; the Balmer lines are weak in the O-type stars, come to a maximum in the A-type stars, and then fade for later spectral types. However, the details are different. Notice that for the early-type stars the Balmer lines are broader in the dwarfs than in the supergiants, and that in the supergiants the maximum occurs at later spectral types. For instance, in the dwarfs the maximum in the Balmer lines occurs at a spectral type of A2; in the Ib supergiants the maximum is in the late A-type stars, or even at F0. Later than F0 the Balmer lines in the dwarfs and supergiants have essentially the same strengths.

In the A-, F-, and G-type supergiants, the metal lines are, with few exceptions, considerably stronger than the same lines in the dwarfs. This is particularly true for lines of ionized metals; some prominent lines and blends of lines of ionized metals that have significantly different strengths in the dwarfs and supergiants are marked in Figure 2.4.

In the late-type supergiants (Figure 2.5) note the strong CN band in 9 Peg, the G5 Ib standard, and its absence in the G-dwarfs (Figure 2.3). In addition, in the K5 dwarf in Figure 2.3, two molecular bands due to MgH are prominent, whereas these spectral features are weak or absent in the supergiants.

These differences (and others) in the spectra of main-sequence and evolved stars can be exploited in *luminosity classification*. A brief overview of luminosity classification is given in §2.2.4, but the details are best left for later chapters.

2.2.3 Sequences in the Ultraviolet and Infrared

2.2.3.1 The Ultraviolet

Ideally, a star should be classified in the region of the spectrum where its energy distribution peaks. Thus, the hot O- and B-type stars are ideally classified in the ultraviolet, A- through K-type stars in the optical, and M-type and later objects in the red and infrared. Of course, for ground-based telescopes, the ultraviolet and much of the infrared are inaccessible, a fact that in the past dictated that spectral classification was carried out largely in the optical. Other considerations may also require that stars be classified in spectral regions far from their flux peak. For instance,

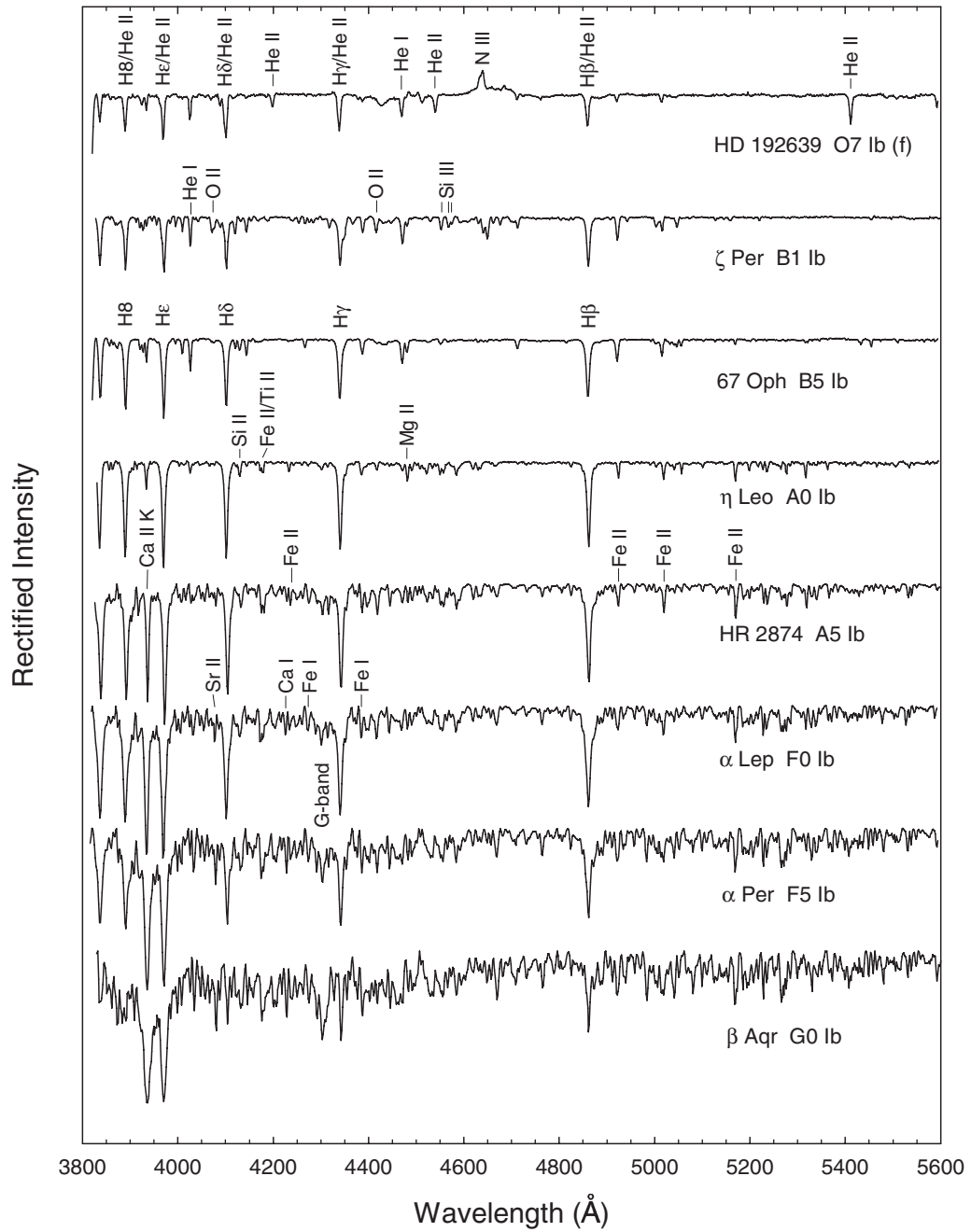


Figure 2.4 Ib Supergiants from O7 to G0. These spectra are rectified, and have been offset vertically by 0.7 continuum units.

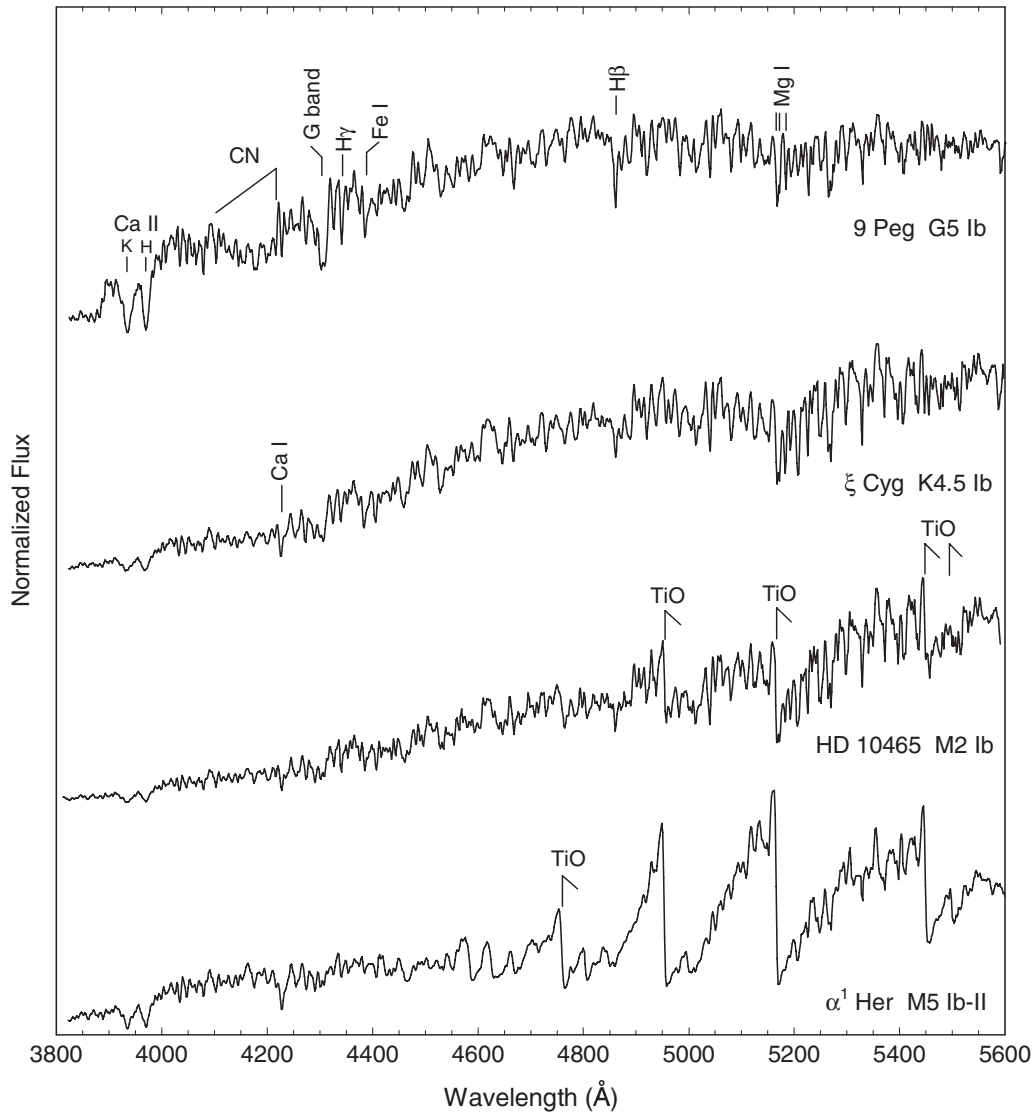


Figure 2.5 Ib Supergiants from G5 to M5. These spectra are in normalized flux format, and have been given integer vertical offsets for clarity.

in star-formation regions, the presence of dust may cause such large extinctions in the ultraviolet and optical that observations in those spectral regions are impossible. In such circumstances, observing and classifying O- and B-type stars in the infrared may be the only option. We will consider one such classification system for the O- and B-type stars in Chapter 3.

Figures 2.6 and 2.7 show spectral sequences for main-sequence stars in the ultraviolet and in the H-band region ($\approx 1.65 \mu\text{m}$) of the infrared. The ultraviolet montage is based on spectra obtained with the International Ultraviolet Explorer

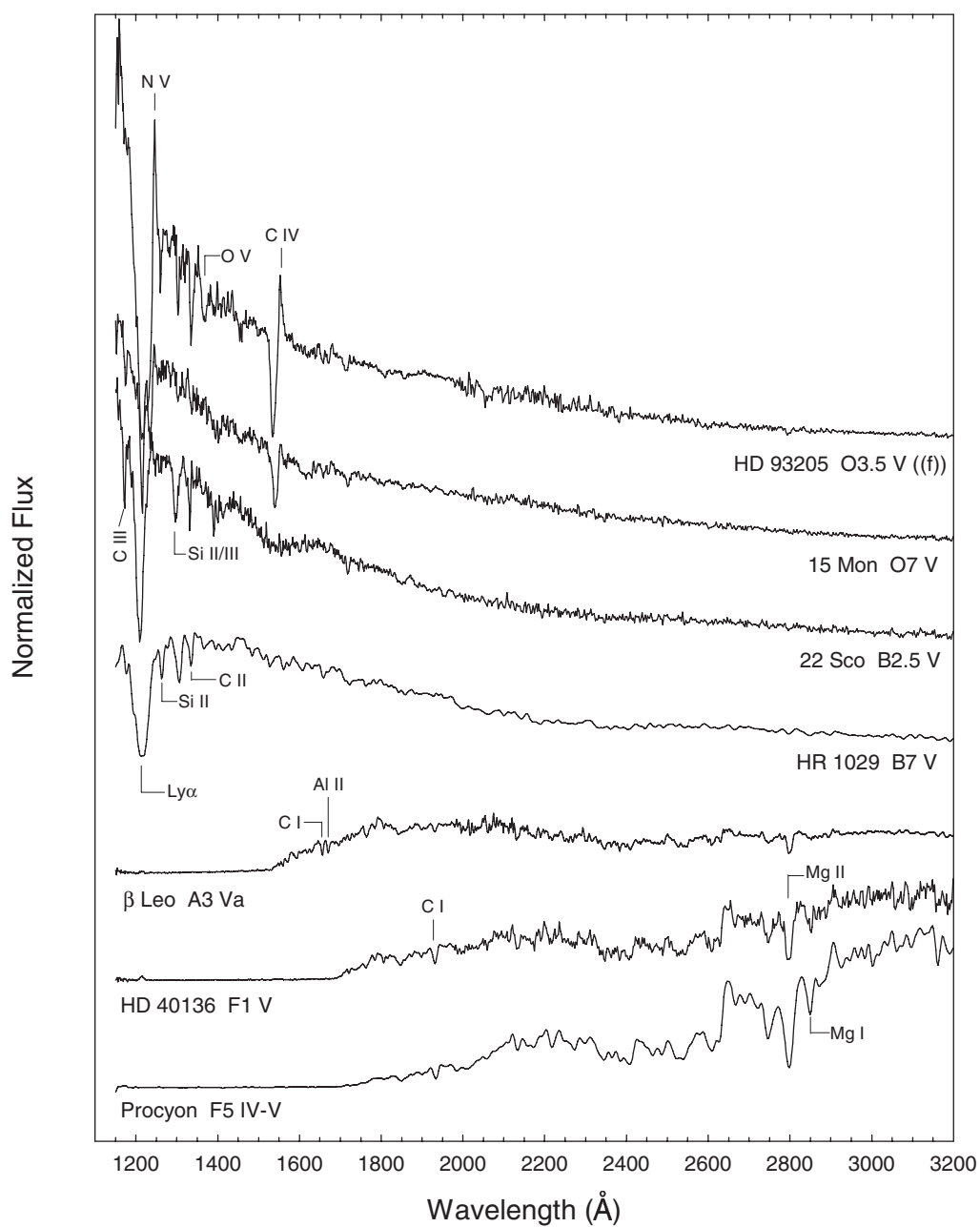


Figure 2.6 The Main Sequence in the ultraviolet. The spectra in this figure are from the International Ultraviolet Explorer data archives (MAST IUE <http://archive.stsci.edu/iue>). The spectra for both HD 93205 and 15 Mon have been dereddened. These spectra have been normalized at a common wavelength and given integer vertical offsets.

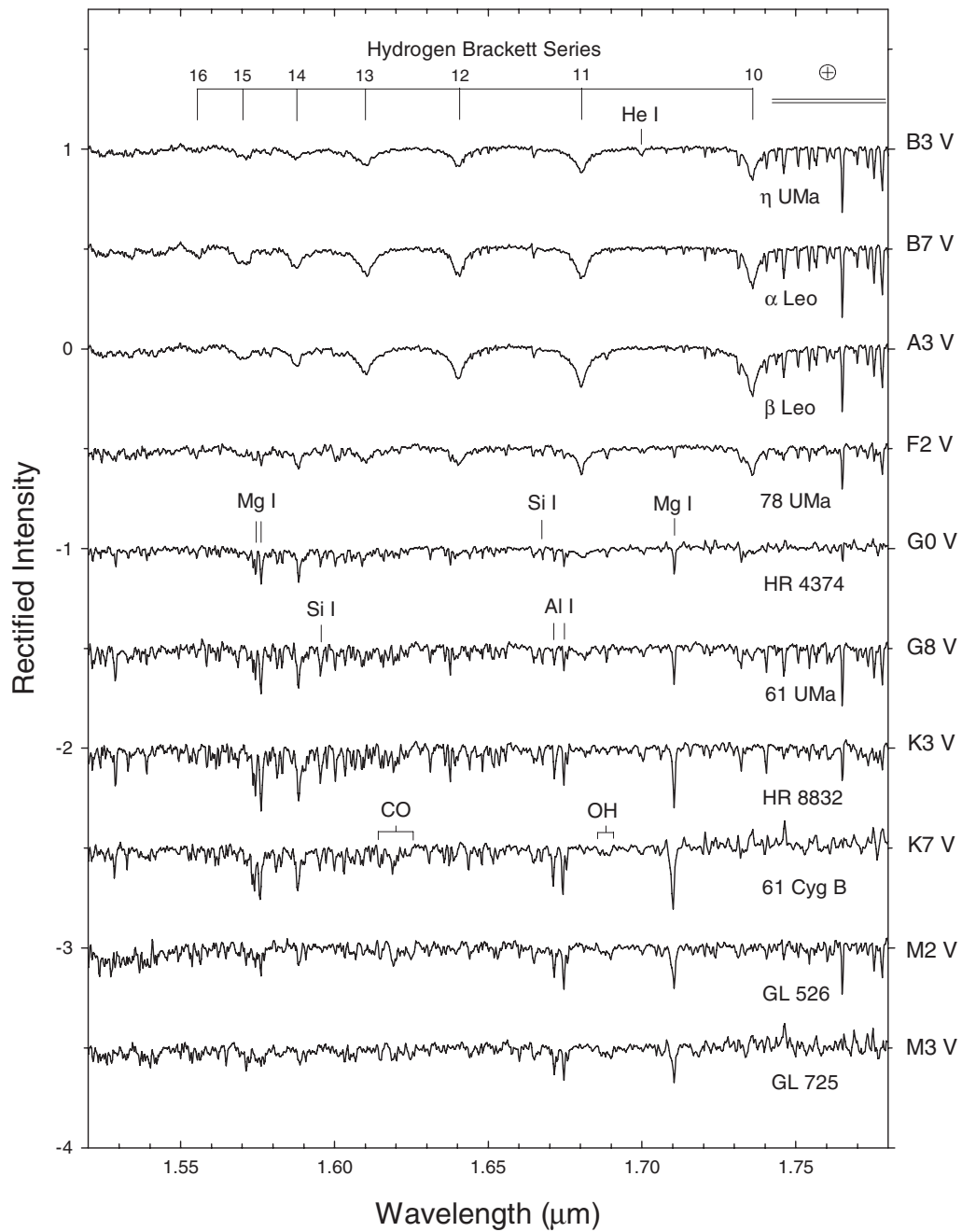


Figure 2.7 The Main Sequence in the H-band infrared. The spectra in this figure are from Meyer et al. (1998) and have been rectified. They have been given half-integer vertical offsets.

spacecraft (IUE) in the low dispersion mode. The infrared sequence is based on spectra obtained by Meyer et al. (1998). In the ultraviolet sequence, we have displayed the spectra in the normalized flux format to illustrate the enormous change in the ultraviolet flux as the temperature decreases. For stars much cooler than the Sun, the photospheric contribution to the ultraviolet region is minimal and instead this region is dominated by chromospheric and coronal emission lines. The strengths of these emission lines depend strongly on factors other than temperature and gravity (for instance, rotation and magnetic field strength), and thus cannot be used in a spectral classification system organized according to temperature and luminosity.

In Chapters 3 and 4 we will consider spectral classification systems for the O- and B-type stars based on high-resolution ultraviolet spectra. Figure 2.6 uses low-resolution IUE spectra, with a resolution of only about 6–9 Å. Even at such a low resolution features useful for spectral classification are visible. Notice in the O3.5 V spectrum the presence of strong lines due to highly ionized species (N V, Fe V, O V, C IV). The C IV feature exhibits a P Cygni profile consisting of a strong, blue-shifted absorption component combined with an emission component. This profile is the signature of a stellar wind; the absorption component is formed in the cylinder of expanding gas that we see in front of the stellar disk and the emission component from the remainder of the expanding shell (see Figure G.2). A similar profile can be seen for the N V line. While nearly all classes of stars have stellar winds, the mass-loss rates decline precipitously along the main sequence, and thus spectral wind features tend to fade toward later types.

The strongest line in the B-type stars in the ultraviolet region is the hydrogen Lyman- α line (1216 Å). Other lines in the Lyman series lie outside of the IUE spectral range but have been observed with the FUSE satellite (see Chapters 3 and 11). It is of interest to note that no lines of He I appear in the IUE spectral range. Lines of ionized helium do appear in this region, but are generally weak and not easily discerned at low resolution.

As we proceed toward cooler types in Figure 2.6, the flux in the far (shortwave) ultraviolet becomes less dominant, and the species that form the strongest lines tend to be in lower ionization states. In the A- and F-type stars, the shortwave ultraviolet vanishes. This is partly a consequence of the cooler temperatures of these stars, but also caused by the presence of both strong continuous and line absorption due to metals (see §2.4) in the atmospheres of these stars. A prominent feature that grows rapidly with declining temperature in the A- and F-type stars is the Mg II line (actually a blend of two strong lines, the Mg II h and k lines). These lines arise from energy levels analogous to those in the Ca II ion that give rise to the Ca II H and K lines and thus behave in a similar way.

2.2.3.2 The Infrared

The infrared is traditionally divided into a number spectral regions accessible from the ground through atmospheric “windows.” The regions or “bands” most often

utilized for stellar spectroscopy include the J-band ($\approx 1.24 \mu\text{m}$), the H-band ($\approx 1.65 \mu\text{m}$), the K-band ($\approx 2.2 \mu\text{m}$) and the L-band ($\approx 3.4 \mu\text{m}$). Other regions in the infrared tend to have too much telluric (terrestrial atmospheric) absorption to make ground-based spectroscopy practical, and thus can be exploited only by space-based instruments (see §13.3).

For pedagogical purposes we will confine our discussion of the infrared in this chapter to the H-band sequence of main-sequence stars presented in Figure 2.7. Detailed spectral sequences in the J-, H-, K-, and L-bands for the different spectral types will be presented in later chapters.

The spectra of early-type stars in the H-band are dominated by lines of hydrogen. In the H-band, these hydrogen lines are members of the Brackett series (which arise from transitions out of the $n = 4$ energy level; the Balmer series, which is visible in the optical and near ultraviolet, arises from transitions out the $n = 2$ energy level in the hydrogen atom). Only the higher lines in the Brackett series are visible here; Brackett- α lies at about $4 \mu\text{m}$ and Brackett- γ is in the K-band. The designation we will use in this book for hydrogen (and He II) lines higher than ϵ in a series is the principal quantum number of the upper energy level of the transition. Thus, Balmer H8 arises from the transition $2 \rightarrow 8$, Brackett-10 from the transition $4 \rightarrow 10$.

The behavior of these hydrogen lines is quite similar to that of the Balmer lines in the optical; the hydrogen lines are relatively weak in the hottest stars, come to a maximum at an intermediate temperature, and then fade in the F- and G-type stars. A comparison with Figure 2.2, however, shows a subtle difference. In the optical, the hydrogen lines come to a maximum at A2 in the dwarf stars. In the H-band we see that B7 and A3 stars have hydrogen-line strengths that are nearly identical, implying that the maximum lies closer to A0, and may even be in the late B-type dwarfs. This difference is easily understood on the basis that the Brackett lines arise from a higher level in the hydrogen atom than the Balmer lines, as we will see in §2.4.

Other features show behaviors similar to the optical. Lines due to neutral metals gradually strengthen as we go toward later types, and come to a maximum at a spectral type of about K7, after which they tend to fade. Molecular absorption is less important in the H-band than in the optical, however. The prominent TiO bands that dominate the spectra of M-dwarfs in the optical extend only to about $1 \mu\text{m}$, and thus do not contribute to the H-band. The only molecules that show absorption features strong enough to be easily visible in these H-band spectra are CO and OH.

2.2.4 Luminosity Classification

The MK System is fundamentally a two-dimensional system, consisting of a temperature dimension (*the spectral sequence*), which we considered in outline in the previous sections, and a luminosity dimension, which separates dwarfs (main-sequence stars) from evolved stars. Table 2.1 lists the main luminosity classes

Table 2.1 Luminosity Class (L.C.) Notation

L.C.	Name	L.C.	name
V	dwarf	Ib	supergiant
IV	subgiant	Ia	bright supergiant
III	giant	0	hypergiant
II	bright giant		

employed in the MK System, but be aware that subdivisions (such as IV–V) are commonly employed, and that the notation for these subdivisions can vary from one spectral class to the next, mostly for historical reasons. The luminosity class VI has been used historically to classify stars that lie below the main sequence in luminosity (i.e. the so-called *subdwarfs*) but this notation is no longer commonly employed (for an exception, see §4.7.1).

Luminosity classification is carried out using spectral criteria that are peculiar to the spectral class, and even, in some cases, spectral subclass, and thus the details of luminosity classification are best left to the later chapters that are devoted to the individual spectral classes.

However, to establish some terminology, let us consider two specific examples. If a spectral feature strengthens with increasing luminosity (i.e., if it strengthens along the sequence $V \rightarrow III \rightarrow I$), then we say that it exhibits a *positive luminosity effect*. On the other hand, if it weakens along the same sequence, we say that it exhibits a *negative luminosity effect*. The hydrogen lines in the early A-type stars exhibit a negative luminosity effect. Compare the width of the hydrogen lines in the A3 V star in Figure 2.2 with the hydrogen lines of the supergiant A0 and A5 stars in Figure 2.4. The marked narrowing of the hydrogen lines with increasing luminosity in the early A-type stars can be used as a sensitive luminosity criterion. On the other hand, lines of Fe II and Ti II in the F-type stars tend to increase in strength with increasing luminosity. For instance, compare the Fe II/Ti II feature at $\lambda\lambda 4172-8$ marked in the dwarf sequence in Figure 2.2 with the same feature in the supergiants in Figure 2.4. This is an example of a luminosity criterion that exhibits a positive luminosity effect.

2.3 MULTICOLOR PHOTOMETRY AND STELLAR CLASSIFICATION

In the previous section, we reviewed the outline of stellar spectral classification. The rest of the book will fill in the details! It should be noted at this point, however, that stellar classification may be carried out using techniques other than spectroscopy. In particular, stars may be classified, or at least characterized, with multicolor photometry. There are many existing systems of multicolor photometry, but all have in common the use of measurements of stellar brightnesses or *fluxes* in certain spectral bands. The isolation of the stellar bands is usually accomplished with glass and/or interference filters, and the flux measurements, traditionally obtained with photomultipliers, are now increasingly being acquired with CCDs.

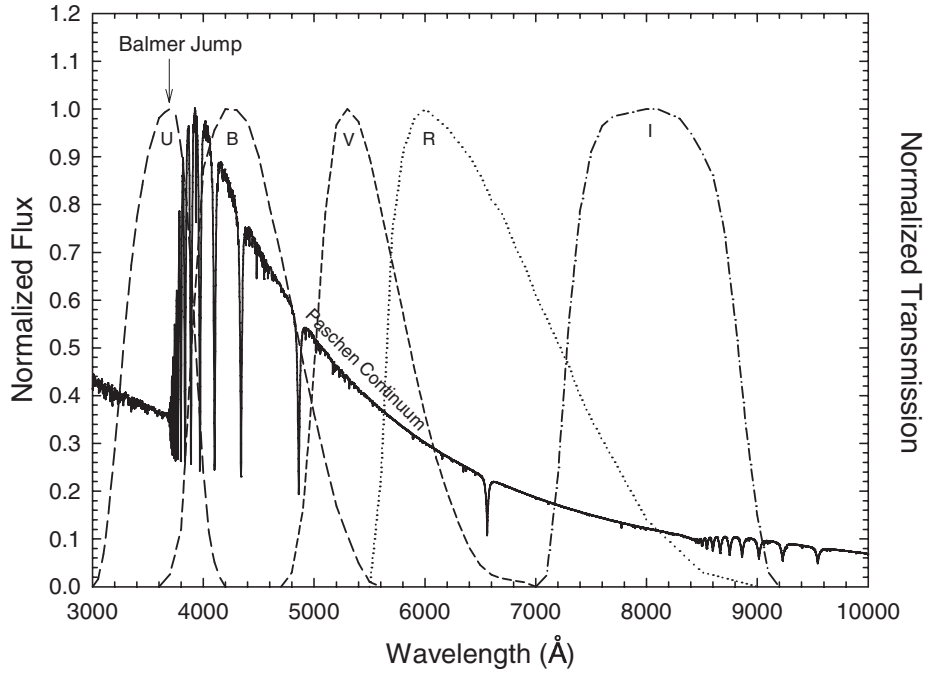


Figure 2.8 The normalized Johnson–Cousins $UBVRI$ photometric passbands (right-hand scale) plotted with the spectral energy distribution of an A0 V star (left-hand scale). The stellar energy distribution has been normalized to unity at the highest point. Notice the positions of the Balmer jump and the Paschen continuum. The Balmer lines are easily visible, and converge at a wavelength of 3646 \AA . The scale of the right-hand vertical axis is identical to the left.

Multicolor photometry has a long and interesting history, but even a precis of that history is beyond the scope of this book. Interested readers are referred to the book *The Measurement of Starlight: Two Centuries of Astronomical Photometry* by Hearnshaw (2005). In the modern era, the most widely used, although not necessarily the best designed, photometric system is the Johnson UBV system (Johnson & Morgan 1953). Figure 2.8 shows the stellar energy distribution (flux spectrum) of an A0 V star plotted with the transmission passbands of the U (ultraviolet), B (blue), and V (“visual” or yellow-green) filters. In normal practice, stellar fluxes measured through these filters are converted to magnitudes, and placed on the standard UBV system via observations of standard stars. These magnitudes may be used to form the *photometric indices* $U-B$ and $B-V$. The $B-V$ index (or color) is a measure of the slope of the Paschen continuum (see Figure 2.8), and as such is quite closely correlated with the *effective temperature* of the star, although dwarfs and giants must be considered separately, and metal-weak stars do not obey the same relation as metal-rich. The $U-B$ index is also related to temperature, and is especially useful in the early-type stars for that purpose, but it is sensitive to other factors as well. Figure 2.8 shows that the U and B filters span and overlap the *Balmer jump*, a spectral discontinuity caused by the

photoionization of hydrogen from the first excited level ($n = 2$; see §2.4 and the discussion of *continuous opacity*), and the convergence of the Balmer series of hydrogen lines. The “height” of the Balmer jump is primarily sensitive to temperature in the early-type stars, but also shows significant sensitivity to pressure (surface gravity) in the A- and F-type stars, and thus $U-B$ is sensitive to both temperature and gravity. But, because the density of spectral lines due to metals is greater shortwards of the Balmer jump than longwards, the $U-B$ index is also sensitive to the overall metal abundance (sometimes called *metallicity*). Combine these various sensitivities with the fact that the short-wavelength cutoff of the U -filter passband is actually set by atmospheric absorption, and it is not surprising that the $U-B$ index can be difficult to interpret and model astrophysically.

UBV photometry is quite often combined with photometry in two other filters in the red and near-infrared, the R and I filters. Figure 2.8 shows the passbands of the R and I filters on the Johnson–Cousins system, which are quite different from the passbands of the R and I filters on the Johnson system. Users of photometry published in the literature must be careful to ascertain which passbands were employed. The Johnson–Cousins system has been carefully standardized by Arlo Landolt (see, for instance, Landolt 1992).

Another commonly used multicolor photometric system is the Strömgren $uvby$ system, designed by Bengt Strömgren in the 1960s (see Strömgren 1966). This system employs filters with narrower passbands than the Johnson UBV system; this enables the color indices on this system to be more easily interpreted astrophysically. Figure 2.9 plots the passbands of the four Strömgren filters with the energy distribution of an A0 V star. Notice that the u (ultraviolet) and v (violet) filters are more intelligently placed with respect to the Balmer jump and convergence than in the UBV system, although the $H\delta$ line lies within the passband of the v filter. The $b-y$ index measures, like the $B-V$ index on the Johnson system, the slope of the Paschen continuum. Two other indices are defined in the Strömgren system. The m_1 index, defined by $m_1 = (v-b) - (b-y)$, was designed to measure the *line blanketing* (absorption by spectral lines) in the v band; the $(b-y)$ term in the definition of the m_1 index helps to remove, to first order, the temperature sensitivity of this index. The c_1 index, defined by $c_1 = (u-v) - (v-b)$, measures the height of the Balmer jump, and is relatively free of the photometric effects of the Balmer convergence, unlike the $U-B$ index. In addition, the $(v-b)$ term in the definition of the c_1 index removes, to first order, the metallicity sensitivity of that index. The c_1 index comes to a maximum in the early A-type stars, like the hydrogen Balmer lines (see §2.2 and Figure 2.10). Strömgren photometry was designed explicitly for the detection and study of metal-weak F- and G-type stars, but has also found applications in the B-, A-, K-, and M-type stars (see, for instance Crawford 1975, 1978, 1979; Olsen 1983; Olsen & Perry 1984; Olsen 1995).

Strömgren $uvby$ photometry is often used with $H\beta$ photometry, which consists of two filters centered on the hydrogen (Balmer) β line. One filter is narrow (full-width $\approx 60 \text{ \AA}$), the other is wider (full-width $\approx 300 \text{ \AA}$; see Crawford & Mander (1966). The inclusion of $H\beta$ photometry helps in the determination of interstellar reddening.

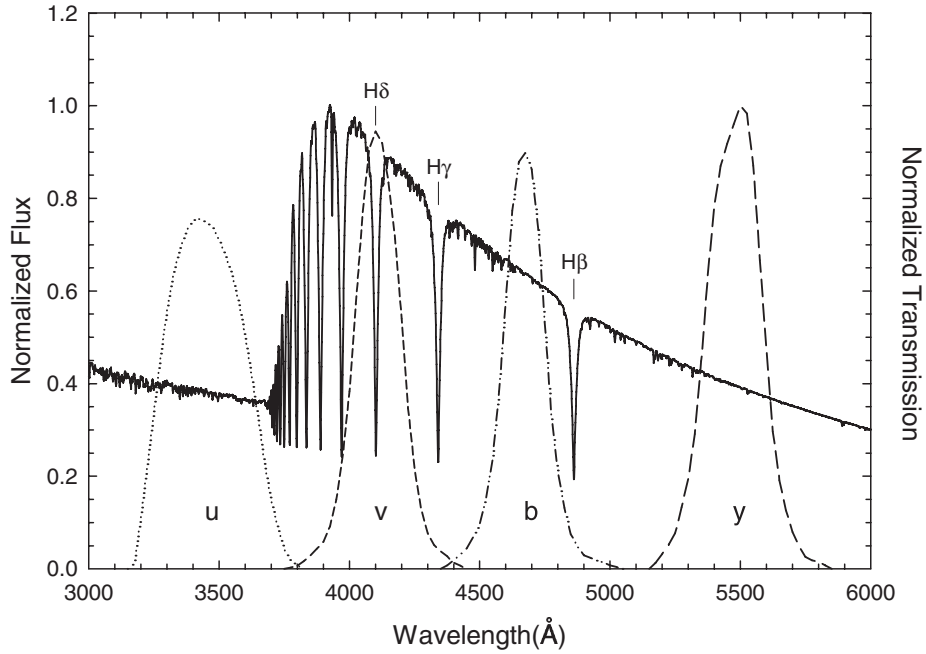


Figure 2.9 The Strömgren *uvby* photometric passbands (right) plotted with the spectral energy distribution of an A0 V star (left). Notice that the narrower bands of the Strömgren system more cleanly sample the Balmer jump than the Johnson *UBV* passbands. The Strömgren passbands in this figure have been normalized to the peak transmission of the *y* band. The scales of the two vertical axes are identical.

A more recent photometric system, combining some of the filter passbands of the Strömgren system with those of the Vilnius system, has been developed, largely through the efforts of Straižys and colleagues (Straižys et al. 1996). This new system is called Strömvil photometry, and time will tell whether it will be widely adopted. Another photometric system that has similar properties to the Strömgren system is Geneva photometry (see, for instance, Nicolet 1996).

Yet another recently developed photometric system is the $u'g'r'i'z'$ Sloan Digital Sky Survey (SDSS) photometric system. The fifth release of data from the SDSS contains photometry of 215 million unique objects, including stars and galaxies. Table 2.2 lists the effective wavelengths of the five Sloan filters. For more information on the survey and $u'g'r'i'z'$ photometry, see <http://www.sdss.org>.

Over the years a large number of photometric systems have been developed, often for special purposes. It is beyond the scope of this book to review these systems, but the following merit mention: the DDO system for the measurement of red giants, incorporating filters to sample the CN molecular bands (McClure 1976); the Wing narrow-band system for late-type stars (White & Wing 1978); and the Washington system for late-type stars (Canterna 1976). Photometric systems have also been defined for the ultraviolet and infrared, such as the 2MASS *JHK* infrared photometric system (Skrutskie et al. 2006).

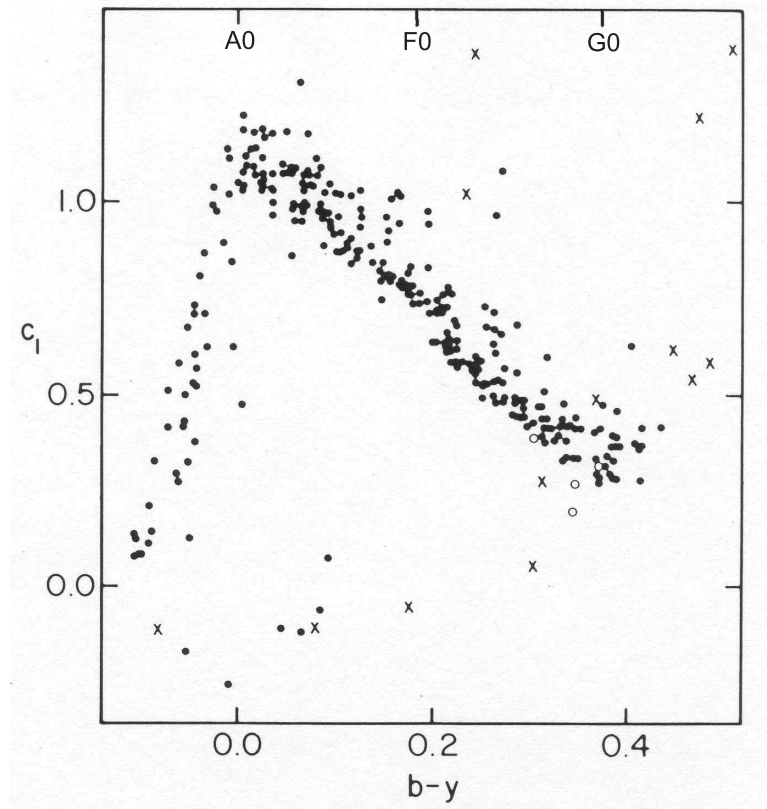


Figure 2.10 The $b-y$ index plotted against the c_1 index for the bright stars. Both indices are on the Strömgren $uvby$ photometric system. The $b-y$ index, in the absence of reddening, measures the temperature, the c_1 index, the Balmer jump. Note that the c_1 index comes to a maximum near $b-y = 0.0$, corresponding to the early A-type stars. The approximate positions of main-sequence spectral types have been added to the top scale for reference purposes. Figure from Crawford (1984) and used with permission from the David Dunlap Observatory.

Every photometric system can be calibrated against MK spectral types; for instance, by observing a large number of A0 V stars, it is possible to find mean $b-y$, m_1 , and c_1 indices for that spectral type. Tabulations of such mean values can be found in a number of sources, including Drilling & Landolt (1999). Some astronomers have been tempted to reverse the process, i.e. to obtain photometric indices for their stars of interest, and then to “derive” MK spectral types via the tabulations. This practice is deprecated (see, for instance, the comments after the paper by Heck 1984), as an MK type is properly determined only through detailed comparison of the unknown spectrum with the MK standards. As will become evident in the following chapters, the combined effects of rotation, metallicity, interstellar reddening, and other *photometric degeneracies* can confuse the translation of photometric indices into MK types, even if such a translation were

Table 2.2 SDSS filter Effective Wavelengths

u'	g'	r'	i'	z'
3551 Å	4686 Å	6165 Å	7481 Å	8931 Å

desirable or legitimate. Rather, the MK type should be regarded as an independent datum of stellar astronomy, capable of yielding insight and information when confronted with other data types, such as photometry. Some of these issues are considered in more detail by Crawford (1984) and Gray (2006).

That is to say, the most productive relationship between MK classification and multicolor photometry is one of *complementarity*. The complementary nature of the interaction between spectral classification and multicolor photometry comes about because these two systems approach the classification of stars in two very different ways. Multicolor photometric systems, for the most part, are confined to measuring continuum features in a stellar spectrum, such as the slope of the Paschen continuum, the Balmer jump, etc. Spectral classification, on the other hand, relies almost entirely on the appearance of the line spectrum. In most cases, the two systems give consistent classifications, but the most interesting comparisons arise when the two systems *disagree*. In that disagreement is often found new information about stellar atmospheres, stellar evolution, or even the interstellar medium. Thus, one's spectral type for a given star should never be influenced by photometric information, because that influence would rob the interface between the two systems of any information content.

The first, and in some ways still the best, example of complementarity between the two systems is the determination of reddening due to the presence of interstellar dust. Interstellar dust *reddens* the light from a star by preferentially scattering out of the line of sight short wavelength light. Reddening, of course, affects the photometric measurement of the color of the star (for instance, the $B-V$ and $b-y$ indices are made more positive), but has little effect on the line spectrum and thus the spectral type. Therefore, if *intrinsic colors* for the different spectral types are found by studying nearby, unreddened stars, the *color excess*, or *reddening*, for a given star may be determined by comparing the measured color index to the intrinsic color index determined from its spectral type. These color excesses take the form

$$E(B-V) = (B-V) - (B-V)_0 \quad (2.3.1)$$

where $(B-V)_0$ is the intrinsic color of the star.

There are many other instances of complementarity between photometry and spectral classification; the history of the Strömgren $uvby\beta$ system is particularly rich in examples. This profitable interaction has been expertly reviewed by Olsen (1994).

2.4 PHYSICAL PRINCIPLES UNDERLYING THE MK SEQUENCE

2.4.1 Physical Conditions in Stellar Photospheres

While a theoretical understanding of the formation of the stellar spectrum is certainly not necessary for the process of spectral classification, it is essential for the *interpretation* of spectral types. It is beyond the scope of this book to develop the theory of stellar atmospheres and spectral-line formation in detail; excellent monographs exist on that subject (i.e. *The Observation and Analysis of Stellar Photospheres*, Gray 2008; and *Stellar Atmospheres*, Mihalas 1978). However, it is possible to gain a physical understanding of the spectral sequence and other aspects of stellar spectral classification by considering some elementary results of statistical physics and radiative transfer.

First, it is necessary to understand that the stellar spectrum is formed only in the surface layers of a star, called the *stellar photosphere*, although in cool stars the chromosphere and the corona also contribute to the emergent spectrum, especially in the far and extreme ultraviolet. The stellar photosphere plays such an important role in the formation of the spectrum because it is here that photons undergo their last few, and thus most critical, interactions with matter before escaping to free space.

Energy in the form of photons, produced in the core of the star by nuclear reactions, reaches the surface of the star only after countless interactions with the material in the interior of the star. The interior of a star is composed of a nearly completely ionized plasma (a gas consisting of electrons and ions). This plasma interacts with the radiation field in the interior through the physical processes of electron scattering and free–free and bound–free (photoionization) absorption and emission by ions. Free–free absorption occurs when a free electron becomes able to absorb a photon when in the vicinity of an ion. Thus a gamma-ray photon produced in the core of the star random walks its way to the surface and, in the process, is degraded into hundreds of lower energy photons (mostly in the UV, optical, and infrared parts of the spectrum). In the interior, because of the high densities, the *mean free path* between interactions is very short—on the order of a centimeter in main-sequence stars. The high densities also mean that in the interior, collisions are extremely effective in coupling the radiation field with the thermal state of the gas. In this condition, the interior is very nearly in a perfect state of thermodynamic equilibrium, and, as a consequence, the material in the interior of the star radiates at the local temperature as a *blackbody radiator*. As we move toward the surface and encounter lower densities, the mean free path of a typical photon becomes much longer. In the stellar photosphere, the mean free path may measure in the kilometers; eventually a level in the stellar photosphere is reached at which it is highly probable that the photon will escape without further interaction. Since at each interaction the energy (wavelength) of the photon may be altered, it is clear that the last few interactions are most important in the formation of the emergent spectrum.

Because the mean free path of a typical photon in the stellar photosphere is quite long, this means that the radiation field is not so tightly coupled to the

local thermal state of the gas, and thus the assumption that the gas is in a state of thermodynamic equilibrium is no longer strictly valid. However, in high-density, high-pressure atmospheres (main-sequence stars), and to a more limited extent in giant and supergiant stars, *local thermodynamic equilibrium*, i.e. the assumption that each layer in the stellar photosphere is characterized thermodynamically and radiatively by the local gas temperature, is an acceptable approximation, at least for the discussion below.

The physical processes of electron scattering and free–free and bound–free absorption by ions are referred to collectively as sources of *continuous opacity*, as these processes can scatter or absorb and emit photons over a wide range of wavelengths. In the stellar atmosphere other forms of opacity come into play. In particular, bound–bound absorption (i.e. absorption in spectral lines, or *line opacity*) is important. As a consequence, opacity in the stellar photosphere is a strong function of wavelength; in the core of a spectral line the opacity is considerably higher than in the surrounding continuum, where the opacity is due only to continuum processes.

There is a temperature gradient in a stellar photosphere; neglecting the possible existence of extended outer layers of the atmosphere—e.g. the corona and the chromosphere—the top (outer layer) of the photosphere is considerably cooler than the “bottom” (inner layer). This temperature gradient is one of the most important factors in the formation of absorption lines in the stellar spectrum. To understand how an absorption line is formed, compare a continuum region of a stellar spectrum with a spectral line. In the continuum region the total opacity is relatively low, as only continuum processes contribute. This means that we can see at those wavelengths deeply into the photosphere to relatively hot layers and thus the emerging radiation flux is high. In the core of a spectral line the opacity is high, and thus the majority of the photons emerge from higher, cooler layers. This leads to a lower radiation flux in the core of the spectral line than in the surrounding continuum, and thus the formation of an absorption line (see Figure 2.11).

The core of an absorption line is therefore formed in the cool upper layers of the stellar photosphere, the surrounding continuum is formed at depth, and the wings of the absorption line in intermediate layers. This implies that if the continuous opacity is relatively high, the spectral line will be formed only over a limited range in the atmosphere, and thus will be weaker than if the continuous opacity were low. This suggests that the strength of a spectral line is in inverse proportion to the continuous opacity and in direct proportion to the line opacity. Factors that contribute to the line opacity include the abundance of the relevant element in the photosphere, the proportion of the atoms that are in the ionization state and the excitation state required for absorption in the spectral line under consideration, and the transition probability associated with the spectral line. If we let κ_λ represent the continuous opacity per unit mass at the wavelength of the spectral line, and I_λ the line opacity, we then have, to a first approximation,

$$\text{Line Strength} \propto \frac{I_\lambda}{\kappa_\lambda}. \quad (2.4.1)$$

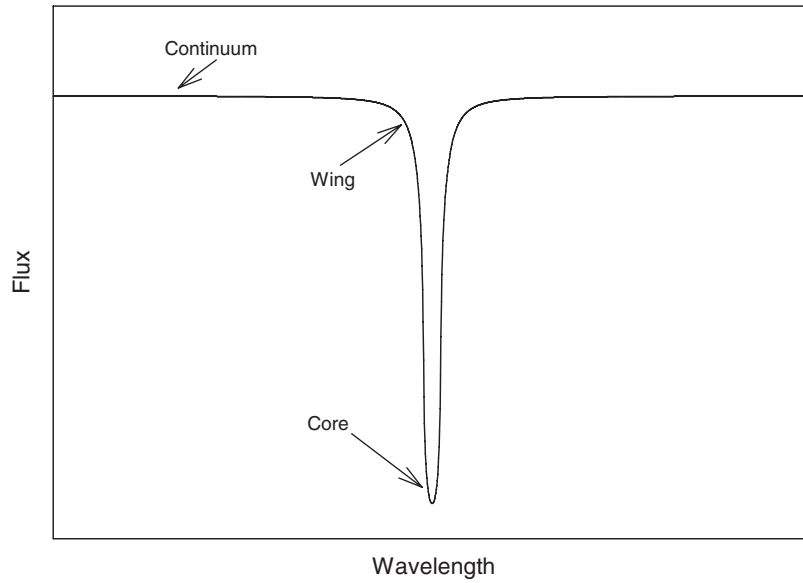


Figure 2.11 The parts of a spectral line.

This relationship is strictly true only for weak spectral lines. For strong lines, effects such as the various line-broadening mechanisms, saturation, and turbulence mean that the line strength will be a nonlinear but monotonically increasing function of I_λ/κ_λ . Details may be found in Gray et al (2003) and Mihalas (1978).

Figure 2.12 shows, graphically, the continuous opacity at $\lambda = 4500 \text{ \AA}$ as a function of the temperature. Some of the important contributors to the continuous opacity are indicated in that figure.

Emission lines, when they are present in stellar spectra, usually, although not always, originate in hotter, outer layers of a stellar atmosphere, such as a chromosphere, a corona, or a stellar wind. These emission lines are usually most evident in regions where the flux in the photospheric spectrum is small, such as the cores of strong absorption lines (the $H\alpha$ line, for example) and, in cool stars, in the short-wavelength ultraviolet.

An understanding of the physical processes that lead to the formation of the stellar spectrum requires some knowledge of representative temperatures, densities, and pressures in the stellar photosphere. The *effective temperature* (T_{eff}) of a stellar photosphere corresponds, roughly, to the temperature of the layer where the spectral continuum is formed. The T_{eff} of a star is defined to be the temperature of a blackbody radiator with the same radius and the same total power output (luminosity) as the star. Effective temperatures range from about 2500 K at the bottom of the stellar main sequence (late M-type dwarfs, not counting the L and T brown dwarfs) to more than 40,000 K at the top (early O-type stars). With a knowledge of the opacity mechanisms in a stellar photosphere, it is possible to compute a theoretical stellar atmosphere model. Theoretical stellar atmosphere models have been computed for effective temperatures all along the main sequence and these

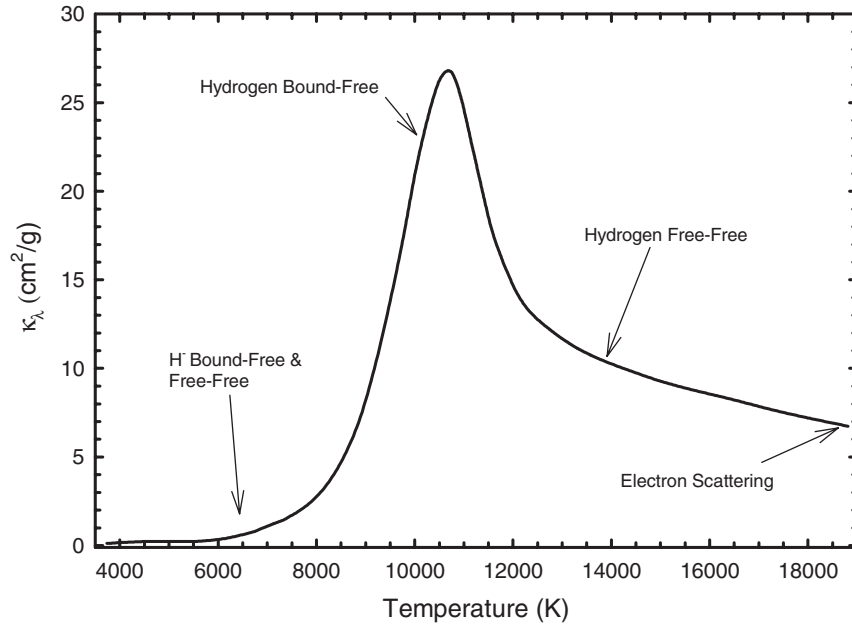


Figure 2.12 Continuous opacity in the optical region (calculated at 4500 \AA at unit *optical depth*) in stellar photospheres along the main sequence as a function of the temperature. The dominant sources of opacity are indicated.

models give us information on the temperature structure and the run of densities and pressures with depth in the photospheres of these stars. Models for giants and supergiants have also been computed.

Along the main sequence, typical pressures in stellar photospheres range from very low values at the surface to about a few $\times 10^5$ or $10^6 \text{ dynes cm}^{-2}$ at the “bottom” (for the purpose of comparison, the pressure of the earth’s atmosphere at sea level is about $10^6 \text{ dynes cm}^{-2}$). Electron number densities are, of course, strongly dependent on the effective temperature, and range from typical values of 10^{12} to 10^{13} cm^{-3} in the late type stars to 10^{14} to 10^{15} cm^{-3} in the early-type stars. These values will be one to two orders of magnitude smaller in the giants, and another one to two orders of magnitude smaller in the supergiants.

2.4.2 The Hydrogen Lines

Let us now use our understanding of spectral-line formation in stellar atmospheres to understand, in physical terms, the broad outline of the spectral sequence. In §2.2 we saw that one of the outstanding features of the spectral sequence is the behavior of the hydrogen lines. In the late-type stars, the hydrogen lines are weak, but become steadily stronger with increasing effective temperature until reaching a maximum in the early A-type stars. At higher temperatures (the B- and O-type stars), the hydrogen lines again become weaker. We saw this behavior in the Balmer lines of hydrogen in main-sequence (Figure 2.2) and supergiant (Figure 2.4) stars and in

the Brackett lines in main-sequence stars (Figure 2.7). We noted, however, that in the supergiants the Balmer lines come to a maximum at a later spectral type than in the main-sequence stars, and the Brackett lines in main-sequence stars come to a maximum at slightly earlier spectral types than the Balmer lines. What are the physical principles underlying this behavior?

The behavior of the Balmer lines in the main-sequence stars may be understood qualitatively as follows. The Balmer series of absorption lines arises from transitions out of the first excited state ($n = 2$) of the hydrogen atom, where n is the principal quantum number of the hydrogen atom. In the late-type stars the photospheric temperatures are low enough that only a very small proportion of the hydrogen atoms have been excited to the $n = 2$ state; most are in the ground ($n = 1$) state. As we move toward earlier types, the photospheric temperatures rise, and a greater proportion of the hydrogen atoms are in the $n = 2$ state. This leads to an increase in the line opacity, l_λ , and the Balmer lines increase in strength. At yet higher temperatures (earlier types), hydrogen begins to become ionized, and so while the proportion of neutral hydrogen atoms in the $n = 2$ state is still increasing, the actual number of atoms in that state is actually declining. This leads to a decline in the line opacity, and a weakening of the Balmer lines. As we shall see later, the continuous opacity plays only a relatively minor role in determining the behavior of the Balmer lines near their maximum.

We can discuss the behavior of the hydrogen lines in a more quantitative way by considering two important equations of statistical physics. The first of these equations is the Boltzmann equation, which is strictly valid only in the condition of thermodynamic equilibrium. The Boltzmann equation relates the number densities of a given species (atom or ion) in two different excitation states:

$$\frac{N_B}{N_A} = \left(\frac{g_B}{g_A} \right) \exp[(E_A - E_B)/kT] \quad (2.4.2)$$

where N_A and N_B are the number densities of the particular species in the two different excitation states, A and B ; E_A and E_B are the excitation energies of those two states, k is the Boltzmann constant, T is the temperature, and g_A and g_B are the statistical weights of the levels A and B (for hydrogen, $g_n = 2n^2$). We can write the ratio $N_n/N_{(0)}$, where N_n is the number density of hydrogen atoms in the n th state and $N_{(0)}$ is the total number density of neutral hydrogen atoms, as

$$\begin{aligned} \frac{N_n}{N_{(0)}} &= \frac{N_n}{N_1 + N_2 + N_3 + \cdots} = \frac{N_n/N_1}{[1 + N_2/N_1 + N_3/N_1 + \cdots]} \\ &= \frac{g_n \exp(-E_n/kT)}{[g_1 + g_2 \exp(-E_2/kT) + g_3 \exp(-E_3/kT) + \cdots]} \\ &= \frac{g_n \exp(-E_n/kT)}{U(T)} \end{aligned} \quad (2.4.3)$$

where $U(T)$ is the partition function for neutral hydrogen. It is defined as

$$U(T) = \sum g_i \exp(-E_i/kT) \quad (2.4.4)$$

where the sum is over all bound states in the hydrogen atom. For $T \lesssim 20,000$ K, $U(T)$ varies between 2.0 and ≈ 2.5 .

The second equation is the Saha equation, again strictly valid only under conditions of thermodynamic equilibrium. The Saha equation relates the number densities of ions in two adjacent ionization states, $N_{(i+1)}$ and $N_{(i)}$:

$$\frac{N_{(i+1)}}{N_{(i)}} = \frac{U_{(i+1)}}{U_{(i)}} \frac{1}{N_e} \frac{2(2\pi mkT)^{3/2}}{h^3} \exp(-E_I/kT) \quad (2.4.5)$$

where E_I is the ionization energy of the i th ion, N_e is the electron number density, m is the electron mass, and $U_{(i+1)}$ and $U_{(i)}$ are the partition functions of the two ionization states. There are only two ionization states for hydrogen: neutral hydrogen and hydrogen that has lost its single electron, i.e. a proton. It turns out that the partition function for a proton, U_p , is identically 1.0. We may therefore write

$$\frac{N_p}{N_{(0)}} = \frac{1}{U(T)} \frac{1}{N_e} \frac{2(2\pi mkT)^{3/2}}{h^3} \exp(-E_I/kT). \quad (2.4.6)$$

Now, according to our discussion in the paragraphs above, the line opacity, l_λ , for a hydrogen line arising from the n th energy level should be proportional to the ratio of the number density of neutral hydrogen atoms in the n th excitation state, N_n , to the total number density of hydrogen, $N_{(0)} + N_p$. Thus for a hydrogen line, we may write

$$l_\lambda \propto \frac{N_n}{N_{(0)} + N_p} = \frac{N_n/N_{(0)}}{N_p/N_{(0)} + 1}. \quad (2.4.7)$$

Substituting from Equations 2.4.3 and 2.4.6, and simplifying we find

$$l_\lambda \propto \frac{N_n}{N_{\text{total}}} = \frac{g_n N_e h^3 \exp(-E_n/kT)}{2(2\pi mkT)^{3/2} \exp(-E_I/kT) + N_e h^3 U(T)}. \quad (2.4.8)$$

What about the continuous opacity? Figure 2.12 shows that the continuous opacity in the vicinity of the Balmer lines peaks strongly at a temperature of about 11,000 K. However, it turns out that the variation in the hydrogen line opacity with temperature is many orders of magnitude greater than the variation in the continuous opacity. Thus, we may safely ignore the effects of the continuous opacity in this calculation, although it must, of course, be taken fully into account in detailed spectral synthesis computations.

Thus, a plot of the quantity N_n/N_{total} given by the equation above versus temperature should mirror the behavior of the hydrogen lines. For the Balmer lines in main-sequence stars, we substitute $n = 2$, $E_2 = 10.2$ eV, $E_I = 13.6$ eV, and $N_e = 1.0 \times 10^{14} \text{ cm}^{-3}$, a typical value for a main-sequence stellar atmosphere near the Balmer maximum.³ The result is shown as the solid line in Figure 2.13. Notice how this curve peaks near $T = 10,000$ K, which is approximately the temperature

³One electron volt (eV) is the energy acquired by an electron when it is accelerated through a potential difference of one volt, and is equal to 1.602×10^{-19} joule or 1.602×10^{-12} erg.

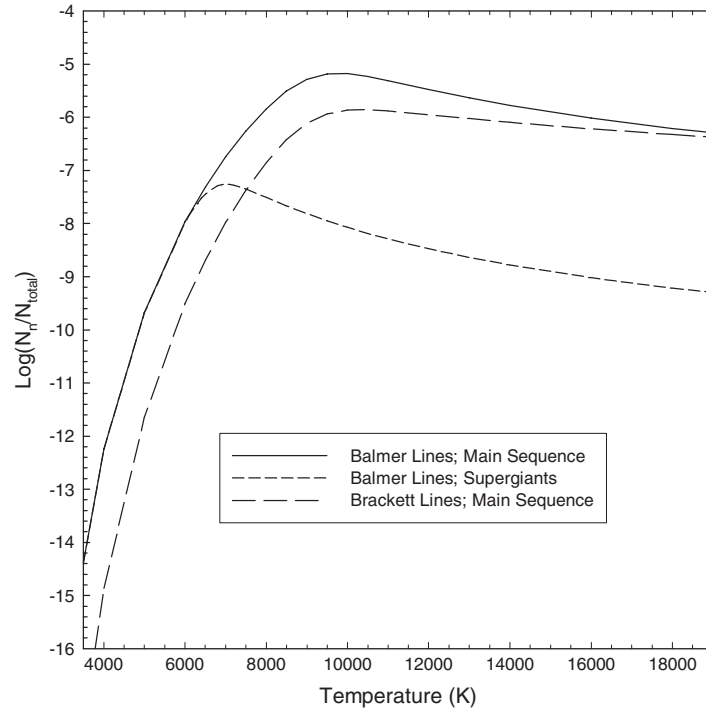


Figure 2.13 Behavior of the hydrogen lines with temperature.

of an A0 star. In main-sequence stars, the actual peak is near 9000 K, but this discrepancy is easily explained by our neglect of a number of more subtle physical effects that can be taken into account only through a full stellar-atmosphere and radiative-transfer treatment. If we use a value of the electron number density more typical of Ib supergiants, say, $N_e = 1.0 \times 10^{11} \text{ cm}^{-3}$, we get the short-dashed curve. Note that this peak is at a significantly cooler temperature, about 7000 K, very close to the maximum near spectral type F0 we observed in Figure 2.4. Finally, again using $N_e = 1.0 \times 10^{14} \text{ cm}^{-3}$, but this time $n = 4$, $E_4 = 12.75 \text{ eV}$, appropriate numbers for the Brackett series of hydrogen lines in main-sequence stars, we obtain the long-dashed curve. Notice that the maximum is at a slightly higher temperature than for the main-sequence Balmer lines, exactly as we observed earlier in this chapter.

A very similar analysis may be carried out for the neutral helium lines; the only difference is that we would have to consider three ionization states (He I, He II, He III) instead of two. Considering that the excitation energies for He I lines in the optical are considerably higher than for the hydrogen lines, and the ionization energy for He I is also higher, it is easy to understand why the maximum for the He I lines occurs at about 22,000 K, instead of 10,000 K.

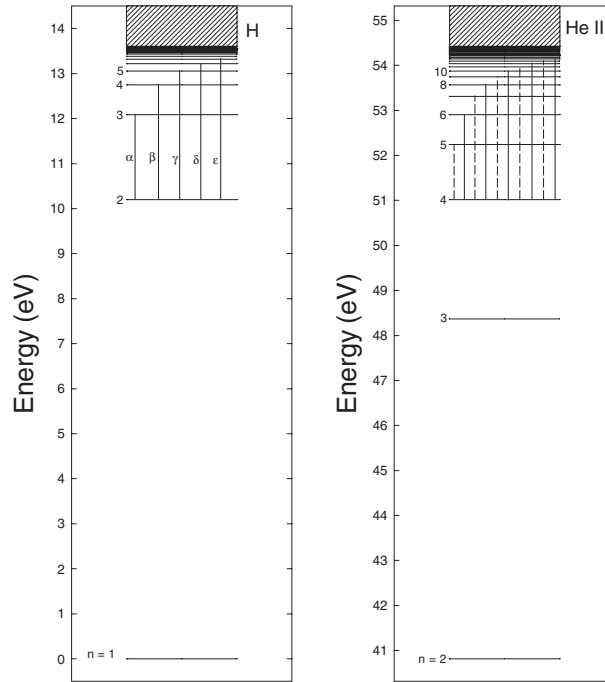


Figure 2.14 Simplified energy-level diagrams for hydrogen (left) and ionized helium (right). The principal quantum numbers for the energy levels are indicated in both panels; $n = 1$ is the ground state. Note that the ground state of He II is not shown in the diagram. In the panel to the left, transitions corresponding to the first few lines of the hydrogen Balmer series are shown. On the right, transitions corresponding to the Pickering series of He II are shown. Note that every other Pickering line (solid lines) corresponds closely in energy to a line of the Balmer series. The hatched area in both diagrams represents the continuum of the two ions.

2.4.3 He II lines

Lines of He II show up in hot stars, not only in the O-type stars (Chapter 3), but also in the Wolf–Rayet stars (Chapter 11). In those chapters, frequent reference is made to the Pickering series of He II, and how it relates to the Balmer series of hydrogen. Ionized helium and neutral hydrogen are one-electron systems, and thus have similar energy-level diagrams, except that the energies for He II are scaled by a factor of Z^2 compared with those for hydrogen, where Z refers to the nuclear charge. Since $Z = 1$ for hydrogen, and $Z = 2$ for He II, the scaling is by a factor of 4. Figure 2.14 shows the energy-level diagrams for hydrogen and He II. In the diagram for hydrogen, transitions corresponding to the first few lines of the Balmer series are shown. In the diagram for He II, transitions corresponding to the Pickering series are shown. Note that the $2 \rightarrow 3$ transition in hydrogen corresponds very closely in energy to the $4 \rightarrow 6$ transition for He II, similarly for the $2 \rightarrow 4$ transition of hydrogen and the $4 \rightarrow 8$ transition for He II and so on. What this

means is that every other line of the Pickering series corresponds very closely in wavelength to a line of the Balmer series. Similar overlaps may be seen in other series. For instance, the Lyman series of hydrogen ($1 \rightarrow m$) overlaps with every other line of the Balmer series of He II ($2 \rightarrow m$). The Paschen series of He II ($3 \rightarrow m$) has one line in the optical, $\lambda 4686$ ($3 \rightarrow 4$), which figures prominently in the classification of the Wolf–Rayet stars.

2.4.4 The Metallic Lines

The behavior of the spectral lines due to metals, which we described in §2.2, obey the same general principles as the hydrogen lines (see §2.4.2). However, careful consideration of Figure 2.15, a temperature sequence of main-sequence stars in the blue-violet region, shows some aspects of this behavior that are not immediately understandable. For instance, the enormous strength of the Ca II K & H lines compared with lines of Fe II is somewhat puzzling considering that iron is nearly 10 times more abundant than calcium in a typical stellar photosphere. Likewise, titanium is about 2.5 orders of magnitude less abundant than iron, and yet Ti II lines in the A5 V star in that figure are of comparable strength to the Fe II lines. The almost complete lack of strong metal lines in the B-type stars also seems curious. For instance, we might expect many strong lines of Fe III or Fe IV in the spectrum of a B3 V star, but none show up in Figure 2.15. The explosive growth of Ca I $\lambda 4226$ toward later types is also notable, and needs further explanation.

2.4.4.1 Resonance Lines

While most spectral lines of metals follow the same pattern of behavior as the hydrogen lines, that is, they come to a maximum at some intermediate temperature depending upon the excitation energy and the ionization energy, *permitted* lines that arise from the ground state of the atom or ion (called *resonance lines*, see Figure 2.16) are an exception. At low temperatures, atoms and ions are preferentially found in the ground state, and hence the strength of these lines, in particular the resonance lines of neutral species, grows dramatically with declining temperature. This is exactly the behavior we noted in the 4226 Å resonance line for Ca I. The resonance lines of ions also tend to grow fairly dramatically with decreasing temperature, but this growth is reversed at temperatures low enough that the ion in question is no longer the dominant ionization state. For instance, the Ca II K & H lines, both resonance lines for the Ca II ion, grow with decreasing temperatures down to a spectral type of about K5 (≈ 4500 K) on the main sequence, and then fade rapidly after that. The reason for this is that Ca I is transitioning to the dominant ionization state in the spectral line-forming region in stellar photospheres on the main sequence for $T_{\text{eff}} \lesssim 4500$ K. This fact also helps to explain the explosive growth of the Ca I resonance line in spectra later than about K5.

It stands to reason, therefore, that the resonance lines for a given atom or ion will usually figure prominently among the strongest lines of that species in a stellar spectrum. It turns out, however, that for many species the resonance lines are

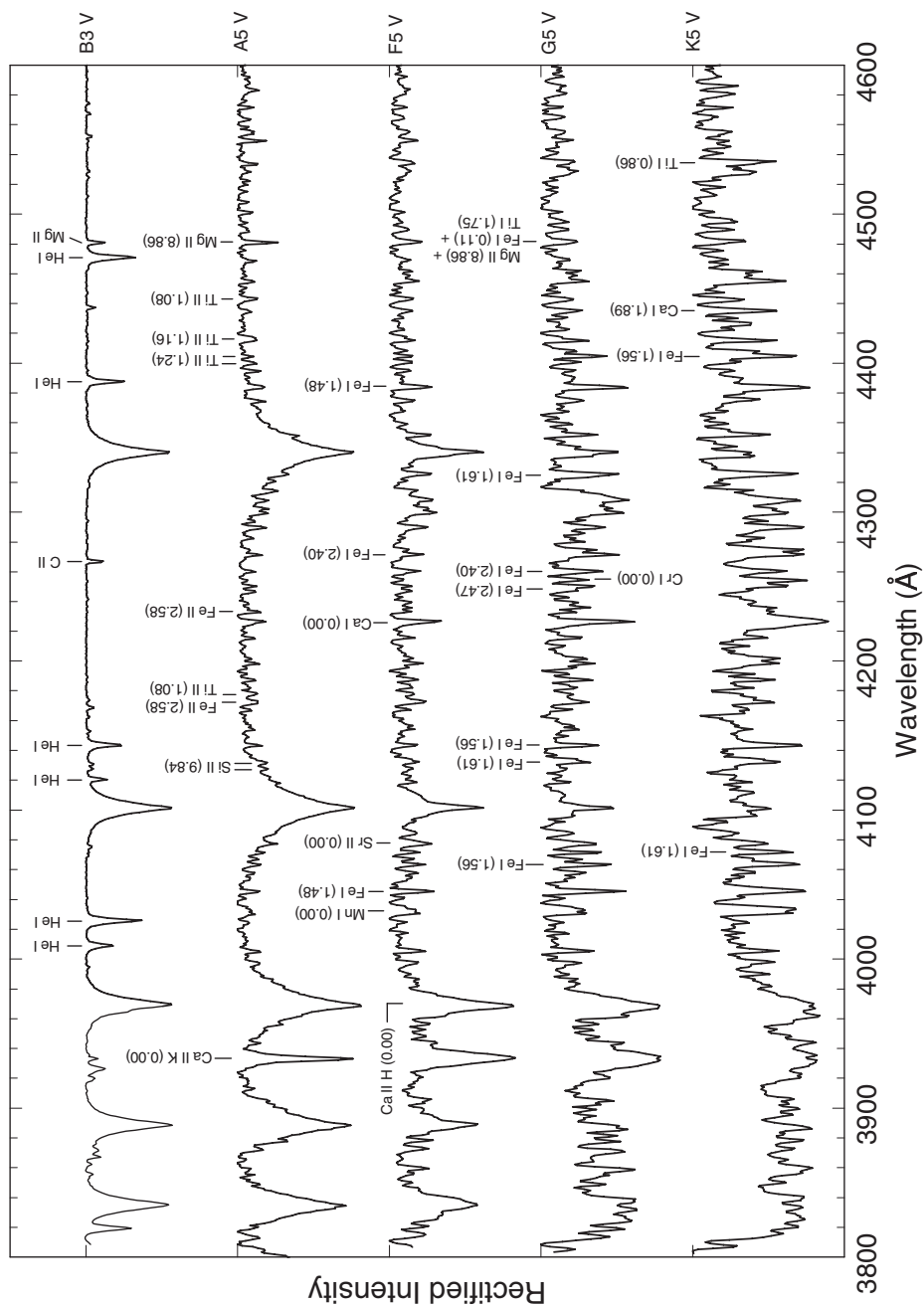


Figure 2.15 Main Sequence stars B3–K5 with a resolution of 1.8 \AA . Many of the strongest lines in these spectra are identified. The numbers in parentheses indicate the excitation energy in electron volts (eV) of the lower state for these transitions. These spectra have been rectified and offset vertically by 0.7 continuum units.

It is important to understand, however, that not all lines that arise from the ground level are resonance lines or are particularly strong. For instance, the Ca I $\lambda 6573$ line arises from the ground state, but is not a resonance line (see Figure 2.16). This line is an example of an *intercombination line*, in that the upper

Table 2.3 Longest Wavelength Resonance Lines and Ionization Potentials

Ion	$\lambda_{\text{RL}}(\text{\AA})$	I.P.(eV)	Ion	$\lambda_{\text{RL}}(\text{\AA})$	I.P.(eV)
H I	1216	13.6	He II	304	54.4
He I	584	24.6	C II	1335	24.4
C I	1657	11.2	C III	977	47.9
Na I	5890	5.1	Mg II	2802	15.0
Mg I	2852	7.6	Ca II	3968	11.9
Ca I	4226	6.1	Ti II	3383	13.6
Ti I	5173	6.8	Fe II	2599	16.2
Fe I	3860	7.9	Fe III	1123	30.7

level is a triplet state (3P_1 with a total electronic spin $S = 1$),⁴ and the lower state, the ground state, is a singlet (1S_0 with a total electronic spin $S = 0$). This transition violates the quantum mechanical *selection rule* $\Delta S = 0$, which states that the total electronic spin should not change during a radiative transition.⁵ As a consequence, Ca I $\lambda 6573$ has a relatively low *transition probability*, and thus is an inconspicuous line. Another quantum mechanical selection rule involves the angular momentum quantum number, l . Transitions that violate $\Delta l = \pm 1$ are called *forbidden lines* and are almost always very weak in stellar spectra. They can, however, be quite strong under low-density conditions (see, for examples, §4.6.1 and §12.3.1). On the other hand, the Ca I $\lambda 4226$ line arises from the ground state and obeys both of these selection rules. It thus has a high transition probability, and is one of the strongest lines of Ca I in a stellar spectrum.

2.4.4.2 Excitation and Ionization

In the spectrum of Fe II, the longest wavelength resonance line is located at 2599 \AA in the ultraviolet. What this means is that all prominent Fe II lines in the optical region arise from excited states (see Figure 2.17). Lines that arise from excited states are weakened by an additional factor, the Boltzmann factor, relative to the resonance lines, which governs the population of the lower state of the transition:

$$g_i \exp(-E_i/kT)$$

where g_i is the statistical weight of the lower level, and E_i is the excitation energy.

Figures 2.15 and 2.17 help to explain why lines of Fe II are of comparable strength to Ti II lines in the traditional spectral classification region (3800–5000 \AA) in the A-type stars even though iron is 2.5 orders of magnitude more abundant than titanium: note that the strongest Fe II lines in this region have excitation energies that are considerably larger than those of the strongest Ti II lines. The difference in the Boltzmann factors partially cancels the difference in the abundances. Of course, there is another factor that is important here: the ionization energy of Ti I

⁴The *multiplicity* of the term is given by $2S + 1$.

⁵The selection rule $\Delta S = 0$ is strictly valid only under the condition of pure *LS* coupling. The *LS* coupling scheme breaks down for the heavier elements, and so *intercombination lines* can be stronger for those elements. See the Glossary for further details.

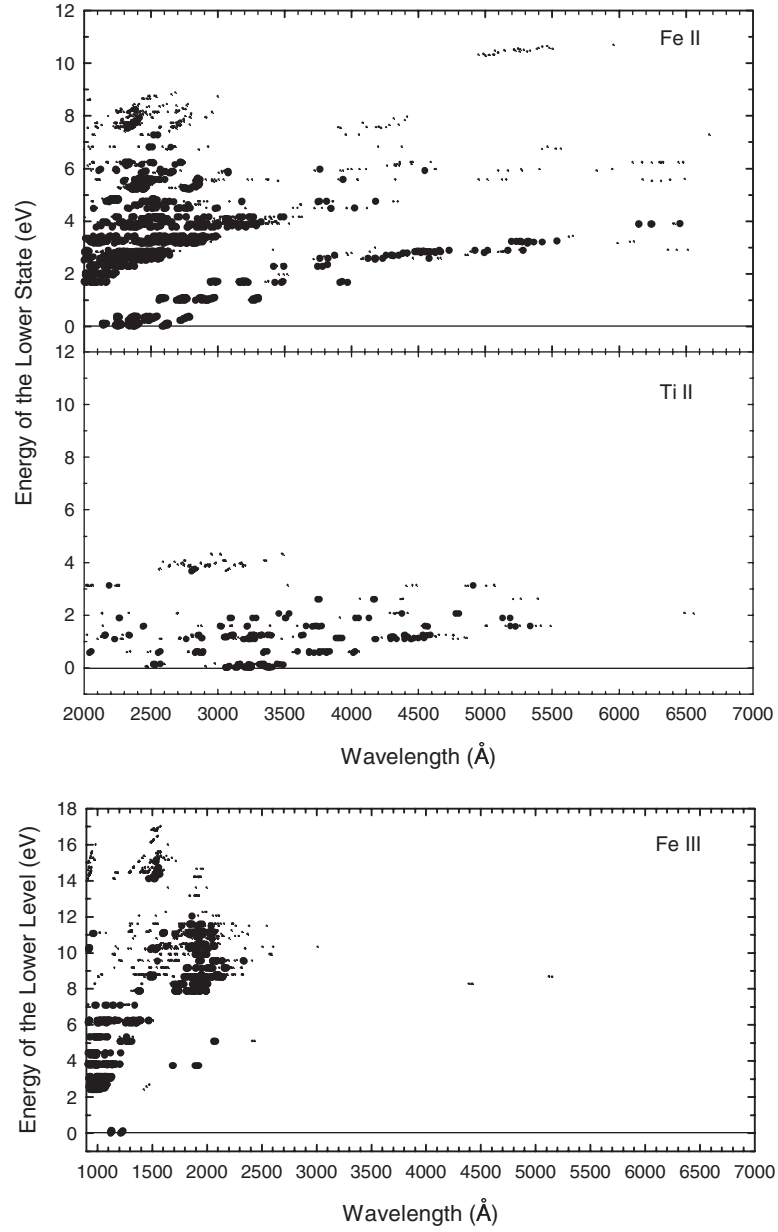


Figure 2.17 Excitation energy of the lower level for spectral lines with *equivalent widths* (W_λ) greater than 10 mÅ of Fe II, Ti II, and Fe III as a function of wavelength. The filled circles represent strong spectral lines ($W_\lambda > 50 \text{ mÅ}$), the dots represent weaker spectral lines. The horizontal line at $E = 0 \text{ eV}$ in each plot represents the energy of the ground state. The line strengths were calculated using the stellar spectral synthesis program SPECTRUM using Kurucz (1993) stellar atmosphere models. A model with an effective temperature of 8500 K (representative of A-type stars) was used for the Fe II and Ti II calculations, and a model with an effective temperature of $15,000 \text{ K}$ (representative of B-type stars) was used for the Fe III calculations.

Table 2.4 Energy, Wavelength and Temperature Equivalents

Energy	1 eV	3 eV	3.4 eV	8 eV	10.2 eV	13.6 eV
$\lambda = hc/E = hc/(kT)$	12398 Å	4133 Å	3647 Å	1550 Å	1216 Å	912 Å
$T = E/k$	11605 K	34814 K	39455 K	92836 K	118366 K	157821 K

is significantly lower than that of Fe I (see Table 2.3), and thus the ionization of titanium is more advanced than that of iron, increasing the abundance of Ti II relative to Fe II.

Notice that the plots in Figure 2.17 for Fe II and for Ti II are quite similar except (1) the range of energies for the lower state of the spectral lines of Ti II is compressed relative to that of Fe II, and (2) the resonance lines of Ti II extend to considerably longer wavelengths than do those of Fe II. Both of these effects can be understood qualitatively on the basis of the scaling of the energy levels of a given ion by the ionization energy.

The Fe II and Ti II lines in the blue-violet region of the spectrum that arise from relatively low-lying excited states play a very special role in spectral classification. These are the strong lines that lie on the lower envelopes of the distributions in the top two panels in Figure 2.17. The lower levels of these lines are classified as *metastable states*, which means, in this context, that a radiative transition between one of these states and any lower level including the ground state would be forbidden as it would violate the selection rule $\Delta l = \pm 1$. As a consequence, in low-density, low-pressure environments (such as the atmospheres of supergiants) where collisions are less important, these states will have higher populations than indicated by the Boltzmann equation. This leads to an enhancement of these lines in supergiant A- and F-type stars (compare Figure 2.4 with Figure 2.2), making them useful in luminosity classification (see §2.2.4). We will discuss these lines in much more detail in Chapter 6 on the F-type stars.

The lack of strong lines of Fe III in the blue-violet region of the spectrum of B-type stars is readily understood on the basis of the lower panel in Figure 2.17. Note that the longest wavelength resonance lines of Fe III lie in the far ultraviolet, and that the few weak lines that do show up in the blue-violet have excitation energies on the order of 8–9 eV. However, this same plot suggests that the ultraviolet region of B-type stars should be richly populated with lines of Fe III, and indeed this is the case. Note as well that the ultraviolet region of A-type stars (top two panels in Figure 2.17) has a high density of Fe II lines. Indeed, the line absorption is so great in this region that the ultraviolet flux is strongly attenuated in the A-type stars (see Figure 2.6).

Table 2.4 is included for the convenience of the reader, and gives energy equivalents in terms of wavelengths and kelvins. For instance, a photon with an energy of 1 eV has a (vacuum) wavelength of 12398 Å (1.2398 μm). A 13.6-eV photon with a wavelength of 912 Å is just able to photoionize a hydrogen atom in the ground state, and a 3.4-eV photon with a wavelength of 3647 Å is just able to photoionize a hydrogen atom in the first excited state ($n = 2$); this corresponds to the

wavelength of the Balmer jump. The factor kT , where k is the Boltzmann constant (8.617×10^{-5} eV/K), is found in many of the equations of statistical physics (including the Boltzmann equation, Eq. 2.4.2 and the Saha equation, Eq. 2.4.5) and has the units of energy. This factor may be used to define a temperature equivalent of the energy ($T = E/k$), which has a number of uses. For instance, if an energy level has an excitation energy of 1 eV, then, according to the Boltzmann equation, the population of that state will be comparable to the population of the ground state at the equivalent temperature of 11605 K. Note from the table that the temperature equivalent of 10.2 eV—the excitation energy of the first excited state in hydrogen, is 118366 K—which implies that at normal photospheric temperatures in stars, the population of the first excited state of hydrogen is a tiny fraction of that of the ground state.

2.4.4.3 *The Continuous Opacity*

One final factor is important in the behavior of the metallic lines in stellar spectra. Note that in the optical the overall strength of the metallic-line spectrum declines sharply with increasing temperature as we move from the K-type stars to the A-type stars. While individual lines will grow and decline in strength as a function of the temperature, according to the principles we have discussed above, this general decline in the strength of the metallic lines is due, in part, to the effect of the continuous opacity. Recall that the line strength is, at least to a first-order approximation, inversely proportional to the strength of the continuous opacity (see Equation 2.4.1). Figure 2.12 shows how this continuous opacity changes with temperature in the optical region of the spectrum. The steep rise in this continuous opacity to a sharp peak at about 11,000 K (the effective temperature of the late B-type stars) is important in the decline of the metallic-line strengths. But should we not, then, expect a rise in the strength of the metallic lines in the B-type stars to coincide with the decline in the continuous opacity with increasing temperature? The answer is that in the B-type stars, the most abundant metals (iron, calcium, etc.) exist predominately in the second (III) or even third (IV) ionization states. We have already seen that in the optical these ions exhibit only very weak lines in stellar spectra. However, in the ultraviolet, the B-type stars do have very rich metallic-line spectra.

Bibliography

- Canterna, R. 1976, AJ, 81, 228
 Crawford, D.L. 1975, AJ, 80, 955
 Crawford, D.L. 1978, AJ, 83, 48
 Crawford, D.L. 1979, AJ, 84, 1858
 Crawford, D.L. 1984, in *The MK Process and Stellar Classification*, ed. R.F. Garrison (David Dunlap Observatory: University of Toronto), p. 191
 Crawford, D.L., & Mander, J. 1966, AJ, 71, 114
 Drilling, J.S., & Landolt, A.U. 1999, in *Allen's Astrophysical Quantities*, 4th edition, ed. A.N. Cox (New York: Springer Verlag), p. 381
 Gray, D.F. 2008, *The Observation and Analysis of Stellar Photospheres*, 3rd edition (Cambridge: Cambridge University Press)
 Gray, R.O. 2006, *Memorie della Società Astronomica Italiana*, 77, 1123
 Hearnshaw, J.B. 2005, *The Measurement of Starlight: Two Centuries of Astronomical Photometry* (Cambridge: Cambridge University Press)
 Heck, A. 1984, in *The MK Process and Stellar Classification*, ed. R.F. Garrison (David Dunlap Observatory: University of Toronto), p. 222
 Johnson, H.L., & Morgan, W.W. 1953, ApJ, 117, 313
 Kurucz, R.L. 1993, CD-Rom 13, ATLAS9 Stellar Atmosphere Programs and 2km/s Grid (Cambridge=SAO)
 Landolt, A.U. 1992, AJ, 104, 340
 McClure, R.D. 1976, AJ, 81, 182
 Meger, M.R., Edwards, S., Hinkle, K.H., & Strom, S.E. 1998, ApJ, 508, 397
 Mihalas, D. 1978, *Stellar Atmospheres*, 2nd edition (New York: W.H. Freeman)
 Nicolet, B. 1996, *Baltic Astronomy*, 5, 417
 Olsen, E.H. 1983, AApS, 54, 55
 Olsen, E.H. 1994, in *The MK Process at 50 Years: A Powerful Tool for Astrophysical Insight*, eds. C.J. Corbally, R.O. Gray, & R.F. Garrison, Astronomical Society of the Pacific Conference Series, Vol. 60 (San Francisco: Astronomical Society of the Pacific), p. 119
 Olsen, E.H., & Perry, C.L. 1984, AApS, 56, 229
 Olsen, E.H. 1995, AA, 295, 710
 Skrutskie, M.F., et al. 2006, AJ, 131, 1163
 Straižys, V., Crawford, D.L., & Philip, A.G.D. 1996, *Baltic Astronomy*, 5, 83
 Strömgren, B. 1966, ARAA, 4, 433
 Valdes, F., Gupta, R., Rose, J.A., Singh, H.P., & Bell, D.J. 2004, ApJS, 152, 251
 White, N.M., & Wing, R.F. 1978, ApJ, 222, 209

Chapter Three

The OB Stars—Nolan R. Walborn

3.1 INTRODUCTION

The OB stars dominate the light (as opposed to the mass) of galaxies in which they exist. They also have major effects on the interstellar medium, star formation, and galactic evolution, by means of their ultraviolet radiation, stellar winds, and final core-collapse supernovae (CCSN). In starburst galaxies, it is not unusual to encounter localized regions that must be powered by hundreds or even thousands of associated O stars; the effects of massive stellar evolution in such regions are truly spectacular. It has now been established that long gamma-ray bursts (LGRB) originate in the CCSN of rapidly rotating massive stars; they correspond to the emission of relativistic jets, likely during the process of black-hole formation. In September 2005, an LGRB was detected at a redshift of 6.3, corresponding to a lookback time of nearly 13 billion years; that is, the death of a single massive star was observed less than 1 billion years after the Big Bang (see Ramirez-Ruiz 2006, and associated reports). Moreover, massive stars are major contributors to nucleosynthesis and chemical evolution, their energy generation and CCSN being the primary sources of numerous elements, including oxygen. ... Thus, the OB stars play a substantial role in cosmic evolution.

The understanding of such processes begins with the study of OB spectra, which are presented in this chapter. It is important to note that “OB” is not synonymous with “O and B.” Rather, the former denotes in the first instance a spectroscopic “natural group” as discussed by Morgan (1951), which at very low resolution may be defined by weakness of the hydrogen Balmer lines, or at somewhat higher resolution by the detection of helium lines. The low-temperature boundary of this group is a diagonal in the Hertzsprung–Russell diagram running from B2 V, through somewhat later types at intermediate luminosity classes, to the latest B Ia supergiants. Subsequently, this empirically defined boundary has been shown to correspond to lower mass and upper age limits of about 8 solar masses and 30 Myr, respectively; and in turn, to the delineation of galactic spiral structure and the occurrence of CCSN.

3.2 THE OPTICAL

3.2.1 Spectral-Type Criteria

The O spectral class was originally defined by the presence of absorption lines of He II at blue-violet wavelengths, particularly the Pickering series (although

these lines are well detected as late as type B0.5 in modern, high-S/N data). The initial one-dimensional (horizontal or temperature) classification was based upon ratios of those lines to He I, primarily He II $\lambda 4541$ /He I $\lambda 4471$, and secondarily He II $\lambda 4200$ /He I(+II) $\lambda 4026$ (Plaskett & Pearce 1931). The former ratio has a value of unity at type O7 and the latter around O6; the original subclass range was O5–O9, with He II dominant at the former, of course, and He I at the latter. These criteria were carried over into the MKK (Morgan, Keenan, & Kellman 1943) and MK (Johnson & Morgan 1953; Abt et al. 1968; Morgan & Keenan 1973; Morgan, Abt, & Tapscott 1978) systems, although with improved photographic material the sequence was extended earlier to type O4, with primary standards HD 46223 in NGC 2244, and ζ Pup. Also half-types, such as O9.5, were increasingly invoked. At late-O types, the weaker He I lines $\lambda\lambda 4387$ and 4144 become more useful substitutes in the above ratios, respectively, which then both have values of unity at type O9. These criteria remain operative in current digital data (Figure 3.1; the spectrum of the historical O7 standard 15 Mon shown here would be classified O7.5 and now appears to be variable).

The early B classification was based upon lines of several metallic ions, primarily C, N, O, and Si, and the behavior of the He I spectrum, which has maximum intensity at type B2.

The OB classification was re-examined, with photographic dispersion and widening each twice those typically used in the MK system, by Walborn (1971a, b, c). The higher information content led to several developments. One was that anomalies among the CNO spectra were discovered, as further discussed later, so primary reliance for the B-type temperature classification was shifted to ionic line ratios of Si: IV to III at the earlier types, and III to II later. Another was that new interpolated spectral types O9.7, B0.2, and B0.7 were introduced, the first defined by equality of He II $\lambda 4541$ to Si III $\lambda 4552$, and the latter two by the Si IV $\lambda 4089$ /Si III $\lambda 4552$ ratio, which has a value near unity at B0.7 (Figure 3.2). Finally, a new earliest O type, O3, was found among the ionizing clusters of the Carina Nebula (NGC 3372), in which no He I lines could be detected in the photographic classification material.

The early limit was subsequently broken once again by Walborn et al. (2002a). The hope had been that with the higher S/N, sky-subtracted digital data, the degeneracy of the O3 subclass (bounded only on the low-temperature side) might be alleviated by the detection of very weak He I features. However, in practice that proved unrealistic, because of the deleterious effects of later-type companions, uncertain subtraction of inhomogeneous nebular He I emission, and sensitivity to the continuum noise level. On the other hand, a considerable range in the ratio of the selective emission lines N IV $\lambda 4058$ and N III $\lambda\lambda 4634$ – 4640 – 4642 (further discussed in the next section) was found among the increasing sample of O3 spectra, which was then subdivided into types O2, O3, and O3.5 on the basis of that criterion (Figure 3.3).

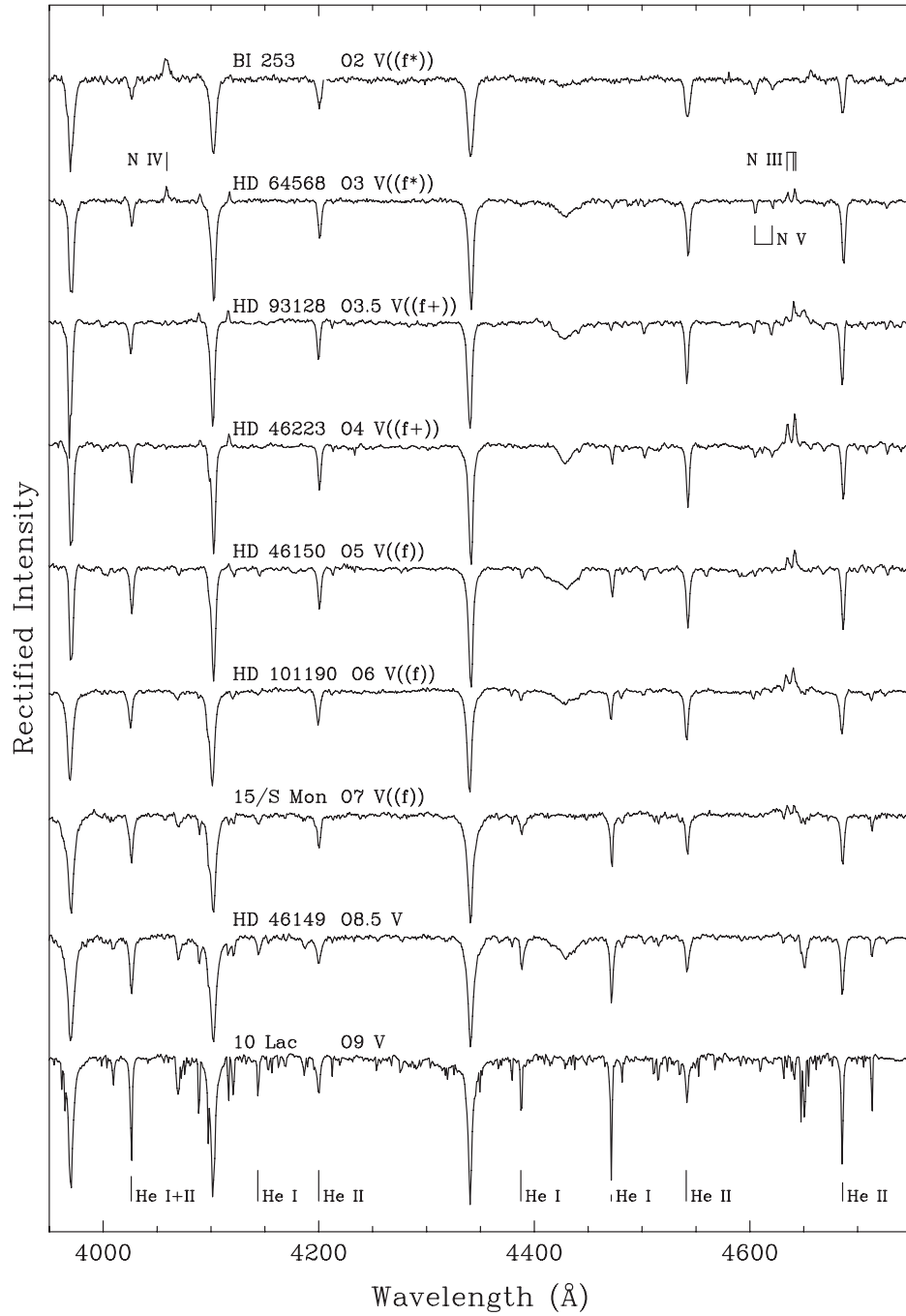


Figure 3.1 O Main Sequence in the Optical. The rectified spectrograms are separated by 0.4 continuum units. The lines identified below are He I+II λ 4026; He I λ 4144, 4387, 4471; and He II λ 4200, 4541, 4686. In the spectrum of HD 64568, they are N IV λ 4058, N V λ 4604–4620, and N III λ 4634–4640–4642. Figure courtesy I. Howarth. The spectrum for BI 253 courtesy P. Massey.

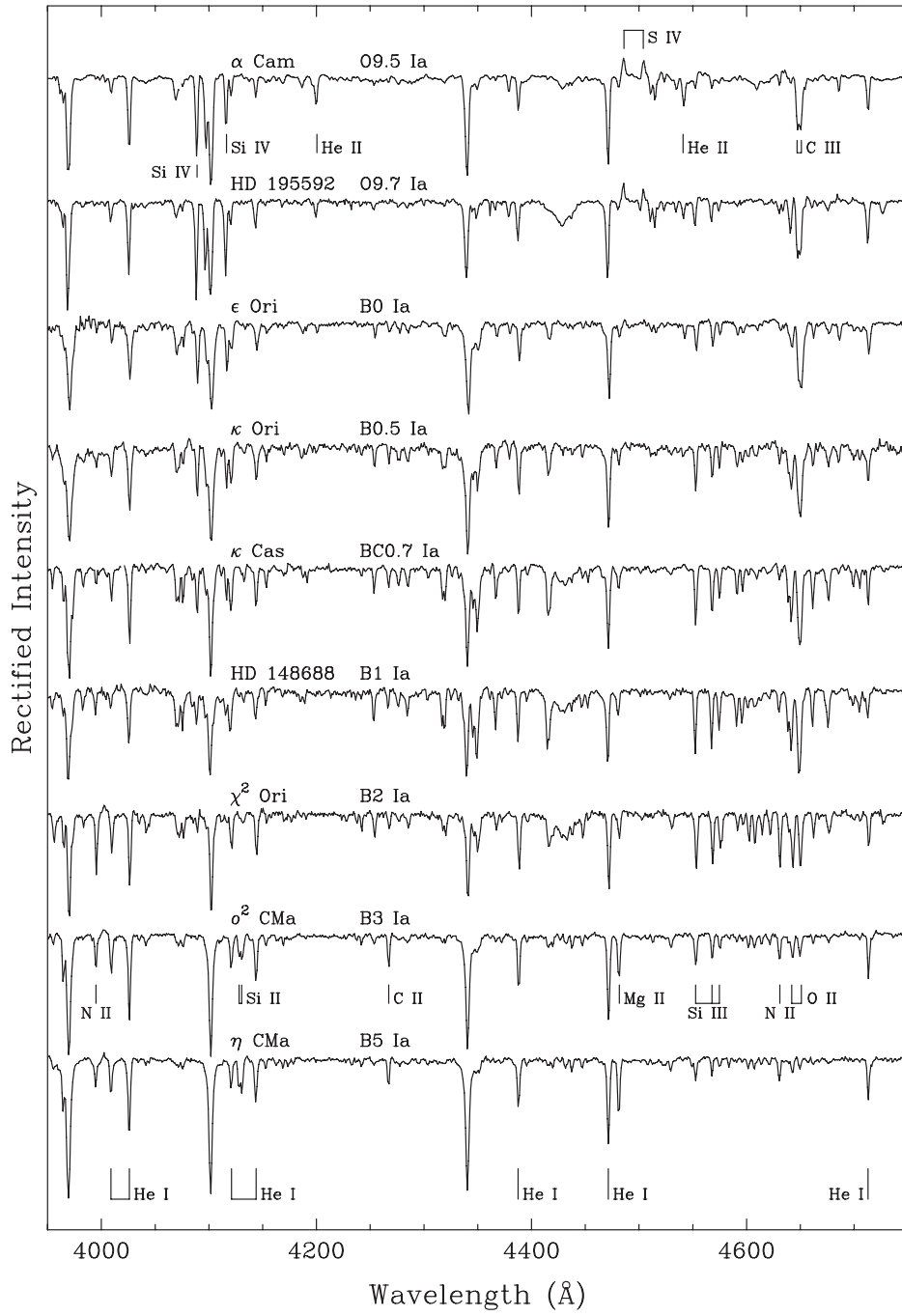


Figure 3.2 Late-O through Mid-B Supergiant Sequence in the Optical. The rectified spectrograms are separated by lines identified below are $\lambda\lambda 4009, 4026, 4121, 4144, 4387, 4471, 4713$. The lines identified in the spectrum of o^2 CMa are N II $\lambda\lambda 3995, 4631$; Si II $\lambda\lambda 4128-4130$; C II $\lambda 4267$; Mg II $\lambda 4481$; Si III $\lambda\lambda 4552-4568-4575$; and O II $\lambda\lambda 4640-4650$. In α Cam, they are Si IV $\lambda\lambda 4089, 4116$; He II $\lambda\lambda 4200, 4541$; S IV $\lambda\lambda 4486-4504$ emission (Werner & Rauch 2001); and the C III $\lambda 4650$ blend. Figure courtesy I. Howarth.

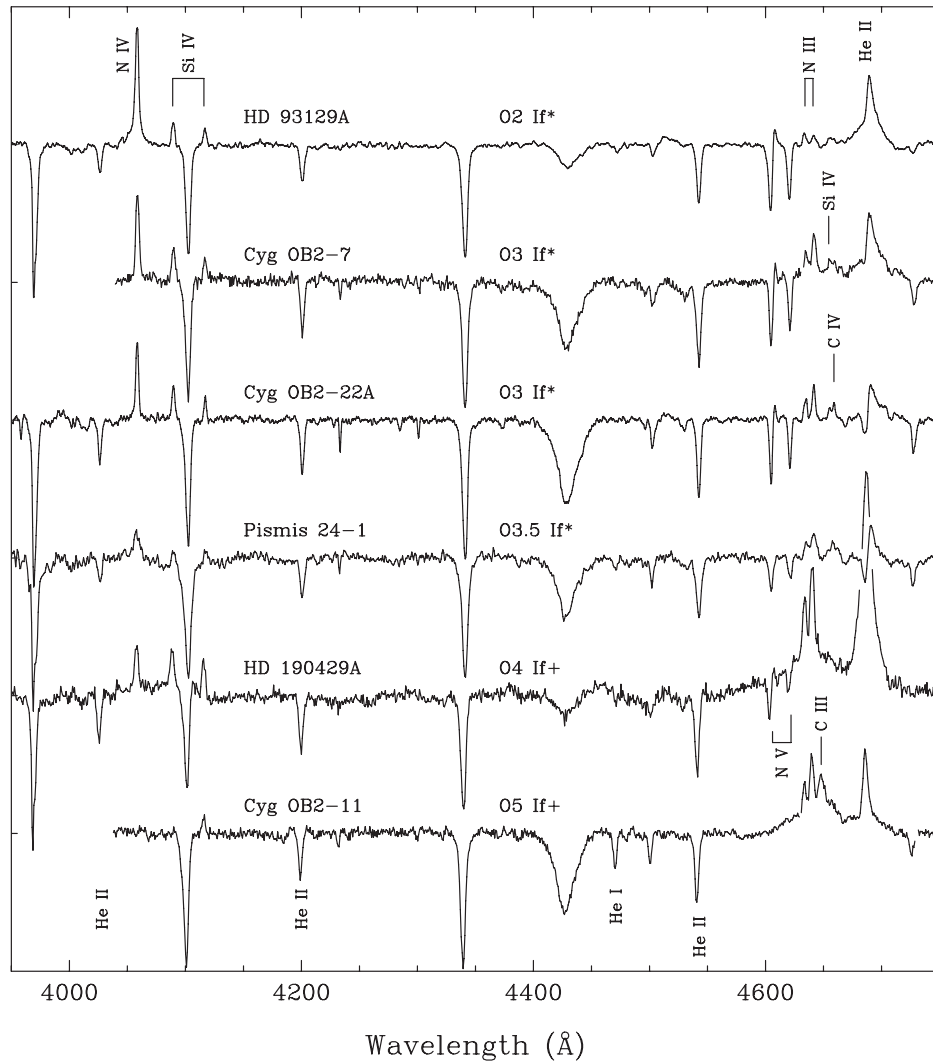


Figure 3.3 Early O Supergiant Sequence in the Optical (Walborn 2003a). The rectified spectrograms are separated by 0.3 continuum units. The lines identified in the spectrum of HD 93129A are N IV λ 4058; Si IV $\lambda\lambda$ 4089–4116; N III $\lambda\lambda$ 4634–4640–4642; and He II λ 4686. In addition, Si IV λ 4654 is identified in Cyg OB2-7, C IV λ 4658 in Cyg OB2-22A, and N V $\lambda\lambda$ 4604–4620 in HD 190429A. The lines identified in Cyg OB2-11 are He II $\lambda\lambda$ 4026 (not covered), 4200, 4541; He I λ 4471; and the C III λ 4650 blend. Figure courtesy I. Howarth and the Astronomical Society of the Pacific. Spectrum for Pismis 24-1 courtesy P. Massey.

3.2.2 Luminosity-Class Criteria

The MK system introduced the second dimension (vertical or luminosity class) for late-O and B types, the principal criteria being positive luminosity effects (i.e., increasing intensity with increasing luminosity class) in the metallic lines. At

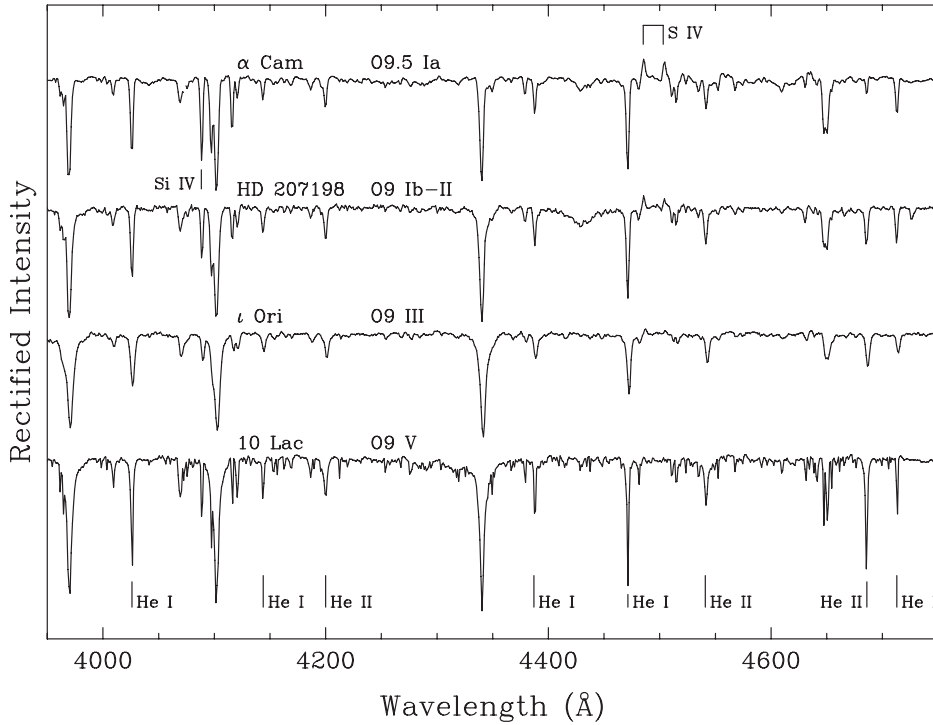


Figure 3.4 Luminosity Sequence at O9–O9.5. The rectified spectrograms are separated by 0.4 continuum units. The lines identified below are He I $\lambda\lambda$ 4026, 4144, 4387, 4471, 4713, and He II $\lambda\lambda$ 4200, 4541, 4686. In the spectrum of α Cam, they are Si IV λ 4089 and S IV $\lambda\lambda$ 4486–4504 emission. Figure courtesy I. Howarth.

B types metal to He I ratios are particularly sensitive, because many of the latter lines have negative luminosity effects, due to the diminishing Stark effect with decreasing pressure in the more extended giant and supergiant atmospheres. Primary luminosity class criteria are the ratios Si IV λ 4089/He I λ 4026 or 4144 and Si IV λ 4116/He I λ 4121 at late O and B0–B0.7 (Figure 3.4), and Si III λ 4552/He I λ 4387 at B0.7–B5 (Figure 3.5).

The MK system did not contain a luminosity classification earlier than type O9 (with a few individual exceptions at O8). However, there was another kind of luminosity criterion at late O and B0 that provided a key to an extension to earlier types. That was the unique negative luminosity effect in the (non-Pickering) He II λ 4686 and N III $\lambda\lambda$ 4634–4640–4642 absorption lines (Figure 3.4). O stars with these two features in emission were denominated Of stars¹ by Plaskett & Pearce (1931), and for many years that category was regarded as peculiar, possibly analogous to the Be stars (Underhill 1966). However, improving data quality and sample sizes revealed gradual, systematic developments of the Of features throughout the early- and mid-O domains, which were divided into ((f)), (f), and f subcategories,

¹That descriptor was chosen because Oa–Oe represented various types of WR and OB spectra in the HD classification nomenclature.

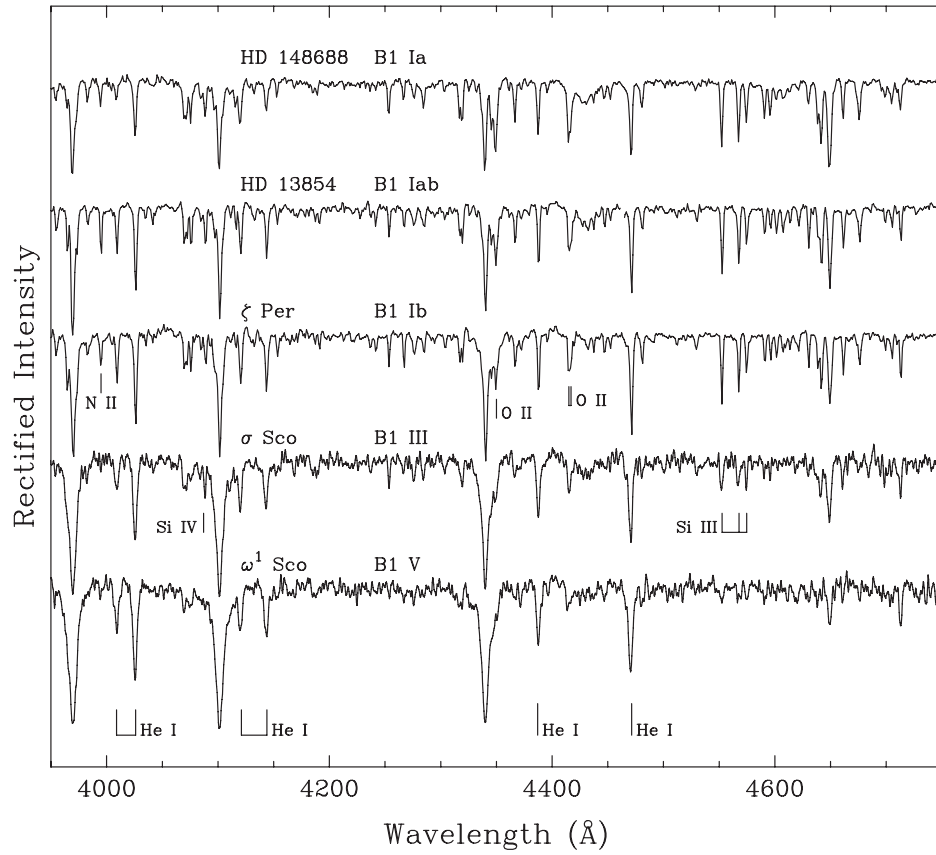


Figure 3.5 Luminosity Sequence at B1. The rectified spectrograms are separated by 0.4 continuum units. The lines identified below are He I $\lambda\lambda$ 4009, 4026, 4121, 4144, 4387, 4471. In the spectrum of σ Sco, they are Si IV λ 4089 and Si III $\lambda\lambda$ 4552–4568–4575, while in ζ Per, they are N II λ 3995 and O II $\lambda\lambda$ 4350, 4415–4417. Figure courtesy I. Howarth.

corresponding to strong He II absorption with weak N III emission, He II absorption weak or neutralized with stronger N III emission, and both features strongly in emission, respectively, that were interpreted as luminosity effects by Walborn (1971a). A key element was the recognition that the negative luminosity effects in these absorption features at late-O types are caused by filling in by the same Of emission mechanisms. Thus, the fully developed Of spectra simply correspond to the earlier O supergiants (Figure 3.6).

Lines such as these that come into emission while others from the same ions remain in absorption are called *selective emission lines*; there is ample evidence from their profiles and systematic behavior that they are formed in the stellar photospheres and diagnose the atmospheric parameters (Walborn 2001). For instance, N III λ 4097 is the next transition down from the λ 4640 triplet but displays a positive luminosity effect in absorption! Physical interpretations of these effects are discussed later. The N IV λ 4058 used in the O2–O3 classification is another

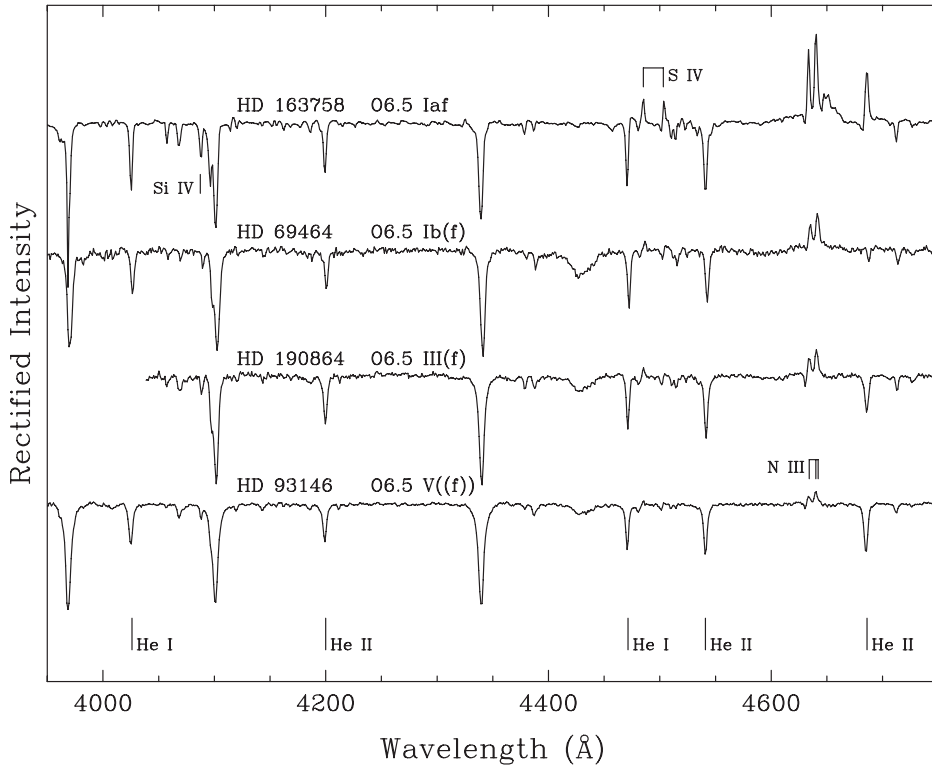


Figure 3.6 Luminosity Sequence at O6.5 in the Optical (Walborn 2007a). The rectified spectrograms are separated by 0.4 continuum units. The lines identified below are He I $\lambda\lambda 4026, 4471$ and He II $\lambda\lambda 4200, 4541, 4686$. N III $\lambda\lambda 4634-4640-4642$ emission lines are also identified in the spectrum of HD 93146, as well as Si IV $\lambda 4089$ and S IV $\lambda\lambda 4486-4504$ emission in HD 163758. Figure courtesy I. Howarth and Editorial Complutense. S. A..

selective emission line; spectra in which it is stronger than the N III emission are denoted f*. The Si IV $\lambda\lambda 4089, 4116$ lines also come into selective emission in early-O spectra, which are denoted f+ in the spectral types; all f* spectra also have these Si IV lines in emission.

Primary standard stars for the two-dimensional OB classification are listed in Appendix A, for each hemisphere as available. A comprehensive digital atlas is presented by Walborn & Fitzpatrick (1990); the extension to O2 is charted by Walborn et al. (2002a). A living online catalogue of Galactic O-type spectra classified in this system, including photometric data from UV through IR and links to other data for each star, is maintained and augmented as described by Maíz-Apellániz et al. (2004).

It is fortunate that the original photographic emulsions were sensitive to blue-violet light, because among those observable from the ground, that wavelength range contains the highest density of spectral lines at all spectral types. Nevertheless, the yellow-red range contains a few features of correlative interest in OB spectra, such as the luminosity-sensitive selective emission in C III $\lambda 5696$

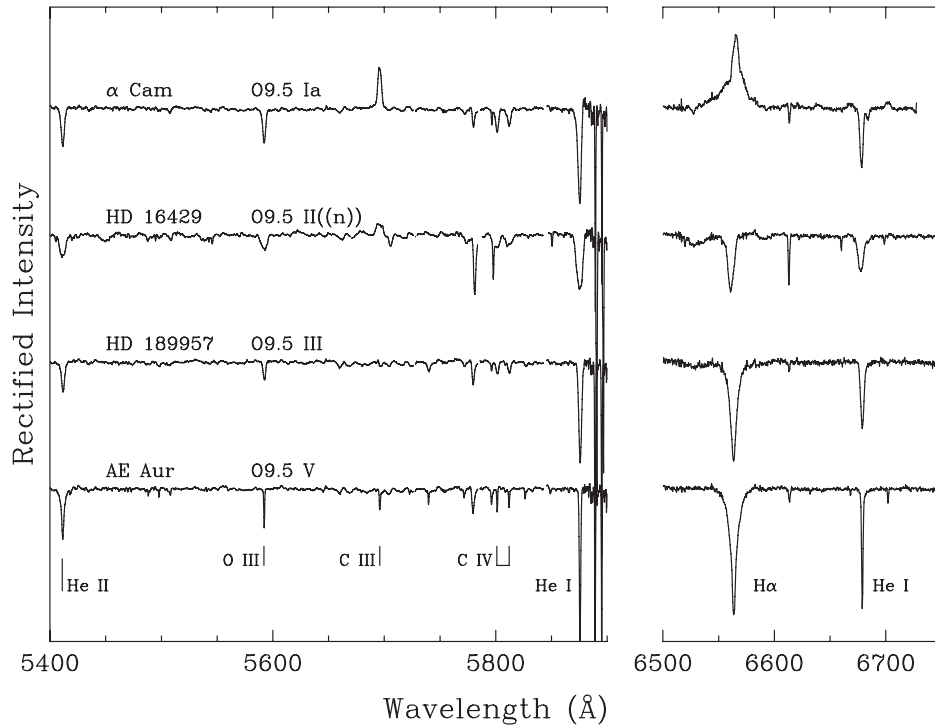


Figure 3.7 Luminosity Sequence at O9.5 in the Yellow-Red (Walborn 2007a). The rectified spectrograms are separated by 0.4 continuum units. The lines identified below are He II $\lambda 5411$; O III $\lambda 5592$; C III $\lambda 5696$; C IV $\lambda\lambda 5801-5812$; He I $\lambda\lambda 5876, 6678$; and H α $\lambda 6563$. Figure courtesy I. Howarth and Editorial Complutense, S.A..

(Walborn 1980, Figure 3.7). Of course, H α displays a rich phenomenology, but it is too sensitive to multiple extraneous effects to provide a useful two-dimensional classification criterion.

As will be emphasized in the next section, the O-type luminosity sequences are also progressions in stellar-wind density. Increasing mass-loss rates also lead to spectroscopic (and arise from evolutionary) relationships among the most massive O stars and one particular type of Wolf-Rayet star, namely the high-luminosity, narrow-line, late-type WN, also denoted WN-A (Hiltner & Schild 1966; Walborn 1974) or WNL, with which they are associated in giant H II regions. (Of course, the spectral morphology is independent of this external information, with which it is correlated subsequently.) For instance, in the Carina and 30 Doradus Nebulae, one finds early Of types associated with WN-A stars that have a range of optical emission-line strengths, but similar luminosities (e.g., Walborn & Blades 1997). The latter correspond to increasing mass loss and wind densities as the stars evolve, which become sufficiently extreme to affect even the optical spectra. There is an interesting intermediate spectroscopic category classified as, e.g., O2 If*/WN6-A, which combines strong, broad emission lines as in WN spectra, especially in He II $\lambda 4686$, with strong, high-ionization absorption lines as in early Of spectra.

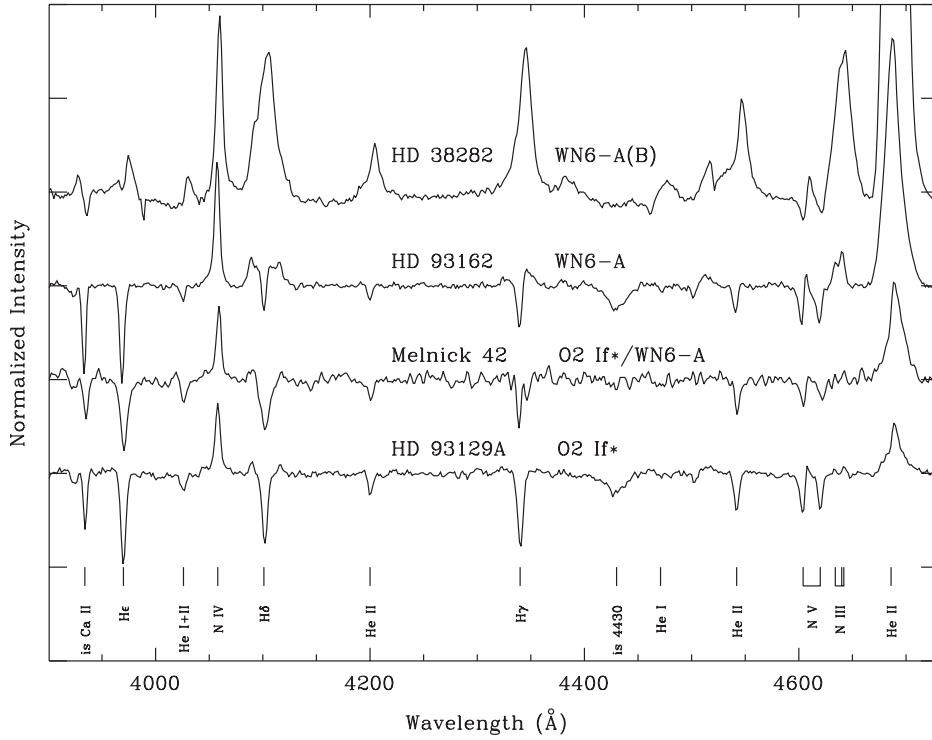


Figure 3.8 Wind Development from Of* through Intermediate to WNL in the Optical. The rectified spectrograms are separated by 0.25 continuum units. The lines identified below are interstellar Ca II λ 3933; H Balmer $\lambda\lambda$ 3970, 4101, 4340; He I+II λ 4026; N IV λ 4058; He II $\lambda\lambda$ 4200, 4541, 4686; λ 4430 unidentified diffuse interstellar band; He I λ 4471; N V $\lambda\lambda$ 4604–4620; and N III $\lambda\lambda$ 4634–4640–4642. Figure courtesy J. Parker.

(Because of the classification notation, these are sometimes referred to as “slash” stars; an unrelated category of cooler slash stars will be discussed under peculiar objects later.) A sequence of early Of through hot slash to WN-A blue-violet spectra of increasing emission-line strengths is shown in Figure 3.8. A complete discussion of WR spectra is beyond the scope of this chapter; see Chapter 11.

3.3 THE ULTRAVIOLET

3.3.1 Relation to the Optical

The spectral energy distributions (SEDs) of the OB stars peak in the space ultraviolet (at 1000 Å for a temperature of 30,000 K), and the dominant ions in their atmospheres have highest line densities near the peaks. Thus, it was expected that access to these wavelengths would prove vital, but it was a surprise when the first rocket data showed that normal OB stars have P Cygni profiles with terminal velocities up to a few thousand km sec⁻¹ in their ultraviolet spectra (Morton, Jenkins, & Bohlin 1968; Carruthers 1968), corresponding to mass-loss

rates significant for their atmospheres and evolution. More extensive objective-prism data were obtained by *SKYLAB* (Henize et al. 1975), the first high-resolution observations by *Copernicus* (e.g., Snow & Morton 1976; Walborn & Bohlin 1996), and definitive samples by the *International Ultraviolet Explorer* (IUE) (Walborn, Nichols-Bohlin, & Panek 1985, hereafter O Atlas; Walborn, Parker, & Nichols 1995, hereafter B Atlas). Many high-quality observations of fainter stars, particularly in the Magellanic Clouds, have been made with the *Hubble Space Telescope* (HST) spectrographs (e.g., Walborn et al. 1995, 2000). Wavelengths between the Lyman limit and $\text{Ly}\alpha$ have been covered for extensive samples by the *Far Ultraviolet Spectroscopic Explorer* (FUSE) (Walborn et al. 2002b, hereafter FUSE Atlas; Pellerin et al. 2002).

It may be useful to clarify some inconsistent, relative terminology here. In the context of groundbased observations, the wavelength range between the violet cut-off of the eye around 3900 Å and the atmospheric cutoff just above 3000 Å is referred to as the near ultraviolet (NUV), or sometimes just the UV. IUE and HST data are divided by the sensitivity of detectors and optical element coatings into NUV ($\sim 3000\text{--}2000$ Å) and FUV (far ultraviolet; $\sim 2000\text{--}1200$ Å). Observations between $\text{Ly}\alpha$ (1215 Å) and the Lyman limit (912 Å) require different technology and are also often called FUV, relative to the longer UV wavelengths. For the OB stars, the space NUV regime contains few spectral features of interest (e.g., Bruhweiler, Kondo, & McCluskey 1981); hence, the discussion in this section will be limited to the two “FUV” ranges.

During the early 1980s, the relationship, or lack thereof, between OB winds and the fundamental stellar parameters was hotly debated. To a large extent, this debate was a result of inadequate sample sizes and uncertainties both in the interpretation of mass-loss diagnostics from different regimes (including infrared and radio) and in the wind models. The negative side of this debate incurred the error of convolving descriptive and uncertain interpretational information as criticized in Chapter 1. However, the O Atlas demonstrated remarkably detailed trends in the morphology of the wind profiles as a function of the optical spectral types, essentially ending the debate. Subsequently, the B Atlas displayed the continuity of these trends into that spectral class, until the disappearance of the winds at lower temperatures; and the FUSE atlases established the same at shorter wavelengths. In the O Atlas, just two exceptions to the very tight correlations between wind profiles and optical types were found among a sample of 89 O stars, preselected to avoid known rapid rotators and interacting binaries; in the B Atlas, the corresponding exception total is 9 stars out of 83, perhaps reflecting the reduced dominance of the radiation fields that drive the winds, with concomitantly increased sensitivity to other effects, although most of the discrepancies are small. The discussion here emphasizes these relationships and trends, as opposed to the definition of independent UV classification criteria. Studies of the latter kind have been presented by Rountree & Sonneborn (1991, 1993)² and Penny, Gies, & Bagnuolo (1996).

²Also see §4.3.

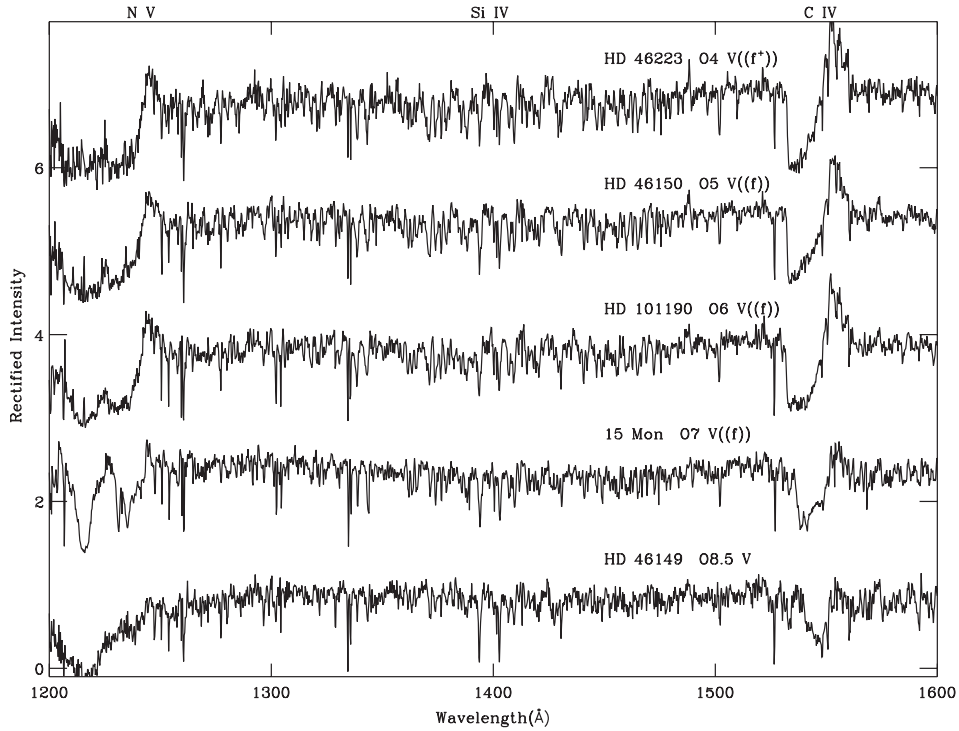


Figure 3.9 O Main Sequence in the IUE FUV. The spectral features identified above are N V $\lambda\lambda$ 1239, 1243; Si IV $\lambda\lambda$ 1394, 1403; and C IV $\lambda\lambda$ 1548, 1551. Figure courtesy D. Lennon.

3.3.2 Spectral-Type Effects

The FUV spectra of the OB stars contain forests of Fe III through Fe VI absorption lines, their ionization increasing and wavelengths of highest density decreasing toward earlier spectral types, analogously to the Fe II and Fe I in the NUV and optical spectra of later types (see the discussion in §2.4.3). However, the appearance of OB FUV spectra is dominated by the spectacular stellar-wind profiles of resonance and a few metastable subordinate lines, whose behavior as a function of the optical spectral types is discussed here.

Three major stellar-wind profiles occur in the IUE FUV spectral range of the O stars, accompanied by three minor ones: the resonance doublets N V $\lambda\lambda$ 1239, 1243; Si IV $\lambda\lambda$ 1394, 1403; C IV $\lambda\lambda$ 1548, 1551; and the subordinate lines O V λ 1371, He II λ 1640, N IV λ 1718, respectively. On the main sequence, the N V and C IV features are saturated from the earliest types until O6.5, at which type they begin to weaken and then decline smoothly thereafter; as further discussed in the next section, there is no Si IV wind feature anywhere on the normal main sequence (Figure 3.9). In the O-type supergiants, Si IV has a moderate wind profile at type O4, which increases at O5–O6 and reaches maximum strength at mid- and late-O types (Figure 3.10). A wind profile in O V λ 1371 is a unique signature of O2–O3 giant and supergiant spectra.

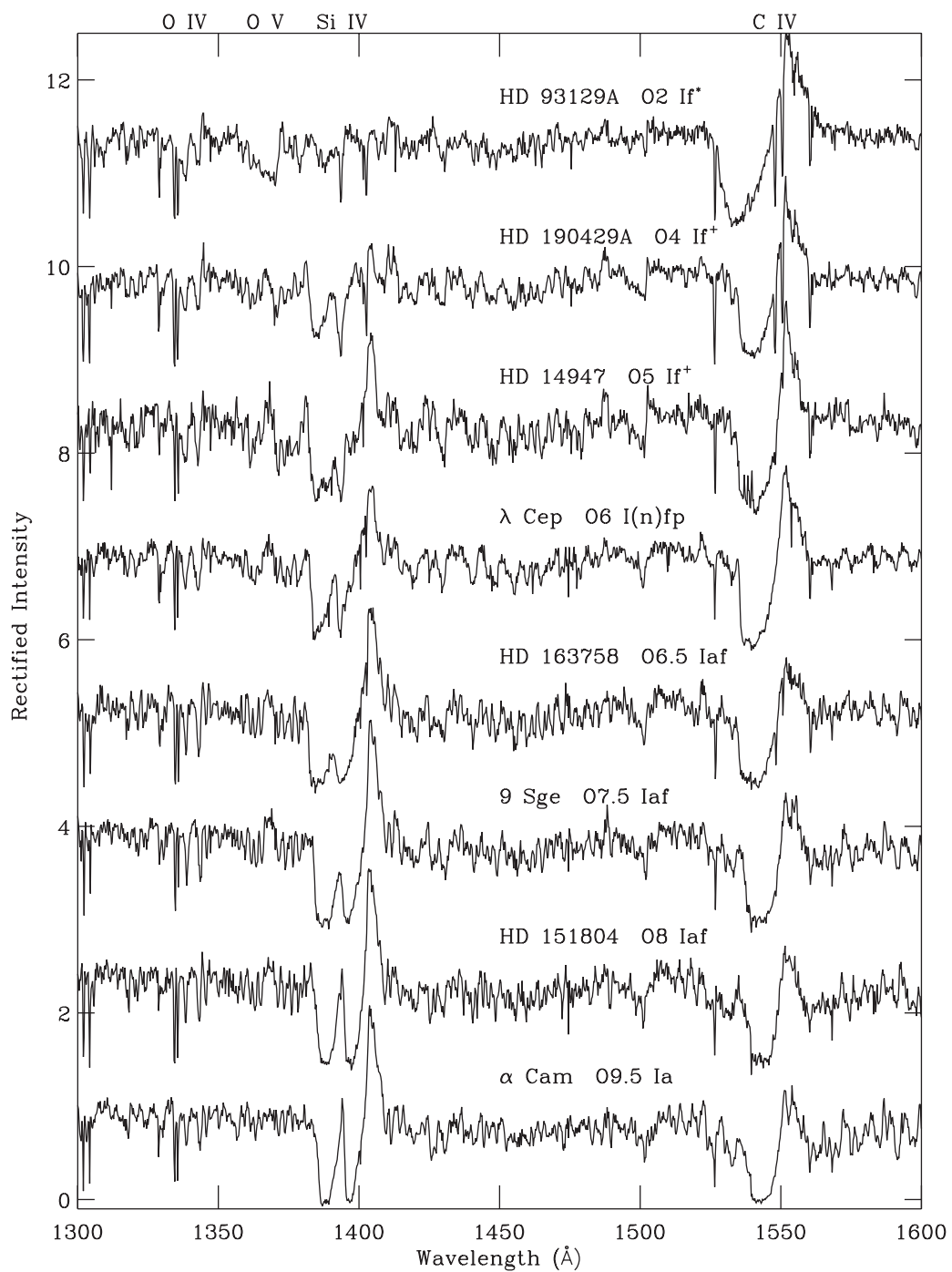


Figure 3.10 O Supergiant Sequence in the IUE FUV. The spectral features identified above are O IV $\lambda\lambda 1339, 1343$; O V $\lambda 1371$; Si IV $\lambda\lambda 1394, 1403$; and C IV $\lambda\lambda 1548, 1551$. Figure courtesy D. Lennon.

The FUSE FUV range offers an even wider array of chemical species and ionization states, which show the expected behavior with spectral type; a representative supergiant sequence in the Large Magellanic Cloud (LMC) is shown in Figure 3.11. At wavelengths below 1100 Å, even moderate interstellar extinction entails virtual obliteration of the stellar spectrum by H_2 , so the less reddened Magellanic Cloud stars provide better information there than their Galactic counterparts, although several interesting features between 1100 and 1200 Å can be well studied in the latter (Pellerin et al. 2002).

Wind features are weak in normal early-B dwarfs, without significant emission components, and even the shortward absorption troughs disappear by B1 V (Figure 3.12). In the supergiants, however, the wind profiles remain strong in the IUE FUV throughout the B-type sequence (Figure 3.13). N V persists until type B0.7 and C IV until B3. At B0.7, C II $\lambda\lambda$ 1334, 1335 and Al III $\lambda\lambda$ 1855, 1863 wind profiles make their appearance and reach maximum strength at B1–B2. Also between types B0.5 and B0.7, the wind profiles undergo an abrupt transition to lower terminal velocities and deeper absorptions, best appreciated in Si IV. This effect may be related to the bistability “jump” described by Lamers, Snow, & Lindholm (1995), although Crowther, Lennon, & Walborn (2006) found a more gradual trend in the physical parameters. At B8 Ia, Si II $\lambda\lambda$ 1260, 1265 and Al II λ 1671 wind features become prominent. In keeping with the relation between wavelengths of SED peaks and density of spectral features, the wind spectra of the B stars in the FUSE FUV are less spectacular, and indeed there are no emission components later than B1 Ia.

3.3.3 Luminosity-Class Effects

As implied by the discussion of the previous section, the OB stellar-wind profiles have strong positive luminosity effects, which in the IUE FUV range are most dramatic in Si IV $\lambda\lambda$ 1394, 1403 (Walborn & Panek 1984a, O Atlas). These effects are caused by the increasing wind densities with luminosity, modulo the ionization potentials of specific features (Drew 1989; Pauldrach et al. 1990). In early O spectra, the high-ionization N V (98 eV) and C IV (64 eV) wind profiles are saturated (i.e., the absorption components are black) at all luminosity classes until spectral type O6.5. However, the lower ionization of Si IV (45 eV) interacts with the prevailing physical parameter range to produce a beautifully sensitive luminosity/density behavior, from zero wind effects on the main sequence, through intermediate profiles at intermediate luminosity classes, to fully developed wind profiles in the supergiants (Figure 3.14). At later O and early B types, when the N V and C IV strengths have declined on the main sequence, they display analogous luminosity effects.

The *Copernicus* atlas of Snow & Morton (1976) already showed a luminosity effect similar to that of Si IV in C III λ 1176 (48 eV), which has a very similar ionization potential. The FUSE Atlas adds S IV (47 eV) $\lambda\lambda$ 1063, 1073 and P V (65 eV) $\lambda\lambda$ 1118, 1128 to the list of wind features displaying sensitivity to luminosity (Figure 3.15). Interestingly, in the case of P V, saturation is prevented by the low abundance of P, rather than the ionization potential.

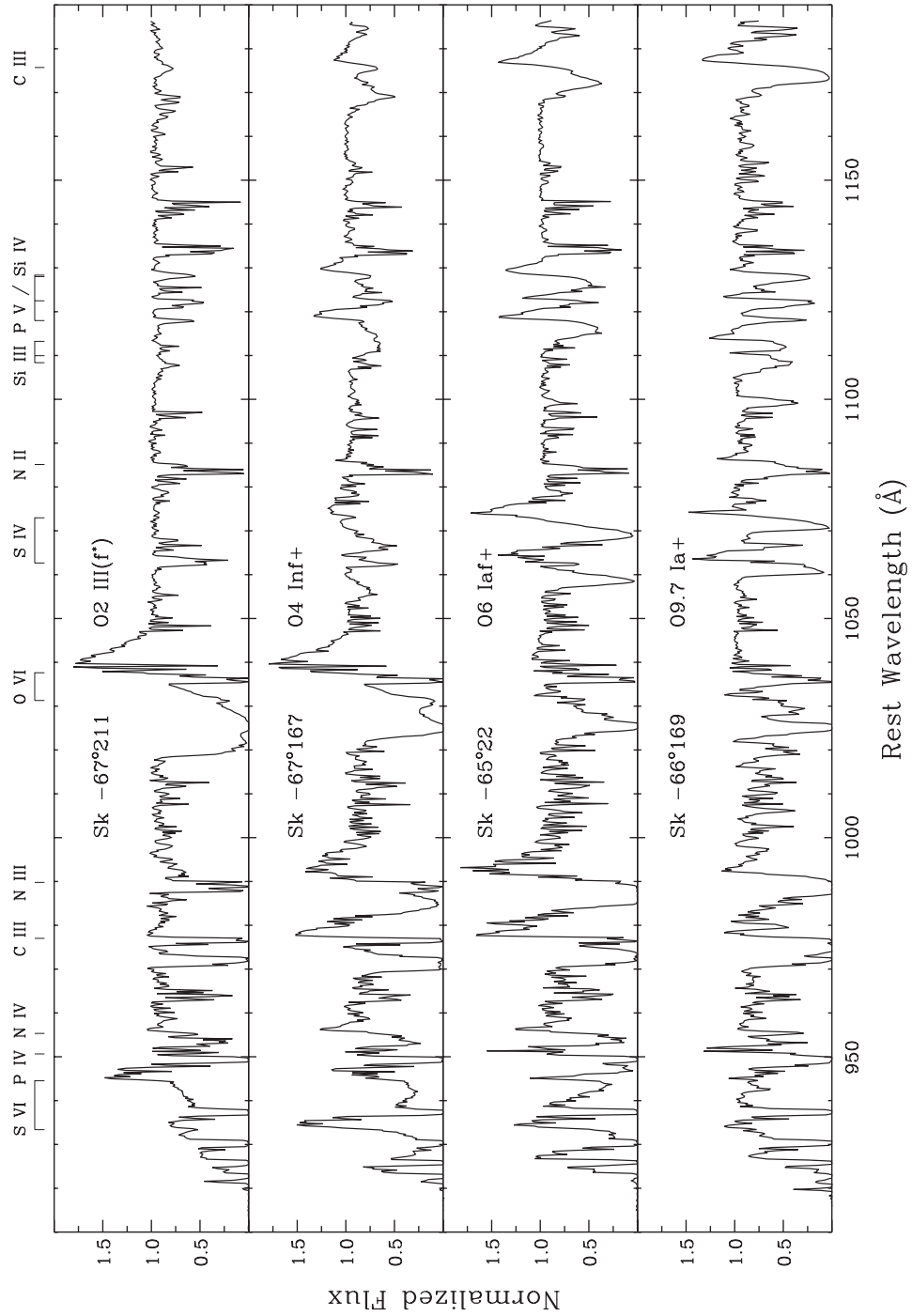


Figure 3.11 LMC Supergiant Sequence in the FUSE FUV (Walborn et al. 2002b). The stellar-wind features identified at the top are, from left to right, S VI $\lambda\lambda 933, 944$; P IV $\lambda 951$; N IV $\lambda 955$; C III $\lambda 979$; N III $\lambda 991$; O VI $\lambda\lambda 1032, 1038$; S IV $\lambda\lambda 1063, 1073$; N II $\lambda 1085$; Si III $\lambda\lambda 1108, 1110, 1113$; P V $\lambda\lambda 1118, 1128$; Si IV $\lambda\lambda 1122, 1128$; and C III $\lambda 1176$. Note the opposite, monotonic trends in the O VI and C III $\lambda 1176$, while some other features peak within this spectral-type range. Figure courtesy A. Fullerton and reproduced by permission of the AAS.

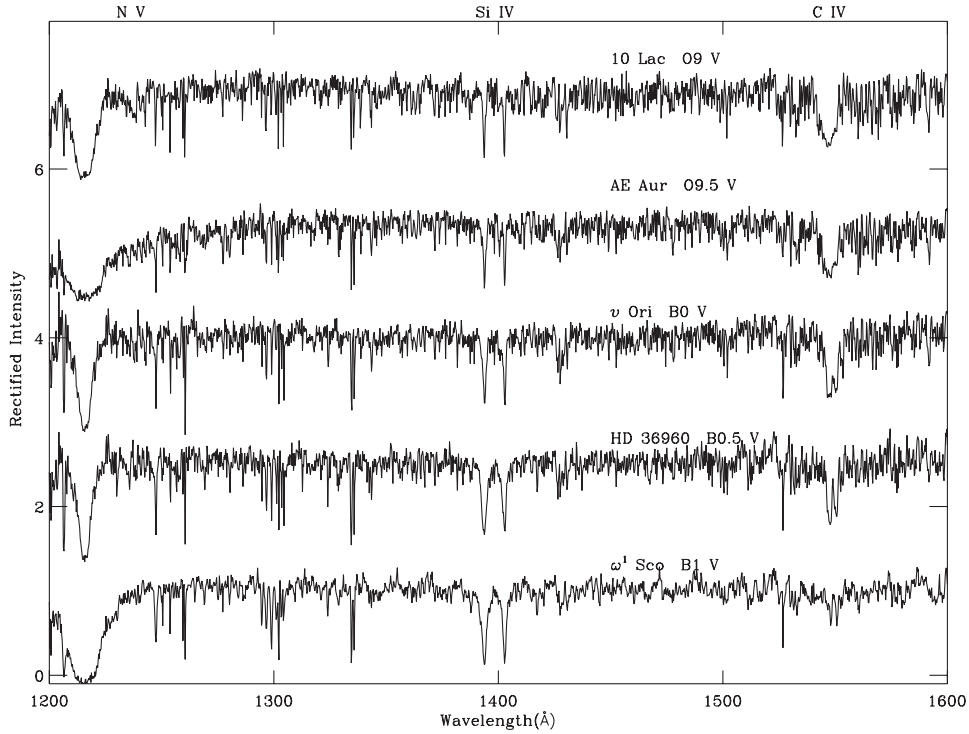


Figure 3.12 Late-O/Early-B Main Sequence in the IUE FUV. The spectral features identified above are N V $\lambda\lambda$ 1239, 1243; Si IV $\lambda\lambda$ 1394, 1403; and C IV $\lambda\lambda$ 1548, 1551. Figure courtesy D. Lennon.

The UV counterpart to Figure 3.8 for hot slash and WN-A stars is given in Figure 3.16. The great strength of the subordinate He II and N IV wind emission profiles in these spectra is noteworthy, as is the saturation of the very sensitive C IV feature, despite the reduced C abundances in these winds.

3.4 THE INFRARED—MARGARET M. HANSON

The earliest near-infrared spectra of hot, massive stars dates back to Swings & Hose (1950), extending redward to $0.86\ \mu\text{m}$ and Miller (1954), extending a bit past $1\ \mu\text{m}$. Both of these studies were of Wolf-Rayet type stars, whose broad, strong emission lines could be detected with early simple instruments. OB star lines are typically many, many times weaker than those seen in WR stars. Demonstrating this point, one of the earliest near-infrared spectra of an OB star, made by Barnes, Lambert, & Potter (1974), showed ζ Pup to be almost featureless to the limit of their signal-to-noise (about 25) between 0.8 and $1.7\ \mu\text{m}$. Only Paschen β and He II $1.01236\ \mu\text{m}$ were detected (all wavelengths listed in this section will be in air). At about that time, Mihalas & Lockwood (1972) and a series of papers by Andrillat & Vreux (1975, 1979) and Vreux & Andrillat (1979) closely studied the

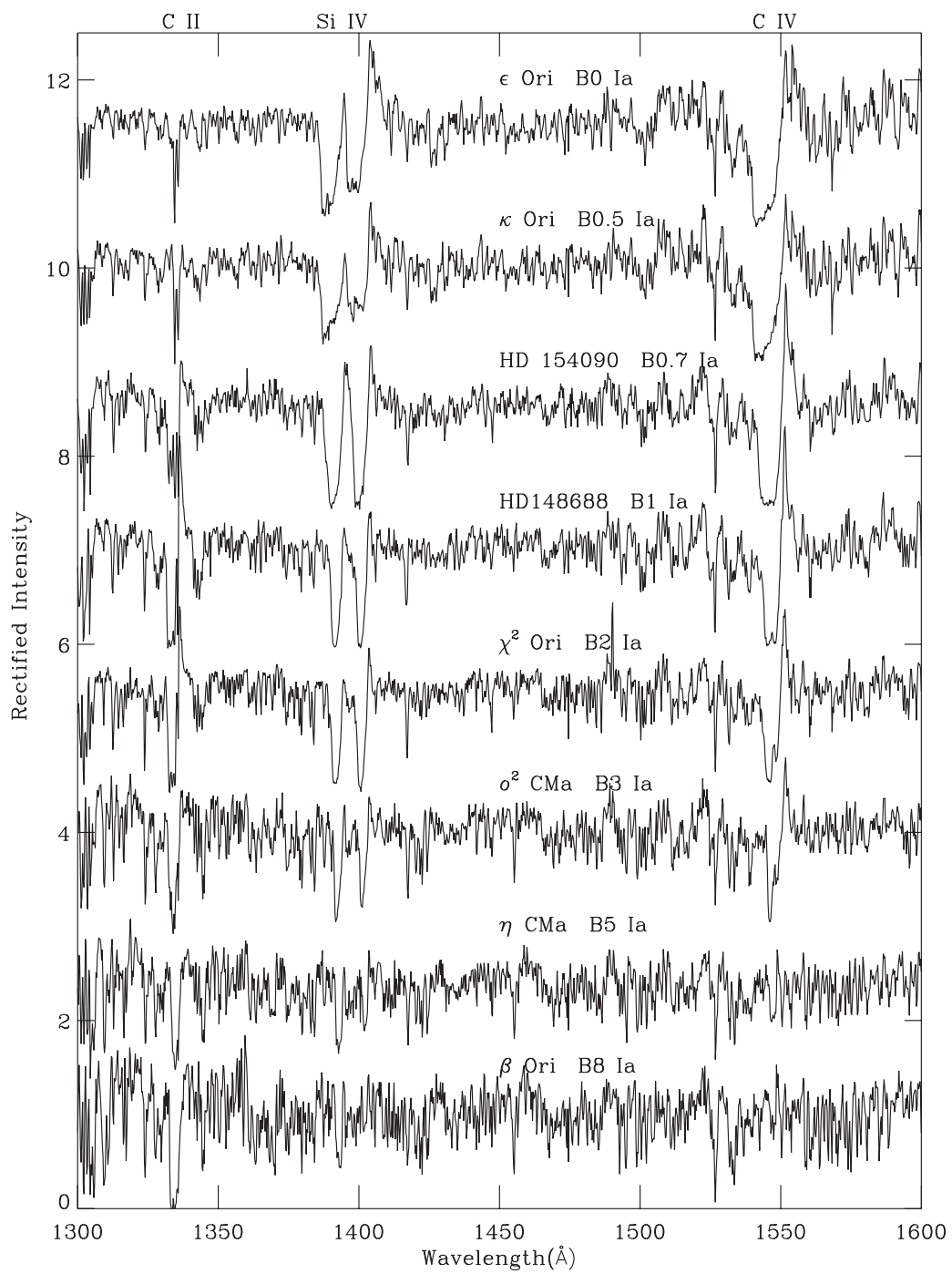


Figure 3.13 B Supergiant Sequence in the IUE FUV. The spectral features identified above are C II $\lambda\lambda$ 1334, 1336; Si IV $\lambda\lambda$ 1394, 1403; and C IV $\lambda\lambda$ 1548, 1551. Figure courtesy D. Lennon.

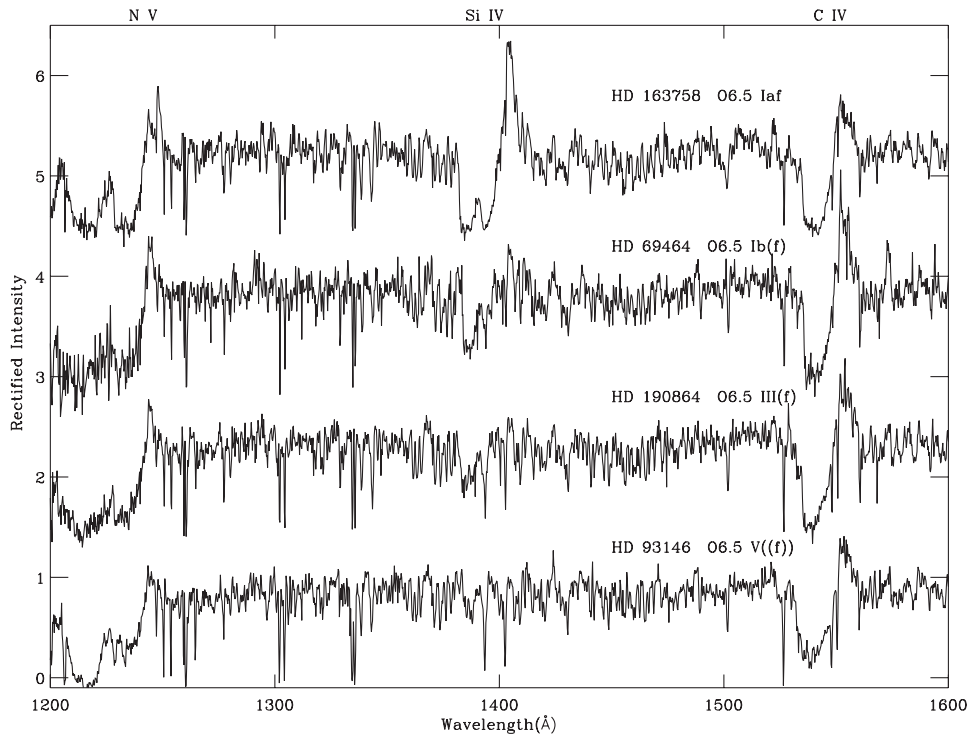


Figure 3.14 Luminosity Sequence at O6.5 in the IUE FUV (Walborn 2007a). These are the same stars shown optically in Figure 3.6. The spectral features identified above are N V $\lambda\lambda$ 1239, 1243; Si IV $\lambda\lambda$ 1394, 1403; and C IV $\lambda\lambda$ 1548, 1551. Figure courtesy D. Lennon and Editorial Complutense, S. A.. Reproduced from *UV Astronomy: Stars from Birth to Death*, with the permission of Editorial complutense, 2007.

behavior of the $1.012\ \mu\text{m}$ He II and $1.08303\ \mu\text{m}$ He I lines in O supergiant stars. These early studies were critical to the early advancement of model atmosphere calculations in OB stars (such as first presented by Auer & Mihalas 1974).

Later, in the 1980s, the advent of near-infrared focal plane arrays and new semiconductor materials highly sensitive to longer wavelengths, such as mercury–cadmium–telluride (HgCdTe) and indium–antimonide (InSb), allowed high quality infrared spectra to be obtained on a large number of objects. Now scores of OB stars could be observed with sufficient signal-to-noise and resolution to allow their spectral nature to be characterized. Among the first high quality near-infrared spectral atlases of stars were presented by Lancon & Rocca-Volmerange (1992) and Dallier, Boisson, & Joly (1996). However, Hanson, Conti, & Rieke (1996) were the first to exclusively present near-infrared spectra of a large number of massive stars with the singular purpose of developing a near-infrared spectral classification system. This classification system has since been broadly accepted by the OB star community as the current near-infrared standard and will be presented here.

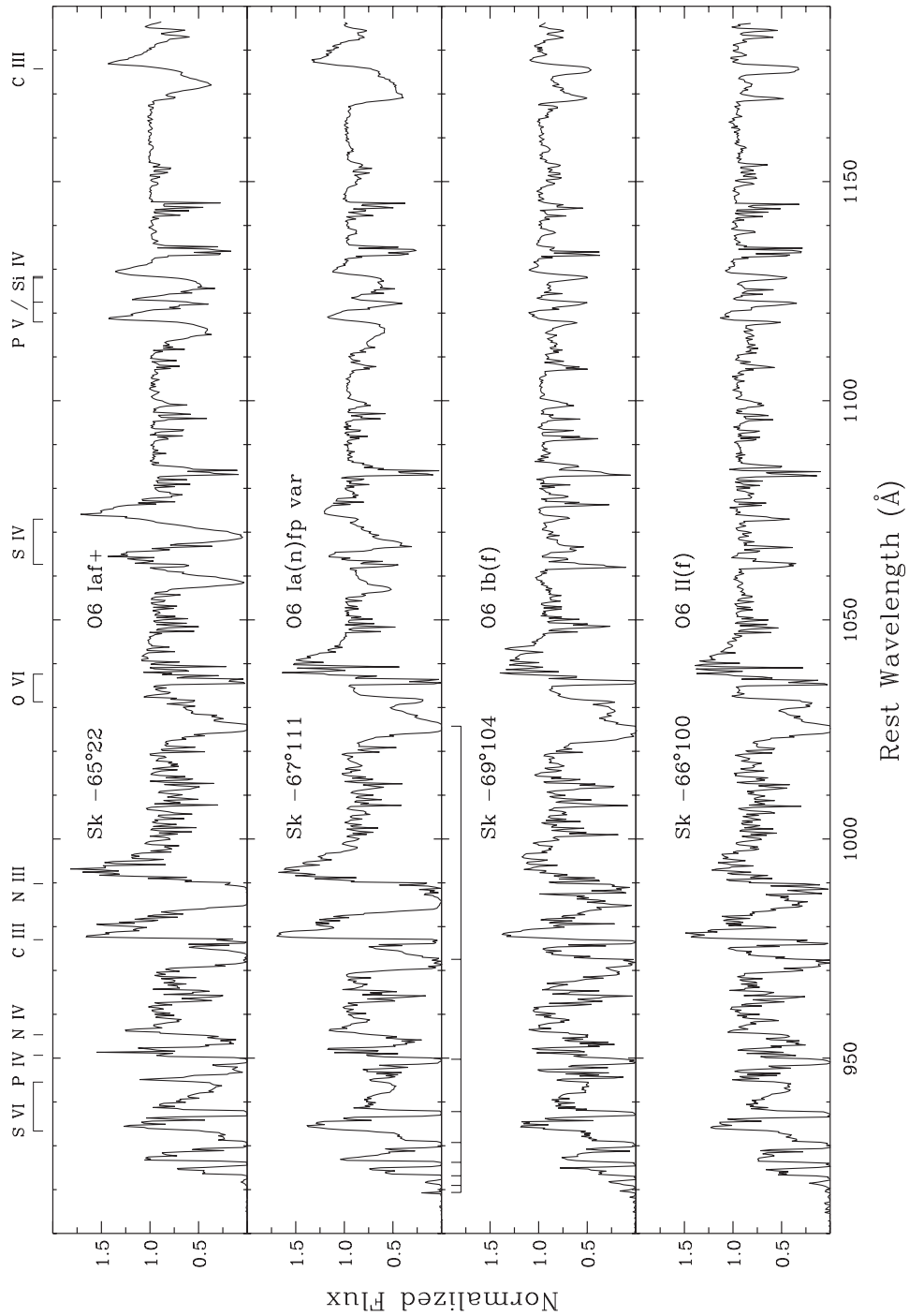


Figure 3.15 Luminosity Effects in the FUSE FUV (Walborn 2002a). See Figure 3.11 caption for line identifications. The comb marks the H I Lyman series beginning with $\text{Ly}\beta$ $\lambda 1026$, which is primarily interstellar in these spectra. Most wind features display positive luminosity effects, but in contrast, the weakening of the O VI in the most luminous star is surprising and may indicate a density and/or temperature threshold for its formation. Figure courtesy A. Fullerton and reproduced by permission of the AAS.

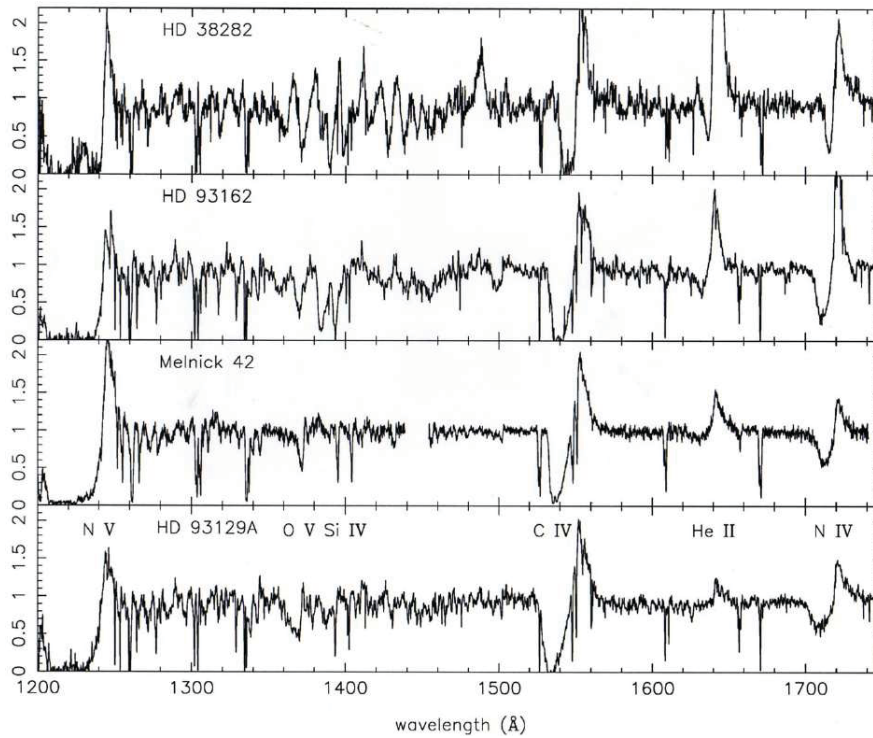


Figure 3.16 Wind Development from Of* through Intermediate to WNL in the FUV. The data for Melnick 42 in 30 Doradus are from HST, while the others are from IUE; cf. Walborn et al. (1992). See Figure 3.8 for corresponding optical data and spectral types. The spectral features identified in the bottom panel are N V $\lambda\lambda$ 1239, 1243; O V λ 1371; Si IV $\lambda\lambda$ 1394, 1403; C IV $\lambda\lambda$ 1548, 1551; He II λ 1640; and N IV λ 1718. Figure courtesy J. Nichols.

3.4.1 Relation to the Optical

Because of its long history in astronomy and the large number of stars with optical classification, the success of a near-infrared classification system is partly dependent on its ability to map back to the optical classification system. Unfortunately, there are far fewer atomic transitions at near-infrared energies (below 1 eV) than in the optical regime. Moreover, many infrared lines form in a different region of the atmosphere than optical lines, either in the uppermost photosphere or in the stellar wind. Note also that due to the combination of non-LTE effects and the strong influence of stimulated emission (low transition energies), emission lines are much more easily created in the IR than the optical/UV, even without the presence of a significant wind (e.g., Mihalas 1978; Najarro et al. 1998). Despite these differences, the classification of O and early-B stars with reasonably direct comparisons to classification systems used in the optical is possible using near-infrared spectra alone.

The lack of lines at near-infrared energies makes near-infrared classification less exact than optical classification. The only reason one would attempt to determine

classification in the near-infrared is because the optical bands are not observable. In the majority of cases, this situation has been driven by large extinction (either local or along the line of sight to the star), which preferentially attenuates the optical photons relative to the near-infrared photons coming from the star. Compared to the B-band region where optical classification is obtained, the near-infrared K-band, centered at $2.2\ \mu\text{m}$, reduces the extinction (in magnitudes) by a factor of 12 (Rieke & Lebofsky 1985). Among the quickest to benefit from a near-infrared spectral classification system for massive stars was the field of massive star formation. Since its introduction more than ten years ago, tens of studies of massive stars in young star forming regions, primary stars of massive X-ray binaries and even normal massive stars deeply hidden through out the galaxy, including the Galactic center, have successfully used the classification system.

Finally, the overall strength of the lines forming in the near-infrared is much weaker than those formed in the optical. While the resolution used for near-infrared classification is about the same as used for the optical ($R \gtrsim 1000$), higher signal-to-noise (S/N) is required to detect these weak photospheric features. We recommend observers strive for a S/N of 100. With a S/N below 70, near-infrared classification is seriously compromised.

3.4.2 Spectral-Type Criteria

As with the optical, the primary temperature classification of O-type stars in the near-infrared is based on the ionization of helium. From 2.0 to $2.2\ \mu\text{m}$, a few “well-behaved,” photospheric lines of He I and He II exist, namely, He I $2.1120/1\ \mu\text{m}$ ($3p^3P^o - 4s^3S$, triplet) and $2.11320\ \mu\text{m}$ ($3p^1P^o - 4s^1S$, singlet) and He II $2.18852\ \mu\text{m}$ ($n = 7-10$). As in the optical, He II is seen to disappear later than O9, while He I disappears earlier than O4. Early B stars then show no He II, just He I, though unlike in the optical, He I is seen to disappear in dwarf B stars as soon as B3. Figure 3.17 presents an array of near-infrared spectra of O and early B dwarfs, their optical spectral types given. The smooth variation of He II and He I lines with temperature is clearly observed. There is another fundamental He I line in the K-band, $2.05813\ \mu\text{m}$ ($2s^1S - 2p^1P^o$). This line is shown in just one spectrum in Figure 3.17, that of the B2 Ia star. Unfortunately, this line is problematic both observationally and theoretically. It falls in a messy spectral region of the Earth’s atmosphere (Kenworthy & Hanson 2003), dominated by rovibrational transitions of CO_2 . But more so, the line is corrupted by complex non-LTE effects and strongly affected by line-blocking effects, since the upper level is coupled to the FUV He I resonance line at $584\ \text{\AA}$. Both in supergiants but also in dwarfs He I $2.058\ \mu\text{m}$ is seen to go into emission for spectral types roughly at or cooler than O7 (most frequently showing a P Cygni profile in case of stronger index OB-type stars, normal!infrared!wind features winds). Because the line reacts most strongly to the wind strength and not so much to changes in the photosphere, it is not (very) suitable for classification purposes (see discussion in Najarro et al. 1994).

A second set of He lines is also seen in the H-band, from 1.4 to $2.0\ \mu\text{m}$, namely He I $1.70023\ \mu\text{m}$ ($3p^3P^o - 4d^3D$, triplet) and He II $1.691837\ \mu\text{m}$ ($n = 7-12$). These

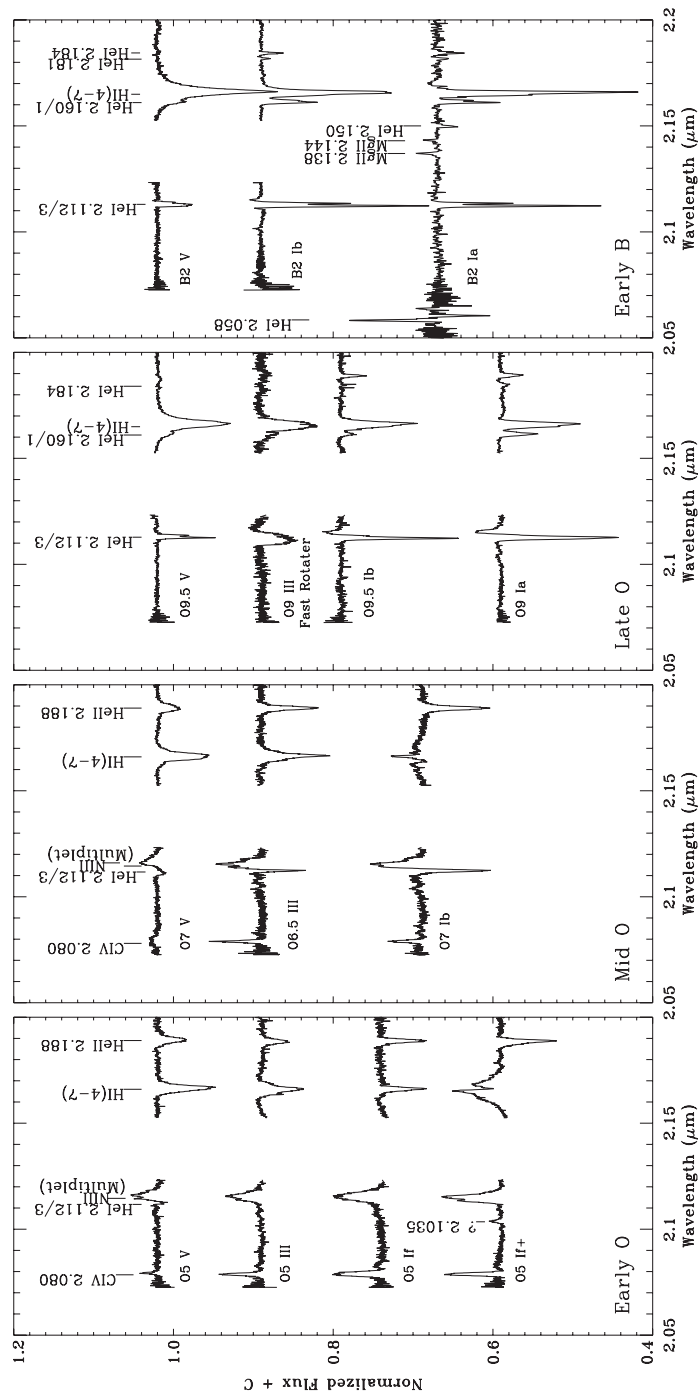


Figure 3.17 High-Quality Near-infrared Spectra of O and Early B Stars Illustrating the Salient Lines Used for Classification. For all spectra, $R \sim 12000$ except for the B2 Ia star for which $R \sim 8000$. The S/N of the spectra is also extremely high for typical near-infrared work, ranging from 150 to over 300. Spectral classification is possible with lower quality spectra, but the observer is advised to stay above $R \sim 1000$ and $S/N = 100$. Luminosity classification will require $R \sim 5000$ and $S/N > 150$. A full set of high-quality near-infrared spectra are presented by Hanson et al. (2005).

lines are, in fact, better behaved than the K-band lines, as they are fully formed in the photosphere and are the most sensitive to temperature and gravity changes. Observationally, however, they are typically less desirable. The H-band lines are even weaker than those found in the K-band; the He II $1.69\ \mu\text{m}$ line is exceedingly weak in late-O stars. Moreover, when extinction in the optical is particularly high ($A_v > 20$), the K-band is again preferred because of its lower extinction relative to the H-band.

There are only a few additional near-infrared lines available to help near-infrared spectral classification and these are seen only in O-type stars. In the hottest O stars, two important features are noted in the K-band: a C IV doublet ($3d^2D - 3p^2P^o$) at $2.0700, 2.0796, 2.0836\ \mu\text{m}$, and a strong, broad feature centered at about $2.1155\ \mu\text{m}$. The exact nature of this transition is not presently known. It has been suggested to be the (7-8) transition of either N III (Hanson, Conti, & Rieke 1996) or C III. Regardless of its lack of identification, its behavior, as well as the behavior of the C IV doublet, is well correlated with temperature. C IV appears in emission over a fairly tight spectral range, being found in most O4s, all O5s, and most O6 dwarfs and O7 dwarfs, if very high S/N is available. Again, if very high S/N is available, the C IV line (predominately the strongest feature at $2.08\ \mu\text{m}$) can be seen in absorption in O3 dwarfs. The unidentified feature at $2.1155\ \mu\text{m}$ is seen to appear in all O dwarf stars hotter than O8; in the hotter O stars it dominates over their weak, nearby He I lines. The strength of the $2.1155\ \mu\text{m}$ line appears to be fairly flat, until it begins to taper off in O7 dwarfs, becoming nearly (depending on the S/N) undetected in the O8 dwarfs.

3.4.3 Luminosity-Class Criteria

Luminosity indicators are very subtle in the near-infrared, requiring higher quality spectra to be measured well. In the lower-resolution atlas of Hanson, Conti, & Rieke (1996), only inappreciable changes in stellar luminosity could be seen most of the time. However, the recent high S/N and higher-resolution atlas of Hanson et al. (2005) provides sufficient evidence to outline luminosity criteria using near-infrared lines alone.

Four temperature ranges are shown in the composite Figure 3.17, representing O5, O7, O9.5, and the B2 spectral classes. While the lines may be different, similar effects on the line profile are seen to occur with the evolution to an extended atmosphere. With decreasing gravity, the spectral features become narrower (except He I, which has no significant Stark-broadening) and deeper. When sufficient resolution and signal-to-noise are available, lines of He I at $2.149, 2.160, 2.181$, and $2.184\ \mu\text{m}$ are seen to emerge for the most luminous O9 and early-B supergiants. Moreover, a pair of Mg II lines at 2.1375 and $2.1438\ \mu\text{m}$ appear in the B2 Ia spectrum. These last two lines are seen in emission in the most extreme supergiants, such as Luminous Blue Variables and P Cygni stars (see Morris et al. 1996). In early and mid-O stars, the Brackett γ feature at $2.16553\ \mu\text{m}$ in the most luminous Ia supergiants goes into emission. While this emission effect would be seen in even moderate resolution spectra, it is clear that the most important

luminosity effect in typical O and early B stars, the depth and narrowness of the lines, can be measured only with spectra of relatively high spectral resolution, $R \sim 5000$ and $S/N > 150$.

However, there may be a way to determine relative luminosities in OB stars via moderate quality infrared spectra, if the temperature is already well constrained. Because many of the spectral features in stars with extended atmospheres become deeper, their total equivalent width increases with decreased $\log g$. This result was first noted empirically by Hanson, Rieke, & Luhman (1998) in the H-band spectra of B supergiants. This behavior—an increase in the equivalent width of the line with decreased gravity—is completely opposite to what is seen in the optical. In the optical, H and He lines become weaker with decreased gravity. This differing effect is now fully understood. Regarding hydrogen and He II, it is caused by the specific behavior of Stark-broadening as a function of electron density, which differs for lines with low (optical) and high (IR) lying upper levels. On the other hand, the strengthening of the He lines with lower gravities is driven by non-LTE effects (Repolust et al. 2005). Thus, if one can make very accurate measurements of the equivalent widths of some of these $\log g$ sensitive H and He lines (as discussed in Repolust et al. 2005) and correct for the temperature dependency of those lines, in principle it should be possible to extract a relative luminosity estimate even with low-resolution spectra. The reliability of such a method has yet to be tested, however.

3.5 PECULIAR CATEGORIES

3.5.1 The OBN and OBC Stars

Opposite anomalies in the intensities of N vs. (C, O) in absorption-line OB spectra were described by Walborn (1971b), and an OBN/OBC classification dichotomy analogous to that for the WR stars was introduced. However, as discussed and referenced in subsequent reviews (Walborn 1976, 1988, 2003), the interpretation has turned out rather differently. Both the spectral morphology and quantitative analyses clearly indicate that the OBC category corresponds to normal, main-sequence abundances, while the morphologically normal majority of OB supergiants already have CNO-cycled material mixed into their atmospheres and winds, and the OBN category displays an even higher degree of such mixing (in some cases due to mass transfer in close binary systems). Analyses of He/H ratios are in agreement with that interpretation (Smith, Crowther, & Prinja 1994; Maeder & Conti 1994). Again, the ultraviolet stellar-wind profiles are strongly correlated with the optical CNO anomalies (O Atlas, B Atlas).

Some typical late-ON/OC supergiant spectra are illustrated in Figure 3.18. The most prominent anomalies are the weakening of C III $\lambda 4650$ relative to N III $\lambda 4640$ in the ON spectra, and the weakening of N III $\lambda 4097$ in the OC. However, the detailed discussion of these same spectra by Walborn & Howarth (2000) emphasizes the plethora of weak CNO lines that faithfully track the inverse ON/OC dichotomy. In BC supergiant spectra, it is N II $\lambda 3995$ that is strikingly deficient.

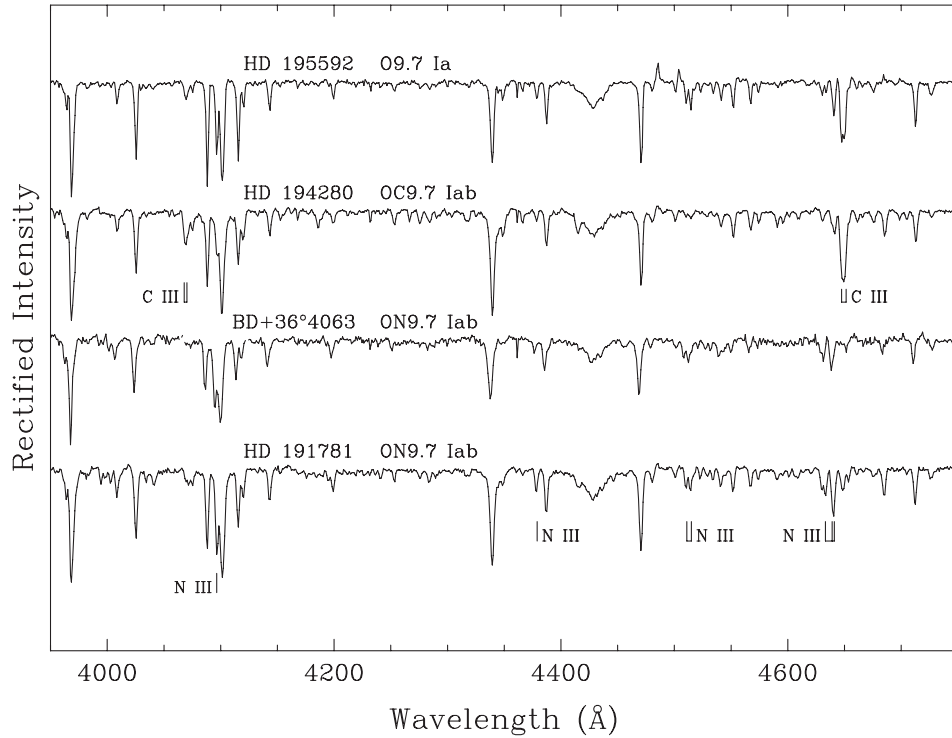


Figure 3.18 Late ON/OC Spectra (Walborn 2007a). The rectified spectrograms are separated by 0.4 continuum units. The lines identified below are N III $\lambda\lambda$ 4097, 4379, 4511–4515, and 4634–4640–4642. In the spectrum of HD 194280, they are the C III $\lambda\lambda$ 4070 and 4650 blends. Figure courtesy I. Howarth and Editorial Comptense S.A.. Reproduced from *UV Astronomy: Stars from Birth to Death*, with the permission of Editorial Comptense, 2007.

Evidence for N/(C, O) differences among O2 spectra in both the optical (Figures 3.19, 3.20) and the FUV (Figure 3.21) has been found more recently (Walborn et al. 2004a; Morrell, Walborn, & Arias 2005), initially from a survey of N IV and O IV features in the little-studied 3400 Å region (the “groundbased NUV”). These very massive objects have small absolute ages and lie near the main sequence, indicating more rapid mixing processes than contemplated in current models, and/or very rapid initial rotations perhaps inducing homogeneous evolution back toward the main sequence (Maeder & Meynet 2000). In the context of evolutionary models for massive stars with rotation, the CNO phenomena are a challenge and eventually a critical diagnostic, as discussed further later.

3.5.2 Rapid Rotators

The rotational systematics of the O stars was surveyed by Conti & Ebbets (1977). The distribution is very strongly peaked around $v \sin i$ of 100 km s⁻¹, with no very slow rotators among the supergiants (indicating that the line widths are dominated

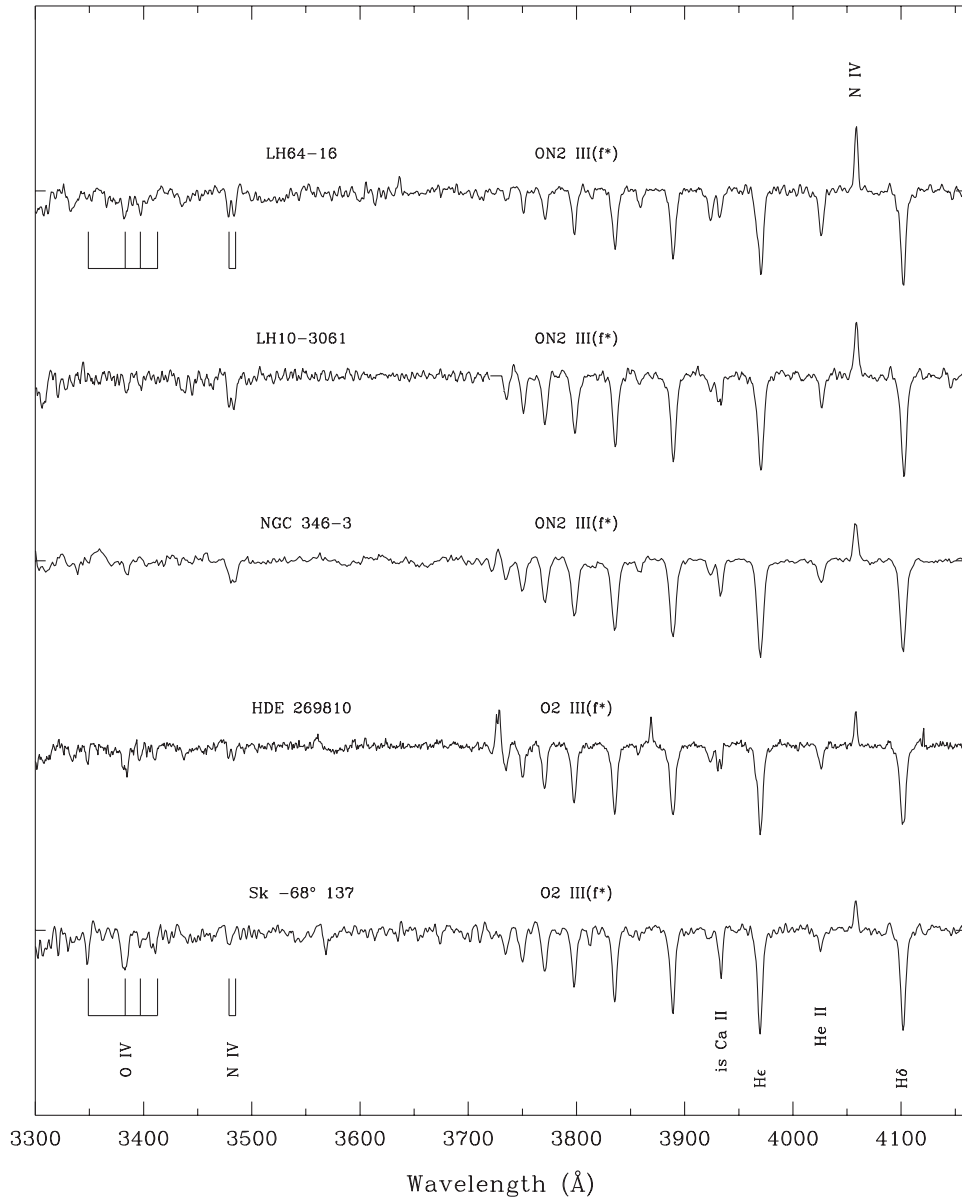


Figure 3.19 Magellanic Cloud ON2 and O2 Spectra in the Groundbased NUV (Walborn et al. 2004a). The rectified spectrograms are separated by 0.5 continuum units. The lines identified below are O IV $\lambda\lambda 3348/49-3381/85-3397-3410/14$; N IV $\lambda\lambda 3479-3485$; interstellar Ca II $\lambda 3933$; H Balmer $\lambda\lambda 3970, 4101$; and He II $\lambda 4026$. N IV $\lambda 4058$ emission is identified above. Figure courtesy N. Morrell and reproduced by permission of the AAS.

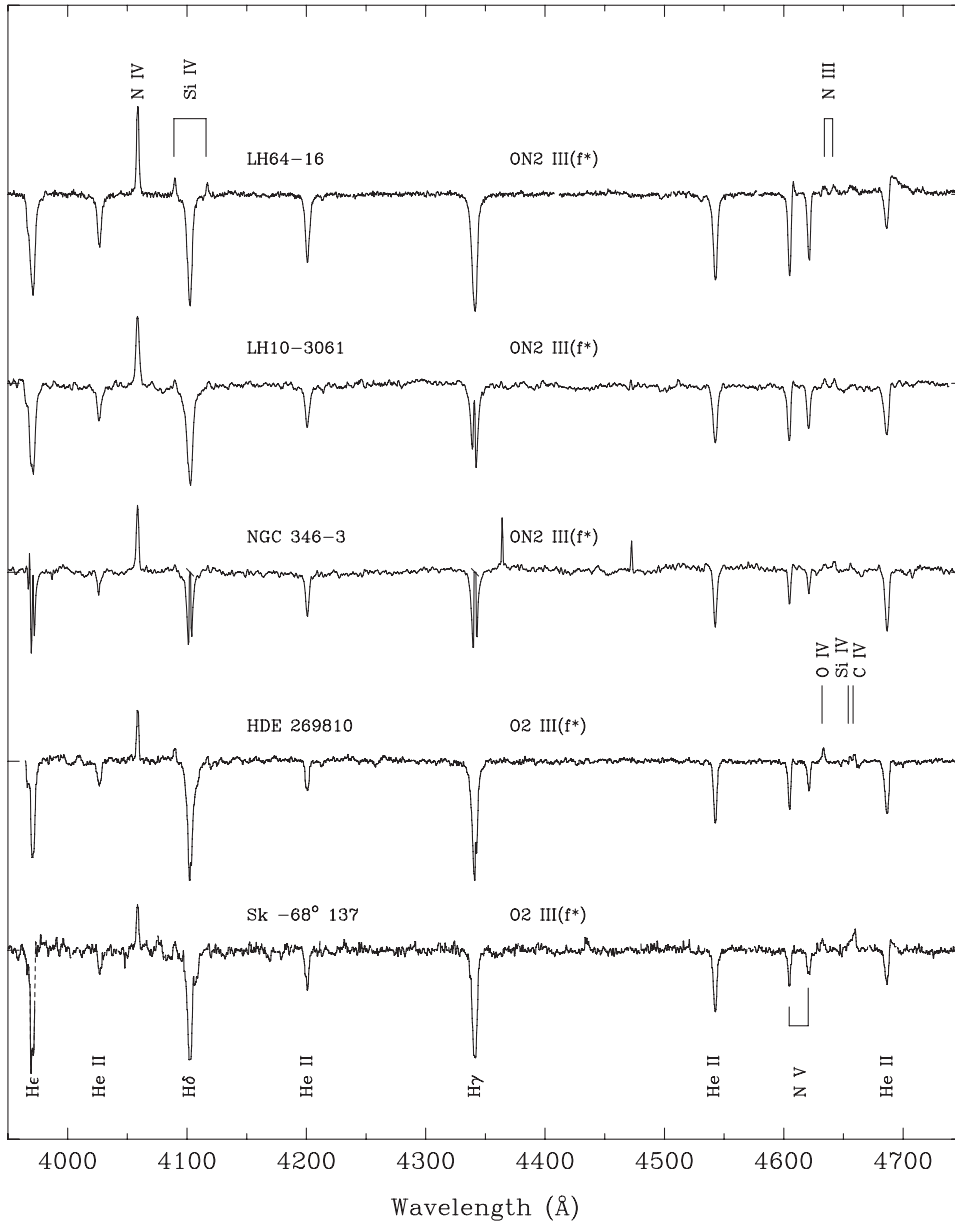


Figure 3.20 Magellanic Cloud ON2 and O2 Spectra in the Optical Violet/Blue/Green (Walborn et al. 2004a) The stars and format are the same as in Fig. 3.19. The lines identified below are H Balmer $\lambda\lambda$ 3970, 4101, 4340; He II $\lambda\lambda$ 4026, 4200, 4541, 4686; and N V $\lambda\lambda$ 4604–4620. In the spectrum of HDE 269810, O IV λ 4632, Si IV λ 4654, and C IV λ 4658 emission lines are identified. Further emission lines identified above are N IV λ 4058, Si IV $\lambda\lambda$ 4089–4116, and N III $\lambda\lambda$ 4634–4640–4642. Figure courtesy I. Howarth and reproduced by permission of the AAS.

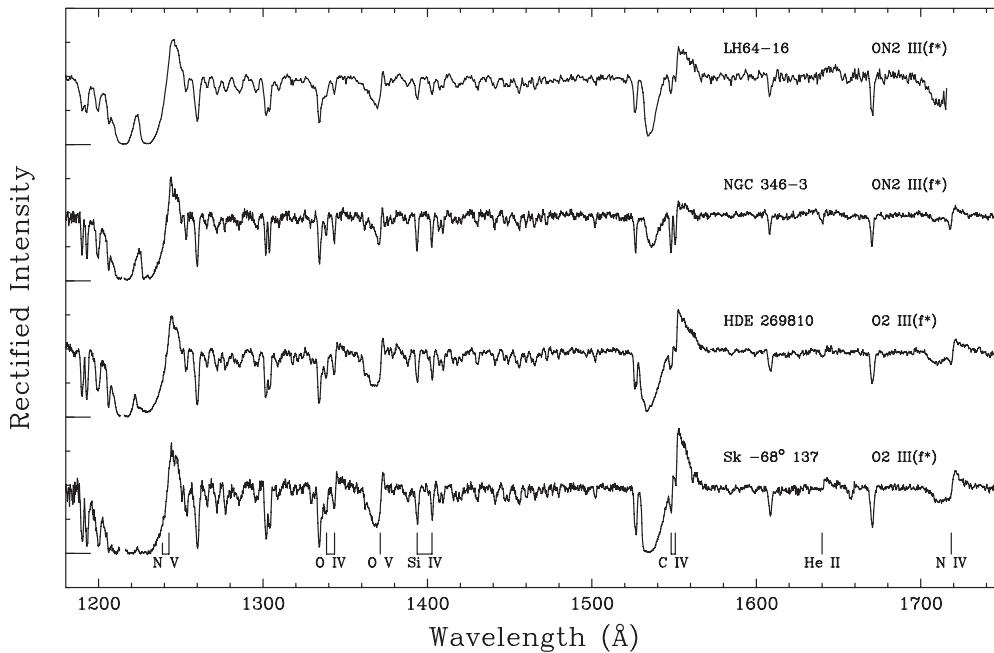


Figure 3.21 Magellanic Cloud ON2 and O2 Spectra in the HST FUV (Walborn et al. 2004a). The longer ordinate tick marks give the zero levels, and the continua are normalized to 1.0. The spectral features identified below are N V $\lambda\lambda$ 1239, 1243; O IV $\lambda\lambda$ 1339, 1343; O V λ 1371; Si IV $\lambda\lambda$ 1394, 1403; C IV $\lambda\lambda$ 1548, 1551; He II λ 1640; and N IV λ 1718. Figure courtesy I. Howarth and reproduced by permission of the AAS. Spectrum for LH64-16 courtesy P. Massey.

by “turbulence,” or more likely velocity gradients in latter-day terms), and with a higher velocity tail at the lower luminosity classes. At least three kinds of peculiar, rapidly rotating O-type stars are known (Figure 3.22): the Oe analogues of the Be stars, with evidence of rotating disks in the Balmer profiles (Walborn 1971a, 1980; Conti & Leep 1974; Conti & Ebbets 1977; Negueruela, Steele, & Bernabeu 2004); the Onfp (Walborn 1972, 1973) or Oef (Conti & Leep 1974) class, in which such evidence appears in terms of an absorption reversal in the broadened He II λ 4686 emission; and a recently defined class of N-rich rapid rotators, the ONn stars (Howarth & Smith 2001; Walborn 2003; Howarth 2004), which are likely of strong evolutionary significance, directly revealing rotationally enhanced mixing. The [n] notation in the spectral type of HD 155806 denotes hydrogen-line broadening greater than that of the He lines; evidently the ((f)) qualifier must be added to the classification of the digital data in Figure 3.22. The very luminous Ofnp! class is currently growing rapidly in the Magellanic Clouds; these intriguing objects may be candidates for stellar merger remnants and/or gamma-ray burst progenitors.

3.5.3 Magnetic Rotators

The Of?p designation was introduced by Walborn (1972, 1973) to distinguish the peculiar spectra of HD 108, 148937, and 191612 (the last newly discovered) from

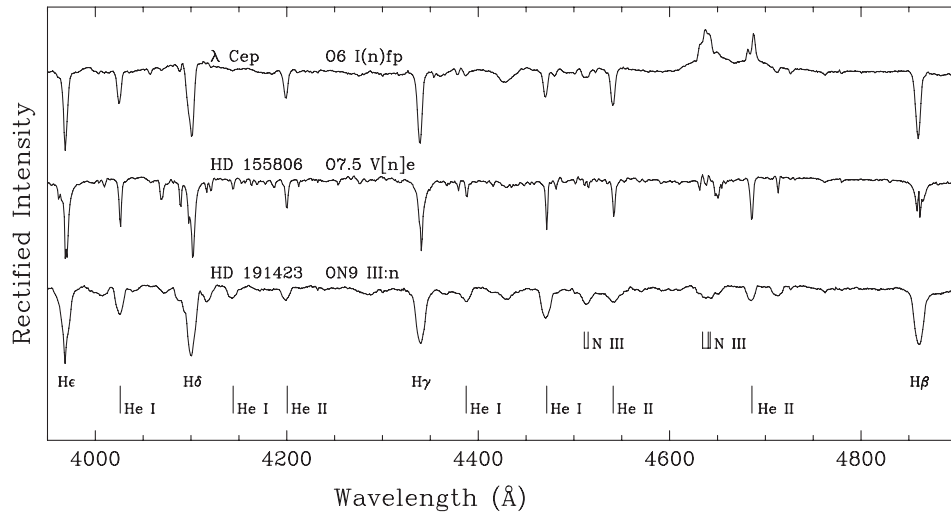


Figure 3.22 Three Categories of O-Type Rapid Rotators (Walborn 2007a). The rectified spectrograms are separated by 0.4 continuum units. The lines identified below are H Balmer $\lambda\lambda$ 3970, 4101, 4340, 4861; He I $\lambda\lambda$ 4026, 4144, 4387, 4471; He II $\lambda\lambda$ 4200, 4541, 4686; and N III $\lambda\lambda$ 4511–4515, 4634–4640–4642. Figure courtesy I. Howarth and Editorial Complutense S. A.. Reproduced from *UV Astronomy: Stars from Birth to Death*, with the permission of Editorial Complutense, 2007.

normal Of spectra. The question mark was intended to emphasize that these objects were not believed to be normal Of supergiants, as the latter had just been interpreted. The defining peculiarity in the blue spectra is C III $\lambda\lambda$ 4647–4650–4651 emission lines of comparable intensity to N III $\lambda\lambda$ 4634–4640–4642; the former are usually much weaker than the latter when present at all in normal Of spectra. Other line-profile peculiarities in the Of?p spectra are suggestive of shell phenomena or dilute (circumstellar) material. Subsequent IUE observations confirmed that these stars are not supergiants, in terms of the behavior of the Si IV resonance lines. Spectral variations had been reported in HD 108 and have been well documented by Nazé, Vreux, & Rauw (2001); the C III/N III emission-line ratio and emission components at H and He lines change on a timescale of decades. The spectral (in)stability of HD 148937 is less known, but it is surrounded by spectacular axisymmetric, N-rich ejected nebulosities (NGC 6164–6165), reminiscent of Luminous Blue Variable nebulae (references in Walborn et al. 2003). The latter reference reports the surprising discovery of large, recurrent spectral variations in HD 191612. The C III emission disappears, the apparent spectral type changes from O6.5 to O8, and the profiles of other features such as He II λ 4686 and H α change entirely, the latter from a strong P Cygni emission to predominantly absorption. Photometry from the *Hipparcos* satellite provided the breakthrough datum of a 538 d period in a very low-amplitude lightcurve (Nazé 2004), which satisfies the spectroscopic variations (Walborn et al. 2004b). Figure 3.23 shows

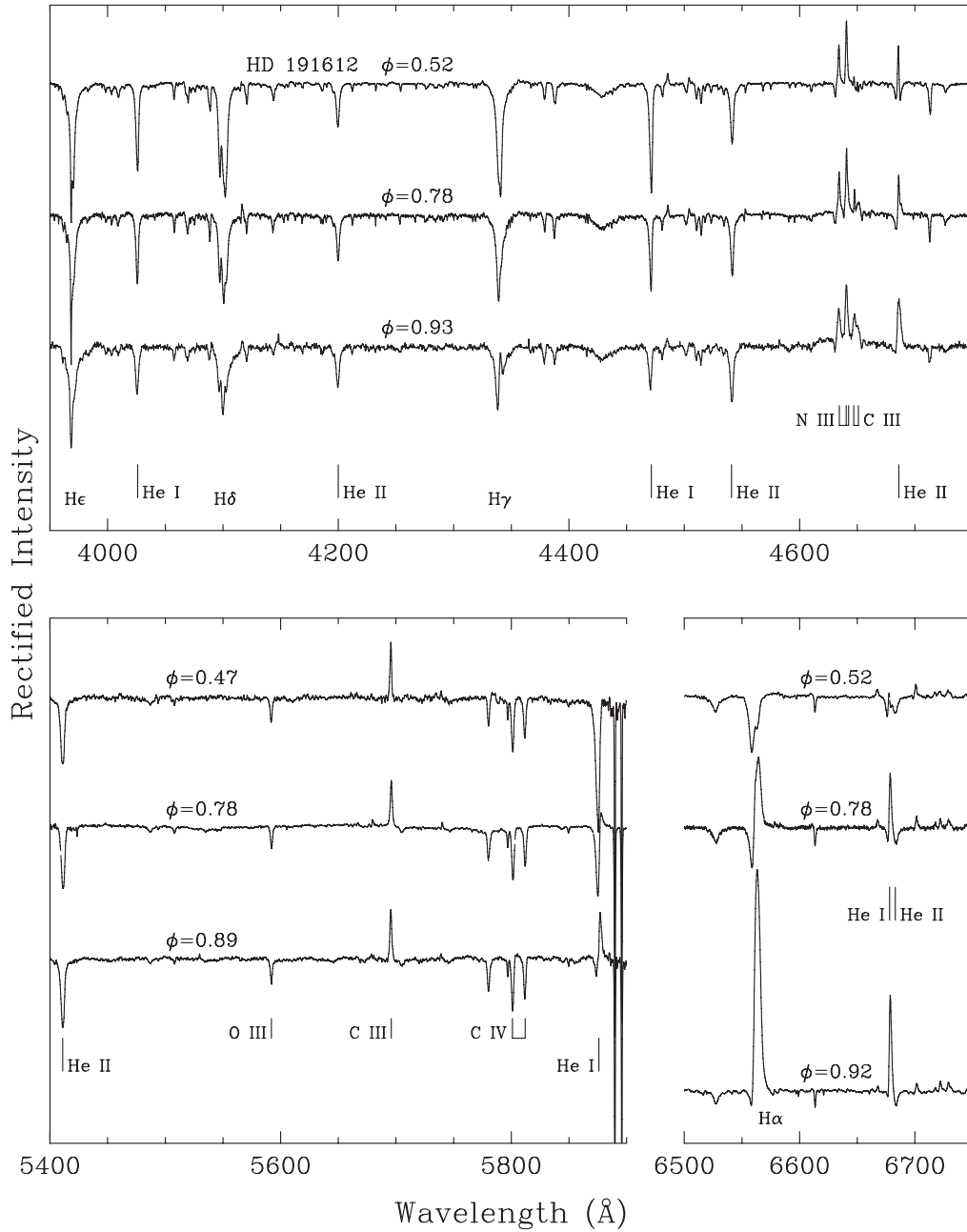


Figure 3.23 Blue-Violet (top) and Yellow-Red (bottom) Spectra of the Of?p Magnetic Oblique Rotator HD 191612 at Different Phases of the 538 d Rotational Period (Walborn 2007a). The rectified spectrograms are separated by 0.4 continuum units, except at lower right by twice that amount. The spectral lines identified in the upper panel are H Balmer $\lambda\lambda 3970, 4101, 4340$; He I $\lambda\lambda 4026, 4471$; He II $\lambda\lambda 4200, 4541, 4686$; N III $\lambda\lambda 4634-4640-4642$; and C III $\lambda\lambda 4647-4650/52$. In the lower panel, they are He II $\lambda\lambda 5411, 6683$; O III $\lambda 5592$; C III $\lambda 5696$; C IV $\lambda\lambda 5801-5812$; He I $\lambda\lambda 5876, 6678$; and H α $\lambda 6563$. Figure courtesy I. Howarth and Editorial Compleutense S.A.. Reproduced from *UV Astronomy: Stars from Birth to Death*, with the permission of Editorial Compleutense, 2007.

the drastic phase dependence of the spectrum in both the blue-violet and yellow-red. Subsequent analysis of extensive optical data with complete phase coverage demonstrated that the spectral-type variation is caused by filling in of the He I lines in the O6.5 state rather than an effective-temperature change, and that the O8 spectrum, while still peculiar, is the baseline (Howarth et al. 2007).

The bizarre phenomena exhibited by HD 191612 are unprecedented in an O-type star and challenged physical interpretation. A breakthrough was the second-only detection of a magnetic field in an O-type star, by Donati et al. (2006a). While phase coverage remains to be obtained, this observation suggests that the variations may be caused by an oblique rotator configuration with a magnetically confined wind disk, and that the very long rotational period is a result of magnetic braking. Comparison with the first known O-type magnetic oblique rotator, θ^1 Orionis C, is thus also suggested (Donati et al. 2002; Smith & Fullerton 2005; Gagné et al. 2005; Wade et al. 2006). Although of similar mass, this star is much younger, consistent with its shorter period of 15 d. θ^1 Ori C displays large, phase-dependent variations in its UV wind features (Walborn & Nichols 1994; Stahl et al. 1996), which have provided key diagnostics for the physical models. UV-spectroscopic phase coverage of HD 191612 now depends upon restoration of appropriate capabilities to HST in a final servicing mission scheduled for 2008.

It is remarkable that all four of the hottest magnetic stars known to date were isolated as peculiar from their optical and/or UV spectra in advance of the magnetic detections. The other two are τ Sco (Walborn & Panek 1984b; O and B Atlases; Donati et al. 2006b) and ξ^1 CMa (Rountree & Sonneborn 1991, 1993; B Atlas; Hubrig et al. 2006). This circumstance suggests the strong magnetic candidacy of other OB stars with unexplained spectral peculiarities and/or variations: in addition to the other two Galactic Of?p stars above, they are HD 36879 (Walborn 1984, O Atlas), θ Car (B Atlas, Lloyd, Stickland, & Walborn 1995), and 15 S Mon (§3.2.1 above). The FUV spectra of τ Sco, ξ^1 CMa, and θ Car are compared with those of normal standards in Figure 3.24; all three peculiar objects display marked anomalies in their wind profiles, including a unique main-sequence Si IV effect in τ Sco. θ Car is also N-enhanced and C-deficient.

A significant unity of interpretation of magnetic oblique rotators is emerging, in which the phenomenology changes as a function of increasing temperature and winds. At A types, they are the Ap stars; at late B, where He sinks, they are the He-weak stars; at early B, where He rises and winds begin to play a role, they are the He-strong stars of which the prototype is σ Ori E (Townsend, Owocki, & Groote 2005); and now the first O types have been added, with extensive disks caused by magnetic wind focusing and confinement toward the equator. Magnetic observations of the other Of?p stars will be of interest; and one can speculate that θ^1 Ori C may join that class as it matures.

3.5.4 ZAMS OB Stars

An “inverse Of effect,” i.e. He II $\lambda 4686$ absorption *stronger* relative to the other He lines than in normal class-V spectra, has been recognized in very young regions;

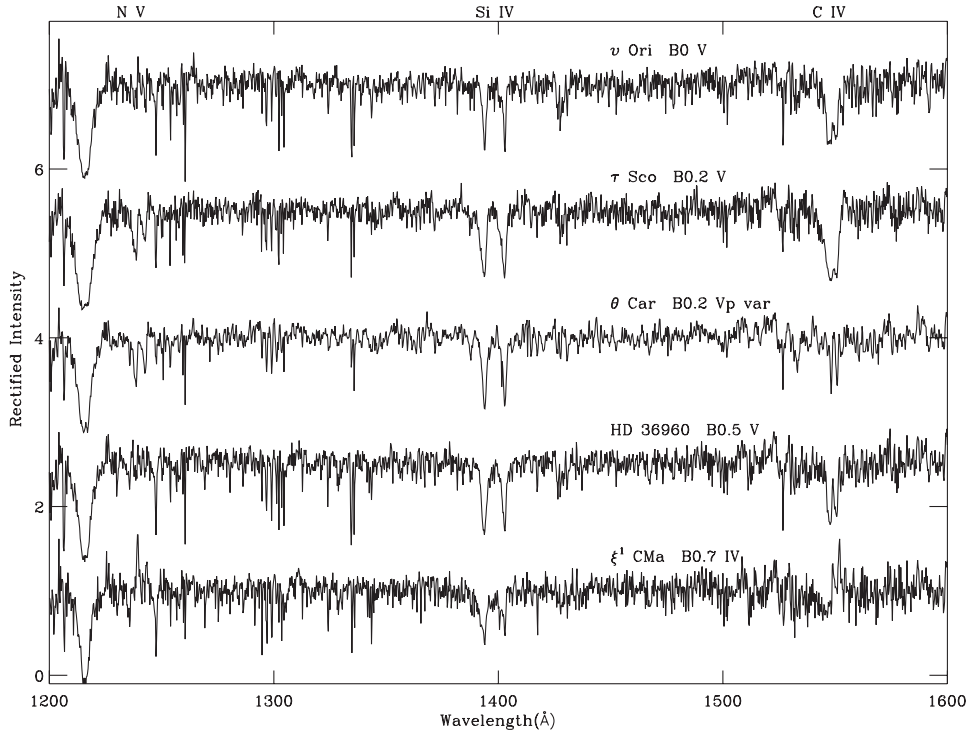


Figure 3.24 Three Peculiar Spectra and Two Standards in the IUE FUV. τ Sco and ξ^1 CMa have detected magnetic fields, while the peculiarities of θ Car are currently unexplained. The spectral features identified above are N V $\lambda\lambda$ 1239, 1243; Si IV $\lambda\lambda$ 1394, 1403; and C IV $\lambda\lambda$ 1548, 1551. Figure courtesy D. Lennon.

such spectra are classified “Vz.” The idea is that typical class-V spectra may already have some emission filling in that line, which is weaker or absent in Vz spectra. Some examples in the LMC association Lucke-Hodge 10, which ionizes the H II region Henize N11B, are shown in Figure 3.25 (Walborn & Parker 1992; Parker et al. 1992). It has been hypothesized that these objects may have lower (visual) luminosities and smaller ages than those of class V. They may be near or on the zero-age main sequence (ZAMS), contrary to some expectations that such would not be optically observable at high masses, because the embedded phases might be comparable to the main-sequence evolutionary timescales.

A misunderstanding of the Vz definition in late-O spectra should be clarified. At early O types, the He II λ 4686 absorption should be stronger than He II λ 4541. At type O7, He II λ 4541 is equal to He I λ 4471, so that λ 4686 is stronger than both in a Vz spectrum. At later O types, however, λ 4541 weakens more rapidly with advancing type than λ 4686 in normal class-V spectra; thus, a late-O Vz spectrum must have λ 4686 *stronger than He I λ 4471*.

Another spectroscopic peculiarity that may be related to sublumosity and extreme youth is broader Balmer lines than in normal class-V spectra, with profiles that do not appear to be rotational. The original examples were reported in the Orion Nebula Cluster (Morgan & Keenan 1973); however, investigation of the

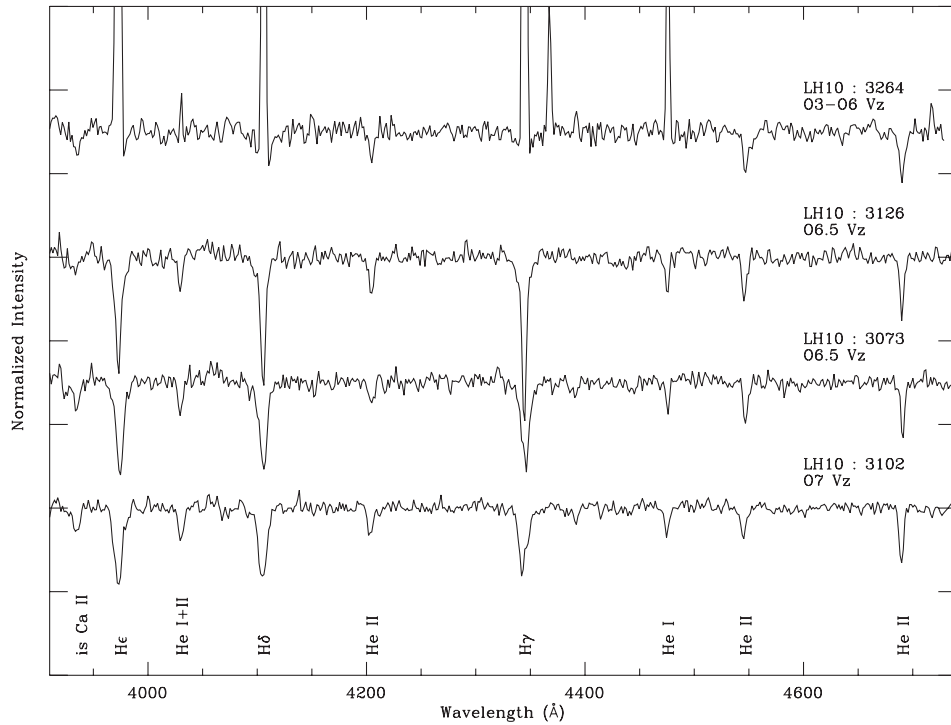


Figure 3.25 ZAMS O Stars in Lucke-Hodge 10 (Walborn 2007a). The rectified spectrograms are separated by 0.25 continuum units. The lines identified below are interstellar Ca II λ 3933; H Balmer $\lambda\lambda$ 3970, 4101, 4340; He I+II λ 4026; He II $\lambda\lambda$ 4200, 4541, 4686; and He I λ 4471. Figure courtesy J. Parker and Editorial Complutense S. A.. Reproduced from *UV Astronomy: Stars from Birth to Death*, with the permission of Editorial Complutense, 2007.

effect in the prototype θ^1 Ori C may be complicated by its more recently discovered magnetic and spectral variations discussed in the previous section. Abt (1979) and Levato & Malaroda (1981, 1982) presented further examples among B- and A-dwarf spectra in very young clusters, and the former introduced the notation “Vb” for their classification.

A third spectroscopic category that may correspond to extreme youth displays weak UV stellar wind profiles for their spectral types. Several examples are shown in the O Atlas, including the variable case of θ^1 Ori C. Some cases may be in common with the optical peculiarities described above, but most examples currently lack UV data.

This topic has been more extensively reviewed Walborn (2007b), in which fifty morphologically selected candidate ZAMS O stars are listed. It is a promising subject for future astrophysical investigation, which is required to establish or otherwise the interpretational hypotheses discussed, as well as the relationships among the different categories.

3.5.5 Metal Deficiency

The normal classification criteria discussed at the beginning of this chapter have been derived from spectra in the solar neighborhood, and they depend on its typical metallicity. At different metallicities, the classification will be affected directly by the different metal line strengths, as well as possibly indirectly by systematic differences in the atmospheric and wind structures. If one wishes to classify spectra with a significantly different metallicity, whether higher as in the Galactic Center and other metal-rich systems, or lower as in the Galactic Anticenter, the Magellanic Clouds, and starburst galaxies, the precepts discussed in Chapters 1 and 6 apply. In principle, the available criteria and their ranges must be investigated and local standards defined; the relationship between the physical parameters corresponding to given spectral types at different metallicities can be investigated subsequently.

In practice, LMC spectra can be classified on the standard system, although there may be small systematic effects in some supergiant luminosity classes (Walborn 1977; Fitzpatrick 1991). In contrast, OB stars in the SMC definitely require special procedures. Some results from relatively small samples have been presented by Walborn (1983); Walborn et al. (1995, 2000). An excellent systematic study of SMC OB supergiant spectra with appropriate methodology was performed by Lennon (1997), who thereby resolved several discrepancies and inconsistencies in previous work.

3.5.6 The OB/LBV Zoo

The diversity of peculiar, hot spectra displayed by massive stars is indeed astounding (Walborn & Fitzpatrick 2000, and references therein), and we are far from understanding the significance and interrelationships of all of them. A cooler category of intermediate “slash” spectra was isolated in the LMC and designated Ofpe/WN9 (Walborn 1977, 1982; Bohannon & Walborn 1989). These objects, together with Galactic extreme O Iafpe stars (Figure 3.26), were subsequently reclassified into a WN9-11 (WNVL) sequence by Crowther & Smith (1997) (Figure 3.27); see also Crowther & Bohannon (1997). In the UV, most of these objects display relatively low-ionization, shortward-shifted absorption features, indicative of very dense, low-velocity winds (Pasquali et al. 1997). One of the original prototypes of this category, HDE 269858 or Radcliffe 127, entered a classical Luminous Blue Variable outburst state in 1982 (Stahl et al. 1983). Other category members have LBV-like, axisymmetric, N-rich circumstellar nebulae (Walborn 1982; Nota et al. 1995; Pasquali, Nota, & Clampin 1999), evidently ejected in prior events. Thus, some or all of these objects correspond to quiescent phases of LBVs, an important insight into the still mysterious, rapid transitions during the late evolution of massive stars. It is plausible that they may subsequently reach WNE and/or WC states, following the extensive LBV mass loss.

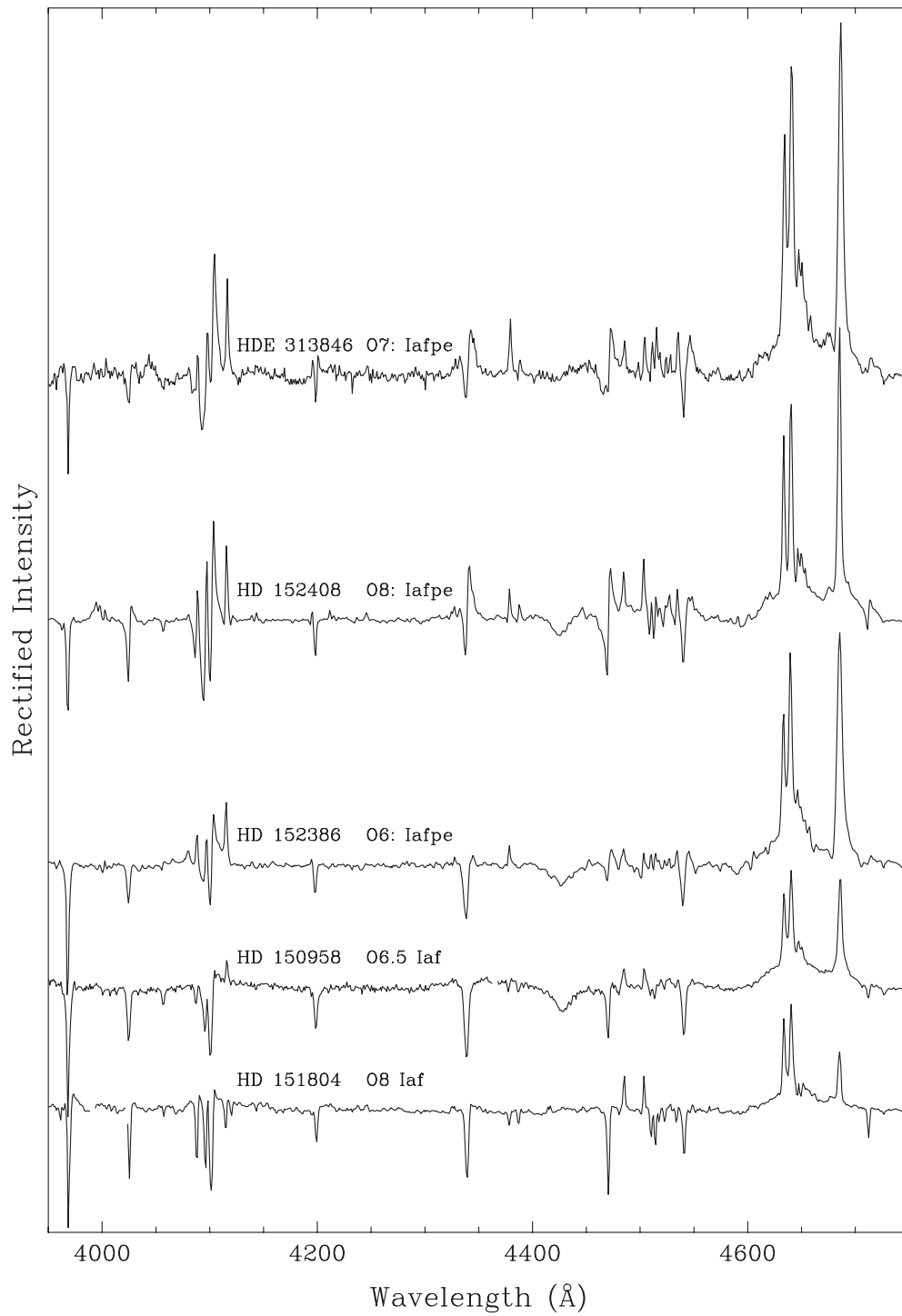


Figure 3.26 Two Normal Of Spectra and Three O Iafpe with Enhanced Winds. All of these objects are Galactic. The lower rectified spectrograms are separated by 0.4 continuum units and the upper ones by twice that amount. The spectral lines are identified in Figure 3.27. Figure courtesy I. Howarth.

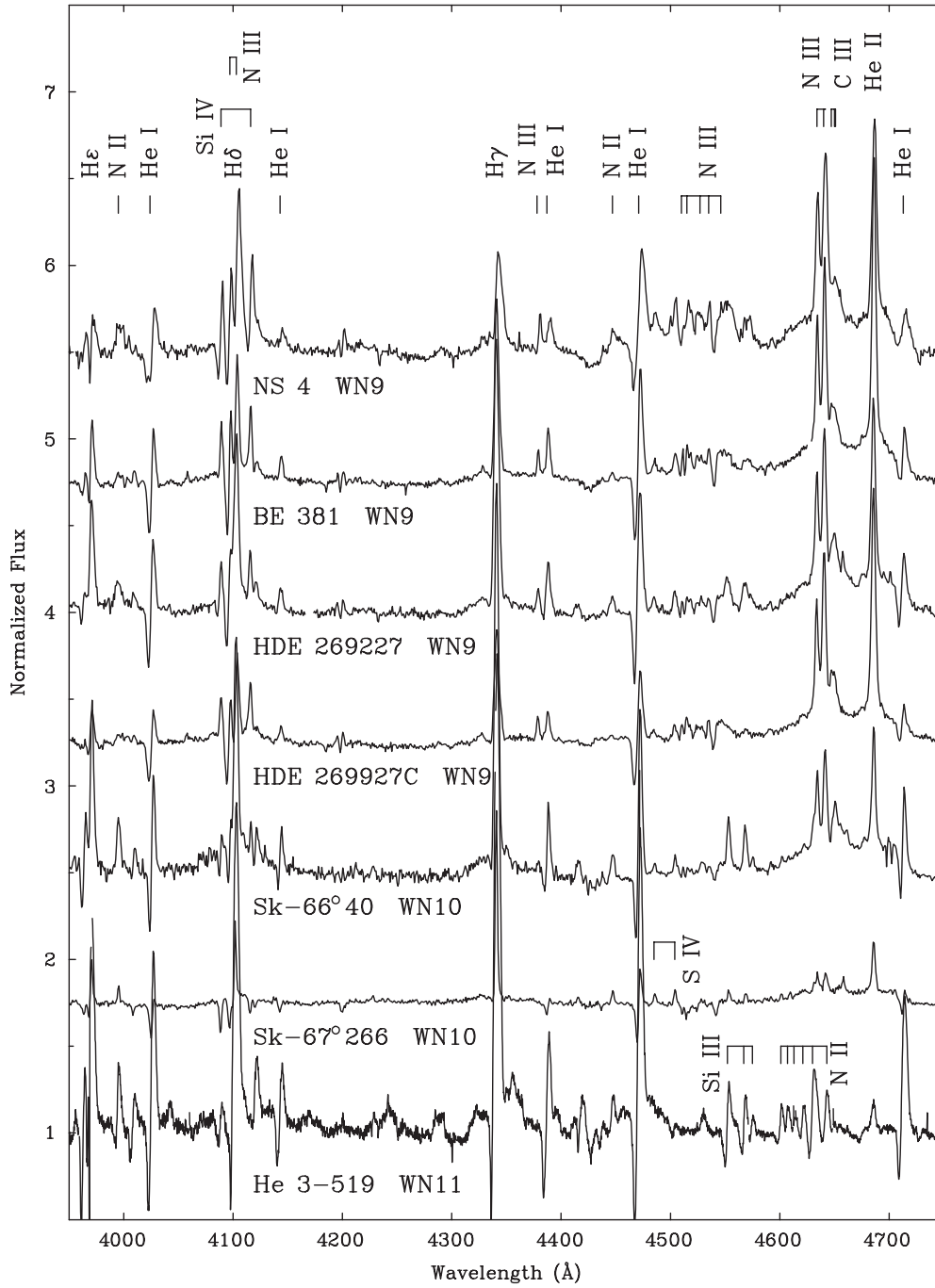


Figure 3.27 Ofpe/WN9 or WNVL Spectra. NS 4 and He 3-519 are in the Galaxy, while the other objects belong to the LMC. The spectral lines identified above are H Balmer $\lambda\lambda$ 3970, 4101, 4340; N II $\lambda\lambda$ 3995, 4447; He I $\lambda\lambda$ 4026, 4144, 4387, 4471, 4713; Si IV $\lambda\lambda$ 4089–4116; N III $\lambda\lambda$ 4097–4103, 4379, 4511–4515–4528–4535–4546, 4634–4640–4642; C III $\lambda\lambda$ 4647–4650/52; and He II λ 4686. In Sk-67° 266, S IV $\lambda\lambda$ 4486–4504 are marked, while in He 3-519, Si III $\lambda\lambda$ 4552–4568–4575 and N II $\lambda\lambda$ 4601–4607–4614–4621–4631–4643 are identified. Figure courtesy P. Crowther.

3.6 X-RAY LINE SPECTRA

The spectroscopic capabilities of the *Chandra* (and *XMM-Newton*) X-ray observatories permit for the first time the extension of the morphological techniques described above in the optical and UV domains to the X-ray line spectra of the OB stars. A *Chandra* program (PI W. Waldron) to fill gaps in the archival HR Diagram coverage has been conducted. Although such coverage to date remains sparse, it is now sufficient to support a preliminary investigation of the X-ray spectral systematics in relation to the optical spectral types of the stars. To that end, supergiant/(giant) and main-sequence/(giant) X-ray spectral sequences from *Chandra* HETGS data are displayed in Figures 3.28 and 3.29, respectively. It should be emphasized that these stars have been selected as normal representatives of their spectral types; e.g., the magnetic stars previously discussed also have peculiar X-ray spectra and must be omitted from the search for fundamental morphological trends.

The existence of such trends is readily apparent in the figures. First, the strongest lines migrate toward longer wavelengths with advancing spectral type, which is an ionization effect. Second, the ratios of the close pairs of He- and H-like ionic lines from Si, Mg, Ne, and O display correlations with the spectral types. For instance, the rapid declines in Mg XII/Mg XI in the early O supergiants, and of Si XIV/Si XIII on the early O main sequence, are noteworthy. (The weakness of the Mg XII line in the main-sequence spectra may be a luminosity effect, although current coverage is inadequate to establish that; the weakness of the Si XIV line in HD 93129 is a surprising anomaly for further investigation.) The reversal of the Ne X/Ne IX ratio in both sequences, despite interference from Fe XVII at the later types, is remarkable. Several of these objects are believed to be colliding-wind binaries, which nevertheless does not appear to obstruct the observed trends; neither does the range of extinctions among these stars, to which the ratios of close line pairs should be particularly insensitive.

These trends in the X-ray spectra of the OB stars as a function of the optical spectral types (and by implication, of the fundamental stellar parameters) are unexpected in some views of their origin, and they have not emerged from previous studies because of inadequate samples and current modeling uncertainties. In effect, the history of the discovery of the UV wind-profile systematics (O and B Atlases) appears to be repeating in the X-ray domain. The importance of pure morphological investigation of such trends, as emphasized in Chapter 1, is being demonstrated once again. Most likely, the physical origin of these correlations will be found in the winds themselves; in retrospect, that may not be so surprising in view of known relationships between bolometric and X-ray luminosities, as recently demonstrated in detail in NGC 6231 by Sana et al. (2006). These morphological results will provide strong guidance to further developments in physical models of the phenomena. Progress will likely be accelerated if astrophysics emulates some of the morphological techniques, e.g., by defining standard objects that are homogeneously reanalyzed whenever there are substantial revisions to the models, and by emphasizing the modeling of the powerfully

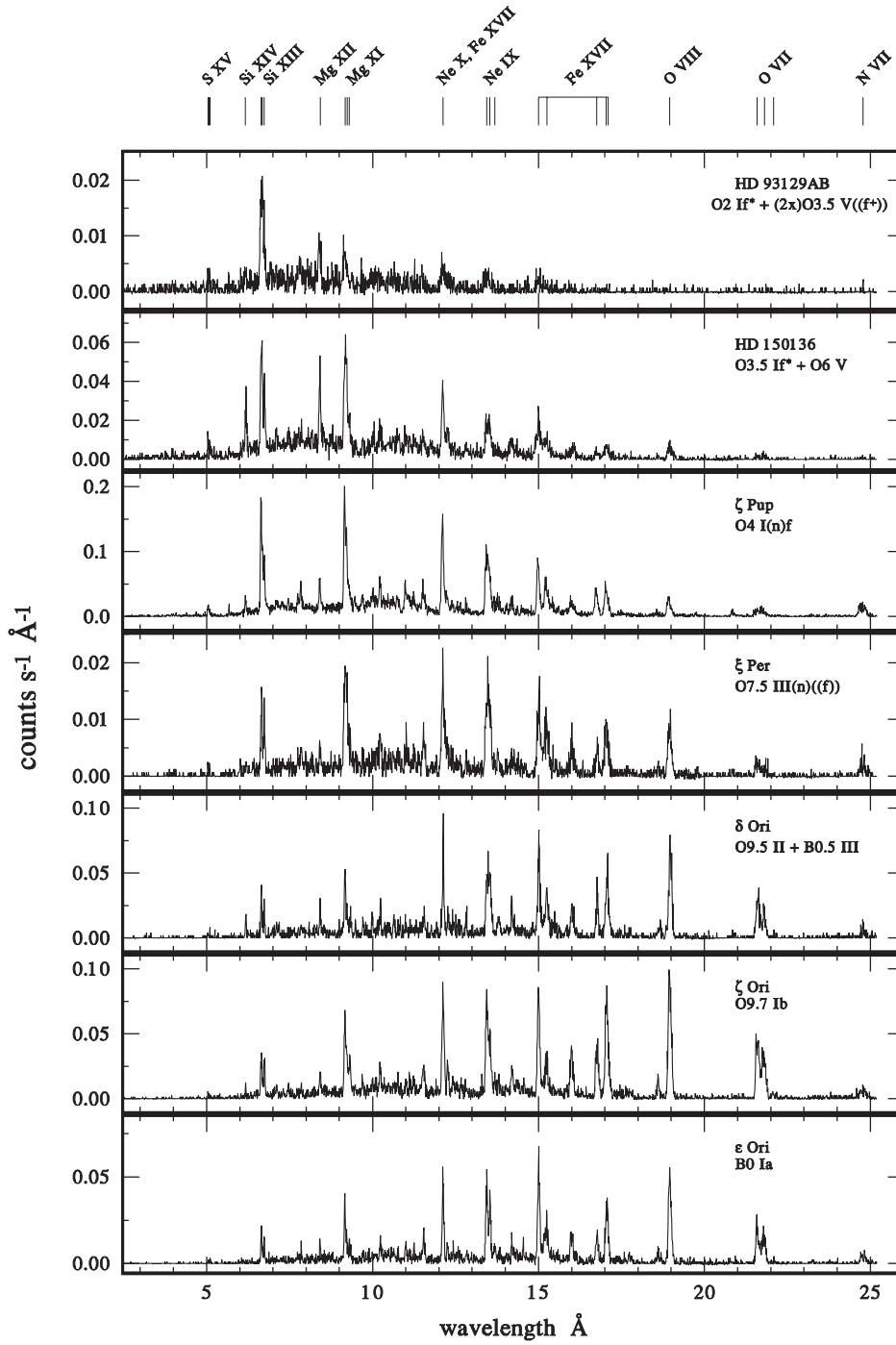


Figure 3.28 Sequence of OB Supergiant/(Giant) X-ray Spectra from *Chandra* (Walborn 2007a). The spectral lines identified (all with component substructure) are S XV $\lambda 5.1$, Si XIV $\lambda 6.2$, Si XIII $\lambda 6.7$, Mg XII $\lambda 8.4$, Mg XI $\lambda 9.2$, Ne X $\lambda 12.1$, Fe XVII $\lambda 12.2$, Ne IX $\lambda 13.5$, Fe XVII $\lambda\lambda 15.0$ – 15.3 – 16.8 – 17.1 , O VIII $\lambda 19.0$, O VII $\lambda 21.6$ – 21.8 – 22.1 , and N VII $\lambda 24.8$. Figure courtesy W. L. Waldron and Editorial Complutense S.A.. Reproduced from *UV Astronomy: Stars from Birth to Death*, with the permission of Editorial Complutense, 2007.

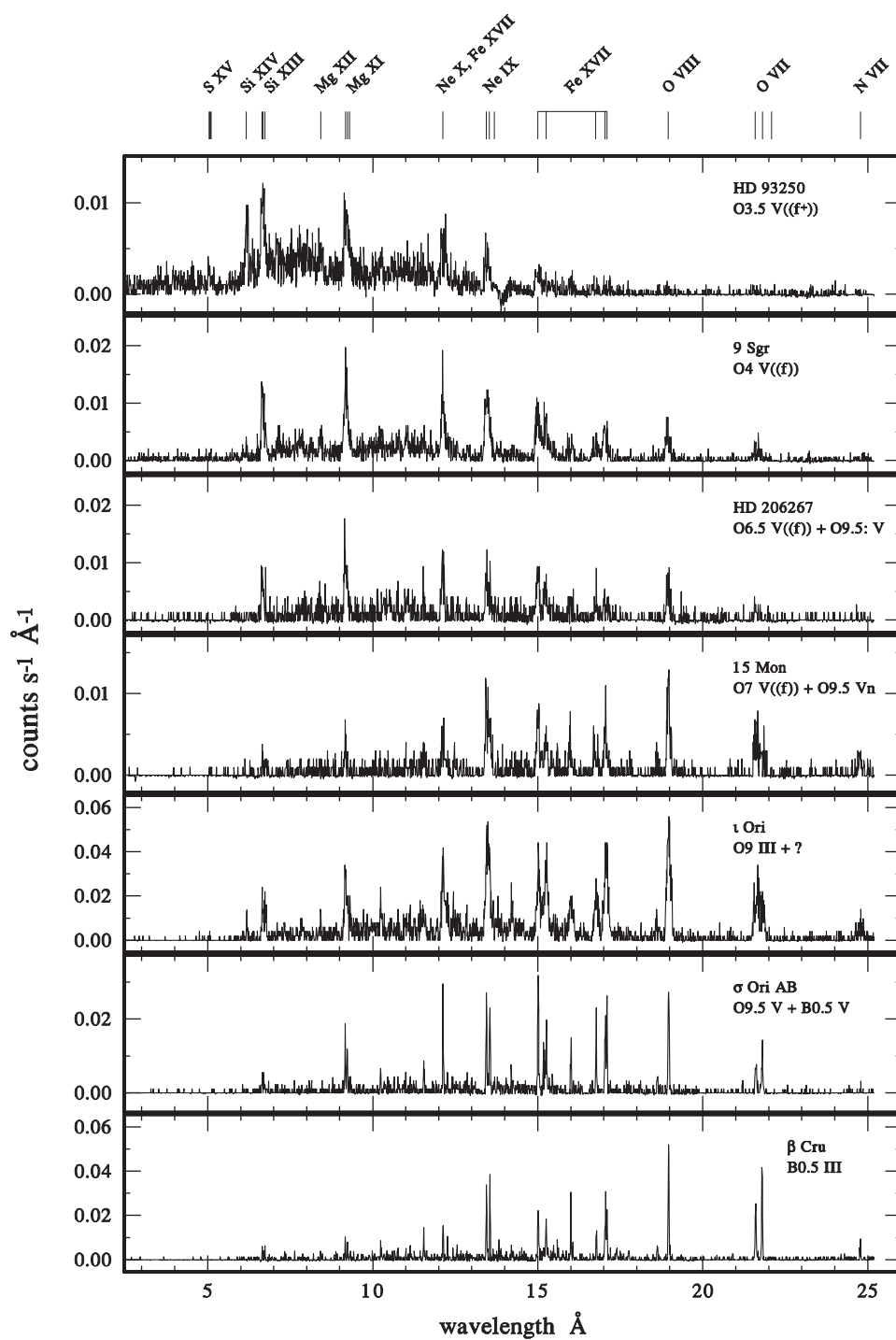


Figure 3.29 OB Main-Sequence/(Giant) X-ray Spectra from *Chandra* (Walborn 2007a). The identified line wavelengths are given in the Figure 28 caption. Figure courtesy W.L. Waldron and Editorial Complutense S. A.. Reproduced from *UV Astronomy: Stars from Birth to Death*, with the permission of Editorial Complutense, 2007.

Table 3.1 Averaged Absolute Magnitude Calibration for the O-type Stars

SpT	V	IV	III	II	Ib	Iab	Ia
O2-3	-5.6	...	-6.0	-6.8
O4	-5.5	...	-6.4:	-7.0
O5	-5.5	...	-6.4	-7.0
O6	-5.3	...	-5.6	...	-6.3:	...	-7.0
O6.5	-5.3	...	-5.6	...	-6.3:	...	-7.0
O7	-4.8	...	-5.6	-5.9	-6.3:	...	-7.0
O7.5	-4.8	...	-5.6	-5.9	-6.3:	...	-7.0
O8	-4.4	...	-5.6	-5.9	-6.2:	-6.5	-7.0
O8.5	-4.4	...	-5.6	-5.9	-6.2:	-6.5	-7.0
O9	-4.3	-5.0	-5.6	-5.9	-6.2	-6.5	-7.0
O9.5	-4.1	-4.7	-5.3	-5.9	-6.2	-6.5	-7.0
O9.7	-5.9	-6.2	-6.5	-7.0

diagnostic, relative trends in the HRD, as opposed to exclusive, absolute studies of one or a few objects in isolation.

3.7 CALIBRATION AND ASTROPHYSICAL MODELING

3.7.1 Atmospheres and Stellar Winds

The refined OB spectral classification system was calibrated in terms of absolute visual magnitudes by Walborn (1972, 1973, Table 3.1). A contemporaneous program led by P. Conti classified the O stars by means of measured equivalent-width ratios; although the MK notation was used in this work, it is operationally distinct from morphological classification. However, the measurements are essential for comparison with models, and ultimately good agreement between these parallel approaches was obtained (Conti & Leep 1974, and references therein). The selective-emission behavior of the N III $\lambda\lambda 4634-4640-4642$ triplet as a function of temperature and gravity was strikingly reproduced theoretically by Mihalas, Hummer, & Conti (1972) and Mihalas & Hummer (1973). Unfortunately, comparable explications of the other selective-emission effects (Walborn 2001) have not been published, although many of them are reproduced by state-of-the-art atmospheric/wind models; understanding of both the classification and the physics will be advanced when they are. The best physical calibrations to that time were presented by Vacca, Garmany, & Shull (1996).

Recently, the effective-temperature scale for the O stars has been revised downward from analyses with line-blanketed atmospheric and wind models (Martins, Schaerer, & Hillier 2002; Crowther et al. 2002; Herrero, Puls, & Najarro 2002; Bianchi & Garcia 2002; Hillier et al. 2003; Bouret et al. 2003; Lanz & Hubeny 2003; Repolust, Puls, & Herrero 2004; Evans et al. 2004; Mokiem et al. 2004). The derived bolometric luminosities and masses are reduced commensurately; some results of Martins, Schaerer, & Hillier (2005) are excerpted in Table 3.2.

Table 3.2 Stellar Parameters for O-type Stars

SpT	T_{eff} [K]	B.C.	$\log(L/L_{\odot})$	T_{eff} [K]	B.C.	$\log(L/L_{\odot})$
Luminosity Class V Stars				Luminosity Class I Stars		
O3	44852	-4.05	5.84	42233	-3.87	5.99
O4	42857	-3.91	5.67	40422	-3.74	5.93
O5	40862	-3.77	5.49	38612	-3.61	5.87
O5.5	39865	-3.70	5.41	37706	-3.54	5.84
O6	38867	-3.62	5.32	36801	-3.46	5.81
O6.5	37870	-3.55	5.23	35895	-3.39	5.78
O7	36872	-3.47	5.14	34990	-3.31	5.75
O7.5	35874	-3.39	5.05	34084	-3.24	5.72
O8	34877	-3.30	4.96	33179	-3.16	5.68
O8.5	33879	-3.22	4.86	32274	-3.08	5.65
O9	32882	-3.13	4.77	31368	-2.99	5.61
O9.5	31884	-3.04	4.68	30463	-2.91	5.57

3.7.2 Evolution

The recent advent of evolutionary models with rotation for O stars (Maeder & Meynet 2000) provides an important advance toward reality, while simultaneously complicating the interpretation of observations, since tracks with different initial rotations cross in the H-R Diagram and a given point no longer corresponds to a unique mass. In this context, the CNO abundances become an essential diagnostic, because the degree of mixing also depends on rotation. Accurate absolute abundance determinations in hot supergiants and causal enrichment predictions by the evolutionary models will be prerequisites to the full realization of their potential. When the former become available for a large sample of supergiants, it will be of interest to compare their CNO abundance distributions with that of rotational velocities on the main sequence. Such a connection is intuitively appealing: the evolved OC stars may have been atypically slow rotators on the main sequence, while the morphologically normal majority were typical, and the ON stars were the most rapid rotators. Those OB associations in which OBC spectra dominate the supergiant populations may have had systematically low initial rotations. Of course, care must be taken to discriminate post-red supergiants at lower masses, and mass-transfer binaries at all masses. Further observational and theoretical work is required to substantiate these possibilities, but they offer good prospects for improved understanding.

Meanwhile, some progress toward understanding pairs of contrasting objects in the above terms has already been made. For instance, a pair of stars in the SMC sharing the same HRD location but with OC7.5 III((f)) vs. (morphologically normal) O7 Iaf+ spectral types has been described by Walborn et al. (2000) and analyzed by Hillier et al. (2003). The analysis finds normal SMC abundances in the first star but greatly enhanced N in the second. Both can be understood as

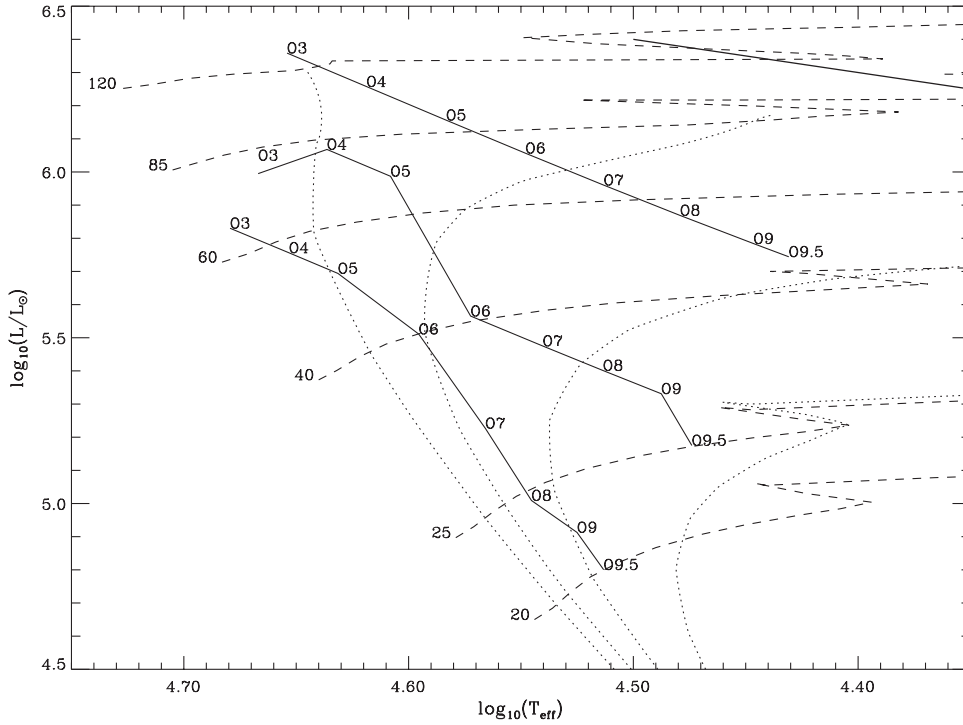


Figure 3.30 Spectral-Type Calibration for Luminosity Classes V, III, Ia (solid lines) Plotted onto Nonrotating Geneva Evolutionary Tracks (dashed lines) and Isochrones (dotted lines) (Walborn & Lennon 2003). The tracks are labeled in solar masses and the isochrones correspond to 1.6, 2.5, 4.0, and 6.3 Myr. The bold line at upper right is the Humphreys–Davidson Limit. See Walborn & Lennon (2003) for further details. Figure courtesy D. Lennon and reproduced by permission of the Astronomical Society of the Pacific.

initially $40M_{\odot}$ objects, with the OC star a slow rotator that has lost only about $1M_{\odot}$ and the O star an initially fast rotator that has lost about $10M_{\odot}$.

A first attempt to interpolate and extrapolate these analyses to all O spectral types and luminosity classes was made by Walborn & Lennon (2003), who plotted the calibrations onto nonrotating and 300 km sec^{-1} rotating Geneva evolutionary tracks and isochrones, as reproduced in Figures 3.30 and 3.31, respectively. Analyses to calibrate the new O2 spectral type are still in progress. Some outstanding inferences from these figures are that all nonrotating O spectral types are burning hydrogen in the core, whereas in contrast, rotating giants are near the hydrogen-exhaustion locus, and rotating supergiants are post-hydrogen burning. However, the latter stages are rapid and are believed to actually correspond to Wolf–Rayet spectra, so a possible implication is that O-type supergiants may derive only from initially slow rotators. (That interpretation appears to conflict with the one in the previous paragraph; however, those two stars have the same luminosity, which is unusually discrepant with the relative luminosity classifications, particularly for the supergiant.) The region between the O supergiant sequence and

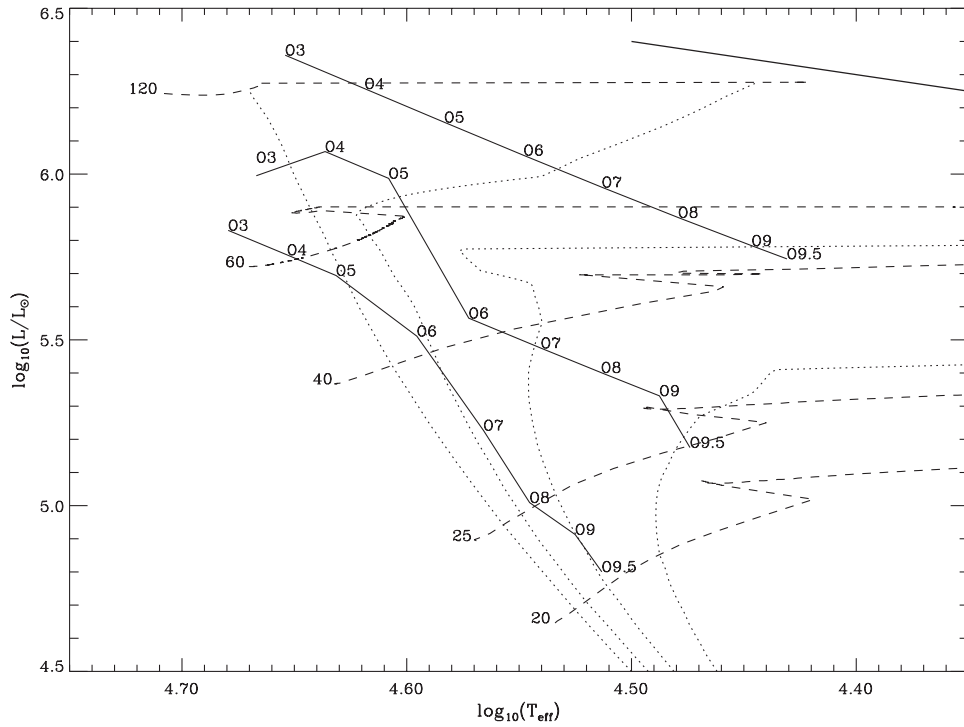


Figure 3.31 As Figure 3.30, but with Geneva Rotating Models (initial rotational velocity 300 km sec^{-1}) (Walborn & Lennon 2003). Figure courtesy D. Lennon and reproduced by permission of the Astronomical Society of the Pacific.

the Humphreys–Davidson Limit (Humphreys & Davidson 1979, 1994) in the figures is presumably the domain of some of the peculiar categories discussed in previous sections.

The O2–O3 spectral types display an unusually large range of luminosities and inferred masses at a given luminosity class (Walborn et al. 2002a). These types have strong spectral and spatial relationships with WN stars, which also have large ranges of stellar parameters at a given subtype. The latter can be understood in terms of their diverse formation channels, at least three of which are very massive single stars in giant H II regions, post-red supergiants at lower masses, and mass-transfer binaries down to still lower masses. If the O2–O3 stars are immediate WN progenitors in all of these channels, their large ranges of parameters can be similarly explained. Alternatively, the ON2 objects may diagnose homogeneous, blueward stellar evolution caused by very rapid rotation and consequent enhanced mixing (Walborn et al. 2004a, and references therein). The results of Morrell, Walborn, & Arias (2005) provide evidence for observable mixing effects on the O-type main sequence, which are not contemplated even in current rotating models.

The foregoing emphasizes the fact that many uncertainties and peculiar situations persist in the fundamental parameters of the O stars, let alone their

evolution. In addition, masses derived from evolutionary tracks tend to be higher than those from atmospheric analyses and spectroscopic binaries. The line-blanketed atmospheric models and evolutionary models with rotation have alleviated these discrepancies, but they are not completely resolved as discussed in the modeling references cited above. Of course, the large differences between initial and current masses due to mass loss, which are functions of metallicity and initial rotation, must be kept in mind. Moreover, some early O stars in close binary systems have remarkably low current masses, with the hotter component often the less massive (e.g., Morrell et al. 2003; Harries, Hilditch, & Howarth 2003); their structures are likely produced by evolution with mass transfer. The ongoing, developmental nature of current OB calibrations and modeling emphasizes the continuing vitality of morphological spectral classification, which provides precise descriptions of the phenomena that are independent of these uncertainties.

Bibliography

- Abt, H.A. 1979, ApJ, 230, 485
- Abt, H.A., Meinel, A.B., Morgan, W.W., & Tapscott, J.W. 1968, *An Atlas of Low-Dispersion Grating Stellar Spectra* (Tucson: Kitt Peak National Observatory)
- Andrillat, Y., & Vreux, J.M. 1975, AA, 41, 133
- Andrillat, Y., & Vreux, J.M. 1979, AA, 76, 221
- Auer, L.H., & Mihalas, D. 1974, ApJS, 24, 193
- Barnes, T.G., Lambert, D.L., & Potter, A.E. 1974, ApJ, 187, 73
- Bianchi, L., & Garcia, M. 2002, ApJ, 581, 610
- Bohannon, B., & Walborn, N.R. 1989, PASP, 101, 520
- Bouret, J.-C., Lanz, T., Hillier, D.J., Heap, S.R., Hubeny, I., Lennon, D.J., Smith, L.J., & Evans, C.J. 2003, ApJ, 595, 1182
- Bruhweiler, F.C., Kondo, Y., & McCluskey, G.E. 1981, ApJS, 46, 255
- Carruthers, G.R. 1968, ApJ, 151, 269
- Conti, P.S., & Ebbets, D. 1977, ApJ, 213, 438
- Conti, P.S., & Leep, E.M. 1974, ApJ, 193, 113
- Crowther, P.A., & Bohannon, B. 1997, AA, 317, 532
- Crowther, P.A., Hillier, D.J., Evans, C.J., Fullerton, A.W., De Marco, O., & Willis, A.J. 2002, ApJ, 579, 774
- Crowther, P.A., Lennon, D.J., & Walborn, N.R. 2006, AA, 446, 279
- Crowther, P.A., & Smith, L.J. 1997, AA, 320, 500
- Dallier, R., Boisson, C., & Joly, M. 1996, AA, 116, 239
- Donati, J.-F., Babel, J., Harries, T.J., Howarth, I.D., Petit, P., & Semel, M. 2002, MNRAS, 333, 55
- Donati, J.-F., Howarth, I.D., Bouret, J.-C., Petit, P., Catala, C., & Landstreet, J. 2006a, MNRAS, 365, L6
- Donati, J.-F., Howarth, I.D., Jardine, M.M., Petit, P., Catala, C., Landstreet, J.D., Bouret, J.-C., Alecian, E., Barnes, J.R., & Forveille 2006b, MNRAS, 370, 629
- Drew, J.E. 1989, ApJS, 71, 267
- Evans, C.J., Crowther, P.A., Fullerton, A.W., & Hillier, D.J. 2004, ApJ, 610, 1021
- Fitzpatrick, E.L. 1991, PASP, 103, 1123
- Gagné, M., Oksala, M.E., Cohen, D.H., Tonnesen, S.K., ud-Doula, A., Owocki, S.P., Townsend, R.H.D., & MacFarlane, J.J. 2005, ApJ, 628, 986
- Hanson, M.M., Conti, P.S., & Rieke, M.J. 1996, ApJS, 107, 281
- Hanson, M.M., Rieke, G.H., & Luhman, K.L. 1998, AJ, 116, 1915
- Hanson, M.M., et al. 2005, ApJS, 161, 154
- Harries, T.J., Hilditch, R.W., & Howarth, I.D. 2003, MNRAS, 339, 157

- Heap, S.R., Lanz, T., & Hubeny, I. 2006, *ApJ*, 638, 409
- Henize, K.G., Wray, J.D., Parsons, S.B., Benedict, G.F., Bruhweiler, F.C., Rybski, P.M., & Ocallaghan, F.G. 1975, *ApJ*, 199, L119
- Herrero, A., Puls, J., & Najarro, F. 2002, *AA*, 396, 949
- Hillier, D.J., Lanz, T., Heap, S.R., Hubeny, I., Smith, L.J., Evans, C.J., Lennon, D.J., & Bouret, J.C. 2003, *ApJ*, 588, 1039
- Hiltner, W.A., & Schild, R.E. 1966, *ApJ*, 143, 770
- Howarth, I.D. 2004, in *IAU Symp. 215, Stellar Rotation*, ed. A. Maeder & P. Eenens (San Francisco: ASP), 33
- Howarth, I.D., & Smith, K.C. 2001, *MNRAS*, 327, 353
- Howarth, I.D., et al. 2007, *MNRAS*, 381, 433
- Humphreys, R.M., & Davidson K. 1979, *ApJ*, 232, 409
- Humphreys, R.M., & Davidson K. 1994, *PASP*, 106, 1025
- Hubrig, S., Briquet, M., Schöller, M., De Cat, P., Mathys, G., & Aerts, C. 2006, *AA*, 369, L61
- Johnson, H.L., & Morgan, W.W. 1953, *ApJ*, 117, 313
- Kenworthy, M.A., & Hanson, M.M. 2003, *PASP*, 116, 97
- Lamers, H.J.G.L.M., Snow, T.P., & Lindholm, D.M. 1995, *ApJ*, 455, 269
- Lancon, A., & Rocca-Volmerange, B. 1992, *AA*, 96, 593
- Lanz, T., & Hubeny, I. 2003, *ApJS*, 146, 417
- Lennon, D.J. 1997, *AA*, 317, 871
- Levato, H., & Malaroda, S. 1981, *PASP*, 93, 714
- Levato, H., & Malaroda, S. 1982, *PASP*, 94, 807
- Lloyd, C., Stickland, D.J., & Walborn, N.R. 1995, *PASP*, 107, 1030
- Maeder, A., & Conti, P.S. 1994, *ARAA*, 32, 227
- Maeder, A., & Meynet, G. 2000, *ARAA*, 38, 143
- Maíz-Apellániz, J., Walborn, N.R., Galué, H.A., & Wei, L.H. 2004, *ApJS*, 151, 103
- Martins, F., Schaerer, D., & Hillier, D.J. 2002, *AA*, 382, 999
- Martins, F., Schaerer, D., & Hillier, D.J. 2005, *AA*, 436, 1049
- Mihalas, D. 1978, *Stellar Atmospheres*, 2nd Edition (San Francisco: Freeman)
- Mihalas, D., & Hummer, D.G. 1973, *ApJ*, 179, 827
- Mihalas, D., Hummer, D.G., & Conti, P.S. 1972, *ApJ*, 175, L99
- Mihalas, D., & Lockwood, G.W. 1974, *ApJ*, 175, 757
- Miller, F.D. 1954, *ApJ*, 120, 265
- Mokiem, M.R., Martín-Hernández, N.L., Lenorzer, A., de Koter, A., & Tielens, A.G.G.M. 2004, *AA*, 419, 319
- Morgan, W.W. 1951, *Pub. Michigan Obs.*, 10, 33
- Morgan, W.W., Abt, H.A., & Tapscott, J.W. 1978, *Revised MK Spectral Atlas for Stars Earlier than the Sun* (Williams Bay, WI: Yerkes Observatory)
- Morgan, W.W., & Keenan P.C. 1973, *ARAA*, 11, 29
- Morgan, W.W., Keenan, P.C., & Kellman, E. 1943, *An Atlas of Stellar Spectra* (Chicago: University of Chicago Press)
- Morrell, N., Ostrov, P., Massey, P., & Gamen, R. 2003, *MNRAS*, 341, 583

- Morrell, N.I., Walborn, N.R., & Arias, J.I. 2005, *PASP*, 117, 699
- Morris, P.W., et al. 1996, *ApJ*, 470, 597
- Morton, D.C., Jenkins, E.B., & Bohlin, R.C. 1968, *ApJ*, 154, 661
- Najarro, F., et al. 1994, *AA*, 285, 573
- Najarro, F., et al. 1998, *Proc. 2nd Boulder-Munich Workshop*, *PASPC* 131, 57
- Nazé, Y. 2004, thesis, Université de Liège
- Nazé, Y., Vreux, J.-M., & Rauw, G. 2001, *AA*, 372, 195
- Negueruela, I., Steele, I.A., & Bernabeu, G. 2004, *AN*, 325, 749
- Nota, A., Livio, M., Clampin, M., & Schulte-Ladbeck, R. 1995, *ApJ*, 448, 788
- Parker, J.Wm., Garmany, C.D., Massey, P., & Walborn, N.R. 1992, *AJ*, 103, 1205
- Pasquali, A., Langer, N., Schmutz, W., Leitherer, C., Nota, A., Hubeny, I., & Moffat, A.F.J. 1997, *ApJ*, 478, 340
- Pasquali, A., Nota, A., & Clampin, M. 1999, *AA*, 343, 536
- Pauldrach, A.W.A., Kudritzki, R.P., Puls, J., & Butler, K. 1990, *AA*, 228, 125
- Pellerin, A., Fullerton, A.W., Robert, C., Howk, J.C., Hutchings, J.B., Walborn, N.R., Bianchi, L., Crowther, P.A., & Sonneborn, G. 2002, *ApJS*, 143, 159
- Penny, L.R., Gies, D.R., & Bagnuolo, W.G., Jr. 1996, *ApJ*, 460, 906
- Plaskett, J.S., & Pearce, J.A. 1931, *Pub. Dominion Ap. Obs.*, 5, 99
- Ramirez-Ruiz, E. 2006, *Nature*, 440, 154
- Repolust, T., Puls, J., & Herrero, A. 2004, *AA*, 415, 349
- Repolust, T., et al. 2005, *AA*, 440, 261
- Rieke, G.H., & Lebofsky, M.J. 1985, *ApJ*, 288, 618
- Rountree, J., & Sonneborn, G. 1991, *ApJ*, 369, 515
- Rountree, J., & Sonneborn, G. 1993, *Spectral Classification with the International Ultraviolet Explorer: An Atlas of B-Type Spectra*, NASA RP 1312
- Sana, H., Rauw, G., Nazé, Y., Gosset, E., & Vreux, J.-M. 2006, *MNRAS*, 372, 661
- Smith, K.C., & Howarth, I.D. 1994, *AA*, 290, 868
- Smith, M.A. & Fullerton, A.W. 2005, *PASP*, 117, 13
- Snow, T.P., Jr., & Morton, D.C. 1976, *ApJS*, 32, 429
- Stahl, O., Kaufer, A., Rivinius, Th., Szeifert, Th., Wolf, B., Gäng, Th., Gummersbach, C.A., Jankovics, I., Kovács, J., Mandel, H., Pakull, M., & Peitz, J. 1996, *AA*, 312, 539
- Stahl, O., Wolf, B., Klare, G., Cassatella, A., Krautter, J., Persi, P., & Ferrari-Toniolo, M. 1983, *AA*, 127, 49
- Swings, P., & Jose, P.D. 1950, *ApJ*, 111, 513
- Townsend, R.H.D., Owocki, S.P., & Groote, D. 2005, *ApJ*, 630, L81
- Underhill, A.B. 1966, *The Early Type Stars* (Dordrecht: Reidel)
- Vacca, W.D., Garmany, C.D., & Shull, J.M. 1996, *ApJ*, 460, 914
- Vreux, J.M., & Andriolat, Y. 1979, *AA*, 75, 93
- Wade, G.A., Fullerton, A.W., Donati, J.-F., Landstreet, J.D., Petit, P., & Strasser, S. 2006, *AA*, 451, 195
- Walborn, N.R. 1971a, *ApJS*, 23, 257
- Walborn, N.R. 1971b, *ApJ*, 164, L67
- Walborn, N.R. 1971c, *ApJ*, 167, L31

- Walborn, N.R. 1972, *AJ*, 77, 312
- Walborn, N.R. 1973, *AJ*, 78, 1067
- Walborn, N.R. 1974, *ApJ*, 189, 269
- Walborn, N.R. 1976, *ApJ*, 205, 419
- Walborn, N.R. 1977, *ApJ*, 215, 53
- Walborn, N.R. 1980, *ApJS*, 44, 535
- Walborn, N.R. 1982, *ApJ*, 256, 452
- Walborn, N.R. 1983, *ApJ*, 265, 716
- Walborn, N.R. 1984b, *ApJ*, 286, 718
- Walborn, N.R. 1988, in *IAU Colloq. 108, Atmospheric Diagnostics of Stellar Evolution* (Lecture Notes in Physics, Vol. 305), ed. K. Nomoto (Berlin: Springer), 70
- Walborn, N.R. 2000, *PASP*, 112, 50
- Walborn, N.R. 2001, in *ASP Conf. Ser., 242, Eta Carinae & Other Mysterious Stars*, ed. T. Gull, S. Johansson, & K. Davidson (San Francisco: ASP), 217
- Walborn, N.R. 2003a, in *A Massive Star Odyssey-From Main Sequence to Supernova*, Proceedings of IAU Symposium 212, eds. K. van der Hucht, A. Herrero & C. Esteban (San Francisco-ASP), 13
- Walborn, N.R. 2003b, in *ASP Conf. Ser., 304, CNO in the Universe*, ed. C. Charbonnel, D. Schaerer, & G. Meynet (San Francisco: ASP), 29
- Walborn, N.R. 2007a, in *UV Astronomy-Stars from Birth to Death* Joint Discussion 4, IAU XXVIth General Assembly, Prague, ed. A.I. Gómez de Castro & M.A. Barstow (Madrid-Editorial Complutense, S.A.), 45
- Walborn, N.R. 2007b, arXiv:astro-ph/0701573
- Walborn, N.R., & Blades, J.C. 1997, *ApJS*, 112, 457
- Walborn, N.R., & Bohlin, R.C. 1996, *PASP*, 108, 477
- Walborn, N.R., Ebbets, D.C., Parker, J.Wm., Nichols-Bohlin, J., & White, R.L. 1992, *ApJ*, 393, L13
- Walborn, N.R., & Fitzpatrick, E.L. 1990, *PASP*, 102, 379
- Walborn, N.R., & Fitzpatrick, E.L. 2000, *PASP*, 112, 50
- Walborn, N.R., Fullerton, A.W., Crowther, P.A., Bianchi, L., Hutchings, J.B., Pellerin, A., Sonneborn, G., & Willis, A.J. 2002b, *ApJS*, 141, 443
- Walborn, N.R., & Howarth, I.D. 2000, *PASP*, 112, 1446
- Walborn, N.R., Howarth, I.D., Herrero, A., & Lennon, D.J. 2003, *ApJ*, 588, 1025
- Walborn, N.R., Howarth, I.D., Lennon, D.J., Massey, P., Oey, M.S., Moffat, A.F.J., Skalkowski, G., Morrell, N.I., Drissen, L., & Parker, J.Wm. 2002a, *AJ*, 123, 2754
- Walborn, N.R., Howarth, I.D., Rauw, G., Lennon, D.J., Bond, H.E., Negueruela, I., Nazé, Y., Corcoran, M.F., Herrero, A., & Pellerin, A. 2004b, *ApJ*, 617, L61
- Walborn, N.R., & Lennon, D.J. 2003, in *IAU Symp. 215, Stellar Rotation*, ed. A. Maeder & P. Eenens (San Francisco: ASP), 512
- Walborn, N.R., Lennon, D.J., Haser, S.M., Kudritzki, R.-P., & Voels, S.A. 1995, *PASP*, 107, 104

- Walborn, N.R., Lennon, D.J., Heap, S.R., Lindler, D.J., Smith, L.J., Evans, C.J., & Parker, J.Wm. 2000, PASP, 112, 1243
- Walborn, N.R., Morrell, N.I., Howarth, I.D., Crowther, P.A., Lennon, D.J., Massey, P., & Arias, J.I. 2004a, ApJ, 608, 1028
- Walborn, N.R., & Nichols, J.S. 1994, ApJ, 425, L29
- Walborn, N.R., Nichols-Bohlin, J., & Panek, R.J. 1985, *International Ultraviolet Explorer Atlas of O-Type Spectra from 1200 to 1900 Å*, NASA RP 1155
- Walborn, N.R., & Panek, R.J. 1984a, ApJ, 280, L27
- Walborn, N.R., & Parker, J.Wm. 1992, 399, L87
- Walborn, N.R., Parker, J.Wm., & Nichols, J.S. 1995, *International Ultraviolet Explorer Atlas of B-Type Spectra from 1200 to 1900 Å*, NASA RP 1363
- Werner, K., & Rauch, T. 2001, in ASP Conf. Ser. 242, *Eta Carinae & Other Mysterious Stars*, ed. T. Gull, S. Johansson, & K. Davidson (San Francisco: ASP), 229

Chapter Four

The B-type Stars

4.1 INTRODUCTION

The B-type stars have played important roles in the development of the MK Classification system, stellar astrophysics, and our knowledge of Galactic structure. The first large-scale classification surveys of stars on the MK System were of the bright B-type stars, largely carried out by Morgan and collaborators in the 1950s and Hiltner, Garrison, and Schild in the 1960s. Those classification studies of thousands of B-type stars led to the discovery and mapping of the spiral structure of the Milky Way. Garrison's work on the MK classification of B-type stars in open clusters was important for the determination of both distances and ages of those clusters. The emission-line B-type stars—the Be stars—have long been favorite subjects of investigation by stellar astronomers, and have stimulated studies of circumstellar environments. Finally, B-type stars, with their “simple” radiative atmospheres, were important in the early development of stellar-atmosphere models under the assumption of local thermodynamic equilibrium (LTE) and later in the development of non-LTE atmosphere models and theories of spectral-line formation.

4.2 OPTICAL CLASSIFICATION

4.2.1 Temperature Classification

The B spectral class was originally defined as being comprised of those stars that show lines of He I in the absence of lines of He II in the blue-violet. However, as was mentioned in the previous chapter, modern, high S/N spectra show lines of He II as late as B0.5 (see, for instance, the B0 spectrum in Figure 4.1); while, at the cool end of the B-type stars, some A0 stars show weak lines of He I. The blue-violet spectra of B-type stars are dominated by the Balmer lines of hydrogen and lines of neutral helium (He I). The Balmer lines strengthen through the B-type stars into the A-type stars, coming to a maximum at a spectral type of A2 in the dwarfs, but also show a marked luminosity sensitivity, especially in the late B-type stars. Lines of neutral helium first show up in the O-type stars, strengthen through the O-type stars, come to a maximum at a spectral type of B2 on the main sequence, and then weaken toward later (cooler) types, finally disappearing from classification spectra at a spectral type of about A0 (see Figures 4.1 and 4.2).

Were it not for the fact that a significant proportion of B-type stars show helium-abundance anomalies (see §4.4), the combination of the behavior of the He I lines

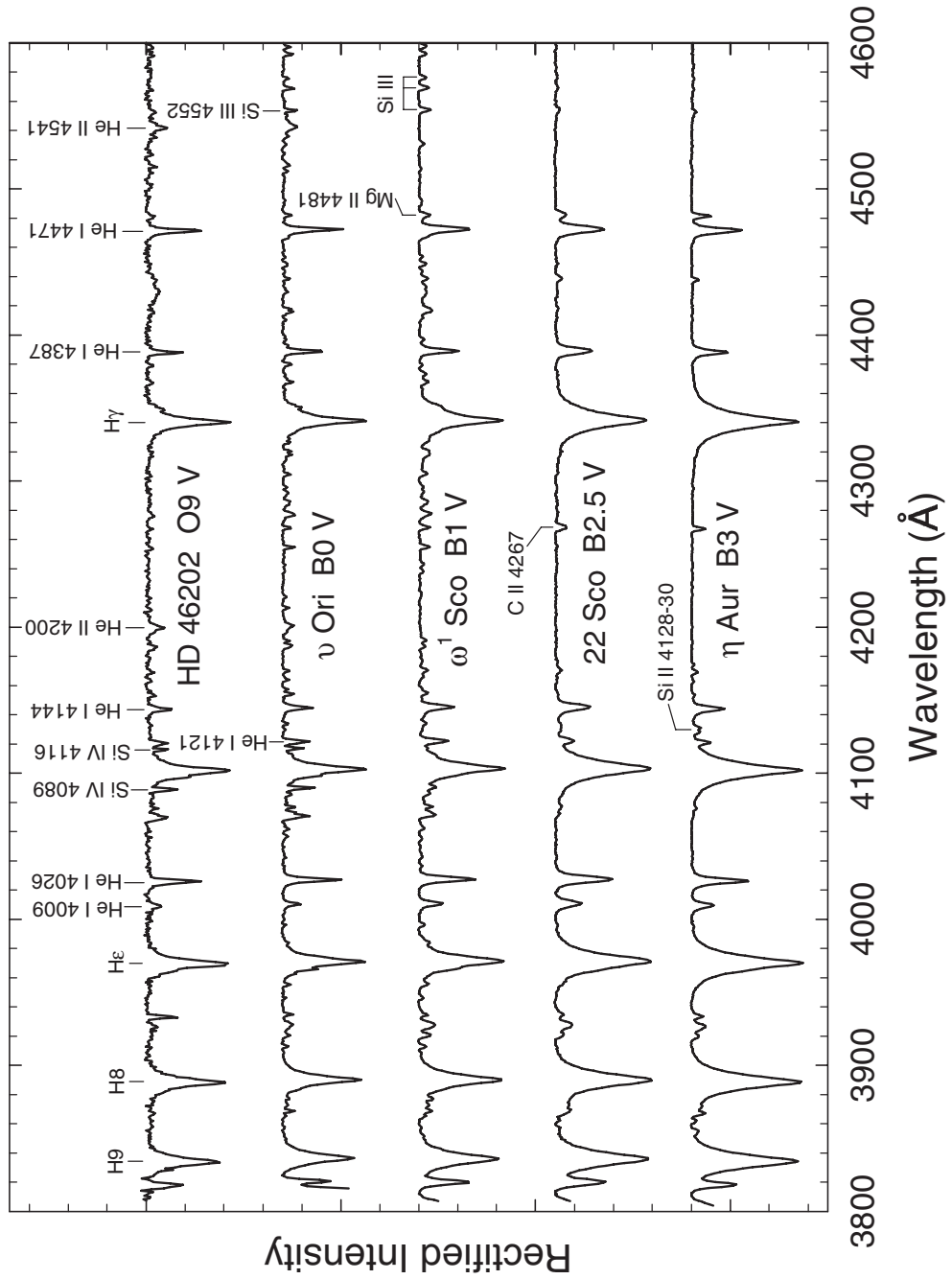


Figure 4.1 The main sequence from O9 to B3 in the blue-violet. Features useful in temperature classification are labeled; note the behavior of the He I lines that come to a maximum at B2. Spectra obtained at the Dark Sky Observatory. Spectra are offset vertically by 0.7 continuous units.

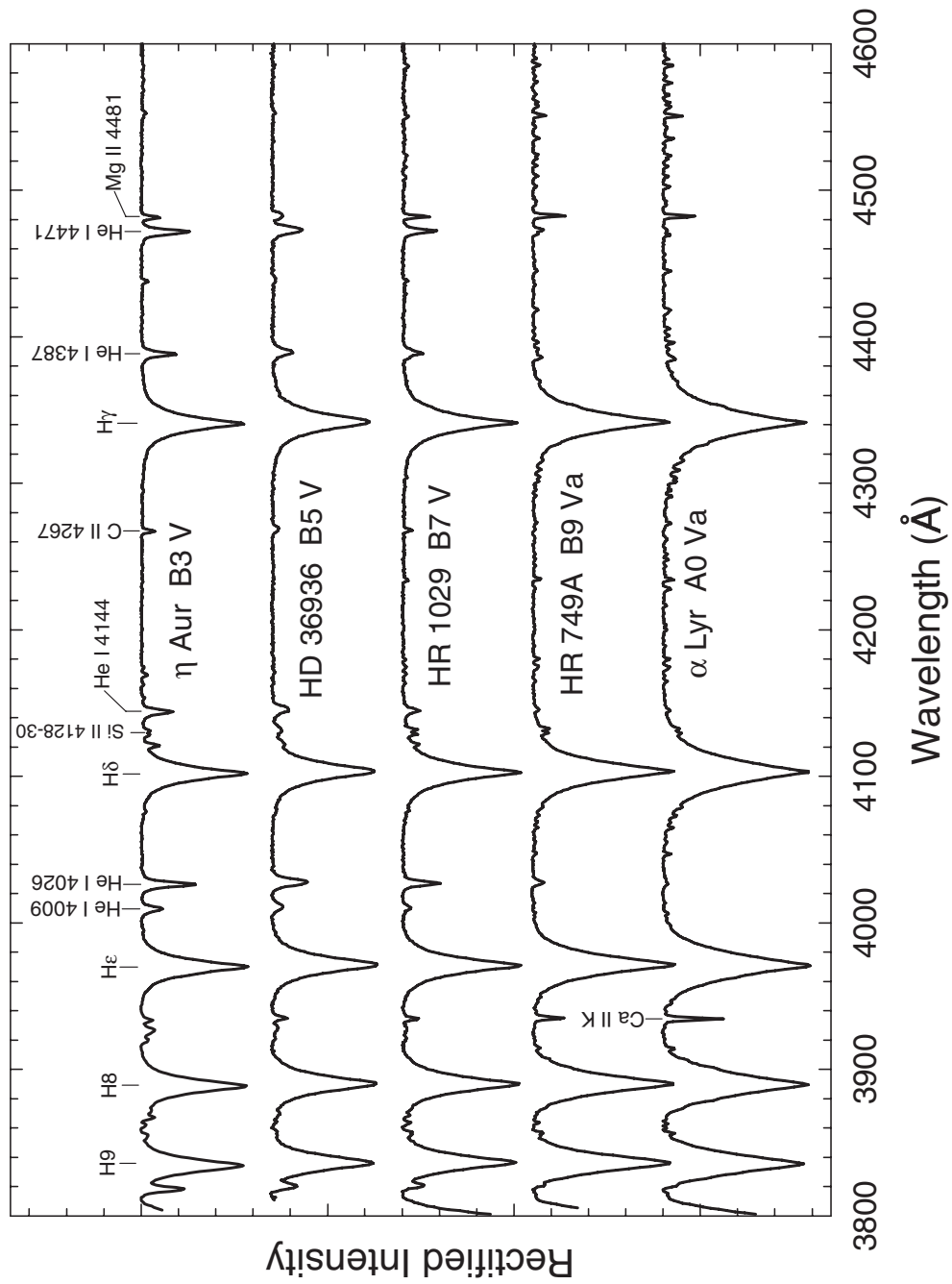


Figure 4.2 The main sequence from B3 to A0 in the blue-violet. Features useful in temperature classification are labeled. Note the behavior of the hydrogen lines that come to a maximum at about A2. Spectra obtained at the Dark Sky Observatory.

and the strengthening of the Balmer lines (despite the luminosity sensitivity of both features) would allow the precise temperature classification of the B-type stars. However, the presence of helium abundance anomalies forces classifiers to rely in the early B-type stars on ratios of lines of silicon ions to determine the temperature type. In particular, as described in Chapter 3, to distinguish between temperature classes B0, B0.2, B0.5, B0.7, and B1, Si IV/Si III ratios, especially Si IV $\lambda 4089$ /Si III $\lambda 4552$, which is about unity at B0.7, should be used. Between B1 and B3, Si III/Si II ratios, in particular Si III $\lambda 4552$ /Si II $\lambda 4128-32$, are employed. It should be noted that the Si IV/Si III and the Si III/Si II ratios are also luminosity sensitive, so the temperature type and the luminosity type must be determined iteratively. These lines are fairly weak in classification spectra, and so high S/N spectra are required for precise classification.

The high-excitation line Mg II $\lambda 4481$ slowly strengthens through the B-type stars, and so a useful ratio for judging the temperature type in helium-normal stars later than B3 is He I $\lambda 4471$ /Mg II $\lambda 4481$. Figures 4.1 and 4.2 illustrate a temperature sequence for the main-sequence B-type stars. Notice in both these figures that the lines of Si IV and Si III, seen in the spectra of early B-type stars, fade completely from view in classification spectra for main-sequence stars of spectral type B3 and later. The weakening of the He I lines contrasted with the strengthening of the Balmer lines with declining temperature is thus the prime classification criterion for the late B-type stars.

While the temperature classification of helium-normal B-type stars is relatively straightforward, the classifier must be aware of a number of subtleties. One of these, which commonly causes confusion, is the so-called “diagonal effect.” It is important to understand that the dominant broadening mechanism for both the Balmer lines and the He I lines is the *Stark effect*, due to the interaction of the atom with electrons and ions (see §5.2.4 for a more detailed explanation of this effect). As a consequence, in the early B-type stars, both the Balmer lines and the He I lines are narrower and shallower at higher luminosities (see §4.2.2 and Figure 3.5; in the mid B-type stars, the He I lines actually narrow and *deepen* with increasing luminosity—see Figure 4.4). Therefore, in the early B-type stars, where both the Balmer lines and the He I lines strengthen with declining temperature, an evolved B-type star can appear superficially like that of a hotter B dwarf. This *spectroscopic degeneracy* can be resolved by relying on other criteria, namely the Si IV/Si III and the Si III/Si II ratios mentioned above and also a detailed inspection of the hydrogen-line profiles. Other effects the classifier must look out for are the helium-strong and the helium-weak stars. While the helium-strong stars are usually unmistakable, helium-weak stars can mimic cooler B-type stars and fool the unwary classifier. Details on the classification of such stars can be found in §4.4.1 and §4.4.2 below.

SYSTEMATIC EFFECTS WITH ROTATION

Rapid rotation can lead to systematic effects in the classification of the B-type stars. Figure 4.3 shows how the ratio He I $\lambda 4471$ /Mg II $\lambda 4481$, useful in the tem-

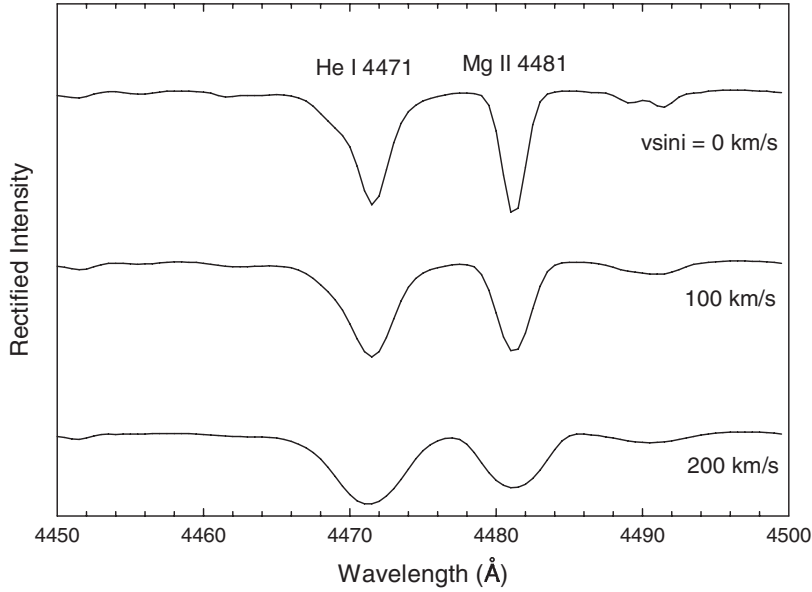


Figure 4.3 The effect of rotation on the He I $\lambda 4471$ /Mg II $\lambda 4481$ line ratio. This figure is based on synthetic spectra.

perature classification of the late B-type stars, is affected by rotation. This figure shows a synthetic spectrum calculated at $T_{\text{eff}} = 13,000$ K, $\log(g) = 4.0$, and rotationally broadened. Notice that at this effective temperature, at low projected rotational velocities ($v \sin i$), the ratio of the line *depths* is <1 , whereas at high rotational velocities the ratio reverses. This happens because He I $\lambda 4471$ has an intrinsically broader profile than Mg II $\lambda 4481$. This can lead to serious systematic effects in spectral classification. One solution is to look at the line *areas* (e.g., equivalent widths) rather than line depths. An even better solution is to use rapidly rotating standards to classify rapidly rotating program stars. Garrison & Gray (1994) have designated a number of rapidly rotating standards for the late B-type stars, but this has not yet been done for stars earlier than B7. See §5.2.3 for a more general discussion on rotation and spectral classification.

4.2.2 Luminosity Classification

The spectral criteria used in the luminosity classification of the B-type stars depend on the spectral type. Throughout the B-type stars the width and strength of the Balmer lines are useful luminosity criteria, although the luminosity sensitivity of the Balmer lines is greatest in the late B-type stars. In the early B-type stars (B2 and earlier) the O II lines ($\lambda 4070$, $\lambda 4076$, $\lambda 4348$, and $\lambda 4416$) are quite strong and increase in strength with increasing luminosity. These lines, when used in ratio with the Balmer lines and the He I lines (both of which weaken with increasing luminosity), constitute quite sensitive luminosity criteria. The ratios He I $\lambda 4026$ /O II $\lambda 4070$, $\lambda 4076$, He I $\lambda 4387$ /O II $\lambda 4416$, and $H\gamma$ /O II $\lambda 4348$ are useful.

However, since the discovery of CNO peculiarities in O and early B-type stars (see §3.5.1), the luminosity classification of the early B-type stars has shifted to ratios of lines of silicon ions to He I. In particular (see §3.2.2) Si IV $\lambda 4116$ /He I $\lambda 4121$ is used for stars as late as B0.7, and Si III $\lambda 4522$ /He I $\lambda 4387$ for stars as late as B5. Figure 3.5 illustrates these criteria in a luminosity sequence at B1.

In the late B-type stars (B3 and later), the luminosity-sensitive O II and Si IV lines mentioned above are very weak and cannot be used for luminosity classification. While the Si III $\lambda 4522$ line continues to be useful until about B5, and the N II $\lambda 3995$ line may be used to separate the supergiant classes at B5, luminosity classification of the late B-type stars relies on the negative luminosity effect of the Balmer lines (see Figure 4.4). The profiles of these Balmer lines are sensitive to both luminosity and temperature, and so even in helium-strong and helium-weak stars, where the He I lines cannot be used in temperature classification, the Balmer lines may be used (except in the more extreme helium-anomaly cases) to determine both the temperature class and the luminosity class. Indeed, the best procedure to follow in the late B-type stars is an iterative one. First, use the Balmer lines in an iterative fashion to obtain a temperature and luminosity class. Then, check to see if the strengths of the He I lines are consistent with this spectral type; if they are, they can then be used to refine the spectral type. If not, this means that the star has a peculiar helium abundance, and may possibly show other spectral peculiarities. See §4.4 to learn how to treat chemical peculiarities in the classification of B-type stars.

4.3 THE ULTRAVIOLET

4.3.1 History and Relation to the Optical

The development of the classification of B-type stars in the ultraviolet was similar to that for O-type stars as access to this spectral region grew through rocket- and satellite-borne instruments (see §3.3). The motivation was also the same: to observe these stars near their peak in the Planck energy curve. Early satellite studies, such as Panek & Savage (1976), showed a correlation between UV line features and MK classification types in the optical. That correlation remained true for Heck et al. (1984) when they published an atlas of over 200 low-dispersion International Ultraviolet Explorer (IUE) spectra from O3 to G5. They listed lines characteristic of O- and B-type stars and some that showed a luminosity effect in B-type stars. More precision was achieved by Rountree & Sonneborn (1991) when they developed spectral type and luminosity criteria that applied to far-UV (FUV) B-type spectra with the same resolution, namely 0.25 \AA or about $R = 5000$, as used by Nolan Walborn and his collaborators. To maintain consistency with MK types, they found it important to use only photospheric absorption lines in their classification and not the resonance lines originating in stellar winds that would occasionally show anomalous strengths in the early- to mid-B type stars. Thus they improved the scheme proposed in Heck et al.'s low-dispersion spectral atlas.

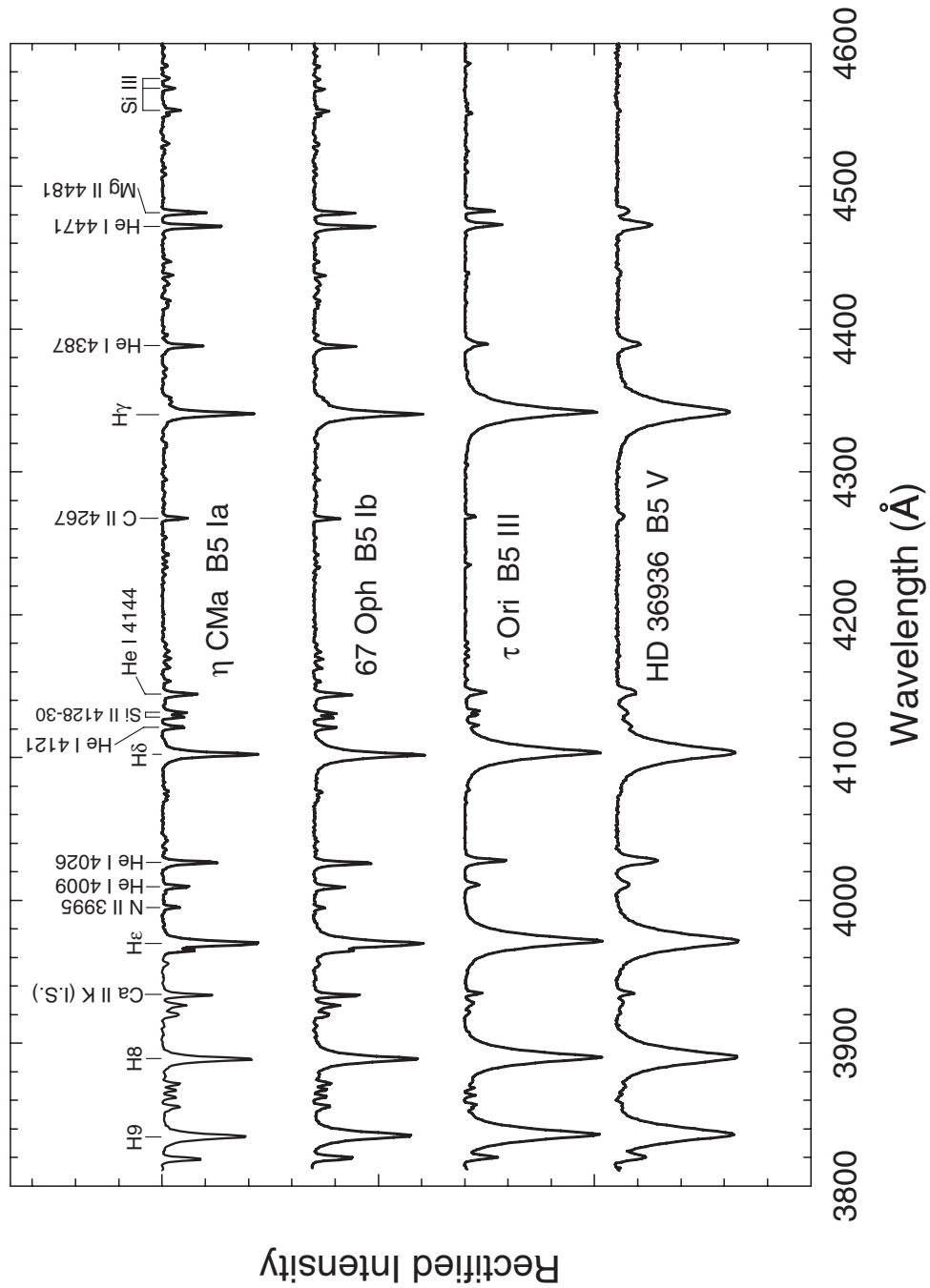


Figure 4.4 Luminosity effects at B5. The primary luminosity discriminant at B5 are the hydrogen Balmer lines. However, lines of N II and Si III may be used to discriminate between supergiant classes. Spectra obtained at the Dark Sky Observatory.

Slettebak (1994) did a careful analysis of FUV lines in normal B and Be stars and, by plotting the ratios of equivalent-widths with spectral types, showed the basis for the Rountree & Sonneborn classification scheme.

“FUV” has been used in the sense of §3.3, namely the region 1200–2000 Å. In the even further UV, that covered by the FUSE satellite (900–1200 Å), there has been analysis of individual B-type stars, but no proposal for a systematic classification scheme, at least of the less evolved stars. Part of the reason for this was pointed out in §3.3.2, namely the interstellar extinction produced by even moderate amounts of H_2 .

4.3.2 Temperature Criteria

Figures 4.5, 4.6, and 4.7 show temperature sequences for B-type dwarfs in the low and high resolutions. For both resolutions the most useful ratios are Si II λ 1264/Si III λ 1299, Si II λ 1265/Si III $\lambda\lambda$ 1341–1343, C II $\lambda\lambda$ 1334, 1335/C III $\lambda\lambda$ 1175, 1176, and Al II λ 1671/Al III λ 1863. These ratios keep to the photospheric lines. One can also see the Ly- α λ 1216 line strengthening considerably toward later types, while the He II λ 1640 line disappears at about B2, depending on the resolution.

Resonance lines, of which the strongest are C IV λ 1550, Si IV λ 1400, and N V λ 1240, arise in the stellar winds and may correlate with the photospheric features, but they are better used to look for departures from the “normal” correlation. In such cases, the addition of “w” to the classification indicates an abnormal, generally stronger, wind strength, as well illustrated in Figure 4.8. Rountree and Sonneborn point out that these stars mostly turn out to have Be or shell characteristics.

For supergiant stars wind features persist consistently into the late B-types, and a sequence of these was given in Figure 3.13.

Stars in the Magellanic Clouds can extend studies to stars of lower metallicity than solar. Smith, Neubig, & Bruhweiler (1997, 1999) selected internal standards in these galaxies to make SMC and LMC classification sequences for O- and B-type stars. These low-resolution IUE sequences are calibrated to MK notation and have about 75% consistency with MK to 1 subclass, even though they are technically new systems.

4.3.3 Luminosity Criteria

Luminosity sequences at B0, B2, and B8 for FUV spectra are shown in Figures 4.9–4.13. For the earlier-type stars the Al III features (λ 1855, λ 1863) increase most clearly with luminosity, while for later-type stars the Al II λ 1671 is best, though these can have an interstellar contribution. Si II has a positive luminosity effect, and the cluster of Fe III lines from λ 1891– λ 1988, arising from metastable states, works well throughout the B-type range.

The high-resolution FUV spectra for B0, B2, and B5 in Figures 4.9, 4.11, and 4.12 respectively show luminosity sensitivity in the C II, C III, and Si III lines. The Si II/III ratio is particularly useful for the B5 luminosities. As in the case of temperature-type criteria, wind lines (N V and Si IV) should be avoided in luminosity classification.

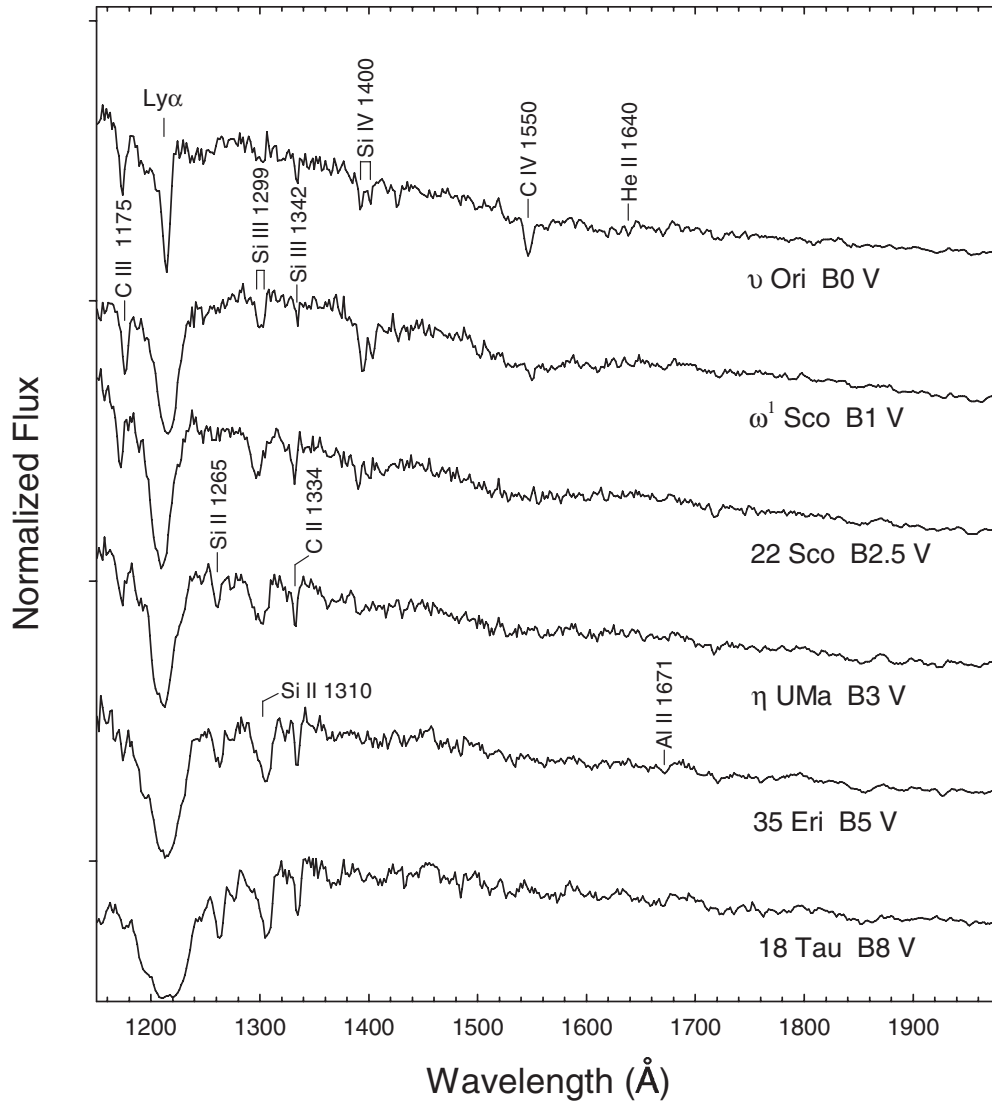


Figure 4.5 A spectral sequence for B-type dwarfs in the low-resolution IUE ultraviolet. For classification criteria in this and Figures 4.6 and 4.7, the Si II/Si III, C II/C III, and Al II/III ratios are favored over the C IV, Si IV, and N V lines, which arise in stellar winds. The spectra are from the IUE data archives (MAST IUE <http://archive-stsci.edu/iue>). The spectra have been normalized at a common wavelength and given integer vertical offsets.

4.4 CHEMICALLY PECULIAR B-TYPE STARS

4.4.1 The Helium-Strong Stars

A handful of early B-type stars (B3 and earlier) have extraordinarily strong lines of neutral helium; these stars are called the helium-strong stars. The prototype of this class is σ Ori E, a star in the young σ Ori cluster. Another bright helium-strong

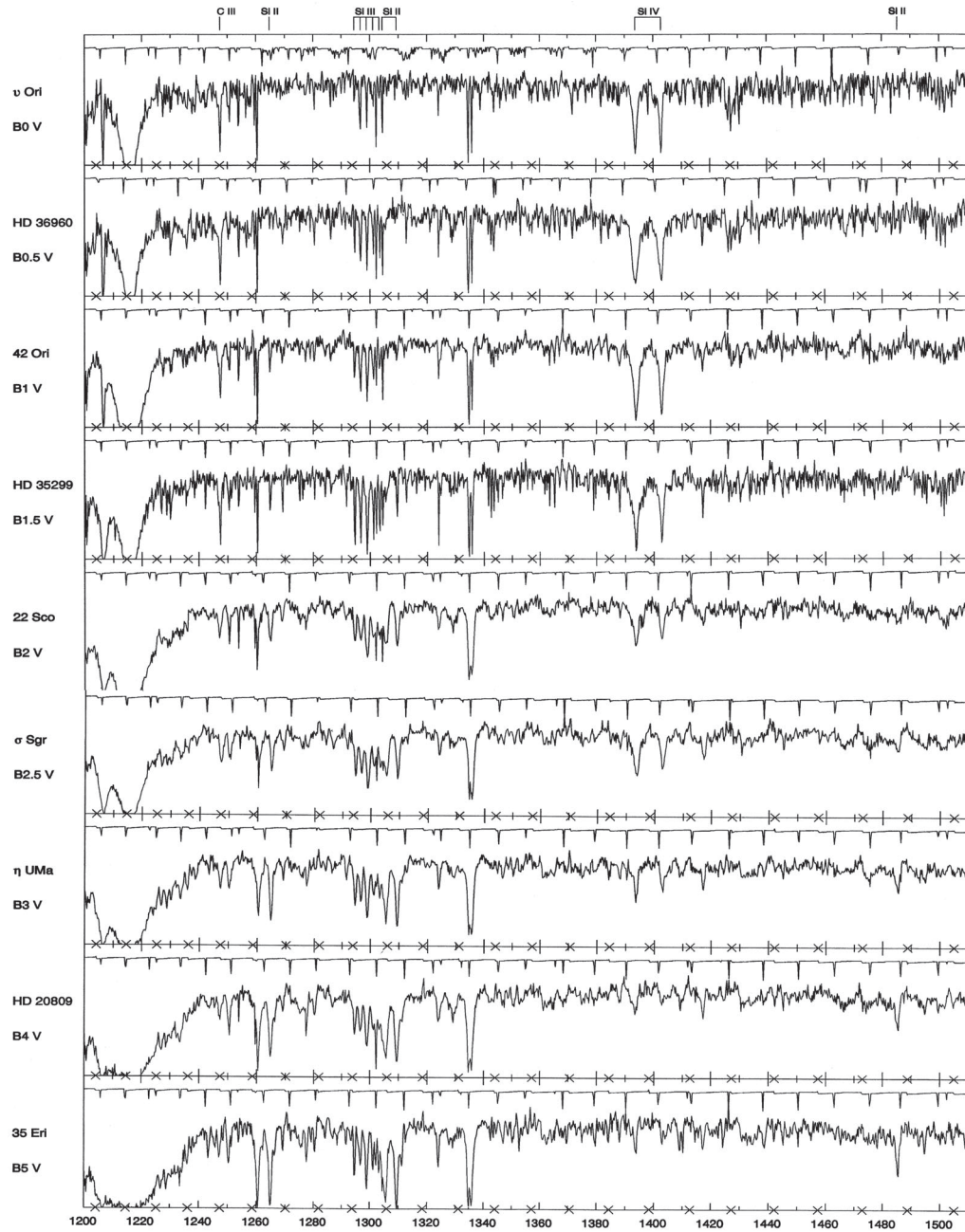


Figure 4.6 A spectral sequence for B-type dwarfs in the high-resolution IUE ultraviolet, B0–B5.
Figure from Rountree & Sonneborn (1991) and reproduced by permission.

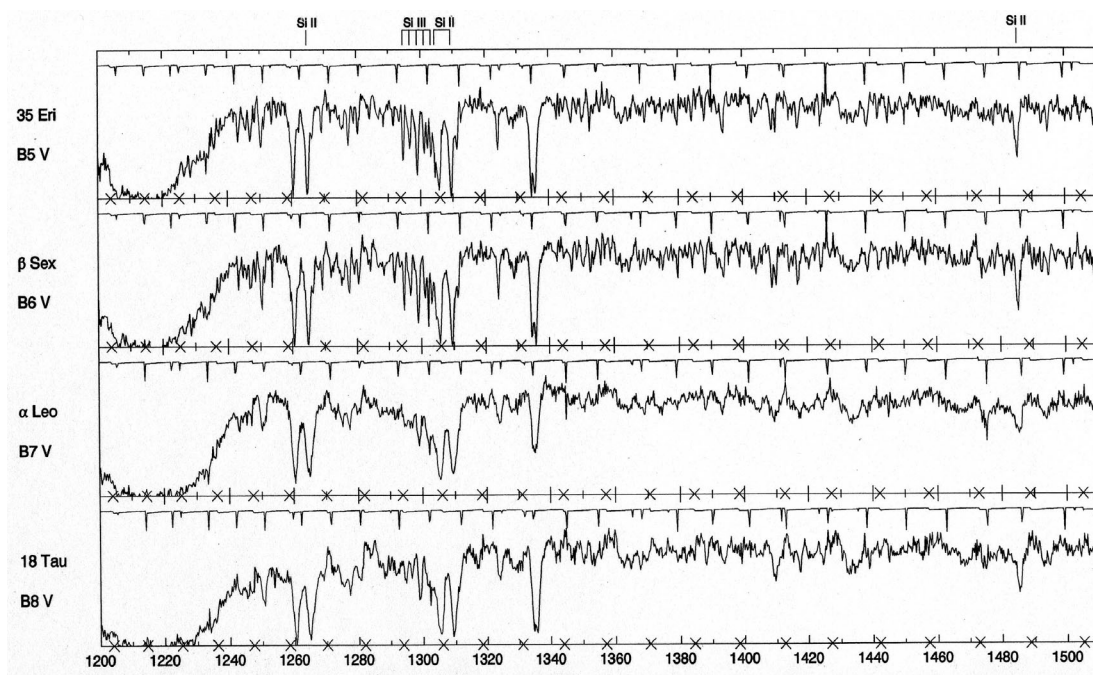


Figure 4.7 A spectral sequence for B-type dwarfs in the high-resolution IUE ultraviolet, B5–B8. Figure from Rountree & Sonneborn (1991) and reproduced by permission.

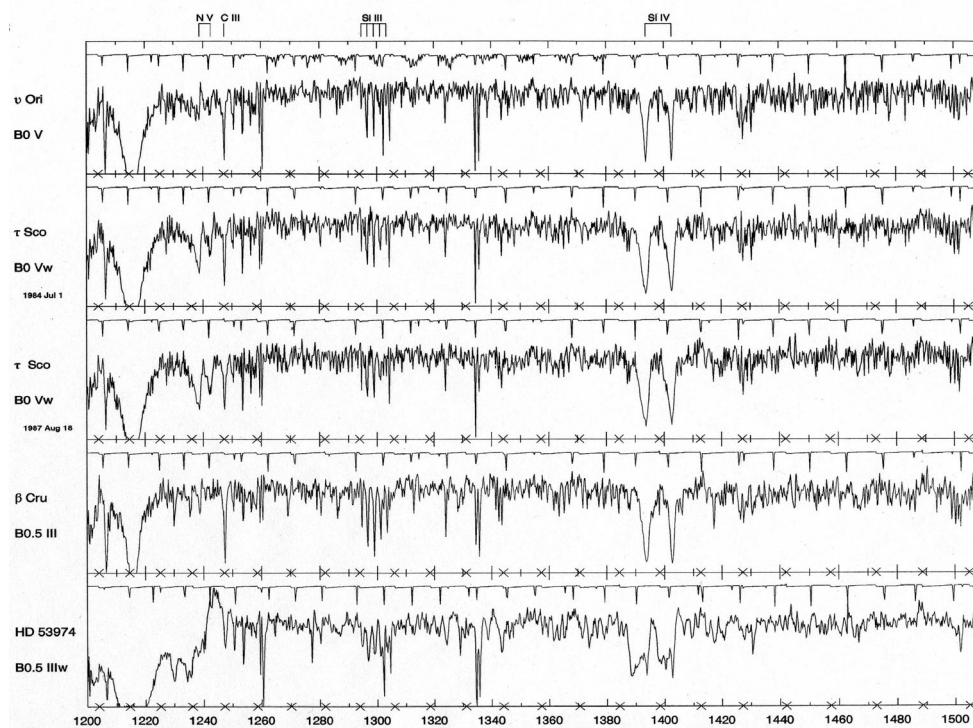


Figure 4.8 Wind effects in the ultraviolet spectra of B-type stars. Figure from Rountree & Sonneborn (1991) and reproduced by permission.

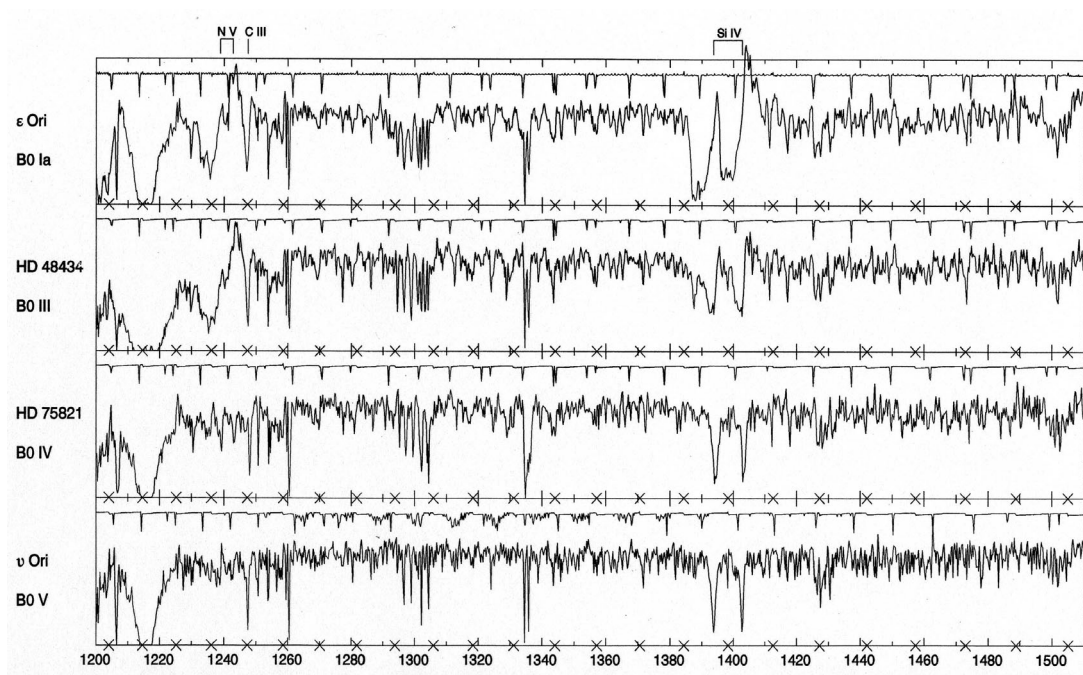


Figure 4.9 A luminosity sequence at B0 composed of high-resolution IUE spectra. Figure from Rountree & Sonneborn (1991) and reproduced by permission.

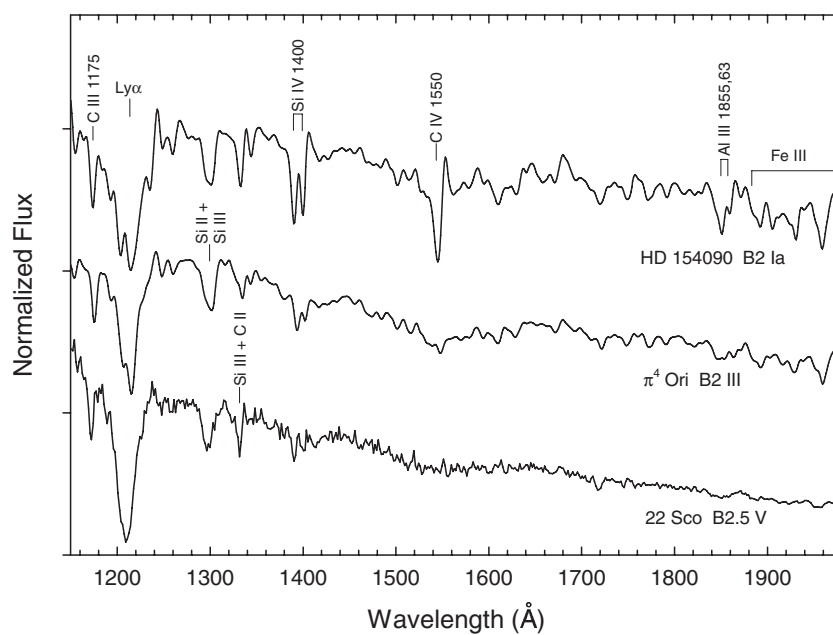


Figure 4.10 Luminosity effects at B2 in the low-resolution IUE ultraviolet. The Al III and Fe III features increase dramatically with luminosity. Spectra from the MAST archive.

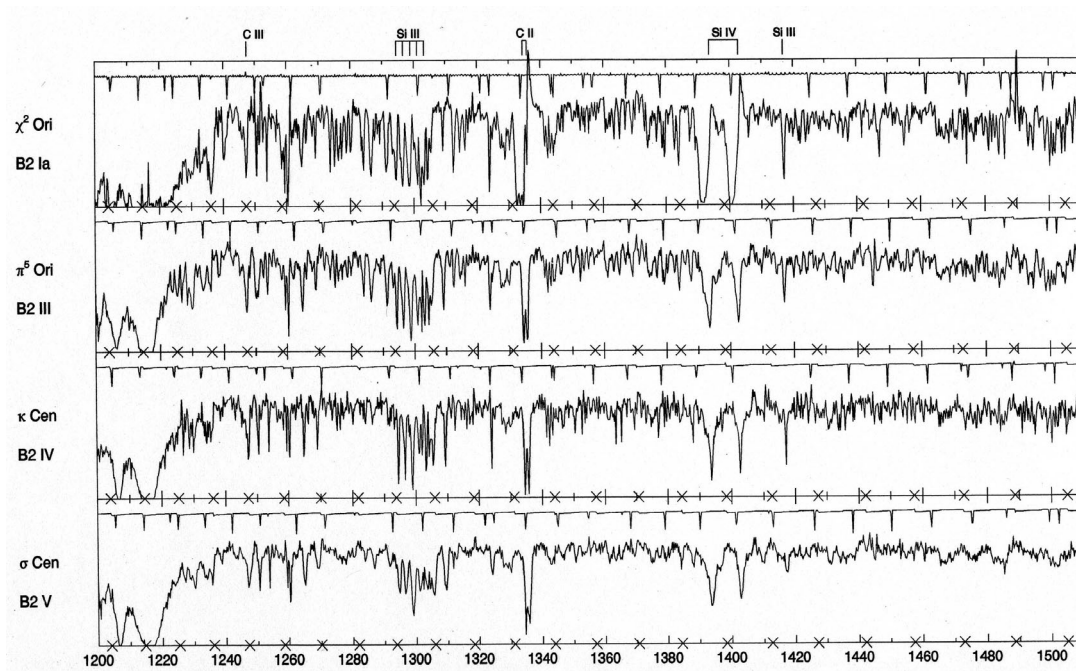


Figure 4.11 A luminosity sequence at B2 composed of high-resolution IUE spectra. Figure from Rountree & Sonneborn (1991) and reproduced by permission.

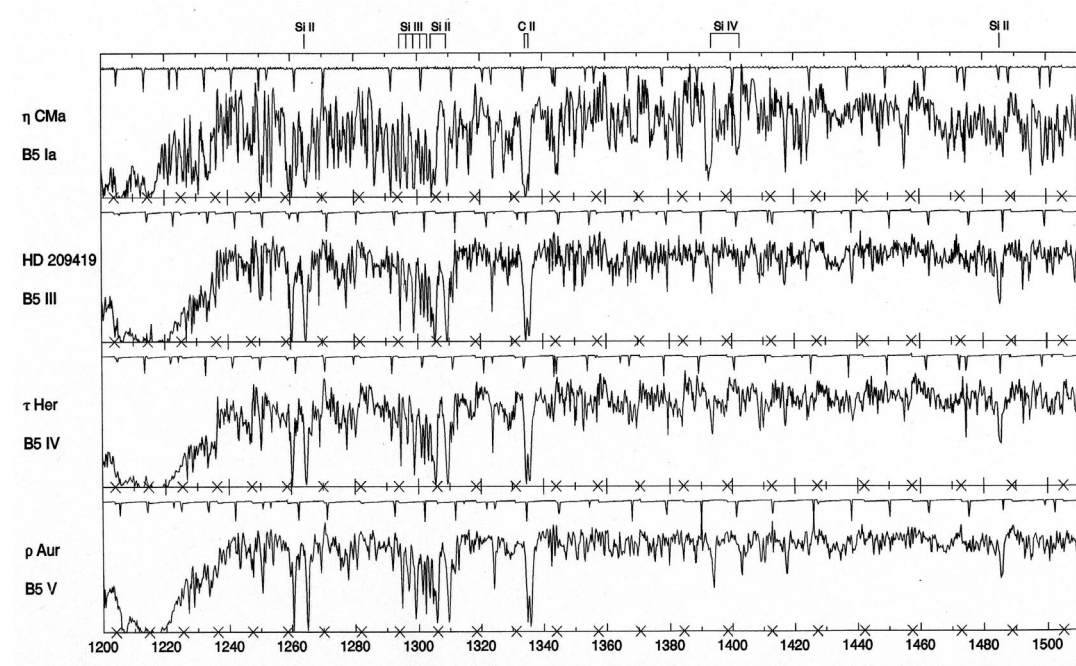


Figure 4.12 A luminosity sequence at B5 composed of high resolution IUE spectra. Figure from Rountree & Sonneborn (1991) and reproduced by permission.

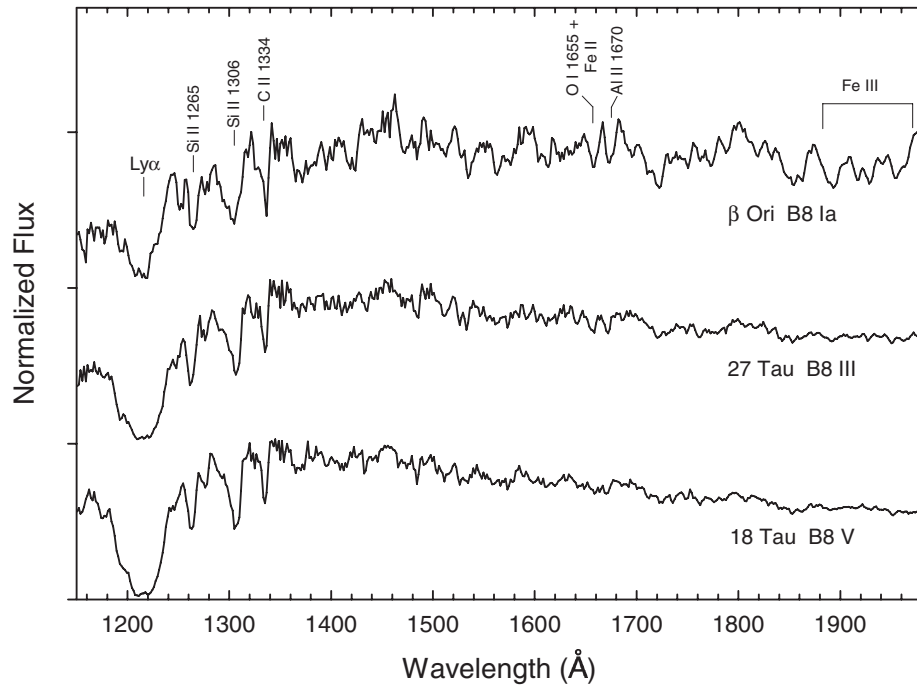


Figure 4.13 Luminosity effects at B8 in the low-resolution IUE ultraviolet. Al II and Fe III features increase dramatically with luminosity. Spectra from the MAST IUE archives.

B-type star is δ Ori C. These two stars are illustrated in Figure 4.14 along with the B0 V and B2.5 V MK standards. The spectral type of δ Ori C is fairly easy to assign, as the hydrogen-line profiles are only slightly narrower, but have the same depth as the B2.5 V standard. However, in addition to the very strong lines of He I, certain other spectral peculiarities are evident, including a very strong C II $\lambda 4267$ line. Morgan, Abt, & Tapscott (1978) classified this star as B2 Vh, with the “h” signifying “helium-strong.” We prefer a slightly cooler type, B2.5 IV-Vh. Assigning a spectral type to σ Ori E is somewhat more problematical, as the hydrogen lines do not match those of any standard well. Perhaps the best match is at B0 V, although the cores of the hydrogen lines are too shallow and the profiles slightly too broad. The spectral morphology of σ Ori E does not fit well at B0 V; the Si IV and Si III lines used in both temperature and luminosity classification in the early B-type stars (see Figure 4.1) are extremely weak, and suggest a spectral type closer to B2 V. Abt & Levato (1977) have classified this star as B2 IV-Vp (He st), and Garrison (private communication) has classified it as B2 Vp. One possible explanation, of course, for the slightly weak Balmer lines of σ Ori E could be its lower than normal hydrogen abundance. Surprisingly, however, it can be shown that the effect of increasing the helium abundance at the expense of hydrogen is to *increase* the width of the hydrogen lines (Böhm-Vitense 1967; Corbally & Gray 1994).

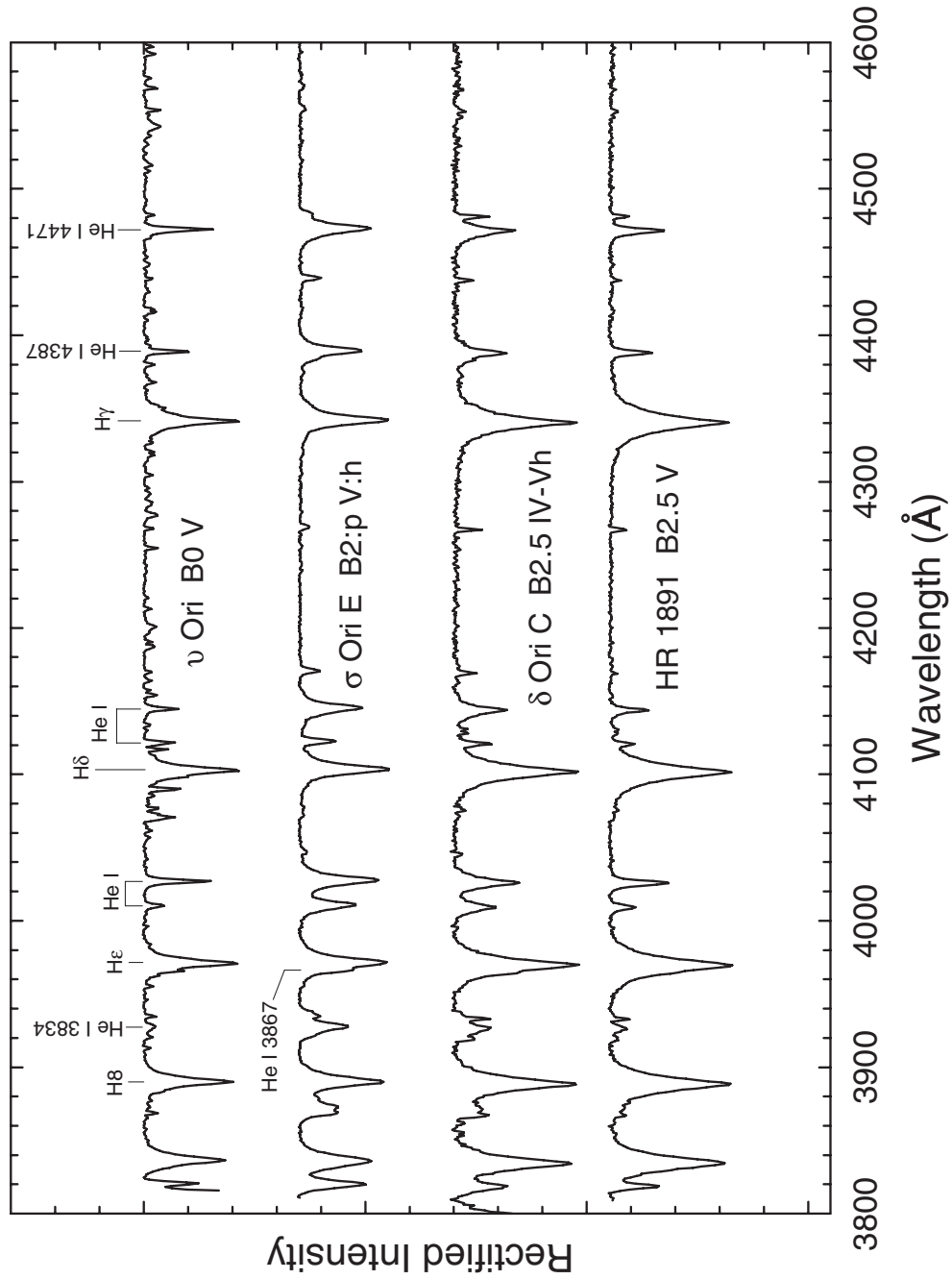


Figure 4.14 Two helium-strong B-type stars, σ Ori E and δ Ori C, compared with two MK standards. Note the extraordinary strength of the He I lines in the two helium-strong stars, even compared with the MK standard at B2.5, near to the He I maximum. Spectra obtained at the Dark Sky Observatory.

A number of helium-strong B-type stars are photometric and spectroscopic variables, some showing large changes in the strengths of the He I lines. Bidelman (1965) was the first to discover variability in the helium-strong stars; he found that HR 5378 (a Cen) has He I line strengths that vary from helium strong to helium weak. HD 184927 is another star that shows strong variation in the He I line strengths, in this case varying between helium-strong and helium-normal strengths (Bond & Levato 1976; Levato & Malaroda 1979); Levato & Malaroda found a period for the variations of 9.536 days. Wade et al. (1997) measured the longitudinal magnetic field of HD 184927 and found that it varied from -0.7 kG to 1.8 kG with a period closely agreeing with that of Levato & Malaroda (1979) (although see Shore & Brown 1990, for comments on the reality of this period). They concluded that “a patch of enhanced helium may exist in the photosphere of HD 184927 near the positive magnetic pole.” Their model suggests that the magnetic axis is inclined with respect to the rotational axis, bringing the enhanced helium patch in and out of view, accounting for the spectroscopic and photometric variability (this model, called the *oblique rotator model*, is also used to explain the spectroscopic variations of the classical magnetic Ap stars).

Strong magnetic fields appear to be a common, although perhaps not universal, feature of the helium-strong B-type stars (Bohlender et al. 1987), with magnetic field strengths averaging up to 3 times larger than the classical magnetic Ap stars (see §5.4.2). Two helium-strong stars without detected magnetic fields are HD 60344 and HD 133518. Quite a large fraction of the helium-strong B-type stars have constant magnetic fields, suggesting, contrary to the case of HD 184927, that the inclination between the magnetic-field axis and the rotational axis is quite small; these stars show little or no photospheric or spectroscopic variations. δ Ori C is an example of an essentially non-variable helium-strong star.

The difficulty in assigning a spectral type for σ Ori E, which is certainly one of the most extreme helium-strong stars, and the explanation for its peculiar hydrogen-line profiles may have something to do with its strong magnetic field (nearly 3 kG at maximum, Bohlender et al. 1987). Such a strong magnetic field can have significant effects on the structure of the stellar atmosphere and lead to spectroscopic peculiarities (see the discussion in §5.4.2).

Despite the fact that there are no strong He I lines in the IUE ultraviolet, many helium-strong stars also show spectral variations there. These spectral variations are most marked in the C IV and Si IV resonance doublets and may be related to circumstellar plasma trapped in the stellar magnetosphere (Shore & Brown 1990).

In the next section we discuss the helium-weak B-type stars and their possible relationship with the helium-strong stars.

4.4.2 The Helium-Weak Stars

The helium-weak stars constitute a class of B-type stars that are characterized by hydrogen-line spectral types (e.g. spectral types based only on the hydrogen-line profiles) of, usually, B3 and later, but for which the He I lines are peculiarly

weak. Osawa (1965) introduced the use of a He I line spectral type (determined by reference to the normal MK standards) for the helium-weak stars, and this practice was followed by Garrison & Gray (1994). Some of these stars show an unusually rich metallic-line spectrum, and in such cases, one can assign a metallic-line type as well.

The helium-weak stars were found early on to display a *color-spectrum* discrepancy (see Sharpless 1952; Garrison 1973) in that the $U - B$ and $B - V$ colors are too blue for the He I line strengths. This criterion has been used in the discovery of new helium-weak stars (Bernacca 1968; Jaschek, Jaschek, & Arnal 1969).

High-resolution studies of the helium-weak B-type stars have demonstrated—if one omits the classical magnetic Ap stars (see §5.4.2) and the mercury–manganese stars (§4.4.3), both of which are often helium-weak—the existence of three subclasses. These subclasses are the Si stars (characterized by enhanced lines of Si II, but generally at hotter temperatures than the classical silicon Ap stars), the phosphorus–gallium (PGa) stars, and the strontium–titanium (SrTi) stars. The Si helium-weak stars may not, in fact, be distinct from the Ap Si λ 4200 stars, which represent the hot end of the silicon Ap stars. In the case of the SrTi helium-weak stars, both strontium and titanium are enhanced, but at spectral types significantly earlier than the classical Ap strontium stars. Examples of these three classes of helium-weak stars are shown in Figure 4.15. A minority of helium-weak B-type stars may not show any additional peculiarity; a possible example is HD 37129.

As a matter of fact, even though these three subclasses of helium-weak stars were first recognized in high-resolution studies (see, for instance, Norris 1971), they can be detected in high S/N classification spectra with resolutions better than 2 Å. Both Ga II and P II have lines in the blue-violet; the insets in Figure 4.15 illustrate that these lines can be observed in good quality classification spectra, at least in the more extreme PGa stars. These species also have “prominent” lines in the red, including Ga II λ 6334 and P II λ 6302, and resonance lines in the UV (Ga II λ 1414 and P II λ 1532).

The He I lines in the helium-weak stars can often show peculiar profiles; this is most readily evident in Figure 4.15 in the star 3 Sco in which the He I lines, especially He I λ 4471, appear to have broad triangular profiles. This recalls the comment by Garrison (1973) that helium-weak stars often show broad “washed-out” He I lines. The stars 3 Cen A and ι Ori B and some other helium-weak stars reportedly have unusually high abundances of the ^3He isotope. This may be responsible, at least at high resolution, for unusual He I profiles because of the isotope shift between ^3He and the normally more abundant ^4He isotope (see Sargent & Jugaku 1961; Dworetzky 1973; Hartoog & Cowley 1979).

Like the helium-strong B-type stars, many but not all helium-weak stars have detectable magnetic fields, although these fields are generally much weaker than in the helium-strong stars (Borra, Landstreet, & Thompson 1983). The existence of these magnetic fields suggests a link between the helium-weak B-type stars and the magnetic Ap stars; indeed it is now generally accepted that the magnetic helium-weak B-type stars represent the hot end of the magnetic Ap

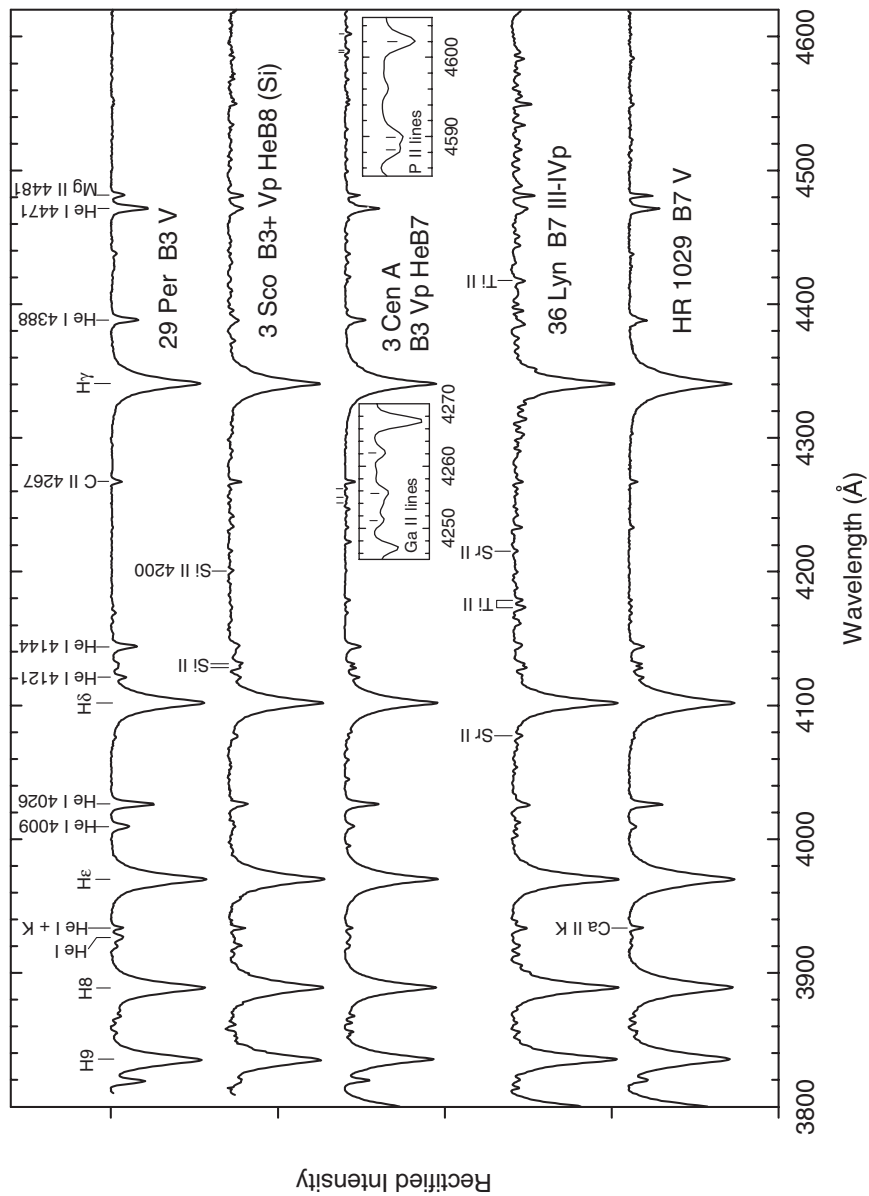


Figure 4.15 The spectra of three helium-weak B-type stars compared with two MK standards. 3 Sco is a hot helium-weak star of the Si variety, 3 Cen A of the PGa variety, and 36 Lyn, a relatively cool He-weak star, of the SrTi variety. Lines of Ga II and P II in 3 Cen A are identified in the insets. The spectrum of 3 Cen A is adapted from the Paranal Observatory library (Bagnulo et al. 2003), whereas the spectrum of 36 Lyn is adapted from the Indo-US Coudé-feed library (Valdes et al. 2004). The other spectra are from the Dark Sky Observatory.

phenomenon. However, the PGa helium-weak stars may instead represent the hot end of the non-magnetic HgMn stars (see below), as Borra, Landstreet, & Thompson (1983) were unable to detect magnetic fields in any of their four observed PGa stars.

The helium-strong stars generally have spectral types of B3 and earlier, while the helium-weak stars have types of B3 and later, and thus there is little overlap in effective temperature between the two groups. On the other hand, the helium-variable stars have spectral types and colors that bridge the gap between these two classes, in particular the star α Cen (HR 5378) that varies from being a helium-strong star to a helium-weak star (Bond & Levato 1976). For a time-series montage of this star, see Garrison (1973).

4.4.3 Other Chemically Peculiar B-type Stars

We delay the discussion of the classical magnetic Ap stars to Chapter 5 (§5.4.2) because, even though many of these stars have effective temperatures that place them in the B-star range, they are traditionally classified as A-type stars because of the absence of He I lines in their spectra. It is now recognized that the lack of He I lines in the classification spectra of the classical magnetic Ap stars is due to the fact that these stars are helium weak; we outline techniques in §5.4.2 that enable the correct (often late B-type) temperature type to be assigned to these stars.

It turns out that there are parallel tracks of chemically peculiar stars: one, the magnetic chemically peculiar stars (mCP), the other the nonmagnetic chemically peculiar stars (nmCP). The mCP stars involve, beginning at the hot end, the helium-strong stars (§4.4.1), some types of helium-weak stars (the Si and SrTi stars), and then the classical magnetic Ap stars, including the Si, SiCrEu, SrCrEu, and the Sr stars. The nmCP stars, beginning with the hottest, are the PGa helium-weak stars, the mercury-manganese (HgMn) stars, the hot-Am, the Am, and, finally, the ρ Puppis stars. There are, however, some doubts about the reality of the magnetic/nonmagnetic divide, as some claims for the detection of magnetic fields in the nmCP stars have been made (see Hubrig & Castelli 2001, and references therein). It may be that the real difference between the two groups is that the magnetic CP stars have geometrically simple fields, while the so-called nonmagnetic CP stars have complex fields that essentially cancel from an observational point of view. A good discussion of this may be found in Wahlgren (2004). Further, when examined at a sufficiently high resolution, nearly every slowly rotating late-B and A-type star will probably show some type of chemical peculiarity. In the remainder of this section we will discuss the HgMn stars; discussions of the other types of upper-main-sequence chemically peculiar stars may be found elsewhere in this chapter, Chapter 5, and Chapter 6.

THE MERCURY-MANGANESE (HGMN) STARS

The HgMn stars are typically found in the narrow spectral-type range from B7 to B9, and have luminosity types from V to III. They are characterized by unusually

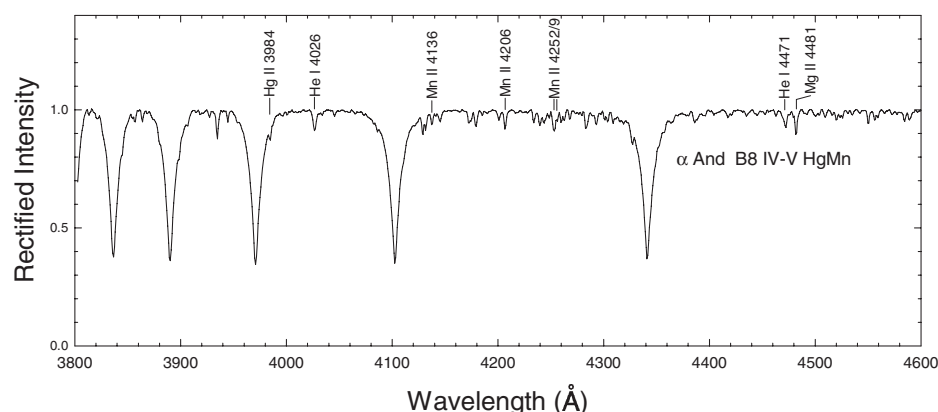


Figure 4.16 A blue-violet spectrum of the mercury–manganese star α And. The most prominent lines of Hg II and Mn II are marked; the Mn II $\lambda 4252$ line may be blended with Ga II in α And. Spectrum obtained at the Dark Sky Observatory.

strong lines of Hg II and Mn II; in the traditional blue-violet, Hg II can be detected only at $\lambda 3984$, whereas enhanced Mn II is most readily seen at $\lambda 4136$, $\lambda 4206$ (be careful not to confuse with Eu II $\lambda 4205$ —see §5.4.2), and $\lambda 4252$. For some stars Hg II is not seen, in which case the star is referred to as a “manganese” star, and for other stars manganese is normal and mercury is enhanced. The HgMn stars often show mild helium deficiencies, and sometimes the presence of other peculiarities. For instance, the well-studied HgMn star χ Lup (Leckrone et al. 1999) shows marked overabundances for most elements with $Z \geq 38$ (strontium and above on the periodic table; manganese has a near-normal abundance) including overabundances of 2 dex and greater for the rare earths, and very large overabundances of platinum, gold, and mercury. In the IUE ultraviolet, the Mn II resonance lines ($\lambda 2594$, $\lambda 2606$) in HgMn stars are clearly strengthened, and in the far IUE ultraviolet, these stars show a marked flux deficiency, presumably due to added line blanketing and bound–free continuous opacity. HgMn stars also show interesting isotopic anomalies in, for instance, platinum and mercury. Figure 4.16 shows the classification spectrum of a prototypical HgMn star, α And, in the traditional blue-violet.

The HgMn stars were first recognized as a group (the “manganese” stars) by Morgan (1931), although at that time the Hg II $\lambda 3984$ line was unidentified. This line was first identified with Hg II by Bidelman, who also suggested the presence of isotopic anomalies in mercury in the HgMn stars (see Whitford 1962).

As discussed above, HgMn stars are considered nonmagnetic chemically peculiar stars, although that picture has been changing recently. For instance, Mathys & Hubrig (1995) proposed a field strength on the order of 1 kG for σ Peg, and similar fields have been detected in a number of other HgMn stars. The fact that some HgMn stars show periodic spectral variations (for instance, profile changes in Hg II $\lambda 3984$ in α And) is also suggestive of a nonuniform distribution of abundances on the stellar surface, and thus of the presence of magnetic fields.

Interesting recent work has been done on the connection between the HgMn stars and the hot-Am stars (those with early-A hydrogen-line types). Many elements, for instance the rare-earth lanthanides, show a continuous trend in abundance anomalies across the HgMn–Am boundary, whereas others show discontinuous behavior (see Dolk, Wahlgren, & Hubrig 2003). Adelman, Adelman, & Pintado (2003) have suggested that there is a direct evolutionary connection between the HgMn stars and the hot-Am stars. In common with the Am stars, the HgMn stars appear to have a high incidence of binarity (perhaps >67%, according to Mathys & Hubrig 1995), with many of the companions possible Am stars (Ryabchikova 1998).

4.5 Be STARS AND B SHELL STARS

The Be stars are B-type stars that are characterized (or have been characterized in the past) by emission in one or more of the Balmer lines of hydrogen, sometimes accompanied by emission in lines of singly ionized metals, most commonly Fe II. The Be class usually excludes B-type supergiants, which commonly show emission at $H\alpha$, as it is generally believed that the mechanism leading to the emission in B supergiants is fundamentally different from that seen in Be stars. Also excluded from the class of Be stars are the B[e] stars (see next section) which show forbidden emission lines, the Herbig Ae/Be stars, which are pre-main-sequence stars (see §5.5), and other peculiar emission objects, such as Algol systems, the P Cygni type stars, and other luminous objects. Be stars have luminosity classes that range from V to III and rarely to II, and thus are mostly main-sequence, hydrogen-burning stars.

The classification of the Be stars began at the dawn of spectral classification; Angelo Secchi in 1866 discovered emission in the $H\beta$ line of γ Cas, now perhaps the best studied Be star, and devoted an entire class of his spectral classification system (class V) to stars showing emission lines (Secchi 1867). The history of the study of the Be stars is a long one, and is well summarized in Hearnshaw (1986). Likewise the literature on Be stars is enormous; the early literature is reviewed in Underhill & Doazan (1982) and Slettebak & Snow (1987), whereas more recent review papers on the Be stars can be found in Smith, Henrichs, & Fabregat (2000). A recent general review of the Be stars is given by Porter & Rivinius (2003). We will not make an attempt to review the vast literature on the Be stars; our treatment here will concentrate on spectral classification.

Observations indicate that a Be star is a rapidly rotating star that somehow produces a disk in its equatorial plane. The emission lines in a typical Be star spectrum are thought to arise from the hot circumstellar gas in this disk, with shell lines appearing when the disk is seen edge-on. How this disk is produced is still a matter of debate; it is now thought that most Be stars are not rotating at break-up velocity, and thus Struve's original idea (Struve 1931) that the disk is formed by mass thrown off from the equator centrifugally needs modification. The mass loss may be aided by pulsation or by a radiatively-driven wind. Magnetic fields may

also be important in confining the disk to the equatorial plane and in transferring angular momentum to the disk.

There are essentially two goals for spectral classification in the study of the Be phenomenon. The first goal is to classify the underlying star by using “photospheric” spectral features (i.e., spectral lines that are formed in the photosphere of the star and are not adversely affected by the circumstellar matter). The second goal is to characterize the emission spectrum. Spectral and photometric variability are key features of the Be phenomenon; while the spectral type of the underlying star should remain constant, the nature of the emission can vary on timescales of minutes to decades. Short-term variations (minutes to days) are more characteristic of the hottest Be stars, but all Be stars can show variations on timescales of years and decades. At times the emission-line spectrum can entirely disappear and the star can appear normal. At other times, a Be star can enter a “shell phase” in which the emission-line spectrum is replaced with a shell spectrum (see below).

Mild Be stars—those that show only emission or infilling in the cores of $H\alpha$ and $H\beta$ and no other emission features—can be classified on the MK system with little difficulty, except for the fact that almost all Be stars are rapid rotators (see §4.2.1). In stars with more developed Be spectra, the classifier must rely on features that are most likely to be photospheric. These features include the wings of the Balmer lines, especially the wings of the higher lines in the series, as these are the ones least likely to be seriously affected by emission, and lines of He I, the Mg II $\lambda 4481$ line, and other absorption lines. The He I lines are usually not involved in the emission, but check to ensure the spectral type implied by the hydrogen-line wings is consistent with the ratio He I/Mg II $\lambda 4481$. Lines of ionized species, in particular lines of Fe II, should be treated with great caution, as these often appear in emission in Be stars. The Mg II $\lambda 4481$ line is relatively safe, as it is a high-excitation line (~ 9 eV) and is unlikely to be affected by line emission in the circumstellar material. Another complication is the possible presence of continuum emission which can “veil” the photospheric lines, making them appear weaker than normal; under such a circumstance, line ratios should be used and not absolute line strengths. Spectral classification becomes more difficult and uncertain with a stronger expression of the Be phenomenon. Finally, in extreme Be stars in which there is intense emission in all of the Balmer lines in the blue-violet, and strong emission in the Fe II lines, the determination of the spectral type of the underlying star may be almost impossible or at least highly uncertain.

Even if the spectral type of the underlying star cannot be determined, or only with significant uncertainty, the emission spectrum itself can be classified. While there is no universally accepted classification system for characterizing the emission-line spectrum, the one most often used is the one designed by Lesh (1968) for the blue-violet (3800–5000 Å, including $H\beta$ but not $H\alpha$). This system adds an “emission parameter” to the MK type, based primarily on emission in the Balmer lines but also depending on the appearance of Fe II emission. Lesh’s six emission classes were described by her as follows:

- e₁ *No overt hydrogen emission.* Prototypes 66 Oph, 1H Cam. The H β absorption line is partially or completely filled in but is not reversed. H γ may also show some filling-in. The Fe II lines are usually absent.
- e₁₊ Prototype 48 Per. H β has a narrow emission core while remaining predominantly an absorption line.
- e₂ *H β in emission.* Prototypes ψ Per, 120 Tau. H β is an emission line. H γ is also filled in but not reversed, while the other Balmer lines are not affected. The Fe II lines are often, but not always, present.
- e₂₊ Prototype HD 45995. H γ shows a narrow emission core, and higher Balmer lines are slightly filled in. The Fe II lines are usually rather marked.
- e₃ *Complete hydrogen emission spectrum.* Prototypes 11 Cam, HD 58050. H β is an emission line and the higher Balmer lines, at least through H ϵ , have emission cores. The Fe II lines are usually present, except in the earliest spectral types, but they do not dominate the spectrum.
- e₃₊ Prototype HD 41335. The Fe II lines are more prominent than at e₃, but the hydrogen emission strength is less than at e₄.
- e₄ *The extreme Be stars.* Prototype χ Oph. There is intense emission in all the Balmer lines plus very strong Fe II lines (except in the earliest types). This group is similar to the Bex class discussed by Schild (1966).

Figure 4.17 illustrates some of the above emission classes. While in the above descriptions Lesh gives prototype stars, it should be realized that Be spectra can be highly variable, and so stars can change classes. For instance, χ Oph above is given as the prototype for class e₄, whereas in the spectrum displayed in Figure 4.17 it clearly is of class e₃. It is worthwhile mentioning that the Lesh system is compatible with the MK system, as it is not based on a theoretical model, and uses only information available in the spectrum. However, we emphasize that since the Be phenomenon is intrinsically variable, a Lesh-type classification should always be accompanied by the date of observation. Papers using the Lesh system include Lesh (1968); Hiltner, Garrison, & Schild (1969); Garrison, Hiltner, & Schild (1977).

An alternate and quite complex classification system for Be stars was worked out by Jaschek et al. (1980), using spectra from 3900 to 6700 Å of 140 stars obtained over a period of 20 years. In this system, Be stars are assigned to 4 (5) groups based on the appearance of their optical spectra, multicolor photometry, polarization, rotational velocities, and time variability. The motivation behind this system was to predict future behavior of a Be star based on its group membership. We do not have sufficient space to describe this system in detail; the interested reader may consult the original paper. Later quantitative comparisons between the group memberships assigned by Jaschek et al. (1980) and equivalent widths of H α showed that the Jaschek et al. system basically orders stars according to H α equivalent width, with the width decreasing from group I to V (see Dachs 1987). In addition, there are serious doubts about the ability of the system to predict Be star behavior; one of the characteristics of Be stars is their individuality and lack of predictability (see comments in Underhill & Doazan 1982).

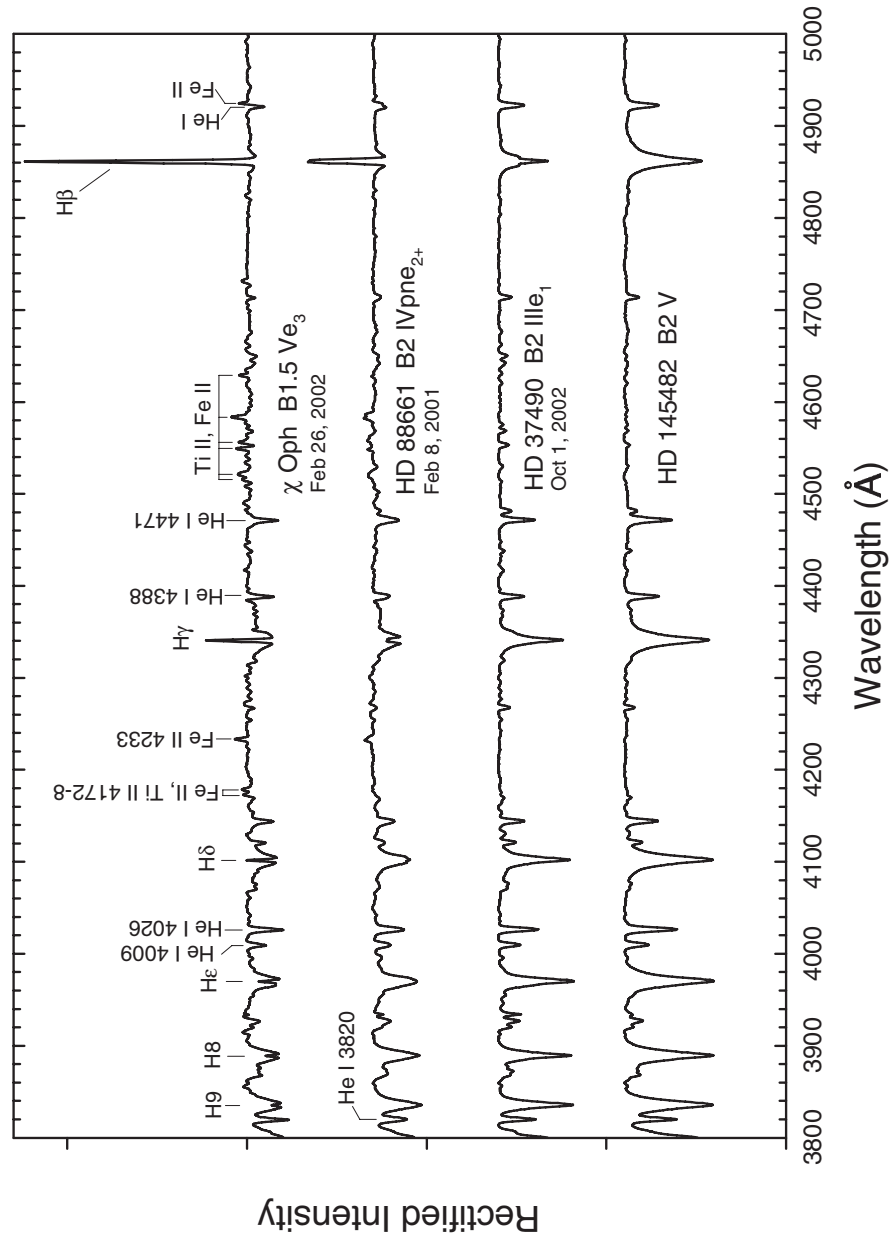


Figure 4.17 A selection of Be stars compared with a B2 V secondary standard, HD 145482. The spectral types are on the Lesh68 system and are based on those of either Lesh (1968) or Hiltner, Garrison, & Schild (1969) but with emission classes estimated from the displayed spectra. Some veiling is probably present in the spectrum of HD 88661. Notice the structure in the core of $H\beta$ in HD 37490. All the spectra in this figure were adapted from the Paranal Observatory spectral library (Bagnulo et al. 2003), smoothed to a resolution of 1.8 \AA . Notice that the wavelength range in this figure has been extended to include $H\beta$.

The profiles of Be-star emission lines, especially the profiles of $H\alpha$ and the Fe II lines, contain significant amounts of information and have been the subject of a number of classification systems. Dachs et al. (1986) and Dachs (1987) devised a classification system based on Balmer emission-line shapes. The first two categories are for symmetrical line profiles, the “symmetric double-peak profiles” and the “wine bottle-type profiles.” The third and fourth categories deal with asymmetric emission lines and shell lines (see Figure 4.18 for some examples). Emission lines that have central absorption components that extend below the continuum level are usually called “shell lines” in the context of Be stars. These profiles are interpreted in terms of the characteristics of the circumstellar envelopes.

More recently, Hanuschik et al. (1996) have published an extensive high-resolution atlas of emission and shell lines in Be stars. They have derived a classification system for the profiles of these lines based on three parameters: inclination of the circumstellar disk, optical depth, and disk kinematics. The kinematics of the disk determine whether the line profile is symmetric (class 1) or asymmetric (class 2). Hanuschik et al. (1996) consider both optically thick ($H\alpha$) and optically thin (Fe II $\lambda 5317$) emission lines in this classification system. Figure 4.19 shows how these profiles change with inclination. For pole-on disks, the $H\alpha$ profile has a characteristic “wine bottle” profile. At higher inclinations, the line evolves into a double-peaked profile and then finally develops a deep V-shaped central depression for disks seen in edge-on. These profiles are designated with four inclination classes, labeled P, L, H, and E, in order of increasing inclination. Stars are assigned a “profile code” according to where they fit into this scheme; some stars, of course, evolve from one profile code to another. Typical codes are, for instance, H2, for an asymmetric line profile showing a double peak, and E1 for a symmetric profile showing a deep V-shaped central depression.

B-TYPE SHELL STARS

It is not uncommon for Be stars to undergo a “shell phase” in which a shell spectrum replaces the Be emission-line spectrum. The shell spectrum can include deep, narrow cores in the Balmer lines and absorption lines of singly ionized metals, such as Fe II and Ti II arising from metastable states. These lines, which are usually enhanced only in supergiants, arise in the extended circumstellar shell that forms a low-density “pseudo-photosphere.” ζ Tau is a well-known early B-type shell star. Pleione (28 Tau), a star in the Pleiades, is a well-known Be star that undergoes shell phases (see Gulliver 1977, for a review of the spectral changes in Pleione from 1938 to 1975). 4 Her is another such star, although it appears to be in an interacting binary system (Koubský et al. 1997). Figure 4.20 illustrates spectra of all three stars.

THE ULTRAVIOLET AND THE INFRARED

In the ultraviolet, Be stars, especially those with broad emission lines, can show enhanced wind lines (notably in the resonance lines of Si IV and C IV—see §4.3). In a shell phase, the UV spectrum is dominated by narrow shell lines.

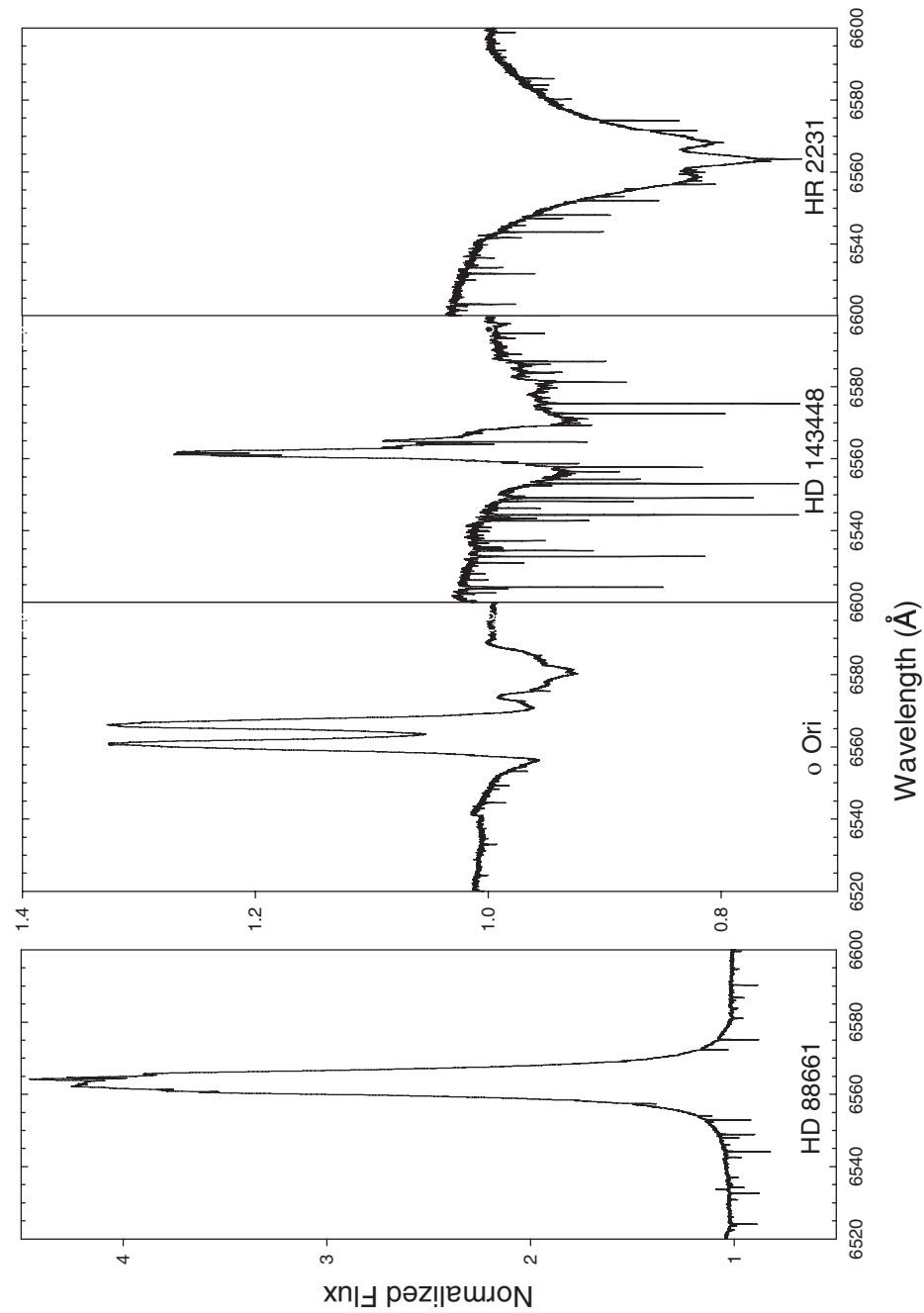


Figure 4.18 Some examples of H α profiles in Be stars. All these spectra have been adapted from the Paranal Observatory spectral library (Bagnulo et al. 2003) with no smoothing, but each profile has been normalized at a consistent point. Note the different flux scale for the H α profile of HD 88661. These spectra have not been corrected for telluric absorption, the source of most of the narrow absorption lines in these spectra.

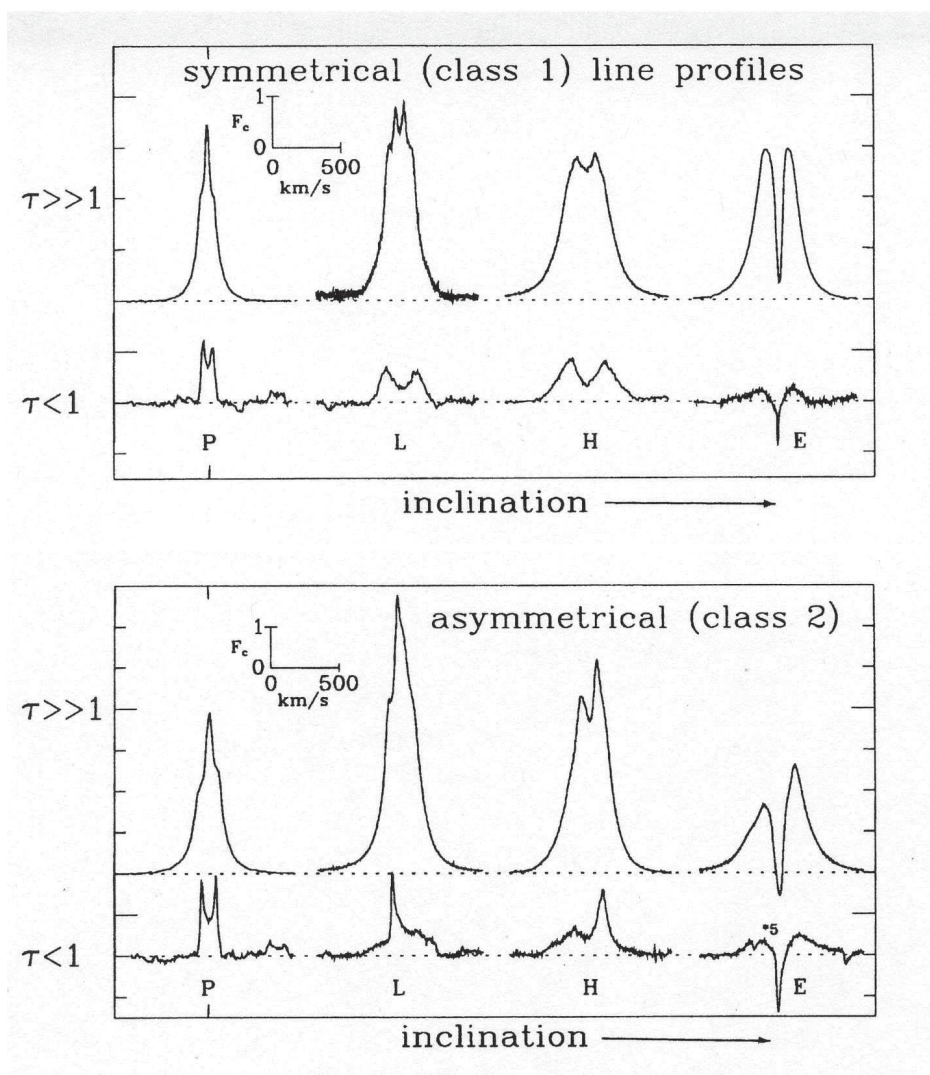


Figure 4.19 Typical emission-line shapes for symmetrical (class 1, top panel) and asymmetrical (class 2) profiles on the Hanuschik et al. (1996) classification system for Be stars. In both panels, the top profiles are for the $H\alpha$ line, the bottom for Fe II. The inclination parameters, P, L, H, and E, are indicated below the profiles. Reproduced by permission of *Astronomy and Astrophysics*.

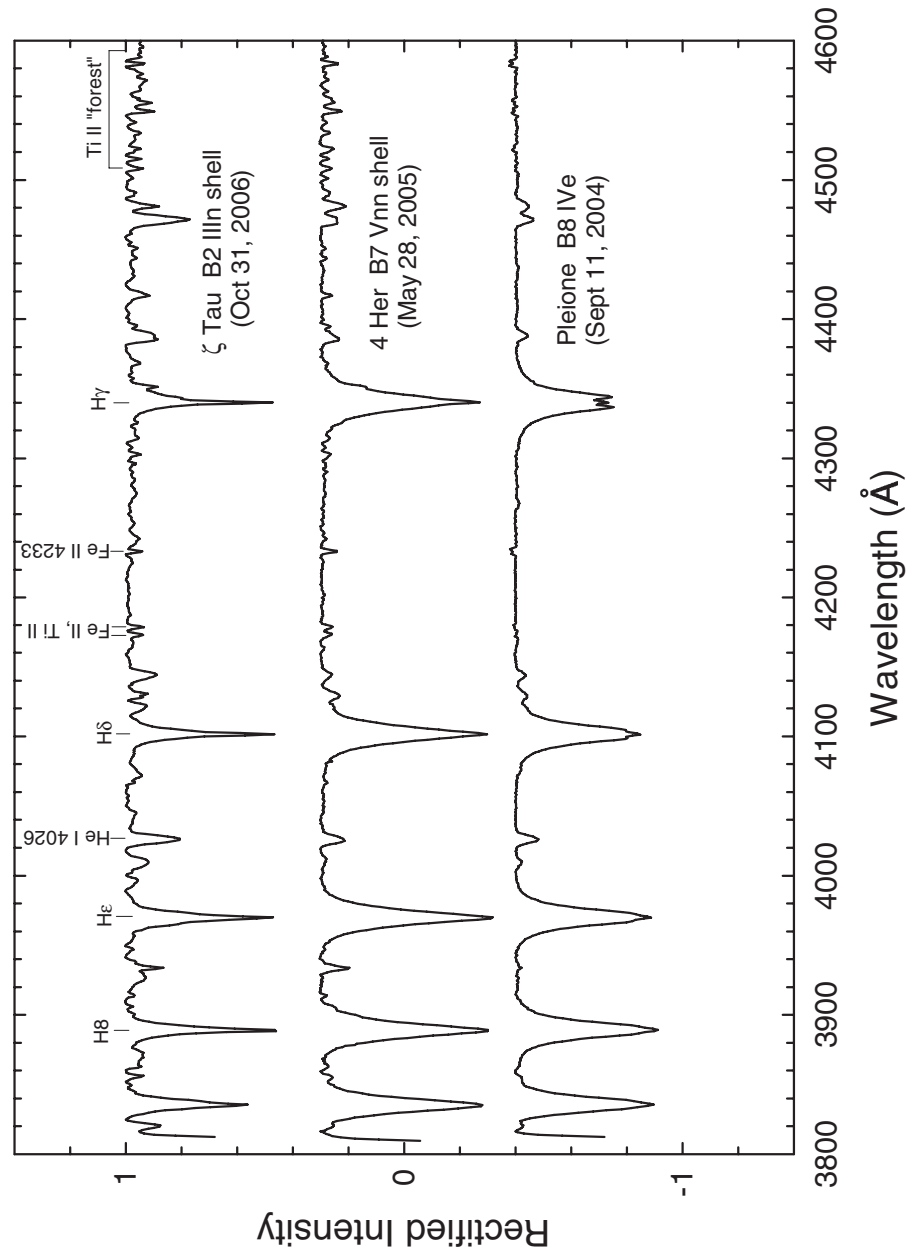


Figure 4.20 Three B-type shell stars. Two of these stars, ζ Tau and 4 Her, were in a shell phase when their spectra were obtained on the dates indicated. Note the deep, narrow cores to the hydrogen Balmer lines in ζ Tau and, to a lesser extent, 4 Her, as well as the narrow Fe II and Ti II shell lines. Pleione (28 Tau), a member of the Pleiades, was in a Be-state at the time of this exposure; note the self-reversed emission in the core of $H\gamma$. Spectra obtained at the Dark Sky Observatory.

In the near- to mid-infrared region, the spectra of Be stars (both Be and B shell) can be dominated by free–free and free–bound emission from the disk.

4.6 OTHER B-TYPE EMISSION-LINE STARS

4.6.1 B[e] Stars

B[e] stars are B-type stars that show *forbidden* emission lines in their spectra, largely lines of [Fe II] and [O I], as well as a strong near-/mid-infrared excess due to hot circumstellar dust. (The square brackets indicate a line’s forbidden status.) This class of stars is very inhomogeneous, because the physical conditions that can give rise to the forbidden emission (which requires an extended region of low density gas exposed to strong UV radiation) can occur in a number of circumstances, such as in the circumstellar material around pre-main-sequence stars, in symbiotic stars under certain conditions, in compact planetary nebulae, and around luminous B-type supergiants undergoing mass loss. In early objective-prism studies, B-type stars with “abnormal spectra” characterized by forbidden emission lines were often classified as “Bq” stars.

As in the Be stars, a major goal for classification is determining the nature of the underlying star. In the B[e] stars this task is especially difficult because there are often few, if any, photospheric features in the spectra of these stars (examples of spectra of B[e] stars may be found in Figure 4.21). In some cases the spectral type can be estimated only from the shape of the continuum, and this can be made doubly uncertain by the presence of circumstellar and interstellar extinction. Often external information, such as luminosities, the presence and nature of infrared excesses, etc., are required to derive even a basic understanding about the nature of the underlying star. A classification system for the B[e] stars has recently been proposed by Lamers et al. (1998) that is an interesting first attempt at using information, both internal and external to the stellar spectrum, to gain clues about the evolutionary state of the underlying star. We give a summary of this system below, but first begin with criteria for including objects in the class of B[e] stars (from Allen & Swings 1976; Zickgraf 1998):

1. The presence of strong Balmer emission lines.
2. Low-excitation permitted emission lines, predominantly singly ionized metals such as Fe II.
3. Forbidden emission lines of [Fe II] and [O I] in the *optical* spectrum.
4. The presence of a strong near- or mid-infrared excess due to hot circumstellar dust (in contrast to Be stars where the infrared excess is due to free–free and free–bound emission from gas in the disk).

Because these criteria can appear in a wide variety of physical situations, Lamers et al. (1998) proposed abandoning the B[e] designation and replacing it with 5 classes. These classes are

- (i) B[e] supergiants or “sgB[e] stars,”
- (ii) pre-main sequence B[e]-type stars, or “HAeB[e] stars,”

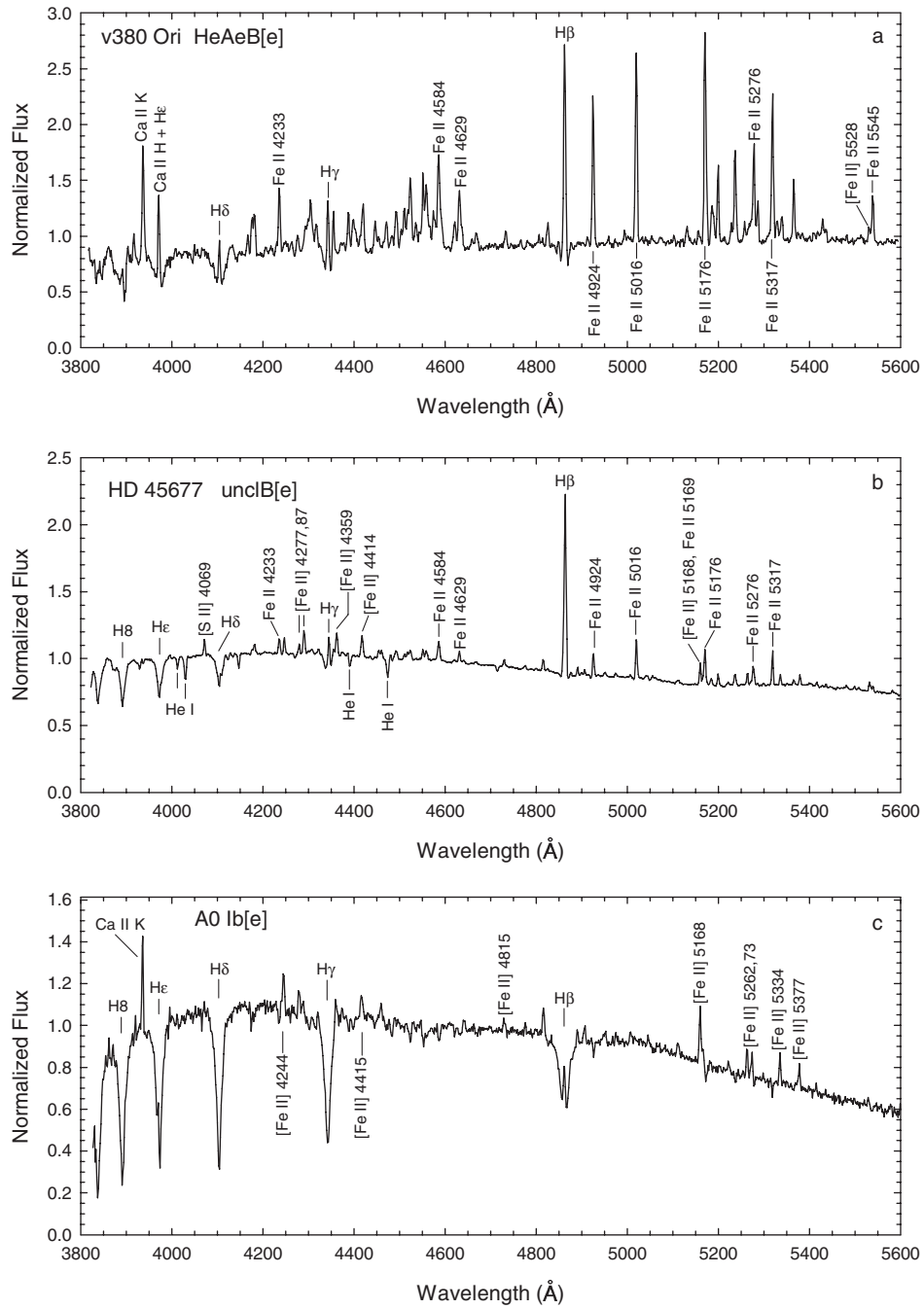


Figure 4.21 Three B[e] stars, including (a) V380 Ori, a Herbig; AeB[e] star; (b) HD 45677, the prototypical B[e] star, but still unclassified (unclB[e]); and (c) a newly discovered A[e] star. Note that the [Fe II] lines of V380 Ori are extremely weak in our spectrum. See Lamers et al. (1998) for a spectrum that shows stronger [Fe II] lines. Spectra obtained at the Dark Sky Observatory.

- (iii) compact planetary nebulae B[e]-type stars or “cPNB[e] stars,”
- (iv) symbiotic B[e]-type stars or “SymB[e] stars,” and
- (v) unclassified B[e]-type stars or “unclB[e] stars.”

Zickgraf (2000) has proposed a possible sixth class, that of main-sequence or near-main-sequence B[e] stars, MSB[e], which could represent a link with the classical Be stars.

As stated above, it is often impossible to decide which class a B[e] star belongs to on the basis of classification-resolution spectra alone. Let us consider, in each case, the type of information required in order to make a secure classification:

SUPERGIANT B[E] STARS (SGB[E])

For a star to belong to this class, it obviously must be a highly luminous object; a number of such objects exist in the Large and Small Magellanic Clouds (LMC and SMC), where they all have luminosities greater than $10^4 L_{\odot}$. In the Galaxy, determining the luminosity of candidate sgB[e] stars can be difficult, but certain other characteristics, in particular mass-loss indicators such as P Cygni profiles in the Balmer lines, or asymmetric double-peaked Balmer emission lines with $V/R < 1$, can be indicative, but of course must be backed up with evidence about the luminosity of the object. See Lamers et al. (1998) for other secondary indicators. A likely example of a supergiant B[e] star in our Galaxy is MWC 300.

PRE-MAIN-SEQUENCE B[E] STARS (HAEB[E])

The criteria for a B[e] star to be a HAeB[e] star are the same as the criteria for Herbig AeBe stars (see §5.5), plus the presence of forbidden emission in their spectra. Two examples are HK Ori and V380 Ori (see Figure 4.21).

COMPACT PLANETARY NEBULA B[E] STARS (cPNB[E])

Certain stars that are in the process of evolving into planetary nebulae (PPNe) can have spectra that show striking similarities to B[e] stars (Swings & Andrillat 1979). For instance, some compact planetary nebulae have optical spectra that show strong Balmer emission lines, Fe II emission, and [Fe II] emission, as well as a strong IR excess. These objects are often not obvious planetary nebulae on images, but the presence of a nebula must be evident from the spectrum (for instance the presence of [O III] nebular lines). A bright but atypical example of this class is OY Gem, the central star of a planetary nebula.

SYMBIOTIC B[E] STARS (SYMB[E])

Symbiotic stars are stars that show evidence in their spectra of both hot and cool components; in a quiescent state, a typical symbiotic star will show TiO bands longwards of 5000 \AA with strong emission lines of hydrogen and He I. Near maximum light many symbiotic stars also show permitted and forbidden Fe II emission. In most cases the presence of TiO bands in the spectrum is a sure indication

of membership in the SymB[e] class, but in some cases, if the optical spectrum is heavily obscured, or the cool star is not sufficiently luminous, the TiO bands may not be obvious. The presence of the cool star may be more evident in the infrared. See §8.5 for more on the symbiotic stars.

UNCLASSIFIED B[e] STARS (UNCLB[e])

Many B[e] stars do not clearly fit the criteria for any of the four above classes, and so are temporarily placed in the unclB[e] class. Some of the best studied B[e] stars are unclassified, including the prototypical example HD 45677, which may actually be an “extreme” Be star, as its Hipparcos parallax places it near to the main sequence. It may thus be a member of Zickgraf’s MSB[e] class.

The fact that the most populated class in the above scheme is unclB[e] points out the limitations of the system of Lamers et al., but it is also indicative of the difficulties astronomers face when studying these stars. Many of the unclB[e] stars have recently been placed in the new FS CMa class of nonsupergiant dust-forming B[e] stars (Miroshnichenko 2007).

It turns out that the B[e] phenomenon extends into the A-type stars. One of the stars in Figure 4.21 is an A[e] star, its ID is cleverly missing from the figure as this object has not yet been published.

4.6.2 Luminous B Supergiants and the Transition to LBVs

An examination of the most luminous stars in the Milky Way and other nearby galaxies led Humphreys & Davidson (1979) to identify the existence of an empirical upper boundary to the luminosities of stars across the HR diagram (the Humphreys–Davidson limit—see Figure 11.15). For the most massive stars, the sloping part of this empirical limit coincides with the Eddington limit, beyond which radiation pressure exceeds the gravitational acceleration; stars at or beyond this limit are highly unstable. For stars with $T_{\text{eff}} < 8000$ K, the boundary represents a temperature-independent upper luminosity limit for late-type hypergiants, and probably corresponds to the highest mass ($\approx 40M_{\odot}$) for which a star may evolve across the HR diagram to become a red supergiant. Above this mass, the star encounters instabilities (corresponding to the Luminous Blue Variable stage) which prevent the star becoming a red supergiant. The Luminous Blue Variables (LBVs) are considered in more detail in §11.2. In the B- and A-type stars, the stars at or near this limit are the massive, luminous supergiants and hypergiants (luminosity classes Ia, Ia⁺, and 0), including some of the Luminous Blue Variables such as P Cygni, and S Doradus in the SMC. These stars all show evident signs of mass loss, including, for the hotter stars, strong P Cygni profiles in the ultraviolet Si IV and C IV resonance lines (see Chapter 3 on the OB stars) and P Cygni profiles at H α . In the cooler late-B and early-A luminous supergiants, the main ultraviolet indicators of mass loss are short-shifted components in lines of Mg II, Fe II, C II, Si II, and Al II, including the resonance lines of those species (Talavera & Gómez de Castro 1987), as well as P Cygni profiles at H α (Verdugo et al. 1999), although

these indicators fade rapidly with declining temperature. In the most luminous late-B and early A-type supergiants and hypergiants a P Cygni profile may be present at $H\beta$ as well, although this is highly dependent on the temperature; α Cyg (A2 Ia), for instance, has an entirely normal $H\beta$ profile. The lower-luminosity late B- and early A-type Ib supergiants, on the other hand, usually show near-normal $H\alpha$ profiles. Verdugo et al. (1999) have published an atlas of $H\alpha$ and IUE spectra of luminous early A-type stars, showing the strong dependence of wind features on luminosity class.

Figure 4.22 shows a montage of $H\alpha$ profiles of a number of late B-, early A-type Ia supergiants, hypergiants, and “low luminosity” LBVs, including the supergiants HD 183143 and α Cyg, the dusty hypergiant AS 314 (Miroshnichenko et al. 2000), the “low-luminosity” LBV candidate HD 168607, and the low-luminosity LBV HD 160529 (Chentsov et al. 2003).

A characteristic of these stars is their variability, both spectroscopic and photometric. The amplitudes of these variations, both in brightness and in temperature, are strong functions of the luminosity, with the most luminous stars of this type, the LBVs, showing enormous spectral and brightness changes over time scales of years and centuries (see discussion in Chapter 11).

4.7 B-TYPE STARS IN ADVANCED EVOLUTIONARY STATES

4.7.1 OB Subdwarfs

4.7.1.1 Introduction and Relation to Other OB Stars

Interest in hot, subdwarf OB stars (sdOB) is high (see conference papers in *Baltic Astronomy*, vol. 15, 2006) and so their known numbers are growing rapidly, with over 2300 in 2004 (Ostensen 2004). In terms of stellar evolution they fall into two groups: the stars at the extreme blue end of the horizontal-branch (EHB stars—see Figure 5.26) and those post-planetary nebula stars that are approaching the top of the white dwarf sequence (pre-WD stars). The EHB stars are core helium burning with extremely thin hydrogen envelopes, presumably resulting from extensive mass loss during the red giant stage at the time of the helium flash, and they constitute the majority of the two groups combined. The pre-WD stars have exhausted their capacity for nuclear burning in their cores. The extremely rare, He-rich subdwarf B-stars, found in the Galactic field as well as in some globular clusters, may be the result of binary white dwarf mergers (Ahmad & Jeffery 2004). The majority of EHB stars, at least in the field, seem to be close binary stars (Moni Biden et al. 2006), and so are an excellent tool for studying mass transfer and mass loss in the evolution of such systems. Some EHB stars are pulsators and thus susceptible to asteroseismology, while for all, their hot atmospheres are the result of weak stellar winds, radiative levitation, and gravitational settling. So both groups of sdOB stars are rich in stellar physics and provide the counterpart to similar astrophysical interest in the very low temperature end of the HR diagram.

Identifying these sdOB stars from spectra was first clearly outlined in the Palomar Green (PG) survey (Green, Schmidt, & Liebert 1986). The aim then became to

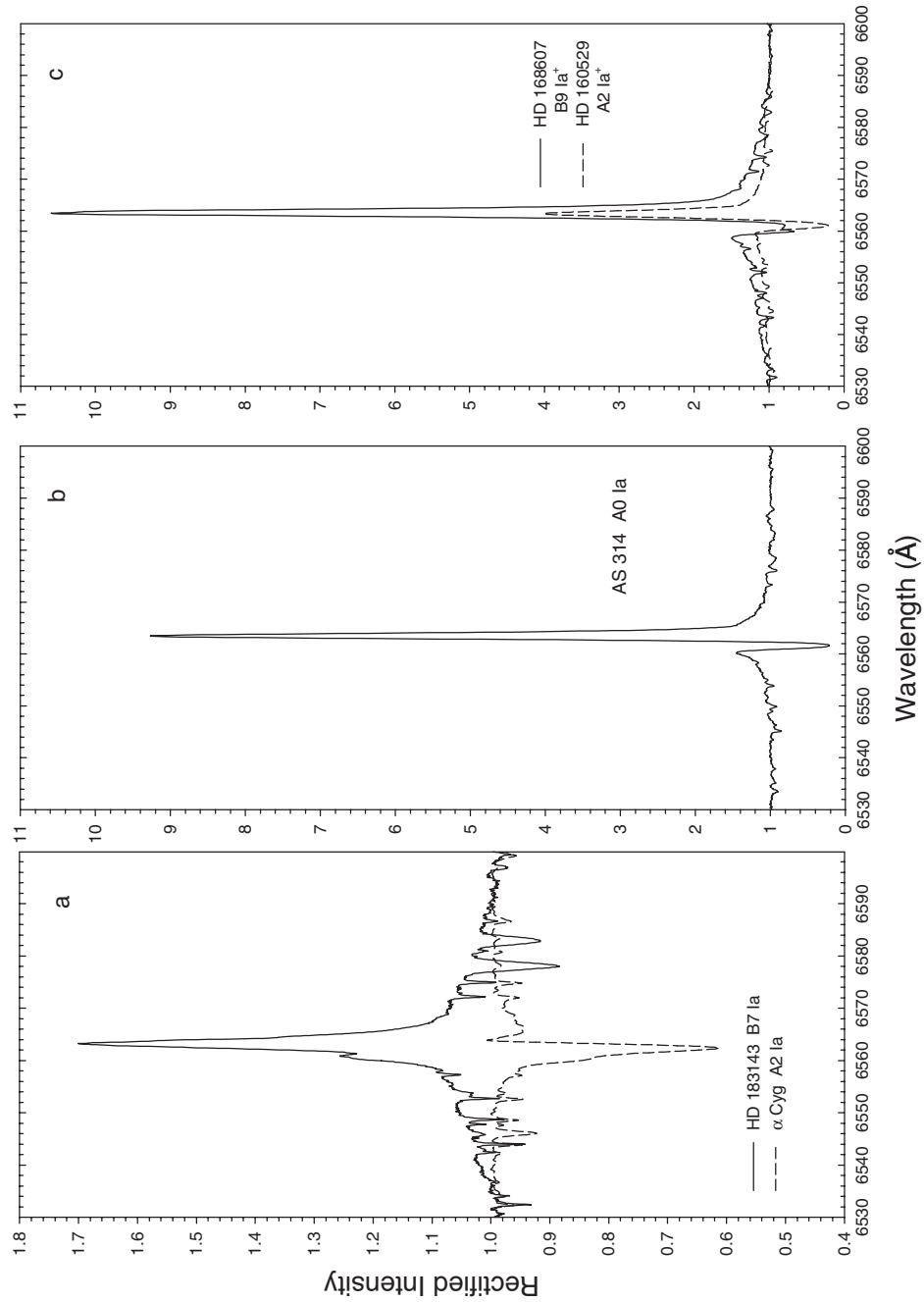


Figure 4.22 Some examples of H α profiles in luminous late B and early A supergiants and hypergiants. In panel (a), α Cyg is compared with HD 183143; in (b), the H α profile of AS314, a dusty A0 hypergiant and LBV candidate, is displayed; and in (c) the H α profile of the LBV star HD 160529 is compared with the candidate LBV HD 168607. Note the vertical scaling in (a) is different from that in (b) and (c). All profiles have been normalized to the local continuum. The spectrum for α Cyg has been adapted from the Paranal spectral library (Bagnulo et al. 2003) whereas all others are from the atlas of Chentsov et al. (2003). The resolution is 0.4 Å.

establish a fixed set of standards, as done in MK for the higher luminosity OB stars, so as to define the system. A standard network for the blue-green spectral region was presented by John Drilling and colleagues in 2002 at the Garrison Festschrift meeting (Drilling et al. 2003). The UV and IR regions are apparently not yet utilized for sdOB classification, save occasional IUE spectra and even Voyager 1's contribution of two stars (Drilling et al. 1984).

Work remains to be done on linking the sdOB stars to the PG 1159 class of star (see §12.2.4). These latter are higher temperature stars with helium and carbon, but no apparent hydrogen in their spectra, giving a broad absorption dip around $\lambda 4670$, sometimes with emission line cores (Werner & Heber 1991).

4.7.1.2 sdOB Classification

Spectra of about 2.5 Å resolution in the wavelength region of about 4000–4900 Å were used by Drilling et al. (2003) to set up the classification system for sdOB stars. With these spectra, three dimensions of spectral type can be distinguished: temperature class, luminosity class, and helium class. The temperature classes follow roughly the same ratios of He I/He II, Si III/Si II and the absolute strength of Mg I $\lambda 4481$ as for MK standards of class V, and this is for the same physical reasons. These classes are, however, defined by a spectral sequence, not by the numeric value of these ratios. Figure 4.23 is an arrangement of temperature classes for relatively H-rich hot subdwarfs that merge into blue HB stars. This smooth sequence allows stars with weaker helium or metallic line strengths to be classified. Notice how “sd” is prefixed to all the classifications to indicate they are not MK types.

In Figure 4.23 the helium class is appended to the spectral type since it is always included in sdOB classes. The colon before the helium class is just a separator for clarity. For those with weaker helium the class is roughly equal to the following function of line depths:

$$20 \frac{\text{He I } \lambda 4471 + \text{He II } \lambda 4541}{\text{H}\gamma - 0.83 \text{ He II } \lambda 4541}.$$

For the stronger helium stars, the helium class is roughly equal to the following function of line depths:

$$40 - 20 \frac{\text{H}\gamma - 0.83 \text{ He II } \lambda 4541}{\text{He I } \lambda 4471 + \text{He II } \lambda 4541}.$$

So the helium classes can run from 0 for stars showing no helium lines to 40 for those showing no Balmer lines. Again, these helium indices are defined by a sequence of spectra, not primarily by these ratios. Such a sequence is shown in Figure 4.24 for stars at sdB1.

The upper two spectra in Figure 4.24 have classifications beginning sdBC. The “C” indicates that the carbon lines are strong compared with the equivalent temperature class in MK spectra. Figure 4.25 shows a temperature sequence for spectra of hot subdwarfs that are both extremely He-rich and C-rich. So besides the

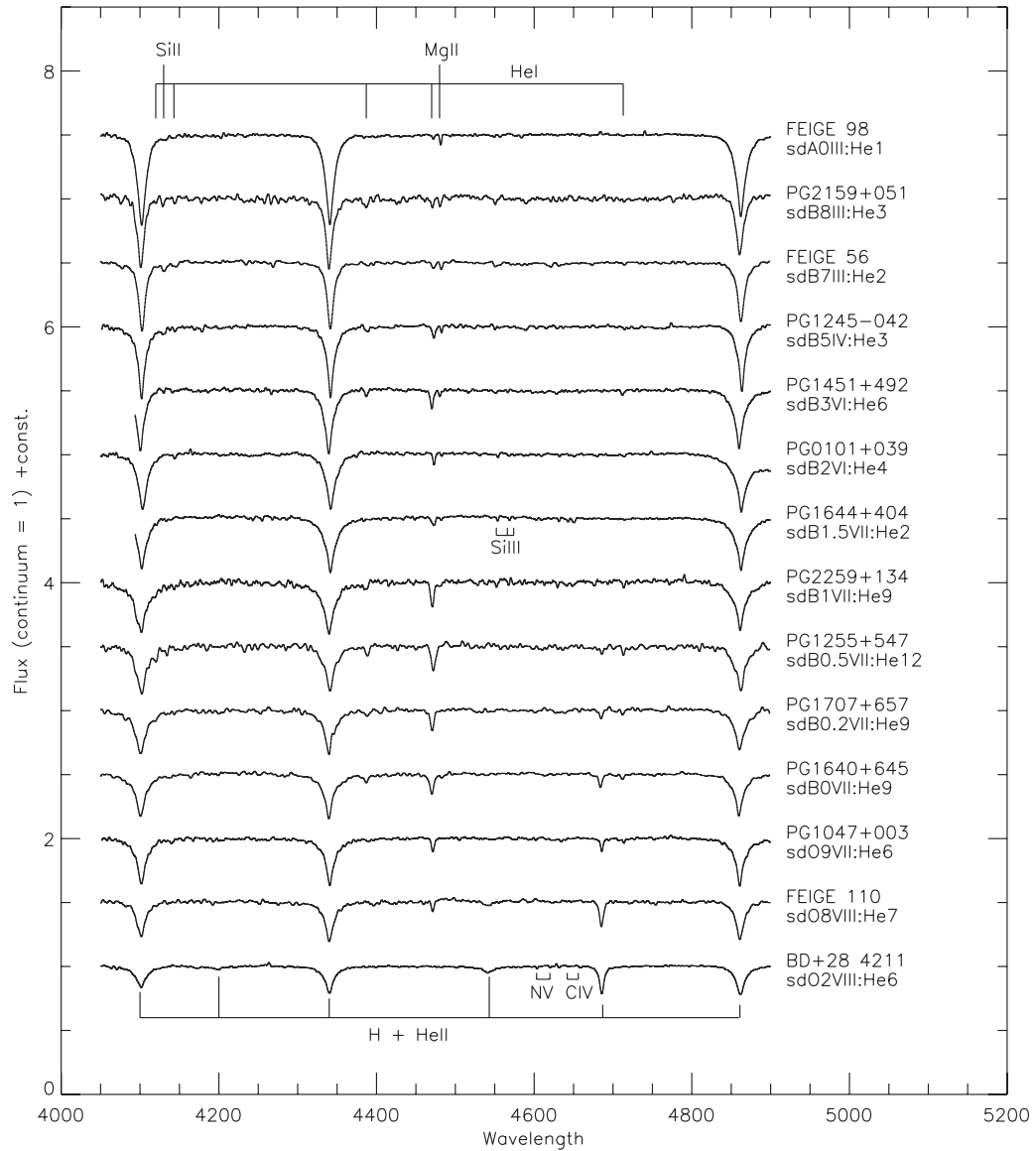


Figure 4.23 A temperature sequence of H-rich hot subdwarfs merging into blue horizontal-branch stars. Note that the hottest stars are at the bottom. The rather minimal spectral features marked—those of both stages of helium ionization and some ionized metallic lines—are useful in temperature classification. All spectra illustrated in this section are taken from Drilling et al. (2003) and reproduced by permission of L. Davis Press.

variation in helium abundances, sdOB stars also range from carbon-rich to carbon-poor. Also note that this figure extends the sequence to sdO1, which is earlier than for more massive stars.

The luminosity class is determined by the line widths. If the line widths at a given temperature class are average, then the standard luminosity class VII is

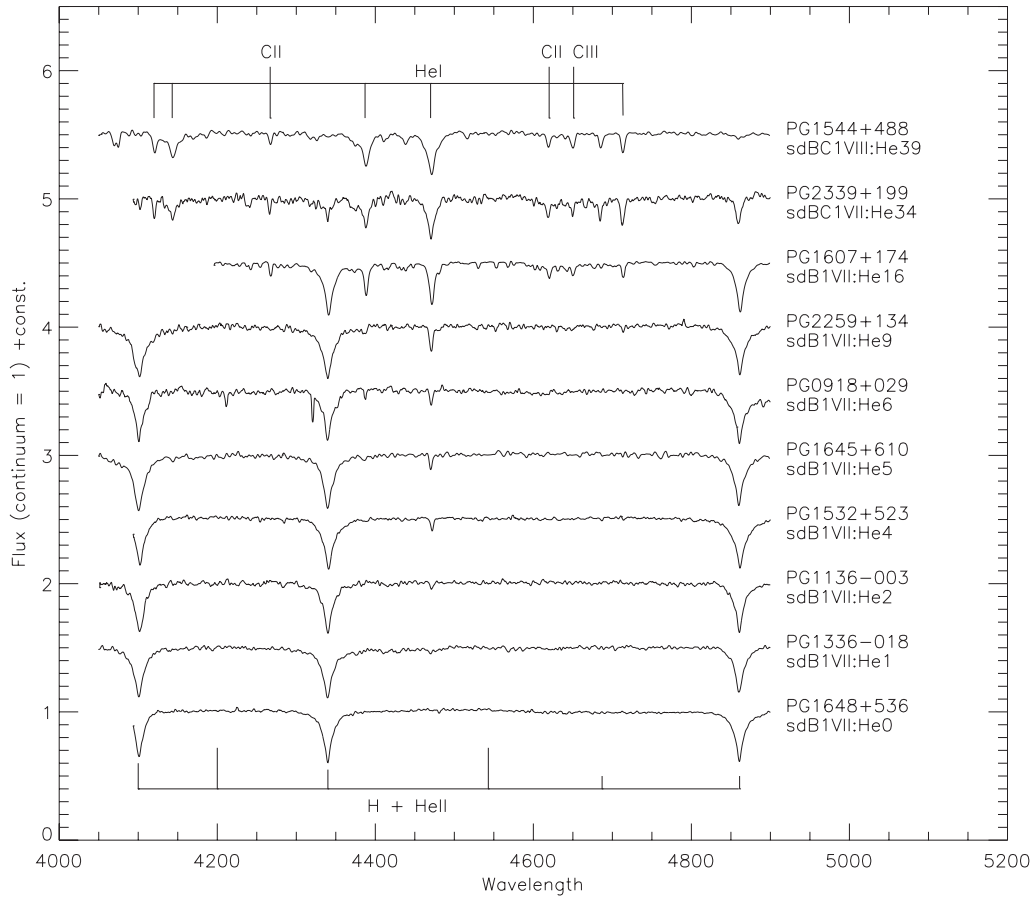


Figure 4.24 sdOB spectra at B1 showing sequence of increasing helium line strengths. The upper two stars are also carbon rich.

assigned. If they are noticeably broader, then it is a class VIII, and if noticeably narrower, then class VI. For spectra with line widths near the equivalent temperature MK class, then the star is assigned that MK class and luminosity. Figures 4.26 and 4.27 show luminosity sequences for sdO stars and sdB stars, respectively.

Some abundance effects are included, particularly in Figure 4.26, and these are inevitable with this group of diverse stars. What is remarkable is that these spectral sequences tie in successfully with the blue end of the horizontal-branch stars. Drilling et al. (2003) also show (in their Figure 10) the good correlation between their new sdOB types and those in the PG survey.

4.7.2 The Nature of the High-Galactic-Latitude “Normal” B-type Stars

The existence of faint blue stars at high Galactic latitudes has been known for many years (Humason & Zwicky 1947; Bidelman 1948), and these stars have been the subject of a series of “Faint Blue Stars” conferences (see, for instance, Philip,

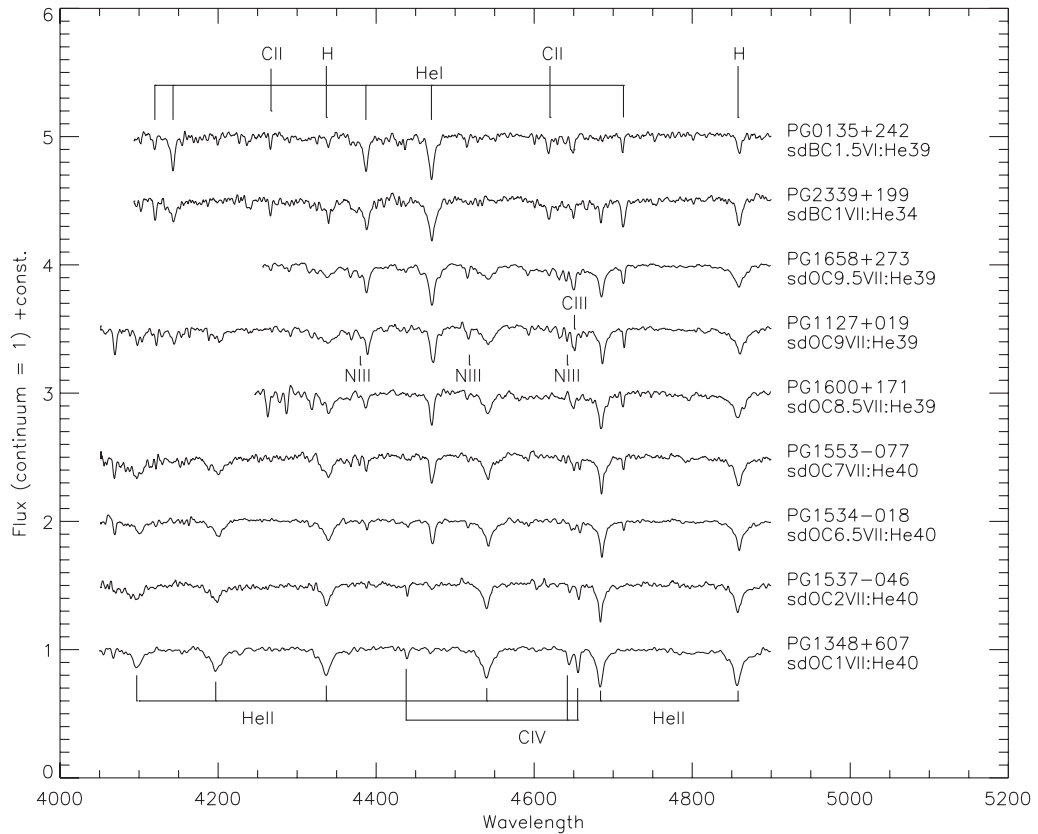


Figure 4.25 sdOB temperature sequence for extremely helium-rich and carbon-rich subdwarfs. NIII reaches its maximum strength at sdO9, which is also true for MK class V standards.

Liebert, & Saffer 1997). Most of these faint blue stars are white dwarfs (see Chapter 12), subdwarf OB stars (see the preceding section), and blue horizontal-branch (BHB) stars (see §5.6.1). However, there remain a handful of B-type stars at high Galactic latitudes, many of which have high velocities, that appear, at least superficially, to be normal B-type stars. Some examples include HD 137569, a late B-type peculiar supergiant at $l = +52^\circ$, HD 149363, an apparently normal B0.5 III star (Morgan, Code, & Whitford 1955) with $V_r = 146$ km/s and $l = +27^\circ$, and HD 220787, a mid B-type giant at $l = -64^\circ$. A listing of a number of such stars may be found in Martin (2004), a recent study of these stars.

Eliminating the categories of sdOB and BHB stars, there are three possible scenarios to explain these high Galactic latitude B-type stars:

1. Young, massive stars formed in the Galactic halo;
2. Massive Population I stars ejected from the Galactic disk; or
3. Old, evolved stars such as post asymptotic-giant-branch (post-AGB) stars.

How might these three classes of high-latitude B-type stars be distinguished? All three classes will likely have high velocities. Young, massive stars formed

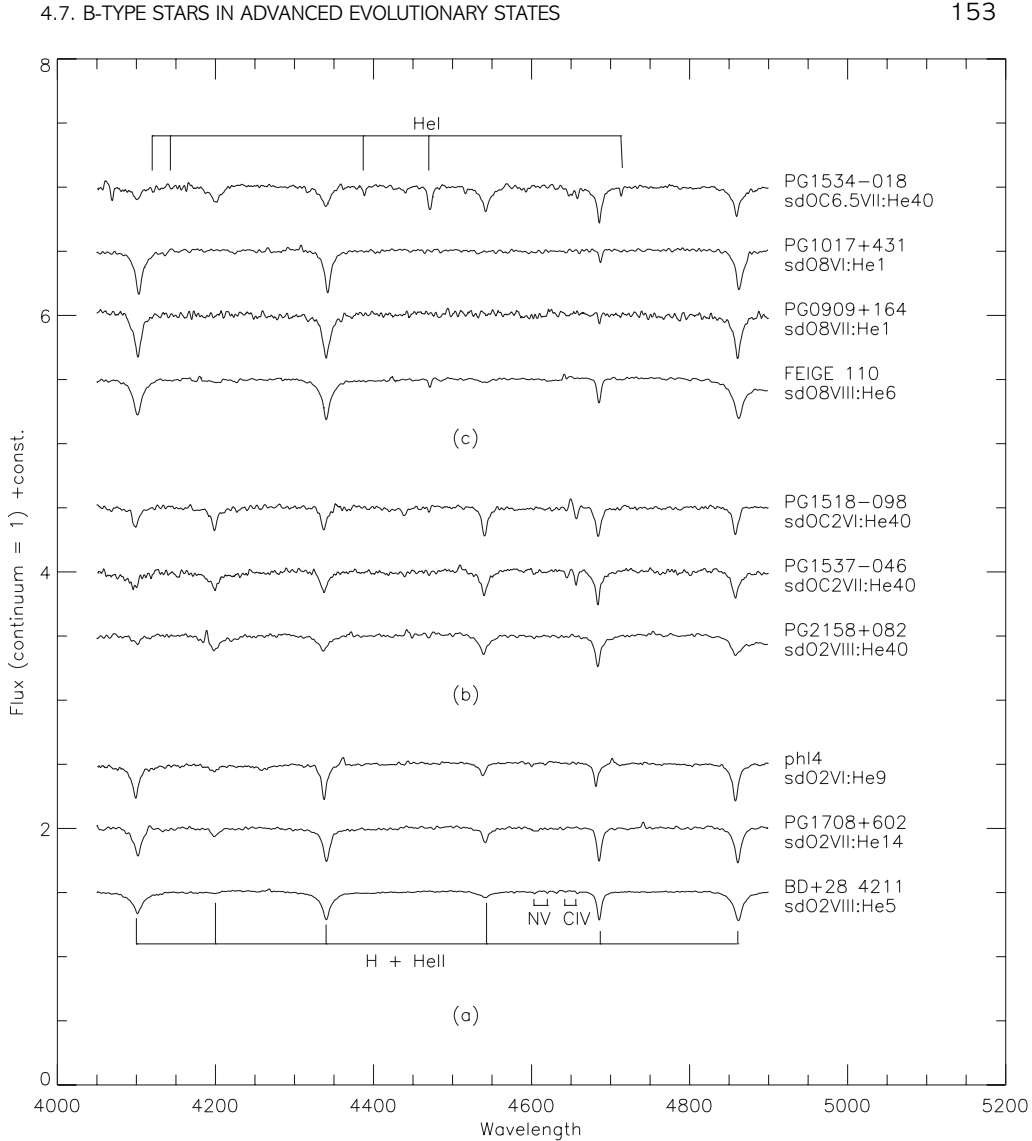


Figure 4.26 Luminosity sequence (a) for H-rich sdO2 stars, (b) for He-rich sdO2 stars, and (c) for sdO8 stars. The luminosity classes follow the broadening of the hydrogen and helium lines. Some abundance effects are also shown.

in the Galactic halo may be the progeny of the high-velocity gas clouds (HVC) observed at high Galactic latitudes in our Galaxy (see Van Woerden 1993). The chemical abundances of such stars would reflect the abundances of the HVCs for which there are very few data, although it is probably safe to assume that such stars would be metal-weak, and would have velocities similar to those of the HVCs. On the other hand, massive stars ejected from the disk should have normal Pop I abundances. A number of such stars are known, including AE Aur and μ Col, both of which have high space velocities in excess of 100 km/s, are moving in

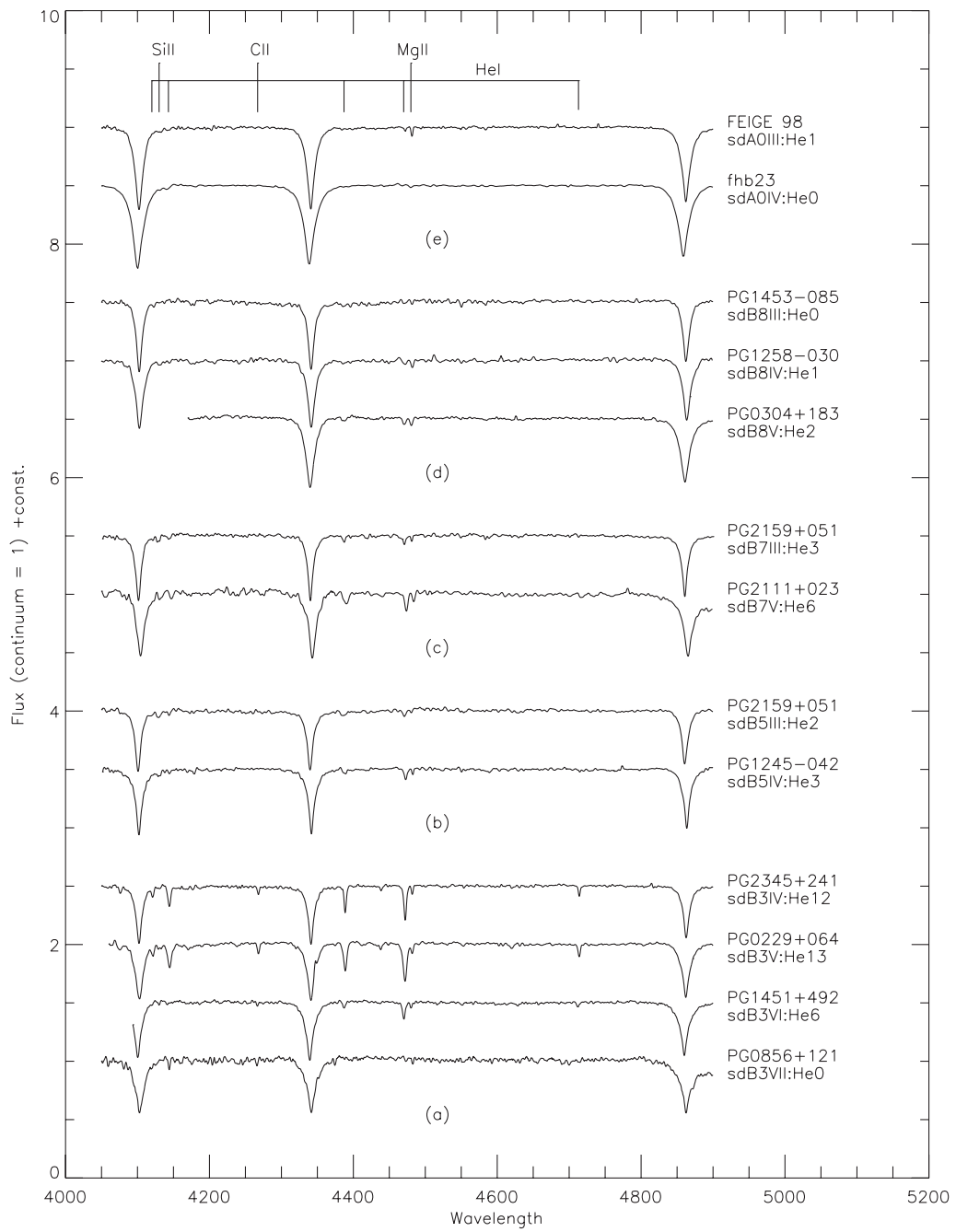


Figure 4.27 Luminosity sequence for sdB and sdA0 stars. The luminosity classes follow the broadening of the Balmer lines.

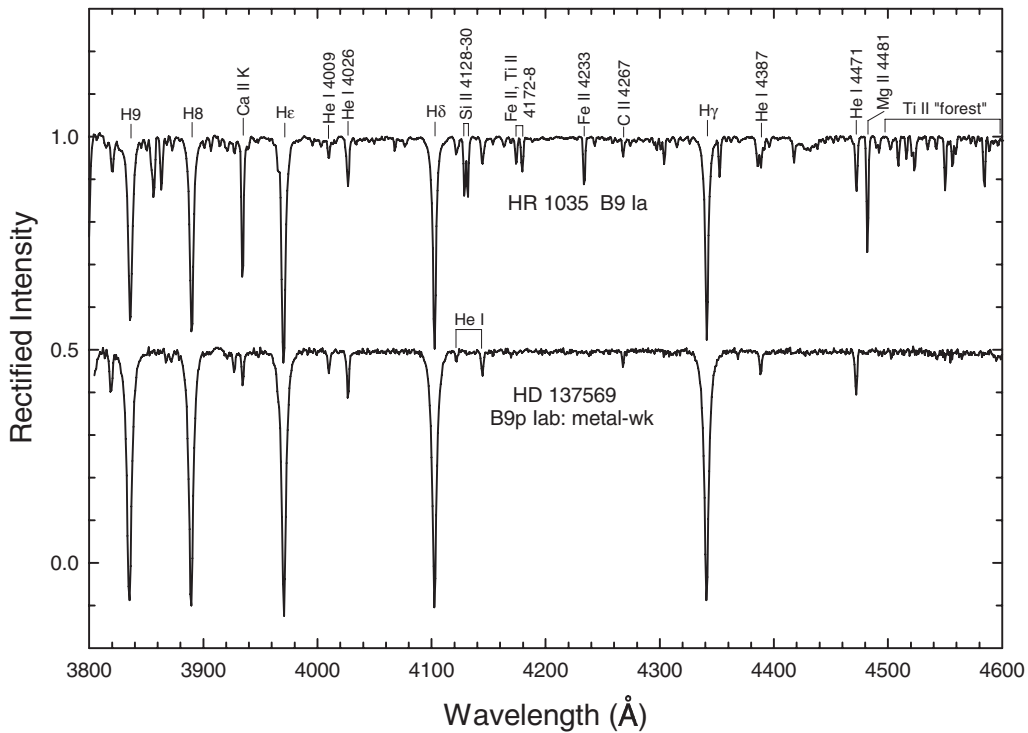


Figure 4.28 The high-Galactic-latitude, post-AGB star HD 137569 compared with the B9 Ia MK standard. Note the similarity of the two spectra, except that the metal lines in HD 137569 are all very weak. The one exception is C II $\lambda 4267$, which is of similar strength in the two spectra, indicating a near-solar abundance of carbon in HD 137569. Spectra obtained at the Dark Sky Observatory.

opposite directions, and which probably originated in the Orion Nebula about two million years ago (Blaauw & Morgan 1953, 1954). Such “runaway” stars may have acquired their high velocities through the disruption of a tight binary system (perhaps when the more massive component became a supernova, Blaauw 1961; Zwicky 1957) but an extensive study of the binary frequency and other properties of these runaway stars (Gies & Bolton 1986) suggests that the high velocities are the result of “single-binary, binary-binary, or n -body close encounters during the early dynamical evolution of associations.” Finally, stars in a post-AGB stage of evolution—a short-lived state in which a low-mass star evolves rapidly toward the blue from the tip of the *asymptotic giant branch* (AGB) in the process of the formation of a planetary nebula—should not only show enhancements of CNO and s -process elements (mixed to the surface during the AGB phase), but also infrared excesses due to dust ejected during the AGB phase. An example of such a post-AGB B-type star is Barnard 29, in the globular cluster M13. Essentially all high-latitude post-AGB B-type stars are Population II stars, and would also be metal-weak. Post-AGB stars are discussed in further detail elsewhere in this book.

What are the classifications of the high-latitude B-type stars mentioned at the beginning of this section? HD 137569 is generally regarded as a post-AGB star even though an infrared excess has not been detected, either with IRAS or at submillimeter wavelengths (van der Veen et al. 1994). However, an abundance analysis (Danziger & Jura 1970) showed that magnesium and silicon are underabundant by factors of 100 and 20, respectively, but carbon has a near-solar abundance. The high relative abundance of carbon strongly suggests this star is in the post-AGB phase. The metal-weak nature of HD 137569 and the overabundance of carbon relative to the other metals is clearly evident in the classification spectrum shown in Figure 4.28. This interesting star is in need of a modern abundance analysis. Its normally quoted spectral type of B5 III is completely spurious; see Figure 4.28 for our best effort at classifying this star. Finally, both HD 149363 and HD 220787 appear to be massive Population I stars ejected from the disk (Gies & Bolton 1986; Martin 2004), and have essentially normal spectra. There is no good evidence for the *in situ* formation of massive B-type stars in the Galactic halo (Martin 2006).

Bibliography

- Abt, H.A., & Levato, H. 1977, *PASP*, 89, 797
- Adelman, S.J., Adelman, A.S., & Pintado, O.I. 2003, *AA*, 397, 267
- Ahmad, A., & Jeffery, C. S. 2004, *Ap&SS*, 291, 253
- Allen, D.A., & Swings, J.P. 1976, *AA*, 47, 293
- Bagnulo, S., Jehin, E., Ledoux, C., Cabanac, R., Melo, C., Gilmozzi, R., & the ESO Paranal Science Operations Team 2003, *Messenger* 114, 10
- Bernacca, P.L. 1968, *Contr. Oss. Astrofiz. Univ. Padova*, No. 202
- Bidelman, W.P. 1948, *PASP*, 60, 264
- Bidelman, W.P. 1965, *AJ*, 70, 667
- Blaauw, A. 1961, *Bull. Astr. Inst. Netherlands*, 15, 265
- Blaauw, A., & Morgan, W.W. 1953, *Bull. Astr. Inst. Netherlands*, 12, 76
- Blaauw, A., & Morgan, W.W. 1954, *ApJ*, 119, 625
- Bohlender, D.A., Brown, D.N., Landstreet, J.D., & Thompson, I.B. 1987, *ApJ*, 323, 325
- Böhm-Vitense, E. 1967, *ApJ*, 150, 483
- Bond, H.E., & Levato, H. 1976, *PASP*, 88, 905
- Borra, E.F., Landstreet, J.D., & Thompson, I. 1983, *ApJS*, 53, 151
- Chentsov, E.L., Ermakov, S.V., Klochkova, V.G., Panchuk, V.E., Bjorkman, K.S., & Miroshnichenko, A.S. 2003, *AA*, 397, 1035
- Corbally, C.J., & Gray, R.O. 1994, in *Hot Stars in the Galactic Halo*, eds. S.J. Adelman, A.R. Upgren, & C.J. Adelman (Cambridge: Cambridge University Press), p. 253
- Dachs, J. 1987, in *IAU Colloquium #92 Physics of Be Stars*, eds. A. Slettebak & T.P. Snow (Cambridge: Cambridge University Press), p. 149
- Dachs, J., Hanuschik, R., Kaiser, D., & Rohe, D. 1986, *AA*, 159, 276
- Danziger, I.J., & Jura, M.A. 1970, *ApJ*, 161, 997
- Dolk, L., Wahlgren, G.M., & Hubrig, S. 2003, *AA*, 402, 299
- Drilling, J.S., Holberg, J.B., & Schoenberger, D. 1984, *ApJL*, 283, 67
- Drilling, J.S., Moehler, S., Jeffery, C.S., Heber, U., & Napiwotzki, R. 2003, in *The Garrison Festschrift*, eds. R.O. Gray, C.J. Corbally, & A.G.D. Philip (Schenectady: L. Davis Press), p. 27
- Dworetsky, M.M. 1973, *ApJL*, 184, 75
- Garrison, R.F. 1973, in *IAU Symposium #50 Spectral Classification and Multi-colour Photometry*, eds. Ch. Fehrenbach & B.E. Westerlund (Dordrecht: Reidel)
- Garrison, R.F., Hiltner, W.A., & Schild, R.E. 1977, *ApJS*, 35, 111

- Garrison, R.F., & Gray, R.O. 1994, *AJ*, 107, 1556
- Gies, D.R., & Bolton, C.T. 1986, *ApJS*, 61, 419
- Green, R.F., Schmidt, M., & Liebert, J. 1986, *ApJS*, 61, 305
- Gulliver, A.F. 1977, *ApJS*, 35, 441
- Hanuschik, R.W., Hummel, W., Sutorius, E., Dietle, O., & Thimm, G. 1996, *AApS*, 116, 309
- Hartoog, M.R., & Cowley, A.P. 1979, *ApJ*, 228, 229
- Hearnshaw, J.B. 1986, *The Analysis of Starlight* (Cambridge: Cambridge University Press)
- Heck, A., Egret, D., Jaschek, M., & Jaschek, C. 1984, *IUE Low Dispersion Spectra Reference Atlas*, ESA SP-1052
- Hiltner, W.A., Garrison, R.F., & Schild, R.E. 1969, *ApJ*, 157, 313
- Hubrig, S., & Castelli, F. 2001, *AA*, 375, 963
- Humason, M.L., & Zwicky, F. 1947, *ApJ*, 105, 85
- Humphreys, R.M., & Davidson, K. 1979, *ApJ*, 232, 409
- Jaschek, M., Hubert-Delplace, A.-M., Hubert, H., & Jaschek, C. 1980, *AApS*, 42, 103
- Jaschek, M., Jaschek, C. & Arnal, M. 1969, *PASP*, 81, 650
- Koubský, P., Harmanec, P., Kubát, J., Hubert, A.-M., Božić, H., Floquet, M., Hadrava, P., Hill, G., & Percy, J.R. 1997, *AA*, 328, 551
- Lamers, H.J.G.L.M., Zickgraf, F.-J., de Winter, D., Houziaux, L., & Zorec, J. 1998, *AA*, 340, 117
- Leckrone, D.S., Proffitt, C.R., Wahlgren, G.M., Johansson, S.G., & Brage, T. 1999, *AJ*, 117, 1454
- Lesh, J.R. 1968, *ApJS*, 16, 371
- Levato, H., & Malaroda, S. 1979, *PASP*, 91, 789
- Martin, J.C. 2004, *AJ*, 128, 2474
- Martin, J.C. 2006, *AJ*, 131, 3047
- Mathys, G., & Hubrig, S. 1995, *AA*, 293, 810
- Miroshnichenko, A.S. 2007, *ApJ*, 667, 497
- Miroshnichenko, A.S., Chentsov, E.L., & Klochkova, V.G. 2000, *AApS*, 144, 379
- Moni Bidin, C., Mendez, R.A., Moehler, S., Piotti, G., Recio-Blanco, A., & Momany, Y., 2006, *Baltic Astronomy*, 15, 53
- Morgan, W.W. 1931, *ApJ*, 73, 104
- Morgan, W.W., Abt, H.A., & Tapscott, J.W. 1978, *Revised MK Spectral Atlas for Stars Earlier than the Sun* (Chicago and Tucson: Yerkes Observatory, University of Chicago, and Kitt Peak National Observatory)
- Morgan, W.W., Code, A.D., & Whitford, A.E. 1955, *ApJS*, 2, 41
- Norris, J. 1971, *ApJS*, 23, 213
- Osawa, K. 1965, *Ann. Tokyo Astron. Obs.*, Ser. 2, 9, 123
- Ostensen, R.H. 2004, *Ap&SS*, 291, 263
- Panek, R.J., & Savage, B.D. 1976, *ApJ*, 206, 167
- Philip, A.G.D., Liebert, J.W., & Saffer, R.A., eds. 1997, *The Third Conference on Faint Blue Stars* (Schenectady: L. Davis Press)

- Porter, J.M., & Rivinius, T. 2003, *PASP*, 115, 1153
- Rountree, J., & Sonneborn, G. 1991, *ApJ*, 369, 515
- Ryabchikova, T. 1998, *Contr. Astron. Obs. Skalnaté Pleso*, 27, 319
- Sargen, W.L., & Jugaku, J. 1961, *ApJ*, 134, 777
- Schild, R.E. 1966, *ApJ*, 146, 142
- Secchi, A. 1867, *Astron. Nachr.*, 68, 63
- Sharpless, S. 1952, *ApJ*, 116, 251
- Shore, S.N., & Brown D.N. 1990, *ApJ*, 365, 665
- Slettebak, A. 1994, *ApJS*, 94, 163
- Slettebak, A., & Snow, T.P., eds. 1987, *Physics of Be Stars*, Proceedings of the 92nd Colloquium of the IAU, Boulder, CO 18–22 Aug 1986 (Cambridge: Cambridge University Press)
- Smith, M.A., Henrichs, H.F., & Fabregat, J., eds. 2000, *The Be Phenomenon in Early-Type Stars*, IAU Colloquium 175, Astronomical Society of the Pacific Conference Series No. 214 (San Francisco: Astronomical Society of the Pacific)
- Smith Neubig, M.M., & Bruhweiler, F.C. 1997, *AJ*, 114, 1951
- Smith Neubig, M.M. & Bruhweiler, F.C. 1999, *AJ*, 117, 2856
- Struve, O. 1931, *ApJ*, 73, 94
- Swings, J.P., & Andriolat, Y. 1979, *AA*, 74, 85
- Talavera, A., & Gómez de Castro, A.I. 1987, *AA*, 181, 300
- Underhill, A., & Doazan, V. 1982, *B Stars With and Without Emission Lines*, in the Monograph Series on Nonthermal Phenomena in Stellar Atmospheres (Washington DC: NASA)
- Valdes, F., Gupta, R., Rose, J.A., Singh, H.P., & Bell, D.J. 2004, *ApJS*, 152, 251
- van der Veen, W.E.C.J., Waters, L.B.F.M., Trams, N.R., & Matthews, H.E. 1994, *AA*, 285, 551
- Van Woerden, H. 1993, in *Luminous High-Latitude Stars*, ed. D.D. Sasselov, ASP Conference Series No. 43, p. 11
- Verdugo, E., Talavera, A., & Gómez de Castro, A.I. 1999, *AApS*, 137, 351
- Wade, G.A., Bohlender, D.A., Brown, D.N., Elkin, V.G., Landstreet, J.D., & Romanyuk, I.I. 1997, *AA*, 320, 172
- Wahlgren, G.M. 2004, in *The A-Star Puzzle*, IAU Symposium # 224, eds. J. Zverko, J. Žižňovský, S.J. Adelman, & W.W. Weiss (Cambridge: Cambridge University Press), p. 291
- Werner, K., & Heber, U. 1991, *AA*, 247, 476
- Whitford, A.E. 1962, *AJ*, 67, 640
- Zickgraf, F.-J. 1998, in *B[e] stars*, Astrophysics and Space Science Library, Vol. 233, eds. A.M. Hubert & C. Jaschek (Dordrecht: Kluwer Academic Publishers), p. 1
- Zickgraf, F.-J. 2000, in *The Be Phenomenon in Early-Type Stars*, IAU Colloquium 175, Astronomical Society of the Pacific Conference Series No. 214, eds. M.A. Smith, H.F. Henrichs, & J. Fabregat (San Francisco: Astronomical Society of the Pacific)
- Zwicky, F. 1957, *Morphological Astronomy* (Berlin: Springer), p. 258

Chapter Five

The A-type Stars

5.1 INTRODUCTION

On first acquaintance, spectra of the A-type stars appear to be, apart from the strong hydrogen lines of the Balmer series, nearly featureless and thus uninteresting. In reality, however, the A-type stars encompass a bewildering array of stellar types. Over 30% of A-type stars show some sort of chemical peculiarity, ranging from the Ap stars with bizarre abundance patterns that vary from star to star, often involving large overabundances of certain elements, to the λ Bootis stars with large *underabundances* of most metals. At high resolution all slowly rotating A-type stars may prove to be peculiar in one way or another. Vega (A0 Va), one of the brightest stars in the sky and a prime standard for photometry, spectrophotometry, and the MK System, is now known to be a rapidly rotating star seen pole-on. The A-type star region in the H–R diagram contains stars in a range of evolutionary states. Many horizontal-branch stars—stars that have been through the red-giant stage and are now burning helium in their cores—are A-type stars. In addition, a brief phase of evolution, immediately before the planetary-nebula stage, can produce stars that look like peculiar A-supergiants.

We will begin this chapter by considering the spectral classification of the *normal* A-type stars. It turns out that many A-type stars are rapid rotators, and this rapid rotation can introduce, unless care is taken, important systematic effects into the classification system. We will then move on to consider the zoo of chemically peculiar A-type stars, the pre-main-sequence Herbig Ae/Be stars, A-type stars in advanced stages of evolution, and then, finally, the A-type shell stars.

5.2 OPTICAL SPECTRAL-TYPE CRITERIA

5.2.1 Temperature Criteria

The original definition of the boundary between the A-star class and the B-star class was based on the disappearance of lines of He I from the classification spectrum, although it turns out that in high S/N digital spectra some A0 MK standard stars show weak lines of He I. Figure 5.1 shows a spectral (i.e. temperature) sequence of *normal* A-type main-sequence stars in the traditional blue-violet region of the spectrum. An examination of this sequence reveals a number of features that can be used in the temperature classification of the A-type stars. These features are, first, the hydrogen Balmer lines that go through a broad maximum at about A2, second, the Ca II K-line which grows dramatically in strength toward

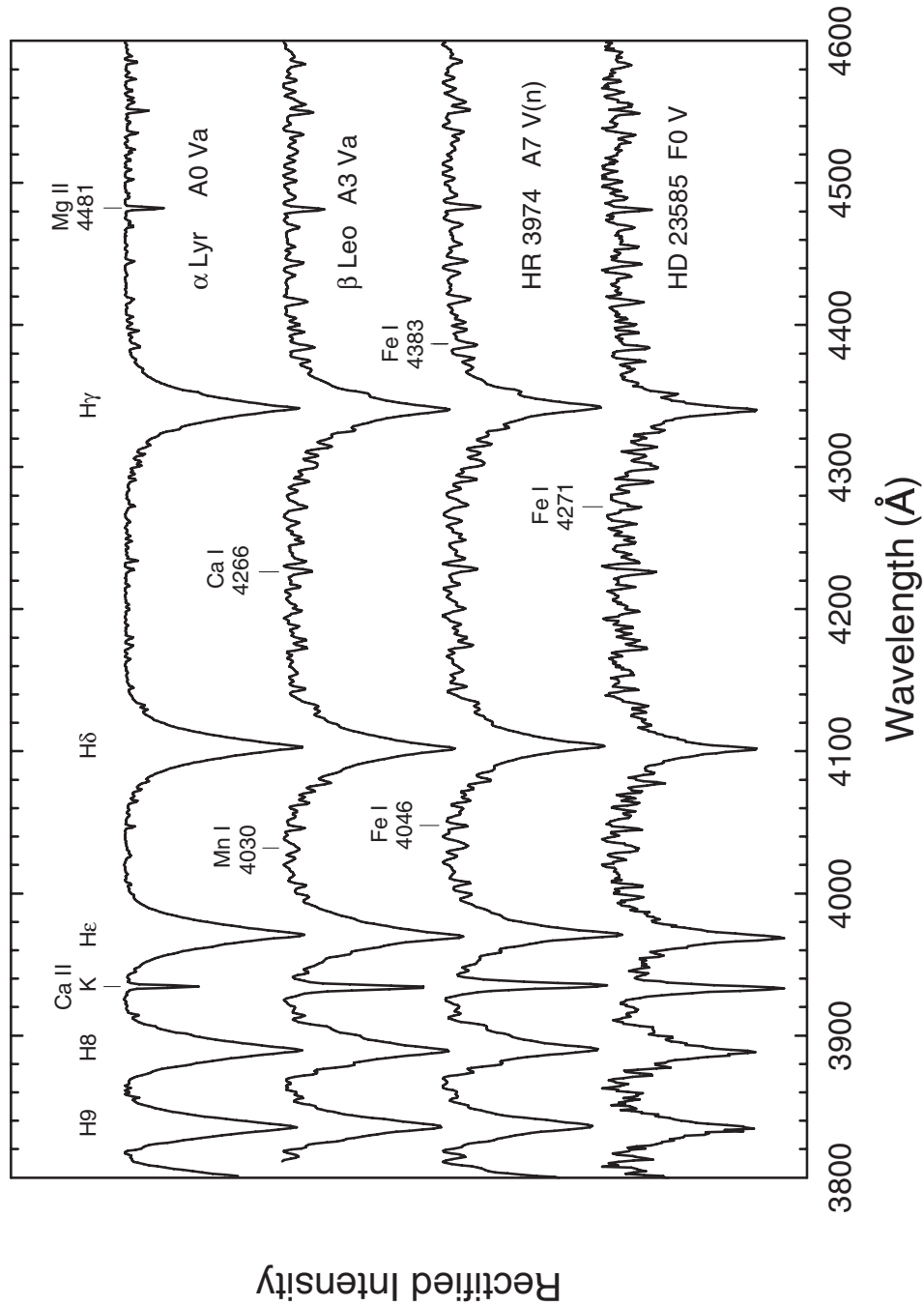


Figure 5.1 A temperature sequence for the main-sequence A-type stars. The spectral features marked are useful in temperature classification of the A-type stars (see text). Unless otherwise specified, all spectra in illustrated in this chapter have a resolution of 1.8 \AA , and were obtained at the Dark Sky Observatory. These spectra have been rectified and vertically offset by 0.7 continuum units.

later types, and third, the general metallic-line spectrum which also strengthens toward later types.

It turns out, as we shall see in the next section, that the hydrogen lines and certain metal lines, especially lines of ionized iron and titanium (Fe II and Ti II), are also sensitive to luminosity in the A-type stars. The strength of the Ca II K-line (or better, especially in the late A-type stars, its ratio with H ϵ or H δ) is therefore the prime temperature criterion in the A-type stars, but classifiers must be aware that in certain peculiar A-type stars the Ca II K-line may be unusually weak. Only in the so-called “normal” A-type stars do all three criteria—the Ca II K-line, the hydrogen lines, and the general metallic-line spectrum—give a consistent spectral type. Metal lines due to neutral species such as Fe I and Ca I are relatively insensitive to luminosity, and therefore can be quite useful in temperature classification. These lines include the Ca I λ 4226 line, the Fe I blend at λ 4271, and certain other Fe I lines, especially those that arise from low-lying states, such as Fe I λ 4046 and Fe I λ 4383. The broad Mn I λ 4030 blend is also useful. These features increase in strength with declining temperature. The classifier must be aware, however, that even these lines can have abnormal strengths in chemically peculiar stars. For instance in the Am stars (see §5.4.1), both the Ca II K-line and the Ca I λ 4226 line are anomalously weak, whereas most lines due to iron-peak elements are enhanced.

5.2.2 Luminosity Criteria

The primary luminosity criterion, at least in the early A-type stars (earlier than A6), is the wings of the hydrogen lines. Figure 5.2 shows a luminosity sequence at a spectral type of A0; note the exquisite sensitivity of the hydrogen-line profiles to luminosity class. However, by spectral type A7 (see Figure 5.3), the hydrogen lines show a much reduced sensitivity to luminosity, and by F2 the hydrogen-line profiles are essentially completely insensitive to luminosity, except possibly for the separation of the supergiant classes. It should be noted that the shape of the hydrogen-line profile is a function of both luminosity (surface gravity) and temperature, and so in the A-type stars the luminosity class must be determined simultaneously with the temperature class (usually an iterative process). This is especially important in the metal-weak A-type stars, such as the λ Bootis stars (§5.4.3) and the horizontal-branch stars (§5.6.1), as the general metal-weak nature of those spectra can fool the novice classifier into assigning too early a spectral type, which in turn can lead to too luminous a luminosity type.

In the early A-type stars, *zero-age main-sequence* stars have noticeably broader hydrogen-line wings than the A0 dwarf standard, Vega (α Lyrae). Such stars are given a luminosity class of Vb, while Vega is assigned a luminosity class of Va. This notation is used for stars with spectral types between B9 and A3 (it is also commonly utilized for G-type dwarfs). For instance, β Leo and α PsA are both A3 Va MK standards. With good high S/N spectra, it is possible in the early A-type stars to make even finer distinctions in the luminosity class. Thus, a luminosity

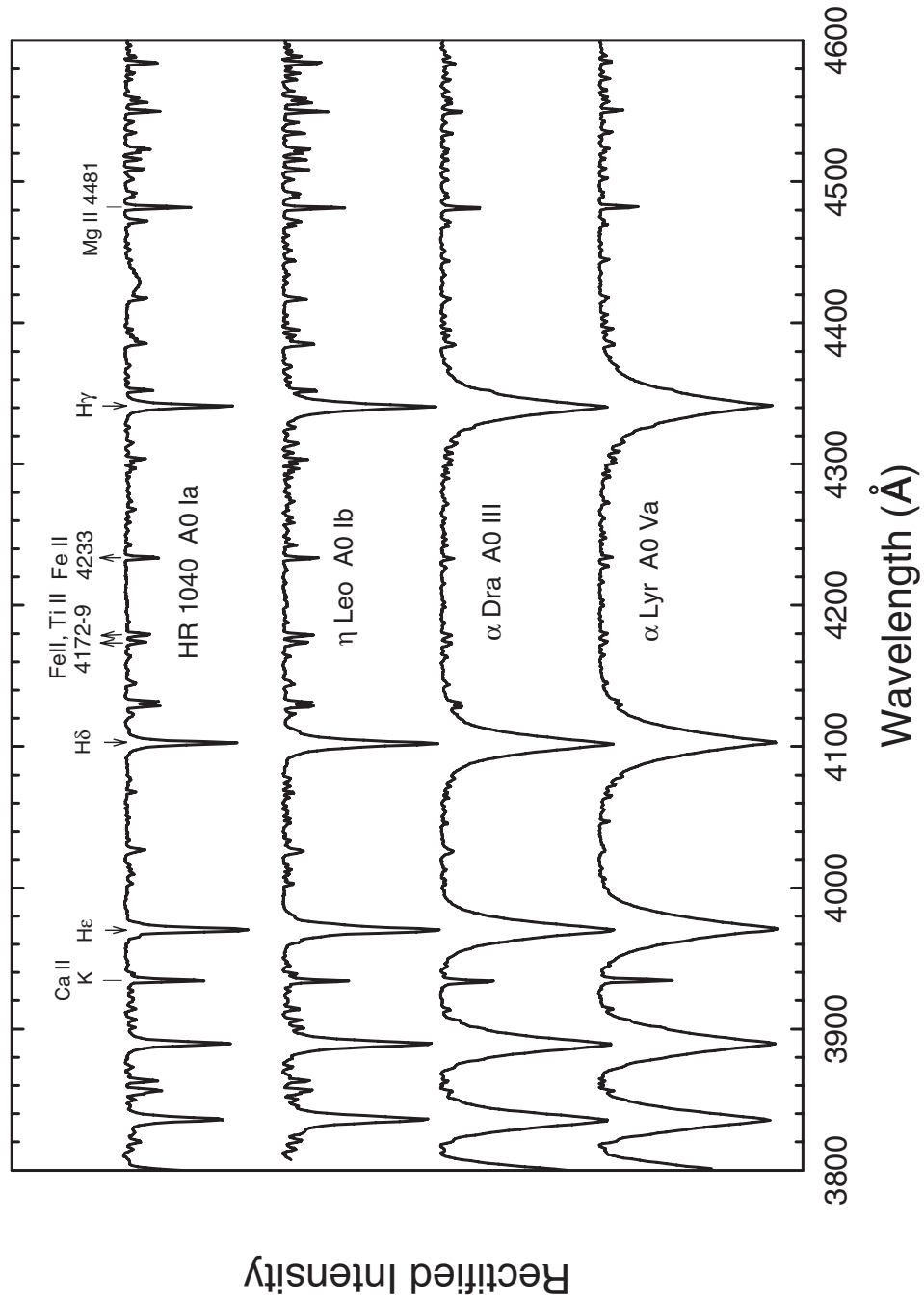


Figure 5.2 Luminosity effects at A0. Spectral features marked with upward arrows show a positive luminosity effect, while the downward arrows indicate spectral features that show a negative luminosity effect. Spectral features marked with a line are insensitive to luminosity. Spectra obtained at the Dark Sky Observatory.

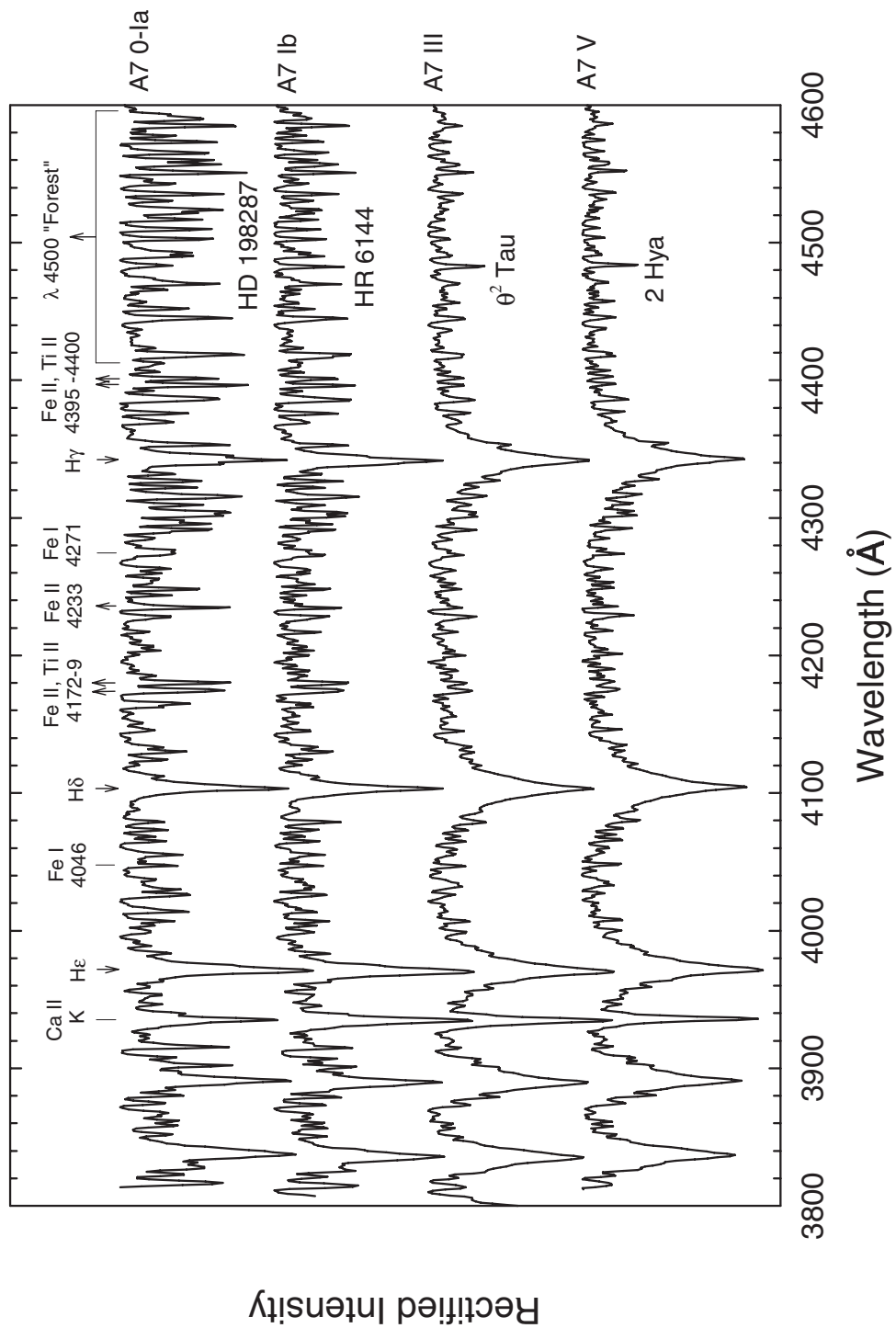


Figure 5.3 Luminosity effects at A7. See Figure 5.2 for an explanation of the symbols. Notice the difficulty in discriminating an A7 giant from an A7 dwarf on the basis of both the hydrogen lines and lines of ionized metals. Note that neither HD 198287 nor HR 6144 is an MK standard. Spectra obtained at the Dark Sky Observatory.

type between Va and IV–V is commonly indicated by Va^+ , and between Va and Vb, Va^- .

Because the luminosity sensitivity of the hydrogen lines fades with declining temperatures, the luminosity type in the late A-type stars must be judged from the enhancement of certain lines of ionized iron and titanium. In the blue-violet, useful luminosity-sensitive lines include the $\lambda\lambda 4172\text{--}4179$ blend of Fe II and Ti II, and the $\lambda 4395$ and $\lambda 4400$ blends, also due primarily to Fe II and Ti II. Indeed, there is an entire forest of Fe II and Ti II lines in the vicinity of $\lambda 4500$ that is enhanced in luminous stars. The strengths of these blends are best estimated in ratio with the Fe I features mentioned in the previous section. In the early A-type stars these blends are enhanced only in the supergiant classes, but in the late A-type stars (later than A7), they begin to become useful in separating dwarfs from giants, and, in the early F-type stars, these same blends are sensitive enough to allow a very fine discrimination between the luminosity classes. What this means is that in the mid A-type stars, especially around A7, luminosity classification (especially the separation of dwarfs from giants) is quite difficult, as the hydrogen lines have lost most of their luminosity sensitivity, whereas lines of ionized iron and titanium have not yet gained the full sensitivity they exhibit in the early F-type stars (see Figure 5.3).

5.2.3 The Effects of Rotation

Rapid rotation can affect stellar spectral classification in two important ways. First, rapid rotation broadens the spectral lines and thus effectively reduces the resolution of the spectrum. This can complicate the comparison between the standard stars and the program star and can lead to the introduction of systematic effects in the spectral types of rapid rotators. This problem used to be particularly serious in the classification of photographic spectra (which were generally classified directly from the glass plates using a dissecting microscope or a spectra comparator), and this led Gray & Garrison (1987, 1989a, b) to define parallel systems of low and high rotational-velocity standards for the A-type stars. However, today with the availability of modern digital spectra and fast computers, it is possible, with the appropriate software, to artificially rotationally broaden the standard to match the rotational velocity (actually the *projected* rotational velocity, $v \sin i$, where v is the equatorial rotational velocity and i is the inclination of the rotational axis) of the program star.

The second effect comes about because rotation actually introduces physical changes into the stellar atmosphere. With rapid rotation, both the local effective temperature and the gravity vary over the surface of the star. For instance, the equator will have a lower effective temperature and gravity than the polar regions. What this means is that the spectrum of a rapidly rotating star, whether seen in the equatorial plane or pole-on, is actually a composite spectrum. This suggests that an artificially rotationally broadened spectrum of a standard star will never be a perfect match with the spectrum of a true rapid rotator, and thus the Gray & Garrison parallel systems of A-type standards are still useful in precision classification.

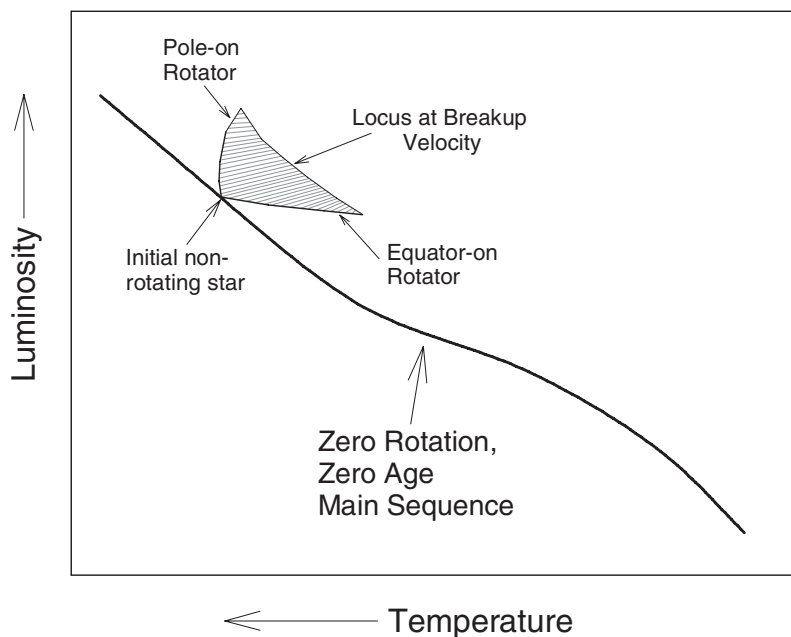


Figure 5.4 A schematic representation of how rotation affects the position of a star in the H–R diagram. An initially non-rotating star, if spun up, would move into the shaded area of the diagram; the boundaries of the shaded area represent the extreme situations of viewing the star either exactly pole-on, or exactly equator-on. In any case, a rotating star generally appears to be above the main sequence.

Rotation displaces a star in the H–R diagram. Consider a star seen in the equatorial plane. If it were possible to increase this star's rotational velocity, we would see it move to the right and down (toward cooler temperatures and lower luminosities). On the other hand, a star seen pole-on would move generally upwards in the H–R diagram (toward higher luminosities). Neither of these paths is necessarily parallel to the main sequence, and so a rapidly rotating main-sequence star, no matter the orientation, tends to lie above the main sequence (see a schematic illustration in Figure 5.4). These effects have been investigated theoretically in a number of papers (e.g., Collins & Sonneborn 1977; Slettebak, Kuzma, & Collins 1980; Collins & Smith 1985). Gray & Garrison (1987, 1989a, b) have investigated these effects empirically in the A- and early F-type stars and have detected subtle *differential effects* in the spectra and photometry of rapid rotators, even those that are seen pole-on.

A case in point is Vega, one of the brightest stars in the sky and the MK A0 Va standard. It has been known for some decades (see Petrie 1964) that Vega is over-luminous (by 0.7 magnitudes) for its spectral type. Petrie suggested that it might be a binary, but radial velocity studies and interferometric observations effectively ruled that out (see Hanbury Brown et al. 1967). Gray (1985, 1988) suggested that Vega might be a rapid rotator seen pole-on. This was later established with

high-resolution spectroscopy by Gulliver et al. (1991) and more recently by optical interferometry (Aufdenberg et al. 2006; Peterson et al. 2006).

5.2.4 The Physical Basis of Classification in the A-type Stars

STARK BROADENING OF THE HYDROGEN LINES

The enormous width of the hydrogen lines achieved in the A-type stars is due to the interaction of electrons and ions with the neutral hydrogen atom. The energy levels in an isolated hydrogen atom are degenerate; each level, characterized by the principal quantum number n , actually has a $2n^2$ -fold degeneracy. When the hydrogen atom is subjected to an external electric field, this degeneracy is lifted, and the level is split into $2n^2$ sublevels. This means that under the influence of an external field, the line profile will consist of a number of discrete *Stark components* that arise from transitions between the various sublevels of the lower and upper states. In general, the shift, $\Delta\lambda$, of these components from the undisturbed line center will be proportional to the external field strength. In a stellar atmosphere, this external field is produced by electrons and ions in the vicinity of the atom. Since these perturbers are moving, the external field will be fluctuating, and the $\Delta\lambda$ for each component will be constantly changing. Consider the ensemble of hydrogen atoms in the stellar atmosphere, each experiencing a different, fluctuating, external field: the net result will be a spectral line spread out into a broad profile. The width of this profile will depend on the characteristic ion and electron density in the atmosphere. This process, which is the dominant broadening mechanism for hydrogen lines in the B- and A-type stars, is called the *Stark effect*. A more quantitative treatment of the Stark effect can be found in Mihalas (1978). The Stark effect is primarily responsible for the sensitivity of the hydrogen lines to gravity (luminosity) in the B- and early A-type stars, and also helps to explain why the hydrogen lines narrow with decreasing temperature.

Considering the above explanation of the Stark effect, it may be difficult to understand why the sensitivity of the hydrogen lines to luminosity is much reduced by a spectral type of A7, and has nearly vanished by F0. At A7 and F0 the predominant broadening mechanism for the hydrogen lines is still the Stark effect. An answer to this mystery may be found in Figure 5.5. In this figure the width of the hydrogen lines is plotted as a function of both the temperature and the gravity. Main sequence (dwarf stars) have $\log g \approx 4.2$, whereas $\log g \approx 3.0$ for giant stars. For supergiant stars, $\log g \lesssim 1.5$. The width of the hydrogen line plotted in this figure corresponds to the full width at a level 0.8 continuum units above zero intensity of the $H\gamma$ line. In the early A-type stars (A3 and earlier, corresponding to $T_{\text{eff}} \geq 8500$ K), the width of the hydrogen lines at any given temperature is a strong function of the gravity, and the curves for the different gravities are well separated. However, beginning at $T_{\text{eff}} \sim 8500$ K, the high-gravity curves begin to merge, and then with declining temperature the curves representing lower and lower gravities begin to overlap. By 7000 K, the hydrogen-line widths are practically the same for values of $\log g$ between 2.0 and 4.5. The main cause of this steady decline in

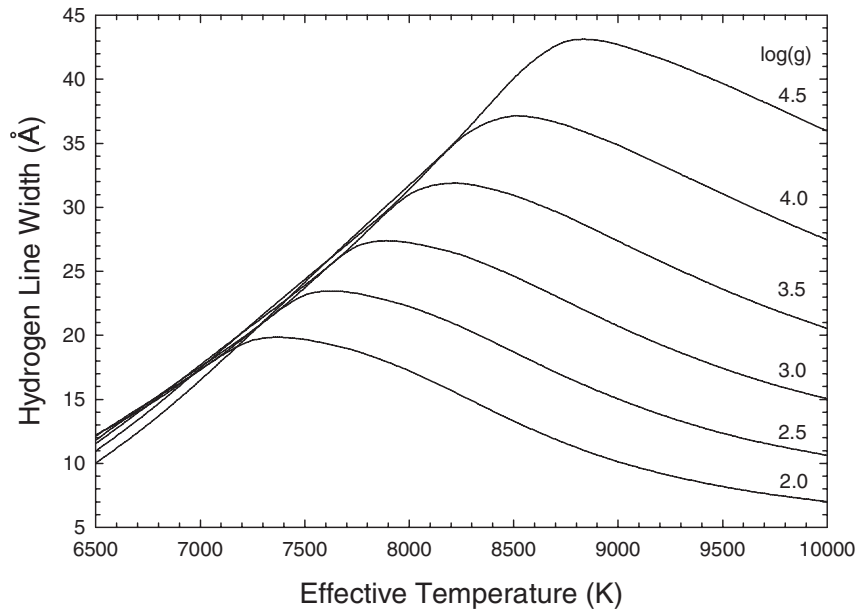


Figure 5.5 The dependence of hydrogen-line width on effective temperature and gravity ($\log g$). The gravity is labelled for each curve. Note that as the gravity (pressure) declines, the Balmer maximum migrates to lower temperatures. It is mainly this effect that reduces the sensitivity of the hydrogen lines to luminosity in the late A- and F-type stars. A spectral type of A7 corresponds to $T_{\text{eff}} \approx 7700$ K. Note that the ability to discriminate between dwarfs ($\log g \approx 4.2$) and subgiants ($\log g \approx 3.5$) is lost first with declining temperature. At cooler temperatures, even the giants cannot be distinguished from the dwarfs. The hydrogen-line widths were computed with SPECTRUM and the latest Castelli & Kurucz (2003) models.

the sensitivity of the hydrogen lines can be seen to be the migration of the Balmer maximum toward lower temperatures with decreasing $\log g$, an effect we explored semi-quantitatively in §2.4.2. This migration conspires with the natural decline in the Stark width with decreasing temperature to almost exactly cancel the variation in hydrogen-line width with gravity.

However, not all is lost. While the hydrogen-line width loses its sensitivity to luminosity in the late A-type stars, the actual shape of the hydrogen-line profile is still slightly different for dwarfs and giants, even at F0. In solar abundance stars, it is difficult to take advantage of this, because line blanketing obscures the true hydrogen-line profile, but in metal-weak stars, such as the horizontal-branch stars (see §5.6.1), with good S/N spectra, the hydrogen lines may be used for luminosity classification throughout the A-type stars.

SENSITIVITY OF Fe II AND Ti II LINES TO LUMINOSITY

We will discuss the physics behind the luminosity criteria based on lines of Fe II and Ti II in much more detail in Chapter 6 on the F-type stars. Here, we discuss the

reason why these lines are relatively insensitive to luminosity (gravity) in the early and mid A-type stars and become useful luminosity criteria only in the late-A type stars. In the early to mid F-type stars, these lines constitute the prime luminosity criteria and allow a very fine discrimination between the luminosity classes.

The basic physics behind the luminosity, or gravity, sensitivity of these lines may be understood from the ionization equilibrium:



In giant and supergiant atmospheres the lower electron density (due to the lower density of the atmosphere overall) drives this equation to the right, thus increasing the abundance of Fe II relative to Fe I (and similarly for titanium). This behavior may also be deduced from the Saha equation (Equation 2.4.5), which indicates that $N_{(i+1)}/N_{(i)} \propto 1/N_e$, where $N_{(i+1)}$ and $N_{(i)}$ are the number densities of adjacent ionization states, and N_e is the electron number density. This pressure sensitivity of the Fe II/Fe I ratio (and likewise the Ti II/Ti I ratio) constitutes the basic physics behind the sensitivity of these features to luminosity.

However, as we mentioned above, the luminosity criteria based on Fe II and Ti II lines are much more sensitive, and provide much greater luminosity discrimination, in the early F-type stars than in the A-type stars. The reason for this is not entirely clear, but it appears to be related to the phenomenon of *microturbulence*. Microturbulence desaturates the core of a spectral line, and can thus lead to strengthening of the line. As we explain in §6.2.3, in the F-type stars, the microturbulent velocity (ξ_t) increases monotonically with increasing luminosity, and this behavior is necessary to explain fully the sensitivity of Fe II and Ti II lines to luminosity. In the A-type stars, however, the microturbulent velocity does not change monotonically with increasing luminosity; Gray, Graham, & Hoyt (2001) found that giants and even bright giants have essentially the same microturbulent velocity as dwarfs. This behavior may be related to the lack of convection in the atmospheres of A-type stars, but it apparently is the main reason why the Fe II and Ti II lines are not very sensitive to luminosity in the A-type stars. Read §6.2.3 for a fuller explanation of the importance of microturbulence to the behavior of metallic-line-based luminosity criteria.

5.3 ULTRAVIOLET AND INFRARED CLASSIFICATION SCHEMES

5.3.1 Ultraviolet

Spectral classification systems in the ultraviolet (primarily using IUE spectra) have been developed by Walborn for the OB-type stars (see Chapter 3) and by Lesh for the B-type stars (see Chapter 4). However, very little work has been done on the classification of A-type stars in the ultraviolet. There are a number of reasons for this. First, the vast majority of IUE spectra were obtained of O, B, and other classes of hot stars, and so the amount of spectral material, especially in the high-resolution mode of that satellite, is much more limited for the A-type stars. Second,

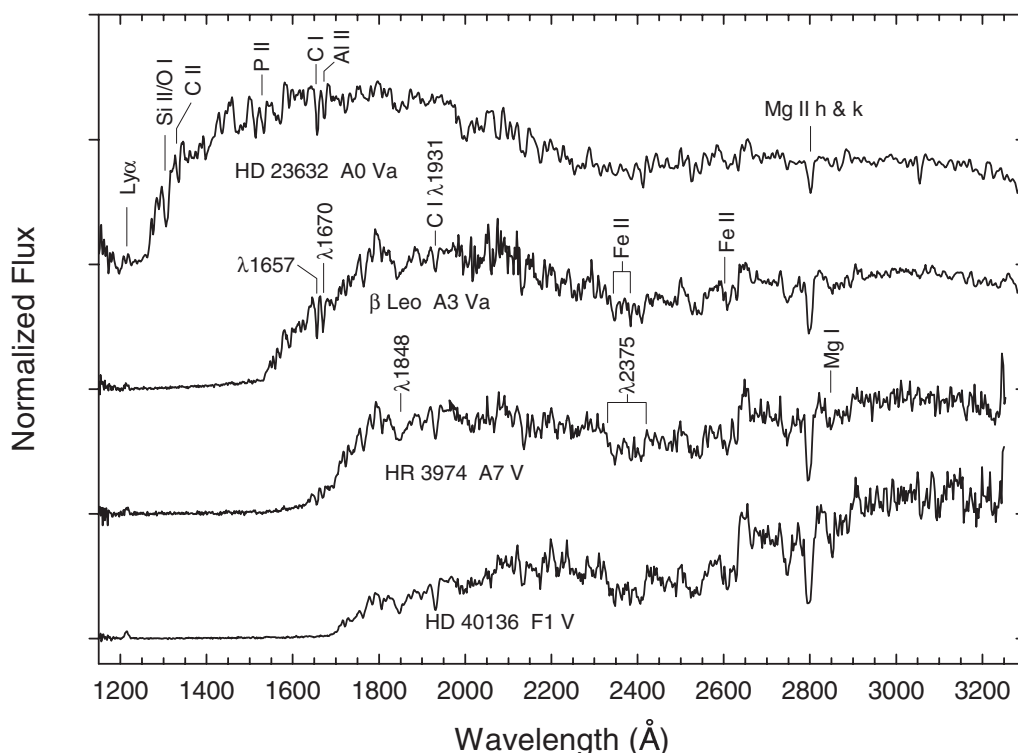


Figure 5.6 A spectral sequence in the IUE ultraviolet. The spectral types given were determined in the blue-violet. The spectra were normalized at 2650 Å, and given an integer vertical offset for clarity. The spectra are from the MAST IUE archive (<http://archive.stsci.edu/iue>).

initial attempts to set up a classification system for the A-type stars in the IUE ultraviolet (see Heck et al. 1984) were somewhat discouraging, with complaints that luminosity criteria were few and far between.

As a matter of fact, the IUE ultraviolet (1100–3200 Å) contains a number of spectral features useful in the characterization of A-type stars. Ultimately, when more spectral material becomes available for A-type stars in the ultraviolet (alas, not from the IUE satellite, as it was turned off in 1996), spectral classification in that region will, we predict, prove to be a highly useful adjunct to optical-region classification.

To illustrate the potential of a classification system for the A-type stars in the ultraviolet, two spectral montages are presented in Figures 5.6 and 5.7.

Before we discuss these two figures in detail, it may be useful to review some of the properties of the IUE satellite and IUE spectra. The IUE satellite, which incorporated a 45-cm Cassegrain telescope, was deployed in a synchronous orbit and equipped with two UV-sensitive echelle spectrographs, one optimized for the shortwave UV (1100–2000 Å) and the other for the longwave UV (1800–3200 Å).

In the echelle mode, the spectra (recorded with a SEC Vidicon) had a resolution of about 0.2 \AA , whereas in the low-dispersion mode (obtained by replacing the echelle grating by a concave mirror) the resolution was $6\text{--}9 \text{ \AA}$. Many more spectra were obtained in the low-dispersion mode than in the high-dispersion mode. In the low-dispersion mode (the only one we consider in this section), both shortwave (SW) and longwave (LW) spectra are available, although not necessarily for every observed star. IUE spectra are available on the **Multimission Archive at STScI (MAST)** IUE website,¹ and are flux calibrated. In the best possible case (which is not too uncommon), a star will have multiple SW and LW spectra, and these two parts will join smoothly together with no inconsistencies in the flux calibration. More commonly, however, only one spectrum of each variety will exist, or possibly only a single wavelength region will have been exposed. In some cases, the flux calibrations of the two wavelength sections are inconsistent, and then it is necessary to scale the fluxes for, say, the LW spectrum to match the fluxes of the SW spectrum in the overlap region. Of course, when this happens, the correct absolute flux calibration is unknown. Quite often, for a given star, the LW spectrum has a lower S/N than the SW spectrum.

In the A-type stars, rectification of the IUE spectrum is impractical because of the enormous density of spectral lines; i.e. there are no or very few “true” continuum points. Thus, in the UV, A-type stars are analogous to K-type stars in the optical, and the most practical spectral format for spectral classification is the *normalized-flux* format (see §2.2.1). There is always the question of where the normalization should be applied. One practical choice is to choose a continuum point (or at least a point where the line blanketing is at a minimum) in the observed spectral region and normalize there. There are a few choices for such a point in the A-type stars in the UV; for Figures 5.6 and 5.7 a point at 2650 \AA has been used. Another possibility is to normalize the spectra using the flux at a point outside the observed spectrum—for instance, the flux in the Strömgren y band or the Johnson V band. This has the advantage of normalizing in a region where the line blanketing is much less, and is probably the preferred method for classifying metal-weak stars. However, with this normalization, the relative UV fluxes in the late A-type stars are then much lower than those in the early A-type stars, and this makes it difficult to pick up systematic trends in spectral features with temperature.

It is important to understand that at a resolution of $6\text{--}9 \text{ \AA}$ almost all features in these spectra are blends of literally hundreds of spectral lines. In a few cases, very prominent lines—usually resonance lines or a resonance multiplet of an abundant species—dominate a spectral feature; most of these have been marked in Figure 5.6. Other features cannot be ascribed to a single species, but may still have value as spectral classification criteria.

¹<http://archive.stsci.edu/iue/>

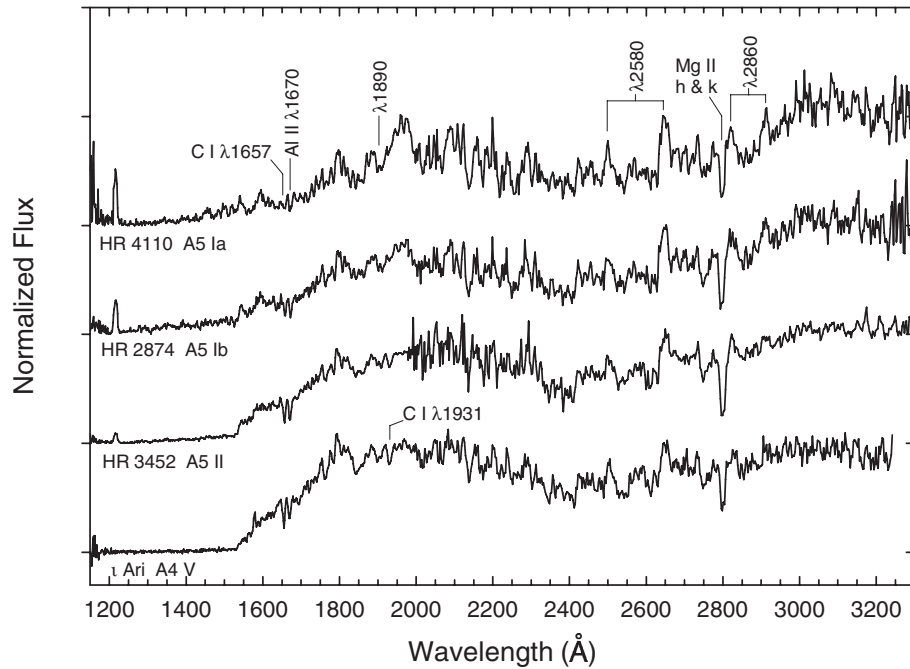


Figure 5.7 Luminosity effects at A5 in the IUE ultraviolet. The spectral types given were determined in the blue-violet. Spectra from the MAST IUE archive.

A temperature classification scheme for the A-type stars in the UV could be based on the following four criteria:

1. The overall shape of the stellar energy distribution (SED) in the UV, including the wavelength at which the flux goes to essentially zero. This criterion, of course, will be affected by interstellar reddening.
2. The increasing strength of the Mg II h & k blend, which behaves similarly to the Ca II K & H lines in the blue-violet.
3. The morphology and strength of the $\lambda 1848$ feature in ratio with C I $\lambda 1931$. In early A-type stars $\lambda 1848$ has a double profile, which changes to a “tooth” shaped feature in the late A-type stars. The central depth of this feature is approximately equal to C I $\lambda 1931$ at A7, but is stronger earlier and weaker later.
4. The morphology of the $\lambda 2375$ feature changes in a consistent manner with temperature, developing into a flat-bottomed broad absorption feature by early F.

Figure 5.7 shows a luminosity sequence at A5. A number of ratios appear to be luminosity sensitive: C I $\lambda 1657$ /Al II $\lambda 1670$ changes smoothly with luminosity type, as does the ratio of the $\lambda 1890$ feature to C I $\lambda 1931$. In addition to these two ratios, the morphologies of the $\lambda 2580$ region and the $\lambda 2860$ region show some

sensitivity to luminosity. Similar luminosity criteria apply at F0, but at A0 the spectra show only subtle differences with luminosity.

5.3.2 Infrared

THE NEAR INFRARED

The near-infrared (NIR), which we define for the purposes of Chapters 5–8 to extend from roughly $H\alpha$ to $1\ \mu\text{m}$ ($10000\ \text{\AA}$), holds some promise for spectral classification of stars across the HR diagram. Torres-Dodgen (1994) and Danks & Dennefeld (1994) have produced low-resolution ($\sim 15\ \text{\AA}$) NIR spectral atlases, and discuss the classification of A-type stars. Figure 5.8 gives a bird's eye-view of this region. The dominant spectral features for the A-type stars in the NIR include the $H\alpha$ line; the O I triplet ($\lambda\lambda 7772, 7774$, and 7775); the higher Paschen-series hydrogen lines, including the Paschen convergence at $8210\ \text{\AA}$; and the Ca II triplet lines ($\lambda\lambda 8498, 8542$, and 8662) which, in the A-type stars, are blended with Paschen lines P16, P15, and P13 respectively. Unfortunately, this region is also intersected by some quite strong telluric bands, including the $7605\ \text{\AA}$ O_2 feature.

In the dwarf A-type stars, the most outstanding spectral trend in this region is the changing appearance of the Paschen lines. In the early A-type stars, the Paschen lines are much stronger than the lines of the Ca II triplet, but in later A-type stars, and in the F-type stars, the Ca II triplet begins to dominate. This leads to a distinctive pattern in which the P13, P15, and P16 lines become increasingly strong relative to the neighboring unblended Paschen lines as one moves toward later types. In addition to this, the strengths of the $H\alpha$ line and the Paschen lines in general decrease with declining temperature. The O I triplet is fairly insensitive to temperature in the A-type stars.

In the lower panel of Figure 5.8, a temperature sequence of supergiants is shown. The outstanding luminosity sensitive features available in this spectral region are marked, including Si II $\lambda\lambda 6347, 6371$, $H\alpha$, the O I triplet, and the Paschen lines. Notice that in the supergiants the Paschen lines are narrower, and the highest line in the series visible in the supergiants is P22 or P23, whereas in the dwarfs, only P16 or P17 can be readily discerned. These luminosity-sensitive features can be used to discriminate between the supergiant classes but, according to Torres-Dodgen, are not sensitive enough to distinguish between V, IV, and III.

Better classification discrimination can be obtained by using spectra of normal MK resolution ($\sim 2\ \text{\AA}$) in this region. In particular, Andriolat, Jaschek, & Jaschek (1995) have published a spectral atlas (resolution $\sim 2.4\ \text{\AA}$) of the higher Paschen-line region ($8375\text{--}8770\ \text{\AA}$) and have used it to map out classification criteria. Munari & Tomasella (1999) have published a spectral atlas of the Ca II triplet region (based on $0.4\ \text{\AA}$ -resolution echelle spectra obtained at Asiago observatory), pointing out that this region is remarkably telluric-free and also contains a number of spectral features that permit precise spectral classification, at least for F-type and later stars. Munari & Tomasella (1999) and Marnese, Boschi, & Munari (2003) have explored the possibility of using this region to perform spectral classification

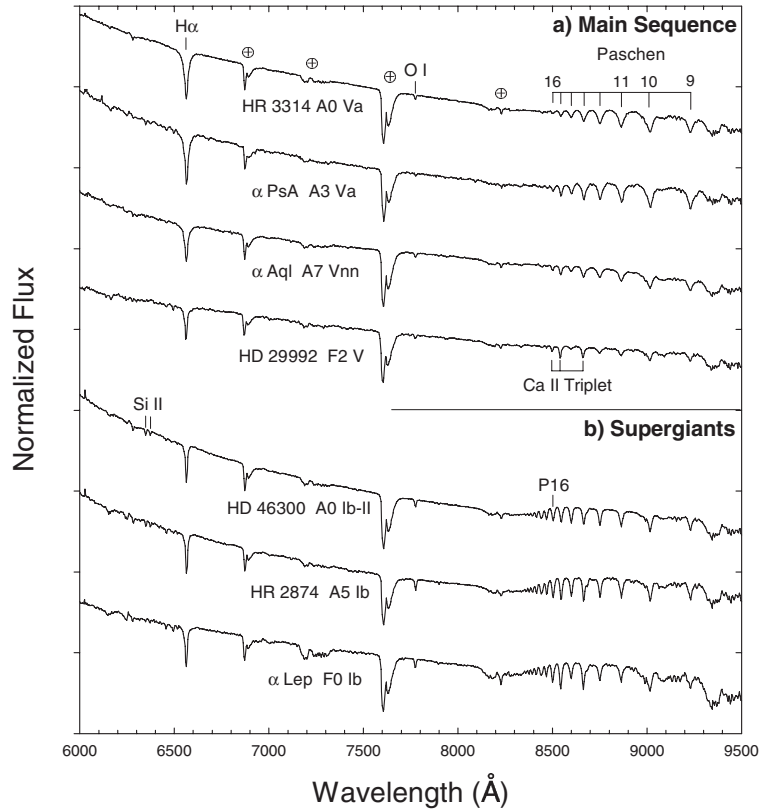


Figure 5.8 (a) A temperature sequence for A-type main sequence stars in the near-infrared part of the spectrum. (b) A temperature sequence for A-type supergiants in the near-infrared. The \oplus symbols represent telluric absorption (absorption by the Earth's atmosphere), and so are not intrinsic features of the stellar spectrum. Spectra from Danks & Dennefeld (1994). These spectra have been offset by one continuum unit for clarity.

with spectra from the *Gaia* spacecraft. As noted above, the interplay between the strengths of the Ca II triplet lines and the P13, P15, and P16 lines yields a sensitive temperature discriminant in the A-type stars. In addition, a number of N I lines and the O I λ 8446 line show luminosity sensitivity in the A-type stars in this region (see Figure 5.9 based on spectra from Andrillat, Jaschek, & Jaschek 1995). However, a glance at this figure shows that the Paschen lines of the A0 giant are actually stronger and deeper than those of the dwarf! This rather surprising and scandalous behavior complicates the use of the higher Paschen lines for luminosity classification, and needs to be carefully mapped out.

Frémat, Houziaux, & Andrillat (1996) have investigated the higher Paschen lines and have shown that this behavior can be understood via spectral synthesis. The Paschen lines in question lie quite near the Paschen convergence, and as a consequence there is considerable overlap in the wings of these lines; indeed at any one point in this spectral region, a dozen or more Paschen lines contribute significant absorption. In the dwarfs, these overlapping wings combine

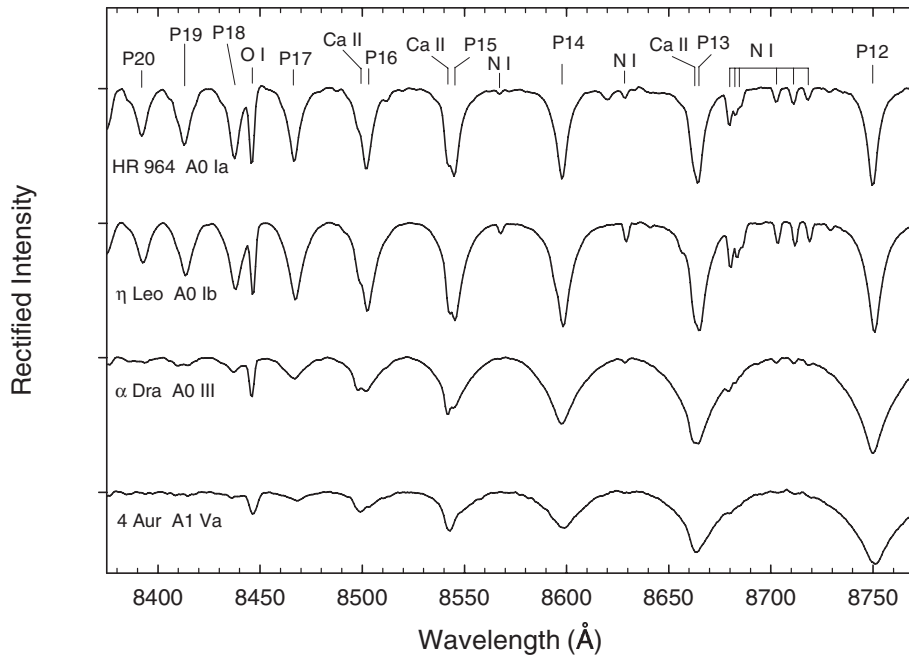


Figure 5.9 Luminosity effects at A0 in the vicinity of the higher Paschen lines in the near-infrared. Note that the Paschen lines of the A0 giant are deeper, stronger, and nearly as broad as those of the dwarf. See text for explanation. The spectra in this figure are vertically offset by half the continuum intensity. Figure based on spectra from Andrillat, Jaschek, & Jaschek (1995).

to produce a strong “pseudo” continuous opacity, with the result that the higher Paschen lines are formed in a limited region of the upper atmosphere, where the electron density is relatively low. In contrast, this opacity source is considerably smaller in the giants, the Paschen lines are formed over a larger depth of the atmosphere, and thus are considerably stronger and deeper than in the dwarfs. This extra opacity due to the overlapping of the hydrogen-line wings is important only in the vicinity of the hydrogen-line convergence (Paschen in this case; a similar effect can be seen in the higher Balmer lines). This behavior must be taken into account when one is using this spectral region for the classification of A- and B-type stars.

THE INFRARED J, H, K, AND L BANDS

The Earth’s atmosphere is partially transparent in the J (1.05–1.34 μm), H (1.55–1.75 μm), K (2.0–2.4 μm), and L (3.3–4.2 μm) infrared bands, making it possible for these spectral regions, to be utilized for spectroscopy with ground-based telescopes. The recent development of efficient detectors, as well as the construction of high-resolution spectrographs for these spectral regions, has opened the door to spectral classification. Spectral classification for O- and B-type stars in the

K-band was reviewed in Chapter 3; the motivation there was to develop K-band spectroscopy as a tool to classify hot, young stars in regions of high extinction. Of course, these bands are the natural spectral regions for the classification of L and T dwarfs, which are reviewed in Chapters 9 and 10 respectively. During the past decade, however, grids of MK standards across the H–R diagram have been observed in the J, H, K, and L-bands and spectral classification criteria have been noted in each of these bands. The relevant papers are, for the J-band, Wallace et al. (2000); the H-band, Meyer et al. (1998); the K-band, Wallace & Hinkle (1997); and the L-band, Wallace & Hinkle (2002).

Apart from hydrogen lines, the spectra of A-type stars are mostly featureless in the J, H, K, and L-bands. Figure 5.10 illustrates temperature sequences for A-type dwarfs, giants, and supergiants in the J-band. The Paschen β and γ lines dominate this spectral region, and behave in the fashion of the Balmer lines in the optical. This means that they can be used for temperature and luminosity classification. But at the resolution of these spectra ($R \approx 3000$), lines of metals do not really show up until the early F-type stars. One exception is the C I doublet at $1.07\mu\text{m}$, which grows only slowly with declining temperature. A ratio of C I $1.07\mu\text{m}$ to $\text{P}\gamma$ should be a fairly sensitive indicator of the temperature type.

The H-band in the A-type stars (see Figure 2.7) is dominated by the higher members of the hydrogen Brackett series; again lines of metals do not show up until the early F-type stars. The K-band is dominated by the single Brackett γ line (see Figure 6.11). Apart from this feature, the K-band is almost featureless in the A-type stars. An exception, in the supergiants, is the appearance of the weak higher members of the hydrogen Pfund series. The L-band, likewise, is almost featureless in the A-type stars, except for the following hydrogen lines: Brackett α ($4.05\mu\text{m}$), Pfund γ ($3.74\mu\text{m}$), and a number of very weak lines of the Humphreys series (see Figure 5.11). As we will see in later chapters, the J, H, K, and L-bands have much more utility for the late-type stars.

5.4 CHEMICALLY PECULIAR STARS

5.4.1 The Am Stars

The Am or *metallic-line* A-type stars are defined, in a spectral classification sense, as A-type and early F-type stars in which the Ca II K-line type is *earlier* than the metallic-line type by at least five spectral subclasses. For instance, an A-type star with a K-line type of A5 and a metallic-line type of F2 (as determined by comparison with the appropriate MK standards) is classified as an Am star. Stars with a similar discrepancy between the K-line type and the metallic-line type, but for which the difference between the two types is less than five spectral subclasses, have been termed by Morgan, Abt, & Tapscott (1978) as “proto-Am” stars. We generally will not make a distinction between the two in this chapter.

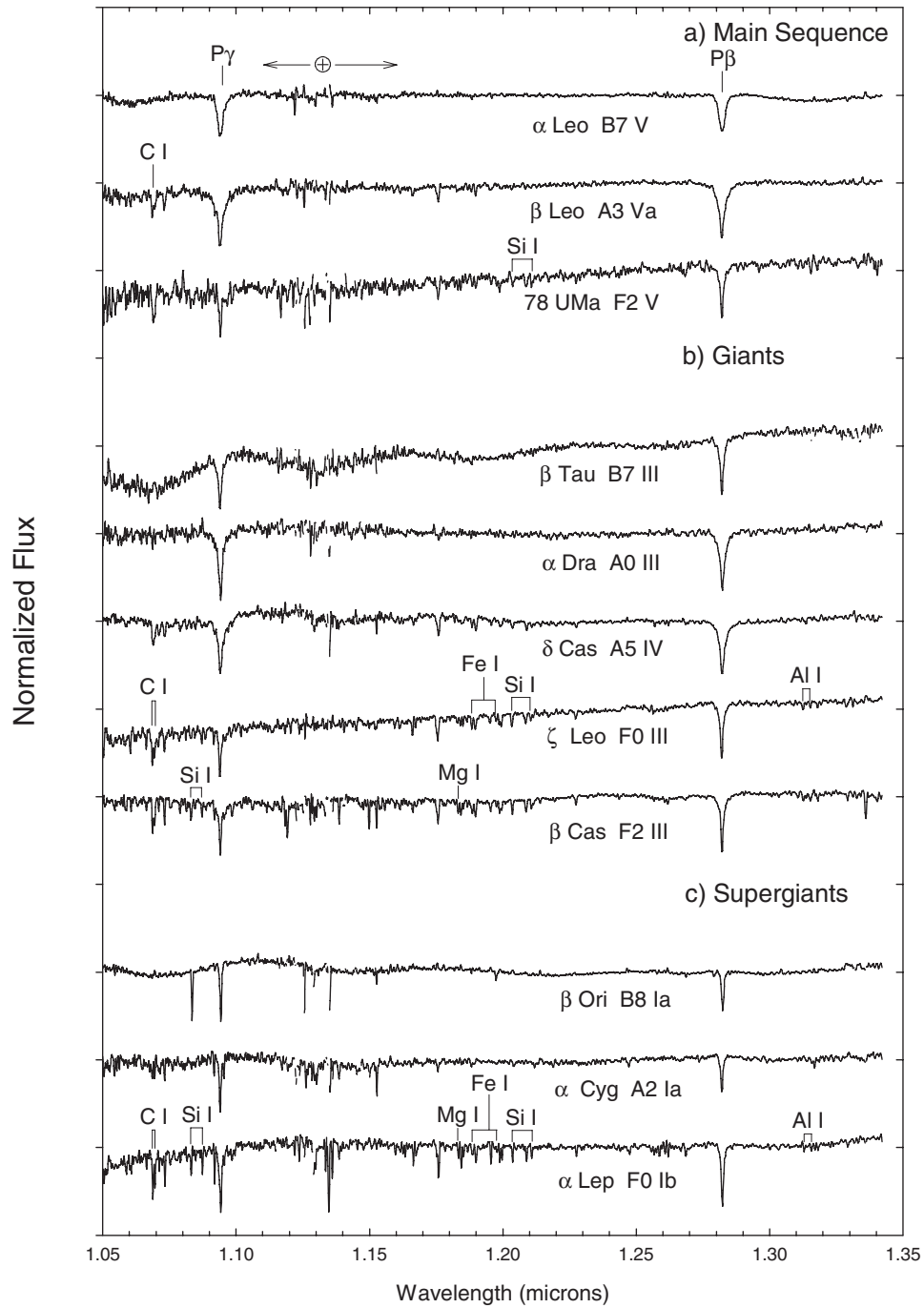


Figure 5.10 Temperature sequences for a) A-type dwarfs, b) giants, and c) supergiants in the infrared J-band (1.05–1.34 μm). The two strongest lines are Paschen β and Paschen γ . These spectra, taken from Wallace et al. (2000), have been slightly smoothed from the originals and given integer vertical offsets for clarity. The wavy shape of the continuum for some of these stars is a purely instrumental effect.

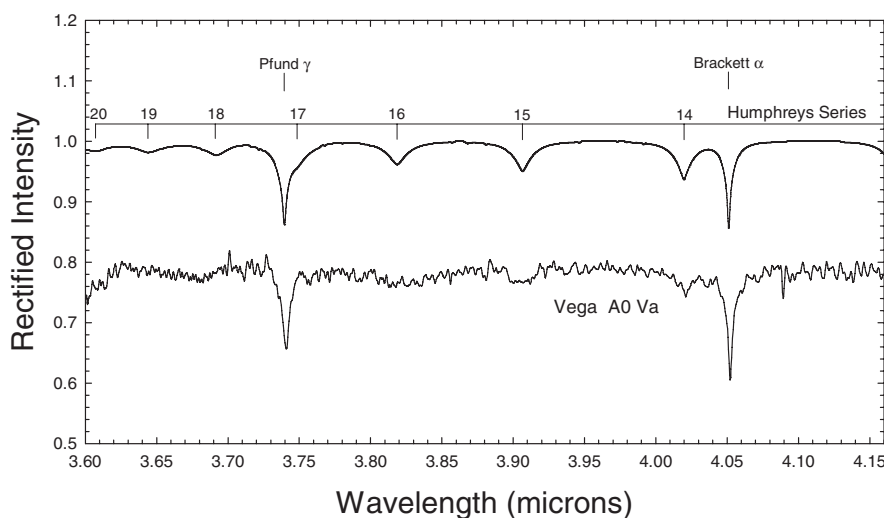


Figure 5.11 Vega in the L-band. The top spectrum is a synthetic spectrum included to show clearly the major absorption lines for the A-type stars in the L-band. The lower spectrum of Vega is from Wallace & Hinkle (2002). The two spectra are separated vertically by 0.2 continuum units.

The discovery of the Am stars can be attributed to Harvard classifiers Antonia Maury and Annie J. Cannon who noted a number of stars, including δ Nor, τ UMa, and τ^3 Eri, that have weak K-lines, but metallic-line strengths resembling those of the F stars. However, the recognition of the existence of a class of Am stars was first made explicit by Titus & Morgan (1940) who classified a number of such stars in the Hyades cluster. The Am class was formalized in the MKK atlas (Morgan, Keenan, & Kelleman 1943) which illustrated 63 Tau as the type star.

63 Tau is shown in Figure 5.12 in comparison with two normal stars: 30 LMi, an A9 III star; and β Cas, the F2 III MK standard. Notice that the metallic-line spectrum appears slightly later than the F2 III standard, but the K-line is much weaker. Indeed, the K-line of 63 Tau is weaker than that of the A2 MK standard. The hydrogen lines, on the other hand, are an excellent match with those of 30 LMi. This leads to the spectral type, expressed in the special notation designed for the Am stars:

$$\text{kA1.5 hA9 mF3(III)}$$

in which the K-line type, the hydrogen-line type, and the metallic-line type are listed sequentially and indicated with the lower-case letters k, h, and m. The luminosity class is based on the normal luminosity criteria of the F-type stars (see below and Chapter 6), but close inspection of the spectrum of 63 Tau shows that the metallic-line spectrum differs from that of the F2 III standard in a number of important ways. First, notice that the Sr II $\lambda 4077$ line is much stronger in the Am star than in the F2 III standard (the Sr II $\lambda 4077$ line is used for luminosity classification in the late F, G, and K-type stars). In addition to the weakness of the Ca II K-line, the Ca I $\lambda 4226$ line is peculiarly weak. The Fe II/Ti II $\lambda\lambda 4172-9$

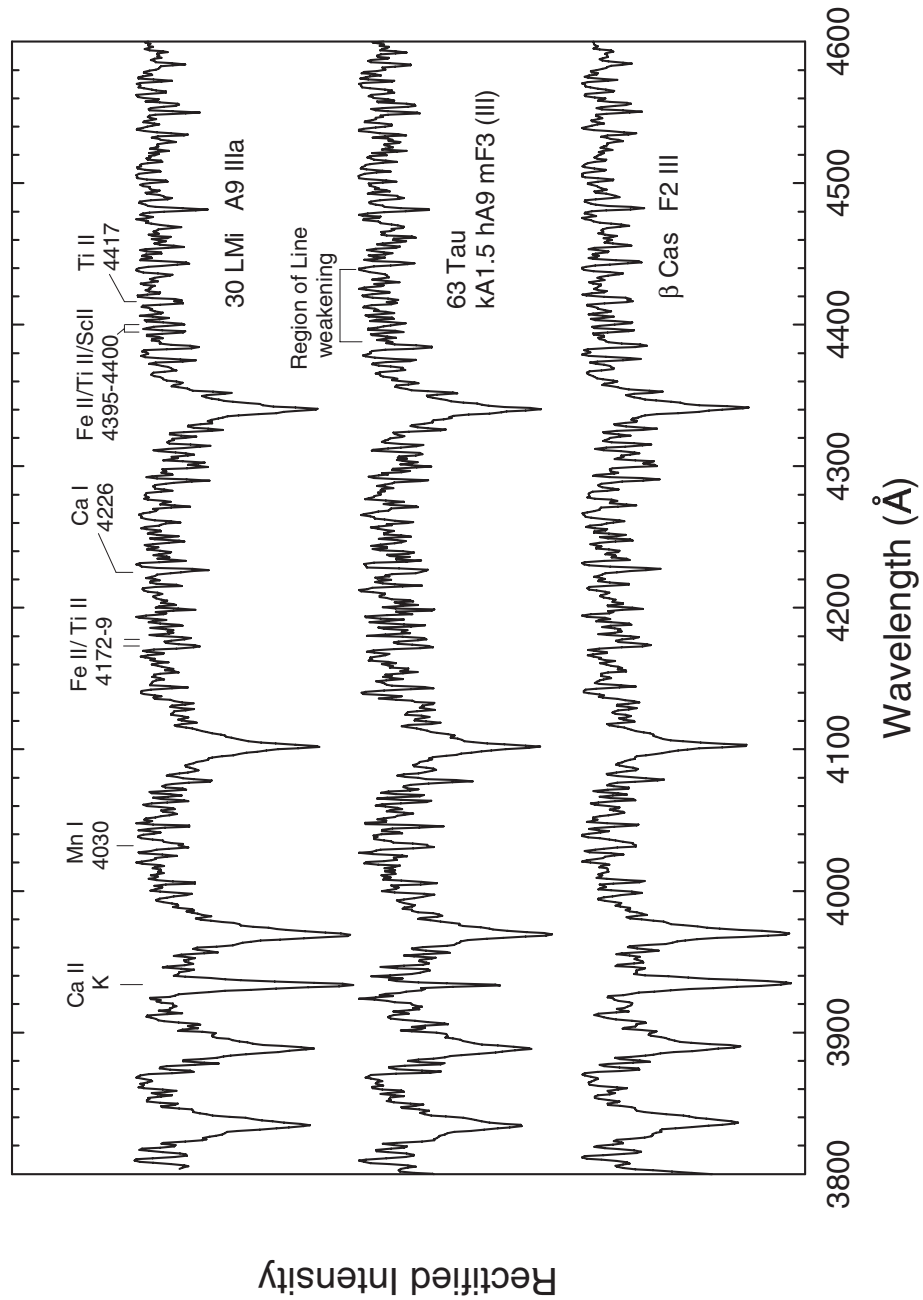


Figure 5.12 The spectrum of an Am star, 63 Tau, compared with two normal stars: 30 LMi, an A9 giant; and β Cas, the MK F2 III standard. The hydrogen-line profiles of 63 Tau are an excellent match with 30 LMi, but the metallic-line spectrum looks slightly later than that of the F2 III. Note the weak K-line in 63 Tau. Spectra from the Dark Sky Observatory.

blend, an important luminosity criterion in the late A and the F-type stars, is similar in strength to the F2 III standard, which suggests that 63 Tau is a giant. However, the 4395–4444 Å region, which also contains a number of luminosity criteria, bears a closer resemblance to dwarf spectra. Note especially the weakness of $\lambda\lambda 4395\text{--}4400$ and $\lambda 4417$. This discrepancy in the luminosity criteria, a common feature of Am stars, is termed the *anomalous luminosity effect*. The anomalous luminosity effect was first noted by Barry (1970, 1971), who pointed out features in the near-UV spectrum of Am stars that indicated “spurious” luminosities, but it was Abt & Morgan (1976) who placed this effect in the context of the MK system. Abt & Morgan compared features in the violet (3850–4078 Å) region to the blue (4260–4340 Å) region and showed that luminosities derived from criteria in those two regions were often in disagreement. For instance, they found that some Am stars show giant (in the most extreme cases supergiant) characteristics in the violet region (especially if Sr II $\lambda 4077$ is employed as a luminosity criterion), whereas the same stars show dwarf characteristics in the blue region. We prefer to contrast the $\lambda\lambda 4172\text{--}9$ blend with the 4395–4444 Å region, and assign the luminosity type based on the $\lambda\lambda 4172\text{--}9$ blend. If the anomalous luminosity effect is present in a star, we indicate that fact by enclosing the luminosity type in parentheses.

We note that 63 Tau has the absolute magnitude of a dwarf A9 star, and thus the luminosity given by the $\lambda\lambda 4172\text{--}9$ blend is spurious. But the weakness of the lines in the 4395–4444 Å region in many Am stars often implies a sub-dwarf luminosity, also completely spurious. The abundance pattern in the Am stars is quite peculiar; calcium and scandium are underabundant, whereas the iron-peak elements and heavier elements tend to be overabundant. The underabundance of scandium helps in understanding the line weakening in the 4395–4400 Å region; the blends at $\lambda 4400$ and $\lambda 4417$ involve lines of Sc II. However, the cause of the spurious luminosity given by the $\lambda\lambda 4172\text{--}9$ blend and in general the violet and near-UV region is still a mystery. The ρ Puppis stars—a class of late, apparently evolved Am stars (see §6.5.1)—can show the anomalous luminosity effect to an extreme; a case in point is the ρ Puppis star HD 103877.

Photometric colors (such as $B - V$ or Strömgren $b - y$) show a large amount of scatter when plotted against the K-line types of Am stars; the conclusion is that the K-line type is not a good indicator of the effective temperature. The correspondence between the metallic-line types and photometric colors is better. However, the hydrogen-line types are least affected by the abnormal elemental abundances in the atmospheres of Am stars, and thus are the best indicators of the effective temperature. It turns out that the excessive *line blanketing* present in the Am stars reddens the photometric colors (absorption lines are more densely spaced in the blue than the red), and thus, for a given effective temperature or hydrogen-line type, Am stars tend to be redder than normal A-type stars.

CHEMICAL SEPARATION AS THE MECHANISM FOR PRODUCING AM STARS

The abundance peculiarities seen in Am stars may be understood on the basis of chemical separation driven by radiative and gravitational acceleration. We say that

a stellar atmosphere is in *hydrostatic equilibrium* when the pressure forces (due to gas pressure and radiation pressure) are exactly balanced by the gravitational force. A stellar atmosphere can be in hydrostatic equilibrium, but individual atoms or ions may still feel an unbalanced force. The reason for this is that every time an atom absorbs a photon, the momentum of that photon is transferred to that atom. Because the net radiation field in a stellar photosphere is in the outward direction, this push is, on the average, outwards. Since the momentum of a photon is inversely proportional to its wavelength, atoms or ions that have many spectral lines in the ultraviolet will feel a strong outward push. If this outward acceleration is greater than the inward gravitational acceleration ($g_{\text{rad}} > g$), those atoms and ions will be pushed toward the surface of the star. Atoms and first and second ions of most transition metals (iron, chromium, nickel, etc.) have rich ultraviolet spectra,² so these elements tend to rise in the stellar photosphere. Elements that have “poor” UV spectra (examples are many light elements, including helium, magnesium, and calcium, but also the first transition metal, scandium) tend to sink because $g_{\text{rad}} < g$ for all or most of the relevant ionization states. This process leads to *chemical separation* in the stellar atmosphere.

In normal A-type stars, chemical separation operates, but it is completely overwhelmed by the effects of rotation. A rotating star, because it is not spherically symmetric, cannot be in hydrostatic equilibrium and radiative equilibrium simultaneously. As a consequence, the flow of radiation out of a rotating star is not isotropic and this means that surfaces of constant pressure do not coincide with surfaces of constant temperature. This produces imbalances in the pressure that in turn lead to large-scale flows in the interior of the star called *meridional circulation*. For rotational velocities greater than 90 km s^{-1} , meridional circulation dominates chemical separation and can completely mix the envelope of a star (Charbonneau 1993). Thus, in normal A-type stars, which are “all” rapid rotators, no chemical separation is visible. For stars that are slow rotators, however, chemical separation can occur, and the results can be seen in the spectrum.

It turns out that all Am stars (at least as far as we know) are slow rotators. The reason for this is that almost all Am stars are members of fairly close binaries. Tidal forces in these systems have synchronized the rotation of the stars with their orbital periods and, as a consequence, all known Am stars have $v \sin i < 100 \text{ km s}^{-1}$ (Abt & Hudson 1971). In these stars, chemical separation dominates mixing by meridional circulation, and helium tends to sink, leading to the disappearance of the *helium convection zone* (see Figure 5.13). With the disappearance of the helium convection zone, chemical separation can operate all the way up to the base of the superficial *hydrogen convection zone*. The peculiar

²The transition metals, the most abundant of that coincide with the iron-peak elements, consist of elements which involve the filling of a d subshell. In the series from Sc to Zn, including Fe, the electron configuration of the ground state fills from $3d^1 4s^2$ to $3d^{10} 4s^2$. Because there are a large number of quantum states associated with a d^w subshell (as compared to p or s subshells), the spectra of the transition metals are much richer than those of the lighter elements. The two series of rare earths, on the other hand, involve the filling of an f subshell, which leads to even richer spectra. See Cowan (1981) for a more quantitative treatment of this matter.

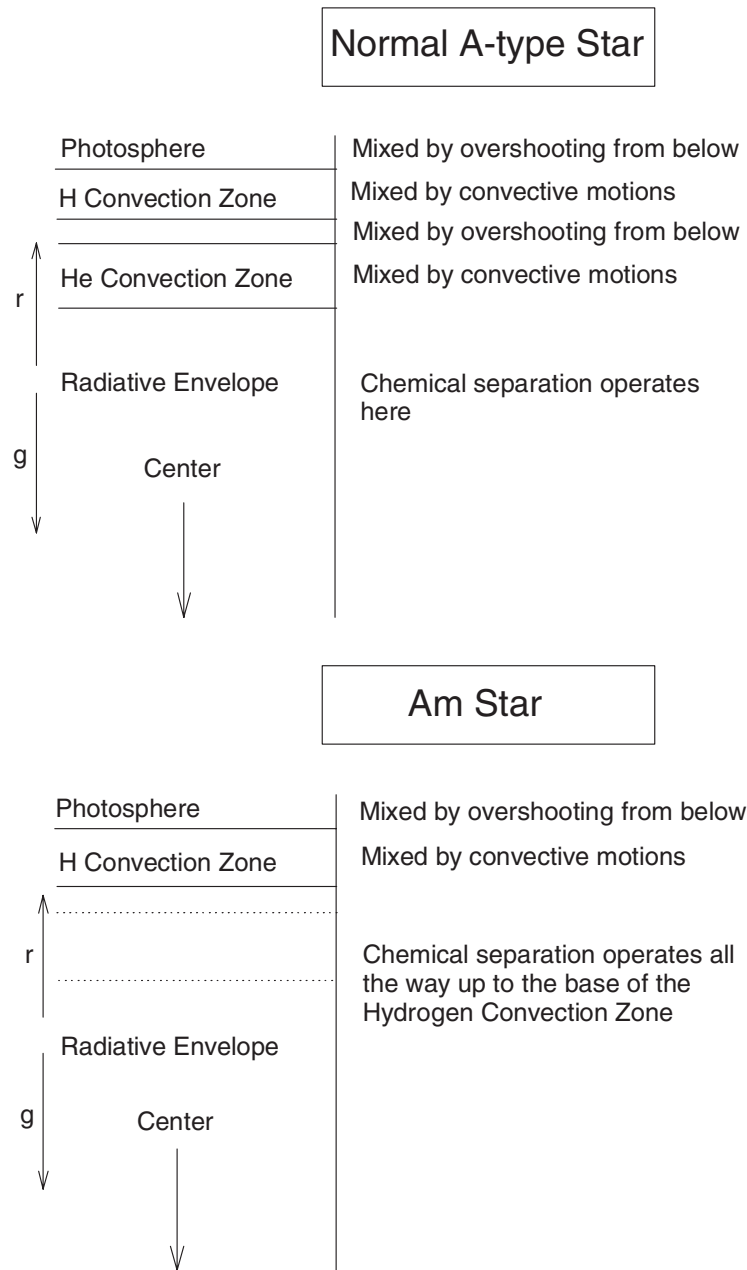


Figure 5.13 A schematic representation of the outer layers of a normal A-type star (top) and an Am star (bottom). The normal star has two superficial convection zones due to the ionization of hydrogen (upper zone) and the first ionization of helium (lower zone). The Am star has only one zone, due to gravitational settling of helium. This allows chemical separation to occur all the way up to the base of the hydrogen convection zone in Am stars. Figure adapted from Charbonneau (1993) with permission from the Astronomical Society of the Pacific.

abundances may then be mixed into the photosphere via convective motions in the hydrogen convection zone and by *overshooting* at the top of this zone.

While we have very good theoretical reasons to expect that all Am stars will be slow rotators, it is important for the classifier to keep her mind open on this matter. Abt (1979) claimed to have found four Am stars in the Orion association with $v \sin i > 200 \text{ km s}^{-1}$, although these types have not been confirmed by later studies.

Most Am stars have hydrogen-line types earlier than F2; a very few have hydrogen-line types as late as F5 (see the discussion on the ρ Puppis stars in Chapter 6). The reason why the Am phenomenon does not penetrate into the late F-type stars is because with decreasing temperatures the hydrogen and helium convection zones deepen and expand, leading to a convective envelope. In the F-type stars, convection becomes increasingly important in the stellar atmosphere with decreasing temperatures. The effect of convection is to thoroughly mix the convective envelope of the star, completely overwhelming chemical separation. Thus chemical peculiarities of any sort in main-sequence stars are extremely rare for stars later than F5. However, for an example of a G-type “Am” star (the primary star in α Leo), see Griffin (2002) and Michaud et al. (2005). This star has retained its Am abundance peculiarities because it is currently in a very rapid phase of evolution, and convection has not yet had a chance to completely mix its envelope.

5.4.2 The Ap Stars

If the Am or *metallic-line* stars are A-type stars in which nearly all heavy elements (with a few special exceptions) are enhanced in the stellar photosphere, then the Ap or *peculiar A-type* stars are stars in which only selected elements have greatly enhanced abundances. In reality, most of the Ap stars are actually B-type stars in terms of effective temperature, but as the coolest are early F-type stars, it seems most appropriate to treat them in this chapter. We have already covered some related stars: the helium-weak and helium-strong B-type stars and the mercury-manganese stars in Chapter 4.

The classification of the Ap stars has a long history. Antonia Maury (Maury & Pickering 1897) classified nearly a dozen northern Ap stars, and remarked on the peculiarity of α^2 CVn, noting the very strong $\lambda\lambda 4128\text{--}30$ (Si II) doublet in that star. In the Draper catalog, Annie J. Cannon (Cannon & Pickering 1901) recognized the existence of two classes of Ap stars: those with enhanced silicon (including ν For, τ^9 Eri and α Dor) and those with enhanced strontium (including ξ Phe, θ^1 Mic and ι Phe). Later, Cannon (1912a, b) added 25 stars to these classes. The first systematic work on the Ap stars was that of W.W. Morgan who, in a series of eight papers printed in the *Publications of the Yerkes Observatory* from 1931 to 33 (see also Morgan 1933), identified five groups of peculiar A-type stars: the Mn II, $\lambda 4200$, Eu II, Cr II, and Sr II stars, with considerable overlaps between these classes. He also noted that the Si II $\lambda\lambda 4128\text{--}30$ stars overlapped the first

three groups. The Jascheks (Jaschek & Jaschek 1958) extended and modified this to six groups—the $\lambda 4200$, Mn, Si, Si–Cr–Eu, Eu–Cr–Sr, and Sr groups. Bidelman (1962) pointed out that $\lambda 4200$ is a high-excitation line of Si II, and so the $\lambda 4200$ stars are now recognized as part of the Si group. Osawa (1965), in a major classification study, divided the Ap stars into 16 peculiarity classes. Osawa’s classifications tend to be quite detailed and usually indicate not only the predominant chemical peculiarities, but also separate spectral types for the Ca II K-line and the hydrogen lines. Garrison & Gray (1994) adopted a similar notation, but also, for the peculiar B-type stars, gave a separate spectral type based on the strength of the He I lines.

Figure 5.14 illustrates four “typical” Ap stars, beginning with a hot Si II Bp star (ϕ Dra); a SiEu star, HD 224801; and two SrCrEu stars, HD 2453 and the relatively cool β CrB.

The classification of an Ap star begins with a specification of the MK class of the star. Historically, the temperature class has usually been based on the strength of the Ca II K-line, but as this line is often peculiarly weak or strong, or has an unusual profile, the correlation with effective temperature is quite poor. As mentioned above, Osawa (1965) specified spectral types for both the Ca II K-line and for the hydrogen lines; if carefully done, the hydrogen-line type should be a better indicator of the actual effective temperature. For mild Ap stars, obtaining the hydrogen-line type is fairly straightforward, as the hydrogen-line profiles do not differ greatly from those of normal stars. Even without the guidance of the He I lines (which are often weak in Ap stars), hydrogen lines of equal strength on either side of the Balmer maximum ($\sim A2$) can be distinguished by the actual shape of the line profile, and since in the B- and A-type stars the hydrogen-line profile is sensitive to both temperature and luminosity, the full MK class (both temperature and luminosity) can be derived. However, in extreme Ap stars, the structure of the stellar atmosphere itself is distorted, yielding unusual hydrogen-line profiles, and it may not be possible to match the hydrogen lines with any MK standard. In particular, the rapidly oscillating Ap stars, or *roAp* stars, have very unusual hydrogen-line profiles (Cowley et al. 2001). In such cases only a very approximate type qualified with a “:” should be provided.

Once the MK class of the star has been determined, an attempt can be made to determine the predominant chemical peculiarities. Figures 5.14 and 5.15 and Table 5.1 can help in deciding which species are enhanced. Table 5.1 lists the wavelengths of the strongest lines of Si II, Cr II, Eu II, and Sr II in the blue-violet region of the spectrum. While many other elements may be enhanced in Ap stars (especially the rare-earth elements), they are more difficult to distinguish in the blue-violet than the four elements mentioned above because of the lack of unambiguously identifiable lines. As a consequence, usually only Si, Cr, Eu, and Sr are specified in the spectral type.

Figure 5.15 is essentially a graphical form of Table 5.1, but also gives a good idea of the placement of these lines in the spectrum, relative to other prominent lines such as the Balmer lines and Ca II K. Note that in Ap stars with broad

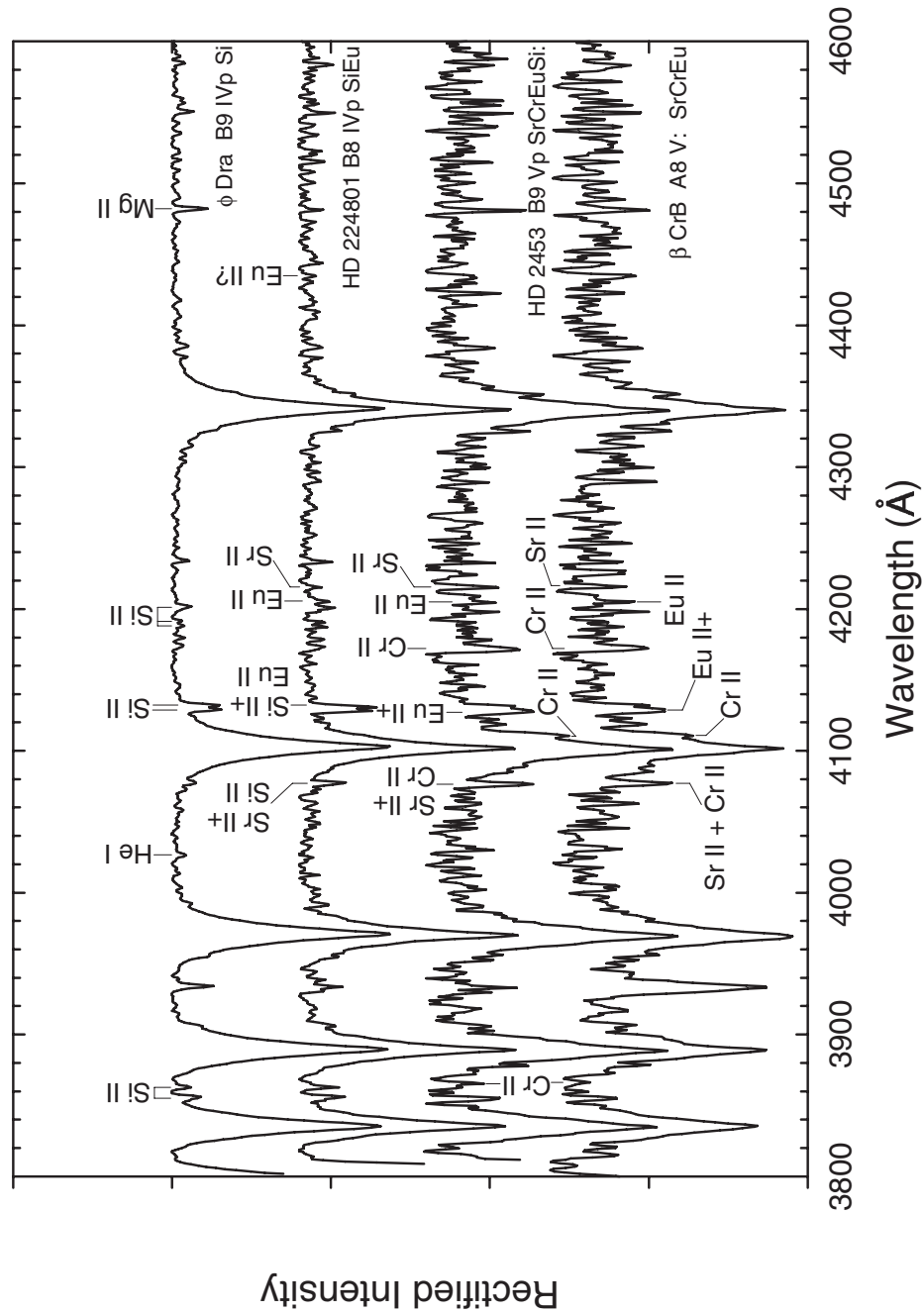


Figure 5.14 Illustrating four “typical” Ap stars, showing enhancements of Si, Cr, Eu, and Sr. See text for how these elements were identified and for cautionary notes regarding the interpretation of features at $\lambda 4078$ and $\lambda 4130$. The blend at $\lambda 4130$ is identified as Eu II+ to indicate that other species besides Eu II are involved in this blend. See text. Spectra from the Dark Sky Observatory.

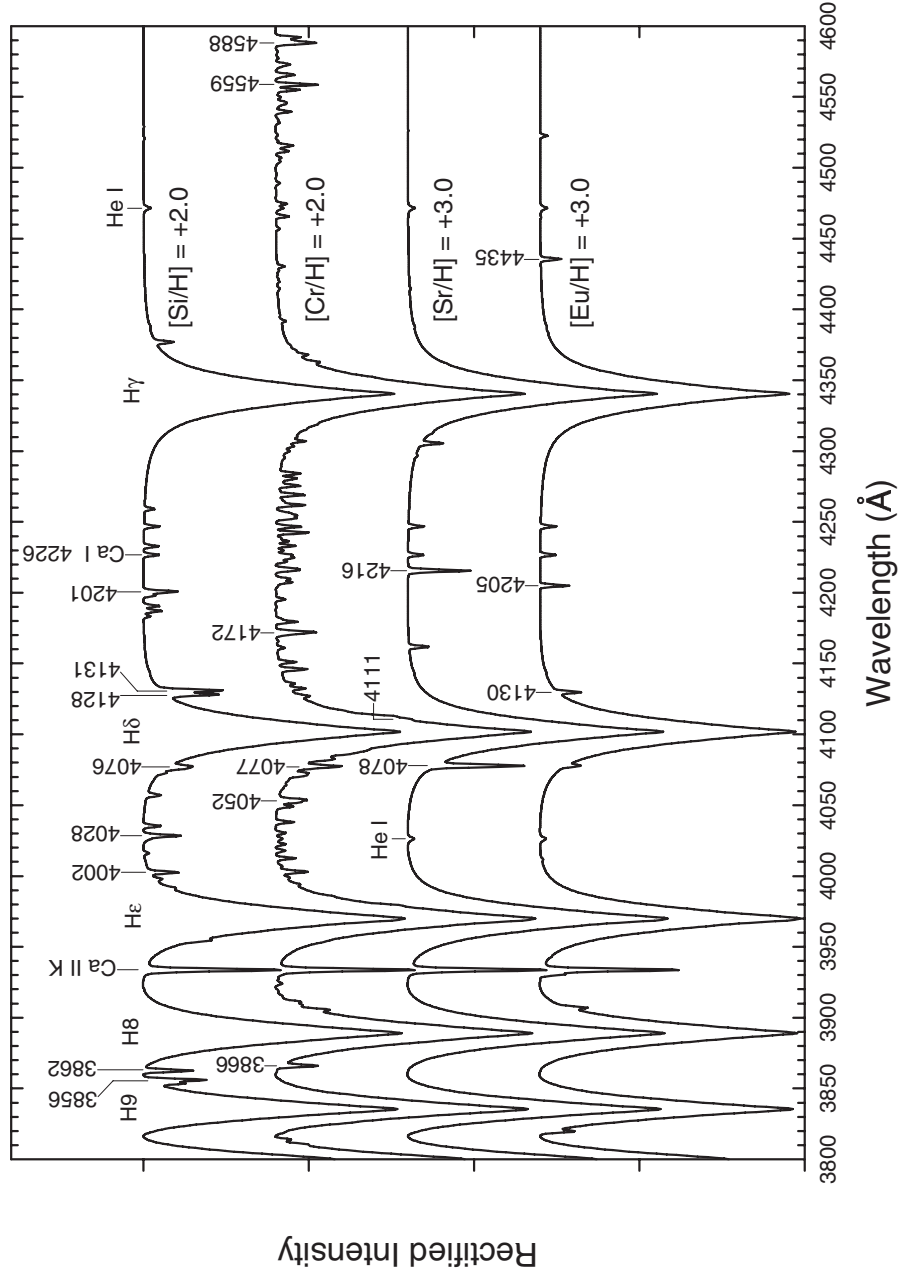


Figure 5.15 Except for a few strong lines of hydrogen, calcium, and helium, which have been included for reference, these synthetic spectra have been computed to show the positions of prominent lines of Si II, Cr II, Sr II, and Eu II respectively, i.e., the first ions of elements that are often enhanced in the spectra of Ap stars. All other spectral lines have been eliminated from these spectra for the purpose of clarity. In the calculations, silicon and chromium have been enhanced by a factor of 100 over solar; strontium and europium by a factor of 1000. The physical parameters of the atmosphere model used were $T_{\text{eff}} = 9500$ K, $\log g = 4.0$, $[\text{M}/\text{H}] = 0.0$. The spectra were smoothed to a resolution of 1.8 Å.

Table 5.1 Prominent Lines in the Blue-Violet Spectra of Ap Stars

Ion	$\lambda(\text{\AA})$	Remarks
Si II	4128 & 4131	Form a close doublet in classification spectra; strongest lines of Si II
	4200	Appears in only the hotter Si II stars
	3856 & 3862	Use to confirm Si peculiarity
	4002, 28 & 76	Note 4076 coincides with Sr II λ 4077
Cr II	4172	Generally strongest line of Cr II
	4111	Blended with H δ ; use to confirm Cr peculiarity
	3866	Use to confirm Cr peculiarity
	4077	Coincides with Sr II λ 4077
Sr II	4077	Strongest line, but can be confused with Si II λ 4076 & Cr II λ 4077
	4216	Always confirm Sr II peculiarity with this line
Eu II	4205	Generally least blended line of Eu II
	4130	Can combine with other lines to form a blend that appears similar to Si II $\lambda\lambda$ 4128–31

hydrogen lines, Cr II λ 4111—an important line that can be used to confirm a chromium peculiarity—can appear as merely a bump in the red wing of H δ . In Ap stars with narrower Balmer lines, this line is more easily distinguished (see HD 2453 and β CrB in Figure 5.14). Table 5.1 also warns against certain confusing blends. For instance, Si II 4076 and Cr II 4077 can combine to give a strong line, easily mistaken for Sr II 4077 in classification spectra. A strontium peculiarity should always be confirmed by noting that Sr II λ 4216 is also strong.

Perhaps the most deceptive feature is the presence of a strong, broad blend centered near λ 4130. Such a blend shows up in all four stars in Figure 5.14. In the two hottest stars (ϕ Dra and HD 224801), this blend is dominated by Si II and appears, at least with spectra of resolution 2 \AA and better, as a closely spaced doublet. In the two coolest stars in that figure (HD 2453 and β CrB), a prominent blend appears at essentially the same wavelength; at a resolution of 1.8 \AA (the resolution of the spectra in Figure 5.14), the morphology of this blend is clearly different from that of the Si II doublet, but with a lower resolution the two would be nearly indistinguishable. Figure 5.16 shows how complex this blend is in the cooler Ap stars. This figure, based on Elodie high-resolution spectra of β CrB and HD 2543, (Moultaka et al. 2004) shows that in β CrB the single most important contributor to this blend is a strong line of Eu II, but many other lines, including lines due to Fe I and Fe II and rare earths Ce II and Gd II, are involved. In β CrB, the coolest Ap star in this figure, Si II plays only a minor role in this blend; in HD 2453, Si II is more important, but is still a minor player. The importance of Si II in these stars can be judged from the Si II $\lambda\lambda$ 3856 & 3862 lines. In β CrB (see Figure 5.14), there is a strong feature near λ 3856, but lack of a feature of similar strength at λ 3862. Things are a bit less clear in HD 2453, which is why “Si:” is included in the list of chemical peculiarities for this star.

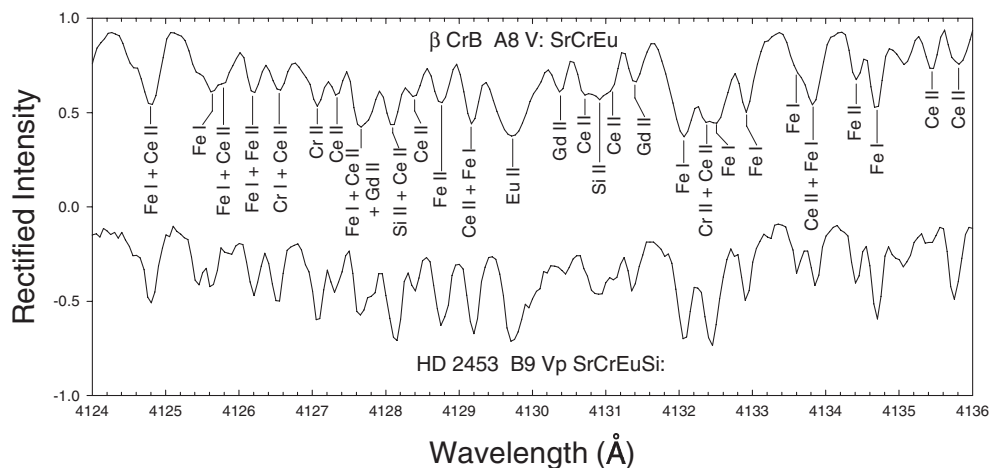


Figure 5.16 Details of the 4130 Å region in two Ap stars, β CrB and HD 2453, illustrating that the $\lambda 4130$ feature in these stars is not dominated by Si II, but rather is a complex blend. The single most important contributor to this blend is the broad Eu II feature. Spectra used by permission from the Elodie archive (Moultaka et al. 2004).

Experience with the spectra of Ap stars shows that the tidy peculiarity groups of the Jascheks are an oversimplification of the actual situation (a statement with which the Jascheks would almost certainly have agreed); there are a number of peculiar A-type stars that are so peculiar they defy classification. Figure 5.17 illustrates three such stars. The first is HR 1094, which shows large overabundances of chlorine, cobalt, gold, mercury, and many rare earths (Nielsen & Wahlgren 2000); the only chemical peculiarity that can be definitely established by spectral classification is chromium. The second, HD 147010, is a very peculiar star in the Sco-Cen Association. It was compared by Garrison (1967) with B8 III and A2 Ib standards and was later classified by Garrison & Gray (1994) as kB8 hB8 II HeA0 mA2 Ib Si. With digital spectra, the hydrogen lines do not match at any spectral type; perhaps the best match is at B9 II, but the far wings in the Ap star are too broad. The metallic-line spectrum of HD 147010 looks superficially like an A2 Ib star (we include a spectrum of HR 2996, A2 Ib for comparison), but the Si II $\lambda\lambda 4128-31$ doublet is too strong and Mg II $\lambda 4481$ is too weak. The hydrogen lines are much too broad for this star to be a Ib supergiant. The spectrum is similar to that of the classical A-type shell stars (see §5.7), except that the Si II doublet is almost always weak in a shell star. Thompson, Brown, & Landstreet (1987) measured the magnetic field for this star, and found that the mean longitudinal magnetic field strength is ~ 5 kG (kilogauss). In the majority of Ap stars (see discussion below), the field strengths range from a few hundred to 2000 gauss. At B8 or B9, this star is located slightly above the main sequence of Sco-Cen; the supergiant appearance of its spectrum suggests an unusual and extended atmospheric structure.

Finally, the third peculiar star in Figure 5.17 is that of Przybylski's star. This star is perhaps the most peculiar Ap star known. Its discoverer (Przybylski 1961)

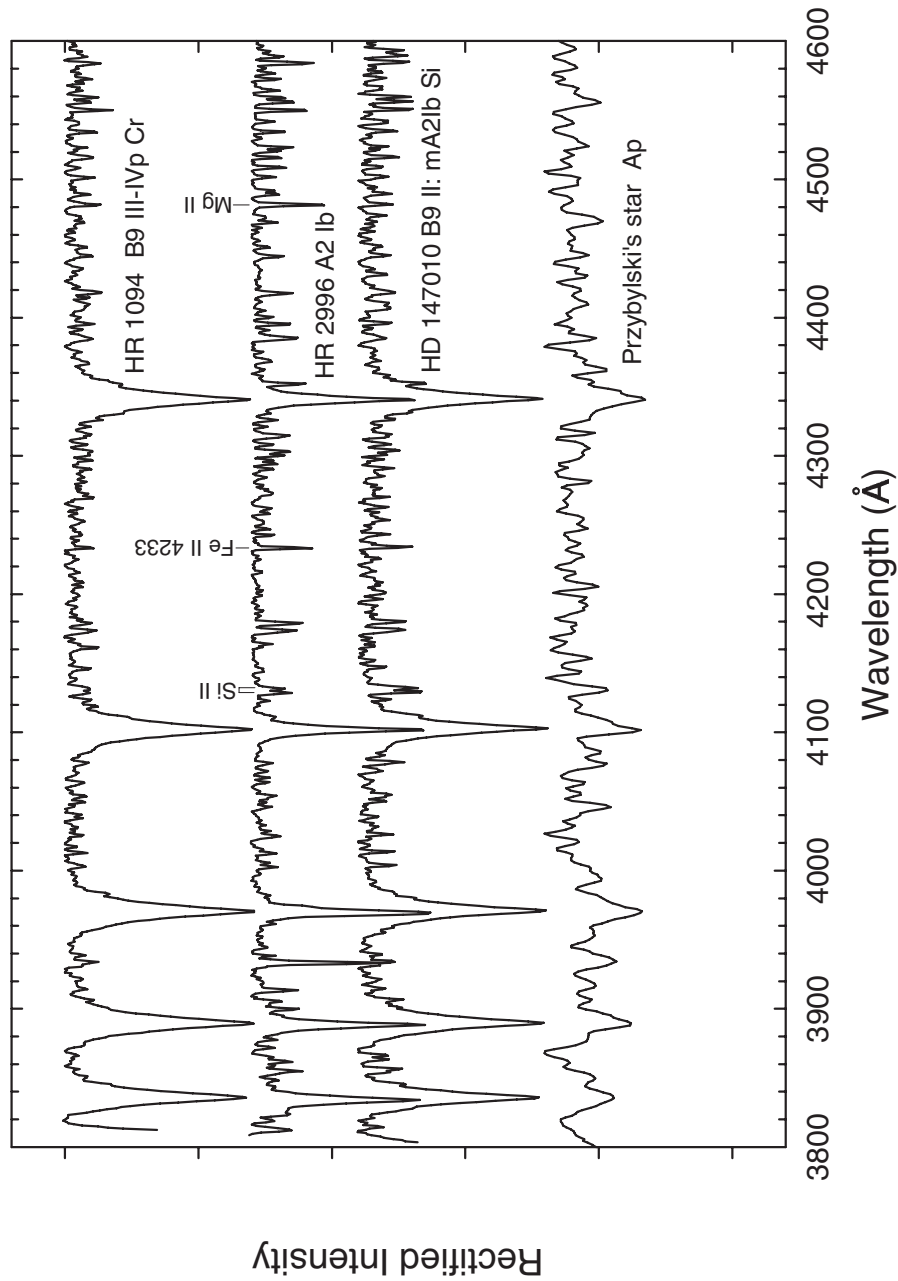


Figure 5.17 This figure illustrates three very unusual Ap stars: HR 1094, which has large overabundances of cobalt and gold; HD 147010, a dwarf Ap star, which shows supergiant features in its spectrum (the A2 Ib MK standard is included for comparison); and Przybylski's star, probably the most peculiar Ap star known—its strongest metal lines are due to the element holmium. The top three spectra are 1.8 Å resolution spectra from the Dark Sky Observatory; the spectrum of Przybylski's star, courtesy M. Grosso and H. Levato, CASLEO Observatory, Argentina, has a resolution of 2.8 Å.

believed it to be a G0 star with unusual abundances; the only lines certainly identified were the Balmer lines and Ca II K & H. Later (see recent papers by Cowley and references therein: Cowley & Mathys 1998; Cowley et al. 2000) it became clear that this is a very unusual Ap star. The strongest lines, other than the hydrogen lines and Ca II K & H, are those of the singly ionized lanthanides; iron is deficient by about a factor of 10 below solar. The lanthanides may have abundances 10^4 times solar. Recently (Cowley et al. 2004), evidence has been presented for the presence of two radioactive rare earths, promethium and technetium, in the spectrum of Przybylski's star and a related star HD 965. The half-life of the most stable isotope of Tc is 4.2×10^6 yr, considerably shorter than the likely evolutionary age of the star, but the half-life of the most stable isotope of Pm, ^{145}Pm , is only 17.7 years! This suggests *in situ* production via nuclear reactions, perhaps at sites of stellar flares associated with the star's rather strong magnetic field. Recent estimates of the effective temperature of the star place it in the mid-F range.

An important point to consider when classifying an Ap star is that at least half of all Ap stars are spectroscopic variables, in that the line strengths associated with the various chemical peculiarities vary with the rotational period of the star. The prevailing view is that this means that the overabundances of these elements are not distributed uniformly on the surface of a typical Ap star, but rather are concentrated in spots. Different elements can be concentrated in different spots on the surface of the star, as the line strengths of different species can vary in different ways. For instance, in α^2 CVn (Pyper 1969) the equivalent widths of the rare-earth elements vary essentially sinusoidally with phase, suggesting these elements are concentrated in a single spot on one hemisphere. The iron-peak elements, however, vary in a much more complex fashion, suggesting the presence of multiple spots. By observing the radial velocity variations of the spectral lines associated with these elements, it is actually possible to map out the position of these spots on the surface of the star.

The origin of these abundance spots or patches is associated with the presence of magnetic fields. It is now known that all "classical" Ap stars (also called the "CP2" stars, comprising the Ap stars considered in this chapter, but not including the HgMn stars that were considered in Chapter 4) have strong magnetic fields, ranging from a few hundred gauss up to a few kilogauss (kG) in most cases. The record magnetic field strength observed on any non-degenerate star is that of the Ap star HD 215441 (Babcock's star, Borra & Landstreet 1978) which at its maximum is 20.5 kG. Magnetic fields were first discovered in Ap stars by Babcock (1947), and have now been measured in some hundreds of Ap stars. How might magnetic fields lead to the presence of abundance spots on Ap stars?

In §5.4.1 we discussed the creation of over- and underabundances of elements in the Am stars on the basis of radiative diffusion. Any given atom or ion feels both an inward gravitational acceleration and an outward radiative acceleration. If the radiative acceleration dominates over the gravitational acceleration, the atom rises in the atmosphere, otherwise it sinks. In an atmosphere with a magnetic field, an additional force can come into play. Neutral atoms will not be affected by a

magnetic field, but ions, which are charged, feel a Lorentz force which, between collisions, compels them to spiral around the magnetic field line. As a consequence, the presence of a magnetic field inhibits the vertical motion of an ion, and reduces the average velocity with which the species migrates or “diffuses” in the vertical direction. The strongest effect occurs when the magnetic field lines are horizontal; when the field lines are vertical, the net magnetic force is much reduced. This can lead to non-homogeneities or spots in the concentration of elements on the surface of the star. For instance, for a simple dipole geometry for the magnetic field, the field lines are nearly vertical at the poles, and horizontal at the magnetic equator. This suggests that chemical separation can occur more readily at the magnetic poles, and one might expect to get abundance spots there. Indeed, in α^2 CVn, the rare earths are concentrated near the negative magnetic pole (Pyper 1969). If the axis of the magnetic field is not aligned with the rotational axis (the basis of the *oblique rotator model* for Ap stars), then this polar spot can come in and out of view, leading to the observed spectral variations.

However, it turns out that in certain circumstances, elemental overabundances can occur at sites on the surface of an Ap star where the magnetic field is horizontal, rather than vertical. Let us consider the case of silicon in the hot Ap stars (Vauclair et al. 1979). In the atmospheres of normal non-magnetic stars, neutral silicon (Si I) feels a strong radiative acceleration, and thus is pushed upwards in the atmosphere. This is because the spectrum of Si I contains a number of strong lines and photoionization edges in the ultraviolet region (see the discussion for the Am stars). However, Si II and Si III have poorer UV spectra, and tend to sink. In normal stars of these spectral types these two tendencies roughly balance, and the abundance of silicon is near the solar abundance. In the presence of a magnetic field, however, in regions where the magnetic field lines are horizontal, the sinking of Si II and Si III is inhibited, and thus the strong radiative acceleration felt by Si I dominates, leading to the development of an overabundance of silicon, at least in a certain range of effective temperatures.

Which elements are supported in a magnetic stellar atmosphere will depend critically on details of atomic physics, the temperature structure of the atmosphere, and the strength and geometry of the magnetic field, as well as a number of other factors, including the action of stellar winds. Most Ap stars, like the Am stars, are slow rotators (some Si II stars can be rapid rotators), but the magnetic field can also help to stabilize the atmosphere, encouraging diffusion.

We must add to the mix the possible *in situ* production of radioactive isotopes on the surface of Ap stars via nuclear reactions (e.g. the short-lived radioactive element promethium, recently discovered in the spectrum of Przybylski’s star, Cowley et al. 2004). Thus, while we understand some of the physics behind the Ap phenomenon, the basic mechanisms leading to the large observed surface inhomogeneities (in some cases rare-earth abundances in spots can be 10,000 times solar) and their placement on the stellar surface are still very poorly understood. A good review of the complexities found in the atmospheres of A-type stars can be found in Landstreet (2004).

AP STARS IN THE ULTRAVIOLET

Figure 5.18 illustrates two classical Ap stars in the ultraviolet. The top panel shows a spectrum of α^2 CVn—a Si II Ap star—compared with the A0 III standard α Dra. The SED (spectral energy distribution) of α^2 CVn is partly shaped by continuous opacity due to Si I; a number of opacity edges for Si I are indicated. Note the very weak Mg II h & k blend in α^2 CVn; magnesium is deficient in α^2 CVn (Lamers & Snijders 1975). β CrB, a cool Ap star, is shown in the bottom panel of Figure 5.18 compared with HR 3974, an A7 Vn MK standard. What is immediately apparent in this diagram is the enormous line blanketing and/or continuous opacity in the spectrum of β CrB between 2400 and 3100 Å. Other cool Ap stars show a similar feature; Przybylski's star, perhaps the most peculiar Ap star, has almost no flux in this region.

CLUSTER ANALYSIS AND THE CLASSIFICATION OF AP STARS

The great diversity of Ap stars, especially when studied at high resolution, has led Cowley & Bord (2004) to seek other ways to classify Ap stars than the methods we have reviewed above. In particular, they suggest adopting the technique of *cluster analysis*, used extensively in evolutionary studies, including the study of the development and the relationships of current human languages, to the classification of Ap stars. They begin with abundances determined for a large number of Ap stars considered as points in an n -dimensional space where n is the number of chemical species considered. An algorithm is then employed to find the closest pair of points, which are then merged into a cluster with coordinates that are the mean of the two points. The algorithm then goes on to find the next closest pair of points, which are likewise merged, and so on. What results is a tree-diagram or *dendrogram* that shows the clusters and illustrates the relationships between them (see Figure 5.19). The vertical cuts in that figure are a first attempt at identifying related groups of stars.

5.4.3 The λ Bootis Stars

The λ Bootis stars are a class of metal-weak, population I A-type stars. The discovery of the class dates from 1943 when the prototype of the class, λ Boo itself, was mentioned in the classic *Atlas of Stellar Spectra* (Morgan, Keenan, & Kellerman 1943). It was described as having a spectral type “near A0,” but with very weak spectral lines, so that the only features easily visible “are a weak K-line and the Balmer series of hydrogen.” This is still a good description of λ Boo, as can be judged from Figure 5.20 where λ Boo and another proto-typical λ Boo star, HR 4881, are shown with two MK standards. It should be noted from that figure that another outstanding feature of the λ Bootis stars is the peculiar weakness of the Mg II λ 4481 line. Indeed, for many years, the operative definition of the class was simply “Stars with spectral types near A0 with weak 4481 lines.” However, that definition turns out to be much too loose, and so over the years after Morgan et al.'s discovery, the class became populated with a wide variety of stars, including

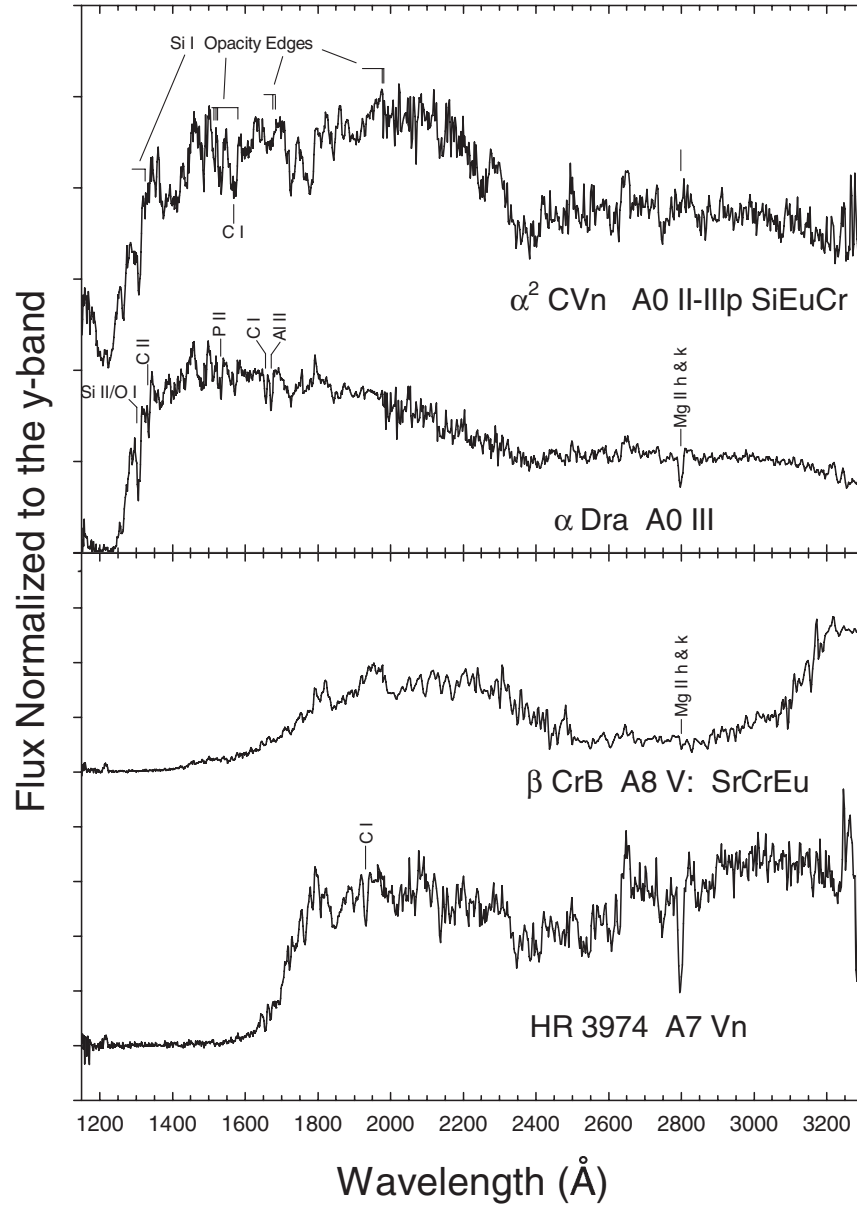


Figure 5.18 Two Ap stars illustrated in the IUE ultraviolet in comparison with MK standards. The top panel illustrates α^2 CVn (a classic Si II Ap star) and the bottom panel, β CrB (a cool SrCrEu Ap star). All the spectra in this figure are presented in the normalized flux format, where the normalization point is taken to be the Strömgren y-band, and were obtained from the MAST IUE archive. Note the enormous line blanketing/continuous opacity between 2400 and 3100 Å in β CrB. In the top panel, α Dra has been shifted downwards by 2 flux units for clarity; in the bottom panel, HR 3974 has been shifted downwards by one flux unit.

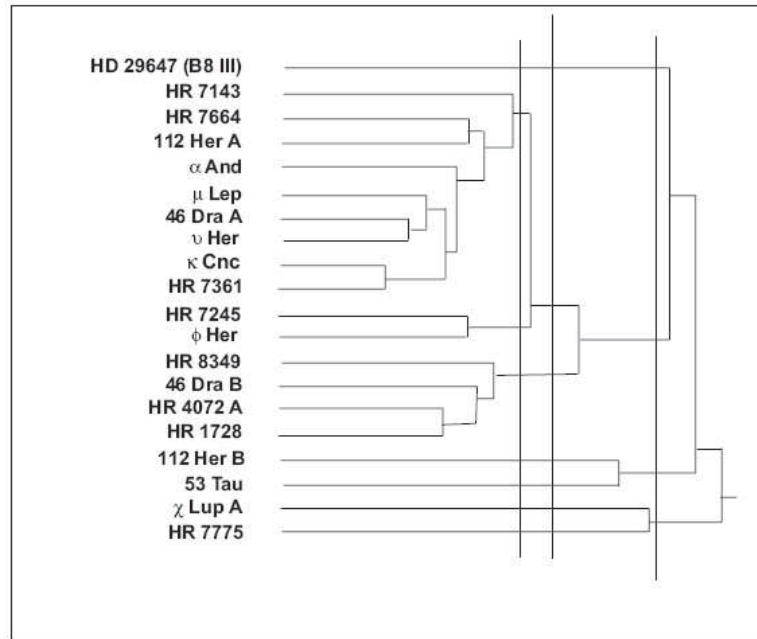


Figure 5.19 The dendrogram of Cowley & Bord (2004) for a sample of Ap stars. The vertical dimension shows the clusters, and the horizontal dimension is a measure of the distance of the clusters from one another. The top cluster, involving among others the stars α and κ Cnc, represents the HgMn stars. Figure used by permission from C. Cowley and Cambridge University Press.

horizontal-branch stars (population II), shell stars, Ap stars, helium-weak B-type stars, and so on (Gray 1988).

Therefore, to advance the study of these astrophysically interesting objects, it is necessary to adopt a clear and unambiguous definition of the class. Such a definition was proposed by Gray (1997) for optical spectra, and the following is based in part on the definition put forward in that paper.

OPTICAL CHARACTERISTICS OF THE λ BOOTIS STARS

In classification-resolution spectra the λ Bootis stars have the following characteristics:

1. The λ Bootis stars are early-A to early-F stars with an approximate spectral-type range (as determined from the hydrogen lines) of B9.5 to F0 with possible members as late as F3.
2. The λ Bootis stars seem to be always characterized by weak Mg II $\lambda 4481$ lines, such that the ratio Mg II $\lambda 4481$ /Fe I $\lambda 4383$ is significantly smaller than in normal A-type stars.
3. In addition to the Mg II $\lambda 4481$ line, the λ Bootis stars show clear signs of a general metal-weak character. In the hottest λ Bootis stars (such as λ Boo

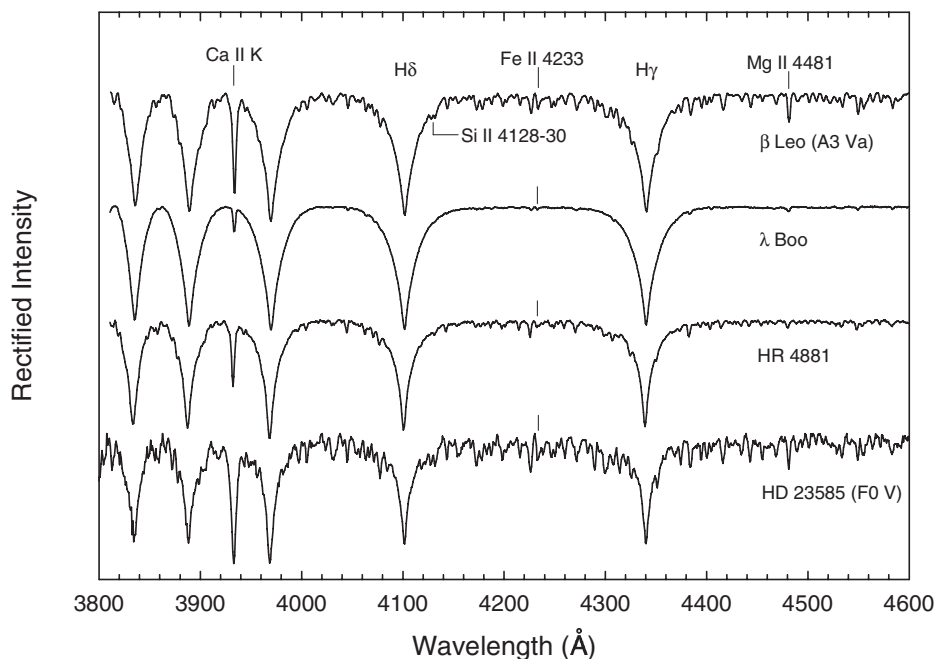


Figure 5.20 The spectrum of two prototypical λ Bootis stars, λ Boo itself and HR 4881, compared with two MK standard stars, β Leo (A3 Va) and HD 23585 (F0 V). These standards were chosen because λ Boo has an A3 temperature type, and HR 4881 an F0 temperature type. Notice the outstanding weakness of the Mg II λ 4481 line. Spectra from the Dark Sky Observatory.

itself) the general metallic-line spectrum can be significantly weaker than in the A0 standards. In late-A and early-F λ Bootis stars, the metallic-line spectrum is clearly weak for the temperature type determined from the hydrogen lines.

4. λ Bootis stars are clearly distinct from classical A-type shell stars (see §5.7 and Figure 5.21). While both types show abnormally weak λ 4481 lines, the typical λ Bootis spectrum does not show the enhanced lines of Fe II and Ti II, such as Fe II λ 4233 and the forest of Fe II and Ti II lines from 4400 to 4600 Å that arise from metastable states. It turns out, however, that a number of λ Bootis stars are β Pictoris shell stars (see §5.7) in that some show narrow absorption components in certain metallic lines, but to see this usually requires high-resolution spectra.
5. λ Bootis stars are also characterized by broad hydrogen lines, and thus appear to be on or near the main sequence.
6. The distribution of rotational velocities of λ Bootis stars cannot be distinguished from that of normal Population I A-type stars. They do not all have $v \sin i > 100 \text{ km s}^{-1}$ as suggested by Jaschek & Jaschek (1990). Stars with high rotational velocities ($v \sin i > 200 \text{ km s}^{-1}$) identified as λ Bootis stars

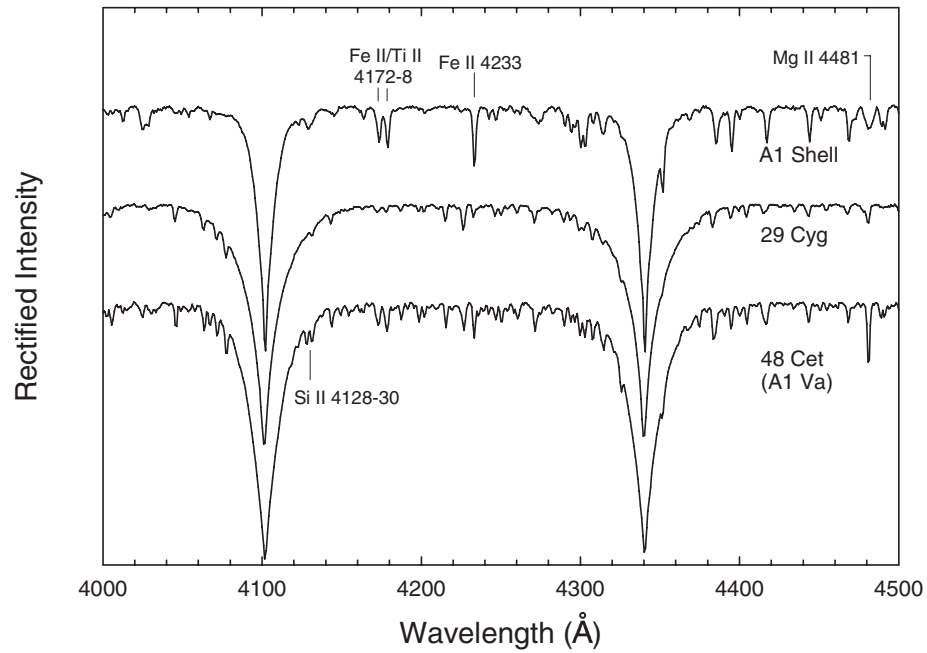


Figure 5.21 The spectrum of 29 Cyg, a λ Bootis star, compared with an A1 classical shell star and the A1 Va standard. Notice the weakness of the Mg II λ 4481 line in the λ Bootis star and the shell star. Spectra from the Dark Sky Observatory.

are necessarily provisional members of the group, as it is difficult to confirm the λ Bootis characteristics in such rapidly rotating stars.

These spectral characteristics are sufficient to distinguish λ Bootis stars from the vast majority of stars. However, there are two regions of confusion that persist, and to resolve the classification of a star in those regions, additional information may be required. These two regions are as follows:

1. It is difficult to distinguish λ Bootis stars from metal-weak horizontal-branch stars (see §5.6.1). Most A-type horizontal-branch stars are metal-weak Population II stars that are burning helium in their cores. As a consequence, space velocities can help to distinguish these two groups. However, Corbally & Gray (1996) found, among a sample of photometrically selected field horizontal-branch stars, a small group of Population II stars that seemed to show λ Bootis-like characteristics. This discovery has never been followed up and the significance of these stars is not clear!

2. The other region of confusion for the λ Bootis class is associated with the low-temperature edge of the distribution of these stars. We can unambiguously distinguish λ Bootis stars as late as F0. However, later than F0 a population of metal-weak, thick-disk (sometimes called “Intermediate Population II”) stars confuse the issue (see Gray 1989). Space velocities can be of some help in distinguishing these two classes, but there are a number of

early F-type metal-weak stars whose status is still unknown, but which may be late λ Bootis stars. The best known of these stars is HD 106223, a star that has been variously classified in the literature as a λ Boo star, a horizontal-branch star, or an Intermediate Population II star. Its spectral type is near F3. A possible way to distinguish the thick-disk stars from λ Bootis stars is to determine the abundances of carbon, nitrogen, oxygen, and sulfur. It turns out that many λ Bootis stars, while showing significant underabundances of the heavier elements, have nearly solar abundances of C, N, O, and S (see Venn & Lambert 1990).

When possible, λ Bootis stars are given three spectral types, the first based on the hydrogen lines, the second on the K-line, and the third on the general strength of the metallic-line spectrum—i.e. the procedure is quite similar to that used in the Am stars, see §5.4.1. However, in order to distinguish the classification notation for the λ Bootis stars (and metal-weak stars in general) from that of the Am stars, the classification is written as follows, for example, for HR 4881:

F0V kA1mA1.5 λ Boo

Here F0 V represents the hydrogen-line type, which is usually the best indicator of the effective temperature. The fact that the K-line and metallic-line types are *earlier* than the hydrogen-line type implies the star is metal-weak.

In the case of the early λ Bootis stars in which the hydrogen-line type corresponds to an early A-type star, but the exact type is indeterminate (this might arise because the early-A type stars span the Balmer maximum, and so the hydrogen-line profile does not change rapidly with effective temperature), it is acceptable to simply write the type as A0 Va λ Boo, for instance. However, with modern digital spectra, it is often possible to assign a hydrogen-line type even among the early A-type stars. Thus, the best spectral type for λ Boo itself is A3 Va kB9.5mB9.5 λ Boo. Note that the B9.5 types for the K-line and the metallic-line spectrum do not imply the presence of He I in the spectrum.

λ Bootis stars are quite rare. Gray & Corbally (2002) have shown that they constitute only 2% of the field A-type stars, and they seem to be curiously absent from star clusters. Paunzen (2001) has published a handy list of confirmed λ Bootis stars.

ULTRAVIOLET CHARACTERISTICS OF λ BOOTIS STARS

The λ Bootis stars are easily distinguished in the ultraviolet in that they have significantly higher relative fluxes in the ultraviolet than normal A-type stars. The reason for this is that in normal A-type stars, the UV flux is considerably reduced because of strong absorption, due both to metal lines (*line blanketing*) and to continuous opacity due to metals. Because λ Bootis stars are metal weak, both of these types of opacity are much reduced, and so the ultraviolet fluxes are higher. Figure 5.22, in which the relative fluxes of 29 Cyg (a λ Bootis star with an A7 hydrogen-line type) and two A7 standard stars are plotted, shows this very clearly. This figure also shows that in the λ Bootis stars, carbon is often of nearly solar abundance;

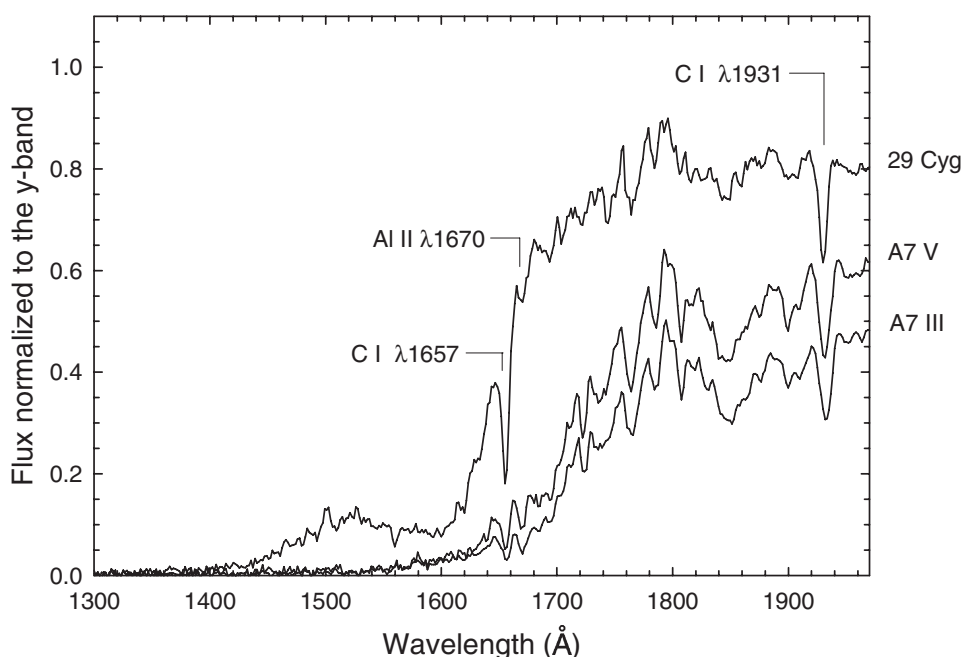


Figure 5.22 The IUE ultraviolet spectrum of 29 Cyg, a λ Boo star compared with that of the A7 V and A7 III MK standards. 29 Cyg has an A7 temperature type. Notice that the fluxes of the λ Boo star are much higher in this region than the MK standards, due to the much lower metallic-line blanketing. Note the broad absorption feature near 1600 Å in the λ Boo star. All the spectra in this figure have been normalized to unity in the Strömgren y-band. Spectra are from the MAST IUE archive.

C I λ 1931 is nearly equally strong in all three stars; and the ratio of C I λ 1657 to Al II λ 1670 is much higher in the λ Bootis star, illustrating that aluminum (like almost all other metals) is deficient in the λ Bootis star (see Faraggiana, Gerbaldi, & Boehm 1990).

Most λ Bootis stars also show a broad absorption feature at 1600 Å—a characteristic they share with A-type horizontal-branch stars and even some white dwarfs. This has been shown by Holweger, Koester, & Allard (1994) to be caused by quasi-molecular absorption by hydrogen, leading to a satellite in the Lyman- α profile due to perturbations by neutral hydrogen. This feature is normally invisible in A-type spectra because of the enormous line-blanketing; as a result, it is characteristic of metal-weak A-type stars in general, and not λ Bootis stars in particular.

λ BOOTIS STARS IN THE IR

In the near-infrared, λ Bootis stars generally show features similar to the optical: strong hydrogen lines with metal-weak spectra. Andriillat, Jaschek, & Jaschek (1995) illustrate a number of λ Boo stars in the near-infrared between 7600 and 10800 Å, but their sample also includes a number of stars that are not λ Bootis

stars, so their overall conclusions about the nature of λ Boo stars in the NIR are somewhat suspect.

There have been a number of studies of the λ Bootis stars in the far infrared. Sadakane & Nishida (1986) were the first to find, using observations from the *Infrared Astronomical Satellite* (IRAS), infrared excesses in three λ Bootis stars: HD 31295, λ Bootis itself, and HD 218396 (HD 218396 was discovered to be a λ Bootis star only later—see Gray & Kaye 1999). Later Cheng et al. (1992) reported another λ Bootis star, HD 110410 (ρ Vir), to have an infrared excess. Most recently, Paunzen et al. (2003) have compiled a comprehensive list of observations of λ Boo stars in the infrared, as well as making new observations with the *Infrared Space Observatory* (ISO) and in the submillimeter spectral region. They found that 23% of the λ Bootis stars they observed show infrared excesses. This should be compared with a proportion of 18% for normal A-type stars (Cheng et al. 1992). Hence, λ Bootis stars do not seem to be unusual in this way. The infrared excesses are due to warm dust in circumstellar clouds or disks associated with the stars.

CIRCUMSTELLAR GAS

It turns out that a number of λ Bootis stars show evidence for circumstellar gas. The first report of circumstellar gas associated with a λ Bootis star, deduced by the presence of narrow absorption components superimposed on photospheric absorption lines, such as Ca II K, was by Gray (1988) who noticed a weak, narrow absorption component in the Ca II K-line of HR 4881. Later, Holweger, & Stürenburg (1991) and Holweger & Rentzsch-Holm (1995) discovered narrow absorption components in the spectra of a number of λ Bootis stars. Bohlender & Walker (1994) discovered shell lines in HD 38545 (131 Tau), although it now appears that this star was misclassified by Gray (1988) as a λ Boo star and is better classified as an A-type shell star. However, Bohlender et al. (1996) went on to demonstrate the presence of strong circumstellar features in the Na I D lines in a number of other λ Bootis stars. Thus there is ample evidence for gas around many but not all λ Bootis stars. It is possible that this gas is in the form of a circumstellar disk and that those stars without detections have disks that are inclined to the line of sight. Stars that show such narrow absorption components are referred to as β Pictoris shell stars and should be distinguished from the *classical shell stars* (see §5.7).

WHY ARE λ BOOTIS STARS INTERESTING?

λ Bootis stars are interesting to astronomers because the metal deficiencies in these Population I stars—which should be metal-rich—are still not explained. It is beyond the scope of this book to explore in detail the theories that have been advanced to explain these metal deficiencies; good summaries are given by Gray & Corbally (2002) and Paunzen et al. (2004). The theory that best seems to account for the characteristics of these stars is the accretion/diffusion theory, first put forward by Venn & Lambert (1990) who noticed that the chemical abundance patterns

in λ Bootis stars mimicked those in the interstellar medium where refractory metals are incorporated into dust grains and C, N, O, and S remain in the gas phase. If gas and dust can be separated near the star and the metal-depleted gas accreted by the star while the dust is blown away, the chemical abundances in the photosphere will be diluted, making the star look metal-weak. Turcotte & Charbonneau (1993) and Turcotte (2002) have shown that an accretion rate of at least $10^{-14} M_{\odot} \text{ yr}^{-1}$ is required to produce the observed abundances. Gray & Corbally (2002) suggest that the gas is associated with a circumstellar disk (the observation of discrete accretion events—see Holweber & Rentzsch-Holm 1995—suggests the gas might come from cometary bodies), while Kamp & Paunzen (2002) have suggested that accretion occurs when the star wanders into an interstellar cloud.

5.5 HERBIG Ae/Be STARS

The identification of the Herbig Ae/Be stars as a class of pre-main-sequence (PMS) A- and B-type stars was first made by Herbig (1960). In that seminal paper, Herbig reasoned from the time scales involved in the contraction of a protostar to the main sequence and nuclear burning on the main sequence that there should be a small (but not vanishingly small) number of observable PMS stars with masses from 3 to $20 M_{\odot}$ (corresponding to spectral types A and B). He suggested that those stars would meet the following conditions: (1) a spectral type of A or earlier with emission lines, (2) a location in an “obscured region” (i.e., the star would be associated with a dark cloud) and (3) the star would illuminate a bright reflection nebula in its immediate vicinity. The first condition followed by analogy from the characteristics of the already known PMS G- and K-type stars—the T Tauri stars, whose spectra are characterized by emission lines (see §7.5). The purpose of points (2) and (3) was to eliminate emission-line stars that were not in the PMS phase of evolution. For instance, planetary nebula nuclei and old novae are generally not found in obscured regions. The ordinary Be stars (see §4.5) are main-sequence B-type stars with emission lines, but are only rarely seen in regions of obscuration or nebulosity. Point (3) also ensured that the star was not simply seen in projection against a dark cloud. Herbig proposed a list of 26 objects that met these criteria, many of which have turned out to be PMS stars.

Of course, an emission-line A- or B-type star that is not found in an obscured region or in association with nebulosity may still be a PMS star. Indeed, a number of such objects are now known, and these stars, in common with other PMS Ae and Be stars, are characterized by the presence of an infrared excess due to thermal re-radiation by circumstellar dust. Generally, these stars show evidence of the presence of either cool or hot circumstellar dust, or both. While many “classical” Be stars show an IR excess, this is due to free-free and free-bound emission from ionized gas in a circumstellar disk, and is easily distinguished from thermal re-emission. This distinction led Malfait, Bogaert, & Waelkens (1998) to suggest replacing points (2) and (3) with the condition that the star show a “broad” infrared excess.

It is beyond the scope of this book to review all of the characteristics of Herbig Ae/Be stars, including details of their infrared excesses, their photometric variability, and the presence of strong intrinsic and variable polarization. We refer the reader to the review of Herbig Ae/Be stars by Waters & Waelkens (1998), even though that review is becoming quickly outdated with new results from the *Spitzer Space Telescope* and other observatories. Instead, we concentrate in this section on the application of spectral classification to the Herbig Ae/Be stars.

Spectral classification plays very important roles in the study of Herbig Ae/Be stars. Because many of these stars show large extinction due both to the presence of dust in the star formation region and to the presence of significant amounts of dust in a shell or disk around the star, spectral classification may be the only way or the best way to determine the nature of the underlying star (including its mass and luminosity). A determination of the spectral type of the star, and thus its intrinsic color, can help determine the total extinction due to dust, as well as some of the characteristics of that dust. For instance, Hernández et al. (2004) used spectral typing to show that R , the ratio of total to selective extinction, can be larger than its canonical value of 3 in the environments of Herbig Ae/Be stars. Finally, the presence of peculiarities in the spectra of Herbig Ae/Be stars (for instance the emission lines) may provide information on the physical conditions of the photosphere and the stellar environment, including the presence of gas accretion or outflows.

It turns out that most Herbig Ae/Be stars may be readily classified on the MK system (Gray & Corbally 1998). However, there are a number of features in the spectra of Herbig Ae/Be stars that are unusual, and contain valuable astrophysical information. Many of these features can be profitably incorporated into a classification system for the Herbig Ae/Be stars.

There are a surprising number of attempts in the literature to devise spectral classification systems for the Herbig Ae/Be stars, a reflection of how important spectral classification is to this field. These systems may be divided into two categories. The first category includes systems that either apply MK classification (with its emphasis on standard stars) to the Herbig Ae/Be stars or extend the MK system to include the spectral features peculiar to the Herbig Ae/Be stars. Two examples include the work by Gray & Corbally (1998) on extending the MK system to PMS A-type stars, and the more recent work by the EXPORT group (Mora et al. 2001) to classify Vega-type and PMS stars. The second category consists of a number of classification systems that utilize the measurement of line strengths or equivalent widths to determine the spectral type of the underlying star. Examples include Cohen & Kuhi (1979), Hillenbrand (1995), and most recently Hernández et al. (2004). Each of these have used different spectral regions and different spectral indices.

It turns out that in the spectra of most Herbig Ae/Be stars, many of the normal MK criteria used to judge the temperature type are not strongly affected by the presence of circumstellar material. Thus, the general strength of the metallic-line spectrum, especially the strengths of lines due to neutral species, such as Ca I $\lambda 4226$, Fe I $\lambda 4271$, etc., can be useful criteria for determining the spectral type of

the underlying star. The cores of the hydrogen lines may, of course, be affected by emission or by shell absorption, but the wings, especially of the higher Balmer lines, are generally photospheric. Other MK criteria must be treated with some caution. The Ca II K-line is often unreliable; its variability in many Herbig Ae spectra attests to the fact that it is often at least partially formed in the circumstellar material. Likewise, He I lines may vary and thus can be unreliable indicators of the spectral type. This of course greatly complicates the classification of Herbig Be stars. Some guidance as to which MK criteria are reliable in a given star may come from looking at a time sequence of spectra. If the star is a spectrum variable, those features that are constant are more likely (but are not guaranteed) to be primarily photospheric. Of course, if a star has a nonvariable spectrum, that does *not* imply that all features are photospheric! Luminosity criteria are more problematic than temperature criteria, but in the B- and early A-type PMS stars, the wings of the hydrogen lines can help determine the luminosity class. All criteria based on lines of ionized species, especially those arising from metastable states, are however suspect.

It should be noted that in some extreme cases of Herbig Ae/Be stars, line and continuum emissions are so strong that no spectral features due to the underlying star can be identified. These stars, of course, cannot be classified. Even if spectral features from the underlying star can be identified, continuum emission can veil the spectrum and weaken the spectral lines. Spectral criteria based on ratios of spectral lines should then be given preference.

The Gray & Corbally system uses the above guidance to determine the underlying MK type of the star, but then extends the MK system to include in the spectral type information on the following points:

1. The presence of emission or shell cores in the Balmer lines, and whether these cores are shifted to the blue or red with respect to the line center.
2. The strength of the Balmer decrement.
3. The presence of non-photospheric contributions (either in the form of emission or enhanced absorption) to certain lines due to ionized metals, in particular lines of the Fe II (42) multiplet $\lambda\lambda 4923, 5018, \text{ and } 5169$.

These points are included in the MK type with the addition of indices and symbols, as follows:

Hydrogen-line emission:

- e** Strong emission, at least in $H\beta$
- (e)** Marginal emission, usually visible only in $H\beta$ as a distortion of the core of the hydrogen line
- r** Hydrogen-line emission core, shifted to the red with respect to the photospheric absorption line
- b** Hydrogen-line emission core, shifted to the blue with respect to the photospheric absorption line

Balmer decrement:

- Bd**> Balmer decrement very strong, going from emission in $H\beta$ to strong shell absorption in higher hydrogen lines
- Bd** \geq Balmer decrement not quite as strong
- Bd**= Normal Balmer decrement (if $H\beta$ is in emission, emission is weak in $H\gamma$ and absent in $H\delta$; if shell absorption is visible in $H\beta$, the profile is normal by $H\delta$). This index is usually not written.
- Bd** \leq Weak Balmer decrement
- Bd**< Very weak Balmer decrement (if $H\beta$ is in emission, filling-in of the cores of the hydrogen lines can be seen to quite high in the Balmer series—say, to $H8$ and $H9$; if $H\beta$ has a strong shell absorption core, shell absorption cores can be seen to quite high in the Balmer series)

Non-photospheric contributions to lines of ionized species (these indices are taken as a mean of the Fe II multiplet 42 lines $\lambda\lambda 4923, 5018, \text{ and } 5169$):

- Nab** These three lines are strongly in absorption (i.e. more strongly in absorption than in the relevant MK standard)
- Nem** These lines are in emission
- Npc** These lines show a P Cygni profile
- Nipc** These lines show an inverse P Cygni profile

These symbols may be used with a numerical index to indicate strength of emission or absorption, judged relative to the relevant MK standard:

- Nem0** \equiv Nab0; normal strength for these lines (not written)
- Nem2** Emission just fills lines to the continuum
- Nem4** Emission strength above continuum = normal absorption strength below the continuum
- Nem6** ... Using the same scale to designate stronger emission
- Nab2** Absorption is to a depth twice that of normal absorption strength
- Nab4** Absorption is to a depth three times that of normal absorption strength, etc.

Figure 5.23 helps to demonstrate the use of some of these extensions to the MK system. Gray & Corbally used 3.6-Å-resolution (2 pixel) spectra in the violet-green (3800–5600 Å) spectral region to set up their system.

One problem with the Gray & Corbally system is that the resulting spectral type is quite long and unwieldy. However, the advantage is that at a single glance, one can get a very good feel for the nature of the spectrum, certainly better than one might get by running one's eye down columns of equivalent widths. A time series of spectral types for a single star reveals very clearly the nature of the spectral variability and, if the dates are included with the spectral type (something we advocate very strongly), a rough time scale for the variations may be deduced.

A more serious criticism of the Gray & Corbally system is that it was set up using the traditional blue-violet part of the spectrum, and thus does not include the important $H\alpha$ line. Stars with very high extinctions may be difficult to observe in the blue-violet. If the spectra available do not contain the Fe II (42) lines, or

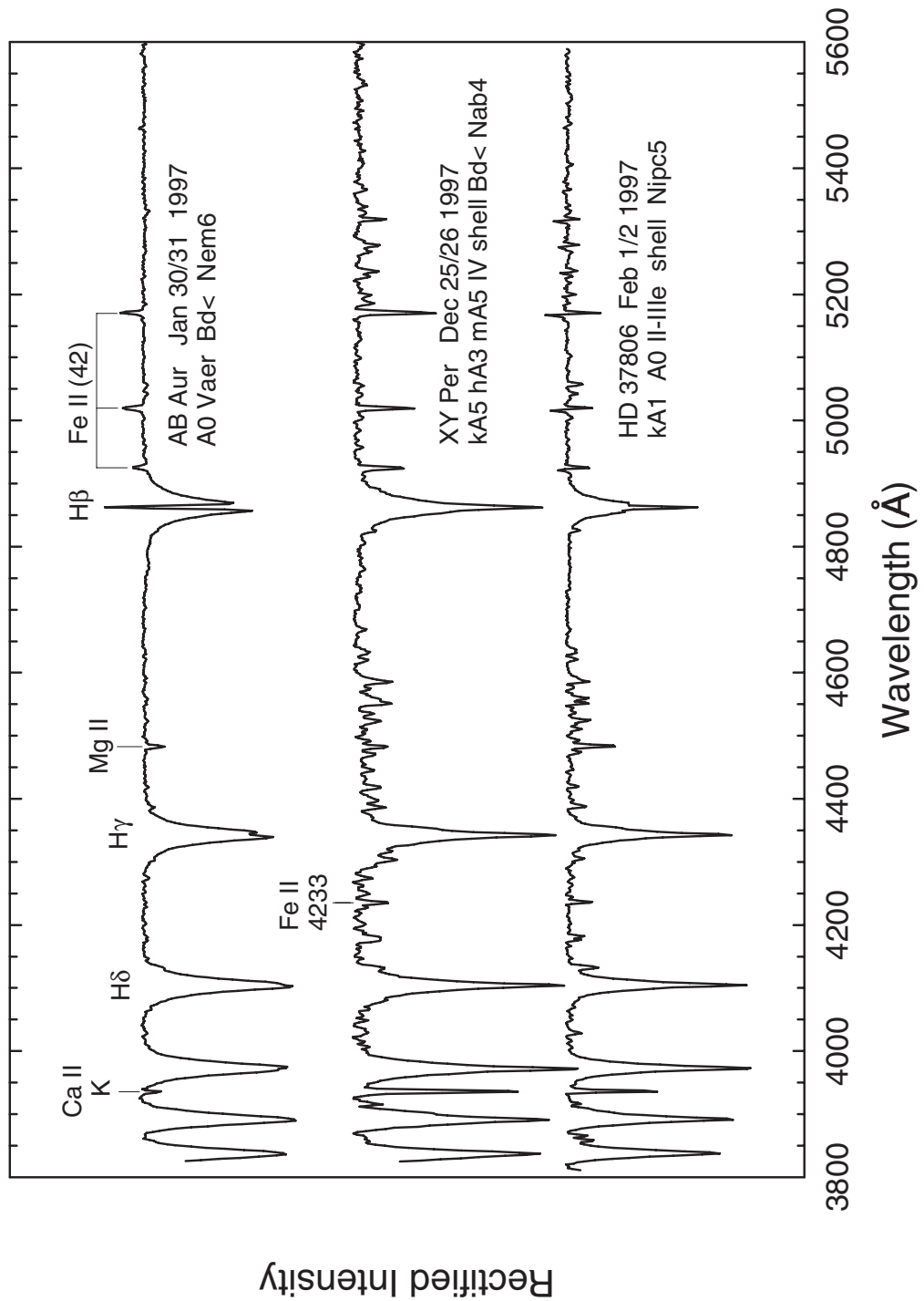


Figure 5.23 Spectra of three Herbig Ae stars. Note that lines of multiplet 42 of Fe II are in emission in AB Aurigae, in deep absorption in XY Per, and exhibit inverse P Cygni profiles in HD 37806. Both XY Per and HD 37806 show pronounced shell features, including a strong Fe II λ 4233 line. These spectra were obtained at the Dark Sky Observatory, and have a resolution of 3.6 Å.

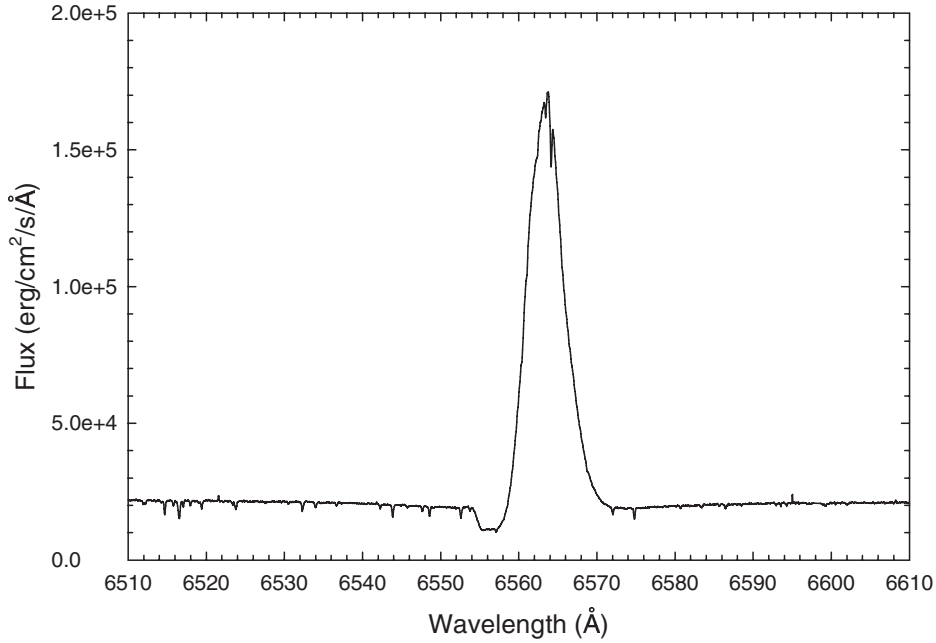


Figure 5.24 A high-resolution $H\alpha$ profile of AB Aur, a Herbig Ae star. This is a P Cygni profile, and corresponds to class IVB on the Reipurth et al. classification scheme. Only the far wings of this profile are photospheric. The spectrum is taken from the Elodie archive (Moultaka et al. 2004).

if these lines are not resolved, then much of the extended system cannot be used. In addition, for early B-type stars, the Fe II (42) lines do not show up in the MK standards, and so the numerical indices cannot be used.

The EXPORT group (Mora et al. 2001) have developed a classification system for *Vega-type* and PMS stars (including Herbig AeBe and T Tauri stars) that appears to have been carefully executed and conceived. The basic spectral material was spectra from the Isaac Newton Telescope with a spectral range of 5854–6728 Å, and a resolution of about 1 Å. Spectra were obtained for both program stars and MK standards. In this spectral range, the group identified lines that are basically photospheric (the Na I D lines, Ca I $\lambda\lambda$ 6102, 6122, and 6162, Fe I λ 6495, and Li I λ 6708). Those lines were used to determine, in comparison with the MK standards, the spectral type of the underlying star. $H\alpha$, He I λ 5875, and a number of *diffuse interstellar bands* (DIBs) were identified as features that may be formed, at least partially, in the interstellar or circumstellar environment (the Na I D lines may also have a non-photospheric component). Luminosity classes were obtained by comparison with the MK standards, although not many satisfactory luminosity criteria for B- and A-type stars are located in their spectral range (emission at $H\alpha$ is often so strong that the photospheric wings are overwhelmed or unusable for classification—see Figure 5.24). The EXPORT group did not devise extensions to the MK type like Gray & Corbally, but such extensions could be added to their system in the future. They did take careful note of how the non-photospheric

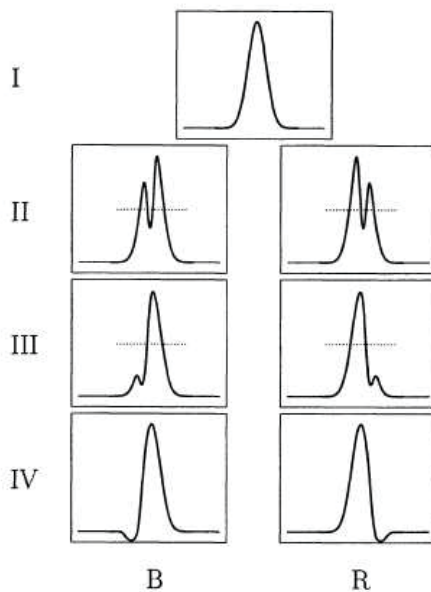


Figure 5.25 The classification scheme of Reipurth, Pedrosa, & Lago (1996) to classify $H\alpha$ profiles of PMS stars. The dotted line corresponds to 50% of maximum line intensity. Reproduced by permission of *Astronomy and Astrophysics*.

features appeared in their spectra, and made use of nonvariable features in selecting photospheric criteria for determining the spectral type of the underlying star.

The classification systems devised by Cohen & Kuhi (1979), Hillenbrand (1995), and Hernández et al. (2004) have in common that they use measurements of line strengths or equivalent widths to determine the spectral type of the underlying star, and not direct comparisons with the MK standards. Hernández et al. (2004), for instance, used 6-Å resolution spectra taken with the FAST spectrograph (Fabricant et al. 1998) with a spectral range from 3800 to 7200 Å. In this spectral region, they identified 33 spectral features sensitive to the effective temperature, including many in common with Gray & Corbally and the EXPORT group (some features, however, appear to have been misidentified). These 33 features were measured in a grid of spectral standards, and then used to determine the spectral type of the underlying star. The luminosity type was not determined. Note was taken of how the Herbig Ae/Be stars deviated from the standards, especially in [O I] $\lambda 6300$, He I $\lambda\lambda 5876$ and 6678, the Na I D-lines, lines of multiplet 42 of Fe II (see above), and $H\alpha$.

CLASSIFICATION OF HERBIG Ae/Be STARS AT $H\alpha$

Finkenzeller & Mundt (1984) surveyed the $H\alpha$ profiles of 57 Herbig Ae/Be stars and candidates, and found that 50% showed double-peaked $H\alpha$ profiles, 25% were

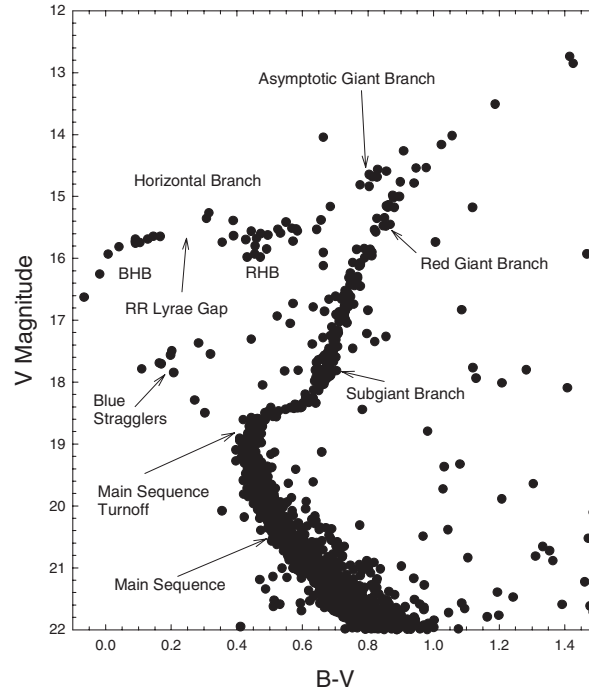


Figure 5.26 A color-magnitude (H-R) diagram of the globular cluster M3, with features mentioned in the text pointed out. Data from Rey et al. (2001).

single peaked, and 20% had P Cygni profiles at $H\alpha$ (see Figure 5.25 for the $H\alpha$ profile of AB Aurigae, which shows a P Cygni profile). Reipurth, Pedrosa, & Lago (1996) published an atlas of $H\alpha$ profiles of PMS stars, including 18 Herbig Ae/Be stars, and found that most had double-peaked $H\alpha$ profiles. They proposed a scheme to classify $H\alpha$ profiles in PMS stars consisting of four categories, illustrated in Figure 5.25.

5.6 A-TYPE STARS IN ADVANCED EVOLUTIONARY STAGES

5.6.1 Horizontal-Branch Stars

Horizontal-branch stars are intermediate-mass stars that are currently burning helium in their cores. For metal-rich stars, the helium-burning phase takes place while the star is a red giant and occurs in the *red-giant clump*, but for metal-poor stars, helium burning occurs during an extended “blue loop” in the H-R diagram. These blue-loop stars, which are B-, A-, and F-type stars, are known as *horizontal-branch stars* (HB), and are a common feature in the H-R diagrams of globular clusters (see Figure 5.26). The helium burning phase, like hydrogen burning on the main sequence, is relatively long-lived. Where a star ends up on the horizontal branch depends on its history of mass loss while it was a red giant. Upon helium ignition in the core, the remnant envelope of the red giant collapses and the

star moves onto the horizontal branch. Those stars with fairly massive envelopes become *red horizontal-branch* (RHB) stars but those with less massive envelopes become *blue horizontal-branch* (BHB) stars. The blue and red parts of the horizontal branch are separated by the RR Lyrae instability strip. RR Lyrae variable stars are horizontal-branch stars that pulsate. When helium is exhausted in the core, HB stars evolve upward and to the right in the H–R diagram toward the red giant branch. This evolutionary phase is very short-lived, and so only a few stars are caught evolving off of the HB. These stars are known as *Supra Horizontal-Branch* (SHB) stars or, sometimes, as *post-HB* stars. Finally, the second visit to the giant branch occurs along the *Asymptotic Giant Branch* (AGB). AGB stars will be considered in Chapter 8.

HB stars have gravities comparable to those of B-, A-, and F-type subgiants and giants. What distinguishes them spectroscopically from Population I B-, A-, and F-type giants is their metal-weak nature. Most HB stars are found in the ancient, Population II massive clusters—the globular clusters. But many are also found as field stars in the Galactic halo, and can as well be distinguished from Population I stars on the basis of their *kinematics*, i.e. they are high-velocity stars; these stars are commonly referred to as *field horizontal-branch* (FHB) stars.

From a spectral classification point of view, we attempt to identify and classify BHB stars on the basis of the information present in the classification spectrum. Figure 5.27 shows a montage of three A-type FHB stars (HD 109995, HD 86986, and HD 161817), one BHB star from the globular cluster M3 (K851), and, for comparison purposes, a metal-weak Population I A dwarf, the λ Bootis star 29 Cyg (see §5.4.3).

Almost all BHB stars are metal-weak, and thus care is required in their classification. As described in §5.4.3 on λ Bootis stars, the spectral types of such stars consist of a hydrogen-line type, followed by types for the Ca II K-line and the general metallic-line spectrum. The hydrogen-line type, which consists of both a temperature type and a luminosity type, based on the sensitivity of the hydrogen-line profile to both temperature and gravity in the B and A-type stars, is the “leading” spectral type, as it is the one that should be best correlated with the effective temperature. The K-line and metallic-line types will be earlier than the hydrogen-line type for metal-weak stars, and this will alert the user of the spectral type to the fact that the star is, indeed, metal-weak. For example, the spectral type of HD 109995, a FHB star illustrated in Figure 5.27 is written

$$A2\text{ IVs kA0mA0},$$

where the A2 IV is the spectral type deduced from the hydrogen-line profile. B-type HB stars have been included in the OB subdwarf classification system of Drilling et al. (2003), which is presented in §4.7.1. See Corbally & Gray (1996) for spectral classifications of 67 HB and HB-candidate stars.

It may be well at this point to finally lay to rest a misunderstanding about the appearance of the spectra of HB stars that has been floating about the literature for some years and unfortunately was not entirely dispelled by

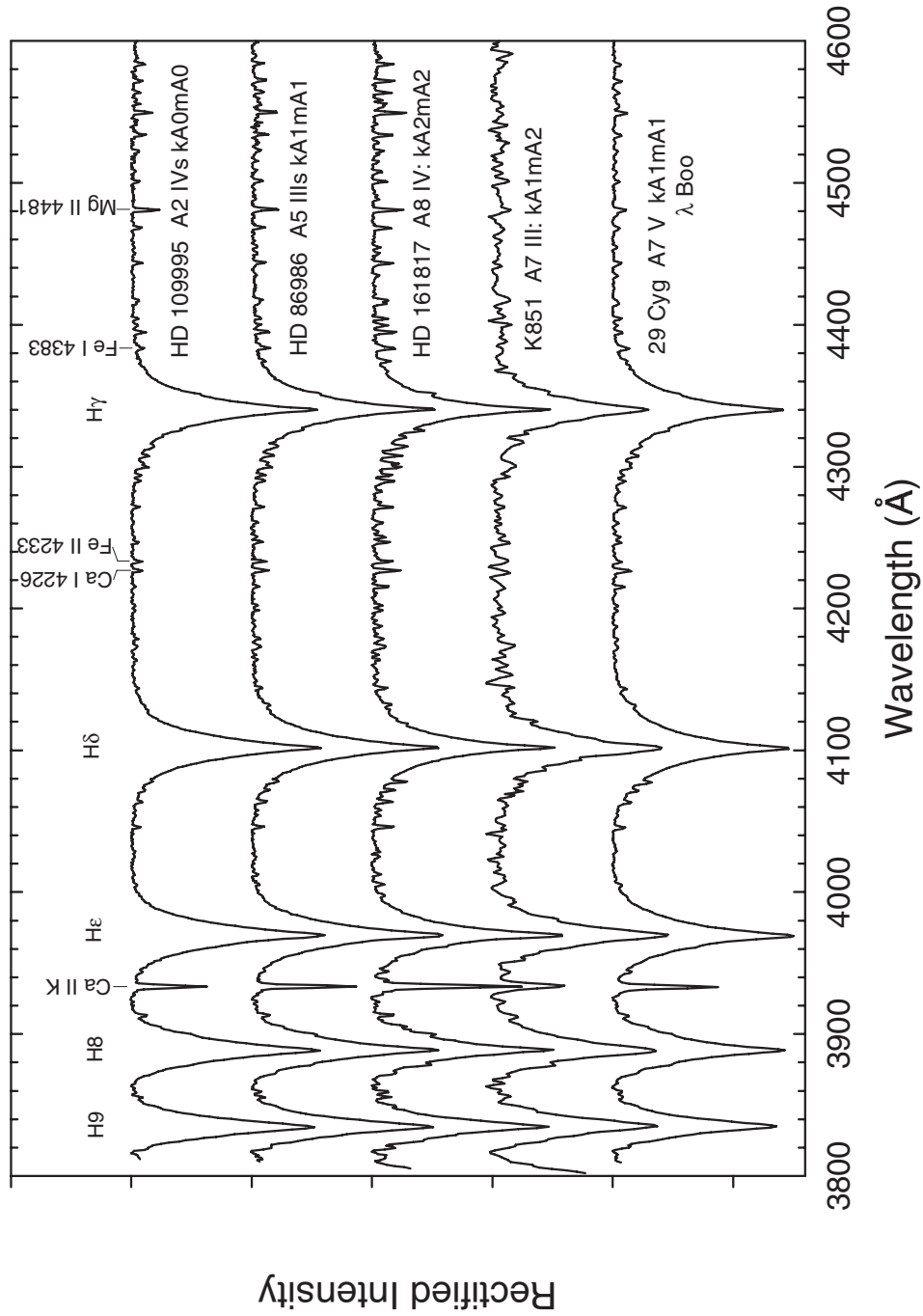


Figure 5.27 A montage of three field horizontal-branch stars, one cluster BHB star (from the globular cluster M3), and, for comparison, one late-type λ Bootis star. All these spectra were obtained at the Dark Sky Observatory and have a resolution of 1.8 \AA , except for the M3 star, which was observed with the Bok 2.3-m telescope (Steward Observatory), and has a resolution of 2.8 \AA .

Jaschek & Jaschek (1990). This is the idea that the spectra of HB stars are characterized by weak, narrow Balmer lines, similar to those seen in supergiant A-type stars. This misunderstanding apparently began with Slettebak et al. (1961) who used the stars BD+32° 2188 and BD+39° 4926 as prototypical HB stars. As a matter of fact, these stars are post-AGB stars, not HB stars, and do indeed have gravities similar to A-type Ib supergiants (see §5.6.2 below).

A glance at Figure 5.27 indicates that the spectra of BHB stars and λ Bootis stars are very difficult to distinguish in the blue-violet. Indeed, successful separation of these two classes using classification techniques requires excellent S/N and good resolution, preferably better than 2 Å. Careful examination of Figure 5.27 shows a number of features that can be used to discriminate between the two classes. First, note that the three FHB stars in Figure 5.27 have very sharp lines, whereas the lines of the λ Bootis star are noticeably broadened by rotation (this distinction is not clear in the case of K851 because of the poorer resolution and S/N of that spectrum). This is not a sufficient criterion as some λ Bootis stars are also slow rotators. Second, note that in the BHB stars the ratio of Mg II λ 4481 to Fe I λ 4383 is always unity or greater. This is not the case in the large majority of bona fide λ Bootis stars. Third, Fe II λ 4233 is always considerably weaker than Ca I λ 4226 in the λ Bootis stars, even when compared with the coolest BHB star in the montage (Figure 5.27); this is probably largely a luminosity effect. Finally, the hydrogen-line wings of the λ Bootis star are noticeably broader than those of the FHB stars, a reflection of the higher gravity in the λ Bootis star. Note that this difference in the hydrogen-line profiles can be perceived even at a spectral type of A7, where the hydrogen-lines have only a fraction of the sensitivity to gravity seen at A0. The small line blanketing in these metal-weak spectra makes the hydrogen-line profiles easier to use in luminosity classification. Clearly, however, these differences are subtle, and require good quality spectra and a sharp eye.

Using external information, discriminating between the two types becomes easier. First, BHB stars are high-velocity stars, whereas the Population I λ Boo stars are not. Second, in the Strömberg [c₁], H β diagram, BHB stars are well separated from λ Boo stars, reflecting their larger Balmer jumps. Better discrimination can also come from other parts of the spectrum. For instance, it will be recalled that λ Boo stars, while showing large metal deficiencies, have nearly solar abundances of C, N, and O. Thus, a comparison of the two in the ultraviolet (compare Figure 5.28 with Figure 5.22) shows that the C I $\lambda\lambda$ 1657 and 1931 lines are much weaker in the BHB spectra than in the λ Boo spectra. A similar comparison can be made at the near-infrared O I triplet. Note from Figure 5.28 that in the IUE ultraviolet, many BHB stars share the very broad 1600-Å absorption feature with the λ Boo stars. This feature, as explained in §5.4.3, is due to Lyman- α H-H⁺ and H-H quasi-molecular absorption. Another similar feature at 1400 Å can just be seen in the spectrum of HD 109995.

RR LYRAE STARS

The RR Lyrae stars are pulsating, variable HB stars with A and F spectral types. Their spectra are similar to those of the cooler BHB stars except, during rising

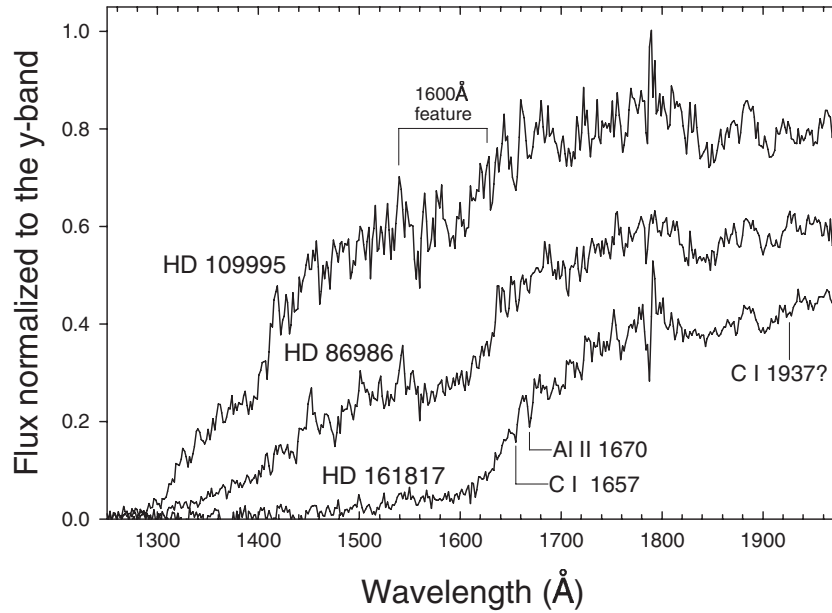


Figure 5.28 The shortwave IUE spectra of the three FHB stars in Figure 5.27. The C I and Al II features have been marked in the spectrum of HD 161817. It is instructive to compare this spectrum with that of 29 Cyg (Figure 5.22) to confirm that λ Boo stars are easy to distinguish from BHB stars in the UV. Note the broad 1600 Å absorption feature also found in the spectra of λ Boo stars. See §5.4.3 for an explanation of this feature. The spectra are from the MAST IUE archive and have been normalized to unity in the Strömgren y -band.

light, the lower Balmer lines may go into emission. Figure 5.29 shows a time sequence of spectra of SU Dra through rising light. Note that an emission core appears in $H\beta$ and line profile changes are visible all the way up to $H9$. Also note the change in the strength of the Ca II K-line, and the implied change in the spectral type as the star progresses through rising light.

POST-HB OR SUPRA HORIZONTAL-BRANCH STARS

As noted in the introduction to this section, once helium exhaustion has occurred in a HB star, it evolves rapidly upward and to the right toward the Asymptotic Giant Branch (AGB). Very few stars are caught in this transition from the HB to the AGB; they are known as post-HB or Supra Horizontal-Branch (SHB) stars. A handful are known in globular clusters, for instance ZNG 4 in M13 (Ambika et al. 2004), V4 and ZNG 5 in NGC 6656, and K260, K996, and K1082 in NGC 7078 (Jasniewicz et al. 2004).

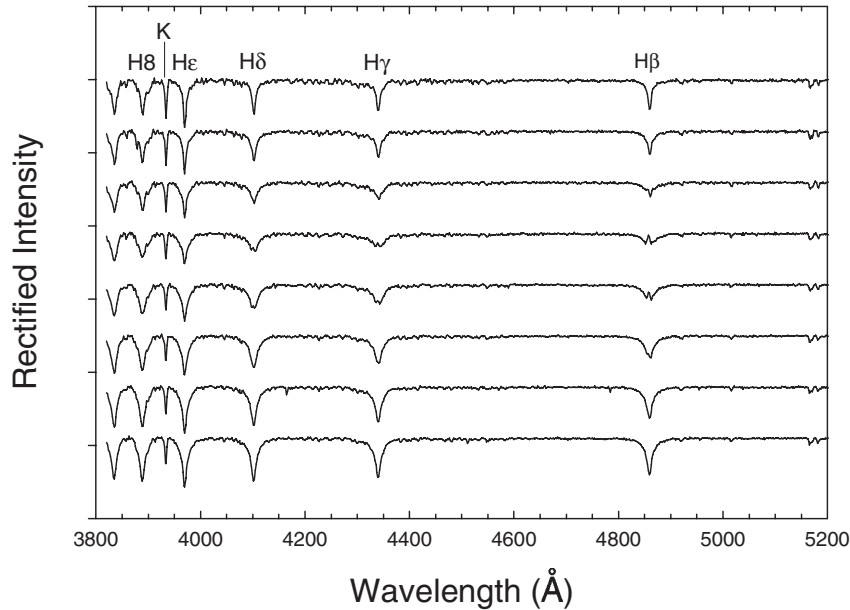


Figure 5.29 A sequence of spectra of SU Dra, an RR Lyrae star through rising light. These spectra were obtained at the Dark Sky Observatory, and have a resolution of 3.6 \AA .

5.6.2 Post-AGB Stars

Post-AGB stars, which are also known as proto-planetary nebulae (PPNe), are intermediate-mass stars that have evolved off the AGB, and are in the process of ejecting shells of gas (and dust) that will eventually become planetary nebulae, once the central star has become hot enough to ionize the gas. This evolutionary phase is very short-lived, and the central star evolves very quickly through the spectral sequence $K \rightarrow G \rightarrow F \rightarrow A \rightarrow OB \rightarrow \text{Planetary Nebula nucleus}$. In the A-star part of this sequence, these stars appear as luminous A-supergiants, often with peculiar abundances. For instance, many of these stars appear deficient in the refractory elements (Fe, Mg, etc.), but have near-solar abundances of C, N, O, S, and Zn. The similarity of this abundance pattern to the λ Bootis stars suggests a somewhat similar mechanism—i.e., removal of the refractory elements from the photosphere through grain formation and subsequent mass loss (Bond 1991). Because of the presence of this dust, many of these objects show large infrared excesses, due to the presence of circumstellar dust shells or disks formed during the mass loss.

Figure 5.30 shows three well-known metal-weak post-AGB A-type stars in comparison with the A0 Ib MK standard. The metal-weak nature of these stars is immediately evident. Waelkens et al. (1991) found HR 4049 and HD 52961 to have iron abundances nearly a factor of 10^5 below solar, and HD 44179 (also known as the “Red Rectangle” for the thick, dusty nebula it has ejected) down by a factor of 1000. An important thing to remember about post-AGB stars is that even though

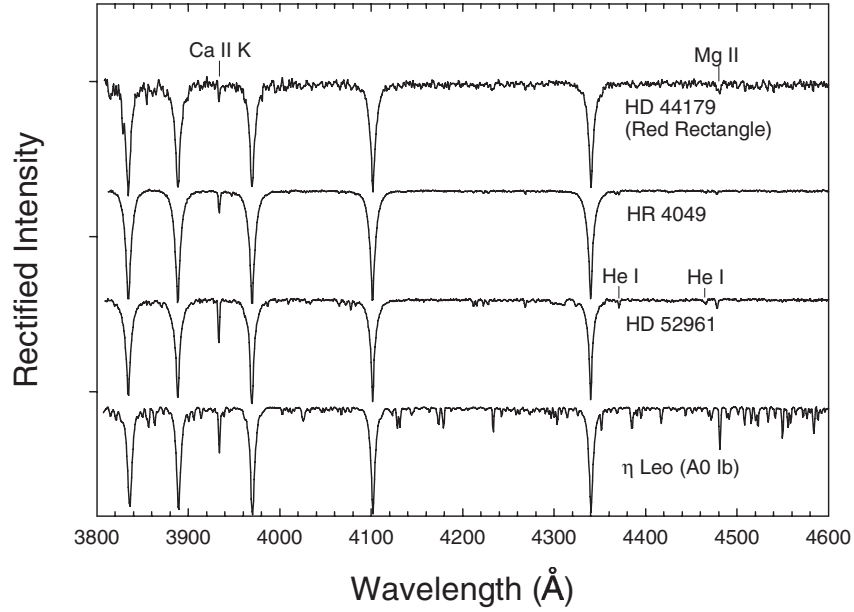


Figure 5.30 Three post-AGB stars compared with the A0 Ib MK standard, η Leo. The spectra from the Dark Sky Observatory, have been vertically shifted by 0.7 continuum units for clarity. HD 44179 is slightly noisier than the other spectra.

their spectra mimic the spectra of massive supergiant stars, at this stage in their evolution their masses are on the order of $1 M_{\odot}$ or less. Their spectral similarity to massive supergiants comes about because of their extended atmospheres. See also the sections on post-AGB stars in Chapters 4, 6, and 7.

5.7 A-TYPE SHELL STARS

Figure 5.31 shows a montage of four well-known A-type shell stars, along with η Leo, the MK A0 Ib standard for comparison. The first three shell stars in this montage have the property of having some spectral features (in particular the wings of the Balmer lines) that are characteristic of late B-, A-, or early F-type subgiants or giants (or even dwarfs), but other spectral features that are reminiscent of A-type supergiants, in particular, strongly enhanced lines of Fe II and Ti II. These Fe II and Ti II lines, referred to as *shell lines*, are the same lines involved in luminosity classification in the A- and F-type stars. The shell stars can also be readily recognized by the strongly enhanced lines of the Fe II multiplet 42 (see panel b of Figure 5.31). The hotter shell stars may also show strong absorption cores in the Balmer lines and quite often a strong Ca II K-line with an unusual profile. A close inspection of the spectra of the first two shell stars in Figure 5.31 shows broad, weak Mg II $\lambda 4481$ lines and broad lines of He I. 14 Com, the early-F shell star, also shows a broad Mg II line. At H α the hotter shell stars can show emission with strong central self-absorption, but the cooler shell stars generally have normal H α profiles.

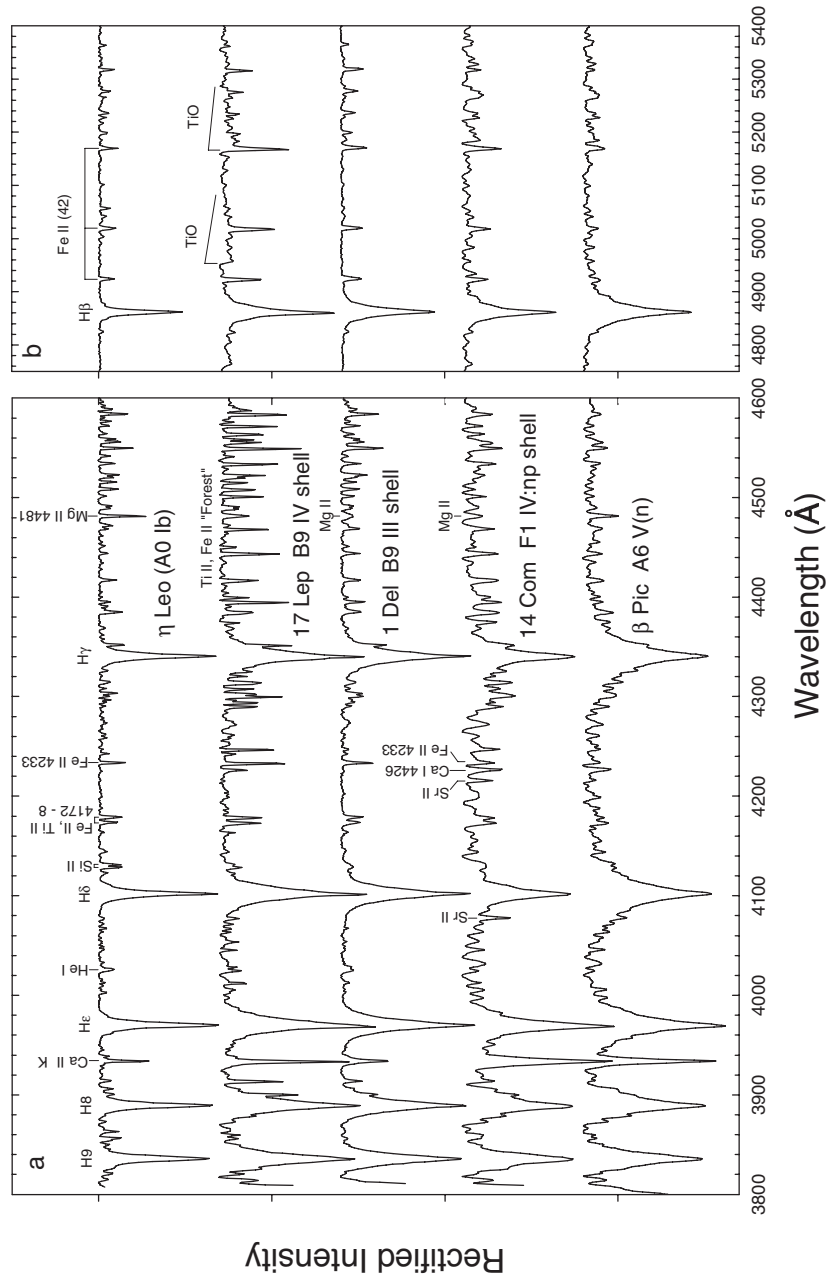


Figure 5.31 A montage of four shell stars with the A0 Ib MK standard, η Leo for comparison. Panel (a) shows the 3800–4600 \AA spectral region at a resolution of 1.8 \AA . Panel (b) shows the 4750–5400 \AA region, including the important Fe II multiplet 42 lines and H β , at a resolution of 3.6 \AA . All spectra were obtained at the Dark Sky Observatory with the exception of the spectra of β Pic, which were derived from the UVES Paranal Observatory Project (<http://www.sc.eso.org/santiago/uvespop/>, Bagnulo et al. 2003) and smoothed to the appropriate resolutions.

As the name implies, the shell features—the enhanced Fe II and Ti II lines and the shell cores in the Balmer lines—arise in a circumstellar shell. In extreme cases the shell features can almost completely overwhelm the spectrum of the underlying star. The main goal of spectral classification, as in the Herbig Ae/Be stars, is to determine the spectral type of the underlying star. This can be done, with greater or lesser success depending upon the strength of the shell features, by considering only photospheric features. In the blue-violet region, these photospheric features include the wings of the Balmer lines, which can usually be matched successfully with an MK standard, and the He I lines (especially $\lambda\lambda 4026$ and 4471). The Mg II $\lambda 4481$ line is unaffected by the shell as it is a high-excitation line (~ 9 eV), but it is not very sensitive to either temperature or luminosity.

The first three shell stars shown in Figure 5.31 have very well-developed shells, but this is not the case for all shell stars. Quite often, the shell nature shows up only in the Fe II (42) lines and Fe II $\lambda 4233$, which are slightly enhanced, with little or no evidence of a shell in the Balmer lines, except possibly at $H\alpha$. The strength of a shell is roughly indicated in spectral classification notation by parentheses: “shell” denotes a strong shell spectrum, “(shell)” a moderate shell spectrum, and “((shell))” a marginally visible shell. Numerical indices could be devised to indicate the strength of a shell spectrum, in analogy to the system devised for the Herbig Ae/Be stars by Gray & Corbally (1998), but this has not been done yet.

Once such an analysis is made it turns out that most of the so-called A-type shell stars are actually late-B (B5 and later), usually rapidly-rotating dwarfs, subgiants, and giants. The rapid rotation of the underlying star can be deduced from the profile of Mg II $\lambda 4481$; see in particular this line in the spectrum of 1 Del, in Figure 5.31, panel a. There *are* A-type shell stars, even early-F shell stars, but their numbers are relatively small.

We term the type of shell star described in the paragraphs above a *classical A-type shell star*. The mechanism producing these shells is still unknown, although it is generally assumed that these stars represent the cool end of the Be/Bshell phenomenon. That this is the case is by no means established; a marked feature of Be stars is their variability, whereas many of the classical A-type shell stars have spectra that have not changed in decades. Some classical A-type stars do, however, show variable spectra. A case in point is 17 Lep, which shows enormous variations in the strength of the shell lines. This star is in a binary system; the companion is an early M-type giant. In the blue-green spectrum of this star (see panel b of Figure 5.31) TiO bands from the M-star are visible (see Welty & Wade 1995).

Useful papers on the classical A-type shell stars include Abt & Moyd (1973); Slettebak (1982, 1983, 1986); Gulliver (1981).

The fourth shell star in Figure 5.31 is the prototype of a group we term the *β Pictoris shell stars*. β Pic is an A6 V star surrounded by a protoplanetary disk that contains gas in addition to dust. Its spectrum shows weak, narrow absorption components in Ca II K and other lines. These absorption components appear and disappear, and often show variable radial velocities. The origin of these components is not entirely clear, but may be connected with the presence of “Falling,

Evaporating, [cometary] Bodies” (FEBs, Ferlet, Vidal-Madjar, & Hobbs 1987). From a spectral classification point of view, most β Pictoris stars look like entirely normal, usually rapidly rotating A-type dwarfs in the blue-violet; only a few show a slightly enhanced Fe II λ 4233 line in classification spectra. High-resolution spectra are required in order to detect the narrow absorption components. Other members of the β Pictoris class show similar variable spectral features and include HD 256, HR 2174, HD 85905, and a number of λ Bootis stars. We presume these members of the class possess protoplanetary disks, but this has not been shown in all cases.

There is very little doubt that these two distinct classes of A-type shell stars exist, although they are often confused in the literature under the heading “A-type shell stars.” There may be other physical mechanisms that can lead to the formation of a circumstellar shell; see, for instance, Abt (2004). Unfortunately, there is no way to distinguish using classification spectra classical A-type shell stars with weak shells from β Pictoris shell stars, and recourse must be made to the infrared to search for evidence of a dusty disk.

Bibliography

- Abt, H.A. 1979, ApJ, 230, 485
Abt, H.A. 2004, ApJ, 603, L109
Abt, H.A., & Hudson, K.I. 1971, ApJ, 163, 333
Abt, H.A., & Morgan, W.W. 1976, ApJ, 205, 446
Abt, H.A., & Moyd, K.I. 1973, ApJ, 182, 809
Ambika, S., Parthasarathy, M., & Aoki, W. 2004, AA, 417, 293
Andrillat, Y., Jaschek, C., & Jaschek, M. 1995, AA, 299, 493
Aufdenberg, J.P. 2006, ApJ, 645, 664
Babcock, H.W. 1947, ApJ, 105, 105
Bagnulo, S., et al. 2003, *Messenger*, 114, 10
Barry, D.C. 1970, ApJS, 19, 281
Barry, D.C. 1971, AJ, 76, 324
Bidelman, W.P. 1962, ApJ, 135, 651
Bohlender, D.A., Gonzalez, J.-F., & Kennelly, E.J. 1996, AA, 307, L9
Bohlender, D.A., & Walker, G.A.H. 1994, MNRAS, 266, 891
Bond, H.E. 1991, in *IAU Symposium 145*, p. 341
Borra, E.F., & Landstreet, J.D. 1978, ApJ, 222, 226
Cannon, A.J. 1912a, *Harvard Ann.* 56, 65
Cannon, A.J. 1912b, *Harvard Ann.* 56, 115
Cannon, A.J., & Pickering, E.C. 1901, *Harvard Obs. Ann.* 28 (part II), 131
Castelli, F., & Kurucz, R.L. 2003, in *Modelling of Stellar Atmospheres, Poster Contributions*, Proceedings of IAU Symposium 210, eds. N. Piskunov, W.W. Weiss, & D.F. Gray (San Francisco: Astronomical Society of the Pacific), p. A20.
Charbonneau, P. 1993, in *Peculiar versus Normal Phenomena in A-type and Related Stars*, eds. M.M. Dworetsky, F. Castelli, & R. Farragiana, ASP Conference Series, Vol. 44, p. 474
Cheng, K.-P., Bruhweiler, F.C., Kondo, Y., & Grady, C.A. 1992, ApJ, 396, L83
Cohen, M., & Kuhi, L.V. 1979, ApJS, 41, 743
Collins, G.W., II, & Smith, R.C. 1985, MNRAS, 213, 519
Collins, G.W., II, & Sonneborn, G.H. 1977, ApJS, 34, 41
Corbally, C.J., & Gray, R.O. 1996, AJ, 112, 2286
Cowan, R.D. 1981, *The Theory of Atomic Structure and Spectra* (Berkeley: University of California Press)
Cowley, C.R., Bidelman, W.P., Hubrig, S., Mathys, G., & Bord, D.J. 2004, AA, 419, 1087

- Cowley, C.R., & Bord, D.J. 2004, in *The A-Star Puzzle*, IAU Symposium # 224, eds. J. Zverko, J. Žižňovský, S.J. Adelman, & W.W. Weiss (Cambridge: Cambridge University Press), p. 265
- Cowley, C.R., Hubrig, S., Ryabchikova, T.A., et al. 2001, AA, 367, 939
- Cowley, C.R., & Mathys, G. 1998, AA, 339, 165
- Cowley, C.R., Ryabchikova, T.A., Kupka, F., Bord, D.J., Mathys, G., & Bidelman, W.P. 2000, MNRAS, 317, 299
- Danks, A.C., & Dennefeld, M. 1994, PASP, 106, 382
- Drilling, J.S., Moehler, S., Jeffrey, C.S., Heber, U., & Napiwotski, R. 2003, in *The Garrison Festschrift*, eds. R.O. Gray, C.J. Corbally, & A.G.D. Philip (Schenectady: L. Davis Press), p. 27
- Fabricant, D., Cheimets, P., Caldwell, N., & Geary, J. 1998, PASP, 110, 79
- Faraggiana, R., Gerbaldi, M., & Boehm, C. 1990, AA, 235, 311
- Ferlet, R., Vidal-Madjar, A., & Hobbs, L. M. 1987, AA, 185, 267
- Finkenzeller, U., & Mundt, R. 1984, AA, 55, 109
- Frémat, Y., Houziaux, L., & Andriolat, Y. 1996, MNRAS, 279, 25
- Garrison, R.F. 1967, ApJ, 147, 1003
- Garrison, R.F., & Gray, R.O. 1994, AJ, 107, 1556
- Gray, R.O. 1985, JRASC, 79, 237
- Gray, R.O. 1988, JRASC, 82, 336
- Gray, R.O. 1989, AJ, 98, 1049
- Gray, R.O. 1997, in *The Third Conference on Faint Blue Stars*, eds. A.G.D. Philip, J. Liebert, R. Saffer, & D.S. Hayes (Schenectady: L. Davis Press)
- Gray, R.O., & Corbally, C.J. 1998, AJ, 116, 2530
- Gray, R.O., & Corbally, C.J. 2002, AJ, 124, 989
- Gray, R.O., & Garrison, R.F. 1987, ApJS, 65, 581
- Gray, R.O., & Garrison, R.F. 1989, ApJS, 69, 301
- Gray, R.O., & Garrison, R.F. 1989, ApJS, 70, 623
- Gray, R.O., Graham, P.W., & Hoyt, S.R. 2001, AJ, 121, 2159
- Gray, R.O., & Kaye, A.B. 1999, AJ, 118, 2993
- Griffin, R.E. 2002, AJ, 123, 988
- Gulliver, A.F. 1981, ApJ, 248, 222
- Gulliver, A.F., Adelman, S.J., Cowley, C.R., & Fletcher, J.M. 1991, ApJ, 623, 460
- Hanbury Brown, R., Davis, J., Allen, L.R., & Rome, J.M. 1967, MNRAS, 137, 393
- Heck, A., Egret, D., Jaschek, M., & Jaschek, C. 1984, *IUE Low Dispersion Spectra Reference Atlas*, ESA SP-1052
- Herbig, G.H. 1960, ApJS, 4, 337
- Hernández, J., Calvet, N., Briceño, C., Hartmann, L., & Berlind, P. 2004, AJ, 127, 1682
- Hillenbrand, L.A. 1995, Ph.D. thesis, Univ. Massachusetts
- Holweger, H., Koester, D., & Allard, N.F. 1994, AA, 290, L21
- Holweger, H., & Rentzsch-Holm, I. 1995, AA, 303, 819
- Holweger, H., & Stürenburg 1991, AA, 252, 255

- Jaschek, C., & Jaschek, M. 1990, *The Classification of Stars* (Cambridge: Cambridge University Press)
- Jaschek, M., & Jaschek, C. 1958, *Z. Astrophys.*, 45, 35
- Jasniewicz, G., de Laverny, P., Parthasarathy, M., et al. 2004, *AA*, 423, 353
- Kamp, I., & Paunzen, E. 2002, *MNRAS*, 335, 45
- Lamers, H.J.G.L.M., & Snijders, M.A.J. 1975, *AA*, 41, 259
- Landstreet, J.D. 2004, in *The A-Star Puzzle*, IAU Symposium # 224, eds. J. Zverko, J. Žižňovský, S.J. Adelman, & W.W. Weiss (Cambridge: Cambridge University Press), p. 423
- Malfait, K., Bogaert, E., & Waelkens, C. 1998, *AA*, 331, 211
- Marnese, P.M., Boschi, F., & Munari, U. 2003, *AA*, 406, 995
- Maury, A.C., & Pickering, E.C. 1897, *Harvard Obs. Ann.* 28 (Part I), 1
- Meyer, M.R., Edwards, S., Hinkle, K.H., & Strom, S.E. 1998, *ApJ*, 508, 397
- Michaud, G. Richer, J., & Richard, O. 2005, *ApJ*, 623, 442
- Mihalas, D. 1978, *Stellar Atmospheres*, 2nd edition (New York: W.H. Freeman)
- Mora, A. et al. 2001, *AA*, 378, 116
- Morgan, W.W. 1933, *ApJ*, 77, 330
- Morgan, W.W., Abt, H.A., & Tapscott, J.W. 1978, *Revised MK Atlas for Stars Earlier than the Sun* (Chicago and Tucson: Yerkes Observatory, University of Chicago, and Kitt Peak National Observatory)
- Morgan, W.W., Keenan, P.C., & Kellman, E. 1943, *An Atlas of Stellar Spectra* (Chicago: University of Chicago Press)
- Moultaka, J., et al. 2004, *PASP*, 821, 693
- Munari, U., & Tomasella, L. 1999, *AApS*, 137, 521
- Nielsen, K., & Wahlgren, G.M. 2000, *AA*, 356, 146
- Osawa, K. 1965, *Ann. Tokyo Astron. Obs.*, Ser. 2, 9, 123
- Paunzen, E. 2001, *AA*, 373, 633
- Paunzen, E. 2004, in *The A-star Puzzle*, eds. J. Zverko, J. Ziznovsky, S.J. Adelman, & W.W. Weiss, IAU Symposium No. 224 (Cambridge, UK: Cambridge University Press), pp. 443–450
- Paunzen, E., Kamp, I., Weiss, W.W., & Wiesemeyer, H. 2003, *AA*, 404, 579
- Peterson, D.M., et al. 2006, *Nature*, 440, 896
- Petrie, R.M. 1964, *Publications of the Dominion Astrophysical Observatory Victoria*, 12, 317
- Przybylski, A. 1961, *Nature*, 189, 739
- Pyper, D.M. 1969, *ApJS*, 18, 347
- Reipurth, B., Pedrosa, A., & Lago, M.T.V.T. 1996, *AApS*, 120, 229
- Rey, S.C., Yoon, S.J., Lee, Y.W., Chaboyer, B., & Sarajedini, A. 2001, *AJ*, 122, 3219
- Sadakane, K., & Nishida, M. 1996, *PASP*, 98, 685
- Slettebak, A. 1982, *ApJS*, 50, 55
- Slettebak, A. 1983, *ApJS*, 53, 869
- Slettebak, A. 1986, *PASP*, 98, 867
- Slettebak, A., Bahner, K., & Stock, J. 1961, *ApJ*, 134, 195

- Slettebak, A., Kuzma, T.J., & Collins, G.W., II 1980, *ApJ*, 242, 171
Thompson, I.B., Brown, D.N., & Landstreet, J.D. 1987, *ApJS*, 64, 219
Titus, J., & Morgan, W.W. 1940, *ApJ*, 92, 256
Torres-Dodgen, A.V. 1994, in *The MK Process at 50 Years*, ASP Conference Series # 60, eds. C.J. Corbally, R.O. Gray, & R.F. Garrison (Tucson: Publications of the Astronomical Society of the Pacific), p. 253
Turcotte, S. 2002, *ApJ*, 573, 129
Turcotte, S., & Charbonneau, P. 1993, *ApJ*, 413, 376
Vauclair, S., Hardorp, J., & Peterson, D.M. 1979, *ApJ*, 227, 526
Venn, K.A., & Lambert, D.L. 1990, *ApJ*, 363, 234
Waelkens, C., Van Winckel, H., Bogaert, E., et al. 1991, *AA*, 251, 495
Wallace, L., & Hinkle, K. 1997, *ApJS*, 111, 445
Wallace, L., & Hinkle, K. 2002, *ApJ*, 124, 3393
Wallace, L., Meyer, M.R., Hinkle, K., & Edwards, S. 2000, *ApJ*, 535, 325
Waters, L.B.F.M., & Waelkens, C. 1998, *Ann. Rev. Astron. Astrophys.* 36, 233
Welty, A.D., & Wade, R.A. 1995, *AJ*, 109, 326

Chapter Six

The F-type Stars

6.1 INTRODUCTION

The F-type stars span a temperature range in which important physical changes occur in the stellar atmosphere. For instance, the A-type stars have largely radiative atmospheres with only superficial convection zones. In the F-type stars, these superficial convection zones expand and deepen so that by the late F/early G-type stars the stellar atmosphere has become almost entirely convective. This has important consequences for the emergent spectrum: because convection thoroughly mixes the stellar atmosphere and the underlying convective envelope, surface chemical peculiarities, which are so prevalent in the A-type stars, essentially cease to exist for main-sequence stars later than F5. Chemically peculiar stars reappear only in the late-type giants, where the abundance anomalies come about through either the convective dredge-up of nuclear-processed material or mass transfer from an evolved companion. The onset of convection must also lead to the near ubiquity of magnetic fields in the late F-type stars (although these magnetic fields are difficult to detect, it is believed that the stellar dynamo is driven by differential rotation in the convection zone); angular momentum can thus be transported away by stellar winds, and so stellar rotational velocities plummet in the F-type stars. At the effective temperatures encountered in the F-type stars, certain rugged diatomic molecules can form and persist in the stellar atmosphere, leading to the appearance of molecular bands, most notably the G-band due to CH. Finally, the F-type stars are at the main-sequence turn-off of the Thick Disk and the Halo populations, and so Population II main-sequence stars, absent at earlier types, are first seen in the F-type stars.

6.2 OPTICAL CLASSIFICATION

6.2.1 Temperature Criteria

Figure 6.1 shows a temperature sequence of main-sequence F-type stars with the most important temperature criteria indicated. The prime temperature criteria are the strength and the profiles of the hydrogen lines, as they are least affected by differences in metallicity. Using good quality digital spectra, the temperature type of an F-type star may be determined with a precision of better than one subtype using only the hydrogen lines. One may then proceed to examine temperature criteria based on metal lines. In solar-abundance stars these criteria should yield a temperature type consistent with the hydrogen lines, but in metal-weak stars they may

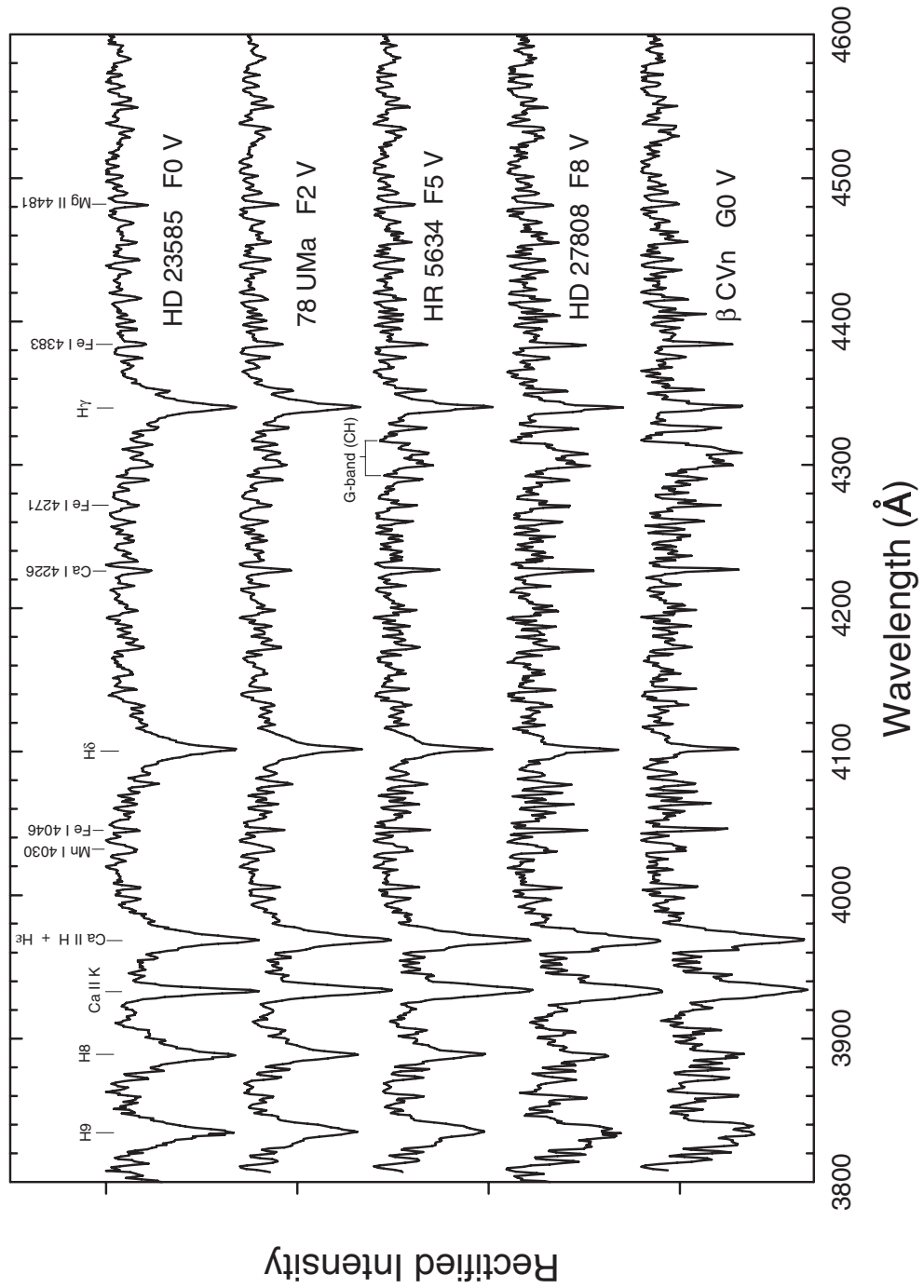


Figure 6.1 A temperature sequence for main-sequence F-type stars. Features useful in the temperature classification of F-type stars are marked. These spectra have been offset vertically by 0.7 continuum units. Unless otherwise stated, all spectra illustrated in this chapter were obtained at the Dark Sky Observatory.

not. We will deal with this situation in §6.4. In Figure 6.1 it can be seen that the strength of the Ca II K-line essentially plateaus in the F-type stars, and is not a useful temperature criterion later than about F3. However, the general metallic-line spectrum continues to strengthen, and low-excitation lines such as Fe I $\lambda\lambda 4046$ and 4383 and the Ca I resonance line $\lambda 4226$ grow rapidly with declining temperature. Note that Ca I $\lambda 4226$ becomes the most prominent line between H δ and H γ . Starting at about F5 on the main sequence, one can use the ratios Fe I $\lambda 4046$ /H δ , Ca I $\lambda 4226$ /(H δ , H γ), and Fe I $\lambda 4383$ /H γ as sensitive indicators of the temperature type. But since these involve a ratio of metallic-line strengths to hydrogen-line strengths, they can give the wrong answer in metal-weak (or metal-rich) stars (see §6.4).

At about F3 or F4, somewhat depending on spectral resolution, the G-band due to the CH diatomic molecule first makes its appearance. This feature grows rapidly with declining temperature, making it a very important temperature criterion in the late F-type stars. Again, this feature is metallicity-dependent and so appears generally weaker in metal-weak stars. There are some rather rare late-F-, early G-type dwarfs with enhanced abundances of *s*-process elements (such as strontium and barium), and in these stars the G-band may be slightly weak or strong (see §6.5.2).

The spectral classifier should be alert to the existence of late Am stars (see §5.4.1). Am stars with hydrogen-line types as late as F2 are common; some rare Am-like stars, known as the ρ Puppis stars (see §6.5.1) persist until about F5. In addition, the latest Ap stars have temperature types of about F2. The classifier should also be alert to the presence of rapid rotation and the problems this can pose for spectral classification (see §5.2.3). As stated above, rotational velocities decline rapidly later than F2, and so a rapidly rotating late F-type star is very rare indeed.

6.2.2 Luminosity Criteria

Figures 6.2 and 6.3 show luminosity sequences at F0 and F8, respectively. The primary luminosity criteria change over the range of effective temperatures represented by the F-type stars. In the early F-type stars (earlier than F6), the primary luminosity criteria are lines of ionized iron and titanium, specifically the blends at $\lambda\lambda 4172-8$, $\lambda\lambda 4395-4400$, $\lambda 4417$, $\lambda 4444$, and indeed the entire Ti II, Fe II “forest” near 4500 \AA . These blends should be used in ratio with lines that do not show a strong luminosity sensitivity, such as Fe I $\lambda 4046$, $\lambda 4271$, and $\lambda 4383$, and Ca I $\lambda 4226$. These blends of Fe II and Ti II reach their maximum sensitivity to luminosity between F0 and F2 (see §5.2.4 for an explanation why), but, with declining temperature, lines of ionized iron and titanium weaken, so these blends cease to be very useful in separating dwarfs from giants later than about F8. However, they continue to be useful in discriminating between the supergiant classes well into the G-type stars.

At F0–F2, lines of Sr II ($\lambda\lambda 4077, 4216$) are marginally useful in luminosity classification, but by F6 and later, continuing well into the K-type stars, the strength

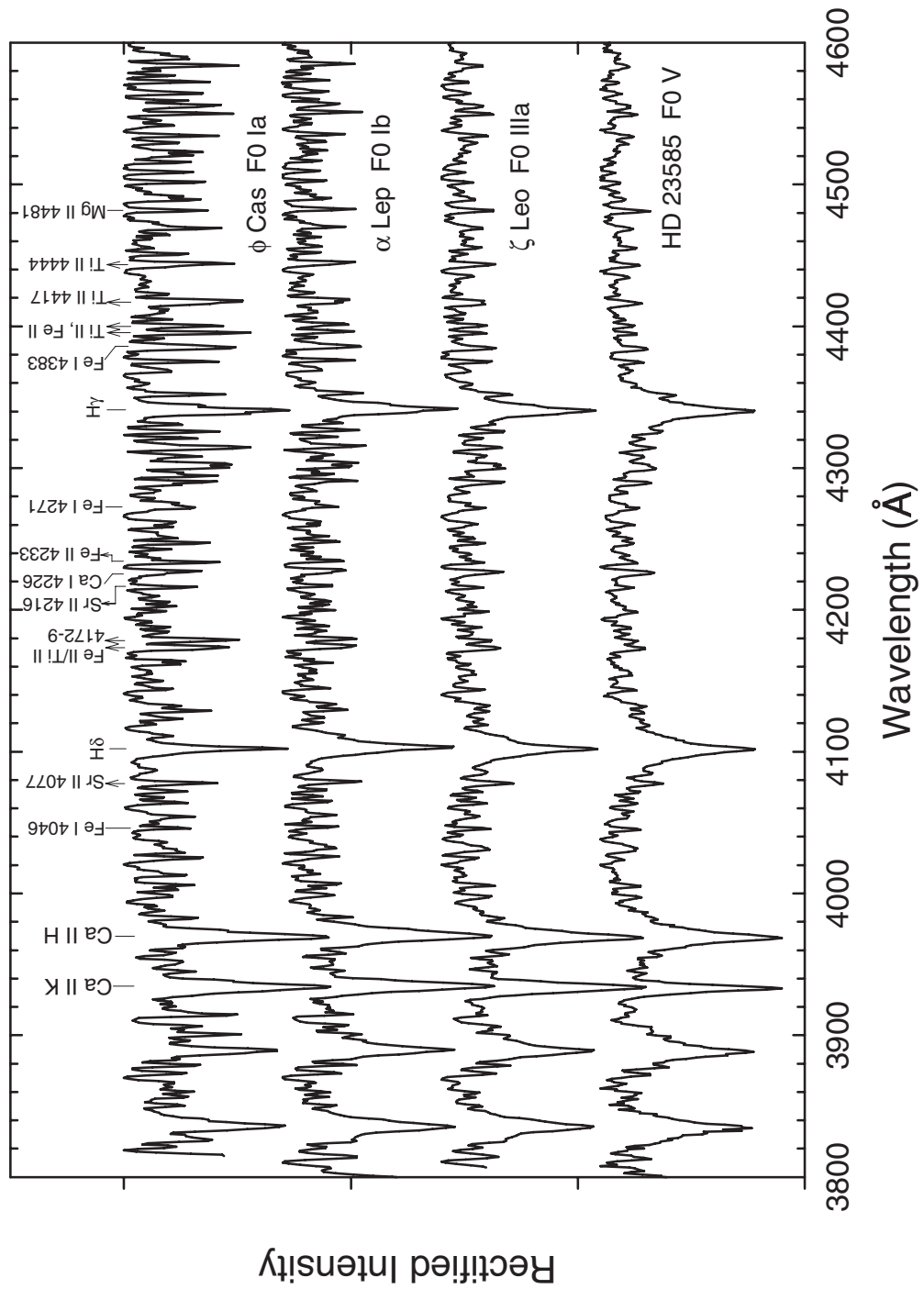


Figure 6.2 Luminosity effects at F0. Spectral features marked with upward arrows show a positive luminosity effect. Spectral features marked with a line are relatively insensitive to luminosity. Note that the hydrogen lines show only a weak negative luminosity effect. These spectra have been vertically offset by 0.7 continuum units.

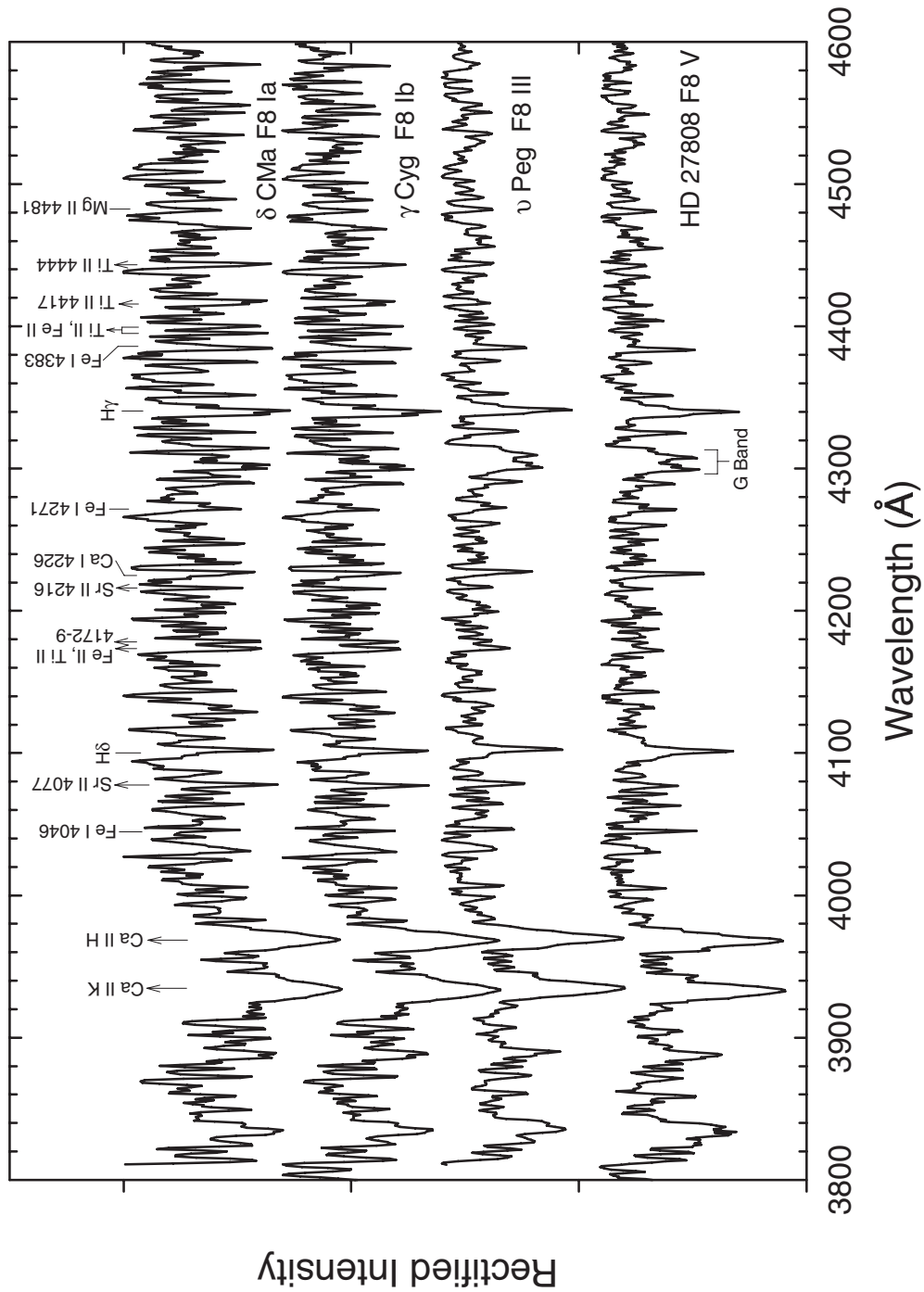


Figure 6.3 Luminosity effects at F8. Spectral features marked with upward arrows show a positive luminosity effect. Spectral features marked with a line are relatively insensitive to luminosity. Notice the change in the morphology of the G band (marked below the F8 V spectrum) with luminosity. These spectra have been vertically offset by 0.7 continuum units.

of these lines in ratio with surrounding Fe I lines (see especially the ratio Sr II $\lambda 4077$ /Fe I $\lambda 4046$, or even $\lambda 4077$ /H δ) constitutes a prime luminosity criterion.

Note that in the F8 stars (see Figure 6.3) the Ca II K & H lines show a mild positive luminosity effect. This broadening of the Ca II K & H lines with increasing luminosity is more pronounced in the G-type stars. Note as well from Figures 6.2 and 6.3 that (1) the hydrogen lines are mildly sensitive to luminosity at F0, but not at all at F8 and (2) the G-band changes morphology with luminosity class.

6.2.3 The Physical Basis of Luminosity Classification

In §5.2.4 we explained that the luminosity sensitivity of lines of ionized species is primarily due to the role of the electron density in the ionization equilibrium. However, in the case of the Fe II and Ti II lines used for luminosity classification in the blue-violet, there is another factor that is very important—the fact that these lines arise from *metastable levels*. In this context, the lower levels of these lines are called metastable because radiative transitions between these levels and lower energy levels including the ground state of the ion are forbidden—they disobey a quantum selection rule (see §2.4.3). Thus if an electron is excited to one of these states, it can decay to the ground state only through a collision. In F-type dwarfs and giants collisions are sufficiently frequent to keep the population of these levels near the equilibrium values predicted by the Boltzmann equation (see Equation 2.4.2), but in the low density atmospheres of supergiants, especially Ia supergiants, collisions are rare, and the populations of these states tend to exceed the Boltzmann predictions. The overpopulation of these states is a fundamental reason for the explosive growth of these lines between the giant and supergiant classes throughout the A- and F-type stars, and also helps to explain why these lines continue to be useful luminosity discriminants for the supergiants well into the G-type stars. It should be noted that the Sr II lines used in luminosity classification ($\lambda 4077$ and $\lambda 4216$) are *resonance lines* and thus arise from the ground state and not metastable levels. For these lines, the role of electron density in the ionization equilibrium is the main physical mechanism behind their luminosity sensitivity.

It is interesting that there is yet another factor that seems to be important in the behavior of the luminosity criteria in the F-, G-, and even K-type stars. It appears that the *microturbulent velocity* plays an important role. Microturbulence refers to a scale of turbulence in the stellar atmosphere in which the turbulent cells are smaller than the *mean free path* of the photon (see §2.4.1 for a discussion of the mean free path). This is important, because if a photon originates in one microturbulent cell, it is probable that it will be absorbed in another microturbulent cell moving relative to the first. The resulting Doppler shift between emission and absorption means that a photon emitted in the spectral line core will be absorbed in the line wing. This has the effect of desaturating the line core and causing the resulting spectral line to be broader and stronger.

Experiments with *spectral synthesis* revealed as early as the 1970s (Bolton 1971) that sequences of synthetic spectra computed with different gravities but the

same microturbulent velocity did not exhibit the correct behavior of the luminosity criteria. Only when the microturbulent velocity was allowed to increase with decreasing gravity (increasing luminosity) did the luminosity criteria based on lines of ionized metals behave in a realistic fashion. Gray, Graham, & Hoyt (2001) carried out a detailed study of this effect in the F- and early G-type stars, and found, using the technique of partial correlation, that “*the microturbulent velocity is as important as, or even more important than, the gravity in the determination of the MK luminosity class.*” They found, for instance, that in the mid F-type stars, a microturbulent velocity of about 2 km/s for the dwarfs and 5–6 km/s for the Ib supergiants led to a realistic behavior of the luminosity criteria. This study points out that unless there is a tight one-to-one relationship between gravity and microturbulent velocity, the fact that the MK luminosity class in the F-, G-, and even K-type stars is partially determined by the microturbulent velocity will lead to “cosmic scatter” in the relationships between the luminosity class and gravity and the luminosity class and absolute magnitude.

What this means, of course, is that astronomers must use the technique of *spectroscopic parallax* with care, as the distances it yields (based on the assumption that each spectral type corresponds to a single value of the absolute magnitude) will be correct only on a statistical basis. This is exactly what Jaschek & Gómez (1998) found when they compared MK luminosity types with absolute magnitudes based on *Hipparcos* (ESA 1997) parallaxes. Does this mean that we should modify the MK spectral classification system so that, say, microturbulent velocity corrections can be made to the luminosity classes? The answer is no, as this would require incorporation of theory into an essentially empirical system, and we would find that each time the theory is changed, the classification system would need to be modified. For instance, our concept of microturbulence may change. Indeed, Asplund and co-workers (Asplund 2000; Asplund et al. 2000a, b) have carried out realistic *ab initio* 3-D hydrodynamical simulations of convection in the solar atmosphere that can, without the use of even the concept of microturbulence, fully account for the observed profiles and strengths of metal lines in the solar spectrum. It turns out that the role of microturbulence is actually played by velocity gradients in the solar granulation convective motions, which serve to desaturate the spectral line cores. Rather, the lesson is that the true power of the MK system lies in its ability to yield astrophysical insights when it is confronted with external data. When we find that an MK type is in conflict with external data, it does not necessarily mean that the MK type is “wrong”; more likely, there is “important information in the interface” (Garrison 2001) that we should exploit to deepen our understanding of stellar physics.

6.3 CLASSIFICATION IN THE ULTRAVIOLET AND INFRARED

6.3.1 The Ultraviolet

No formal effort has been made to set up a classification system for the F- and G-type stars in the IUE ultraviolet, except for some initial efforts by Heck et al.

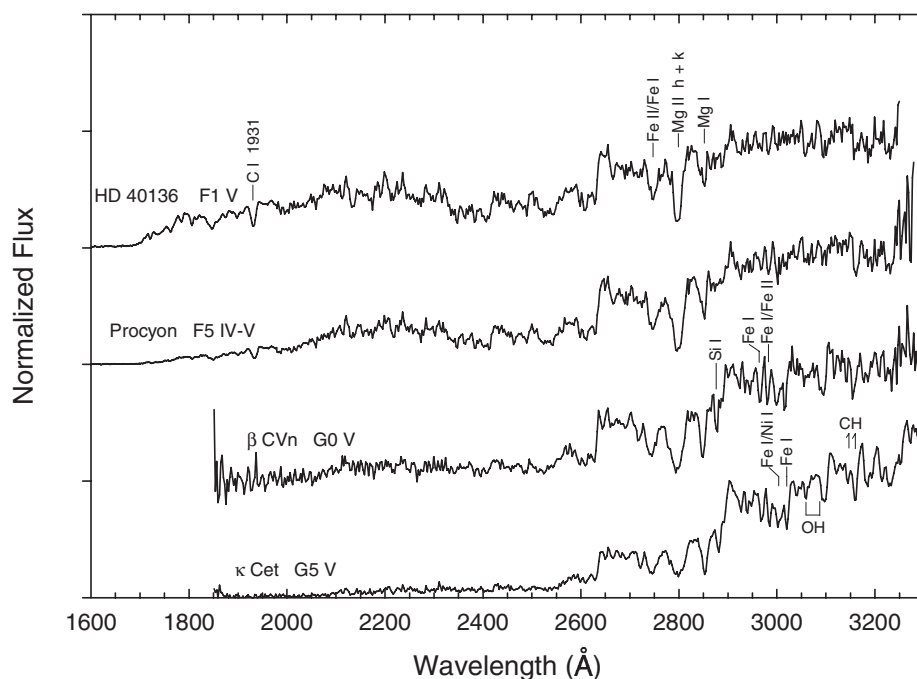


Figure 6.4 A temperature sequence in the IUE ultraviolet for F- and early G-type stars. The features that are identified with one or two species are actually blends of hundreds of lines. The species indicated are simply the dominant contributors to the blend. All spectra have been normalized at a common point (2903 Å) and offset vertically by one unit. Spectra are from the low-resolution MAST IUE archive (<http://archive.stsci.edu/iue/>).

(1984). One of the major barriers to setting up a system is lack of spectral material, as the vast majority of IUE spectra are of O- and B-type stars and other hot objects, such as Wolf-Rayet stars. Consequently, we will be content with making only preliminary comments regarding spectral classification in the ultraviolet for F- and G-type stars until more spectral material becomes available. Figure 6.4 shows a sequence of F- and G-type dwarfs in the IUE ultraviolet. As in the A-type stars (§5.3.1), there are four basic points upon which a classification system could be based. These are:

1. The overall shape of the spectral energy distribution (SED) in the ultraviolet, including the wavelength at which the flux goes to essentially zero. It should be noted, however, that the SED will be strongly dependent on the metallicity, as most of the continuous and line opacity in the shortwave UV in F- and G-type stars is due to metals.
2. The Mg II h & k lines continue to increase in strength and width into the G-type stars. Note the change in the spectral morphology of this region; in the early F-type stars, the region is dominated by three strong features: a blend due to Fe II and Fe I at $\lambda 2745$, the blended Mg II h & k lines, and the Mg I line at $\lambda 2852$. In the late F-type stars, a strong Si I line appears

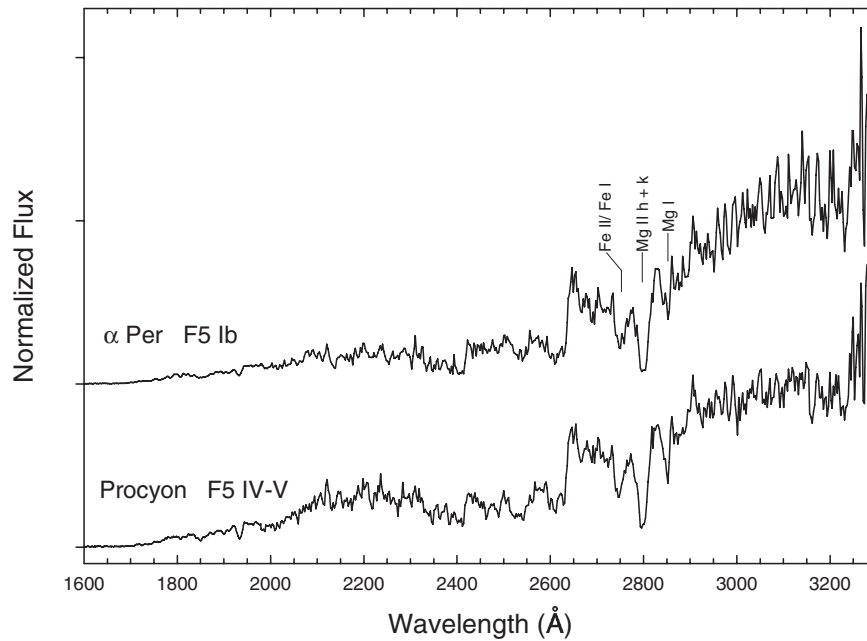


Figure 6.5 A luminosity sequence in the IUE ultraviolet at F5. The spectra of these two stars are surprisingly similar. These spectra have been normalized at a common point (2903 \AA) and offset vertically by one unit. Spectra from the MAST IUE archive.

at $\lambda 2881$, and a relatively weak, but broad feature develops shortwards of the Fe II, Fe I $\lambda 2745$ blend, leading to a quintuplet of strong, broad features dominating this spectral region.

3. In the late F-type stars, four strong features, dominated by Fe I, Fe II, and Ni I, develop near $\lambda 2990$.
4. In the G-type stars, molecular features, primarily due to CH and OH, develop at $\lambda 3066$ (OH) and $\lambda 3092$ (only the short wavelength wing of this broad feature is due to OH) and $\lambda \lambda 3145$ and 3160 (CH).

Thus, it appears there are sufficient criteria in the low-resolution IUE spectra to carry out temperature classification in the F- and G-type stars in the ultraviolet. Figure 6.5 shows, however, that luminosity classification in the F-type stars will be very difficult at this resolution. It is interesting that even the Fe II-dominated feature at $\lambda 2745$ appears to show only a slight positive luminosity sensitivity. It may be that higher resolution ultraviolet spectra would yield better luminosity criteria.

6.3.2 The Infrared

THE NEAR INFRARED

As we noted in Chapter 5 on the A-type stars, the near-infrared (NIR), essentially the region from $H\alpha$ to $1.0 \mu\text{m}$, holds considerable promise for spectral classification. This region includes the $H\alpha$ line, the O I $\lambda 7774$ triplet, the higher

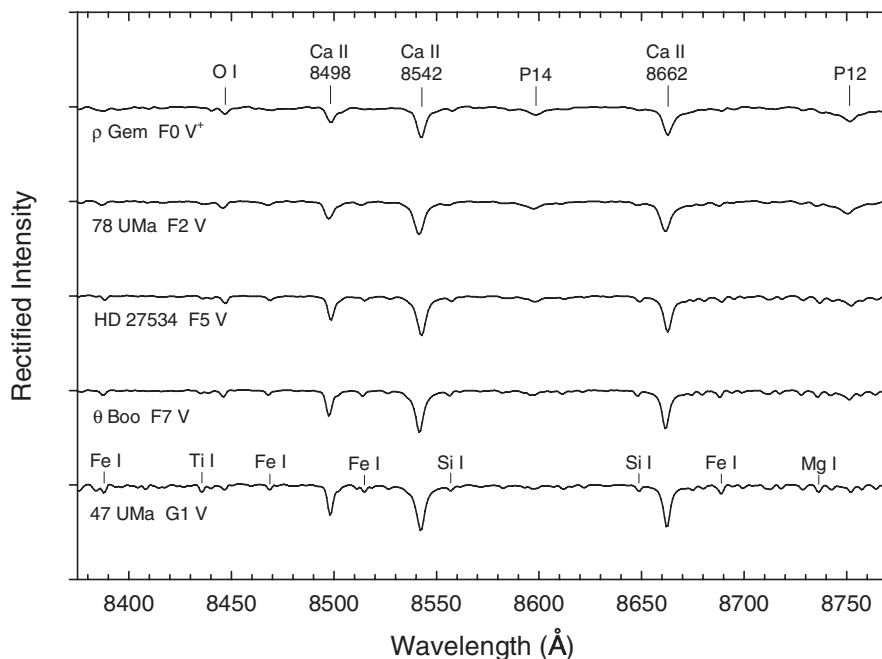


Figure 6.6 A temperature sequence in the near-infrared for F-type main-sequence stars. These spectra have been vertically offset by one continuum unit. Spectra from Andriillat, Jaschek, & Jaschek (1995).

Paschen-series hydrogen lines, and the Ca II ($\lambda\lambda 8498$ – 8662) triplet. Unfortunately, this region is also subject to some quite strong telluric (atmospheric) absorption.

A spectral region of considerable interest within the NIR is the region of the higher Paschen lines, in particular the 8375 – 8770 Å region, explored spectroscopically by Andriillat, Jaschek, & Jaschek (1995) at a resolution of 2.4 Å (1.2 Å/pixel) and later, at higher resolution (0.4 Å), by Munari & Tomasella (1999) and Marnese, Boschi, & Munari (2003). This region is of interest for ground-based work because it is essentially telluric-free, and also contains a rich combination of astrophysically important lines, such as the higher Paschen lines, the Ca II triplet, and the O I $\lambda 8446$ triplet, which mirrors the behavior of the better known O I $\lambda\lambda 7772$ – 7775 triplet. This region has also been selected for the spectroscopy that will be carried out by *Gaia*, the European Space Agency astrometric and radial velocity satellite. However, as we noted in Chapter 5, this region is not suitable for spectral classification earlier than A0, and it turns out that the temperature discrimination offered by this region is only a fraction of that available in the blue-violet for stars earlier than G0. Figure 6.6 points this out very clearly. In the F-type main-sequence stars, the dominant spectral features in this region are the lines of the Ca II triplet; the higher Paschen lines can be seen as only shallow depressions that fade from view by F5. In the early F-type stars, the ratio Ca II/Paschen allows some temperature discrimination, but in the late F-type stars, the spectrum

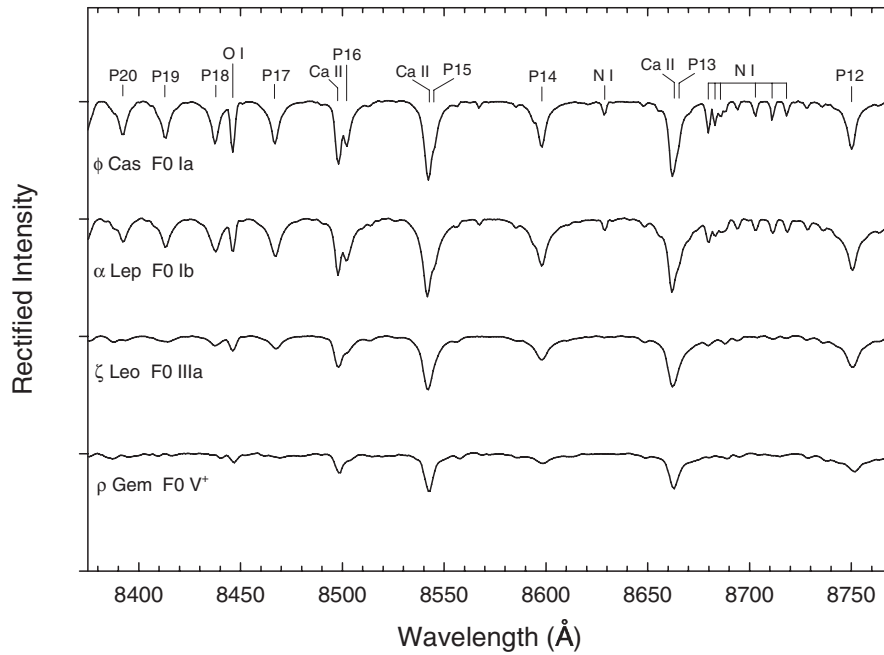


Figure 6.7 A luminosity sequence at F0 in the near-infrared. These spectra have been vertically offset by one continuum unit. Spectra from Andrillat, Jaschek, & Jaschek (1995).

changes in only rather subtle ways with temperature. By G0, some metallic lines are beginning to develop that as we shall see in Chapter 7 will allow reasonably good temperature discrimination in the G- and K-type stars.

Rather surprisingly, luminosity effects in the F-type stars in the higher Paschen region are much more dramatic than the temperature effects. Figure 6.7 shows a luminosity sequence at F0 and Figure 6.8 a luminosity sequence near F6. At F0, both the Ca II triplet and the Paschen lines of hydrogen show a *positive* luminosity effect. The O I $\lambda 8446$ triplet and lines of N I also show dramatic positive luminosity effects. While the N I lines provide discrimination only between the supergiant classes, the O I triplet is useable over the entire range of luminosities. The rather surprising positive luminosity effect of the Paschen lines recalls their curious behavior in the A-type stars (§5.3.2); again the physical cause of this behavior is related to the strong overlap between the wings of the higher Paschen lines, which produces a particularly strong pseudo-continuous opacity in the dwarfs. But we are also seeing the effect of the fact that the hydrogen maximum occurs for the supergiants at a spectral type of about F0 (see §2.4.2).

At F6, the positive luminosity effect of the Paschen lines is much reduced. The Ca II triplet still shows a pronounced positive luminosity effect, although note that it offers little discrimination between the dwarf and giant classes. The same may be said for the O I $\lambda 8446$ triplet. Indeed, the only usable luminosity discriminant between luminosity classes V and III appears to be the slight positive luminosity

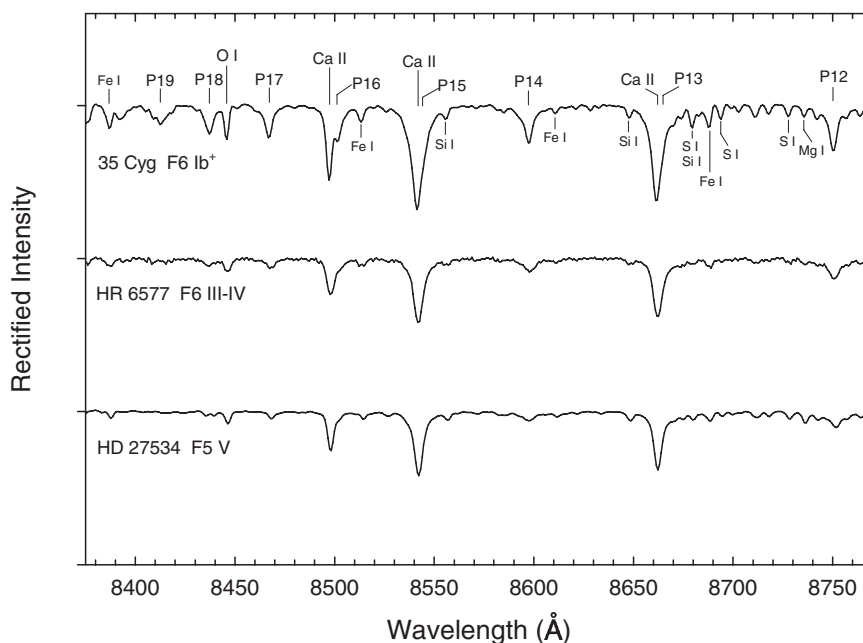


Figure 6.8 A luminosity sequence near F6 in the near-infrared. Note the interesting luminosity sensitivity of the Si I and S I lines in the supergiant. These spectra have been vertically offset by one continuum unit. Spectra from Andriillat, Jaschek, & Jaschek (1995).

effect of the Paschen lines. This lack of luminosity sensitivity coupled with a similar lack of temperature discrimination in the late F-type stars leads to a classification “dead zone” stretching from about F5 to G0 along the temperature dimension, and dwarf to giant along the luminosity dimension within which the spectra are nearly indistinguishable. A further exploration of this “dead zone” may be found in Gray (2006).

J, H, AND K BANDS

Figures 6.9, 6.10, and 6.11 show temperature and luminosity sequences for F-type stars in the infrared J-band ($1.05\text{--}1.34\ \mu\text{m}$), H-band ($1.55\text{--}1.75\ \mu\text{m}$), and K-band ($2.0\text{--}2.4\ \mu\text{m}$) respectively.

In the F-type stars, the J-band (see Wallace et al. 2000) is dominated by the Paschen β and γ lines, which decrease in strength with declining temperature. The metallic-line spectrum in the J-band mimics the optical and increases in strength toward later types. Note, however, that the C I multiplet (1.0682 and $1.0691\ \mu\text{m}$, with excitation energy $\sim 7.5\ \text{eV}$) weakens with decreasing temperature. The ratio C I/Si I (using the Si I lines at 1.0827 and $1.0869\ \mu\text{m}$) should allow precise temperature classification, as well as having the virtue of being, at least to first order, independent of metallicity. In solar metallicity stars, Si I/ $P\gamma$ should also be a useful temperature criterion. Similar ratios can be made with the Mg I line ($1.1828\ \mu\text{m}$) with $P\gamma$ or $P\beta$ and the Si I blends at 1.2032 and $1.2105\ \mu\text{m}$ with $P\beta$.

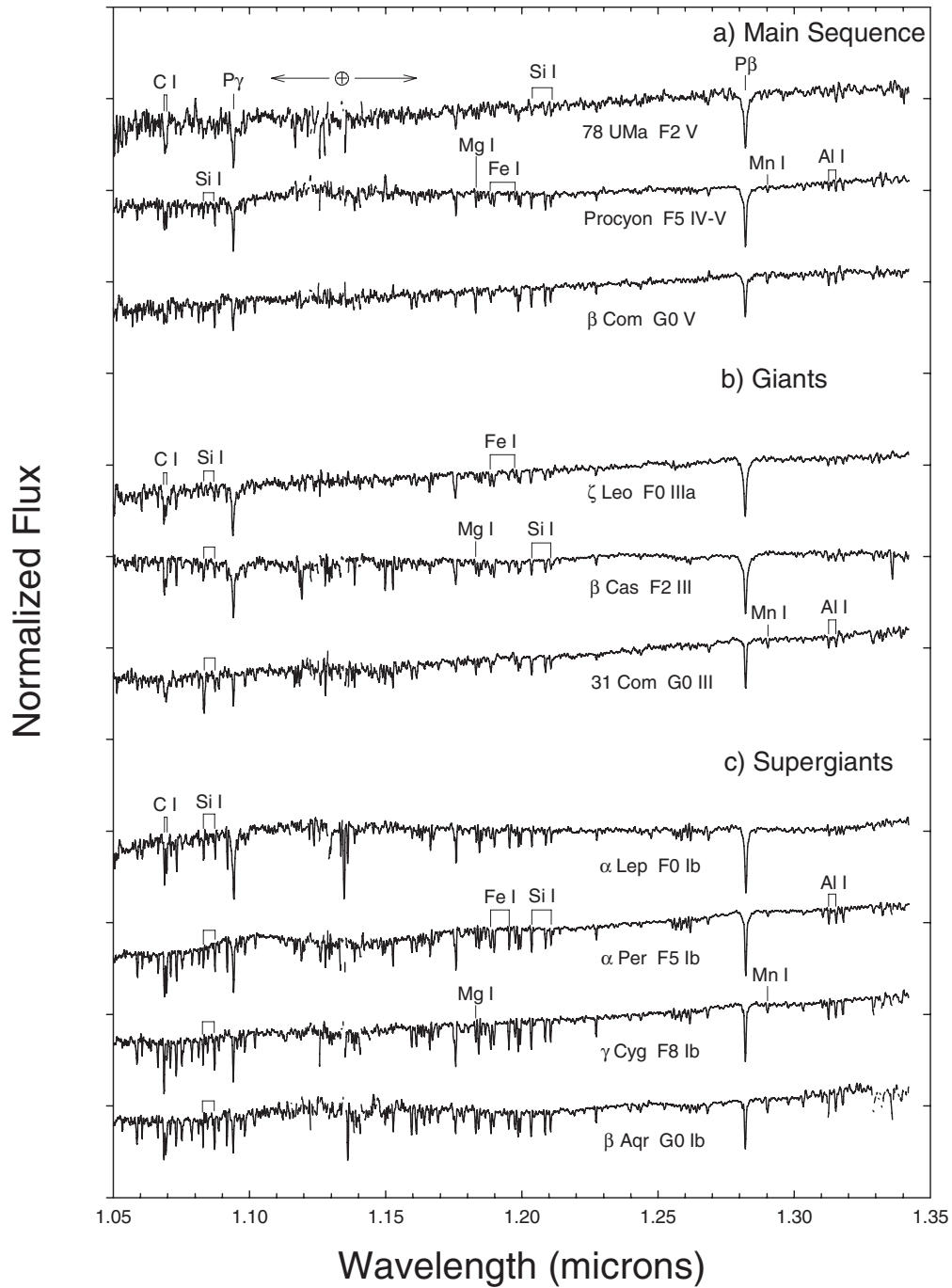


Figure 6.9 Temperature sequences for (a) F-type dwarfs, (b) giants, and (c) supergiants in the infrared J-band (1.05–1.34 μm). The two strongest lines are Paschen β and Paschen γ . These spectra, taken from Wallace et al. (2000), have been slightly smoothed from the originals.

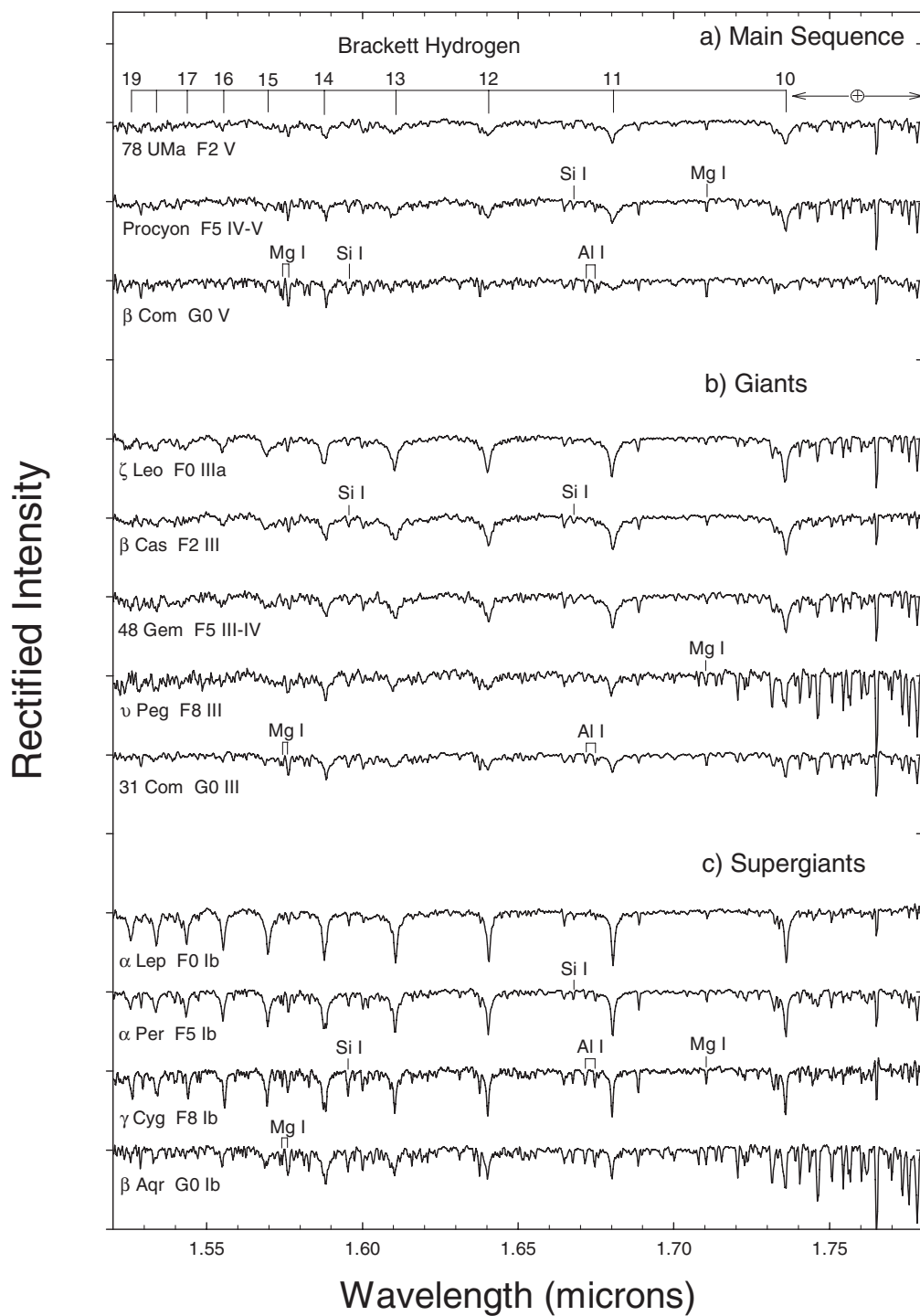


Figure 6.10 Temperature sequences for (a) F-type dwarfs, (b) giants, and (c) supergiants in the infrared H-band (1.52–1.78 μm). This region corresponds with the upper hydrogen Brackett series. Spectra from Meyer et al. (1998).

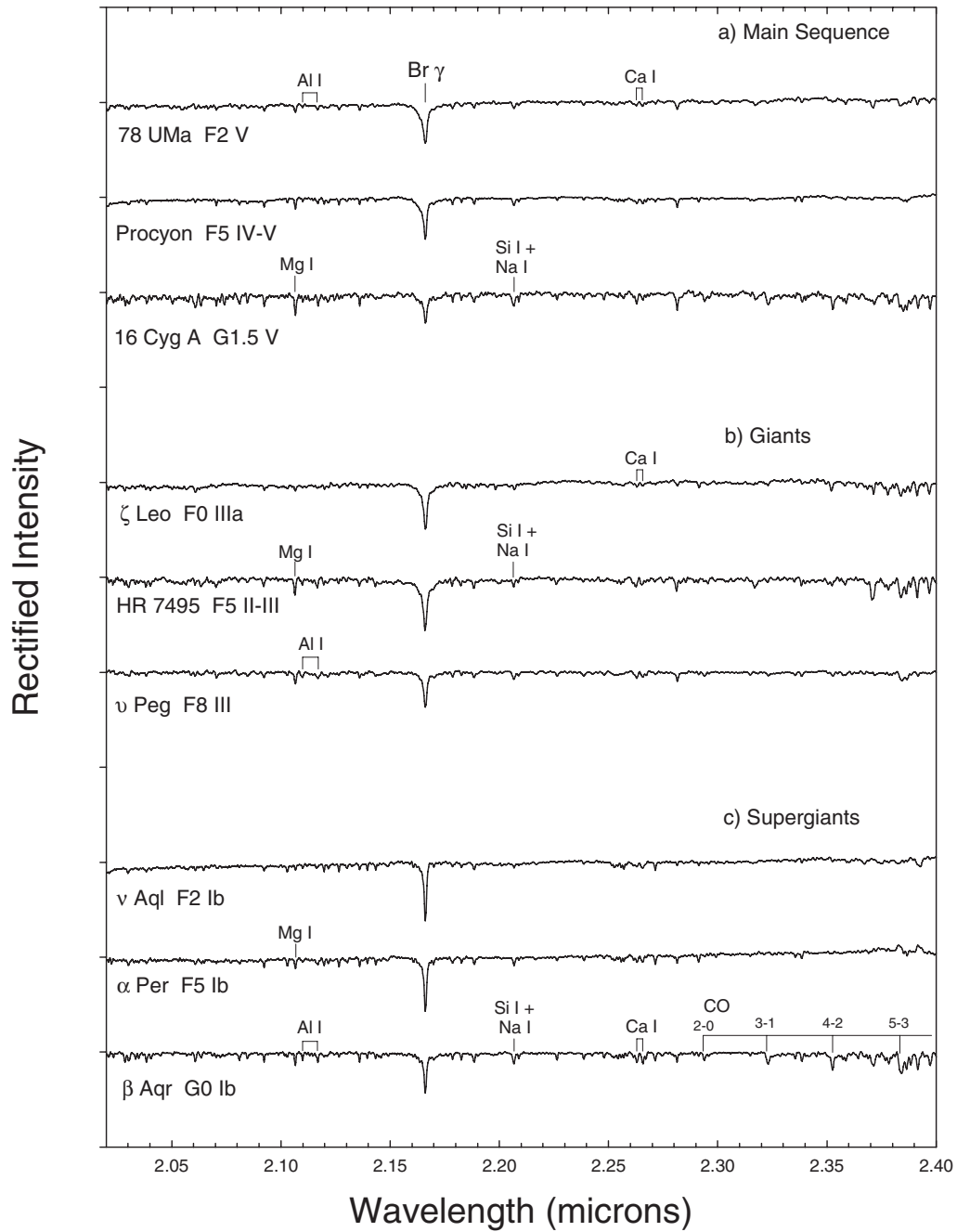


Figure 6.11 Temperature sequences for (a) F-type dwarfs, (b) giants, and (c) supergiants in the infrared K-band (2.02–2.40 μm). Spectra from Wallace & Hinkle (1997).

Wallace et al. (2000) also identify the Al I/Mg I ratio as a temperature criterion in the spectral-type range F5–M2.

The Paschen β and γ lines show a mild luminosity sensitivity in that, while the profiles are moderately broad in the dwarfs and giants, they are narrower and deeper in the supergiants. Very few lines of ionized metals show up in the F-type stars in the J-band; the most prominent is a Ca II line at $1.1839\ \mu\text{m}$. However, nearly every neutral metal line in the J-band region shows a positive luminosity effect, although, unfortunately, this effect does not appear to be sensitive enough to separate clearly the giants from the dwarfs. This situation may possibly be improved with higher S/N spectra.

The H-band (Meyer et al. 1998, see Figure 6.10) is dominated by the higher Brackett lines of hydrogen in the early F-type stars. However, by early G, these lines have weakened considerably. The metallic-line spectrum, dominated by neutral metals with relatively low ionization potentials (e.g., Mg I, Si I, and Al I), strengthens towards later types; by G0 the spectrum is dominated by metals. While ratios of these lines with a nearby Brackett hydrogen line can be useful temperature criteria, these ratios are strongly dependent on the luminosity class, because of the marked *positive* luminosity effect of the higher Brackett lines (see remarks below) and are also dependent on metallicity. Unfortunately, in the H-band there is no convenient high-excitation metal line (such as the C I multiplet in the J-band—see above) that can be used in ratio with lower excitation lines to form a useful temperature criterion; the Al I lines marked in Figure 6.10 have excitation energies of about 4 eV, and the Si I and Mg I lines about 5.5–6 eV, but all of these features increase in strength throughout the F-type stars.

As mentioned above, the higher Brackett lines show a marked positive luminosity effect, in that these lines are deeper and stronger in the giants and supergiants than in the dwarfs. This behavior is reminiscent of, and indeed analogous to, the behavior of the upper Paschen lines in the near-infrared (see above). Many of the neutral-metal lines in the H-band also show a positive luminosity effect, but this is most marked in the late F-type stars.

In the K-band (Wallace & Hinkle 1997, see Figure 6.11) spectra of F-type stars are dominated by the single Brackett γ line of hydrogen and a number of weak lines of low ionization-potential neutral metals. The Br γ line weakens toward later types, and the metals strengthen, yielding useful temperature criteria such as Mg I/Br γ . In the early G-type stars, a number of bandheads of CO become visible; these are marked on the spectrum of the G0 Ib standard in Figure 6.11, but are also marginally visible in the spectrum of the G1.5 V standard.

The Br γ line is narrower (but deeper) in the supergiants, but the metallic-line spectrum does not show a marked luminosity sensitivity.

6.4 POPULATION II F-TYPE STARS

Until fairly recently the MK classification system was a strictly two-dimensional system with its standards drawn from stars of solar composition. The

classification of metal-weak stars was, therefore, technically outside of its purview. This deficiency was recognized early on (see the discussion in *Trans. IAU*, 1961, 11A, 334) and suggestions were made that the MK system could be extended with a “metallicity parameter.” Keenan & McNeil (1976) (see also Keenan 1985) made the first substantial efforts to set up abundance indices to classify the metal-weak and chemically peculiar late-type giants of the solar neighborhood.

The concept of stellar populations originated with Baade (1944); his Population I stars comprised the stars of the Galactic disk, whereas Population II included stars in the Galactic halo. These two groups of stars could be separated by their kinematics, with the Population II stars being synonymous with high-velocity stars, and it was soon realized that Population II stars were substantially older than Population I stars. The connection between population and metallicity was first made by Roman (Roman 1950, 1952, 1954), who showed, using the tool of MK spectral classification, that the old, high-velocity Population II stars were also metal-weak. By the time of the Vatican conference on stellar populations (O’Connell 1958), Baade’s original scheme had been refined to include the extreme (halo) Population II and the intermediate Population II. The intermediate Population II is comprised of objects with kinematics, metallicities, and concentration toward the Galactic plane intermediate to the extreme (halo) Population II and the young (thin) disk population, and corresponds roughly to the population of stars now termed the *thick disk*. Strömgren (1964) led the effort to discover members of this population in the solar neighborhood; to this end he invented the Strömgren *uvby* photometric system that incorporated a metallicity index (m_1) that could be used to identify metal-weak F and G dwarfs (see §2.3).

6.4.1 The Classification of Intermediate Population II F-type Stars

Roman (1950) was the first to consider the spectral classification of F- and G-type stars in what would later be called the intermediate Population II, and her seminal classification papers (Roman 1952, 1954) also included members of this population. After that, the subject languished spectroscopically for over a decade until Bond (1970) carried out an objective-prism survey for metal-weak F5 to G5 stars, and obtained Strömgren *uvby* photometry for 250 stars that appeared metal-weak on his plates. He classified these metal-weak stars on the basis of the hydrogen-line strength, which, as we saw in §6.2.1, is essentially a metallicity-independent temperature indicator. He also introduced the metallicity classes “normal, slight, moderate and extreme (line weakening)” judged visually with respect to the MK standard of the same hydrogen-line type. He compared his metallicity classes with the Strömgren m_1 index and showed that there was a good correlation—a direct confirmation that Strömgren’s photometric system could, indeed, pick out stars that appeared metal-weak spectroscopically.

Nancy Houk has had to classify metal-weak stars in her monumental reclassification of the HD stars (Houk & Cowley 1975; Houk 1978, 1982, 1988; Houk & Swift 1999). Her technique is very simple: a temperature type is assigned

according to the hydrogen-line strength, and then a metallicity-type is assigned by identifying the earlier MK standard with the same general strength of metal lines as the program star. This results in classifications such as G0wF2, where the “w,” in analogy with the notation for Am stars (§5.4.1), indicates metal-weakness.

Erik Olsen, a former student of Strömgren, has carried out a massive, kinematically unbiased, magnitude-limited, photometric survey of nearly 13,500 F-type stars on the Strömgren *uvby* β system (Olsen 1983; Olsen & Perry 1984). Abt (1986) and Corbally (1987) devised schemes to classify metal-weak F-type stars discovered in Olsen’s survey. Abt’s scheme is very similar to that of Houk, although he also introduced a G-band type based on comparison with MK standards. Corbally, on the other hand, introduced a number of refinements. First, he assigned separate metallic-line types for the weak (background) metallic lines and the strong lines based on matches to MK standards. Second, he not only assigned a temperature type based on the hydrogen lines, but also gave consideration to the Cr I resonance triplet ($\lambda\lambda$ 4254, 4275, 4290) in ratio with nearby, subordinate Fe I lines ($\lambda\lambda$ 4250, 4260, 4326; excitation energies ~ 1.5 eV). The Cr I resonance lines grow more rapidly with declining temperature than the subordinate Fe I lines. Because these ratios are based on “iron-peak” elements, they are essentially independent of the metallicity of the star (see Keenan & McNeil 1976).

In an unpublished development of his system, Corbally has derived a formula to convert the difference, Δ , between the hydrogen-line and the metallic-line type (where Δ is the number of spectral subtypes between the hydrogen and metallic-line types, and is defined as positive for metal-weak stars) into a Keenan-like metallicity index (see Chapter 7 for more details on Keenan’s metallicity indices). Thus, for instance, the spectral type G0 V mF2 ($\Delta = 8$) may be written G0 V Fe-1.3. The formula (see Corbally 1987) that yields the “Fe index” is as follows:

$$\text{Fe} = -0.13\Delta - 0.26$$

The shortcoming of all of the classification systems mentioned above is that they depend on comparison of the (metal-weak) program star with solar-composition MK standards. The disadvantage of this is that the program star is often compared with standards of considerably different effective temperatures and metallicities. Thus, with Abt’s and Corbally’s systems, a metal-weak G0 star might have its metallic-line spectrum matched in strength with that of an F2 MK standard. The problem with this is that the morphology of the metallic-line spectrum (meaning the pattern of lines and their relative strengths) is a function of temperature, and thus one can never achieve a completely satisfactory match between the metallic-line spectrum of a metal-weak program star and a solar-composition MK standard. The same can be said for the appearance and strength of the G-band. This means that the derived metallicity-type and G-band type are ambiguous, and this makes it difficult to come to conclusions about the normality of a particular star or the homogeneity of a given population of stars.

It should also be noted that the metallic-line spectrum of a metal-weak star does not simply have metallic-line strengths that are uniformly scaled down from the

solar-abundance standard with the same effective temperature. That is to say, the morphology of the metallic-line spectrum is a function not only of temperature, but also metallicity itself. The reason for this is easy to understand: weak lines grow in strength in proportion to the abundance of the element in question, but once the spectral line starts to saturate in the core, the strength no longer grows linearly with the abundance. This nonlinear regime corresponds to the “flat” and “damping” parts of the classical *curve of growth*. On the flat part of the curve of growth, the line core is essentially saturated, and so the line strength grows very slowly with increasing abundance. Eventually, however, very broad “damping” wings begin to develop; in this regime the line strength grows with the square root of the abundance (for more information on the curve of growth, see Gray 2008). It turns out that in classification spectra of F- and G-type MK standards, most of the strong metallic lines are in the damping regime, whereas most of the weaker “secondary” lines are in the linear regime or on the beginning of the flat part of the curve of growth. Thus, in the transition from solar-abundance to metal-weak F- and G-type stars, the “strong” lines move onto the flat part of the curve of growth, and the “secondary” lines move almost entirely into the linear regime. As a result, the “strong” lines will exhibit a less pronounced weakening than the “secondary” lines, leading to a change in the spectral morphology.

There is another consideration that affects the spectral morphology in metal-weak stars. In late-type stars the electron density is provided primarily not by the ionization of hydrogen, but by the ionization of metals. Thus metal-weak stars have lower electron densities than solar-abundance stars of the same effective temperature. One consequence of this is that the ionization of metals will be more complete in metal-weak stars (see §5.2.4 for an explanation), and thus ratios of ionized to neutral species, such as are used in luminosity criteria, will be affected.

The only way to address this problem (the fact that the spectral morphology is a function of both temperature and metallicity) satisfactorily is to define metal-weak standard stars as an extension of the MK system. This is exactly what Gray (1989) did in his study of the intermediate Population II F-type stars. Gray defined two sequences of metal-weak standards that run parallel in visual terms to the MK standards (which were denoted as “metallicity class 0”). These two sequences were labeled as “−1” and “−2”, the “−2” sequence coinciding with the most metal-weak stars found in the intermediate Population II. The temperature types of these standards were determined by use of the hydrogen lines, the morphology of the overall metallic-line spectrum, and especially the metallicity-independent Cr I, Fe I ratios mentioned above (in particular, the “triplet” of lines, Fe I λ 4250, Cr I λ 4254, and Fe I λ 4260; the Cr I line is a resonance line, the Fe I lines are subordinate lines). Figure 6.12 illustrates a metallicity sequence at F9 on Gray’s system. Gray also set up fragmentary and preliminary sequences at metallicity classes −3, −4, and −5, thus introducing the possibility of incorporating F-type extreme Population II halo stars into the scheme (see comments in the next section). In all, 21 new standards were proposed, including some for subgiants (IV) and giants (III).

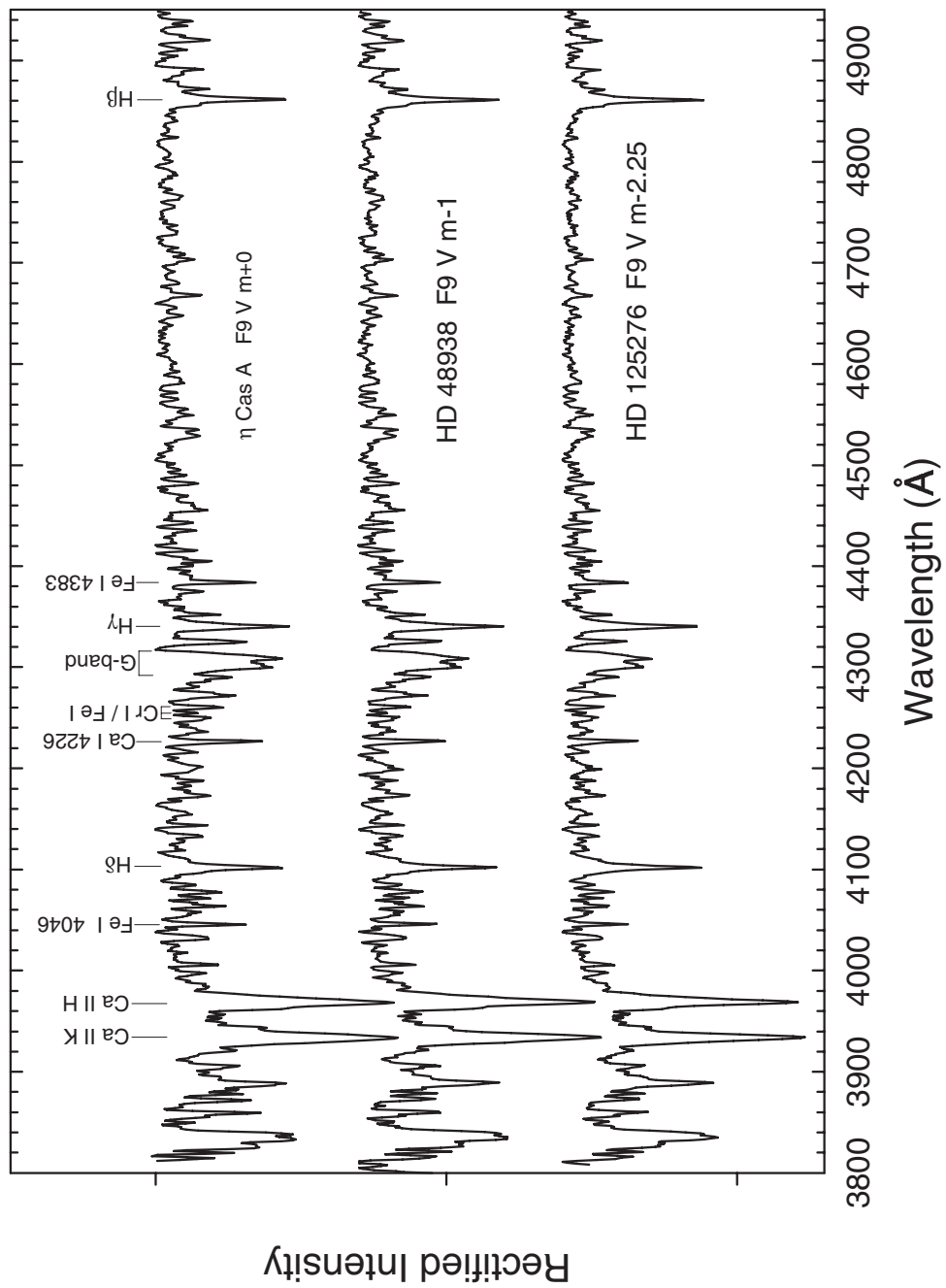


Figure 6.12 A metallicity sequence of F9 main-sequence stars classified on Gray's (1989) system. These spectra were obtained on the Steward Observatory 90" Bok telescope.

Spectral types on this system have the form

$$G0\ V\ m - 2$$

where the number following the “m” is the metallicity class.¹ Interpolations between metallicity classes are allowed and encouraged under this scheme, and so a metallicity class of, for instance, “m–1.5” is possible. Gray showed that his metallicity classes were well correlated with the Strömgren m_1 metallicity index. But, perhaps most importantly, he was able to state that his sample of metal-weak F- and early G-type stars appeared to have “a high degree of homogeneity,” even with respect to the strength of the G-band, which was so consistent with the other spectral criteria it was found it could be used as a sensitive indicator of both the temperature and metallicity classes. This, interestingly, is in contrast to the result of Abt (1986) who felt, on the basis of his classification system (which involved comparisons with MK standards only), that more than one composition parameter would be required to describe this population. Gray’s system was also successful in separating out truly peculiar or unusual stars, such as HD 17576, a G2 dwarf with a hot subdwarf companion, causing the lines of the G2 dwarf to appear “washed out” or “veiled” instead of weak; and HD 184266, a red horizontal-branch star (see §6.6.1).

A practical problem with the implementation of the Gray (1989) system is that it requires the user to obtain spectra of many more standard stars than just the MK standards. Time allocation committees for telescopes are usually averse to assigning telescope time just for the acquisition of standard-star observations (a highly regrettable tendency in our opinion), and so obtaining spectra of many standards can prove to be difficult. The systems of Houk, Abt, and Corbally have the advantage that they require only the MK standards and thus are much easier to implement. Indeed, in Gray, Corbally, & Garrison’s recent classification study of the nearby solar-type stars (Gray et al. 2003, 2006), Corbally’s 1987 system enhanced with “Fe indices” (see above) has been used to classify the limited number of metal-weak F- and G-type stars within 40 parsecs.

Even a cursory examination of the spectral types of Abt, Corbally, or Gray shows that the great majority of metal-weak stars of the intermediate Population II have spectral types of F5 or later; so this spectral type essentially marks the main-sequence turn-off for this population. However, there are a handful of stars as early as F0 that are classified in these papers as metal-weak. These stars, also discovered photometrically by Olsen (see Olsen 1983), are termed *field blue stragglers* (FBS) in analogy with the *blue straggler* stars seen in open and globular clusters. These blue stragglers are stars whose evolution has, for some reason, been “delayed,” and are still on the main sequence even though lower mass stars in the same population have begun to evolve off the main sequence. The coalescence of a close binary star is one possible mechanism that may be able to produce a blue straggler.

¹It turns out that a star with a spectral type of G0 V m–2 on Gray’s system has a metallic-line spectrum similar in strength to the F2 MK standard. Thus, the equivalent spectral type in Abt or Corbally’s system would be G0 V mF2.

6.4.2 Halo Main-Sequence F-type Stars

F-type stars in the Galactic Halo are treated in three different sections in this chapter. The F-type horizontal-branch stars—a late stage of stellar evolution in which the star is burning helium in its core—are discussed in §6.6.1, while the high-latitude F-supergiants, some of which may be post-AGB stars, are dealt with in §6.6.2. In this section, we deal with main-sequence and “turn-off” F-type stars of the halo, often referred to in the earlier literature as F-type “subdwarfs.”

The F-type halo dwarfs were first discussed by Adams & Joy (1922) who noted that these stars seem to lie between the main sequence and the white-dwarf sequence, and were therefore termed by them “intermediate white dwarfs.” In the course of her massive study of nearly 600 high-velocity stars, Roman (1954) isolated a sample of 17 such stars and examined their characteristics. She found, contrary to the conclusions of Adams and Joy, that in these stars “the strength of the hydrogen lines, the behavior of the Balmer jump, and the blue-yellow colors all indicate that these stars are similar to main-sequence stars in the middle or late F-types.” She went on to note, however, that they exhibit large *ultraviolet excesses*. Other authors besides Adams and Joy have noted that when plotted in the HR diagram, these stars tend to lie below the main sequence, and it was this property that led them to being termed “subdwarfs.” The reason why these stars lie below the main sequence is because they are very metal-weak; a typical example, HD 19445, has metal abundances nearly a factor of 100 below solar. Since metal lines are more strongly concentrated in the blue and violet (and ultraviolet) than in the red, metal-weak stars tend to be bluer (as measured by the $B-V$ or $U-B$ indices) than solar-abundance stars of the same effective temperature. This means that these stars are displaced to the left in the HR diagram, and so they define a sequence that appears to lie below the main sequence. However, if this lack of *line blanketing* is accounted for, and the stars are appropriately “reddened” (see Sandage & Eggen 1959), or if they are simply plotted on the basis of their hydrogen-line types, then it can be shown that they are not subluminal, but define essentially the same main sequence as solar-abundance stars. Unfortunately, the term “subdwarf” is still often applied to these stars. As a matter of practice, we never use the term “subdwarf” unless the spectrum clearly shows features indicating an unusually high gravity, although this term is currently in use for the metal-weak M, L, and T dwarfs (see Chapters 9 & 10).

Figure 6.13 illustrates the spectra of three prototypical examples of these stars, HD 19445, HD 140283, and BD +25° 1981. Also included, for comparison, are the F3 V and G2 V MK standards. Even a glance at this figure shows the enormous problems one faces in attempting to classify these stars on the MK system via comparisons with MK standards. The difference in line blanketing between these stars and the MK standards is so large that even comparing hydrogen-line strengths is problematical, as the hydrogen lines are significantly blended with metal lines in the MK standards. To find an MK standard with a general metallic-line spectrum of the same approximate strength as one of these stars, it is necessary to reach

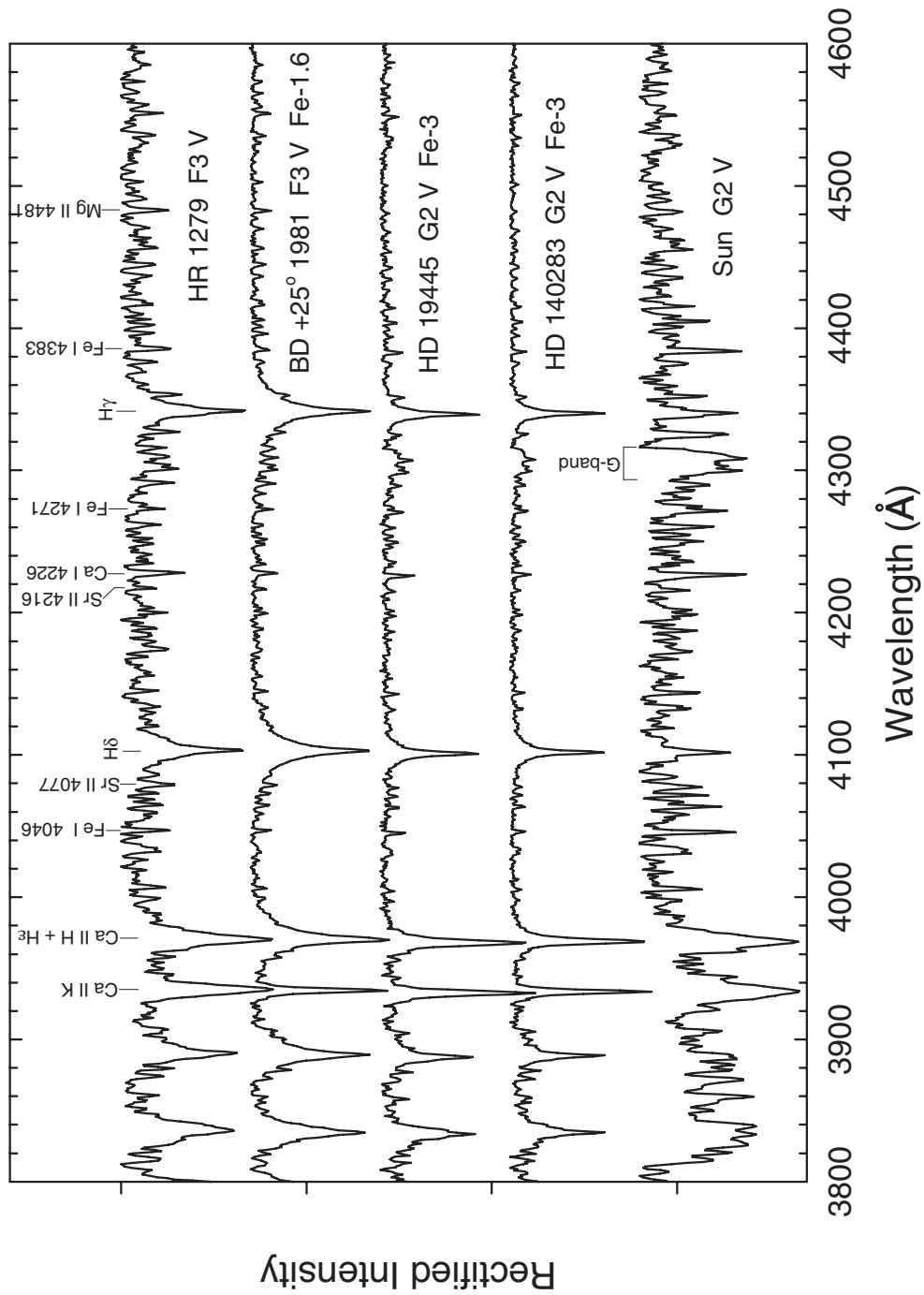


Figure 6.13 Three halo main sequence stars compared with the MK standards HR 1279 (F3 V) and the Sun (G2 V). HD 19445 is a true halo main sequence star, HD 140283 is actually a main-sequence “turnoff” star, while BD+25° 1981 is a halo “field blue straggler.”

back into the A-type stars. The resulting large difference in effective temperatures means that the match is very poor, and the more prominent metal lines indicate quite a different “metallicity type” than the weaker or “background” metallic lines. The cautions and caveats mentioned in the previous section in the context of classifying the intermediate Population II stars are of even greater importance here. In short, these stars really need to be classified on an extension of the MK system that would permit the use of metal-weak standards, such as that of Gray (1989); Gray has provided fragmentary “preliminary sequences” of standards that may be used for halo dwarfs, although new digital spectra indicate that a number of those standards are in need of significant revision. The spectral types in Figure 6.13 are our best efforts based on Corbally’s system (Corbally 1987).

HD 19445, a halo G2 dwarf, is also compared in Figure 6.17 with HD 119516, a halo G0 “giant” (actually, a red horizontal branch star). This comparison shows that the usual luminosity criteria are operative in these halo stars, even though the ionized-to-neutral ratios are somewhat different from what one would expect in Population I stars (i.e. the lines of ionized species are stronger relative to the neutral lines than we see in Pop I stars of the same luminosity class: see discussion in the previous section).

It turns out that HD 140283 is actually slightly evolved off the main sequence; it is properly termed a halo “turn-off” star. Notice that its spectrum is very similar to that of HD 19445, except that some of the prominent low-excitation lines (such as Fe I $\lambda\lambda$ 4046, 4383, and Ca I λ 4226) appear weaker in HD 140283. Apart from this weakening (which may be due to a difference in the gravities of the two stars, as similar effects can be seen in the MK standards), the standard luminosity criteria give no hint that HD 140283 is evolved relative to HD 19445. We have thus classified HD 140283 as a dwarf even though we know, from external information, that it is evolved.

It is immediately clear from hydrogen-line strengths alone that BD +25° 1981 is considerably hotter than the other two halo stars in Figure 6.13. Indeed this star, while on the main sequence, is hotter than the turnoff indicated by other halo dwarfs. It appears that BD+25° 1981 is a good example of a halo field blue straggler (see Carney et al. 2005).

6.5 CHEMICALLY PECULIAR F-TYPE STARS

6.5.1 The ρ Puppis Stars

The ρ Puppis stars are a group of unusually late, probably evolved Am-type stars (see §5.4.1). ρ Puppis, the prototype of the group, used to be classified as a δ Delphini star, but the designation “ δ Delphini” has now been dropped by most astronomers because of confusion over the characteristics of stars that should be included in the “ δ Del” group. Before we discuss the ρ Pup stars in detail, let us review the history of the δ Del group to illustrate why this designation has been dropped.

The δ Del stars were first recognized as a class by Bidelman (1965) who defined them as “metallic-line stars . . . in which the difference between the metallic-line type and the K-line type is rather small.” Stars satisfying such a description would now be included in the group of *proto-Am* stars, another term for stars that show mild Am characteristics. Cowley (1968) classified a number of stars as δ Del, giving a slightly different definition as stars in which “the metallic-line spectrum resembles that of an F2 IV star but the hydrogen and ionized calcium lines are very narrow.” Morgan & Abt (1972) classified a number of δ Scuti variable stars (these are A and early-F main-sequence pulsating stars), including δ Del, and found them to be inhomogeneous spectroscopically. Some of these stars appear normal and others show weak Ca II K & H lines. Later, Malaroda (1973, 1975) classified a number of stars that show similar peculiarities to the peculiar δ Scuti stars as δ Del stars. Houk, in the Michigan reclassification of the HD stars (see references under Houk in the bibliography), has consistently classified stars that appear to be late Am stars as “Fm δ Del”. It is clear from this survey of the literature that different classifiers have meant different things when they have classified stars as δ Del.

Gray (1989) reclassified many of the bright δ Del stars and found that they fall into four groups. A number of these stars appear essentially normal, and were probably put into the δ Del class on the basis of their narrow spectral lines, a consequence of low rotational velocities. Another subset of these stars again look essentially like normal, evolved F-type stars, with, perhaps, a minor strengthening of the metallic-line spectrum. This group includes δ Scu. The third group, including δ Del itself, are *proto-Am* stars. It is interesting to note that δ Del is a high-amplitude double-lined spectroscopic binary, lines of which may be resolved at quadrature in classification spectra. This double-lined nature creates a dramatic change in the appearance of the spectrum of this star. Finally, the only subset of the “ δ Del” stars that appear to form a distinct and interesting class of stars are the stars ρ Pup, θ Gru, HD 103877, and possibly τ UMa.

The three stars ρ Pup (the brightest), θ Gru, and HD 103877 are the prototypes of the ρ Puppis class of stars. These stars, which appear to be late Am stars (all three show the “anomalous luminosity effect,” see §5.4.1) are outstanding because (1) their hydrogen-line types are F5, remarkably late for Am stars, and (2) their luminosity types, as determined from the Fe II, Ti II $\lambda\lambda 4172-9$ blend, and Sr II $\lambda\lambda 4077$ and 4216 lines, are extreme, ranging from II–III to Ib. While these luminosity types probably do not reflect the true evolutionary state of these stars, being due to the anomalous luminosity effect (HD 103877 shows this effect to an extreme), there is little doubt that these stars do lie well above the main sequence, and thus are evolved. For instance, the absolute visual magnitude of ρ Puppis is $M_V = 1.41$, suggesting the star is a subgiant or giant. Figure 6.14 shows the spectral characteristics of these stars, including the very pronounced anomalous luminosity effect in HD 103877.

The star ρ Pup is itself very interesting, and has been the subject of a number of studies. Of great interest is that fact that it is a δ Scuti pulsator with a large amplitude (see Mathias et al. 1997). The star HD 40765, another ρ Pup star, is also

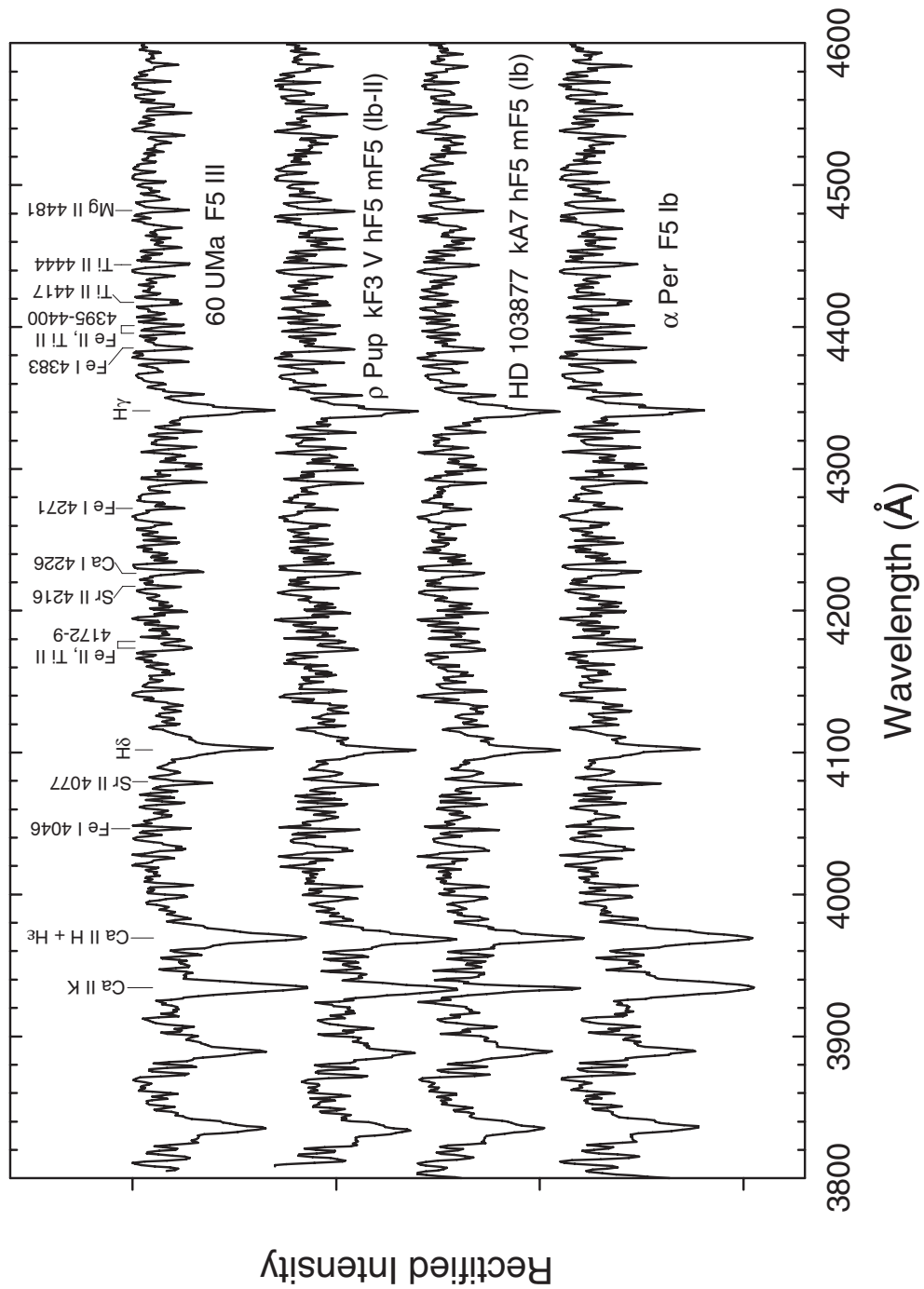


Figure 6.14 Two ρ Puppis stars, ρ Pup itself and HD 103877, compared with two MK standards. The luminosity types of the ρ Pup stars are based on Sr II $\lambda 4077$, $\lambda 4216$, and the Fe II, Ti II $\lambda\lambda 4172-8$ blend. Note the strong anomalous luminosity effect in HD 103877, revealed by strengths of lines of ionized metals between $\lambda\lambda 4383$ and 4444 .

a δ Scu pulsator (Kurtz et al. 1995). This is significant because δ Scu pulsation is generally very rare among Am stars. This is thought to be the case because helium has settled in Am star atmospheres, resulting in the loss of the helium convection zone. The engine for the δ Scuti pulsations is connected with helium ionization in this zone, and so it makes sense that Am stars are generally not δ Scuti pulsators. Thus, the presence of δ Scuti pulsation in ρ Puppis stars suggests this zone is still intact, or has been re-established. Indeed, this observation may be consistent with the scenario that ρ Puppis stars were Am stars during their main-sequence lifetimes, have now evolved off the main sequence and, as a consequence, are developing deep convection zones as they expand and cool (Kurtz 1976). The co-existence of pulsation and the Am phenomenon in these stars suggests that we have caught them at a point before convection has entirely erased their Am abundance peculiarities.

There are not many ρ Pup stars known, and discovering more members of the class would be of great interest. A graduate student of one of us (ROG) is currently working on this problem. Prime candidates for this search would be the Fm δ Del stars classified by Houk.

6.5.2 F-type $\lambda 4077$ Strong Stars and Barium Dwarfs

In the course of an “early result” program undertaken by Bidelman and MacConnell to discover astrophysically interesting stars on the objective-prism plates intended for the Michigan HD reclassification program carried out by N. Houk, Bidelman (1981, 1983, 1985) classified 20 F-type stars as “ $\lambda 4077$ strong,” meaning that the Sr II $\lambda 4077$ line appears abnormally strong in these stars. These stars are distinguished from the late-type Ap Strontium stars (see §5.4.2) on the basis of their temperature types; all of these stars have spectral types between F5 and early G, considerably later than that of any Ap star. Later photometric and spectroscopic analysis by North (see North et al. 1994, and related papers) revealed that some of these stars are late Am or “ δ Del” (ρ Pup—§6.5.1) stars, but that a number are genuine late-F, early-G dwarfs with not only a strontium overabundance, but also overabundances of other *s-process* elements including barium. These stars are now known as *barium dwarfs*. Other barium dwarfs have been discovered and analyzed by Tomkin et al. (1989), Edvardsson et al. (1993), Porto de Mello & da Silva (1997), and Gray & Griffin (2007). Figure 6.15 illustrates the spectra of two of these barium dwarfs, HR 107, an F5 dwarf, and HR 5338, an F8 dwarf.

Inspection of Figure 6.15 shows that the distinguishing classification feature of the F-type barium dwarfs is not an enhanced Ba II $\lambda 4554$ line (the enhancement of this resonance line of Ba II is only marginally detectable in classification-resolution spectra), but exceptionally strong lines of Sr II $\lambda 4077$ and $\lambda 4216$. The reader will recall that Sr II $\lambda 4077$ and $\lambda 4216$ are primary luminosity criteria for the late F-type stars, but the other luminosity criteria indicate that these stars are main-sequence objects. Many of these stars are also slightly metal-weak, and they, as well, can show peculiarities in the G-band, in that the G-band can be slightly strong or weak compared with the hydrogen-line type.

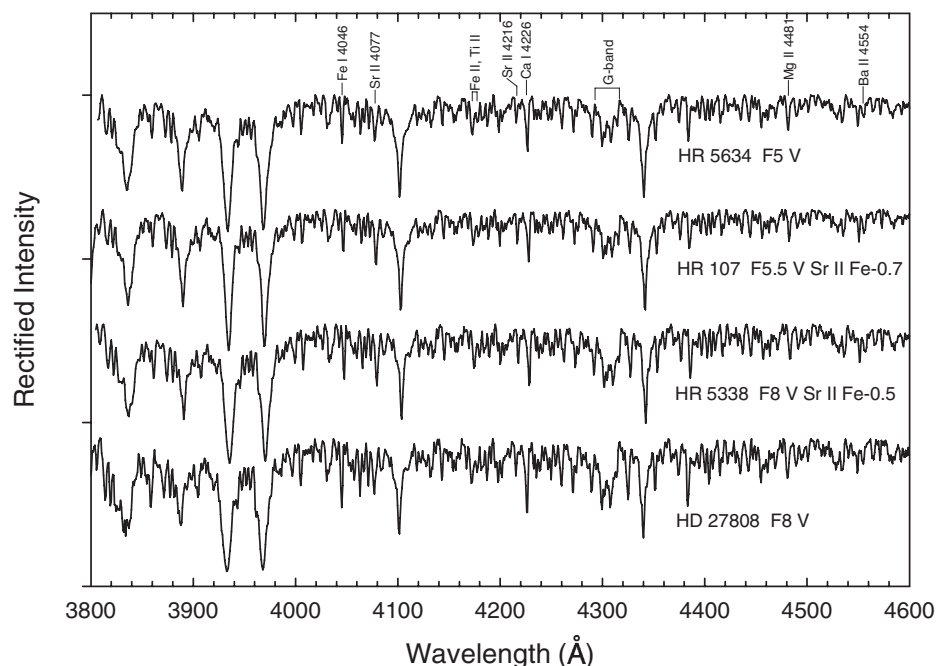


Figure 6.15 Two F-type “strong $\lambda 4077$ stars,” also classified as F-type “barium dwarfs,” compared with two MK standards.

The existence of such spectral peculiarities at spectral types F5–G2 is curious, as the deep convective envelopes of these stars should, in a short period of time, erase any surface chemical peculiarities, so diffusion and chemical separation (§5.4.1) is not a viable mechanism to explain these stars. Elements such as strontium and barium are primarily produced by the *s*-process of nucleosynthesis in the cores of stars on the asymptotic giant branch (AGB) when they can be mixed to the surface by deep convective currents. Such a mechanism, of course, is not possible in dwarf stars. There is one mechanism, however, that is capable of explaining the existence of these stars. McClure (1983) discovered that *barium giants* (see §7.6.3)—G- and K-type giants that show substantial overabundances of barium and other *s*-process elements—are exclusively found in binary systems. In a number of cases, the binary companion has been directly detected in the UV, and has proved to be a white dwarf (see Böhm-Vitense et al. 2000). The scenario outlined by McClure suggests that when the white-dwarf companion was in its AGB phase of evolution it transferred mass, either through Roche-lobe overflow or by wind accretion, onto its companion (the current barium giant), thus contaminating it with *s*-process elements. Such a scenario also works for main-sequence stars, and so actually predicts the existence of barium dwarfs. Indeed, Böhm-Vitense et al. (2000) presented evidence that at least some barium giants are contaminated while on the main sequence, thus establishing a connection between barium dwarfs and barium giants. North et al. (2000) have found that a majority of barium dwarfs

do show radial velocity variations (and thus are binaries), and have also shown statistically that the companions have masses of about $0.6M_{\odot}$, consistent with a white-dwarf status. However, to date, none of these companions has been detected in the ultraviolet.

6.6 F-TYPE STARS IN ADVANCED EVOLUTIONARY STAGES

6.6.1 RR Lyrae and Red Horizontal-Branch Stars

The evolutionary state of the RR Lyrae and Horizontal-Branch (HB) stars was discussed in §5.6.1. RR Lyrae stars are HB stars that lie in the *Instability Strip*, the same instability strip that is responsible for the pulsation of the Cepheids and the main-sequence δ Scuti variables. At the luminosity of the HB, the instability strip spans temperatures from about 7500 to 6000 K, or roughly spectral types A7 to F8. At F8 and later, HB stars, termed red horizontal-branch (RHB) stars, are again pulsationally stable. At later spectral types (roughly G8), the red horizontal branch merges with the Asymptotic Giant Branch (AGB, see Figure 5.24), and thus the spectral type range for RHB stars is about F8 to G8. Where the RHB ends and the AGB begins is ultimately defined in terms of the central energy source of the star; HB stars burn helium in their cores, whereas AGB stars have an inert carbon core. Of course, observationally, and from a spectral classification point of view, the dividing point between the two evolutionary stages is not so clear cut, and deciding whether a particular star is a cool RHB or a warm AGB star may not be easy.

RR Lyrae stars, as discussed in §5.6.1 and illustrated in Figure 5.29, have variable spectra, and thus their spectral types change cyclically. Yet the spectra of F-type RR Lyrae stars do not show outstanding peculiarities in the blue-violet, other than sub-solar metallicities, and they may be readily classified on the MK system using the techniques employed for the intermediate Population II stars—see §6.4 (an exception to this statement is during rising light when many RR Lyrae stars can show peculiar hydrogen lines—see Figure 5.29 and Struve 1948). Figure 6.16 shows the spectra of two typical F-type RR Lyrae stars, RR Lyrae itself and HD 19510, compared with the F6 III-IV MK standard. While these two RR Lyrae stars have similar spectral types (F6 III versus F7 III), they have quite different metallicities, with HD 19510 being considerably more metal weak. The luminosity type for these stars can be easily deduced from the strengths of the Sr II $\lambda 4077$ and $\lambda 4216$ lines relative to neighboring lines of neutral species. HD 19510 has a metallic-line spectrum that has the general strength of an A2 star, but inspection shows that the spectral morphology is quite different; lines of ionized iron and titanium are all very weak compared with an A2 standard, while lines of neutral species dominate. Mg II $\lambda 4481$ is exceptionally weak in HD 19510. The Fe “metallicity indices” in Figure 6.16 are calculated according to the formula given by Corbally (1987) (see above, §6.4.1).

For many years, astronomers have estimated the metallicity of RR Lyrae stars via spectral classification. A ΔS index is used for this purpose; this index is

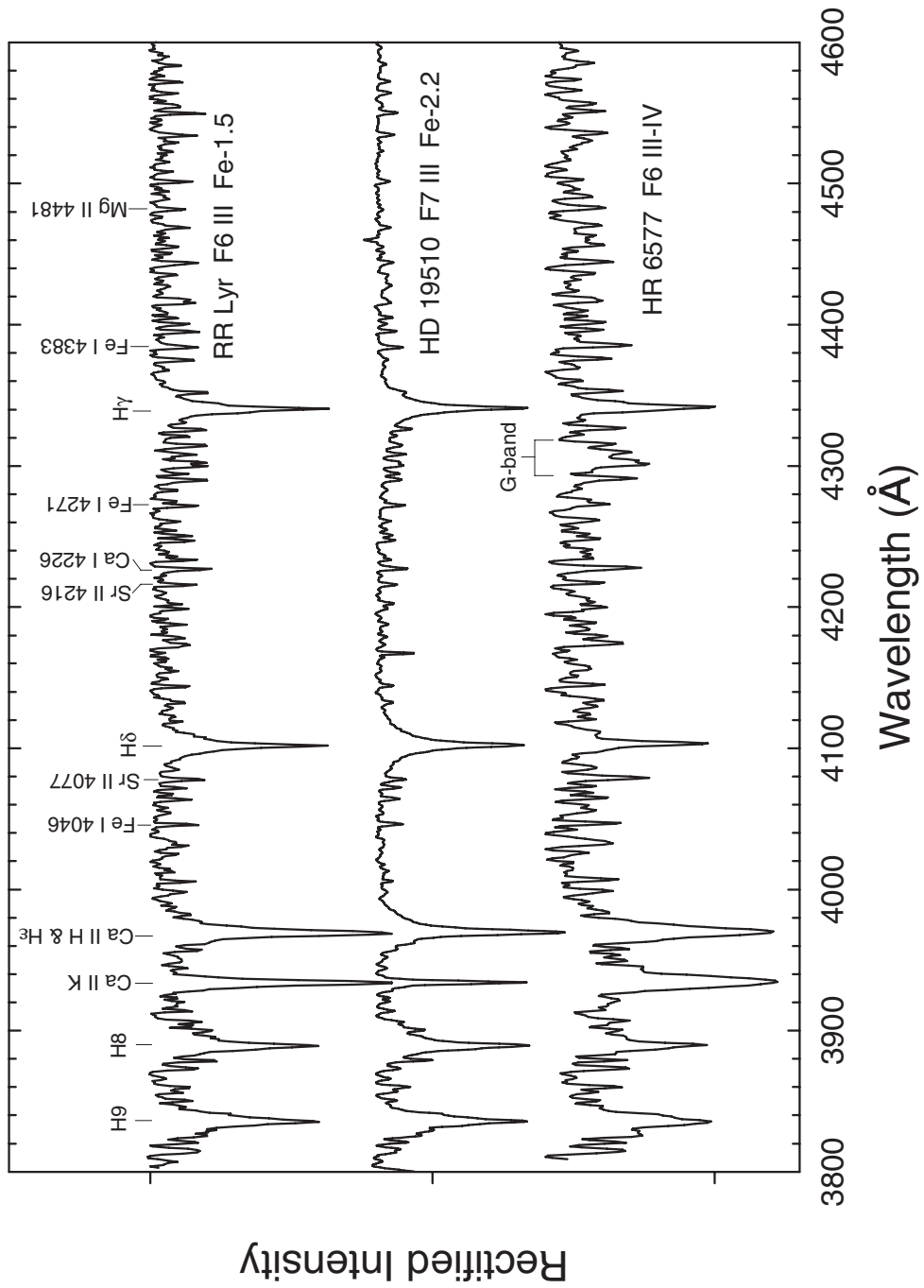


Figure 6.16 Spectra of two RR Lyrae variable stars compared with the F6 III-IV MK standard. The spectra for RR Lyr itself and HR 6577 are from the Dark Sky Observatory and have a resolution of 1.8 Å. The spectrum for HD 19510 is adapted from the Indo-US coudé-fed library (Valdes et al. 2004) and has been smoothed and rectified to match the DSO spectra.

defined as the difference in the number of spectral subtypes between the hydrogen-line type and the Ca II K-line type. For instance, if an RR Lyrae star has an F0 hydrogen-line type, and an A2 K-line type, $\Delta S = 8$. A positive value of this index indicates the star is metal weak. The ΔS index is usually determined at maximum light. See Suntzeff et al. (1994) for a catalog of nearly 500 RR Lyrae stars classified on this system.

RHB stars in the field have traditionally been distinguished from metal-weak red giants and subgiants through the agency of intermediate-band photometry, either Strömgren *uvby* photometry or Vilnius photometry. Bond (1980) used objective-prism plates to discover a number of field metal-weak red giants and subgiants, and then obtained Strömgren photometry for these stars. He identified a number of metal-poor, late F-type stars with large c_1 indices as RHB stars. Tautvaišienė (see references in Tautvaišienė 1994) has more recently isolated a number of RHB candidates using Vilnius photometry, and has gone on to analyze these stars with high-resolution spectroscopy. Other authors who have identified and studied RHB stars in the field include Straižys et al. (1981); Rose (1985), who used his own “quantitative” three-dimensional classification system (Rose 1984) to identify a number of RHB stars (see below); Schuster & Nissen (1989); and Carney et al. (2003). Interestingly, there does not appear to be universal agreement in the literature about which stars should be identified as RHB stars, but the following stars would make it onto most lists: HD 20, HD 6229, HD 6461, HD 79452, HD 82590, HD 119516, HD 184266, HD 195636, HD 208110, HD 214362, and BD + 11° 2998. The stars in this list have temperature types that range from F7 to G8.

Using classification-resolution spectra, we find that the earlier RHB stars are exceptionally easy to distinguish from the lower luminosity, similar metallicity main sequence and turn-off halo stars such as HD 19445 and HD 140283 (see §6.4.2) on the basis of luminosity criteria (see Figure 6.17); indeed there should be no difficulty in picking these stars out from spectral surveys, such as the Sloan Digital Sky Survey.² There are nearly 300,000 stellar spectra available in the SDSS data archive as of June 2007. The later RHB stars, for which the stars HD 6461, HD 79452, and HD 208110 may serve as prototypes, are the particular subject of Rose (1985), who defined criteria by which these stars may be distinguished from main-sequence and giant-branch objects, clump giants, and chemically peculiar G giants. A particularly important criterion is the ratio of the $\lambda 3859$ and $\lambda 3871$ features (marked on Figure 6.17); in late RHB stars, this ratio is always less than unity. This ratio is both luminosity and metallicity sensitive; the luminosity sensitivity arises because CN dominates $\lambda 3871$, whereas Fe I dominates $\lambda 3859$ (for a discussion of luminosity criteria in G stars, see Chapter 7). Rose does not, however, include a discussion of how these cool RHB stars might be distinguished from warm, metal-weak, AGB stars. HD 79452 is compared in Figure 6.17 with the MK G0 V standard, which it superficially resembles. However, even a casual

²<http://www.sdss.org/>

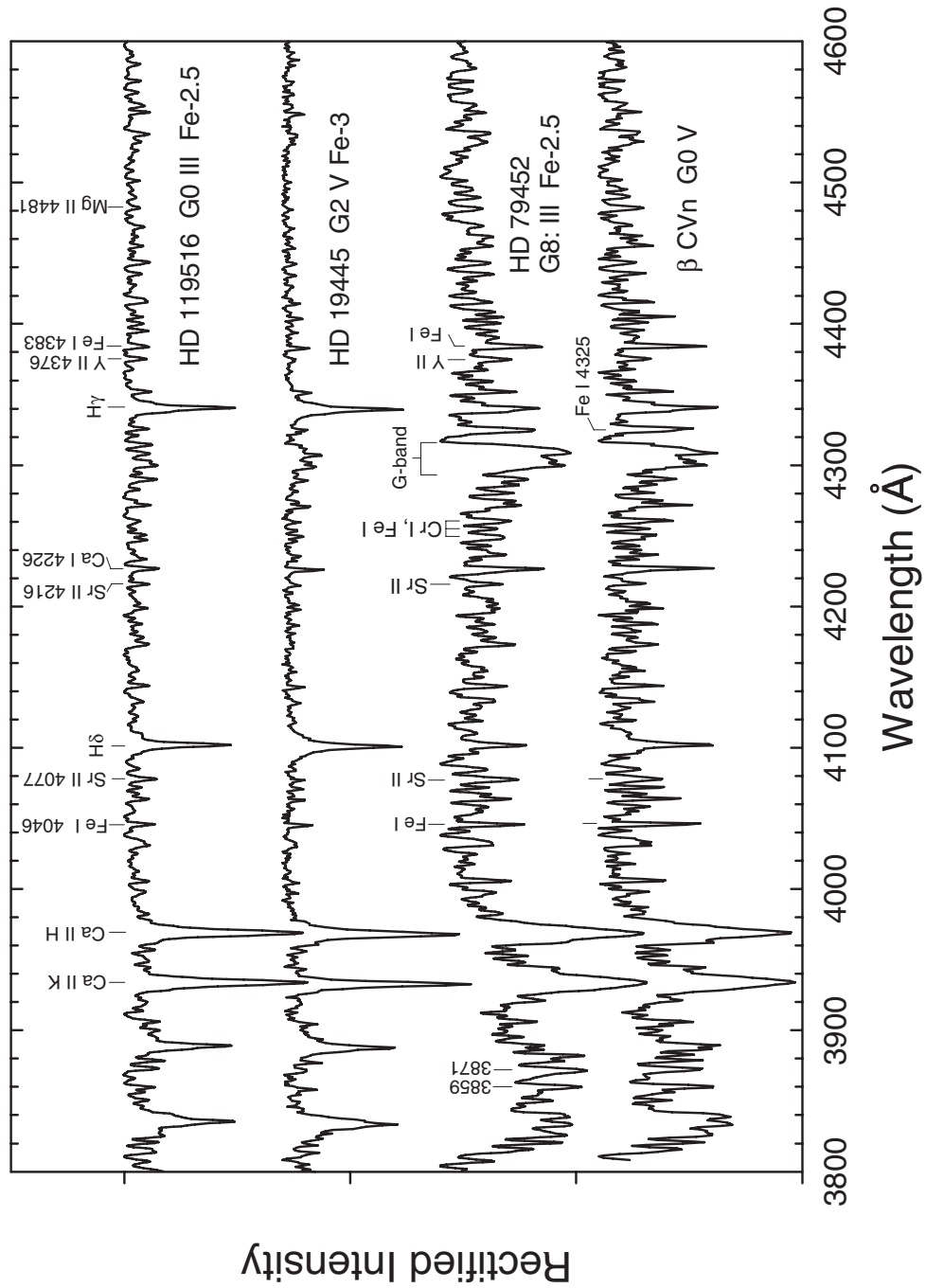


Figure 6.17 Spectra of two RHB stars (HD 119516 and HD 79452) compared, respectively, with the halo dwarf HD 19445 and the MK G0 V standard. The spectra for HD 119516 and HD 79452 have been adapted from the Indo-US coude-feed library (Valdes et al. 2004).

inspection shows many differences between these two spectra, especially in the strength of the hydrogen lines and in the luminosity criteria.

6.6.2 High-Latitude F Supergiants

The vast majority of F-type supergiants are members of the *thin disk*, and are massive, evolved Population I stars. However, there are a few F-type supergiants that appear either essentially normal or metal-weak (on the basis of classification spectra) and are found at high Galactic latitudes (Garrison & Lopez-Cruz 1993). Many of these stars have high velocities, characteristic of the thick disk or even the halo, are metal deficient, and are photometrically and spectroscopically variable. Many also show large infrared excesses. Stars that fall into this category include 89 Her, HD 46703, HD 112374, HD 161796, HD 190390, HR 6144, HR 7671, and UU Her. The variable high-Galactic-latitude F supergiants are often known as either UU Her or 89 Her stars.

Figure 6.18 shows a montage of three of these stars, HD 46703, HD 161796, and HD 190390, in comparison with two MK F-type supergiant standards. These spectra have been classified against MK supergiant standards, using the strengths of the hydrogen lines and the morphology of the metallic-line spectrum to assign a temperature type and luminosity class, and then a comparison of metallic-line strengths with MK standards of the same luminosity class to come up with a “metallicity class.” It should be noted that while HD 46703 and HD 190390 have quite similar spectral types, HD 46703 has a much stronger G-band (CH). This suggests an enhanced carbon abundance in HD 46703, in accordance with the results of Bond & Luck (1987). The MK A5 Ib standard has been included in Figure 6.18 for reference. The spectra of HD 46703 and HD 190390 resemble this star superficially, but close inspection shows that the hydrogen lines of the A5 Ib standard are significantly stronger, and certain details of the metallic-line spectrum differ. For instance, note the relative strengths of the three lines Sr II $\lambda 4216$, Ca I $\lambda 4226$, and Fe II $\lambda 4233$; in the high-latitude F-type supergiants these lines have roughly equal strengths, more similar to what we see in the spectrum of the F8 Ib MK standard than the A5 Ib standard. Other details of the metallic-line spectra of the high-latitude F-type supergiants also suggest a much later type than A5.

The origin and evolutionary state of these stars is still uncertain. The most important question to resolve is whether these stars are high-mass supergiants that happen to find themselves at high Galactic latitudes (i.e., well above the plane of the Milky Way) or are low-mass stars that are “masquerading” as high-mass supergiants. If these stars have high masses like normal F-type supergiants, then we must resolve the problem of how they come to be so far above the Galactic plane, well away from sites of star formation. Since they are high-velocity stars, it is possible that they have been ejected from the plane, for instance through the disruption of a binary system (Leonard 1993). Alternately, they may have been born above the plane; there is, for instance, evidence for high-velocity clouds at high Galactic latitudes that might serve as sites of star formation (see, for instance, the review by

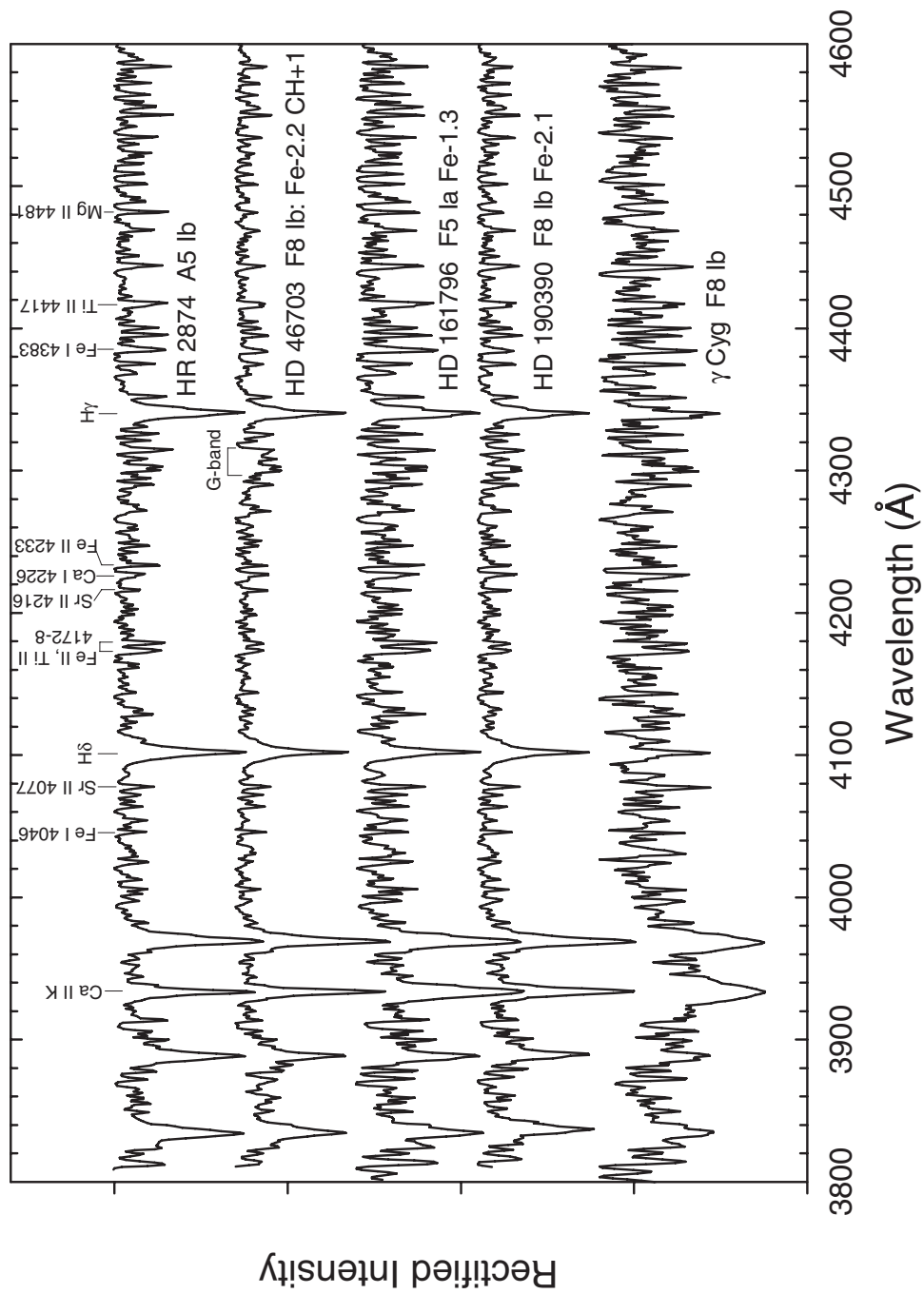


Figure 6.18 Spectra of three high-latitude F supergiants, HD 46703, HD 161796, and HD 190390, compared with two supergiant MK standards. Note the relatively strong G-band in HD 46703.

Van Woerden 1993). Alternately, these stars may be low-mass, Population II stars in the post-AGB phase; this would be in accord with the fact that many of these stars show an infrared excess. Detailed spectroscopic studies can help to resolve the issue. Bond & Luck (1987) found that HD 46703 is overabundant in C, N, O, and S, but otherwise very metal-weak. The overabundance of CNO suggests that the results of hydrogen and helium burning have been dredged to the surface of this star, and the overabundance of S may be due to α -capture during the core helium flash. These considerations suggest that HD 46703 is a post-AGB star. On the other hand, Reyniers & Cuypers (2005) could not come to a conclusion about the evolutionary state of HD 190390, but suggested this star could be either in the post-AGB state or a member of the W Vir (Population II Cepheids—see §7.8.1) class. Luck et al. (1990) suggest, from the lack of enhancements of *s*-process elements, that HD 161796 cannot be a post-AGB star.

Bibliography

- Abt, H.A. 1986, ApJ, 309, 260
- Adams, W.S., & Joy, A.H. 1922, ApJ, 56, 242
- Andrillat, Y., Jaschek, C., & Jaschek, M. 1995, AApS, 112, 475
- Asplund, M. 2000, AA, 359, 755
- Asplund, M., Nordlund, Å., Trampedach, R., Allende Prieto, C., & Stein, R.F. 2000a, AA, 359, 729
- Asplund, M., Nordlund, Å., Trampedach, R., & Stein, R.F. 2000b, AA, 359, 743
- Baade, W. 1944, ApJ, 100, 137
- Bidelman, W.P. 1965, *Vistas Astron.*, 8, 53
- Bidelman, W.P. 1981, AJ, 86, 553
- Bidelman, W.P. 1983, AJ, 88, 1182
- Bidelman, W.P. 1985, AJ, 90, 341
- Böhm-Vitense, E. et al. 2000, ApJ, 533, 969
- Bolton, C.T. 1971, AA, 14, 233
- Bond, H.E. 1970, ApJS, 22, 117
- Bond, H.E. 1980, ApJS, 44, 517
- Bond, H.E., & Luck, R.E. 1987, ApJ, 312, 203.
- Carney, B.W., Latham, D.W. & Laird, J.B. 2005, AJ, 129, 466
- Carney, B.W., Latham, D.W., Stefanik, R.P., Laird, J.B., & Morse, J.A. 2003, AJ, 125, 293
- Corbally, C.J. 1987, AJ, 94, 161
- Cowley, A.P. 1968, PASP, 80, 453
- Edvardsson, B., Andersen, J., Gustafsson, B., Lambert, D.L., Nissen, P.E., & Tomkin, J. 1993, AA, 275, 101
- ESA 1997, *The Hipparcos and Tycho Catalogues* (ESA SP-1200) (Noordwijk: ESA)
- Garrison, R.F. 2001, "Classification of Stellar Spectra" in *Encyclopedia of Astronomy and Astrophysics* (Basingstoke & Bristol: Nature Publishing Group and Institute of Physics Publishing)
- Garrison, R.F., & Lopez-Cruz, O. 1993, in *Luminous High-Latitude Stars*, ed. D.D. Sasselov, ASP Conference Series No. 43, p. 43
- Gray, D.F. 2008, *The Observation and Analysis of Stellar Photospheres*, 3rd edition (Cambridge: Cambridge University Press)
- Gray, R.O. 1989, AJ, 98, 1049
- Gray, R.O. 2006, *Memorie della Società Astronomia Italiana*, 77, 1123
- Gray, R.O., Corbally, C.J., Garrison, R.F., McFadden, M.T., Bubar, E.J., McGahee, C.E., O'Donoghue, A.A., & Knox, E.R. 2006, *in press*

- Gray, R.O., Corbally, C.J., Garrison, R.F., McFadden, M.T., & Robinson, P.E. 2003, *AJ*, 126, 2048
- Gray, R.O., Graham, P.W., & Hoyt, S.R. 2001, *AJ*, 121, 2159
- Gray, R.O., & Griffin, R.E.M. 2007, *AJ*, 134, 96
- Heck, A., Egret, D., Jaschek, M., & Jaschek, C. 1984, *IUE Low Dispersion Spectra Reference Atlas*, ESA SP-1052
- Houk, N. 1978, *Michigan Catalogue of Two-Dimensional Spectral Types for the HD Stars*, Vol. 2 (Ann Arbor: Department of Astronomy, University of Michigan)
- Houk, N. 1982, *Michigan Catalogue of Two-Dimensional Spectral Types for the HD Stars*, Vol. 3 (Ann Arbor: Department of Astronomy, University of Michigan)
- Houk, N. 1988, *Michigan Catalogue of Two-Dimensional Spectral Types for the HD Stars*, Vol. 4 (Ann Arbor: Department of Astronomy, University of Michigan)
- Houk, N., & Cowley, A.P. 1975, *University of Michigan Catalogue of Two-Dimensional Spectral Types for the HD Stars*, Vol. 1 (Ann Arbor: Department of Astronomy, University of Michigan)
- Houk, N., & Swift, C. 1999, *Michigan Catalogue of Two-Dimensional Spectral Types for the HD Stars*, Vol. 5 (Ann Arbor: Department of Astronomy, University of Michigan)
- Jaschek, C., & Gómez, A.E. 1998, *AA*, 330, 619
- Keenan, P.C. 1985, in *Calibration of Fundamental Stellar Quantities*, IAU Symposium No. 111, eds. D.S. Hayes, L.E. Pasinetti, & A.G.D. Philip (Dordrecht: Reidel), p. 121
- Keenan, P.C., & McNeil, R.C. 1976, *An Atlas of Spectra of the Cooler Stars: Types G, K, M, S and C* (Columbus: Ohio State University)
- Kurtz, D.W. 1976, *ApJS*, 32, 651
- Kurtz, D.W., Garrison, R.F., Koen, C., Hofmann, G.F., & Viranna, N.B. 1995, *MNRAS*, 276, 199
- Leonard, P.J.T. 1993, in *Luminous High-Latitude Stars*, ed. D.D. Sasselov, ASP Conference Series No. 43, p. 360
- Luck, R.E., Bond, H.E., & Lambert, D.L. 1990, *ApJ*, 357, 188
- Malaroda, S. 1973, *PASP*, 85, 328
- Malaroda, S. 1975, *AJ*, 80, 637
- Marnese, P.M., Boschi, F., & Munari, U. 2003, *AA*, 406, 995
- Mathias, P., Gillet, D., Aerts, C., & Breittellner, M.G. 1997, *AA*, 327, 1077
- McClure, R.D. 1983, *ApJ*, 268, 264
- Meyer, M.R., Edwards, S., Hinkle, K.H., & Strom, S.E. 1998, *ApJ*, 508, 397
- Morgan, W.W., & Abt, H.A. 1972, *AJ*, 77, 35
- Munari, U., & Tomasella, L. 1999, *AApS*, 137, 521
- North, P., Berthet, S., & Lanz, T. 1994, *AA*, 281, 775
- North, P., Jorissen, A., & Mayor, M. 2000, in *The Carbon Star Phenomenon*, ed. R.F. Wing (Dordrecht: Kluwer Academic Publishers), p. 269

- North, P., & Lanz, T. 1991, AA, 251, 489
O'Connell, D.J.K. 1958, *Ric. Astron. Specola Vaticana*, 5
Olsen, E.H. 1983, AApS, 54, 55
Olsen, E.H., & Perry, C.L. 1984, AApS, 56, 229
Porto de Mello, G.F., & da Silva, L. 1997, ApJL, 476, L89
Reyniers, M., & Cuypers, J. 2005, AA, 432, 595
Roman, N.G. 1950, ApJ, 112, 554
Roman, N.G. 1952, ApJ, 116, 122
Roman, N.G. 1954, AJ, 59, 307
Rose, J.A. 1984, AJ, 89, 1258
Rose, J.A. 1985, AJ, 90, 787
Sandage, A., & Eggen, O. 1959, MNRAS, 119, 279
Schuster, W.J., & Nissen, P.E. 1989, AA, 222, 69
Stražys, V., Bartkevičius, A., & Sperauskas, J. 1981, AA, 99, 152
Strömgren, B. 1964, *Astrophys. Norv.*, 9, 333 (KPNO Contrib. No. 59)
Struve, O. 1948, AJ, 53, 108
Suntzeff, N.B., Kraft, R.P., & Kinman, T. D. 1994, ApJS, 93, 271
Tautvaišienė, G. 1994, *Baltic Astron.*, 3, 168.
Tomkin, J., Lambert, D.L., Edvardsson, B., Gustafsson, B., & Nissen, P.E. 1989, AA, 219, L15
Valdes, F., Gupta, R., Rose, J.A., Singh, H.P., & Bell, D.J. 2004, ApJS, 152, 251
Van Woerden, H. 1993, in *Luminous High-Latitude Stars*, ed. D.D. Sasselov, ASP Conference Series No. 43, p. 11
Wallace, L., & Hinkle, K. 1997, ApJS, 111, 445
Wallace, L., Meyer, M.R., Hinkle, K., & Edwards, S. 2000, ApJ, 535, 325

Chapter Seven

The G- and K-type Stars

7.1 INTRODUCTION

Here we get into familiar territory, since our Sun is the closest example of these stars. Their spectra form an obvious “natural group” (see §13.6), and as such they were picked out by Angelo Secchi as one of his four types. Compared with the hotter stars, they show an abundance of spectral features, with a smooth progression of changes in these to the cooler types. However, the beginner in classification can still find these an easier group to tackle than the A- and F-type spectra because they constitute a more uniform set, though peculiarities do exist. The interest in the dwarf members of these G- and K-types is that some have been found not only to have planets around them but are also the most likely stars to have habitable planets. As for the giants, they dominate the class of evolved stars and some, due to dredge-up anomalies in nuclear-processed material, show peculiarities that drive forward the understanding of stellar evolution. Finally, the supergiant stars can show dramatic changes in spectral type and in luminosity as they reach the final stage of their lives.

In this chapter we shall take the usual look at temperature and luminosity features, both in the optical and infrared regions. Their ultraviolet features have been considered in the previous chapter (§6.3.1). Then we shall ask how to identify the stars most like our Sun and about the effects of chromospheric activity on their spectra. This leads to the very young stars, named after their prototype T Tauri, and the very old ones, the Population II stars, with great significance for Galactic history. Various chemical peculiarities in G and K giants and the variations of the short-lived supergiants will also be considered.

7.2 OPTICAL CLASSIFICATION

7.2.1 Temperature Criteria

In Figures 7.1 and 7.2 are montages of spectra showing the dwarf star sequence for these G- to mid-K types. Their boundary with the F-type stars is not a distinct one, but in the G-type stars the G-band characteristically dominates over other features. This G-band, caused by the diatomic CH molecule, increases in strength until about K2, after which it begins to fade. We can also note that the hydrogen lines fade steadily, while the strength of the general metallic-line spectrum increases. In particular, the Ca I $\lambda 4226$ resonance line grows gradually in strength until the early

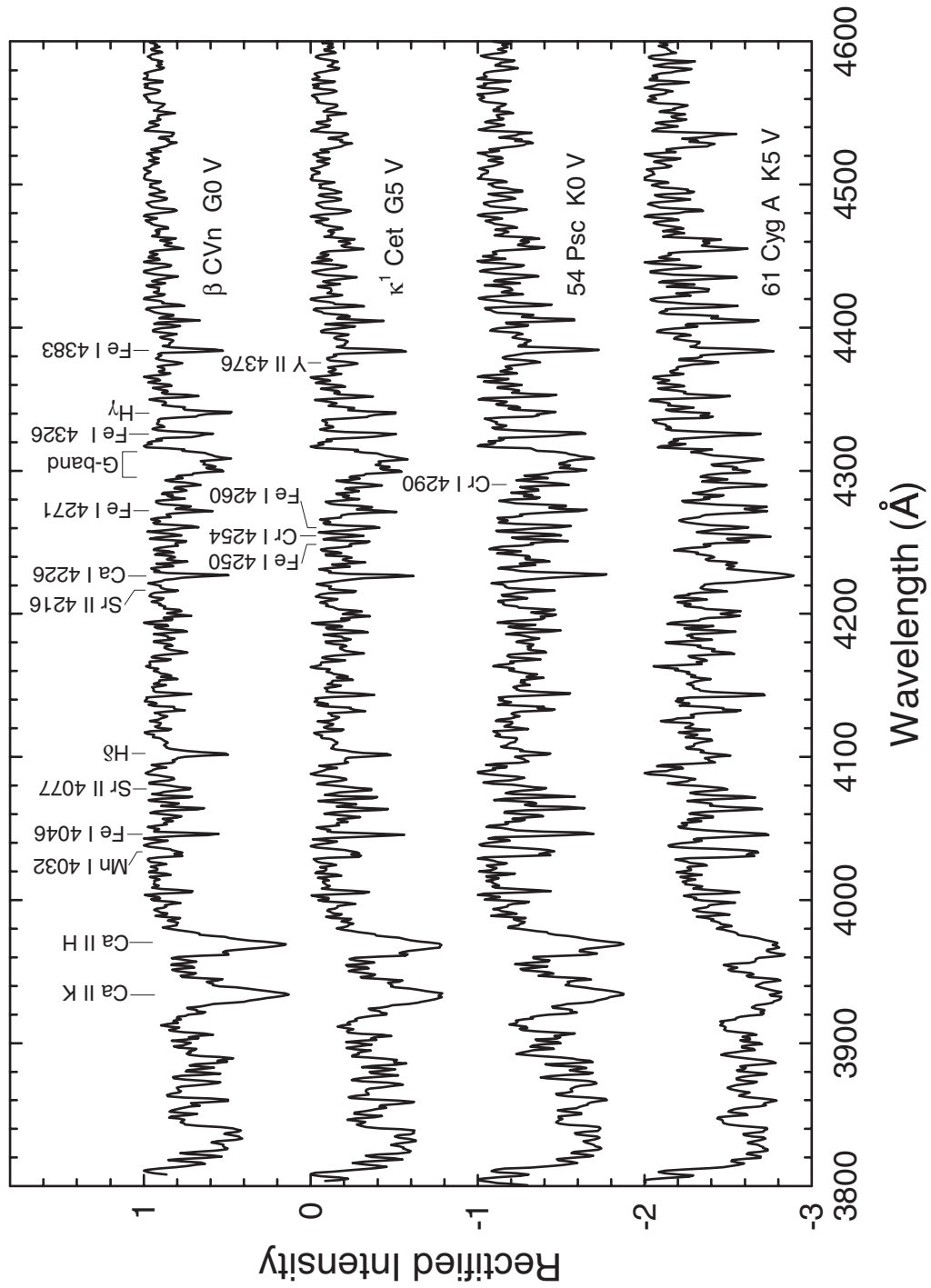


Figure 7.1 A temperature sequence for main-sequence stars from G- to mid-K types. Features useful in the temperature classification of these stars are marked. These spectra have been rectified and offset vertically by 0.7 continuum units. Unless otherwise stated, all spectra in this chapter were obtained at the Dark Sky Observatory.

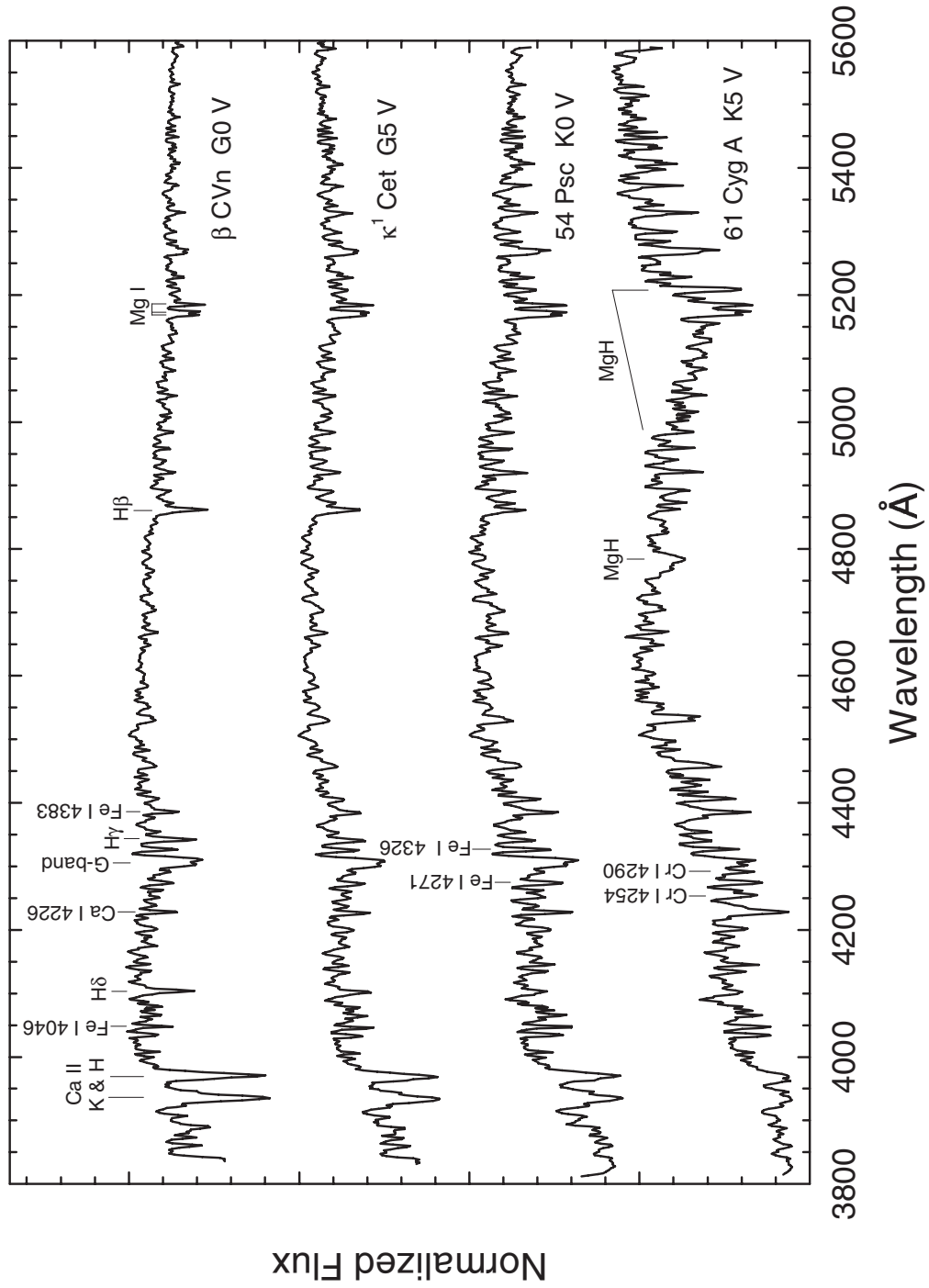


Figure 7.2 The same temperature sequence for main-sequence stars illustrated in Figure 7.1, but with 3.6 Å resolution normalized-flux spectra. Features useful in the temperature classification of these stars are marked.

K-type stars and then becomes dramatically stronger by mid-K. The Ca II H & K lines remain on a plateau and are not useful as temperature criteria, though later in §7.4.2 we shall see they are important as chromospheric activity indicators. As for the F-type spectra, the low-excitation metallic lines can be ratioed with hydrogen lines and used, with caution, as criteria thus: Fe I $\lambda 4046/H\delta$, Fe I $\lambda 4144/H\delta$, and Fe I $\lambda 4383/H\gamma$. $H\beta$ ratioed to the metallic lines just to its red can also be used, if these lie within the spectral range as in Figure 7.2. This lower-resolution montage also shows how the Mg I triplet, $\lambda\lambda 5167, 72, 83$, increases as temperature lowers and how the two MgH bands become significant criteria around K5. However, these are also luminosity sensitive (see §7.2.2).

The caution mentioned above when ratioing metal lines with those of hydrogen applies to stars that are metal-weak or metal-strong. Happily, the abundance of chromium generally follows that of iron and so the ratio of the Cr I triplet ($\lambda 4254, \lambda 4275, \lambda 4290$; resonance transitions) with nearby Fe I can be used with precision to give types for the K-stars. The ratios Cr I $\lambda 4254/Fe I \lambda 4250, \lambda 4260$ and Cr I $\lambda 4290/Fe I \lambda 4326$ are clear up to 4 Å resolution (see Figure 7.2), while the ratio Cr I $\lambda 4275/Fe I \lambda 4271$ can be used around 1 Å resolution. Even with normal metallicity stars the best practice is to use the Fe I and Ca I to hydrogen ratios to determine the initial type, and then, if later than K0, to use the Cr I triplet for a precise type.

7.2.2 Luminosity Criteria

Luminosity effects in the blue-violet are illustrated in Figure 7.3 for G8 stars. The ratio of Sr II $\lambda 4077$ to nearby iron lines (Fe I $\lambda\lambda 4046, 4064, 4072$) remains sensitive to luminosity, as it does for earlier-type stars. The violet system of the CN bands, arising like the G-band from a diatomic molecule, shows a strong positive luminosity effect, giving characteristically deep dips in the spectrum from G5 and into the early-K stars. The bandhead at $\lambda 4215$ is the most useful, but the bandhead at $\lambda 3883$ is also obvious, if often in the lower signal-to-noise part of the spectrum. At K5 and later the MgH/TiO blend near $\lambda 4770$ (see Figure 8.2) becomes very sensitive to luminosity since it is the MgH that dominates in dwarfs, producing a toothlike feature for them.

One can notice that the Ca II H & K lines have extremely broad, damping wings in supergiants, and the G-band also changes morphology in its red edge especially for the supergiants. For the early K-types hydrogen appears to have a positive luminosity effect, in the sense that it is stronger in the higher luminosity stars; however, this is probably just due to the enhancement of blended metallic lines, and anyway the effect is too small and ambiguous (i.e., it is also temperature dependent) to be very useful. The highest luminosity supergiants, like ρ Cas, HR 8752, and RW Cep, are undergoing significant mass loss from their surfaces. In the case of ρ Cas this has led to a variation in its spectrum from F8 Ia, where it was a MK standard, through early-M, and currently to mid-G type. Clearly, caution is needed for classifying these interesting yellow supergiants (Morgan et al. 1981).

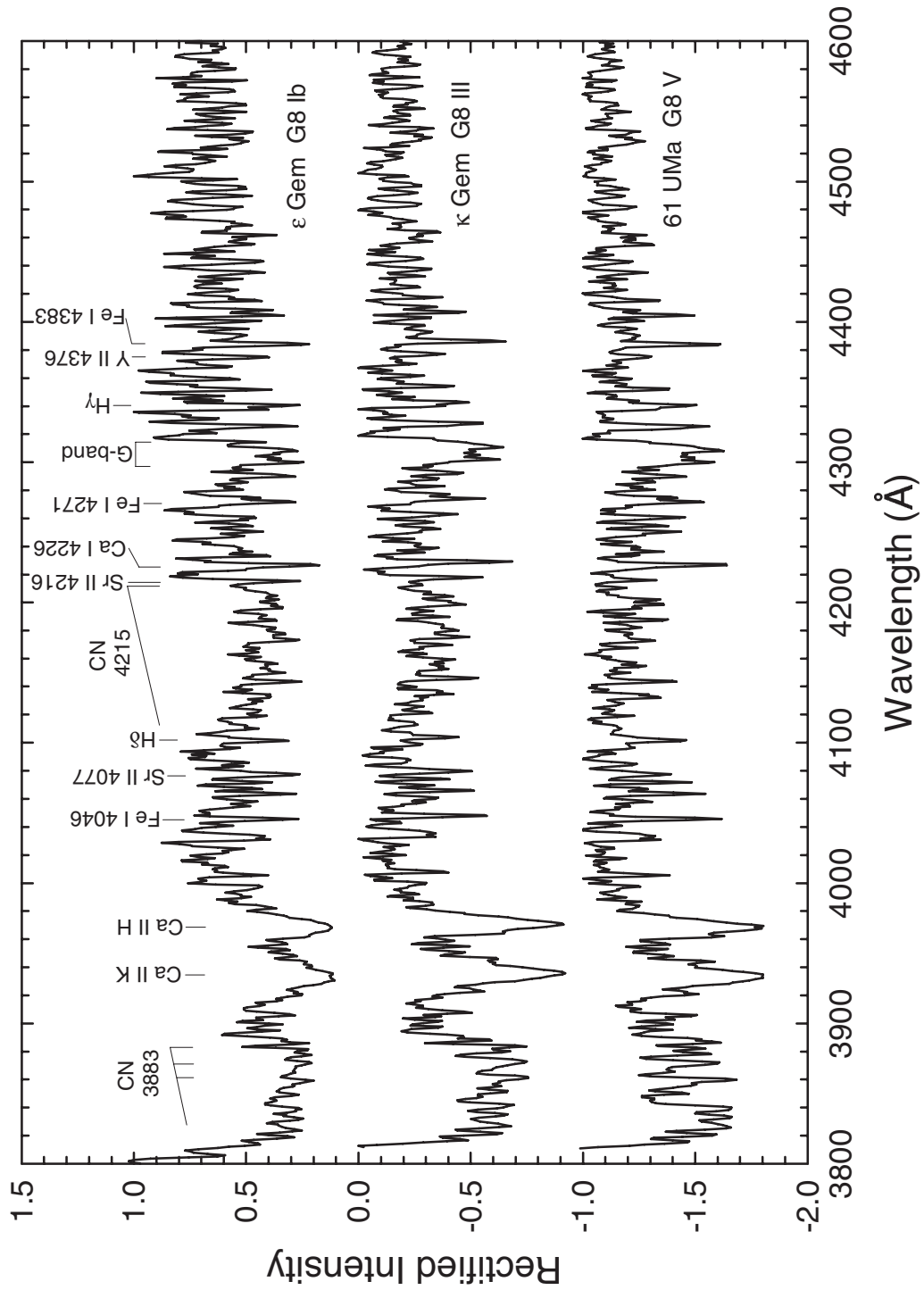
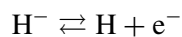
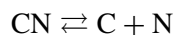
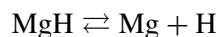


Figure 7.3 Luminosity effects at G8. Principal features are marked. The two CN bands show a positive luminosity effect, while the ratio of the Y II $\lambda 4376$ line to Fe I $\lambda 4383$ is particularly useful since it is the most metallicity independent.

While the resonance lines of Sr II, $\lambda 4077$ and $\lambda 4216$, are often used with nearby Fe I lines as luminosity sensitive ratios, the criterion that offers the most discrimination in the luminosity classes is the ratio of the Y II $\lambda 4376$ line to Fe I $\lambda 4383$. It may also offer the safest discrimination, as the Sr II lines can be significantly enhanced in chemically peculiar G- and K-type stars, as strontium is an *s-process* element. Having said that, Sr and Y are both “light *s-process*” elements, forming with Zr the first of three *s-process* abundance peaks. The observed reliability of the Y II/Fe I ratio for luminosity classification is thus a bit surprising but seems somewhat borne out by Travaglio (2004). Certainly Sr and Y should be used when the molecular bands involving carbon are found to be weak or strong, as is the case for a number of G- and K-type giants like the CN and Ba II stars. Some peculiarities (e.g., in barium stars, see §7.6.3) also involve the Sr II and Y II lines, so one must be careful to look at the whole spectrum for consistency. Further to the red, the Mg I triplet, $\lambda\lambda 5167, 72, 83$, is sensitive to luminosity for the late-G to mid-K stars and conveniently seems *insensitive* to metallicity variations among Population I stars (Guinan & Smith 1984, and references therein).

For astrophysics as well as Galactic structure studies it is worth noting that at high spectral resolution the remarkable *Wilson–Bappu luminosity effect* can be seen in the Ca II K-line core (Wilson & Bappu 1957). In that line core, for cool stars with near-solar metallicity, the emission with a central self-absorption correlates to about 0.6 mag rms with the luminosity, and this happens over a range of about 15 absolute magnitudes (Pace et al. 2003). According to Cheng et al. (1997), the Wilson–Bappu relationship appears to be a combined effect of column mass density and turbulence velocity, so it is important in probing the structure and heating in stellar chromospheres. The effect can also be found in the Mg II h & k lines.

An obvious question is to ask why the CN bands show a positive luminosity effect (i.e., an increase in strength with increasing luminosity) while the hydride molecules (CH and especially MgH and CaH) show a negative luminosity effect in G- and K-type stars. The answer to this question involves both molecular dissociation with declining pressure, and the behavior of the continuous opacity, which, in G- and K-type stars in the optical and infrared, is primarily due to H^- bound–free and free–free absorption (see §2.4.1). The relevant equilibrium equations are as follows:



The lower pressures in giant and supergiant atmospheres drive these dissociation equations toward the right (i.e., toward greater dissociation). But, because MgH has a much lower dissociation energy (1.34 eV) than the CN molecule (7.66 eV), the dissociation of MgH is driven further toward completion than is the case for CN. This is also true for the other hydride molecules, because they, too, have relatively low dissociation energies (CaH, 1.70 eV; CH, 3.47 eV). The reduction

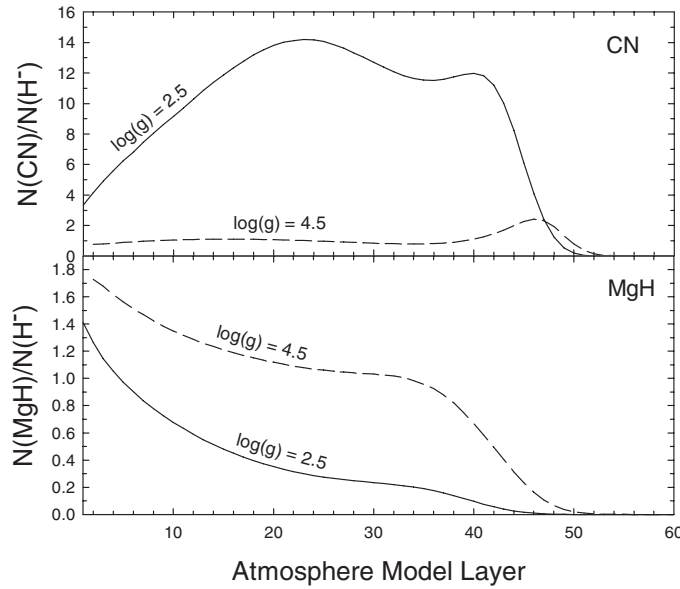


Figure 7.4 The run of the ratios CN/H^- and MgH/H^- in a dwarf ($\log g = 4.5$, dashed lines) and a giant ($\log g = 2.5$, solid lines) atmosphere (both with $T_{\text{eff}} = 4500 \text{ K}$). The “top” of the atmosphere is to the left. Computations made with SPECTRUM and Kurucz (1993) ATLAS9 stellar atmosphere models. See text for explanation.

in the abundance of H^- is also quite pronounced, as this is a very fragile ion, with a dissociation energy of only 0.76 eV . However, because the abundance of free electrons is bolstered in giants and supergiants by the enhanced ionization of metals at low pressure (see §5.2.4), the decline in the abundance of the H^- ion in the transition from dwarf to giant and supergiant is actually intermediate to the declines in MgH and CN . What this means is that the ratio MgH/H^- in the line-formation region in a giant or supergiant atmosphere is much smaller than in a dwarf atmosphere of the same effective temperature. On the other hand, the ratio CN/H^- is actually larger in giant and supergiant atmospheres. Now, since the line strength is related to the ratio of the line opacity to the continuous opacity (see §2.4.1), the behavior of the MgH/H^- and CN/H^- ratios with pressure will track the strengths of the MgH and CN bands. The run of these ratios with depth in giant ($\log g \approx 2.5$) and dwarf ($\log g \approx 4.5$) atmospheres is plotted in Figure 7.4. A brief review of the effect of molecules for the structure of late-type stellar atmospheres was given by Gustafsson (1997).

7.3 THE INFRARED

7.3.1 The Near-Infrared

If for the A- and F-type stars the near-infrared (NIR), the region from $\text{H}\alpha$ to $1.0 \mu\text{m}$, holds considerable promise for spectral classification, then this becomes

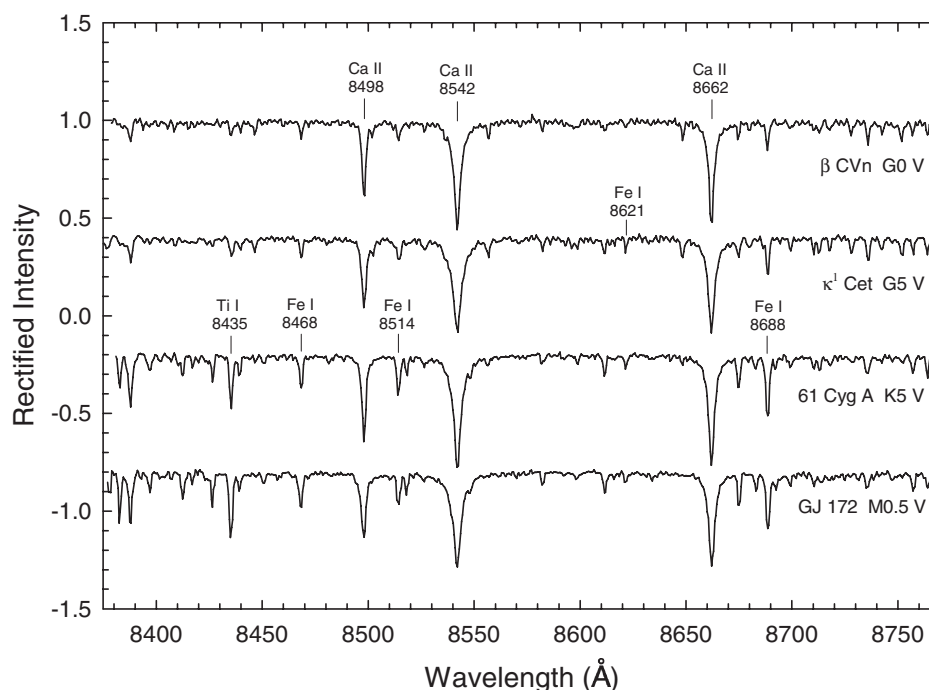


Figure 7.5 A temperature sequence for G–K stars in the near-infrared around the Ca II triplet. The spectra are from Carquillat et al. (1997).

even more true as the temperature decreases, the metallic lines increase in strength, and the maximum of the spectral energy distribution (SED) shifts into this region. As noted in Chapter 6, the strong *telluric* (atmospheric) absorption can be avoided by choosing the 8375–8770 Å region, which offers a rich combination of astrophysically important lines.

This region was explored spectroscopically for the G–M stars by Carquillat et al. (1997) near 2 Å resolution. Earlier and lower resolution atlases were produced by Danks & Dennefeld (1994), based upon southern MK standards (5800–10200 Å at 4 Å resolution), and by Torres-Dodgen & Weaver (1993) (5800–8900 Å at 15 Å resolution). Figure 7.5 shows a montage of dwarf spectra from the Carquillat et al. (1997) atlas. While early-G stars can be distinguished from late-G and K stars by the increase in absolute strength of the Fe I and Ti I lines, the disappearance of the Paschen series around G0 means that these hydrogen lines are not useful for ratios in this region. The line Fe I λ 8621 stays fairly constant in dwarf stars over G–K types, but it is not near other strongly varying lines and so again is of little use. If spectra with the range of Danks & Dennefeld (1994) or Torres-Dodgen & Weaver (1993) are observed, then the ratio of the Balmer H α line with a blend at λ 6497 makes a good temperature discriminant (Figure 7.6).

For luminosity classification the dominant Ca II triplet lines, λ 8498, 8542, and 8662, are the obvious ones to use in the NIR (see Figure 7.7). However, since all

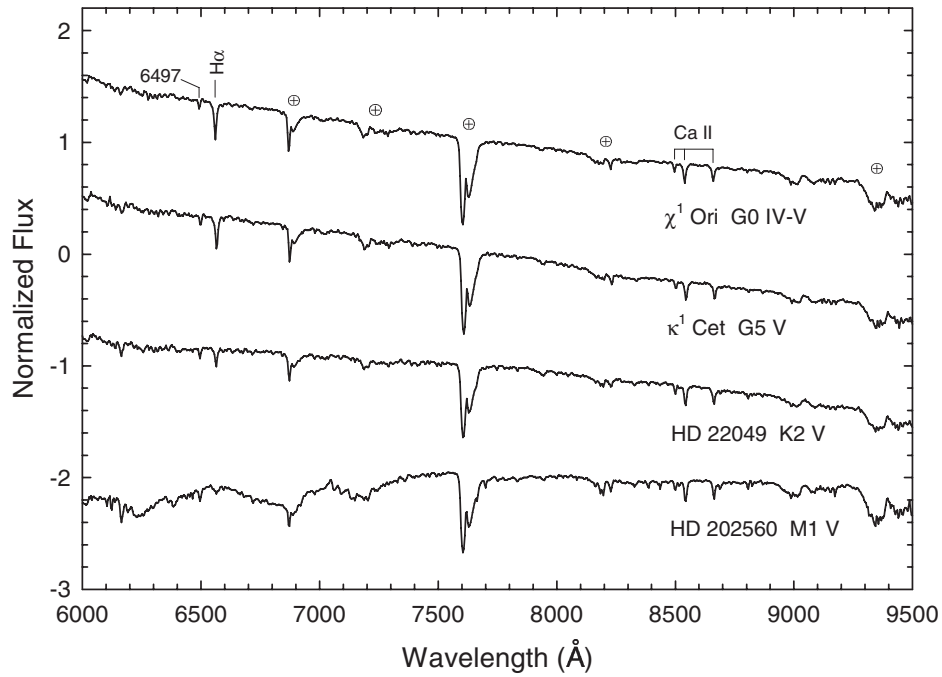


Figure 7.6 A temperature sequence for G-K stars in the near-IR. The \oplus symbols indicate the positions of telluric features. The spectra are from Danks & Dennefeld (1994).

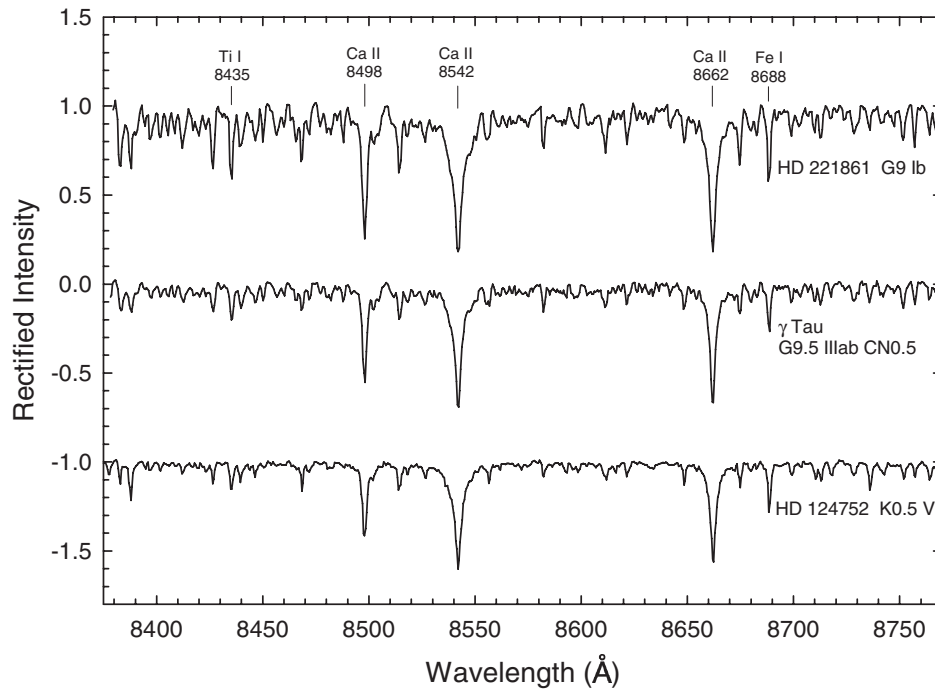


Figure 7.7 Luminosity effects in the near-IR at K0. The spectra are from Carquillat et al. (1997).

low-level lines are also strengthening with higher luminosity, the absolute strength of the triplet has to be taken.

7.3.2 The Infrared J-, H-, K-, and L-bands

In contrast to the NIR, the IR is rather more discriminating for classifying the G–K type stars. Appropriate hydrogen lines are present to mid-K types in the J-band and at least to mid-G types in the H-, K-, and L-bands, while the neutral atomic metallic lines become ever more prominent, so that hydrogen to metallic line ratios can be used for temperature discrimination. From mid-K it is better to switch to the longer wavelength regions where the molecular bands, particularly the first-overtone CO band heads, become stronger. The strongest metallic lines include Mg I, Si I, Ca I, Al I, and Fe I. The relevant papers for the IR regions are the same as for the A-type stars (see §5.3.2), though Ivanov et al. (2004) can be added for the H-, and K-bands and Ali et al. (1995) for main sequence stars in the K-band.

Figure 7.8 shows temperature sequences for G-, K-, and early M-type dwarfs, giants, and supergiants in the J-band. Paschen β remains visible to later spectral types than does Paschen γ and can be used with the adjacent metallic lines for temperature classification. The C I doublet at $1.07\ \mu\text{m}$, which is visible in earlier-type stars, has disappeared. The only obvious luminosity discriminant is the 0–0 band of CN at its R1 and R2 heads around $1.1\ \mu\text{m}$, but this of course is dependent on normal metallicities being present in the atmosphere.

The K-band offers more discriminating criteria for G–K stars than the H-band (see Figure 2.7), both in temperature and in luminosity types. The montage in Figure 7.9 for the K-band shows that the Brackett γ line at $2.166\ \mu\text{m}$ can be ratioed with nearby Na I and Ca I lines for early-G temperature types, while these metallic lines continue to be more sensitive to temperature than other metallic lines as the spectra go to later types. Also for these later types, the rotation–vibration CO bands make good temperature as well as luminosity criteria with, for example, the CO $1.62\ \mu\text{m}$ band (see Figure 2.7) doubling in strength between K5 and M5 types (Kleinmann & Hall 1986; Bell & Briley 1991). Blum et al. (2003) add the myriad blended H₂O bands between the H- and K-regions to compare with the CO bands and so yield two-dimensional classification, while Ivanov et al. (2004) suggest combining ratios of the CO $2.29\ \mu\text{m}$ and CO $1.62\ \mu\text{m}$ bands with nearby neutral metals of Na, Ca, and Mg to give quite sensitive luminosity criteria that are fairly independent of temperature effects.

The L-band, at least by mid-K type, is rich in features for these later classes of stars (see Figure 7.10). Brackett α is still present in early-G dwarfs and can be ratioed with Si I and Mg I lines to give temperature types. For the K-, and M-giants that are oxygen-rich, the vibration–rotation bands of SiO and the *P*-branch features of OH increase in strength. The unblended lines of the latter have characteristic trident shapes, a result of their being composed of four Λ -doubled and spin-split

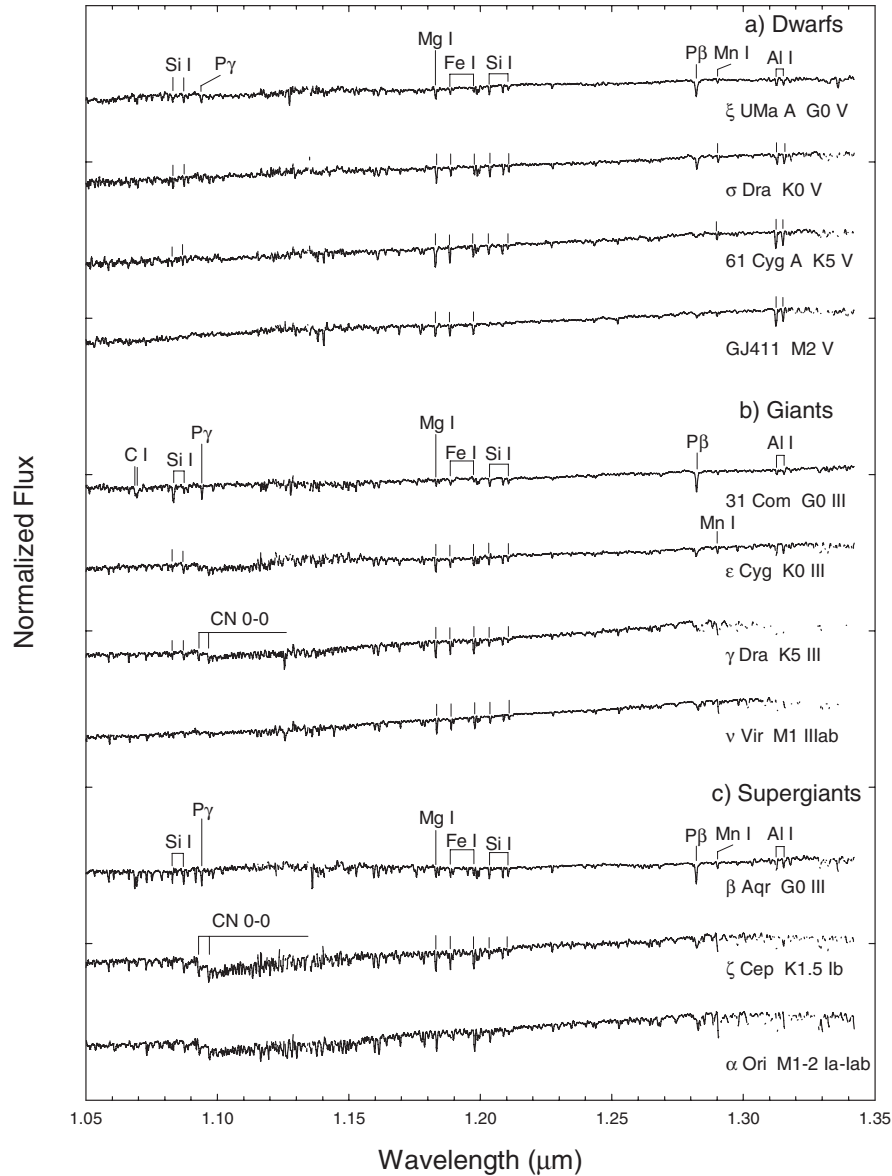


Figure 7.8 Temperature sequences for (a) late-type dwarfs, (b) giants, (c) supergiants in the infrared J-band. These spectra, taken from Wallace et al. (2000), have been slightly smoothed from the originals.

lines, the inner two being stronger and unresolved (see the P19 feature of the 1-0 band). The prominent atomic feature in this temperature range is the Mg I line, which contributes to the blend at $3.87 \mu\text{m}$. Since this is relatively unvarying, it is useful for temperature typing in this wavelength region.

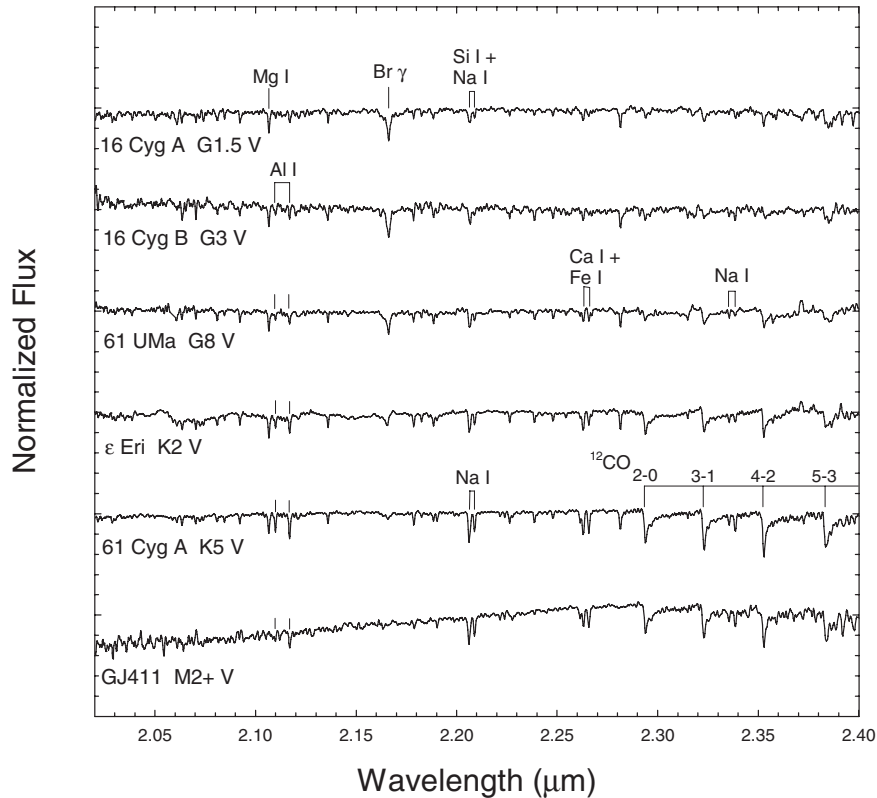


Figure 7.9 A spectral sequence for late-type dwarfs in the K-band. Brackett γ and nearby Na I and Ca I lines are marked. The spectra are from Ivanov et al. (2004) where sequences for giants, with and without metallicity effects, and for supergiants can be found.

7.4 THE SEARCH FOR A SOLAR TWIN; CHROMOSPHERIC ACTIVITY

7.4.1 A Solar Twin

Why do we care about finding stars most like the Sun? Thomas Ayres during a workshop at Lowell Observatory in 1997 gave these reasons: solar twins act as a surrogate for nighttime comparisons and calibrations, they allow the study of the envelope (i.e., range) of rare variability, like the Maunder minimum, and they give a broader perspective of the solar atmosphere's characteristics, such as activity, for what in fact is a complex star. Even the chemical composition of the Sun is under debate (Asplund et al. 2005), so our nearest neighbor star is not at all "simple," and those like it are worth finding and studying. In her classic review, Giusa Cayrel de Strobel (1996) distinguished three classes: *solar-like stars*, "a very broad class of stars, in which is found a mixture of late F, early, middle and, sometimes, late G type dwarfs and sub-giants"; *solar analogs*, "those unevolved, or slightly evolved Pop I disk stars with effective temperatures, degree of evolution, metallicities and kinematic properties not very different from those of the Sun"; and *solar twins*,

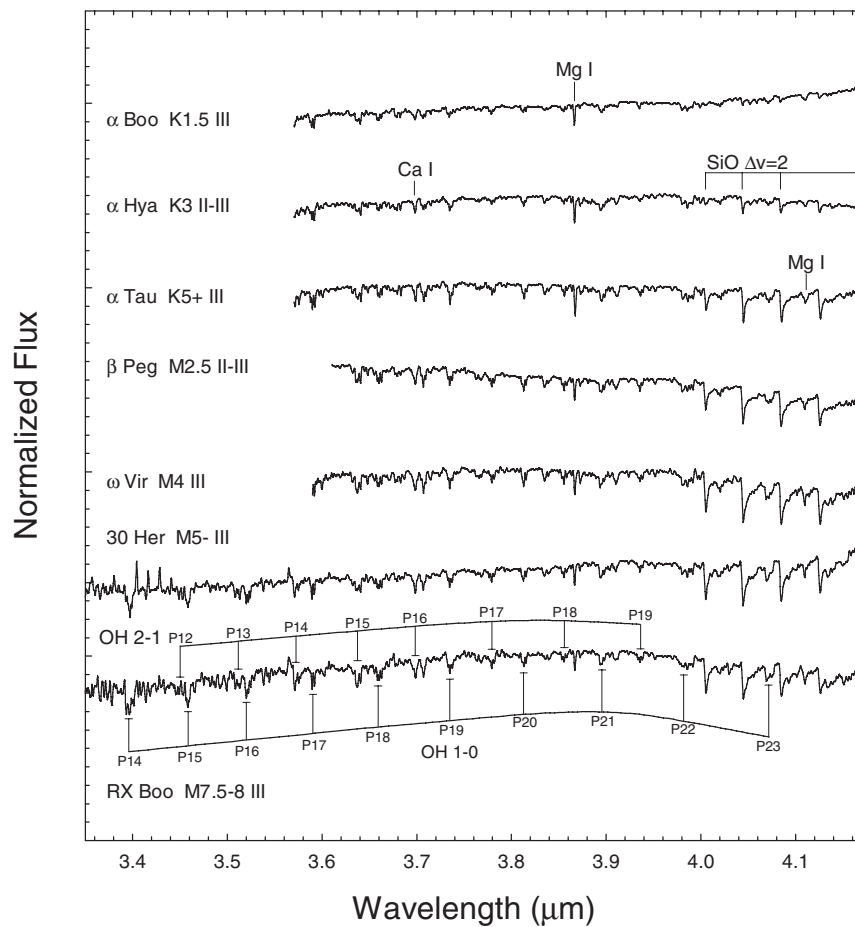


Figure 7.10 A spectral sequence for K- and M-type giants in the L-band. The labeled SiO features are band heads, whereas the OH features are blends of four *P*-branch lines. Spectra are from Wallace & Hinkle (2002).

the “ideal stars possessing fundamental physical parameters (mass, chemical composition, age, effective temperature, luminosity, gravity, velocity fields, magnetic fields, equatorial rotation, etc.) very similar, if not identical to those of the Sun.”

A search has to define its parameters and rank these in importance. Here lies the problem in finding a solar twin. Everyone has his or her own favorite parameters and their specific rankings among these. Then the question arises of how best to measure these parameters. At one stage the debate got testy (e.g., Hardorp 1980—see §1.3.5), but among the issues was that of the MK spectral type of the Sun, which classifiers affirmed, as a philosophical point, is and would always remain G2 V (Garrison 1979). The 1997 Lowell Observatory Workshop significantly advanced the debate by clarifying the issues and by settling on criteria and their ranking. There was even consensus as to the best current solar twin. It is clear from reading the proceedings how humor, as well as good leadership, helped

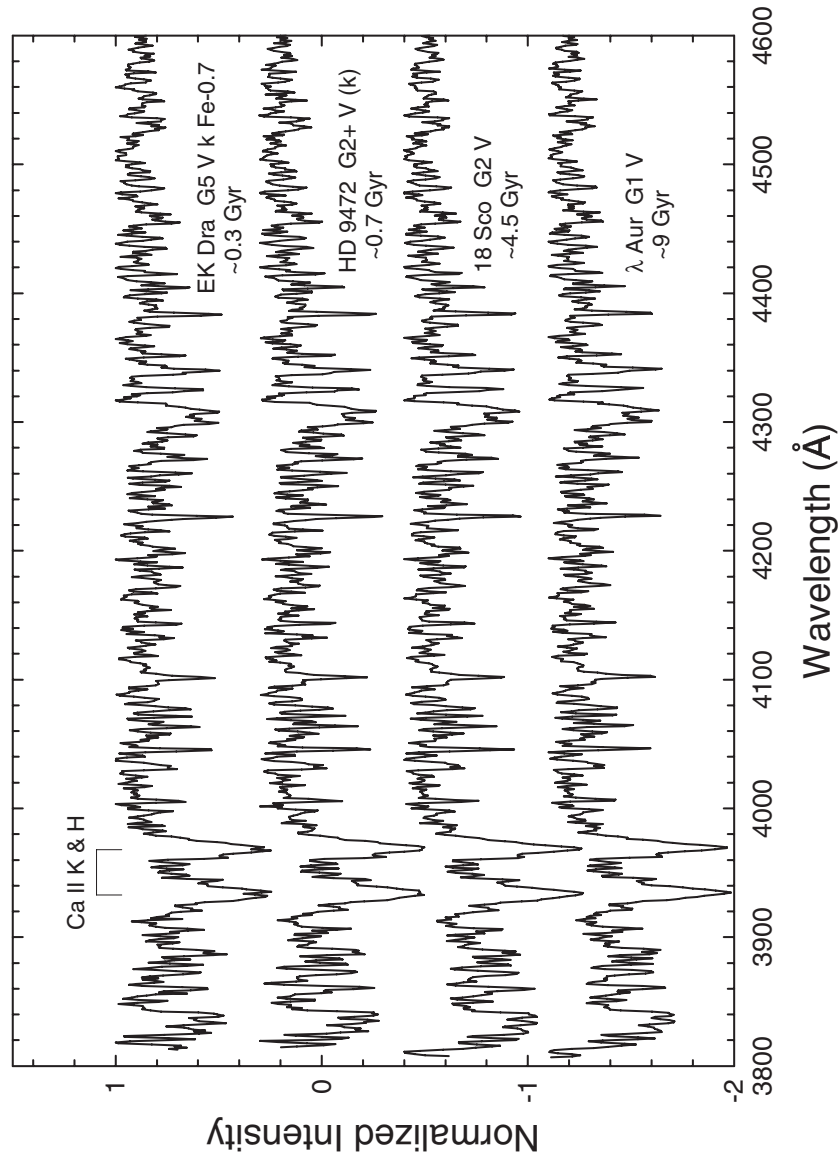


Figure 7.11 A Sun Through Time montage in which solar analogs have been chosen to represent different ages of the Sun. The spectral difference is most obvious in the Ca II H & K line cores. Note that the Lowell Workshop “pick” for the solar twin, 18 Sco, is included.

to keep the balance among participants. For the curious, the Lowell Workshop “pick” for the solar twin was HD 146233 = 18 Sco, while HD 217014 = 51 Peg, HD 186408 = 16 CygA, and HD 186427 = 16 CygB were equally good close analogs (for 18 Sco see Figure 7.11). However, Giusa Cayrel’s parting caution should be remembered, “We are not done.”

Four parameters were regarded as fundamental in characterizing stars and so in determining a twin to any particular star. These, not surprisingly, are

temperature, luminosity, metallicity, and activity, and all are equally ranked. There are, of course, a variety of ways to measure these, some more fundamental than others; and the value of the search data depends on the integrity of the measurements and the clarity of databases with respect to the origins, and so the reliability, of the data contained in them. The examination of medium-resolution spectra of stars is a powerful way to pick out analogs and twins. This will first give a precise spectral classification and then, when coupled with atmospheric models and photometric data, provide the parameters of T_{eff} , $\log g$, $[M/H]$, and chromospheric activity. From this methodology a Nearby Stars survey (Gray et al. 2003, and further papers in series) is offering examples of solar analogs and of candidates for having earth-like planets around them.

7.4.2 Chromospheric Activity

The search for a solar twin has raised the question of *stellar activity*. A difference in activity within the chromosphere between two otherwise similar stars indicates a difference in the nonthermal chromospheric heating, brought about by local magnetic fields, which in turn generally indicates a difference in age. The qualifier “generally” is used since a member of an old, tidally-locked binary system, such as ξ UMa B (Cayrel de Strobel et al. 1994), can keep a relatively high level of activity as a result of a higher than normal rotation speed.

For solar-type stars the best indicators of stellar activity are the emissions in the cores of the Ca II H & K lines, in the core of the H α line, and in the cores of the Ca II triplet lines, $\lambda\lambda 8498, 8542, \text{ and } 8662$. Other useful chromospheric lines for indicating activity are the Na I D lines and the Mg I b triplet. Accompanying their classifications in the blue-green spectral region Gray et al. (2003) have indicated different levels of chromospheric activity with the following notation added to the spectral types: “(k)” indicates that slight emission reversals or infilling of the Ca II K and H lines is visible; “k” indicates that emission reversals are clearly evident in the Ca II K and H lines but these emission lines do not extend above the surrounding (pseudo-) continuum; “ke” indicates emission in the Ca II K and H lines above the surrounding (pseudo-) continuum, usually accompanied with infilling of the H β line; and “kee” indicates strong emission in Ca II K and H, H β , and perhaps even H γ and H δ . Figure 7.12 shows examples of spectra with these different activity levels. Because chromospherically active stars tend also to be variable, the chromospheric activity type will also vary. Therefore the observation date should be noted when an activity indicator is given as part of the spectral type.

The standard *quantitative* measure of chromospheric emission is $\log(R'_{\text{HK}})$, which is essentially independent of the star’s effective temperature. This quantity was derived by Noyes et al. (1984) from the Mount-Wilson index (Baliunas et al. 1995), which is a measure of the depths of the Ca II H & K lines in relation to the nearby continuum. In such measurements of activity attention must be paid to metallicity and luminosity effects, the more important being the former (Chmielewski 2000).

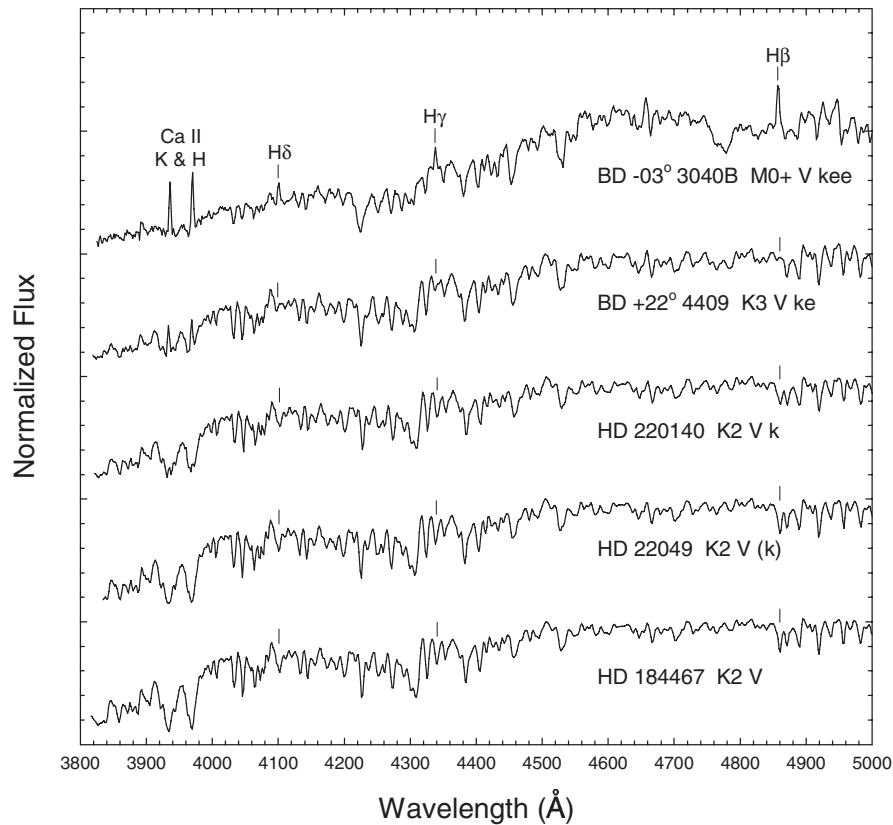


Figure 7.12 Spectra showing increased chromospheric activity, starting at the bottom with the normal, inactive star HD 184467. The Gray et al. (2003) notation for the different levels of activity is given after the spectral type.

The fruit of well-determined measures of chromospheric activity is in having an estimate of the star's age, though Soderblom et al. (1991) find some ambiguity over what relationship gives the best fit. Other age estimators are the comparison of a star's luminosity and temperature with a grid of isochrones and the depletion of its original lithium abundance. For the former, obviously a measure is first needed of its metallicity since different compositions produce different isochrone sets. The latter, Li-depletion, is not as straightforward an indicator of age as might be expected, and besides it continues to have conflicting theoretical explanations (Cayrel de Strobel 1996) (e.g., Mallik et al. 2003). There remains interesting work to be done here. Meanwhile, Figure 7.11 gives a spectral montage of how the Sun might appear at different ages.

7.4.3 RS CVn Binary Stars

The RS CVn binary stars fit among the late-type active stars. Their hotter component is of F- or G-type and luminosity class V or IV. While at classification

dispersion their spectra are relatively normal, they have emission in their Ca II H & K lines and often at H α also. They show velocity and light variations characteristic of binaries with large star spots on their surfaces, so their definition is not purely spectroscopic (Hall 1976). In the UV they have strong emission in the Mg II lines around 2800 Å and in the chromospheric lines between 1200 and 1900 Å. They also have strong radio and X-ray emissions, all of which indicate active coronae (Ramsey 1990).

The spectrum of TZ CrB, a good example of an RS CVn-type, is shown in Figure 7.13. While at first glance it may appear a normal star, the quite strong emission in the core of the Ca II H & K lines is obvious. There is also an overall *veiling*, or weakening of the lines, including those of hydrogen. Hence the weakening is not due to an abundance effect, but to a non-normal temperature structure in its atmosphere. The temperature type, G1, comes from the ratio of the temperature-sensitive lines rather than from their absolute strength, as its luminosity does from the respective ratios too. The overall spectral morphology is of an early-G, slightly evolved star.

7.5 T TAURI STARS

The systematic study of T Tauri stars (TTS) was initiated by Alfred Joy (1945), who recognized them as a distinct class of emission-line variable stars, occurring in association with nebulosity. It was gradually realized that they are the pre-main sequence (PMS) precursors of solar-type stars (Herbig 1962). They are the cool counterparts to the Herbig Ae/Be stars (see §5.5) and share the importance of these in the study of star formation. Like them they are characterized by emission features in their spectra, so spectral classification plays an important role in finding the T Tauri stars. Traditionally, as in the classic review of Appenzeller & Mundt (1989), they are divided into “weak-line T Tauri” stars (WTTS) and those with stronger Balmer-line emission, the “classical T Tauri” stars (CTTS). The WTTS are sometimes called the Naked T Tauri stars (NTTS), and the boundary between the WTTS and the CTTS is somewhat arbitrary since it is based on differing measures of the H α equivalent width; some use $W(\text{H}\alpha) < 10 \text{ \AA}$ for defining the WTTS whereas others use $W(\text{H}\alpha) < 5 \text{ \AA}$ (Martín 1997). As well as in the hydrogen lines, the emission can also be seen in Ca II, Fe II, Na I, and fluorescent Fe I ($\lambda\lambda$ 4063, 4132), and sometimes in [O I] and [S II] lines. Hence the emission lines resemble those from the solar chromosphere. Underlying these is an absorption spectrum, generally veiled, which can be anything from G to M. If the absorption spectrum is earlier and between F0 and G2, then they would be called early-type T Tauri stars (ETTS) according to Mora et al. (2001) of the EXPORT group. Abnormally strong Li absorption at $\lambda 6708$ and P Cygni-type line profiles, especially for the H α and the Ca II K-lines, are also characteristic of TTS (Herbig 1962). The former indicates that these are young objects, and the latter that they have mass outflow.

All the TTSs share an ambiguity with their early-type cousins, the Herbig Ae/Be stars, in that the original definition of this group included their association with

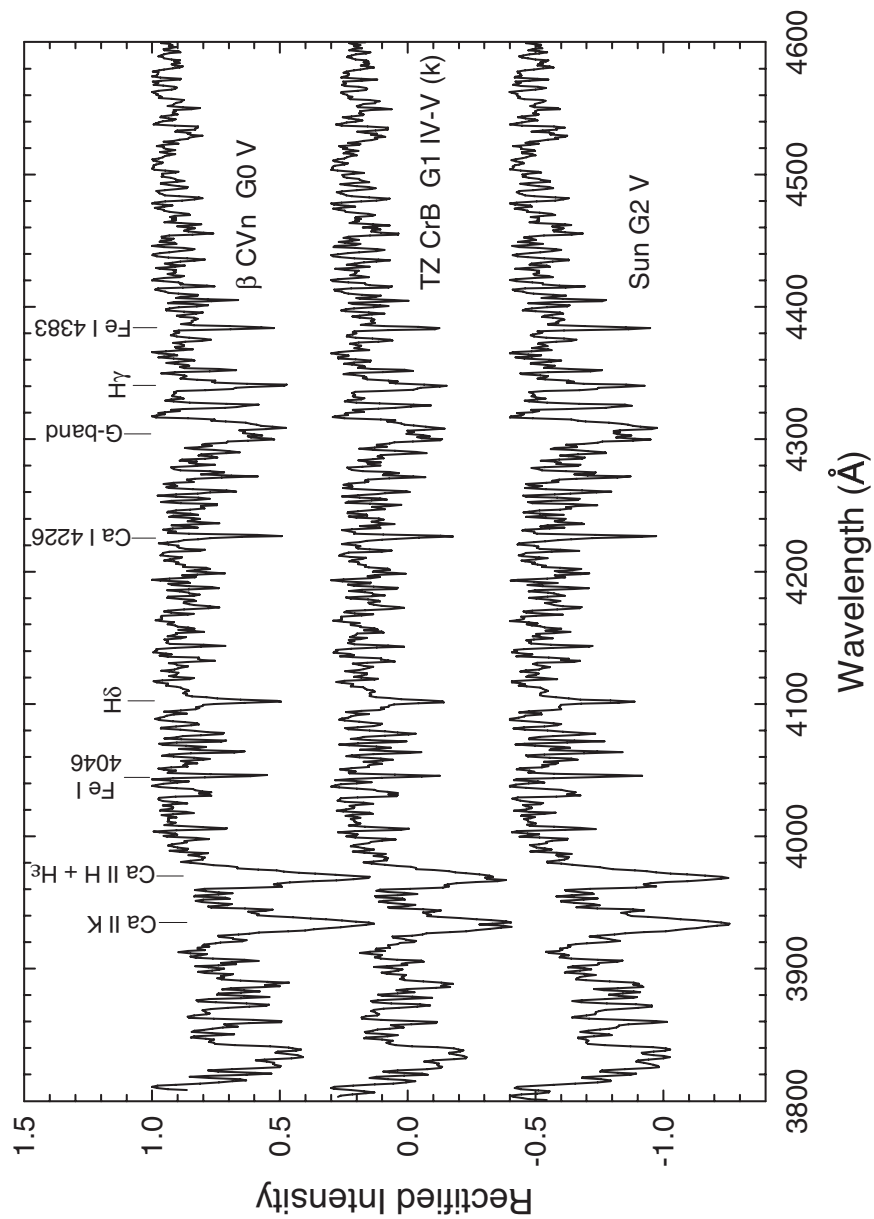


Figure 7.13 The RS CVn-type binary star, TZ CrB, is shown between G0 V and G2 V standard star spectra. Marked are the spectral features useful for typing. Note the emission reversals in the cores of the Ca II H & K lines of TZ CrB. Its spectrum also shows slight veiling in all lines, including the hydrogen lines. These 1.8-Å resolution spectra were taken at the Dark Sky Observatory.

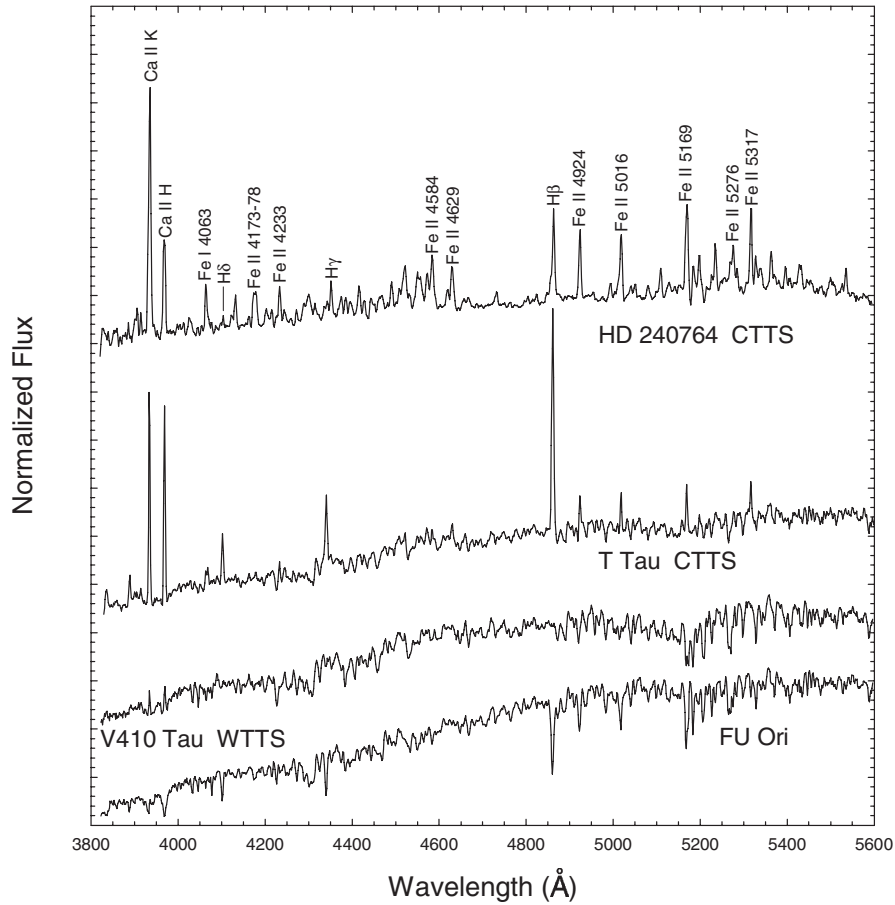


Figure 7.14 A montage of T Tauri stars and the FUor prototype.

nebulous regions of the Galaxy, and so the characterization has not been purely a spectroscopic one. Yet there are examples of late-type emission stars with no nebula nearby or even with no infrared excess. The incidence of disks and IR excess associated with CTTSs and WTTSs has been discussed by Lada et al. (2006) based on *Spitzer Telescope* IR observations. Here we are more concerned with their spectral classification characteristics.

TTSs are identified most readily from the emission in the Ca II H & K lines and, for spectra of K5 and later, from the emission in the H α line (Walter et al. 1988). These emission lines sometimes show P Cygni profiles. A montage of several TTSs and a FUor (see below) is shown in Figure 7.14.

Before leaving the T Tauri stars, the small FU Ori group should be mentioned (see review by Hartmann & Kenyon 1985). Post-eruption these stars show a mixture of supergiant spectra that gradually change to later types. One of them, V1057 Cyg, had a TTS spectrum before its outburst, and given their

association with nebulosity these “Fuors” must also be young objects. The contending explanations for their outbursts include accretion from a circumstellar disk, from a companion star, and the influence of a massive planet, so they remain enigmatic.

7.6 CHEMICALLY PECULIAR G- AND K-GIANTS

From the PMS stars we turn to those evolved away from the main sequence. For some the progress through the giant phase has been relatively tranquil; for others deep dredge-up of the products from interior nuclear burning has occurred via their convective envelopes, and so the abundance of elements in their atmospheres has changed from its original state. These abundance effects are seen particularly in carbon and the *s-process elements*. The “mixing” can be considerably enhanced within a binary scenario, as depicted in Figure 8.25. This reference to the next chapter indicates that the carbon-enhanced G- and K-giants are the hot extension of what appears as the carbon-star phenomenon in the M-stars.

The classification of chemically peculiar yellow giants has a history strongly associated with Philip Keenan and his collaborators. This work culminated in the Revised MK System for stars G0 and later. A large set of standard stars (Keenan & Yorka 1988; Keenan & McNeil 1995) defined the System and its indices of peculiarity, e.g., CN-1, CN-2, CH+1, CH+2, etc.

7.6.1 Strong-CN Stars

The top two spectra in Figure 7.15 are of strong-CN stars, identified most obviously by their enhanced CN-band features but also with the C_2 band strong. For illustration, a star with a slightly weak CN band, 16 Aur, is also included. Classification, both of temperature and luminosity, is first made independently of the carbon features (see §7.2.1 and §7.2.2) and then an index of the carbon-feature strength is given.

Strong-CN stars became a hot topic in the 1970s and 1980s after they were labelled super-metal-rich (SMR) by Spinrad & Taylor (1969). Through attention to improved standards and methods by, e.g., Schmitt (1971, careful CN classification), Keenan et al. (1987, use of the Revised MK System), and Griffin & Holweger (1990, caution w.r.t. parameter determination, especially T_{eff}), the numbers of abnormal stars were considerably reduced and their metallicity then compared more closely with the Sun’s. Thus the “super” label was dropped. Still, there are indeed G- and K-stars with higher than solar metallicities, and classification of these should be treated with caution.

7.6.2 Weak-lined Stars

Carbon-poor stars are also found, and they have an origin related to internal changes in the star itself rather than to external factors as in barium stars

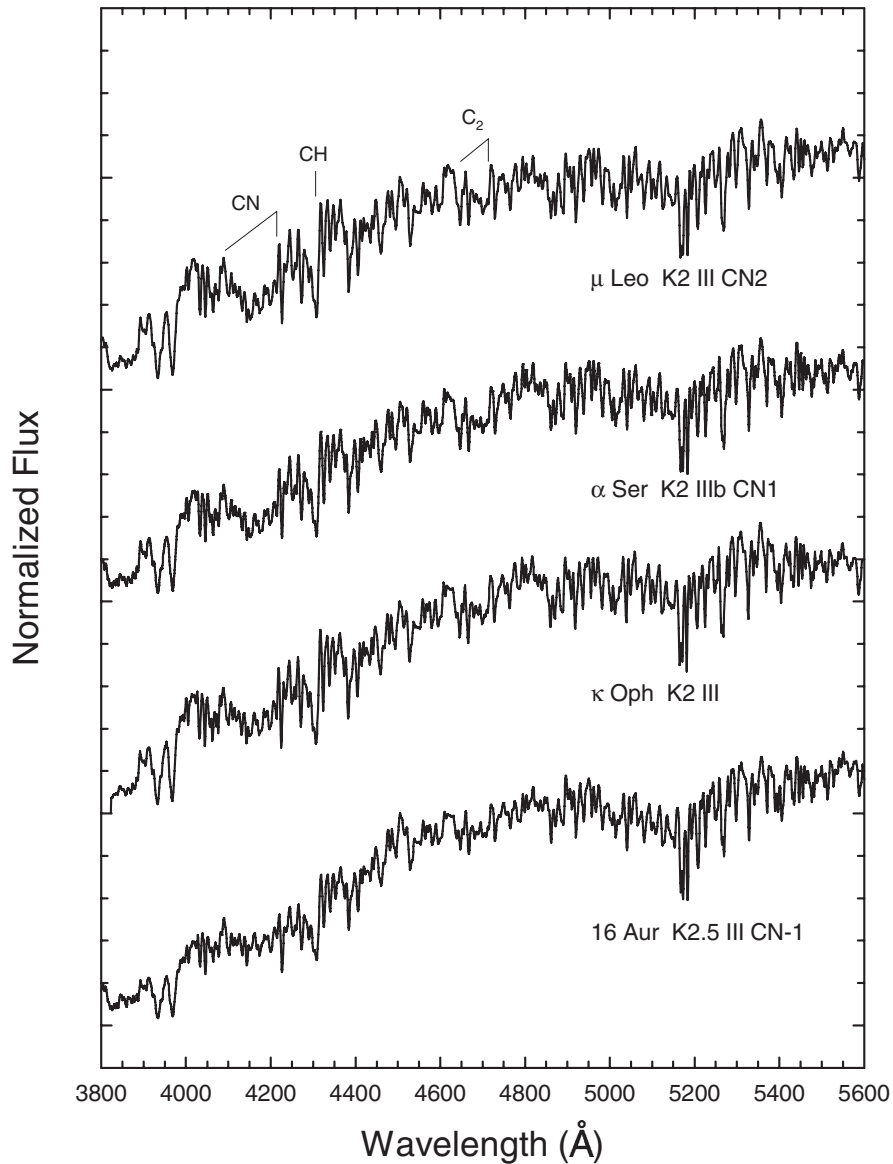


Figure 7.15 Giant stars, grouped around the normal K2 III standard, with different CN and C_2 band strengths. The luminosities of such chemically peculiar stars are determined independently of these bands.

(see §7.6.3). We have seen 16 Aur in Figure 7.15, and we can look at two further typical manifestations of a carbon-poor star at the bottom of the next figure (7.16). HR 6791 has only a slightly weakened CN $\lambda 4216$ band but a very weak G-band (CH). This can be explained since carbon preferentially forms the CN molecule over the CH molecule. In 37 Com it is only the G-band that is somewhat weak, and hence this suggests that carbon is more abundant than in HR 6791,

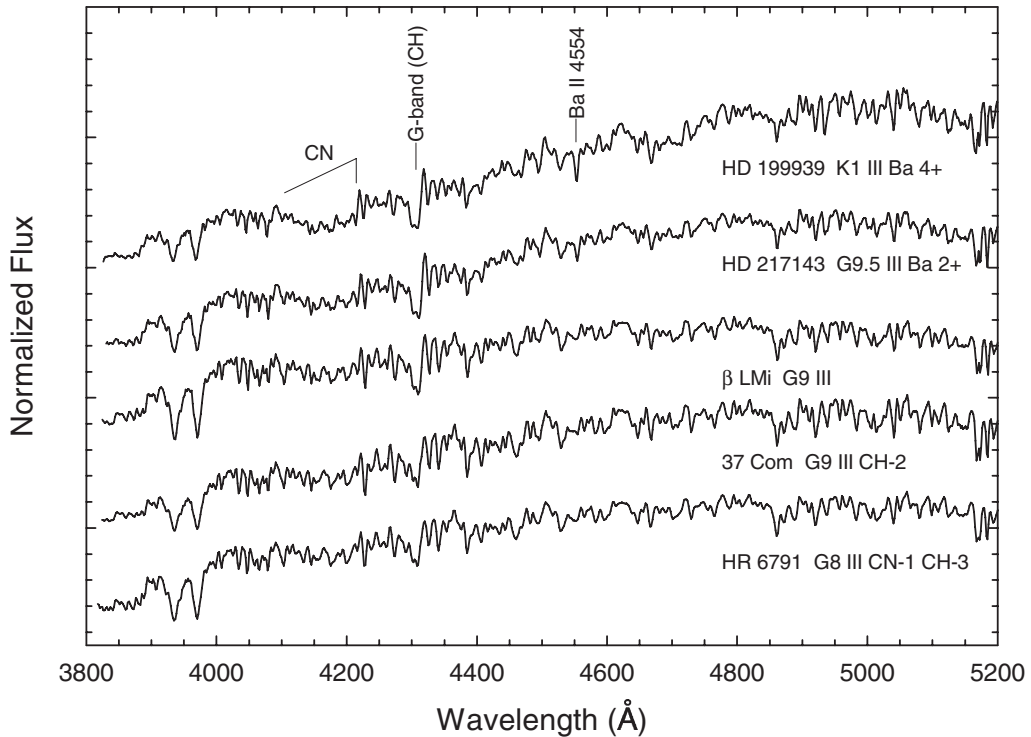


Figure 7.16 A late-type giant, HR 6791, with a slightly weak CN $\lambda 4216$ band but a rather weak G-band (CH) is compared with a slightly less weak G-band star above it and a normal standard. Above these are two more late-type giants showing enhanced Ba II $\lambda 4554$ lines, among other strong features. Note the strong CN of HD 199939, which is even stronger than the top star in the previous figure (7.15).

though Lambert & Ries (1981) and Luck (1991) indicate $[C/H] \approx -0.70$ for both. The former reference links the first dredge-up phase in a red giant star, a period after $C \rightarrow N$ processing has occurred, with an expected depletion of carbon in its atmosphere, just as is shown by these two carbon-weak evolved stars.

7.6.3 Barium Stars

The top two peculiar stars in Figure 7.16, HD 217143 and HD 199939, are typical “barium star,” which were first called the “Ba II stars” in the announcement of this new class by Bidelman & Keenan (1951). This announcement built on investigations of Ba II $\lambda 4554$ strengths by such as Merrill (1926) and Morgan (1933). Cora Burwell (1938) at Mt. Wilson was noticing abnormally strong barium lines, including those of the red triplet (Ba II $\lambda\lambda 5854, 6142, 6497$), in A-type stars, subsequently recognized as the Am stars, as well as in some late-type stars.

In barium stars an enhanced resonance line of Ba II $\lambda 4554$ is accompanied by enhanced Sr II $\lambda\lambda 4077, 4216$ lines and, less noticeably, the Y II $\lambda 4376$ line. Notice

how the strength of the CN band and, less obviously, the G-band of CH are also enhanced. These enhancements of the *s*-process elements barium, strontium, and yttrium, and of carbon, are presently understood to be due to “dredge-up” by deep convection currents of the advanced products of nuclear burning from the interior to the surface of asymptotic giant branch (AGB) stars. This enriched material is then transferred from the AGB star to its now “barium star” companion, as described for barium giants in §8.4.3, and for barium dwarfs in §6.5.2.

Barium star spectra also show the Bond–Neff depression (Bond & Neff 1969), which is a broad drop in the continuum between 3500 and 4500 Å. The fine review of barium stars by McClure (1984), in pointing out that the abundance of elements determined from lines in this region is lower than normal, indicates that the origin of this depression is in the line-forming region of the photosphere, rather than above this in a circumstellar shell. However, its explanation is still not clear. What can be said from the fact that barium stars show *JHK*-band excesses, but not at 12 μm and farther into the infrared (Chen 2001), is that the flux from the Bond–Neff depression becomes redistributed into the IR. It was thought that the IR excess in a barium star might mainly be due to thermal emission from circumstellar material caused by the mass transfer scenario from what is now its WD binary companion (as above and in Figure 8.25). However, this would give excess flux *throughout* the infrared region, and this is not seen.

Classifying the carbon-peculiar and barium stars follows that of normal G- and K-stars, save that Sr II lines and the violet-system CN bands cannot be used for luminosity (see §7.2.2). It appears better to rely instead on the Y II λ4376 line, ratioed to nearby neutral species like Fe I λ4383. For the barium stars one should also be aware of less extreme barium enhancement both in the “mild barium stars,” with Ba II and Sr II only slightly enhanced, and in the “marginal” or “strontium” stars with just Sr II enhanced. This nomenclature follows a suggestion of Bond (see McClure 1984). In addition, *Dwarf* barium stars can be found among the F- and G-type stars (§6.5.2), and the exchange of processed material in a binary scenario also appears to be the best explanation for them.

7.7 POPULATION II AND III STARS

What are the oldest, most primitive stars in the Galaxy? This is a question that bears strongly on Galactic history because according to standard Big Bang nucleosynthesis the first stars had zero abundance of metals, the true “Population III” stars. Even those with slightly higher abundances, the extreme Population II stars, are important tracers of the early epochs of Galactic formation, help understand nucleosynthesis products and their mixing, and give insight into the nature and interplay of various stellar populations (Beers 2000). The hunt for the most metal-weak stars has a natural focus in G- and K-types. The giants are relatively luminous and so reach to large distances, despite the disadvantage that giant stars are subject to dredge-up and hence display non-primitive abundances; while the metal-weak dwarfs and subgiants have not been neglected (Kraft 1987),

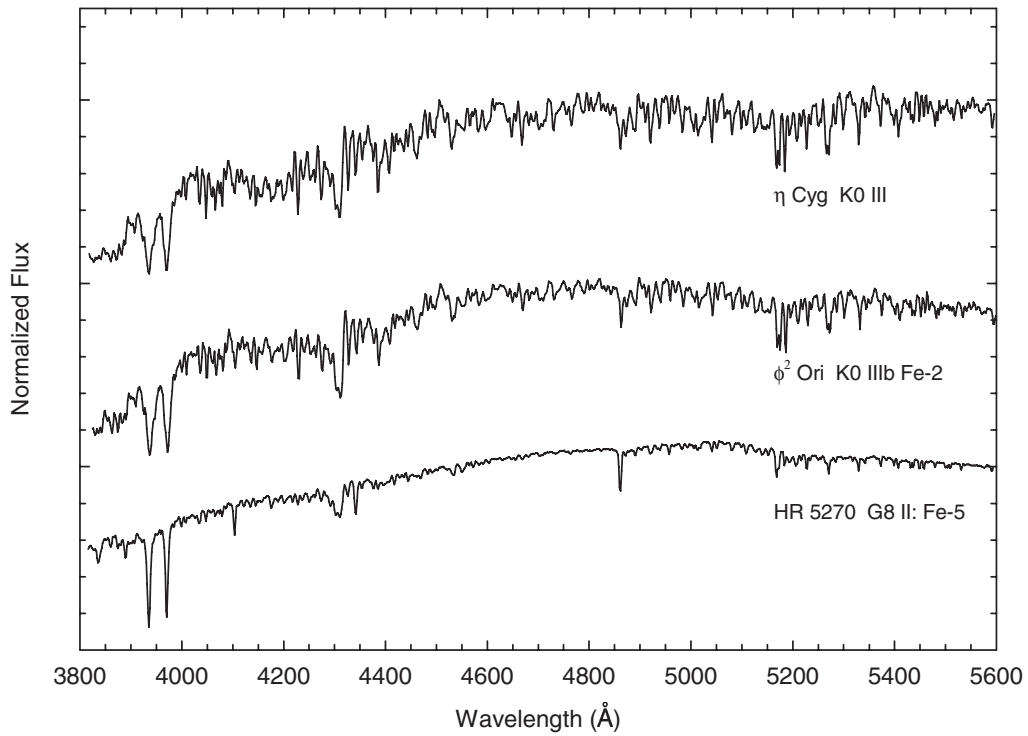


Figure 7.17 Two metal-weak giants shown under a normal K0 III standard. The classifications and Fe indices are those of Keenan & McNeil (1995).

since their ages can come close to that of the Galaxy. Given the stakes, it is not surprising that a certain amount of controversy has attended the hunt, as also happened with the strong-lined or SMR stars of §7.6.1. Pitfalls in the way of achieving true abundance determinations include line equivalent-width measures, transition probabilities or gf-value determinations both in the laboratory and for solar lines, besides the all-important T_{eff} parameter (see Peterson et al. 1990).

With respect to classification, the spectra of the late-type metal-weak stars have had a similar history to those in the F-type range (see §6.4), and not surprisingly the same remarks apply to their classification as in §6.4.1. They are illustrated in Figure 7.17, where HR 5270 is clearly an extremely metal-weak star with an $[\text{Fe}/\text{H}]$ of about -2.7 , while the intermediate ϕ^2 Ori is at about -0.5 . Their temperature types are derived from the absolute strength of their hydrogen lines, and their luminosities come mainly from the Y II 4376/Fe I 4383 ratio (but, as in §7.2.2, beware of using this if s -process elements are enhanced). For the G-class of hydrogen types the “Fe index” can be derived from the difference in subtypes between the hydrogen-line type and the metallic-line type according to the “Corbally 1987” formula given in §6.4.1. The Keenan metallicity index given for the classifications in the figure is an arbitrary, while smooth indication of progressive weakness of the metallic features in a spectrum. After K0 the calibration

of the Corbally Fe index with metallicity is less certain, so the better indication of weakness becomes that of giving the average of the metallic-line type. Thus, “K2 V mG5” would be a spectrum showing K2 hydrogen strength and averaging G5 in its strong and weak metallic lines, with no indication that the star is evolved from the main sequence.

After K5, even the metallic-line type index breaks down since some increasing continuum opacity in the blue-violet weakens the metal lines so that comparison with earlier types becomes inappropriate. This weakening can be seen in Figure 8.1 of the next chapter. This caution recalls the remarks in §6.4.1 that concern the problems of making a convincing match of the weakened lines in a spectrum to an earlier-type, normal spectrum. For the later-type weak-lined stars the real solution is again to have a grid of appropriate metal-weak standards, as in the “Gray 1989” system. Philip Keenan and collaborators have laid the groundwork for such a grid, as can be seen by selecting the “Fe-” stars in (Keenan & McNeil 1995). This is a task remaining to be completed, but one that promises accompanying astrophysical insights.

Of course, stars maintain an ability to surprise, so one should be aware of two very metal-poor giants, CS 22948-27 and CS 29497-34, which have $[\text{Fe}/\text{H}] \approx -3$, but large C and N (and *s*-process elements, and Eu) abundances relative to that of Fe (Hill et al. 2000). Explanations include mass-transfer from a binary companion, accretion from passage through interstellar clouds, and anomalies in the initial material of formation. The alert classifier can be the first to find and probe such mysteries.

7.8 THE HIGH LUMINOSITY, YELLOW VARIABLES

7.8.1 Cepheid Variables

If Henrietta Leavitt and Edwin Hubble are associated with the discovery in 1909 and the exploitation from 1923 of Cepheid variables as “standard candles” for extragalactic distances via their period–luminosity relation, then Harlow Shapley and Cecilia Payne can be associated, among their many significant studies, with the early classification of these variable supergiants, so named after their prototype, δ Cephei. As a prime instance, C. J. Krieger (1934), while doing a careful study of δ Cephei’s line variations, cites Shapley and Payne as finding that it had an average range in spectral type between F2 at maximum to G4 at minimum light. Figure 7.18 shows its current variation is less, but this is assessed according to the MK system rather than the earlier one of Harvard.

At this point it is well to distinguish the classical Cepheids, which belong to Population I stars and so are found in the Galactic plane, from the type II Cepheids, often called “W Virginis variables” after their prototype, which being from Population II belong in the Galactic halo and typically are found in globular clusters. This distinction was recognized by Baade (1952) and of course led to the separation of the period–luminosity relations for the two kinds of Cepheids. Since the classical Cepheids turned out to be about a magnitude brighter for the same period than the

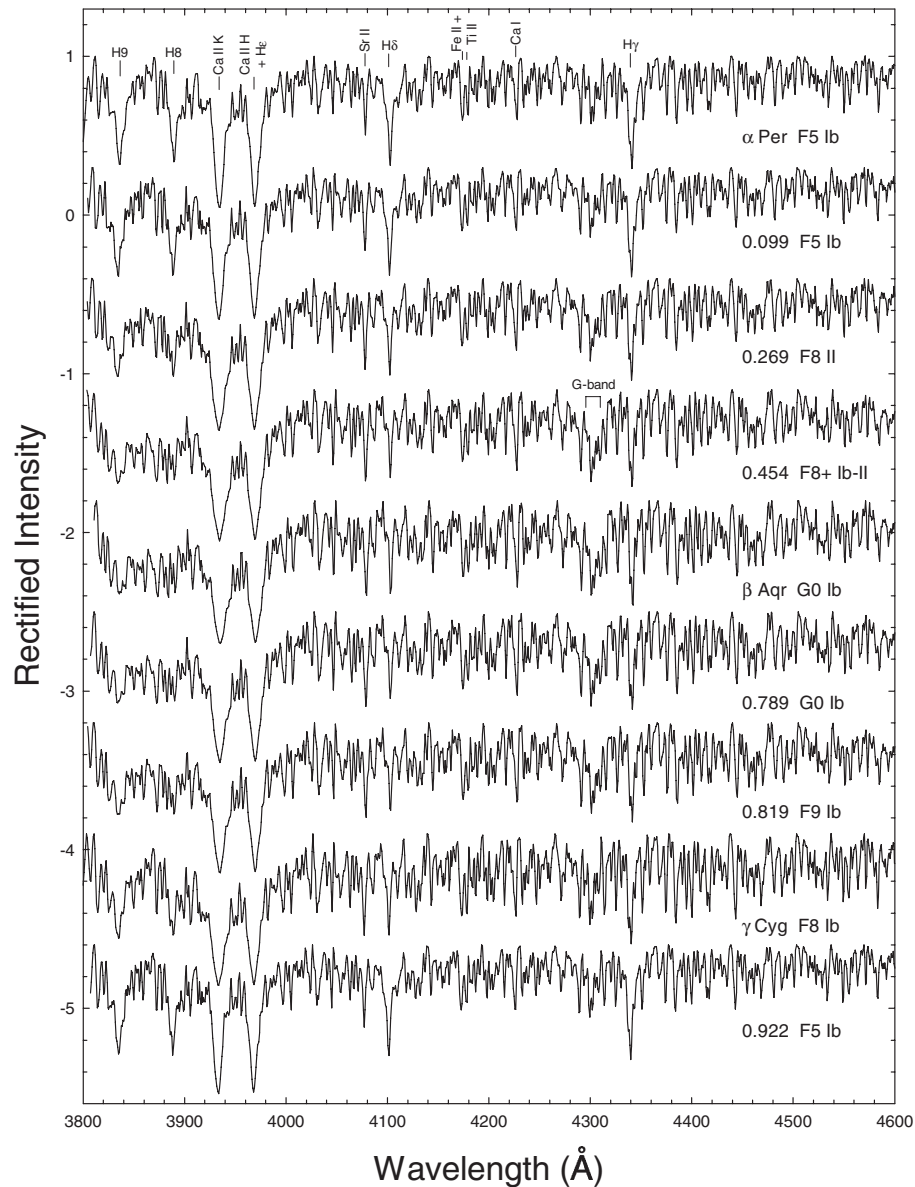


Figure 7.18 Spectral variations with phase for δ Cephei. Its spectra closely match that of the standards, though at G0 Ib its hydrogen lines are slightly weak. Spectra are from the Dark Sky Observatory.

type II Cepheids, the distance to the Andromeda Galaxy, which was based on the former, doubled overnight and with it the scale of the universe. Classical Cepheids have periods between 2 to 50 days, while type II Cepheids range between 0.75 to about 30 days (Wallerstein & Cox 1984). The type II Cepheids with periods up to 5 days are also called BL Her stars. Those with periods longer than 20–30 days are the RV Tauris (see §7.8.2).

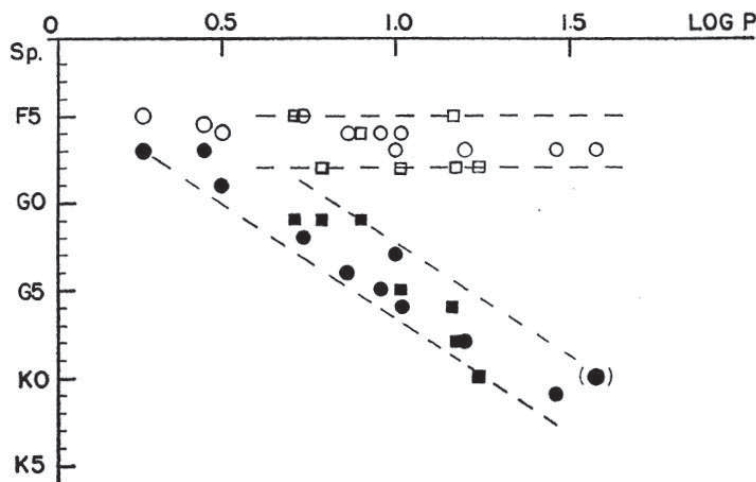


Figure 7.19 Spectral types at maximum (open symbols) and minimum phases for classical Cepheid variables plotted against their periods (Code 1947). Circles are observations by Code; squares are those by Struve. Gauthier & Garrison (1984) confirmed that at maximum light the spectral types fall in the narrow range F5 to F8. Figure reproduced by permission of the AAS.

Classical Cepheids have been classified spectroscopically since the HD Catalogue days, but precision studies of the spectral variations through their luminosity cycles had to await the MKK atlas with its grid of supergiant spectral standards. Otto Struve (1944) took first advantage of these, closely followed by Art (Code 1947). In the latter paper we find the figure reproduced here as Figure 7.19. This shows the spectral types of classical Cepheids at their maximum and minimum light plotted against their periods. At maximum light their spectra fall in the narrow range of F5 to F8, an observation confirmed by Gauthier & Garrison (1984), while their spectral types at minimum get later as the period increases. Gauthier refined Struve and Code's study with the aid of updated supergiant spectral sequences. His work (Gauthier 1983) showed that, while the weaker metal lines throughout the period variations could always be found to match with those of nonvariable supergiants, the strong lines and the $H\delta$ and $H\gamma$ lines increased in their departures from the normal as both the amplitudes and periods of the light variations increased. In the spectral montage for different phases of δ Cephei (Figure 7.18) the only really noticeable departures from the norm are near minimum light, phase 0.789, when the hydrogen lines are slightly weak compared with the G0 Ib standard, β Aquarii.

The spectral characteristics of type II Cepheids, the W Vir variables, while also those of supergiants, are markedly different from those of the classical Cepheids. The hydrogen emission characteristic of W Vir was first noted by Joy (1937). To complete their characteristics we can now list that the type II Cepheids are metal-weak stars; their spectral ranges are earlier and wider than the classical Cepheids,

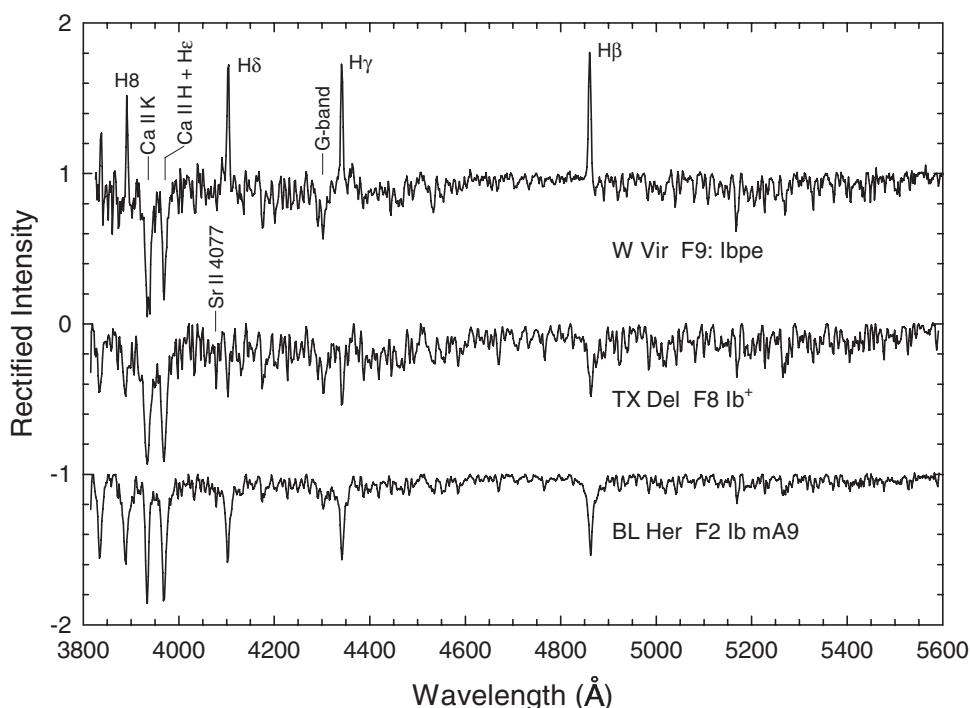


Figure 7.20 A spectral montage of type II Cepheids in increasing temperature. W Vir shows the hydrogen emission characteristic of type II Cepheids, and there is also an emission reversal in the core of its Ca II K-line. The line strengths of TX Del, sometimes called a type II Cepheid, are nonetheless normal for a Pop I supergiant, while those of the short period, type II Cepheid, BL Her, are certainly slightly weak for its F2 temperature type. Spectra are from the Dark Sky Observatory.

going from mid-A to G0, and with no clear spectrum–period relation; most notably, their hydrogen lines are in emission during increasing light and partially filled-in thereafter, so their atomic metal species (Fe I, Ca I, Cr I, and Ca II for earlier types) must be used for typing them; even He I $\lambda 5876$ has been observed in W Virginis during rising light from phase 0.84 to 1.01; Mg II 4481 is generally weak; also Fe, Sr, Sc can be weak to varying degrees. Wallerstein (1958) concluded from these characteristics that greater individualism exists among these type II Cepheids than for the classical Cepheids.

A spectrum of W Vir is shown in Figure 7.20. The “p” and the uncertainty in temperature type, notated by the colon, are due to the morphology of its spectrum not being a good match to a late-F supergiant. Clearly the strong emission in the Balmer lines not only shows that it was observed near maximum light, but indicates why the temperature structure of its atmosphere was not at all normal then. The bottom star in the montage, BL Her, is a short-period type II Cepheid and has a spectrum more like an early-F, metal-poor supergiant. An extensive abundance analysis of the W Vir stars in contrast to the BL Her stars was given by

Maas et al. (2007), and this study also showed that both kinds of variables give evidence for atmospheres contaminated with triple- α -process and CN-cycling products.

The middle star in Figure 7.20, TX Del, looks like a normal-metallicity supergiant, as if it is a classical Cepheid near maximum light. It is generally cited in the literature as a type II Cepheid, following the criteria of Harris (1985), but Balog & Vinko (1995) argue from its derived radius being three times that expected of such that it is instead a classical Cepheid. The spectrum shown here supports that conclusion. If not, TX Del certainly participates in the “greater individualism” of the type II as opposed to classical Cepheids.

No systematic spectral classification of Cepheids and their variations has been done in the spectral regions beyond the optical. However, these are important in their study. For example, the Mg II features in the UV are particularly helpful for the study of atmospheric shocks and/or chromospheric activity in these stars with highly extended atmospheres, and the two classical Cepheids, Polaris and β Dor, show strong C III ($\lambda\lambda 977, 1176$) and O VI ($\lambda\lambda 1032, 1038$) emissions in FUSE spectra, indicative of plasma well above the photospheric temperatures (Engle et al. 2006). As for the infrared, while radial-velocity and line-profile variations appear similar to those in the optical region (Butler & Bell 1997), their circumstellar dusty disks have great potential for study in this spectral region (Kervella et al. 2006).

7.8.2 RV Tauri Stars

RV Tau stars are a set of rare, pulsating red supergiants. The classic study of Preston et al. (1963) distinguishes three groups, as illustrated in Figure 7.21. Group A stars, the GK variables, have G- or K-type spectra, but some irregularities may be seen, such as TiO bands at deep light minima. Group B stars, the Fp(R) variables, range from F5 to G0, but their Ca II H & K lines are weaker or earlier than their hydrogen-line type, and the CH and CN bands vary considerably with phase of the variable. Group C stars, the Fp variables, have hydrogen-line types and weak Ca II lines like group B, but without the variations in CH and CN bands, which are weak or absent at all phases.

The yellow semiregular variable stars, “SRd,” are distinguished from the RV Tau stars by having strong emission in the Balmer lines at maximum. Such emission is rarely seen in RV Tau stars and is then always weak. Like the Fp variables, the CN bands are weak or absent, but the overall morphology indicates types later than F, so these are often just classed as “Gp” or “Kp.”

Further peculiarities can occur in individual RV Tau or SRd stars. These peculiarities may also be a phenomenon associated with a specific phase in their history. For instance, R Scuti is a group A RV Tau star, whose G-K Ia absorption spectrum turned at one deep minimum in 1981 into strong TiO bands and an array of narrow emission lines of the neutral metals, as if one were looking at a reversed photospheric spectrum and suggesting a purely chromospheric origin of these neutral

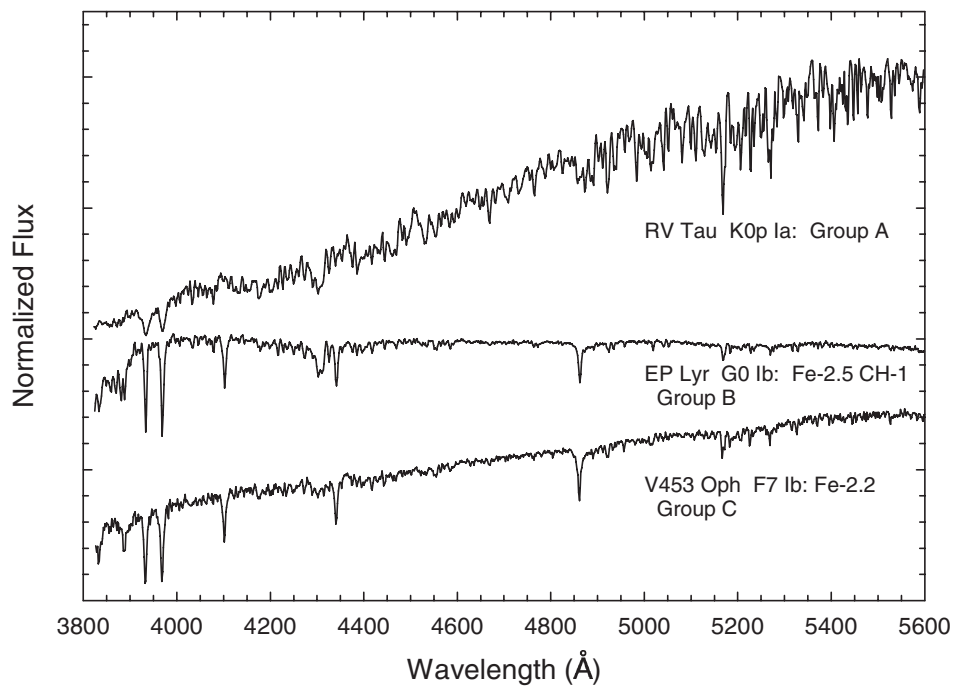


Figure 7.21 The three groups of RV Tau stars are illustrated.

lines (Howell et al. 1983). Modelling these stars gives scope for understanding complex velocity structures and shock fronts, as well as circumstellar shells from mass loss in their AGB stage of evolution.

7.8.3 Post-AGB Stars

In addition to the Cepheid variables and the RV Tau stars, there are other pulsating, yellow supergiant stars. These are the *post-Asymptotic-Giant-Branch* (post-AGB) stars, which are losing mass and quickly evolving to hotter stars, so to form planetary nebulae, and then onto becoming white dwarf stars (see §12.1 and the review of van Winckel (2003)). Typical of these transition objects among late-type stars are V1027 Cyg and HD 179821, whose spectra are shown in Figure 7.22.

V1027 Cyg as seen here in the blue-violet region is a G7 Ia supergiant, but in the NIR Winfrey et al. (1994) classify it as later, a K2-4 supergiant. HD 179821 is in the Perkins Catalogue (Keenan & McNeil 1995) as G4 0-Ia, but not as a dagger or standard-type star. The metallicity of both stars seems normal at classification dispersion, though hotter post-AGB stars can appear selectively metal-weak, imitating the λ Bootis-type stars abundances (§5.6.2).

Given their cool, dusty disks/shells, it is not surprising that the post-AGBs show infrared luminosity excesses, and so this provides a way to discover them, as demonstrated by Suárez et al. (2006). This paper also contains an atlas of

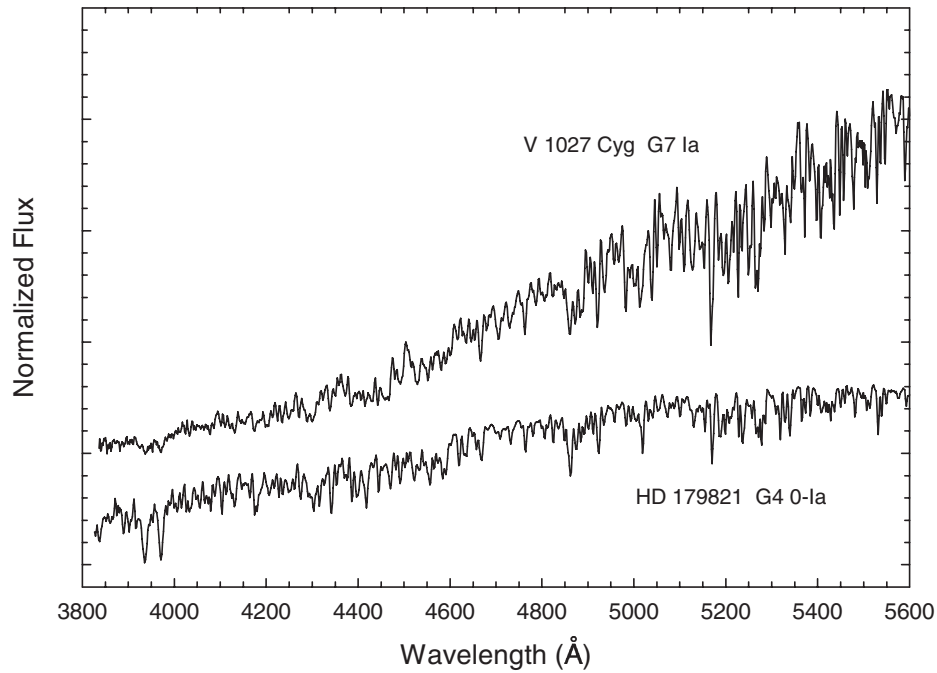


Figure 7.22 Two yellow post-Asymptotic Giant Branch stars.

low-resolution optical and NIR spectra for many post-AGBs, transition objects, and planetary nebulae.

The post-AGBs have low-to-intermediate masses and are in an evolutionary stage subsequent to the equally luminous but higher mass stars, the AGBs and RV Tauris. The luminosities of post-AGBs are not particularly variable, in contrast with the RV Tauri stars, whose spectra show significant peculiarities and variations (see §7.8.2). The post-AGBs are clearly in a more tranquil transition to their final stages than those stars still on the AGB.

Bibliography

- Ali, B., Carr, J.S., Depoy, D.L., Frogel, J.A., & Sellgren, K. 1995, *AJ*, 110, 2415
- Appenzeller, I., & Mundt, R. 1989, *Astron. Astrophys. Rev.*, 1, 291
- Asplund, M., Grevesse, N., & Sauval, A.J. 2005, *ASPC*, 336, 25
- Baade, W. 1952, *Trans. IAU*, 8, 397
- Baliunas, S.L., et al. 1995, *ApJ*, 438, 269
- Balog, Z., & Vinko, J. 1995, *IBVS*, 4150, 1
- Beers, T.C. 2000, in *The First Stars*, eds. A.Weiss, T. Abel, & V. Hill (Berlin: Springer), p. 3
- Bell, R.A., & Briley, M.M. 1991, *AJ*, 102, 763
- Bidelman, W.P., & Keenan, P.C. 1951, *ApJ*, 114, 473
- Blum, R.D., Ramírez, S.V., Sellgren, K., & Olsen, K. 2003, *ApJ*, 597, 323
- Bond, H.E., & Neff, J.S. 1969, *ApJ*, 158, 1235
- Burwell, C.G. 1938, *ApJ*, 88, 278
- Butler, R.P., & Bell, R.A. 1997, *ApJ*, 480, 767
- Carquillat, M.J., Jaschek, C., Jaschek, M., & Ginestet, N. 1997, *AApS*, 123, 5
- Cayrel de Strobel, G. 1996, *Astron. Astrophys. Rev.*, 7, 243
- Cayrel de Strobel, G., Cayrel, R., Friel, E., Zahn, J.P., & Bentolila, C. 1994, *AA*, 291, 505
- Chen, P.S. 2001, *AA*, 372, 245
- Cheng, Q.-Q., Engvold, O., & Elgaroy, O. 1997, *AA*, 327, 1155
- Chmielewski, Y. 2000, *AA*, 353, 666
- Code, A.D. 1947, *ApJ*, 109, 309
- Danks, A.C., & Dennefeld, M. 1994, *PASP*, 106, 382
- Engle, S.G., Guinan, E.F., & Evans, N.R. 2006, *AAS*, 209, 2908
- Garrison, R.F. 1979, in *Spectral Classification of the Future*, IAU Coll. 47, eds. M.F. McCarthy, A.G.D. Philip, & G.V. Coyne (Vatican: Vatican Observatory) RA, 9, 23
- Gauthier, R.P. 1983, PhD thesis, 33 (University of Toronto)
- Gauthier, R.P., & Garrison, R.F. 1984, in *The MK Process and Stellar Classification*, ed. R.F. Garrison (David Dunlap Observatory: University of Toronto), p. 362
- Gray, R.O., Corbally, C.J., Garrison, R.F., McFadden, M.T., & Robinson, P.E. 2003, *AJ*, 126, 2048
- Griffin, R.E.M., & Holweger, H. 1990, *AA*, 214, 249
- Guinan, E.F., & Smith, G.H. 1984, *PASP*, 96, 354
- Gustafsson, B. 1997, *Ap&SS*, 255, 241

- Hall, D.S. 1976, IAU Coll, 29, p.287
- Hardorp, J. 1980, AA, 91, 221
- Harris, H.C. 1985, AJ, 90, 756
- Hartmann, L., & Kenyon, S.J. 1985, ApJ, 299, 462
- Herbig, G.H. 1962, *Adv. Astr. Astrophys.*, 1, 47
- Hill, V. et al. 2000, in *The First Stars*, eds. A.Weiss, T. Abel, & V. Hill (Berlin: Springer), p. 62
- Howell, S.B., Noah, P.V., & Bopp, B.W. 1983, PASP, 95, 762
- Ivanov, V.D., Rieke, M.J., Engelbracht, C.W., Alonso-Herrero, A., Rieke, G.H., & Luhman, K.L. 2004, ApJS, 151, 387
- Joy, A.H. 1937, ApJ, 86, 363
- Joy, A.H. 1945, ApJ, 102, 168
- Keenan, P.C., & McNeil, R.C. 1995, *VizieR On-line Data Catalog: III/150*. Originally published in: 1989, ApJS, 71, 245
- Keenan, P.C., & Yorka, S.B. 1988, BICDS, 35, 37
- Keenan, P.C., Yorka, S.B., & Wilson, O.C. 1987, PASP, 99, 629
- Kervella, P., Mérand, A., Perrin, G., & Coudé Du Foresto, V. 2006, AA, 448, 623
- Kleinmann, S.G., & Hall, D.N.B. 1986, ApJS, 62, 501
- Kraft, R.P. 1987, JAA, 8, 89
- Krieger, C.J. 1934, ApJ, 79, 98
- Kurucz, R. 1993, KurCD, 13
- Lada, C.J., et al. 2006, AJ, 131, 1574
- Lambert, D.L., & Ries, L.M. 1981, ApJ, 248, 228
- Luck, R.E. 1991, ApJS, 75, 579
- Maas, T., Giridhar, S., & Lambert, D.L. 2007, arXiv0706.2029
- Mallik, S.V., Parthasarathy, M., & Pati, A.K. 2003, AA, 409, 251
- Martín, E.L. 1997, AA, 321, 492
- McClure, R.D. 1984, PASP, 96, 117
- Merrill, P.W. 1926, ApJ, 63, 13
- Mora, A., et al. 2001, AA 378, 116
- Morgan, W.W. 1933, ApJ, 77, 291
- Morgan, W.W., Keenan, P.C., Abt, H.A., & Tapscott, J.W. 1981, ApJ, 243, 894
- Noyes, R.W., Hartmann, L.W., Baliunas, S.L., Duncan, D.K., & Vaughan, A.H. 1984, ApJ, 279, 763
- Pace, G., Pasquini, L., & Ortolani, S. 2003, AA, 401, 997
- Peterson, R.C., Kurucz, R.L., & Carney, B.W. 1990, ApJ, 350, 173
- Preston, G.W., Krzeminski, W., Smak, J., & Williams, J.A. 1963, ApJ, 137, 401
- Ramsey, L.W. 1990, ASPCS 9, 195
- Schmitt, J.L. 1971, ApJ, 163, 75
- Soderblom, D.R., Duncan, D.K., & Johnson, D.R.H. 1991, ApJ, 375, 722
- Spinrad, H., & Taylor, B. 1969, ApJ, 157, 1279
- Struve, O. 1944, Obs, 65, 257
- Suárez, O., García-Lario, P., Manchado, A., Manteiga, M., Ulla, A., & Pottasch, S. R. 2006, AA, 458, 173

- Torres-Dodgen, A.V., & Weaver, W.B. 1993, *PASP*, 105, 693
- Travaglio, C., Gallino, R., Arnone, E., Cowan, J., Jordan, F., & Sneden, C. 2004, *ApJ*, 601, 864
- van Winckel, H. 2003, *ARA&A*, 41, 391
- Wallace, L., & Hinkle, K. 2002, *AJ*, 124, 3393
- Wallace, L., Meyer, M.R., Hinkle, K., & Edwards, S. 2000, *ApJ*, 535, 325
- Wallerstein, G. 1958, *ApJ*, 127, 583
- Wallerstein, G., & Cox, A.N. 1984, *PASP*, 96, 677
- Walter, F.M., Brown, A., Mathieu, R.D., Myers, P.C., & Vrba, F.J. 1988, *AJ*, 96, 297
- Wilson, O.C., & Bappu, M.K.V. 1957, *ApJ*, 125, 661
- Winfrey, S., Barnbaum, C., Morris, M., & Omont, A. 1994, *AAS*, 185, 4515

Chapter Eight

The M-type, S-type, and Carbon Stars

8.1 INTRODUCTION

There are more M-type dwarf stars than any other class, while the luminosity and radius differences between the dwarfs and the supergiants are the most extreme to be found on the H–R diagram. Of further interest for the M-type stars, the ages of their dwarfs can reach back to the beginning of the Milky Way Galaxy, while those of the supergiants are very short, giving rapid changes in type, like HV 11423 which moved more than a letter-type and back in a matter of months (Massey et al. 2007). Again, their giants can have the slowest brightness variations, the *long-period-variables*, famous for their prototype, Mira (*o Ceti*).

The spectra of these M stars are dominated in the visible by the molecular bands of TiO, and as such they are “cousins” to the other stars that have atmospheres cool enough for fragile molecular species to dominate. These cousins include the *carbon stars* and the *S-type stars*, both of which are treated later in this chapter. The story of the M dwarfs and their transition to the cooler L-type objects is continued in the next chapter; whereas in this chapter we conclude with those close binary stars whose composite spectra include a late-type giant star, the *symbiotic stars*, and the *Algol systems*. So we are now turning to a set of stars, showing rich variety and having great astrophysical importance.

8.2 THE M-TYPE STARS

8.2.1 History

The M-type stars were first discovered in the year 1866 by Father Angelo Secchi, a Jesuit astronomer who built an observatory on the roof of the Collegio Romano in Rome. Using a visual spectrograph, Secchi observed stars down to magnitude 8 and established a classification system in which he sorted stars into types I, II, and III, adding two years later type IV (see §1.1.1). The type III stars are the M-type stars, and the type IV stars are the carbon stars.

Classification of the M-type stars historically progressed smoothly after Secchi. The “Harvard types” in the Draper catalogues ordered the spectra in terms of the visibility of the TiO bands (Ma, Mb, Mc, Md), while the greater resolution of the “Mount Wilson” spectra introduced luminosity-sensitive line pairs and the decimal subdivisions (M0, M1, . . . M6). These stages underlay the introduction of the MKK system in 1943 (see §1.1.5). The recent developments in tackling the late-M and even cooler objects well merit their own story. So in Chapter 9 will be found a

complementary treatment of the M-type dwarfs, particularly emphasizing the red and infrared regions, and this will lead on to the classification of the L-type objects. Chapter 10 continues with the even cooler T-type dwarfs. Classification of the carbon stars and the S-type stars was a much less straightforward proposition than for the M-type stars, and the historical steps and current status are treated in their appropriate sections later in this chapter, §8.3 and §8.4.

8.2.2 The Spectral Classification of M-type Stars

8.2.2.1 Temperature Criteria

For using the TiO molecular bands as classification criteria in these late-type stars, it is helpful to have spectra further into the green than $H\beta$, and indeed the spectral range shown in Figure 8.1, a main-sequence montage, is quite ideal. It will also be noticed that this figure's ordinate is in terms of "normalized flux" rather than "rectified intensity." This is done partly so that the change in the shape and slope of the continuum can be seen as a function of spectral type and partly because consistency in delineating the continuum, and so producing the rectification, is hard to achieve for these so-deeply-lined spectra. The K-type spectra are included in the montage to show the transition to the M-types. There is in fact only one full spectral subtype between K5 and M0, since here the criteria are very sensitive to small differences in temperature (Keenan 1984).¹

While the ratio Ca I $\lambda 4226$ to Fe I $\lambda 4383$ starts off as a useful temperature criterion, since it grows toward later types, the dramatic change in the TiO band strengths is the most obvious one to use in the M-type stars. The Cr I triplet, so helpful as an abundance-independent temperature criterion for K-type stars (see §7.2.1), loses its sensitivity by early-M, so instead the ratios of TiO band strengths should be employed for metal-weak stars. An example is the relatively slowly increasing TiO $\lambda 4804$ band to the rapidly strengthening $\lambda 4955$ TiO band.

In dwarf stars, but not giants, one can also use the development of the MgH feature at $\lambda 4780$. At mid-K-type dwarfs it begins as a pointed tooth-like absorption feature, which becomes progressively more flat-bottomed as the nearby TiO $\lambda 4761$ band dominates. The progression of the MgH band at $\lambda 5198$ is similar, losing its temperature sensitivity around M1 and thereafter becoming dominated by the TiO band at $\lambda 5166$. If the spectral range allows, the band at $\lambda\lambda 5500\text{--}5560$ of CaOH, a tri-atomic molecule, can be used from its appearance at about M3 and for later types.

Many M dwarfs have active chromospheres and exhibit strong flares many times more energetic than solar flares. This shows itself as emission in hydrogen and Ca II lines, such as for the M4.5 star, σ^2 (40) Eri C. Strong X-ray emission is

¹What is actually happening is that in terms of effective temperature, the jump from K5 to M0 is small, and is comparable to that between M0 and M1. Hence, when one is plotting spectral type against effective temperature, the curve will have a kink in it unless K5 to M0 is taken as a unit change, similar to that between M0 and M1. In reality, the temperature criteria are so sensitive in this region that we can, with classification techniques, insert a number of partial subtypes between K5 and M0, even though these temperature divisions cannot yet be measured by the techniques used to find effective temperatures.

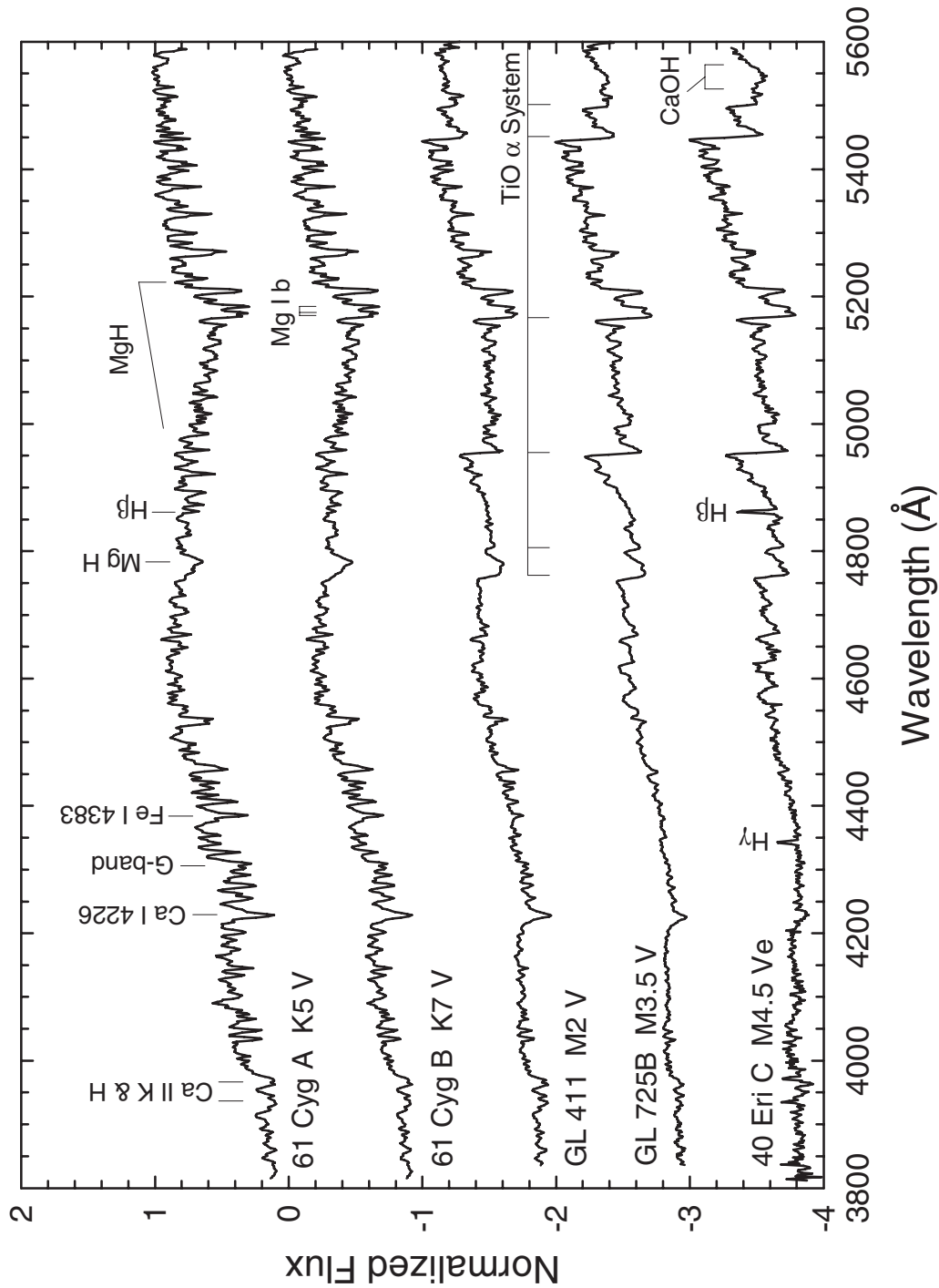


Figure 8.1 A temperature sequence of main sequence stars from late-K to mid-M, with the principal features labelled. Notice how the TiO band strengths increase dramatically, while the morphology of the MgH and Mg b regions changes. The Ca I λ 4226 to Fe I λ 4383 ratio is also useful as a temperature criterion, providing one is sure of the luminosity class. Spectra obtained at the Dark Sky Observatory.

associated with such stellar activity. These flare stars will be treated in detail in the next Chapter (§9.5.2), while emission-line M giants come in the following section, §8.2.3.

The temperature classification of the M giants, shown in the montage of Figure 8.2, is, like the dwarfs, based on the rapidly increasing strength of the TiO bands. At K7, the TiO $\lambda 4955$ can just be detected, while after M3 the strongest bands become saturated and the temperature type is assigned on the basis of the strength of the fainter bands. The increase in Ca I $\lambda 4226$ strength, especially after M5, helps for classifying the later M-giants, as does the appearance of VO bands at M9. For these giants as for the M dwarfs, to avoid abundance or “veiling” (see §8.2.3.2) complications, the spectral type is best judged from the ratios of the strengths of these bands.

We noted that the metallic lines reach a maximum strength in the early-M types and then decline despite the lowering of T_{eff} . This decline occurs because the extraordinary strength of the molecular features progressively removes the background continuum. However, the Ca I $\lambda 4226$ line continues to increase in strength for the M giants, especially after M5. Again one must carefully compare any program spectrum with standards to determine whether the weakness of metallic lines seen in the spectrum is due to the above continuum effect or also to an actual metal-weakness.

Finally, we show an unpublished table of temperature criteria for the MK classification of M giants (Figure 8.3). It was put together by Philip Keenan from all his papers, and we include it as a tribute to his many years of dedicated work on these types of stars.

8.2.2.2 Luminosity Criteria

The most striking luminosity indicator in M-type stars is the negative luminosity effect in the Ca I $\lambda 4226$ line (see Figure 8.4). At the resolution of the spectra in this figure (3.6 \AA), the morphology of the MgH/TiO blend near $\lambda 4770$ is also very sensitive to luminosity since it is the MgH that dominates in dwarfs, producing a tooth-shaped feature for them.

The ratio of the $\lambda 5250/\lambda 5269$ blends makes another luminosity sensitive indicator. The blend at $\lambda 5250$ is mainly due to lines of an intersystem Fe I triplet, and it gains considerably in strength as the luminosity increases (Fitch & Morgan 1951). Scarfe (1966) showed this triplet is also very luminosity sensitive in the late-G and K giants.

The low flux at the blue-violet end of the spectrum makes relatively weak atomic species difficult to see at this resolution, so instead one can look at the general morphology of the region between $\lambda\lambda 4900\text{--}5200$, which changes quite distinctively with luminosity. However, if the resolution is 2 \AA or better, then the negative luminosity effects in the Ca I triplet at $\lambda\lambda 4425, 35, 55$ and in the Cr I triplet $\lambda\lambda 4254, 60, 90$ are additional useful indicators.

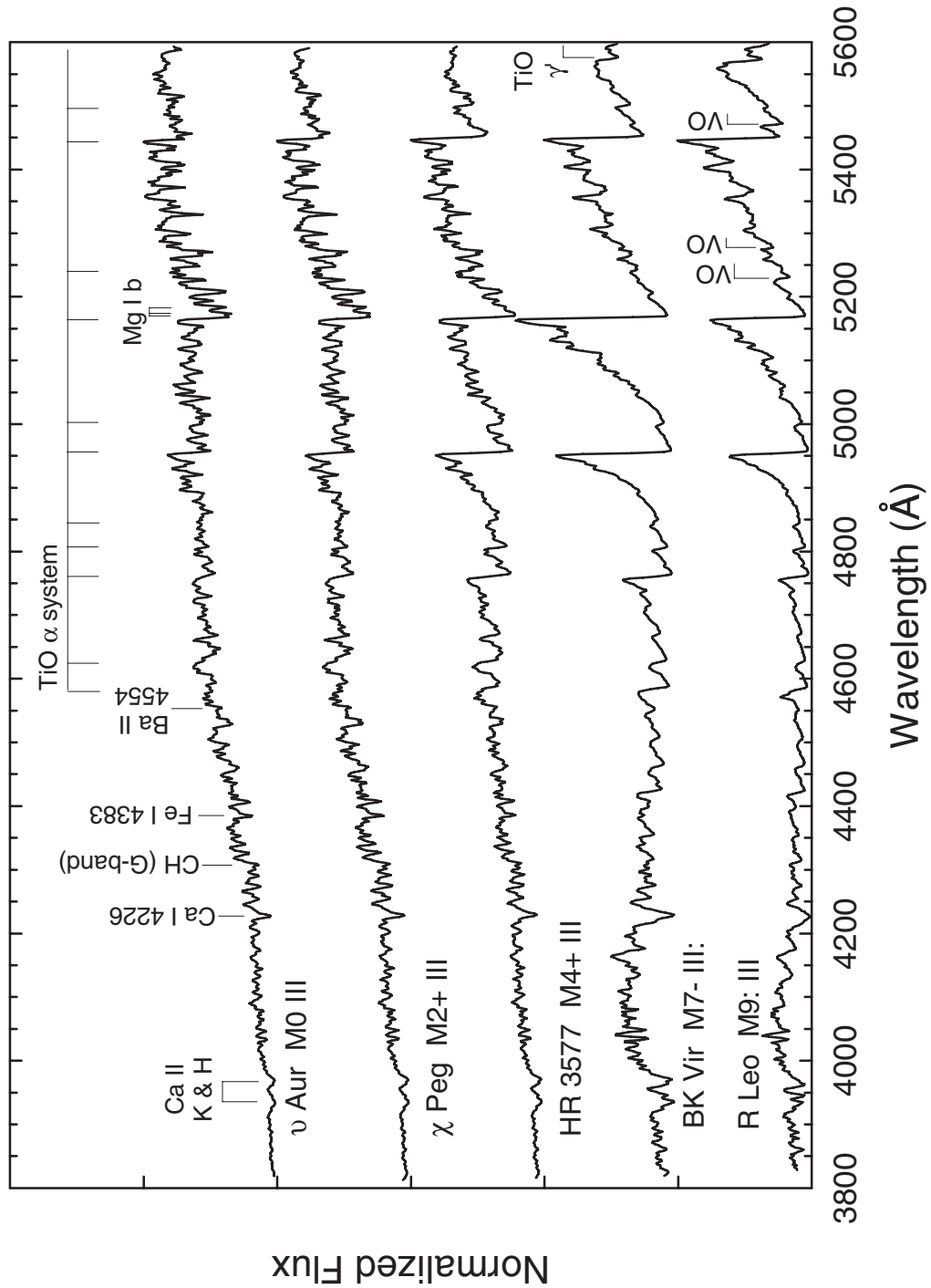


Figure 8.2 A temperature sequence for M giants. The blue-green (α) system of TiO bands has been marked, as well as the bluest bandhead in the orange-red (γ') system of TiO at $\lambda 5569$. Note the appearance of weak VO bands in the M9 giant. These spectra are presented in a normalized flux format, and have all been normalized at a common point, 5445 Å. Spectra obtained at the Dark Sky Observatory.

CRITERIA FOR TYPES M0 TO M9		
Type	Blue Region	Visual Region
M0	$\lambda 4954$ clearly seen. The marginal appearance of this band at scales ≈ 100 A/mm helps define type K5.	$\lambda 6159$ clearly seen $\lambda 5448$, $\lambda 5167$ present
M1	$\lambda 4761$ present.	$\lambda 5448$ clearly seen. $\lambda 5167$ is now strong enough to form a distinct break in spite of the strong atomic lines nearby.
M2	$\lambda 4804$ present. Broadening of $\lambda 4667$ noticeable.	$\lambda \lambda 5448$, 6159 stronger.
M3	$\lambda 4584$ present; 4667 , 4804 clearly seen.	$\lambda \lambda 5597$, 5847 present.
M4	$\lambda \lambda 4626$, 4667 distinct; $\lambda 4848$ present.	$\lambda \lambda 5759$, 5810 distinct.
M5	$\lambda \lambda 4352$, 4462 distinct.	V0 5736 present.
M6	$\lambda 4395$ present and becomes distinct at M6.5. $\lambda 4422$ distinct on plates of larger scale.	V0 5736 slightly weaker than $\lambda 5759$.
M7	$\lambda \lambda 4082$, 4310 present.	V0 5736 = $\lambda 5759$ $\lambda \lambda 5591$, 5615 fairly strong.
M8	All of the spectrum longward from $\lambda 4100$ presents banded appearance. $\lambda \lambda 4082$, 4310 fairly strong.	V0 5736 = $\lambda 5759$ $\lambda 5591$ comparable with $\lambda 5597$.
TiO Band heads		

Figure 8.3 Philip Keenan's table of criteria for the MK classification of M giants. In his hand the obvious criterion, "TiO band heads," is added at the bottom. This original page from a working document was kindly provided by P. Boeshaar.

8.2.2.3 NIR and IR Classification

The classification in the NIR and IR of the early-M types overlaps that for the late-K stars and so these are treated in §7.3, while that for the later-M types comes in Chapter 9. However, to begin an extension of classification into this spectral region for M-types, Figure 8.5 illustrates the effect of luminosity on NIR spectra at M2. In the dwarf star GL 411 the Na D doublet (unresolved at this resolution) is greatly enhanced, but becomes increasingly overwhelmed by the nearby TiO band for the giants at M2 and later. CaH, in its A-band ($\lambda 6946$, $\lambda 6908$) and B-band ($\lambda 6385$) systems, is very sensitive to luminosity changes between dwarfs and giants. Even though the CaH A-bands are blended with the atmospheric O₂ B-band, it is still a useful luminosity indicator. Just to the blue of the CaH B-band ($\lambda 6385$) is the blend near $\lambda 6362$ consisting of Ti, Fe, and Cr (from β Peg line identifications by Davis (1947)). As CaH disappears with increasing luminosity, so this blend becomes more visible even through the surrounding TiO.

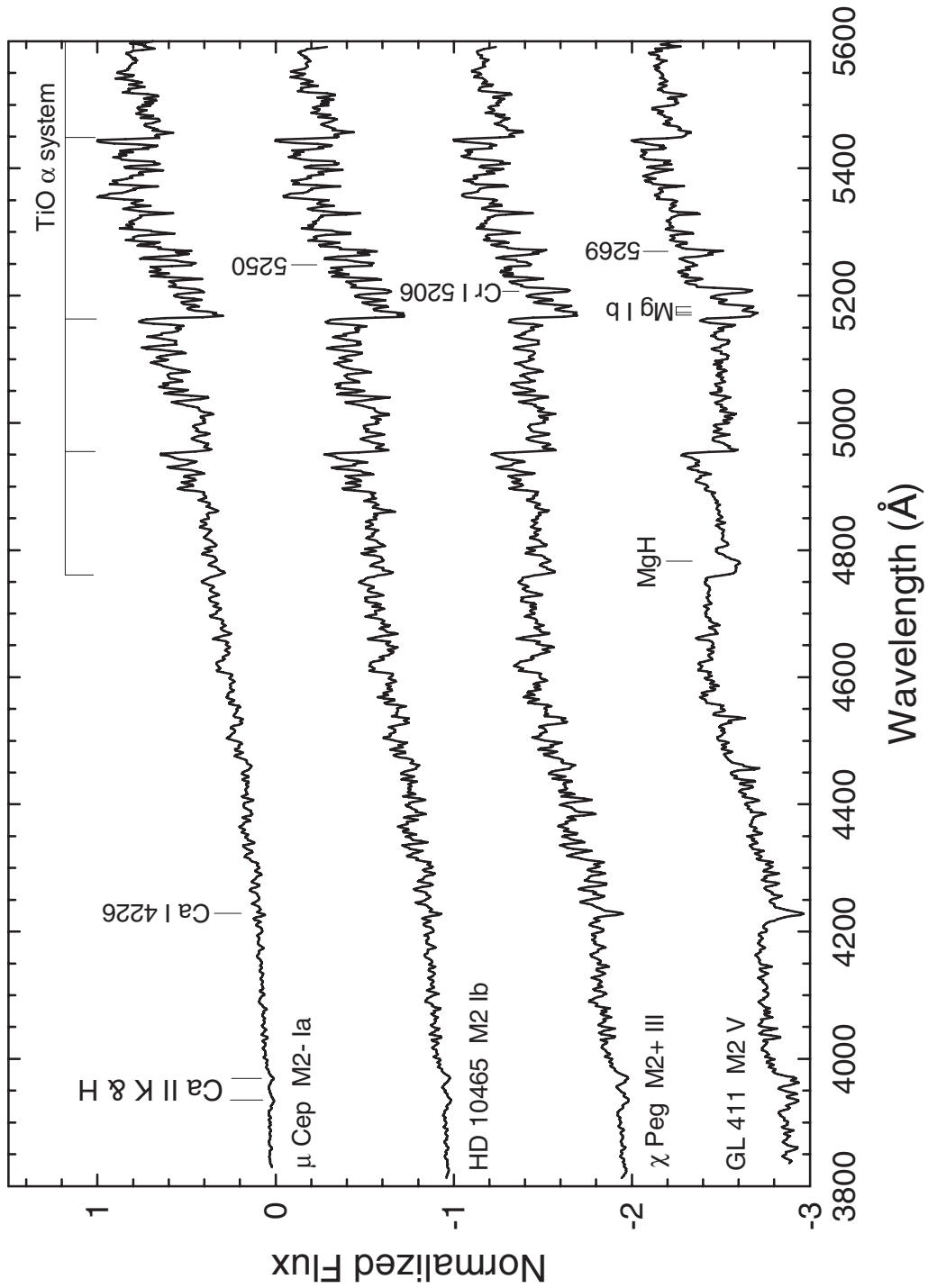


Figure 8.4 A luminosity montage for giant stars at M2. The most striking feature is the negative luminosity effect in Ca I $\lambda 4226$. Also, at the resolution of these spectra (3.6 \AA), the morphology of the MgH/TiO blend near $\lambda 4770$ is very sensitive to luminosity, as is that in the region between $\lambda\lambda 4900$ and 5200 .

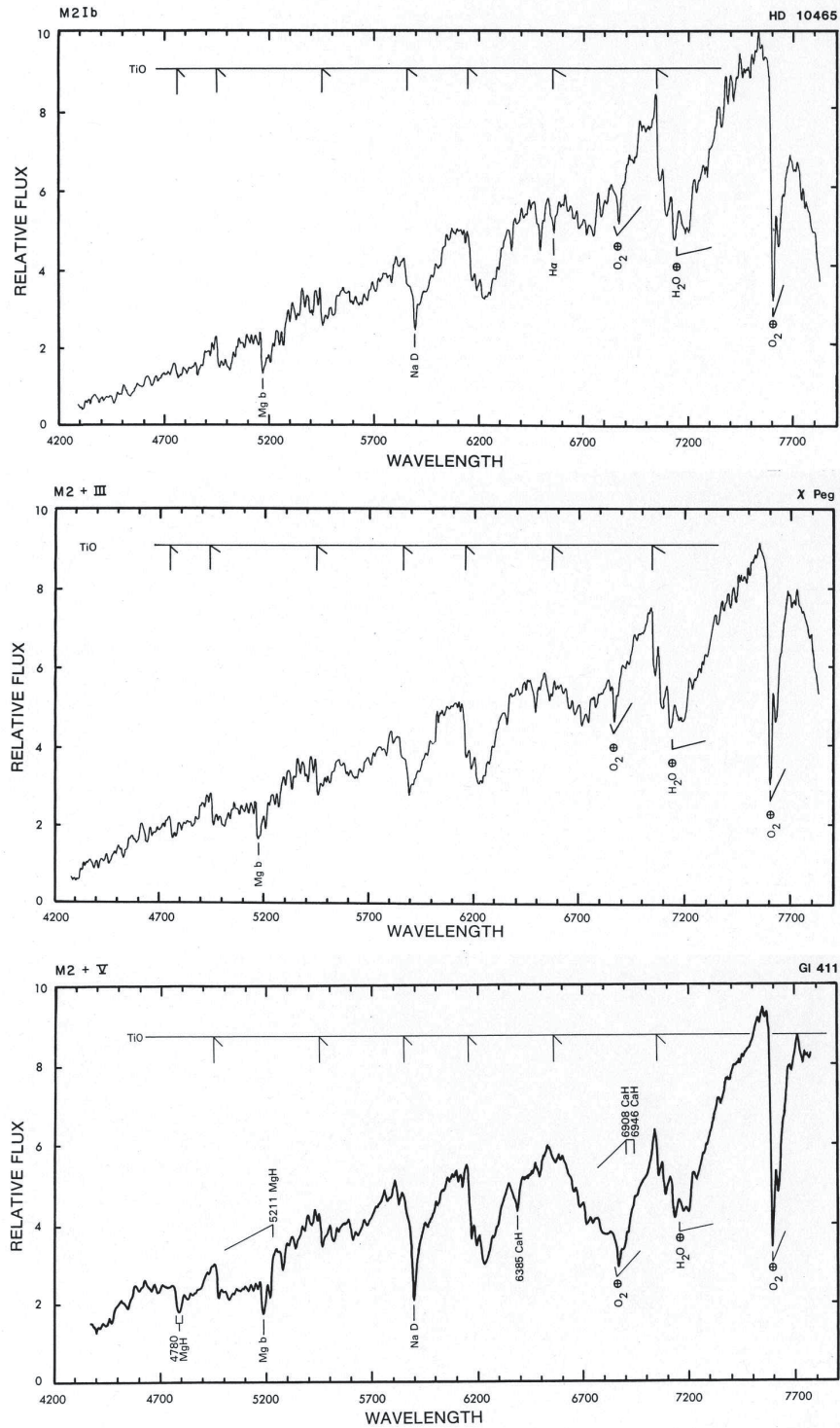


Figure 8.5 A luminosity montage for M2 stars in the NIR. There is a marked negative luminosity effect in the Na D doublet and in the CaH bands, and this persists to later M-types. The spectra are courtesy of Turnshek et al. (1985).

For temperature classification, the increasing strength of the TiO bands toward later M-types, for all luminosities, is the dominant feature, as has been emphasized for the optical region spectra. The K I lines at $\lambda 7665$ and $\lambda 7699$ become clear in dwarfs by M3 and increase in strength to later types, though these lines are much weaker in giants. So these K I lines can be used iteratively to confirm both temperature and luminosity for the mid and later M-type stars. From M7 and later the VO bands around $\lambda 7400$ and $\lambda 7900$ join TiO in usefulness, since their strength also increases with declining temperature in both dwarfs and giants (see Figure 8.6). These and other features in the NIR are illustrated and described in the NIR atlas of cool stars by Turnshek et al. (1985).

Looking further into the IR, the CO bands dominate the spectral features in the K-band. This is shown by Figure 8.7 in which the two uppermost spectra are of M giants. In the L-band, spectra of M-type giants are dominated by the vibration-rotation bands of SiO as well as the *P*-branch of the OH 1–0 and 2–1 bands (see Figure 7.10).

8.2.3 The Classification of the Mira Variables

The cooler and more luminous the star, the more likely is it to have an unstable interior and atmosphere and so to vary in temperature and luminosity. The variations can be “irregular” or “semi-regular” (see §8.2.3.3) or fairly regular. Among the last are the *Mira* or *long-period* class of giant star variables. The amplitude in luminosity for Miras is at least 2.5 magnitudes and can be up to 10, though usually it is around 5. While their periods are indeed fairly regular and range between 80 and 1000 days, the amplitude of the luminosity variations for an individual star may change considerably. It comes as no surprise that all this variation gives rise to fascinating spectra, which change throughout their light cycles and from cycle to cycle, and so they amply live up to their prototype’s name, Mira (= *o* Ceti), which means “the wonderful.”

8.2.3.1 History

The minimum period to qualify as a long period variable (LPV) was in some dispute initially. It ranged from 6 months for Pickering in 1881 to 40 days for Payne-Gaposhkin and Gaposhkin in 1938 (Merrill 1940, pp. 1–2). From the mention of these authors it is clear that these stars were well monitored at Harvard over several eras and featured in various of its catalogues. Given that the upper range for their periods can be several years, their monitoring needed the long-term commitment suited to such a classical observatory.

Merrill (*ibid.*, p. 6) distinguishes three great periods of understanding the spectra of LPVs: the visual observation period from the 1860s in which the pioneering work of Angelo Secchi was outstanding, the period from 1885 of photography with objective prisms, and then photography with slit spectrographs from 1896 onwards. Visually, bright molecular bands were seen in the spectra, but it is probable that the emission in the hydrogen lines was never clear until the first

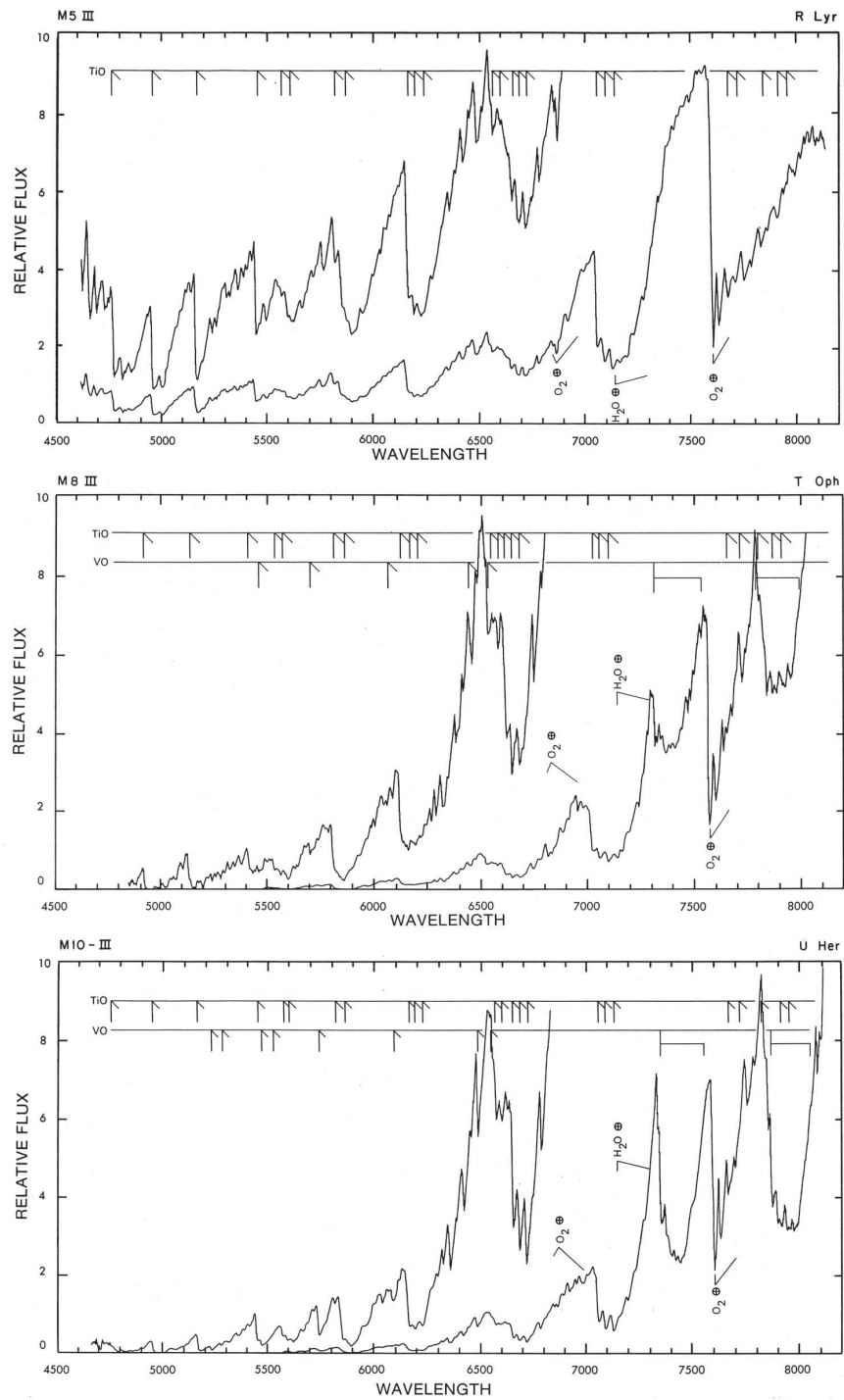


Figure 8.6 A temperature montage for late M-star giants in the NIR. The spectra in each pair that are offset higher are duplicates of the lower, but at a scale to bring out the low-flux features. The strength of the TiO bands increases with decreasing temperature, and so does that of the VO bands that appear around M7. The spectra are courtesy of Turnshek et al. (1985).

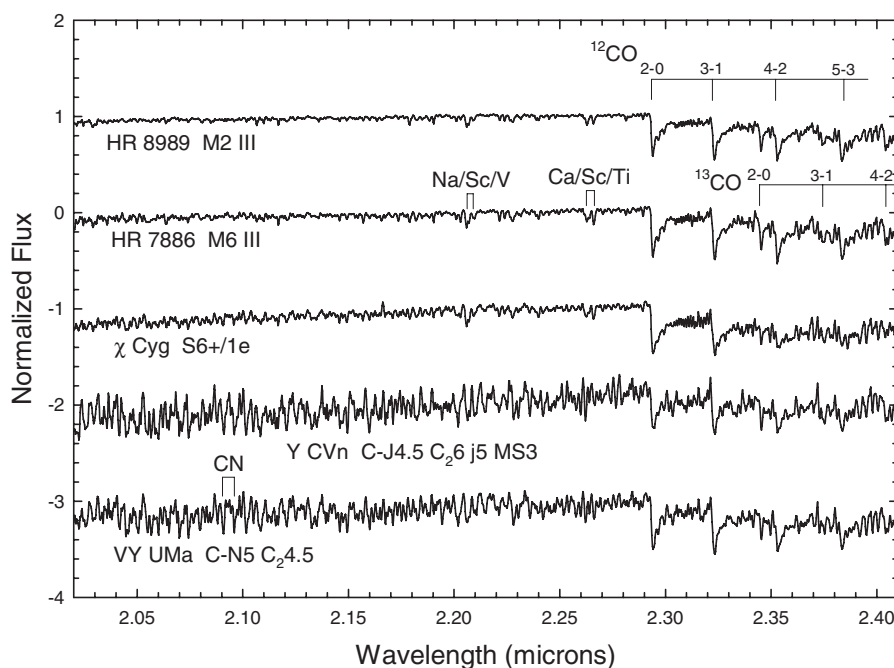


Figure 8.7 A montage of two M-giants, a mild S-type star (χ Cyg), and two carbon stars in the infrared K-band. Note these three types are quite similar in the K-band, all with strong CO bands, although the carbon stars show stronger line blanketing. Spectra from Wallace & Hinkle (1997).

photographs were taken at Harvard. From these photographic spectrograms Williamina P. Fleming and Antonia C. Maury were able to characterize and subdivide these Md stars, later called Me, or emission-line M-stars. It was A. Fowler in 1904 who first showed that the spectral bands of M stars, particularly clear in those of α Ceti and α Her, were due to the “flutings of titanium” compounded with oxygen (Fowler 1904). The work in the 1920s of A. H. Joy, using slit spectra, brought a significant conclusion to this classical period of the study of Mira variables. It was during this time that Joy discovered Mira itself to be a binary star, thus explaining asymmetries in its spectrum at minimum light, the most favorable phase to detect its companion.

In the 1960s an intense study of Miras, carried out by Merrill, Deutsch, Keenan, and Garrison, gathered 900 slit spectrograms of 150 variables and enabled the detailed description of the phenomenon of veiling and of the unusual behavior of the AlO absorption bands (Merrill et al. 1962; Keenan et al. 1969). Today digital slit spectroscopy, with polarimetry and access to the UV and IR, seems to be giving rise to another great period in the understanding of Mira variables. Extensive photometric surveys in the optical for MACHOs or in the infrared, like 2MASS, have been adding to these spectroscopic studies.

Miras, particularly the longer-period ones which are younger and more massive, give insight into stars in the thermally pulsing part of the asymptotic giant branch

(AGB), the period involving an internal mixing process between the nuclear burning region and the surface of a star that is called a “dredge-up.” Explanations of the variations in Mira spectra were initially based on a hot shell around the star, but they were replaced by models in which the pulsations produced “shocked” atmospheres of enormous extension (e.g., Bowen 1988). At the stellar surface, not only are their atmospheres becoming understood in such terms as extended water vapor layers (Ohnaka et al. 2006), but also the importance of their dusty winds in contributing to the ISM is being well realized (Willson 2000; Bieging et al. 2006).

A review of the ever-wonderful Miras in the context of other AGB stars is given by Habing & Olofsson (2003), and the treatment of them continues in later chapters of the book edited by these authors. The study of Miras will, for the patient, yield understanding of the structure of giant stars, of their pulsation and evolution, of their contribution to the formation of the next generation of stars, and of the morphology and history of their parent galaxy, and so there have always been those fascinated by and willing to investigate them.

8.2.3.2 Classification

We saw in §8.2.2.1 that the temperature type of M giants is well correlated with the strengthening of the absorption bands of TiO, along with a strengthening of atomic lines, particularly Ca I $\lambda 4226$, all with decreasing temperature. Garrison (1972) expertly describes how this also applies to the spectra of Mira variables, but how their spectra can be distinguished from those of the “normal” M-giants by the presence of high-excitation emission lines, such as H and Fe II, as well as a number of fluorescence lines produced in the rarefied Mira atmospheres by the population of excited levels being governed by radiative processes (see the two Miras, S Leo and R Leo, in Figure 8.8 and the description in Crowe & Garrison (1988)). These emission lines vary around the luminosity cycle, but they are strongest at and after maximum, weakest after minimum.

The Balmer decrement in the hydrogen emission is often quite unusual. For instance, as in the spectrum of S Leo in Figure 8.8, $H\beta$ can be almost absent due to absorption in the TiO band, while $H\gamma$ and $H\delta$ emissions are quite strong. This implies that the emission is occurring lower in the atmosphere than the strong TiO absorption, whereas usually emission is associated with the top of an extended atmosphere or surrounding shells. In the phase of R Leo’s variations shown in Figure 8.8, the hydrogen lines are not strong in emission, but emission lines of Fe I ($\lambda 4202$, $\lambda 4308$, $\lambda 4376$) and Mg I $\lambda 4571$ are quite visible. In many of these stars the hydrogen-line emission strength is in antiphase with the emission lines of Fe I and Mg I. As mentioned above, Fe II emissions can be present in Miras too, except for a few weeks after minimum light.

Mira variables can show interesting phenomenon in their spectra other than the presence of emission lines. Many will show a “washed-out” appearance to their absorption lines. This can be the line-weakening associated with an overall abundance effect, and this is well understood in terms of the Intermediate

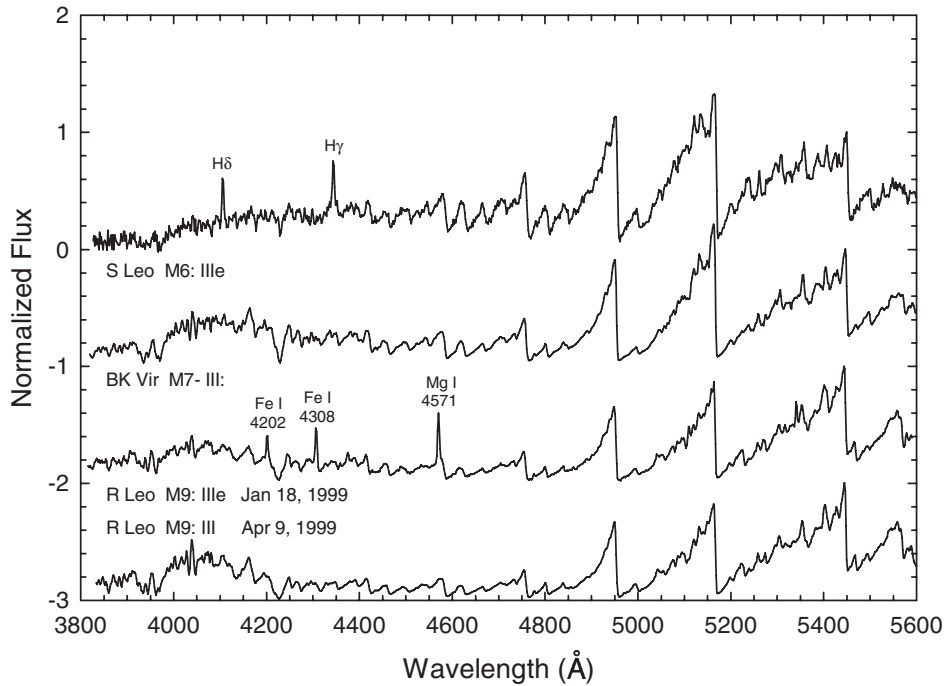


Figure 8.8 The two Mira-type stars, S Leo and R Leo, illustrated between two giant M-type spectra, including the MK standard BK Vir. They are distinguished from normal M-giants by emission in the hydrogen lines and in the atomic species marked in the montage. The bottom spectrum is that of R Leo, observed during a phase in which its spectrum is essentially normal with a spectral type near M9 III. Spectra obtained at the Dark Sky Observatory.

Population I or Population II stars from an older generation in the Galaxy or in nearby ones. Or the line-weakening can vary from cycle to cycle and be selective: for instance, certain lines, but not all of a given element, are weakened; or the atomic lines in the blue-violet region of the spectrum are weakened, but not those in the ultraviolet. This latter kind of line-weakening, not due to an abundance effect, is called “veiling.” There must be some difference from normal in the structure of the temperature and/or density in the atmospheres of these stars, which has even been ascribed to high-level atmospheric clouds.

Another interesting phenomenon in Miras is the behavior of the AIO molecular bands. The main bandhead is at $\lambda 4842$, near $H\beta$ (Figure 8.9), and in normal stars it appears near M4 and increases with decreasing temperature-type. In Miras, for the same star at the same phase in different cycles, so presumably at the same surface temperature, the AIO can be extremely strong or weak, in absorption or emission. This behavior was discovered first in Mira (Joy 1926) and then seen in a few others like R Cnc, RR Boo, and RV Cas. Keenan et al. (1969) saw no trend between the strength of the resonance Al I lines at $\lambda 3944$ and $\lambda 3961$ and the AIO bands, so it is not an abundance effect. However, they did find a correlation between

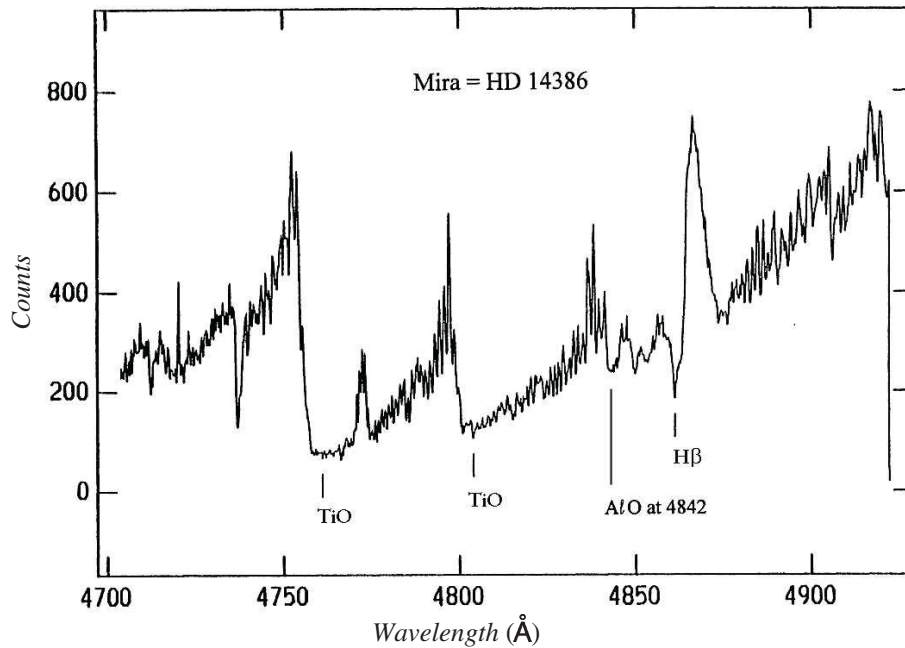


Figure 8.9 Spectrum of Mira taken in August 1966. The main AlO bandhead is at $\lambda 4842$ near the mark for H β . Figure by kindness of Garrison (1997) and the *Journal of the American Amateur Variable Star Observers*.

the veiling extent and the AlO bands, in the sense of strong-line cycles yielding strong AlO bands and vice versa, with AlO emission only in the most veiled cycles, so perhaps there are high-level clouds of AlO floating around in some Mira atmospheres. Again, more monitoring is needed—in all wavelength and dispersion combinations—to understand the very individual atmospheric phenomena of these LPVs.

8.2.3.3 Irregulars and Semiregulars

Photometrically the irregular and semiregular variables are less regular and less extreme, with maximum amplitudes of 2.5 magnitudes, than the LPVs. Spectroscopically, they exhibit milder and fewer Mira characteristics; e.g., the emission is weaker.

8.3 THE CARBON STARS

The classical carbon stars are stars with temperatures and luminosities corresponding to late-G, K, and M giants but with large overabundances of carbon relative to oxygen. These stars have spectra that are dominated by strong molecular bands due to molecules including carbon, namely CH, CN, and C₂, and, in the cooler stars, SiC₂, C₃, and other carbon-rich molecules. While most known carbon stars are giants or bright giants, there are also dwarf carbon stars, and these may

actually prove to be the most common type. The classification of dwarf carbon stars is considered in §9.5.1.

The essential difference between the M-type stars and the carbon stars is in the relative abundances of carbon and oxygen. In the oxygen-rich stars (the M-type stars), most of the carbon is consumed in the formation of the CO molecule, and thus little carbon remains to produce other carbon molecules, such as CN and C₂. On the other hand, carbon stars are enriched in carbon relative to oxygen, and thus essentially all the oxygen is used up in the formation of CO, leaving little oxygen to form oxides such as TiO (which dominate the spectra of the M-type stars), and much carbon to form the molecules that characterize the spectra of the carbon stars. This matter is discussed in some detail in §8.4.2.

8.3.1 History

As mentioned in §8.2.1, the carbon stars were first discovered and studied by Father Angelo Secchi of the Collegio Romano. Of his four spectral types, I, II, III, and IV, type IV, the carbon stars, with their spectacular molecular bands, were apparently his favorite. This is evident from the following passage by Secchi:

Schjellerup No. 152. . . . A splendid object of type IV which is truly outstanding for its vividness; the spectrum is composed of three zones which are strong and broad. One zone is yellow, another green and the third is blue. These are all vivid with a cutoff on the violet side and a fading tapering from the red side. The ridge of each zone is strengthened by vivid lines at the edge. In the yellow these lines are like two most beautiful threads of gold. So too there are strong features in the green and in the blue, though this last is not so prominent. We also see some lesser streaks. . . . In addition we note a characteristic which differentiates this type IV from type III: in type IV the light curve inclines towards the cut off at the violet side, whereas in type III the curves incline more steeply towards the red; besides they are only half as broad. Thus the two types are essentially different. . . . (translation from McCarthy 1994).

Secchi noted a “marked analogy with the reversed spectrum of carbon” and thus was the first to identify the molecular bands in the spectra of these stars with carbon molecules.

Carbon stars were also considered in the Henry Draper classification scheme and appeared in the first volume of the Henry Draper Catalog (Cannon & Pickering 1918) as R and N stars. The N stars encompassed most of Secchi’s type IV stars, and were divided into types Na and Nb on the basis of the redness of their energy distributions. Type Nc was added later to include stars that had essentially no flux shortwards of H β . Williamina Fleming (Pickering 1896) was the first to notice the existence of stars with strong carbon molecular bands but with spectra that extended much further into the violet than Secchi’s type IV stars. These stars were

designated as type R stars. In the first volume of the HD catalog, the R-type was used in the sequence R0, R3, R5, and R8, in order of decreasing violet flux, with a certain amount of overlap or confusion between R8 and Na.

In the R-type stars, because of the appreciable violet flux in the spectrum, many of the classification criteria defined for G and K giants could be used, and thus a temperature sequence was relatively easy to define. In the N-type spectra, however, it was realized that the divisions Na, Nb, and Nc did not represent a temperature sequence, but rather reflected the degree of excess abundance of carbon over oxygen. As a consequence, Keenan & Morgan (1941) attempted a reclassification of the carbon stars into a single temperature sequence. This is referred to in the literature as the “C-system” or the “C-classification.” Numerical temperature types were assigned on the basis of the spectral features Keenan & Morgan believed to be temperature sensitive, and a C_2 strength index was added to indicate the strength of the Swan bands. The N and R types were not used in the C-classification system. This system was used extensively by Yamashita (1972, 1975) who also introduced some modifications, and was illustrated in the Keenan–McNeil atlas (Keenan & McNeil 1976).

However, even the C-classification system was not in satisfactory agreement with later temperature determinations for the N-type stars. One reason for this was given by Tsuji (1981) who pointed out that the strength of the Na I D-lines (one of the prime temperature criteria in the C-system) is strongly influenced by pseudo-continuous opacity due to overlapping molecular bands. Furthermore, it was realized (Sanford 1944; Gordon 1968; Dean 1976) that R- and N-type stars are of different populations, with different scale heights (the N stars are more closely concentrated to the Galactic plane) and velocity dispersions. In addition to this, many N stars show abundance enhancements of the *s*-process elements such as Ba, Sr, Y, Zr, and La, whereas the R-type stars generally do not. And thus it appeared that the R/N dichotomy had some physical basis.

These considerations and others led Keenan to realize the need to revise and make more flexible the spectral classification system for the carbon stars. His new system, first introduced in Keenan (1993), not only distinguishes between R and N type stars (the C-R and C-N stars), but also includes carbon stars showing unusually low isotope ratios $^{12}\text{C}/^{13}\text{C}$ (the C-J stars), the hydrogen deficient carbon stars (type C-Hd), and the CH stars. This system, which forms the basis for our discussion of the classification of the carbon stars in the following section, was further enhanced with information from high-resolution spectra by Barnbaum (1994) and illustrated with low- and medium-resolution spectra in Barnbaum, Stone, & Keenan (1996).

8.3.2 The Spectral Classification of the Carbon Stars

8.3.2.1 The C-classification System

The C-classification system for the carbon stars, devised by Keenan & Morgan (1941), has now been superseded by the Keenan (1993) system. However, there

Table 8.1 Carbon Sequence Equivalent Types (Keenan & Morgan 1941)

Equivalent Types	Carbon Sequence	Equivalent Types	Carbon Sequence
	Type		Type
G4 – G6	C0	K3 – K4	C4
G7 – G8	C1	K5 – M0	C5
G9 – K0	C2	M1 – M2	C6
K1 – K2	C3	M3 – M4	C7

is an extensive literature associated with the C-classification system, and so we give a brief outline of this system. More details can be found in the original paper (Keenan & Morgan 1941) and in the Keenan–McNeil spectral atlas (Keenan & McNeil 1976).

As mentioned in the previous section, the C-classification system was devised in an attempt to find an ordering of the carbon stars more consistent with observed effective temperatures. To do this, Keenan and Morgan abandoned the R, N notation for the carbon stars, and placed all carbon stars in a single sequence. The primary temperature criteria in this system were as follows:

1. Atomic-line ratios in the blue region of the spectrum: The lines used in these ratios lie between the strong molecular bands in the carbon stars, and so can be compared with normal abundance G-, K-, and M-type stars. In particular, the ratios Fe I $\lambda\lambda 4045$ /Mn I $\lambda\lambda 4032-4$ and Fe I $\lambda\lambda 4250, 4260$ /Cr I $\lambda 4254$ were found useful.
2. Color: Relative intensities of the continuum in the orange part of the spectrum, in particular near $\lambda\lambda 5190, 5670$, and 6150 , were used to judge the temperature.
3. Absolute strength of the Na I D-lines.
4. Band-intensity gradients: The relative intensities of different vibration bands in a given sequence are temperature sensitive. For instance, the ratio of the Swan bands (C_2) at $\lambda 5635$ and $\lambda 5585$ increases with declining temperature.

A numerical type on the C-system was assigned according to equivalent types in the G, K, and M-stars, as given in Table 8.1.

A C_2 strength parameter was then added to the spectral type to designate the strength of the Swan bands. A value of “1” refers to Swan bands that are just barely distinguishable in classification-resolution spectra, up to “5” for the strongest observed bands. The spectral types have the following format: C2,2 for a star with a G9 – K0 equivalent spectral type, and Swan bands with a strength of 2 on the scale of 1 to 5. In the Keenan–McNeil atlas, additional composition parameters were added to indicate, for instance, strong or weak CH bands, enhanced *s*-process abundances (with a Ba or Y index), or an enhanced abundance of the isotope ^{13}C . Due to the great difficulty in using luminosity criteria in the carbon stars, luminosity types were not assigned.

Table 8.2 Carbon Star Notation on the Keenan (1993) System

Equivalent types for oxygen stars	R Sequence	N sequence	CH sequence
G4 – G6	C-R0		C-H0
G7 – G8	C-R1	C-N1	C-H1
G9 – K0	C-R2	C-N2	C-H2
K1 – K2	C-R3	C-N3	C-H3
K3 – K4	C-R4	C-N4	C-H4
K5 – M0	C-R5	C-N5	C-H5
M1 – M2	C-R6	C-N6	C-H6
M3 – M4		C-N7	
M5 – M6		C-N8	
M7 – M8		C-N9	

8.3.2.2 The Revised MK Carbon-star Classification System (Keenan 1993)

In the decades since the C-classification system was devised, it has become clear that the carbon stars encompass a wide variety of objects of different populations and origins. Modern detectors and telescopes have made it possible to observe carbon stars in external galaxies and in both the central regions and outlying fringes of our own Milky Way Galaxy. Keenan realized that a much more flexible system was required than the C-classification system, which rather artificially squeezed all carbon stars into a single sequence. In his “Revised MK Carbon-star Classification system” (or for short, the Keenan 1993 system), five types of carbon stars are recognized, the C-R stars and the C-N stars (corresponding roughly with the Harvard R and N stars), the C-J stars, the C-H stars, and finally, the hydrogen-deficient carbon stars (C-Hd). We discuss the classification of these five types below. Our treatment is based on that of Barnbaum, Stone, & Keenan (1996).

PRELIMINARY REMARKS

Spectral synthesis with an enhanced carbon abundance shows very clearly that the entire spectral region from 4000 to 10,000 Å in cool stars is blanketed with lines due to the carbon molecules CH, CN, and C₂. What this means is that the normal classification criteria used in the G-, K-, and M-type giants are, except in the hottest carbon stars, either strongly affected by this blanketing, or completely obscured. This fact makes both quantitative analysis and spectral classification difficult in the carbon stars. Having said that, it is possible to assign temperature types using criteria detailed below for the different categories of carbon stars. The temperature types for the R and N types have the equivalent G-, K-, and M-types given in Table 8.2 (from Keenan 1993). Luminosity types may be assigned for some carbon stars.

A C₂ index is also included in the spectral type for every carbon star, based on the strength of the C₂ Swan bands. This index runs from 1 to 5, where 1 indicates that the Swan bands at 4737 Å and 5135 Å are just discernible in classification-resolution spectra. Following the practice in the C-classification system, additional

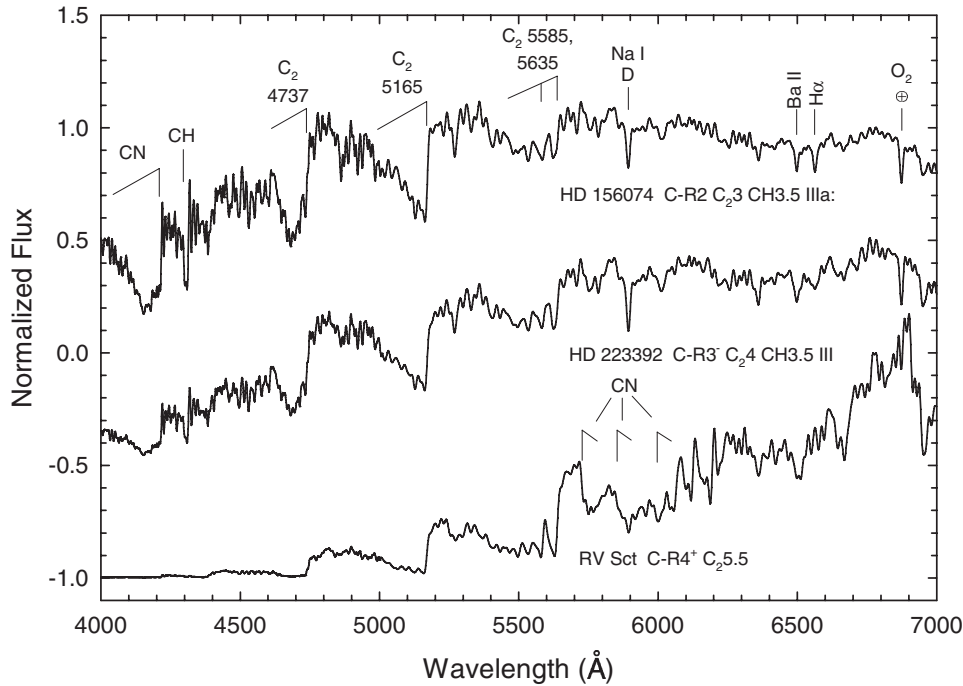


Figure 8.10 A low-resolution temperature sequence for the carbon R-type stars on the Keenan (1993) system. The most prominent features have been labeled, including the Swan bands of C_2 . Note the CN bands in the vicinity of the Na I D lines. Spectra and spectral types from Barnbaum, Stone, & Keenan (1996).

composition parameters are included in the classification when required; a CH index of 3.5 or greater, for instance, is defined as a C-H star on this system. Many carbon stars show $^{12}C/^{13}C$ isotope ratios significantly smaller than solar (92), and this is indicated with a j -index, again running from 1 to 5, where 1 indicates a solar ratio, and 5 a ratio of about 3. How this j -index is determined is explained below; the j -index is usually not included in the spectral type unless $j > 3.5$. Some carbon stars show the Merrill–Sanford bands of SiC_2 , and for these stars an MS index is appended to the spectral type. Accurate classifications on this system are possible using classification-resolution spectra ($\sim 3 \text{ \AA}$), although high-resolution spectra can help to increase the precision and discrimination (Barnbaum 1994).

As an aside, the appearance of the carbon stars in the infrared K-band may be judged from Figure 8.7. The K-band in cool stars is dominated by CO bands, and it thus turns out that carbon stars in this region look remarkably like M-type stars. The reason for this may be discovered in §8.4.2.

THE C-R STARS

The C-R stars are the warmest of the carbon stars, and the early C-R stars are generally characterized by appreciable flux in the blue-violet. While a prominent CN band at $\lambda 4215$ and C_2 Swan bands at $\lambda 4737$ and $\lambda 5165$ obscure parts of the blue and blue-violet (see Figure 8.10), in the early C-R stars a few of the standard

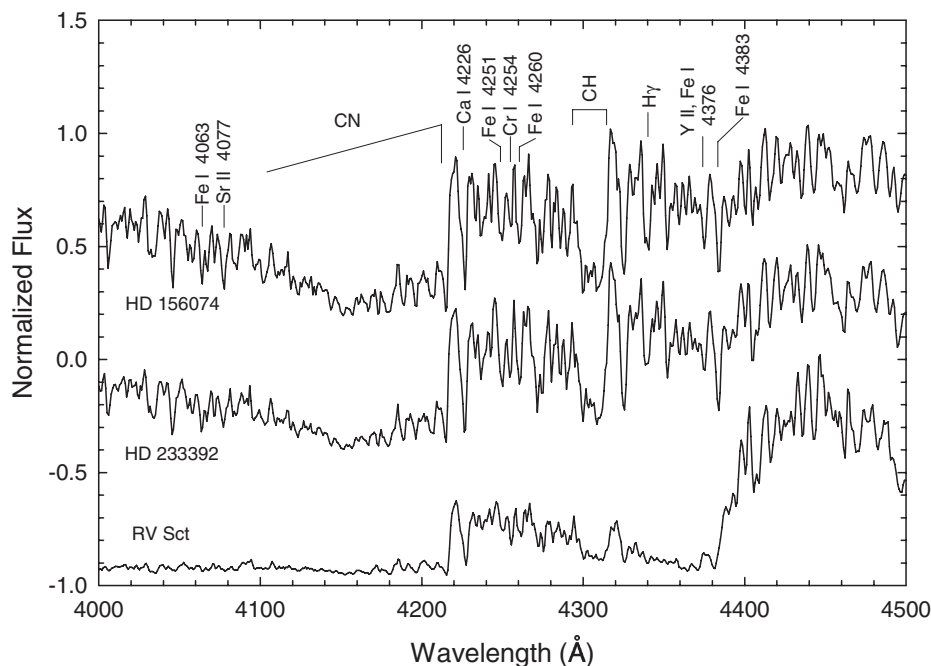


Figure 8.11 A temperature sequence in the violet for carbon R-type stars at higher resolution than Figure 8.10; see that figure for the spectral types of the illustrated stars. In the early C-R stars, the equivalent “oxygen” temperature type may be judged from the ratio of the Cr I $\lambda 4254$ line to the neighboring Fe I lines, and the $H\gamma$ /Fe I $\lambda 4383$ ratio. The luminosity sensitive ratios, Sr II $\lambda 4077$ /Fe I $\lambda 4063$ and Y II $\lambda 4376$ /Fe I $\lambda 4383$, are indicated. Spectra from Barnbaum, Stone, & Keenan (1996).

temperature classification criteria used in the G- and K-type giants may be employed to judge the equivalent “oxygen” temperature type (see Figure 8.11). Of particular use is the metallicity-independent ratio of the Cr I $\lambda 4254$ resonance line with neighboring higher excitation Fe I lines. The strength of the Balmer lines in ratio with neighboring Fe I lines ($H\gamma$ /Fe I $\lambda 4383$, for instance) may also be used as a general guide to the temperature type. In the cooler C-R stars, the weakness or absence of the Balmer lines indicates a later equivalent oxygen type. However, opacity from overlapping carbon bands generally makes the Cr I/Fe I ratio unreliable in these stars. In the red, the strength of the Na I D doublet is unreliable at any type because of an overlapping CN band. The *s*-process elements (including Sr, Y, and Ba) are generally not enhanced in the C-R stars, and thus the luminosity criteria Sr II $\lambda 4077$ /Fe I $\lambda 4063$, 4071 and Y II $\lambda 4376$ /Fe I $\lambda 4383$ may be employed, but only in the early C-R stars (see Figure 8.11). In the late C-R stars, these lines are generally too obscured and thus these ratios are either unusable or unreliable. Note in figure 8.11 that the Y II/Fe I ratio in HD 156074 is slightly larger than in HD 233392, indicating that HD 156074 is more luminous. The Sr II/Fe I and Y II/Fe I luminosity criteria are not useable in the later C-R star RV Sct,

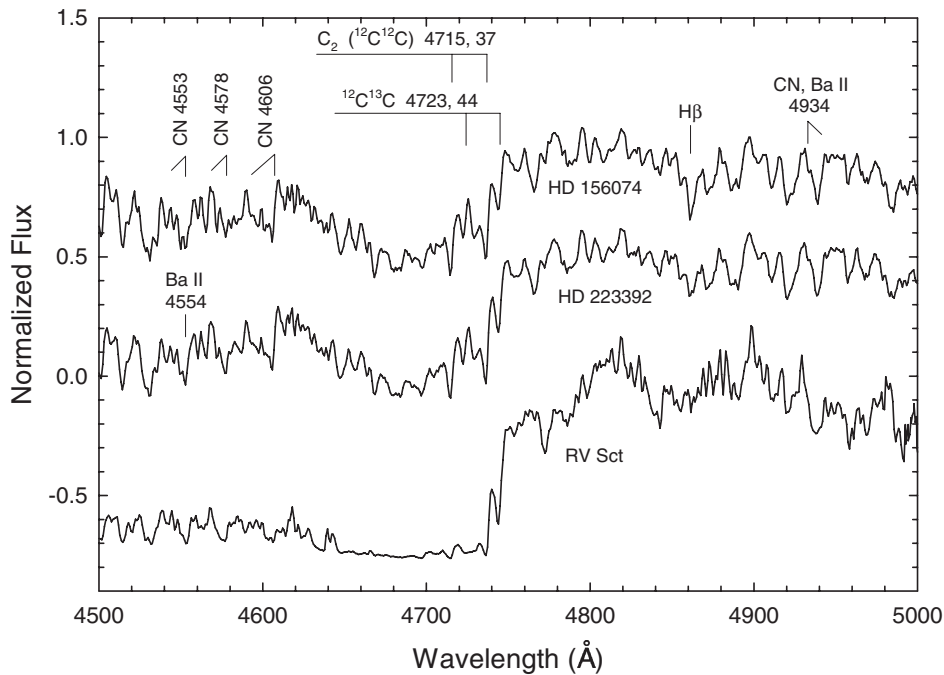


Figure 8.12 A temperature sequence in the blue for carbon R-type stars. See Figure 8.10 for the spectral types of the displayed stars. Note the temperature sensitivity of the $H\beta$ line, and the decreasing flux in the blue-violet with decreasing temperature. The broad C_2 band, labeled in Figure 8.10 as the $C_2 \lambda 4737$ band, is actually a blend of a number of bands, including one with band head at $\lambda 4715$, and the analogous isotopic bands of $^{12}C^{13}C$. The two Ba II lines in this region are blended with CN bands. Spectra from Barnbaum, Stone, & Keenan (1996).

because of both the reduced flux in the far violet and the enhanced blanketing due to carbon molecules.

Figure 8.12 is a high-resolution view in the blue of the same stars displayed in Figures 8.10 and 8.11. This figure illustrates that the isotopic bands of C_2 , especially those of $^{12}C^{13}C$ (which are most easily seen near the $\lambda 4737$ bandhead), are usually quite prominent in the C-R stars. Two Ba II lines are visible in this figure, but are heavily blended with nearby CN bands. If barium were enhanced in these stars, as it is in many C-N stars, the Ba II lines would dominate these blends. As it is, these spectra indicate that the barium enhancement is small or nonexistent, in accordance with the general tendency of s -process elements to have near-normal abundances in C-R stars.

Figure 8.13 shows a carbon abundance sequence for the early C-R stars at low resolution. HD 112127 shows carbon bands (including CN $\lambda 4215$ and $C_2 \lambda 4737$) just slightly stronger than an early K (K1–K2) giant; indeed the $C_2 \lambda 5165$ band can barely be discerned. HD 123821, although slightly warmer than HD 112127, shows stronger carbon bands, and in HD 76846, blanketing due to carbon molecules has significantly suppressed the violet-end flux.

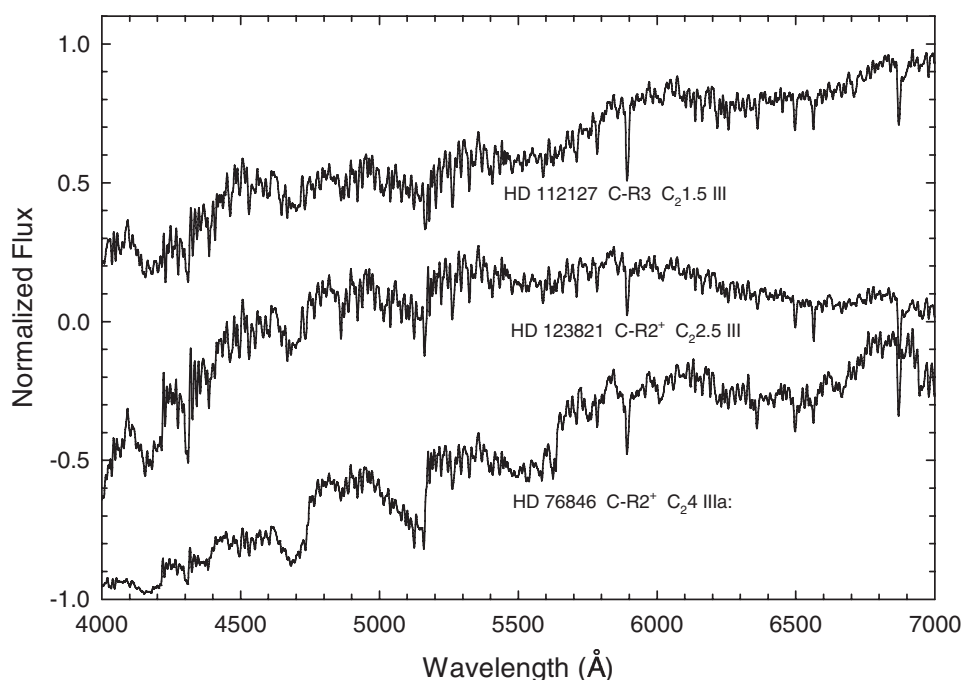


Figure 8.13 A low-resolution carbon-abundance sequence for the early carbon R-type stars. For an identification of the most prominent spectral features, see Figure 8.10. Spectra and spectral types from Barnbaum, Stone, & Keenan (1996).

THE C-N STARS

The C-N stars (Figure 8.14) can be distinguished from the C-R stars by their extreme redness and by strong absorption in the blue, with generally little or no flux shortward of 4400 Å. The C₂ isotopic bands in the C-N stars are generally weaker than in the C-R stars, and lines of *s*-process elements are more enhanced than in the C-R stars.

The temperature criteria used in the early C-R stars, namely the Cr I λ 4254/ Fe I ratio, and the strength of the Balmer lines are generally unusable in the C-N stars because of the lack of violet flux. H β is weak in the earliest C-N star displayed in Figures 8.14 and 8.15, while H α tends to be filled in or in emission in most C-N stars. Instead, the primary temperature criterion used in the C-N stars is the ratio Ba II λ 4554/Sr I λ 4607. It is important to note that these lines are blended with CN bands, but because these CN bands are of very similar strengths, this ratio is not strongly affected by the carbon abundance.

Figure 8.15 illustrates a temperature sequence for C-N stars in the blue region (compare with Figure 8.12, which shows the same region for C-R stars). Note that the CN-Ba II λ 4554 and CN-Sr I λ 4607 blends in the C-N stars are stronger than the λ 4578 CN blend, whereas in the C-R stars these blends have similar strengths. In the red, the Ba II λ 6497 line (Figure 8.14) is clearly stronger in the C-N stars.

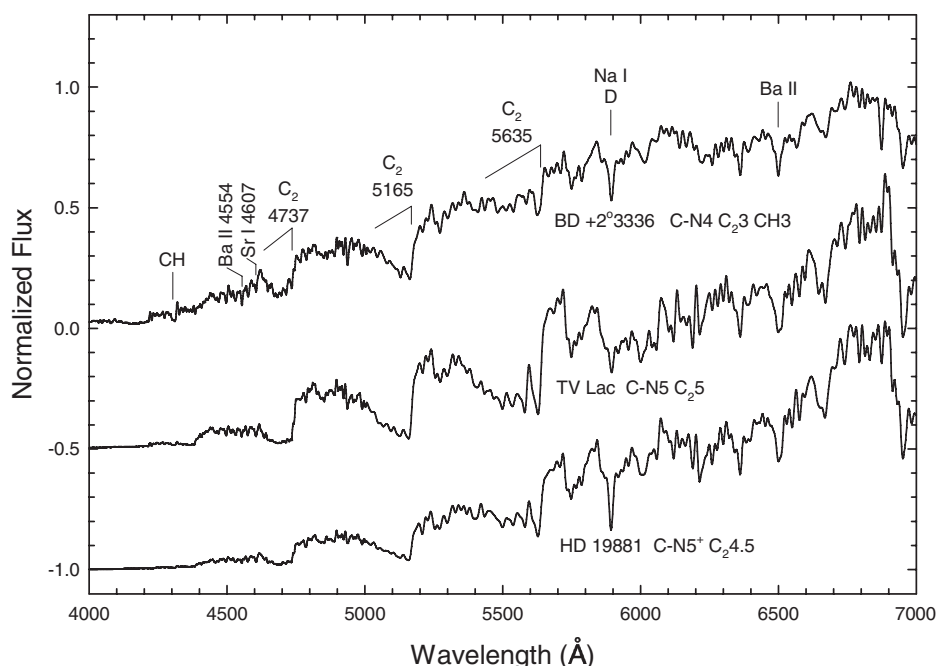


Figure 8.14 A low-resolution temperature sequence for the carbon N-type stars on the Keenan (1993) system. The most prominent features have been labeled, including the Swan bands of C_2 . Spectra and spectral types from Barnbaum, Stone, & Keenan (1996).

The enhancement of these *s*-process elements is an important way to distinguish between C-R and C-N stars of the same equivalent type.

In Figure 8.15 it is clear that BD + 2° 3336 is the earliest star of the three displayed; this is made evident by the fairly strong $H\beta$ line and by the Ba II/Sr I ratio exceeding unity. It is interesting to note that the vast majority of C-N stars lie in a fairly narrow temperature range; in Barnbaum, Stone, & Keenan (1996) 119 carbon stars are classified on the Keenan (1993) system. The earliest C-N star in that catalog has a spectral type of C-N4, and the latest C-N6, with 77% having spectral types between C-N5⁻ and C-N5.5. Having said that, the C-N stars do show a considerable diversity in the strength of the carbon molecular bands, and the earlier C-N stars have a slightly greater tendency to show the Merrill–Sanford bands (see below).

Keenan (1993) states that the CN/ C_2 ratio may be used to estimate the luminosity class in the C-N stars, as CN shows a positive luminosity effect, while C_2 (like CH) fades as the luminosity increases. But Barnbaum, Stone, & Keenan (1996) caution that luminosity classification in the C-N stars is difficult and unreliable, and indeed only a few of the earlier C-N stars have luminosity types in their catalog. The C-R luminosity criteria (Sr II $\lambda 4077$ /Fe I and Y II $\lambda 4376$ /Fe I) tend not to be useable in the C-N stars because of the lack of violet flux.

Figure 8.16 illustrates a carbon-abundance sequence for the C-N stars.

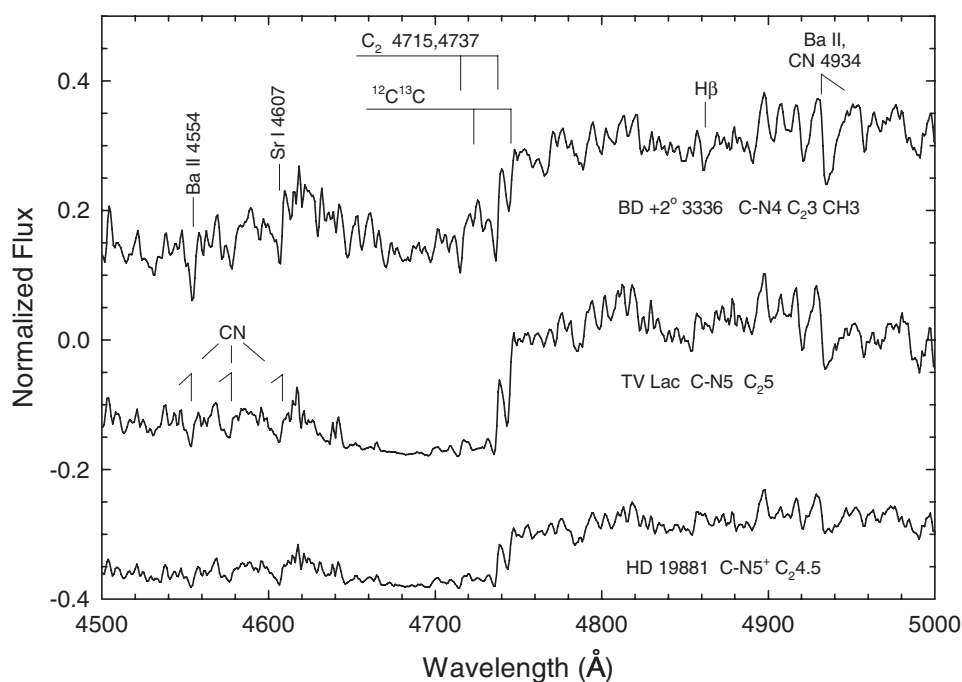


Figure 8.15 A temperature sequence in the blue for carbon N-type stars at higher resolution than Figure 8.14. In these stars the Sr I $\lambda 4607$ /Ba II $\lambda 4554$ ratio is a prime temperature criterion, although note that these lines are blended with CN bands. The strength of lines of the *s*-process elements (barium and strontium, in this figure) is one of the main ways to distinguish C-N stars from C-R stars of the same equivalent type. Compare with Figure 8.12. Spectra and spectral types from Barnbaum, Stone, & Keenan (1996).

THE C-J STARS

The C-J stars are carbon stars that show a remarkably large abundance of the isotope ^{13}C ; in these stars the $^{12}\text{C}/^{13}\text{C}$ ratio is generally less than 13 (Lambert et al. 1986), as compared to 92 in the solar system. The presence of isotopic bands of carbon molecules was first noted in certain carbon stars by Shane (1928) and also by McKellar (1949), but the appellation “J-type star” was first applied by Bouigue (1954), who noted bands of $^{13}\text{C}^{14}\text{N}$ and $^{12}\text{C}^{13}\text{C}$ in a number of carbon stars including HD 52432, WX Cyg, and WZ Cas. There is no indication in Bouigue (1954) why the letter “J” was chosen to designate these stars. Bouigue assigned a star the designation J on the basis of the ratio of $^{13}\text{CN } \lambda 6260$ to $^{12}\text{CN } \lambda 6206$; later Gordon (1967) defined a J-type star as one in which the strength of the $\lambda 6168$ $^{12}\text{C}^{13}\text{C}$ band is one-half the strength of the $\lambda 6122$ $^{12}\text{C}^{12}\text{C}$ band. The C-J stars are occasionally referred to as “ $\lambda 6168$ ” stars in the earlier literature.

The C-J stars may be readily recognized in the blue as the normally very weak $\lambda 4752$ $^{13}\text{C}^{13}\text{C}$ bandhead is conspicuous (see Figure 8.17) in these stars. However, to estimate the $^{12}\text{C}/^{13}\text{C}$ ratio and to assign the *j*-index on the Keenan (1993) system, it is better to use the $^{13}\text{CN } \lambda 6260$ / $^{12}\text{CN } \lambda 6206$ and $^{12}\text{C}^{13}\text{C } \lambda 6168$ / $^{12}\text{C}^{12}\text{C}$

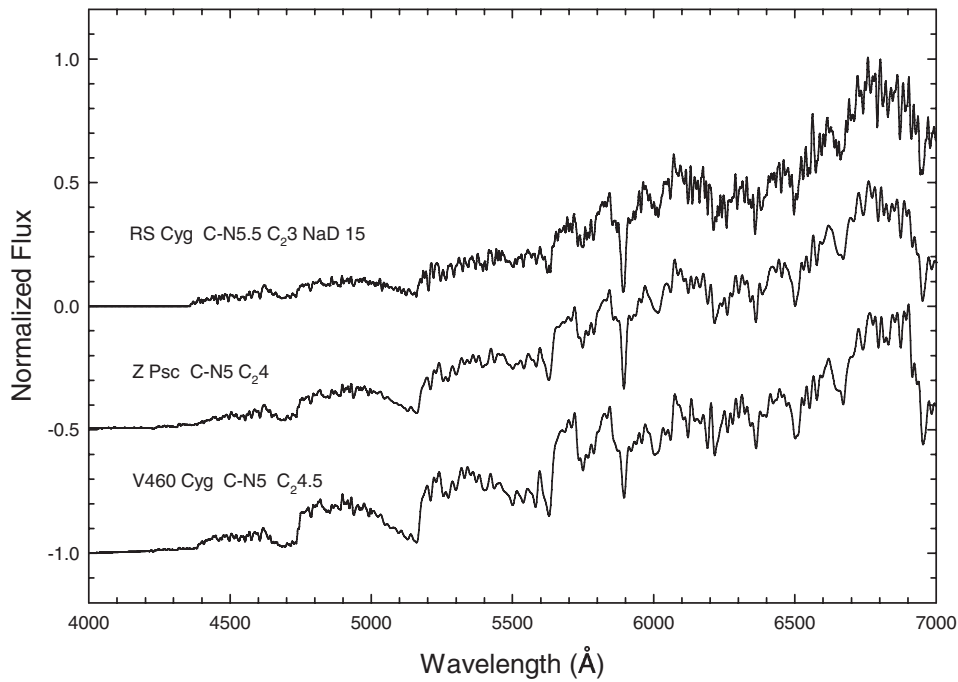


Figure 8.16 A low-resolution carbon-abundance sequence for the carbon N-type stars. For an identification of the most prominent spectral features, see Figure 8.14. RS Cyg has some characteristics of an SC star (see §8.4). Spectra and spectral types from Barnbaum, Stone, & Keenan (1996).

$\lambda 6122$ ratios (see Figure 8.18). The reason for this is that the $\lambda 4737$ $^{12}\text{C}^{12}\text{C}$ band is at or near saturation in these stars, making it difficult to compare with the $\lambda 4752$ $^{13}\text{C}^{13}\text{C}$ bandhead. The Keenan (1993) j -index ranges from 1 to 5 (and beyond in extreme cases); stars with $j > 3.5$ are considered C-J stars on this system. The assignment of equivalent “oxygen” types for the C-J stars may be accomplished using the temperature criteria for the C-R and C-N stars; indeed, the C-J stars generally have temperature types intermediate to those of the majority of C-R and C-N stars. It turns out that the C-J stars comprise most of the stars previously classified as late R or early N stars, and also those stars provisionally assigned by Keenan (1993) to the C-RN class.

The Merrill–Sanford bands of SiC_2 occur most commonly in the C-J and the early C-N stars. Figure 8.19 shows the spectra of two stars with strong Merrill–Sanford bands. The presence and strength of these bands is indicated in the Keenan 1993 system with an MS index, again running from 1 to 5. A recent examination of the Merrill–Sanford bands in carbon stars was carried out by Sarre, Hurst, & Lloyd Evans (2000); interestingly they concluded that the M-S bands are formed 2–3 stellar radii from the star, at a temperature substantially below the photospheric temperature. In the Barnbaum, Stone, & Keenan (1996) catalog, nearly 20% of the C-J and C-N stars show Merrill–Sanford bands. In the Large Magellanic Cloud, Morgan, Hatzidimitriou, & Cannon (2004) found a proportion closer to 27%.

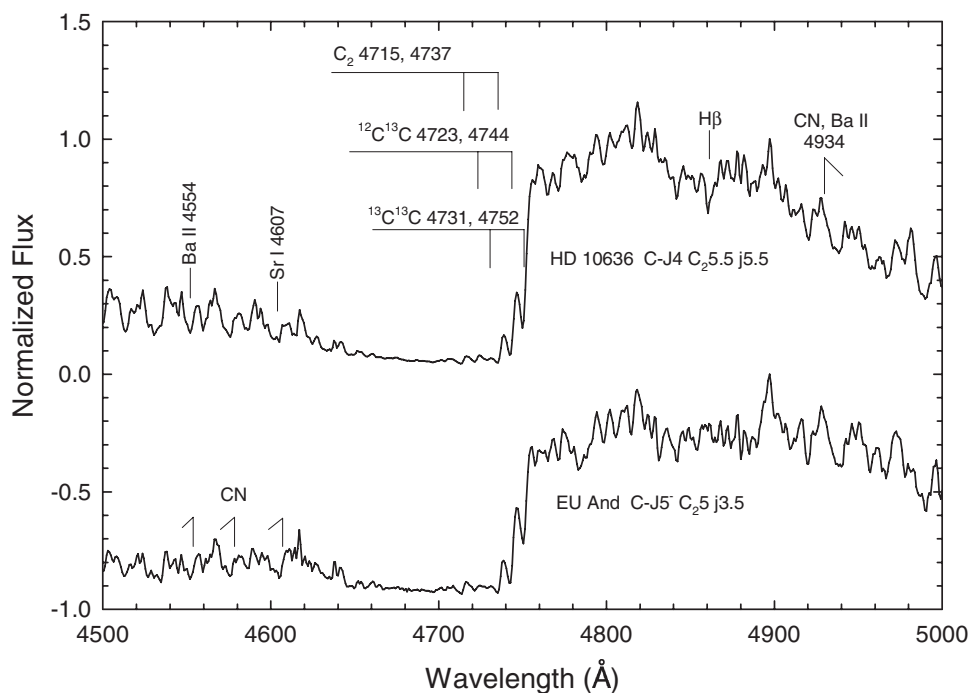


Figure 8.17 A temperature sequence of C-J stars in the blue. Note the strong isotopic $^{13}\text{C}^{13}\text{C}$ band-head at $\lambda 4752$ visible in both these stars. Note as well that the Ba II and Sr I lines are not enhanced in these stars (compare with Figure 8.15 for the C-N stars). Spectra and spectral types from Barnbaum, Stone, & Keenan (1996).

In the spectra of the C-J stars lines of the s -process elements are generally much weaker than in the C-N stars, a feature they share with the C-R stars.

The intermediate nature of the C-J stars may lead some to dismiss the separation of carbon stars into C-R, C-J, and C-N classes as artificial. However, it turns out that other physical characteristics correlate with these spectral classes. For instance, the C-N stars are more closely concentrated to the Galactic plane than the C-R stars. Many C-J stars show infrared excesses associated with oxygen-rich dust shells (Little-Marenin 1986; Willems & Jong 1986). And we have seen above that only the C-N stars show overabundances of the s -process elements. These differences suggest that the C-R, C-J, and C-N division reflects different evolutionary states. We will discuss current ideas on the origin of the different classes of carbon stars in §8.4.3 below.

THE C-H STARS

The spectra of the C-H stars are dominated by bands of CH in the blue-violet region of the spectrum. While the G-band (which is formed from the Q -branches of the CH A-X 0-0 and 1-1 bands located near 4300 \AA) is exceptionally strong in these stars, this is not unusual for early carbon stars; indeed the G-band is quite often

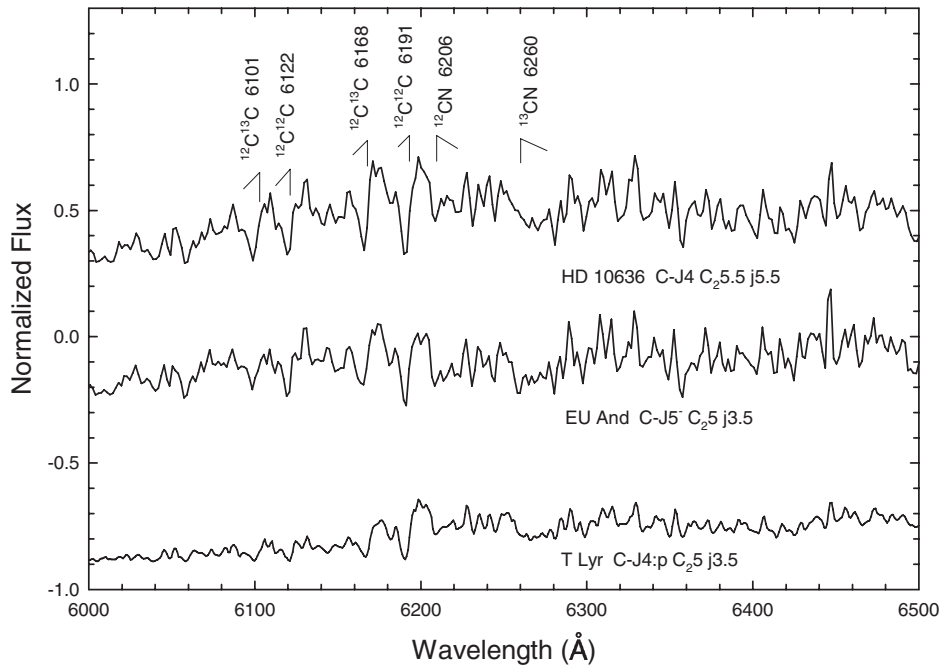


Figure 8.18 A temperature sequence of C-J stars in the red showing spectral features that may be used in the estimation of the isotopic j -index. Note in HD 10636 the isotopic bands involving ^{13}C are of nearly the same strength as those involving only ^{12}C , yielding a j -index of 5.5. Spectra and spectral types from Barnbaum, Stone, & Keenan (1996).

saturated in the spectra of early carbon stars. Instead, the distinguishing spectral feature of these stars is the strength of the P -branches of these same CH bands, which are visible as a broad depression longwards of the G-band (see Figures 8.20 and 8.21). The strength of the CH bands is indicated in the spectral type with a CH index, which runs from 1 (for a barely noticeable enhancement) to 5, although Barnbaum, Stone, & Keenan (1996) extend this range to 6 for stars with exceptionally strong CH features. Generally speaking, any star with a CH index greater than 4 is classified as a C-H star on the Keenan 1993 system (Barnbaum, Stone, & Keenan 1996), even though the C-H stars have been traditionally recognized as high-velocity, halo objects (see below).

While the C-H stars overlap the C-R stars and the early C-J stars in temperature, they differ from both of these types of carbon stars in that they generally show enhancements of the s -process elements. The C-H stars also show quite a wide range in the $^{12}\text{C}/^{13}\text{C}$ ratio, which generally varies between 4 and 25 (Vanture 1992a, b). Some C-H stars are early enough that the luminosity criteria, described above for the C-R stars, may be used, although the Y II $\lambda 4376/\text{Fe I } \lambda 4383$ ratio can be obscured by the strength of the CH-band P -branches.

THE C-HD STARS

The C-Hd stars are hydrogen-deficient carbon stars. These stars are distinguished by the almost complete absence of the G-band of CH and lines of hydrogen, but

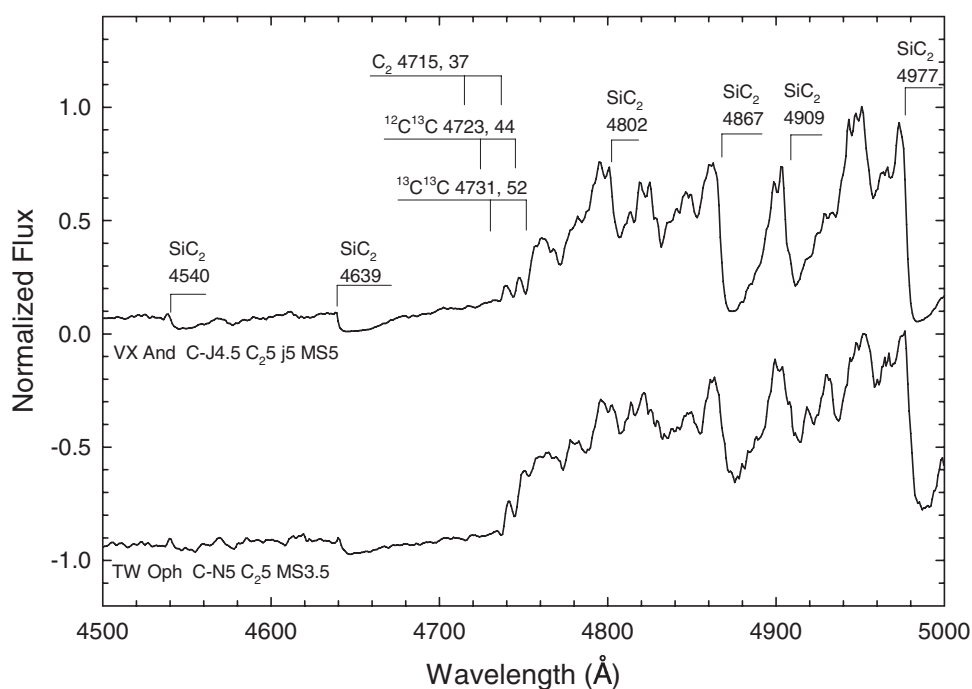


Figure 8.19 Two stars showing strong Merrill–Sanford bands. Compare with Figures 8.15 and 8.17. Spectra and spectral types from Barnbaum, Stone, & Keenan (1996).

are also characterized by stronger than normal bands of CN and C_2 . There are two types of hydrogen-deficient carbon stars. The most common are the R CrB variables, which spend most of their time at maximum light, but at irregular intervals undergo dramatic fadings during which the visual magnitude can decrease by up to 8 magnitudes in the course of a few weeks. There is an exceptionally rare class of nonvariable (or weakly variable) C-Hd stars that appear to be G-type Ib supergiants but show bands of CN and C_2 and exceptionally weak hydrogen lines and G-band (CH). Figure 8.22 shows spectra of two C-Hd stars, R CrB taken both at maximum light and during the early stage of a decline, and the weakly variable C-Hd star, HD 182040.

The dramatic fadings of the R CrB stars apparently occur when thick dust clouds are formed in their upper atmospheres, which can completely obscure the photosphere of the star. At maximum light the spectrum of these stars appears to be that of a hydrogen-deficient, carbon-rich F or G supergiant, but during the dust formation episodes the spectrum of the star can change from an absorption-line spectrum to one dominated by emission lines. During the early part of the decline in brightness, the emission-line spectrum consists of narrow emission lines of neutral and singly ionized species (see Figure 8.22). As the decline continues, this emission-line spectrum fades and is replaced by one consisting of a few strong, broad emission lines due, for the most part, to resonance transitions, namely Ca II H & K, the Na I D-lines, and Mg II h & k. An excellent review of the spectral and photometric variability of R CrB stars is given by Clayton (1996).

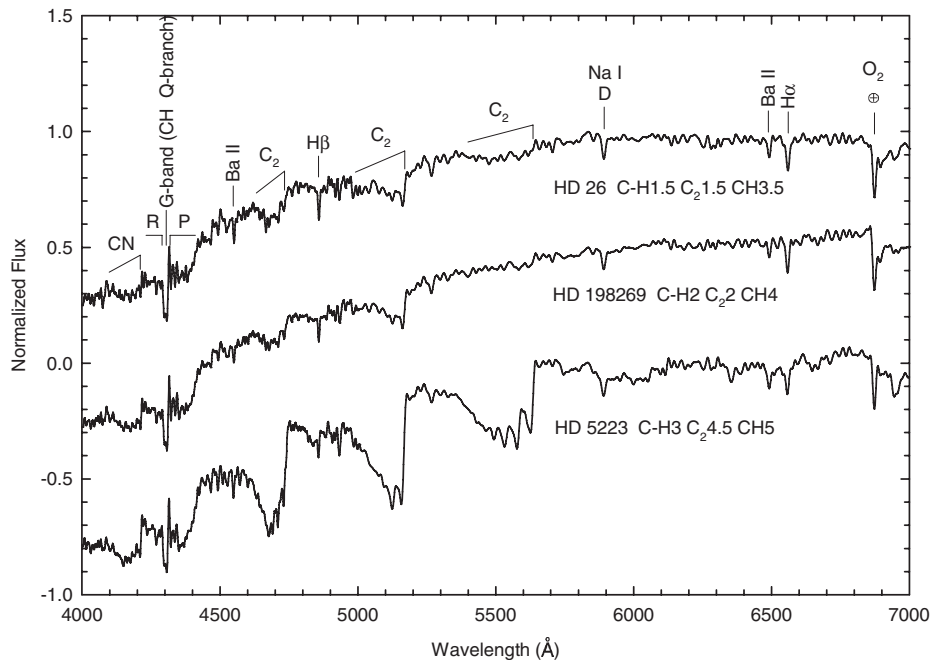


Figure 8.20 A low-resolution temperature sequence for the C-H type stars on the Keenan (1993) system. The most prominent features have been labeled, including the Swan bands of C_2 . Note the strength of the P -branch of the CH band, a distinguishing feature of these stars. Spectra and spectral types from Barnbaum, Stone, & Keenan (1996).

8.4 THE S-TYPE STARS

The S-type stars are late-type giant stars, many of which are long-period variables, that show bands of zirconium oxide (ZrO) in their spectra. Bright examples of this class include R Gem, R Cyg, and U Cas. The distinct nature of the spectra of these stars was first recognized in the early 1920s by Cannon & Pickering (1923) and Merrill (1922). Merrill was the first to propose that the peculiar nature of the spectra of these stars was due to the presence of ZrO. Many of these stars also show bands of TiO in their spectra, and thus it is clear that the S-type stars cover the same range of temperatures as the M-type giants. Other molecular bands of metallic oxides—such as VO, YO, and LaO—also often appear in the spectra of S-type stars.

Interestingly, the S-type stars form a bridge between the M-type stars and the carbon stars. The transition from the M-type stars to the pure S-type stars, which show only bands of ZrO and no TiO, it turns out, is only marginally related to the increased abundances of the s -process elements (of which zirconium is one) that characterize the S-type stars. Molecular dissociation calculations (Scalo & Ross 1976) have demonstrated that the sequence $M \rightarrow MS \rightarrow S \rightarrow SC \rightarrow C$ instead represents an increase in the ratio of carbon to oxygen; this ratio passes through a value of unity in the SC stars (see Keenan & Boeshaar 1980, and §8.4.2).

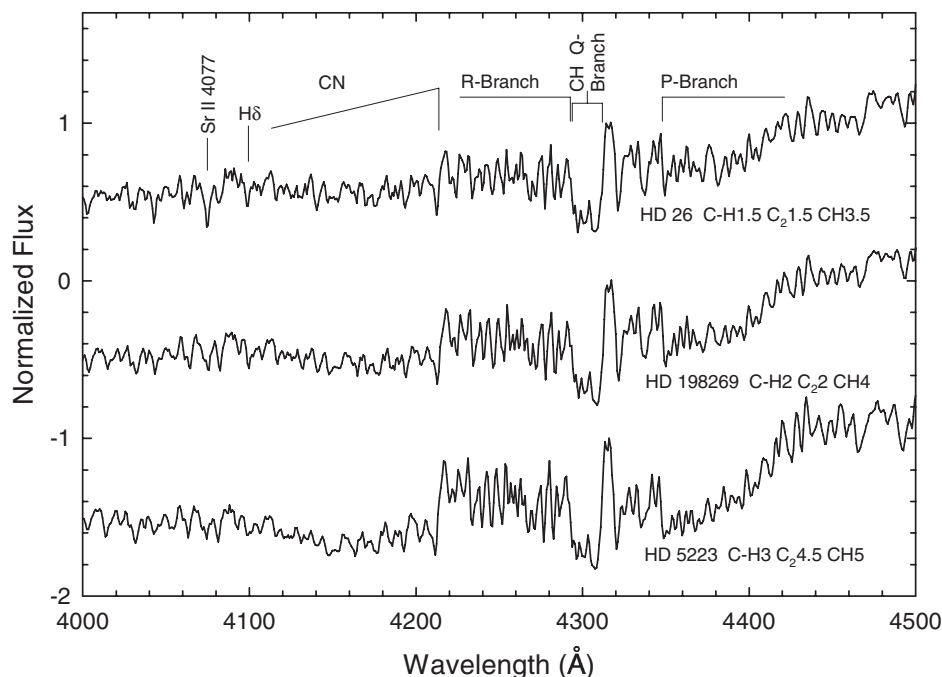


Figure 8.21 A temperature sequence in the violet for C-H type stars at higher resolution than Figure 8.20. Note the strength of the *R* and *P* branches of the CH band; the G-band is the *Q*-branch of the CH band. Compare with Figure 8.11. Spectra and spectral types from Barnbaum, Stone, & Keenan (1996).

The earliest systematic attempt to devise a classification system for the S-type stars was made by Keenan (1954), and was based on the relative strengths of the TiO and ZrO bands. However, the recognition of the SC class of stars, sometimes called the D-line stars (Gordon 1967) from the great strength of their Na I D-lines, necessitated a revision of this system. The first step in this process was taken by Ake (1979) with the introduction of a C/O index. This idea was taken up by Boeshaar & Keenan (1979) and Keenan & Boeshaar (1980) and plays a central role in the modern S-classification system that they devised. This system forms the basis of our discussion below.

8.4.1 The Boeshaar–Keenan S-Classification System

The classification of the S-type stars on the Boeshaar–Keenan (BK) system involves the designation of a C/O index, a temperature type, and, when possible, intensity estimates for the ZrO bands, the TiO bands, the Na I D-lines, the YO bands, and the Li I 6708 line. Practically speaking, what this means is that in order to fully classify a star on the BK system, it is necessary to have spectra in both the blue and red parts of the spectrum, and preferably these spectra should be obtained as close as possible in time, because of the variable nature of many of these stars.

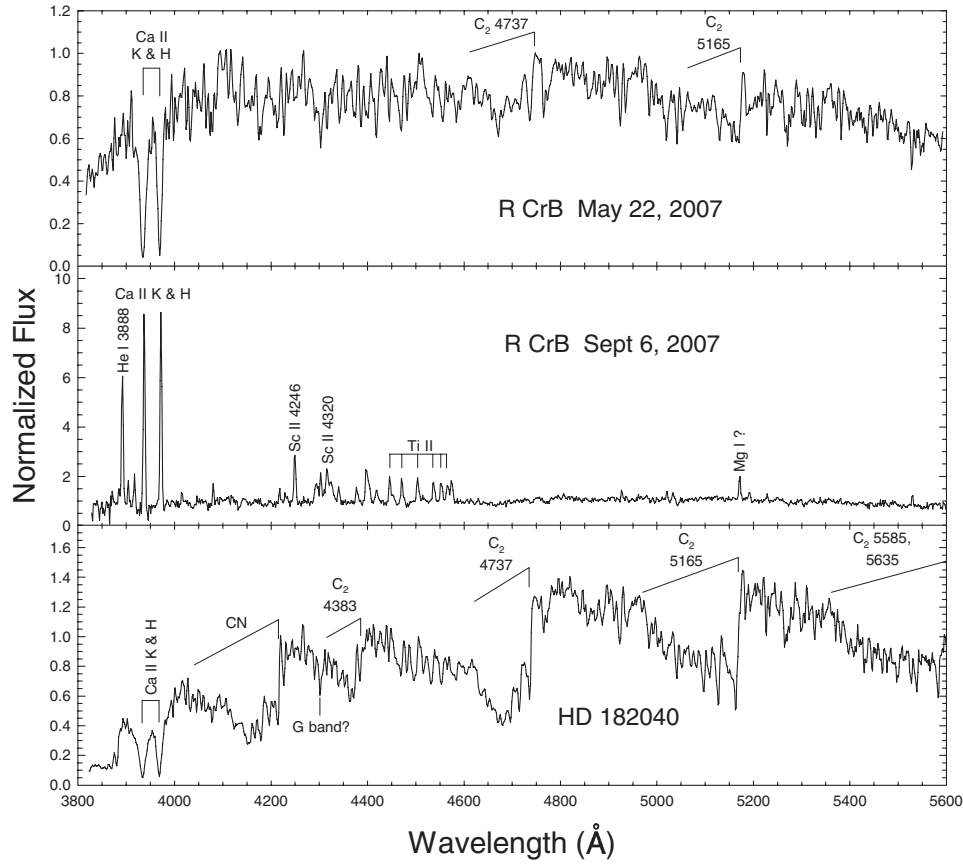


Figure 8.22 The spectra of two hydrogen-deficient carbon stars, including R CrB taken at maximum light (top panel) and during the early stage of a dropout (middle panel), as well as HD 182040, a weakly variable C-Hd star (bottom panel). R CrB has an early G Ib spectral type, but notice the absence of the hydrogen Balmer lines and the G-band in the spectrum taken at maximum light. Note as well the narrow emission lines in the early decline spectrum of R CrB. Line identifications for that spectrum are based on those in Alexander et al. (1972). HD 182040 shows very strong bands of C_2 , but the G-band is very weak or nonexistent. Spectra obtained at the Dark Sky Observatory. Thanks to C. E. McGahee for obtaining the early decline spectrum of R CrB.

Keenan & Boeshaar (1980) did not specify S-type standard stars, because most are spectrum variables, but instead gave spectral types for over 100 S-type stars with many at a number of different phases. These spectral types, plus the specification of the classification criteria below, should enable the accurate classification of most S-type stars. The format of a BK type is given below:

$$SX/n[e] \text{ ZrO TiO D YOLi}$$

where the “X” stands for the temperature type on the scale of the M-giants; thus an S6 star should have roughly the effective temperature of an M6 giant; the “n”

stands for the C/O index, which runs from 1 to 10, where 7–10 correspond to the SC stars, and 10 represents the transition to mild C-N type stars; an “e” is appended to the spectral type if emission lines of any type are observed (emission lines normally occur only in the variable S-type stars, and may not be present at all phases; see §8.2.3); finally, when possible, numerical estimates, on an arbitrary scale, of the strengths of various molecular and atomic features are included in the spectral type. These indices must be assigned on the basis of the spectral types in Keenan & Boeshaar (1980).

THE C/O INDEX

The C/O ratio cannot be measured directly in classification spectra, but its value may be estimated in the form of a C/O index from the relative strengths of TiO and ZrO, and the strength of the Na I D-lines (we will examine the physical basis for this statement below, in §8.4.2). The C/O-index criteria are outlined in Table 8.3, adopted from Keenan & Boeshaar (1980). The SC stars ($7 \leq \text{C/O index} \leq 10$) are best identified through the absence or near absence of molecular bands involving carbon or oxygen, and the excessive strength of the Na I D-lines. The estimated values for the C/O ratio in Table 8.3 are derived from Scalo & Ross (1976), and are included to show the extreme sensitivity of the S-star spectral morphology to the C/O ratio. It should be emphasized that this classification system does not depend on knowledge of the exact relationship between the theoretical C/O ratio and the C/O index. Figure 8.23 shows a sequence of blue spectra of S-type stars with increasing C/O index.

THE TEMPERATURE TYPE

In the MS stars, and S-type stars with a C/O index of 2 or less, the temperature criteria for the M-type giants, discussed in §8.2.2.1, can be used essentially unchanged, including those criteria involving the TiO bands. Of course, because the TiO bands fade with increasing C/O index, it is always best to use *ratios* of bands rather than the absolute strength of bands. Keenan & Boeshaar (1980) recommend the use of ratios of bands of TiO arising from different vibrational states, thus a ratio such as $\text{TiO}[\alpha(1, 3)\lambda 5810/\gamma'(1, 0)\lambda 5847]$ can be used in stars with a C/O index of 4 or less. In S-type stars in which the ZrO strengths \approx the TiO strengths (C/O indices 2–4), the total “intensity” of the ZrO and TiO bands combined is also a useful temperature criterion. However, as ZrO bands begin to dominate, it is best to abandon the use of the TiO bands, and rely on other temperature criteria. Keenan & Boeshaar (1980) have found that the ratio $\text{ZrO } \lambda 5305/\lambda 5552$ is very sensitive to temperature in pure S-type stars (C/O index 5–7), even though the $\lambda 5305$ band may be blended with other species. An important temperature criterion, usable throughout the S-type stars, but especially in those with C/O indices > 3 , including the SC stars, is the ratio $\text{Sr I } \lambda 4607/\text{Ba II } \lambda 4554$. This ratio is certainly also sensitive to luminosity, but luminosity criteria have not yet been worked out for the S-type stars. Finally, in the red, a ratio of two blended features, $\lambda 6450/\lambda 6456$,

Table 8.3 Classification Criteria for S-type Stars on the Boeshaar–Keenan System

Spectral Type	Criteria for C/O Index	Estimated C/O	Temperature Criteria
MXS	Strongest ZrO bands just visible, also YO		M-giant criteria
SX/1	TiO \gg ZrO, YO	<0.95	M-giant criteria
SX/2	TiO > ZrO	0.95:	M-giant criteria plus total intensity ZrO + TiO
SX/3	TiO = ZrO, YO strong	0.96	ZrO + TiO, Sr I λ 4607/ Ba II λ 4554 from S0 to S5, ZrO λ 5305/ λ 5551. IR LaO strong after S5
SX/4	ZrO > TiO	0.97	Same as SX/3
SX/5	ZrO \gg TiO		ZrO intensity and same ratios as above
SX/6	ZrO strong, no TiO	0.98	Same as SX/5
SX/7 = SC X/7	ZrO weaker, D lines strong	0.99	Same as above, and λ 6456/ λ 6450.
SC X/8	No ZrO or C ₂ D-lines very strong	1.00	λ 4607/ λ 4554, λ 6456/ λ 6450
SC X/9	C ₂ very weak, D-lines very strong	1.02	Same as above
SC X/10 = C-N C ₂ 1	C ₂ weak, D-lines strong	1.1:	λ 4607/ λ 4554

constitutes a useful temperature criterion, especially for the SC stars. These temperature criteria are summarized in Table 8.3. Figure 8.24 shows the spectra of three selected S-type stars, including the SC star VX Aql, in the red and near-infrared. Note in WX Cam the strength of the LaO bands, especially the infrared LaO bands at $\lambda\lambda$ 7880 and 7910. These bands are useful temperature criteria for S-type stars later than S5.

8.4.2 The Physical Basis of the M \rightarrow MS \rightarrow S \rightarrow SC \rightarrow C Sequence

The spectral sequence M \rightarrow MS \rightarrow S \rightarrow SC \rightarrow C involves a strengthening of ZrO bands at the expense of the TiO bands that dominate the spectra of M-type stars, followed by the fading of the ZrO bands and strengthening of the Na I D-lines, and finally the appearance of bands of C₂ and other carbon molecules. This sequence can be explained in a fairly straightforward way (Scalo & Ross 1976) by an increase of the C/O ratio through the value of unity. There are two physical effects involved here, first a change in the nature of the mean opacity in the cool

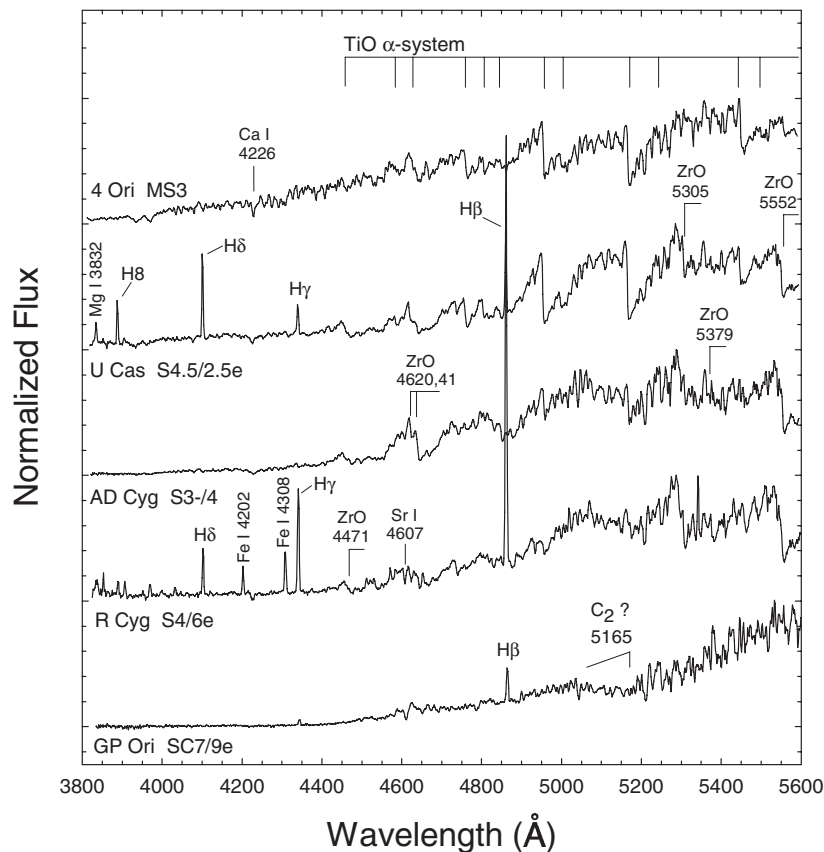


Figure 8.23 A sequence of S-type stars with increasing C/O index. Some of these stars are Mira variables and show emission lines at certain phases. Spectra obtained at the Dark Sky Observatory.

atmospheres of these stars, and second, a molecular dissociation effect. Let us first examine how the mean opacity changes with a change in the C/O ratio.

In the cool atmospheres of M- and S-type stars, typical temperatures are on the order of 2000–3000 K. At these temperatures, H_2O is a major contributor to the mean opacity, which sets the level of the formation of the continuum. As the C/O ratio increases toward unity, oxygen becomes less available (as most of the oxygen becomes locked up in the robust molecule CO),² and thus the abundance of H_2O begins to decrease. This reduces the mean opacity, which means that the spectral continuum is formed at a greater depth, and thus there is a greater mass (or column density) in the spectral-line forming layers above the continuum formation depth. The effect of this change in the mean opacity is to generally strengthen spectral

²The CO molecule has a dissociation energy of 11.08 eV, much higher than any of the other common diatomic molecules involving carbon or oxygen in stellar atmospheres. This high dissociation energy drives the equilibrium equation $\text{C} + \text{O} \rightleftharpoons \text{CO}$ almost completely toward the right, meaning that CO will take up almost all the available carbon or oxygen, depending on which is less abundant.

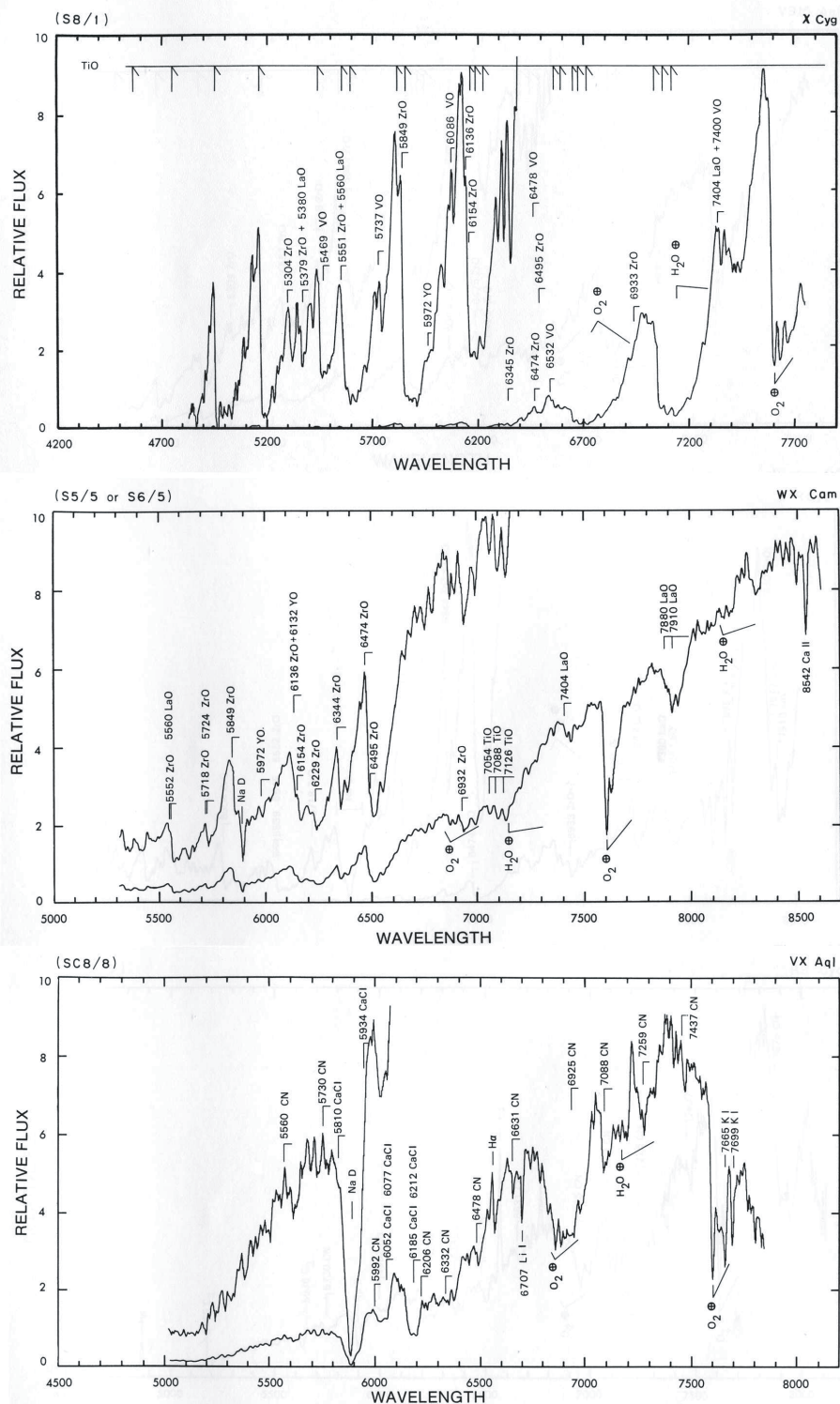


Figure 8.24 A montage of three S-type stars from Turnshek et al. (1985). Note the very strong Na I D-line in the SC star VX Aql.

lines as the C/O ratio increases towards unity. This is the major contributing factor to the strengthening of the Na I D-lines, but this effect also tends to strengthen the molecular bands.

However, for the metallic oxides, such as TiO, ZrO, AlO, VO, LaO, and YO, there is another important effect. As the C/O ratio increases toward unity, the abundance of free oxygen declines, and the equilibrium of the metallic oxides is driven toward dissociation. The metallic oxides with dissociation energies less than 7 eV (TiO, AlO, and VO) are relatively fragile and experience the greatest dissociation; for these molecules dissociation wins over the general line-strengthening effect due to the change in the mean opacity, and their molecular bands fade. On the other hand, the more robust metallic oxides—those with dissociation energies greater than 7 eV (ZrO, LaO, and YO)—suffer less dissociation, and at least at first, the general line strengthening dominates, and the bands of these molecules become more prominent. Eventually, however, as C/O approaches unity, even these robust molecules dissociate, leading to the SC stars in which bands of metallic oxides and carbon molecules are essentially absent. When C/O exceeds unity, carbon molecules, such as C₂ and CN, begin to dominate the spectrum, leading to the carbon stars.

8.4.3 Stellar Evolution and the Nature of the Carbon and S-type Stars

It should be clear from the previous sections in this chapter that the N-type carbon stars and the S-type stars have a number of characteristics in common. Both types of star are, of course, red giants, and a significant fraction of C-N and S-type stars are either semiregular pulsating variables or Mira variables (see §8.2.3). Another important common feature is that both types of star have enhanced abundances of carbon and *s*-process elements. Both carbon and the *s*-process elements are products of advanced nuclear burning. Carbon can be produced at two stages of nuclear burning, first during core helium burning (which occurs, in Population I stars, on the red giant branch), and then, considerably later, during shell helium burning on the *Asymptotic Giant Branch* (AGB). Carbon from core helium burning is very difficult to bring to the surface of a star, but deep convective currents that form in the envelopes of AGB stars can dredge nuclear-processed, carbon-rich material from the helium-burning shell region to the surface. Alpha capture by ¹³C nuclei can yield neutrons during helium-shell burning ($^{13}\text{C} + \alpha \rightarrow ^{16}\text{O} + n$), which then can lead to the production of many heavy elements via the slow or *s*-process of neutron capture. Examples of *s*-process elements are strontium, yttrium, barium, zirconium, technetium, and lanthanum. Helium-shell burning in AGB stars is subject to a thermal instability that leads to the development of thermal pulses in the helium-burning shell that eventually result in the ejection of the stellar envelope and the creation of a planetary nebula. Before this happens, the thermal pulses cause the episodic formation of deep convective currents that are able to dredge the carbon-rich, *s*-process-rich material up to the surface. Successive dredge-ups thus increase the C/O ratio in the atmosphere of the star as well as the abundance

of *s*-process elements, moving the star through the spectral-type sequence $M \rightarrow MS \rightarrow S \rightarrow SC \rightarrow C-N$. The presence of radioactive technetium (for which all isotopes have relatively short half-lives, on the order of 10^5 – 10^6 yrs) in the atmospheres of many of the *variable* S-type stars (Merrill 1952) is direct evidence of the active dredge-up of nuclear-processed material in these stars and is strong observational support for this scenario.

However, this scenario does not explain the whole range of carbon star and S-star types. For instance, many of the nonvariable S-type stars do not show technetium (Tc) in their spectra, leading to the realization that two groups of S-type stars exist: the “intrinsic” Tc-rich S-type stars that are AGB stars undergoing thermal pulses and the “extrinsic,” Tc-poor S-type stars, which have presumably acquired their abundance peculiarities in another way (see Jorissen & van Eck 2000, and references therein). In addition, the C-R stars and the C-J stars, while carbon-rich, do not show strong enhancements of the *s*-process elements, and so really do not fit into this scenario.

A characteristic of the Tc-poor S-type stars is that essentially all of these stars are binaries. It turns out that these stars have the same distribution of orbital periods, eccentricities, and mass ratios as the strong barium stars (§7.6.3), and this immediately suggests a relationship between the two groups. The enhanced abundances of *s*-process elements and carbon seen in the barium stars are believed to have been acquired by mass transfer from an AGB companion that has since evolved into a white dwarf (see §6.5.2). Thus both binarity and abundance characteristics point to a relationship, most probably evolutionary, between the two groups. Figure 8.25 summarizes the probable evolutionary scenarios for both Tc-rich and Tc-poor S-type stars. The transfer of nuclear-processed material from the AGB companion to the main-sequence predecessor of the barium stars and Tc-poor S-type stars is indicated in step (4) of that figure.

The Tc-rich and Tc-poor S-type stars cannot be distinguished at classification resolutions, as identification of the Tc I lines requires high resolution. Jorissen & van Eck (2000) discuss various ways that these two types may be distinguished without recourse to high-resolution spectroscopy.

Most C-H stars, as mentioned above (§8.3.2.2), are high-velocity stars and are most likely halo and/or thick-disk objects. Like the C-N and S-type stars, the high-velocity C-H stars show overabundances of the *s*-process elements relative to iron. The exceptions to this general picture are the “CH-like” stars, which, according to Yamashita (1975) who defined them, are low-velocity stars, usually without *s*-process enhancements. If these CH-like stars are neglected, it turns out that the remaining C-H stars have a very high binary frequency (McClure 1984). Thus a mass-transfer scenario can also be used to explain these stars.

What about the carbon stars such as the C-R and C-J stars that do not have significant enhancements of *s*-process elements? This abundance pattern is not entirely consistent with these stars being on the AGB. In the case of the C-R stars, Dominy (1984) suggests that the enhanced carbon is derived from the core helium flash rather than shell helium burning, but how carbon from the core is mixed to

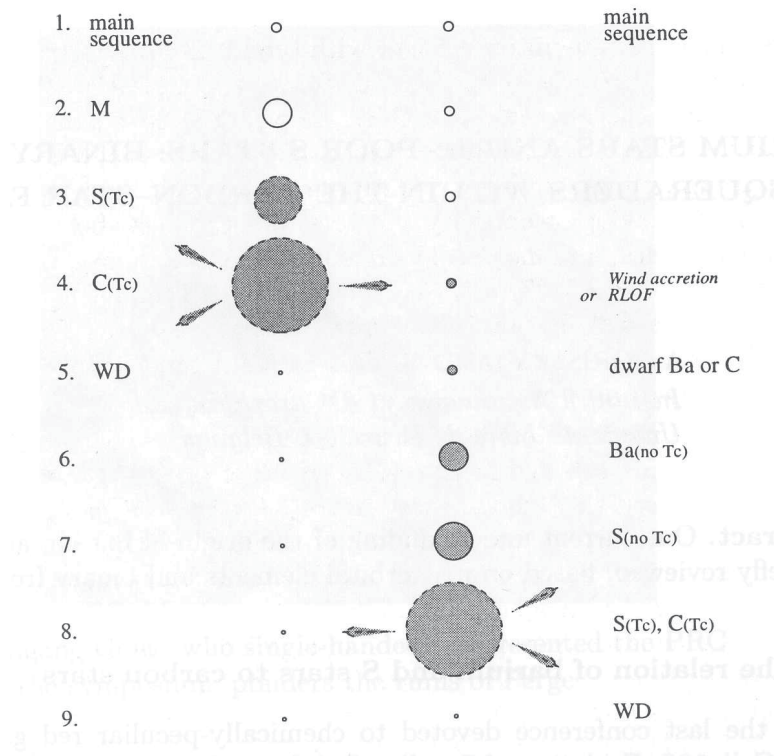


Figure 8.25 Evolutionary sequences for Tc-rich and Tc-poor S-type stars. Grey symbols represent *s*-process enriched stars and dashed boundaries indicate Tc-rich stars. The left column depicts the normal (i.e. not requiring binarity) $M \rightarrow S \rightarrow C$ evolution on the AGB whereas the right column represents the evolution of a companion star. Note that later evolution of the Tc-poor companion may transform it into a Tc-rich S-star on the AGB. Figure and caption reproduced from Jorissen & van Eck (2000) with permission from Kluwer Academic Publishers.

the surface is not known. The mass-transfer scenario in the case of the C-R stars is particularly problematical, not only because of the lack of *s*-process enhancements, but also because these stars have a very low binary frequency. McClure (2000) suggests that the C-R stars were once all close binaries that then merged; the merger would have mixed the interior of the combined star thoroughly, mixing some of the helium-flash or post-helium-flash carbon in the core to the surface. The likelihood, then, is that C-R stars are on the red giant branch (RGB) instead of the AGB.

The C-J stars—carbon stars that show very strong isotopic bands of C_2 and CN—have a number of interesting characteristics. For instance, a significant fraction of C-J stars have been discovered to have oxygen-rich dust shells, and some are even associated with OH and/or H_2O masers. This phenomenon is not understood. The origin of the relatively large abundance of the ^{13}C isotope is also somewhat mysterious. Normal 4He burning in the shell via the triple- α process

actually increases the $^{12}\text{C}/^{13}\text{C}$ ratio. The primary nuclear reaction that can increase the abundance of ^{13}C at the expense of ^{12}C is the CN cycle (hydrogen burning); if the CN cycle is active in the hydrogen-burning shell, deep convective currents may be able to dredge this material to the surface. This is called Hot Bottom Convective Envelope (HBCE) burning, and can occur when the star is on the AGB. Curiously, observations of C-J stars in M31 (Brewer, Richer, & Crabtree 2000) and the LMC (Richer, Olander, & Westerlund 1979; Smith et al. 1995) indicate that these stars are one to two magnitudes fainter than models predict for HBCE burning; the reason for this is that in models with initial masses less than $4M_{\odot}$ the bottom of the convective envelope is too cool to develop CN burning. Wasserburg, Boothroyd, & Sackmann (1995), however, pointed out that in low-mass RGB and AGB stars, deep convective currents might penetrate below the bottom of the standard convective envelope to regions where some CN processing takes place. Thus, the evolutionary state of the C-J stars is not yet clear. See Abia & Isern (2000) for a good discussion of these issues.

8.5 SYMBIOTIC AND ALGOL STARS

There are two kinds of composite stars that belong in this chapter. Though their dominant spectral morphology is often earlier than the M-type stars, their peculiarities can be understood in the light of the evolutionary scenario just outlined for interacting binary stars.

8.5.1 Symbiotic Stars

First come the *symbiotic stars* (SySs), which have been identified as a spectroscopically peculiar class of stars since the pioneering work of Mrs. Fleming and Miss Cannon on the HD catalogue early in the twentieth century. Miss Cannon (1916) assigned Z Andromedae to the class Ocp, thinking it to be a peculiar member of the Wolf–Rayet class of stars. Detailed work was done on Z And by H. H. Plaskett and later by P. W. Merrill, who eventually coined the name “symbiotic,” since their spectra seemed to be a combination of a cool giant with a planetary nebula. They were first thought to be single stars with peculiar atmospheres, but Frank Hogg, building on the work of Pol Swings, Otto Struve, and Merrill (1933), suggested they were binaries (Hogg 1934).

The SySs are now indisputably recognized to be interacting binaries, those with the largest orbital separations (Mikolajewska 2003). Their UV spectra bear the signature of a hot component, generally a WD star, while their optical spectra are dominated by that of a cool giant primary. In these spectral regions they are distinguished from normal stars by strong emission in the hydrogen lines and in those relatively highly ionized species that are usually found in planetary nebulae. These species regularly include He II and [O III], and sometimes [Ne III], [Fe V], C III, and N III. Figures 8.26 and 8.27 illustrate their spectra in the UV and optical.

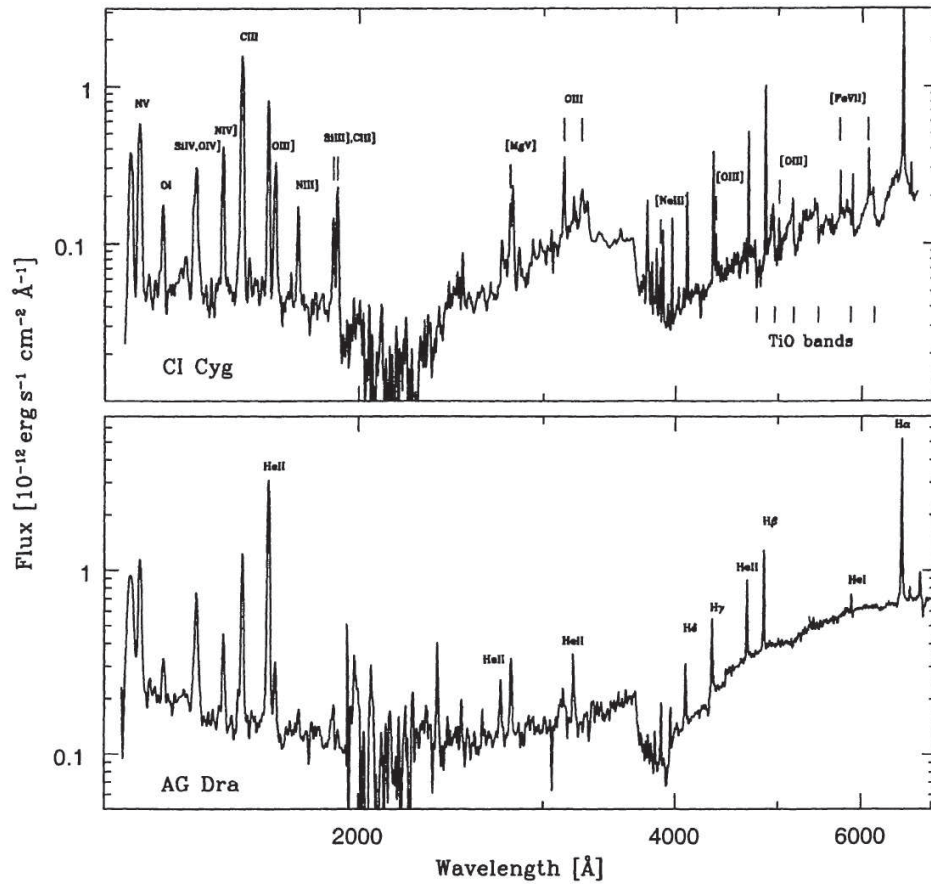


Figure 8.26 Quiescent optical and UV spectra for symbiotic stars. Strong TiO bands in the red spectrum of CI Cyg indicate an M4-5 III primary; they are absent in the yellow, Galactic halo system AG Dra with a K3 II-III primary. The intensity of the UV continuum and He II emission lines requires a similar temperature and luminosity of the hot component in both systems, whereas the CNO emission lines in AG Dra are systematically weaker than those in CI Cyg, which reflects the low metallicity of AG Dra. Another difference is the presence of strong, high-excitation forbidden lines in CI Cyg that are not visible in AG Dra. Figure taken from Mikolajewska (2003) and reproduced with permission of the Astronomical Society of the Pacific.

The latter figure for CH Cyg shows that they are indeed variables, having variations in spectra as well as in light, with the latter sometimes very large in amplitude (3 magnitudes in U for CH Cyg) and short in period (a few months). Eyres et al. (2002) describe how CH Cyg is in fact a triple system, with a symbiotic pair orbited by a G-K giant. Periodic mass outflows and resulting nebulosity complicate the picture, though prior to its outburst in 1963 CH Cyg was used as an M6 III standard spectrum. Nothing should be taken for granted with respect to these SySs.

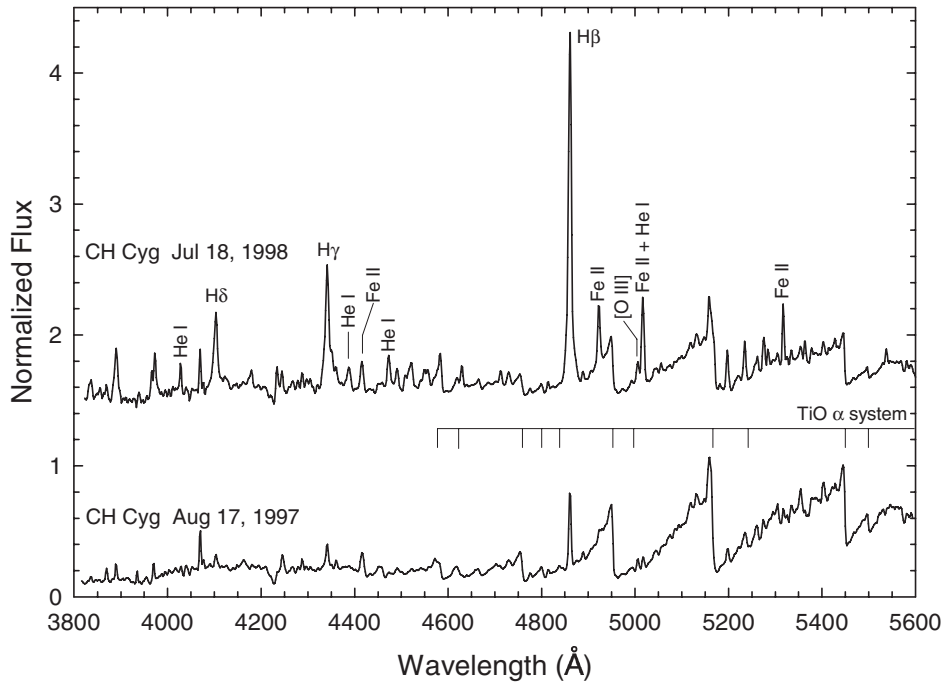


Figure 8.27 CH Cyg is an unusual s-type symbiotic star that undergoes occasional outbursts. The lower spectrum was obtained during quiescence, but the upper spectrum was obtained just after an outburst in mid-1998. Note the presence of He I, Fe II, and [O III] lines in the outburst spectrum. High-resolution spectra taken during this outburst also show weak lines of He II (Eyres et al. 2002). These two spectra are normalized at a common “continuum” point, and offset vertically by 1 continuum unit. Note, from the flux scale, that this implies considerable excess continuum *emission* in the outburst spectrum, causing veiling of the photospheric features, such as the TiO bands. Spectra obtained at the Dark Sky Observatory.

Allen (1982) distinguished two types of SySs, each with two subtypes, from their *JHK*L photometry and their 2- μ m spectroscopy. Those SySs with a stellar infrared continuum (s-type) and G or K primaries—the yellow s-types—have low metallicities and high space velocities, and thus are Galactic halo objects (Jorissen 2003). The red s-type SySs have M-giant primaries, and they may belong to the Galactic bulge. Figure 8.26 compares these two types. The red dusty d-type SySs—those showing IR excesses indicating a complex circumstellar environment—seem mostly to include a Mira in their binary composition (Whitelock 2003). The subset of yellow dusty SySs with a hotter, G-type spectrum (the infrared d’-types) are Galactic disk objects and have cooler dust, presumably at a greater distance from their G-star hosts than those with M-star hosts. S and D are also used for the two types of SySs, though the lowercase nomenclature will help distinguish these from the S-type stars of the previous section, §8.4.

Kenyon & Fernandez (1987) make a good case for classifying SySs in the NIR, for there prominent TiO and VO bands can be used for spectral types, providing

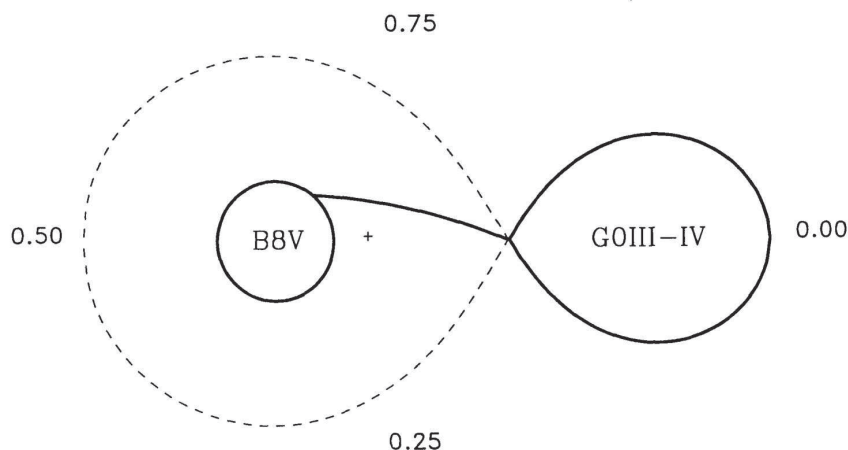


Figure 8.28 Model of an Algol-type binary system in which the cool secondary star has filled its Roche lobe and is transferring material through the inner Lagrangian point onto the hot, compact primary star. The model shows the predicted path of the gas stream, the range of spectral types, the spectral classes, and the lines of sight for different orbital phases. Figure from Richards & Albright (1999) and reproduced by permission of the AAS.

observations are made throughout at least one orbital cycle and the results averaged. Luminosity types are more problematic, but the CN bands at $\lambda\lambda 8026, 44, 68$ are useful, while that at $\lambda 9190$ may hold the best promise for determining luminosities in SySs when CN $\lambda 4215$ is filled in by the hot binary component (O'Connell 1973).

8.5.2 Algol Systems

Akin to the composite SySs are the Algol-type stars, named after their prototype β Per. These are close-interacting binary stars, whose components eclipse each other, as shown first in the case of Algol by the pioneering spectroscopist Vogel (1890). The “classical” Algols consist of a mid-B to mid-F main-sequence primary star, rather than a WD as for SySs, and an F to K giant or subgiant secondary. In general, the star eclipsed at the primary minimum is the more massive component. This picture gave rise to the well-known Algol paradox: an unevolved more massive primary is somehow accompanied by an evolved low-mass secondary (Struve 1948). This oddity was resolved by realizing there had been mass transfer between the components when the initially more massive star had overflowed its Roche lobe, a “semi-detached” configuration (Crawford 1955; Kopal 1955; Batten 1973). A model of an Algol system is shown in Figure 8.28. RZ Cnc and BL Tel have giant *primaries* and so are examples of non-classical Algols.

The spectra of classical Algols are those of a composite system that is dominated by the hotter component (Figure 8.29, and see §13.2). Emission lines, principally in hydrogen but also rather fainter in the Ca II K-line, Mg II $\lambda 4481$,

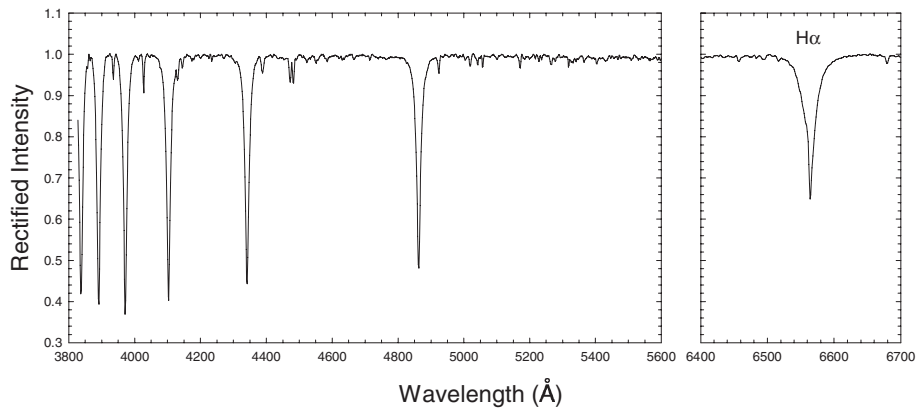


Figure 8.29 The spectrum of β Per (Algol) in the blue-violet (left) and in the vicinity of $H\alpha$ (right). The wavelength scale of the $H\alpha$ panel is twice that of the blue-violet. Note the shallowness and asymmetry of the $H\alpha$ profile; this is due to mass transfer in this interacting binary system. Spectra obtained at the Dark Sky Observatory.

Fe II, and other atomic species, can be observed just before and after total eclipse (Joy 1942). Given the interacting nature of these binaries, it is not surprising that the absorption line strengths can also vary, even from cycle to cycle at the same phase of the light curve. Happily, there have been careful high-resolution studies of line-profile variations with phase and the application of Doppler tomography to these (e.g., Richards & Albright 1999 for a summary of $H\alpha$ variations in 18 systems). However, there still seems plentiful opportunity for a systematic study at medium spectral resolution, one that looks carefully at the classification of Algols and their variations. Of course, today such a study that emphasized the UV and the IR could be very fruitful.

Bibliography

- Abia, C., & Isern, J. 2000, in *The Carbon Star Phenomenon*, ed. R.F. Wing (Dordrecht: Kluwer Academic Publishers), p. 89
- Ake, T. 1979, *ApJ*, 234, 538
- Alexander, J.B., et al. 1972, *MNRAS*, 158, 305
- Allen, D.A. 1982, IAU Coll 70, *The Nature of Symbiotic Stars*, ed. M. Friedjung & R. Viotti (Dordrecht: Reidel), p. 27
- Barnbaum, C. 1994, *ApJS*, 90, 317
- Barnbaum, C., Stone, R.P.S., & Keenan, P.C. 1996, *ApJS*, 105, 419
- Batten, A.H. 1973, *Binary and Multiple Systems of Stars* (Oxford: Pergamon), p. 226ff
- Bieging, J.H., Schmidt, G.D., Smith, P.S., & Oppenheimer, B.D. 2006, *ApJ*, 639, 1053
- Boeshaar, P.C., & Keenan, P.C. 1979, *Richerche Astronomiche*, 9, 39
- Bouigue, R. 1954, *Ann. d'Astrophys.*, 17, 104
- Bowen, G.H. 1988, *ApJ*, 329, 299
- Brewer, J.P., Richer, H.B., & Crabtree, D.R. 2000, in *The Carbon Star Phenomenon*, ed. R.F. Wing (Dordrecht: Kluwer Academic Publishers), p. 59
- Cannon, A.J. 1916, *Harvard Ann.*, 76, 3
- Cannon, A.J., & Pickering, E.C. 1918, *Harvard Ann.*, 91, 10
- Cannon, A.J., & Pickering, E.C. 1923, *Harvard Ann.*, 98, 258
- Clayton, G.C. 1996, *PASP*, 108, 225
- Crawford, J.A. 1955, *ApJ*, 121, 71
- Crowe, R.A., & Garrison, R.F. 1988, *ApJS*, 66, 69
- Davis, D.N. 1947, *ApJ*, 106, 28
- Dean, C.A. 1976, *AJ*, 81, 364
- Dominy, J.F. 1984, *ApJS*, 55, 27
- Eyres, S.P.S., et al. 2002, *MNRAS*, 335, 526
- Fitch, W.S., & Morgan, W.W. 1951, *ApJ*, 114, 548
- Fowler, A. 1904, *MNRAS*, 64, 16
- Garrison, R.F. 1972, *JAVSO*, 1, 39
- Garrison, R.F. 1997, *JAVSO*, 25, 70
- Gordon, C.P. 1967, Ph.D. thesis, Univ. Michigan
- Gordon, C.P. 1968, *ApJ*, 153, 915
- Habing, H.J., & Olofsson, H. 2003, *Asymptotic Giant Branch Stars* (New York: Springer), p. 1
- Hogg, F.S. 1934, *PASP*, 8, 14

- Jorissen, A. 2003, ASPC, 303, 25
- Jorissen, A., & van Eck, S. in *The Carbon Star Phenomenon*, ed. R.F. Wing (Dordrecht: Kluwer Academic Publishers), p. 259
- Joy, A.H. 1926, ApJ, 63, 281
- Joy, A.H. 1942, PASP, 54, 35
- Keenan, P.C. 1954, ApJ, 120, 484
- Keenan, P.C. 1984, in *The MK Process and Stellar Classification*, ed. R.F. Garrison (Toronto: David Dunlap Observatory), 29
- Keenan, P.C. 1993, PASP, 105, 905
- Keenan, P.C., & Boeshaar, P.C. 1980, ApJS, 43, 379
- Keenan, P.C., Deutsch, A.J., & Garrison, R.F. 1969, ApJ, 158, 261
- Keenan, P.C., & McNeil, R.C. 1976, *An Atlas of Spectra of the Cooler Stars: Types G, K, M, S, and C* (Columbus: Ohio State University Press)
- Keenan, P.C., & Morgan, W.W. 1941, ApJ, 94, 501
- Kenyon, S.J., & Fernandez-Castro, T. 1987, AJ, 93, 938
- Kopal, Z. 1955, AnAp, 18, 379
- Lambert, D.L., Gustafsson, B., Eriksson, K., & Hinkle, K.H. 1986, ApJS, 62, 373
- Little-Marenin, I.R. 1986, ApJ, 307, L15
- Massey, P., Levesque, E.M., Olsen, K.A.G., Plez, B., & Skiff, B.A. 2007, ApJ, 660, 301
- McCarthy, M.F. 1994, in *The MK Process at 50 Years. A Powerful Tool for Astrophysical Insight*, eds. C.J. Corbally, R.O. Gray, & R.F. Garrison, ASP Conference Series No. 60, p. 224
- McClure, R.D. 1984, ApJ, 280, L31
- McClure, R.D. 2000, in *The Carbon Star Phenomenon*, ed. R.F. Wing (Dordrecht: Kluwer Academic Publishers), p. 249
- McKellar, A. 1949, PASP, 61, 34
- Merrill, P.W. 1922, ApJ, 56, 457
- Merrill, P.W. 1933, ApJ, 77, 44
- Merrill, P.W. 1940, *Spectra of Long Period Variable Stars* (Chicago: University of Chicago Press)
- Merrill, P.W. 1952, ApJ, 116, 21
- Merrill, P.W., Deutsch, A.J., & Keenan, P.C. 1962, ApJ, 136, 21
- Mikolajewska, J. 2003, ASPC, 303, 9
- Morgan, D.H., Hatzidimitriou, D., & Cannon, R.D. 2004, MNRAS, 355, 1196
- O'Connell, R.W. 1973, AJ, 78, 1074
- Ohnaka, K., Scholz, M., & Wood, P.R. 2006, AA, 446, 1119
- Pickering, E.C. 1896, *Harvard Circ.*, 9
- Richards, M.T., & Albright, G.E. 1999, ApJS, 123, 537
- Richer, H.B., Olander, N., & Westerlund, B.E. 1979, ApJ, 230, 724
- Sanford, R.F., 1944, ApJ, 99, 145
- Sarre, P.J., Hurst, M.E., & Lloyd Evans, T. 2000, MNRAS, 319, 103
- Scarfe, C.D. 1966, MNRAS, 133, 99
- Scalo, J.M., & Ross, J.E. 1976, AA, 48, 219

- Shane, C.D. 1928, *Lick Obs. Bull.*, 396, 123
- Smith, V.V., Plez, B., Lambert, D.L., & Lubowich, D.A. 1995, *ApJ*, 441, 735
- Struve, O. 1948, *AnAp*, 11, 117
- Tsuji, T. 1981, *J. Astrophys. Astron.*, 2, 95 and 253
- Turnshek, D.E., Turnshek, D.A., Craine, E.R., & Boeshaar, P.C. 1985 *An Atlas of Digital Spectra of Cool Stars* (Tucson: Western Research Company)
- Wallace, L., & Hinkle, K. 1997, *ApJS*, 111, 445
- Wasserburg, G.J., Boothroyd, A.I., & Sackmann, I.-J. 1995, *ApJ*, 447, L37
- Whitelock, P.A. 2003, *ASPC*, 303, 41
- Willems, F.J., & Jong, T. 1986, *ApJ*, 309, L39
- Willson, L.A. 2000, *ARA&A*, 38, 573
- Vanture, A.D. 1992a, *AJ*, 104, 1986
- Vanture, A.D. 1992b, *AJ*, 104, 1997
- Vogel, H.C. 1890, *AN*, 123, 289
- Yamashita, Y. 1972, *Tokyo Obs. Ann.*, (2) 13, 169
- Yamashita, Y. 1975, *Tokyo Obs. Ann.*, (2) 14, 47

Chapter Nine

M Dwarfs and L Dwarfs—J. Davy Kirkpatrick

9.1 INTRODUCTION

“At which spectral type does the sequence of hydrogen-burning stars end and the sequence of brown dwarfs begin?” This often asked question has no direct answer simply because the spectral type (i.e., temperature) of a low-mass star or brown dwarf depends upon the object’s mass and age. A young brown dwarf can have the same temperature as an older, higher mass star, making the two kinds of objects at first glance appear spectroscopically indistinguishable.

Main sequence types of O, B, A, F, G, and K are comprised wholly of hydrogen-burning stars, and the T spectral type is comprised wholly of brown dwarfs. Types in between represent an admixture of both, meaning that this co-existence of stars and substellar objects at the same spectral subclasses is a phenomenon unique to M and L dwarfs. The further complication of gaseous molecule formation and, at cooler temperatures, grain formation add even more complexity to the physical decipherment of M and L dwarfs. The richness of features that give rise to the intricate and complex spectra of these objects also provides an abundance of diagnostics with which to study physical effects. This chapter addresses how the art and science of empirical spectroscopic classification can be used as the framework against which to decode the physics of these cool atmospheres.

9.2 THE DISCOVERY OF M DWARFS AND L DWARFS

9.2.1 M Dwarfs

Stars now classified as type M have been recognized since the days of Father Angelo Secchi. Secchi (1866) classified stars into four types based on the appearance of their spectra. These types—referred to as I, II, III, and IV—were further subdivided, renamed, and augmented by Williamina Fleming during her classification of 10,351 stars for the Henry Draper Memorial Catalogue (Pickering 1890). It was stars of Secchi’s class III that became Fleming type M, which is still used today. Secchi noted that the spectra of these stars were dominated in the photographic region by dark “lines” and striated “columns” that were later identified by Fowler (1904) as absorptions due to molecules of titanium oxide (TiO).

Astronomical spectroscopy in Secchi’s day was limited to the brightest objects, so the only M-type stars observed were M giants and supergiants like Betelgeuse (α Orionis), Ras Algethi (α Herculis), and Menkar (α Ceti) (Secchi 1868). In fact this remained the case for nearly the next fifty years. The Henry Draper Memorial

Catalogue (limited to declinations north of -25°) contained stars as faint as V -band magnitude of ~ 6.5 , yet despite the large number cataloged, just missed the brightest M dwarf, Lacaille 9352, in both magnitude ($V = 7.34$) and sky location ($\text{Dec} \approx -36^\circ$).¹

With the advent of precision astrometric measurements, the parallaxes for many proper motion stars were determined. A few of these were discovered to lie close to the Sun despite their relatively faint magnitudes. One of these, Lalande 21185, was extensively monitored by Winnecke (1858), Kapteyn (1890), Flint (1895), and Russell (1905). Another of these closely monitored stars was Groombridge 34, which in 1913 became the first M dwarf to have its spectrum acquired (Adams 1913). This was followed closely by the spectrum of Lalande 21185 a few months later (Adams & Kohlschütter 1914). By the middle of the next decade, almost one hundred M dwarfs had been classified (Adams et al. 1926), the latest of which— α^2 Eridani C—was typed as mid-M.

9.2.2 L Dwarfs

The discovery of L dwarfs is separated from the study of Secchi's M-type stars by over 120 years. It was during a near-infrared imaging search around white dwarfs that Becklin & Zuckerman (1988) discovered a very red companion to the star GD 165. An optical spectrum of the companion, GD 165B, was first obtained by Kirkpatrick et al. (1993), who noted that TiO absorption, which is the hallmark of the M spectral class, was not seen. Other observed absorption bands were found not to match methane or ammonia features seen in Jupiter and Saturn. The two independent temperature estimates for GD 165B (Zuckerman & Becklin 1992; Kirkpatrick et al. 1993) supported a temperature between that of known M dwarfs and the giant planets of our Solar System.

In the years following this initial discovery, other objects later in type than M9.5 dwarfs and spectroscopically akin to GD 165B were discovered. The first of these was announced by Kirkpatrick et al. (1997). This was followed closely by the discovery of three more objects by Delfosse et al. (1997), one apiece by Ruiz et al. (1997), Rebolo et al. (1998), Martín et al. (1998), and Delfosse et al. (1999), and nineteen others by Kirkpatrick et al. (1999). Most of these discoveries were made possible by the advent of larger-format infrared array detectors that allowed not only searches for cooler companions but also vaster areal surveys of generic sky. Two examples of the latter are the Two Micron All Sky Survey (2MASS, Skrutskie et al. 2006) and the Deep Near-infrared Sky Survey (DENIS, Epchtein et al. 1999).

It is interesting to note that in the history of M dwarf spectroscopy, approximately thirteen years elapsed between the first classified M dwarf and the 100th. In the history of the L spectral type, on the other hand, that same length of time has produced ~ 500 classified L dwarfs (<http://DwarfArchives.org>).

¹Some references list Lacaille 8760 as the brightest M dwarf although it is more often regarded as a late-K dwarf. With $V = 6.68$ and $\text{Dec} \approx -39^\circ$, it was also not included in the Henry Draper Memorial Catalogue.

9.3 SPECTROSCOPIC CLASSIFICATION

9.3.1 M Dwarfs in the Optical and Near-infrared

At the turn of the twentieth century, stellar spectra were traditionally taken in the visible region not just because hotter stars have their peak flux in this region but also because detectors (the human eye and the photographic plate) operated in this wavelength regime. M dwarfs actually have their peak flux at near-infrared wavelengths,² but technological advances allowing faint spectra to be recorded in this region were still decades away. Therefore, M dwarf classifications were based on features available in the visible. Because of the richness of features at these wavelengths—particularly the many transitions of TiO and other molecules—this proved to be an excellent choice.

Figure 9.1 shows line and band identifications for a mid- and a late-M dwarf between 4000 and 9000 Å. Immediately apparent in the figure is the fact that most of this region is blanketed by TiO absorption. Only a few areas such as the pseudo-continuum peaks near 7000 Å, 7300–7500 Å, and 8100–8200 Å lie clear of TiO bands. In addition to this dominant molecule, absorption from molecules of VO, MgH, CaH, CrH, FeH, and CaOH and lines of Ca II, Mg I, Na I, K I, Rb I, and Cs I are noted. Also remarkable is the dramatic change in the slope of the spectrum between mid- and late-M, with the latter showing a rapid rise in flux at the longest wavelengths shown.

9.3.1.1 Temperature Classification

Using the strength of the TiO bands as the primary indicator of the M subtype (Morgan 1938), researchers by the early-1940s had classified some 138 M dwarfs within ~10 pc of the Sun (Kuiper 1942). Around this same time the MK classification system was announced (Morgan et al. 1943) but it defined dwarf standards only as late as M2. This left individual researchers no framework against which to classify later M dwarfs, and as a result different and somewhat conflicting systems were invented to fill the void.

The two main systems were those of Kuiper (1942) and Joy (1947). Both classified M dwarfs based on TiO band strengths. However, the latter system tied types to the M-giant classification scheme and the former established M dwarf classifications completely independently of M giants. As the published types for Wolf 359 show—M8 on the Kuiper system and M6 on that of Joy—this led to substantial differences for mid- to late-M dwarfs. Part of this discrepancy was a result of the fact that Kuiper's spectra were taken at slightly longer wavelengths (the photographic yellow-red region) than those of Joy (the blue region), and he mistakenly assumed that the molecular band near 6200 Å was attributable to TiO alone. This

²Readers should be aware that the terms “optical,” “near-infrared,” “infrared,” etc. are used in somewhat different ways in this chapter and the next than in the rest of the book. See the Important Note on Terminology and Units at the beginning of the book for more details.

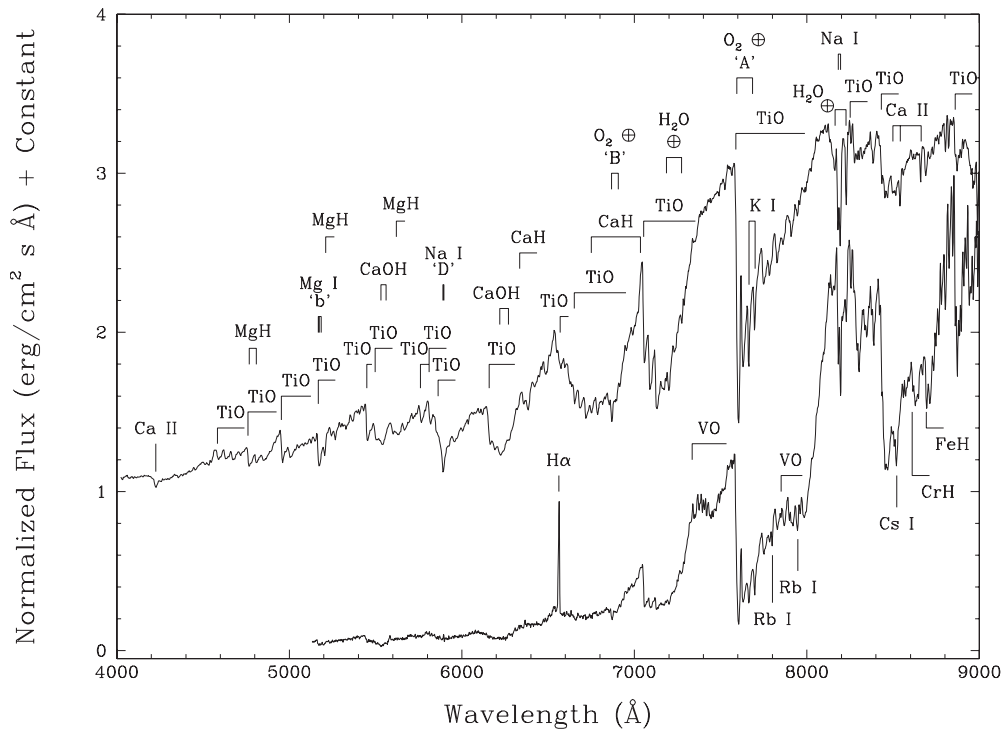


Figure 9.1 Optical spectra of the M4.5 dwarf ν And B (Lowrance et al. 2002) and the M9 dwarf LHS 2065 (Kirkpatrick et al. 1997). Line and band identifications are marked on the mid-M dwarf. Additional features appearing at cooler temperatures are marked on the spectrum of the late-M dwarf. These spectra have not been telluric subtracted; bands of H_2O and O_2 caused by the Earth's atmosphere are marked with a \oplus sign. Fluxes are normalized to unity at 7500 \AA and the normalized fluxes of the M4.5 dwarf have been offset by one unit to separate it vertically from the M9 spectrum.

band is, in fact, contaminated by CaOH in the dwarfs, leading him to measure TiO strengths in the dwarfs that were stronger than they really were (Boeshaar 1976).

This discrepancy was rectified by Boeshaar (1976), who established spectral standards from M0 through M6.5 over the wavelength region $4400\text{--}6800 \text{ \AA}$. Classification itself was done via the appearance of particular TiO bands for early M dwarfs, and via the ratio of 5736 \AA VO to 5759 \AA TiO and via the strength of the 5530 \AA CaOH for later M dwarfs. In a later paper, Boeshaar & Tyson (1985) published M7, M8, and M9 standards to further extend the classification to cooler types.

The classification of the entire M-dwarf sequence was reanalyzed at longer wavelengths— 6300 to 9000 \AA —by Kirkpatrick et al. (1991), who established spectral standards in agreement with those of Boeshaar (1976) and Boeshaar & Tyson (1985). The totality of the spectrum was used to order the spectra into a temperature sequence. Primary spectral standards were chosen to represent anchor points for the sequence, as illustrated in Figure 9.2. Note in particular the

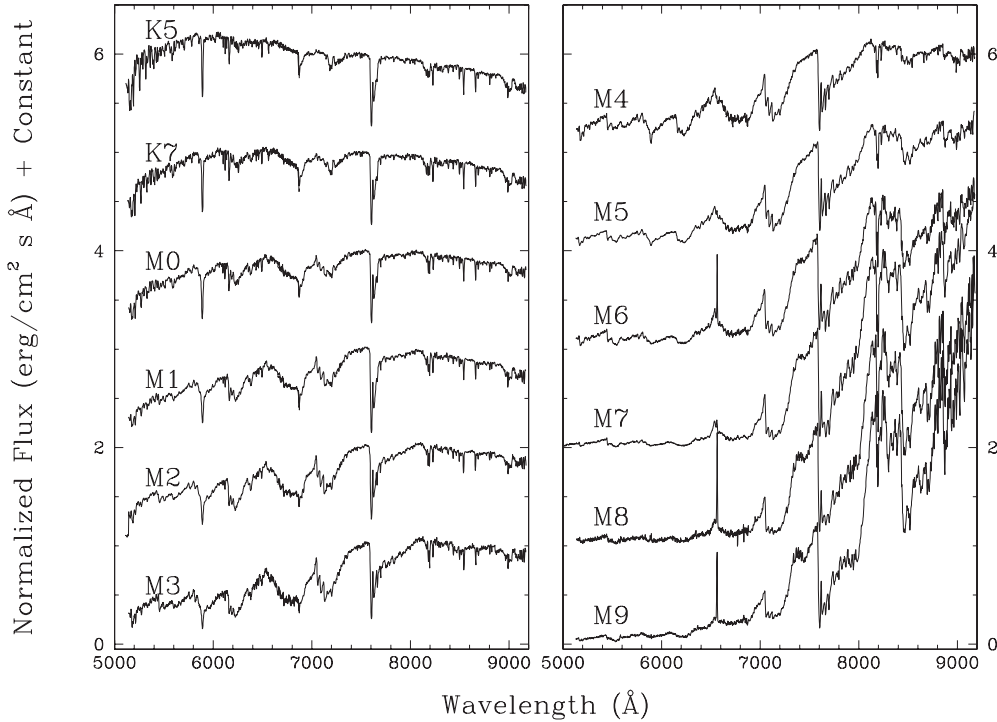


Figure 9.2 The K5–M9 dwarf sequence at red-optical wavelengths. For feature identifications please refer to Figure 9.1. The spectra shown here were taken as part of the classification program described in Kirkpatrick et al. (1997). The fluxes of all spectra have been normalized to unity at 7500 Å and an integer offset has been added to separate the spectra vertically.

strengthening of the TiO bands from mid-K until M6, and then for later types the strengthening of the VO bands along with the increasing slope of the pseudo-continuum toward longer wavelengths.

Primary standards for M dwarfs are listed in Table 9.1. The spectra plotted in Figure 9.2 are those of the full-integer subtypes listed in the table, shown along with spectra of the two primary late-K dwarf standards 61 Cyg A (Gl 820A; K5) and 61 Cyg B (Gl 820B; K7). These objects represent on-sky anchor points and are the grid against which the spectra of other target objects are classified. Ideally, these standards would be observed with the same instrument and telescope used for the target spectra, as this methodology helps to eliminate any systematic effects introduced when comparing data taken, reduced, and calibrated through different means. Although a number of recipes for classification can be used—among them a least-squares minimization to spectra in the standard grid or a suite of spectral ratios calibrated using the anchor stars—the important point is that new targets be typed relative to this same set of on-sky fiducials. In most cases, the standards are among the brightest examples of their subtype and are located sufficiently close to the celestial equator to be observed from either the northern or southern hemisphere.

Table 9.1 Primary M Dwarf Spectral Standards in the Optical Region

Optical Spectral Type	2MASS Designation (J2000 Coordinates encoded as Jhh[:]:mm[:]:ss[.]:ss ± dd[:]:mm[:]:ss[.]:s)	Other Name	Reference
M0	2MASS J07193126 + 3249482	Gl 270	1,3
M0.5	2MASS J22021026 + 0124006	Gl 846	1,2,3
M1	2MASS J06103462 − 2151521	Gl 229A	1,3
M1.5	2MASS J05312734 − 0340356	Gl 205	1,3
M2	2MASS J11032027 + 3558203	Gl 411	1,3
M2.5	2MASS J06521804 − 0511241	Gl 250B	1,3
M3	2MASS J19165526 + 0510086	Gl 752A	1,3
M3.5	2MASS J18424688 + 5937374	Gl 725B	2,3
M4	2MASS J10505201 + 0648292	Gl 402	1,3
M4.5	2MASS J02001278 + 1303112	Gl 83.1	1,3
M5	2MASS J01031971 + 6221557	Gl 51	1,3
M5.5	2MASS J19535443 + 4424541	GJ 1245AC	2,3
M6	2MASS J10562886 + 0700527	Gl 406	1,3
M6.5	2MASS J08294949 + 2646348	GJ 1111	1,3
M7	2MASS J16553529 − 0823401	Gl 644C = vB 8	2,3
M7.5	2MASS J12465176 + 3148104	LHS 2632	4
M8	2MASS J19165762 + 0509021	Gl 752B = vB 10	2,3
M8.5	2MASS J15010818 + 2250020	TVLM 513-46546	4
M9	2MASS J14284323 + 3310391	LHS 2924	2,3
M9.5	2MASS J00242463 − 0158201	BRI 0021 − 0214	4,5

Reference: 1 = Boeshaar (1976); 2 = Boeshaar & Tyson (1985); 3 = Kirkpatrick et al. (1991); 4 = Kirkpatrick et al. (1995); 5 = Kirkpatrick et al. (1999).

Many of the same species seen in the optical reappear in the near-infrared spectra of M dwarfs. Figure 9.3 shows that features in the 0.95–2.35 μm region are attributable to neutral atomic lines of Ti, Ca, Fe, Si, Mg, Al, Na, K, and Mn along with molecules of FeH, CO, and H₂O. At the earliest M types these near-infrared spectra are dominated by atomic lines, but by mid-M the H₂O bands have begun to strengthen markedly. By late-M the H₂O bands are the most prominent features in the spectrum, and absorption by neutral alkali lines (Na and K) and FeH are also much stronger than in earlier types.

Oddly, M-dwarf spectral standards have yet to be defined in the near-infrared. This is primarily because of insufficient need. Most authors have found that the M-dwarf standards used to define the benchmarks for optical classification also define a monotonic morphological sequence in the near-infrared, obviating the need for a second set of standards (Jones et al. 1994; Kirkpatrick 1995; Leggett et al. 1996).

9.3.1.2 Gravity/Luminosity Classification

DWARFS VS. GIANTS

Even as early as the 1920s it became clear that M stars were comprised of at least two different sequences. The parallax data then available suggested that there

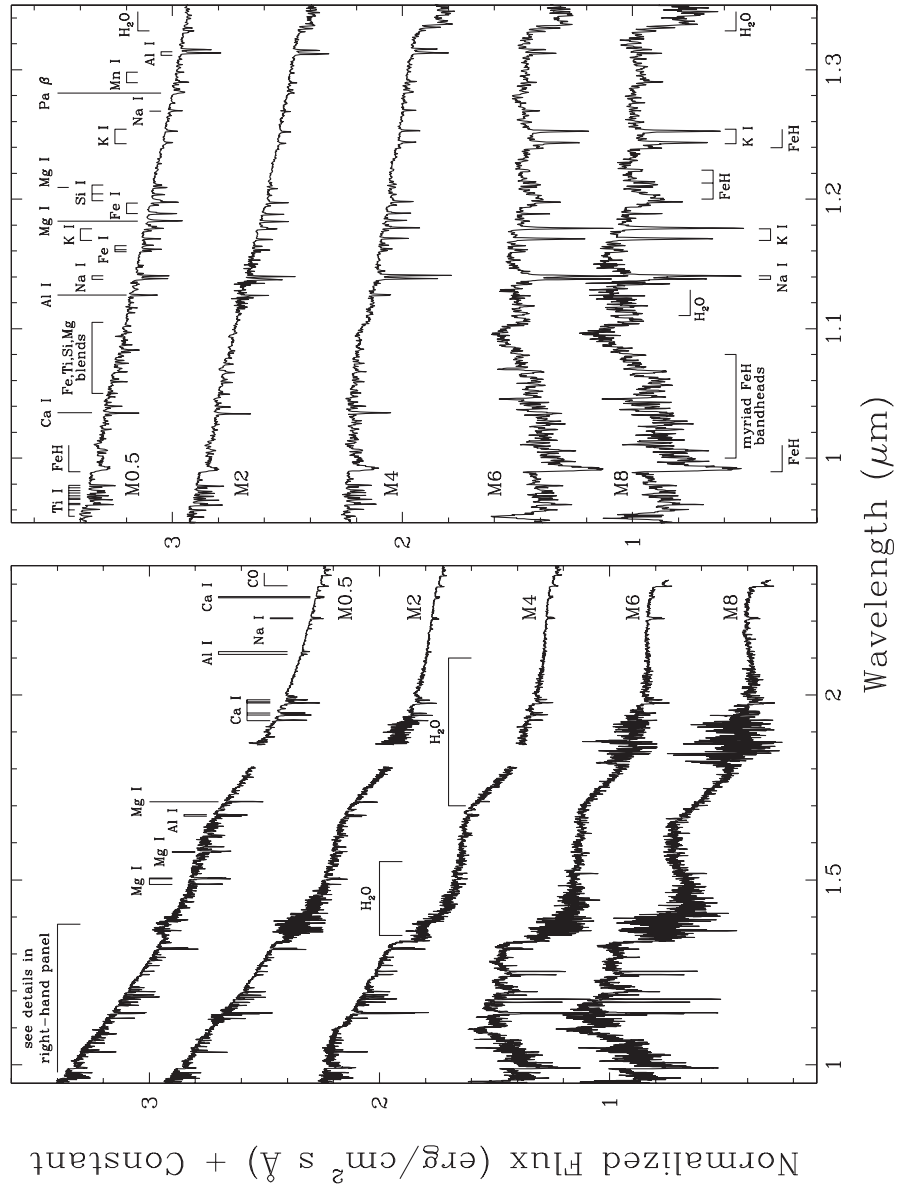


Figure 9.3 The near-infrared spectra of M dwarfs. In the left panel is shown the complete 0.95–2.35 μm region; in the right panel is an expanded view of the 0.95–1.35 μm portion. Spectral types are those assigned in the optical for the same objects. The spectra are those of Gl 846 (M0.5), Gl 411 (M2), and Gl 213 (M4) from Cushing et al. (2005) and Gl 406 (M6) and Gl 752B (M8) from McLean et al. (2003). The flux values of each spectrum have been normalized to unity at 1.28 μm and an integral or half integral offset added to separate the spectra vertically.

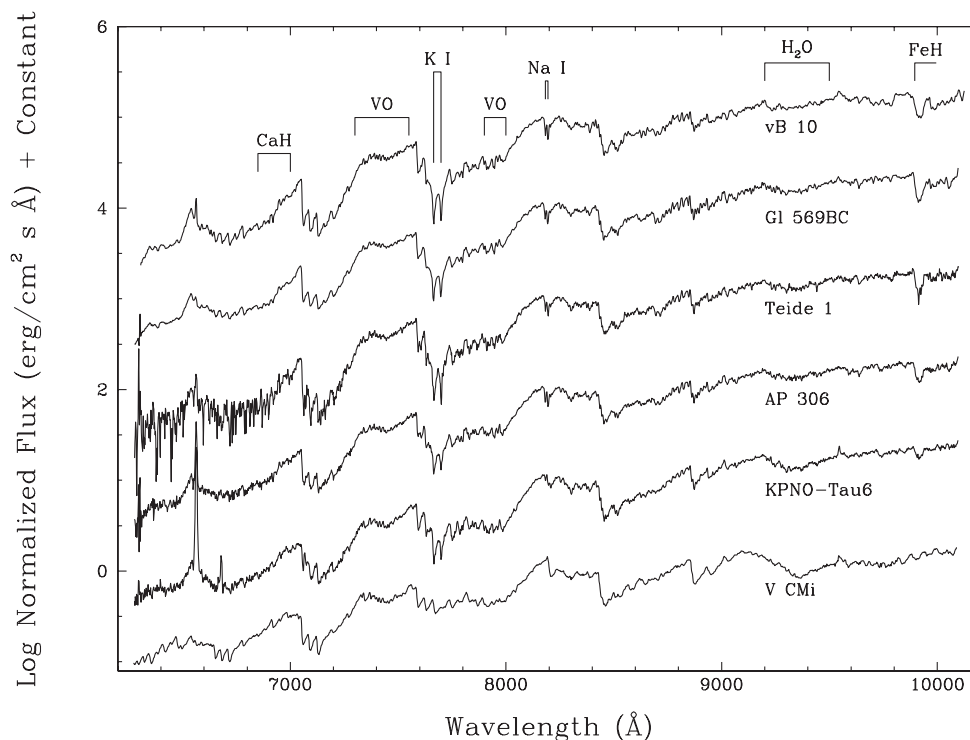


Figure 9.4 Late-M spectra showing gravity effects in the optical. From top to bottom are shown the old (several Gyr) companion star vB 10, the 300-Myr-old companion object Gl 569B, the 100-Myr-old Pleiades brown dwarf Teide 1, the 90-Myr-old α Persei cluster brown dwarf AP 306, the 1-Myr-old Taurus–Auriga association brown dwarf KPNO-Tau 6, and the giant star V CMi. From top to bottom note the subtle but nonetheless clear weakening of the hydride and alkali strengths despite similar VO band strengths. All spectra have their fluxes normalized to unity at 7500 Å, converted to a logarithmic scale and separated vertically by integer offsets. All are unpublished data from the author.

were M stars (the dwarfs) some ten thousand to fifty thousand times dimmer than the other sequence of M stars (the giants) (see Lundmark & Luyten 1923 and Luyten 1923b for discussion). In the absence of distance measurements, were there spectroscopic characteristics that could distinguish between the dwarf and giant sequences? Luyten (1923a) noted that the low ionization potential of Na I should translate into a distinct difference in line strength given the change in gas densities between the two types of objects. He obtained spectra to test this, and showed that the sodium D lines were indeed stronger in dwarfs than in giants. Burwell (1930) noted the same effect for calcium lines. The strengths of hydride bands were also shown to be excellent luminosity discriminants by Öhman (1934, 1936a, b) and Iwanowska & Wayman (1952).

Figure 9.4 shows the late-M dwarf standard, Gl 752B (vB 10), at the top compared to a late-M giant, V CMi, at the bottom. (The four spectra sandwiched in between these will be discussed further below.) Most notable in the giant is the

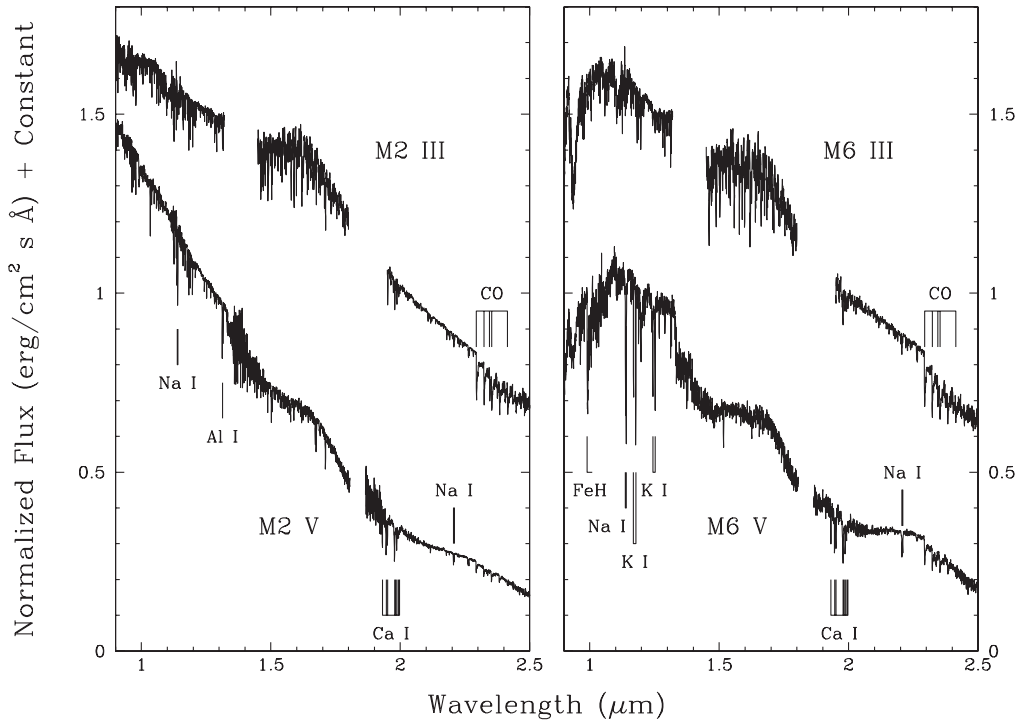


Figure 9.5 M dwarfs compared to M giants in the near-infrared. Fluxes have been normalized to unity at $1.28 \mu\text{m}$ and an offset of 0.5 has been added to the fluxes of the giants to separate them vertically from the dwarfs. These data are from Cushing et al. (2005) and Rayner et al. (2007).

weakness in line strengths for the K I and Na I doublets. Also weaker in the giant are band strengths of the hydrides CaH and FeH. As shown in Kirkpatrick et al. (1991), for earlier M giants, not only are the CaH and Na I strengths weaker, but the Ti I (at 7358 \AA) and the Ca II triplet (at 8498 , 8542 , and 8662 \AA) are stronger relative to dwarfs of the same spectral subclass.

In the near-infrared, spectra also reveal clear diagnostics with which to distinguish M giants from M dwarfs. Figure 9.5 illustrates the differences at early- and mid-M types. The CO bands are stronger in the giant than in the dwarf whereas the Na I and Ca I lines are stronger in the dwarf. At early-M, the dwarf also shows stronger Al I. At mid-M, the strengths of FeH and K I can also be used to distinguish dwarfs and giants.

These optical and near-infrared discriminants have been often referred to as luminosity dependent, but more accurately could be described as gravity dependent. M-dwarf stars are small objects with radii typically less than $0.7 R_{\odot}$ and masses below $0.6 M_{\odot}$ (Lane et al. 2001; Ségransan et al. 2003; Berger et al. 2006; López-Morales 2007), whereas M giants are large stars with masses of $\sim 1\text{--}2 M_{\odot}$ (Lebzelter & Hron 2003; Wittkowski et al. 2004, 2006b) and radii from 40 to $100 R_{\odot}$ for early- to mid-M (Dyck et al. 1996; van Belle et al. 1999; Wittkowski

et al. 2006a) or radii from a few to several hundred R_{\odot} for late-M (Mira) types (Dyck et al. 1998; Hofmann et al. 2000; van Belle et al. 2002). Resulting $\log(g)$ values (in cgs units) are around 4.5 dex for early-M dwarfs but around 1.0 dex for early-M giants. These three and a half orders of magnitude difference in the surface gravities lead to very disparate physical conditions in the photospheres in the two types of objects, leading to the observed spectroscopic differences.

STARS VS. BROWN DWARFS

In addition there is another type of M “star” that shows gravity-dependent features intermediate between the M-type dwarf stars and M-type giants. These are young brown dwarfs whose temperatures, because they have had insufficient time to cool, still fall within the range of older, higher-mass M stars. In these cases the M-type brown dwarfs are not only lower in mass than an M-dwarf star of the same spectral type, but they are also larger because they are still contracting to their final radius. Theory (e.g., Burrows et al. 1997) shows that both low-mass stars and brown dwarfs shrink to a radius of around $0.1 R_{\odot}$, but higher-mass brown dwarfs take roughly 200 Myr to contract to this value. Hence, young brown dwarfs masquerading as M-type stars will also show spectroscopic signatures of lower gravity. Whereas a late-type M giant can have a value of $\log(g)$ of -1.0 dex (in cgs units), a 1-Myr brown dwarf at the stellar–substellar break will have $\log(g)$ of ~ 4.5 dex, much closer to the $\log(g)$ values of 5.0–5.5 dex typical of old, late-M dwarf stars. Therefore, the effect on gravity-dependent spectral features should be reduced relative to the effect in late-M giants, but nonetheless identifiable.

Figure 9.4 illustrates these gravity effects. Between the spectrum of the old late-M dwarf star at the top and the spectrum of the late-M giant at the bottom are four spectra of late-M brown dwarfs of various ages; from top to bottom these four have ages of ~ 300 Myr, ~ 100 Myr, ~ 90 Myr, and ~ 1 Myr. Note the gradual weakening of the alkali lines (K I and Na I) and the hydride bands (CaH and FeH) despite similar VO strengths. These are the same gravity-dependent behaviors seen in the spectrum of the late-M giant at the bottom of the plot, but as expected the amplitude of the difference is much reduced. Such gravity diagnostics have been used in the past to verify brown-dwarf candidates in young clusters (Steele & Jameson 1995; Martín et al. 1996; Luhman et al. 1997).

Near-infrared spectra of an M-dwarf star and an M-type brown dwarf are compared in Figure 9.6. In this wavelength regime, the differences between two objects typed similarly in the optical are very evident. The old M dwarf at top shows stronger alkali lines and hydride bands, mimicking the behavior seen at optical wavelengths. Most surprising, however, is the vast difference in H₂O band strengths, which are greatly increased in the lower gravity brown dwarf at the bottom of the plot, along with the triangular spectral shape near $1.75 \mu\text{m}$ and the surprisingly weak CO bands at $2.3 \mu\text{m}$.

9.3.1.3 Metallicity Classification

Some M dwarfs exhibit unusually strong band strengths of hydride molecules in their optical spectra. As Greenstein (1965) pointed out, a reduction in the

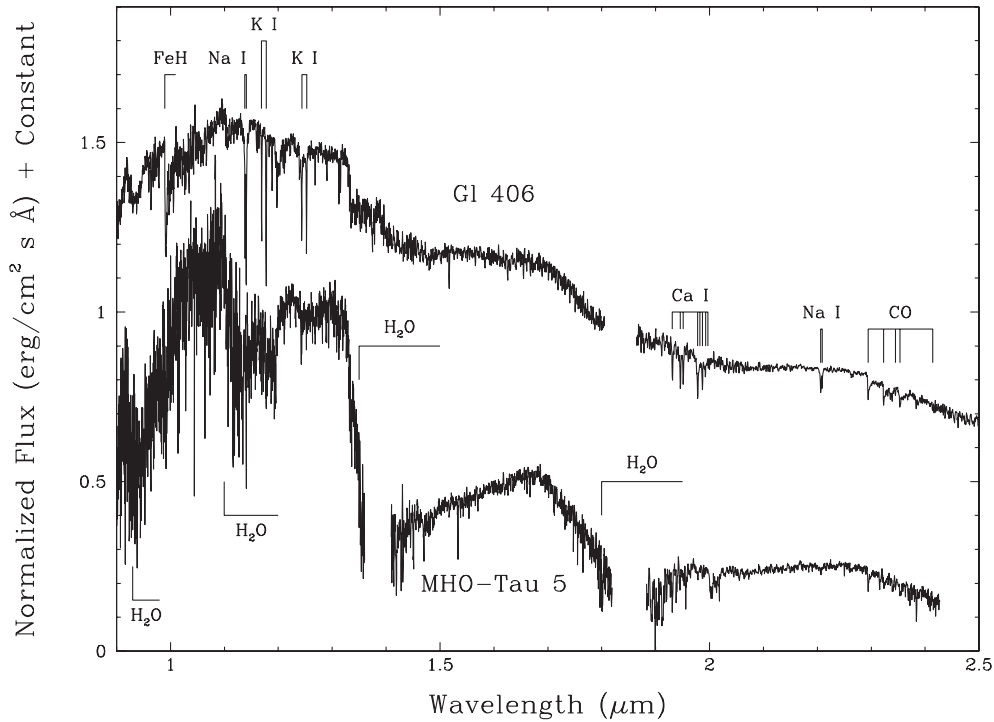


Figure 9.6 Near-infrared spectral comparison between a M-type star (top) and an M-type brown dwarf (bottom) having similar spectral types in the optical. The top spectrum is that of Wolf 359 (Gl 406; Cushing et al. 2005) and the bottom spectrum is that of a ~ 1 -Myr-old brown-dwarf member of the Taurus–Auriga association (courtesy of Dagny Looper and the author). The flux of both spectra has been normalized to unity at $1.28\ \mu\text{m}$ and an offset of 0.5 has been added to the top spectrum to separate it vertically from the other.

abundance of metals in an M dwarf atmosphere would lead to a more severe abundance reduction for an oxide molecule like TiO (metal + metal) than for a hydride molecule like MgH, CaH, FeH, or CrH (metal + hydrogen). Thus, for a fixed TiO band strength the more metal-poor star would have stronger hydride bands than a metal-rich star.

Historically, these objects have come to be known as *subdwarfs* (Kuiper 1939) even though this term can also be applied to stars whose kinematics indicate an old disk or halo origin or whose location on the observational Hertzsprung–Russell diagram places them below the normal main sequence. For the ensuing discussion, this term will be used only for objects whose spectra show anomalies consistent with low metal content. As an example, Barnard’s Star (Gl 699) does not show gross spectroscopic anomalies at low resolution in the red optical region, yet it has been referred to as a subdwarf for other reasons (Joy 1947; Eggen 1950).

Figure 9.7 shows two slices through the metallicity sequence near M4 and M7. The prefixes refer to normal metallicity (dwarfs, or “d”), metal-poor (subdwarfs, or “sd”), and extremely metal-poor (extreme subdwarfs, or “esd”) objects. The

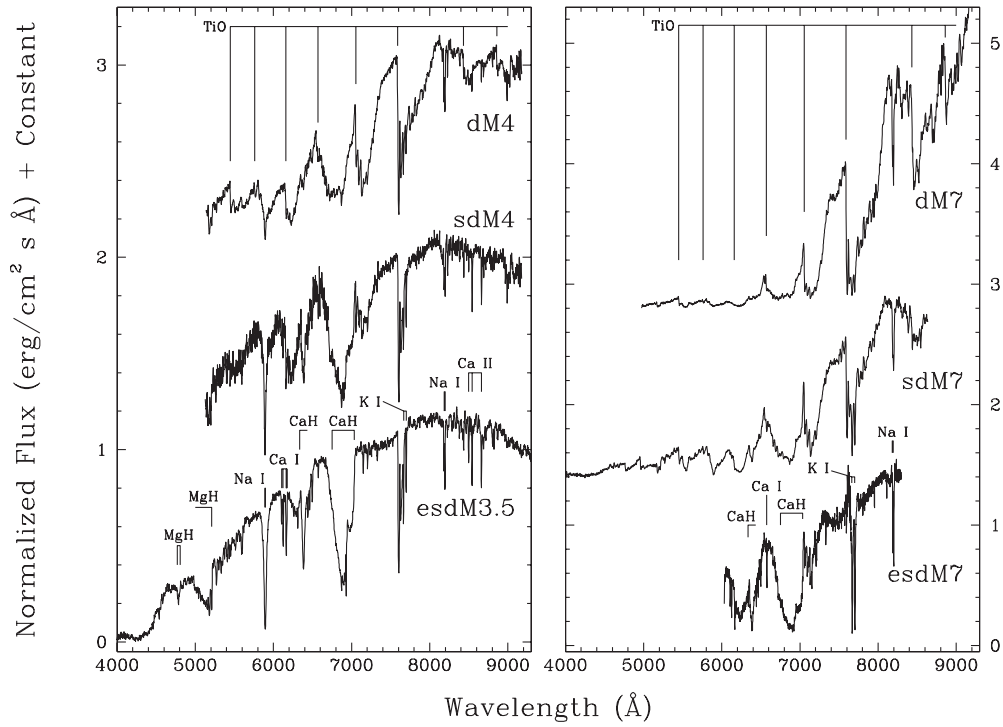


Figure 9.7 Slices through the d/sd/esdM sequence. The left panel shows a comparison of dwarf, subdwarf, and extreme subdwarfs near M4, and the right panel shows the same comparison at M7. Locations of prominent TiO absorptions are shown at the top of each panel, and other non-TiO features are noted in the spectra of the extreme subdwarfs. Note the weakening or outright disappearance of TiO and the relative strengthening of hydride molecules in the subdwarfs and extreme subdwarfs. The flux of each spectrum has been normalized to unity at 7500 Å and constants added to separate the spectra vertically. These spectra come from Kirkpatrick et al. (1995), Reid et al. (2000), and Burgasser & Kirkpatrick (2006).

hallmark TiO bands of the dM stars weaken for the sdM stars and the hydride molecules strengthen, most spectacularly the CaH band near 6950 Å. For the esdM stars, TiO is extremely weak or absent. With the disappearance of the blanketing TiO absorption, other line absorptions become more prominent. These include Na I, Ca I, Ca II, and K I.

An M spectral sequence of extreme subdwarfs is shown in Figure 9.8. Note the strength of the 6950 Å CaH band (and the 5200 Å MgH band for spectra covering the shortest wavelengths). Anchor points for both the subdwarf and extreme subdwarf sequences have not yet been established. Rather, these objects are classified relative to normal M dwarfs using the prescription of Gizis (1997), which uses the ratios of the 6400 and 6950 Å CaH band strengths to that of 7150 Å TiO. Using fits of atmospheric models to the spectra of M dwarfs, Gizis (1997) found that the M-dwarf sequence has $[M/H] \approx 0.0$, the M-subdwarf sequence has $[M/H] \approx -1.2$, and the extreme M-subdwarf sequence has $[M/H] \approx -2.0$.

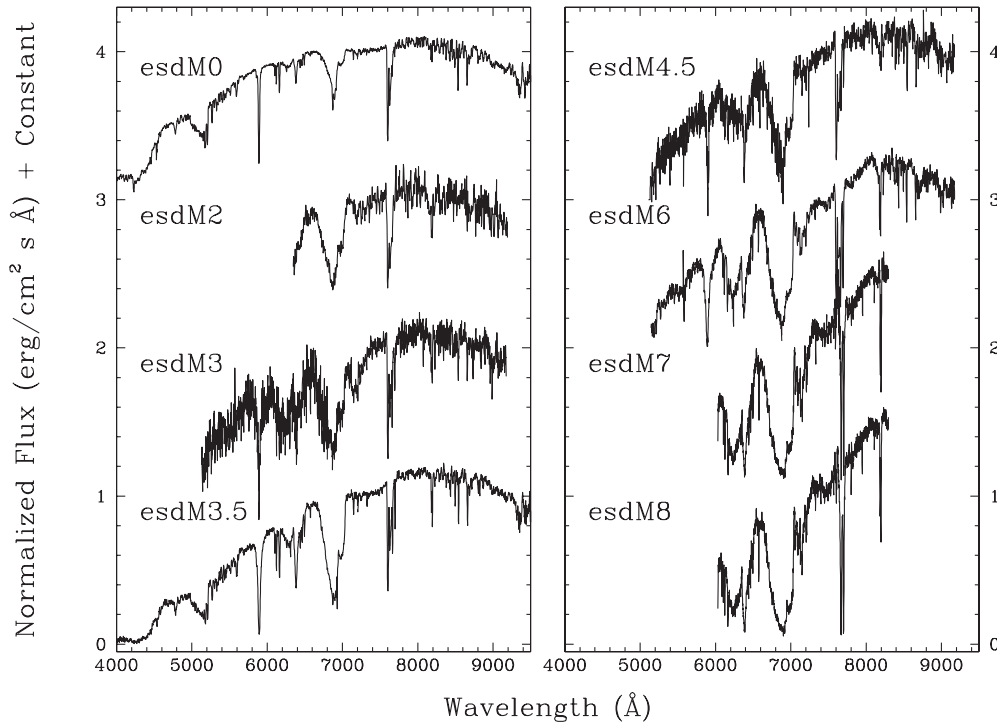


Figure 9.8 Optical spectra illustrating the extreme M-subdwarf sequence from esdM0 through esdM8. Fluxes have been normalized to unity at 7500 Å and integer offsets have been used to separate the spectra vertically. These spectra are taken from Kirkpatrick et al. (1995), Reid et al. (2000), and Burgasser & Kirkpatrick (2006).

In the near-infrared, subdwarfs are characterized by a flattening of the spectrum, as shown in Figure 9.9. In metal-poor atmospheres, the dominance of hydrogen means that collision-induced absorption (CIA) by H_2 is the primary shaper of the spectrum in the near-infrared. As shown in Borysow et al. (1997), this absorption is omnipresent in the 1.0–2.5 μm region and is strongest at the longest of those wavelengths. This has the effect of making the subdwarfs and extreme subdwarfs much bluer than normal M dwarfs in near-infrared colors.

9.3.2 L Dwarfs in the Optical and Near-infrared

9.3.2.1 Temperature Classification

Early-L dwarfs show a mélange of atomic and molecular bands in the optical, the most prominent being the neutral alkali lines (Na I, K I, Rb I, Cs I, and sometimes Li I), oxide bands TiO and VO, hydride bands CrH and FeH, and CaOH (see Figure 9.10). By mid-L the ground-state (resonance) Na I and K I lines have grown tremendously in strength; the hydrides MgH, CaH, CrH, and FeH have also strengthened, whereas the oxides TiO and VO have largely disappeared. By late-L

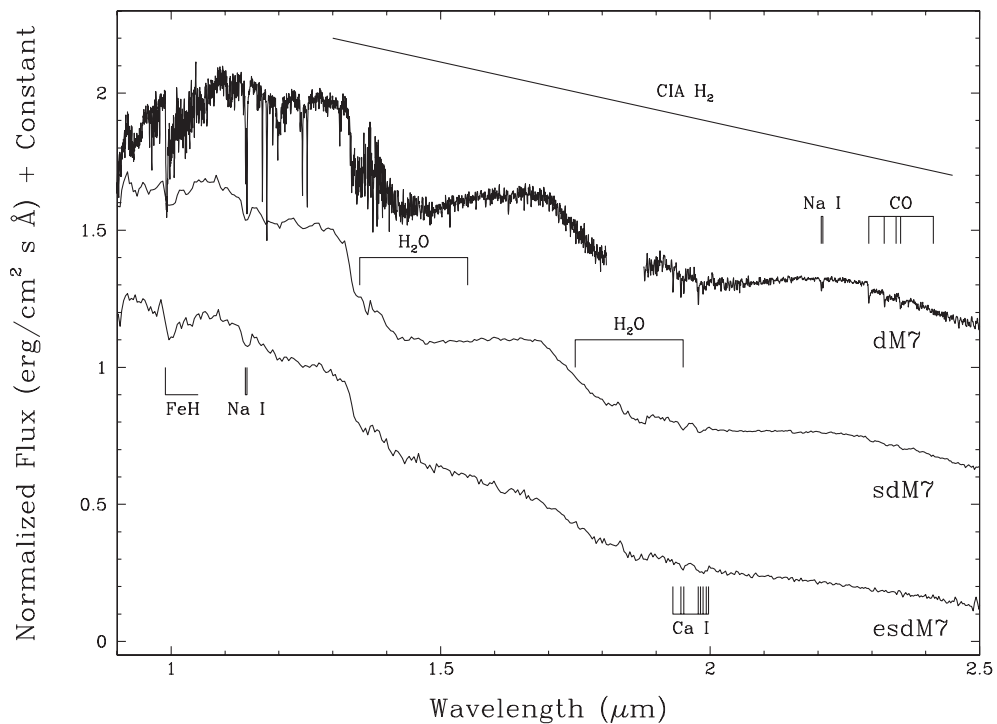


Figure 9.9 Slices through the dM7/sdM7/esdM7 sequence in the near-infrared. Note the increasing relative importance of collision-induced absorption by H_2 as the metallicity drops. The fluxes have been normalized to unity at $1.28 \mu\text{m}$ and integral or half integral offsets added to separate the spectra vertically. The spectrum of the dM7 has about ten times better resolution than the other two spectra, but all were taken with the same instrument. The data are taken from Cushing et al. (2005), Burgasser (2004a), and Burgasser & Kirkpatrick (2006).

H_2O has increased in strength, the neutral alkali lines are still strong, and the hydrides are much reduced in prominence.

Optical classifications have been established for L dwarfs by Kirkpatrick et al. (1999). This paper identified a set of reference objects (“anchor points”) to serve as the on-sky classification standards for the typing scheme. These anchors are listed for convenience in Table 9.2. Although readers are referred to this paper for discussion of line/band strengths and spectral ratios useful for typing, it should be noted that the establishment of anchors is the single most important step in constructing a classification scheme. As with M-dwarf classifications, details of how those anchors are used to classify a new set of objects—whether it be through automated methods or simply through by-eye fits (see, e.g., the discussion in Hawley et al. 2002)—are of secondary importance as long as those classifications are judged against the same set of standards.

Optical spectra of L-dwarf standards at each integral subtype are shown in Figure 9.11. These spectra are plotted with a logarithmic flux scale so that

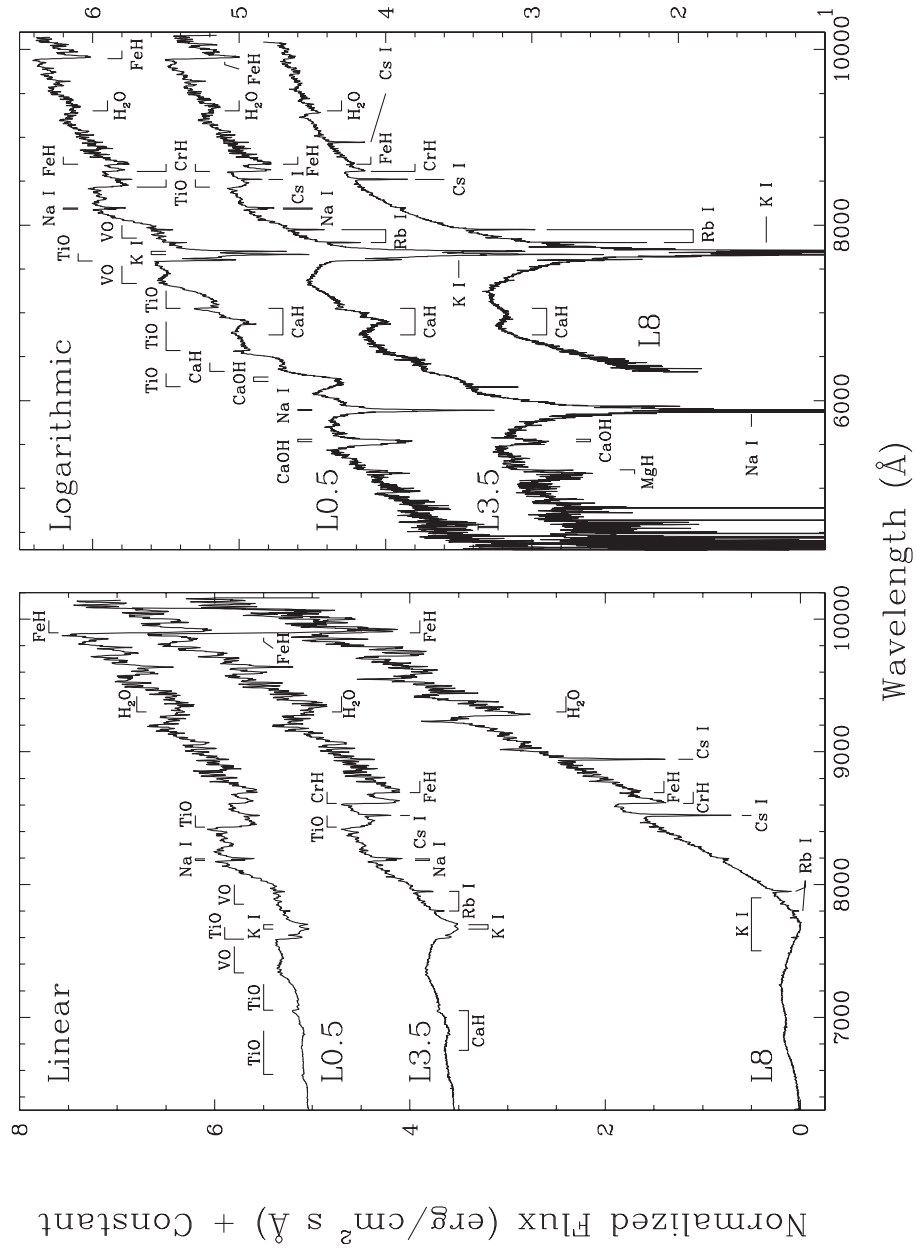


Figure 9.10 Line and band identifications for L dwarfs. Shown are an early-, mid-, and late-L dwarf on both a linear (left) and logarithmic (right) flux scaling. All spectra have had their fluxes normalized to unity at 8250 Å and offsets added to separate the spectra vertically. In the left panel the offsets are 5, 3.5, and 0; in the right panel there are integer offsets between spectra. Data come from Reid et al. (2000) and unpublished work by the author.

Table 9.2 Primary L Dwarf Spectral Standards in the Optical Region

Optical Spectral Type	2MASS Designation (J2000 Coordinates encoded as Jhh[:]:mm[:]:ss[.].ss \pm dd[:]:mm[:]:ss[.].s)	Other Name	Reference
L0	2MASS J03454316 + 2540233	—	1
L0.5	2MASS J07464256 + 2000321	—	2
L1	2MASS J14392836 + 1929149	—	1
L1.5	2MASS J08320451 – 0128360	—	2
L2	2MASS J13054019 – 2541059	Kelu-1	1
L2.5	2MASS J13382615 + 4140342	—	2
L3	2MASS J11463449 + 2230527	—	1
L3.5	2MASS J00361617 + 1821104	—	2
L4	2MASS J11550087 + 2307058	—	1
L4.5	2MASS J22244381 – 0158521	—	2
L5	2MASS J12281523 – 1547342	DENIS-P J1228.2 – 1547	1
L5.5	2MASS J15532142 + 2109071	—	1
L6	2MASS J08503593 + 1057156	—	1
L6.5	2MASS J09201223 + 3517429	—	2
L7	2MASS J02052940 – 1159296	DENIS-P J0205.4 – 1159	1
L7.5	2MASS J08251968 + 2115521	—	2
L8	2MASS J16322911 + 1904407	—	1

Note: 1 =Kirkpatrick et al. (1999); 2 =Kirkpatrick et al. (2000).

features at shorter wavelengths can be easily seen. (For the same spectra shown in linear flux units, see Figures 6 and 7 of Kirkpatrick et al. 1999). The optical L-dwarf sequence presently ends at L8; there are no objects yet identified with optical types of L8.5, L9, or L9.5. Just beyond L8 there is an abrupt change in spectral morphology in the optical leading to the cooler dwarfs of type T. Refer to Chapter 10 for a full discussion of the transition from late-L to early-T.

Near-infrared spectra of a subset of L dwarfs are shown in Figure 9.12. L dwarfs are characterized by strong bands of H₂O, bands of FeH and CO, and neutral atomic lines of Na, Fe, and K. At the time of this writing there has still not been a set of spectral standards established in the near-infrared for L dwarfs, so the objects shown here are labeled with the types derived for them based on their optical data.

It should not be assumed *a priori* that a set of objects classified on optical spectroscopic morphology alone will necessarily fall into the same ordering based on near-infrared morphology. This is because the two spectral regions sample different physical environments in the atmosphere of the object. This fact is clearly seen in the left panel of Figure 9.12, as the sequence of objects here hardly falls in the same orderly, monotonic progression seen in the optical sequence of Figure 9.11.

If we consider only the sequence of 0.95–1.35 μ m spectra in the right panel of Figure 9.12 we see a much smoother, monotonic ordering. This is perhaps not surprising since these wavelengths are not far removed from the optical wavelengths at which the ordering was established and thus sample similar atmospheric physics.

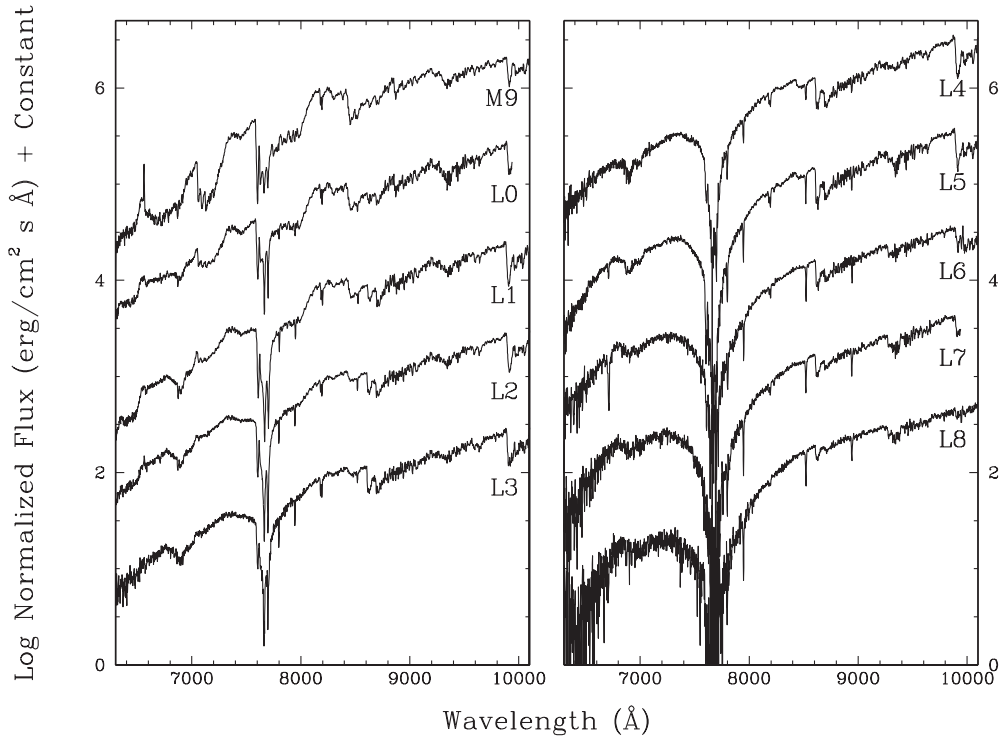


Figure 9.11 Optical spectra from M9 to L8. The L dwarfs shown here are the optical standards from Table 9.2. The flux of each spectrum has been normalized to unity at 8250 Å and integer offsets added to separate the spectra vertically. All data are from Kirkpatrick et al. (1999). For feature identifications, please refer to Figure 9.10.

It is only when looking at the longer wavelengths, 1.5–2.3 μm , that we see clear discrepancies in the ordering. In particular, the difference in overall color between the L2 and the L4 is much larger than the color difference between the L0 and the L2. Also, the shape of the peak near 1.65 μm does not change smoothly from L2 through L8. These longer wavelengths, being farther removed from the optical, may be sampling different physical conditions in the atmosphere, or other effects such as unresolved binarity or dust may be more easily noticeable here.

There is a lot of information available in the near-infrared spectra of these objects, some of which samples physics not addressed by the optical portion of the spectra. For this reason a separate, independent, near-infrared classification system for L dwarfs needs to be established. It is worth keeping in mind that if most objects have optical and near-infrared types that are identical and only a handful of others have discordant types, then it should not be interpreted that either the optical or near-infrared type of the discordant objects is “wrong.” Instead, this should be viewed as a clue to the atmospheric physics of those objects—that is, something about *those* objects makes them different from the majority. Part of the power of spectral classification is its ability to flag such differences for further study.

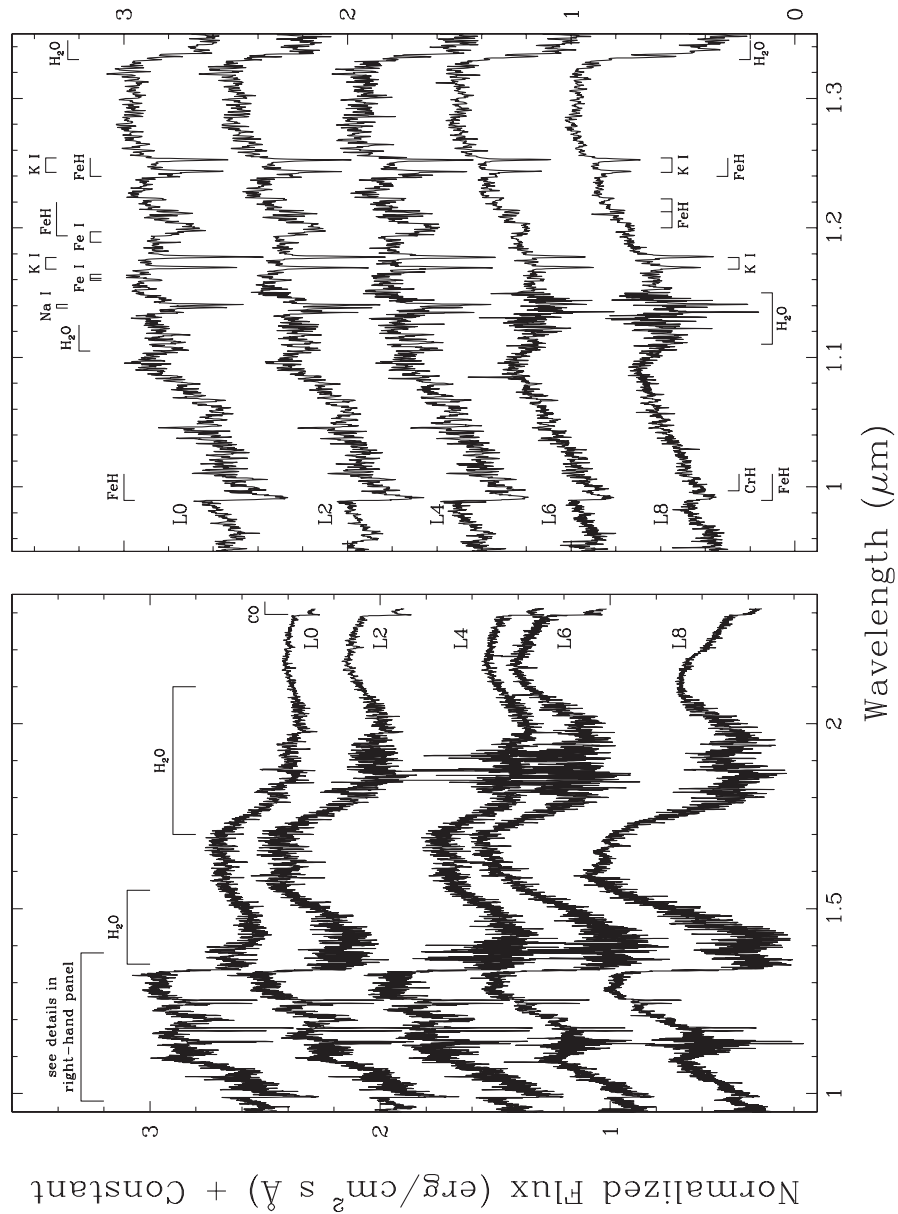


Figure 9.12 Near-infrared spectra of L dwarfs. Fluxes are normalized to unity at $1.28\,\mu\text{m}$ and half integer offsets have been added to separate the spectra vertically. The data shown here are from McLean et al. (2003).

9.3.2.2 Gravity Classification

As we will explain in a later section, there is no such thing as an L giant or supergiant, but L-type stars and brown dwarfs do show spectroscopic features that vary with gravity. Figure 9.13 shows the optical spectrum of a low-gravity L dwarf compared to a normal, higher-gravity L dwarf and a normal late-M giant. The

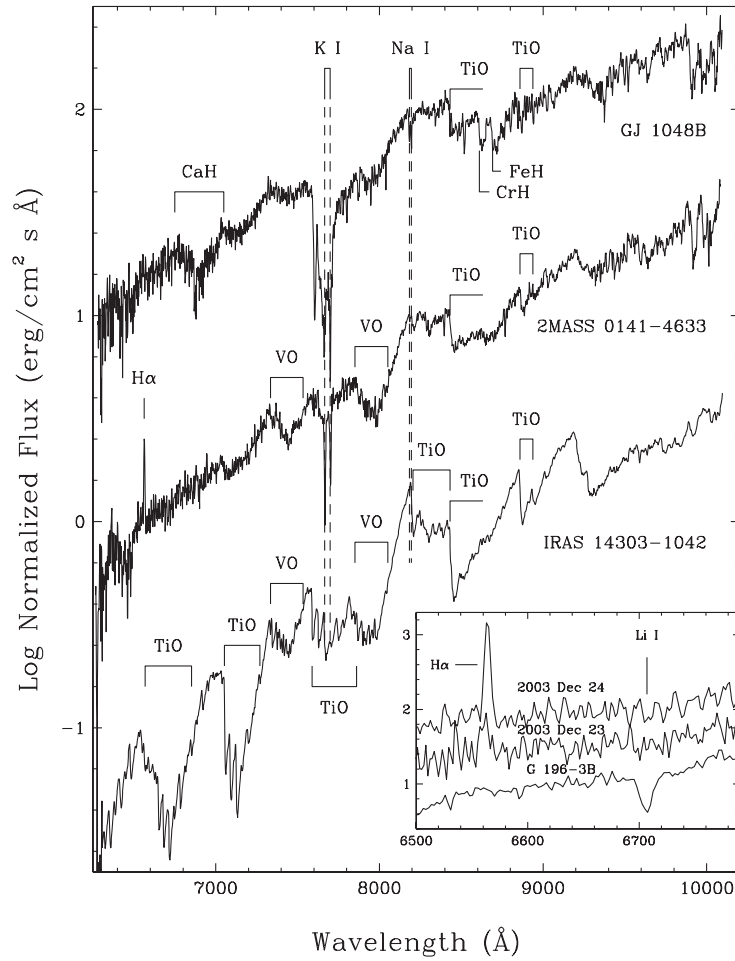


Figure 9.13 Gravity effects in the optical at early-L types. Plotted are the spectra of a normal L1 dwarf GJ 1048B (top), the peculiar L dwarf 2MASS 01415823 – 4633574 (center), and the very late type M giant IRAS 14303 – 1042 (bottom). Spectra have been normalized to unity at 8250 Å and separated vertically by 1 dex for ease of comparison. In the spectrum of 2MASS 0141 – 4633, the strength of the sodium and potassium lines, as well as the strength of the vanadium oxide bands, falls between the strengths seen in the dwarf and the giant. The titanium oxide strengths, on the other hand, are very similar to those of the dwarf and quite unlike those of the giant. The inset shows an expanded version of the 2MASS 0141 – 4633 spectrum (top) along with a spectrum of the same object taken one night earlier (middle). Note the change in H α emission strength between the two nights. Also shown in the inset for comparison is the low-gravity L2 dwarf G 196-3B. Unlike G 196-3B, the spectrum of 2MASS 0141–4633 shows no indication of Li I absorption. All three spectra in the inset have been normalized to unity at 6650 Å, displayed in linear flux units, and separated vertically from one another by units of 0.5. Plot taken from Kirkpatrick et al. (2006), and reproduced by permission of the AAS.

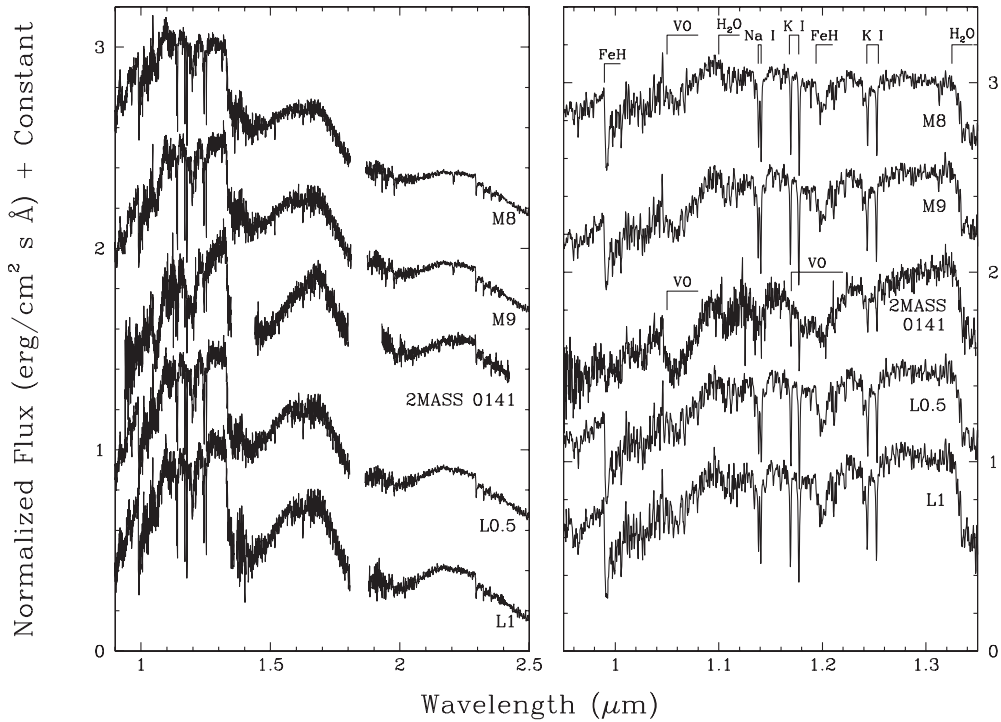


Figure 9.14 Gravity effects in the near-infrared at early-L types. Near-infrared spectra of normal field late-M and early-L dwarfs (top two and bottom two) and the peculiar L dwarf 2MASS 01415823–4633574 (middle). The comparison spectra are vB 10 (M8), LHS 2924 (M9), 2MASS J0746425 + 200032AB (L0.5), and 2MASSW J1439284 + 192915 (L1) from Cushing et al. (2005). All spectra have been normalized to unity at $1.30\ \mu\text{m}$. Spectra have been separated vertically in units of 0.5 for clarity. Most notable in the spectrum of 2MASS 0141 – 4633 is the triangular-shaped appearance of the pseudo-continuum near $1.7\ \mu\text{m}$. Also notable are two deep VO bands centered near 1.06 and $1.18\ \mu\text{m}$ that are not present in spectra of the normal late-M/early-L dwarfs. As can also be seen in this figure, the near-infrared spectrum of 2MASS 0141 – 4633 is much redder than spectra of normal late-M/early-L dwarfs. Plot taken from Kirkpatrick et al. (2006), and reproduced by permission of the AAS.

weakness or absence of TiO bands along with the presence of VO bands make this an L dwarf, but the alkali lines (K I and Na I) and hydride bands (CaH, CrH, FeH) are all weak, as one would expect in a lower-gravity environment. Curiously, the VO bands are much stronger than in a normal L dwarf and in fact appear to have similar strengths to the VO bands in the late-M giant.

Figure 9.14 shows a near-infrared comparison of this same L dwarf with normal late-M and early-L dwarfs. This L dwarf is again anomalous due to the weakness of its FeH bands and Na I and K I lines, and it again has anomalously strong VO band strengths. Moreover, the shape of its spectrum between 1.5 and $1.8\ \mu\text{m}$ is much more peaked compared to the more rounded spectra of normal dwarfs. It also has a redder overall flux, meaning that there is more emergent flux at $2.2\ \mu\text{m}$ relative to that at $1.3\ \mu\text{m}$ than in the normal dwarfs.

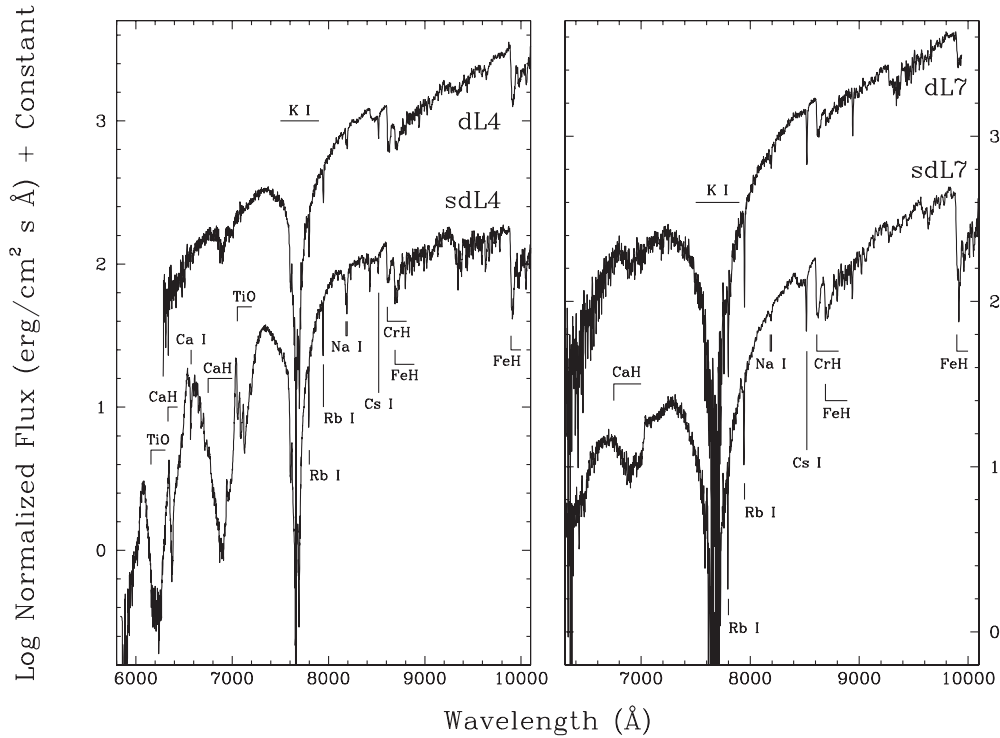


Figure 9.15 Optical spectral comparison of L dwarfs and L subdwarfs. In the left panel is a comparison of the L4-dwarf standard with the sdL4 2MASS J16262034 + 3925190. In the right panel is a comparison between the standard L7 and the sdL7 2MASS J05325346 + 8246465. Note the strong CaH, FeH, and TiO bands in the subdwarfs. Fluxes have been normalized to unity at 8250 Å and offsets of 1.0 dex added to the standards to separate them vertically from the subdwarfs. Data for the standards are from Kirkpatrick et al. (1999) and data for the subdwarfs are from Burgasser et al. (2003) and Burgasser et al. (2007).

To date the only L dwarfs with clear signs of lower gravity have been those with early-L spectral types. This is because at the distance of young clusters and star-formation regions such as the Pleiades, Orion, and Taurus-Auriga, later L dwarfs are still beyond the range of detailed spectroscopic follow-up. Therefore we are reliant on the occasional discovery of low-gravity L dwarfs in the field because these tend to be much closer, brighter, and more easily observed. A few of these are beginning to be uncovered and may turn out to be members of very nearby (a few $\times 10$ pc), young (5–50 Myr) associations like the TW Hydrae Association and the β Pictoris Moving Group (Kirkpatrick et al. 2006; Cruz et al. 2007).

9.3.2.3 Metallicity Classification

Other anomalous L dwarfs appear to be the cooler equivalents of M subdwarfs; that is, they have feature strengths most consistent with a low-metallicity explanation. Figure 9.15 shows two L subdwarfs. The subtypes of both have been

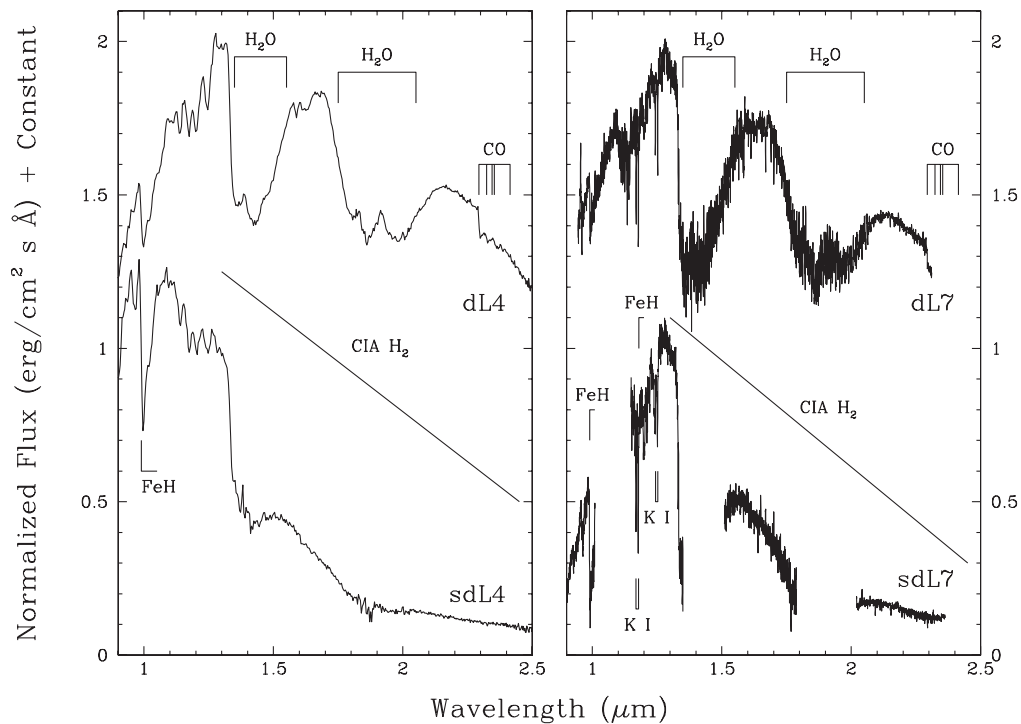


Figure 9.16 Near-infrared comparison of L dwarfs and subdwarfs at L4 and L7. The left panel compares the low-resolution spectrum of an L4 dwarf to that of the sdL4 from the previous figure. The right panel shows the higher-resolution spectrum of an L7 dwarf compared to that of the sdL7 from the previous figure. Note the increase in the FeH band strengths of the subdwarfs but more notably the dramatic reduction in emergent flux at the longest wavelengths shown here. All spectra have been normalized to unity at $1.28 \mu\text{m}$. Integer offsets have been used to separate the spectra vertically. Data are from Cushing et al. (2005), McLean et al. (2003), Burgasser et al. (2003), and Burgasser (2004a).

assigned based on their overall best match to the normal L-dwarf standards. So few L subdwarfs are currently known (Burgasser et al. 2007) that there are not enough to define subdwarf anchor points yet. For both objects the hydride bands, particularly CaH and FeH, are enormously strong, as are the TiO bands. For M subdwarfs, TiO band strengths are actually much weaker than the hydride band strengths, but the opposite appears to be true for L subdwarfs. The reason has to do with the defining characteristic of L dwarfs themselves—the disappearance of the oxide bands in the optical, which is a consequence of condensate (dust) formation. In a lower metallicity atmosphere, there will be fewer available species out of which to form dust. It is believed that the TiO, which generally disappears into grains starting at late-M, instead remains in its gaseous state for L subdwarfs and is still a significant source of opacity. (See §9.4.2 for more discussion on condensation in general.)

In the near-infrared between 0.95 and $2.5 \mu\text{m}$, strong FeH bands are again seen in the L subdwarfs, but the most prominent trait of the subdwarfs is the suppres-

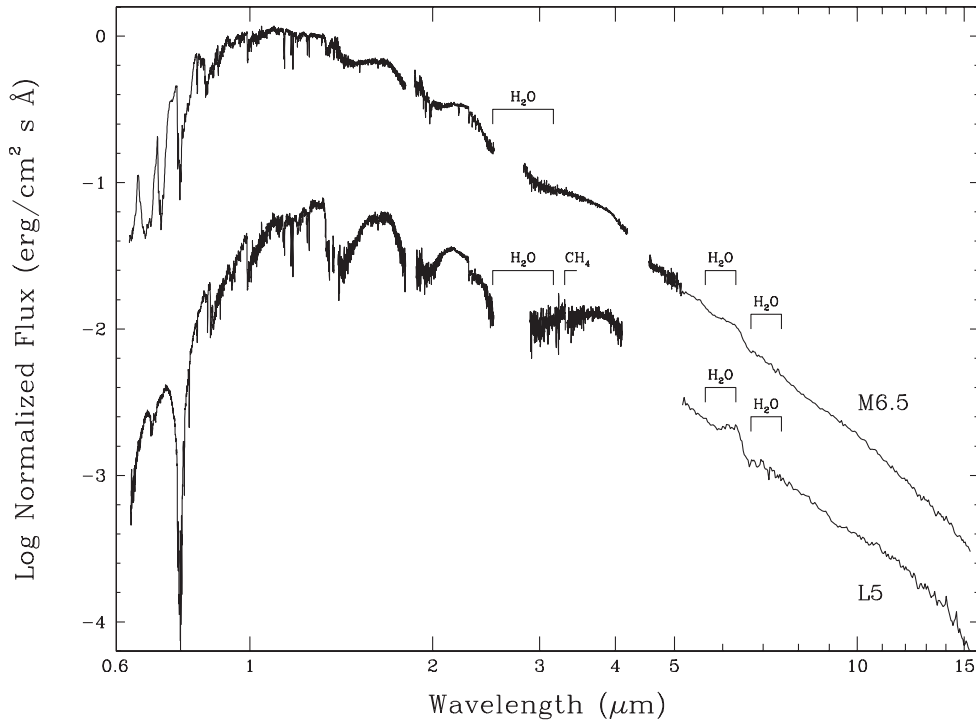


Figure 9.17 Full (0.6–15 μm) spectra of a mid-M and a mid-L dwarf. Features longward of 2.5 μm are marked. These data have been normalized so that the relative flux between these two objects, if observed from the same distance from the observer, is preserved. The top object is GJ 1111 and the bottom one is 2MASS J15074769 – 1627386. These spectra are taken from Cushing et al. (2006).

sion of their flux longward of 1.5 μm (Figure 9.16). This suppression is probably due to the overwhelming influence of collision-induced absorption by H_2 , which is enhanced in a low-metallicity atmosphere relative to opacities by metallic molecules. This means that L subdwarfs have much bluer $J - K_s$ colors than L dwarfs of the same spectral subclass.

9.3.3 M Dwarfs and L Dwarfs beyond 2.5 Microns

Independent classification of M and L dwarfs at wavelengths longward of 2.5 μm is not currently feasible due to the faintness of the objects at these wavelengths and the difficulty of observing this wavelength regime from the ground. As a result relatively few objects have been spectroscopically observed longward of 2.5 μm .

Figure 9.17 shows complete 0.6–15 μm spectra for a mid-M dwarf and a mid-L dwarf. Longward of 2.5 μm the M dwarf is largely featureless except for H_2O bands at 2.5, 5.5, and 6.5 μm (Roellig et al. 2004); otherwise, the flux plummets as expected for the Rayleigh–Jeans tail of a blackbody of the same effective temperature. The L dwarf, on the other hand, shows more interesting behavior longward

of $2.5\ \mu\text{m}$. In addition to the H_2O bands, which are now more prominent, the CH_4 fundamental band at $3.3\ \mu\text{m}$ has just begun to appear (Noll et al. 2000). Here the decline in flux with increasing wavelength has less resemblance to a Rayleigh–Jeans tail. Roellig et al. (2004) show spectra of M and L dwarfs between 15 and $35\ \mu\text{m}$ (not shown here), but the continua are quite featureless.

One other interesting aspect to Figure 9.17 is that the spectra have been scaled relative to one another so that they represent the true relative luminosities if both the mid-M dwarf and the mid-L dwarf were located at the same distance from the observer. At all wavelengths the M dwarf is brighter, but the difference ($\sim 4\times$ in flux) is at a minimum near $4.0\ \mu\text{m}$ and again between $10\text{--}15\ \mu\text{m}$. The difference is largest in the core of the K I doublet at $0.77\ \mu\text{m}$, where the flux in the L dwarf is reduced by $\sim 1000\times$.

9.3.4 M Dwarfs below 4000 Angstroms

As was true for longer-wavelength observations, spectra shortward of $4000\ \text{\AA}$ have also been difficult to obtain for late-M and L dwarfs due to their faintness at these wavelengths and our inability to observe below $\sim 3300\ \text{\AA}$ from the surface of the Earth. Figure 9.18 shows a sequence of late-K through mid-M dwarfs with coverage in this region. Some line absorption is seen in this region, namely by neutral Fe, Ca, and Cr. More obvious are the many emission lines attributable to the Balmer series of hydrogen and the Ca II H and K transitions. These lines originate in the chromospheres of these objects, a topic that is further discussed in §9.5.2 below.

9.4 PHYSICAL INTERPRETATION OF TYPES

9.4.1 Effective Temperatures

Using our empirical spectroscopic classifications we can begin to understand the physical processes responsible for shaping the spectra. For higher-mass main-sequence stars of solar metallicity, temperature is the most important parameter determining spectral appearance. Is the same true of M and L dwarfs? Using the Stefan–Boltzmann law, $L = 4\pi R^2 \sigma T_{\text{eff}}^4$, we can measure temperatures directly if the bolometric luminosity and radius are known.

9.4.1.1 Measuring R

A growing number of M dwarfs have had their radii measured directly either because they are members of an eclipsing binary system or they are bright enough and close enough to the Sun that their angular extent on the sky is measurable via current interferometric methods. (See López-Morales 2007 for a summary.) The latest M-type dwarf for which a radius has been directly measured is the M5.5 star Proxima Centauri. Later M-type dwarfs are too faint for current interferometric measurements, and no late-M eclipsing systems are recognized so far.

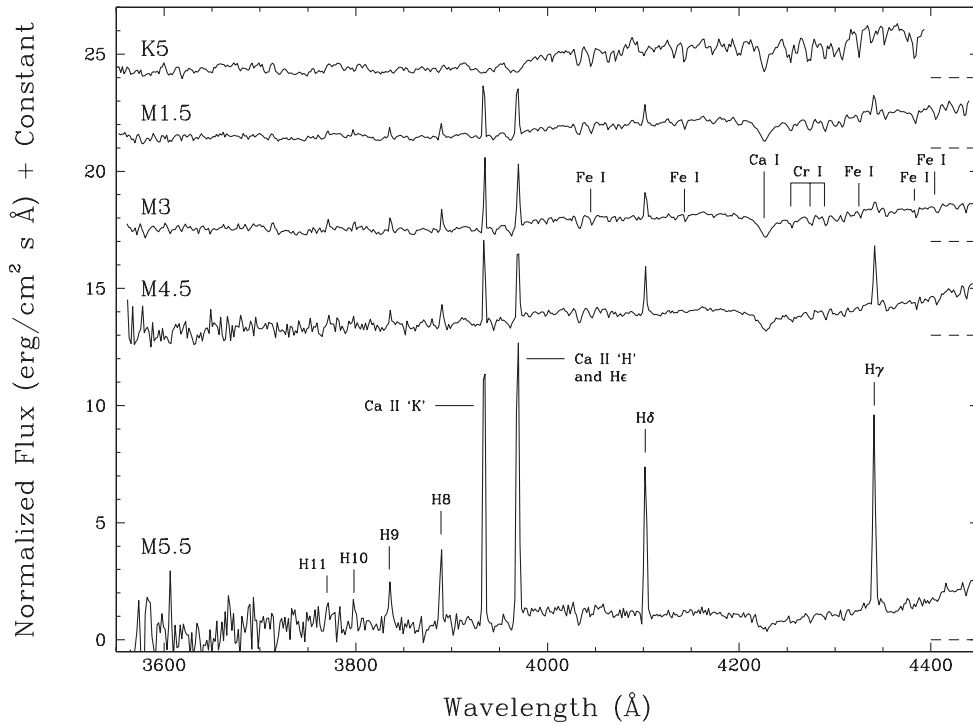


Figure 9.18 Optical spectra of late-K through mid-M dwarfs from 3550 to 4450 Å. From top to bottom are shown Gl 820A (61 Cyg A), Gl 494 (DT Vir), Gl 388 (AD Leo), Gl 234AB (V577 Mon), and Gl 473AB (FL Vir). The fluxes have been normalized to unity at 4200 Å and offsets added to separate spectra from each other. Dashed lines along the right side show the zero points of each spectrum. These data come from Pettersen & Hawley (1989), the digital versions of which were courteously provided by Suzanne Hawley.

No L dwarfs are known in eclipsing systems either, so direct measurements of their radii are not yet possible. Interior models, on the other hand, indicate that field-age L dwarfs have very similar radii. Assuming a constant birthrate and a mass function of the form $dN \propto M^{-1}dM$, Monte Carlo simulations using the Burrows et al. (1997) evolutionary models show a total range in radius of $\sim 0.75\text{--}1.05 R_{\text{Jup}}$ for field L (and T) dwarfs drawn from a sample with $1 \text{ Myr} < \text{age} < 1 \text{ Gyr}$ and $1 M_{\text{Jup}} < M < 100 M_{\text{Jup}}$ (Burgasser 2001). In the absence of empirical measures we will assume a mean radius of $0.90 R_{\text{Jup}}$ for L dwarfs.

9.4.1.2 Measuring *L*

To measure luminosity, both the distance and the apparent flux summed over all wavelengths must be known. For field M and L dwarfs, highly accurate trigonometric parallaxes have been obtained through concentrated astrometric monitoring campaigns such as those by Monet et al. (1992), van Altena et al. (1995), Tinney

et al. (1995), Tinney (1996), Dahn et al. (2002), and Vrba et al. (2004). In addition, the distances to several M- and L-dwarf companions have been deduced from common proper motion with a primary star whose trigonometric parallax has already been measured.

The apparent bolometric luminosity is usually deduced through a combination of empirical spectra and photometry supplemented where needed by spectral models. These models are generally needed only to estimate the small contribution by the unobserved short- and long-wavelength tails of the flux distribution. Researchers often compute a correction value for a particular subclass of object (for example, an M2 dwarf or a dwarf of specific $R-I$ color) so that similar objects may have band-specific luminosities converted to total luminosities without the need for measurements across many different wavelengths. (The assumption here is that the bolometric flux will be the same for objects classified similarly or having similar colors.) This is called a bolometric correction. Bolometric corrections for M, L, and T dwarfs can be found in Bessell (1991) and Golimowski et al. (2004).

9.4.1.3 Calculating T_{eff}

Using R and L from above, we can deduce T_{eff} for M and L dwarfs. The results are shown graphically in Figure 9.19. The values of T_{eff} for M dwarfs are taken from López-Morales (2007) and for L and T dwarfs from Vrba et al. (2004). These temperatures are plotted against optical spectral type. (See section 4.1 of Kirkpatrick 2005 for more on the construction of the L and T dwarf portion of this diagram.) A simple linear least squares fit to the M- and L-dwarf data gives the relation

$$T_{\text{eff}}(K) = 3759 - 135x$$

where x is the optically defined spectral type, valid for optical types M0 through L8, with $x = 0$ for M0, $x = 5$ for M5, $x = 10$ for L0, $x = 18$ for L8, etc. Empirically measured radii for dwarfs later than mid-M are badly needed not only to fill in the gap from mid- through late-M but also to check the model assumptions implicit to the radius calculation for L and T dwarfs. Nonetheless, the extant data point to a tight, linear relation between T_{eff} and optical spectral types, but this relation breaks down completely at the transition between late-L and mid-T dwarfs. See Chapter 10 for a discussion of the L-to-T transition.

9.4.2 Chemistry of the Atmosphere

The spectra of M and L dwarfs are very complex, but they are part of a continuum of types describing main-sequence stars and brown dwarfs. The simplified explanation of the entire sequence is that at the highest temperatures the atoms of the gas favor an ionized state, then at lower values of T_{eff} favor a neutral state, at even lower temperatures begin to form molecular compounds, and finally at the coolest values of T_{eff} form into solid and liquid condensates along with more complex molecules. Which molecules and condensates form is a function of gas pressure, metallicity, and other factors such as turbulent mixing. During the cooling process

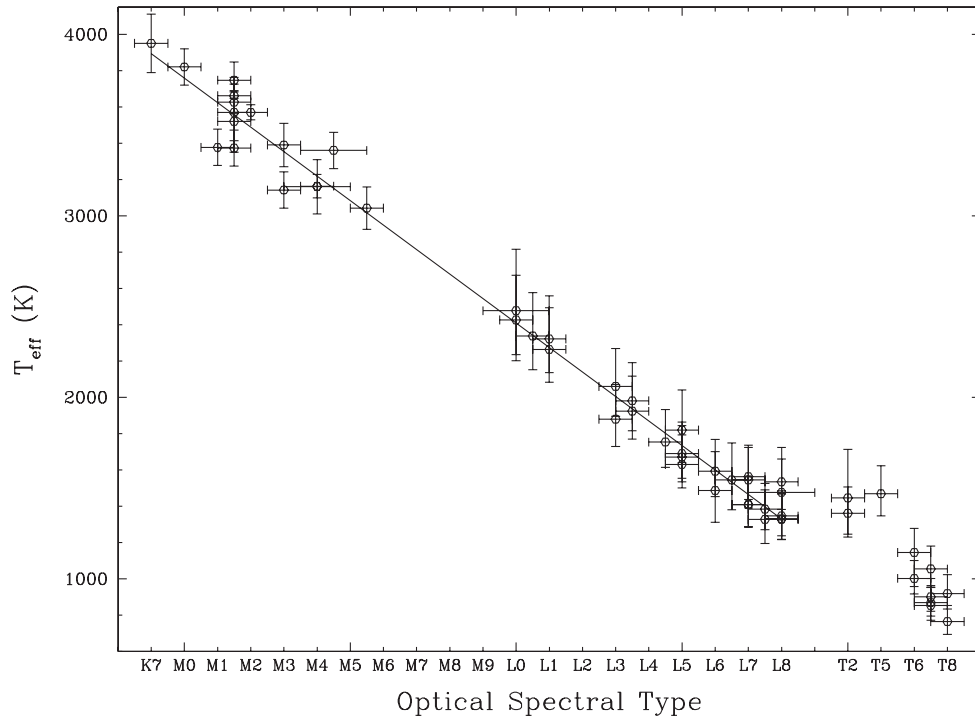


Figure 9.19 Empirically determined effective temperature versus optical spectral type from late-K through late-T. Data for the early- to mid-M dwarfs are taken from Metcalfe et al. (1996), Torres & Ribas (2002), Ribas (2003) Ségransan et al. (2003), and Berger et al. (2006). The K and M dwarfs plotted are Gl 380 (K7); Gl 278C = YY Gem (M0); Gl 514 (M1); Gl 15A, Gl 191, Gl 205, Gl 526, Gl 880, Gl 887 (all M1.5); Gl 411 (M2); Gl 687, Gl 752A (both M3); Gl 699 = Barnard's Star, GJ 2069A = CU Cnc (both M4); Gl 630.1 = CM Dra (M4.5); Gl 551 = Proxima Cen (M5.5). Larger error bars have been placed on the optical spectral types for the eclipsing systems Gl 630.1 and GJ 2069A because their published types, unlike the others plotted here, may not be on the Kirkpatrick et al. (1999) system. See Kirkpatrick (2005) for details concerning the L and T dwarfs.

(which never ends for brown dwarfs), the sequence of molecule and condensate formation is also very important because condensation robs the atmosphere of elemental constituents that would otherwise be available for molecule formation at even lower temperatures.

Simple gas-phase chemistry has provided an adequate description of the spectra of main-sequence stars warmer than type M, but problems arise when attempting to fit such models to later M-type dwarfs. The difficulty lies in the omission of condensation, or “dust” formation, in the models themselves, as described in Tsuji et al. (1996a, b) and Fegley & Lodders (1996). Jones & Tsuji (1997) showed that the TiO bands in the latest M dwarfs do not strengthen as expected for cooler temperature objects (as is also seen in the spectra of the latest M-type giants), and likewise can not be adequately modeled with synthetic spectra that are dust-free.

Moving to cooler temperatures, we find for early- to mid-L dwarfs an almost complete disappearance of TiO and VO molecules. Chemical equilibrium calculations by Lodders (1999), Burrows & Sharp (1999), and Allard et al. (2001) suggest that TiO disappears from the spectra because it converts to TiO_2 or condenses into perovskite (CaTiO_3) and other titanium-bearing molecules ($\text{Ca}_4\text{Ti}_3\text{O}_{10}$, $\text{Ca}_3\text{Ti}_2\text{O}_7$, Ti_2O_3 , Ti_3O_5 , and Ti_4O_7) at temperatures near the boundary between late-M and early-L. Vanadium is less refractory than titanium, so VO is removed from the gas at slightly lower temperatures than the removal of TiO. Lodders (2002) argues that the VO is removed via formation of VO_2 and a condensate not of pure VO as others have stated, but instead as a solid solution with titanium-bearing condensates.

Condensate formation is a function of gas pressure, which is dependent upon the gravity, and this determines the temperature at which the TiO and VO condensates form. For lower-gravity objects, the formation of TiO and VO condensates is pushed to lower temperatures. The reason why the young L dwarf in Figures 9.13 and 9.14 shows such unusually strong VO bands is that it still retains more of its VO in molecular form than does a higher gravity L dwarf of the same subtype. Further, objects of much lower gravity (the M giants) will have the onset of condensation pushed to even cooler temperatures. Late-M giants show no condensation of either TiO or VO, which is why those bands are so strong (for reference, see the giant spectrum displayed in Figure 9.13). Giant stars, in fact, never reach temperatures cool enough for the condensation of TiO and VO to take place. There are no objects known as “L giants” because of this lack of TiO and VO disappearance, which is the defining characteristic of spectral class L.

The TiO and VO condensates mentioned above have a very noticeable effect on the emergent spectrum since they clear the photosphere of two of its main absorbers. Other condensates have a much less obvious, but no less important, effect. Excellent review papers by Burrows et al. (2001), Lodders (2002), and Lodders & Fegley (2002) explain this “behind the scenes” dust formation. Al-bearing condensates such as corundum (Al_2O_3) and Ca aluminates like hibonite ($\text{CaAl}_{12}\text{O}_{19}$), grossite (CaAl_4O_7), and gehlenite ($\text{Ca}_2\text{Al}_2\text{SiO}_7$) form at even higher temperatures than the Ti-bearing condensates mentioned above. These first condensates remove Ca that might otherwise go toward perovskite formation, and this determines the rate at which the atmosphere is robbed of its TiO. Likewise, forsterite (Mg_2SiO_4) and enstatite (MgSiO_3), which are somewhat less refractory than the Ca and Al silicates and thus form at slightly cooler temperatures, sequester some of the O and prohibit it from forming other compounds at cooler temperatures. As one specific example, if elements such as Al, Ca, and Si were not removed at higher temperatures, neutral K would not be seen as a major absorber in late-L dwarfs because it would have been removed by Si condensates like orthoclase (KAlSi_3O_8 , sometimes referred to as high sanidine).

As the Ti-bearing condensates form at late-M and early-L, the opacity of the oxide bands weakens and the contrast of the alkali lines and hydride bands against the relative continuum is increased. By mid- to late-L the resonance lines of Na I and K I are the dominant absorbers in the optical, their wings covering thousands

of Å. Burrows & Volobuyev (2003) point out that the rainout of condensates clears the atmosphere of most of its metals and leaves the less refractory neutral alkali metals as the only major sources of opacity between 4000 and 10000 Å. Sodium and potassium are the most abundant of the alkali metals at solar metallicity and they have the most influence on the shape of the spectral energy distribution in the optical. These Na and K atoms have their energy levels perturbed by the potential field of H_2 , which is the dominant molecule in a gas at L-dwarf temperatures. Burrows & Volobuyev (2003) find that the influence of K I on the continuum shape extends out to 9500–10000 Å, and the wings of Na I extend out to ~ 8000 Å. These results explain the shape of the optical continua of mid- to late-L dwarfs (see Figure 9.10).

At early-L through late-L, absorptions by hydride molecules are also seen in the optical and near-infrared. The empirical spectra at early- to mid-L show the strength of first FeH, then CrH reaching a peak, with both beginning to weaken and disappear around early-T. Chemical equilibrium calculations imply that CrH should remain at temperatures cooler than the disappearance of FeH (Burrows et al. 2001).

At mid-L the methane fundamental band at $3.3 \mu\text{m}$ is first seen (Noll et al. 2000; Cushing et al. 2005), indicating that the conversion of carbon monoxide to methane as the dominant carbon-bearing molecule via the reaction $\text{CO} + 3\text{H}_2 \rightarrow \text{CH}_4 + \text{H}_2\text{O}$ has begun. This reaction produces more H_2O , so water bands also continue to strengthen. Methane is also seen at $7.8 \mu\text{m}$ in late-L dwarfs, which is not surprising since this band should have a strength comparable to that of the $3.3 \mu\text{m}$ feature (Roellig et al. 2004). The overtone bands of methane at 1.6 and $2.2 \mu\text{m}$ are also sometimes seen in late-L dwarfs (e.g., McLean et al. 2001; Nakajima et al. 2004) but are not clearly detected at low resolution until type T0. This unambiguous detection of CH_4 at the H- and K-bands is the defining characteristic of T dwarfs (see Chapter 10).

9.4.3 Stars or Brown Dwarfs?

During the formation of a low-mass star, contraction is halted by radiation pressure when the contraction produces core densities and temperatures capable of igniting hydrogen fusion. For an object of lower mass, electron degeneracy is reached in the core before central densities and temperatures have reached the hydrogen fusion point. As first postulated by Kumar (1963) and Hayashi & Nakano (1963) the degeneracy of such an object, now known as a “brown dwarf,” is what supports it from collapsing further. As a consequence of the lack of a stable energy source, such a brown dwarf continues to cool with time.

Theoretical evolutionary tracks of low-mass stars and brown dwarfs with solar metallicity are shown in Figure 9.20. This plot illustrates the evolution of the effective temperature with time for models running from a mass of $0.6 M_\odot$ to $0.002 M_\odot$ (or ~ 600 to ~ 2 Jupiter masses, since $1 M_\odot \approx 1000$ Jupiter masses). Tracks shown by solid lines represent objects that become normal stars because they eventually reach stable hydrogen burning in their cores and have hence reached the main

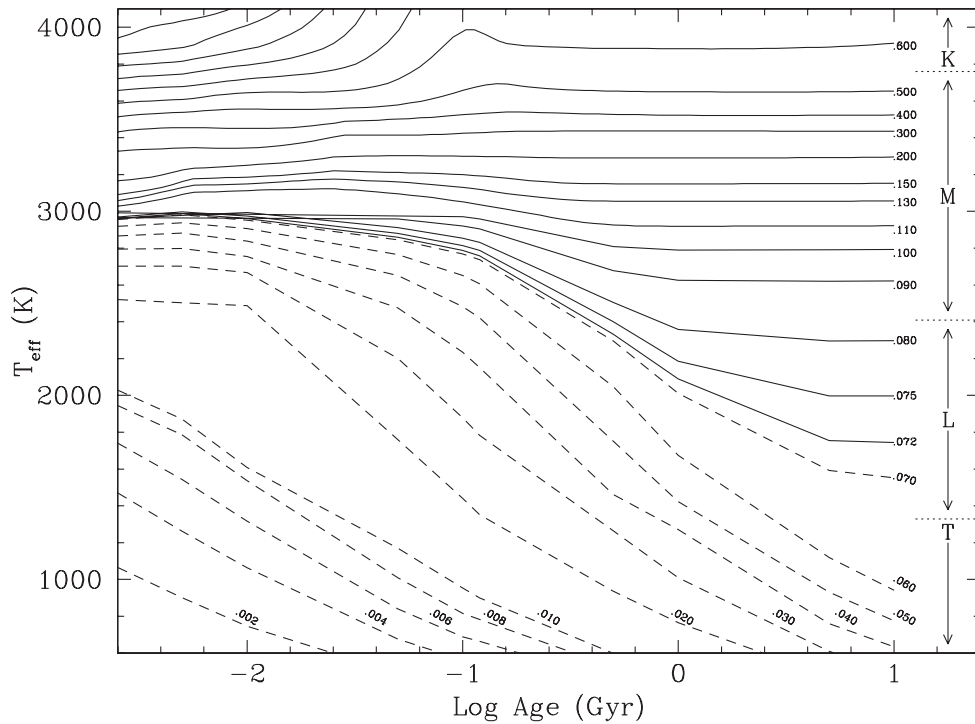


Figure 9.20 Theoretical evolutionary diagram (T_{eff} vs. age) for low-mass stars and brown dwarfs of solar metallicity. These models come from Baraffe et al. (1998) and Baraffe et al. (2003). In these models, the break between hydrogen-burning stars (solid tracks) and brown dwarfs (dashed tracks) occurs near $0.072M_{\odot}$. Shown along the right side of the diagram are the temperature ranges for old field K, M, L, and T dwarfs as determined in Figure 9.19.

sequence. Tracks shown by the dashed lines represent brown dwarfs, whose temperatures continue to drop with time because they never undergo normal hydrogen burning.³

Also marked on Figure 9.20 are the approximate temperature ranges at old ages (several Gyr) spanned by the optical M- and L-spectral classes. Matching these ranges of T_{eff} to the evolutionary models suggests that early- to mid-M dwarfs are comprised completely of hydrogen-burning stars whose temperatures change very little after their first few Myr. (The earliest stages of a star's life are not depicted on this plot, as the physics of star formation is far more uncertain than for subsequent evolution.) Mid- to late-M dwarfs are comprised of old, low-mass stars (masses between ~ 0.120 and $\sim 0.085M_{\odot}$) and young brown dwarfs (ages \sim few Myr). Early- to mid-L dwarfs are a mixture of low-mass stars ($< 0.085M_{\odot}$) that are fairly old (> 300 Myr) and brown dwarfs generally younger than ~ 3 Gyr. The

³Objects above $\sim 0.013M_{\odot}$ are thought to burn heavy hydrogen (deuterium) for periods of < 100 Myr early in their lives, but this does not halt further collapse for very long since the primordial abundance of deuterium is low (Burrows et al. 1997).

latest L dwarfs are, however, all brown dwarfs—spanning the range from very high-mass ones ($\sim 70 M_{\text{Jup}}$) that are as old as the Sun to very low-mass ones that are still very young.

Researchers should thus be cautious when using terms such as “M stars” and “L stars.” For dwarfs, the term “M stars” implies a star in which stable hydrogen burning is taking place. Young-cluster brown dwarfs should strictly not be called “M stars” because they are not stably burning hydrogen as a star does; these should be called “M-type brown dwarfs” instead. Specificity is generally not needed, however, in which case the term “M dwarf” is preferred because of its conveniently ambiguous nature. The same logic applies to the terms “L star,” “L-type brown dwarf,” and “L dwarf,” the latter being the phrasing of choice in most situations.

We need not rely totally on theory to determine the stellar or substellar nature of objects. By definition, distinguishing a brown dwarf from a star requires knowledge that the object is not burning hydrogen in its core. There is no direct way to probe the interiors of these objects, but the most common indirect method used is the “lithium test” (Rebolo et al. 1992). This test recognizes the fact that the temperature needed to sustain core hydrogen fusion in the lowest-mass stars ($T > 3 \times 10^6$ K; Burrows et al. 1997; Nelson et al. 1993) is only slightly higher than that needed to burn lithium ($T \approx 2 \times 10^6$ K; Pozio 1991). If lithium does not burn, that means hydrogen is also not being fused. Once destroyed, lithium is not easily manufactured again in stellar interiors, so stars and brown dwarfs will never have more than their natal abundance of this element. In principle, the presence or absence of lithium in the spectrum can thus provide an indirect probe of inner temperatures.

In practice, there are several drawbacks when applying the lithium test to real data. First, the Li I resonance line at 6708 \AA is located in a portion of the spectrum where the flux is quite low. Large telescopes with moderate-resolution optical spectrographs are required. Second, searching for the Li I line should prove futile below $T_{\text{eff}} \approx 1500$ K due to the formation of Li-bearing molecules like LiCl and LiOH (Lodders 1999). Third, in young brown dwarfs low gravity will weaken the Li I line, making it much harder to detect than in older, higher-mass brown dwarfs of the same temperature (Kirkpatrick et al. 2006). The first point is illustrated in Figure 9.13, which shows detections of the 6708 \AA Li I absorption line in an L5 dwarf (weak) and L6 dwarf (stronger) despite the low flux levels at these wavelengths. The third point is illustrated in Figure 9.13 (inset), which shows the complete lack of a Li I detection in a low-gravity early-L dwarf suspected of being a low-mass brown dwarf.

The second point is best demonstrated via analysis of optical spectra of 123 field L dwarfs taken by Kirkpatrick et al. (in prep.). This paper reports that the percentage of L dwarfs with discernible lithium absorption (equivalent widths $\geq 4 \text{ \AA}$) is $\sim 10\%$ at early-L then slowly rises to $\sim 65\%$ by L6. At later types the percentage drops, declining to $\sim 40\%$ by L8. Measures of the lithium equivalent width also appear to reach a maximum around L6 and then diminish at later types. This corresponds to the temperatures where monatomic lithium is expected to disappear into

molecular form, and the seeming agreement between observations and theory is reassuring. It should be kept in mind, however, that such measurements are made against a relative continuum that is strongly modulated by the strong Na I D line to the blue and strong K I line to the red. Increasing absorption by the broad wings of these two strong bands can weaken the contrast between the Li I line and the continuum, too.

9.4.4 Space Density

Early- to mid-M dwarfs within a few parsecs of the Sun are relatively bright and easily distinguished. The vast majority of these have measured trigonometric parallaxes so their distances are known precisely. In this case, calculating a space density involves nothing more than counting the number of objects within a specified volume of space. We will refer to this as method #1.

For the majority of late-M through late-L dwarfs, however, distances are not yet accurately known but can be estimated using the small numbers of late-M and L dwarfs with measured parallaxes. In this case, distance estimation biases such as unresolved binarity, which gives an object the appearance of being closer than it actually is, need to be taken into account before calculating a true space density. We will refer to this as method #2.

Traditionally, method #1 has used the volume of sky within 8 pc of the Sun. This volume has been thoroughly scoured for early- to mid-M dwarfs, except for some possible incompleteness in the southern hemisphere where the proper motion and photometric surveys necessary to identify these objects have lagged. If we therefore restrict ourselves to the portion of that volume having $\text{Dec} > -30^\circ$ (corresponding to a space volume of $\sim 1600 \text{ pc}^3$), we find 107 M dwarfs with types earlier than M7 and 6 M dwarfs typed as M7 or later. The space density for the M0–M6.5 sample is found to be $6.7 \times 10^{-2} \text{ pc}^{-3}$. For the full list of stars in this volume, see the compilation in Reid & Gizis (1997) and subsequent updates in Reid et al. (1999), Reid et al. (2003), and Reid et al. (2004).

The best estimate for the space density of late-M through late-L dwarfs comes from Cruz et al. (2007), who performed an exhaustive photometric search using the Two Micron All Sky Survey (2MASS) and supplemented with their own spectroscopic follow-up. Based on the known optical spectral type versus magnitude relation and using their measured optical spectral types for the objects in their sample, these authors were able to compute space densities via method #2. For late-M dwarfs (optically typed as M7–M9.5) they measure a space density of $4.9 \times 10^{-3} \text{ pc}^{-3}$. For L dwarfs, the survey was slightly hindered by incompleteness at the latest types, so their measured space density of $3.8 \times 10^{-3} \text{ pc}^{-3}$ for L0–L8 should be considered a lower limit. For even cooler objects the most robust determination comes from Metchev et al. (2007), who combined subsets of data from the Sloan Digital Sky Survey and 2MASS. Also using method #2 they find a lower limit of $\sim 7.2 \times 10^{-3} \text{ pc}^{-3}$ for the space density of T0–T8 dwarfs, or twice that of L0–L8 dwarfs.

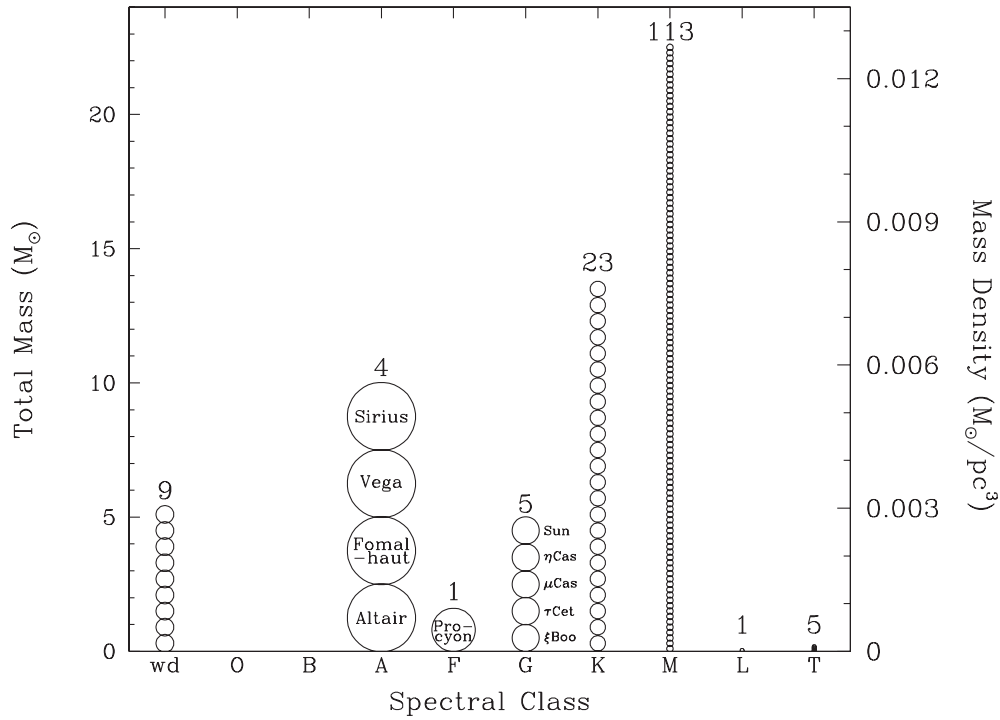


Figure 9.21 Previously catalogued stars and brown dwarfs within 8 pc of the Sun and north of Dec = -30° . Symbol size scales with mass so that total mass or mass density can be read off the vertical axes. Common names of the bright (A-, F-, and G-type) stars are also marked.

We illustrate the constituents of the 8-pc volume in Figure 9.21. Early-type stars are, of course, rare—there are no O or B stars and only 4 A dwarfs, 1 F dwarf, and 5 G dwarfs in that volume of space (the earlier type stars that *had* been present are represented by the 9 white dwarfs). Dimmer than that are 23 K dwarfs, 113 M dwarfs, 1 L dwarf, and 5 T dwarfs. The census of late-M, L, and T dwarfs in this volume may still be short a few not-yet-discovered objects based on the space densities quoted above, and the prevalence of objects cooler than T8 (not shown) awaits all-sky surveys at longer wavelengths.

Despite their similarities, M dwarfs and L dwarfs are very different in their prevalence and in their importance to the mass budget of the Galaxy. Note that in Figure 9.21 M dwarfs dominate both the numbers and the mass density in this slice of the Solar Neighborhood. L dwarfs, on the other hand, are among the rarest of objects and contribute very little to the Galactic mass budget. This paucity of L dwarfs is a consequence of two facts: (1) The rapid cooling of brown dwarfs through the temperature range encompassing L dwarfs means that L-type brown dwarfs should be rare relative to other, cooler brown dwarfs (Burgasser 2004b). (2) As shown in the models of Figure 9.20, the mass range spanned for hydrogen-burning L dwarfs, $\sim 0.07\text{--}0.08 M_\odot$, is much narrower than that spanned by M dwarfs, $\sim 0.08\text{--}0.55 M_\odot$. Hence, depending upon the shape of the mass function at

those masses, proportionately fewer stars—only those at the very lowest masses—settle onto the main sequence as L dwarfs.

9.5 PECULIAR OBJECTS

9.5.1 Dwarf Carbon Stars

With the introduction of Secchi's spectroscopic class IV (Secchi 1868), prominent carbon bands were recognized as a distinguishing feature in the spectra of some stars. More detailed study of these carbon stars revealed them to be evolved objects occupying the giant or subgiant branches of the H–R diagram (see Chapter 8). Such stars have enhanced carbon abundances in their upper atmospheres presumably because of post-main sequence dredge-up of material from nuclear-processed layers deep within the star. See Chapter 8 and Wallerstein & Knapp (1998) for a detailed review.

Over 100 years after the identification of carbon giants, Dahn et al. (1977) identified a carbon star whose measured parallax and space motion indicated that it was a relatively nearby, low-luminosity object residing near the M-dwarf sequence in the H–R diagram. This object, G 77-61 (LHS 1555), is now recognized as the prototype of a class of object known as carbon dwarfs (dC). At face value, the existence of such a main-sequence object with processed material in its atmosphere is a puzzle. Dahn et al. (1977) hypothesized that this object was in fact a double star. Presumably the former, now invisible primary evolved off the main sequence and, during its asymptotic giant branch (AGB) phase, dumped dredged-up, processed material onto the surface of its lower mass, main-sequence companion. The former AGB star has now become a cool white dwarf and is much fainter than the carbon dwarf “secondary” now seen. Subsequent observations have proven the existence of an unseen component in G 77-61 from radial-velocity variations (Dearborn et al. 1986). Two other carbon dwarfs that show telltale signs of the white-dwarf component in the composite spectrum (Heber et al. 1993; Liebert et al. 1994) are also now recognized.

Even a generous amount of carbon deposited onto the atmosphere of a normal K or M dwarf would not give rise to a spectrum like that of G 77-61. Dearborn et al. (1986) showed that it was necessary for the mass-receiving dwarf to be of very low metallicity itself in order for the carbon not to be overwhelmed by the oxygen-bearing constituents already present. Such a scenario means that this would have to be a Population II halo binary system with low Z . Model fits to the atmosphere of G 77-61 (Gass et al. 1988; Plez & Cohen 2005) along with its measured UVW space motion (Dahn et al. 1977) indicate that it is indeed a low-metallicity member of the Galactic halo. On the other hand, some dC examples such as PG 0824 + 289 are known to have characteristics of Population I (Heber et al. 1993).

Carbon dwarfs are rare objects if one uses normal M dwarfs to define a common star. The dC nearest the Sun is at 59 pc (Harris et al. 1998), yet there should be some 50,000 M dwarfs located within that same distance. Nonetheless, car-

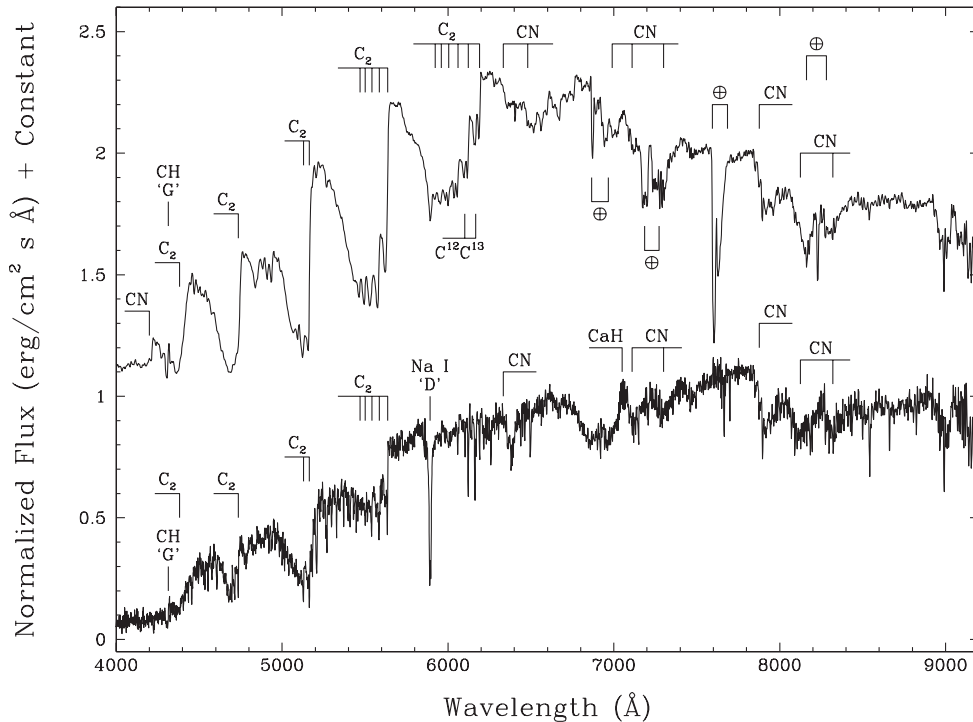


Figure 9.22 Line and band identifications for two dwarf carbon stars. At the top is shown a spectrum of the dC prototype G 77-61 from Lowrance et al. (2003) and below a spectrum of the dC star SDSS J152702.75 + 434517.4 from Downes et al. (2004). Both spectra have been normalized to unity at 7500 Å and an integer offset added to the fluxes of G77-61 to separate it vertically from the SDSS object. Line and band identifications are shown for each.

bon dwarfs almost certainly outnumber their better-known carbon-giant counterparts and hence constitute the majority of carbon stars in the Galaxy (Green 2000). Figure 9.22 shows sample optical spectra of two dwarf carbon stars with features identified. At the time of this writing, over 120 dC stars are now recognized (Margon et al. 2002; Lowrance et al. 2003; Downes et al. 2004) and these show a wide range of spectroscopic morphologies (Figure 9.23). Continuing searches through the Sloan Digital Sky Survey, the Two Micron All Sky Survey, and other deep surveys of large areal coverage are sure to reveal many more.

The holy grail of dC spectroscopy is finding a discriminant that faithfully distinguishes a carbon dwarf from a carbon giant. Dahn et al. (1977) cited differences in strength and shape of the Na D line between G 77-61 and carbon giants, but this feature falls within a sometimes very strong C₂ absorption trough. Green et al. (1992) suggested the use of a ¹²C to ¹³C ratio (using the strength of the C₂ band at 6191 Å) to distinguish luminosity classes, but counterexamples have since been found (Green & Margon 1994; Margon et al. 2002). The strength of the Ca II triplet at 8498, 8542, and 8662 Å has been suggested by Kirkpatrick (1992)

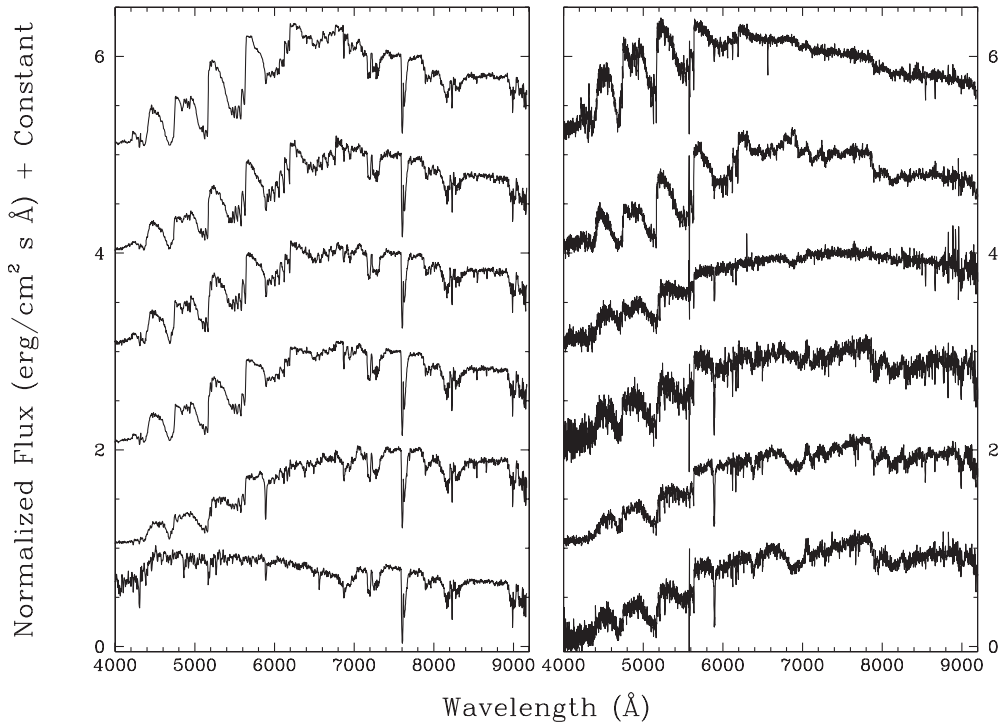


Figure 9.23 Examples of dwarf carbon stars. Shown on the left are non-telluric-corrected spectra from Lowrance (priv. comm.), and on the right are telluric-corrected spectra from Downes et al. (2004). All spectra have been normalized to unity at 7500 Å, except for the one at lower left which was normalized arbitrarily, and integer offsets added to the fluxes to separate them vertically. Note that although most spectra exhibit both C₂ and CN bands, there are examples that show only C₂ (see third spectrum from the top in the right panel) or only CN (bottom spectrum in left panel).

as another luminosity discriminant, although examples of giants and dwarfs with very similar Ca II strengths are also now known (see Figure 9.24). Green & Margon (1994) noted enhanced Ba II lines in the spectra of carbon dwarfs, but these are also sometimes confused by much stronger, overlapping C₂ bands. Margon et al. (2002) suggested that in the cooler objects, the presence of CaH absorption could be used as an indicator of a low-gravity dwarf. This suggestion is still unproven (Downes et al. 2004) and if confirmed would still be useful for only the coolest types. The presence of a very strong CN band at 7900 Å can be used to identify carbon giants (Downes et al. 2004), but a weak 7900-Å CN band does not necessarily mean that the object is a dwarf.

Given the fact that most optical spectroscopic discriminants either fail or are of limited usefulness, it is worth considering other spectroscopic or photometric criteria at longer wavelengths. Near-infrared photometry, optical photometry, or a combination of the two appear to offer some help in distinguishing the two luminosity classes, but all such color-color diagrams suffer from the same limited

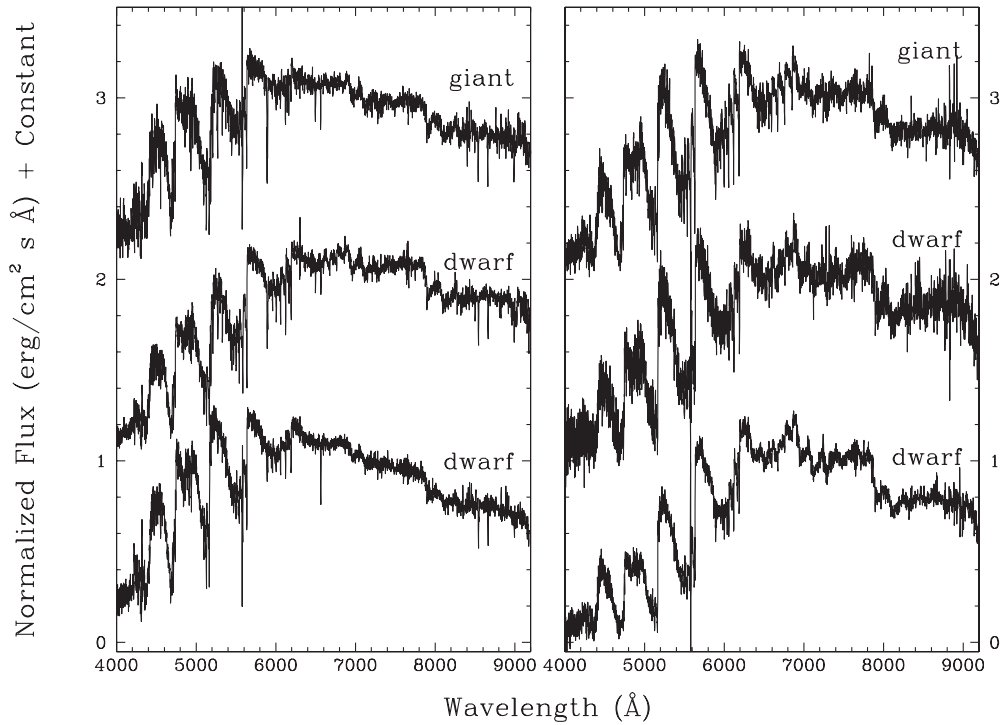


Figure 9.24 Comparison of carbon dwarfs to carbon giants. Shown here are two carbon-giant and four carbon-dwarf spectra from Downes et al. (2004). All fluxes have been normalized to unity at 7500 Å and integer offsets used to separate the spectra vertically. Note that giants and dwarfs sometimes look more alike than dwarfs do with each other. The spectra shown here are, from top to bottom, SDSS J144841.80 + 042844.5, SDSS J112034.87 + 555937.2, and SDSS J1009587.0 + 010313.2 on the left and SDSS J125520.36 + 631326.7, SDSS J073621.29 + 390725.2, and SDSS J012150.28 + 011302.8 on the right.

usefulness as the spectroscopic discriminants. See Downes et al. (2004) for a summary and Joyce et al. (1998) for a discussion of near-infrared spectroscopic traits.

9.5.2 Flare Stars

Flare stars were discovered by accident in 1924 by Ejnar Hertzsprung (of H–R diagram fame). He was examining a series of nine successive photographic plates of the η Carinae region when he discovered one star that suddenly increased in brightness by 1.8 magnitudes on the third plate and faded rapidly on the following plates. Upon examining 37 other plates of the same region taken over 19 different nights, he found that the star was otherwise steady in brightness.⁴ Although now

⁴The uniqueness of this event led Hertzsprung to postulate that a small planet might have fallen into its parent star, thus explaining the sudden outburst of energy. We know now, however, that stellar flares are very common, particularly among M dwarfs. Curiously, a similar physical scenario has been proposed to explain the “unique” nova-like behavior of V838 Monocerotis (Soker & Tylenda 2007; Retter et al. 2006). Now that V838 Mon has also lost its unique status (see Bond & Siegel 2006; Kimeswenger 2006), will history repeat itself?

recognized as an O-type emission-line star, this was the first indication that stars could suddenly flare and then quickly return to a normal state.

The first low-luminosity star seen to flare was the faint, M5.5 dwarf Lalande 21258 (Gl 412B; van Maanen 1940). A few years later, van Maanen (1945) discovered another flaring M dwarf, this time the M4-dwarf Ross 882 (Gl 285). Luyten (1949) reported three different outbursts on the M6-dwarf L 726-8B (Gl 65B, UV Cet), calculating that it spends about 4% of its time in the flaring state. Joy & Humason (1949) obtained the first optical spectroscopic observation of an M dwarf during a flare, again a flare on L 726-8B, and noted that there was not only an increase in continuum flux at the shortest wavelengths but also a strengthening of emission by the hydrogen Balmer lines as well as an appearance of emission in lines of He I and He II.

The top four panels of Figure 9.25 show the spectra of a late-M dwarf caught during the declining phase of a spectacular flare. The bottom panel shows a spectrum of the same dwarf during quiescence. During the flare, emission lines of hydrogen (from both the Paschen and Balmer series), He I, Ca II, Ba II, K I, and O I are seen. At the shortest wavelengths note also the filling-in of the continuum (called “veiling”), which obscures the normally prominent TiO bands. For the event witnessed here, the energy released in the burst may have matched or exceeded the total bolometric luminosity of the star in quiescence (Liebert et al. 1999).

Figure 9.26 shows the ultraviolet spectra of four early- to mid-M dwarfs known to exhibit frequent flaring events. Identification of the emission-line species seen here gives even more clues about the nature of the flares themselves. Note the presence of highly ionized atoms like C IV, O IV, O V, N V, and even Fe XXI in these spectra. How could M dwarfs, known to have effective temperatures no hotter than ~ 3800 K, show such lines? We believe that these stars, like our own Sun, have outer atmospheres consisting of chromospheres, transition regions, and coronae powered by magnetic fields anchored within the dwarf itself. An early-M dwarf’s chromosphere, which has a temperature range of $\sim 4,000$ – $20,000$ K, lies closest to the photosphere and produces lines primarily seen in the optical. The transition region lies between the chromosphere and the corona, has a temperature range of $20,000$ – $200,000$ K, and is primarily responsible for the lines seen at ultraviolet wavelengths. (See Linsky et al. 1982 for more discussion.) The corona has a temperature as high as a few million K and produces lines seen at X-ray wavelengths. See Osten et al. (2006) for a detailed study of the flare star Gl 873(EV Lac) from X-ray/ultraviolet to radio wavelengths and Reid & Hawley (2000) for a detailed review of stellar magnetic activity.

Despite a basic understanding of the atmospheric anatomy of these objects, the exact physical processes under which the magnetic fields transfer energy to the chromosphere, transition region, and corona are not well understood; they are likely different for M dwarfs of different masses and temperatures. A possible empirical measure of this—though it is also fraught with measurement biases that must be accounted for—is the ratio of the number of dMe objects (those showing

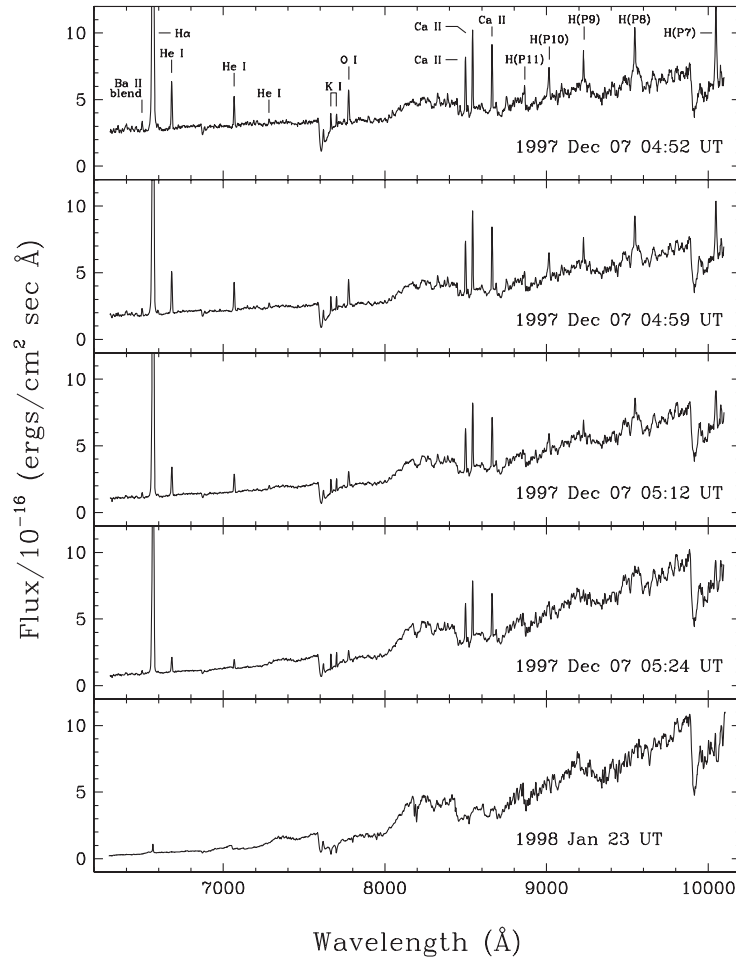


Figure 9.25 Time series of a decaying flare on the M9.5 dwarf 2MASS J01490895 + 2956131. All spectra are plotted with the same flux range. The top four panels represent the decaying flare seen on 1997 Dec 07 (UT), and the bottom panel shows the star in quiescence a month later. This figure comes from Liebert et al. (1999), and is reproduced by permission of the AAS.

the Balmer series of hydrogen in persistent emission) to the number of dM's not having hydrogen in emission. This percentage is $\sim 5\text{--}10\%$ at early-M and steadily rises to $\sim 75\text{--}100\%$ at M7–M8 before dropping off dramatically at late-M and early-L (Gizis et al. 2000; West et al. 2004). For L dwarfs, the values are $\sim 30\%$ for early-L and $\sim 0\%$ for mid- to late-L, at least for objects showing $H\alpha$ equivalent widths of 2 \AA or more (Kirkpatrick et al. 2000).

Nonetheless, it appears that even L dwarfs are capable of flaring events. Figure 9.27 shows an L5 dwarf with $H\alpha$ emission enhanced relative to its quiescent state, which shows no detectable $H\alpha$ emission line. In this figure, a series of spectroscopic exposures show the $H\alpha$ line decaying as if ramping down

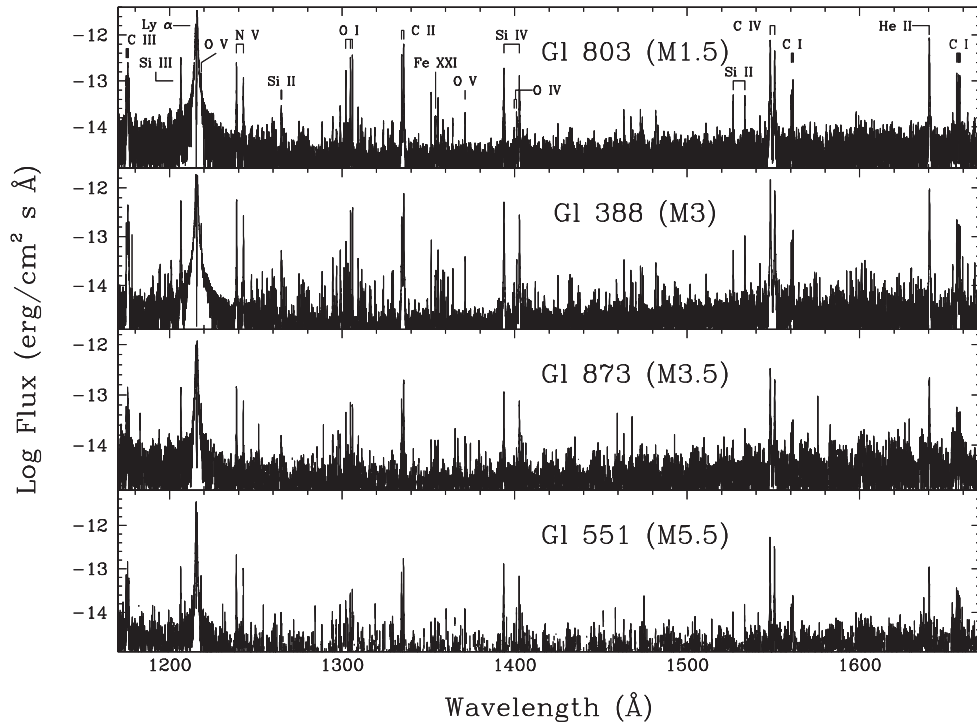


Figure 9.26 Ultraviolet spectra of M-dwarf flare stars between 1170 and 1670 Å. From top to bottom these are G1 803 (AU Mic), G1 388 (AD Leo), G1 873 (EV Lac), and G1 551 (Proxima Cen). These spectra come from the CoolCAT catalog of Thomas Ayers (<http://casa.colorado.edu/~ayers/CoolCAT>).

from a flare. Still, L dwarfs may flare only $\sim 1\%$ of the time (Liebert et al. 2003), in contrast to the $\gtrsim 7\%$ rate seen for M dwarfs (Gizis et al. 2000).

9.5.3 Pre–Main-Sequence Objects

The classification of pre–main-sequence objects has followed a different path from that of other low-mass stars. This is primarily because these objects are in the early stages of their evolution and are still surrounded by dust envelopes or disks that make them extremely faint or invisible at the optical wavelengths traditionally used for spectroscopic classification. Therefore, fluxes at longer wavelengths have been used to set up a typing scheme for these objects.

Sources are generally classified using the parameter α , defined as $\alpha = d \log(\lambda F_\lambda) / d \log(\lambda)$ over the wavelength interval from roughly 2 to 25 μm (Lada 1987; see also Lada & Wilking 1984). Three classes of objects have been established based on the value of α : Class I has a steeply rising continuum and $0 < \alpha < 3$, Class II has “flat” spectra and $-2 < \alpha < 0$, and Class III has falling spectra and $-3 < \alpha < -2$. There are also Class 0 sources that are defined as having very little emission shortward of 10 μm , submillimeter (i.e., wavelengths

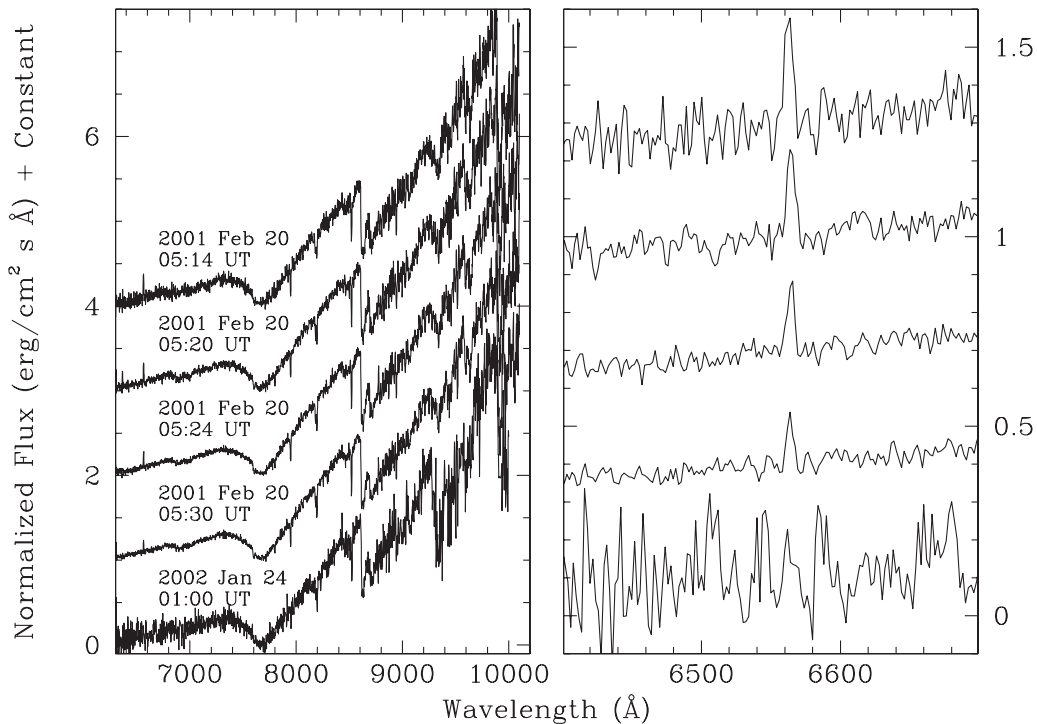


Figure 9.27 Time series of a decaying flare on the L5 dwarf 2MASS J01443536 – 0716142. The top four spectra represent the decaying flare seen on 2001 Feb 20 (UT), and the bottom spectrum shows the star in quiescence a year later. The left panel shows the entire far-optical spectrum; the right panel is a blow-up of the region around $H\alpha$, using a compressed vertical scale to highlight the decline in strength of the emission line. Spectra are taken from Liebert et al. (2003). Left panel reproduced from Liebert et al. (2003) by permission of the AAS.

longward of $350\ \mu\text{m}$) luminosities $>0.5\%$ of the bolometric luminosity, and a few other non-spectroscopic characteristics as summarized in Andre et al. (2000). Examples of each class are shown in Figure 9.28.

Alternatively, the classes can be defined by a “bolometric temperature,” T_{bol} , which is the temperature of a blackbody having the same mean frequency as the source’s observed spectral energy distribution (Myers & Ladd 1993). When using this parameter, the classes roughly fall as follows: Class 0 has $T_{\text{bol}} < 70\ \text{K}$, Class I has $75\ \text{K} < T_{\text{bol}} < 650\ \text{K}$, Class II has $650\ \text{K} < T_{\text{bol}} < 2880\ \text{K}$, and Class III has $T_{\text{bol}} > 2880\ \text{K}$ (Chen et al. 1995). It should be noted that Class I sources are sometimes referred to as embedded protostars, Class II sources are known as classical T Tauri stars, and Class III sources are known as weak-lined T Tauri stars (see also §7.5).

These classes were established in an attempt to approximate an evolutionary sequence. The scenario as envisioned runs as follows: Class 0 sources are cloud cores just beginning their collapse into stars. Class I sources are stars lying in a cocoon of circumstellar material that is assembling itself into a disk and being

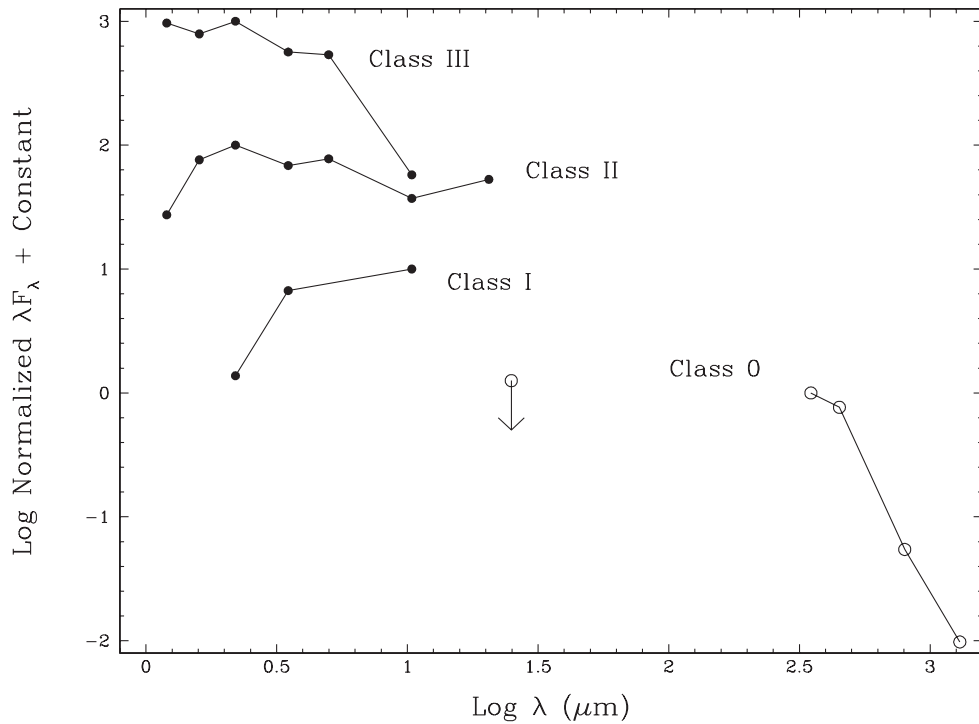


Figure 9.28 Typical spectral energy distributions of Class 0, I, II, and III sources, as observed in the ρ Ophiuchi star-formation region. Each spectrum has been normalized to its peak flux and integral offsets added to separate the spectra vertically. Shown by open circles are broad-band photometry for the Class 0 source VLA 1623 from Ward-Thompson (1993) and Andre et al. (1993). Shown by solid circles are photometric measures of the Class I source LFAM 26, Class II source SR 24S, and Class III source SR 20 from Greene et al. (1994). The Class 0 source is undetected at the shorter wavelengths where the Class I, II, and III sources are easily seen.

funneled onto the star. Class II sources are more mature stars undergoing normal disk accretion but having little residual material in the envelope. Class III sources are stars that have moved beyond the accretion stage but have yet to reach the main sequence.

Several wrinkles exist in this clean scenario, however. Some Class I sources assumed to have spherically symmetric dust envelopes can be just as easily modeled with nearly edge-on flared disks (e.g., Chiang & Goldreich 1999). Not only is the viewer's line of sight an important consideration, but changing the size of the aperture used for flux summing can also cause gross differences in the shape of the measured spectrum, thus altering its assigned classification (e.g., Whitney et al. 2003). In summary, even if our understanding of the basic steps in star formation is correct, mapping observed objects back to their proper step in the sequence is far from straightforward.

As stated in White et al. (2007), the most unambiguous determination of a pre-main-sequence star's atmospheric properties and accretion signature is to acquire

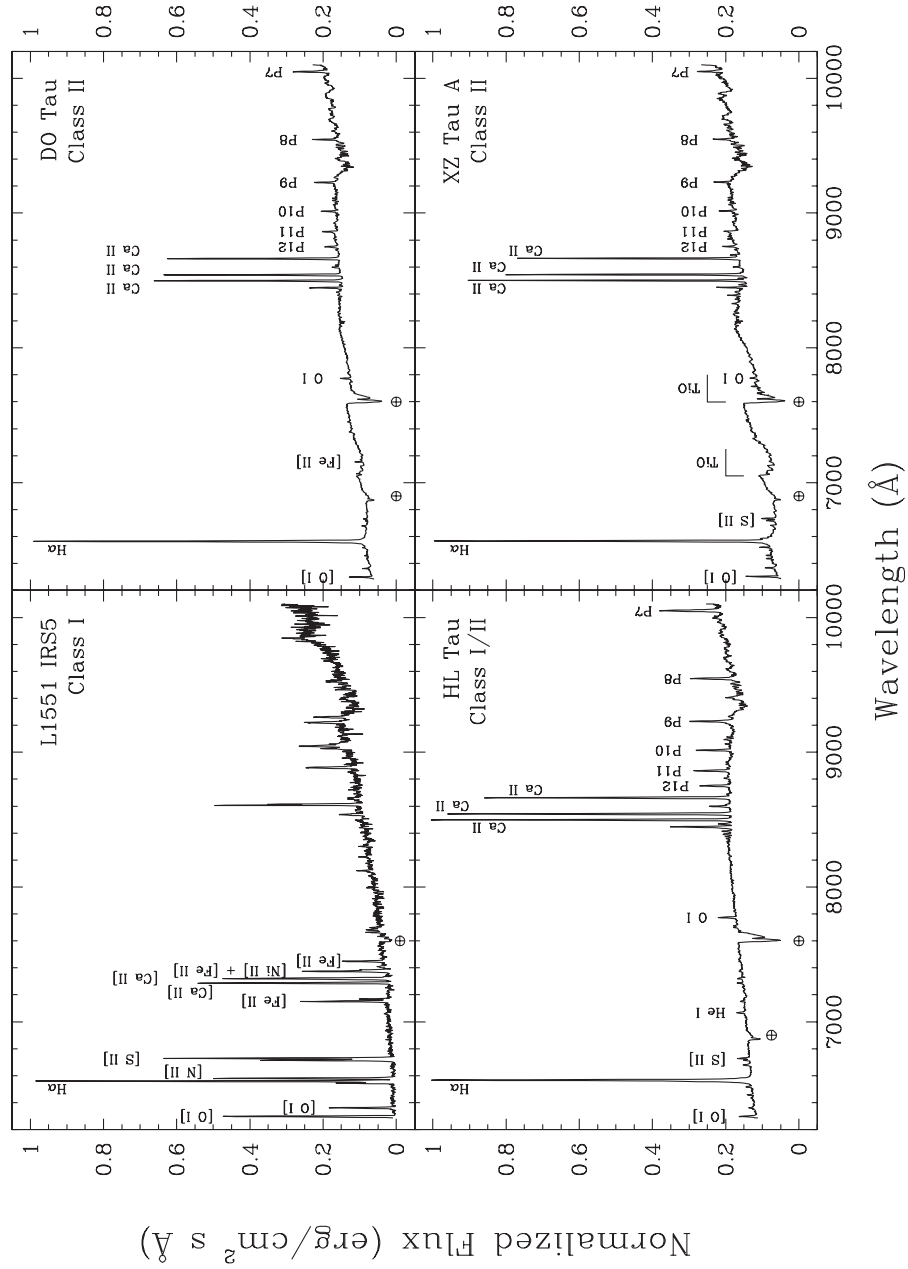


Figure 9.29 Optical spectra of Class I, I/II, and II sources. The flux of each spectrum is normalized to unity at the peak of $H\alpha$ emission. In the Class I and I/II sources, the only absorptions seen are from the earth's atmosphere and are not intrinsic to the sources themselves. In the two Class II sources, intrinsic absorption by TiO in the star's photosphere begins to be seen. Data are unpublished spectra from the author.

spectroscopy in the optical or near-infrared where the emitted photospheric flux is maximum. For Class III and II sources, this is relatively easy with modern spectrographs on large-aperture telescopes, but Class I sources are very difficult, with Class 0 sources still beyond reach. Figure 9.29 shows optical spectra for a few Class I, I/II, and II sources. In the Class I source the emission is probably dominated by a jet of collimated material associated with the young protostar. In the Class I/II source the spectrum is dominated by emission from the accretion disk or scattering off the circumstellar envelope. The Class II sources show less obscuration and veiling so that true photospheric features such as the familiar TiO bands of an M dwarf begin to appear.

Bibliography

- Adams, W.S. 1913, PASP, 25, 258
- Adams, W.S., Joy, A.H., & Humason, M.L. 1926, ApJ, 64, 225
- Adams, W.S., & Kohlschütter, A. 1914, *Contributions from the Mount Wilson Observatory*, Carnegie Institution of Washington, 79, 1
- Allard, F., Hauschildt, P.H., Alexander, D.R., Tamanai, A., & Schweitzer, A. 2001, ApJ, 556, 357
- Andre, P., Ward-Thompson, D., & Barsony, M. 1993, ApJ, 406, 122
- Andre, P., Ward-Thompson, D., & Barsony, M. 2000, *Protostars and Planets IV*, 59
- Baraffe, I., Chabrier, G., Allard, F., & Hauschildt, P.H. 1998, AA, 337, 403
- Baraffe, I., Chabrier, G., Barman, T.S., Allard, F., & Hauschildt, P.H. 2003, AA, 402, 701
- Becklin, E.E., & Zuckerman, B. 1988, *Nature*, 336, 656
- Berger, D.H., et al. 2006, ApJ, 644, 475
- Bessell, M.S. 1991, AJ, 101, 662
- Boeshaar, P.C. 1976, Ph.D. Thesis, Ohio State Univ.
- Boeshaar, P.C., & Tyson, J.A. 1985, AJ, 90, 817
- Bond, H.E., & Siegel, M.H. 2006, AJ, 131, 984
- Borysow, A., Jorgensen, U.G., & Zheng, C. 1997, AA, 324, 185
- Burgasser, A.J. 2001, Ph.D. Thesis, California Institute of Technology
- Burgasser, A.J., et al. 2003, ApJ, 592, 1186
- Burgasser, A.J. 2004a, ApJL, 614, L73
- Burgasser, A.J. 2004b, ApJS, 155, 191
- Burgasser, A.J., Cruz, K.L., & Kirkpatrick, J.D. 2007, ApJ, 657, 494
- Burgasser, A.J., & Kirkpatrick, J.D. 2006, ApJ, 645, 1485
- Burrows, A., et al. 1997, ApJ, 491, 856
- Burrows, A., Hubbard, W.B., Lunine, J.I., & Liebert, J. 2001, *Reviews of Modern Physics*, 73, 719
- Burrows, A., & Sharp, C.M. 1999, ApJ, 512, 843
- Burrows, A., & Volobuyev, M. 2003, ApJ, 583, 985
- Burwell, C.G. 1930, PASP, 42, 351
- Chen, H., Myers, P.C., Ladd, E.F., & Wood, D.O.S. 1995, ApJ, 445, 377
- Chiang, E.I., & Goldreich, P. 1999, ApJ, 519, 279
- Cruz, K.L., Kirkpatrick, J.D., Burgasser, A.J., Looper, D., Mohanty, S., Prato, L., Faherty, J., & Solomon, A. 2007, in the *14th Cambridge Workshop on Cool Stars, Stellar Systems, and the Sun*, in press

- Cushing, M.C., Rayner, J.T., & Vacca, W.D. 2005, *ApJ*, 623, 1115
- Cushing, M.C., et al. 2006, *ApJ*, 648, 614
- Dahn, C.C., Liebert, J., Kron, R.G., Spinrad, H., & Hintzen, P.M. 1977, *ApJ*, 216, 757
- Dahn, C.C., et al. 2002, *AJ*, 124, 1170
- Dearborn, D.S.P., Liebert, J., Aaronson, M., Dahn, C.C., Harrington, R., Mould, J., & Greenstein, J.L. 1986, *ApJ*, 300, 314
- Delfosse, X., Tinney, C.G., Forveille, T., Epchtein, N., Borsenberger, J., Fouqué, P., Kimeswenger, S., & Tiphène, D. 1999, *AApS*, 135, 41
- Delfosse, X., et al. 1997, *AA*, 327, L25
- Downes, R.A., et al. 2004, *AJ*, 127, 2838
- Dyck, H.M., Benson, J.A., van Belle, G.T., & Ridgway, S.T. 1996, *AJ*, 111, 1705
- Dyck, H.M., van Belle, G. T., & Thompson, R.R. 1998, *AJ*, 116, 981
- Eggen, O.J. 1950, *ApJ*, 112, 141
- Epchtein, N., et al. 1999, *AA*, 349, 236
- Fegley, B.J., & Lodders, K. 1996, *ApJL*, 472, L37
- Flint, A.S. 1895, *Publications of the Washburn Observatory*, 9, 208
- Fowler, A. 1904, *The Observatory*, 27, 197
- Gass, H., Wehrse, R., & Liebert, J. 1988, *AA*, 189, 194
- Gizis, J.E. 1997, *AJ*, 113, 806
- Gizis, J.E., Monet, D.G., Reid, I.N., Kirkpatrick, J.D., Liebert, J., & Williams, R.J. 2000, *AJ*, 120, 1085
- Golimowski, D.A., et al. 2004, *AJ*, 127, 3516
- Green, P.J. 2000, *The Carbon Star Phenomenon*, 177, 27
- Green, P.J., & Margon, B. 1994, *ApJ*, 423, 723
- Green, P.J., Margon, B., Anderson, S.F., & MacConnell, D.J. 1992, *ApJ*, 400, 659
- Greene, T.P., Wilking, B.A., Andre, P., Young, E.T., & Lada, C.J. 1994, *ApJ*, 434, 614
- Greenstein, J.L. 1965, *Galactic Structure*, 361
- Harris, H.C., et al. 1998, *ApJ*, 502, 437
- Hawley, S.L., et al. 2002, *AJ*, 123, 3409
- Hayashi, C., & Nakano, T. 1963, *Progress of Theoretical Physics*, 30, 460
- Heber, U., Bade, N., Jordan, S., & Voges, W. 1993, *AA*, 267, L31
- Hofmann, K.-H., Balega, Y., Scholz, M., & Weigelt, G. 2000, *AA*, 353, 1016
- Iwanowska, W., & Wayman, P.A. 1952, *ApJ*, 115, 129
- Jones, H.R.A., Longmore, A.J., Jameson, R.F., & Mountain, C.M. 1994, *MNRAS*, 267, 413
- Jones, H.R.A., & Tsuji, T. 1997, *ApJl*, 480, L39
- Joy, A.H. 1947, *ApJ*, 105, 96
- Joy, A.H., & Humason, M.L. 1949, *PASP*, 61, 133
- Joyce, R.R., Hinkle, K.H., Wallace, L., Dulick, M., & Lambert, D.L. 1998, *AJ*, 116, 2520
- Kapteyn, J.C. 1890, *Astronomische Nachrichten*, 123, 105
- Kimeswenger, S. 2006, *Astronomische Nachrichten*, 327, 44

- Kirkpatrick, J.D. 1992, Ph.D. Thesis, Univ. Arizona
- Kirkpatrick, J.D. 1995, *The Bottom of the Main Sequence—and Beyond*, Proceedings of the ESO Workshop held in Garching, Germany, 10–12 August 1994, ed. Christopher G. Tinney. Berlin Heidelberg New York: Springer-Verlag. Also ESO Astrophysics Symposia, 1995, p. 140
- Kirkpatrick, J.D. 2005, ARAA, 43, 195
- Kirkpatrick, J.D., Barman, T.S., Burgasser, A.J., McGovern, M.R., McLean, I.S., Tinney, C.G., & Lowrance, P.J. 2006, ApJ, 639, 1120
- Kirkpatrick, J.D., Beichman, C.A., & Skrutskie, M.F. 1997, ApJ, 476, 311
- Kirkpatrick, J.D., Henry, T.J., & Liebert, J. 1993, ApJ, 406, 701
- Kirkpatrick, J.D., Henry, T.J., & McCarthy, D.W., Jr. 1991, ApJS, 77, 417
- Kirkpatrick, J.D., Henry, T.J., & Simons, D.A. 1995, AJ, 109, 797
- Kirkpatrick, J.D., et al. 1999, ApJ, 519, 802
- Kirkpatrick, J.D., et al. 2000, AJ, 120, 447
- Kirkpatrick, J.D., et al. 2007, in prep.
- Kuiper, G.P. 1939, ApJ, 89, 548
- Kuiper, G.P. 1942, ApJ, 95, 201
- Kumar, S.S. 1963, ApJ, 137, 1121
- Lada, C.J. 1987, *Star Forming Regions*, 115, 1
- Lada, C.J., & Wilking, B.A. 1984, ApJ, 287, 610
- Lane, B.F., Boden, A.F., & Kulkarni, S.R. 2001, ApJL, 551, L81
- Lebzelter, T., & Hron, J. 2003, AA, 411, 533
- Leggett, S.K., Allard, F., Berriman, G., Dahn, C.C., & Hauschildt, P.H. 1996, ApJS, 104, 117
- Liebert, J., Kirkpatrick, J.D., Cruz, K.L., Reid, I.N., Burgasser, A., Tinney, C.G., & Gizis, J.E. 2003, AJ, 125, 343
- Liebert, J., Schmidt, G.D., Lesser, M., Stepanian, J.A., Lipovetsky, V.A., Chaffe, F.H., Foltz, C.B., & Bergeron, P. 1994, ApJ, 421, 733
- Liebert, J., Kirkpatrick, J.D., Reid, I.N., & Fisher, M.D. 1999, ApJ, 519, 345
- Linsky, J.L., Bornmann, P.L., Carpenter, K.G., Hege, E.K., Wing, R.F., Giampapa, M.S., & Worden, S.P. 1982, ApJ, 260, 670
- Lodders, K. 1999, ApJ, 519, 793
- Lodders, K. 2002, ApJ, 577, 974
- Lodders, K., & Fegley, B. 2002, *Icarus*, 155, 393
- López-Morales, M. 2007, ApJ, 660, 732
- Lowrance, P.J., Kirkpatrick, J.D., & Beichman, C.A. 2002, ApJL, 572, L79
- Lowrance, P.J., Kirkpatrick, J.D., Reid, I.N., Cruz, K.L., & Liebert, J. 2003, ApJL, 584, L95
- Luhman, K.L., Liebert, J., & Rieke, G.H. 1997, ApJL, 489, L165
- Lundmark, K., & Luyten, W.J. 1923, AJ, 35, 93
- Luyten, W.J. 1923a, PASP, 35, 175
- Luyten, W.J. 1923b, PASP, 35, 209
- Luyten, W.J. 1949, PASP, 61, 179
- Margon, B., et al. 2002, AJ, 124, 1651

- Martín, E.L., Basri, G., Zapatero-Osorio, M. R., Rebolo, R., & López, R. J. G. 1998, *ApJL*, 507, L41
- Martín, E.L., Rebolo, R., & Zapatero-Osorio, M. R. 1996, *ApJ*, 469, 706
- McLean, I.S., McGovern, M.R., Burgasser, A.J., Kirkpatrick, J.D., Prato, L., & Kim, S.S. 2003, *ApJ*, 596, 561
- McLean, I.S., Prato, L., Kim, S.S., Wilcox, M.K., Kirkpatrick, J.D., & Burgasser, A. 2001, *ApJL*, 561, L115
- Metcalfe, T. S., Mathieu, R.D., Latham, D.W., & Torres, G. 1996, *ApJ*, 456, 356
- Metchev, S.A., Kirkpatrick, J.D., Berriman, G.B., & Looper, D. 2007, *ApJ*, submitted
- Monet, D.G., Dahn, C.C., Vrba, F.J., Harris, H.C., Pier, J.R., Luginbuhl, C.B., & Ables, H.D. 1992, *AJ*, 103, 638
- Morgan, W.W. 1938, *ApJ*, 87, 589
- Morgan, W.W., Keenan, P.C., & Kellman, E. 1943, *An Atlas of Stellar Spectra*, Chicago: University of Chicago Press
- Myers, P.C., & Ladd, E.F. 1993, *ApJL*, 413, L47
- Nakajima, T., Tsuji, T., & Yanagisawa, K. 2004, *ApJ*, 607, 499
- Nelson, L.A., Rappaport, S., & Joss, P.C. 1993, *ApJ*, 404, 723
- Noll, K.S., Geballe, T.R., Leggett, S.K., & Marley, M.S. 2000, *ApJL*, 541, L75
- Öhman, Y. 1934, *ApJ*, 80, 171
- Öhman, Y. 1936a, *Stockholms Observatoriums Annaler*, 12, No. 3
- Öhman, Y. 1936b, *Stockholms Observatoriums Annaler*, 12, No. 8
- Osten, R.A., Hawley, S.L., Allred, J., Johns-Krull, C.M., Brown, A., & Harper, G.M. 2006, *ApJ*, 647, 1349
- Pettersen, B.R., & Hawley, S.L. 1989, *AA*, 217, 187
- Pickering, E.C. 1890, *Annals of Harvard College Observatory*, 27, 1
- Plez, B., & Cohen, J.G. 2005, *AA*, 434, 1117
- Pozio, F. 1991, *Memorie della Societa Astronomica Italiana*, 62, 171
- Rayner, J.T., Vacca, W.D., & Cushing, M.C., 2007, in prep.
- Rebolo, R., Martín, E.L., & Magazzu, A. 1992, *ApJL*, 389, L83
- Rebolo, R., Zapatero Osorio, M.R., Madrugá, S., Bejar, V.J.S., Arribas, S., & Licandro, J. 1998, *Science*, 282, 1309
- Reid, I.N., & Gizis, J.E. 1997, *AJ*, 113, 2246
- Reid, N., & Hawley, S.L. 2000, *New Light on Dark Stars: Red Dwarfs, Low Mass Stars, Brown Dwarfs*, New York: Springer (Springer-Praxis series in astronomy and astrophysics)
- Reid, I.N., Kirkpatrick, J.D., Gizis, J.E., Dahn, C.C., Monet, D.G., Williams, R.J., Liebert, J., & Burgasser, A.J. 2000, *AJ*, 119, 369
- Reid, I.N., et al. 1999, *ApJ*, 521, 613
- Reid, I.N., et al. 2003, *AJ*, 125, 354
- Reid, I.N., et al. 2004, *AJ*, 128, 463
- Retter, A., Zhang, B., Siess, L., & Levinson, A. 2006, *MNRAS*, 370, 1573
- Ribas, I. 2003, *AA*, 398, 239
- Roellig, T.L., et al. 2004, *ApJS*, 154, 418

- Ruiz, M.T., Leggett, S.K., & Allard, F. 1997, *ApJL*, 491, L107
- Russell, H.N. 1905, *MNRAS*, 65, 787
- Secchi, A. 1866, *CR Acad. Sci. Paris*, 63, 621
- Secchi, A. 1868, *MNRAS*, 28, 196
- Ségransan, D., Kervella, P., Forveille, T., & Queloz, D. 2003, *AA*, 397, L5
- Skrutskie, M.F., et al. 2006, *AJ*, 131, 1163
- Soker, N., & Tylenda, R. 2007, *Astronomical Society of the Pacific Conference Series*, 363, 280
- Steele, I.A., & Jameson, R.F. 1995, *MNRAS*, 272, 630
- Tinney, C.G. 1996, *MNRAS*, 281, 644
- Tinney, C.G., Reid, I.N., Gizis, J., & Mould, J.R. 1995, *AJ*, 110, 3014
- Torres, G., & Ribas, I. 2002, *ApJ*, 567, 1140
- Tsuji, T., Ohnaka, K., & Aoki, W. 1996, *AA*, 305, L1
- Tsuji, T., Ohnaka, K., Aoki, W., & Nakajima, T. 1996, *AA*, 308, L29
- van Altena, W.F., Lee, J.T., & Hoffleit, E.D. 1995, *The General Catalogue of Trigonometric Stellar Parallaxes*, 4th ed., New Haven: Yale University Observatory
- van Belle, G.T., Thompson, R.R., & Creech-Eakman, M.J. 2002, *AJ*, 124, 1706
- van Belle, G.T., et al. 1999, *AJ*, 117, 521
- van Maanen, A. 1940, *ApJ*, 91, 503
- van Maanen, A. 1945, *PASP*, 57, 216
- Vrba, F.J., et al. 2004, *AJ*, 127, 2948
- Wallerstein, G., & Knapp, G.R. 1998, *ARAA*, 36, 369
- Ward-Thompson, D. 1993, *MNRAS*, 265, 493
- West, A.A., et al. 2004, *AJ*, 128, 426
- White, R.J., Greene, T.P., Doppmann, G.W., Covey, K.R., & Hillenbrand, L.A. 2007, *Protostars and Planets*, V, 117
- Whitney, B.A., Wood, K., Bjorkman, J.E., & Cohen, M. 2003, *ApJ*, 598, 1079
- Winnecke, A. 1858, *Astronomische Nachrichten*, 48, 289
- Wittkowski, M., Aufdenberg, J.P., Driebe, T., Roccatagliata, V., Szeifert, T., & Wolff, B. 2006b, *AA*, 460, 855
- Wittkowski, M., Aufdenberg, J.P., & Kervella, P. 2004, *AA*, 413, 711
- Wittkowski, M., Hummel, C.A., Aufdenberg, J.P., & Roccatagliata, V. 2006a, *AA*, 460, 843
- Zuckerman, B., & Becklin, E.E. 1992, *ApJ*, 386, 260

Chapter Ten

The T-type Dwarfs—Adam J. Burgasser

10.1 INTRODUCTION

The T-dwarf class is the latest-type spectral class currently studied, encompassing the lowest luminosity and lowest effective temperature (T_{eff}) brown dwarfs identified to date. These sources are distinguished from L dwarfs (and indeed all other stellar classes) by the presence of CH_4 absorption in their near-infrared spectra,¹ in addition to strong H_2O and NH_3 bands, prominent neutral metal-line features, collision-induced H_2 absorption, and spectral energy distributions that are increasingly peaked at near-infrared and mid-infrared wavelengths. The strong, overlapping molecular bands present in T dwarf spectra result in complex (non-blackbody) spectral morphologies, and lead to stronger dependencies on secondary parameters such as surface gravity or metallicity. The spectra of T dwarfs are thought to be similar in appearance to those of short-period extrasolar giant planets, the so-called “Hot Jupiters” (e.g., Mayor & Queloz 1995), making them important empirical templates for exoplanet atmosphere models and direct detection studies (e.g., Baraffe et al. 2003).

This chapter will discuss the spectral characteristics of the T-dwarf class and current methods for classification in the near-infrared ($1\text{--}2.5\ \mu\text{m}$), red-optical ($0.6\text{--}1.0\ \mu\text{m}$), and mid-infrared ($5\text{--}15\ \mu\text{m}$) wavebands, based largely on low-resolution data. §10.2 provides a brief history of the early reconnaissance of T dwarfs. §10.3 reviews their general spectral properties from optical to mid-infrared wavelengths. §10.4 describes the primary means of T-dwarf classification using low-resolution near-infrared spectral data, including a discussion on the development leading up to the current scheme and a comparison of spectral subtypes to measured physical parameters (including luminosity and T_{eff}). §10.5 examines T-dwarf classification based on red-optical spectra, which provides a direct tie with the current L-dwarf classification scheme (Chapter 9). §10.6 examines T-dwarf classification based on mid-infrared spectra. §10.7 touches upon additional considerations for classification, including the influence of multiplicity, surface gravity, and metallicity effects, and limits on temporal variations in spectral types. This is followed by a brief discussion in §10.8 on what may define the end of the T spectral class.

¹Readers should be aware that the terms “optical,” “near-infrared,” “infrared,” etc. are used in somewhat different ways in this chapter and the previous than in the rest of the book. See the Important Note on Terminology and Units at the beginning of the book for more details.

10.2 RECOGNITION OF THE T DWARF CLASS AND EARLY DISCOVERIES

The first T dwarf to be identified was Gliese 229B (Nakajima et al. 1995; Oppenheimer et al. 1995), a low luminosity companion to the nearby M1 star Gliese 229 (an M dwarf spectral standard; Kirkpatrick, Henry, & McCarthy 1991; see Chapter 9) and one of the first brown dwarfs to be discovered. The rapid acceptance of this source as a bona-fide brown dwarf was due primarily to the detection of CH₄ absorption in its near-infrared spectrum (Oppenheimer et al. 1995; Geballe et al. 1996), a species seen only in solar planetary spectra at that time (although predicted to be present in cool brown dwarf spectra by Tsuji 1964). The presence of this feature, in addition to bolometric luminosity measurements, indicated an effective temperature of ≈ 1000 K for this source (Oppenheimer et al. 1995; Fegley & Lodders 1996; Marley et al. 1996; Matthews et al. 1996), far cooler than predicted for a hydrogen-burning star (Burrows et al. 1997; Chabrier & Baraffe 1997). Early-on, it was speculated that Gliese 229B might prove to be the first extrasolar planet to be directly detected. While this idea has now been largely discounted (i.e. it is more likely to be a brown dwarf than a planet), methane-bearing brown dwarfs such as Gliese 229B provide a conceptual bridge between stellar and planetary spectra.

Like the prototype L dwarf GD 165B—another low-luminosity companion source (Becklin & Zuckerman 1988; Kirkpatrick et al. 1993)—it was recognized early on that Gliese 229B did not match the spectral morphological types of the coolest dwarfs known at that time. This is illustrated in Figure 10.1, reproduced from Kirkpatrick et al. (1999), which compares the K-band spectra ($1.7\text{--}2.5\ \mu\text{m}$) of two late-type L dwarfs and Gliese 229B. The CH₄ band at $2.2\ \mu\text{m}$ clearly distinguishes the latter source. At both optical and near-infrared wavelengths, the unique spectral morphology of Gliese 229B distinguishes it from the L dwarfs, warranting its own spectral designation. Kirkpatrick et al. (1999), in their definition of the L dwarf spectral class, suggested the letter “T” for Gliese 229B and its (future) counterparts.²

The first analogs to Gliese 229B were identified as nearby solivagant³ field sources in 1999 by researchers using the Sloan Digital Sky Survey (hereafter SDSS; York et al. 2000) and the Two Micron All Sky Survey (hereafter 2MASS; Skrutskie et al. 1997, 2006). Both of these wide-field imaging surveys employed near-infrared filters ($z'JHK_s$) measuring to the peak spectral energy distributions of low-temperature brown dwarfs, were substantially more sensitive than previous work (e.g., the Two Micron Sky Survey, Neugebauer & Leighton 1969), and imaged a wide region of sky. All of these characteristics are essential to the identification of T dwarfs, given their extremely low luminosities and faint magnitudes at all wavelengths, particularly the optical bands.

²Other studies suggested the use of “L_{CH₄” or “H” to distinguish CH₄-bearing brown dwarfs (e.g., Martín et al. 1999). However, the “T” designation became widespread as the first field counterparts to Gliese 229B were identified (Strauss et al. 1999; Burgasser et al. 1999; Tsvetanov et al. 2000).}

³From the Latin *solus* alone + *vagans* wandering.

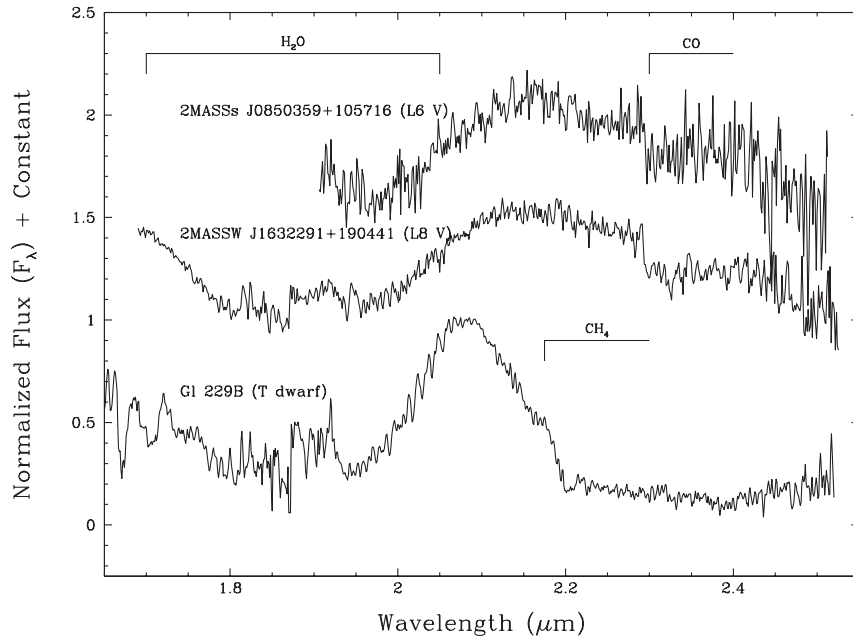


Figure 10.1 K-band spectra of the L dwarfs 2MASS J08503593 + 1057156 (L6) and 2MASS J16322911 + 1904407 (L8) compared to the prototype T dwarf Gliese 229B. The strong absorption feature at $2.2\ \mu\text{m}$ in the spectrum of Gliese 229B, one of several CH_4 bands found in the near-infrared, distinguishes this source from the L dwarfs, which do not exhibit CH_4 absorption. The distinct spectral character of Gliese 229B led Kirkpatrick et al. (1999) to propose a new T-dwarf class to encompass it and its forthcoming counterparts (reproduced from Kirkpatrick et al. 1999 by permission of the AAS).

Early searches for T dwarfs using these wide-field surveys were primarily magnitude-limited and color-selected, using Gliese 229B and the latest-type L dwarfs known at that time as templates. The first success came from the SDSS, with the discovery of SDSS J162414.37+002915.6 (Strauss et al. 1999), a source that would ultimately become the T6 spectral standard (see §10.4.3).⁴ This was followed promptly by the discovery of four T dwarfs in the 2MASS database (Burgasser et al. 1999), a faint and distant T dwarf in the NTT Deep Field (Cuby et al. 1999), and a second T dwarf by SDSS (Tsvetanov et al. 2000). New detections followed quickly thereafter, primarily based on 2MASS and SDSS searches, but also in deep field surveys (e.g., Liu et al. 2002), companion searches (e.g., Scholz et al. 2003; Luhman et al. 2006), searches toward distant star-forming regions (e.g., Zapatero Osorio et al. 2002), and near-infrared proper motion surveys (e.g., Artigau et al. 2006). As of May 2007, there are over 100 T dwarfs known. An up-to-date list is maintained by Chris Gelino and collaborators on the DwarfArchives website (<http://dwarfarchives.org>).

⁴It is interesting to note that the period between the first reported spectrum of a companion prototype and the subsequent discovery of a field counterpart was roughly same (~ 4 years) for both the L and T spectral classes.

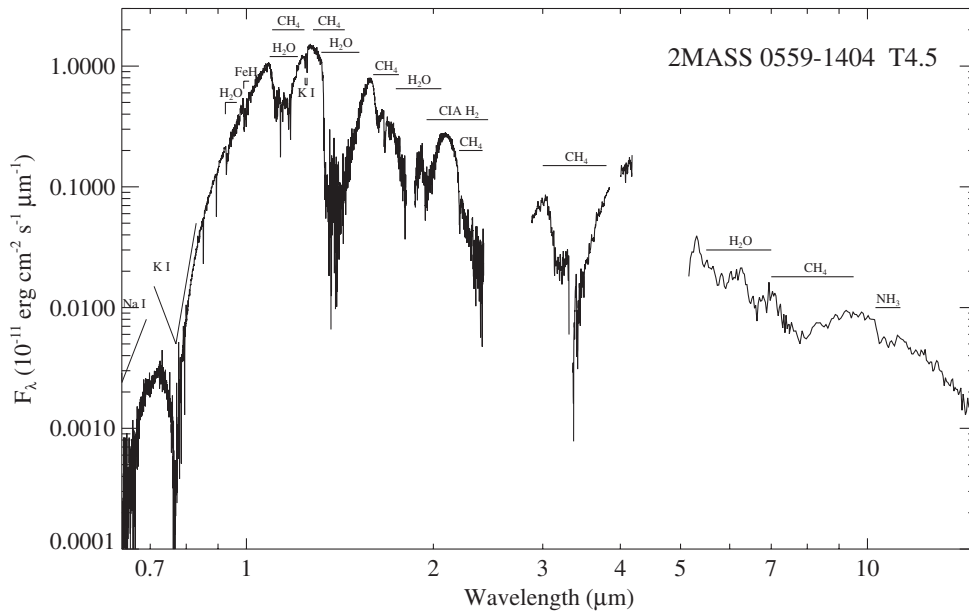


Figure 10.2 Observed spectrum of the T4.5 2MASS J05591914 – 1404488 spanning wavelengths 0.63–15 μm . Data are from Burgasser et al. (2003b); Cushing, Rayner, & Vacca (2005); and Cushing et al. (2006), and are scaled to the absolute flux density of this source at 10 pc. Prominent atomic and molecular features are labeled.

10.3 T DWARF SPECTRAL CHARACTERISTICS

Figures 10.2 through 10.4 display the spectrum of a typical mid-type T dwarf spanning 0.6–15 μm , in this case the bright T4.5 2MASS J05591914 – 1404488 (Burgasser et al. 2000c, 2003b; Cushing, Rayner, & Vacca 2005; Cushing et al. 2006). Molecular and atomic features identified over this wavelength range are listed in Tables 10.1 and 10.2, respectively. The primary distinguishing spectral traits of T dwarfs are the near-infrared CH_4 absorption bands centered at 1.15, 1.35, 1.65, 2.2, and 3.3 μm . The last, and strongest, ν_3 overtone band is also present in the spectra of late-type L dwarfs (Noll, Geballe, & Marley 1997). There are also strong H_2O bands at 1.15, 1.4, and 1.8 μm , which are present (but weaker) in the near-infrared spectra of M and L dwarfs. The earliest-type T dwarfs exhibit CO absorption at 2.3 μm (Leggett et al. 2000), although this feature weakens and is absent in the mid- and late-type T dwarfs, as predicted by chemical equilibrium models (Fegley & Lodders 1996; Burrows & Sharp 1999). CO absorption at 4.7 μm has also been identified in the spectra of Gliese 229B (Noll, Geballe, & Marley 1997; Oppenheimer et al. 1998) and 2MASS J05591914 – 1404488 (Burgasser 2001), and is notably stronger than expected from chemical equilibrium models.

An additional molecular opacity source present in the near-infrared spectra of T dwarfs is collision-induced H_2 absorption (CIA H_2 ;

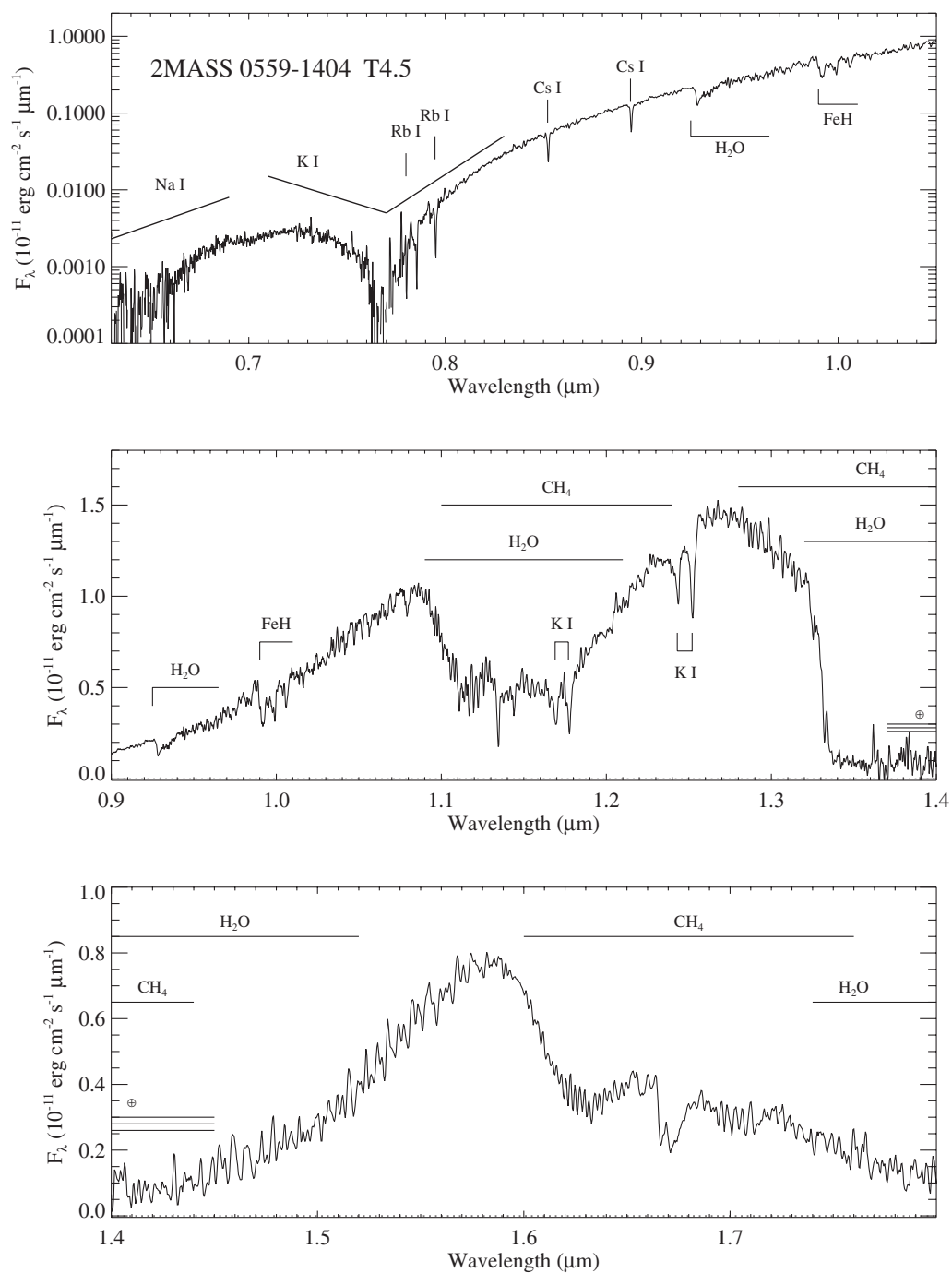


Figure 10.3 Close-up views of Figure 10.2 in the red-optical (0.63–1.05 μ m, top), J-band (0.9–1.4 μ m, middle), and H-band (1.4–1.8 μ m, bottom) regions. Prominent atomic and molecular features are labeled, as are regions of strong telluric absorption (circle-plus symbols).

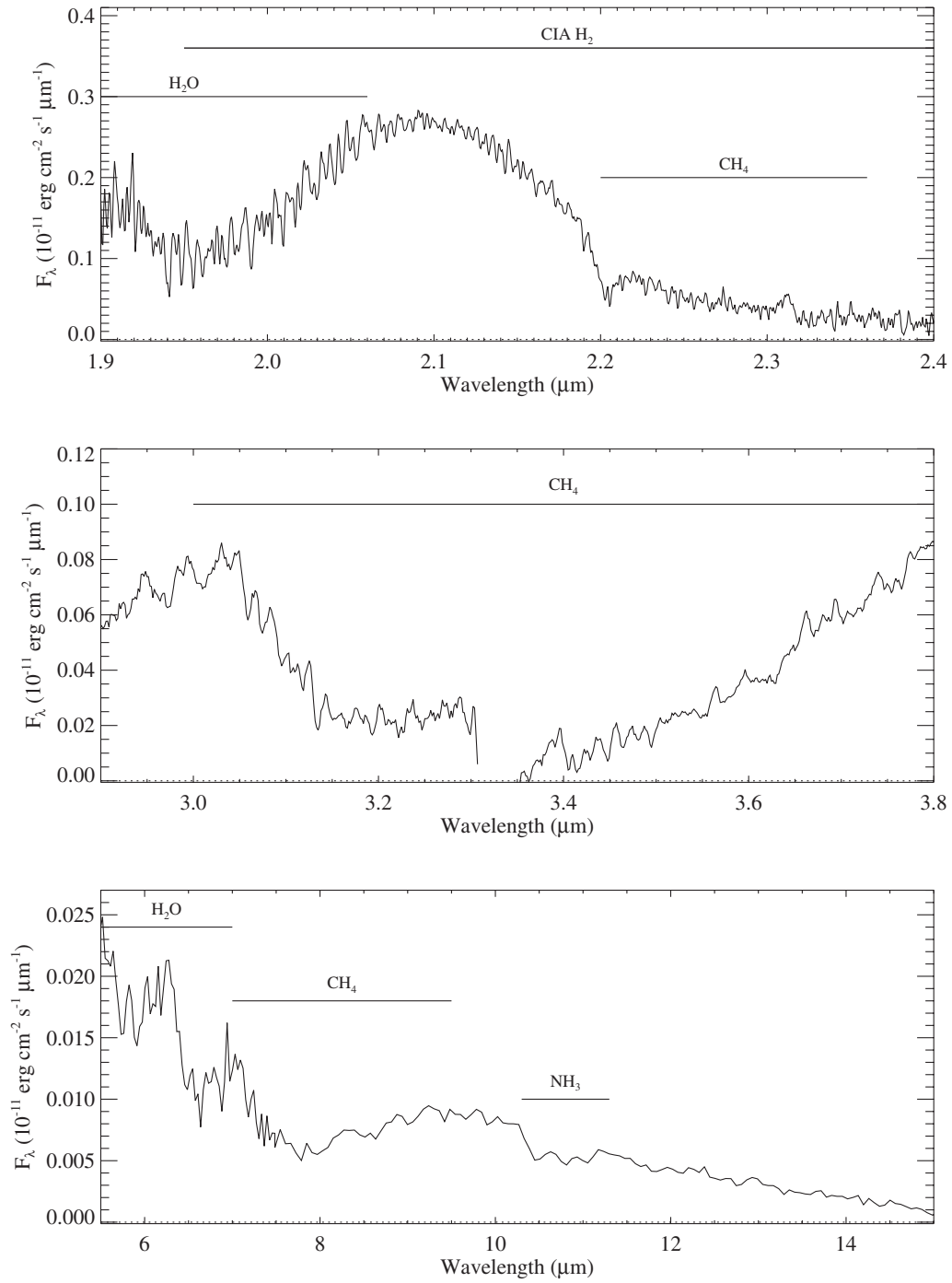


Figure 10.4 Same as Figure 10.3 for the K-band (1.9–2.4 μm , top), L-band (2.9–3.8 μm , middle), and mid-infrared (5.5–15 μm ; bottom) regions.

Table 10.1 Molecular Features Identified in T-Dwarf Spectra

Species	λ (μm)	Transition
CaH ^a	0.675 bandhead	0–0 band of $A^2\Pi-X^2\Sigma$
CrH	0.8611 bandhead	0–0 band of $A^6\Sigma^+-X^6\Sigma^+$
FeH	0.8692 bandhead	1–0 band of $A^4\Delta-X^4\Delta$
CH ₄ ^b	0.88–0.92	$4(\nu_1, \nu_3)$
H ₂ O	0.925–0.98	$3(\nu_1, \nu_3), \nu_1+2\nu_2+\nu_3, 2\nu_1+2\nu_2$
FeH	0.99 bandhead	0–0 band of $F^4\Delta-X^4\Delta$
H ₂ O	1.09–1.20	$\nu_2+2(\nu_1, \nu_3), 3\nu_2+\nu_3, \nu_1+2\nu_2$
CH ₄	1.10–1.24	$3\nu_3$
H ₂ O	1.30–1.51	$2\nu_3, \nu_1+\nu_2, 2\nu_1, 2\nu_2+\nu_3, \nu_1+2\nu_2$
CH ₄	1.6–1.8	$2\nu_3, 2\nu_2+\nu_3$
H ₂ O	1.75–2.05	$\nu_2+\nu_3, \nu_1+\nu_2, 3\nu_2$
CH ₄	2.15–2.6	$\nu_3+\nu_4, \nu_2+\nu_3$
H ₂ O	2.3–3.2	$\nu_1, \nu_3, 2\nu_2$
CO	2.29–2.42 bandheads	bands of $X^1\Sigma^+-X^1\Sigma^+$
H ₂	1.8–2.8	1–0 quadrupole (CIA)
OH	3.4–4.2 bandheads	$\Delta\nu = +1, +2$ bands
CH ₄	3.0–3.8	ν_3
CO	4.6–5.0	1–0 bands of $X^1\Sigma^+-X^1\Sigma^+$
H ₂ O	5.5–7.0	ν_2
H ₂ O	6.5–7.0	$2\nu_2$
CH ₄	7.0–9.5	ν_4
NH ₃	10.3–11.2	ν_2

^aHas also been associated with a satellite feature of the K–H₂ interaction (pressure broadening); see Allard, Spiegelman, & Kielkopf (2007).

^bDetection of this feature is ambiguous and may arise from the broadened wings of the 0.8943 μm Cs I line or weak H₂O absorption; see Oppenheimer et al. (1998) and Burgasser et al. (2003b).

Table 10.2 Atomic Features Identified in T-Dwarf Spectra

Species	λ (μm)	Transition
Na I	0.5890 ^a	$3s\ ^2S_{1/2} - 3p\ ^2P_{3/2}$
Na I	0.5896 ^a	$3s\ ^2S_{1/2} - 3p\ ^2P_{1/2}$
H α ^b	0.6563	$3d\ ^2D_{5/2} - 2p\ ^2P_{3/2}$
K I	0.7665 ^a	$4s\ ^2S_{1/2} - 4p\ ^2P_{3/2}$
K I	0.7699 ^a	$4s\ ^2S_{1/2} - 4p\ ^2P_{1/2}$
Rb I	0.7800	$5s\ ^2S_{1/2} - 5p\ ^2P_{3/2,1/2}$
Rb I	0.7948	$5s\ ^2S_{1/2} - 5p\ ^2P_{3/2,1/2}$
Cs I	0.8521	$6s\ ^2S_{1/2} - 6p\ ^2P_{3/2}$
Cs I	0.8943	$6s\ ^2S_{1/2} - 6p\ ^2P_{1/2}$
K I	1.169	$4p\ ^2P_0 - 3d\ ^2D$
K I	1.178	$4p\ ^2P_0 - 3d\ ^2D$
K I	1.244	$4p\ ^2P_0 - 5s\ ^2S$
K I	1.252	$4p\ ^2P_0 - 5s\ ^2S$

^aPressure-broadened over $>1000\ \text{\AA}$.

^bObserved in emission in four magnetically active T dwarfs (Burgasser et al. 2000a, 2002a, 2003b; Cruz et al. 2003).

Saumon et al. 1994; Borysow, Jørgensen, & Zheng 1997), arising from an induced quadrupolar moment of the symmetric H_2 molecule from gas collisions at the photosphere. CIA H_2 produces a broad but featureless “band” centered near $2.3\ \mu\text{m}$, along with weaker absorptions at 0.8 and $1.3\ \mu\text{m}$. The $2.3\ \mu\text{m}$ band is largely responsible for the blue near-infrared colors of mid- and late-type T dwarfs, in addition to the strong H_2O and CH_4 features. CIA H_2 absorption is also pressure-sensitive, and as such serves as a useful surface gravity diagnostic (Burgasser et al. 2002c; Burgasser et al. 2006a; Knapp et al. 2004, see §10.7).

Atomic line absorption at near-infrared wavelengths is largely limited to K I lines present in the $1.1\text{--}1.25\ \mu\text{m}$ region, although these disappear in the spectra of the latest-type T dwarfs. High-resolution spectroscopy indicate that these lines are considerably pressure-broadened (Zapatero Osorio et al. 2006; McLean et al. 2007), although not as strongly as their counterparts at optical wavelengths.

The red-optical spectra of T dwarfs (Figure 10.3) are dominated by the pressure-broadened wings of the $4s\ ^2\text{S}_{1/2} \rightarrow 4p\ ^2\text{P}_{1/2,3/2}$ K I resonance doublet, centered at $0.7665/0.7699\ \mu\text{m}$. This feature and its stronger $0.5890/0.5896\ \mu\text{m}$ Na I doublet counterpart (the solar D-lines) continue to deepen and broaden from the end of the L-dwarf sequence (Kirkpatrick et al. 1999; Reid et al. 2000), ultimately dominating the whole of the optical opacity (Tsuji, Ohnaka, & Aoki 1999; Burrows, Marley, & Sharp 2000; Allard et al. 2003; Burrows & Volobuyev 2003). A slight peak-up in flux between the Na I and K I doublets is commonly referred to as the “blue bump” (Liebert et al. 2000). Superimposed on the red wing of K I are other alkali lines arising from Rb I (0.7800 and $0.7948\ \mu\text{m}$) and Cs I (0.8521 and $0.8943\ \mu\text{m}$). The $0.6708\ \mu\text{m}$ Li I line, a powerful discriminant of substellarity for M and L dwarfs (Rebolo, Martín, & Magazzu 1992; Magazzu, Martín, & Rebolo 1993), is neither expected nor commonly observed in the spectra of T dwarfs, as this species is predicted to be depleted by LiCl and LiOH formation at temperatures typical of T-dwarf photospheres (Lodders 1999). Indeed, Li I has been detected only in the T0 SDSSp J042348.57 – 041403.5 (Geballe et al. 2002; Cruz et al. 2003), and likely arises from the L6.5 primary of this brown dwarf binary (Burgasser et al. 2005).

Molecular H_2O absorption over $0.925\text{--}0.98\ \mu\text{m}$ is present in all of the T dwarf spectra, while the $0.99\ \mu\text{m}$ Wing–Ford band of FeH, prominent in mid-type L dwarf spectra, is weakly present in the spectra of mid-type T dwarfs but not, surprisingly, in early- and late-type T dwarf spectra. There is some evidence for weak CH_4 absorption at $0.89\ \mu\text{m}$ (Oppenheimer et al. 1998; Burgasser et al. 2003b), a common feature in planetary spectra (Dick & Fink 1977), although coincidence with the $0.8943\ \text{\AA}$ Cs I line and possible H_2O absorption in this region makes this identification uncertain (Cushing, Rayner, & Vacca 2005). There is also evidence of a weak feature at $0.675\ \mu\text{m}$ that has been attributed to CaH absorption (Burgasser et al. 2003b), and a satellite feature from K– H_2 interaction (pressure-broadening; Allard, Spiegelman, & Kielkopf 2007). $\text{H}\alpha$ emission, resulting from magnetic activity, is rare in T-dwarf spectra, and is seen weakly in only a few cases. One such case is the T6.5 2MASS J12373919 + 6526148, which exhibits strong

and steady emission possibly arising from an interaction with a faint, unseen companion (Burgasser et al. 1999, 2000a, 2002a; Liebert & Burgasser 2007).

At mid-infrared wavelengths, characterization of T dwarfs has been made possible by the Infrared Spectrograph (IRS, Houck et al. 2004) on board the *Spitzer Space Telescope* (Werner et al. 2004). Molecular opacity from H_2O (5.5–7.0 μm), and CH_4 (7.0–9.5 μm) dominates this region, while the ν_2 band of NH_3 is present at 10.5 μm (Roellig et al. 2004; Cushing et al. 2006). The latter band adds another species to the menu of low-temperature dwarf molecular diagnostics, and it appears that this feature is particularly sensitive to non-equilibrium atmospheric mixing in cool brown dwarf atmospheres (Saumon et al. 2006; Leggett et al. 2007a; Mainzer et al. 2007). Expectations are that longer-wavelength spectra are largely featureless (with the possible exception of LiCl at 15 μm ; Weck et al. 2004), although suitable spectral data at such wavelengths have yet to be obtained.

10.4 NEAR-INFRARED CLASSIFICATION

While classification schemes for M and L dwarfs are based largely on features and overall spectral shape in the red-optical spectral region (nominally 0.6–1.0 μm), the optical spectra of T dwarfs are exceedingly faint (Figure 10.3), and there are far fewer features available for classification. T dwarfs are also considerably brighter in the near-infrared, and the prominent molecular bands present at these wavelengths make for ideal classification diagnostics. Hence, both initial and more currently used spectral classification schemes have been based on near-infrared data.

10.4.1 Early Near-Infrared Classification Schemes and the Development of the Unified Scheme

The first attempts to tease out a spectral sequence for T dwarfs followed on the heels of the first discoveries of field counterparts to Gliese 229B. It was recognized early on that the primary molecular absorbers— H_2O , CH_4 , and CIA H_2 —would be essential in defining a sequence. Burgasser et al. (1999) proposed a preliminary scheme based on the relative flux between the H- and K-bands for four 2MASS T dwarf discoveries and Gliese 229B, arguing that CIA H_2 strengthens in lower temperature atmospheres, resulting in weaker K-band flux (Saumon et al. 1994; Borysow, Jørgensen, & Zheng 1997). The subsequent identification of T dwarfs with H_2O and CH_4 bands that were significantly weaker than those of Gliese 229B (Burgasser et al. 2000c; Leggett et al. 2000) made it clear that these features exhibited greater variation than H_2 and were therefore more useful in segregating T dwarf near-infrared spectra.⁵ First attempts at defining more robust spectral classification schemes for T dwarfs were made in 2002, independently by Burgasser et al. (2002c) and Geballe et al. (2002), using low-resolution near-infrared data. By that time, over two dozen T dwarfs were known, many reported for the first time in these two studies.

⁵Variation in H_2 absorption turns out to be a useful diagnostic of secondary parameters (§10.7).



Figure 10.5 The author in 2001, setting up one of the first near-infrared T-dwarf classification schemes.

One of the first steps in defining a spectral sequence is to determine the number of unique subtypes, or “boxes,” a class can be adequately defined by. For the scheme of Burgasser et al. (2002c), this was done by visual inspection, literally spreading paper printouts of spectra for a sample of 24 T dwarfs onto the floor (Figure 10.5) and selecting a sequence of seven subgroups that appeared to “evenly represent the spectral variation seen.” These subgroups were assigned integer subtypes T1 through T8, with later types corresponding to stronger H_2O and CH_4 bands. Subtypes T0 and T4 were left as apparent “gaps” in this sequence. Representative standards for each subtype were then selected (Figure 10.6). The remaining T dwarf spectra in the Burgasser et al. sample were then classified using eight spectral indices sampling the H_2O and CH_4 bands, spectral peak flux ratios, and the shape of the K-band flux peak, with the types assigned by comparing these indices to the standards.

There were two critical limitations to the Burgasser et al. study. First, only three sources out of the sample of 24 were assigned types earlier than T5, the three early-type T dwarfs identified by Leggett et al. (2000) assigned to be the T1, T2, and T3 standards. Hence, half of the T dwarf sequence was poorly represented. The second limitation was the use of spectral data from a variety of instrumentation, with resolutions ranging over $100 \lesssim \lambda/\Delta\lambda \lesssim 1200$. The sample was therefore inhomogeneous.

Geballe et al. (2002) proposed a qualitatively similar sequence, again based on the depth of H_2O and CH_4 bands. This study examined a homogenous spectral sample of 17 T dwarfs, all observed using the Cooled Grating Spectrometer 4

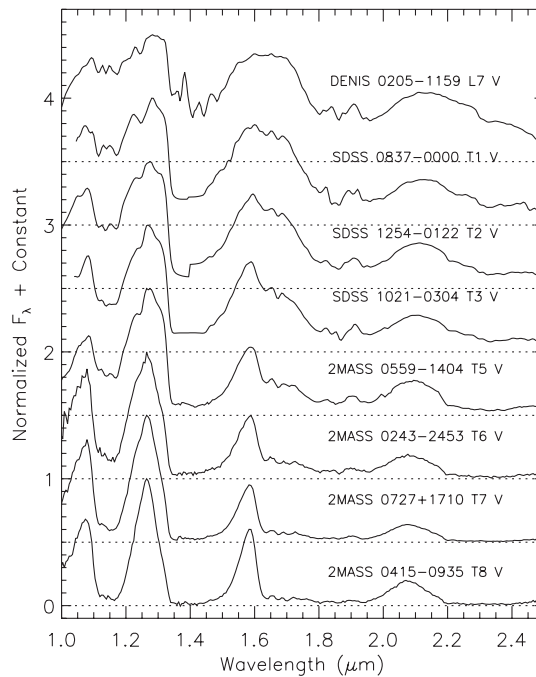


Figure 10.6 An early sequence of T-dwarf spectral standards from Burgasser et al. (2002c), based on low resolution ($\lambda/\Delta\lambda \approx 100$) near-infrared data. Spectra are normalized at $1.27 \mu\text{m}$ and offset by constants (dotted lines). Reproduced by permission of the AAS.

(CGS4; Wright et al. 1993) mounted on the United Kingdom Telescope (UKIRT). These data had a typical resolution of $\lambda/\Delta\lambda \approx 400$. By examining the breadth of spectral morphologies in this sample, Geballe et al. constructed a sequence spanning subtypes T0 to T8—the same basic range used by Burgasser et al. However, no explicit standards were chosen to represent these subtypes. Classifications were instead determined from four spectral indices sampling H_2O and CH_4 bands, and predetermined ranges for these indices based on measured values in the sample (see Table 5 in Geballe et al.). The sources in this sample provided a far better representation of earlier subtypes, with over half of the sources being classified earlier than T5. Most notably, Geballe et al. defined the start of the T dwarf class by the appearance of CH_4 absorption at both 1.6 and $2.2 \mu\text{m}$, denoting those sources with only the latter band as L9 dwarfs. This was the first clear delineation between the L and T spectral classes.

Neither the Burgasser et al. nor Geballe et al. schemes adequately adhered to the MK Process. The inhomogeneous spectral sample of the former, the lack of spectral standards of the latter, and the small samples in both studies were all limiting factors. In addition, the existence of two separate classification schemes for T dwarfs led to redundancies and confusion in the literature (e.g., Scholz et al. 2003). Yet, despite their subtle differences, classifications of sources common to both studies differed by no more than 0.5 subtypes. Hence, the authors of these



Figure 10.7 Members of the T-dwarf classification collaboration in 2002, working to combine the Burgasser et al. and Geballe et al. near-infrared schemes. Clockwise from bottom left: Sandy Leggett, Adam Burgasser, Tom Geballe, and David Golimowski. Not present in the photo is J. Davy Kirkpatrick.

studies initiated a collaboration (Figure 10.7) to identify ways of unifying the two classification schemes. Their objectives included the selection of improved spectral standards (e.g., eliminating peculiar or faint sources), definition of refined spectral indices, examination of homogeneous data sets, and a comparative study of the different classification methods already proposed. The resulting scheme (Burgasser et al. 2006a) is now considered to be the primary method of T-dwarf classification, and is discussed in detail below.

10.4.2 Characteristics of Near-Infrared Classification Data

The classification of T dwarfs is based primarily on low resolution data ($\lambda/\Delta\lambda \approx 100\text{--}400$) spanning the $1\text{--}2.5\ \mu\text{m}$ near-infrared window most readily accessible from the ground. The use of such data in the studies of Burgasser et al. and Geballe et al. was motivated largely by the intrinsic faintness of T dwarfs and sufficiency in resolving the broad H_2O and CH_4 bands that were central to both schemes.

10.4.3 Spectral Standards

10.4.3.1 Primary Standards

T dwarf near-infrared classification is defined by nine primary spectral standards spanning subtypes T0–T8. These sources were chosen to conform to the following criteria:

1. reasonably bright, to facilitate observation at a variety of telescopes;
2. not known to be spectroscopically peculiar;

3. not known to be significantly variable from photometric or spectroscopic observations;
4. not known to be a resolved multiple system, to the limit of high-angular resolution imaging (Burgasser et al. 2003d, 2006b; McCaughrean et al. 2004; Liu et al. 2006), and
5. within $\sim 25^\circ$ of the ecliptic, to facilitate observation from both Northern and Southern hemispheres.

Several of the T dwarf standards are identical to those from the Burgasser et al. (2002c) scheme, with additions to cover the subtype gaps in that study and to replace identified binaries. Coordinates and photometric measurements are given in Table 10.3; detailed descriptions are as follows:

SDSS J120747.17+024424.8 (T0): Identified in SDSS by Hawley et al. (2002) and classified T0 by Knapp et al. (2004) on the Geballe et al. scheme, this source is favored over the brighter T0 SDSS J042348.57 – 041403.5 (Geballe et al. 2002) which is a known binary (Burgasser et al. 2005). No high-angular resolution imaging or parallax observations have been reported for this source.

SDSS J083717.21–000018.0 (T1): One of the first “L/T transition objects” discovered by Leggett et al. (2000), this source was the T1 spectral standard on the Burgasser et al. scheme and classified T0.5 by Geballe et al. (2002). It is unresolved in *Hubble Space Telescope* (HST) observations (Burgasser et al. 2006b) and has a poorly constrained parallactic distance of 29 ± 12 pc (Vrba et al. 2004).

SDSS J125453.90–012247.4 (T2): Also identified by Leggett et al. (2000), this relatively bright source ($J = 14.66 \pm 0.03$) was the T2 standard in the Burgasser et al. scheme and classified likewise on the Geballe et al. scheme. It is unresolved in HST images. Three parallax distance measurements have been made for SDSS J125453.90 – 012247.4, one in the optical (11.8 ± 0.3 pc, Dahn et al. 2002) and two in the near-infrared (13.7 ± 0.4 , Tinney, Burgasser, & Kirkpatrick 2003; and 13.2 ± 0.5 pc, Vrba et al. 2004); note the disagreement. Artigau, Nadeau, & Doyon (2003) have reported statistically significant variability in the J-band flux of SDSS J125453.90 – 012247.4, albeit at a very low level (< 0.05 mag).

2MASS J12095613–1004008 (T3): Identified in 2MASS by Burgasser et al. (2004b), this source replaces the binary SDSS J102109.69 – 030420.1AB (Leggett et al. 2000; Burgasser et al. 2006b) as the T3 standard on the Burgasser et al. system. No high-angular resolution imaging or parallax measurements of this source have yet been reported.

2MASS J22541892+3123498 (T4): While outside of the declination constraint listed above, the spectrum of this relatively bright T dwarf ($J = 15.01 \pm 0.03$) fits ideally between those of the T3 and T5 standards. Identified by Burgasser et al. (2002c) and originally classified T5 on that scheme (Knapp et al. 2004 classify it T4 on the Geballe et al. scheme), it is unresolved in HST observations. No parallax measurement has been reported for this source.

Table 10.3 T Dwarf Spectral Standards

Source Designation ^a	SpT	MKO Photometry ^b				d (pc) ^c	Ref.
		J	$J - H$	$H - K$	$K - L'$		
Primary Standards							
SDSS J120747.17 + 024424.8	T0	15.38 ± 0.03	0.75 ± 0.04	0.47 ± 0.04	1.54 ± 0.06	...	1,2
SDSS J083717.21 − 000018.0	T1	16.90 ± 0.05	0.69 ± 0.07	0.23 ± 0.07	...	29 ± 12	3
SDSS J125453.90 − 012247.4	T2	14.66 ± 0.03	0.53 ± 0.04	0.29 ± 0.04	1.59 ± 0.06	13.7 ± 0.4	3
2MASS J12095613 − 1004008	T3	15.55 ± 0.03	0.31 ± 0.04	0.07 ± 0.04	4
2MASS J22541892 + 3123498	T4	15.01 ± 0.03	0.06 ± 0.04	−0.08 ± 0.04	1.79 ± 0.06	...	5
2MASS J15031961 + 2525196	T5	13.55 ± 0.03	−0.35 ± 0.04	−0.09 ± 0.04	2.08 ± 0.06	...	6
SDSS J162414.37 + 002915.6	T6	15.20 ± 0.03	−0.28 ± 0.04	−0.13 ± 0.04	2.01 ± 0.05	11.00 ± 0.15	7
2MASS J07271824 + 1710012	T7	15.19 ± 0.03	−0.48 ± 0.04	−0.02 ± 0.04	2.01 ± 0.06	9.09 ± 0.17	5
2MASS J04151954 − 0935066	T8	15.32 ± 0.03	−0.38 ± 0.04	−0.13 ± 0.04	2.55 ± 0.06	5.57 ± 0.10	5
Alternate Standards							
SDSS J015141.69 + 124429.6	T1	16.25 ± 0.05	0.71 ± 0.07	0.36 ± 0.07	1.64 ± 0.07	21.3 ± 1.4	8
SDSS J102109.69 − 030420.1AB	T3	15.88 ± 0.03	0.47 ± 0.04	0.15 ± 0.04	1.62 ± 0.07	29 ± 4	3
2MASS J07554795 + 2212169	T5	15.46 ± 0.03	−0.24 ± 0.04	−0.16 ± 0.04	5
2MASS J15530228 + 1532369AB	T7	15.34 ± 0.03	−0.42 ± 0.04	−0.19 ± 0.04	2.11 ± 0.06	...	5

^aSource designations include the J2000 sexagesimal right ascension and declination at an epoch around 2000.0, as 2MASS Jhhmmss.ss±ddmmss[.]s or SDSS Jhhmmss.ss±ddmmss.s. *JHKL'* photometry on the Mauna Kea Observatory (MKO) System.

^b*JHKL'* photometry on the Mauna Kea Observatory (MKO) System (Simons & Tokunaga 2002; Tokunaga, Simons, & Vacca 2002) from Strauss et al. (1999); Leggett et al. (2000, 2002, 2007a); Geballe et al. (2002); Golimowski et al. (2004); and Knapp et al. (2004).

^cParallax distance measurements from Dahn et al. (2002); Tinney, Burgasser, & Kirkpatrick (2003); and Vrba et al. (2004).

References: (1) Hawley et al. (2002); (2) Knapp et al. (2004); (3) Leggett et al. (2000); (4) Burgasser et al. (2004b); (5) Burgasser et al. (2002c); (6) Burgasser et al. (2003c); (7) Strauss et al. (1999); (8) Geballe et al. (2002).

Enoch, Brown, & Burgasser (2003) report a marginally significant rise of 0.5 ± 0.2 mag in the K-band flux of this object over the course of three nights, but this possible detection of variability has yet to be confirmed.

2MASS J15031961 + 2525196 (T5): This bright source ($J = 13.55 \pm 0.03$) was identified by Burgasser et al. (2003c) and originally classified T5.5 on the Burgasser et al. scheme. While at a slightly higher declination than the selection criteria listed above, the brightness of this source and lack of a visible companion make it an excellent choice as a spectral standard. No parallax distance measurement has been reported.

SDSS J162414.37 + 002915.6 (T6): The first identified field T dwarf Strauss et al. (1999), this source was classified T6 on both the Burgasser et al. and Geballe et al. schemes; SDSS J162414.37 + 002915.6 is a representative and easily accessible standard. It is unresolved in HST imaging observations, and has a parallax distance measurement of 11.00 ± 0.15 pc (Tinney, Burgasser, & Kirkpatrick 2003, see also Dahn et al. 2002; Vrba et al. 2004). Nakajima et al. (2000) report very low levels (1–3%) of variability in fine H₂O features between 1.53 and 1.58 μ m in the spectrum of the source, but not significant enough to affect its gross spectral morphology.

2MASS J07271824 + 1710012 (T7): Identified by Burgasser et al. (2002c) and selected as the T7 standard in that scheme (Knapp et al. 2004 classify it T8 on the Geballe et al. scheme), this source remains an excellent spectral standard. No high-angular resolution imaging observations have been reported, but the source has a parallax distance measurement of 9.09 ± 0.17 pc (Vrba et al. 2004).

2MASS J04151954 – 0935066 (T8): The coldest ($T_{\text{eff}} \approx 700$ K; Golimowski et al. 2004; Vrba et al. 2004; Saumon et al. 2006) and latest-type T dwarf currently known, this source was initially identified by Burgasser et al. (2002c) and selected as the T8 standard in that scheme. It is the sole T9 on the Geballe et al. scheme (Knapp et al. 2004). 2MASS J04151954 – 0935066 is unresolved in HST imaging observations, and has a parallax distance measurement of 5.75 ± 0.10 pc (Vrba et al. 2004).

Figures 10.8 and 10.9 display two spectral sequences of these standards, plus the L8 optical standard 2MASS J16322911 + 1904407 (Kirkpatrick et al. 1999) and the L9 dwarf (near-infrared classification; Geballe et al. 2002) 2MASS J03105986 + 1648155 (Kirkpatrick et al. 2000), based on $\lambda/\Delta\lambda \approx 150$ and 400 data obtained with the SpeX (Rayner et al. 2003) and CGS4 instruments, respectively. The standard spectra shown here define the T-dwarf class. The emergence of CH₄ absorption at 1.6 μ m designates the start of the T-dwarf sequence (Geballe et al. 2002), and early-type T dwarfs exhibit weak CH₄ bands, strong H₂O bands, and waning CO absorption at 2.3 μ m. In later types, H₂O and CH₄ bands

progressively strengthen; the 1.05, 1.25, 1.6, and 2.1 μm peaks become more pronounced and acute; and the K-band peak becomes increasingly suppressed relative to J. The end of the currently known T-dwarf class is exemplified by the spectrum of 2MASS J04151954 – 0935066, with nearly saturated H_2O and CH_4 bands, and sharp triangular flux peaks emerging between these bands. The range of spectral morphologies encompassed by the standards spans the full spectral variety of the currently known T-dwarf population.

10.4.3.2 Alternate Standards

In addition to the primary standards, four alternate standards are defined and listed in Table 10.3. These sources have nearly identical near-infrared spectral energy distributions as the primary standards (Figure 10.10), but are well-separated on the sky to facilitate the observation of a spectral comparator at any time of the year. Note that these alternate standards do not strictly adhere to the constraints listed above. They are as follows:

SDSS J015141.69 + 124429.6 (T1 alternate): Identified by Geballe et al. (2002), this faint source ($J = 16.25 \pm 0.05$; Leggett et al. 2002) was classified T1 on that study's scheme. It is unresolved in HST images and has a parallax distance measurement of 21.4 ± 1.6 pc (Vrba et al. 2004). Enoch, Brown, & Burgasser (2003) report significant K-band variability from this source (0.42 ± 0.14 mag peak-to-peak) with a possible period of 2.97 hours. The faintness and apparent variability of SDSS J015141.69 + 124429.6 relegate it as an alternate standard.

SDSS J102109.69 – 030420.1AB (T3 alternate): Identified by Leggett et al. (2000), this source was the original T3 standard on the Burgasser et al. scheme (also classified T3 by Geballe et al. 2002). However, it has been resolved as an unequal-brightness binary in HST observations, and appears to have T1 + T5 components (Burgasser et al. 2006b). Nevertheless, this source remains a viable alternative to the primary standard 2MASS J12095613 – 1004008, although it is separated by only 28° on the sky. SDSS J102109.69 – 030420.1AB has a parallax distance measurement of 29 ± 4 pc (Tinney, Burgasser, & Kirkpatrick 2003, see also Vrba et al. 2004).

2MASS J07554795 + 2212169 (T5 alternate): Identified by Burgasser et al. (2002c) and classified T5 on that system, this source has a spectrum nearly identical to that of the brighter primary standard 2MASS J15031961 + 2525196 (see also Figure 10.11). It is unresolved in HST images. No parallax measurement has been reported.

2MASS J15530228 + 1532369AB (T7 alternate): This late-type T dwarf identified by Burgasser et al. (2002c) and classified T7 on that system has a near-infrared spectrum identical to that of the primary standard 2MASS J07271824 + 1710012.

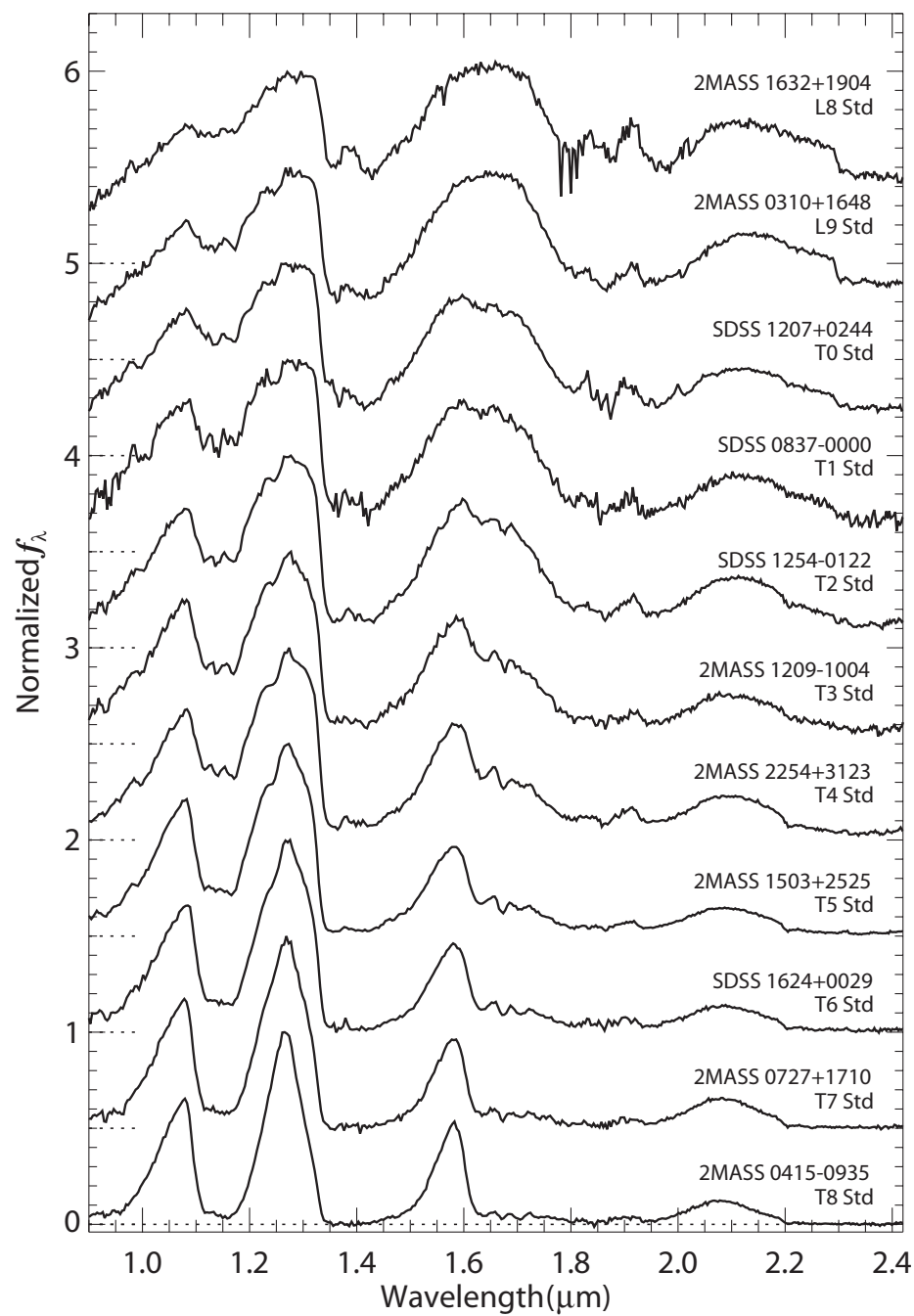


Figure 10.8 T-dwarf spectral standards measured at resolution $\lambda/\Delta\lambda \approx 150$. Data are from Burgasser et al. (2006a), and Looper, Kirkpatrick, & Burgasser (2007). L8 and L9 comparison sources are shown at top. All spectra are normalized at 1.27 μm and offset by constants (dotted lines).

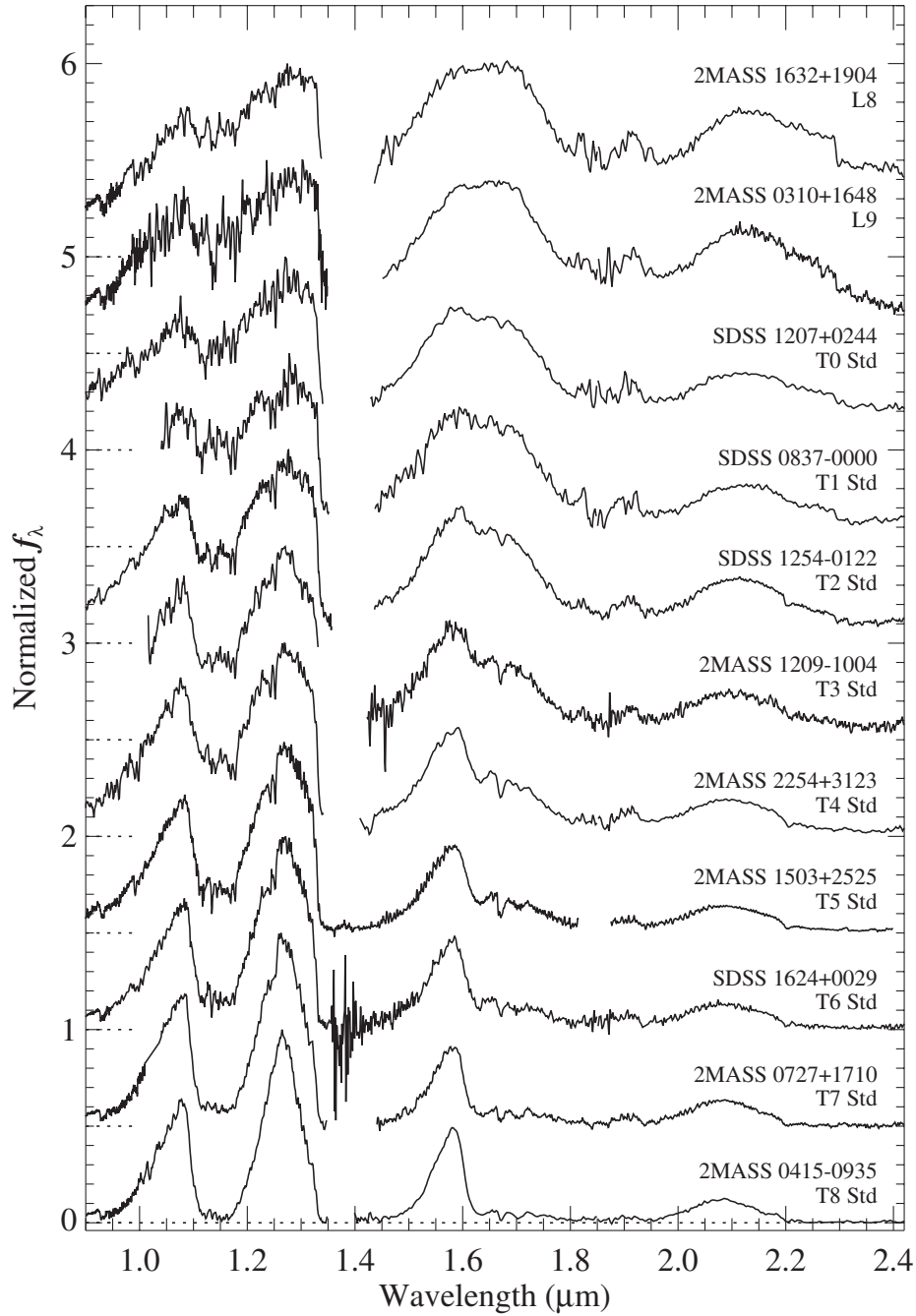


Figure 10.9 T-dwarf spectral standards measured at resolution $\lambda/\Delta\lambda \approx 400$. Data are from Geballe et al. (2002); Burgasser et al. (2004b); and Knapp et al. (2004). Note that the spectrum of 2MASS J15031961 + 2525196 was measured at higher resolution ($\lambda/\Delta\lambda = 1200$), and data are smoothed to match the other spectra. Finer structure seen in the 1.1–1.3 μm region is due in part to alkali absorption lines. All spectra are normalized at 1.27 μm and offset by constants (dotted lines).

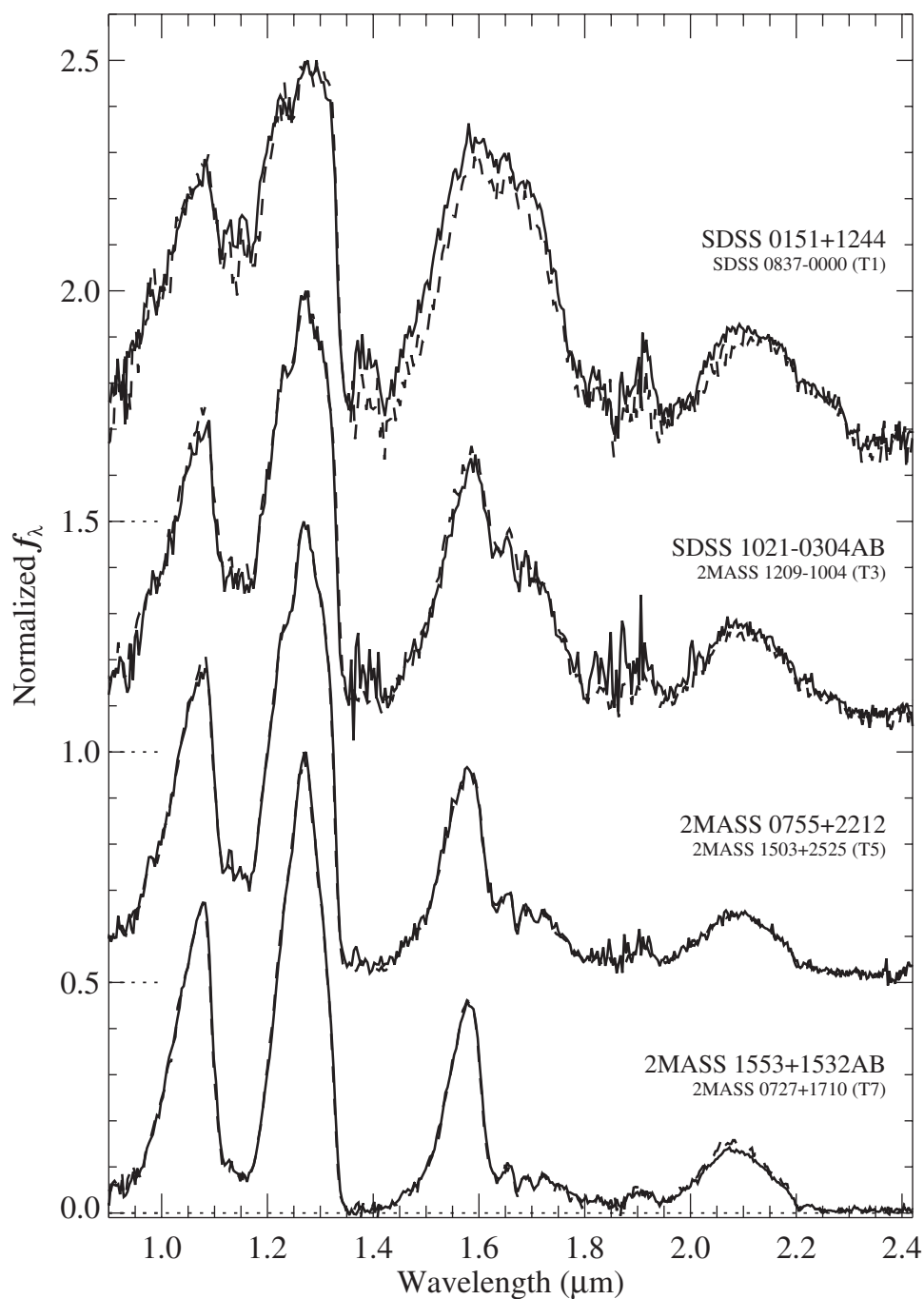


Figure 10.10 Low-resolution spectra of alternate T-dwarf spectral standards (solid lines) compared to their primary standard counterparts (dashed lines). Data are from Burgasser et al. (2004b, 2006a); and Looper, Kirkpatrick, & Burgasser (2007). All spectra are normalized at $1.27 \mu\text{m}$ and offset by constants (dotted lines).

Resolved into an equal-magnitude, co-moving pair with HST and ground-based observations, 2MASS J15530228 + 1532369AB appears to be composed of two similarly-typed T dwarfs, making it a viable comparison source. No parallax measurement has been reported for this system.

10.4.4 Methods of Classification

10.4.4.1 Direct Spectral Comparison

The classification of T dwarfs is optimally done by direct comparison of near-infrared spectral data to equivalent data for the spectral standards listed above, with spectra optimally obtained over a similar wavelength range (nominally 1–2.5 μm) and resolution ($\lambda/\Delta\lambda \approx 150\text{--}400$ for the spectra shown in Figures 10.8 and 10.9). Burgasser et al. (2006a) outlined two methods for this comparison, as illustrated in Figures 10.11 through 10.13. For single-order dispersion spectrographs (such as SpeX in prism mode), the overall spectral energy distributions of sources and standards can be compared directly, after normalizing to the flux peak at 1.27 μm . Such comparisons enable immediate classification of “normal” T dwarfs (e.g., Figure 10.11) that fit within the standard sequence, and ready identification of “peculiar” sources that exhibit conflicting band strengths or substantially inconsistent broadband colors (e.g., Figure 10.12). Peculiar T dwarf spectra are discussed in further detail in §10.7.

More commonly, near-infrared spectroscopic data are acquired in multiple dispersion orders or separate exposures to span the full 1–2.5 μm range. As merging of multi-order spectral data is prone to scaling errors (see McLean et al. 2003 for a discussion of this issue) a more reliable method for classifying these data is to compare individual dispersion orders separately, as illustrated in Figure 10.13. Both methods yield consistent classifications to within 0.5 subtypes. This limit is consistent with the formal limit for spectral-classification uncertainty on the near-infrared scheme, since spectral standards are defined in integer subtype steps.

10.4.4.2 Spectral Indices

While direct spectral comparison provides the most robust method for spectral typing, there are situations in which the use of *spectral indices*—ratios of the average or integrated flux density measured at different wavelengths on a spectrum—may be preferred as an estimator for spectral type. Examples include classification measurements of noisy spectral data, in which case coarse binning can improve signal-to-noise; or automated classification of very large datasets (e.g., Burgasser 2007b). In addition, spectral indices enable the quantification of peculiarities seen in some spectra, and hence a potential starting point for segregating sources with, e.g., low surface gravity or subsolar metallicity (see §10.7.2).

Useful spectral indices sample strong features that vary monotonically with spectral subtype. It is clear from Figures 10.8 and 10.9 that the 1.1, 1.4, and 1.8 μm H₂O and 1.3, 1.6, and 2.2 μm CH₄ absorption bands are the most useful

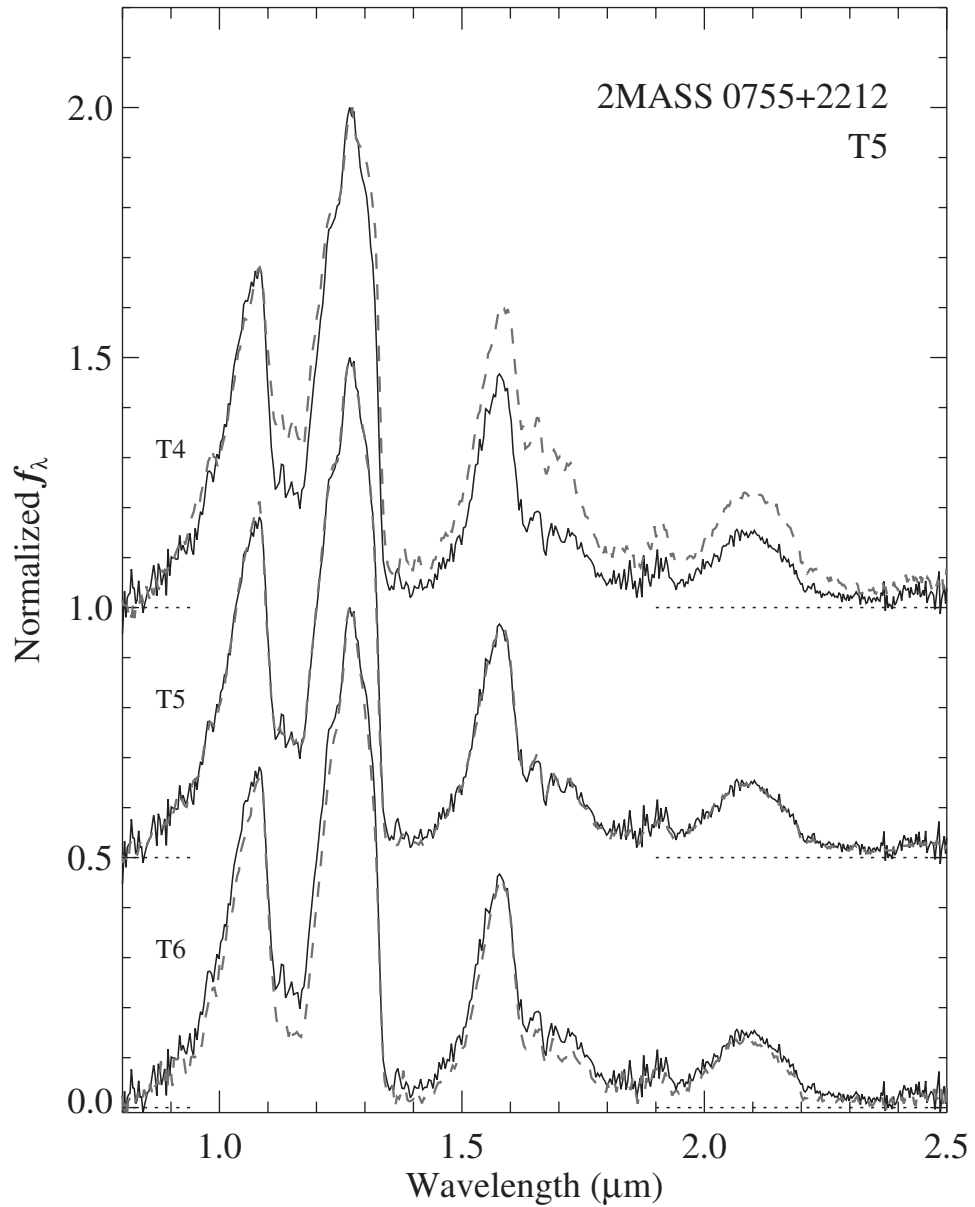


Figure 10.11 An example of spectral classification via direct spectral comparison for low-resolution ($\lambda/\Delta\lambda \sim 150$) data of the T5 2MASS J07554795 + 2212169 (repeated solid lines). These data were measured in a single dispersion order, so comparison of the spectral energy distribution across the full near-infrared waveband can be made. The spectrum of 2MASS J07554795 + 2212169 closely matches that of the T5 standard 2MASS J15031961 + 2525196 (middle dashed line), and is an inferior match to either the T4 or T6 standards (upper and lower dashed lines). All spectra are normalized at the J-band flux peak ($1.27 \mu\text{m}$) and offset by constants (dotted lines). Reproduced from Burgasser et al. (2006a) by permission of the AAS.

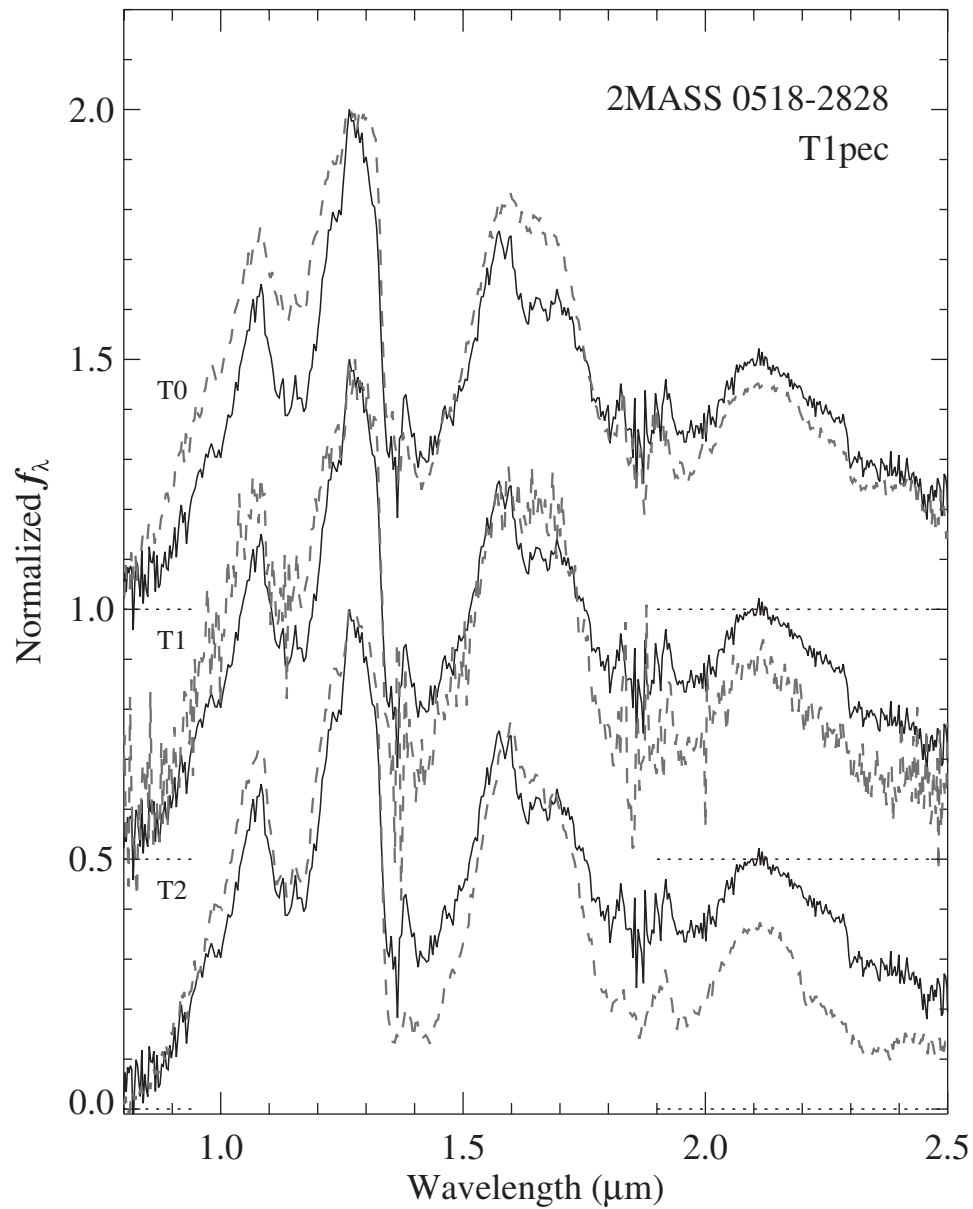


Figure 10.12 Same as Figure 10.11 for the peculiar T1 2MASS J05185995 – 2828372 (repeated solid lines), whose spectrum fails to align with any of the closest matching T-dwarf standards (dashed lines). This source has been resolved as a probable L-dwarf/T-dwarf binary (Burgasser et al. 2006b); see §10.7.1. Reproduced from Burgasser et al. (2006a) by permission of the AAS.

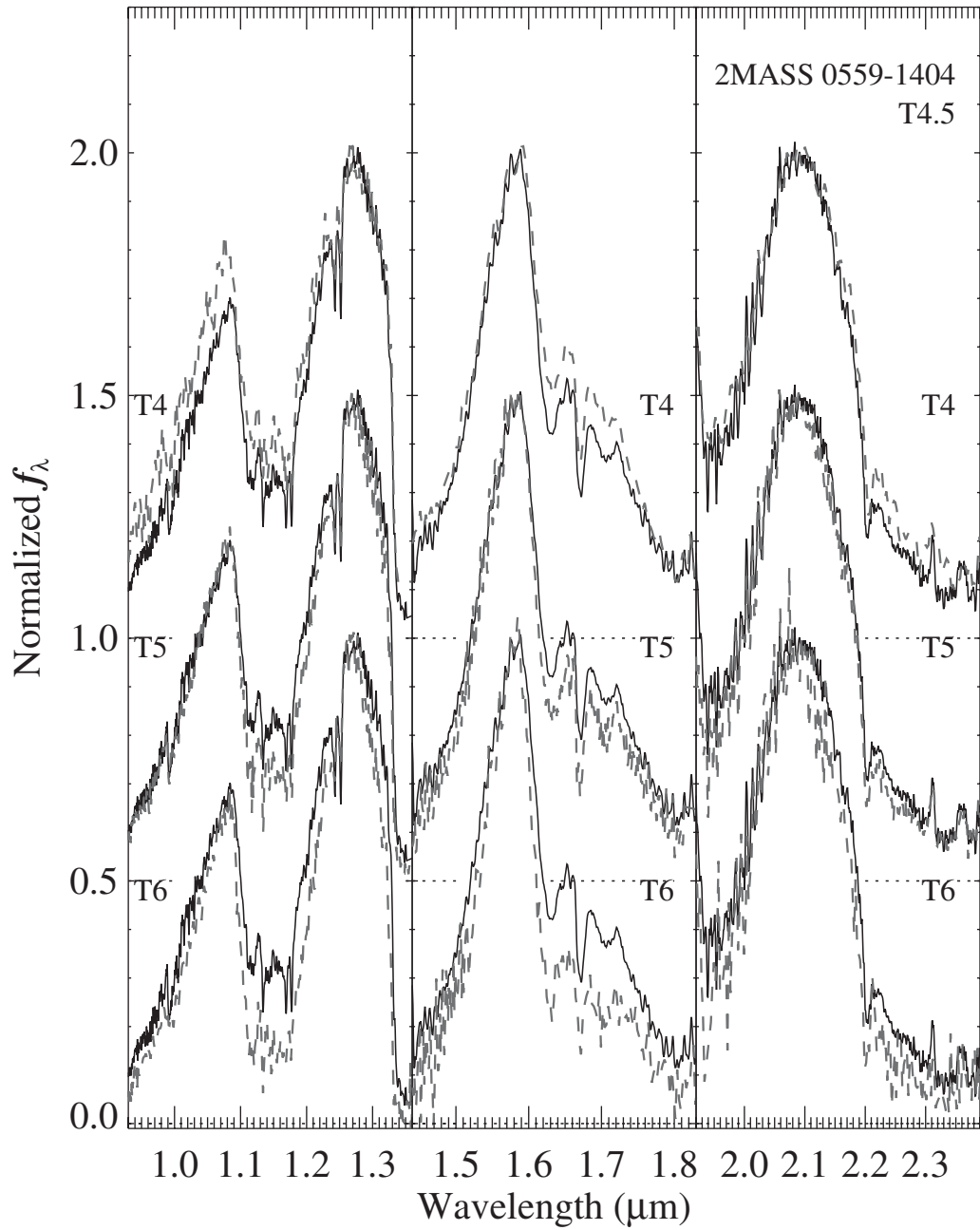


Figure 10.13 Example of spectral classification through direct spectral comparison for the T4.5 2MASS J05591914 – 1404488, based on higher-resolution ($\lambda/\Delta\lambda \sim 400$) CGS4 data. These data were measured in three separate orders, from left to right: 0.95–1.35, 1.45–1.8, and 1.9–2.4 μm , corresponding roughly to the J, H, and K photometric bands. In order to minimize scaling errors between the orders, spectra of the source (repeated solid lines) and standards (dashed lines) are normalized at the local flux peak in each order. Note how features in the spectrum of the T4.5 2MASS J05591914 – 1404488 fall midway in strength between those of the T4 and T5 standards. Reproduced from Burgasser et al. (2006a) by permission of the AAS.

Table 10.4 Definitions of Near-Infrared Spectral Classification Indices

Index	Numerator (μm)	Denominator (μm)	Feature Measured
H ₂ O-J	$\int F_{1.140-1.165}$	$\int F_{1.260-1.285}$	1.15 μm H ₂ O
CH ₄ -J	$\int F_{1.315-1.340}$	$\int F_{1.260-1.285}$	1.32 μm CH ₄
H ₂ O-H	$\int F_{1.480-1.520}$	$\int F_{1.560-1.600}$	1.4 μm H ₂ O
CH ₄ -H	$\int F_{1.635-1.675}$	$\int F_{1.560-1.600}$	1.65 μm CH ₄
CH ₄ -K	$\int F_{2.215-2.255}$	$\int F_{2.080-2.120}$	2.2 μm CH ₄

Note: $\int F_{\lambda_1-\lambda_2}$ denotes integrated flux measured over the wavelength interval λ_1 to λ_2 .

for this purpose. These bands strengthen throughout the standard sequence and are well correlated. These bands are also broad enough to be measured at the low spectral resolutions that define the sequence.

Table 10.4 lists the five spectral indices recommended by Burgasser et al. (2006a) to estimate T-dwarf subtypes. These indices are defined as the ratio of the integrated flux over a waveband located within an absorption feature to the integrated flux over an identically sized waveband (in wavelength units) in the neighboring pseudocontinuum.⁶ With this definition, smaller index values correspond to stronger absorption, which minimizes large fluctuations arising from poor signal-to-noise at the bottom of strong bands (e.g., in the latest-type T dwarfs). The choice of spectral wavebands sampled was optimized to avoid regions of strong telluric absorption, as illustrated in Figure 10.14, helping to minimize variations between data obtained at different sites. Finally, the spectral ratio wavebands were defined to be broad enough to facilitate use with low resolution spectral data.

Figure 10.15 illustrates how the five classification spectral indices vary with spectral type for L8–T8 dwarfs. All five indices decline monotonically with later spectral type, although the CH₄-H index exhibits more obvious trends for subtypes T2 and later, while CH₄-K index values saturate around type T7. It is clear that these indices can provide a useful mapping to spectral type for the T dwarfs.

Two methods to estimate spectral subtypes using spectral indices were examined by Burgasser et al. (2006a), based on the methods originally outlined in the Burgasser et al. (2002c) and Geballe et al. (2002) studies. The first method starts from the values of the spectral indices for the standard sources, listed in Table 10.5 for both SpeX and CGS4 datasets. By measuring the same indices on the spectrum of the source to be classified, individual index subtypes are determined as the closest match to the standard values. Indices with values intermediate between two standard values can be assigned a half-subtype. Final classifications are then estimated as the average of the index subtypes, except for the earliest standard types (T0 and T1) where the H₂O-J and CH₄-H indices are generally omitted due to their slight degeneracies. Sources with a large scatter amongst the index subtypes (>1 subclass) are noted as having an uncertain classification (indicated

⁶Absorption from various opacity sources is present at all wavelengths in the near-infrared spectra of T dwarfs; hence, the brightest regions do not probe the blackbody continuum ($T_{\text{brightness}} = T_{\text{eff}}$), but a local “pseudocontinuum.”

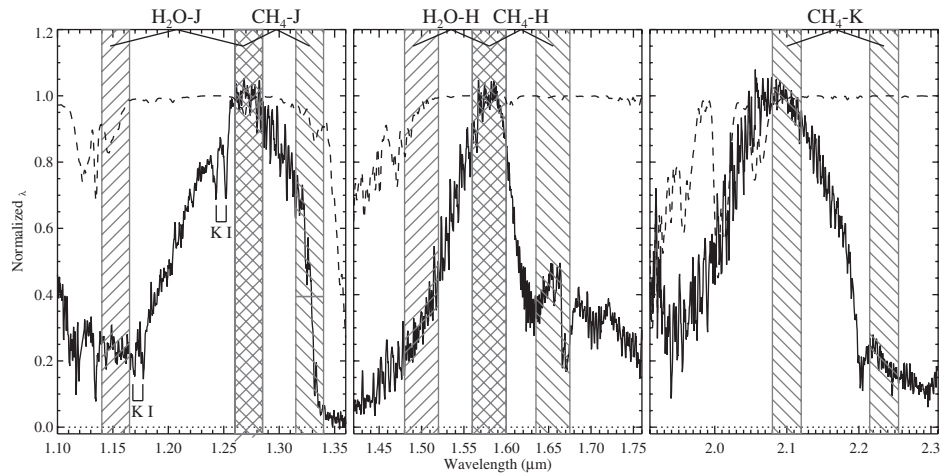


Figure 10.14 Spectral regions sampled by the five H_2O and CH_4 classification indices defined in Table 10.4, plotted over the near-infrared spectrum of the T5 standard 2MASS J15031961 + 2525196. A telluric transmission spectrum typical for Mauna Kea is also shown (dashed lines). Spectral data in each panel are normalized at the local flux peak. Reproduced from Burgasser et al. (2006a) by permission of the AAS.

by a “:”) if the spectral data have particularly low signal-to-noise. Sources with high quality data but scattered index subtypes are noted as peculiar (indicated by a “p” or “pec”; see Figure 10.12).

As an example, consider the SpeX prism spectrum of the T dwarf 2MASS J19010601 + 4718136 (Burgasser et al. 2004b). The measured spectral index values are $\text{H}_2\text{O-J} = 0.285$, $\text{CH}_4\text{-J} = 0.450$, $\text{H}_2\text{O-H} = 0.355$, $\text{CH}_4\text{-H} = 0.435$, and $\text{CH}_4\text{-K} = 0.237$. Comparison to the standard values in Table 10.5 finds best agreements of T4.5, T4.5, T5, T4.5, and T4.5, for an average of T4.5. Comparison of the spectrum of this source to the T4 and T5 standards shows that its morphology is indeed intermediate between these integer subtypes.

A second method, based on Geballe et al. (2002), involves the comparison of measured spectral indices to predefined ranges. Table 10.6 lists these ranges, determined as the typical values for each spectral subtype as measured for a large sample of CGS4 data. Because of their degeneracy, ranges for the $\text{H}_2\text{O-J}$ and $\text{CH}_4\text{-K}$ indices are defined only for spectral types $\geq \text{T2}$ and $\leq \text{T6}$, respectively. Using this method, index subtypes for a given source are assigned according to the range in which the measured value for this source’s spectrum falls; half-subtypes are again allowed for values within 25% of the range borders. An average type is determined from all of the applicable index types, with uncertain or peculiar sources notes as above.

Burgasser et al. (2006a) compared the estimated subtypes derived from the two spectral index methods described above to each other and to classifications based on direct comparison of spectral data. Consistency was found between all three methods, with differences of less than 1 subtype between index and direct

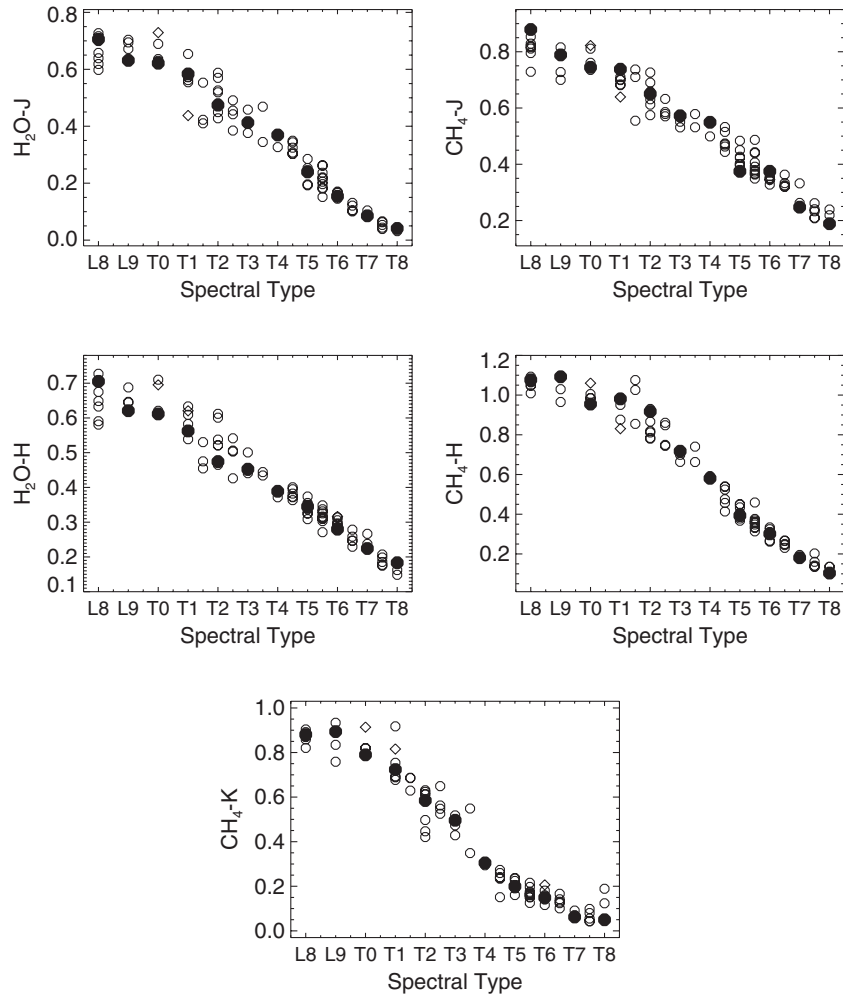


Figure 10.15 Values of spectral classification indices versus spectral type for 96 SpeX prism spectra of sources with published classifications of L8 and later. Spectral types are based on optical data for L8 dwarfs and near-infrared data for L9 and T dwarfs. Standards (Table 10.3) are indicated by solid circles, known peculiar sources by open diamonds, and all others by open circles. Note the generally monotonic decline in all five indices as a function of spectral type.

comparison classifications for the same spectral data; typical deviations were 0.3 subtypes. This is consistent with the formal 0.5 subtype uncertainty of the scheme set by the integer type standards, so the use of spectral indices as an estimator of spectral type appears to be robust. It is important to stress, however, that such results should be considered as proxies for the true classification of a source, determined by direct spectral comparison of that source's spectrum to a grid of standards observed at the same resolution and over the same spectral range.

Table 10.5 Near-Infrared Spectral Indices for T-Dwarf Spectral Standards

Name	SpT	H ₂ O-J	CH ₄ -J	H ₂ O-H	CH ₄ -H	CH ₄ -K
SpeX Prism Data, $\lambda/\Delta\lambda \approx 150$						
2MASS J16322911 + 1904407 ^a	L8	0.706	0.879	0.705	1.077	0.881
2MASS J03105986 + 1648155 ^a	L9	0.631	0.789	0.621	1.092	0.894
SDSS J120747.17 + 024424.8	T0	0.621	0.745	0.612	0.955	0.790
SDSSp J083717.22 – 000018.3	T1	0.584	0.738	0.563	0.981	0.724
SDSSp J125453.90 – 012247.4	T2	0.474	0.650	0.474	0.917	0.585
2MASS J12095613 – 1004008	T3	0.413	0.572	0.453	0.717	0.496
2MASS J22541892 + 3123498	T4	0.369	0.549	0.389	0.581	0.305
2MASS J15031961 + 2525196	T5	0.240	0.375	0.345	0.393	0.200
SDSSp J162414.37 + 002915.6	T6	0.154	0.375	0.280	0.301	0.149
2MASS J07271824 + 1710012	T7	0.085	0.247	0.224	0.181	0.062
2MASS J04151954 – 0935066	T8	0.041	0.189	0.183	0.104	0.050
CGS4 Data, $\lambda/\Delta\lambda \approx 400$						
2MASS J16322911 + 1904407 ^a	L8	0.701	0.834	0.705	1.036	0.888
2MASS J03105986 + 1648155 ^a	L9	0.675	0.835	0.645	1.064	0.786
SDSS J120747.17 + 024424.8	T0	0.628	0.707	0.597	0.944	0.812
SDSSp J083717.22 – 000018.3	T1	0.646	0.714	0.586	0.936	0.689
SDSSp J125453.90 – 012247.4	T2	0.501	0.603	0.491	0.870	0.564
2MASS J12095613 – 1004008	T3	0.439	0.612	0.462	0.687	0.495
2MASS J22541892 + 3123498	T4	0.411	0.514	0.416	0.547	0.302
2MASS J15031961 + 2525196 ^b	T5	0.239	0.398	0.332	0.381	0.200
SDSSp J162414.37 + 002915.6	T6	0.156	0.314	0.320	0.318	0.158
2MASS J07271824 + 1710012	T7	0.090	0.243	0.227	0.168	0.060
2MASS J04151954 – 0935066	T8	0.030	0.171	0.173	0.105	0.043

^aLate L dwarf comparison source.^bData obtained with SpeX cross-dispersed mode ($\lambda/\Delta\lambda \approx 1200$) smoothed to the resolution of the CGS4 data ($\lambda/\Delta\lambda \approx 400$).

10.4.5 Alternate Near-Infrared Classification Schemes

The low-resolution classification scheme described above provides a consistent, reliable method for determining T-dwarf spectral types. However, alternate schemes may be preferable when data have higher resolution or wavelength coverage is limited. McLean et al. (2003) examined this case for a sample of 16 T dwarfs with $\lambda/\Delta\lambda \approx 2000$ near-infrared spectral data confined to the 1.15–1.35 μm range (a single dispersion order for the Near Infrared Spectrometer or NIRSPEC; McLean et al. 1998, 2000). These data were sufficient to resolve several of the atomic lines present in T-dwarf near-infrared spectra, in particular the 1.169/1.178 and 1.244/1.252 K I doublets. Figure 10.16 shows a sequence of these spectra, which include several of the spectral standards. The strengthening molecular absorptions around 1.15 and 1.3 μm observed in the low-resolution data are reproduced in these data. Indeed, the authors of this study found good agreement between spectral types based on a set of narrow-band (40 Å) spectral indices sampling this region mapped onto the standard grid, and published types (within

Table 10.6 Numerical Ranges of Near-Infrared Spectral Indices for T-Dwarf Subtypes

NIR SpT	H ₂ O-J	CH ₄ -J	H ₂ O-H	CH ₄ -H	CH ₄ -K
T0	...	0.73–0.78	0.60–0.66	0.97–1.00	0.75–0.85
T1	>0.55	0.67–0.73	0.53–0.60	0.92–0.97	0.63–0.75
T2	0.45–0.55	0.58–0.67	0.46–0.53	0.80–0.92	0.55–0.63
T3	0.38–0.45	0.52–0.58	0.43–0.46	0.60–0.80	0.35–0.55
T4	0.32–0.38	0.45–0.52	0.37–0.43	0.48–0.60	0.24–0.35
T5	0.18–0.32	0.36–0.45	0.32–0.37	0.36–0.48	0.18–0.24
T6	0.13–0.18	0.28–0.36	0.26–0.32	0.25–0.36	0.13–0.18
T7	0.07–0.13	0.21–0.28	0.20–0.26	0.15–0.25	<0.13
T8	0.02–0.07	0.15–0.21	0.14–0.20	0.07–0.15	...

1 subclass). This results suggests that the J-band region is largely representative of the full near-infrared spectral morphology (however, see Burgasser et al. 2003a). On the other hand, the K I lines show a more complex behavior, initially strengthening in the early-T spectral types and then declining toward the end of the sequence (see also Figure 14 in McLean et al. 2003). In addition, a few sources (e.g., 2MASS J09373487 + 2931409, discussed below) exhibit peculiar K I strengths compared to sources with similar spectral types. As stressed by McLean et al. (2003), broader spectral coverage is generally preferred to superior resolution in the classification of T dwarfs.

10.4.6 Near-Infrared Spectral Types and Physical Parameters

With a well-defined sequence based on spectromorphological criteria, it is worth examining how T-dwarf spectral types correlate with other observational properties. Figure 10.17 compares absolute J and K_s magnitudes for unresolved and binary-component late-L and T dwarfs based on 2MASS photometry and measured parallaxes. In general, later spectral types correspond to fainter absolute magnitudes, particularly for the mid- and late-type T dwarfs in the K_s -band. At the J-band, early-type T dwarfs appear to be as bright as late-type L dwarfs, an effect known as the “J-band bump” (Dahn et al. 2002; Tinney, Burgasser, & Kirkpatrick 2003; Knapp et al. 2004; Burgasser et al. 2006b; Liu et al. 2006). A similar effect is seen in the $1.05\ \mu\text{m}$ Y-band (Liu et al. 2006; Burgasser et al. 2006b). The J-band bump appears to be related to the depletion of photospheric condensate dust clouds across the L-dwarf/T-dwarf transition (Ackerman & Marley 2001; Cooper et al. 2003; Burrows, Sudarsky, & Hubeny 2006), a process that appears to occur rapidly (on a time scale of ~ 100 Myr—Burgasser et al. 2006b; Liu et al. 2006; Burgasser 2007b) and has a direct impact on the frequency and nature of early-type T-dwarf multiples (see §10.7.1).

Golimowski et al. (2004) have examined trends in T_{eff} as a function of spectral type, based on luminosity determinations from parallax and broadband photometric measurements (e.g., Leggett et al. 2002; Vrba et al. 2004). The spectral types of T dwarfs typed \sim T4 and later appear to correlate well with T_{eff} (see Figure 10.18),

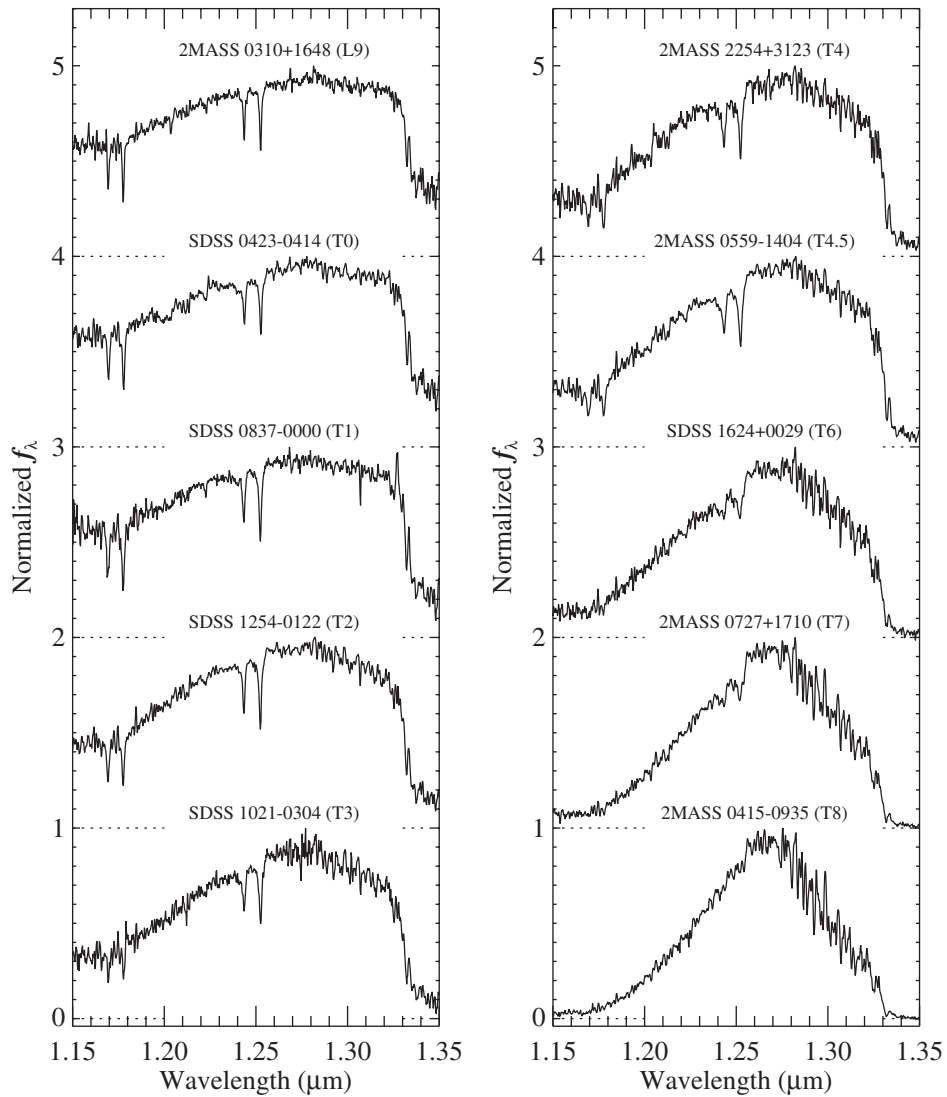


Figure 10.16 Moderate resolution ($\lambda/\Delta\lambda \approx 2000$) spectral sequence of T dwarfs, including several of the standards shown in Figures 10.8 and 10.9, based on data from McLean et al. (2003). Spectra are normalized at their $1.27 \mu\text{m}$ flux peaks and offset by constants (dotted lines). In addition to the trend toward increasing molecular absorption at 1.15 and $1.3 \mu\text{m}$ observed in the low-resolution data, K I lines at 1.244 and $1.252 \mu\text{m}$ are seen to vary in strength, although in a non-monotonic manner.

consistent with the expectation that stronger molecular bands should be found in cooler photospheres. However, the early-type T dwarfs appear to have roughly the same temperatures as the late-type L dwarfs. This flattening in the T_{eff} relation (and equivalently the bolometric-luminosity relation) has important implications for the evolution of condensate clouds across the L/T transition. However, the

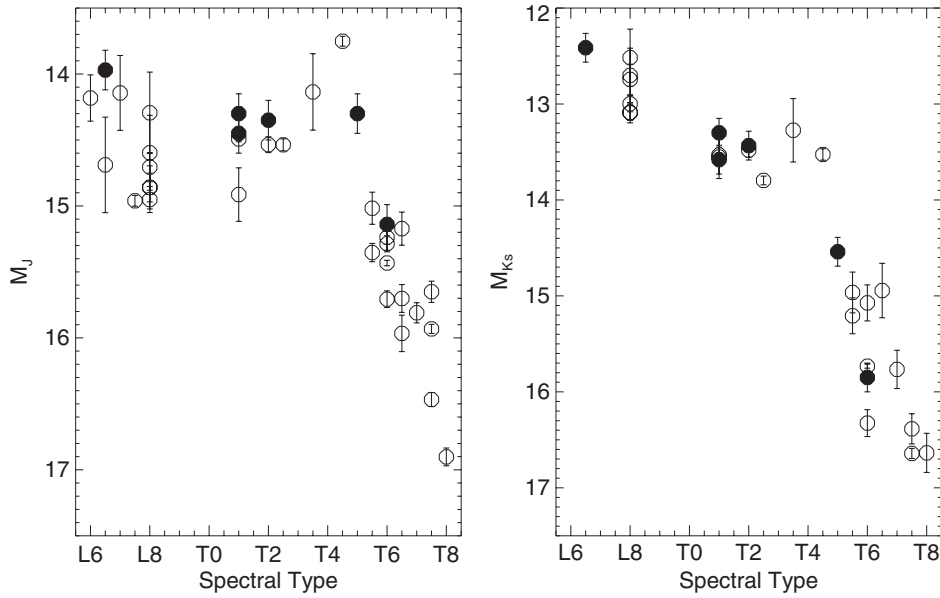


Figure 10.17 Absolute J (left) and K_s (right) magnitudes for 30 L and T dwarfs as a function of spectral type. Photometric data are from 2MASS; parallax data are from Dahn et al. (2002); Tinney, Burgasser, & Kirkpatrick (2003); and Vrba et al. (2004) for field sources, and from ESA (1997) for brown dwarf companions to nearby stars. Components of resolved binary systems are indicated by filled circles, unresolved systems by open circles.

flattening of the T_{eff} relation does not translate into difficulties in distinguishing spectral subtypes among the early-type T dwarfs, as the spectral morphology does change considerably in this spectral-type range.

10.5 OPTICAL CLASSIFICATION

The near-infrared is the optimal waveband for classifying T dwarfs, due to their relative brightness and the presence of strong H_2O and CH_4 bands at these wavelengths. On the other hand, L-dwarf classification is fundamentally defined at red-optical wavelengths (6000–10000 Å; Chapter 9), while definition of a robust near-infrared classification scheme for L dwarfs has been stymied due in large part to cloud effects. In order to provide a continuum of classifications from the M dwarfs through the T dwarfs, and in particular map the properties of dwarfs spanning the L-dwarf/T-dwarf transition, it is useful to consider classification of T dwarfs at red-optical wavelengths.

The red-optical spectra of T dwarfs are of interest in their own right. This spectral band encompasses unique and in some cases dramatic features, most notably the deep and strongly pressure-broadened atomic-line absorptions arising from the 5890/5896 Å Na I and 7665/7699 Å K I doublets (Tsuji, Ohnaka, & Aoki

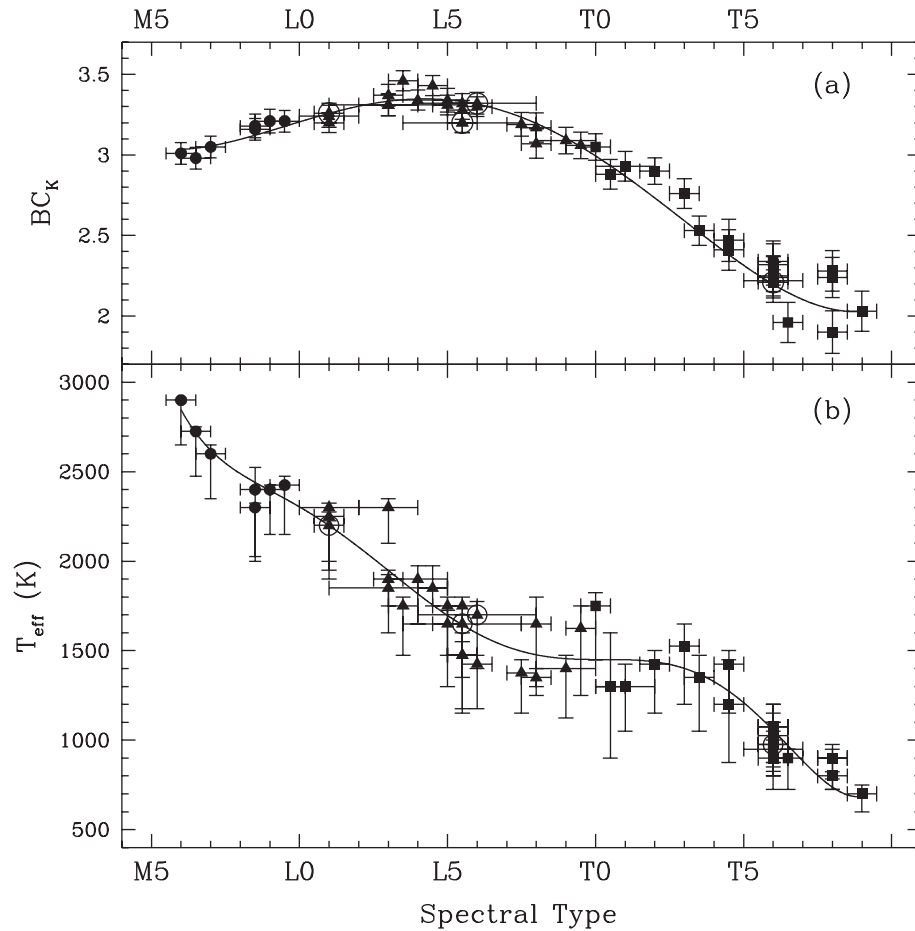


Figure 10.18 K-band bolometric correction (top) and derived T_{eff} (bottom) for a large sample of late-type M, L, and T dwarfs with parallax and broadband photometric measurements. Note the flattening in the T_{eff} relation from late-L to mid-T, while late-type T dwarfs are progressively cooler. Reproduced from Golimowski et al. 2004 and with permission of the AAS.

1999; Burrows, Marley, & Sharp 2000), which span much of the optical band and give rise to the extremely red spectral slope from 8000 to 11000 Å. The resulting extremely red-optical/near-infrared colors of T dwarfs have been exploited in the search for T dwarfs by SDSS and 2MASS. Other features of note include alkali lines of Rb I and Cs I in the 7800–9000 Å region, a weak Wing–Ford band of FeH at 9896 Å, and H₂O absorption spanning 9250–9800 Å (CH₄ and CaH bands have also been suggested; Oppenheimer et al. 1998; Burgasser et al. 2003b).

The classification of T dwarfs at red-optical wavelengths has been examined in detail by Burgasser et al. (2003b), who developed a one-dimensional scheme tied to the near-infrared spectral standards listed in Table 10.3. This section summarizes the results of that study.

10.5.1 Characteristics of Classification Data

The difficulty in using red-optical data to classify T dwarfs is their extreme faintness at these wavelengths, with spectral energy distributions dropping over four orders of magnitude in flux (10 magnitudes) from the $1.27\ \mu\text{m}$ peak to the core of the K I doublet. This means that red-optical observations of T dwarfs have generally been limited to the brightest examples and have required significant investments in 8–10 m telescope time to acquire sufficient data. For this reason, the red-optical classification scheme for T dwarfs developed by Burgasser et al. (2003b) is based on data acquired with the Low Resolution Imaging Spectrograph (LRIS; Oke et al. 1995) mounted on the Keck 10-m Telescope. These data span a wavelength range of 6300–10100 Å with a resolution of $\lambda/\Delta\lambda \approx 1200$. An example of these data for the bright T4.5 2MASS J05591914 – 1404488 is shown in Figure 10.3. Comparable data have been reported for 19 T dwarfs to date (Oppenheimer et al. 1998; Burgasser et al. 2000a, 2002a, 2003b, Kirkpatrick et al., in preparation), all using LRIS. Hence, the dispersion and wavelength coverage of this instrument sets the *de facto* requirements for spectral classification.

10.5.2 Spectral Standards

The sparsity of available red-optical data restricts the definition of spectral subtypes to a coarser grid. Four standards define the optical classification, chosen amongst the near-infrared standard sequence: SDSS J125453.90–012247.4 (T₀2), 2MASS J15031961 + 2525196 (T₀5), SDSS J162414.37 + 002915.6 (T₀6), and 2MASS J04151954 – 0935066 (T₀8). Here, the subscript T₀ is used to differentiate optical from near-infrared classifications.

Spectra for these standards, in addition to the L8 optical standard 2MASS J16322911 + 1904407 (Kirkpatrick et al. 1999), are shown in Figures 10.19 and 10.20 using both linear and logarithmic vertical scales, respectively. Despite choosing standards on the basis of their near-infrared types, these spectra exhibit clear trends in their optical spectra, including a steepening of the 8000–10000 Å slope, strengthening of the 9250 Å H₂O band, and a weakening of the 8521 and 8943 Å Cs I lines. In addition, FeH and CrH bands at 8611 and 8692 Å decline from L8 to T₀2, and are absent from T₀5 on; while the 9896 Å Wing–Ford band strengthens somewhat from L8 to T₀5, only to fade again in the later T dwarfs. These readily apparent trends, and the distinct spectral morphology of the optical standards, indicates a robust framework for the definition of an optical scheme.

10.5.3 Classification Methods

10.5.3.1 Direct Spectral Comparison

Classification of T-dwarf red-optical spectra can again be accomplished via direct comparison to the spectra of the standards listed above. The optimal means of doing this is by comparison on a logarithmic scale (e.g., Figure 10.20), which

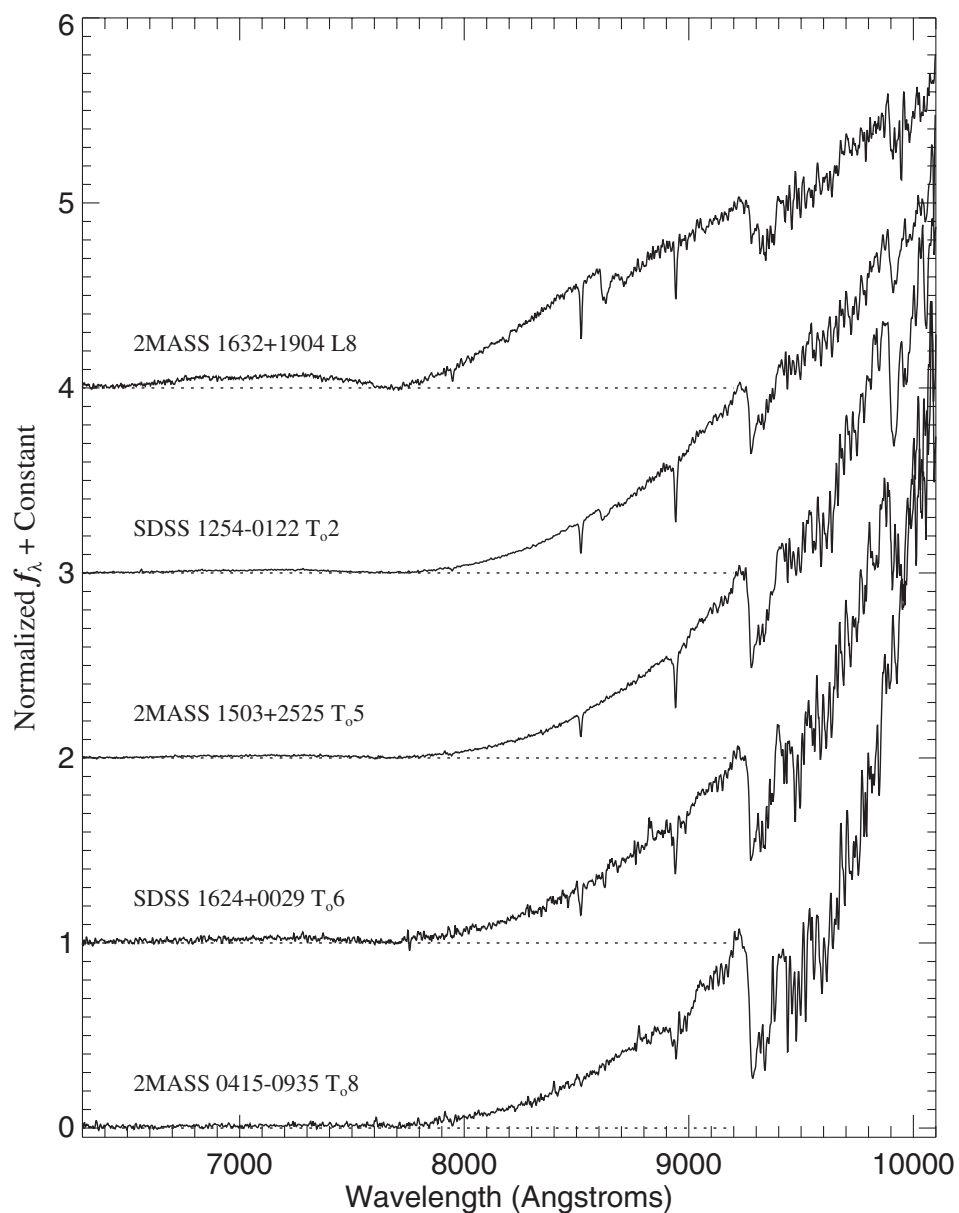


Figure 10.19 LRIS spectra of optical spectral standards 2MASS J16322911 + 1904407 (L8), SDSS J125453.90 - 012247.4 ($T_{0.2}$), 2MASS J15031961 + 2525196 ($T_{0.5}$), SDSS J162414.37 + 002915.6 ($T_{0.6}$), and 2MASS J04151954 - 0935066 ($T_{0.8}$). All spectra are normalized at 9250 Å and plotted on a linear scale, with constant additive offsets indicated by dotted lines.

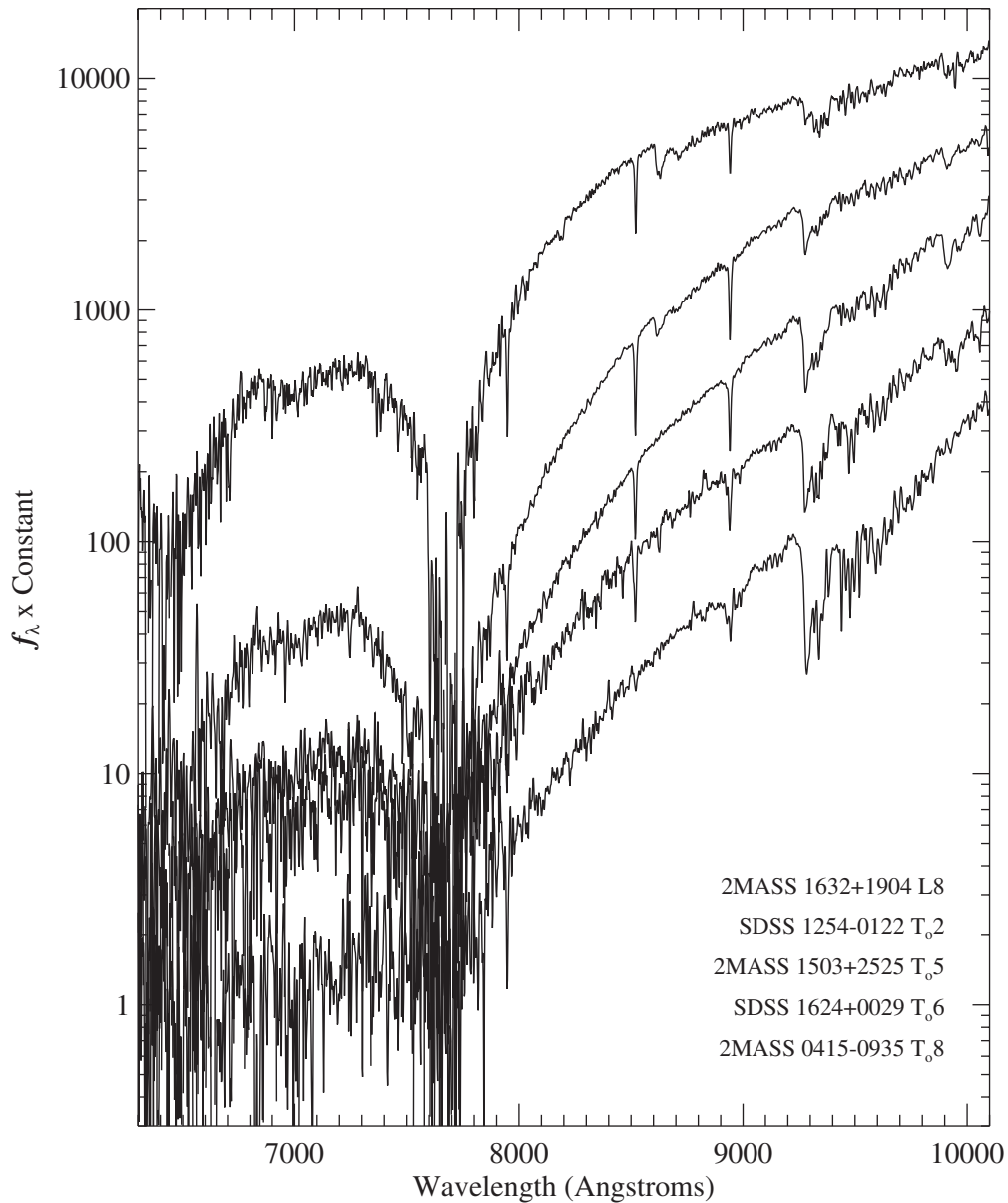


Figure 10.20 Same as Figure 10.19, but with spectra shown on a logarithmic scale. Data are normalized at 9250 Å and offset by a constant factor.

permits simultaneous examination of steep spectral slopes with weaker molecular and atomic features. The coarse sampling of the standard grid implies that intermediate types are generally limited to integer subclasses, as opposed to the half-integer subclass resolution of the near-infrared scheme. Nevertheless, Figure 10.21 illustrates how such intermediate types can be readily distinguished. Note that the current absence of standards between types L8 and T₀.2 implies even

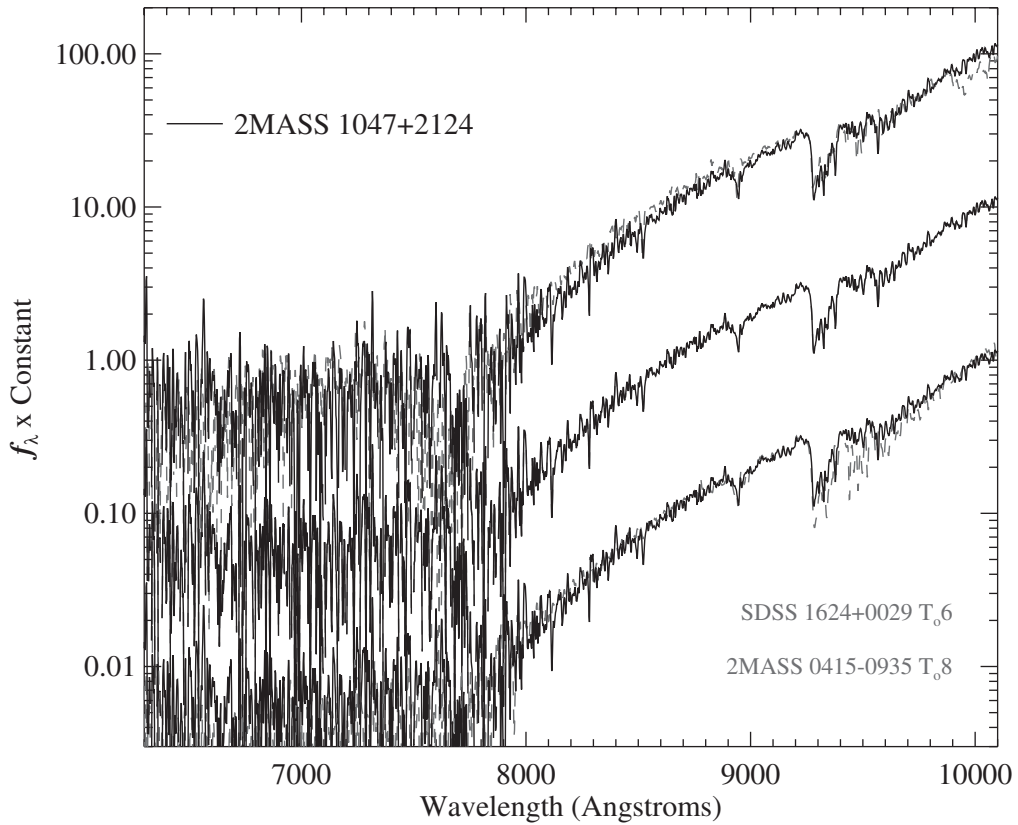


Figure 10.21 An example of red-optical spectral classification via direct comparison. The black lines trace data for the T_{6.5} (near-infrared classification) 2MASS J10475385 + 2124234, and are compared to the T_{0.6} and T_{0.8} optical standards (top and bottom grey dashed lines, respectively). All spectra are initially normalized at 9200 Å and offset by a constant factor. Note how 2MASS J10475385 + 2124234 has a steeper red-optical slope and weaker 9896 Å FeH absorption as compared to the T_{0.6} standard, but weaker 9250 Å H₂O absorption as compared to the T_{0.8} standard. This comparison justifies its intermediate T_{0.7} optical classification.

coarser sampling across the L dwarf/T dwarf transition, a situation that remains to be remedied.

10.5.3.2 Spectral Indices

As with the near-infrared data, spectral indices can provide a useful means of estimating spectral subtypes, particularly for noisy data. Burgasser et al. (2003b) identified five spectral indices useful for this purpose that are listed in Table 10.7. The CsI(A) index is essentially identical to an index defined by Kirkpatrick et al. (1999), measuring the strength of the 8521 Å Cs I line. The H₂O index samples the 9250 Å band, which is particularly strong for the latest spectral subtypes. This index can be affected by telluric absorption, although it has been defined to avoid

Table 10.7 T-Dwarf Spectral Classification Indices in the Red-Optical

Index	Numerator (Å)	Denominator (Å)	Feature Measured
CsI(A)	$\langle F_{8496.1-8506.1} \rangle + \langle F_{8536.1-8546.1} \rangle$	$2 \times \langle F_{8516.1-8526.1} \rangle$	8521 Å Cs I
H ₂ O	$\int F_{9220-9240}$	$\int F_{9280-9300}$	9250 Å H ₂ O
CrH(A)	$\int F_{8560-8600}$	$\int F_{8610-8650}$	8611 Å CrH
FeH(B)	$\int F_{9855-9885}$	$\int F_{9905-9935}$	9896 Å FeH
Color-e	$\langle F_{9140-9240} \rangle$	$\langle F_{8400-8500} \rangle$	Spectral Slope

Note: $\langle F_{\lambda_1-\lambda_2} \rangle$ denotes the average flux density and $\int F_{\lambda_1-\lambda_2}$ the integrated flux measured over the wavelength range λ_1 to λ_2 .

Table 10.8 Classification Index Values for Optical Spectral Standards

Object	SpT	CsI(A)	CrH(A)/H ₂ O	FeH(B)	Color-e
2MASS J16322911 + 1904407	L8	1.70	1.02	1.11	1.88
SDSSp J125453.90 – 012247.4 ^a	T ₀ 2	2.01	0.78	1.13	4.02
2MASS J15031961 + 2525196	T ₀ 5	1.77	0.63	1.37	4.24
SDSSp J162414.37 + 002915.6	T ₀ 6	1.68	0.47	1.15	3.83
2MASS J04151954 – 0935066 ^a	T ₀ 8	1.19	0.25	0.94	4.20

^a Measured from combined spectrum averaged over multiple epochs.

the strongest absorption longward of 9300 Å (Stevenson 1994). The CrH(A) index measures the strength of the 8611 Å CrH band which disappears around type T₀2, after which the index essentially measures spectral slope. Burgasser et al. (2003b) combine the H₂O and CrH(A) indices into a “super-ratio,” CrH(A)/H₂O, to extend its use across the full range of subtypes. The FeH(B) index measures the 9896 Å Wing–Ford band which, as discussed above, exhibits complex behavior. Finally, the Color-e index measures the red spectral slope due to K I absorption, but is defined at longer wavelengths than the Color-d (Kirkpatrick et al. 1999) or PC3 (Martín et al. 1999) indices because of the absence of detectable flux shortward of 8000 Å in many of the spectra.

Ratio values for the four T-dwarf spectral standards and the L8 standard 2MASS J16322911 + 1904407 are listed in Table 10.8, while trends for the full observed optical sample are shown in Figure 10.22. Of the four classification indices defined by Burgasser et al. (2003b), only the CrH(A)/H₂O ratio shows the clearest trend with spectral type, with excellent correlation across the range of spectral types shown. CsI(A) and Color-e appear sufficient to segregate T dwarfs from late-type L dwarfs, but trends within the T spectral class are not obvious. Color-e in particular appears to “saturate” in the late-type T dwarfs, although there is at least one clear outlier, the peculiar T6 2MASS J09373487 + 2931409 (Burgasser et al. 2002c; see below). The FeH(B) index shows unusual behavior, related in large part to the reappearance and disappearance of this feature in the early- and mid-type T dwarfs, and is useful only for segregating the late-type T dwarfs. Nevertheless, despite these less than optimal trends, Burgasser et al. (2003b) were able to derive

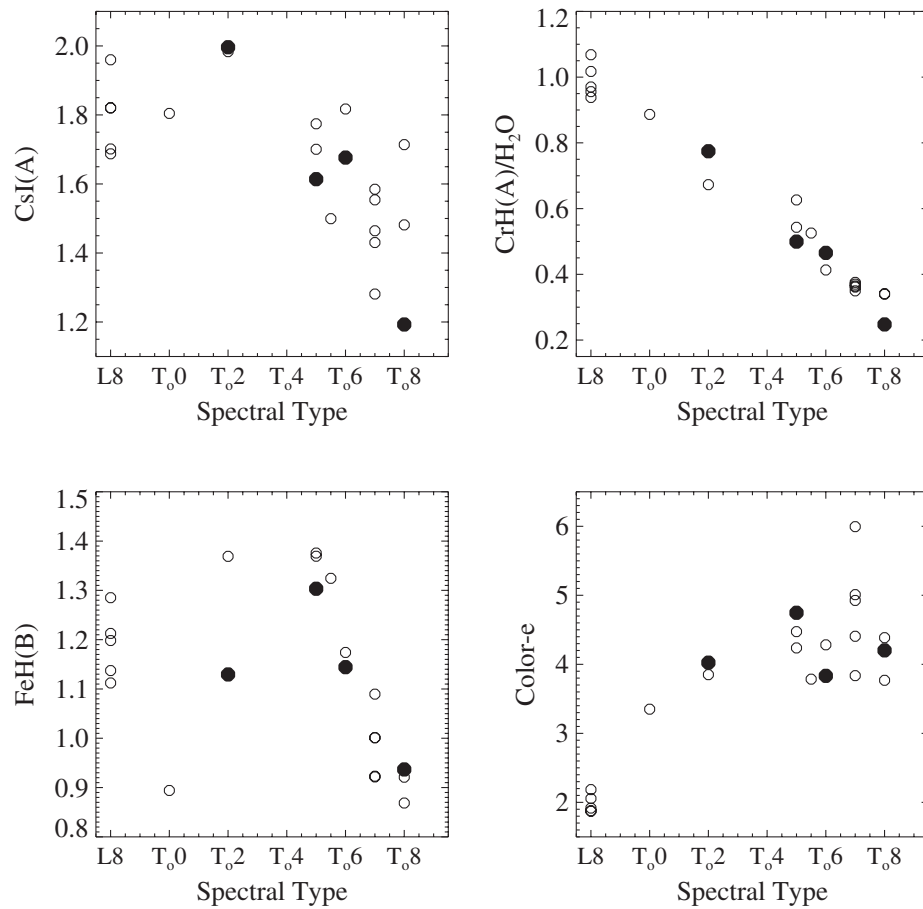


Figure 10.22 Optical spectral index values versus optical spectral type for 17 T dwarfs from Burgasser et al. (2003b) and five L8 dwarfs from Kirkpatrick et al. (1999, 2000). Standards are indicated by the solid circles, all others by open circles.

spectral type estimates for source by comparing indices to the standard values, finding agreements with the direct comparison classifications to within ~ 1 sub-type.

10.5.4 Comparison to Near-Infrared Classification

The optical types inferred for the sources in the Burgasser et al. (2003b) study are largely consistent with their near-infrared classifications, within the 1 sub-type formal uncertainty of the optical scheme. This indicates that optical and near-infrared spectral morphologies for T dwarfs are well correlated, unlike the situation for L-dwarf optical and near-infrared types where differences of several subclasses are seen (Geballe et al. 2002; Knapp et al. 2004; see §9.3.2). The disagreements in the L-dwarf regime are largely attributed to condensate cloud effects

(Knapp et al. 2004; Burgasser et al. 2007a), so the agreement between optical and near-infrared types in the T-dwarf regime may stem from the depletion of photospheric condensates in the latter.

However, agreement is not universal. One important case in point is the bright T dwarf SDSSp J042348.57 – 041403.5, classified T0 in the near-infrared (Geballe et al. 2002) but L7.5 in the optical (Cruz et al. 2003). While this was initially seen as a problem for stitching together the L- and T-dwarf classes at red-optical wavelengths, it is now known that SDSSp J042348.57 – 041403.5 is a binary likely composed of L6.5 and T2 components (Burgasser et al. 2005). The disagreement therefore arises in the dominance of the L-dwarf primary at optical wavelengths and the T dwarf secondary at near-infrared wavelengths. Other systems with divergent optical and near-infrared types have similarly been identified as binaries or binary candidates (Cruz et al. 2004; Burgasser et al. 2006b; Burgasser 2007c, see §10.7.1). Future optical spectroscopic studies of the earliest T dwarfs will aid in delineating the transition between the L and T classes in the spectral band in which the L dwarfs are defined.

10.6 MID-INFRARED CLASSIFICATION

10.6.1 Spectroscopic Observations of T Dwarfs at Mid-Infrared Wavelengths

While T dwarfs are exceedingly faint at wavelengths shortward of the near-infrared waveband, they are well-detected at longer wavelengths, particularly in the 4–10 μm mid-infrared region (Figure 10.4). However, this spectral region is notoriously difficult to observe from the ground due to strong telluric absorption and thermal backgrounds. Spectral observations in this region from the ground are relatively sparse, limited primarily to 3–5 μm studies of a handful of notable sources, including the prototype T dwarf Gliese 229B (Noll, Geballe, & Marley 1997; Oppenheimer et al. 1998), the bright T4.5 dwarf 2MASS J05591914 – 1404488 (Burgasser 2001; Cushing, Rayner, & Vacca 2005), the T2 dwarf SDSSp J125453.90 – 012247.4 (Cushing, Rayner, & Vacca 2005), and the latest-type T dwarf (currently known) 2MASS J04151954 – 0935066 (Saumon et al. 2007). However, the launch of the *Spitzer Space Telescope* in 2003 (Werner et al. 2004), with instrumentation sensitive over 3.5 to 160 μm , has provided an opportunity to explore the mid-infrared properties of cool dwarf stars and brown dwarfs. In particular, the Infrared Spectrograph (IRS; Houck et al. 2004) has enabled the first mid-infrared spectroscopic studies of T dwarfs.

Initial observations of the bright, nearby, early-type T-dwarf binary ϵ Ind Ba/Bb with IRS produced the first detection of the 10.5 μm NH_3 band in the spectrum of a brown dwarf (Roellig et al. 2004, see Figure 10.4). This was followed by a comprehensive investigation of M, L, and T dwarfs with IRS by Cushing et al. (2006), including the first spectroscopic sequences of these sources in the mid-infrared. The remainder of this section is devoted to reviewing the findings of this study as it pertains to T-dwarf classification.

Table 10.9 T-Dwarf Spectral Ratios in the Mid-Infrared

Index	Numerator (μm)	Denominator (μm)	Feature Measured
IRS-H ₂ O	$\langle F_{6.125-6.275} \rangle$	$0.562 \langle F_{5.725-5.875} \rangle + 0.474 \langle F_{6.675-6.825} \rangle$	6–6.5 μm H ₂ O bands
IRS-CH ₄	$\langle F_{9.925-10.075} \rangle$	$\langle F_{8.425-8.575} \rangle$	7.65 μm CH ₄ band
IRS-NH ₃	$\langle F_{9.925-10.075} \rangle$	$\langle F_{10.725-10.875} \rangle$	10.5 μm NH ₃ band

Note: Indices as defined in Cushing et al. (2006). $\langle F_{\lambda_1-\lambda_2} \rangle$ denotes the average flux density measured over the wavelength range λ_1 to λ_2 .

10.6.2 Characteristics of Mid-Infrared Classification Data

The 11 T-dwarf sample examined by Cushing et al. (2006) (including data from Roellig et al. 2004) was observed using the “Short-Low” mode of the *Spitzer* IRS instrument, which provides low resolution ($\lambda/\Delta\lambda \approx 90$) spectroscopy over the range 5.3–15.3 μm . This is the most efficient spectroscopic mode of IRS, so any forthcoming T-dwarf data obtained with this instrument are likely to have the same spectral coverage and resolution (e.g., Saumon et al. 2007; however, see Mainzer et al. 2007).

Figure 10.23 shows a sequence of the T-dwarf spectra obtained by Cushing et al. (2006), including two of the near-infrared spectral standards, SDSSp J125453.90 – 012247.4 (T2) and SDSSp J162414.37 + 002915.6 (T6). These spectra are dominated by three molecular absorbers: H₂O over 6–6.5 μm , CH₄ at 7.65 μm , and NH₃ at 10.5 μm . As with their near-infrared equivalents, the H₂O and CH₄ bands increase in strength with later type, although the latter begins to overwhelm the former in the latest-type T dwarfs. NH₃ is faintly present at T0 and strengthens considerably through the sequence shown. These three bands therefore appear to map out a sequence that is qualitatively consistent with the near-infrared classifications.

10.6.3 Spectral Indices

To quantify the trends observed in the spectral sequence shown in Figure 10.23, Cushing et al. (2006), defined three indices to measure the relative strengths of the primary H₂O, CH₄, and NH₃ molecular bands. These indices are listed in Table 10.9 and illustrated in the spectrum of 2MASS J05591914 – 1404488 in Figure 10.24. Note that the indices are defined in an inverse manner to those listed above for near-infrared and optical data; namely, stronger absorption leads to larger index values.

Figure 10.25 illustrates how the mid-infrared indices vary with spectral type across the entire M-, L-, and T-dwarf sequence. Focusing on the T dwarfs (where types shown are based on near-infrared classifications), it is seen that the IRS-H₂O index provides a poor discriminant of spectral type, due largely to the competing influence of CH₄ absorption at the long wavelength side of this feature. Both IRS-CH₄ and IRS-NH₃, however, show clear increases with later spectral type starting

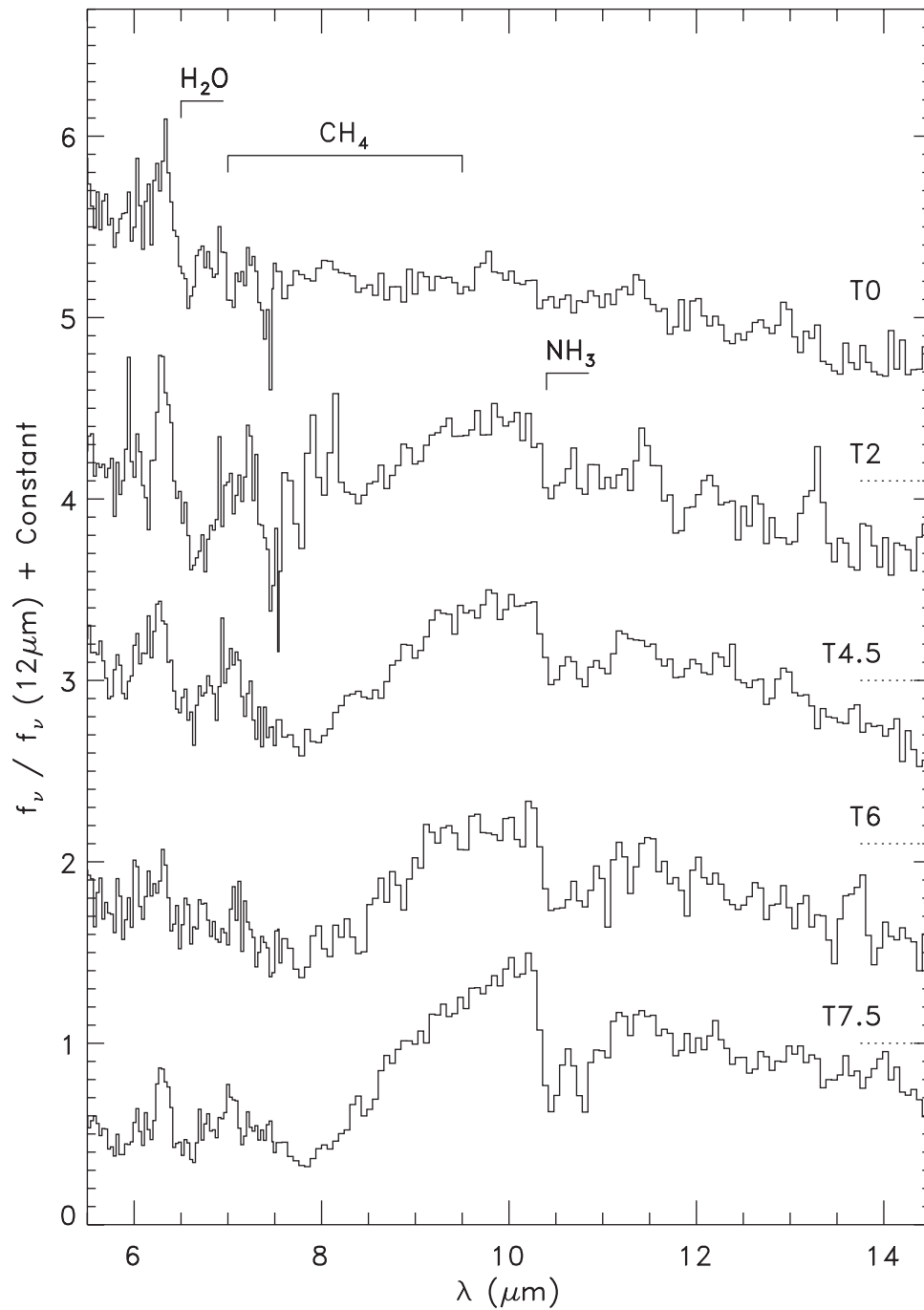


Figure 10.23 A sequence of T-dwarf spectra in the 5.5–14.5 μm range, based on data from Cushing et al. (2006). Sources shown are (from top to bottom): SDSSp J042348.57 – 041403.5 (T0), SDSSp J125453.90 – 012247.4 (T2), 2MASS J05591914 – 1404488 (T4.5), SDSSp J162414.37 + 002915.6 (T6), and Gliese 570D (T7.5). Spectra are normalized at 12 μm and offset by constants (dotted lines) (reproduced from Cushing et al. 2006 with permission of the AAS).

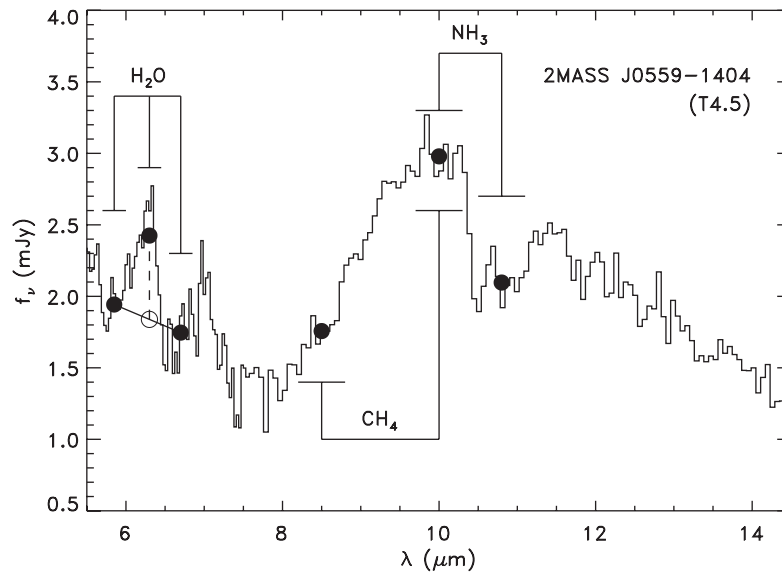


Figure 10.24 Location of mid-infrared spectral indices defined in Table 10.9 on the IRS spectrum of 2MASS J05591914 – 1404488 (reproduced from Cushing et al. 2006 with permission of the AAS).

at the end of the L-dwarf sequence, with the NH_3 index appearing to be nearly linear with type across the entire T sequence.

Despite the clear delineation of mid-infrared features and spectral indices with near-infrared spectral type, Cushing et al. (2006) did not pursue the prospect of mid-infrared classification any further in their study. Yet, the ingredients for defining a mid-infrared sequence are nevertheless in place. Future work toward this aim should include the observation of additional spectral standards—preferably those sources that comprise the near-infrared standard sequence—and an examination of how significant spectral differences are in the mid-infrared between the near-infrared standards.

The *Spitzer* cryogen reserve is expected to be depleted by 2008, rendering IRS unusable. However, the Mid-Infrared Instrument (MIRI), planned to be implemented on the James Webb Space Telescope, will provide similar spectral capabilities to IRS ($\lambda/\Delta\lambda \approx 100$ over 5–10 μm). Hence, future studies of T dwarfs, including the classification of distant sources, are likely to benefit from the well-defined sequence constructed from IRS data.

10.7 ADDITIONAL CONSIDERATIONS FOR T-DWARF CLASSIFICATION

The one-dimensional T-dwarf classification scheme outlined in §10.4 broadly encapsulates the gross spectral variations observed in these sources, in particular the correlated H_2O and CH_4 bands and overall trends in broadband color. In addition, the sequence defined shows reasonable correlation with fundamental parameters,

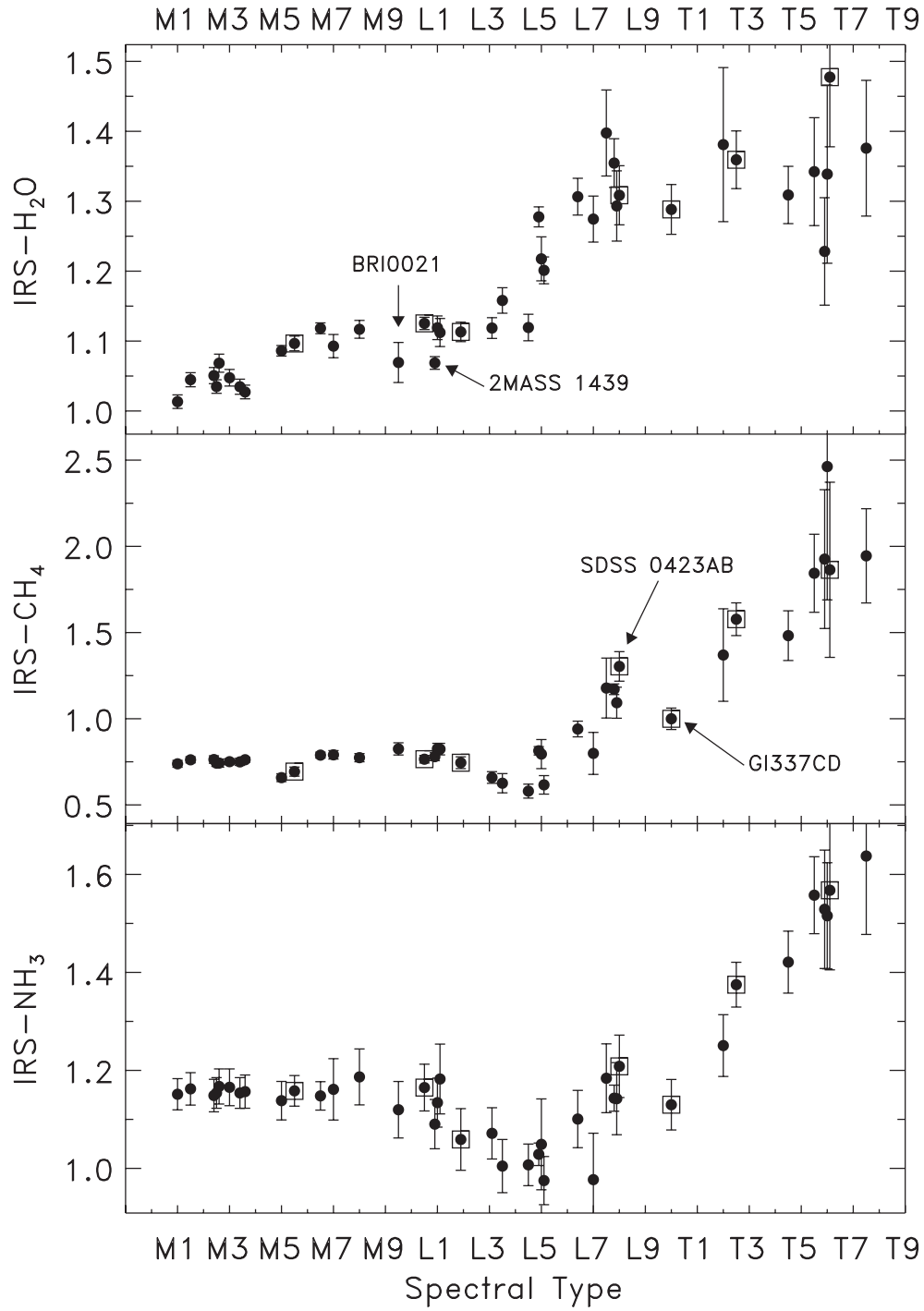


Figure 10.25 From top to bottom, variation in $\text{IRS-H}_2\text{O}$, IRS-CH_4 , and IRS-NH_3 mid-infrared indices with spectral type. The H_2O index appears to be a poor discriminant of spectral type for T dwarfs, while the other two indices show excellent monotonic trends, increasing with later spectral type. Known binaries are highlighted by open squares (reproduced from Cushing et al. 2006 with permission of the AAS).

including absolute brightness and T_{eff} , at least for the mid- and late-type T dwarfs. However, peculiar T dwarfs, whose spectra do not appear to conform to the smooth sequence defined by the standards, have been identified (e.g., Figure 10.12); and certain spectral traits, such as the relative brightness between the 1.6 and 2.1 μm flux peaks, show variations that are uncorrelated with spectral type (Knapp et al. 2004; Burgasser et al. 2006a). These secondary effects likely arise from three primary sources: unresolved multiplicity, surface gravity/metallicity effects, and condensate cloud effects, which are considered here in turn.

10.7.1 Unresolved Multiplicity

Roughly 20% of field brown dwarfs observed at high-angular resolution are resolved into binary systems (e.g., Bouy et al. 2003; Close et al. 2003; Burgasser et al. 2007b), including the T dwarfs. This number is certainly a lower limit to the true binary fraction, as an unknown percentage of binaries may be too closely separated to be resolved (e.g., Maxted & Jeffries 2005; Burgasser 2007c). If the two components of such a system have differing spectral types, the combined light spectrum can appear to be a blend of the two component spectra scaled by their relative brightness, and as such may appear peculiar.

Multiplicity-induced spectral peculiarities are most often discerned amongst the early-type T dwarfs, due to several converging factors. First, the transition between the L- and T-dwarf classes encompasses a dramatic shift in near-infrared spectral morphology, with the emergence of strong CH_4 bands and a shift toward bluer near-infrared colors. Moreover, this transition appears to occur over a narrow range of absolute brightness and effective temperature (Figures 10.17 and 10.18) allowing later-type secondaries to contribute significantly to the combined light spectrum. The flattening of the near-infrared brightness relation is likely related to the apparent rapidity of the transition between the L and T classes, as traced by shallow luminosity and T_{eff} trends (Golimowski et al. 2004; Vrba et al. 2004). Population simulations based on these trends indicate a substantial decrease in the space density of (single) early-type T dwarfs as compared to late-type L and mid-type T dwarfs (Burgasser 2007b). As a result, a large fraction ($\sim 40\%$ observed) of early-type T dwarfs are in fact L-dwarf/T-dwarf or T-dwarf/T-dwarf binaries (Liu et al. 2006; Burgasser et al. 2006b), exhibiting peculiar combined-light spectral morphologies.

Figure 10.12 illustrates an example of one such L-dwarf/T-dwarf binary, 2MASS J05185995 – 2828372 (Cruz et al. 2004). The near-infrared spectrum of this source was noted as peculiar due to the presence of CH_4 absorption at 1.1 and 1.6 μm but not at 2.2 μm (L9 dwarfs show the opposite behavior). Its H_2O bands are also unusually weak for a source with CH_4 absorption, and the overall near-infrared spectral energy distribution is redder than the early T-dwarf standards. 2MASS J05185995 – 2828372 has been resolved in HST observations, and the relative magnitudes are marginally consistent with an L-dwarf/T-dwarf binary (Burgasser et al. 2006b). Other early-type T dwarfs exhibiting peculiar spectra,

including sources with highly divergent optical and near-infrared spectral classifications (e.g., §10.5.4), have also been successfully resolved (Burgasser et al. 2005, 2006b; Liu et al. 2006; Reid et al. 2006b) and/or reproduced as the combined light of an L-dwarf/T-dwarf binary (Burgasser 2007c).

The apparently high frequency of binaries amongst early-type T dwarfs is problematic with regards to the definition of the standard sequence. Two sources originally considered as early-type standards (the T0 SDSSp J042348.57 – 041403.5 and the T3 SDSS J102109.69 – 030420.1) were both resolved as unequal-brightness binaries (Burgasser et al. 2006b). Could one or more of the current T-dwarf spectral standards be an unresolved binary as well? Ongoing high-angular resolution imaging studies, including use of ground-based adaptive optics systems, are underway for those sources not yet observed, and several groups have begun high-resolution spectroscopic studies to look for closely separated binaries (e.g., McLean et al. 2007). Furthermore, as the sample of T dwarfs with parallax measurements increases, it may be possible to weed out any overluminous binary contaminants that may be present. Fortunately, this problem does not appear to be significant for the later-type T dwarfs, which have a lower resolved binary fraction ($\sim 20\%$) and steeper spectral-type/absolute-magnitude relations, implying that unseen companions with different spectral characteristics are both more rare and less likely to contaminate the spectrum of the primary.

10.7.2 Surface Gravity and Metallicity Effects

Variations in the near-infrared spectral features of T dwarfs are generally synchronized with spectral type; later subtypes exhibit both stronger H_2O and CH_4 bands and bluer near-infrared colors. However, slight deviations from these trends are nevertheless seen amongst apparently single sources, and are readily apparent when one directly compares sources with similar spectral types. Figure 10.26 illustrates this effect with one of the first T dwarfs noted as peculiar, the T6 dwarf 2MASS J09373487 + 2931409 (Burgasser et al. 2002c). The spectrum of this source is consistent with the T6 standard in the J- and H-bands, but there are notable discrepancies at the 1.05 and 2.1 μm peaks, where 2MASS J09373487 + 2931409 is 10% brighter and 40% fainter, respectively. The weak emission at K-band is responsible for the unusually blue near-infrared colors of this source, with $J - K_s = -0.62 \pm 0.13$ as compared to the typical $J - K_s \approx 0$ color of mid- to late-type T dwarfs (Burgasser et al. 2002c; Vrba et al. 2004). The red-optical spectrum of 2MASS J09373487 + 2931409 also exhibits the steepest spectral slope from 0.8–1.0 μm amongst all T dwarfs observed at these wavelengths (Burgasser et al. 2003b).

The weak K-band emission of this source has been attributed to enhanced collision-induced H_2 absorption in an unusually high pressure photosphere. CIA H_2 opacity (κ) arises from kinematic perturbations, and is therefore enhanced in higher-pressure photospheres, scaling roughly as $\kappa \propto P$. Similarly, Burgasser, Burrows, & Kirkpatrick (2006) have argued that the bright 1.05 μm peak and

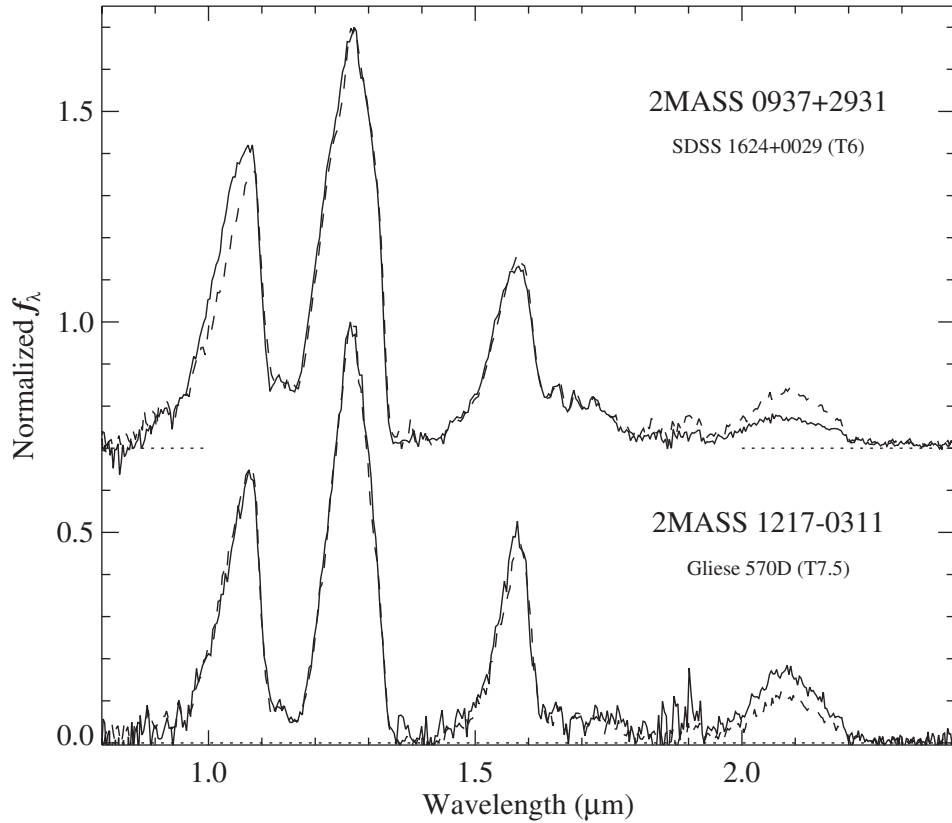


Figure 10.26 Low-resolution near-infrared spectra of the peculiar T dwarfs 2MASS J09373487 + 2931409 (top) and 2MASS J12171110 – 0311131 (bottom, solid lines) overlain on the spectra of the T6 standard SDSSp J162414.37 + 002915.6 and T7.5 companion brown dwarf Gliese 570D (dashed lines). Spectra are normalized at $1.27\ \mu\text{m}$. Note the discrepancies at the 1.05 and $2.1\ \mu\text{m}$ flux peaks.

steep red-optical spectral slope of 2MASS J09373487+2931409 may be related to changes in the pressure-broadened (and hence pressure-sensitive) wings of the $0.77\ \mu\text{m}$ K I doublet (see also Burrows & Volobuyev 2003). Photospheric gas pressure varies with both the surface gravity (g) and mean opacity (κ_R), scaling as $dP/d\tau \approx P/\tau \approx g/\kappa_R$, where $\tau = 2/3$ is the photospheric optical depth. Hence, an older and more massive brown dwarf (increased g) and a metal-poor brown dwarf (reduced κ) both exhibit signatures of enhanced photospheric gas pressure. Indeed, analysis by Burgasser et al. (2003b); Knapp et al. (2004); and Burgasser, Burrows, & Kirkpatrick (2006) all indicate that 2MASS J09373487 + 2931409 may have both a higher surface gravity *and* a slight metal-deficiency.

Several other sources have also been reported to share the same spectral peculiarities as 2MASS J09373487+2931409, suggesting that they too may be older and/or metal-poor brown dwarfs (Burgasser et al. 2004b; Knapp et al. 2004; Burgasser, Burrows, & Kirkpatrick 2006; Liebert & Burgasser 2007). In addition, a

handful of T dwarfs are suspected of having low surface gravities and/or metal-rich atmospheres, based on their relatively bright K-band peaks. Examples include the T7.5 HD 3651B (Luhman et al. 2006; Mugrauer et al. 2006), a wide brown dwarf companion to an old ($\sim 3\text{--}12$ Gyr, Valenti & Fischer 2005), and metal-rich star ($[\text{Fe}/\text{H}] = 0.12 \pm 0.04$, (Santos, Israelian, & Mayor 2004)). Independent analyses by Burgasser (2007a) and Liu et al. (2007) conclude that the high metallicity of this source (assuming coevality) compensates for the increased H_2 absorption from its probably high surface gravity. Another source, 2MASS J12171110 – 0311131 Burgasser et al. (1999), also shows a bright K-band peak, and while originally believed to be a low surface gravity object (Knapp et al. 2004; Burgasser, Burrows, & Kirkpatrick 2006) may in fact also be metal-rich (Saumon et al. 2007). Finally, there is the case of the young-cluster brown dwarf candidate S Ori 053810.1 – 203626 (S Ori 70; Zapatero Osorio et al. 2002; Martín & Zapatero Osorio 2003), a potential planetary-mass object (2–8 Jupiter masses) whose red near-infrared colors lend support to a low-gravity interpretation. However, spectroscopic evidence of this remains controversial (Burgasser et al. 2004a).

While analyses such as these have revealed much about the physical properties of T dwarfs, the spectral peculiarities found in sources such as 2MASS J09373487 + 2931409 also indicate how T-dwarf classification is likely to evolve from its current one-dimensional sequence to a multi-dimensional system common to hotter stellar classes. Roughly, these morphological dimensions may map to physical parameters such as temperature, surface gravity, and/or metallicity, although these mappings need not be one-to-one or consistent through the entire sequence. Defining additional classification dimensions must wait for new examples of T dwarfs with consistent spectral peculiarities that may serve as appropriate standards.

10.7.3 Condensate Clouds and Temporal Variations

Condensates strongly influence the near-infrared spectra of L dwarfs and early-type T dwarfs, but appear to be largely absent in mid- and late-type T-dwarf photospheres (e.g., Tsuji et al. 1996; Allard et al. 2001). The depletion of condensates is believed to play a significant role in the transition between the L- and T-dwarf classes (Ackerman & Marley 2001; Burgasser et al. 2002c; Tsuji & Nakajima 2003), although the mechanism for this depletion remains under considerable debate (Burgasser et al. 2002b; Knapp et al. 2004; Tsuji 2005). The composition and abundance of condensate dust species, and the thickness, density, and surface distribution of condensate cloud structures (Ackerman & Marley 2001) are likely to be complex functions of T_{eff} , surface gravity, metallicity, rotation, and other parameters (e.g., Helling et al. 2001; Lodders 2002; Woitke & Helling 2003); hence, substantial spectral variations among dust-dominated sources might be expected.

Such spectral variations may include temporal variations of condensate-sensitive spectral features, including the 1.05 and $1.27\text{ }\mu\text{m}$ spectral flux peaks (Ackerman & Marley 2001). Such variations are relevant to the stability of

the spectral standards. While a number of studies have measured photometric variability of up to 0.5 mag in a handful of T dwarfs (e.g., Enoch, Brown, & Burgasser 2003; Koen 2003, 2004; Koen et al. 2005), only one T dwarf has been monitored for spectral variations to date, conveniently the T6 spectral standard SDSSp J162414.37 + 002915.6 (Nakajima et al. 2000). The spectral variations observed, of the order of a few percent in the H₂O bands, were sufficiently small that no change in the overall classification of this source would have been discerned. However, more work is needed, particularly for the early-type T dwarfs in which condensate clouds play a more important role in determining the spectral energy distribution.

10.8 BEYOND THE T DWARFS

The classification schemes for T dwarfs discussed in this chapter so far encompass the full range of spectral morphologies observed for the currently known population, extending down to $T_{\text{eff}} \approx 700$ K (Golimowski et al. 2004; Vrba et al. 2004; Saumon et al. 2007). Yet the T dwarfs observed today will eventually cool further still, while lower mass brown dwarfs with comparable ages have already evolved to have lower temperature photospheres (indeed, such objects may be more plentiful than T dwarfs; see Burgasser 2004; Allen et al. 2005). How do we incorporate these objects into the current classification scheme? Defining new T subtypes is one possibility, with the requirement that these subtypes follow the same spectral trends as the currently defined T class, namely progressively stronger bands of H₂O and CH₄ in the near-infrared, and/or progressively stronger NH₃ at mid-infrared wavelengths. As the near-infrared bands are already near saturation in the spectra of T8 dwarfs (e.g., Figure 10.8, although Leggett et al. 2007b suggest that the weaker CH₄ band at 1.00–1.03 μm may be a useful indicator for dwarfs cooler than 700 K), it is possible that the number of additional *readily distinguishable* T subtypes may be limited, and later T subtypes may encompass much broader T_{eff} intervals. However, there is no *a priori* reason that T subtypes could not extend to T10 and beyond, as is the case for the M giant sequence (Chapter 8).

On the other hand, if the near-infrared spectral features of a cold brown dwarf discovery were significantly and systematically different from those examined here, a new spectral class, already referred to in the literature as the Y dwarf class (e.g., Kirkpatrick 2005), would be required. How will these spectra differ? Theoretical atmosphere models predict several effects, including the emergence of distinct NH₃ bands at 1.5, 1.95, 3, and 4 μm below $T_{\text{eff}} \sim 600$ K (in addition to the 10.5 μm band already observed), the disappearance of the strong pressure-broadened Na I and K I doublets below $T_{\text{eff}} \sim 500$ K, the condensation of H₂O vapor around 400–500 K, and the gradual transition to red near infrared spectral energy distributions around 300–400 K (Burrows, Sudarsky, & Lunine 2003). Any of these near-infrared spectral transitions could result in a clear spectromorphological break between the T and (putative) Y spectral classes. Such a break may also be detected in spectral regions other than the near-infrared, where T dwarf

classification is currently performed, just as T dwarfs are distinguished from optical classified L dwarfs by near-infrared CH_4 bands. Mid-infrared features, such as the 3 and 4 μm NH_3 bands or broad H_2 features beyond 10 μm , may ultimately distinguish the Y class (Saumon et al. 1994; Burrows, Sudarsky, & Lunine 2003). However, Leggett et al. (2007b) point out that at least down to $T_{\text{eff}} \sim 500$ K detector sensitivities are such that obtaining a near-infrared spectrum remains much more practical than obtaining a similar S/N mid-infrared spectrum.

Until examples of these cold brown dwarfs are actually identified, delineating the end of the T dwarf class is largely an exercise in speculation. Yet near-term wide-field near-infrared and mid-infrared sky surveys conducted with *Spitzer*, the UKIRT Infrared Deep Sky Survey (UKIDSS; Dye et al. 2006), and the Wide-Field Infrared Survey Explorer (WISE; Duval et al. 2004) may soon uncover such objects, necessitating yet another addition (and chapter!) to the MK spectral sequence.

The author of this chapter would like to thank Michael Cushing, Sandy Leggett, and Dagny Looper for providing spectral data, and Sandy and Davy Kirkpatrick for helpful comments.

Bibliography

- Ackerman, A.S., & Marley, M.S. 2001, *ApJ*, 556, 872
- Allard, F., Hauschildt, P.H., Alexander, D.R., Tamanai, A., & Schweitzer, A. 2001, *ApJ*, 556, 357
- Allard, N.F., Allard, F., Hauschildt, P.H., Kielkopf, J.F., & Machin, L. 2003, *AA*, 411, L473
- Allard, N.F., Spiegelman, F., & Kielkopf, J.F. 2007, *AA*, 465, 1085
- Allen, P.R., Koerner, D.W., Reid, I.N., & Trilling, D.E. 2005, *ApJ*, 625, 385
- Artigau, É, Doyon, R., Lafrenière, D., Nadeau, D., Robert, J., & Albert, L. 2006, *ApJ*, 651, L57
- Artigau, É, Nadeau, D., & Doyon, R. 2003, in *Brown Dwarfs*, Proceedings of IAU Symposium 211, ed. E. Martín (ASP: San Francisco), p.451
- Baraffe, I., Chabrier, G., Barman, T., Allard, F., & Hauschildt, P.H. 2003, *AA*, 382, 563
- Becklin, E.E., & Zuckerman, B. 1988, *Nature*, 336, 656
- Borysow, A., Jørgensen, U.G., & Zheng, C. 1997, *AA*, 324, 185
- Bouy, H., Brandner, W., Martín, E.L., Delfosse, X., Allard, F., & Basri, G. 2003, *AJ*, 126, 1526
- Burgasser, A.J. 2001, Ph.D. Thesis, California Institute of Technology
- Burgasser, A.J. 2004, *ApJS*, 155, 191
- Burgasser, A.J. 2007a, *ApJ*, 658, 617
- Burgasser, A.J. 2007b, *ApJ*, 659, 655
- Burgasser, A.J. 2007c, *AJ*, submitted
- Burgasser, A.J., Burrows, A., & Kirkpatrick, J.D. 2006, *ApJ*, 639, 1095
- Burgasser, A.J., Geballe, T.R., Leggett, S.K., Kirkpatrick, J.D., & Golimowski, D.A. 2006a, *ApJ*, 637, 1067
- Burgasser, A.J., Kirkpatrick, J.D., Burrows, A., Liebert, J., Reid, I.N., Gizis, J.E., McGovern, M.R., Prato, L., & McLean, I.S. 2003a, *ApJ*, 592, 1186
- Burgasser, A.J., Kirkpatrick, J.D., Cruz, K.L., Reid, I.N., Leggett, S.K., Liebert, Burrows, A., & Brown, M.E. 2006b, *ApJ*, 637, 1067
- Burgasser, A.J., Kirkpatrick, J.D., Liebert, J., & Burrows, A. 2003b, *ApJ*, 594, 510
- Burgasser, A.J., Kirkpatrick, J.D., McElwain, M.W., Cutri, R.M., Burgasser, A.J., & Skrutskie, M.F. 2003c, *AJ*, 125, 850
- Burgasser, A.J., Kirkpatrick, J.D., McGovern, M.R., McLean, I.S., Prato, L., & Reid, I.N. 2004a, *ApJ*, 604, 827
- Burgasser, A.J., Kirkpatrick, J.D., Reid, I.N., Brown, M.E., Miskay, C.L., & Gizis, J.E. 2003d, *ApJ*, 586, 512

- Burgasser, A.J., Kirkpatrick, J.D., Reid, I.N., Liebert, J., Gizis, J.E., & Brown, M.E. 2000a, *AJ*, 120, 473
- Burgasser, A.J., Liebert, J., Kirkpatrick, J.D., & Gizis, J.E. 2002a, *AJ*, 123, 2744
- Burgasser, A.J., Looper, D.L., Kirkpatrick, J.D., Cruz, K.L., & Swift, B. 2007a, *ApJ*, submitted
- Burgasser, A.J., Marley, M.S., Ackerman, A.S., Saumon, D., Lodders, K., Dahn, C.C., Harris, H.C., & Kirkpatrick, J.D. 2002b, *ApJ*, 571, L151
- Burgasser, A.J., McElwain, M.W., Kirkpatrick, J.D., Cruz, K.L., Tinney, C.G., & Reid, I.N. 2004b, *AJ*, 127, 2856
- Burgasser, A.J., Reid, I.N., Leggett, S.J., Kirkpatrick, J.D., Liebert, J., & Burrows, A. 2005, *ApJ*, 634, L177
- Burgasser, A.J., Reid, I.N., Siegler, N., Close, L.M., Allen, P., Lowrance, P.J., & Gizis, J.E. 2007b, in *Planets and Protostars V*, eds. B. Reipurth, D. Jewitt, and K. Keil (Tucson: Univ. Arizona Press), p. 427
- Burgasser, A.J., et al. 1999, *ApJ*, 522, L65
- Burgasser, A.J., et al. 2000b, *AJ*, 120, 1100
- Burgasser, A.J., et al. 2002c, *ApJ*, 564, 421
- Burrows, A., Marley, M.S., & Sharp, C.M. 2000, *ApJ*, 531, 438
- Burrows, A., & Sharp, C.M. 1999, *ApJ*, 512, 843
- Burrows, A., Sudarsky, D., & Hubeny, I. 2006, *ApJ*, 640, 1063
- Burrows, A., Sudarsky, D., & Lunine, J.I. 2003, *ApJ*, 596, 587
- Burrows, A., & Volobuyev, M. 2003, *ApJ*, 583, 985
- Burrows, A., et al. 1997, *ApJ*, 491, 856
- Chabrier, G., & Baraffe, I. 1997, *AA*, 327, 1039
- Close, L.M., Siegler, N., Freed, M., & Biller, B. 2003, *ApJ*, 587, 407
- Cooper, C.S., Sudarsky, D., Milson, J.A., Lunine, J.I., & Burrows, A. 2003, *ApJ*, 586, 1320
- Cruz, K.L., Burgasser, A.J., Reid, I.N., & Liebert, J., 2004, *ApJ*, 604, L61
- Cruz, K.L., Reid, I.N., Liebert, J., Kirkpatrick, J.D., & Lowrance, P.J. 2003, *AJ*, 126, 2421
- Cuby, J.G., Saracco, P., Moorwood, A.F.M., D'Odorico, S., Lidman, C., Comerón, F., & Spyromilio, J. 1999, *AA*, 349, L41
- Cushing, M.C., Rayner, J.T., & Vacca, W.D. 2005, *ApJ*, 623, 1115
- Cushing, M.C., et al. 2006, *ApJ*, 648, 614
- Dahn, C.C., et al. 2002, *AJ*, 124, 1170
- Dick, K.A., & Fink, U. 1977, *J. Quant. Spectrosc. Radiat. Trans.*, 18, 433
- Duval, V.G., Irace, W.R., Mainzer, A.K., & Wright, E.L. 2004, *SPIE*, 5487, 101
- Dye, S., et al. 2006, *MNRAS*, 372, 1227
- Enoch, M.L., Brown, M.E., & Burgasser, A.J. 2003, *AJ*, 126, 1006
- ESA, 1997, *The Hipparcos and Tycho Catalogues*, ESA SP-1200
- Fegley, B., & Lodders, K. 1996, *ApJ*, 472, L37
- Geballe, T.R., Kulkarni, S.R., Woodward, C.E., & Sloan, G.C. 1996, *ApJ*, 467, 101
- Geballe, T.R., et al. 2002, *ApJ*, 564, 466

- Golimowski, D.A., et al. 2004, *AJ*, 127, 3516
- Hawley, S.L. et al. 2002, *AJ*, 123, 3409
- Helling, C., Oevermann, M., Lüttke, M.J.H., Klein, R., & Sedlmayr, E. 2001, *AA*, 376, 194
- Houck, J.R. 2004, *ApJS*, 154, 18
- Kirkpatrick, J.D. 2005, *ARAA*, 43, 195
- Kirkpatrick, J.D., Henry, T.J., & McCarthy, D.W., Jr. 1991, *ApJS*, 77, 417
- Kirkpatrick, J.D., Kelly, D.M., Rieke, G.H., Liebert, J., Allard, F., & Wehrse, R. 1993, *ApJ*, 402, 643
- Kirkpatrick, J.D., Reid, I.N., Liebert, J., Gizis, J.E., Burgasser, A.J., Monet, D.G., Dahn, C.C., Nelson, B., & Williams, R.J. 2000, *AJ*, 120, 447
- Kirkpatrick, J.D., et al. 1999, *ApJ*, 519, 802
- Knapp, G., et al. 2004, *ApJ*, 127, 3553
- Koen, C. 2003, *MNRAS*, 346, 473
- Koen, C. 2004, *MNRAS*, 354, 378
- Koen, C., Tanabé, T., Tamura, M., & Kusakabe, N. 2005, *MNRAS*, 362, 727
- Leggett, S.K., Marley, M.S., Freedman, R., Sauman, D., Liu, M.C., Geballe, T.R., Golimowski, D.A., & Stephens, D.C. 2007, *ApJ*, in press (astrop-ph/0705.2602)
- Leggett, S.K., Saumon, D., Marley, M.S., Geballe, T.R., Golimowski, D.A., Stephens, D., & Fan, X. 2007, *ApJ*, 655, 1079
- Leggett, S.K., et al. 2000, *ApJ*, 536, L35
- Leggett, S.K., et al. 2002b, *ApJ*, 564, 452
- Liebert, J., & Burgasser, A.J. 2006, *ApJ*, 655, 522
- Liebert, J., Reid, I.N., Burrows, A., Burgasser, A.J., Kirkpatrick, J.D., & Gizis, J.E. 2000, *ApJ*, 533, L155
- Liu, M.C., Leggett, S.K., & Chiu, K. 2007, *ApJ*, 660, 1507
- Liu, M.C., Leggett, S.K., Golimowski, D.A., Chiu, K., Fan, X., Geballe, T.R., Schneider, D.P., & Brinkmann, J. 2006, *ApJ*, 647, 1393
- Liu, M.C., Wainscoat, R., Martín, E.L., Barris, B., & Tonry, J. 2002, *ApJ*, 568, L107
- Lodders, K. 1999, *ApJ*, 519, 793
- Lodders, K. 2002, *ApJ*, 577, 974
- Looper, D.L., Kirkpatrick, J.D., & Burgasser, A.J. 2007, in preparation
- Luhman, K.L., et al. 2006, *ApJ*, in press
- Magazzu, A., Martín, E.L., & Rebolo, R. 1993, *ApJ*, 404, L17
- Mainzer, A.K. et al. 2007, in press
- Marley, M.S., Saumon, D., Guillot, T., Freedman, R.S., Hubbard, W.B., Burrows, A., & Lunine, J.I. 1996, *Science*, 272, 1919
- Martín, E.L., Delfosse, X., Basri, G., Goldman, B., Forveille, T., & Zapatero Osorio, M.R. 1999, *AJ*, 118, 2466
- Martín, E.L., & Zapatero Osorio, M.R. 2003, *ApJ*, 593, L113
- Matthews, K., Nakajima, T., Kulkarni, S.R., & Oppenheimer, B.R. 1996, *AJ*, 112, 1678
- Maxted, P.F.L., & Jeffries, R.D. 2005, *MNRAS*, 326, L45

- Mayor, M., & Queloz, D. 1995, *Nature*, 378, 355
- McCaughrean, M., Close, L.M., Scholz, R.-D., Lenzen, R., Biller, B., Brandner, W., Hartung, M., & Lodieu, N. 2004, *AA*, 413, 1029
- McLean, I.S., Graham, J.R., Becklin, E.E., Figer, D.F., Larkin, J.E., Levenson, N.A., & Teplitz, H.I. 2000, *SPIE*, 4008, 1048
- McLean, I.S., McGovern, M.R., Burgasser, A.J., Kirkpatrick, J.D., Prato, L., & Kim, S. 2003, *ApJ*, 596, 561
- McLean, I.S., Prato, L., McGovern, M.R., Burgasser, A.J., Kirkpatrick, J.D., Rice, E.L., & Kim, S.S. 2007, *ApJ*, 658, 1217
- McLean, I.S., et al. 1998, *SPIE*, 3354, 566
- Mugrauer, M., Seifahrt, A., Neuhäuser, R., & Mazeh, T. 2006, *MNRAS*, in press
- Nakajima, T., Oppenheimer, B.R., Kulkarni, S.R., Golimowski, D.A., Matthews, K., & Durrance, S.T. 1995, *Nature*, 378, 463
- Nakajima, T., Tsuji, T., Tamura, M., & Yamashita, T. 2000, *PASJ*, 52, 87
- Neugebauer, G., & Leighton, R.B. 1969, *Two-Micron Sky Survey, A Preliminary Catalogue* (Washington: NASA)
- Noll, K.S., Geballe, T.R., & Marley, M.S. 1997, *ApJ*, 489, L87
- Oke, J.B., et al. 1995, *PASP*, 107, 375
- Oppenheimer, B.R., Kulkarni, S.R., Matthews, K., & Nakajima, T. 1995, *Science*, 270, 1478
- Oppenheimer, B.R., Kulkarni, S.R., Matthews, K., & van Kerkwijk, M.H. 1998, *ApJ*, 502, 932
- Rayner, J.T., Toomey, D.W., Onaka, P.M., Denault, A.J., Stahlberger, W.E., Vacca, W.D., Cushing, M.C., & Wang, S. 2003, *PASP*, 155, 362
- Rebolo, R., Martín, E.L., & Magazzu, A. 1992, *ApJ*, 389, L83
- Reid, I.N., Kirkpatrick, J.D., Gizis, J.E., Dahn, C.C., Monet, D.G., Williams, R.J., Liebert, J., & Burgasser, A.J. 2000, *AJ*, 119, 369
- Reid, I.N., Lewitus, E., Cruz, K.L., & Burgasser, A.J. 2006b, *ApJ*, 639, 1114
- Roellig, T.L., et al. 2004, *ApJS*, 154, 418
- Santos, N.C., Israelian, G., & Mayor, M. 2004, *AA*, 415, 1153
- Saumon, D., Bergeron, P., Lunine, J.I., Hubbard, W.B., & Burrows, A. 1994, *ApJ*, 424, 333
- Saumon, D., Marley, M.S., Cushing, M.C., Leggett, S.K., Roellig, T.L., Lodders, K., & Freedman, R.S. 2006, *ApJ*, 647, 552
- Saumon, D., et al. 2007, *ApJ*, 656, 1136
- Scholz, R.-D., McCaughrean, M.J., Lodieu, N., & Kuhlbrodt, B. 2003, *AA*, 398, L29
- Simons, D.A., & Tokunaga, A.T. 2002, *PASP*, 114, 169
- Skrutskie, M.F., et al. 1997, in *The Impact of Large-Scale Near-IR Sky Surveys*, ed. F. Garzon (Dordrecht: Kluwer), p. 25
- Skrutskie, M.F., et al. 2006, *AJ*, 131, 1163
- Stevenson, C.C. 1994, *MNRAS*, 267, 904
- Strauss, M.A., et al. 1999, *ApJ*, 522, L61
- Tinney, C.G., Burgasser, A.J., & Kirkpatrick, J.D. 2003, *AJ*, 126, 975

- Tokunaga, A.T., Simons, D.A., & Vacca, W.D. 2002, *PASP*, 114, 180
- Tsuji, T. 1964, *Ann. Tokyo Astron. Obs. Ser. II*, 9, 1
- Tsuji, T. 2005, *ApJ*, 621, 1033
- Tsuji, T., & Nakajima, T. 2003, *ApJ*, 585, L151
- Tsuji, T., Ohnaka, K., & Aoki, W. 1999, *ApJ*, 520, L119
- Tsuji, T., Ohnaka, K., Aoki, W., & Nakajima, T. 1996, *AA*, 308, L29
- Tsvetanov, Z.I., et al. 2000, *ApJ*, 531, L61
- Valenti, J.A., & Fischer, D.A. 2005, *ApJS*, 159, 141
- Vrba, F.J., et al. 2004, *AJ*, 127, 2948
- Weck, P.F., Schweitzer, A., Kirby, K., Hauschildt, P.H., & Stancil, P.C. 2004, *ApJ*, 613, 567
- Werner, M.W. 2004, *ApJS*, 154, 1
- Woitke, P., & Helling, C. 2003, *AA*, 339, 297
- Wright, G.S., Mountain, C.M., Bridger, A., Daly, P.N., Griffin, J.L., & Ramsay-Howat, S.K. 1993, *Proc. SPIE*, 1946, 547
- York, D.G., et al. 2000, *AJ*, 120, 1579
- Zapatero Osorio, M.R., Béjar, V.J.S., Martí, E.L., Rebolo, R., Barrado y Navascuès, D., Mundt, R., Eislöffel, J., & Caballero, J.A. 2002, *ApJ*, 578, 536
- Zapatero Osorio, M.R., Martín, E.L., Bouy, H., Tata, R., Deshpande, R., & Wainscoat, R.J. 2006, *ApJ*, 647, 1405

Chapter Eleven

Wolf–Rayet Stars and the Luminous Blue Variables

11.1 THE WOLF–RAYET STARS

The Wolf–Rayet stars are hot, luminous stars whose spectacular spectra are dominated by emission lines formed in a massive stellar wind. They are the evolved descendants of the most massive stars of the main sequence, namely the O-type stars. The minimum mass a star must have to be a Wolf–Rayet progenitor is about $25 M_{\odot}$, but a typical Wolf–Rayet star has a mass in the range $10\text{--}25 M_{\odot}$. The discrepancy is due to the massive winds of both the Wolf–Rayet stars and their progenitors, with mass loss rates in the Wolf–Rayet stars on the order of $10^{-5} M_{\odot} \text{ yr}^{-1}$. This wind is optically thick over the optical and ultraviolet parts of the spectrum, and thus the bizarre spectra of these stars are characterized by broad, strong emission lines superimposed on a weak but hot continuum. This continuum is actually formed in the wind (Crowther 2007) and thus photospheric features are not visible in the spectra of single Wolf–Rayet stars. Various evolutionary paths lead to and through the Wolf–Rayet phase, but almost all of these stars (probably) end their lives in a supernova explosion. There are two sequences of Wolf–Rayet stars—the nitrogen sequence (WN) and the carbon sequence (WC); the winds of these stars are enriched chemically by the products of the CNO cycle (hydrogen burning) in the case of the WN stars, and the triple- α process (helium burning) in the case of the WC stars. Thus even though the Wolf–Rayet stars are exceedingly rare, they are important in the chemical enrichment of the interstellar medium and also play important roles in the energetics of the interstellar medium.

11.1.1 History

In 1867, two French astronomers, Charles Wolf and Georges Rayet, using a visual spectroscope, discovered three faint emission-line stars in the constellation of Cygnus. According to the description of Wolf and Rayet, the spectra of those three stars (HD 191765, HD 192103, and HD 192641) were characterized by several bright bands (i.e. broad emission lines) superimposed on a continuous background (Wolf & Rayet 1867). Some years later Vogel (Vogel 1883) noted that the blue band in HD 191765 was displaced slightly to the red relative to the other two stars discovered by Wolf and Rayet. This was the first indication that the Wolf–Rayet stars actually fall into two main classes, the WN (nitrogen-strong) and the WC (carbon-strong) stars, although identification of the ions responsible for the prominent emission lines in the Wolf–Rayet stars had to wait for the analysis of Edlén (1932). In the original HD classification scheme, Wolf–Rayet stars were

included in type O. Indeed, in that scheme, all O-type stars (except for the Oe5 stars) were emission-line stars, and class O was divided into 5 groups, Oa, Ob, Oc, Od, and Oe. Most of the stars that were classified in the first three groups are now recognized as Wolf–Rayet stars (Cannon & Pickering 1901).

The modern era in the study and classification of the Wolf–Rayet (WR) stars began with the work of Carlye Beals, an astronomer at the Dominion Astrophysical Observatory. Although not the first to recognize the existence of two sequences of WR stars, Beals certainly played the major role in establishing a spectral classification system for these stars based on that fact. He wrote, in a letter to the editor of the *Observatory*:

A noteworthy advance in our understanding of Wolf-Rayet spectra has recently been made by Edlen, who successfully identified a majority of the emission bands of hitherto unknown origin with the highly ionized atoms of oxygen, nitrogen and carbon. The existence of two parallel sequences of Wolf-Rayet spectra... seems to be established beyond reasonable doubt by the new identifications, which indicate one group of spectra containing bands due to C III, C IV, O IV, O V and possibly O VI, to the exclusion of nitrogen, and a separate group containing nitrogen in various stages of ionization to the exclusion of oxygen and carbon. He I and He II are common to both groups, which... may be referred to as the carbon sequence and the nitrogen sequence respectively (Beals 1933).

Beals (1934, 1938) followed this letter with papers outlining in detail a classification system for the WR stars, including division of the WC stars into subclasses 6–8, and 5–8 for the WN stars. This classification system formed the foundation for the Smith (1968) classification system, which is still used, at least in some form, for the classification of the WR stars today. Hiltner & Schild (1966) presented a modified Beals classification system that divided the WN stars into two parallel sequences—the WN-A stars and the WN-B stars—based on emission-line widths. They recognized that many of the narrow-line WN-A stars are binaries. The Smith (1968) system, however, has been much more widely used. Unfortunately, the classification of the WR stars is in somewhat of a state of flux at the present time, as a number of revisions and refinements of the Smith (1968) classification scheme have been proposed, but none of these has been universally adopted. However, the Smith, Shara, & Moffat (1996) system (a modification of the WN classification scheme of Smith 1968) is widely used, and this system is treated in some detail in §11.1.2.2. There are two current schemes for the classification of the WC stars, but fortunately both give similar spectral types.

It should be stated at the outset that devising a classification system based solely on emission lines presents problems entirely different from those encountered by the MK system, which is based on photospheric lines. As mentioned above, the emission-line spectrum of a WR star originates entirely in the stellar wind, and so the spectrum depends not only on the temperature and luminosity of the underlying

star, but also on the mass-loss rate, the wind velocity law, and a number of other factors that will be discussed later in this chapter. So, it is perhaps not surprising that the WR classification systems are still in a state of flux, as astronomers sort through the complex phenomenology of these stars!

Many new avenues for the classification of the WR stars have opened through the availability of spectra in the ultraviolet and the far ultraviolet, and the ability to observe WR stars in other galaxies as well as toward the Galactic center. A recent wide-ranging review of the WR stars is given by Crowther (2007), and an up-to-date catalog of WR stars is available both in print (van der Hucht 2001) and online.¹

11.1.2 The Optical Classification of Wolf–Rayet Stars

11.1.2.1 The Smith 1968 System

Both the Beals (1938) and the Smith (1968) classification systems were based on photographic spectra, and both are one-dimensional systems, classifying the WR stars on the basis of ionization. In the Beals system the most important classification criterion for establishing the ionization class, for both the WN and the WC stars, was the ratio He I $\lambda 5875$ /He II $\lambda 5412$. In the WN stars, ratios of lines of nitrogen ions to lines of He II were also important. Smith (1968), however, pointed out that WR stars with otherwise identical spectra could have very different helium-line strengths, and in some cases the helium lines could be so weak as to make the use of the He I/He II ratio difficult to use. As a consequence, Smith (1968) proposed a revision to the WR classification system in which the ionization class was determined largely by ratios of blends of N III, N IV, and N V for the WN stars, and ratios of C III, C IV, and O V for the WC stars. While the Smith 1968 system has been largely supplanted by the Smith et al. 1990 and 1996 systems, there is an extensive literature based upon the earlier scheme, and so we present it in some detail below.

THE WN STARS

On the Smith 1968 system, the classification of the WN stars is based on a judgment of which ionization state of nitrogen predominates in the spectrum. The following lines and blends of nitrogen are used to make that judgment:

N III: $\lambda 4634$ – $\lambda 4641$ (blend), $\lambda 5314$

N IV: $\lambda 3479$ – $\lambda 3484$ (blend), $\lambda 4057$

N V: $\lambda 4603$, $\lambda 4619$, $\lambda 4933$ – $\lambda 4944$ (blend)

The criteria based on these features are summarized in Table 11.1.

¹<http://cdsweb.u-strasbg.fr/viz-bin/Cat?III/215>; see addendum.txt which gives recent discoveries of WR stars

Table 11.1 Classification Criteria for the WN Stars on the Smith 1968 System

Class	Ratios	Criteria
WN3	$N\ V \gg N\ IV$	N III absent
WN4	$N\ V \approx N\ IV$	N III very weak or absent
WN4.5	$N\ IV > N\ V$	N III very weak or absent
WN5	$N\ III \approx N\ IV \approx N\ V$	N III $\lambda\lambda 4634\text{--}41$ band present
WN6	$N\ III \approx N\ IV$	N V present but weak N III $\lambda\lambda 4634\text{--}41$ band present
WN7	$N\ III \gg N\ IV$	He I weak, N III $\lambda 4640 < \text{He II } \lambda 4686$
WN8	$N\ III \gg N\ IV$	He I strong with violet absorption edges N III $\lambda 4640 \approx \text{He II } \lambda 4686$ N III $\lambda 5314$ present

It should be noted that on this system, criteria based on helium are used only in discriminating between WN7 and WN8. This is in contrast to the Smith, Shara, & Moffat (1996) system summarized in §11.1.2.2. Figure 11.1 shows a sequence of WN stars based on the criteria listed in Table 11.1. Hamann, Koesterke, & Wessolowski (1995a) have introduced a number of minor modifications to the Smith 1968 system, including addition of an “a” to the spectral type, indicating the presence of absorption lines in a WN spectrum that have not been attributed to the presence of a companion, and the addition of a “-w” or “-s” indicating weak or strong emission lines. The “-s” is added if the equivalent width of He II $\lambda 5412$ is greater than $37\ \text{\AA}$, “-w” if it is less; the dividing point at $37\ \text{\AA}$ is somewhat arbitrary, but ensures that WR91 and WR149 fall into the strong-line group (Hamann, Koesterke, & Wessolowski 1995b).

THE WC STARS (INCLUDING CHANGES TO 1998)

The classification of the WC stars is relatively straightforward and was defined by Smith (1968) on the basis of three main criteria—the C III $\lambda 5696/\text{O V } \lambda 5590$ and C III $\lambda 5696/\text{C IV } \lambda 5808$ ratios and the width of the C III, IV $\lambda 4650$ blend. However, the definition of the WC classes, especially for the early WC classes, has tended to drift with time (see the discussion in Smith et al. 1990). Part of the reason for this is that the WC classes (likewise the WN classes) have never been defined in terms of *standards*, but rather in terms of criteria. Such criteria-based definitions should be fairly stable, but problems with the interpretation of the criteria (for instance, should the ratios be defined in terms of peak flux or equivalent widths?) and the transition from photographic to digital detectors have contributed to this drift and also to some confusion over time. A comparison of the WC spectral types in the van der Hucht catalog (van der Hucht 2001) and Smith (1968) clearly shows this drift toward earlier types. Smith et al. (1990) have gone a long way toward placing the definition of the WC classes on a firm foundation, although the classification system is not yet standards-based. Our treatment here is based on the Smith et al. 1990 system.

The Smith et al. 1990 system for the WC stars is based on two ratios of three lines, C IV $\lambda 5808$, C III $\lambda 5696$, and O V $\lambda 5590$. The two ratios are C III/O V

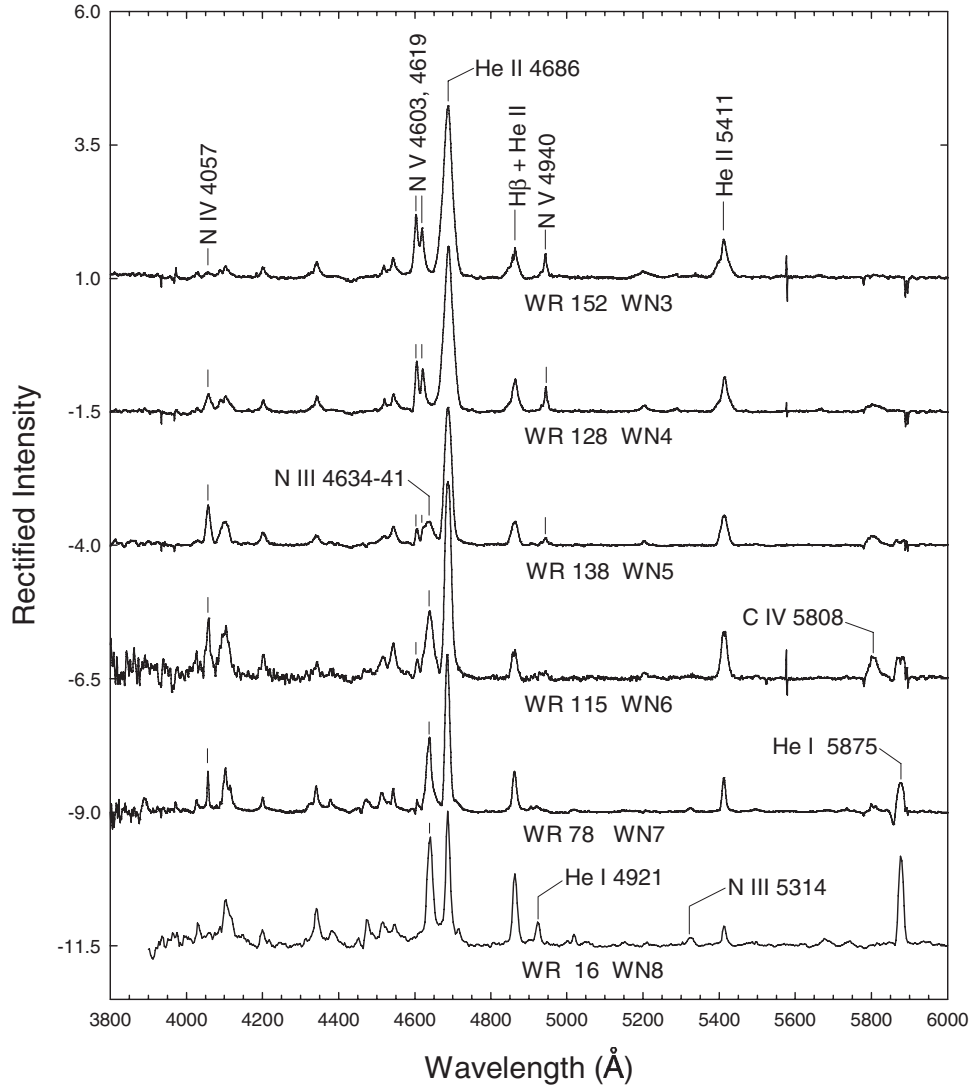


Figure 11.1 A sequence of WN stars classified on the Smith 1968 system. The line marked N V 4940 refers to the N V $\lambda\lambda 4933$ – $\lambda 4944$ blend. All of these stars are narrow-line WN stars on the Smith et al. 1996 system. On that system the spectral types are WR 152, WN3(h); WR 128, WN4(h) + OB?; WR 138, WN5 + B?; WR 115, WN6 + OB?; WR 78, WN7h; WR 16, WN8. Spectra courtesy of Hamann, Koesterke, & Wessolowski (1995a).

and C IV/C III. The definition of the WC classes is given by Smith et al. (1990) in terms of ratios of the equivalent width (or flux) and the peak flux (i.e., the flux measured at the peak of the lines relative to the continuum). The defining table for the WC classes (Table 11.2) is adapted from Smith et al. (1990).

The criteria listed in Table 11.2 require the measurement of either equivalent widths or peak fluxes, and then the calculation of ratios, but in practice, classification with similar precision can be carried out by eye (see Figure 11.2). It is clear

Table 11.2 Classification Criteria for the WC Stars on the Smith et al. 1990 System

Subclass	C IV $\lambda 5808$ /C III $\lambda 5696$		C III $\lambda 5696$ /O V $\lambda 5590$	
	log(EW or Flux)	log(Peak Flux)	log(EW or Flux)	log(Peak Flux)
WC4	> 0.6	> 0.75	< -0.05	< -0.2
WC5	> 0.6	> 0.75	-0.05 to $+0.2$	-0.2 to $+0.05$
WC6	> 0.6	> 0.75	> 0.2	> 0.05
WC7	0.1 to 0.6	0.25 to 0.75	(> 0.15)	(> 0.35)
WC8	-4.4 to 0.1	-0.25 to $+0.25$	(> 0.15)	(> 0.35)
WC9	< -0.4	< -0.25	(> 0.15)	(> 0.35)

from this figure that C III $\lambda 5696$ is weaker than O V $\lambda 5590$ in WC4 stars, the ratio of these two lines passes through unity in the WC5 class, and is greater than unity in WC6 stars. In WC7 stars and later, the O V line disappears. C IV $\lambda 5808$ is much stronger than C III $\lambda 5696$ in the early WC stars, and the ratio of these two lines passes through unity in the WC8 class. This ratio is especially sensitive to the spectral type for stars with types WC7 and later. The transition from the C III/O V ratio as the primary classification criterion to the C IV/C III ratio at about WC6 is an important feature of the Smith et al. 1990 system, and enables unambiguous classification.

Crowther et al. (1998) have proposed an alternate WC classification scheme, based largely on the C IV $\lambda 5808$ /C III $\lambda 5696$ ratio. They point out that the C III/O V ratio used by Smith et al. (1990) is subject to variations in the C/O abundances. Fortunately, their system results in only a small number of reclassifications of the Smith et al. (1990) types, but they also use their scheme to extend the WC classification system to W10 and W11 types. In the range WC8–WC11, they advocate using, as secondary criteria, the C IV $\lambda 5808$ /C II $\lambda 4267$ ratio and the He II $\lambda 4686$ /He I $\lambda 5876$ ratio. Many of these late WC (WCL) stars are, in fact, not classical high-mass Wolf–Rayet stars, but rather central stars of planetary nebulae (CSPNe). The spectral types of such stars are written enclosed in brackets, for instance, [WC10]. But, as a matter of fact, the spectra of these CSPNe are very similar to those of the massive WC stars, except that they show a greater range of line strength and widths than the massive WC stars of the same ionization class. As it turns out, the latest WC classes (WC10 and WC11) are exclusively CSPNe stars. Some CSPNe stars are WO stars (see below); these stars have, on the average, narrower C IV $\lambda 5808$ lines than the massive WO stars. [WN] stars are exceedingly rare. The central star of the planetary nebula LMC-N66 has been classified as [WN4.5]. This fascinating object was the subject of a recent study (Hamann et al. 2003). A [WN] spectral type has also been suggested for the central star of a Galactic planetary nebula (Morgan, Parker, & Cohen 2003).

THE WO STARS

Sanduleak (1971) pointed out the existence of five stars discovered in the course of an objective prism survey that show exceptionally strong O IV $\lambda 3818$ emission.

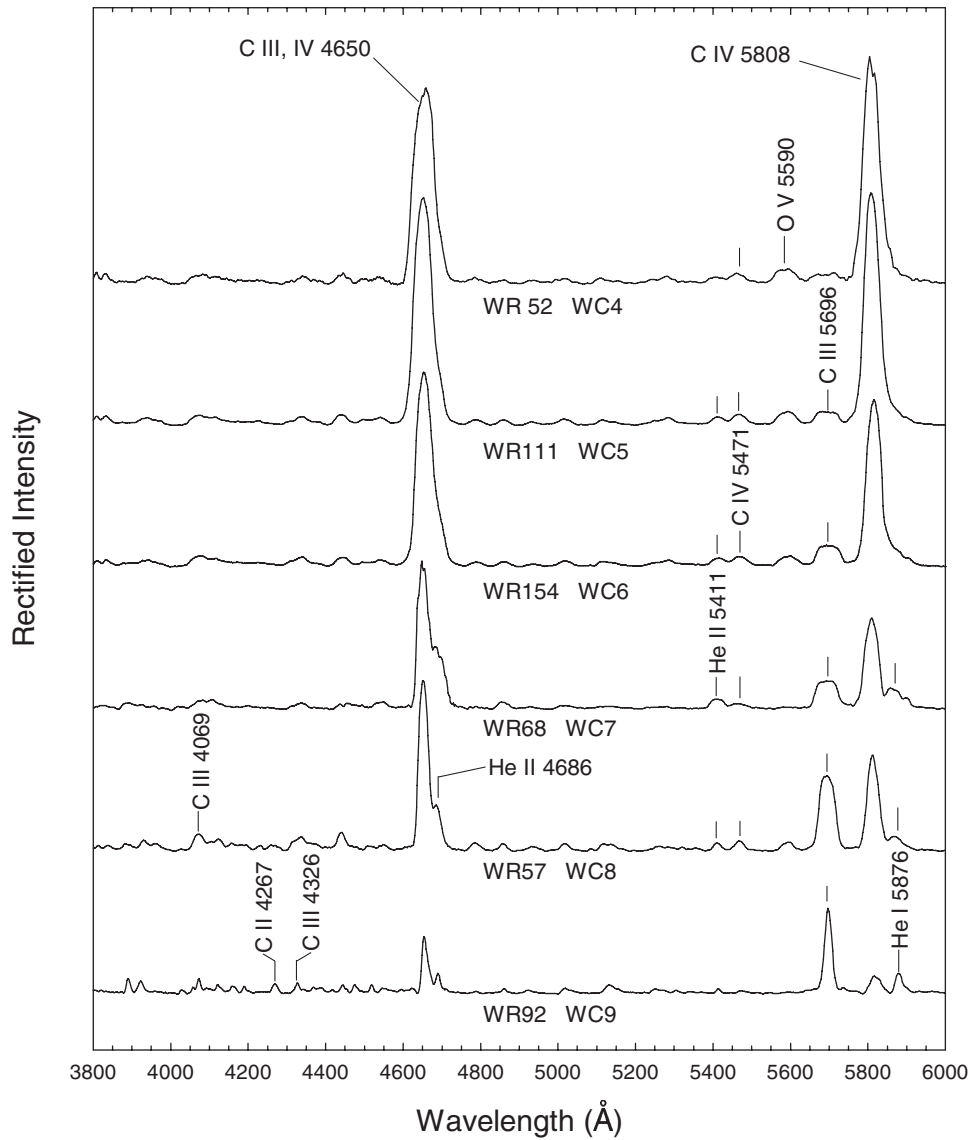


Figure 11.2 A sequence of WC stars classified on the Smith et al. 1990 system. Spectral types from van der Hucht (2001). Spectra from Torres & Massey (1987).

Barlow & Hummer (1982) suggested that four of the five should be placed in a distinct WR class (the WO stars) as lines of O IV, O V, and O VI are present, but only one ion of carbon, C IV, is represented. They argued that the abundance of oxygen is enhanced in these stars. Their proposed classification system for the WO stars was based on lines of O IV, O V, O VI, and C IV.

This system was later “quantified” by Kingsburgh, Barlow, & Storey (1995), who also changed the numbering scheme to run from WO1 to WO5. Crowther et al. (1998) introduced a revision of the WO classification system. They argued

Table 11.3 Classification Criteria for the WO Stars (Crowther et al. 1998)

Class	C IV $\lambda 5808$ FWHM(\AA)	O VI $\lambda 3818$ /O V $\lambda 5590$ $\log(W_\lambda)$ Primary criterion	O VI $\lambda 3818$ /C IV $\lambda 5808$ $\log(W_\lambda)$ Secondary criterion	O VII $\lambda 5670$ /O V $\lambda 5590$ $\log(W_\lambda)$ Additional
WO1 ¹	40 ± 10	≥ 1.1	$\geq +0.2$	≥ 0.0
WO2	160 ± 20	$+0.6$ to $+1.1$	$\geq +0.2$	≤ 0.0
WO3	90 ± 30	$+0.25$ to 0.6	-1 to $+0.2$	$\ll 0.0$
WO4	60 ± 30	-0.3 to $+0.25$	-1.5 to -1	$\ll 0.0$

To exclude O-type and weak emission line stars from the WO class, require $W_\lambda(\text{C IV } \lambda 5808) \geq 10 \text{ \AA}$ and O VI in emission.

¹WO1 also shows the presence of O VIII $\lambda 6068$.

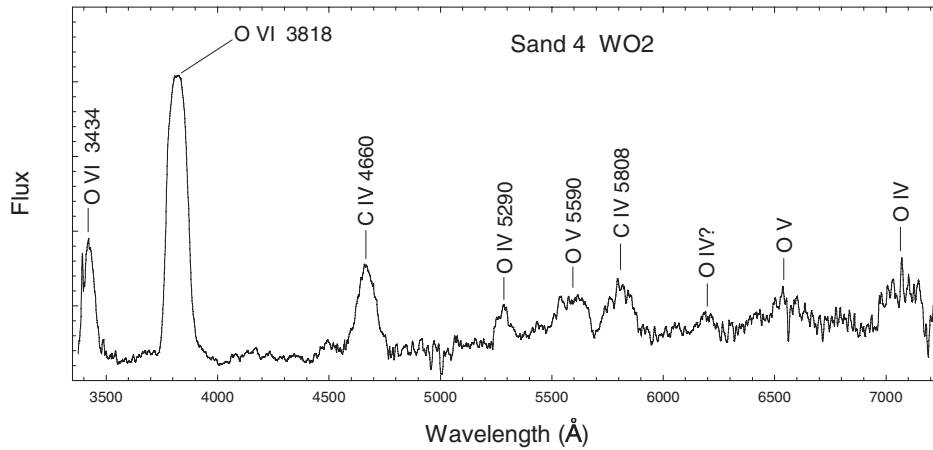


Figure 11.3 The spectrum of the WO2 star Sand 4. The identifications without wavelength labels are tentative. The red end of this spectrum is somewhat noisy. Spectrum from Torres & Massey (1987).

that the strength of the oxygen lines in WO stars is primarily a result of higher ionization, rather than dramatically increased oxygen abundances, and thus the WO stars are, in reality, the high-ionization extension of the WC class. If this is indeed the case, then it makes sense, as Crowther et al. (1998) argued, that the classification system (and the numbering scheme) for the WO stars should merge continuously with that for the WC stars. Crowther et al. proposed a numbering scheme from WO1 to WO4, with the transition from WO4 to WC4 marked by the appearance of C III $\lambda 5696$. Their classification criteria are presented in Table 11.3. Figure 11.3 illustrates the spectrum of a WO2 star.

11.1.2.2 WN Star Classification on the Smith et al. 1996 System

Classification of the WN stars on the Smith 1968 system has never been entirely satisfactory as there are a high proportion of stars that do not fit easily with the system, and thus have been deemed peculiar. There are a number of reasons for this.

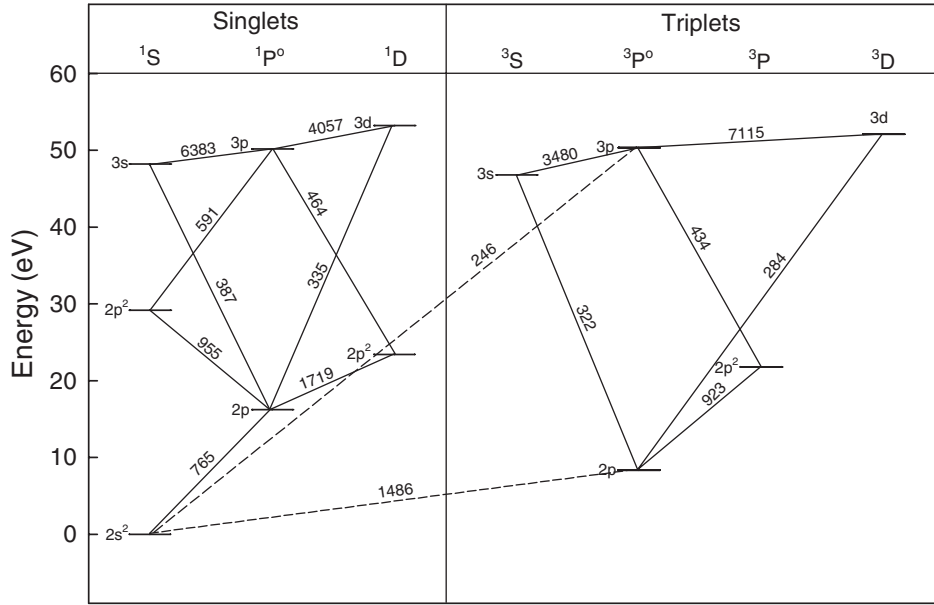


Figure 11.4 A simplified Grotrian diagram of N IV. Only the strongest permitted transitions are shown (solid lines), along with two important intercombination lines (dashed lines). Each transition is labeled with the wavelength in angstroms of the corresponding spectral line.

First, within a single ionization class, there are both narrow-line and broad-line WN stars. In the WC stars, this is not the case, as the line width is strongly correlated with the ionization class (Torres, Conti, & Massey 1986), with the caveat that there is some dependency on the metallicity. Second, from an examination of the Pickering series of He II lines, every other one of which is blended with a hydrogen line, it is clear that the H/He abundance ratio varies from star to star. Finally, the Smith 1968 system relies on ratios of N III, N IV, and N V lines to estimate the dominant ionization state, but Conti, Massey, & Vreux (1990) show that in the relationship between the strengths of the N IV $\lambda 4057$ and $\lambda 3480$ lines, both of which are important in the Smith 1968 system (and likewise for the corresponding isoelectronic transitions of C III, $\lambda 5696$ and $\lambda 4650$), there is evidence for factors other than ionization.

Factors other than ionization that can affect the strength of the nitrogen and carbon lines in the spectra of WR stars include selective excitation processes, such as dielectronic recombination and autoionization, and optical depth effects in the WR wind. For instance, Hillier (1989) and Conti, Massey, & Vreux (1990) have shown that the strength of the N IV $\lambda 4057$ line depends on the optical depth in the wind. This can be understood in the following way: the upper level of the N IV $\lambda 4057$ line is the $2s3d$ 1D state (see Figure 11.4). This state can decay either to the $2s2p$ $^1P^\circ$ state, via the $\lambda 335$ transition, or to the $2s3p$ $^1P^\circ$ state, via the $\lambda 4057$ transition. The branching ratio (A_{335}/A_{4057}) is about 280, and thus under normal

Table 11.4 The Ionization Sequence for WN Stars (Smith et al. 1996)

Class	He II $\lambda 5411$ He I $\lambda 5875$	N V $\lambda 4604$ N III $\lambda 4640$	N IV $\lambda 4057$ ¹ N V,III $\lambda\lambda 4603-41$	C IV $\lambda 5808$ He II $\lambda 5411$	C IV $\lambda 5808$ He I $\lambda 5875$
WN2	No He I	No N V	No N IV	No C IV	No C IV
WN3	> 10	No N III	< 0.1	< 0.2	both weak
WN4	$4 - 8 - 10$	> 2	0.6	$0.2 - 0.5 - 0.8$	$2 - 3 - 10?$
WN5	$1.25 - 4 - 8$	$0.5 - 1 - 2$	$1.25 - 2.5$	$0.6 - 0.8 - 2.0$	$1.5 - 2.5 - 5$
WN6	$1.25 - 2 - 4$	$0.2 - 0.3 - 0.5$	0.8	$0.3 - 0.4 - 0.6$	$0.5 - 1 - 1.5$
WN7	$0.65 - 1 - 1.25$	$0.1 - 0.15 - 0.25$	0.6	< 0.5	$0.15 - 0.3 - 0.5$
WN8	$0.1? - 0.4 - 0.65$	$0.05 - 0.17 - 0.25$	0.2	< 0.4	< 0.15
WN9	$< 0.1?$	0	$< 0.1?$		

Figures are based on Peak/Continuum values.

When a value defines an ionization class, the item is boxed; center values are typical.

¹ The peak of the N V,III 4603–41 blend is taken, regardless of which component dominates.

circumstances, the $\lambda 4057$ line is weak. But if the $\lambda 335$ line is optically thick, a greater percentage of the photon decays will take place through the $\lambda 4057$ transition, making that line stronger. The relevance of all of this to spectral classification is that the spectral morphology of the WN stars is more complicated than can be described by a single dimension based on ionization.

Smith, Shara, & Moffat (1996) have attempted to address this situation by defining a three-dimensional classification system for the WN stars. The three dimensions in their new system are (1) ionization, (2) line width, and (3) the hydrogen abundance.

THE IONIZATION DIMENSION

The ionization classification in the Smith et al. 1996 system is primarily based on the He II $\lambda 5411$ /He I $\lambda 5875$ ratio. This choice has a number of advantages. It removes primary dependence for the ionization classification from the nitrogen lines, which have been the main source of inconsistencies in the Smith 1968 system. Second, these He lines are relatively isolated and uncontaminated, and so the blending that afflicts the nitrogen-based classification is removed. But there are disadvantages. When the He II $\lambda 5411$ line is weak (peak/continuum ratio < 0.2), classification by helium fails. In such cases secondary criteria involving the nitrogen lines must be employed. These criteria (see Table 11.4) are similar to those of the Smith 1968 system, but with some changes.

In the new system, absence of He I, N III, N IV, and N V defines the earliest type, WN2. The WN3 class is distinguished from WN2 by the presence of He I, N V, very weak N IV, and the absence of N III, and from WN4 by the absence of the C IV $\lambda 5808$ line. The main way to distinguish between WN4, WN5, and WN6 on the new system (because the He II/He I ratios for these types overlap) is

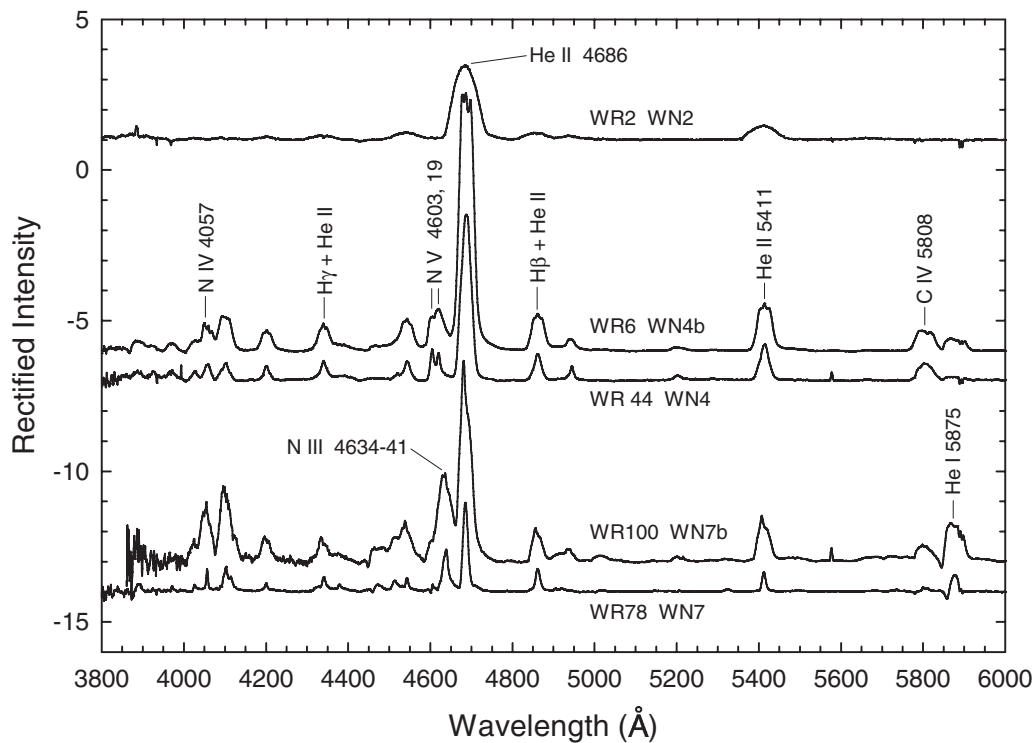


Figure 11.5 A comparison of narrow-line and broad-line WN spectra. Note the triangular profiles of the lines in the narrow-line spectra, and the more rounded profiles in the broad-line spectra, especially at WN4. Spectra courtesy of Hamann, Koesterke, & Wessolowski (1995a).

by the relative strengths of N V $\lambda 4604$ and N III $\lambda\lambda 4634-41$, as measured by the peak/continuum fluxes. In the WN5 stars, N V $\lambda 4604 \sim$ N III $\lambda\lambda 4634-41$, and the N IV $\lambda 4057$ and the C IV $\lambda 5808$ lines both peak. In the WN7 and WN8 types, the He II/He I ratio generally suffices for classification. Unlike the Smith 1968 system, the He II $\lambda 4686$ /N V,III $\lambda\lambda 4603-41$ ratio is not used as a classification criterion. This ratio turns out to be sensitive to both ionization and the initial abundance. Figure 11.1 shows a sequence of single, narrow-line WN stars.

LINE WIDTH

The Smith et al. 1996 system also includes a parameter for the line width; a “b” is appended to the spectral type for stars with FWHM He II $\lambda 4686 > 30 \text{ \AA}$ or, equivalently, when FWHM He II $\lambda 5411 > 40 \text{ \AA}$. Figure 11.5 shows some comparisons between broad and narrow-line WN stars.

HYDROGEN

The presence of hydrogen in a WN spectrum may be detected by the oscillation in the strength of the lines of the He II Pickering series caused by the blending

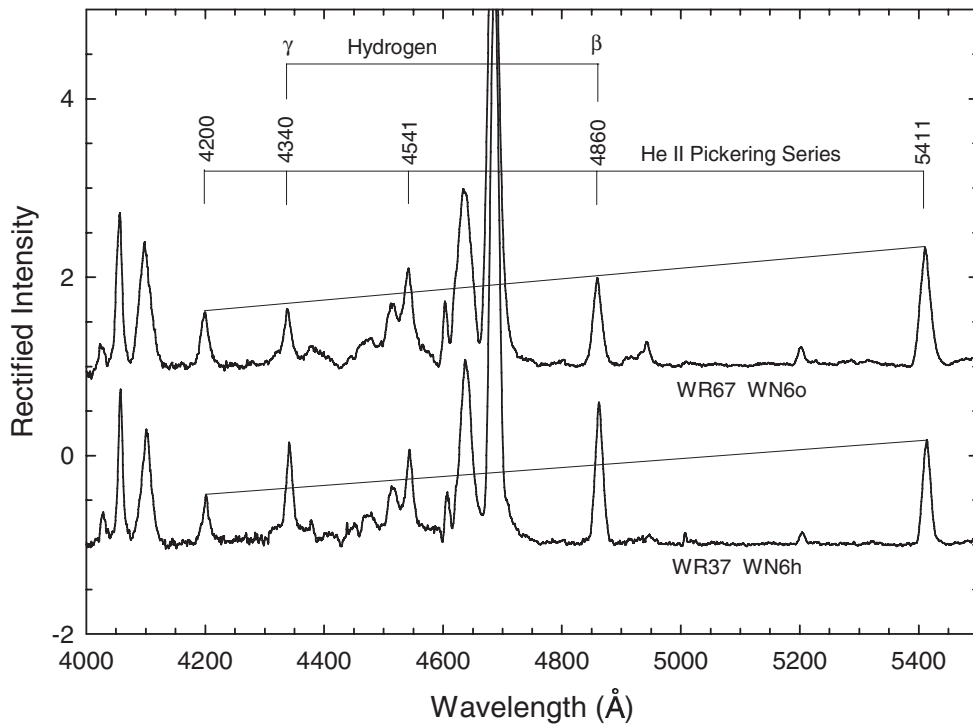


Figure 11.6 A comparison of a WN spectrum with hydrogen and one without. Notice the oscillating Pickering decrement in WR37, indicative of the presence of hydrogen. He II 4541 is blended with other lines. Spectra courtesy of Hamann, Koesterke, & Wessolowski (1995a).

of every other line with a hydrogen Balmer line (see §2.4.2). For instance, the $\lambda\lambda 4200, 4541$, and 5411 lines are pure He II lines in the Pickering series, whereas $\lambda\lambda 4340$ and 4861 are Pickering lines that may be blended with hydrogen ($H\gamma$ and $H\beta$ respectively). If the strengths of these five lines decline monotonically toward the violet, then there is no hydrogen present in the wind. An oscillating Pickering decrement, on the other hand, indicates the presence of hydrogen. Taking the peak/continuum flux, if $\lambda 4861 / (\lambda 4541 \times \lambda 5411)^{1/2} - 1 > 0.5$ (or, equivalently, if $\lambda 4340 / (\lambda 4200 \times \lambda 4541)^{1/2} - 1 > 0.5$) then an “h” should be appended to the spectral type, indicating the presence of hydrogen. If these quantities lie between 0 and 0.5, “(h)” should be appended, and if the Pickering decrement is monotonic, then an “o” (although in practice, the “o” is usually left off). Figure 11.6 shows a comparison between a WN star with and a WN star without hydrogen. WC stars show no evidence for hydrogen.

ABSORPTION LINES

Some WR stars show absorption lines. The origins of these absorption lines fall into three cases. In the first case, the absorption lines are intrinsic to the WR wind and the absorption is displaced to the violet. In the second case the absorption

lines are obviously due either to a companion (usually an O- or B-type star) or to a close optical double. But in the third case the origin of the absorption lines is undetermined. Smith et al. 1996 append an “a” to the spectral type in the first case; in all such stars, hydrogen is always present, and so “a” always appears with “h.” Thus an “ha” star has violet-shifted absorption lines with hydrogen in emission. The “ha” designation, however, is not applied to stars with fully developed WR spectra in which the emission is strong relative to the violet-shifted absorption component. Rather, a typical “ha” star has, in the specific case of the He II + H γ λ 4340 line, nearly equal absorption and emission components. In the second case, “+OB” is appended when the star is an SB2 or hydrogen absorption lines are seen. If the pair can be resolved, then the spectral type of the companion should be appended, enclosed in brackets. Occasionally, evidence for the companion does not show up, and this situation is covered by appending “(+OB)”. In the third case, in which the origin of the absorption lines is unknown, Smith et al. append “+abs.”

THE WN/C STARS

Some WN stars show abnormally strong C IV λ 5808 or C III λ 5969 lines. It is now understood (Massey & Grove 1989) that these spectra are not composites of a WN and a WC star, but rather WN stars with unusually high carbon abundances. This can be deduced from the C IV λ 5808/C IV λ 4650 ratio, which is usually much larger than is found in WC stars. Such stars are known as WN/C stars, and appear to be genuinely intermediate types. The high-excitation WN/C stars are given the designation WN/CE. How the WN/C stars fit into the WR evolutionary scheme will be discussed in §11.3.

THE EXTENSION OF THE WN SYSTEM TO WN9, WN10, AND WN11 TYPES

The WN classification system has been extended by Crowther & Smith (see, e.g., Smith, Crowther, & Prinja 1994; Crowther et al. 1995; Crowther & Smith 1997) to late (WNL) types, incorporating stars formerly classified as Ofpe/WN9 into the WN sequence. These stars can be distinguished from Of stars on the basis of the fact that the only absorption lines that appear are violet shifted P Cygni absorption troughs. In Of stars, there are always some unshifted absorption components present. The optical spectra of WNL stars are characterized by narrow P Cygni He I profiles, usually pure-emission Balmer lines, and moderate to prominent He II, N III, and Si IV emission features. N II features tend to be weak. A montage of WNL stars is shown in Figure 3.26, and further discussed in §3.5.6. This classification system merges continuously with the Smith et al. 1996 system.

THE ADOPTION OF THE SMITH ET AL. 1996 SYSTEM BY THE WOLF–RAYET COMMUNITY

As mentioned in the introduction to this chapter, Wolf–Rayet classification is in a state of flux, with no system of classification having been universally accepted. The Smith et al. 1996 system is widely used by astronomers in the Wolf–Rayet field; almost all modern WN classifications are based on the system, and the latest versions of the van der Hucht Wolf–Rayet catalog (van der Hucht 2001) also list

classifications on that system. But it is generally acknowledged that some stars cannot be classified unambiguously on the system. An excellent example of this is the class of weak-lined WN stars (WNha). Crowther & Dessart (1998) discuss this ambiguity in the context of the Wolf–Rayet stars in HD 97950, Carina OB1, and R136a. They suggest an alternate criterion to distinguish WN stars in the range WN5–7, the equivalent width ratio of N IV λ 4057/N III λ 4634–41, namely $W_{\lambda}(\text{N IV } \lambda 4057)/W_{\lambda}(\text{N III } \lambda 4634-41) \leq 0.4$ for WN7 stars, ≥ 1.0 for WN5 stars, with the WN6 stars falling in between.

Spectral classification clearly plays a vital and dynamic role in the study of the Wolf–Rayet stars and so it is not surprising, and indeed it is to be expected, that the classification systems will continue to be refined and to evolve with developments in the field.

11.1.3 Ultraviolet and Far Ultraviolet Classification

The Wolf–Rayet stars emit most of their radiation in the ultraviolet and the far ultraviolet regions. The ions that are most abundant in the Wolf–Rayet winds have their resonance and other low-excitation transitions in these regions, and thus the ultraviolet should be the prime spectral region for the classification of the Wolf–Rayet stars.

However, no attempt to date has been made to set up independent classification systems for the WR stars in the ultraviolet (UV) and far ultraviolet (FUV). Instead, the optical classifications have been used to order the UV and FUV spectra, and then a search is made for line ratios or other spectral features that reproduce the ordering given by the optical classifications. As will be seen in this section, this approach has not always been successful. We urge the development of independent UV and FUV classification systems for WR stars, as considerable astrophysical insight may be forthcoming from their confrontation with the existing optical systems.

THE IUE ULTRAVIOLET

Low-resolution spectral montages of WN and WC stars in the IUE ultraviolet (1150–3250 Å) are presented in Figures 11.7 and 11.8. Line identifications are given in those figures, and are based on those given in Niedzielski & Rochowicz (1994) and also Nussbaumer et al. (1982). It should be kept in mind that at the resolution (~ 6 Å) of the IUE spectra presented in these two figures, most spectral features are blends of a number of lines, and thus the primary contributor to a given feature may change with the ionization class. A good example of this is the feature marked in the early WC stars as O IV λ 1343; this feature is actually a blend with C II λ 1335. Obviously, O IV dominates in the early WC stars, and C II in the late WC stars.

A cursory glance at the montage for the WN stars (Figure 11.7) shows no obvious trends in line ratios or line strengths with ionization class, at least for WN3–WN7. Of course, a visual search for systematic trends with ionization class is

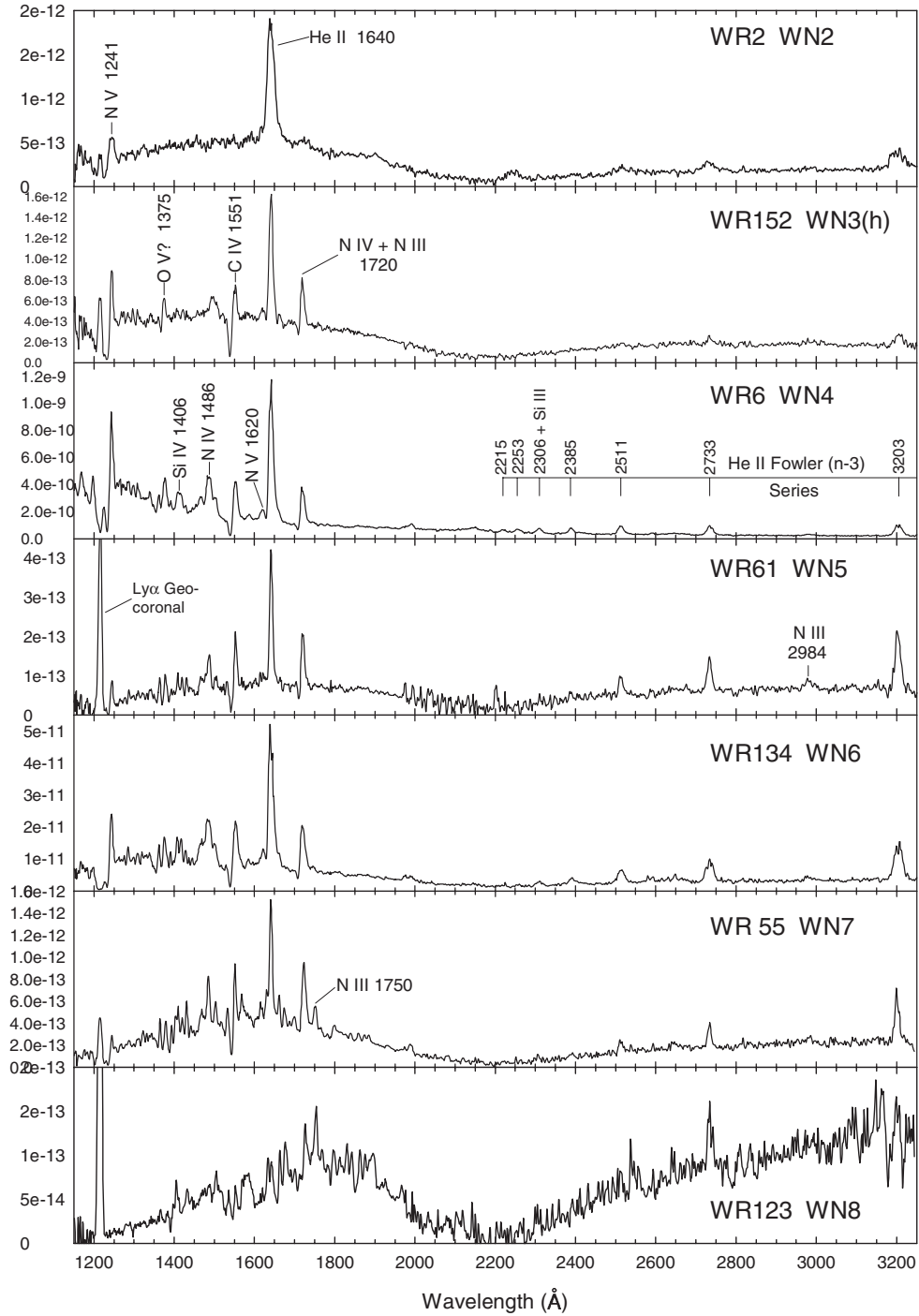


Figure 11.7 Low-resolution ultraviolet IUE spectra of WN stars. Line identifications from Niedzielski & Rochowicz (1994). In each panel, the ordinate is the stellar flux ($\text{erg s}^{-1} \text{cm}^{-2} \text{\AA}^{-1}$), but normalized to the highest point in the stellar spectrum. These IUE spectra, which have a resolution of about 6–9 Å, are from the MAST IUE archives (<http://archive.stsci.edu/ive>).

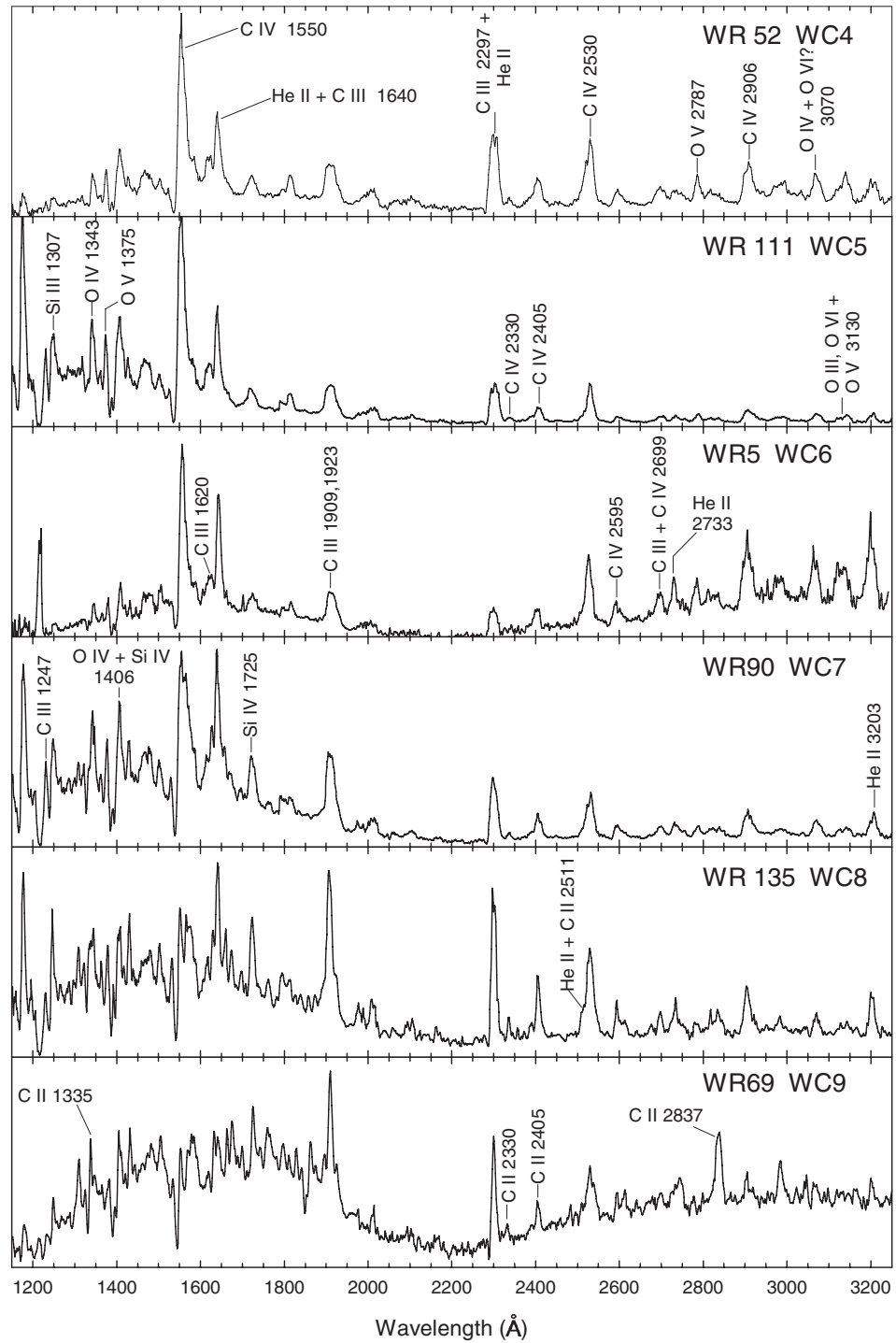


Figure 11.8 Low-resolution ultraviolet IUE spectra of WC stars. Line identifications from Niedzielski & Rochowicz (1994). See caption to Figure 11.7.

complicated by the varying continuum level, which is a function not only of temperature and continuous opacities, but also of interstellar reddening. Most of the stars in both montages are significantly reddened; the “kink” in the spectrum at 2200 Å is due to the interstellar 2200 Å extinction feature. Equivalent widths will, of course, be less sensitive to differences in continuum levels, and so Niedzielski & Rochowicz (1994) investigated correlations between the equivalent widths of a number of features in WN spectra and the WN type; most of the features marked in Figure 11.7 were included in that study. All of the correlations examined showed a large amount of scatter. This is not surprising, as WN stars in the optical show a wide range of line strengths; line ratios in the optical tend to show better correlations with the ionization class. Niedzielski & Rochowicz (1994) did find one UV line ratio, N III λ 1750/N V λ 1241, that shows a good correlation with the WN ionization class. As can be seen from Figure 11.7, however, N III λ 1750 is a weak feature that is difficult to measure or even see in many WNE stars, and thus this ratio cannot be used as the basis for a spectral classification system in the ultraviolet. The WN2 stars do stand out clearly from the later WN stars. The WN8 stars are also quite distinct, with a more subdued, but rich emission line spectrum than the other WN classes. The WN8 spectra are dominated by P Cygni profiles of resonance lines of metallic ions, such as Mg II, Zn II, Al II, Al III, and Fe II (Willis et al. 1986). Apart from these extreme cases, however, it is clearly difficult to classify WN stars in the IUE ultraviolet.

The WC stars show much richer spectra in the IUE ultraviolet than the WN stars, and thus present more opportunities for good classification criteria. Indeed, even a casual glance at Figure 11.8 shows that the ratio C IV λ 1550/He II + C III λ 1640 is a good indicator of the ionization class; this ratio is listed by Niedzielski & Rochowicz (1994) as a prime classification criterion. Note that the C IV λ 1550 line shows a distinct P Cygni absorption component in all WC classes. Another useful ratio is C IV λ 1550/C III $\lambda\lambda$ 1909, 1923, especially for stars later than WC5. The C II lines ($\lambda\lambda$ 1335, 2330, 2405 and 2837) become prominent in the latest WC stars. In general, the equivalent widths of many of the strong lines in ultraviolet WC spectra correlate quite well with ionization class. Niedzielski & Rochowicz (1994) note, however, that WC (as well as WN) LMC stars have a tendency toward stronger lines than their Galactic counterparts.

Willis et al. (1986) have presented a high-resolution IUE atlas of 14 Galactic Wolf–Rayet stars, including 9 WN and 5 WC stars. This atlas represents essentially all of the Wolf–Rayet stars that were observable by the IUE satellite at high resolution. From a spectral classification point of view, moving to high resolution does not seem to help in classifying WN stars in the ultraviolet. Although their sample size is small, Willis et al. (1986) noted that among the 3 WN7 stars in their atlas there is a wide range of line strengths, indicating significant “subclass heterogeneity.” It should be noted, however, that the IUE ultraviolet region has been very important for the determination of Wolf–Rayet wind characteristics, largely due to the fact that many emission lines in the ultraviolet show well-developed P Cygni profiles.

THE FAR ULTRAVIOLET

A number of satellites have been employed to obtain far-ultraviolet spectra (spectra in the wavelength region below 1150 Å) of Wolf–Rayet stars. These satellites include *Copernicus*, the Hopkins Ultraviolet Telescope on the *Astro-1* and *Astro-2* missions, and the *Orbiting Retrievable Far and Extreme Ultraviolet Spectrometer* (ORFEUS) mission. But the launch of the *Far-Ultraviolet Spectroscopic Explorer* (FUSE) mission in 1999 has had far-reaching consequences for the study of the Wolf–Rayet stars. The FUSE spectrograph provides spectra with redundant wavelength coverage from 905 to 1188 Å with a resolution of ~ 0.05 Å. The shortest wavelength region (below 1000 Å) is strongly affected by interstellar absorption, largely due to the Lyman-hydrogen lines, resonance lines of metals, and lines in the Lyman and Werner bands of H_2 .

Figures 11.9 and 11.10 present montages of WN and WC spectra, respectively, obtained by Willis et al. (2004) with the FUSE satellite. Galactic Wolf–Rayet stars tend to have very high extinction in the shortwave FUSE region, and so LMC Wolf–Rayet stars, which show much less extinction than their Galactic counterparts, are used in these montages when possible. However, it turns out that there are no massive WC stars in the LMC later than WC4, and so the WC montage contains two Galactic stars, HD 92809 and HD 164270. While the foreground extinction is comparatively small in the direction of the LMC, the LMC spectra are still strongly affected by interstellar absorption; most of the narrow features in both the Galactic and LMC spectra are interstellar. The broad Lyman-hydrogen interstellar lines have been marked, but the numerous narrow absorption lines due to various metals and H_2 are not. Another thing to keep in mind when examining these spectra is that the radial velocities of the stars have not been removed. That, coupled with the fact that different stars have different wind velocities, result in the P Cygni absorption components appearing at different wavelengths in different stars.

See the original reference (Willis et al. 2004) for more detailed and extensive montages of and descriptions of the WN and WC stars. FUSE spectra may be accessed online at http://archive.stsci.edu/prepds/fuse_wratlas/. The following discussion is based on that of Willis et al. (2004).

THE WN FUSE SEQUENCE

The earliest WN star in this montage (Figure 11.9) is the WN3b LMC star HD 32109. The spectrum of this star is characterized by well-developed P Cygni profiles of resonance lines of high-ionization species such as O VI ($\lambda\lambda 1031.9, 1037.6$) and S VI ($\lambda\lambda 933.4, 944.5$), and well-developed P Cygni absorption features for the resonance transitions of P V ($\lambda\lambda 1118.0, 1128.0$). Weaker P Cygni features may be seen for the C III ($\lambda 977$) and N III ($\lambda 991.0$) resonance lines.

In the WN6(h) LMC star (HD 38282) the P Cygni features of the high ions O VI and S VI are noticeably weakened, but there is a corresponding strengthening of the resonance P Cygni structures of S IV ($\lambda\lambda 1062.7, 1073.0$) and P V with the

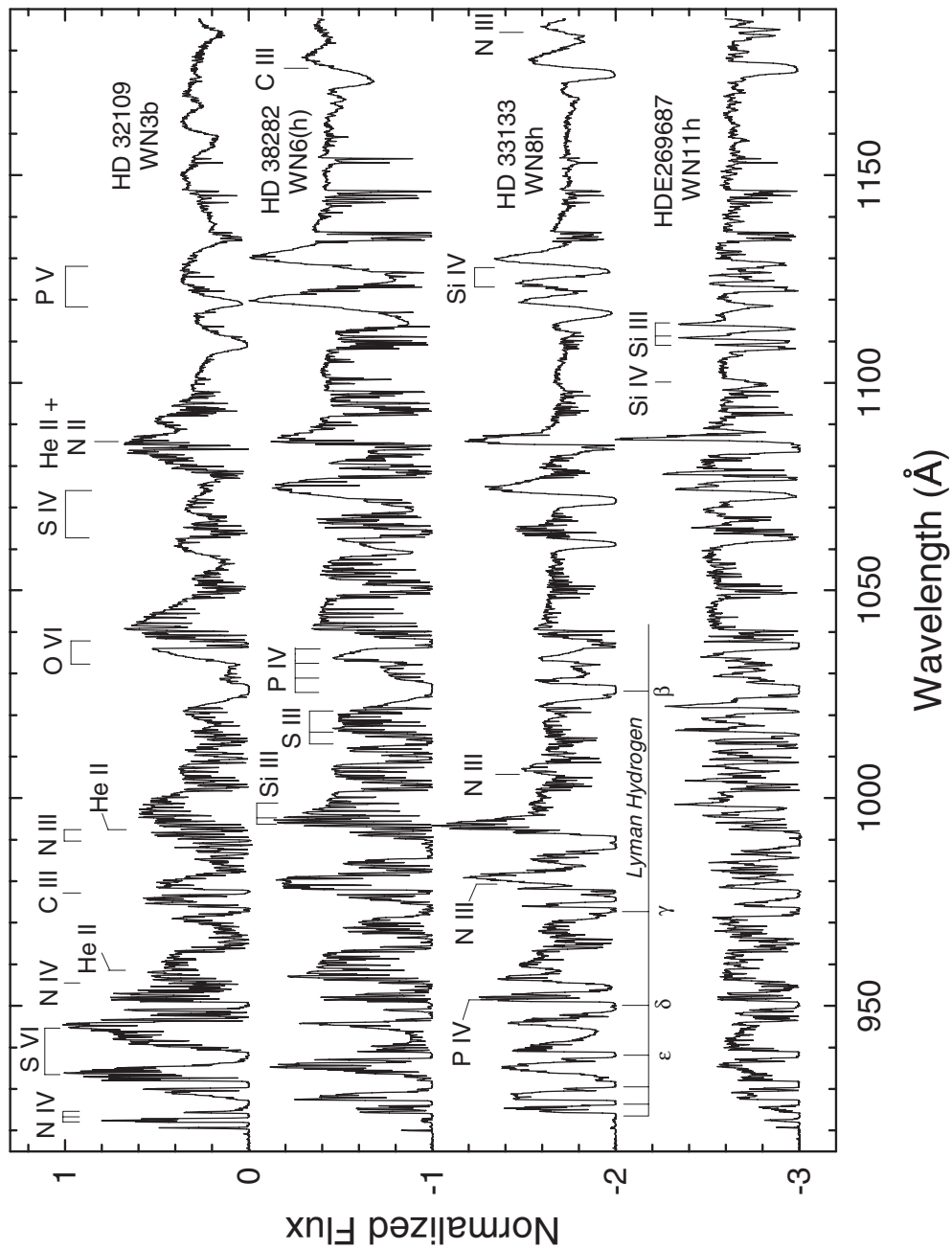


Figure 11.9 An ionization sequence of WN Wolf–Rayet stars in the far ultraviolet. Prominent interstellar features are labeled in *italics*, but most of the narrow features are interstellar. These spectra have a resolution of $\sim 0.05 \text{ \AA}$ and were obtained with the FUSE satellite, courtesy Willis et al. (2004).

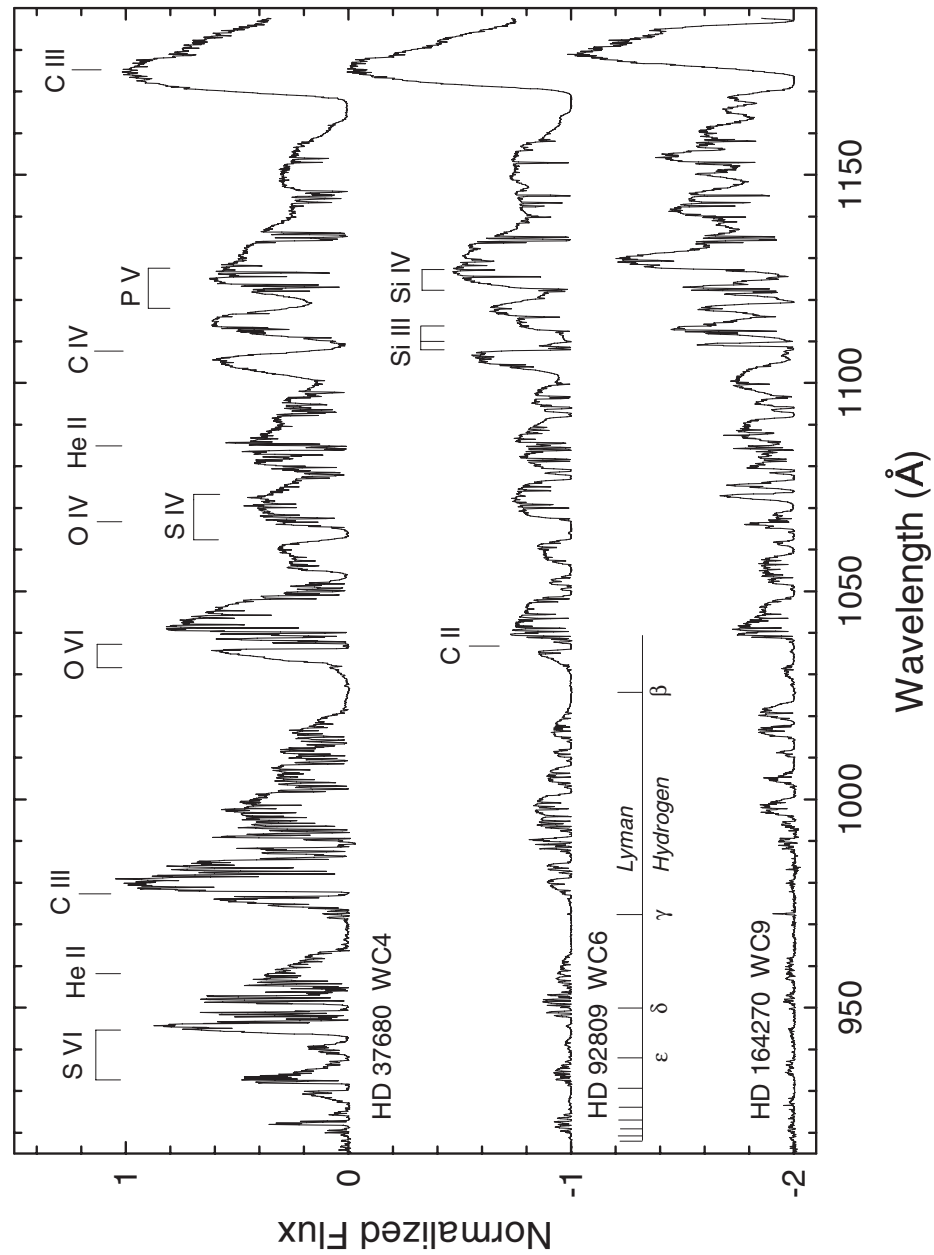


Figure 11.10 An ionization sequence of WC Wolf-Rayet stars in the far ultraviolet. Prominent interstellar features are labeled in italics, but most of the narrow features are interstellar. These spectra have a resolution of $\sim 0.05 \text{ \AA}$ and were obtained with the FUSE satellite, courtesy Willis et al. (2004).

development of strong emission. The subordinate transition of C III ($\lambda 1175$) also shows a well-developed P Cygni profile.

In the WN8h LMC star (HD 33133) the clearest wind features are the P Cygni profiles of the C III ($\lambda 977$) and N III ($\lambda 991$) resonance lines. The S IV resonance lines show saturated P Cygni profiles, there is a strong P Cygni feature at He II $\lambda 1085$, and also well developed P Cygni profiles in the P V resonance lines and the Si IV subordinate transitions at $\lambda\lambda 1122, 1128$. Both the C III $\lambda 1175$ and the N III $\lambda 1184$ features show emission.

Finally, in the WN11h LMC star HDE 269687, features due to lower ionization species dominate. For instance, both C III ($\lambda 977$) and N III ($\lambda 991$) appear strongly, but only as P Cygni absorption features. The Si III ($\lambda\lambda 994, 997$) subordinate transitions show well developed P Cygni profiles, as do the Si III $\lambda\lambda 1108, 1110, 1113$ multiplet and S III ($\lambda\lambda 1016, 1019, 1022$) transitions. The C III $\lambda 1175$ and N III $\lambda 1184$ features appear only in absorption. However, the most outstanding feature in this spectrum is the pronounced P Cygni profile of the He II, N II blend at $\lambda 1085$. In the late WN types, this blend is dominated by N II.

THE WC FUSE SEQUENCE

The WC montage (Figure 11.10) contains one LMC star (HD 37680) and two Galactic stars (HD 92809 and HD 164270). The WC4 star (HD 37680) shows well-developed P Cygni structures in the O VI $\lambda 1031$ and C III $\lambda 977$ resonance lines and in the C III $\lambda 1175$ multiplet. All three of these lines have saturated absorption components. In addition to this, the S VI resonance lines ($\lambda\lambda 933, 944$) also show well-developed P Cygni profiles. The P V resonance lines ($\lambda\lambda 1118, 1128$) show strong, but unsaturated absorption components.

The WC6 star, HD 92809, unfortunately suffers considerable extinction in the shortwave part of the spectrum, but it is still clear that the C III resonance line is present as a saturated P Cygni profile; likewise for the O VI $\lambda 1031$, S VI $\lambda\lambda 933, 944$, and S IV $\lambda\lambda 1062, 1072$ resonance lines. Weak emission is visible at He II $\lambda 1085$. The Si III ($\lambda\lambda 1108–1113$) and Si IV ($\lambda\lambda 1122, 1128$) lines blend with the P V absorption components, and help to distinguish WC5 and later stars from WC4 stars. Finally, the C III $\lambda 1175$ multiplet is still present as a strong P Cygni feature with a saturated absorption component.

The WC9 star in this montage, HD 164270, also suffers from considerable interstellar absorption in the shortwave channel. The most visible feature in this short-wave channel is the strong P Cygni profile of C II $\lambda 1037$. S IV $\lambda\lambda 1062, 1072$ still show up as saturated P Cygni profiles. The P V absorption components, however, are considerably weaker than in earlier types, and this region is now dominated by well-developed, but unsaturated P Cygni structures due to Si IV ($\lambda\lambda 1122, 1128$). C III $\lambda 1175$ emission is slightly weaker at WC9, but the absorption component is still saturated.

11.1.1.4 Classification in the Infrared

Montages of WN and WC stars in the near-infrared (NIR), reproduced from Conti, Massey, & Vreux (1990), are illustrated in Figures 11.11 and 11.12. In the WN sequence, the strongest lines are N IV $\lambda 7115$ and He II $\lambda 10,124$. Other lines of the He II $n=5$ series are seen in this spectral range as well. As we saw in the IUE ultraviolet, spectra at the extreme ends of the WN sequence may be easily recognized in the NIR, WN2 stars from the weakness of the N IV line, and WN7–WN9 stars by the appearance of He I ($\lambda\lambda 6678, 7065$). It is very difficult, however, to classify stars into subtypes between WN3 and WN6 on the basis of NIR spectra alone.

In the WC stars, much the same can be said. The spectra of the WC stars in the NIR are much richer than the WN stars. The latest WC stars (WC8, WC9) can be recognized by the presence of C II $\lambda 7236$, which is clearly the strongest line in WC9 stars. Other strong lines include C III $\lambda 9711$ and C IV $\lambda 7726$. The early WC stars may be identified on the basis of the relative strengths of the C II and C IV lines; the star is a WCE if C IV is strong, or a WCL if C II dominates. But subdivision of the WC stars into their subtypes on the basis of C III/C IV ratios, for instance, is not possible. The reason for this difficulty in classifying mid-WR stars, in both the WN stars and the WC stars, is that some of the lines involved are subject to the selective excitation and optical depth effects that were discussed in §11.1.2.2. More details may be found in Conti, Massey, & Vreux (1990).

In the I, J, H and K infrared bands, the spectra of the WN stars are dominated by emission lines of He I and He II (see Crowther & Smith 1996). In the I-band the ratio He II $1.01236\ \mu\text{m}$ /He I $1.08303\ \mu\text{m}$ appears well-correlated with the ionization class. Similar ratios in the H-band involve He II lines blended with hydrogen Brackett lines, and likewise for the K-band. These ratios are useful for determining the H/He ratio, but not the subtype.

In contrast, the J, H, and K infrared bands are dominated by many lines of carbon ions in the WC stars. Eenens et al. (1991) have set up a tentative classification system for the WC stars in this region, and found, with a few exceptions, that WC subtypes as determined in this region are consistent with the optical types. This classification scheme, however, is based on only eight(!) WC stars, and so it clearly must be re-examined with a larger sample. In the J-band, the C IV $1.191\ \mu\text{m}$ /C III $1.199\ \mu\text{m}$ ratio appears to be able to be used to separate the WCL stars; the WCE stars are characterized by a strong O V $1.111\ \mu\text{m}$ line. Eenens et al. (1991) suggest a He I, He II/C IV ratio as a classification criterion in the H-band, but this will be subject to abundance differences. In the K-band, two C IV/C III ratios, $2.08\ \mu\text{m}/2.11\ \mu\text{m}$ and $2.43\ \mu\text{m}/2.48\ \mu\text{m}$ appear to have some promise as classification criteria.

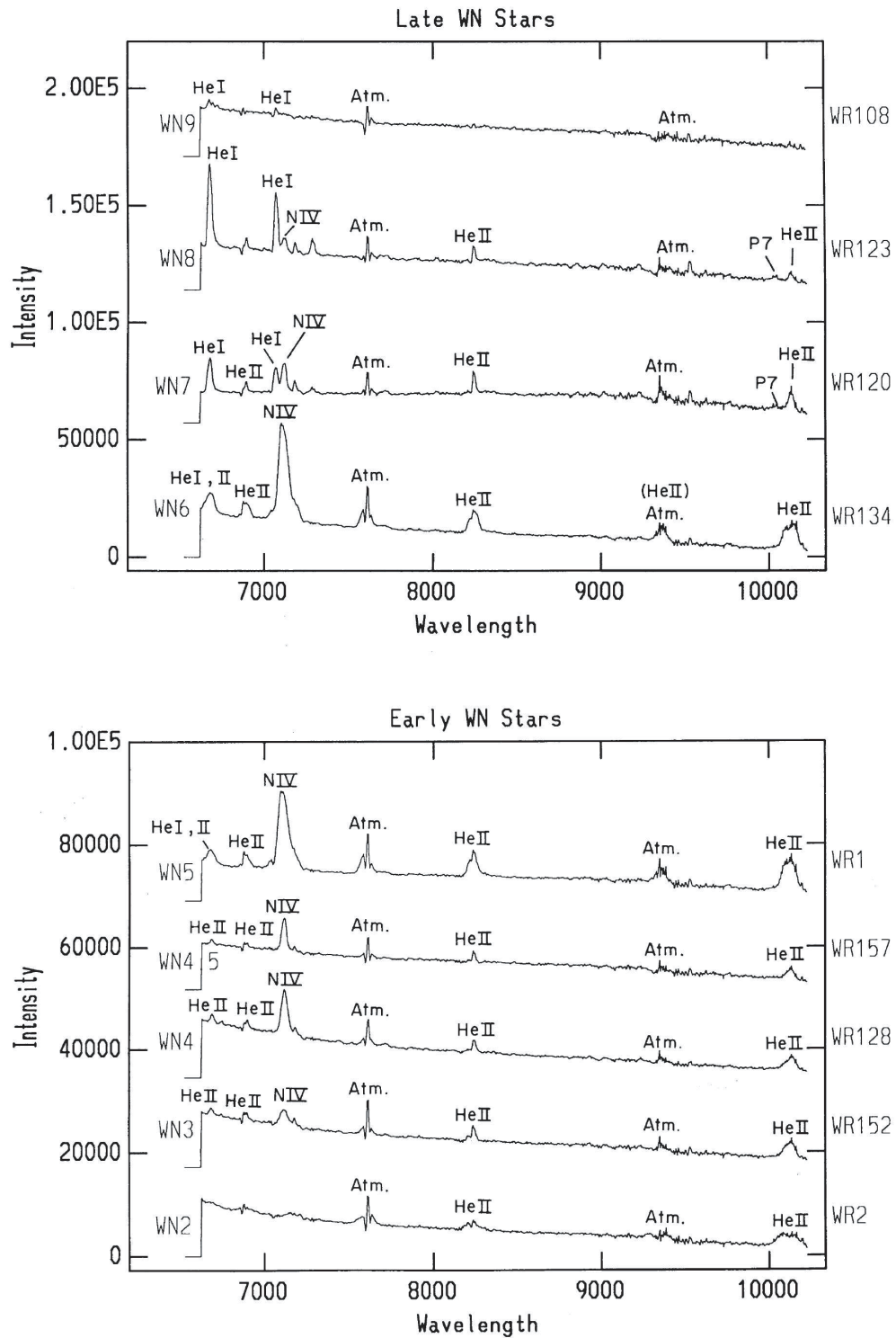


Figure 11.11 A montage of WN Wolf-Rayet stars in the near-IR. Figure from Conti, Massey, & Vreux (1990), and reproduced by permission of the AAS.

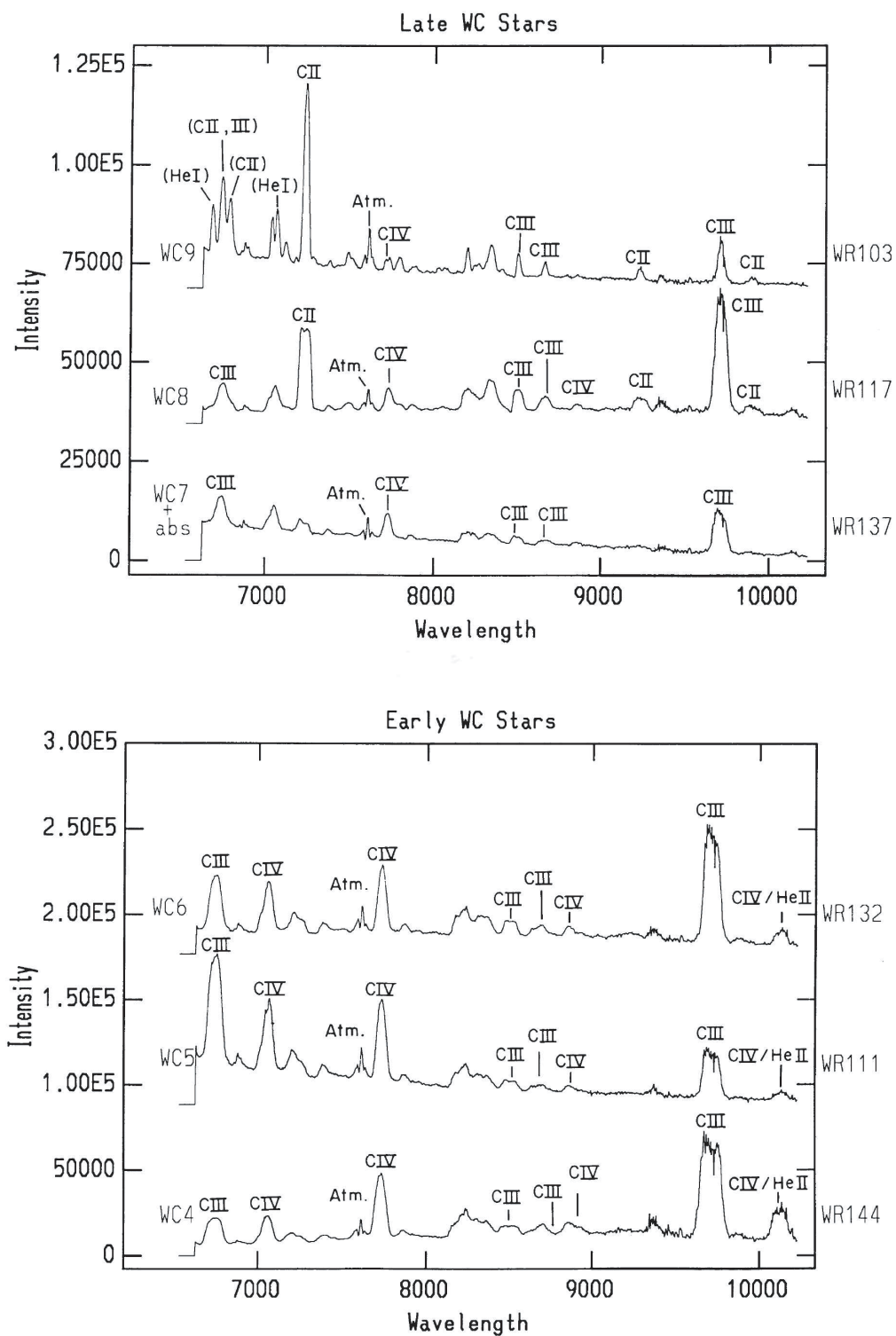


Figure 11.12 A montage of WC Wolf-Rayet stars in the near-IR. Figure from Conti, Massey, & Vreux (1990), and reproduced by permission of the AAS.

11.2 LUMINOUS BLUE VARIABLES

A Luminous Blue Variable (LBV), also called an S Doradus variable, is an evolved, massive, extremely luminous supergiant that is subject to instabilities that results in eruptions of various sorts. The most famous LBV is η Carinae, which suffered a “giant eruption” during the nineteenth century. Visual observations before the early 1800s (stretching back to the seventeenth century) indicate that its visual magnitude fluctuated between 4th and 2nd magnitudes, but in the late 1830s, η Carinae underwent its “Great Eruption” during which time it became one of the brightest stars in the sky. A lesser outburst occurred in the 1890s. Studies of the complex ejecta that surround the star indicate that such eruptions have taken place in the past as well; there is even a possibility that this variability was noticed by the ancient Sumerians and incorporated into their mythology (Humphreys & Davidson 1994)! Another well-known LBV is P Cyg, which itself underwent a giant eruption in the year 1600, brightened during that eruption to 3rd magnitude, then faded, and then erupted again in mid-century. After this second eruption, it faded to about 7th magnitude, and then brightened to about 5th magnitude at which level it has remained since about the year 1700 (Lamers & de Groot 1992).

The variability pattern of S Dor is more typical of LBVs than the giant eruptions experienced by η Car and P Cyg. S Dor-type variability is characterized by irregular eruptions, with excursions in V of 1 to 2 magnitudes. Both the giant and S Dor-type eruptions involve enhanced rates of mass loss, leading to the formation of an optically thick, expanded atmosphere or “pseudo photosphere.” This causes quite dramatic changes in the spectrum. During the quiescent, or minimum state, the apparent temperature is high ($>15,000$ K), and the star may take on one of many guises as a hot, luminous, emission-line star. R 127, an LBV in the LMC, for instance, was first classified by Walborn (1977) as an Of/WN9 star, and then later underwent an S Dor-like eruption during which its spectrum changed to resemble that of S Dor itself (see the top spectrum in Figure 11.13). AG Car is another LBV that has an Of/WN9 spectrum during minimum light (Stahl 1986) and an S Dor-like spectrum at maximum (see Figure 11.14). This does not imply, however, that all Of/WN9 stars are quiescent LBVs (see Bohannan 1997); to be placed in this category, some evidence of variability and/or past ejections is required.

During maximum light, the apparent temperature of the star (actually the temperature of the pseudo-photosphere) decreases to about 7000–8000 K, and the spectrum takes on the character of a luminous A or F supergiant. The spectrum of S Dor has recently undergone such a change (see Massey 2000, and Figure 11.13). During the famous outburst of η Car in the 1890s, its spectrum also resembled that of an F supergiant. This outburst was an S Dor-like eruption, and not a “giant eruption” like the outburst in the 1830s. Unfortunately, we do not have a spectrum of η Car during the Great Eruption, but we do have spectra of SN 1961V, presumed at the time to be a supernova, but now known to be an LBV undergoing what might properly be called a “hyper-eruption,” as at maximum light

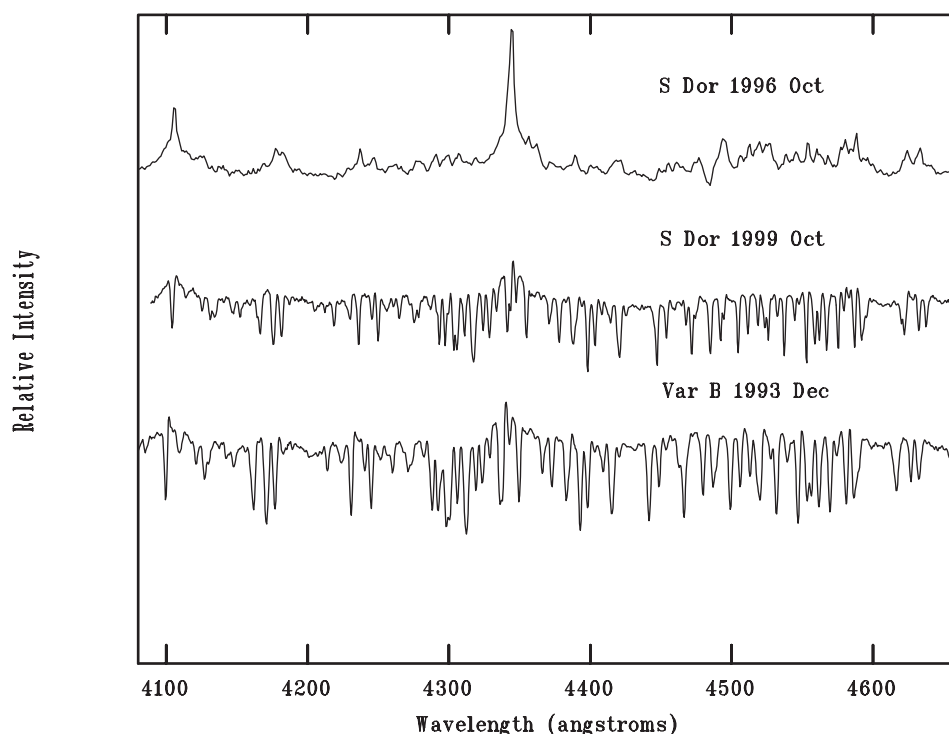


Figure 11.13 A montage showing the normal appearance (top) of the spectrum of S Dor, the prototypical LBV, its appearance after its sudden change in 1999 (middle), and a comparison with the spectrum of Var B in M33, another LBV, at the time of its outburst in 1993. Figure courtesy of P. Massey (Massey 2000), and reproduced by permission of the University of Chicago.

it exceeded η Car during the Great Eruption in absolute visual magnitude by about 1.5 magnitudes. During this maximum phase, its spectrum also appeared similar to that of an F supergiant (Goodrich et al. 1989).

While, it is beyond the scope of this book to cover all of the fascinating details of LBVs (a number of good reviews exist, such as Humphreys & Davidson 1994; van Genderen 2001), it is of interest to understand the implications of the location of these objects on the H–R diagram. Figure 11.15 plots the position of many of the known LBVs on the HR diagram, both at minimum light and at outburst maximum. Many of the known luminous cool hypergiants are also plotted in that Figure. It is interesting to note that during the typical S Dor outburst the LBV remains at constant bolometric luminosity. This is apparently not true for the “giant eruptions” during which the absolute bolometric magnitude may increase by 1–2 magnitudes.

Studies of the most luminous stars in the Milky Way and external galaxies led Humphreys & Davidson (1979, 1984) to define an empirical upper luminosity boundary in the HR diagram, now known as the Humphreys–Davidson limit, illustrated as the solid line in Figure 11.15. The sloping part of this empirical limit

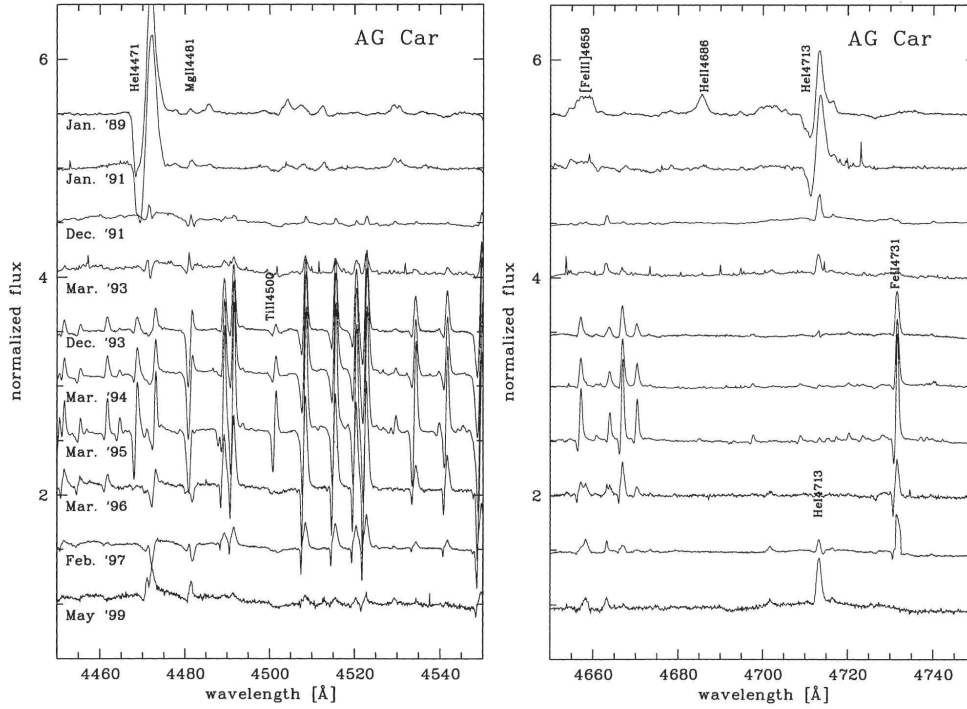


Figure 11.14 A time sequence showing the change in the appearance of the spectrum of AG Car, an LBV, during its outburst in 1995. During the outburst, the spectrum was dominated by lines of Fe II. At minimum, He I emission is very strong. Also at minimum, forbidden lines of [Fe III] are observed. Figure courtesy of O. Stahl (Stahl 2001), and reproduced by permission of the Astronomical Society of the Pacific.

corresponds roughly to the Eddington Limit, which is defined as the luminosity at which the radiation pressure (assuming the dominant form of opacity is electron scattering) exceeds the gravitational attraction, leading to disruption of the star. Note that the position of the LBVs coincides quite closely with the Eddington limit. In that same figure, the horizontal part of the Humphreys–Davidson limit is the temperature-independent upper luminosity limit for late-type hypergiants ($T_{\text{eff}} \leq 8000 \text{ K}$). The proximity of the LBVs to the Eddington limit and the existence of the temperature-independent upper luminosity limit suggest (see Humphreys & Davidson 1979, 1994) that above a certain critical mass ($\sim 40 M_{\odot}$) post main-sequence stars encounter instabilities, leading to episodes of very high mass-loss rates, and that these episodes correspond to the LBV phase. These high mass-loss rates probably prevent the star from evolving to the red supergiant stage; this is the most likely explanation for the existence of the temperature-independent upper luminosity limit for late-type hypergiants. During outburst, it is interesting that LBVs not only have a uniform apparent temperature ($\sim 8000 \text{ K}$), but also lie at or *beyond* the Humphreys–Davidson limit. Bear in mind that at outburst we are seeing the opaque pseudo-photosphere, and the underlying star, which remains at a constant bolometric luminosity, still lies to the left of the empirical limit.

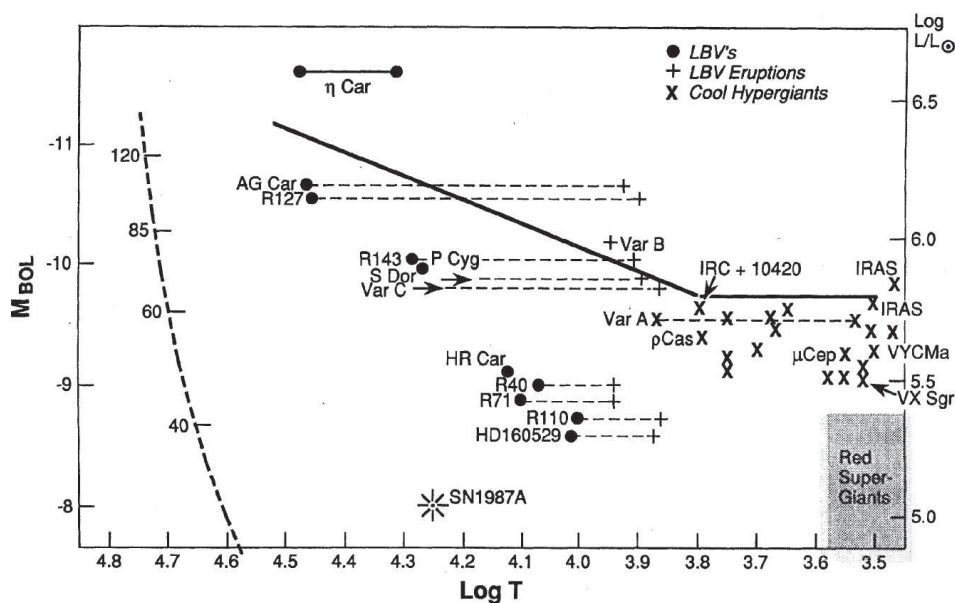


Figure 11.15 A plot of luminous stars, including LBVs and cool hypergiants, in the upper H-R diagram. The positions of the LBVs at quiescence are indicated with filled circles, and during outburst with +’s, the two connected with dashed lines. The solid line is the Humphreys–Davidson empirical upper luminosity limit. The horizontal part of this limit is the temperature-independent upper luminosity limit for late-type hypergiants (X’s). The upper main-sequence can be seen to the left, with initial masses indicated in units of solar masses. Figure reproduced by permission of Humphreys & Davidson (1994), and the University of Chicago.

Note in Figure 11.15 the existence of a group of low-luminosity LBVs (including HD 160529 and HR Car). These stars show many of the same characteristics as the more luminous LBVs, although they display lower mass-loss rates and lower variability amplitudes. They undoubtedly are lower mass stars and thus may currently be evolving toward the red supergiant stage or have already been through this stage and are now on a “blue loop” moving across the H–R diagram. In quiescence, these stars appear to be luminous emission-line B supergiants. The spectra of some of these stars are discussed in §4.6.2.

11.3 EVOLUTIONARY CONNECTIONS

Conti (1976) was the first to propose that a massive Of star may lose enough mass through stellar winds to first reveal hydrogen-burning products (primarily enhanced nitrogen via the CNO cycle) and then He-burning products (carbon and oxygen), thus transforming itself first into a WN star, and then a WC star. This “peeled onion skin” model for the origin of the WR stars is now known as the “Conti scenario,” and gains credence through the existence of intermediate types, including the Of/WN9 stars and the WN/C stars.

High rates of mass loss, high luminosities, and close association with recent star-formation activity are three characteristics shared by WR stars and LBVs. These similarities, plus the fact that many LBVs in quiescence have late WN (WNL) spectral types suggest an evolutionary connection between WR stars and LBVs. The nature of that connection is not yet clear. How might the LBV stars fit into the “Conti scenario”?

Schild & Maeder (1984) and Massey, DeGioia-Eastwood, & Waterhouse (2001) have investigated the initial masses of WR stars by observing the occurrence of the different types of WR stars in massive young clusters. These studies found a wide range of progenitor masses for WR stars. For instance, for the WNE stars, progenitor masses ranging from 20 to $100M_{\odot}$ were found, but interestingly, the hydrogen-rich WNL stars have the highest progenitor masses, ranging from 50 up to or even exceeding $120M_{\odot}$. These hydrogen-rich WNL stars are believed to be evolved, but still core-hydrogen burning (see Conti et al. 1995). These stars are found in clusters as young as 1 Myr, in two cases also containing an LBV or LBV candidate. The WC, mid-WN, and WO stars appear to have lower progenitor masses. These points, together with the absence of red supergiant stars (RSG) at the highest luminosities (see Figure 11.15), suggest the following evolutionary scenarios (Crowther 2007):

For stars more massive than $\sim 75 M_{\odot}$:

$$\text{O} \rightarrow \text{WN(H-rich)} \rightarrow \text{LBV} \rightarrow \text{WN(H-poor)} \rightarrow \text{WC} \rightarrow \text{SNIc}$$

while for stars with initial masses from ~ 40 to $75 M_{\odot}$:

$$\text{O} \rightarrow \text{LBV} \rightarrow \text{WN(H-poor)} \rightarrow \text{WC} \rightarrow \text{SNIc}$$

and for stars of the lowest mass range $25\text{--}40M_{\odot}$:

$$\text{O} \rightarrow \text{LBV/RSG} \rightarrow \text{WN(H-poor)} \rightarrow \text{SNIb}$$

The end point for each of these scenarios is a hydrogen-poor supernova (see Chapter 12). The exact role of the LBV in these scenarios is not entirely clear; for some mass ranges the LBV phase may not be involved at all, in others it may dominate. Only further observations will reveal the true story.

Bibliography

- Barlow, M.J., & Hummer, D.G. 1982, in *Wolf-Rayet Stars: Observations, Physics, Evolution*, eds. C.W.H. de Loore & A.J. Willis, IAU Symp 99 (Dordrecht: Reidel), p. 387
- Beals, C.S. 1933, *Observatory*, 56, 196
- Beals, C.S. 1934, *Pub. Dominion Astrophys. Obs. Victoria*, 6, 95
- Beals, C.S. 1938, *Trans. IAU*, 6, 248
- Bohannon, 1997, in *Luminous Blue Variables: Massive Stars in Transition*, ASP Conference Series, Vol. 120, eds. A. Nota & H. Lamers, p. 3
- Cannon, A.J., & Pickering, E.C. 1901, *Harvard Obs. Annals*, 28, 131
- Conti, P.S. 1976, in *Proc. 20th Colloq. Int. Ap. Liège*, Liège, University of Liège, p. 193
- Conti, P.S., Hanson, M.M., Morris, P.W., Willis, A.J., & Fossey, S.J. 1995, *ApJ*, 445, L35
- Conti, P.S., Massey, P., & Vreux, J-M. 1990, *ApJ*, 354, 359
- Crowther, P.A. 2007, *ARAA*, 47, in press
- Crowther, P.A., De Marco, O., & Barlow, M.J. 1998, *MNRAS*, 296, 367
- Crowther, P.A., & Dessart, L. 1998, *MNRAS*, 296, 622
- Crowther, P.A., Hillier, D.J., & Smith, L.J. 1995, *AA*, 293, 172
- Crowther, P.A., & Smith, L.J. 1996, *AA*, 305, 541
- Crowther, P.A., & Smith, L.J. 1997, *AA*, 320, 500
- Edlén, B. 1932, *Observatory*, 55, 115
- Eenens, P.R.J., Williams, P.M., & Wade, R. 1991, *MNRAS*, 252, 300
- van Genderen, A.M. 2001, *AA*, 366, 508
- Goodrich, R.W., Stringfellow, G.S., & Penrod, G.D. 1989, *ApJ*, 342, 908
- Hamann, W.-R., Koesterke, L., & Wessolowski, U. 1995a, *AApS*, 113, 459
- Hamann, W.-R., Koesterke, L., & Wessolowski, U. 1995b, *AA*, 299, 151
- Hamann, W.-R., Pena, M., Graefener, G., & Ruiz, M.T. 2003, *AA*, 409, 969
- Hillier, D.J. 1989, *ApJ*, 347, 392
- Hiltner, W.A., & Schild, R.E. 1966, *ApJ*, 143, 770
- Humphreys, R.M., & Davidson, K. 1979, *ApJ*, 232, 243
- Humphreys, R.M., & Davidson, K. 1984, *Science*, 223,
- Humphreys, R.M., & Davidson, K. 1994, *PASP*, 106, 1025
- Kingsburgh, R.L., Barlow, M.J., & Storey, P.J. 1995, *AA*, 295, 75
- Lamers, H.J.G.L.M., & de Groot, M.J.H. 1992, *AA*, 257, 153
- Massey, P. 2000, *PASP*, 112, 144
- Massey, P., DeGioia-Eastwood, K., & Waterhouse, E. 2001, *AJ*, 121, 1050

- Massey, P., & Grove, K. 1989, *ApJ*, 344, 870
- Morgan, D.H., Parker, Q.A., & Cohen, M. 2003, *MNRAS*, 346, 719
- Niedzielski, A., & Rochowicz, K. 1994, *AApS*, 108, 669
- Nussbaumer, H., Schmutz, W., Smith, L.J., & Willis, A.J. 1982, *AApS*, 47, 257
- Sanduleak, N. 1971, *ApJ*, 164, L71
- Schild, H., & Maeder, A. 1984, *AA*, 136, 237
- Smith, L.F. 1968, *MNRAS*, 138, 109
- Smith, L.F., Shara, M.M., & Moffat, A.F. 1990, *ApJ*, 358, 229
- Smith, L.F., Crowther, P.A., & Prinja, R.K. 1994, *AA*, 281, 833
- Smith, L.F., Shara, M.M., & Moffat, A.F. 1996, *MNRAS*, 281, 163
- Stahl, O. 1986, *AA*, 164, 321
- Stahl, O. 2001, in *Eta Carinae and Other Mysterious Stars: The Hidden Opportunities of Emission Spectroscopy*, ASP Conference Series Vol. 242, eds. T.R. Gull, S. Johansson, & K. Davidson, p. 163
- Torres, A.V., Conti, P.S., & Massey, P. 1986, *ApJ*, 300, 379
- Torres, A.V., & Massey, P. 1987, *ApJS*, 65, 459
- van der Hucht, K.A. 2001, *New Astronomy Reviews*, 45, 135
- Vogel, H.C. 1883, *Publ. Astrophys. Obs. Potsdam*, 4, 17
- Walborn, N.R. 1977, *ApJ*, 215, 53
- Willis, A.J., van der Hucht, K.A., Conti, P.S., & Garmany, D. 1986, *AApS*, 63, 417
- Willis, A.J., Crowther, P.A., Fullerton, A.W., Hutchings, J.B., Sonneborn, G., Brownsberger, K., Massa, D.L., & Walborn, N.R. 2004, *ApJS*, 154, 651
- Wolf, C., & Rayet, G. 1867, *Comptes Rendus*, 65, 292

Chapter Twelve

Endpoints of Stellar Evolution

12.1 PROTO-PLANETARY NEBULAE AND PLANETARY NEBULA NUCLEUS STARS

In other places in this book, we have described the appearance of the spectra of stars in the *post-Asymptotic-Giant-Branch* (post-AGB) stage of evolution (see §4.7.2, §5.6.2, §6.6.2, and §7.8.3 for examples of B-, A-, F-, and G-type post-AGB spectra). Post-AGB stars, also known as proto-planetary nebula stars (PPNe), are intermediate-mass stars that have evolved from the *Asymptotic Giant Branch* (AGB), and are in the process of ejecting shells of gas and dust that will eventually become planetary nebulae, once the stars become hot enough to ionize the gas. A famous example of such a star is the Red Rectangle (HD 44179) (see Figure 5.30). This evolutionary phase is very short-lived, as these stars are in a state of rapid mass-loss and core contraction, which transforms them into the extremely hot nuclei (central stars) of planetary nebulae (PNN, or CSPNe). These hot CSPNe can have a variety of spectra, and generally fall into the following categories: subdwarf O-type stars (§4.7.1), Wolf–Rayet stars, including the [WO] and [WC] types (see §11.1.2.1), and the very hot, proto-white dwarf PG 1159 stars (§12.2.4). All of these types of stars rapidly evolve to the white-dwarf stage, which is the subject of the next section.

12.2 WHITE DWARF STARS

12.2.1 Introduction and History

These highly compact, white dwarf (WD) stars are important for various reasons. They mark the most common endpoint of stellar evolution. Their internal structure contains a detailed record of the stages undergone since leaving the main sequence; e.g., the composition of their deep interiors is determined by the core helium burning when they were red giants, while the profile of their outer cores is set by the various shell burnings and mixing processes experienced. Their dense atmospheres provide “laboratories” for studying radiation and absorption among atoms and molecules in conditions unobtainable on the Earth. This same high surface gravity ($\log g \sim 8$) leads to significant diffusion and separation of the elements in their outer layers, and particularly the light hydrogen or helium dominates their upper atmospheres. Pulsation sets in as they cool through the instability strip, so that asteroseismology can probe their interior structure (Metcalfe 2005).

Significant traces of the heavier elements, the metals, in their otherwise hydrogen-dominated atmospheres seem to have been accreted from the ISM and so provide information about the ISM local to the Sun (Koester & Wilken 2006).

The recognition of the class of WD stars started in 1910 when Henry Norris Russell of Princeton University Observatory prompted Williamina Fleming via Edward Pickering, both at Harvard Observatory, to look at the spectrum of the companion to α^2 Eridiani (= 40 Eri).¹ She described the spectrum of 40 Eri B as being “Class A” (Russell 1944), while all other known faint absolute magnitude stars were class G or later. Confirmation came from Walter Adams (1914), who a little later managed to get a spectrum of the companion to Sirius, which also turned out to be “A0.” This “bombshell,” as later described by William Luyten (1956), of finding such an early type for such a faint star was explained by Arthur Stanley Eddington (1924) in Cambridge, who coined the term “white dwarfs” for these compact objects with mean density some 10,000 times that of the Sun. The explanations continued via quantum mechanics with R.H. Fowler (1926) showing that a degenerate electron gas would provide the support that has to be far in excess of that given by thermal gas pressure, and with S. Chandrasekhar (1935) working out the details of white dwarf structure.

Despite these exciting beginnings the spectral classification of WDs was long in evolving. This was partly since their faintness made good quality spectra difficult to come by, but principally because the composition of their atmospheres did not fit the run of other stars on the H–R diagram. Thus, those WD stars showing a dominance of hydrogen lines in their spectra could cover an enormous range of surface temperatures, virtually that of the H–R diagram not just that of the normal A-type stars.

Liebert & Sion (1994) give Gerard Kuiper (1941) the honor of the first systematic attempt to classify WD stars. He distinguished the dominant elemental features in their atmospheres (hydrogen lines = “A”; Ca II lines = “F”; weaker metallic blends = “G”; featureless spectrum = “Con”) with the prefix of “w” signifying a WD. That prefix was changed by Luyten (1952) to the capital “D,” and he also added those showing only He I, the “B” type. To the elemental variations, signified by the letters, Luyten added a numeric subtype to indicate temperature, but in fact these do not correlate well with T_{eff} . Jesse Greenstein was fortunate to have an avid interest in WDs coupled with access to the largest telescope in the 1950s, the Palomar Hale 200-in. His extensive review of WDs (Greenstein 1960) introduced the DO type for those showing just He II, and the $\lambda 4135$ type and the $\lambda 4670$ type for those showing respectively the initially mysterious Minkowski bands and the Swan bands of carbon. Greenstein also dropped Luyten’s temperature subtype in favor of a color index or a spectrophotometric indication of temperature (e.g., equivalent width of $H\gamma$). This system of classification remained in place for the next couple of decades during which time the sample size grew and manifested increased complexities and diversities. An improved classification system was needed.

¹A fuller account of WD history will be found in J.B. Hearnshaw, *The Analysis of Starlight* (CUP 1986).

The Sion et al. (1983) paper, confirmed in the Palomar-Green catalogue (Green et al. 1986), can claim to initiate the current WD classification scheme, replacing or modifying the ones mentioned above. It uses information on the effective temperature of the stars to give an index from 1 to 9, thus introducing non-morphological information in the attempt to distinguish different types of WD star. This is a practical expedient, dependent on theory, but Sion et al. (1983) remark that “the classification of individual objects in other, more descriptive systems also changes with the passage of time.” Maybe so, but the discussants at the key presentation of this scheme during the MK50 conference (Liebert & Sion 1994) emphasized that the power of the MK system is in “anchoring” the primary classification standards precisely to gauge the change in theory rather than vice versa. We can note that Jim Liebert and Ed Sion did volunteer that a WD standard would be model-independent, i.e., not change in subtype if a better estimate of its temperature became available (*op.cit.*, p. 68). The remarks given that same year in Wesemael et al. (1993) about readjusting this index for some types in their atlas puts this in doubt, so we might be better to consider the defining of WD standards to be a work in progress.

12.2.2 Current Classification

If you find a spectrum that is fundamentally unlike those of other stars, it could well be that of a WD. Particularly if it has extremely broad hydrogen lines, indicating the very high gravities characteristic of the atmospheres in these degenerate stars, it is certainly a WD of type DA (see Figure 12.1). The “D” denotes a degenerate star, while the “A” shows its primary spectroscopic characteristic. The primary symbols and their characteristics are given in Table 12.1, which follows the definitions in McCook & Sion (1999). The primary symbol DA denotes that hydrogen is the most abundant element in the atmosphere of these WDs, while DB and DO denote it is helium. Helium also dominates in the DZ and DQ atmospheres, but for DC it could either be hydrogen or helium, depending whether the temperature is high enough for hydrogen to be seen in the spectrum.

To the primary type can be added one or more secondary composition symbols (A, B, C, O, Z, or Q), indicating a trace of an element defined as for the primary ones. Thus DQAB describes a spectrum dominated by carbon, but also showing weak hydrogen and neutral helium lines. Then can be appended one or more of the “additional symbols” from Table 12.1. Clearly “X” can be a somewhat desperate description. As “V” indicates photometric variability, it is optional as an addition to the spectroscopic symbols.

Since the Sion et al. (1983) paper appeared, a revised numeric index of temperature is now added to the morphological description of the WD spectrum. It is assigned on the basis of a color temperature determined from photometric indices that are calibrated from model atmospheres, and sometimes from direct comparison of the spectrum with those model atmospheres. The index is given as ten times the model “theta,” i.e., $50400/T_{\text{eff}}$. Hence a hydrogen-dominated WD with

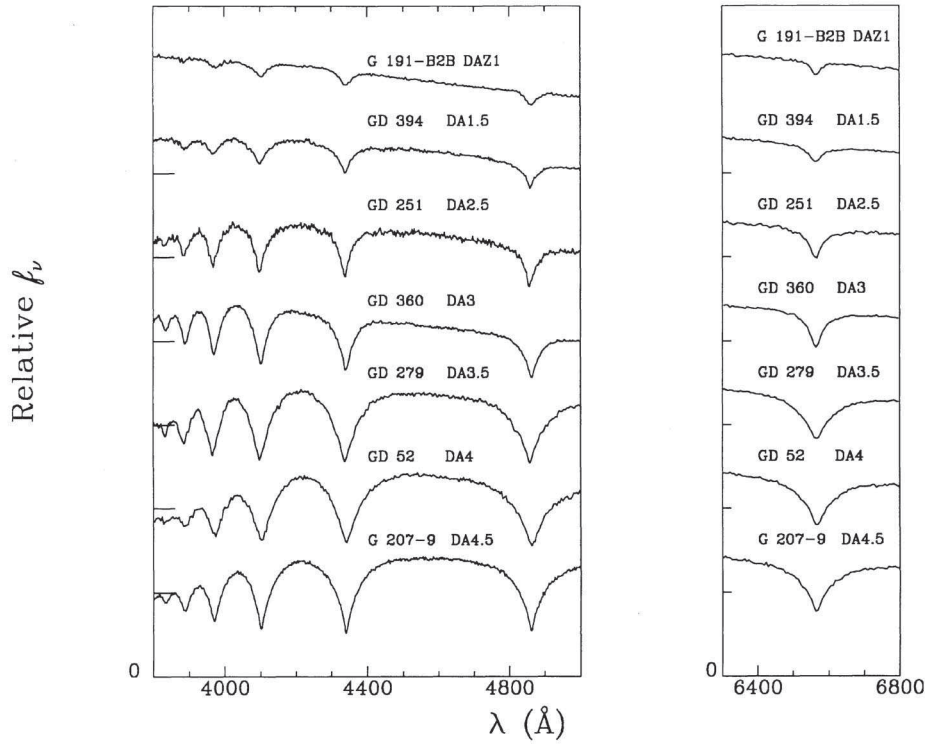


Figure 12.1 DA white dwarfs at the hot end of the sequence. The spectra are ordered with the hottest at the top. Note the strong, broad Balmer lines. This and Figures 12.2–12.7 and 12.10 of WD spectra are courtesy of Wesemael et al. (1993), and are reproduced by permission of the University of Chicago.

a temperature near 13,000 K is called a DA4 star. The range of spectra with various temperatures for a particular primary type can be seen in the montages shown from Figures 12.1 to 12.7, which are courtesy of Wesemael et al. (1993). It will be noticed that expanded and refined indices of temperature are used in these montages. The expansion refers to “.9” to “.1” being used for temperatures hotter than 50,400 K ($= 10 \times \theta_{\text{eff}}$) and to the index of cool temperatures stretching down to 13. The refinement refers to the decimal half-integer indices rather than a plus symbol (“+”) for temperatures less than 50,400 K. Thus, the full sequence for DA stars could, in principle, be DA.1, DA.2, . . . DA.9, DA1, DA1.5, DA2, DA2.5, . . . DA13.

A final indicator for WD spectra is that of gravity. Their gravities ($\log g$) can run from 9 to 7, a range comparable to that between giants and supergiants. Early indicators of corresponding differences in the width of lines in the spectra used symbols such as “d” for diffuse from broadening due to high gravity and “n” for narrow or “s” for sharp from lower gravity. An example of lines a little too sharp to be a WD can be seen in the top spectrum of Figure 12.3, that of the sdO star PG 1628 + 554. Recent WD catalogues (e.g. Kleinman et al. 2004) have started

Table 12.1 Definition of Spectral Symbols for White Dwarfs

<i>Spectral Type Symbols and Characteristics</i>
DA – Only Balmer lines; no He I or metals present
DB – He I lines; no H or metals present
DC – Continuous spectrum, no lines deeper than 5% in any part of the electromagnetic spectrum
DO – He II strong; He I or H present
DZ – Metal lines only; no H or He lines
DQ – Carbon features, either atomic or molecular in any part of the electromagnetic spectrum
<i>Additional Symbols</i>
P – Magnetic white dwarfs with detectable polarization
H – Magnetic white dwarfs without detectable polarization
X – Peculiar or unclassifiable spectrum
E – Emission lines are present
? – Uncertain assigned classification; a colon (:) may also be used
V – Optional symbol to denote variability
d – Circumstellar dust
C I, C II, O I, O II – added within parentheses to hot DQ star types to indicate presence of these atomic species

This table is an updated version of the one in McCook & Sion (1999).

to use a numeric indicator of gravity for DA and DB stars. Thus a DB1.3_ 7.9 has a temperature of about 38,800 K and a log g of 7.9. Notice how the decimal half-integer indices for temperature have been further “refined,” as is the wont for computer-derived classifications.

Stemming from the discovery by Zuckerman & Becklin (1987) of a pronounced infrared excess for a white dwarf, it is now becoming clear that a new class of “dusty DAZ” white dwarfs is needed (von Hippel et al. 2007). These white dwarfs show photospheric Balmer lines and metal lines, but are also surrounded by dusty circumstellar disks, and hence they are denoted as “DAZd” types. The lower-case “d” indicates that the dust is circumstellar, not photospheric. Its accretion onto the WD surface probably accounts for the metallic lines in its spectrum. Spectroscopically the dust appears as an excess in the normal SED after about $2\ \mu\text{m}$.

Another recent discovery is of “hot DQ” white dwarfs. Previously, DQ white dwarfs as a class were cooler than 12,000 K and showed C₂ Swan molecular bands, and sometimes atomic lines of C I. The hotter ones show C I, C II, and even O I and O II, as seen in Figure 12.8. The discoverers, Liebert et al. (2003), suggest it may be that massive white dwarfs in the DB and DO temperature range of 12,000–30,000 K, with no hydrogen left, dredge up carbon into their atmospheres.

The spectra shown in this section’s montages are the simple ones. WD spectra, with all their possibilities for showing various trace elements in their atmospheres, can take on seemingly infinite variety. Illustrations of various combinations of primary and secondary characteristics, including the more heavily-blanketed DZs, can be found in papers on WDs such as Wesemael et al. (1993), Harris et al. (2003),

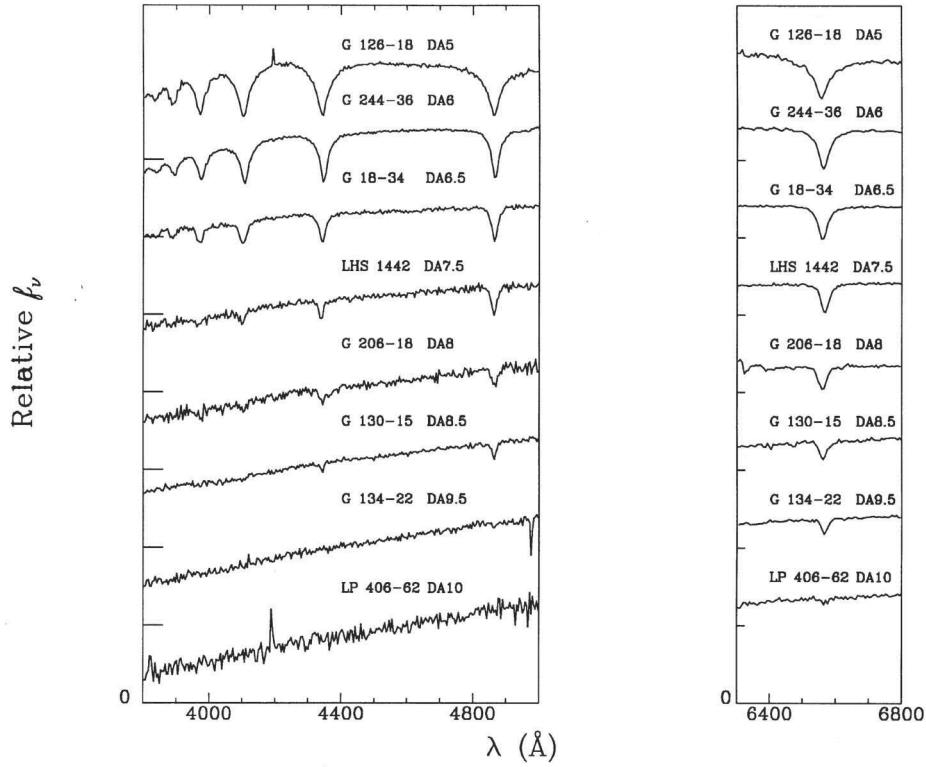


Figure 12.2 DA white dwarfs, as for Figure 12.1 but at the cool end of the sequence. The strong, broad Balmer lines become sharper and weaker, almost disappearing around DA9 save at H α in the right-hand panel.

and Zuckerman et al. (2003). The field, after a survey like SDSS has provided such an enormous increase in WD identifications (e.g., Eisenstein et al. 2006), is ripe for new experts in the endless spectral possibilities for WDs.

12.2.3 White Dwarfs in the UV and IR

The ultraviolet is an obvious region in which to explore WD spectra. For the hottest WDs, the energy peaks here, making it best for effective temperature determinations and so abundance ratios; metallic-line features can appear stronger than in the visible, such as C IV, Mg I λ 2852, Mg II λ 2796, 2803, and Ca II λ 1840; and interesting spectral features can be discovered. An example of the last point is the occurrence of broad bands around 1400 and 1600 Å for WDs of certain temperatures (see Figure 12.9). These bands were explained by Koester et al. (1985) as due to quantum-mechanical effects in a hydrogen atom and its perturber, such that the absorption is not zero beyond the “satellite” frequency, but decreases exponentially. The quasi-molecules in question are H $_2^+$ for 1400 Å and H $_2$ for

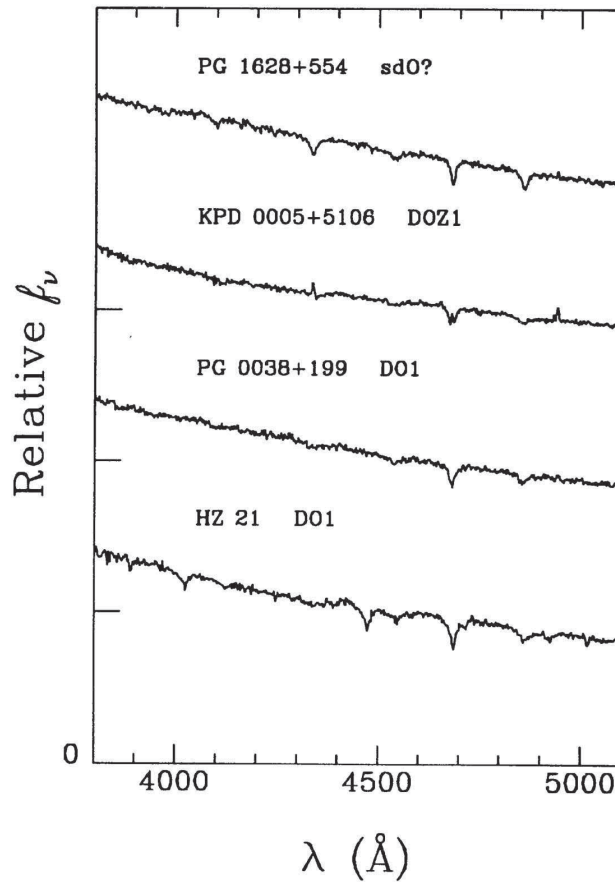


Figure 12.3 DO white dwarf sequence, as for Figure 12.1. The bottom three spectra, despite the assignment of the same temperature index “1,” form an approximate temperature sequence, with the prototype of the cool DO stars, HZ 21, at the bottom. This last shows He I $\lambda 4471$, along with the He II lines, particularly He II $\lambda 4686$, which dominate this DO class. The top object, PG 1628 + 554, is included for contrast since it looks very similar to the hot DO stars, but its slightly narrower lines probably indicate a lower gravity, and so an sdO star. The next spectrum, KPD 0005 + 5106, shows an emission core to He II $\lambda 4686$ as well as other emission features, and may be a transition object to the PG 1159 stars (see §12.2.4).

1600 Å. Other montages illustrating IUE spectra for WDs will be found in the atlas of Holberg et al. (2003).

The far-ultraviolet has no equivalent atlas to date, but studies such as Petitclerc (2005) on FUSE spectra show the importance of this spectral region in analyzing and explaining trace elements. In this example it is the trace of carbon in helium-rich DB stars that could be the sign of a weak wind in the outer atmospheres of these WDs.

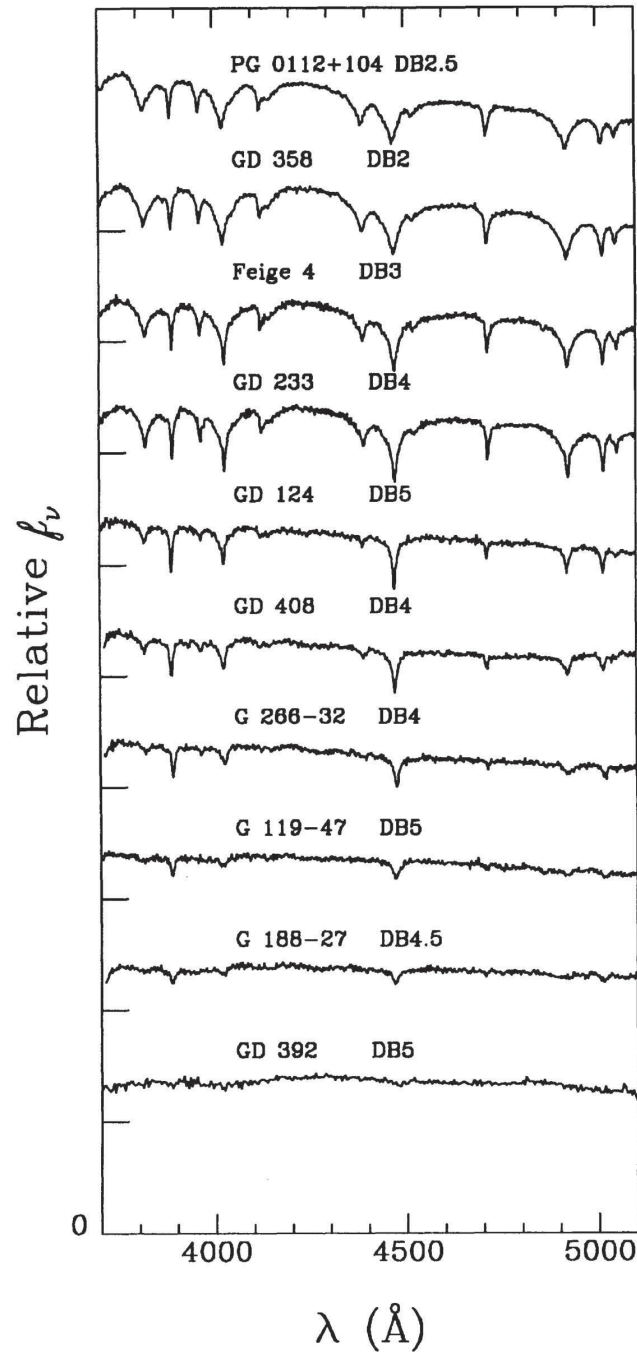


Figure 12.4 DB white dwarf sequence, as for Figure 12.1. The He I $\lambda 4471$ line shows strongly in the hottest at the top, and it has almost disappeared in the coolest at the bottom. In the red spectrum (not shown) $\lambda\lambda 5876$ and 6678 will be somewhat stronger at the cool end of the sequence. These coolest spectra merge smoothly with the helium-rich DQ spectra. Additions of hydrogen, metals, or both lines are frequent among DB spectra.

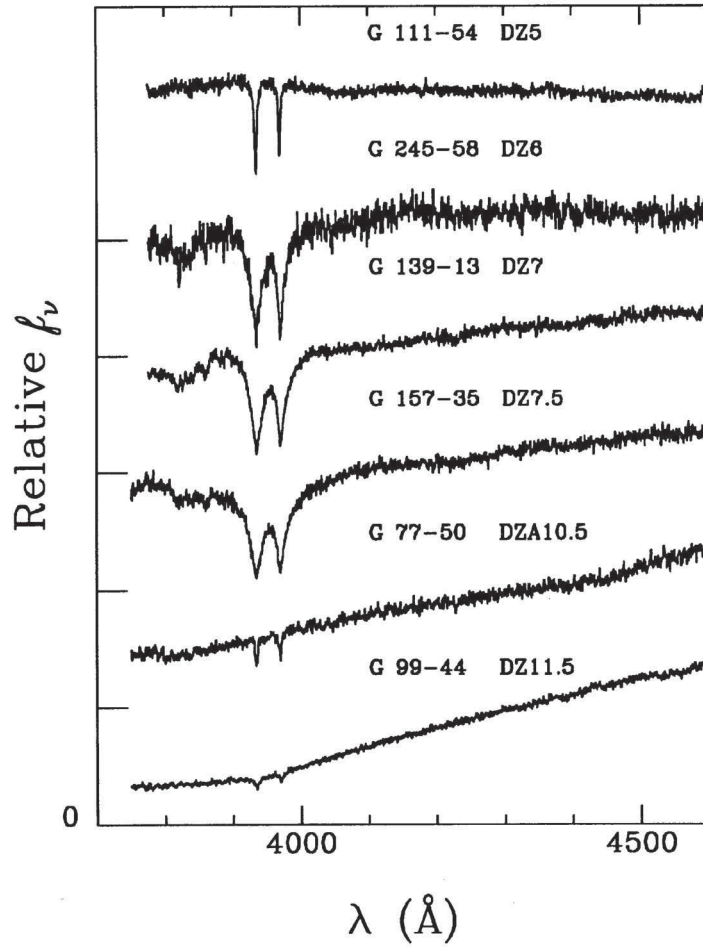


Figure 12.5 DZ white dwarfs, as for Figure 12.1. These cool, helium-rich stars are characterized by prominent Ca II H & K lines. They can also show other metallic lines, e.g., Mg I λ 3835 and lines of Fe I such as λ 3730.

The infrared, similarly to the FUV, also lacks any systematic spectral atlas of WDs. More usually, the identifying and investigating the cool companion to a hot WD is the concern for IR spectra.

12.2.4 PG 1159 Stars

The pulsating “PG 1159” stars are the hot extension of the white-dwarf sequence and were first recognized as a class by Wesemael et al. (1985). They are pre-white dwarfs in which gravitational diffusion has not yet had time to produce an outer pure-helium layer.

They are characterized by having no H or He I features and by a very distinctive He II plus C IV blend in the 4650–90 Å region. In showing atomic oxygen they

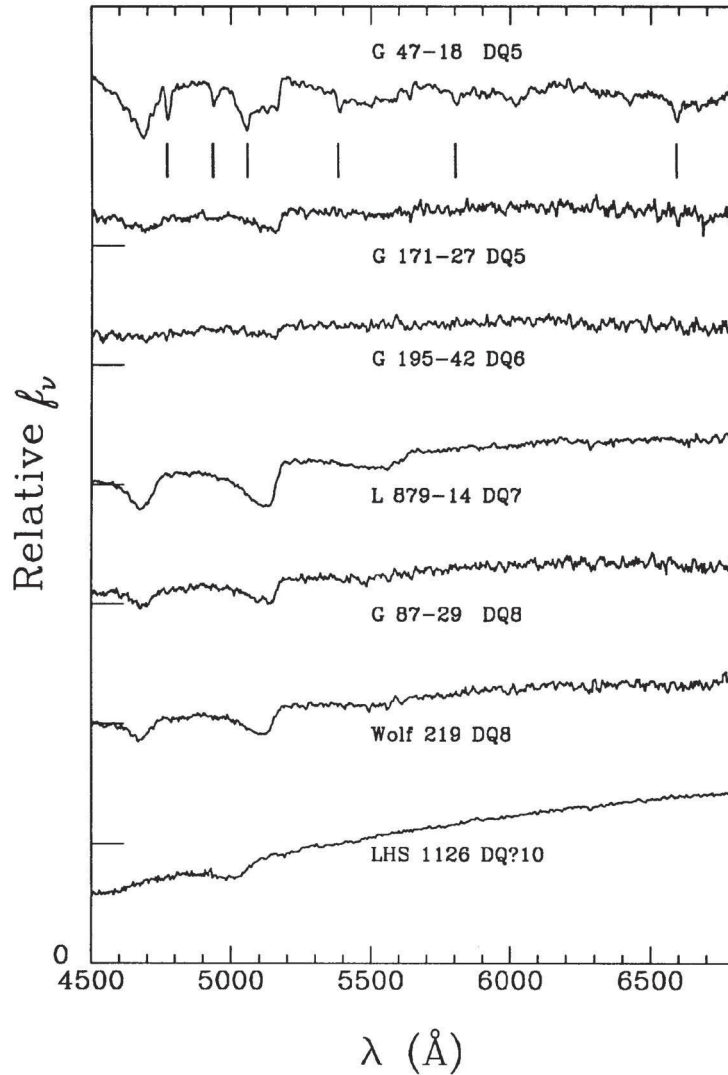


Figure 12.6 DQ white dwarfs, as for Figure 12.1. Like the DZs these are also cool, helium-rich stars, but are dominated by molecular carbon bands, notably the triplet system Swan bands (2, 0) at $\lambda 4382$, (1, 0) at $\lambda 4737$, (0, 0) at $\lambda 5165$, and (0, 1) at $\lambda 5635$, but for some also the Deslandres–d’Azambuja bands [$\lambda\lambda 3600, 3852, 4102, \dots$], a singlet transition system in the violet. Other stars, like G 47-18, show C I features too (as marked). The bottom spectrum, LHS 1126, a very cool star, has heavily shifted and broadened C_2 bands.

have similarities to the hot DQ star spectra, but are even hotter. Werner (1992) has divided the PG 1159 stars into three groups of increasing temperature: the A group; the E group with emission cores in the main features, among which is the prototype PG 1159; and the IgE group with emission features but sharper absorption wings denoting lower gravities. These groups are illustrated in Figure 12.10.

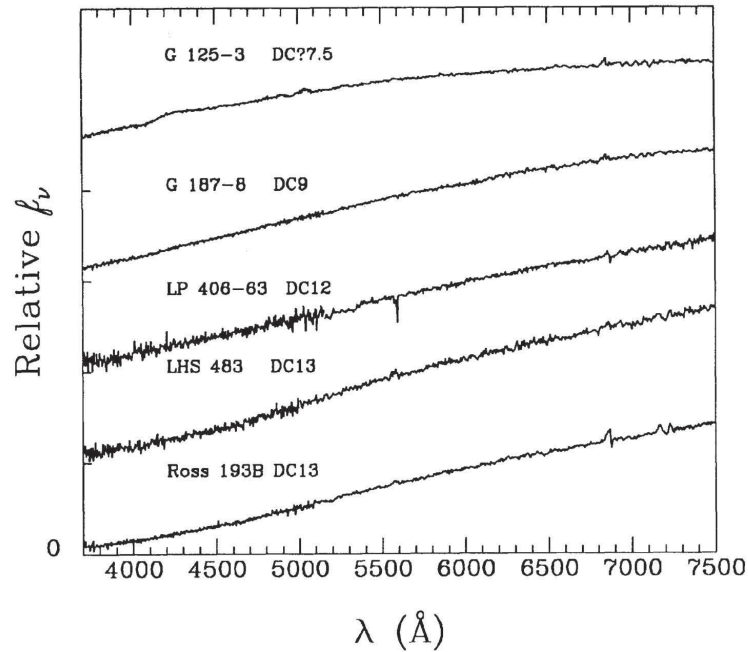


Figure 12.7 DC white dwarfs, as for Figure 12.1. These are completely featureless at the 5% of continuum level, even showing no sign of H α λ 6563. The glitches near 5577, 6800, and 7200 Å are due to an incomplete correction for atmospheric O₂ and night-sky lines.

12.3 NOVAE

12.3.1 Classical Novae

The term “nova,” which derives from the Latin term *nova stella*, has been used for centuries to describe the sudden appearance and brightening of a “new star.” We now realize there are a number of physical phenomena that can lead to the sudden brightening of a star, including those that lead to a supernova explosion (§12.4) and the instabilities that result in the outburst of a luminous blue variable (LBV, §11.2), such as the “Great Eruption” of η Carinae during the nineteenth century. In this section we concentrate on the *classical novae*, a class of stars characterized by an explosion that leads to an increase in brightness in the optical by 7–16 magnitudes, although Nova Cygni 1975 increased by over 19 magnitudes! This increase is usually sudden, and takes place over only one or a few days, although in some cases the increase is more gradual. After reaching maximum brightness, the decline is usually much more gradual than the brightening, and can sometimes last for years.

The classical novae actually belong to a group of related stars known as the *Cataclysmic Variable* (CV) stars. The CVs will be described briefly in §12.3.2. We now know that the classical novae and the CVs in general are close binary systems with a white dwarf as the primary and (usually) a lower main-sequence star as the

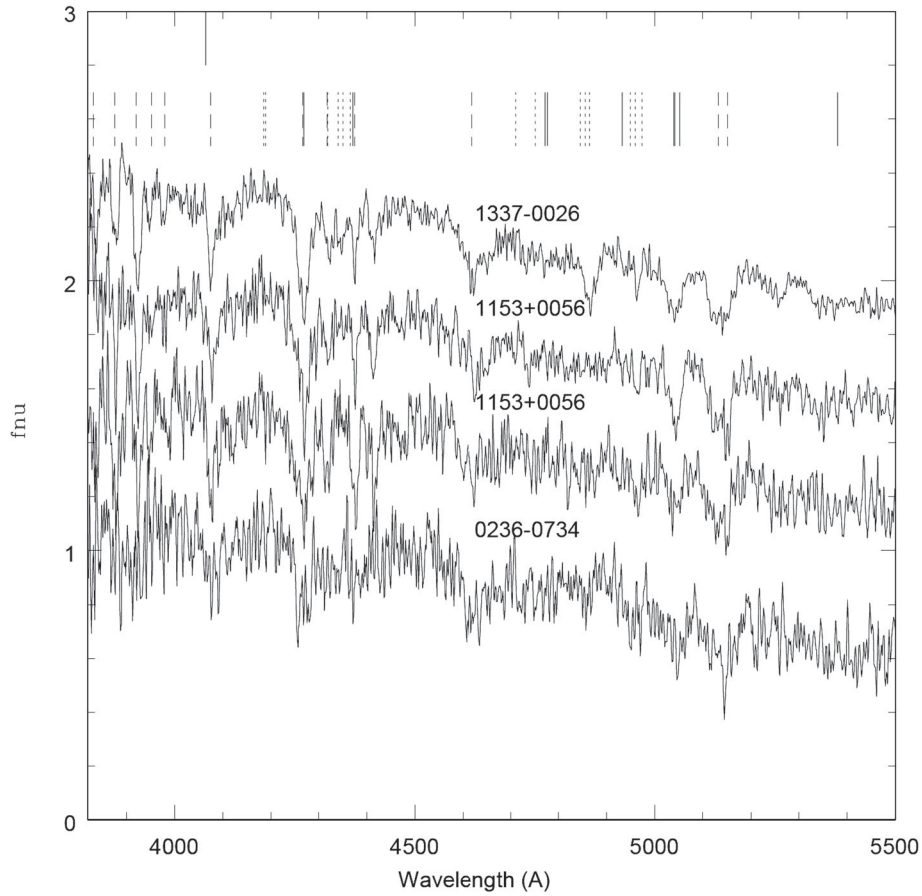


Figure 12.8 DQ white dwarfs, but with temperatures $\geq 28,000$ K. These hot DQs show C I (solid tick marks), C II (dashed ticks), and possible O II (dotted ticks) in the top spectrum. Two independent spectra of SDSS J1153 + 0056 are displayed to give an idea of the reliability of features at this low S/N. No H or He features are visible. The figure is from Liebert et al. (2003), and is reproduced by permission of the AAS.

secondary. In these systems, the main-sequence star loses hydrogen-rich material to an accretion disk around the white dwarf. In a classical nova, hydrogen-rich material from the accretion disk forms a layer on the surface of the white dwarf. Once this hydrogen-rich layer becomes sufficiently massive, a runaway thermonuclear reaction takes place, leading to the violent ejection of much of this material, forming an expanding shell. Model calculations suggest that the remaining material on the white-dwarf surface is hot enough to sustain thermonuclear reactions, meaning that the luminosity of the white dwarf remains at or near the Eddington limit. This causes the surface layers to expand, forming an extended envelope that may even encompass the companion star; a wind arises from this extended envelope (Williams 1992). Both the wind and the expanding shell are sites for the

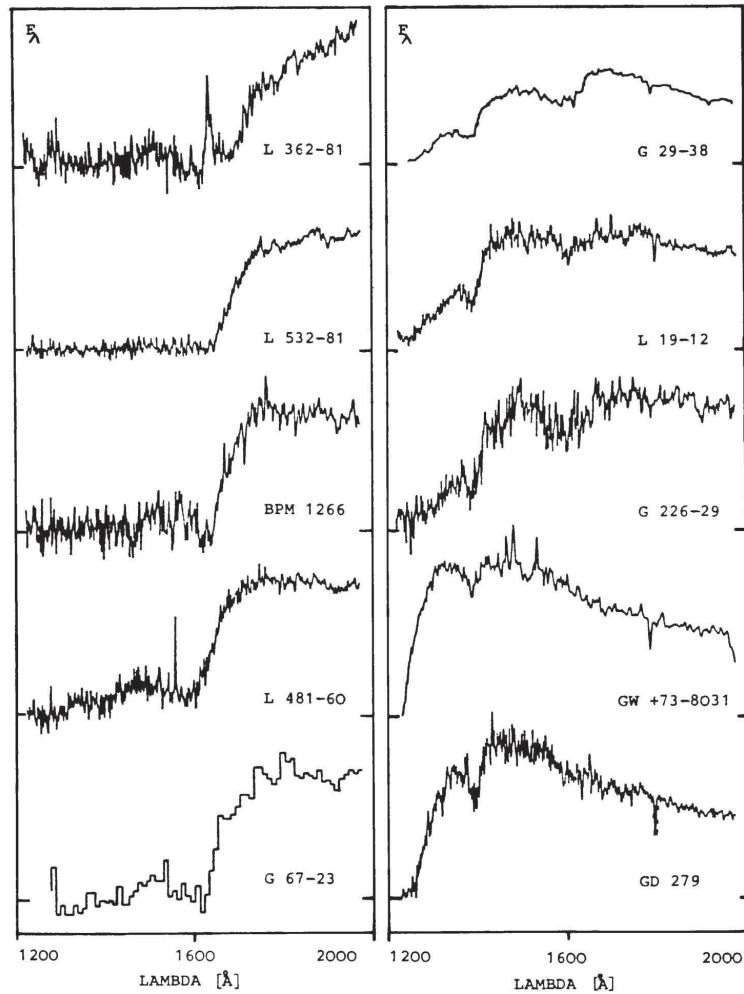


Figure 12.9 DA white dwarfs observed by IUE and arranged, from top to bottom and left to right, according to increasing temperature. Note the appearance and disappearance of the broad bands around 1400 Å and 1600 Å. Montage from Koester et al. (1985), and reproduced by permission of *Astronomy and Astrophysics*.

formation of the emission lines that characterize the spectrum of a nova. The evolution of these two entities leads to the dramatic and complex changes observed in the spectra of novae.

A classical nova can be recognized by its light curve and spectrum. Classical novae may be classified by the shape of their light curves (Woronzow-Weljaminow 1953; Duerbeck 1981). While a detailed description of these light-curve classification schemes is beyond the scope of this book, very briefly, novae are classified into very fast and fast novae with smooth light curves and fast, slow, and very slow novae with irregular light curves, often involving an extended rise period, multiple

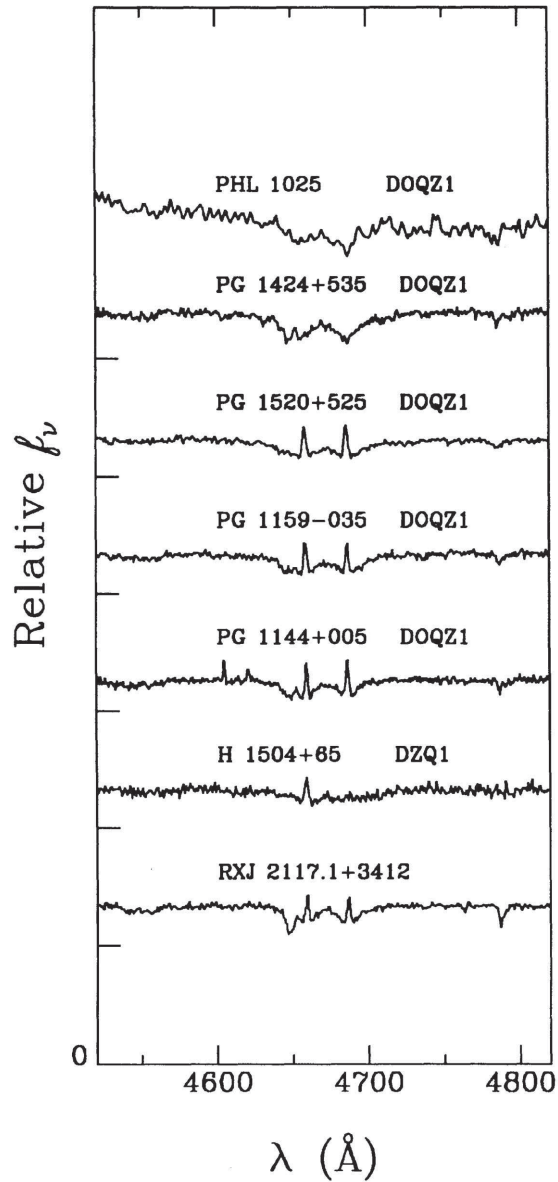


Figure 12.10 PG 1159 stars, as for Figure 12.1. These are very hot, degenerate, or pre-degenerate stars. Their spectra lack H or He I and have a He II plus C IV blend in the 4650–90 Å region. The top two spectra are in the A group, as defined by Werner (1992), showing only absorption features. The middle four belong to the E group, showing emission in the cores of the defining He II plus C IV blend. The bottom spectrum illustrates the sharper lined, lower gravity, and still with emission features, lgE group.

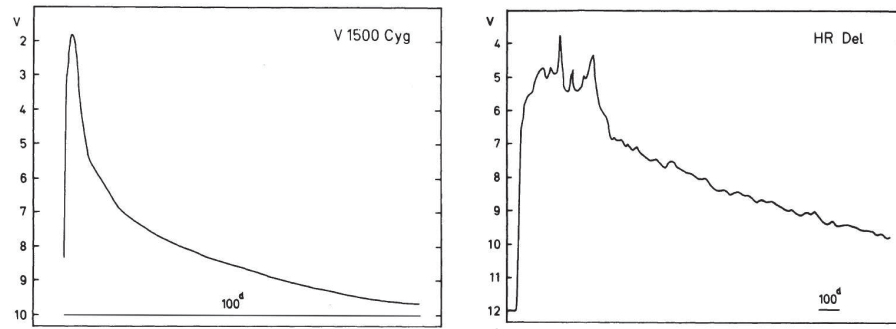


Figure 12.11 Two typical classical-nova light curves. The one on the left is a featureless light curve of a fast nova; on the right, a slow, irregular light curve. The bar on the bottom of each graph represents 100 days. Reproduced from Duerbeck (1981) by permission of the University of Chicago.

maxima, an extended maximum, oscillations during decline, and/or a deep, rapid decline followed by a partial recovery. Figure 12.11 shows two typical nova light curves.

We concentrate in this section on the spectral classification of the classical novae. The first detailed examination of the evolution of nova spectra was carried out by Payne-Gaposchkin (1957) in her classic and pioneering book *The Galactic Novae*. In that book, Payne-Gaposchkin described and illustrated in detail the spectral evolution of a number of novae, but did not propose a classification system, admitting that “the spectral development of all novae is complex, and the observations are very difficult to interpret.” McLaughlin, in a detailed and still useful treatise (McLaughlin 1960) devised a complex system for categorizing nova spectra. He broke the spectral evolution down into a number of phases, including “premaximum,” “principal,” “diffuse enhanced,” “orion,” “nebular,” and finally “post nova.” For each of these phases he looked at the velocities and strengths of certain lines, and the appearance and disappearance of certain absorption and emission features. This system is really a blend of classification and detailed analysis and as such is difficult to apply. In 1991 a simpler and more versatile classification system was proposed by Robert Williams and his colleagues (Williams et al. 1991; Williams, Phillips, & Hamuy 1994). We will confine our discussion of nova spectral classification to the Williams et al. system, also known as the “Tololo Nova Spectral Classification System.”

THE TOLOLO SYSTEM FOR THE CLASSIFICATION OF CLASSICAL NOVA SPECTRA

The Tololo system concentrates on the spectral classification of *post-outburst* spectra. It is, of course, difficult to obtain spectra of novae at maximum light, not only because of the short time spent at maximum, but also due to difficulties in mobilizing a telescope and spectrograph for these unpredictable events. No spectra at maximum light were obtained during the Tololo nova project

(Williams et al. 1991; Williams, Phillips, & Hamuy 1994). As a result, there is still some uncertainty about the appearance of the spectrum of a classical nova at maximum. Payne-Gaposchkin (1957) and McLaughlin (1960) published photographic spectra of a number of novae at maximum, including V 603 Aql, DQ Her, and Nova Pictoris. Interestingly, at maximum, these novae had absorption spectra that resembled A or F supergiants. Williams et al. (1991), however, expressed doubt that the maximum-light spectrum is a purely absorption spectrum, pointing out that photographic spectra were usually exposed to bring the continuum to optimal density, which would have suppressed any weak emission present. Their nova spectra, even those obtained shortly after maximum light, all show the presence of emission features.

The post-outburst spectrum of a classical nova goes through a number of phases. Immediately after maximum light, when the expanding shell is still at relatively high density, the spectrum is dominated by emission lines arising from permitted transitions; the Balmer lines are almost always the strongest emission features at this stage. In the permitted phase, nova spectra fall into two distinct classes. The “Fe II” novae, which evolve relatively slowly spectroscopically, are dominated by Fe II permitted lines and other low-ionization transitions due to Na I, O I, Mg I, etc. The He/N novae, which usually evolve rapidly, are characterized by higher excitation transitions, including He II $\lambda 4686$, He I $\lambda 5876$, N II $\lambda\lambda 5001, 5679$, and/or N III $\lambda 4640$. The He/N novae also usually show broader emission lines.

As the densities of the emitting regions fall, forbidden emission lines begin to appear, first the higher-excitation “auroral” lines (such as [N II] $\lambda 5755$, [O III] $\lambda 4363$, and [O II] $\lambda\lambda 7319, 7330$) that have relatively high critical densities;² then, as the densities continue to decrease, the more familiar, lower-excitation “nebular” forbidden lines ([O III] $\lambda 5007$, [N II] $\lambda 6584$, [Ne III] $\lambda 3869$, and [Fe VII] $\lambda 6087$) appear.

The He/N novae generally develop differently from the Fe II novae. After the permitted phase, they either (a) fade away without developing any forbidden emission lines, (b) go through a high-excitation coronal phase characterized by the appearance of the coronal [Fe X] $\lambda 6375$ line, or (c) develop strong forbidden lines of [Ne III] and [Ne V] in the nebular stage, resulting in a “neon” nova (Williams 1992).

Eventually, the ionization level drops, and the spectrum becomes that of the quiescent system. The spectral evolution of three novae are illustrated in Figures 12.12 to 12.14.

On the Tololo classification system, a nova spectrum is classified as belonging to either the permitted (P), auroral (A), nebular (N), or coronal (C) phase. These phases are defined in the spectral region 3400–7500 Å as follows:

Phase C: A spectrum is considered to be in the coronal phase if the coronal [Fe X] $\lambda 6375$ emission line is present and stronger than the nebular [Fe VII] $\lambda 6087$ line, regardless of the strengths of any other line.

²The critical density for a forbidden spectral line is the density at which the collisional de-excitation rate is equal to the spontaneous radiative de-excitation rate. The ratio of the two rates will vary from line to line.

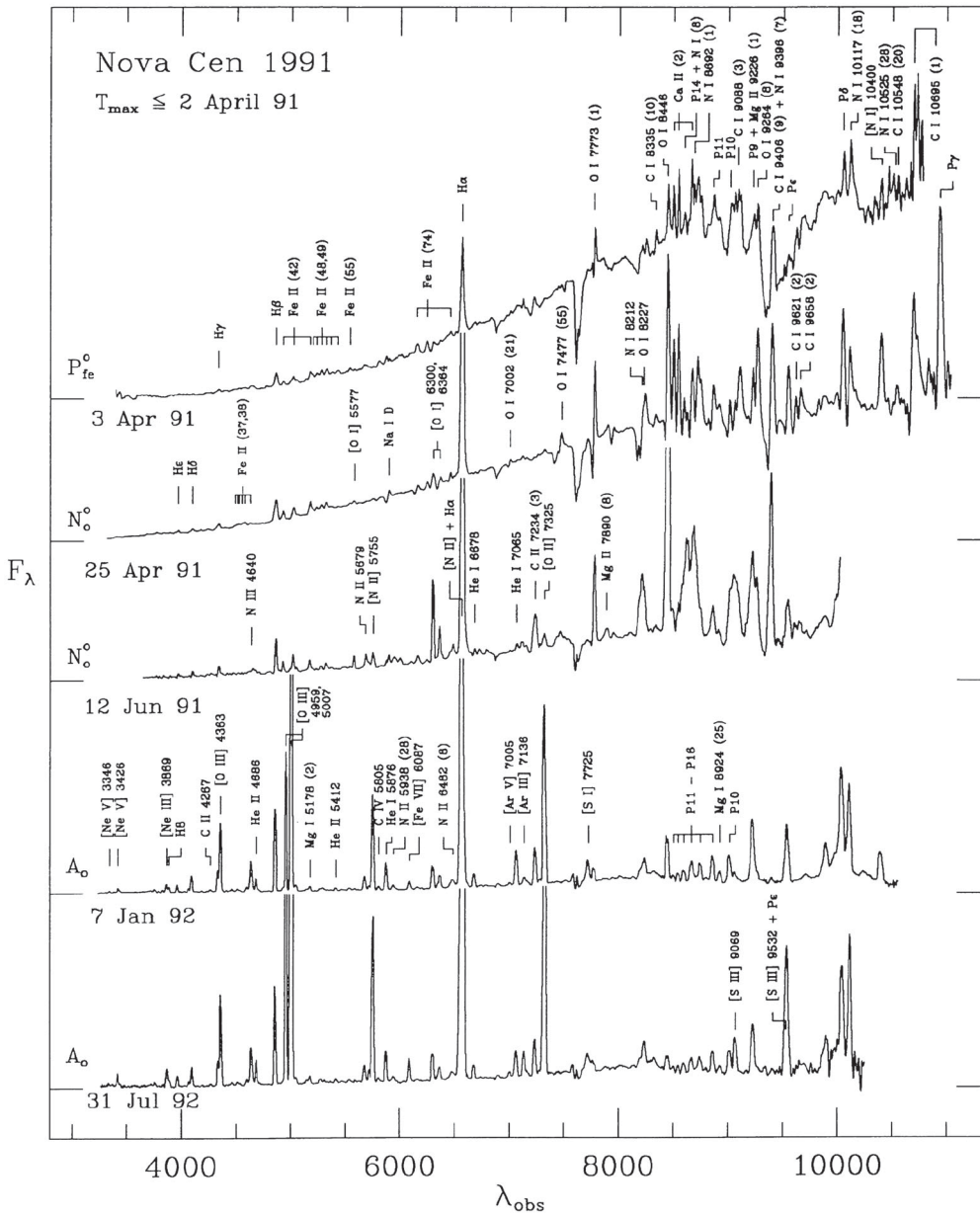


Figure 12.12 Time development of the spectrum of Nova Cen 1991, an “Fe II γ ” nova that developed a “standard” nebular spectrum, and then entered an auroral phase. This figure along with Figures 12.13 and 12.14 reproduced courtesy of Williams, Phillips, & Hamuy (1994) and by permission of the AAS.

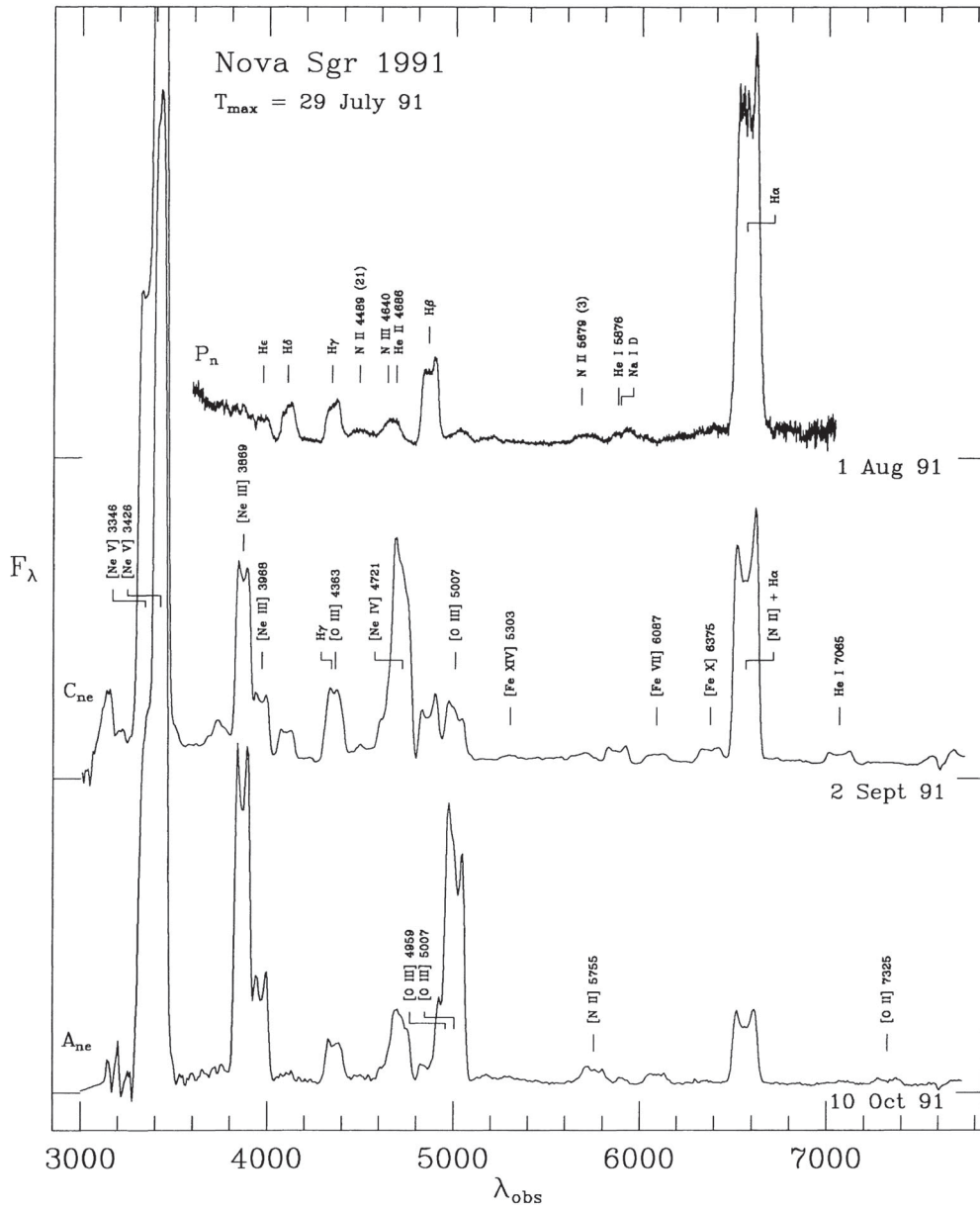


Figure 12.13 Optical spectra of the very fast “He/N” Nova Sgr 1991. This nova developed a coronal spectrum (note the presence of [Fe X] $\lambda 6375$), and faded very rapidly. Reproduced by permission of the AAS.

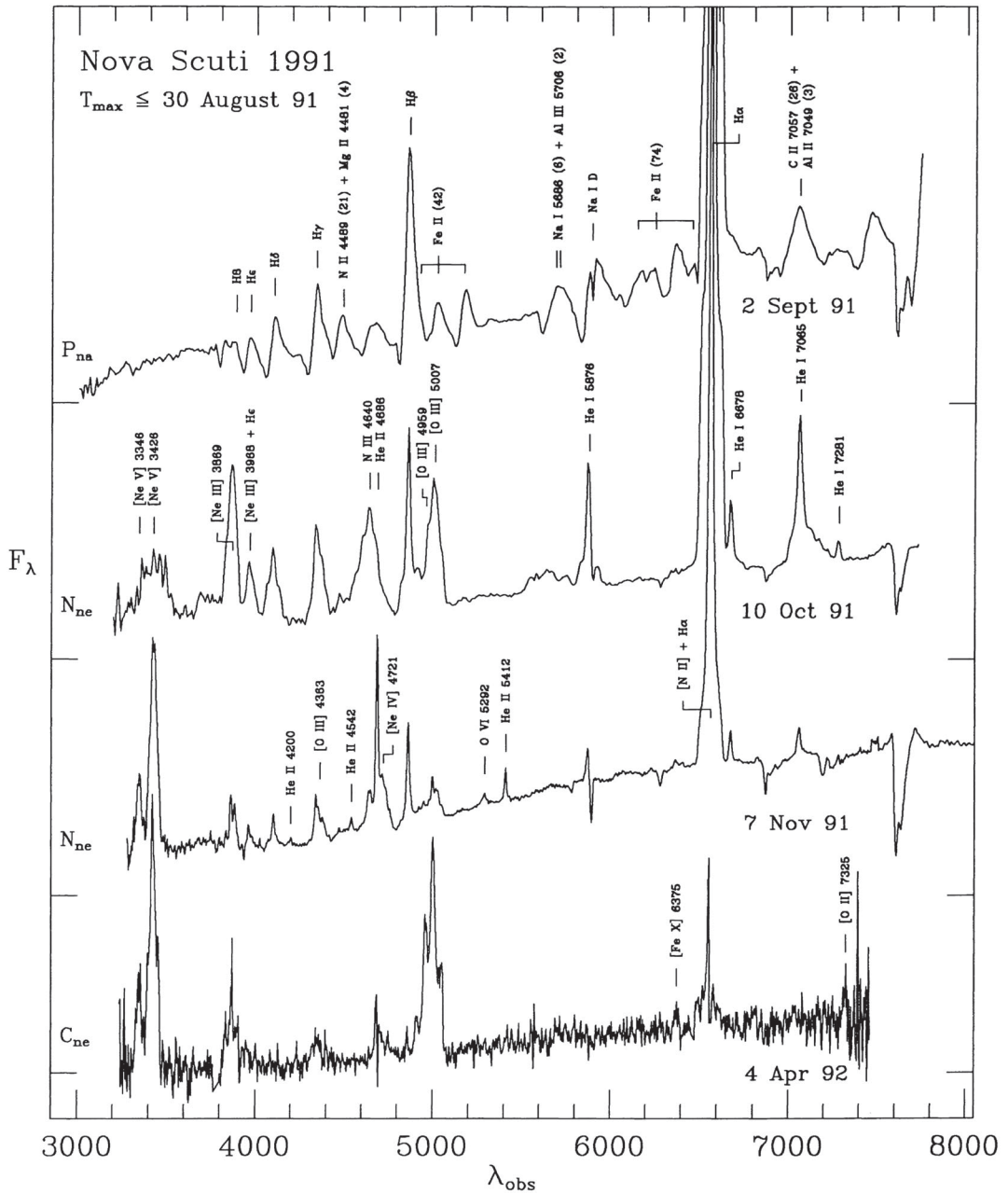


Figure 12.14 Optical spectra of the broad-lined “Fe IIb” Nova Scuti 1991. Note the development of strong neon forbidden lines and the development of a coronal phase. Also note that the width of the emission lines decreased with time. Reproduced by permission of the AAS.

Phase P: If the spectrum is not in the coronal phase, then it is in the permitted phase if the strongest non-Balmer line is a permitted transition.

Phase A: If the spectrum is not in the coronal phase, then it is in the auroral phase whenever any forbidden auroral line has a flux greater than that of the strongest non-Balmer permitted line, regardless of any nebular line strengths.

Phase N: If the spectrum is in neither the coronal nor the auroral phase, it is in the nebular phase if the strongest non-Balmer line is a forbidden nebular line.

A subclass is defined for each phase depending upon the stronger non-Balmer lines; this subclass is denoted by a subscript to the spectral phase. These subclasses are defined as follows:

Phase C subclasses (assigned from the strongest non-Balmer line in the spectrum, and selected from one of the following):

a = auroral transition :[N II] $\lambda 5755$; [O I] $\lambda 5577$; [O II] $\lambda 7319, \lambda 7330$;

[O III] $\lambda 4363$

he = He I $\lambda 5876, \lambda 7065$

he⁺ = He II $\lambda 4686$

n = N III $\lambda 4640$; N II $\lambda 5679$; [N II] $\lambda 6584$

o = [O III] $\lambda 5007$

ne = [Ne III] $\lambda 3869$; [Ne V] $\lambda 3426$

fe = [Fe X] $\lambda 6375$; [Fe XIV] $\lambda 5303$

Phase P subclasses (assigned from the strongest non-Balmer line in the spectrum):

he = He I $\lambda 5876, \lambda 7065$

he⁺ = He II $\lambda 4686$

c = C IV $\lambda 5805$; C II $\lambda 7234$

n = N II $\lambda 5679, \lambda 5001$; N III $\lambda 4640$; N V $\lambda 4605$

fe = Fe II $\lambda 5018, \lambda 5169, \lambda 5317$

na = Na I $\lambda 5892$

ca = Ca II H&K

Phase A subclasses (modified in Williams, Phillips, & Hamuy 1994, assigned from the strongest auroral line in the spectrum):

n = [N II] $\lambda 5755$

o = [O I] $\lambda 5577$; [O II] $\lambda 7325$; [O III] $\lambda 4363$

ne = [Ne III] $\lambda 3343$; [Ne IV] $\lambda 4721$

s = [S I] $\lambda 7725$; [S III] $\lambda 6312$

Phase N subclasses (assigned from the strongest nebular line in the spectrum):

n = [N II] λ 6584
 o = [O I] λ 6300; [O III] λ 5007
 ne = [Ne III] λ 3869; [Ne V] λ 3426
 fe = [Fe II] λ 4244, λ 5159; [Fe III] λ 4658, λ 5270; [Fe V] λ 4072;
 [Fe VI] λ 5176; [Fe VII] λ 6087

Additional subclasses that may be assigned provided the spectral coverage (extending into the near-infrared) is available (these subclasses are indicated with a superscript):

o = flux of O I λ 8446 exceeds that of H β
 s = the clear presence of red continuum from a late-type secondary.

Notes to the classification system:

1. Unless [N II] λ 6584 is clearly resolved from H α , the H α + [N II] emission feature is always considered to be due entirely to H α . Similarly for the [O III] λ 4363 + H γ blend, the [O III] contribution is that component that exceeds the geometrical mean of H β and H δ .
2. Provisional phase assignments may be made on the basis of the spectral region from H γ to H α during the period before the spectrum develops forbidden lines.

One of the advantages of the succinctness of the Tololo notation is that it can be used to write “evolutionary sequences.” Let us suppose, for instance, that a nova passed through the phases P_n, C_{ne}, and A_{ne} (such as Nova Sgr 1991, Figure 12.13; Williams, Phillips, & Hamuy 1994). We may then write its evolutionary sequence as P_nC_{ne}A_{ne}. Such evolutionary sequences allow one to understand the spectral evolution at a glance, but they can also yield certain insights such as the following points (from Williams et al. 1991; Williams, Phillips, & Hamuy 1994):

1. within a month after outburst, recurrent novae (see §12.3.2) enter a high-ionization phase, marked either by coronal [Fe X] emission, or very strong He II.
2. the presence of coronal lines is often accompanied by lines due to species in low ionization states, such as O I λ 8446.
3. the neon novae (those with strong [Ne III] or [Ne V] lines) evolve directly from the permitted phase to the nebular phase, without an intermediate coronal or auroral phase (although see point 4, below).
4. the spectral evolution of a nova is correlated with its spectrum at or near maximum light. As mentioned above, most novae can be placed into one of two classes. These two classes are based on the stronger emission lines

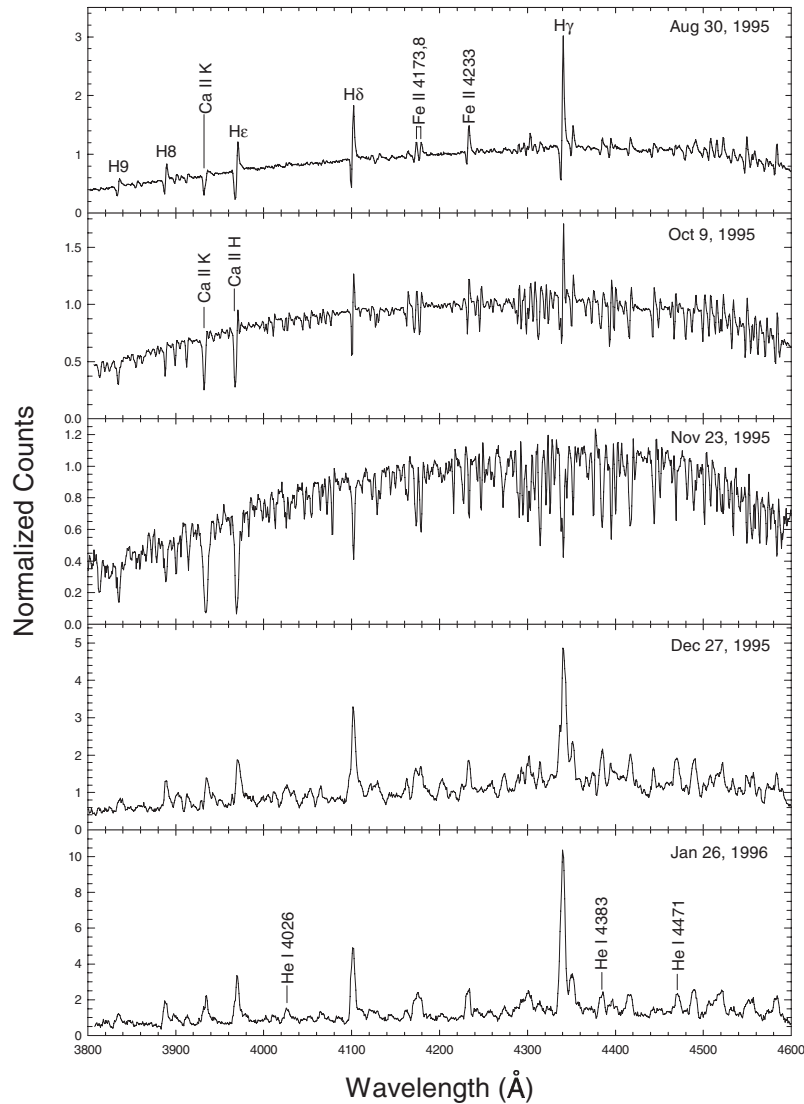


Figure 12.15 Blue-violet non-flux-calibrated spectra (1.8 \AA resolution) of the unusual Nova Cas 1995. The first spectrum was obtained 5 days after discovery, and shows well-developed P-Cygni profiles for not only the Balmer lines, but also for many Fe II lines. Later, just before the first “flare,” the spectrum took on the character of a luminous F supergiant. The final two spectra in the montage show much broader lines of hydrogen, iron, and neutral helium. Spectra obtained at the Dark Sky Observatory.

present at the time of visual maximum, e.g. either Fe II lines or lines of He and N. Almost all He/N novae have high expansion velocities and thus tend to develop neon or coronal forbidden spectra; an example is Nova Sgr 1991 (V4160 Sgr, Figure 12.13), which went through a $P_n C_{ne} A_{ne}$ evolutionary sequence. On the other hand, low velocity Fe II novae, which are characterized by narrow emission lines (and thus are designated Fe II_n), go on to develop

auroral lines of N and O, followed by a nebular phase with forbidden nebular transitions of the same elements—known as the “standard” development (example, Nova Sgr 1992, No. 1; $P_{\text{Fe},n}A_n$, also see Figure 12.12). Finally, high-velocity Fe II novae (characterized by broad lines, and thus designated Fe IIb) generally go on to develop a forbidden neon spectrum, similar to some He/N novae. Fe IIb novae can also pass through a coronal phase (example, Nova Sct 1991, Figure 12.14; $P_{\text{Na}}N_{\text{ne}}C_{\text{ne}}$), again suggesting a closer relation to the He/N novae than to the Fe II_n novae.

Classical novae may also be classified as either CNO or ONeMg novae, according to the composition of the ejecta. Such differences probably reflect the composition of the underlying white dwarf (Sparks et al. 1999).

Some novae simply do not fit into the normal evolutionary patterns outlined above. A case in point was Nova Cas 1995, which was discovered on August 24, 1995, while it was still brightening. It shortly thereafter leveled out in brightness at about $V = 9$ –10, where it remained until Dec 17, 1995, on which date it flared to nearly $V = 7$, after which it rapidly declined back to $V = 9$ –10. Over the next few years, the brightness slowly declined, but this decline was interrupted by a number of 1–1.5 m flares. An early spectrum (see Figure 12.15), obtained 5 days after discovery, shows P Cygni profiles in the Balmer lines (up to H9) and in numerous Fe II lines. Over the following three months, the Balmer emission lines and the Fe II emission components faded, and the spectrum took on the appearance of a luminous A or F supergiant. After the Dec 17, 1995 flare, the emission lines reappeared, but this time were broader and without P Cygni profiles. The Balmer lines continued to broaden and the other emission lines to fade. Very late spectra (obtained in 1997 and 1998) show strong Balmer and He II emission.

12.3.2 Other Cataclysmic Variables

As mentioned in the previous section, the classical novae are members of a broader class of interacting binaries called the Cataclysmic Variables (CV). In addition to the classical novae, the CVs include the recurrent novae, dwarf novae, nova-like variables, helium CVs, and the polar variables.

The classical novae are novae that have undergone only one outburst, and the recurrent novae are, by definition, systems that have been *observed* to have undergone more than one outburst. The operative word here is “observed” as many classical novae may have undergone repeated outbursts, except that the characteristic time between outbursts may be longer than a few hundred years. In classical novae the outburst has been attributed to a runaway thermonuclear event on the surface of the white dwarf; in most recurrent novae that is probably the case as well. However, in some recurrent novae, the outburst may be related to an episodic mass transfer event. One of the best-known recurrent novae is T CrB, also known as the “Blaze Star.” A spectrum of T CrB in the quiescent state is shown in Figure 12.16;

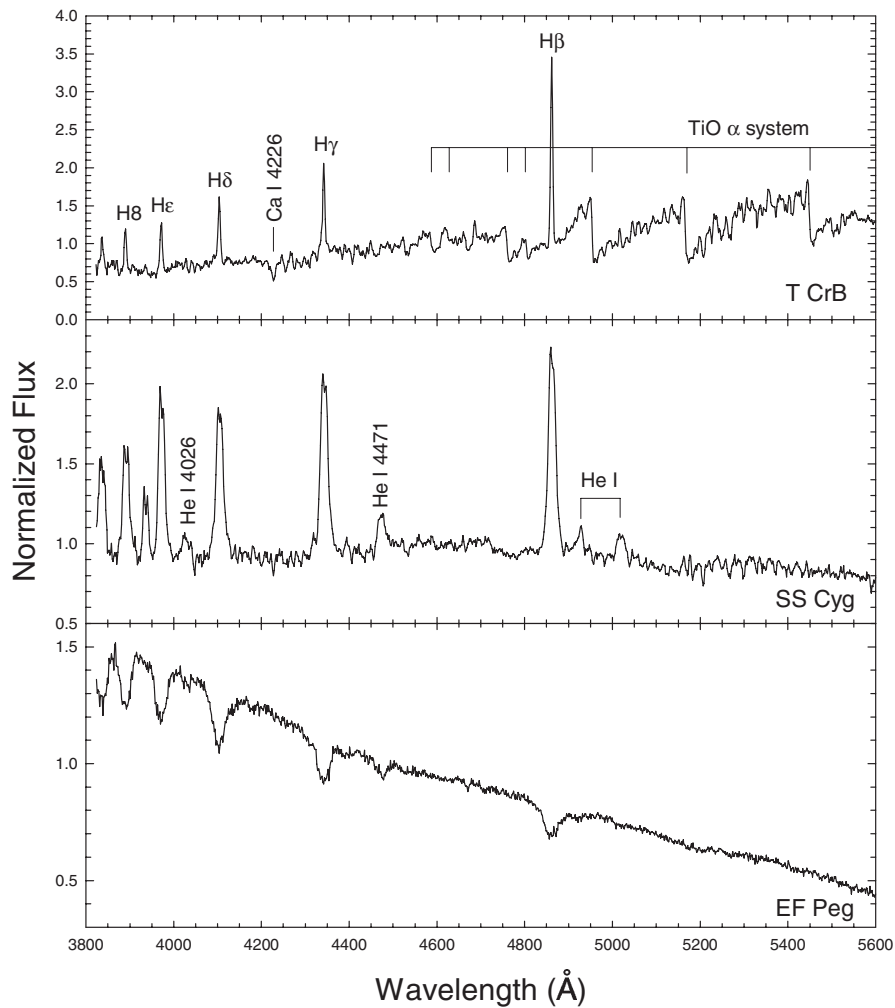


Figure 12.16 Spectra of three cataclysmic variables. Beginning at the top, T CrB, a recurrent nova, at quiescence; SS Cyg, a U Gem-type dwarf nova, also at quiescence; and EF Peg, an SU UMa-type dwarf nova, caught during a superoutburst. Spectra obtained at the Dark Sky Observatory.

note that the underlying spectrum is that of an M-giant, with superimposed Balmer emission lines.

Dwarf novae are stars that undergo a periodic brightening, usually with an amplitude of 2–5 mag. The time scale involved is usually weeks to years. In quiescence, dwarf novae usually have emission-line spectra, but during an outburst, the spectrum is transformed to absorption-line. The underlying cause of the outburst is thought to be due to an instability in the accretion disk. The prototype is U Gem, but recognized subclasses involve the SU UMa stars that show occasional outbursts of very large amplitude (superoutbursts), and the Z Cam stars that show

occasional standstills during the decline after an outburst. Figure 12.16 shows a spectrum of SS Cyg, a U Gem dwarf nova, during quiescence, and EF Peg, an SU UMa variable, during a superoutburst.

The nova-like variables are probably quiescent classical novae that have not been observed in outburst. In helium CVs the mass transfer involves helium-rich instead of hydrogen-rich material to the white dwarf. Finally, the polar variables involve systems with strong magnetic fields. The magnetic field funnels the accreting mass onto a spot—a magnetic pole—on the surface of the white dwarf (thus the name *polar*). In the AM Herculis systems, an accretion disk does not form because of the presence of a strong magnetic field and because the white dwarf spin is synchronous with the orbital period of the accreting material. Systems with weaker magnetic fields do, however, form a partial accretion disk with the white dwarf spinning more rapidly than the orbital period of the disk. These systems, which are intermediate to the non-magnetic CVs and the strongly magnetic polars, are called *intermediate polars* or DQ Her systems.

Recently, much attention has been paid to what appears to be a new class of eruptive variables that are neither novae nor supernova. The best known example of this class is V838 Mon, which erupted in January 2002 (Brown 2002), and reached optical maximum in February of that year. By May, it had returned to pre-outburst levels in the optical. This eruption did not, however, follow the usual pattern for classical novae. Instead, after developing an A–F supergiant spectrum at the optical maximum, the effective temperature declined sharply. By April, it had almost disappeared from the optical, but it continued to remain bright in the infrared, and the spectrum evolved into that of a very cool supergiant; Evans et al. (2003) even classified it as an L supergiant (see Figure 12.17).³ After the eruption of V838 Mon, it was realized that two other objects were likely in the same class: M31 RV (discovered September 1988) and V4332 Sgr, discovered at the end of February 1994. These three eruptive variables, all of which, after maximum light, had spectra similar to a luminous M supergiant, are now becoming known as V838 Mon objects.

The mechanism underlying the V838 Mon outbursts is still not known. A number of thermonuclear models have been proposed, including a nova-like outburst on a white dwarf, a thermonuclear shell event in an evolved massive star approaching carbon ignition, or a very late He-shell flash in a post-AGB star. Other scenarios include stellar mergers or a collision between a gas-giant planet and a star. The recent discovery (Afşar & Bond 2007) that V838 Mon is the member of a young stellar cluster, and that the progenitor was not a luminous object, effectively rules out the thermonuclear models. Thus a stellar or planetary merger seems the most likely mechanism.

³The classification of V838 Mon as an L-type supergiant does not stand up to scrutiny. Evans et al. (2003) based their classification on the strength of the water bands in the near-infrared. However, the depth of the H₂O bands has nothing to do with the definition of the L class (see Chapter 9). Indeed, the optical spectrum of V838 Mon shows extremely strong and saturated TiO and VO bands, and thus clearly is a late M supergiant, with no indication whatsoever of TiO and VO condensation as would be characteristic of an L-type object (see §9.4.2; private communication, J. Davy Kirkpatrick).

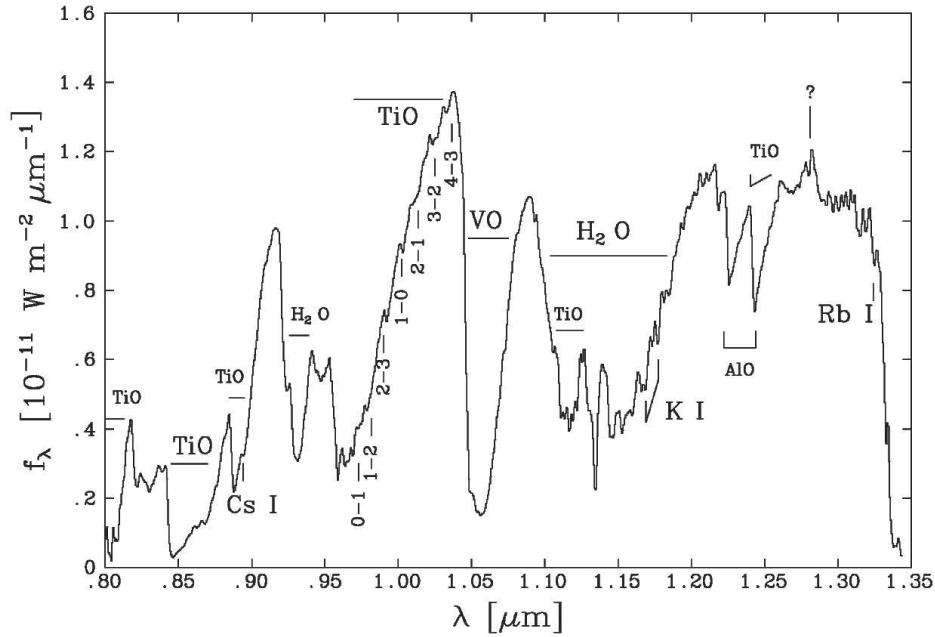
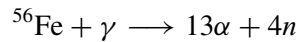


Figure 12.17 A near-infrared spectrum of V838 Mon, obtained in Oct 2002. Note the deep H₂O molecular bands, and the strong lines of alkali metals. Figure reproduced courtesy of Evans et al. (2003) and Blackwell Publishing, Ltd.

12.4 SUPERNOVAE

A supernova is a cataclysmic explosion that ends the life of a star. For a short period of time, the luminosity of a supernova can exceed that of an entire galaxy. With the exception of certain types of gamma-ray bursts (some of which may actually be associated with supernovae), a supernova represents the single most energetic event in the current Universe. There are at least two mechanisms that can lead to supernova explosions. In the first, a massive star ($M > 8M_{\odot}$) develops, through a series of nuclear reactions, an iron core. Instead of fusing, ^{56}Fe photodisintegrates:



This is an *endothermic* reaction, resulting in the catastrophic collapse of the iron core. This leads, via various mechanisms that are not yet completely understood, to a supernova explosion. The second occurs in a mass-transfer binary system in which one of the stars is a carbon–oxygen white dwarf near the *Chandrasekhar limit* ($\approx 1.39M_{\odot}$), which is the maximum mass that can be supported by the pressure of degenerate electrons. Material from the companion star falls on the white dwarf, increasing its mass. As the white dwarf nears the Chandrasekhar limit, the entire star collapses, resulting in a carbon–oxygen detonation that destroys the

Supernova Classification System

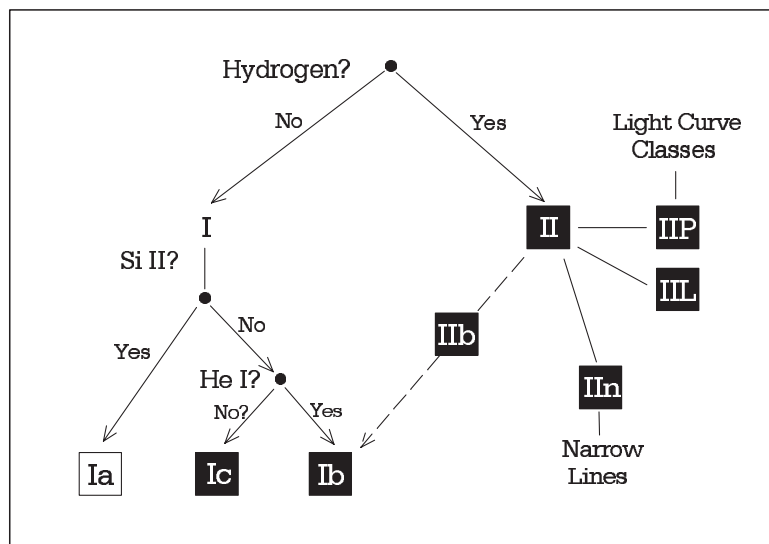


Figure 12.18 Schematic plan of the supernova spectral classification system. Supernova classes represented by filled-in boxes are thought to derive from core-collapse events. Figure adapted from Turatto (2003) and published by permission of Springer.

white dwarf. The exact details of how this detonation occurs have yet to be worked out (see Hillebrandt & Niemeyer 2000, for a recent review.)

Supernova spectra come in essentially two types, those without hydrogen (Type I) and those with hydrogen (Type II), a fact that was first established by Minkowski (1941). The classification scheme was further developed by Zwicky (1965) who added classes III, IV, and V, although those types of supernovae are now generally included in class II. The general scheme of supernova classification is presented in Figure 12.18. For obvious reasons, the classification of a supernova is usually made from spectra obtained around the time of maximum light, but it turns out that, with a few exceptions, an accurate classification may be carried out at any time. Only occasionally do supernovae change types. For instance, the spectra of certain Type II supernovae have been observed to evolve to resemble those of Type Ib supernovae. Recent reviews of the supernova classification scheme (which is still under development) include Filippenko (1997) and Turatto (2003).

Figure 12.19 shows a montage of both Type I and Type II supernova spectra obtained within approximately a week of maximum light. The features in these spectra, some of which show well-developed P-Cygni profiles, are all broad due to the very high ejection velocities, which typically are in excess of 10,000 km/s. The presence of hydrogen in the Type II spectrum and its lack in the Type I spectra

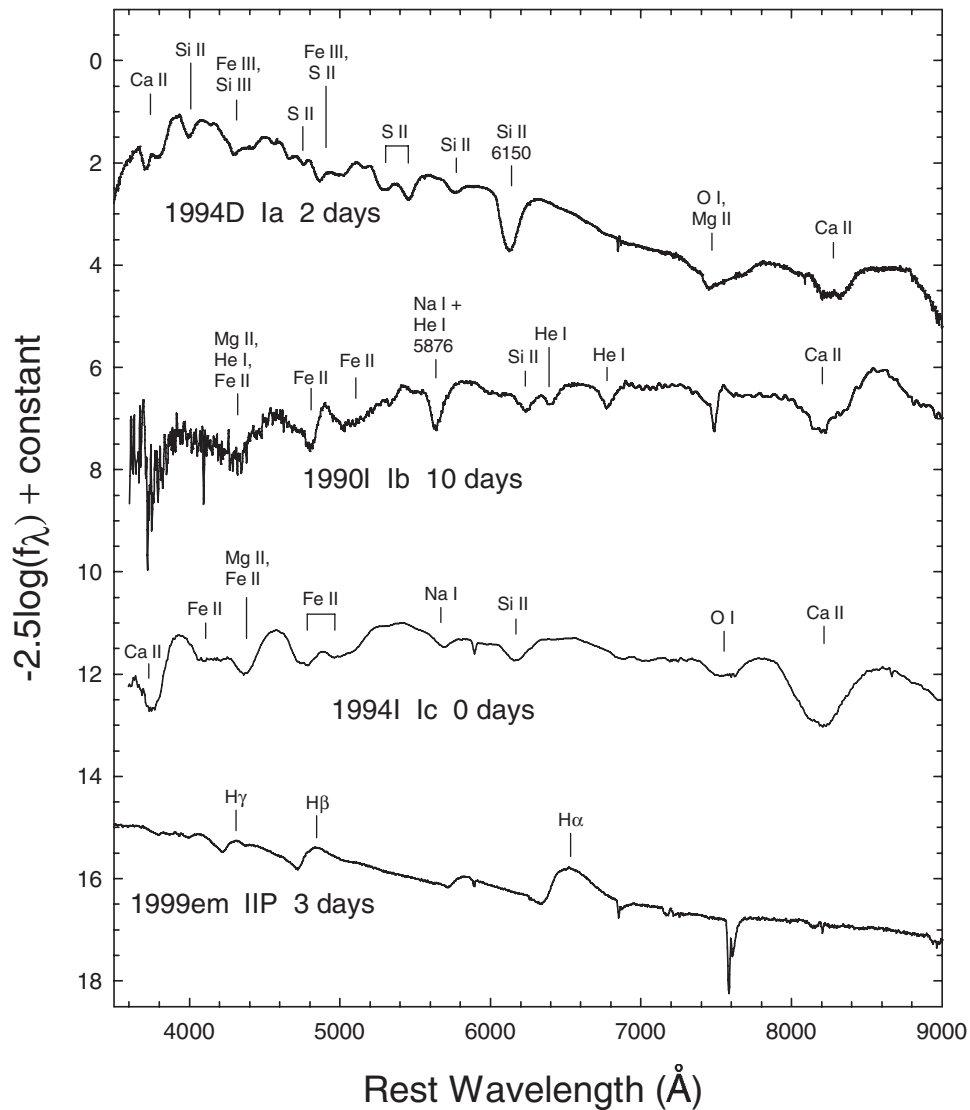


Figure 12.19 A montage of spectra of supernovae of Types Ia, Ib, Ic, and IIP captured shortly after maximum light. Spectra courtesy of the Online Supernova Spectrum Archive (<http://bruford.nhn.ou.edu/suspect/index1.html>). Individual spectra from the Asiago Supernova Catalogue (Barbon, Cappellaro, & Turatto 1989) and Elmhamdi et al. (2004).

are evident. Early-time Type I spectra are dominated by broad absorption features due to Si II, Fe II, Ca II, and O I. Type Ia spectra may be distinguished from those of Type Ib and Ic by the presence of strong absorption due to Si II, especially the deep absorption feature at $\lambda 6150$. Early-time Type Ib spectra show strong lines of He I, especially He I $\lambda 5876$, whereas He I is weak or absent in Type Ic spectra. The distinction between Ib and Ic types is not always clear-cut, and sometimes a supernova is given a hybrid type (Ib/c).

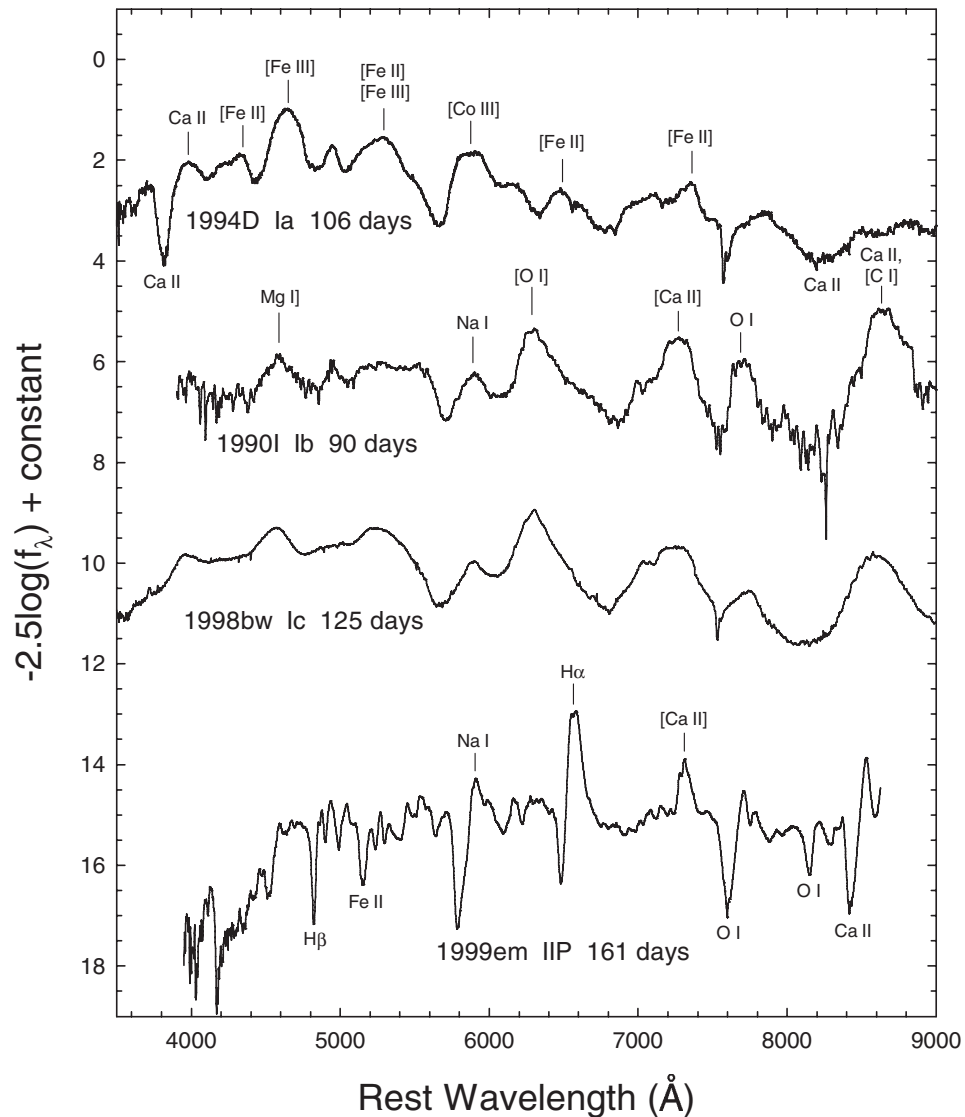


Figure 12.20 A montage of spectra of supernovae of Types Ia, Ib, Ic, and IIP captured more than three months after maximum light. Emission components are labeled above the spectrum; some of these also show P-Cygni absorption components. Absorption features are labeled below the spectrum. Spectra courtesy of the Online Supernova Spectrum Archive. Individual spectra from the Asiago Supernova Catalogue (R. Lopez), Elmhamdi et al. (2004), Leonard et al. (2002).

A late-time montage of supernovae ($\gtrsim 3$ months, Figure 12.20) shows additional features that can be used in the classification process. Type Ia spectra at this point show a complex of Fe and Co emission lines, primarily due to forbidden transitions, indicating that these objects have, by this epoch, entered the “nebular phase.” Type Ib and Ic spectra, on the other hand, are dominated by strong emission

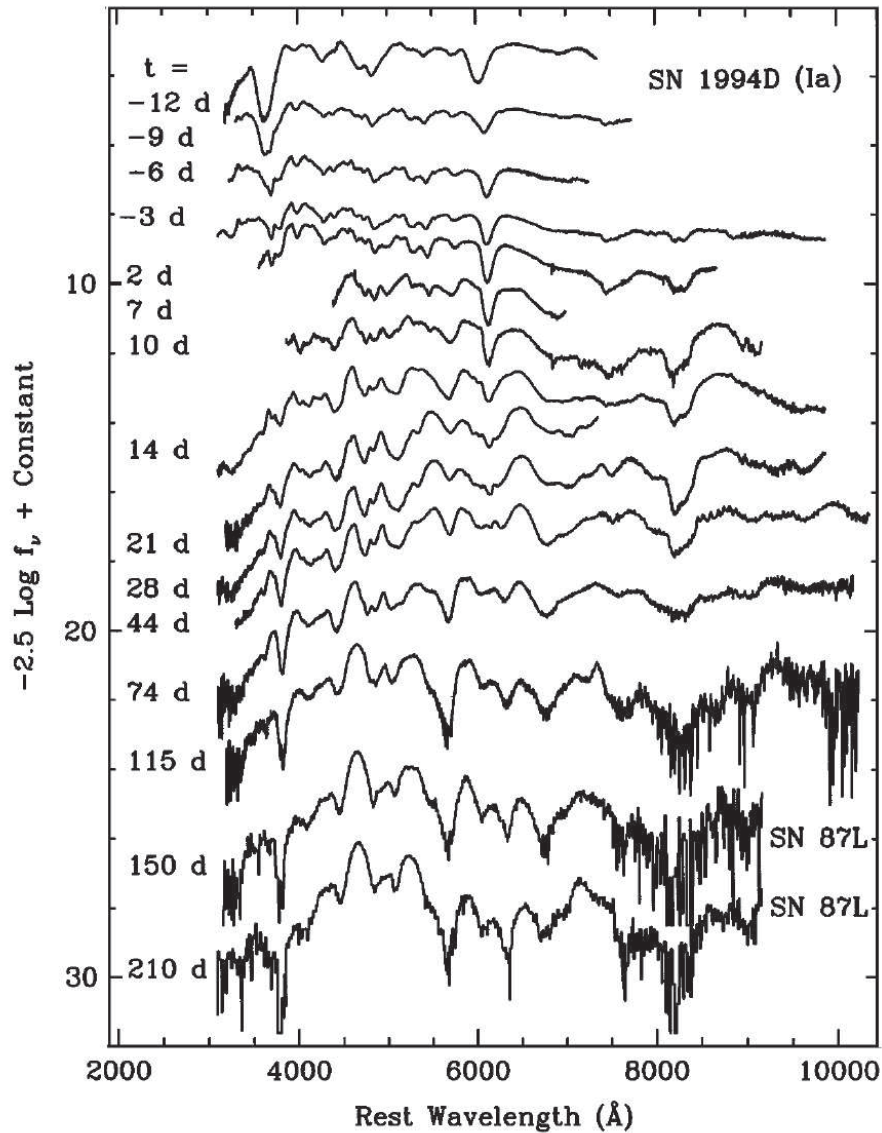


Figure 12.21 A montage of spectra of the Type Ia SN1994D from Filippenko (1997). Epochs (days) are given relative to maximum light in the *B* band. The last two spectra are of the similar SN 1987L. Reprinted, with permission, from the *Annual Review of Astronomy and Astrophysics*, volume 35 c 1997 by Annual Reviews www.annualreviews.org.

features due to light elements, in particular C I, O I, Mg I, Na I, and Ca II, including forbidden transitions of C I, O I, and Ca II, and the intersystem line Mg I $\lambda 4562$ (Mg II). Types Ib and Ic are difficult to distinguish at this epoch, as the He I lines in Ib supernovae, prominent in early-time spectra, fade with time. In particular, the He I $\lambda 5876$ line fades and blends with the nearby strengthening Na I D-line.

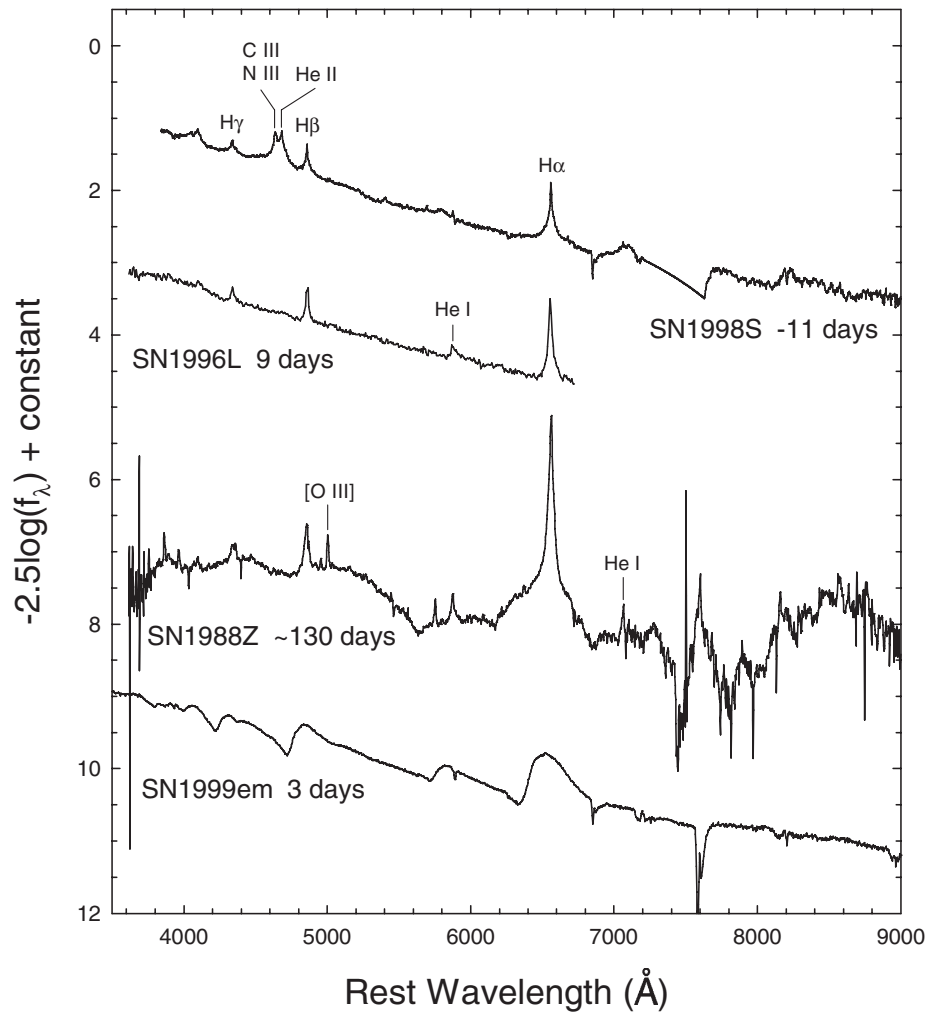


Figure 12.22 A montage of spectra of narrow-lined Type II_n supernovae obtained at different epochs relative to maximum light. SN1988Z was a peculiar, high-luminosity supernova. See Stathakis & Sadler (1991) for more details. The normal broad-lined Type II SN1999em is included for comparison. Spectra courtesy of the Online Supernova Spectrum Archive, with individual spectra from the Asiago Supernova Catalogue, Fassia et al. (2001) and Hamuy et al. (2001).

Type II spectra are still dominated by hydrogen at this epoch; H α usually shows a well-developed P-Cygni profile. Note that the infrared Ca II triplet (≈ 8600 Å) is prominent and also shows a well-developed P-Cygni profile in late-time Type II spectra.

Supernova spectra may be used not only to assign a spectral type, but also to estimate the epoch of the spectrum in terms of time elapsed since maximum light. This is carried out with time-series montages, such as Figure 12.21, reproduced from Filippenko (1997). Time-series montages for other types of supernovae are

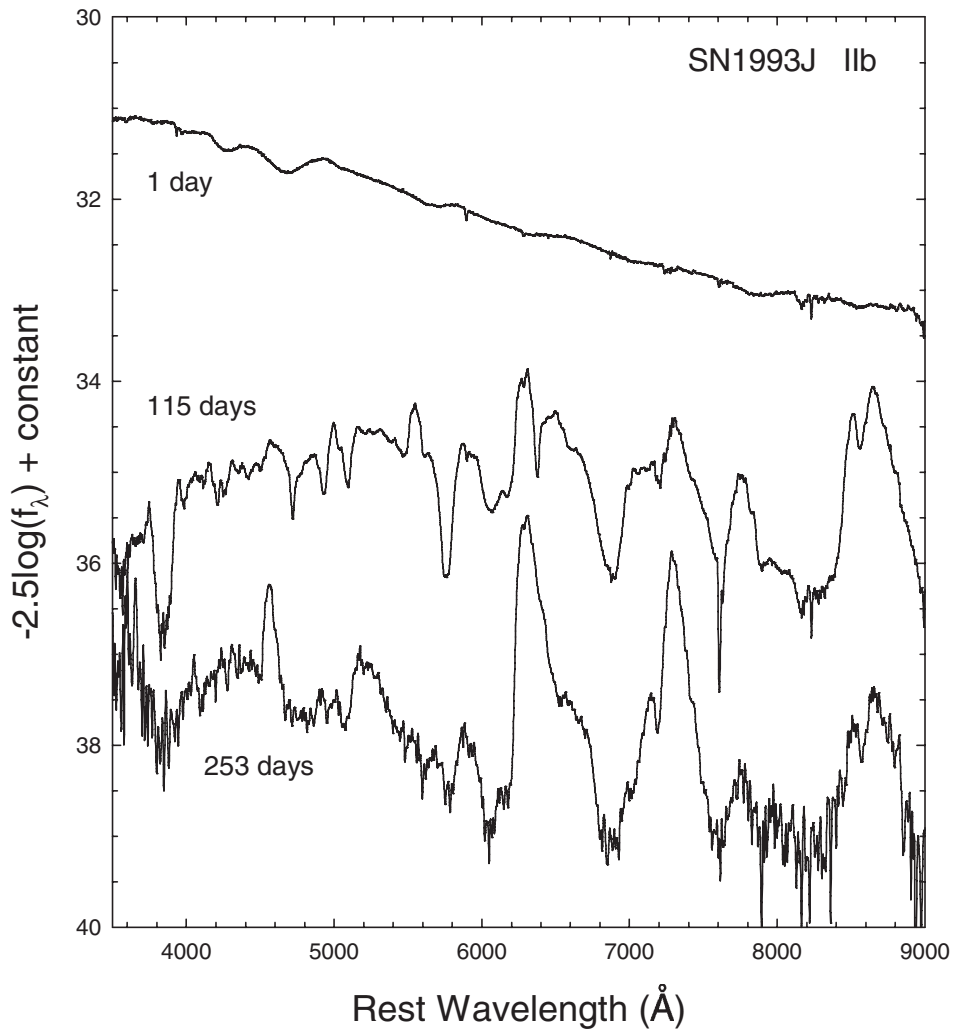


Figure 12.23 A time series of spectra of the unusual supernova SN1993J. Near maximum light, the spectrum resembled that of a normal Type II supernova, but later evolved to resemble that of a Type Ib supernova. Compare with the Ib supernova spectrum in Figure 12.20. Such supernovae are classified as IIb. Spectra courtesy of the Online Supernova Spectrum Archive. Individual spectra from the Asiago Supernova Catalogue.

available from that source and from Weaver & Benetti (1999) as well as from papers on individual stars.

There are a number of subtypes for Type II supernovae. Two of these subtypes are based on the appearance of the light curve. Type IIL supernovae have a single maximum followed by a fairly steep but linear (L) decline; after about 100 days, the rate of decline lessens, but the light curve is still linear. The light curve of a Type IIP supernova, on the other hand, shows, shortly after the maximum, a

distinct “plateau” (P) about 1 magnitude below maximum brightness, followed by a short, steep decline, before assuming a shallower, approximately linear decline. The slope of the late-time linear decline for both types is consistent with the radioactive decay of ^{56}Co , which is produced in large quantities in Type II events.

Type II supernovae also show spectral diversity. The typical early-time Type II supernova spectrum is characterized by broad line profiles, but a subset show much narrower lines (Type IIn). Figure 12.22 shows spectra of three Type IIn supernova. Finally, as mentioned above, a subset of Type II supernovae have spectra that evolve to resemble those of Type Ib supernovae. Such supernovae are classified as Type IIb; a time series spectral montage for one such supernova (SN1993J) is shown in Figure 12.23.

Type II supernovae are believed to result from core collapse events occurring in massive red supergiant stars. There are a number of lines of evidence pointing to this conclusion. First, Type II supernovae show hydrogen in their spectra; it is thought that this arises from the hydrogen-rich envelope of the red supergiant that is ejected during the supernova explosion. Second, Type II supernovae always occur in spiral galaxies or in irregular galaxies that show evidence for star formation (such as the Large Magellanic Cloud). They almost always occur in or near spiral arms and/or in association with H II regions. This, of course, implies that their progenitors are massive stars. Type Ia supernovae occur in all types of galaxies; when they occur in spiral galaxies, they show no tendency to be associated with the spiral arms. The lack of hydrogen in their spectra is consistent with the detonation of a carbon–oxygen white dwarf. However, both Ib and Ic supernova are hydrogen deficient, but are never seen to occur in elliptical galaxies. Like Type II supernovae, they almost always occur in association with spiral arms or star formation regions. Thus, it is believed that these supernovae also arise from core collapse in massive stars, but apparently after the star has been stripped of its hydrogen-rich envelope. Type Ib and Ic supernovae, therefore, may arise from the massive Wolf–Rayet (WR) stars and/or Luminous Blue Variables (LBV), both of which are characterized by high rates of mass loss. Scenarios that link WR and LBV stars with Type Ib and Ic supernovae are discussed in §11.3.

Bibliography

- Adams, W.S. 1914, PASP, 26, 198
 Afşar, M., & Bond, H.E. 2007, AJ, 133, 387
 Barbon, R., Cappellaro, E., & Turatto, M. 1989, AApS, 81, 421
 Brown, N.J. 2002, *IAU Circ.*, 7785
 Chandrasekhar, S. 1935, MNRAS, 95, 207
 Duerbeck, H.W. 1981, PASP, 93, 165
 Eddington, A.S. 1924, MNRAS, 84, 308
 Eisenstein, D.J., and 15 coauthors 2006, ApJS, 167, 40
 Elmhamdi, A., et al. 2004, AA, 426, 963
 Evans, A., et al. 2003, MNRAS, 343, 1054
 Fassia, A., et al. 2001, MNRAS, 325, 907
 Filippenko, A.V. 1997, ARAA, 35, 309
 Fowler, R.H. 1926, MNRAS, 87, 114
 Green, R.F., Schmidt, M., & Liebert, J. 1986, ApJS, 61, 305
 Greenstein J.L. 1960, *Stars & Stellar Systems, Stellar Atmospheres*, ed. J.L. Greenstein (Chicago: Univ. Chicago), vol. 6, 676
 Hamuy, M., et al. 2001, ApJ, 558, 615
 Harris, H.C., & 37 coauthors 2003, AJ, 126, 1023
 Hillebrandt, W., & Niemeyer, J.C. 2000, ARAA, 38, 191
 Holberg, J.B., Barstow, M.A., & Burleigh, M.R. 2003, ApJS, 147, 145
 Kleinman, S.J., et al. 2004, ApJ, 607, 426
 Koester, D., Weidemann, V., Zeidler-K.T., E.M., & Vauclair, G. 1985, AA, 142, L5
 Koester, D., & Wilken, D. 2006, AA, 453, 1051
 Kuiper, G.P. 1941, PASP, 53, 248
 Leonard, D.C., et al. 2002, PASP, 791, 35
 Liebert, J., & Sion, E.M. 1994, ASPC, 60, 64
 Liebert, J., and 20 coauthors 2003, AJ, 126, 2521
 Luyten, W.J. 1952, ApJ, 116, 283
 Luyten, W.J. 1956, *Vistas in Astron.*, 2, 1048
 McCook, G.P., & Sion, E.M. 1999, ApJS, 121, 1
 Metcalfe, T.S. 2005, MNRAS, 363, L86
 McLaughlin, D.B. 1960, in *Stars and Stellar Systems*, Vol. 6, *Stellar Atmospheres*, ed. J.L. Greenstein (Chicago: Univ. of Chicago Press), 585
 Minkowski, R. 1941, PASP, 53, 224
 Payne-Gaposchkin, C. 1957, *The Galactic Novae* (Amsterdam: North-Holland)

- Petitclerc, N., Wesemael, F., Kruk, J.W., Chayer, P., & Billères, M. 2005, *ApJ*, 624, 317
- Russell, H.N. 1944, *AJ*, 51, 13
- Sion, E.M., Greenstein, J.L., Landstreet, J.D., Liebert, J., Shipman, H.L., & Wegner, G.A. 1983, *ApJ*, 269, 253
- Sparks, W.M., Starrfield, S.G., Sion, E.M., Shore, S.N., Chanmugam, G., & Webbink, R.F. 1999, in *Allen's Astrophysical Quantities*, 4th edition, ed. A.N. Cox (New York: Springer Verlag), p. 429
- Stathakis, R.A., & Sadler, E.M. 1991, *MNRAS*, 250, 786
- Turatto, M. 2003, in *Supernovae and Gamma-Ray Bursters*, Lecture Notes in Physics, ed. K. Weiler (Berlin/Heidelberg: Springer), p. 21
- von Hippel, T., Kuchner, M.J., Kilic, M., Mullally, F., & Reach, W.T. 2007, *ApJ*, 662, 544
- Weaver, J.C., & Benetti, S. 1999, in *Allen's Astrophysical Quantities*, 4th edition, ed. A.N. Cox (New York: Springer Verlag), p. 451
- Werner, K. 1992, in *The Atmospheres of Early-Type Stars*, eds. U. Herber and S. Jeffery (New York: Springer), p. 291
- Wesemael, F., Green, R.F., & Liebert, J. 1985, *ApJS*, 58, 379
- Wesemael, F., Greenstein, J.L., Liebert, J., Lamontagne, R., Fontaine, G., Bergeron, P., & Glaspey, J.W. 1993, *PASP*, 105, 761
- Williams, R.E. 1992, *AJ*, 104, 725
- Williams, R.E., Hamuy, M., Phillips, M.M., Heathcote, S.R., Wells, L., & Navarrete, M. 1991, *ApJ*, 376, 721
- Williams, R.E., Phillips, M.M., & Hamuy, M. 1994, *ApJS*, 90, 297
- Woronzow-Weljaminow, B.A. 1953, *Gasnebel und Neue Sterne* (Berlin: Kultur und Fortschritt)
- Zuckerman, B., & Becklin, E.E. 1987, *Nature*, 330, 138
- Zuckerman, B., Koester, D., Reid, I.N., & Hünsch, M. 2003, *ApJ*, 596, 477
- Zwicky, F. 1965, in *Stars and Stellar Systems*, Vol. 8, *Stellar Structure*, ed. L.H. Aller & D.B. McLaughlin (Chicago: Univ. of Chicago Press), 367

Chapter Thirteen

Further Techniques

13.1 INTRODUCTION

Embedded in earlier chapters, especially Chapters 1 and 2, are techniques for obtaining the most suitable spectra for classification of stars and then doing the actual classification. We have also laid an emphasis on the importance of maintaining the integrity of the grid of standard stars on which all stellar classification depends. While remembering that techniques provide a tool and are not the science itself, it is appropriate now to look at several ways of getting more out of stellar spectral classification. Here we shall consider composite spectra and their deconvolution into the component spectra, modes of spectral classification other than the MK system, namely in the thermal infrared and with the BCD system, automated methods of doing spectral classification, and how to get the faintest in surveys and get the best out of low dispersion, wide field spectra.

13.2 COMPOSITE SPECTRA

More than two-thirds of stars are not alone, but in binary or multiple systems. When the separation of such stars is less than the resolution of the telescope through the atmosphere, then two or more stars will contribute to a single resulting spectrogram in proportion to their relative magnitudes. If the difference between these magnitudes in the spectral region of interest is much more than 3, then to the classifier the primary star will dominate so much that the secondary's spectrum (or tertiary's, etc.) is not noticeable. Digital techniques can extend this range just a little, but there is still a fairly limited range in magnitude difference between the components of unresolved binary systems for which any special technique is needed. However, when one thinks of clusters of stars and particularly of galaxies, then the sheer numbers of stars with lower magnitudes can dominate the integrated spectrum that is seen. Let us take the two cases separately: that of unresolved binary stars and that of clusters and galaxies.

First, however, a reminder on nomenclature may be helpful. Two stars, whether we can resolve them at the telescope or not, may be a physical pair, bound by their mutual gravity and so a true "binary star," or not so bound and just lying along the same line of sight, an "optical pair." A "double star" can refer to either. Binary stars may be "non-interacting" or "interacting." In the latter case, to the spectrum of each star is added that of the excited interacting material. Such symbiotic and Algol stars were treated in §8.5.

13.2.1 History of Composite Spectra Classification

While Angelo Secchi was very familiar with binary stars from his systematic observation of the positions of their components, it was during the expansion of his spectral classification system by the people at Harvard Observatory that the term *composite spectrum* appeared (Pickering 1891; Maury 1897). Rather later, Shaïn (1926) showed from a statistical study that composite spectra could be considered simply as an extension of spectra from close visual doubles to those of unresolved pairs. J. Allen Hynek at Yerkes Observatory devoted considerable effort in his lifetime to the observation and organization of double stars. His catalogue (Hynek 1938) contained not only a useful list of the known stars with composite spectra, but an attempt to divide them into classes according to their probable physical origin. Among his nine classes there were the *visual binaries*, those which could be resolved as double stars; the *spectroscopic binaries*, with one or both components showing sufficient periodic shift in radial velocity so as to be distinguishable as indeed binary; and the *spectrum binaries*, which were neither of the two groups above, but whose spectrum appeared composed of two or more unresolved stars.

The last group in Hynek's catalogue came to contain fewer and fewer members as normal supergiant spectra became understood and as the metallic-line stars were discovered (Titus & Morgan 1940). However, with surveys based on the MK system the number of identified composite spectra has grown considerably. The identification and deconvolution into individual components by MK classification is well represented by the careful study of Markowitz (1969). Stephenson & Sanwal (1969) in their work on visual binary systems made 40 artificial composite spectra to help them determine the spectral type of each component. To these purely spectroscopic methods should be added those that completely or partially use photometric data, a technique that started with Bahng (1958) and continued with, e.g., Beavers & Cook (1980). Those last used spectral indices provided by a scanner, which today of course is replaced by the CCD. In the realm of high dispersion studies, one should certainly note the success of deconvolving composite spectra by digital spectrum subtraction (e.g., Griffin & Griffin 1986).

While the effort to deconvolve composite spectra into their components is both understandable and commendable, at the classification level the comment of William Bidelman (1984) should always be kept in mind: "don't believe anything that anyone, including me, tells you about composite spectra." There has been much nonsense written in relation to composite spectra, and Bidelman well illustrates this point in the rest of his talk at the MK Process conference. In the discussion following he made clear what was the prime task of the classifier: "The important thing for the classifier is to tell others that (the spectrum) is indeed composite. The detailed work can be done by someone else at higher dispersion or with more information."

13.2.2 Optical Classification

Detecting that a spectrum is in fact made up from two stars is easier as the difference in their spectral classes increases and the difference in their magnitudes

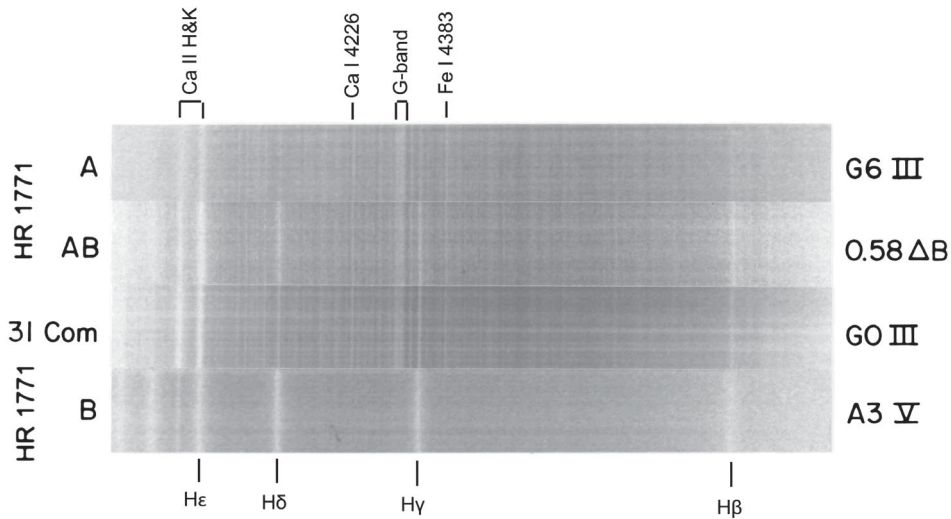


Figure 13.1 A spectral montage for the double star HR 1771, comprising the A and B components, with their authentic composite AB. ΔB gives the B-magnitude difference between the components A and B. The normal standard star, 31 Com, is added for comparison with the composite. Figure from Corbally (1987) and reproduced by permission of the AAS.

decreases. Hence, in the blue-violet region one finds the “characteristic composite” to be made up of a late-type giant primary plus an early-type dwarf secondary. Figure 13.1 shows just such a combination. When compared with the standard spectrum of 31 Com, the composite AB has the three characteristic features: *veiling*, or weakening without decrease in width, of the late-type absorption lines, especially towards the violet end of the spectrum; an unusual Balmer decrement where the higher-series lines are stronger than normal and may, as in HR 1771, show faint wings; and a filled-in Ca II K line, with a just noticeable strong core, giving unequal-looking H & K lines.

A trap for the unwary is that the mid-Am stars also show enriched metallic lines with respect to their K-line strengths, as well as unequal H & K line strengths. That is why early catalogues of composite spectra contained misidentified Am stars, as mentioned above in §13.2.1. Such a misidentification would no doubt have been avoided for the characteristic composite in Figure 13.1. However, combinations of primaries and secondaries that are closer in spectral types and further apart in magnitudes can yield rather more subtle pseudo-Am spectra. Figure 13.2 is one such illustration from the “Atlas of 12 Rather Subtle Composite Spectra” by C.J. Corbally (1987). Here it is revealed that the at-first-seeming, mild-Am star is composed of two normal stars. The hint of a G-band and the slightly strong Fe I $\lambda 4383$ line indicate that is not in fact a true Am star. Of course, genuine Am stars can also appear in composite spectra, as is clear from the illustration of the HR 2482 combination in the same paper (Figure 7 in Corbally 1987) and

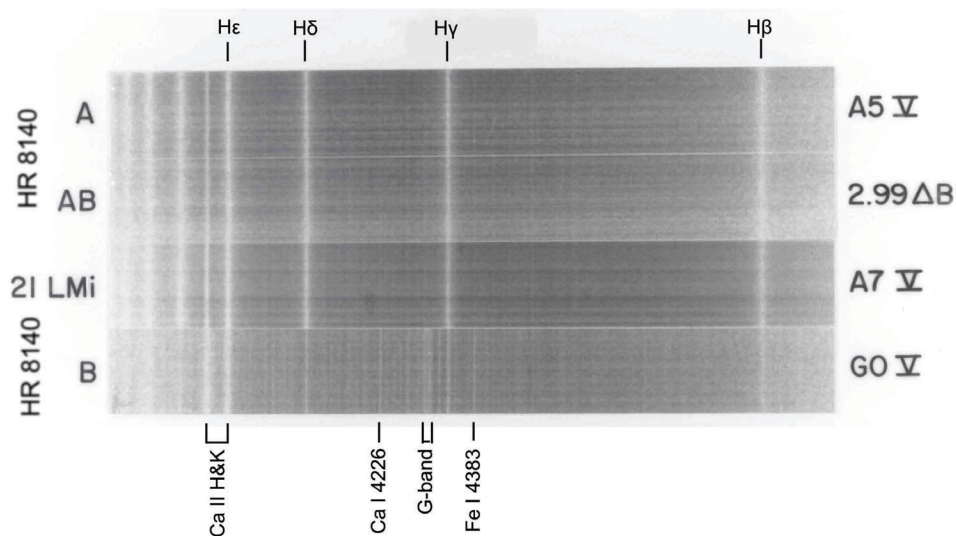


Figure 13.2 A spectral montage for the double star HR 8140, comprising the A and B components, with their authentic composite AB. ΔB gives the B-magnitude difference between the components A and B. The normal standard star, 21 LMi, is added for comparison with the composite. Figure from Corbally (1987) and reproduced by permission of the AAS.

the combination of two Am stars, one of which is evolved, that was revealed by Griffin (2002).

To help the prime role of the classifier—identifying that the spectrum is indeed composite, clues to look for, in addition to the three characteristic features above—are (1) the presence of metal lines or band structure that are uncharacteristic of the first-look type and not expected of the typical peculiar stars in that temperature region; (2) any incompleteness in the characteristic peculiarities for stars which initially seem Am type; (3) inconsistencies in the luminosity discriminants, especially when these are far apart in wavelength and the spectrum is not Am type (see “anomalous luminosity effect” under “Am stars”); and (4) a continuum gradient which does not match the temperature type, although this can be confused by interstellar reddening.

Once a spectrum is identified as composite, an educated guess can be made at the types of the primary and secondary components. Such “education” will be helped by artificially producing a set of composite spectra out of known components and by plenty of classifying experience, a start to which may be found in the “subtle atlas” of Corbally. To go beyond the educated guess needs careful quantitative analysis.

One such quantitative method is to synthesize a composite from two spectra until the observed and the synthesized spectrum agree. Alternately, with the help of Elizabeth Griffin (in Griffin & Griffin 1986) who is an expert guide, the methodology for the subtraction technique can be used to isolate the components of

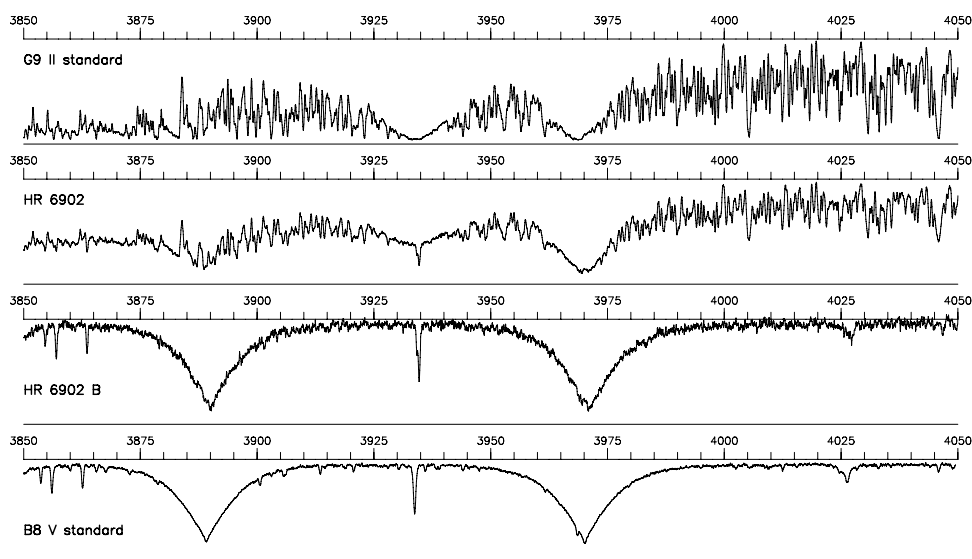


Figure 13.3 Subtraction method to isolate components of a composite spectrum. The spectrum at the top of two G9 II standard and is chosen to match the primary. It is then subtracted from the composite spectrum (HR 6902), leaving the secondary component, HR 6902 B, which may be compared to the B8 V standard at the bottom. Figure courtesy of Elizabeth Griffin. More details on this system may be found in Griffin & Griffin (1986)

composite spectra. As illustrated in Figure 13.3, a close match to the spectrum of the primary is selected from a library of standards, and this is subtracted from the composite spectrum in just the right amount to make the features of the primary spectrum disappear simultaneously. The residual spectrum is presumably that of the secondary star, unless there are clues that it too is composite, and this can be classified and measured for its radial velocity or whatever is of interest. The method demands high signal-to-noise and hence is applicable only to the brighter composite objects. The techniques in the next section can help for the fainter ones.

13.2.3 Ultraviolet and NIR Contributions

The UV and NIR, with the former region emphasizing the hot component and the latter the cool component, are obviously a great help to the deconvolution of composite spectra. For example, Ginestet et al. (1994, and further papers) set up classification criteria in the $\lambda\lambda 8370\text{--}8780$ region at a dispersion of 33 \AA/mm . These criteria were of the kind that have been outlined in previous chapters. In subsequent studies they applied the criteria to obtain the spectral types and luminosities of the cooler components of composites. One curiosity they found was that if the hot companion contributed significantly to the Paschen lines, then the infrared Ca II triplet was also strengthened. However, the hot companion also contributed to raising the continuum and so a veiling of those triplet lines, thus cancelling out what would have been their enhancement. The two principal collaborators in this

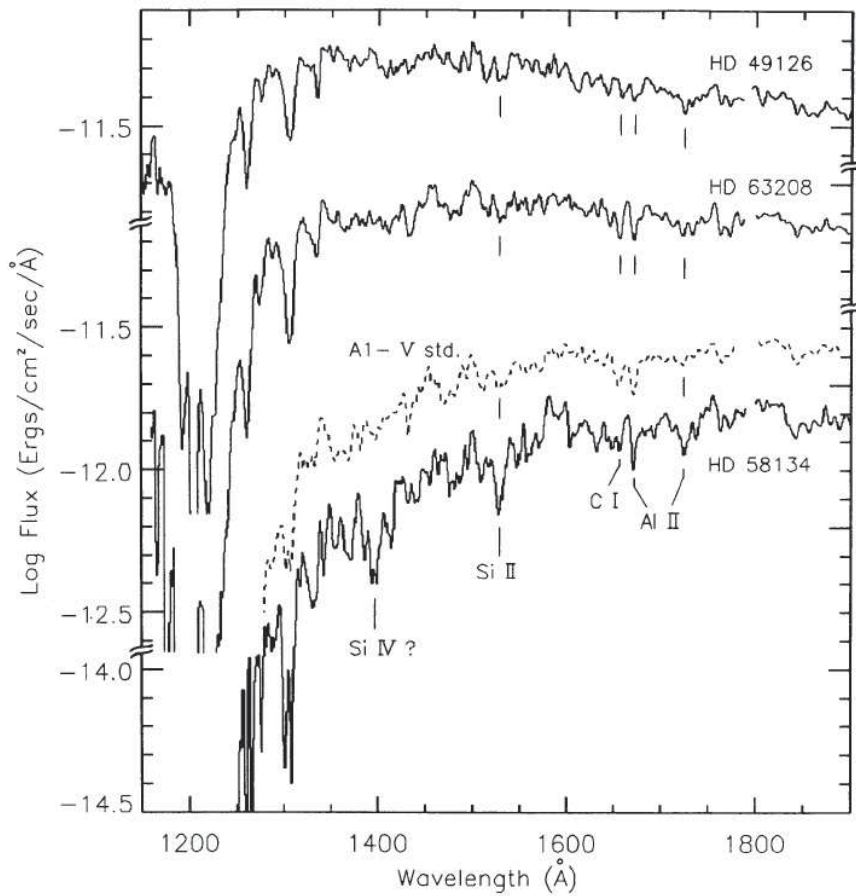


Figure 13.4 IUE far-UV spectra of composite stars showing that the hot component can be classified clearly. The peculiar feature in HD 58134 appears to be Si IV at $\lambda 1400$, probably due to a stellar wind from the cool component or to circumbinary gas. Figure courtesy of Parsons & Ake (1993), and reproduced by permission of the AAS.

study later employed the subtraction method of Griffin on near-UV spectra to determine the classification of the hot component, a neat complement of techniques in the appropriate spectral ranges that reached to fainter magnitudes than possible initially (Ginestet & Carquillat 2002).

In the far-UV very little to no contribution from the cool component of a composite system is expected, so the hot component can be classified unambiguously. Figure 13.4 shows examples of the hot components, whose spectra can be compared with the far-UV spectra in Chapter 5. Parsons & Ake (1993) note that the Si IV feature in the bottom spectrum may be due to a stellar wind from the cool supergiant or from mild interaction of the two components. The Mg II $\lambda 2800$ doublet, formed in high levels of the chromosphere and with its visibility enhanced by a hot companion, also becomes a sensitive feature with which to study

winds in cool stars (Hünsch & Reimers 1993). So, in addition to classifying the hot component, spectra in the UV can contribute information about the winds and circumbinary gas in a system, as in the case of HR 1129 (Griffin et al. 2006).

The use of tomography, or imaging by sectioning, on UV spectra to separate the components of composites has been applied successfully in a series of papers that started with Baguolo & Gies (1991). One advantage of using the UV is that its lines are formed by higher excitations than for the optical and so are more likely to be photospheric than circumstellar. This aids in getting the Doppler shift data for the system, so also the tomographic separation, and in the classification of the components.

NIR spectra, coupled with the automated analysis given by Artificial Neural Networks (see §13.5.2), have been shown by Weaver (2000) to be quite powerful in identifying components of the characteristic composites—those containing a cool giant or supergiant and a hot, near-main sequence secondary—although see the caution by Griffin (2001). The NIR is also vital for studying the cool companions of low-mass systems. These are composed of a white dwarf and a low luminosity, cool object, perhaps that of a brown dwarf as found by Burleigh et al. (2006). They will also include the Post-Common Envelope Binaries (PCEB). The PCEBs have significant potential (see Aungwerojwit et al. 2007) in helping to understand the stages of stellar evolution both immediately before them and that coming afterwards, the Cataclysmic Variables that include the Supernovae Ia.

Even the X-ray region can help. Evans et al. (2006) use such data to enumerate the multiplicity of Polaris, the nearest and brightest classical Cepheid. Other modern techniques for disentangling of the components of multiple systems and their astrophysical applications are reviewed by, e.g., Gies (2004) and Hensberge & Pavlovski (2006). Even with such powerful tools, Bidelman's caution is needed so that the element of judgment and experience is included.

13.2.4 Clusters and Galaxies

Classifying clusters of stars and galaxies has an advantage over doing this for single or multiple stars in having information from their form, at least to moderate distances, as well as from their integrated spectra.¹ While the earliest description of “nebulae” traces back to the era of William Herschel (de Vaucouleurs 1959), investigating the interplay of form and spectrum started with Edwin Hubble's (Hubble 1926) characterization of the appearance of galaxies in the familiar tuning-fork sequence and continued with the spectral classification work of Milton Humason (1936). One does, of course, realize that these two last people were principally concerned with the redshift–distance relation for galaxies.

¹The light from the group of stars as a whole. Integrated spectra for an object larger than the width of the spectrograph slit can be obtained by “drifting” it up and down and across the slit, an exercise that helps the observer appreciate the cluster or galaxy all the more.

After both N. U. Mayall (1946) and W. W. Morgan (1959) had built up experience of the varieties of stellar cluster spectra, they both (Morgan & Mayall 1957) proposed four properties by which to classify galaxy spectra, and they applied these first to characterizing M31, M33, and NGC 4449. The spectrum of M31, depending on which spectral range was taken, looked like that of both yellow and red giants or of early-G dwarfs. So it resembled that of an old cluster, either open or globular. The spectrum of the irregular galaxy NGC 4449 had nebular emission lines and the absorption line characteristics of late-A and mid-F stars. It resembled that of the galactic spiral arms or a young open cluster. The spectrum of M33 was intermediate between these two galaxies. They then classified a number of other galaxies into A-, AF-, F-, FG-, or K-systems, and they found that the form of the galaxies, while showing considerable diversity, nonetheless became more centrally concentrated toward the later galaxy spectral types. That degree of central concentration became a principal criterion in a scheme of classification in terms of stellar population proposed by Morgan (1958). Gérard de Vaucouleurs (1959) gave a fine review of the state of galaxy classification at the end of this productive decade, and he also introduced a revision of the Hubble scheme to take into account recent morphological additions.

This essential correlation found for galaxies of *form* and *stellar content*, as given by the spectral type, continued in subsequent studies, and so the understanding in terms of the various stellar populations within a galaxy deepened. These populations followed the age sequence of stellar cluster spectra, which begin with the Orion-type open clusters and progress to the strong-lined globular clusters. The increased sensitivity of digital detectors allowed the production of a milestone spectrophotometric atlas of galaxies by Kennicutt (1992b). Figures 13.5 and 13.6 are montages of spectra from this atlas, illustrating both normal and peculiar galaxies in two spectral resolutions. The first, at medium resolution, shows a steady progression from the dominance of late-type giant features in the E4 galaxy to early-type and emission features in the Sc and Irr galaxies. The lower resolution of the second montage better shows the range of emission features that are possible in peculiar galaxies.

In recent years the interaction of galaxies has featured strongly in understanding their history and current form. For instance, Conselice (2006) includes interactions, along with galaxy mass and recent star formation, as the fundamental properties on which to build a new physical classification scheme. The availability now of myriads of galaxy spectra from the Sloan Digital Sky Survey provides a fruitful resource with which to investigate these fundamental properties. Interestingly, Yip et al. (2004) find that only 10 eigenspectra enable the reproduction of both quiescent and active galaxy spectra from an observed set of 170,000. Still, there are many parameters of galaxies that can be used in their classification, those from integrated spectra being just one set. That is why it is not intended to give here an exhaustive treatment of galaxy classification but just an indication of how integrated spectra, whether of clusters or galaxies, overlap with stellar classification. For after all, galaxies do include stars.

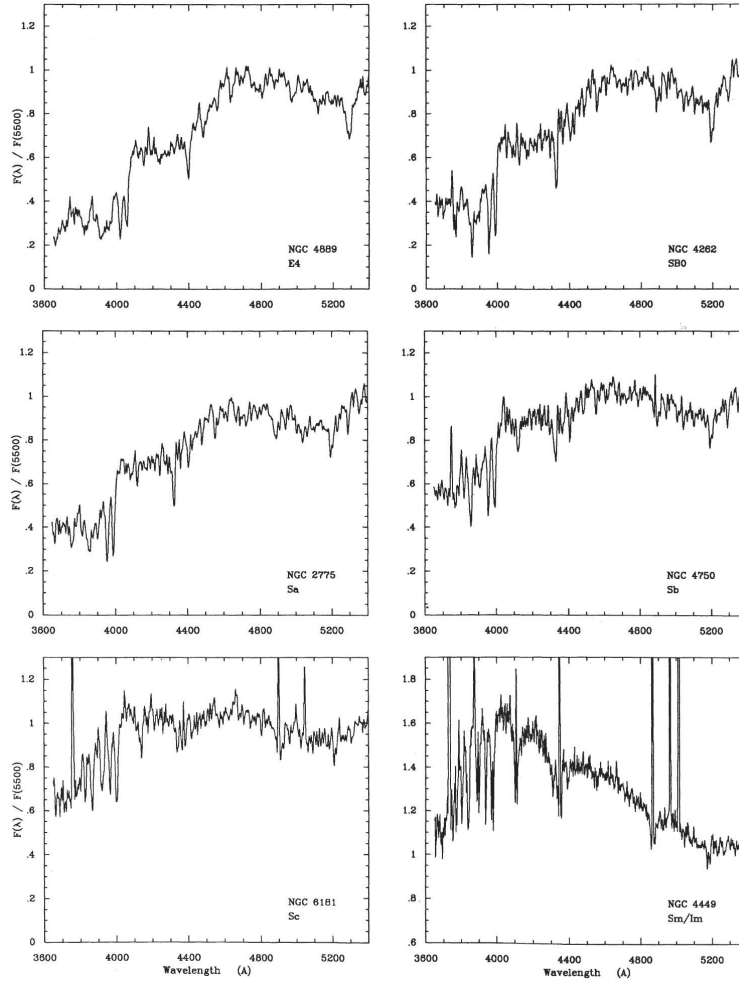


Figure 13.5 Integrated spectra at medium resolution of normal galaxies, arranged in increasing Hubble type. Figure courtesy of Kennicutt (1992a), and reproduced by permission of the AAS.

13.3 CLASSIFICATION SYSTEMS IN THE THERMAL INFRARED

13.3.1 IRAS Spectra

Stellar spectral classification in the wavelength region $5\text{--}50\ \mu\text{m}$, essentially the thermal infrared, is still in its infancy, but holds considerable promise for the investigation of both the earliest and the latest stages of stellar evolution. The largest collection of spectra in this spectral region is from the Low-Resolution Spectrometer (LRS) on the *Infrared Astronomical Satellite* (IRAS). These spectra range from 7.7 to $22.7\ \mu\text{m}$ and have a spectral resolution $R \sim 20\text{--}60$. The database comprises observations of 11,224 sources (Kwok, Volk, & Bidelman 1997). The original LRS classification scheme (IRAS Explanatory Supplement 1988) classified spectra into

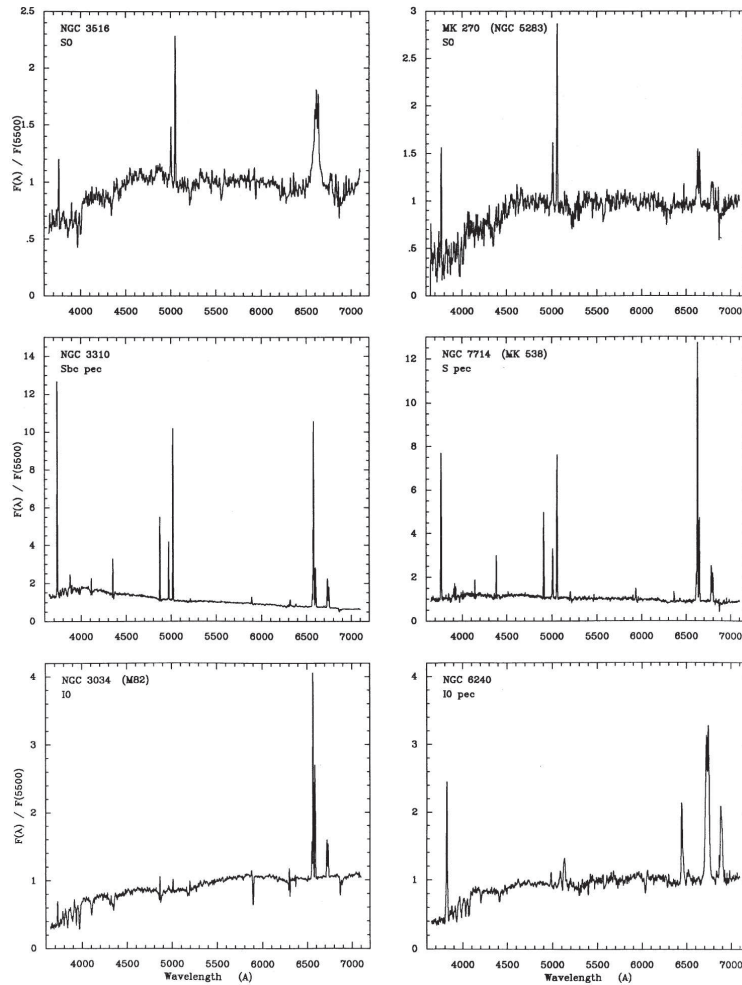


Figure 13.6 Integrated spectra at low resolution of peculiar galaxies, showing active nuclei or star formation. Figure courtesy of Kennicutt (1992a), and reproduced by permission of the AAS.

9 classes, $1n-9n$, where the n subclass (an integer) is defined according to either a spectral index or the strength of the strongest emission or absorption band that characterizes the class. Classes $1n$, $2n$, $3n$, and $4n$ are comprised of sources with blue energy distributions, $5n$, $6n$, and $7n$ with red energy distributions, and classes $8n$ and $9n$ are for sources with spectral lines. A tenth class, $0n$, was reserved for low S/N or unclassifiable sources. Table 13.1, adapted from the IRAS Explanatory Supplement (1988), summarizes the classification scheme, and Figure 13.7 illustrates typical spectra from the LRS database (Joint IRAS Science Working Group 1987) along with their two-digit classifications.

Volk & Cohen (1989); Volk (1993) (see also Kwok, Volk, & Bidelman 1997) devised a parallel classification system for the LRS spectra consisting of ten

Table 13.1 LRS Classification Scheme

Class	Subclass	Typical Objects
0 <i>n</i>	Unclassifiable or low S/N	Unknown
1 <i>n</i>	<i>blue</i> , featureless <i>n</i> given by spectral index	stars earlier than M5
2 <i>n</i>	<i>blue</i> 10- μ m emission <i>n</i> given by band strength	stars with thin, O-rich envelopes
3 <i>n</i>	<i>blue</i> 10- μ m absorption <i>n</i> given by band strength	stars with thick, O-rich envelopes
4 <i>n</i>	<i>blue</i> 11- μ m emission <i>n</i> given by band strength	stars with carbon-rich envelopes
5 <i>n</i>	<i>red</i> no line or band features	unknown
6 <i>n</i>	<i>red</i> 10- μ m emission <i>n</i> given by band strength	stars with very thick O-rich envelopes
7 <i>n</i>	<i>red</i> 10- μ m absorption <i>n</i> given by band strength	stars with extremely thick, O-rich envelopes, and hot spots in molecular clouds
8 <i>n</i>	11.3- μ m emission line <i>n</i> given by strongest line	compact H II regions and planetary nebula
9 <i>n</i>	Emission-line object, but without 11.3- μ m line	unknown

categories defined as follows:

S – LRS spectra are essentially Rayleigh–Jeans tails of the stellar photospheric continuum. These are usually stars with spectral types earlier than M5, without substantial mass loss.

F – LRS spectra show a featureless continuum, flatter than expected for a stellar photosphere. These objects probably represent oxygen- or carbon-rich stars with small amounts of circumstellar dust.

E – LRS spectra show the 9.7- μ m silicate dust feature in emission. This type of spectrum probably originates in the circumstellar envelopes of oxygen-rich AGB stars.

A – LRS spectra show the 9.7- μ m feature in absorption. Again, the sources are probably mostly oxygen-rich AGB stars with thick circumstellar envelopes.

C – LRS spectra show circumstellar 11- μ m SiC dust emission, and are probably evolved carbon stars undergoing mass loss.

P – LRS spectra have a red continuum from 13 to 23 μ m with either a sharp rise at the blue end or 11.3- μ m or 12.5- μ m emission features (attributed to PAH molecules).

H – LRS spectra have a red continuum, as well as either the 9.7 μ m absorption feature or the 11.3 μ m PAH feature. These sources are planetary nebulae, reflection nebulae, or H II regions.

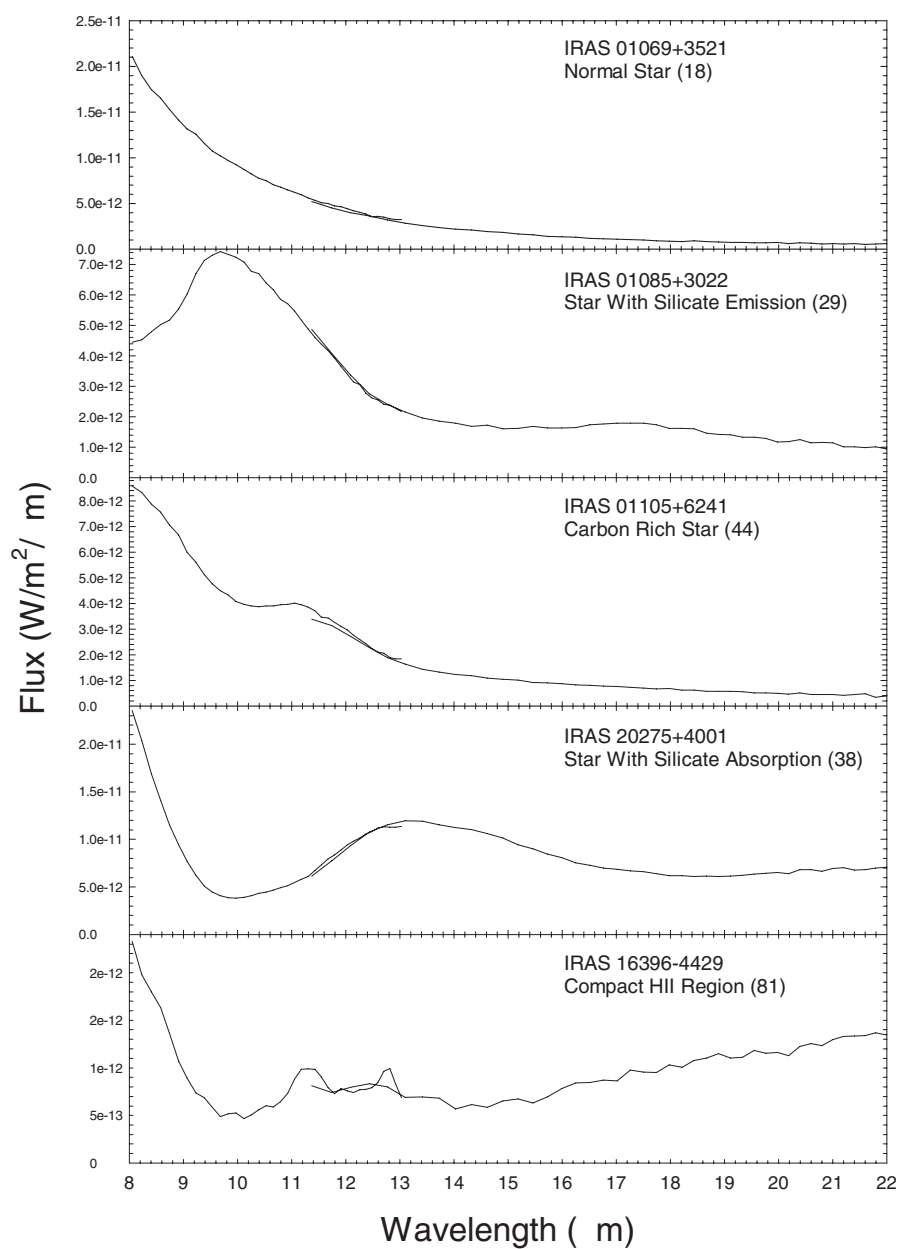


Figure 13.7 Sample spectra from the IRAS LRS database with their two-digit classifications in parentheses, including, from the top, a normal star (LRS class 18), a star with silicate emission (LRS class 29), a star with a carbon-rich envelope (LRS class 44), a star with silicate absorption (LRS class 38), and a compact H II region (LRS class 81). Spectra from the LRS database (Joint IRAS Science Working Group 1987).

Table 13.2 AutoClass LRS Classification Scheme

Metaclass (Classes)	Em./Abs.	Associated Dust
α (0–6)	Em. Em.	Silicon Carbide HAC
β (7–20)	Em.	Silicate
γ (21–22)	Em. Em. Abs.	PAH HAC Silicate
δ (23–31)	—	Blackbodies—some with very weak absorption or emission features
ϵ (32–35)	Em.	Silicate
ζ (36–40)	Em. Em. Abs.	PAH HAC Silicate
η (41–42)	Abs.	Silicate
θ (43)	—	Uncertain
λ (44–79)	Em. Em. Em.	Metal Oxides HAC Silicates

U – Unusual spectra with a flat continuum; most have abnormal silicate emission features.

L – Spectra with evidence of emission lines above a continuum.

I – Noisy or incomplete spectra.

Kwok, Volk, & Bidelman (1997) provide classifications for all 11,224 sources in the LRS database on the Volk & Cohen system.

The LRS database has also been classified with an Bayesian-based automatic technique (Autoclass, Goebel, et al. 1989), which recovered many of the original LRS classes discussed above, but also was able to address subtleties related to band shape and strength not detected by the two above systems. The Autoclass classification is organized hierarchically into metaclasses, classes, and subclasses. Table 13.2, adapted from Goebel, et al. (1989) summarizes the reclassification of the LRS database under the Autoclass system.

13.3.2 ISO SWS Spectra

Spectra obtained with the Short Wavelength Spectrometer (SWS) on the *Infrared Space Observatory* (ISO) have a number of advantages over the IRAS LRS spectra. Their resolution is considerably better ($R \sim 400$) as opposed to 20–60, and the

wavelength range is much greater, stretching from 2.4 to 45.2 μm . The resolution of these spectra is sufficient to resolve important atomic fine-structure lines and to perform a detailed examination of molecular bands. However, the database is much smaller, and consists of only about 910 sources. Nonetheless, Kraemer et al. (2002) have devised a detailed classification system based on these spectra. It is intended for this system to be comprised of three levels. Level 1 classification sorts the spectra into “groups” based on the general morphology of the stellar energy distribution (SED). The Level 2 classification places each spectrum into a self-consistent subgroup based on the most prominent spectral features such as, for instance, silicate dust emission, carbon-rich dust emission, atomic fine-structure lines, etc. The Level 3 classification, which is not yet fully implemented, will arrange the spectra within a given subgroup. The Level 1 groups are defined as follows:

1. Naked stars, i.e. sources without detectable circumstellar dust.
2. Stars with dust. These sources have SEDs that are primarily photospheric at short wavelengths, but show evidence of dust emission at longer wavelengths. Most of these sources are red supergiants or AGB stars.
3. Warm, dusty objects. These sources have spectra that are dominated by emission from warm ($> 150\text{ K}$) dust. Any photospheric contribution is either absent, or very much weaker than the dust emission. Most of these objects are very dusty AGB stars, post-AGB stars, planetary nebulae (PN), or other evolved objects.
4. Cool, dusty objects. These objects have dust emission that peaks longward of $\sim 20\text{ }\mu\text{m}$. Most of these sources are PNs, AGB stars, and post-AGB stars, although many are young stellar objects (YSO).
5. Very red objects. These objects have rising spectra toward longer wavelengths. Most are star-forming regions or PNs.
6. Continuum-free objects with emission lines. These objects have very low continuum levels, making it difficult to place them in any of the above categories. However, these objects are dominated by atomic fine-structure emission lines. Many of these objects are supernova remnants and novae.
7. Flux-free or unusable spectra.

Figures 13.8 and 13.9 show ISO SWS spectra classified on this system.

Level 2 subgroups are summarized in Table 13.3 (taken from Kraemer et al. (2002)).

Since the original publication by Kraemer et al. of the ISO SWS classification system, the scheme has evolved to clarify definitions and to include additional feature combinations observed by other IR spectrometers such as ISOCAM-CVF, ISOPHT-S, and Spitzer’s IRS. New classes include 1.NO– and 1.NC–, naked stars with weak oxygen or carbon features. New combinations include U/SA, E/SA, and UE/SA. Papers detailing these changes include Hodge et al. (2004) and Engelke, Kraemer, & Price (2004).

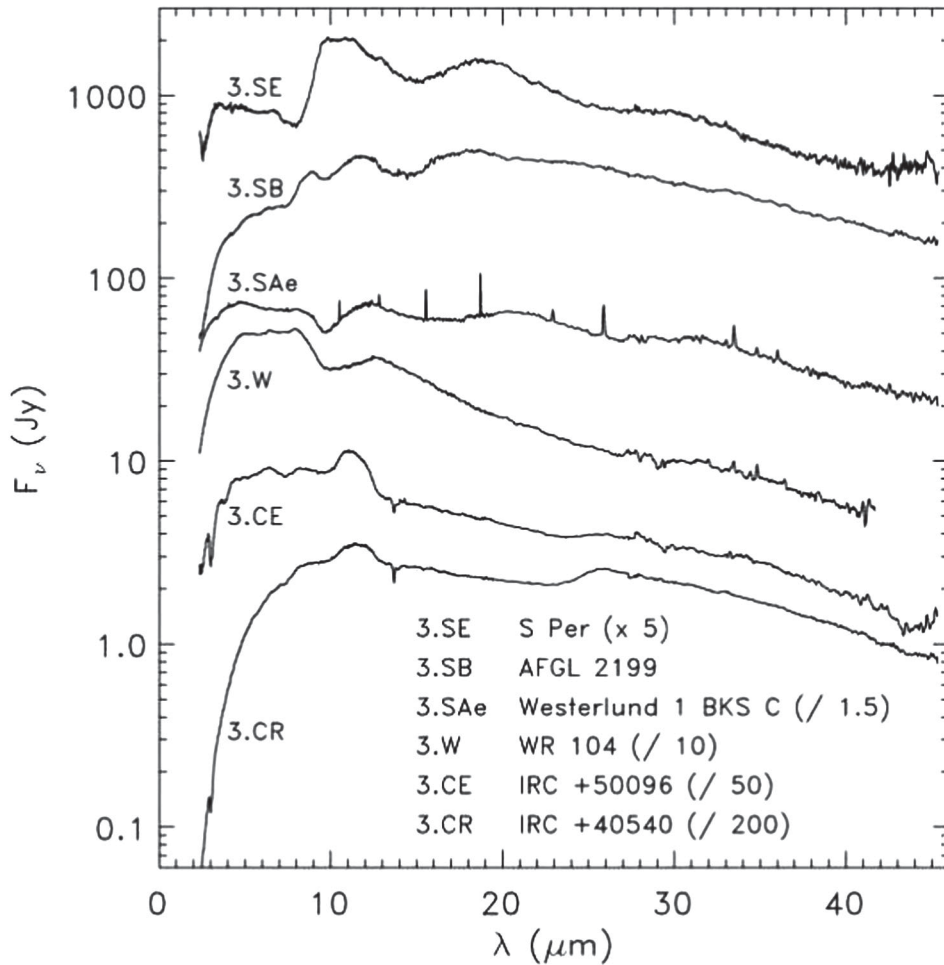


Figure 13.8 Sample spectra from the ISO SWS database in category 3 (warm, dusty objects). Figure from Kraemer et al. (2002), and reproduced by permission of the AAS.

13.3.3 Spitzer, the James Webb Space Telescope, and the Future

The InfraRed Spectrograph (IRS) on the Spitzer Space Telescope provides low and moderate resolution spectra in the 5.2 to 38 μm region. The low resolution spectra ($R \sim 60\text{--}120$) have a spectral range of 5.2–38 μm , whereas the high-resolution spectra ($R \sim 600$) have a spectral range of 9.9–37.2 μm . This instrument provides unrivaled sensitivity in this spectral range. The James Webb Space Telescope (JWST) will carry two infrared spectrographs, the Near Infrared Spectrograph (NIRSpec) and the Mid Infra Red Instrument (MIRI), which will provide both imaging and spectroscopy in the 5–27 μm region. The MIRI medium-resolution spectrograph will have a resolution of about 3000 in this spectral region.

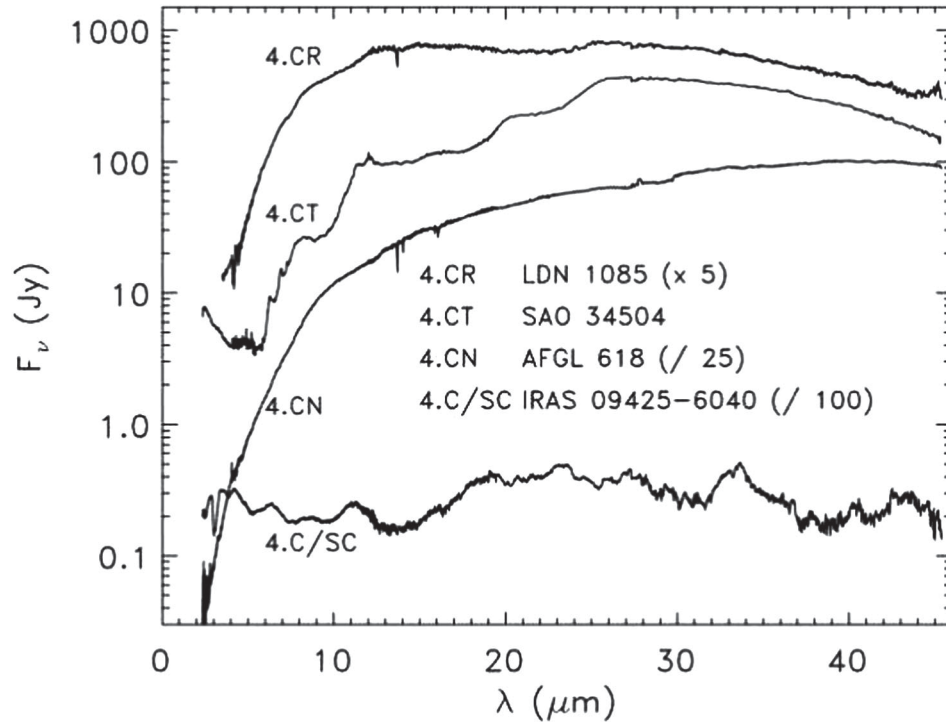


Figure 13.9 Sample spectra from the ISO SWS database of carbon-rich sources in category 4 (cool, dusty objects). Figure from Kraemer et al. (2002), and reproduced by permission of the AAS.

13.4 OTHER CLASSIFICATION SYSTEMS

Besides the new and developing systems in the thermal infrared, we would be remiss if we failed to mention certain stellar classification systems, other than the MK system, that have been used effectively by astronomers over the past years. These classification systems fall into two groups: classification systems, like the MK system, that are based on stellar spectra, and classification schemes that are based on photometric systems. The emphasis of this book is on *spectral* classification schemes, and so we have deliberately limited any discussion of photometric classification systems. However, for completeness, §2.3 does discuss a few of the more important photometric systems, and John Hearnshaw's *The Measurement of Starlight*² is an excellent source for those interested. In the course of this book we mentioned, and in a few places discussed in considerable detail, a number of spectral classification systems that properly lie outside of the purview of the MK system. These include the classification systems for the WR stars (Chapter 11) and white dwarfs, novae, and supernovae (Chapter 12). Below, we discuss a system of significant importance in the history of classification, although not now widely used, the BCD system.

²J.B. Hearnshaw *The Measurement of Starlight* (CUP 1996).

Table 13.3 ISO SWS Level 2 Classification Definitions

Class	Description
SE	Silicate (or oxygen-rich) dust emission (10–12 and 18–20 μm)
SB	Silicate emission in self-absorption (10 μm)
SA	Silicate absorption (10–12 μm)
SX	Silicate emission from crystalline grains (33, 40, 43 μm) ²
SEC	Silicate emission from crystalline grains (11, 19, 23, 33 μm)
CE	Carbon-rich dust emission, primarily from SiC (11.5 μm)
CR	Carbon-rich dust emission in a reddened shell (with features at 11.5 and 26 μm , often 13.7 μm absorption)
CT	8, 11.5, 21, 26 μm , but no 13.7 μm absorption
CN	Carbon-rich nebulae
C/SE	Carbon-rich, plus silicate emission (10–12 μm)
U/SC	Crystalline silicate and UIR ¹ emission features
U	Prominent UIR emission features
PN	Many prominent atomic fine-structure lines typical of PNs
PU	As PN, but with strong UIR emission
W	Emission peaks 6–8 μm
F	Basically featureless
E	Strong emission lines
M	Miscellaneous

¹ UIR features include emission at 3.3, 6.2, ~ 7.7 –7.9, 8.6 and 11.2 μm .

² The SX class was changed from SC to avoid confusion with SC stars.

13.4.1 The Barbier, Chalonge, and Divan (BCD) System

William Huggins was the first to notice a spectral feature called the *Balmer jump* in the spectra of Vega and similar stars. Rather later in the early 1930s Daniel Barbier, Daniel Chalonge, and colleagues exploited the high sensitivity to the near-UV attained at the Jungfraujoch Scientific Station due to its high altitude. They investigated the Balmer jump about the time that Yngve Öhman (1935), who had studied under Bertil Lindblad at the Stockholm Observatory, was concluding that the extreme example of this jump in white-dwarf A stars was related to the Stark broadening effect in strong electric fields. Barbier and Chalonge realized that two parameters derived from the Balmer jump (λ_1 , D ; see Figure 13.10) could characterize the temperature and surface gravity of stars, and so their two-dimensional classification system was born (Barbier & Chalonge 1941). It correlated well both with the Harvard types and with absolute magnitudes. The (λ_1 , D) system was perfected with the help of Mlle R. Canavaggia and applied to both normal and spectrally peculiar stars such as the Ap and Be.

Later the “BCD” classification system was extended with Mlle Lucienne Divan to include the continuum-gradient parameter Φ_b , derived from the 3800–4800 Å spectral region, and marked AB in Figure 13.10. Normal stars defined a surface called Σ in the three-dimensional space of λ_1 , D , Φ_b (see Figure 13.11), and so peculiar stars could be studied by their deviation from this surface. Divan looked

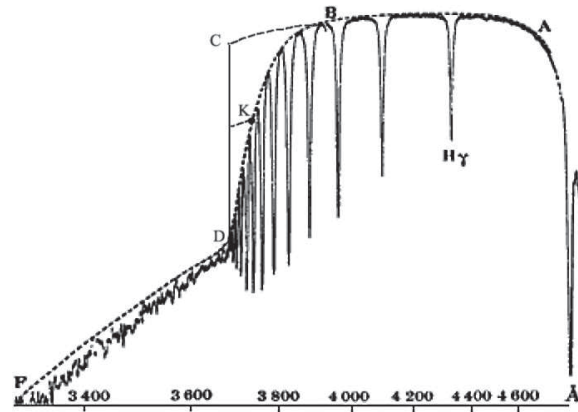


Figure 13.10 The parameters of the BCD system illustrated by a spectrum of Vega (A0 V). The parameter D measures the Balmer jump, C to D, which indicates the effective temperature. The parameter λ_1 gives the wavelength at K, the mean spectral position of the Balmer jump, and is related to surface gravity. The continuum gradient AB is the third parameter, Φ_b , and is a measure of the star's departure from normality. Figure adapted from Barbier & Chalonge (1939) and reproduced by permission of *Astronomy and Astrophysics*.

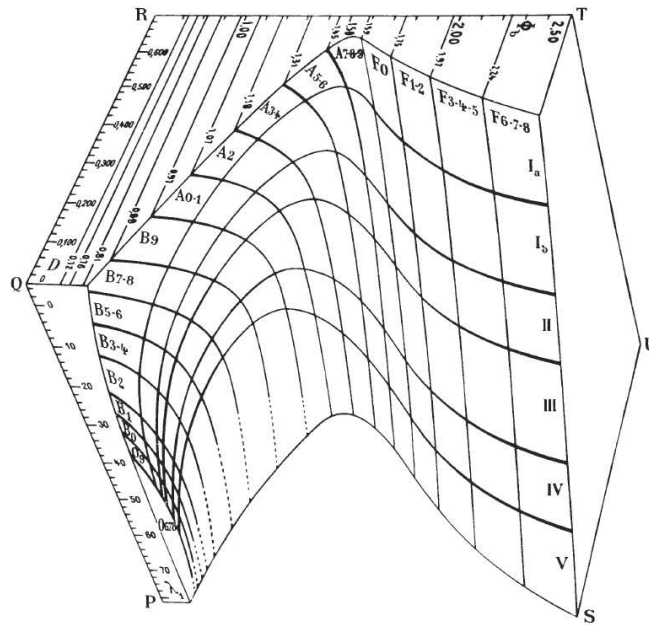


Figure 13.11 The BCD Σ surface in λ_1 , D , Φ_b space, showing where normal stars lie. Figure from Berger et al. (1958) and reproduced by permission from *Astronomy and Astrophysics*.

at dwarf stars with low metal abundances, known often as the subdwarfs, that lay below the normal Σ surface. J. Berger and colleagues also used the BCD system to study strong-lined stars, the Am stars, that lay above this surface (Berger et al. 1958). Work on this classification system, which has been described as really photometry at a point, continued intensively at the Institut d'Astrophysique in Paris for about two further decades, culminating quite logically in the relations of the BCD parameters with absolute magnitude (Chalonge & Divan 1973), temperature (Chalonge & Divan 1977b), and chemical composition (Chalonge & Divan 1977a). Cidale et al. (2007) make a good case for its continued use, but comparable data on the quantitative classification and parameterization of stars are now being obtained automatically from more extensive spectral features (see §13.5.3) or from photometric indices such as those in the Strömgen system.

13.5 AUTOMATED METHODS OF SPECTRAL CLASSIFICATION

13.5.1 Introduction

Traditionally, MK spectral classification has been carried out visually by comparing the program star with spectra of standard stars. In Chapter 1 and from subsequent chapters it is clear that the technique has been successfully transferred to modern digital spectra, and very precise and accurate spectral types result, providing that the spectra of unknowns and standards are obtained under controlled conditions. However, the process can still be very time consuming, and a reliable and accurate way to deal with the flood of spectra from new digital surveys, often employing multi-object spectrographs, is very much needed.

There is some truth to saying that achieving successful automation is the current “holy grail” of spectral classification. An early pioneer remarked, “Contrary to what some astronomers seem to think, spectral classification is a field where automatic methods are very difficult to apply. The reason is that the human classifier is able to see patterns that cannot readily be described mathematically” (Lyngå 1975). More than thirty years later we are still waiting for, say, the pipeline that will classify a spectrum in essentially real time and do it at the telescope as the spectra are being acquired. However, what makes computer-assisted classification of spectra possible is that the classification process is fundamentally not a subjective one, but a matching of the unknown spectrum with those of standard stars.

Here we should, following West (1976), recognize the two ways of approaching automated spectral classification, i.e., criterion evaluation and pattern recognition. The former measures specific spectral features, or criteria, that have been found to be helpful in distinguishing one spectral class from another. It then calibrates these measurements in terms of the desired parameters, such as spectral type and luminosity class or temperature and surface gravity. So the criterion-evaluation approach is what the experienced classifier does visually as *part* of the classification process. The more complete process—that of matching the total morphology of an unknown spectrum to that of a standard—is closer to the second automated

way, i.e., pattern recognition. Examples of pioneering in both ways, and even a mixture of the two, can be found in the review by Schmidt-Kaler (1982), while Rybski (1984) also attempted an evaluation of the two ways.

13.5.2 Recent Progress in Pattern Recognition

Attention over the last two decades on automated classification has on balance been more directed toward the way of pattern recognition or correlation analysis. Two approaches to this have been investigated in detail—the “metric-distance technique” (cf. Kurtz 1984; LaSala 1994); and techniques based on Artificial Neural Networks (ANN) (cf. von Hippel 1994; Bailer-Jones 1997; Weaver 1994; Gulati 1994; Singh et al. 1998). Both techniques show promise even though they are based on quite different philosophies.

The metric-distance technique regards the digitized spectrum as an n -element vector (where n refers to the number of resolution elements in the spectrum) and defines the metric distance between a program spectrum X and a standard S as

$$d_{xs} = \frac{1}{n} \sqrt{\sum_{i=1}^n \alpha^2 (X_i - S_i)^2}, \quad (13.5.1)$$

where the weighting factor α^2 is defined in such a way that the highest weights are given to those features that most strongly discriminate the final spectral type from other surrounding spectral types (cf. LaSala 1994). One advantage of this method is that it is quite close to the original philosophy of the MK system (e.g., that spectral types are determined by comparison with MK standards). A disadvantage is that the method requires that the spectra should be accurately rectified (i.e., the shape of the continuum should be removed). This is straightforward in the early type stars, but is problematical in the late-type stars (say later than K0), as in these stars there are no true continuum points. This problem becomes extreme in the M- and the C-type stars. This should not be an insurmountable problem, but so far this method has been applied only to stars earlier than K0.

Artificial Neural Networks (ANN) have been used quite extensively to distinguish, on digital images, between stars and galaxies and to classify galaxies, and so it is quite natural to apply the technique to stellar classification. Details on the method can be found in the references given at the start of this section and in papers that cite these, but in brief the ANN method uses an artificial neural network consisting of a number of layers of nodes, including a layer for input of the data (in this case, the spectral data), a layer for the output, and one or more “hidden layers” of summation nodes together with weighted connections between the layers (see Figure 13.12). A popular configuration for automatic spectral classification uses a gradient-descent, nonlinear minimization ANN technique, known as back propagation, with a single hidden layer. The ANN must first be trained on a set of spectra with well-determined spectral types; this training changes the weighting used in the connections between the layers. Once trained, the ANN can be used

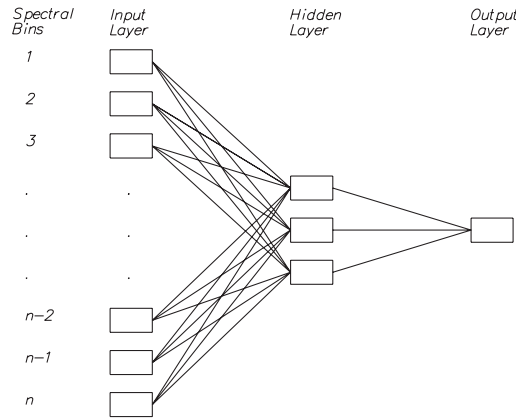


Figure 13.12 A sample ANN architecture with one hidden layer. From Corbally, Garrison & Gray (2003) reproduced by permission of kluwer Academic Publishers.

to classify new data. Errors involved in temperature classification are typically between 1 to 2 spectral subtypes when classifying across the entire H–R diagram. One of the advantages of this method is that rectification of the spectrum is not so critical as in the metric-distance method. Indeed, the ANN can, in principle, be trained with non-rectified spectra with known reddenings, and can be designed to output not only the spectral type but also the reddening. A disadvantage is that the ANN method does not, contrary to the principles of MK classification, classify a star against the standards, but is instead an “expert” system that effectively reproduces the results of an expert classifier (in the case of the work by Ted von Hippel’s group, Nancy Houk, Houk 2001), and thus classifies stars against the “cloud” of stars classified by that expert as a single spectral type.

Refinements in technique have occurred principally for the ANN method. Bailer-Jones (1997, 1998) introduced the use of two hidden layers and of Principal Components Analysis (PCA), which reduces the number of parameters in the network and so the computing required. An example of how as few as 20 Principal Components can reproduce the original spectrum to within 99.9%, with a data compression of 33:1, is given in the work of Singh et al. (1998) (see Figure 13.13). One disadvantage can be that very weak features that show very little correlation across the data set will be lost in a PCA reconstruction. However, not all such weak features are lost, and both noise, including sky noise, and detector artefacts, such as cosmic ray events, can be filtered out. Even so, one problem of such filtering is that unexpected peculiarities, like emission in some lines, will also be rejected. Still, the reconstructed spectrum in this case would have a large error in relation to the original, and this can be flagged to indicate that more refined classification, even by the human eye, is needed.

Given the vast range of stellar peculiarities, which a glance through this book attests, it is no wonder that more work is needed to identify these automatically. Of greater concern is that the subtle process of luminosity classification needs

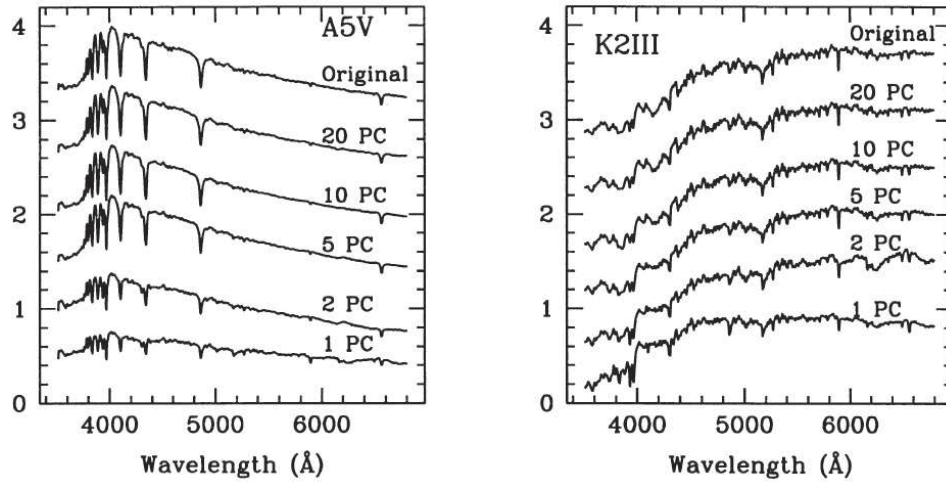


Figure 13.13 Reconstruction of an early and a late spectral type out of the test spectra using the first 20, 10, 5, 2, and 1 principal components. These are compared with the original spectrum at the top. This figure is courtesy of Singh et al. (1998) and reproduced permission of Blackwell Publishing, Ltd.

further refinement. For instance, the ANN of Bailer-Jones (1998), even when the output node was divided into temperature and luminosity class, failed to distinguish mid-G type class IV from classes V and III. Medhi et al. (2007), who tried both cross-correlation and ANN, with separate networks for temperature and luminosity, showed no real improvement. The rather earlier work of Weaver (1994) applied first a coarse then a specialist ANN to 15-Å resolution A-type spectra. This dual-stage method yielded an accuracy to within 0.2 luminosity classes. So this was quite encouraging, though it was not clear whether the method or the use of NIR spectra, or both, was the significant factor. The NIR was also chosen by Malyuto et al. (1997) for their application of the cross-correlation method to the classification of late K- and M-type stars. Here they found accuracies to 0.6 of a spectral subtype and 0.8 of a luminosity class.

The review of Coryn Bailer-Jones (2002) describes one further method of automated classification, that by Gaussian probabilistic models (GPM). This is a statistical approach that uses training on a set of preclassified spectra to determine the probability that an object with a measured feature vector is a member of a particular class. This method could be most useful in surveys where data for particular features, or vectors, are missing. Bailer-Jones also makes the point that the goals of a particular survey may be better achieved by one rather than another automated method, so it is as well to have the choice of several mature techniques. In this regard there are other statistical techniques, like that of Dodd & Legget (1993) whose use of statistical image moments on low-resolution stellar spectra was at least encouraging, and like those that range from the Karhunen–Loève transform to wavelet transforms, which are being applied to such as SDSS galaxy spectra, so the choice is widening (Connolly et al. 2001).

13.5.3 Current Interests and Opportunities in the IR and UV

Current interest is in the automated derivation of physical parameters for objects in large surveys, an interest that is complementary to classification albeit dependent on improvements in models. So we find Snider et al. (2001) investigating ANNs to get not just T_{eff} and $\log g$, but particularly $[\text{Fe}/\text{H}]$ from medium-resolution spectra of F- and G-type stars. They claim that a signal-to-noise down to just 13 will yield useful results, a boon for surveys. Winter et al. (2006) first tried an ANN with a 3-element PCA filter to classify hot subdwarfs from SDSS spectra, and then applied a χ^2 minimizer over a set of LTE model atmospheres to give the parameters. Gupta et al. (2004) were more interested in spectral features in the IR, so they defined 17 such features (e.g., emissions, silicate bumps, featureless spectra, continuum profiles, carbon stars) and automatically classified, using a two hidden-node ANN, the spectra of IRAS sources with respect to these. Work in the IR more closely related to MK classes, i.e., the development of classification from mid-IR CO, SiO, and water molecular bands, has been done with spectra from the Short Wavelength Spectrometer on the Infrared Space Observatory by Heras et al. (2002). The mid-IR spectral characteristics were earlier correlated with the physical parameters of the stars. This work, with its theoretical underpinning of band behavior (Decin et al. 2000), indicates potential for automated classification in the IR when databases have built up in quantity. The UV has not been neglected either, for Gulati et al. (1997) have made extinction determinations of O- and B-type stars from ANNs applied to IUE spectra.

Sunetra Giridhar et al. (2006) have reviewed current methods in automated classification, and she suggests that the input of classical or special photometric indices can help achieve the accuracy that large surveys require and the sensitivity to more complex or peculiar spectra. No doubt these lines of work will continue and hopefully make these methods “robust.” The authors of this book, with Robert Garrison, have pointed out an important role for the smaller telescopes in this process (Corbally et al. 2003). We look forward to the time when automated techniques become widely available and are applicable with ease to large quantities of real data that span the whole H–R diagram.

13.6 LOW DISPERSION TECHNIQUES AND NATURAL GROUPS

13.6.1 Introduction and History

The mention of large surveys in the previous section leads to the obvious remark that these are often searching for very faint stars or other faint objects. Usually the most efficient way to do this spectroscopically is by using low dispersions and wide fields. The Schmidt telescope, a wide-field camera invented in 1930 by Bernhard Schmidt of Hamburg Observatory, was ingeniously designed for such work, but any telescope and disperser combination delivering low dispersion plus wide field will qualify as a spectroscopic survey instrument. For the Schmidt, the disperser is a prism large enough to be put above the aperture, which is the “corrector plate”

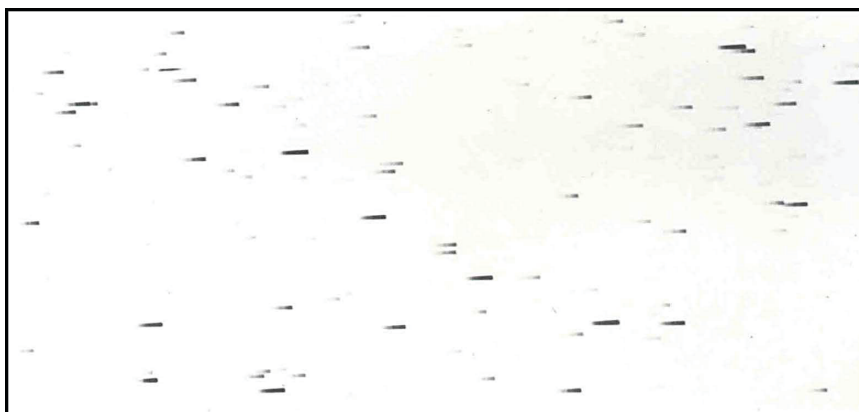


Figure 13.14 Low-dispersion spectra in about a 2 deg square area of the relatively sparse South Galactic Pole. Here are mostly G- and K-dwarfs as evidenced from the many G-bands visible under a microscope (as a guide to the eye, see Figure 13.17). The spectra were taken with the Curtis Schmidt telescope and a 1.8 deg objective prism (Corbally & Garrison 1988) and they are about 2 mm long on the original plate.

of the telescope. These prisms typically have angles from about 1 deg to 12 deg resulting in dispersions between about $5,000$ to 100 \AA mm^{-1} at $H\gamma$. The dispersion depends on the telescope plate scale and the disperser's optical glass. Since the disperser is a prism, the dispersion varies with wavelength, and so it is always quoted at a specific wavelength. The resolution of line features in the spectrum depends on the seeing at the time of the observation, so the best telescope sites give the best efficiency for such work. The typical look of low-dispersion spectra is shown in Figure 13.14.

There are other ingenious ways of delivering multiple, low-dispersion, slitless spectra over a relatively wide field. Martin McCarthy (1979), in his review of classification beyond the MK System, describes the evolution from putting a transmission grating in the converging beam of a telescope to adding a weak prism to the grating, the "grism." For the prime focus at large telescopes, Richardson (1982) makes the case for adding a final lens element, producing the "grens." Currently the slitless approach is being complemented by fiber-fed multiobject slit spectrographs, which are too numerous to list here.

Now some of these survey spectra are of sufficient quality to take classification by the MK System. When there are limitations of seeing and resolution, what method best serves to select the objects of interest? Without a doubt, it is that of "natural groups." In W. W. Morgan's classic paper on natural groups (Morgan 1951) he picks up on a basic principle underlying the classification of stars as stated by Miss Payne (1925): "In classifying a number of objects, an attempt should be made to select criteria that will distribute the material into the most natural groups." Morgan then goes on to define a natural group as "one made up of spectra which have some obvious characteristic in common, and which, at the same time, are confined to a relatively small area of the luminosity class-spectral type (LC-S)

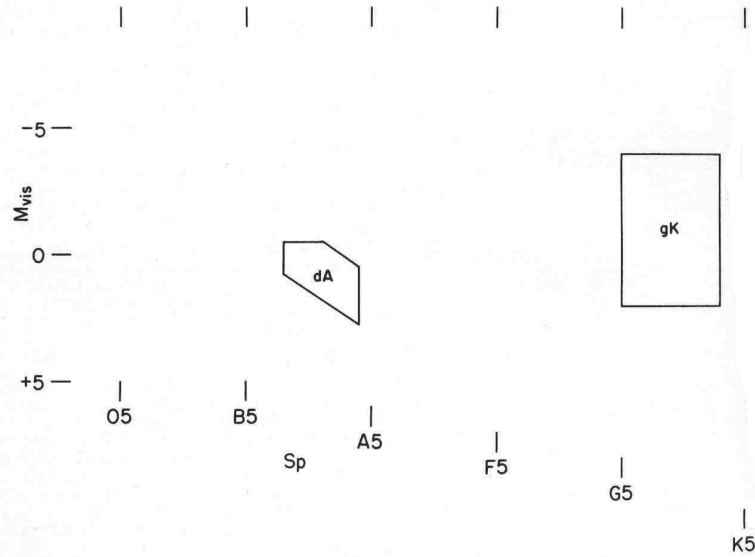


Figure 13.15 Natural groups for a dispersion of $700\text{--}1200\text{ Å mm}^{-1}$ at $H\delta$. The dA group shows strong hydrogen absorption and the gK group has strong CN band absorption. The Figure is from Morgan (1951). Reproduced by permission.

diagram.” One could well say that Father Secchi’s four spectral classes, the A-type, the solar-type, the M-star, and the carbon-star, were the first examples of natural groups.

Morgan himself described sets of natural groups in the HR diagram that were appropriate for different spectral dispersions. At the lowest dispersion that he considered, $700\text{--}1200\text{ Å mm}^{-1}$ at $H\delta$, he identified two classic natural groups: the dA group, consisting of stars showing the strongest hydrogen absorption, and the gK group, distinguished by strong absorption of the CN band near $\lambda 3883$. These two natural groups are shown in Morgan’s “LC-S” diagram of Figure 13.15. His “OB” natural group, identified at a dispersion of 390 Å mm^{-1} at $H\delta$ as having hydrogen and all other lines weak or absent, has been adopted as the name for the earliest-type stars (see Chapter 3). Higher dispersions can allow natural groups for luminosity, as well as temperature, to be distinguished. So a dispersion of around 200 Å mm^{-1} at $H\delta$ for the spectra in Figure 13.16 can show how the gK group (K-giants) is separated from the cK (K-supergiants) and dK (K-dwarfs) groups. However, higher dispersions may not always be needed if properties from the distribution of stars on the H–R diagram are found to help. For example, Corbally & Garrison (1988) distinguished the natural group of early-G dwarf stars from spectra at 1360 Å mm^{-1} at $H\gamma$, regardless of metallicity (Figure 13.17). This group fell under the “Hertzsprung Gap,” so any giant stars in the candidate sample would be very few and anyway interesting.

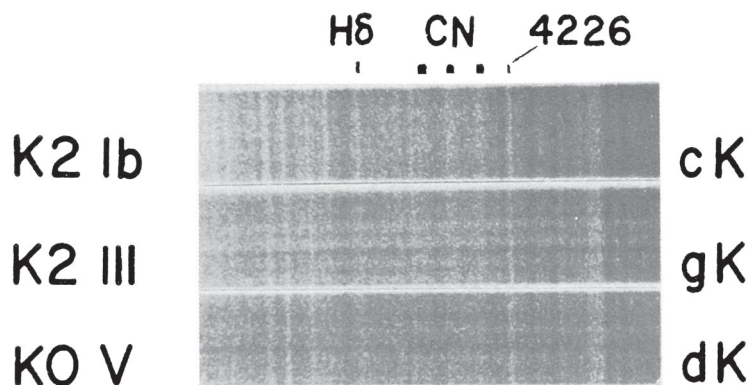


Figure 13.16 Luminosity natural groups for a dispersion of around 200 Å mm^{-1} at $H\delta$ by Morgan (1951). His criteria are: group cK has CN strong, $H\delta$ strong; group gK has CN strong, $H\delta$ weak; group dK has CN weak, with Ca $\lambda 4226$ and the G-band similar in strength to the gK group. Reproduced by permission.

13.6.2 Further Natural Groups and Luminosity Criteria

In mentioning Father Secchi we have touched on some other natural groups of stellar spectra—those with strong molecular bands, the M-type, S-type, and carbon stars of Chapter 8, whose broad bands are obvious and characteristic at low dispersion, especially in the NIR. Late-M stars can be classified by the relative strengths of the TiO $\lambda\lambda 7598, 8432$, and VO $\lambda 7900$ bands, while carbon star spectra show strong blends of CN bands near $\lambda\lambda 7910, 8100$, and 8320 . These criteria have been exploited by Blanco et al. (1978, and related papers) to compare stellar populations within the Magellanic Clouds and the Galaxy. Since their criteria do not discriminate luminosity classes, they take advantage of knowing the distance to their objects, which with the apparent magnitudes can provide luminosities. As explored below, the metal-hydride bands are also useful natural-group criteria for luminosity and temperature type.

Morgan et al. (1981) point out the natural group of super-supergiants around G8–K0 for whom blends, especially 4475 Å , in the $H\beta$ – $H\gamma$ region dramatically change appearance between Ib and 0-Ia. A caution is that this natural group is subject to the variability these stars show. There is also a suggestion by Morgan in the discussion after a talk by McCarthy (1984) that the metastable helium line at $\lambda 3888$ might lead to a group of “wind” stars, but such a group would be stepping beyond the confines of a small area in the H–R diagram and could include WR, Be, interacting binaries, etc. Emission line objects are another set that can occupy various parts of the H–R diagram and so need caution when searches are made for them. Indeed as a further caution, MacConnell & Coyne (1983) had to point out that the continuum between close molecular bandheads can get confused at low dispersion with emission features, an effect with which spectral classification pioneers had had to contend also.

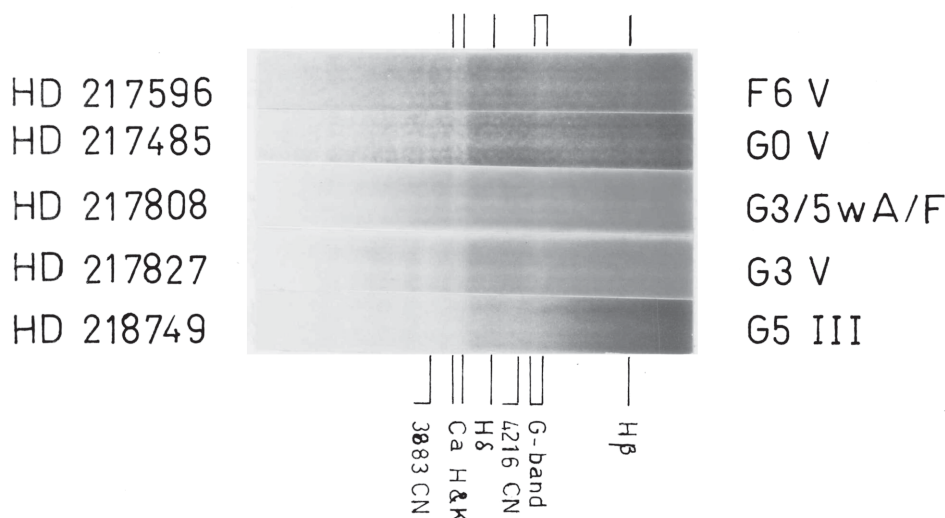


Figure 13.17 The inner set of three spectra form the natural group of early-G dwarfs for a dispersion of 1360 \AA mm^{-1} at $H\gamma$. Four criteria described by Corbally & Garrison (1988) include also the central, weak-lined star in the group, and by lying under the Hertzsprung Gap in the H–R diagram naturally exclude giant stars. Reproduced by permission of the AAS.

It should certainly be mentioned that Bruch et al. (1979), after investigating errors in classifications of spectra at the Bonn Spectral Atlas dispersions of 240, 645, and 1280 \AA mm^{-1} , advocate that straight classifications rather than natural groups be used since the former use more information in the spectra. However, not all survey spectra are of such high quality as those from the Bonn Schmidt telescope and the errors in luminosity at these dispersions may not be acceptable for some surveys.

Luminosity discrimination at low dispersion will be helped by broad features, e.g., the Na-D lines and the metal hydrides (MgH, CaH), and, as mentioned in the previous subsection, the Hertzsprung Gap in the H–R diagram. So we find that Ratnatunga & Freeman (1985), in looking for K-giants to do kinematical studies in the outer Galactic Halo, used the criteria of (1) strong MgH to pick out disk dwarfs, (2) no MgH or the Mg b triplet for metal-weak giants, and (3) no MgH but the Mg b triplet for metal normal giants or some hotter G-dwarfs. As one might expect, the same luminosity sensitivity of the Mg I triplet+MgH features near 5150 \AA in F–K stars was not lost to the photometric community. It is reproduced by the flux in the intermediate-band DDO51 filter, which was introduced to the DDO system by Clark & McClure (1979) (the actual inspiration for the Ratnatunga & Freeman 1985 work) and later combined with Washington system filters by such as Majewski et al. (2000) in studies of Galactic Halo substructure.

13.6.3 Very Low Dispersion, “Tadpoles,” and Automation

Even the spectra in Figure 13.17 are relatively detailed. When it is desired to go as faint as possible in a survey, while putting up with some loss of discrim-

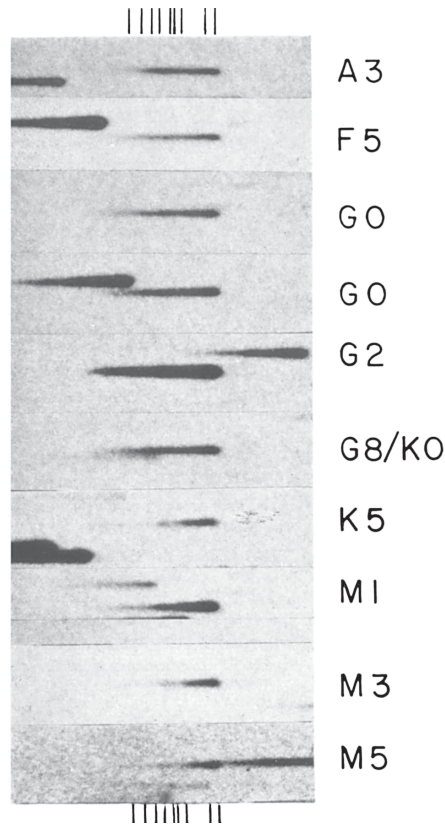


Figure 13.18 Very low-resolution, “tadpole-like” objective-prism spectra from the UK Schmidt telescope of 10 stars used as standards. The long wavelength ends are aligned to avoid confusion with nearby, non-standard spectra. The spectra have a dispersion of 2440 Å/mm at $H\gamma$ and range from $\lambda 3200$ to $\lambda 5400$. Features used in the classification are indicated by the vertical lines. For identifications see the original figure in Krug et al. (1980). Reproduced by permission of Blackwell Publishing, Ltd.

ination, then there is no substitute, if spectroscopy is going to be more suitable than photometry to find the required objects, for very low dispersion. Figure 13.18 shows that this kind of spectra look like nothing so much as tadpoles at first sight. However, the paper does describe criteria that can sort even these spectra within a letter class (as demonstrated by Figure 13.19 from later work on the same UK 1.2 m Schmidt Telescope). Such sorting lends itself to automatic methods, which brings us back to the topic of the previous section, that of automated classification. It was the wealth of data on such as Schmidt telescope plates that encouraged the pioneering of these techniques. Contemporary studies, like that of Bratsolis et al. (2000, and related papers), are continuing to develop and do automatic extraction and classification of low-dispersion objective prism stellar spectra. One difference today, of course, is that the detector of choice is no longer the fine-grained IIIaJ photographic emulsion but the pixels from a mosaic of CCDs.

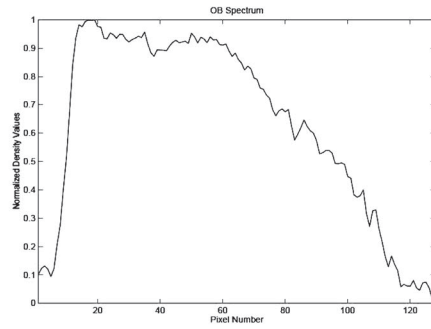
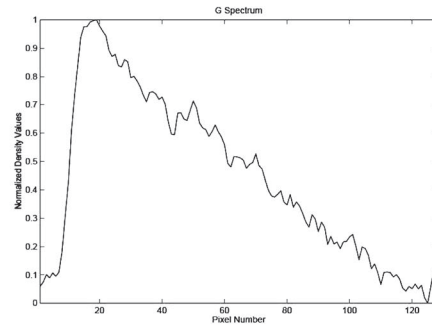
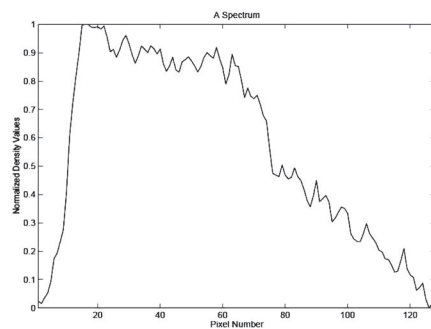
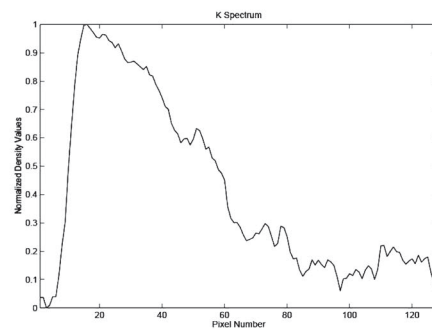
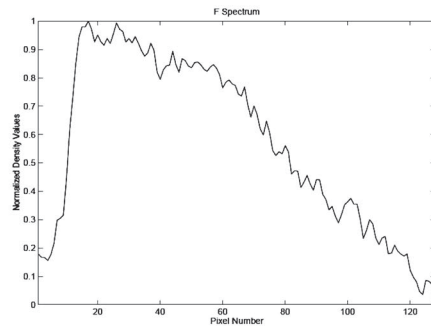
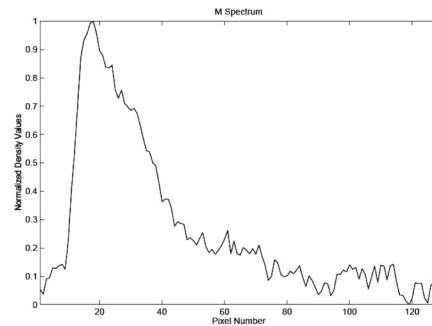
A characteristic 1×128 OB spectrumA characteristic 1×128 G spectrumA characteristic 1×128 A spectrumA characteristic 1×128 K spectrumA characteristic 1×128 F spectrumA characteristic 1×128 M spectrum

Figure 13.19 Characteristic very low-resolution spectra from the sample of Bratsolis et al. (2000). These are digitizations of photographic spectra from the UK Schmidt telescope, similar to those of Figure 13.18, and they show that at least the letter-types can be distinguished. Reproduced by permission of *Astronomy & Astrophysics*.

The Byurakan Schmidt has a 1.5 deg prism that gives a dispersion of 1800 \AA mm^{-1} at $H\gamma$. The plates from the First Byurakan Survey, made famous by Markarian and his discovery of the galaxies named after him, have been digitized and compared with optical identifications of IRAS point sources (Mickaelian & Gigoyan 2006). Their techniques are good enough to distinguish carbon and M stars, planetary nebulae, QSOs, galaxies, and other objects that correspond to infrared sources.

Mention of nebulae and active galaxies is a reminder that stars are not the only interesting objects that turn up in low dispersion work. “Typical” galaxy surveys might include those of Lewis (1983) who showed that the Michigan-Tololo plates were very efficient at finding active galaxies; of Moss et al. (1988, and its series) who were using the Burrell Schmidt to make an objective prism, $H\alpha$ survey of nearby clusters with star-forming galaxies and of like field galaxies; and of Gallego et al. (1995) similarly finding emission objects with the Schmidt telescope at Calar Alto to study the current star formation rate of the local universe, a work that is gaining a considerable number of citations.

13.6.4 Extending the Spectral Range and the Future

What of the future of survey work? While the Byurakan-IRAS Star catalogue (Mickaelian & Gigoyan 2006) demonstrates a neat, complementary approach being followed between the optical and infrared data, the latter is photometric rather than spectroscopic. One might say that searches beyond the optical spectrum, i.e., in the IR and UV, should remain photometric. The areal coverage is made faster than for spectroscopic ones and the potential of going fainter is greater.

Faster-and-fainter is an attractive argument, especially if cheaper is coupled to it. However spectroscopy, even at low dispersion, has the potential for more information elements than photometry—which has been described as the very low-dispersion spectroscopy. That is why large field, low-dispersion spectroscopic searches have persisted and why automated techniques have been developed to get the most out of them. Since low-dispersion spectroscopic searches in the UV and IR are dependent on a large areal size of the respective detectors, then this is for the future. When these large UV and IR detectors do come, it will be interesting to see how the field develops. Extragalactic researchers will be very excited, but how about the further possibilities for stellar and ISM astrophysics in investigating Mira variables obscured by their own dust (see Kerschbaum et al. 2006). And who would like to pick out the natural groups at different dispersions for, say, brown dwarfs?

Bibliography

- Aungwerojwit, A., Gänsicke, B.T., Rodríguez-Gil, P., Hagen, H.-J., Giannakis, O., Papadimitriou, C., Allende Prieto, C., & Engels, D. 2007, AA, 469, 297
- Bagnuolo, W.G., & Gies, D.R. 1991, ApJ, 376, 266
- Bahng, J.D.R. 1958, ApJ, 128, 572
- Bailer-Jones, C.A.L. 1997, PASP, 109, 932
- Bailer-Jones, C.A.L. 1998, MNRAS, 298, 361
- Bailer-Jones, C.A.L. 2002, in *Automated Data Analysis in Astronomy*, eds. R. Gupta, H.P. Singh, & C.A.L. Bailer-Jones (New Delhi: Narosa Pub. House), p. 83
- Barbier, D., & Chalonge, D. 1939, Ann. Ap. 2, 254
- Barbier, D., & Chalonge, D. 1941, AnAp, 4, 30
- Beavers, W.I., & Cook, D.B. 1980, ApJS, 44, 489
- Berger, J., Chalonge, D., Divan, L., Fringant, A-M., & Westerlund, B. 1958, JO, 41, 100
- Bidelman, W.P. 1984, in *The MK Process and Stellar Classification*, ed. R.F. Garrison (Toronto: David Dunlap Observatory), 45
- Blanco, B.M., Blanco, V.M., & McCarthy, M.F. 1978, *Nature*, 271, 638
- Bratsolis, E., Bellas-Velidis, I., Dapergolas, A., Kontizas, E., & Kontizas, M. 2000, AApS, 142, 339
- Bruch, A., Buescher, M., Samson, W., & Seitter, W.C. 1979, RA, 9, 493
- Burleigh, M.R., Hogan, E., Dobbie, P.D., Napiwotzki, R., & Maxted, P.F.L. 2006, MNRAS, 373, L55
- Chalonge, D., & Divan, L. 1973, AA, 23, 69
- Chalonge, D., & Divan, L. 1977a, AA, 55, 117
- Chalonge, D., & Divan, L. 1977b, AA, 55, 121
- Cidale, L.S., Arias, M.L., Torres, A.F., Zorec, J., Frémat, Y., & Cruzado, A. 2007, AA, 468, 263
- Clark, J.P.A., & McClure, R.D. 1979, PASP, 91, 507
- Connolly, A.J., and 12 coauthors, 2001, in *Mining the Sky*, eds. A.J. Banday, S. Zaroubi, & M. Bartelmann (Berlin/Heidelberg: Springer-Verlag), p. 323
- Conselice, C.J. 2006, MNRAS, 373, 1389
- Corbally, C.J. 1987, ApJS, 63, 365
- Corbally, C.J., & Garrison, R.F. 1988, AJ, 95, 739
- Corbally, C.J., Garrison, R.F., & Gray, R.O. 2003, in *The Future of Small Telescopes in the New Millenium*, ed. T.D. Oswalt, Vol. III (Dordrecht: Kluwer Academic Publishers), p. 93

- de Vaucouleurs, G. 1959, *Handbuch der Physik*, 53, 275
- Decin, L., Waelkens, C., Eriksson, K., Gustafsson, B., Plez, B., Sauval, A.J., Van Assche, W., & Vandebussche, B. 2000, AA, 364, 137
- Dodd, R.J., & Legget, S. 1993, Ap&SS, 203, 305
- Engelke, C.W., Kraemer, K.E., & Price, S.D. 2004, ApJS, 150, 343
- Evans, N.R., & 11 coauthors 2006, IAUS, 240, 86 (astro-ph/0609759)
- Gallego, J., Zamorano, J., Aragon-Salamanca, A., & Rego, M. 1995, ApJ, 455, L1
- Gies, D.R. 2004, ASPC, 318, 61
- Ginestet, N., & Carquillat, J.M. 2002, ApJS, 143, 513
- Ginestet, N., Carquillat, J.M., Jaschek, M., & Jaschek, C. 1994, AApS, 108, 359
- Giridhar, S., Muneer, S., & Goswami, A. MmSAI, 2006, 77, 1130
- Goebel, J., et al. 1989, AA, 222, L5
- Griffin, R.E.M. 2001, *The Observatory*, 121, 259
- Griffin, R.E. 2002, AJ, 123, 988
- Griffin, R.E.M., & Griffin, R.F. 1986, JApA, 7, 195
- Griffin, R.E.M., Griffin, R.F., & Stickland, D.J. 2006, MNRAS, 373, 1351
- Gulati, R.K., Gupta, R., Gothoskar, P., & Khobragade, S. 1994, ApJ, 426, 340
- Gulati, R., Gupta, R., & Singh, H. 1997, PASP, 109, 843
- Gupta, R., Singh, H.P., Volk, K., & Kwok, S. 2004, ApJS, 152, 201
- Hensberge, H., & Pavlovski, K. 2006, astro-ph.0611422
- Heras, A.M., Shipman, R.F., Price, S.D., de Graauw, Th., Walker, H.J., Jourdain de Muizon, M., Kessler, M.F., Prusti, T., Decin, L., Vandebussche, B., & Waters, L.B.F.M. 2002, AA, 394, 539
- Hodge, T.M., Kraemer, K.E., Price, S.D., & Walker, H.J. 2004, ApJS, 151, 299
- Houk, N. 2001, Michigan Spectral Catalogue, <http://cdsarc.u-strasbg.fr/viz-bin/Cat?III/31B>
- Hubble, E.P. 1926, ApJ, 64, 321
- Humason, M.L. 1936, ApJ, 83, 18
- Hünsch, M., & Reimers, D. 1993, AA, 276, 161
- Hynek, J.A. 1938, Perkins Contr., 1, No.10, 185
- IRAS Explanatory Supplement 1988, Catalogs & Atlases, Vol. I (Washington DC: NASA)
- Joint IRAS Science Working Group 1987, NASA RP-1190
- Kennicutt, R.C. 1992a, ApJ, 388, 310
- Kennicutt, R.C. 1992b, ApJS, 79, 255
- Kerschbaum, F., Groenewegen, M.A.T., & Lazaro, C. 2006 AA, 460, 539
- Kraemer, K.E., Sloan, G.C., Price, S.D., & Walker, H.J. 2002, ApJS, 140, 389
- Krug, P.A., Morton, D.C., & Tritton, K.P. 1980, MNRAS, 190, 237
- Kurtz, M.J. 1984, in *The MK Process and Stellar Classification*, ed. R.F. Garrison (Toronto: David Dunlap Observatory), 136
- Kwok, S., Volk, K., & Bidelman, W.P. 1997, ApJS, 112, 557
- LaSala, J. 1994, in *The MK Process at 50 Years*, eds. C.J. Corbally, R.O. Gray, & R.F. Garrison, ASPC, 60, 312

- Lewis, D.W. 1983, PhD Thesis, Univ. Michigan
- Lyngå, G. 1975, *Rep. Obs. Lund*, No.5
- Majewski, S.R., Ostheimer, J.C., Kunkel, W.E., & Patterson, R.J. 2000, *AJ*, 120, 2550
- Malyuto, V., Oestreicher, M.O., & Schmidt-Kaler, Th. 1997, *MNRAS*, 286, 500
- Markowitz, A.H. 1969, Ph.D. diss., Ohio State Univ.
- Maurý, A.C. 1897, *Ann. Astron. Obs. Harvard College*, 28, 1
- Mayall, N.U. 1946, *ApJ*, 104, 290
- McCarthy, M.F. 1979, in *Spectral Classification of the Future*, IAU Coll. 47, eds. M.F. McCarthy, A.G.D. Philip, & G.V. Coyne (Vatican: Vatican Observatory) RA, 9, 103
- McCarthy, M.F. 1984, in *The MK Process and Stellar Classification*, ed. R.F. Garrison (Toronto: David Dunlap Observatory), 55
- MacConnell, D.J., & Coyne, G.V. 1983, *VatOP*, 2, 63
- Medhi, B.J., Messina, S., Parihar, Padmakar, S., Pagano, I., Muneer, S., & Duorah, K. 2007, *AA*, 469, 713
- Mickaelian, A.M., & Gigoyan, K.S. 2006, *AA*, 455, 765
- Morgan, W.W. 1951, *POMic*, 10, 33
- Morgan, W.W. 1958, *PASP*, 70, 364
- Morgan, W.W. 1959, *AJ*, 64, 432
- Morgan, W.W., Keenan, P.C., Abt, H.A., & Tapscott, J.W. 1981, *ApJ*, 243, 894
- Morgan, W.W., & Mayall, N.U. 1957, *PASP*, 69, 291
- Moss, C., Irwin, M.J., & Whittle, M. 1988, *MNRAS*, 232, 381
- Öhman, Y. 1935, *StoAn*, 12, 1
- Parsons, S.B., & Ake, T.B. 1993, *ApJ*, 412, 814
- Pickering, E.C. 1891, *Astr. Nach.*, 127, 155
- Ratnatunga, K.U., & Freeman, K.C. 1985, *ApJ*, 291, 260
- Richardson, E.H. 1982, *SPIE*, 331, 252
- Rybski, P.M. 1984, in *The MK Process and Stellar Classification*, ed. R.F. Garrison (Toronto: David Dunlap Observatory), 131
- Schmidt-Kaler, Th. 1982, *BICDS*, 23, 2
- Shaïn, G. 1926, *Astr. Nach.*, 228, 337
- Singh, H.P., Gulati, R.K., & Gupta, R. 1998, *MNRAS*, 295, 312
- Snider, S., Allende Prieto, C., von Hippel, T., Beers, T.C., Sneden, C., Qu, Y., & Rossi, S. 2001, *ApJ*, 562, 528
- Stephenson, C.B., & Sanwal, N.B. 1969, *AJ*, 74, 689
- Titus, J., & Morgan, W.W. 1940, *ApJ*, 92, 256
- Volk, K. 1993, in ASP Conf. Proc. 41, *Astronomical Infrared Spectroscopy* (San Francisco: ASP), 63
- Volk, K., & Cohen, M. 1989, *AJ*, 98, 931
- von Hippel, T., Storrie-Lombardi, L.J., & Storrie-Lombardi, M.C. 1994, in *The MK Process at 50 Years*, eds. C.J. Corbally, R.O. Gray, & R.F. Garrison, *ASPC*, 60, 289

- Weaver, Wm. B. 1994, in *The MK Process at 50 Years*, eds. C.J. Corbally, R.O. Gray, & R.F. Garrison, ASPC, 60, 303
- Weaver, Wm. B. 2000, ApJ, 541, 298
- West, R.M. 1976, in *Proceedings of the Third European Astronomical Meeting*, ed. E.K. Karadzi (Tbilissi: Abastuman Astrophysical Observatory), 23
- Winter, C., Jeffery, C.S., Ahmad, A., & Morgan, D.R. 2006, BaltA, 15, 69
- Yip, C.W., and 14 coauthors, 2004, AJ, 128, 585

Glossary

Anomalous Luminosity Effect: A phenomenon seen in the luminosity criteria of Am and related stars. For those stars exhibiting the anomalous luminosity effect, certain luminosity criteria indicate the star is a giant or even a supergiant, while other luminosity criteria indicate the star is a dwarf. Often, both luminosity classes are in disagreement with the absolute magnitude based on the parallax. See §5.4.1.

Balmer jump: A discontinuity in the stellar energy distribution, most clearly seen in the spectra of B-, A-, and F-type stars. This discontinuity occurs at a wavelength of about 3650 Å, in the near-ultraviolet, and coincides with the convergence of the Balmer series of lines. The cause of this discontinuity is the continuous opacity edge that arises from the photoionization of hydrogen in the $n = 2$ state. The size of the Balmer jump is temperature dependent in the B-type stars, but both gravity and temperature dependent in the A- and F-type stars. Similar discontinuities occur at the convergence of the other series of hydrogen lines. For instance, the Paschen jump occurs at a wavelength of about 8204 Å.

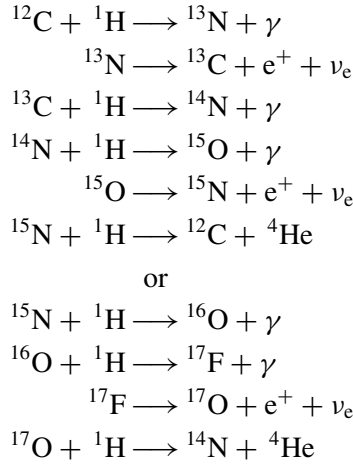
Blue straggler stars: Stars that lie on the main sequence of a cluster, but above the turn-off. See §6.4.1.

Bound-free absorption: The cause of bound-free continuous opacity is photoionization in which the absorption of a photon leads to the removal of a bound electron from an atom or ion. This produces a continuous opacity edge, which can lead to a discontinuity in the stellar energy distribution. The Balmer jump (see above) is an example of such a continuous opacity edge.

Chemical separation: Refers to physical processes that can cause certain elements to migrate either vertically or horizontally (or both) in a stellar atmosphere. These mechanisms are thought to be important in creating the chemical peculiarities seen in the Am and Ap stars. See §5.4.1.

Cluster analysis: The term cluster analysis is used to refer to a number of different methods and algorithms to group objects of similar kind into categories. This type of analysis can give insight into relationships between different groups of objects, and has commonly been used to classify biological organisms and languages.

CN, CNO cycle: The CN and CNO cycles are hydrogen-burning nuclear reactions involving isotopes of carbon, nitrogen, and oxygen, and have the net result of fusing four protons into one ${}^4\text{He}$ nucleus. The relevant reactions are as follows:



The top set of reactions is called the CN cycle, in which isotopes of carbon and nitrogen act as catalysts. The combination of the top and bottom sets of reactions constitutes the complete CNO cycle. The reaction ${}^{14}\text{N}(\text{p}, \gamma){}^{15}\text{O}$ is the slowest reaction in the CNO cycle, which means that if the CNO cycle is allowed to reach equilibrium, essentially all the C and O in the stellar core will be converted to ${}^{14}\text{N}$. In the case of the Wolf–Rayet stars in which the massive stellar wind has excavated down to the level of nuclear-processed material, this nitrogen-enhanced material can appear in the wind, leading to the WN sequence. In general, the different rates of the CNO cycle reactions lead to time-varying abundance ratios of the various isotopes. In particular, the ${}^{13}\text{C}/{}^{12}\text{C}$ ratio may be significantly altered from its usual value (in the solar system, this ratio is about 1/90). If this nuclear-processed material is mixed to the surface, non-standard isotope ratios can appear in the spectrum, such as in the ${}^{13}\text{C}$ -enhanced J-type carbon stars.

Convection; Convection zone: Convection refers to the flow of heat via the bulk movement of matter, usually in fluid form, from a relatively hot to a relatively cool region. Convection is one of the major modes of energy transport in stellar interiors and stellar atmospheres, although the proportion of energy actually carried by convection in a stellar atmosphere is quite small. Convection is essentially absent in the atmospheres of hot stars, but convective transport becomes important in the atmospheres of F-type stars and cooler. Convection will occur whenever the radiative temperature gradient exceeds the adiabatic temperature gradient. This will be true under conditions of high opacity (which steepens the radiative temperature gradient), where ionization occurs (for instance, hydrogen and helium ionization), which leads to a very low adiabatic temperature gradient, or where the gas becomes polyatomic. The occurrence of polyatomic gas

(i.e., when molecules are abundant) in the atmospheres of cool stars likewise reduces the adiabatic temperature gradient.

Curve of growth: The relationship between the equivalent width (W_{eq}) of an absorption line and the number of atoms (N) that produce it. For a weak line, $W_{\text{eq}} \propto N$, but as N increases and the line strengthens, the core begins to saturate and the relationship departs from linearity. At this point, the curve of growth flattens out (the “flat part of the curve of growth”). As N continues to increase, the damping wings of the line begin to develop, and the curve once again steepens and $W_{\text{eq}} \propto N^{1/2}$. This is referred to as the “damping part” of the curve of growth. Microturbulence, which can desaturate the core of the line, delays the onset of the flat part of the curve of growth.

Diffuse Interstellar band: Diffuse interstellar bands (DIBs) are broad absorption features due to interstellar material seen in the spectra of stars and other objects. Reddened stars (stars affected by interstellar reddening) often show strong DIBs. DIBs are most likely caused by large carbon-bearing molecules, but their identity has not yet been determined. There is a particularly strong and broad DIB at $\sim 4430 \text{ \AA}$ that can be seen in certain spectra displayed in this book.

Early-type stars; Late-type stars: The early-type, late-type terms used in stellar spectroscopy are employed to indicate relatively hot and relatively cool stars, respectively. For instance, stars hotter than the sun are commonly called the *early-type stars*, and those cooler than the sun the *late-type stars*. Within a given spectral class, the terms may also be used relatively. For instance, it is possible to refer to the early B-type stars, and the late B-type stars, and so on. This terminology originated early in the development of spectral classification when it was believed that stars evolved down the spectral sequence.

Effective Temperature (T_{eff}): The equivalent blackbody temperature of a star. The effective temperature of a star is the temperature a blackbody of the same radius would need to have the same total luminosity (total power output) as the star.

Equivalent width: A measure of strength of a spectral line. To measure the equivalent width of an absorption line, the surrounding continuum must first be normalized to unity. The area of the spectral line below the continuum is then determined. The width of a rectangular absorption line that is perfectly dark (i.e. has zero intensity) and has the same area as the absorption line in question is the equivalent width of that line.

Flux: Refers to the rate at which radiant energy flows through a unit area in the interior or surface of a star. If this energy flow is measured over the entire electromagnetic spectrum, this is referred to as the *bolometric flux*. Otherwise, if it is measured over a small wavelength interval, $d\lambda$, it is referred to as *monochromatic*

flux. Flux may also be measured at the surface of the earth or the surface of a detector, and then refers to the rate at which energy is received from a distant object per unit surface area (if monochromatic, then also per unit wavelength interval).

Forbidden lines: See glossary entry for *permitted lines*.

Free-free emission (absorption): Free-free emission or absorption of a photon can take place when an electron makes a close approach to an atom or ion. This phenomenon is an important contributor to the continuous opacity. For instance, in the solar atmosphere, H^- free-free opacity is the dominant source of continuous opacity in the infrared.

Galactic Latitude, Longitude: The plane of the Galactic equator corresponds to the great circle on the celestial sphere most closely approximating the plane of the Milky Way. The Galactic latitude, b , is the angular distance perpendicular to the Galactic equator. In the new system of Galactic coordinates ($l^{\text{II}}, b^{\text{II}}$), the Galactic longitude is measured from the Galactic center ($l^{\text{II}} = 0^\circ$, $b^{\text{II}} = 0^\circ$), which has equatorial coordinates (J2000) $\alpha = 17^{\text{h}} 42^{\text{m}}.4$, $\delta = -28^\circ 55'$. In the old system ($l^{\text{I}}, b^{\text{I}}$), the Galactic center was at $l^{\text{I}} = 327^\circ 41'$.

Gravity; surface gravity; log g: This refers to the acceleration of gravity at the “surface” of the star, generally taken to be the photosphere. The gravity is usually measured in cgs units, except that $\log g$ is customarily written with no units indicated. The gravity is, at least to a first approximation, correlated with the MK luminosity class, with main-sequence stars having higher gravities than giants and supergiants.

Hertzsprung Gap: The relative absence of evolved stars just to the left (bluewards) of the *red-giant clump* in the H–R diagram (Figure G.1).

H II region: An H II region is an emission nebula primarily composed of ionized hydrogen (H II). H II regions normally correspond to star-formation regions.

Hipparcos satellite: An astrometric satellite launched by the European Space Agency in 1989. Its purpose was to measure accurate stellar trigonometric parallaxes and proper motions. It observed approximately 120,000 stars.

H–R Diagram: A Hertzsprung–Russell (H–R) diagram is a plot of stellar luminosity against stellar temperature. There are a number of forms of the H–R diagram. The original (devised independently by E. Hertzsprung in Denmark and H. N. Russell in the United States) plotted the absolute visual magnitude against the spectral type. Another observational form of the diagram is a plot of the absolute visual magnitude against a color index, such as Johnson $B - V$; an example of

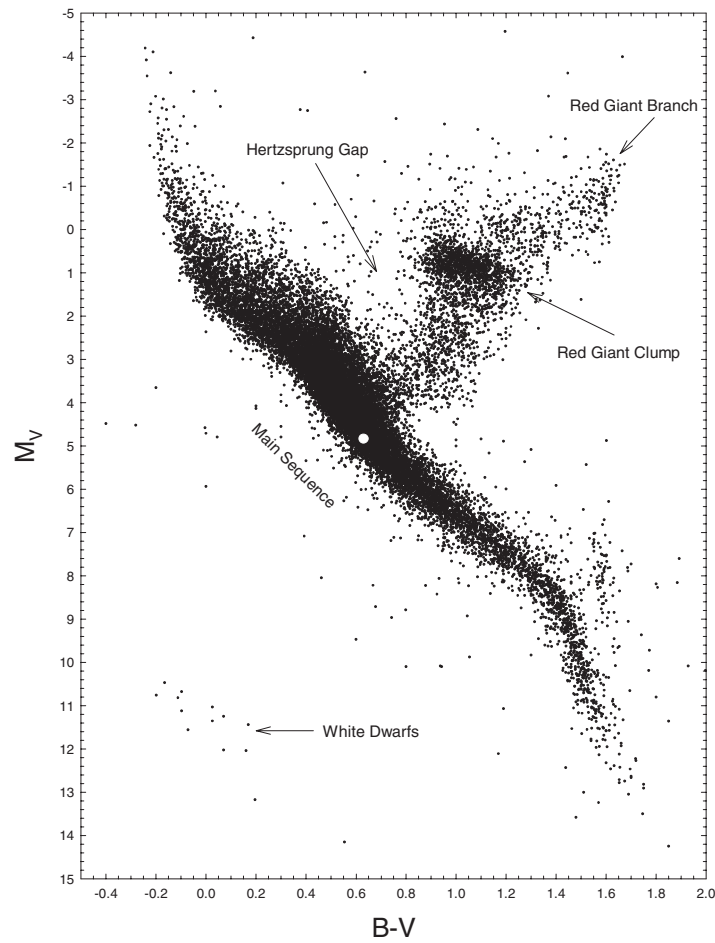


Figure G.1 This Hertzsprung–Russell diagram of stars in the solar neighborhood is based on parallaxes obtained by the *Hipparcos* satellite. The diagonal band is the main sequence. The red-giant branch and the red-giant clump, along with the position of white dwarf stars, are marked. The position of the Sun is indicated by the white circle.

such a diagram is shown in Figure G.1. This H–R diagram is based on *Hipparcos* parallaxes of solar neighborhood stars; as a consequence most of the stars in this diagram are young, metal-rich Population I stars. A comparable H–R diagram for the Population II is shown in Figure 5.26. There is also a theoretical form of the H–R diagram, in which stellar luminosity (usually in solar units) is plotted against the effective temperature.

Humphreys–Davidson Limit: An empirical boundary in the H–R diagram corresponding to the upper luminosity limit for stable stars. For more details, see §11.2.

Hydrostatic Equilibrium: Refers to a balance between the inward gravitational force and the outward gas and radiation pressure in the interior and atmosphere of a star.

Instability Strip: A region in the H–R-diagram in which stars are subject to pulsational instabilities originating in the He II ionization zone. The Cepheid variable stars inhabit this instability strip, as well as the RR Lyrae stars and the δ Scuti stars.

Intercombination lines: Sometimes called *intersystem* lines or *semi-forbidden lines*, these are spectral lines for which the upper and lower levels have different values of S , the total electronic-spin quantum number. These lines thus violate the quantum-mechanical selection rule under LS coupling, $\Delta S = 0$. See §2.4.3 and Figure 2.16 for examples. Atoms and ions for which the condition of LS coupling is valid are those for which the energy contribution of the spin-orbit interaction is much less than the energy involved in the electrostatic electron–electron repulsion. Under this circumstance, the above selection rule is valid, and intercombination lines will have low transition probabilities and will tend to be weak, even if they involve the ground state of the atom. LS coupling is generally valid for light elements, but begins to break down for heavier elements. Thus, in heavier elements, states with different values of S may be “mixed,” and the notion of an intercombination line becomes less meaningful. Intercombination (intersystem) lines can be pressure sensitive, and can therefore serve as useful luminosity criteria.

International Ultraviolet Explorer (IUE) satellite: The IUE satellite was launched as an international collaboration between NASA, the European Space Agency, and the United Kingdom’s Science and Engineering Research Council in 1978. It operated until the latter part of September 1996. During this period, it collected over 70,000 spectra. The IUE science instrument consisted of a 45-cm f/15 telescope coupled with two spectrographs. The long-wavelength spectrograph operated in the range 1850–3300 Å, while the short-wavelength spectrograph operated in the range 1150–2000 Å. Each spectrograph consisted of a high-dispersion mode, employing an echelle grating with cross-disperser, and a low-dispersion mode, using only the cross-disperser. The high-resolution mode gave a resolution of about 0.2 Å, whereas the low-resolution mode had a resolution of about 6 Å. The detectors were SEC Vidicons with ultraviolet converters.

Kinematics: Refers to the motions of stars, usually relative to the sun or the Local Standard of Rest. These motions may be expressed in the form of radial velocities and proper motions, or as the U, V, and W components of the space velocity.

Large Magellanic Cloud (LMC): A satellite galaxy of the Milky Way Galaxy. Both the LMC and the Small Magellanic Cloud (SMC) are irregular galaxies, and are visible to the naked eye in the southern hemisphere. Both the LMC and the SMC

have regions of active star formation. This is fortunate, as active star formation regions in the Milky Way Galaxy lie in the Galactic plane, and thus often suffer from considerable interstellar extinction, especially in the far-ultraviolet. Both the LMC and the SMC are at high Galactic latitudes, and thus Galactic extinction is minimal, although there is some internal extinction in both Clouds. None the less, many types of young and luminous stars may be studied in the Clouds with little extinction. This includes Wolf–Rayet stars, OB stars, and Cepheid variable stars. The period–luminosity relationship for the Cepheid variable stars was discovered by Henrietta Leavitt in the SMC.

Line blanketing: Refers to the combined effect of the (typically) millions of absorption lines on the spectrum and spectral energy distribution of a star. Line blanketing is stronger at shorter wavelengths for all types of stars, as the density of spectral lines increases with decreasing wavelength. As a consequence, increased metal abundance will tend to redden the stellar color, as line blanketing will remove more shortwave light from the spectrum than longwave light. Line blanketing can also have important effects on the structure of the stellar atmosphere. For instance, with increasing line blanketing, the temperature gradient in the atmosphere steepens, due to “backwarming” at depth and cooling at the surface.

Local Thermodynamic Equilibrium (LTE): The assumption that the electron populations, ionization ratios, and all other distribution functions characterizing the local material, including the local radiation field, are determined by the local values of the temperature and density via the relevant thermodynamic equilibrium equations. For instance, the level populations are given by the Boltzmann equation, the ionization ratios by the Saha equation, and the material is assumed to radiate as a blackbody radiator.

Magnitude, Apparent and Absolute: The apparent brightness of star (as viewed from Earth) is expressed in terms of its apparent magnitude. An apparent magnitude is defined in terms of a particular filter passband, such as the V -band of the Johnson UBV system (see §2.3), and is related logarithmically to the stellar flux in that band. If we let S_λ represent the V -filter passband (which should also take into account the reflectivity of the mirrors of the telescope and the transmission of the Earth’s atmosphere, as well as the spectral sensitivity of the detector), and F_λ the flux as a function of wavelength of a certain star as measured on Earth, then the flux in the V -band from that star is given by

$$f_V = \int_0^\infty S_\lambda F_\lambda d\lambda$$

The magnitude system is defined in such a way that if two stars have fluxes in a certain passband that differ by a factor of 100 ($f_1/f_2 = 100$), then they have a

magnitude difference ($m_2 - m_1$) of 5. More generally,

$$m_1 - m_2 = -2.5 \log \left(\frac{f_1}{f_2} \right)$$

Note that on this scale a 1st magnitude star is 100 times brighter than a 6th magnitude star. The zeropoint of the magnitude system is set by reference to a set of photometric standard stars.

The apparent magnitude refers to the brightness of the star as seen from Earth, but in astronomy we are most interested in the intrinsic brightness of the star, which is closely related to its *luminosity*. The apparent magnitude depends both on the luminosity of the star and its distance. If we correct for the distance, we derive a quantity called the *Absolute magnitude*. The absolute magnitude of a star is defined to be the apparent magnitude it would have if it were located at a distance of 10 parsecs. The relationship between the apparent magnitude (m) and the absolute magnitude (M) in any wavelength band is thus given by

$$M = m - 5 \log d + 5$$

where d is the distance of the star in parsecs. If there is interstellar absorption corresponding to A magnitudes of extinction along the line of sight to that star, then the above equation must be modified to

$$M = m - 5 \log d + 5 - A.$$

Mean Free Path: The mean distance between absorption or scattering events for a photon in a stellar interior or photosphere.

Meridional circulation: In a rotating star, circulation that takes place in a meridional plane (that is, a plane containing the rotational axis) is referred to a meridional circulation. Such circulation can occur because a rotating star cannot be simultaneously in hydrostatic and radiative equilibrium. This means that the flow of radiation out of a rotating star is not isotropic, and thus surfaces of constant pressure do not coincide with surfaces of constant temperature. This leads to large-scale flows in the interior of the star.

Metastable states: See glossary entry under *permitted* lines. Absorption lines with metastable states as the lower level tend to be pressure sensitive, and thus can be used in luminosity classification.

Microturbulence: Microturbulence refers to a scale of turbulence in the stellar atmosphere in which the characteristic size of the turbulent cell is smaller than the local mean free path (see above). This means that if a photon is emitted in one microturbulent cell, it will likely be absorbed in another. The relative motions of the two turbulent cells will result in a Doppler shift that will cause a photon emitted in the core of a line to be absorbed in the wing. This will cause the line

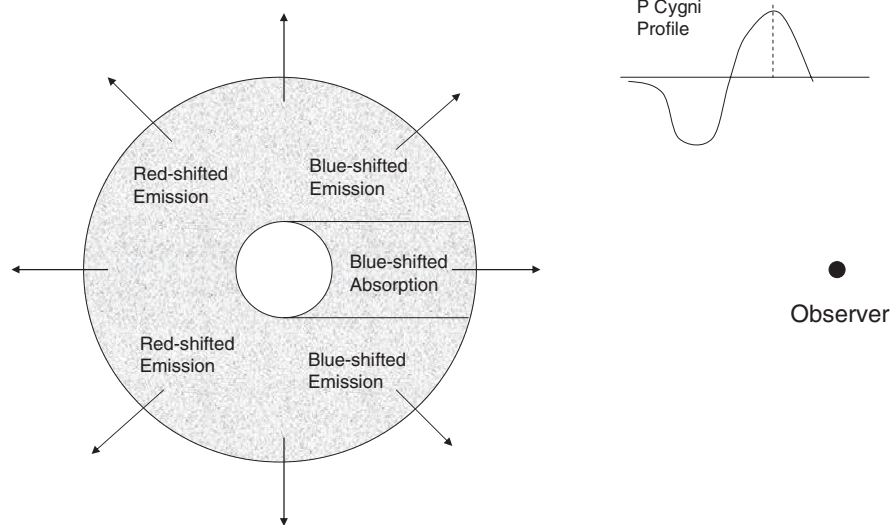


Figure G.2 A star surrounded by an expanding envelope will show P Cygni profiles for the stronger spectral lines. The blue-shifted absorption component is formed in the column of gas between the observer and the star, whereas the emission component is formed in the remainder of the envelope. The form of the P Cygni profile is shown in the upper-right-hand corner; the dotted line shows the rest wavelength for the spectral line.

core to become desaturated, and so the line will be stronger than in the absence of microturbulence.

non-LTE: Pertains to situations and calculations in which the assumption of Local Thermodynamic Equilibrium (LTE) is not valid. For instance, in a stellar atmosphere, the radiation field often departs significantly from the local Planck function. This means that the electron populations, ionization ratios, etc., are not well-determined by the equations of thermodynamic equilibrium.

Oblique Rotator Model: A stellar model in which the rotational and magnetic axes do not coincide. This implies that as the star rotates, the magnetic poles come in and out of view, provided that the star is not seen with the rotational axis pole-on.

P Cygni profile: A P Cygni profile is a line profile characterized by a blue-shifted absorption trough, coupled with an emission component (see Figure G.2). A P Cygni profile originates in an expanding stellar atmosphere, for instance, a stellar wind, and therefore is a spectral diagnostic of the presence of a wind, especially in early-type stars. Some stars show lines with an *inverse P Cygni profile*, which consists of a red-shifted absorption trough combined with an emission component. Such profiles are indicative of mass infall, and are commonly found in pre-main-sequence objects such as the Herbig AeBe stars (see §5.5). Occasionally, only the *P Cygni absorption troughs* are visible in the spectrum, without the appearance of an emission component.

Permitted lines: One of the elementary results of quantum mechanics is that radiative transitions (as opposed to collisional transitions) by electrons between bound states in an atom or ion are subject to certain *selection rules*. In particular, the angular-momentum quantum number (l) of the electron involved in the transition is subject to the selection rule $\Delta l = \pm 1$. The *parity* of a state (i.e., whether it is even or odd) is determined by $\sum l$, taken over all the bound electrons; this selection rule thus requires that the initial and final states must have opposite parities. Another selection rule involves the total angular momentum $\vec{J} = \vec{L} + \vec{S}$ where \vec{L} is total orbital angular momentum, and \vec{S} is the total spin angular momentum, for a given state. The associated total angular momentum quantum number J is subject to the following selection rule:

$$\Delta J = 0, \pm 1, \quad J = 0 \rightarrow J = 0 \text{ not allowed}$$

Transitions that obey these selection rules are termed *permitted* or allowed and correspond to *electric dipole* radiation, and have relatively high transition probabilities. Transitions that violate the selection rules have low transition probabilities and are termed *forbidden*. These forbidden lines are usually extremely weak in normal stellar spectra, but can be very strong under conditions of low density. If the upper state of a forbidden transition cannot decay to a lower energy state by a permitted transition, then that upper state is referred to as *metastable*. In high density conditions, such metastable states are depopulated by collisions, but in low density conditions (for instance, in extended envelopes around stars, in nebulae, in novae, or in the solar corona), metastable states can achieve much higher populations than predicted by the Boltzmann equation; in such a circumstance, the forbidden transition can result in a strong line. Forbidden lines are usually indicated by brackets around the species name, for instance, [O III]. One very strong forbidden line seen in the spectra of nebulae is the [O III] $\lambda 5007$ line. Forbidden transitions generally correspond either to electric quadrupole or magnetic dipole radiation. Permitted transitions that have a metastable state as the *lower* energy level are pressure sensitive, and make good luminosity criteria.

Pickering Series: A series of lines in the spectrum of He II. See §2.4.2.

Pre Main Sequence (PMS): Refers to stars that are still contracting toward the main sequence and have not yet ignited nuclear fusion reactions in their cores.

Projected rotational velocity: The rotational velocity of a star can be deduced from the rotational broadening of its spectral lines due to the Doppler effect. But the velocity so determined is only the *projected* rotational velocity ($v \sin i$, where i is the inclination of the rotational axis) and not the real or *equatorial* rotational velocity, v_{eq} . The equatorial rotational velocity can be determined only if the inclination of the rotational axis is known.

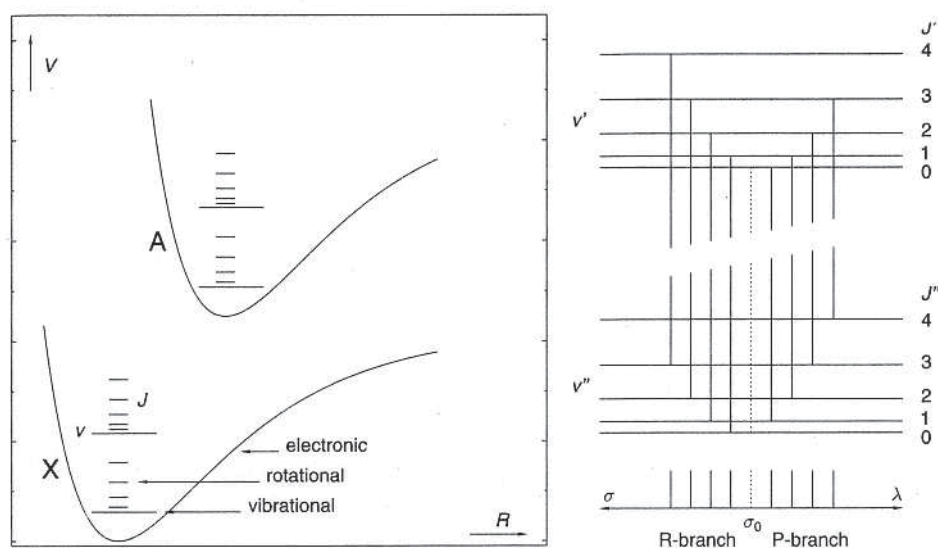


Figure G.3 The left-hand panel shows a schematic energy level structure of a typical diatomic molecule, including two electronic states (the ground state is designated X, and the first excited state A, etc.), and, for each, vibrational energy levels and rotational energy levels. The vibrational quantum number is v , the rotational quantum number J . Electronic bands of molecules (generally found in the ultraviolet, optical, and near-infrared) involve transitions between two different electronic states; individual bands (such as those designated 0–0, 1–0, etc.) involve transitions between a single pair of vibrational states (one from the upper electronic state, one from the lower), and individual lines in the bands are formed via transitions between the rotational levels associated with those vibrational states. Vibrational–rotational bands (right-hand panel) involve transitions between vibrational and rotational levels within a single electronic state. Such bands are usually found in the infrared. Figure from Thorne, Litzén, & Johansson 1999, *Spectrophysics*, Springer, and used by permission.

Q-branch, P-branch, R-branch: Band spectra of diatomic molecules often display structure referred to as the *P*-, *R*- and *Q*-branches. Molecular bands, whether rotational–vibrational bands in the infrared or electronic bands in the ultraviolet, visible, and near-infrared involve transitions between vibrational and rotational states characterized by the vibrational quantum number v and the rotational quantum number J (see Figure G.3). In rotational–vibrational bands J obeys the *selection rule* $\Delta J = \pm 1$. Denoting the J for the upper energy level as J' and the lower as J'' , the *P*-branch consists of transitions with $J' = J'' - 1$ and the *R*-branch of transitions with $J' = J'' + 1$ (see the right-hand panel of Figure G.3). The corresponding wavenumbers (frequencies) for the two branches will fall on either side of the wavenumber for the pure vibrational transition $\sigma_0 = v' - v''$. In the electronic spectra of diatomic molecules, the selection rule for J includes $\Delta J = 0$, although the transition $J' = 0 \leftrightarrow J'' = 0$ is still forbidden. This addition to the selection rule allows for a third branch referred to as the *Q*-branch. The

well-known G-band in the spectra of F, G, and K-type stars is formed from the *Q*-branches of the CH A–X 0–0 and 1–1 bands (see Figure 8.21).

Red-giant clump: A density enhancement in the red giant branch corresponding to red giant stars that are burning helium in their cores. See Figure G.1.

Resonance lines: A resonance line corresponds to a *permitted* transition involving the ground state of an atom or ion.

Small Magellanic Cloud (SMC): See entry for *Large Magellanic Cloud*.

Spectral synthesis: The process of computing the emergent spectrum of a star by employing an appropriate stellar atmosphere model, atomic and molecular data, and the numerical integration of the equation of radiative transfer at each point in the spectrum.

Spectroscopic degeneracy: Refers to the situation in which spectroscopic features in a certain spectral region are of insufficient sensitivity to distinguish adjacent spectral classes (for instance, cannot be used to distinguish dwarfs from giants).

Spectroscopic parallax: Involves the use of the spectral type of a star to infer its distance. This technique requires that the spectral type has been calibrated in terms of absolute magnitude (see Appendix B).

s-process elements: The *s*-process elements are produced by the slow-neutron-capture process (*s*-process) that can occur in the cores of intermediate-mass stars in advanced evolutionary stages, in particular, while the star is on the *asymptotic giant branch* (AGB). Alpha capture by ^{13}C nuclei yields neutrons during helium-shell burning ($^{13}\text{C} + \alpha \rightarrow ^{16}\text{O} + n$). These neutrons can be captured by nuclei, and lead to the build-up of heavier elements. The neutron flux produced by the α -capture reaction yields neutron capture rates that are *slow* compared with the β^- -decay rate. Thus, during the *s*-process, if a nucleus is formed by neutron capture that is unstable to β^- decay, chances are the nucleus will decay before another neutron capture occurs. Thus the neutron-capture cross sections and the β^- decay rates of the various nuclei involved determine the relative abundances of the isotopes produced by the *s*-process. Figure G.4 shows the *s*-process path through the table of isotopes near strontium.

Elements that are primarily produced by the *s*-process include strontium, yttrium, barium, zirconium, technetium, and lanthanum.

Stark Effect; Stark Broadening: A spectral line broadening mechanism caused by the interaction of the atom with free electrons and ions. See §5.2.4.

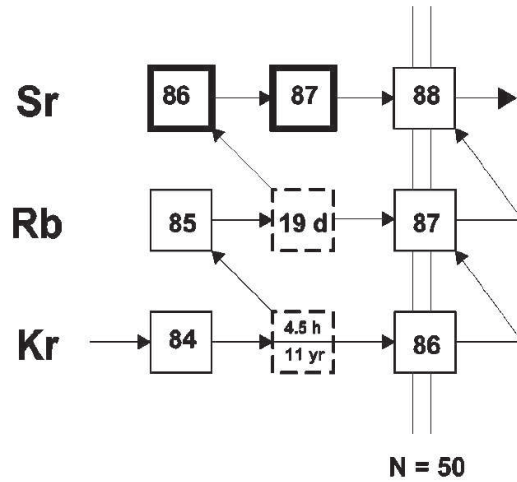


Figure G.4 The *s*-process path in the strontium region. The solid boxes represent stable nuclei, and dashed boxes radioactive ones. The thick boxes indicate that ^{86}Sr and ^{87}Sr are produced solely by the *s*-process. Horizontal arrows represent neutron capture, and diagonal arrows β^- decay (there are nuclei beyond the right-hand side of the diagram not shown). Diagram used by permission from Koehler et al. 2000, *Phys. Rev. C*, 62, 055803.

Stellar Energy Distribution (SED): The stellar (or spectral) energy distribution is a plot of the stellar monochromatic *flux* as a function of the wavelength or frequency across the electromagnetic spectrum.

***R*:** Spectral resolution, defined to be $R = \lambda/\Delta\lambda$ where $\Delta\lambda$ is the resolution, in wavelength units, of the spectrograph. $\Delta\lambda$ is the full width at half maximum (FWHM) of the line-spread function of the spectrograph. Since spectrographs are (usually) designed so that $\Delta\lambda$ corresponds to 2 pixels on the detector, the resolution of the spectrograph is often quoted as “2 pixel” resolution, such as 1.8 Å (2 pixels).

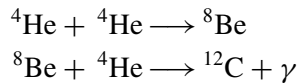
Subdwarf: This term was originally introduced to describe Population II dwarf stars that define a sequence running parallel to but below the main sequence for Population I stars in the H–R diagram. Because for a given color the Population II dwarfs have a lower luminosity than the Population I main-sequence stars, they were called subdwarfs. In actual fact, the Population II sequence actually lies to the blue of the Population I sequence because of their metal-weak nature. Metal-weak stars have less *line blanketing*, and thus for a given effective temperature have bluer colors and emit more ultraviolet light (and are thus said to have an *ultraviolet excess*). More recently, the term has been used for helium-burning OB stars (see §4.7.1) and for low-mass stars with either higher than normal gravities or low metal abundances.

Subordinate lines: This term generally refers to non-resonance permitted lines, i.e., lines that arise from excited states.

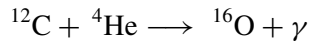
Telluric lines: Absorption lines formed in the atmosphere of the earth.

Thick disk: The Thick disk refers to one of a number of spatial/kinematical components of the Milky Way Galaxy, including the Extreme disk (comprised of the very youngest stars which are also confined closely to the Galactic plane), the Thin disk, the Thick disk, and the Galactic Halo, each comprised of populations of stars successively older and less confined to the Galactic plane. These components are also distinguished by metallicity (for instance, on the average, Thick disk stars have lower metallicities than Thin disk stars) and kinematics with, for instance, the Thick disk stars having a higher velocity dispersion than the Thin disk stars. The sun is a member of the Thin disk. The Intermediate Population II (see §6.4.1) corresponds roughly with the Thick disk population.

Triple- α process: The triple- α process refers to the set of reactions for helium fusion in stars. The products of the triple- α process include carbon and oxygen:



Once ${}^{12}\text{C}$ is formed, ${}^{16}\text{O}$ will be the product of an α -capture



Ultraviolet excess: See entry for *Subdwarf*.

Veiling: A situation that occurs when the spectral lines of a star are filled in or *veiled* by continuum emission or light from a companion star. This phenomenon is commonly found in chromospherically active stars (see Figure 7.13), in late-type stars with an early hot companion (for instance, HD 17576, a G2 dwarf with a hot subdwarf companion), and in other situations.

Zero-age Main Sequence (ZAMS): The zero-age main sequence is the locus of points in the H–R diagram where hydrogen ignition occurs in the cores of stars upon contraction from an interstellar cloud. ZAMS stars are therefore young stars which have just begun their main-sequence lives.

Appendix A: MK Standard Stars

ANCHOR POINT STANDARDS—ROBERT F. GARRISON

The table of Anchor Points for the MK System is taken from a paper by the author in the book *The MK Process at 50 Years*, edited by Corbally, Gray, and Garrison (ASP Conference Series, vol. 60, 1994), pp. 3–14.

The “Anchor Points” is the subset of standard stars that have survived through the years with no change and therefore represent the most stable points in the System. They do not form a complete grid. I am working on defining the set of “Primary Standards” that are the best current standards to use in terms of accessibility and suitability and will represent a complete grid.

The first three columns in Table A.1 are self-explanatory. Column four is a list of classifications from the tables in the introductory booklet of the MKK Atlas (Morgan, Keenan, & Kelleman 1943). In parentheses are listed types from the Atlas that were not listed in the tables (only one star in this subset: HR 617), or differed slightly from the types in the tables (only one star in the final list: HR 5191 and the only difference is that an “n” was added in the Atlas).

Column five is a list of classifications from Morgan’s table of MK standard stars given in the UBV definition paper by Johnson & Morgan (1953). The types in the parentheses are from Morgan (1951).

Column six is a list of types from the 1973 Annual Reviews in Astronomy and Astrophysics article by Morgan and Keenan.

The types listed in columns seven, eight, and nine are taken from several modern lists. The seventh and eighth columns include types for stars cooler than the Sun, from various publications by Keenan and his associates. The ninth column includes types for GK stars by Morgan from an unpublished list as well as Walborn’s (1973) types for O stars and Gray’s (1987, 1989a, b, and 1994) types for B8–F2 stars.

Finally, all the types were checked for consistency with my own plate file. Thus, the Anchor Points represent the MK System as it was in 1943, as it was in 1953, 1973, 1978, 1989, and as it is now. The Anchor Points are the *de facto* standards, though they may not be the best ones or the ones we wish were standards. However, because of its long history, the MK System now has a life of its own. Instead of trying to manipulate it and distort it, we must listen to it.

Note by Gray and Corbally: We have added a tenth column to this table giving the recommended spectral type for the standards listed in this table. We also note that Walborn has recently found that 15 (S) Mon is a likely spectrum variable, with mean type near O7.5. We also suggest users avoid the star α Ori (Betelgeuse) as it is a spectrum variable. To date, Garrison has not finished his selection of primary standards. We offer the following tables of standards (Tables A.2–A.7) from a number of sources as recommended primary and secondary standards.

Table A.1 MK Standard Stars: Anchor Points September 1993

HD	HR or other	Star Name	MKK43 Table (Atlas)	MK53 Table 1 (Michpub1951)	MK73 Table 1,2 (K76M78 Atlases)	KY88 (KM89)	KY85 (KP80)	WWM GK STD 86 Walborn OB, GRAY BAF	Recommended Type
47839	HR 2456	15 S Mon	O7	(O7)	O7 (V)			O7 V((f))	var?
214680	HR 8622	10 Lac	O9 V	O9 V	O9 V			O9 V	O9 V
36512	HR 1855	ν Ori	BO V	BO V	BO V			BO V	B0 V
37128	HR 1903	ϵ Ori	BO I	BO Ia	BO Ia (BO Ia)			B0 Ia	B0 Ia
41117	HR 2135	χ^2 Ori	B2 I	B2 Ia	B2 Ia (B2 Ia)			B2 Ia	B2 Ia
206165	HR 8279	9 Cep	B2 I	B2 Ib	(B2 Ib)			B2 Ib	B2 Ib
120315	HR 5191	η UMa	B3 V(n)	B3 V	B3 V			B3 V	B3 V
32630	HR 1641	η Aur	B3 V	B3 V	B3 V			B3 V	B3 V
53138	HR 2653	σ^2 CMa	B3 I	B3 Ia	B3 Ia (B3 Iab)			B3 Ia	B3 Ia
58350	HR 2827	η CMa	B5 I	B5 Ia	B5 Ia (B5 Ia)			B5 Ia	B5 Ia
34085	HR 1713	β Ori	B8 Ia	B8 Ia	B8 Ia			B8 Ia	B8 Ia
103287	HR 4554	γ UMa	AO V	AO V	AO V			AO V	A0 V
172167	HR 7001	α Lyr	AO V	AO V	AO V (AO Va)			AO V (AO Va)	A0 Va
87737	HR 3975	η Leo	AO Ib	AO Ib	(AO Ib)			(AO Ib)	A0 Ib
21389	HR 1040	+58° 607	AO Ia	AO Ia	(AO Ia)			AO Ia	A0 Ia
197345	HR 7924	α Cyg	A2 Ia	A2 Ia	A2 Ia (A2 Ia)			A2 Ia	A2 Ia
216956	HR 8728	α PsA	A3 V	A3 V	A3 V			A3 V	A3 Va
89025	HR 4031	ζ Leo	FO III	FO III	FO III (FO III)			FO III	F0 IIIa
36673	HR 1865	α Lep	FO Ib	FO Ib	FO Ib (FO Ib)			FO Ib	F0 Ib
113139	HR 4931	78 UMa	F2 V	F2 V	F2 V (F2 V)			F2 V	F2 V
20902	HR 1017	α Per	F5 Ib	F5 Ib	F5 Ib (F5 Ib)			F5 Ib	F5 Ib
30652	HR 1543	π^3 Ori	F6 V	F6 V	F6 V			F6 V	F6 V
194093	HR 7796	γ Cyg	F8 Ib	F8 Ib	(F8 Ib)(WWM)			(F8 Ib)(WWM)	F8 Ib
54605	HR 2693	δ CMa	F8 Ia	F8 Ia	(F8 Ia)(WWM)			(F8 Ia)(WWM)	F8 Ia

109358	HR 4785	β CVn	GO V	GO V (PCK)	GO V	GO V	GO V	G0 V	G0 V	G0 V
121370	HR 5235	η Boo	GO IV	(GO IV)(PCK)	GO IV	GO IV	GO IV	G0 IV	G0 IV	G0 IV
204867	HR 8232	β Aqr	GO Ib	GO Ib(PCK)(GO Ib)	GO Ib	GO Ib	GO Ib	G0 Ib	G0 Ib	G0 Ib
Sun	Sun	ASTEROIDS	G2 V	G2 V	G2 V	G2 V	G2 V	G2 V	G2 V	G2 V
20630	HR 996	κ Cet	G5 V	(G5 V)	G5 V	G5 V	G5 V	G5 V	G5 V	G5 V
161797	HR 6623	μ Her	G5 IV	G5 IV(G5 IV) note	G5 IV	G5 IV	G5 IV	G5 IV	G5 IV	G5 IV
206859	HR 8313	9 Peg	G5 Ib	G5 Ib	G5 Ib	G5 Ib	G5 Ib	G5 Ib	G5 Ib	G5 Ib
101501	HR 4496	61 UMa	G8 V	(G8 V)	G8 V	G8 V	G8 V	G8 V	G8 V	G8 V
188512	HR 7602	β Aql	G8 IV	G8 IV	G8 IV	G8 IV	G8 IV	G8 IV	G8 IV	G8 IV
62345	HR 2985	κ Gem	G8 III	G8 IIIa	G8 III	G8 III	G8 IIIa	G8 III	G8 III	G8 IIIa
113226	HR 4932	ϵ Vir	G8 III	G8 IIIab (G8 III)	G8 IIIab	G8 IIIab	G8 IIIab	G8 IIIab	G8 IIIab	G8 IIIab
48329	HR 2473	ϵ Gem	G8 Ib	G8 Ib	G8 Ib	G8 Ib	G8 Ib	G8 Ib	G8 Ib	G8 Ib
185144	HR 7462	σ Dra	KO V	KO V	KO V	KO V	KO V	KO V	KO V	KO V
62509	HR 2990	β Gem	KO III	KO IIIb	KO III	KO III	KO III	KO III	KO III	KO III
197989	HR 7949	ϵ Cyg	K0 III	K0- III	K0- III	K0- III	K0- III	K0 III	K0 III	K0- III
222404	HR 8974	γ Cep	K1 IV	K1 IV see notes	K0 III	K0 III	K0- III	K0 III	K0 III	K0- III
22049	HR 1084	ϵ Eri	K2 V	(K2 V)	K2 V	K2 V	K2 V	K2 V	K2 V	K2 V
12929	HR 617	α Ari	(K2III)	K2 IIIab	K2 III	K2 III	K2 III	K2 III	K2 III	K2 IIIab
153210	HR 6299	κ Oph	K2 III	K2 III	K2 III	K2 III	K2 III	K2 III	K2 III	K2 III
127665	HR 5429	ρ Boo	K3 III	K3 III	K3 III	K3 III	K3 III	K3 III	K3 III	K3 III
31398	HR 1577	ι Aur	K3 II	K3 II	K3 II	K3 II	K3 II	K3 II	K3 II	K3 II
201091	HR 8085	61 Cyg A	K5 V	K5 V	K5 V	K5 V	K5 V	K5 V	K5 V	K5 V
164058	HR 6705	γ Dra	K5 III	K5 III	K5 III	K5 III	K5 III	K5 III	K5 III	K5 III
6860	HR 337	β And	M0 III	M0 IIIa	M0 III	M0 III	MO+ IIIa	MO+ IIIa	MO+ IIIa	MO+ IIIa
1013	HR 45	χ Peg	M2 III	M2+ III(M2 III)	M2 III	M2 III	M2+ III	M2+ III	M2+ III	M2+ III
39801	HR 2061	α Ori	M2 Ib	M1-M2 Ia-Ib	M1-M2 Ia-Ib var	M1-M2 Ia-Ib	M1-M2 Ia-Ib	M1-M2 Ia-Ib	M1-M2 Ia-Ib	var
206936	HR 8316	μ Cep	M2 Ia	M2 Ia	M2 Ia	M2 Ia	M2- Ia	M2- Ia	M2- Ia	M2- Ia

WALBORN'S OB PRIMARY STANDARDS

Table A.2 Walborn's Early O-type standards

O2 If*	O3 If*	O3.5 If*	O4 If ⁺
HD 93129A	Cyg OB2-7 Cyg OB2-22A	Pismis 24-1 (HDE228766) (NGC 2044W-9A) (MH 14)	HD 190429A Sk −67° 166 Sk −67° 167
O2 III(f*) HDE 269810 Sk −68° 137 LH 10-3061 LH 64-16 LH 114-7 NGC 346-3 (Sk −66° 172 [+OB])	O3 III(f*)	O3.5 III(f*) Pismis 24-17	O4 III(f ⁺) ST 2-22 W28-23
O2 V((f*)) BI253 (P871)	O3 V((f*)) HD 64568 LH 10-3058 (Sk −71° 51) (P1163) (P1311) (ST 5-52[+OB])	O3.5 V((f ⁺)) HD 93128 HD 93129B (HD 93205) (HD 93250)	O4 V((f ⁺)) HD 46223 HDE 303308 W28-5

Table A.3 Walborn's Late O-type standards

HD 46150	O5 V((f))	HD 15558	O5 III(f)	Cyg OB2-11	O5 If ⁺
HD 93204	O5 V((f))			HD 14947	O5 If ⁺
HD 101190	O6 V((f))	Sk −66° 100	O6 II(f)	Sk −65° 22	O6 Iaf ⁺
		HD 93130	O6 III(f)	Sk −69° 104	O6 Ib(f)
				λ Cep	O6 I(n) fp
HD 93146	O6.5 V((f))	HD 190864	O6.5 III(f)	HD 163758	O6.5 Iaf
HD 165052	O6.5 V(n)((f))			HD 150958	O6.5 Iaf
LH10:3128	O6.5 Vz			HD 69464	O6.5 Ib(f)
LH10:3073	O6.5 Vz				
HD 91824	O7 V((f))	HD 151515	O7 II(f)	Sanduleak 80	O7 Iaf ⁺
LH10:3102	O7 Vz	HD 93222	O7 III((f))		
		ξ Per	O7.5 III(n)((f))	9 Sge	O7.5 Iaf
HD 48279	O8 V	HD 175754	O8 II((f))	HD 151804	O8 Iaf
		λ Ori	O8 III((f))	HD 112244	O8 Iab(f)
				HD 225160	O8 Ib(f)
HD 46149	O8.5 V				
10 Lac	O9 V	ι Ori	O9 III	HD 148546	O9 Ia
HD 93028	O9 V			HD 210809	O9 Iab
HD 46202	O9 V			HD 207198	O9 Ib-II
AE Aur	O9.5 V	HD 189957	O9.5 III	α Cam	O9.5 Ia

Table A.3 Continued

HD 93027	O9.5 V	HD 16429	O9.5 II((n))	19 Cep	O9.5 Ib
		δ Ori	O9.5 II	HD 152249	OC9.5 Iab
		HD 10125	O9.7 II	HD 195592	O9.7 Ia
				Sk $-66^\circ 169$	O9.7 Ia ⁺
				μ Nor	O9.7 Iab
				HD 152003	O9.7 Iab
				HD 47432	O9.7 Ib
				ζ Ori	O9.7 Ib
				HD 152147	O9.7 Ib
				HD 152424	OC9.7 Ia
				HD 104565	OC9.7 Ia
				HD 194280	OC9.7 Iab
				HD 269896	ON9.7 Ia ⁺
				BD $+36^\circ 4063$	ON9.7 Iab
				HD 191781	ON9.7 Iab
				HD 123008	ON9.7 Iab

Table A.4 Walborn's B-type standards

ν Ori	B0 V			HD 48434	B0 III	ϵ Ori	B0 Ia
				HD 150041	B0 III	HD 122879	B0 Ia
						HD 91969	B0 Ia
						HD 156134	B0 Iab
						HD 164402	B0 Ib
τ Sco	B0.2 V	ϕ^1 Ori	B0.2 IV	HD 108639	B0.2 III		
				HD 6675	B0.2 II		
HD 36960	B0.5 V	λ Lep	B0.5 IV	1 Cas	B0.5 III	κ Ori	B0.5 Ia
						HD 152234	B0.5 Ia
HD 201795	B0.7 V	ξ^1 CMa	B0.7 IV	ϵ Per	B0.7 III	HD 154090	B0.7 Ia
						κ Cas	B0.7 Ia
						HD 152235	B0.7 Ia
						HD 109867	B0.7 Ib
						HD 190919	B0.7 Ib
ω^1 Sco	B1 V			β Cen	B1 II-III	HD 169454	B1 Ia ⁺
				$-57^\circ 3506A$	B1 II	HD 148688	B1 Ia
				σ Sco	B1 III	HD 13854	B1 Iab
						ρ Leo	B1 Iab
						ζ Per	B1 Ib
						HD 86606	B1 Ib
HD 36959	B1.5 V			ϵ CMa	B1.5 II	ζ^1 Sco	B1.5 Ia ⁺
HD 154445	B1.5 V			HD 96159	B1.5 II	HD 190603	B1.5 Ia ⁺
				12 Lac	B1.5 III		
HD 42401	B2 V	γ Peg	B2 IV	HD 141318	B2 II	χ^2 Ori	B2 Ia
				γ Ori	B2 III	9 Cep	B2 Ib
22 Sco	B2.5 V			π^2 Cyg	B2.5 III	HD 92964	B2.5 Ia
HD 214432	B2.5 V					55 Cyg	B2.5 Ia
						3 Gem	B2.5 Ib
η Hya	B3 V			HD 21483	B3 III	ϕ^2 CMa	B3 Ia
η Aur	B3 V					κ Cru	B3 Ia
η UMa	B3 V					ι CMa	B3 Ib
						η CMa	B5 Ia
						β Ori	B8 Ia

Table A.5 Morgan and Keenan's Late B-type Revised (1973) MK Standards

ρ Aur	B5 V	18 Tau	B8 V
τ Her	B5 IV	27 Tau	B8 III
η CMa	B5 Ia	β Ori	B8 Ia
19 Tau	B6 IV	α Del	B9 IV
η Tau	B7 III		

Source: Morgan & Keenan (1973).

GRAY AND GARRISON'S LATE-B, A AND EARLY-F STANDARDS

In a series of four papers, Gray & Garrison (Gray & Garrison (1987, 1989a, b; Garrison & Gray 1994) defined parallel sequences of late B, A and early F-type standards. These two sequences (reproduced in Table A.6) are for low- $v \sin i$ and high- $v \sin i$ standards, to reduce systematic trends in spectral classification caused by differing rotational velocities.

Table A.6 Gray and Garrison's Late-B, A and Early-F Standards

Spectral Type	low- <i>v</i> sin <i>i</i> Standards	high- <i>v</i> sin <i>i</i> Standards
B7 V	(HR 1029) ¹	
B8 V	HR 9050	18 Tau
B8 III		27 Tau
B8 II	HR 3571	
B9 Va	ω For A	HR 2328
B9 IV	134 Tau	α Del
B9 III	HR 4712	ϵ Tuc
B9 II	HR 7245	
	(HR 5898)	
A0 Vb	HD 225047	
A0 Va	α Lyr	γ UMa
	(HR 3314)	(HD 201184)
A0 IV	HR 7211	HR 8451
A0 III	α Sex	HR 2969
	(α Dra)	
A0 II	HR 6478	
A0 Ib	η Leo	
A0 Ia	HR 1040	
A1 Va	HR 520	HR 2324
	(48 Cet)	
A1 IV	ρ Peg	δ Hya
A1 III	HR 2925	γ Tra
A1 II	HR 3487	
A2 Va	HR 4023	HR 2758
A2 IV	β Crt	β Ser
A2 III		HR 2751
A2 Ia	α Cyg	
A3 Vb	β Cir	
A3 Va	α PsA	HD 23643
	β Leo	
A3 IV	HR 4293	β Eri
A3 III	HR 3514	
A5 V	HD 23194	HD 23886
A5 II	σ Sco	
A6 II	HR 3426	
A7 V	2 Hyi	21 LMi
A7 IV	HR 3270	ι UMa
A7 III	θ^2 Tau	
A9 V		44 Cet
A9 IIIb		γ Her
F0 V	HD 23585	
F0 IV	57 Tau	HR 8895A
F0 IIIb	η CMi	
F0 IIIa	ζ Leo	
F0 II	HR 292	
	HD 96898	
F0 Ib	α Lep	
F0 Ia	ϕ Cas	
F2 V	78 UMa	
	μ Vir	
F2 IV	32 Tau	
F2 III	β Cas	
F2 Ib	ν Aql	

¹Suitable secondary standards in parentheses.

LATE-TYPE STANDARDS

The best source for late-type standard stars, especially, G and K-type stars and M giants is Keenan's Perkins catalog (Keenan & McNeil 1989). M-dwarf standards are listed in Chapter 9, and L- and T-dwarf standards in Chapters 9 and 10. The large number of standards in the Perkins catalog makes a full listing impossible here. Instead, we offer a table of standards (Table A.7), largely, but not exclusively drawn from the Perkins catalog that we have used in the Nearby Stars Program (Gray et al. 2003, 2006). Please also consult Table 9.1 for the primary M-dwarf standards, Table 9.2 for the primary L-dwarf standards, and tables in Chapter 10 for the primary T-dwarf standards.

Table A.7 Standards Used for the NStars Project

HR 1279	F3 V	HR 1566	F3 IV	HR 7495	F5 II-III	HD 10494	F5 Ia
HD 27524	F5 V	Procyon	F5 IV-V	HR 2706	F5 III-IV	α Per	F5 Ib
HR 5634	F5 V			(60 UMa)	F5 III		
γ Ser	F6 V	α Tri	F6 IV	HR 6577	F6 III-IV		
HD 27808	F8 V			HR 8905	F8 III	δ CMa	F8 Ia
						γ Cyg	F8 Ib
HR 506	F9 V			81 Psc	G0 III	β Aqr	G0 Ib
β CVn	G0 V						
λ Ser	G0- V						
16 Cyg A	G1.5 V					α Aqr	G2 Ib
Sun	G2 V						
16 Cyg B	G3 V			37 LMi	G2.5 IIa		
70 Vir	G4 V	24 UMa	G4 IV	HR 4742	G3 III		
κ Cet	G5 V	ω Sgr	G5 IV	HR 7788	G5 IIIa	HR 8752	G4 0
HR 5209	G5 V	μ Her	G5 IV			9 Peg	G5 Ib
61 UMa	G8 V	β Aql	G8 IV	κ Gem	G8 III	ϵ Gem	G8 Ib
				ϵ Vir			
				71 Oph	G8 III		
				δ Phe	G9 III		
				β LMi	G9 III		
				η Cyg	K0 III		
54 Psc	K0 V			19 Pup	K0 III		
HD 224618	K0 V			δ Cnc	K0 III		
HR 637	K1 V			90 Her	K1 IIIb		
ϵ Eri	K2 V			β Ret	K2 III		
HD 184467	K2 V			κ Oph	K2 III		
HR 753	K3 V						
GI 570A	K4 V			κ Pyx	K4 III		
						ξ Cyg	K4.5 Ib
61 Cyg A	K5 V			γ Dra	K5 III		
GI 529	K6 V						
61 Cyg B	K7 V			α Lyn	K7 III		
				ν Aur	M0 III		
GI 846	M0.5 V			χ Peg	M2+ III	μ Cep	M2- Ia
GI 411	M2 V					HD 10465	M2 Ib
GI 752 A	M2.5 V						
GI 725 B	M3.5 V			HR 3577	M4+ III		
GI 166 C	M4.5 V					EV Car	M4.5 Ia
				BK Vir	M7- III		
				R Leo	M9: III		

Bibliography

- Garrison, R.F., & Gray, R.O. 1994, AJ, 107, 1556
- Gray, R.O., Corbally, C.J., Garrison, R.F., McFadden, M.T., & Robinson, P.E. 2003, AJ, 126, 2048
- Gray, R.O., Corbally, C.J., Garrison, R.F., McFadden, M.T., Bubar, E.J., McGahee, C.E., O'Donoghue, A.A., & Knox, E.R. 2006, AJ, 132, 161
- Gray, R.O., & Garrison, R.F. 1987, ApJS, 65, 581
- Gray, R.O., & Garrison, R.F. 1989, ApJS, 69, 301
- Gray, R.O., & Garrison, R.F. 1989, ApJS, 70, 623
- Johnson, H.L., & Morgan, W.W. 1953, ApJ, 117, 313
- Keenan, P.C., & McNeil, R.C. 1989, ApJS, 71, 245
- Morgan, W.W. 1951, POMic, 10, 33
- Morgan, W.W., & Keenan, P.C. 1973, ARAA, 11, 29
- Morgan, W.W., Keenan, P.C., & Kellman, E. 1943, *An Atlas of Stellar Spectra* (Chicago: University of Chicago Press)
- Walborn, N.R. 1973, AJ, 78, 1067

Appendix B: Calibrations of the MK System

ABSOLUTE MAGNITUDE CALIBRATION

References consulted in compiling Tables B.1 and B.2:

Table B.1 Averaged Absolute Visual Magnitude Calibration for the Early-type Stars

SpT	V	IV	III	II	Ib	Iab	Ia
O2-3	-5.6	...	-6.0	-6.8
O4	-5.5	...	-6.4:	-7.0
O5	-5.5	...	-6.4	-7.0
O6	-5.3	...	-5.6	...	-6.3:	...	-7.0
O6.5	-5.3	...	-5.6	...	-6.3:	...	-7.0
O7	-4.8	...	-5.6	-5.9	-6.3:	...	-7.0
O7.5	-4.8	...	-5.6	-5.9	-6.3:	...	-7.0
O8	-4.4	...	-5.6	-5.9	-6.2:	-6.5	-7.0
O8.5	-4.4	...	-5.6	-5.9	-6.2:	-6.5	-7.0
O9	-4.3	-5.0	-5.6	-5.9	-6.2	-6.5	-7.0
O9.5	-4.1	-4.7	-5.3	-5.9	-6.2	-6.5	-7.0
O9.7	-5.9	-6.2	-6.5	-7.0
B0	-4.1	-4.6	-5.0	-5.6	-5.8		-7.0
B1	-3.5	-3.9	-4.4	-5.1	-5.7		-7.0
B2	-2.5	-3.0	-3.6	-4.4	-5.7		-7.0
B3	-1.7	-2.3	-2.9	-3.9	-5.7		-7.0
B4	-1.4	-2.0	-2.6	-3.9	-5.7		-7.0
B5	-1.1	-1.6	-2.2	-3.7	-5.7		-7.0
B6	-0.9	-1.3	-1.9	-3.7	-5.7		-7.1
B7	-0.4	-1.3	-1.6	-3.6	-5.6		-7.1
B8	0.0	-1.0	-1.4	-3.4	-5.6		-7.1
B9	0.7	-0.5	-0.8	-3.1	-5.5		-7.1
A0	1.4	0.3	-0.8	-2.8	-5.2		-7.1
A1	1.6	0.3	-0.4	-2.6	-5.1		-7.3
A2	1.9	0.5	-0.2	-2.4	-5.0		-7.5
A3	2.0	0.7	0.0	-2.3	-4.8		-7.6
A5	2.1	1.2	0.3	-2.1	-4.8		-7.7
A7	2.3	1.5	0.5	-2.0	-4.8		-8.0
A9	2.5	1.6	0.6	-2.0	-4.8		-8.3

Table B.1 Continued

SpT	V	IV	III	II	Ib	Iab	Ia
F0	2.6	1.7	0.6	-2.0	-4.7		-8.5
F1	2.8	1.8	0.6	-2.0	-4.7		-8.5
F2	3.0	1.9	0.6	-2.0	-4.6		-8.4
F3	3.1	1.9	0.6	-2.0	-4.6		-8.3
F4	3.3	2.0	0.7	-2.0	-4.6		-8.3
F5	3.4	2.1	0.7	-2.0	-4.4		-8.2
F6	3.7	2.2	0.7	-2.0	-4.4		-8.1
F7	3.8	2.3	0.6	-2.0	-4.4		-8.1
F8	4.0	2.4	0.6	-2.0	-4.3		-8.0
F9	4.2	2.6	0.6	-2.0	-4.2		-8.0

Table B.2 Averaged Absolute Visual Magnitude Calibration for the Late-type Stars

SpT	V	IV	IIIb	IIIab	IIIa	II	Ib	Ia
G0	4.4	2.8		0.6		-2.0	-4.1	-8.0
G1	4.5	2.9		0.5		-2.0	-4.1	-8.0
G2	4.7	3.0		0.4		-2.0	-4.0	-8.0
G3	4.9	3.0		0.4		-1.9	-4.0	-8.0
G4	5.0	3.1		0.4		-1.9	-3.9	-8.0
G5	5.2	3.2		0.4		-1.9	-3.9	-8.0
G6	5.3	3.2		0.4		-1.9	-3.8	-8.0
G7	5.5	3.2		0.3		-1.9	-3.8	-8.0
G8	5.6	3.2	0.8	0.3	-0.4	-1.9	-3.7	-8.0
G9	5.7	3.2	0.8	0.25	-0.4	-2.0	-3.7	-8.0
K0	5.9	3.2	0.7	0.2	-0.5	-2.0	-3.6	-8.0
K1	6.1		0.6	0.1	-0.6	-2.1	-3.6	-8.0
K2	6.3		0.6	0.1	-0.7	-2.1	-3.6	-8.0
K3	6.9		0.4	-0.1	-0.8	-2.2	-3.6	-8.0
K4	7.4		0.3	-0.2	-1.0	-2.3	-3.7	-8.0
K5	8.0		0.1	-0.4	-1.1	-2.5	-3.8	-8.0
K7	8.5		0.0	-0.5	-1.2	-2.5	-3.8	-7.7
M0	9.2		-0.2	-0.7	-1.3	-2.6	-3.9	-7.3
M1	9.7		-0.3	-0.8	-1.5	-2.7	-4.1	-7.3
M2	10.6		-0.6	-1.1	-1.7	-2.9	-4.2	-7.0
M3	11.6		-0.8	-1.3	-1.9			
M4	12.9		-1.1	-1.6	-2.2			
M5	14.5							
M6	16.1							

Corbally, C.J., & Garrison, R.F. 1984, in *The MK Process and Stellar Classification*, ed. R.F. Garrison (Toronto: University of Toronto), p. 277

Drilling, J.S., & Landolt, A.U. 2000, in *Allen's Astrophysical Quantities*, 4th Ed., ed. A.N. Cox (New York: Springer-Verlag), p. 381

- Egret, D., Keenan, P.C., & Heck, A. 1982, AA, 106, 115
 Gray, R.O. 1986, Ph.D. Thesis, University of Toronto
 Gotlieb, D.M. 1978, ApJS, 38, 287
 Keenan, P.C. 1973, in *IAU Symposium 54: Problems of Calibration of Absolute Magnitudes and Temperatures of Stars*, ed. B. Hauck & B.E. Westerlund (Dordrecht: Reidel), p. 68
 Keenan, P.C. 1978, in *IAU Symposium 80: The HR Diagram*, ed. A.G.D. Philip & D.S. Hayes (Dordrecht: Reidel), p. 13
 Martins, F., Schaerer, D., & Hillier, D.J. 2005, AA, 436, 1049
 Reid, I.N., & Hawley, S.L. 2000 *New Light on Dark Stars* (Chichester: Springer-Praxis), p. 453

EFFECTIVE TEMPERATURE CALIBRATION

References consulted in compiling Tables B.3 and B.4

Table B.3 Effective Temperature Calibration for the Early-type Stars

SpT	Dwarfs	Giants	Supergiants
O3	44852	42942	42233
O4	42857	41486	40422
O5	40862	39507	38612
O5.5	39865	38003	37706
O6	38867	36673	36801
O6.5	37870	35644	35895
O7	36872	34638	34990
O7.5	35874	33487	34084
O8	34877	32573	33179
O8.5	33879	31689	32274
O9	32882	30737	31368
O9.5	31884	30231	30463
B0	29000	29000	
B1	24500	24500	
B2	19500	21050	18000
B3	16500	16850	
B5	15000	14800	13600
B7	13000	13700	
B8	11500	13150	11100
B9	10700	11731	
A0	9800	10000	9900
A1	9500	9500	
A2	8900	9000	9000
A3	8520	8500	8400
A5	8150	8000	8100
A7	7830	7750	7800
A9	7380	7450	

Table B.3 Continued

SpT	Dwarfs	Giants	Supergiants
F0	7250	7350	7200
F1	7120	7200	7050
F2	7000	7050	6960
F3	6750	6840	6770
F5	6550	6630	6570
F7	6250	6330	6280
F8	6170	6220	6180
F9	6010	6020	5980

Table B.4 Effective Temperature Calibration for the Late-type Stars

SpT	Dwarfs	Giants	Supergiants
G0	5900	5800	5590
G1	5800	5700	5490
G2	5750	5500	5250
G5	5580	5200	5000
G8	5430	4950	4700
G9	5350		
K0	5280	4810	4500
K1	5110	4585	4200
K2	4940	4390	4100
K3	4700	4225	
K5	4400	3955	
K7	4130		3840
M0	3759	3845	3790
M1	3624	3750	3745
M2	3489	3655	3660
M3	3354	3560	3605
M4	3219	3460	
M5	3084	3355	3450
M6	2949	3240	
M7	2814	3100	
M8	2679	2940	
M9	2544	2755	
L0	2409		
L1	2274		
L2	2139		
L3	2004		
L4	1869		
L5	1734		
L6	1599		
L7	1464		
L8	1329		

- Blackwell, D.E., & Lynas-Gray, A.E. 1994, AA, 282, 899
- Castelli, F. 1991, AA, 251, 106
- Crawford, D.L. 1978, AJ, 83, 48
- Drilling, J.S., & Landolt, A.U. 2000, in *Allen's Astrophysical Quantities, 4th Ed.*, ed. A.N. Cox (New York: Springer-Verlag), p. 381
- Gray, R.O., Graham, P.W., & Hoyt, S.R. 2001, AJ, 121, 2159
- Gray, R.O., et al. 2003, AJ, 126, 2048
- Kirkpatrick, J.D. (Chapter 9)
- Levesque, E., et al. 2006, ApJ, 645, 1102
- Martins, F., Schaerer, D., & Hillier, D.J. 2005, AA, 436, 1049
- Richichi, A., Fabbroni, L., Ragland, S., & Scholz, M. 1999, AA, 344, 511
- Venn, K.A. 1995, ApJS, 99, 659

Appendix C: The Book Website

A website has been developed to accompany this book. Its purpose is to act as a site on the Internet where readers can download many of the spectra illustrated in the book and to link to other resources. The website is <http://www.phys.appstate.edu/MK/MKbook.html>.

The spectra directly available on the website are those spectra illustrated in the book that were obtained at the Dark Sky Observatory, the research observatory of Appalachian State University. This observatory is situated in the mountains of northwest North Carolina; its main instrument is a 0.8 m Ritchey-Chretien reflecting telescope equipped with an inhouse spectrograph, the so-called “GM spectrograph.” More information on this spectrograph may be found at <http://www.phys.appstate.edu/spectrum/GM/GM.html>. These spectra may be used freely for education and research. If they are used in a publication, this book should be referenced.

We also include links on the website where readers may pick up spectra from other sources. Of particular interest may be the Nearby Stars Spectra website, <http://stellar.phys.appstate.edu>.

The standard star tables in Appendix A will be posted to the website, and readers may be interested in periodically checking those tables as we continue to update Garrison’s hierarchy of standards with primary and secondary standards for the MK system.

The software that the two main authors use for spectral classification, the program `xmk22`, illustrated in Figure 1.13, is available for download on the website. This program comes in two versions, one for Linux/UNIX and one for Microsoft Windows (`winmk`). These programs may be employed for personal use or use in education, but resale and/or redistribution of these programs is strictly forbidden.

